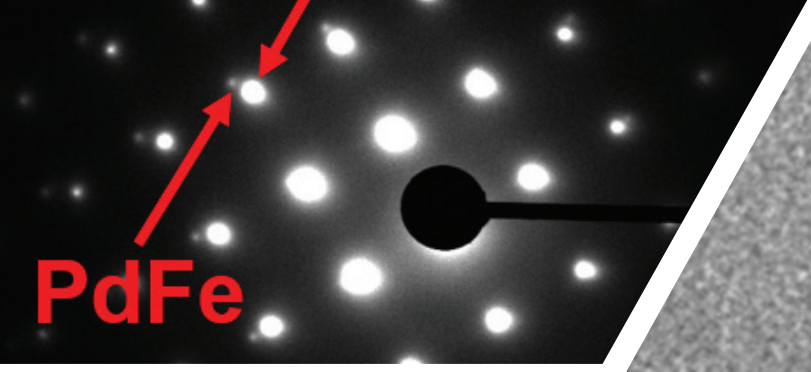

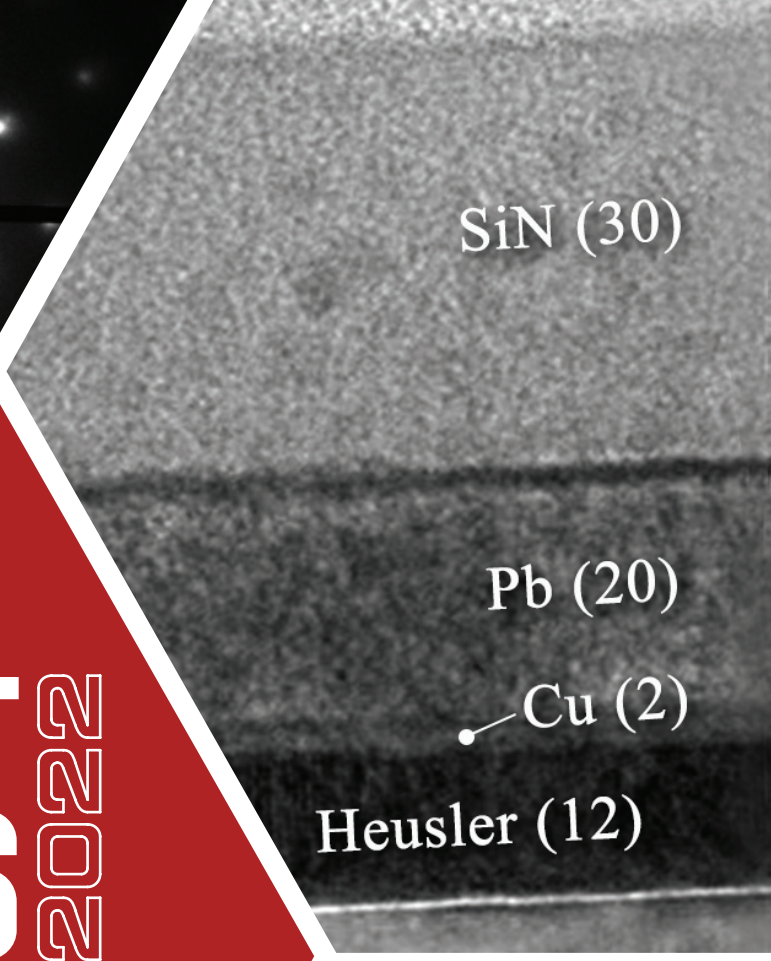

KAZAN

EAST MAG 2022

ABSTRACTS
VOLUME I

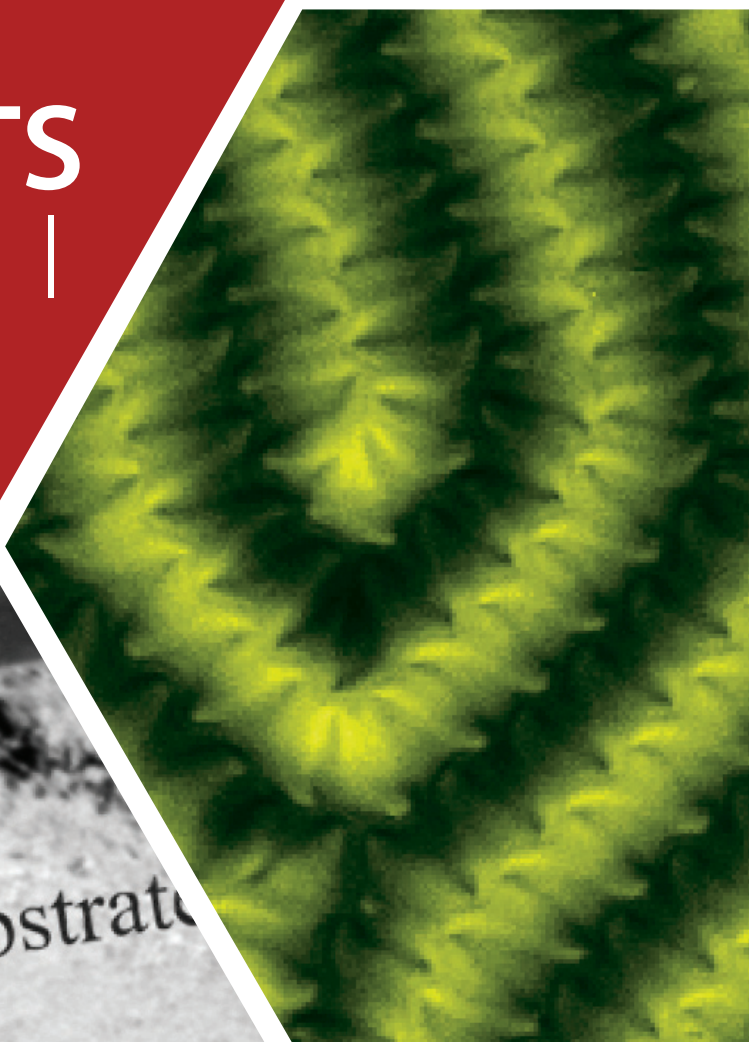

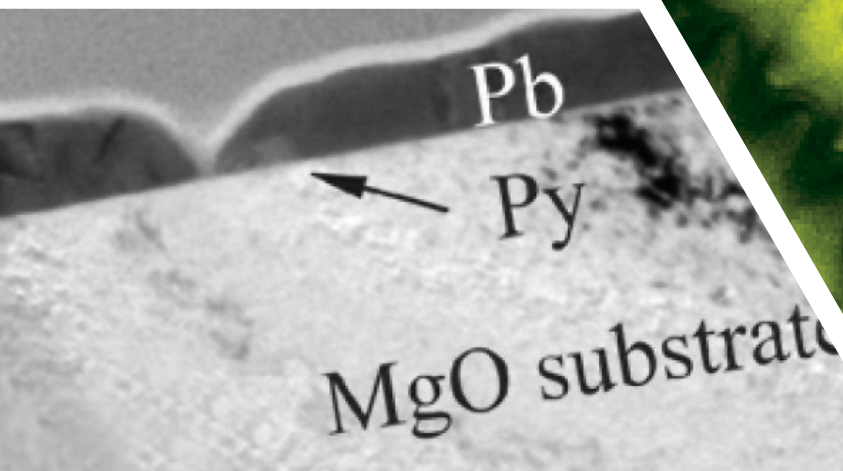

VIII Euro-Asian Symposium «Trends in MAGnetism»

August 22–26, 2022, Kazan, Russia

Zavoisky Physical-Technical Institute FRC Kazan SC RAS

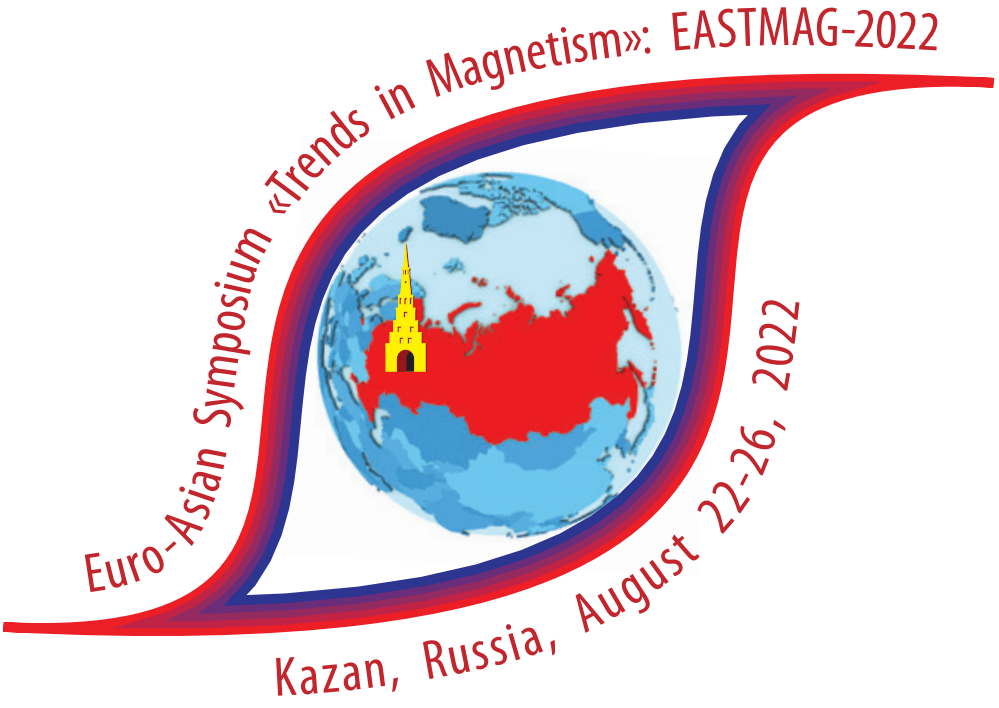

BOOK OF ABSTRACTS

VOLUME I

Symposium is supported by:

Ministry of Science
and Higher Education
of the Russian Federation

Ministry of Education and Science
of the Republic of Tatarstan

Federal Research Center
"Kazan Scientific Center of
the Russian Academy of Sciences"

Zavoisky Physical-Technical
Institute FRC KazanSC RAS

Kazan Federal University

Academy of Sciences
of the Republic of Tatarstan

Symposium is sponsored by:

Government
of the Republic of Tatarstan

"MTEON" Ltd

ORGANIZING COMMITTEE

Vladimir V. USTINOV (Ekaterinburg)	Symposium General Chairman
Alexey A. KALACHEV (Kazan)	Organizing Committee Chairman
Kev M. SALIKHOV (Kazan)	Organizing Committee Co-Chairman
Lenar R. TAGIROV (Kazan)	Organizing Committee Co-Chairman
Rushana M. EREMINA (Kazan)	Program Committee Chairman
Sergey M. KHANTIMEROV (Kazan)	Local Committee Chairman
Dmitrii A. TAYURSKII (Kazan)	Local Committee Co-Chairman
Marat R. GAFUROV (Kazan)	Local Committee Co-Chairman
Sergey M. AKHMIN (Kazan)	Publication Committee Chairman
Sufia A. ZIGANSHINA (Kazan)	Symposium Chief Secretary
Andrey A. KAMASHEV (Kazan)	Symposium Secretary
Ivan V. YATSYK (Kazan)	Symposium Secretary

PROGRAM COMMITTEE

Nikolay G. BEBENIN (Ekaterinburg)
Alexander V. BELUSHKIN (Dubna)
Mikhail V. EREMIN (Kazan)
Nikolay V. ERSHOV (Ekaterinburg)
Andrey A. FRAERMAN (Nizhny Novgorod)
Zukhra V. GAREEVA (Ufa)
Andrei A. GIPPIUS (Moscow)
Oksana A. GOLOVNYA (Ekaterinburg)
Alexander A. GOLUBOV (Dolgoprudny)
Alexander B. GRANOVSKY (Moscow)
Sergey V. GRIGORIEV (Gatchina)
Alexey O. IVANOV (Ekaterinburg)
Alexandra M. KALASHNIKOVA (Saint Petersburg)
Leonid N. KOROTKOV (Voronezh)
Alexander I. KURBAKOV (Gatchina)
Ivan V. LEONOV (Ekaterinburg)
Alexander S. MEL'NIKOV (Nizhny Novgorod)
Mikhail A. MILYAEV (Ekaterinburg)
Elena V. MOSTOVSHCHIKOVA (Ekaterinburg)
Alexander A. MUKHIN (Moscow)
Alexey V. OGNEV (Vladivostok)
Sergei G. OVCHINNIKOV (Krasnoyarsk)
Alexander P. PYATAKOV (Moscow)
Yuriy L. RAIKHER (Perm)
Valeria V. RODIONOVA (Kaliningrad)
Alexander V. SADOVNIKOV (Saratov)
Anatolie S. SIDORENKO (Chisinau)
Alexander I. SMIRNOV (Moscow)
Sergey V. STRELTSOV (Ekaterinburg)
Gregory B. TEITELBAUM (Kazan)
Alexander N. VASILIEV (Moscow)
Evgeniia L. VAVILOVA (Kazan)
Roman V. YUSUPOV (Kazan)
Anatoly E. YERMAKOV (Ekaterinburg)
Svetlana V. YURTAEVA (Kazan)

PUBLICATION COMMITTEE

Sergey G. L'VOV (KPTI FRC KazSC RAS)
Olga B. YANDUGANOVA (KPTI FRC KazSC RAS)
Polina A. AGZAMOVA (IMP UB RAS)

LOCAL COMMITTEE

Tatiana P. GAVRILOVA (KPTI FRC KazSC RAS)
Ilshat I. FAZLIZHANOV (KPTI FRC KazSC RAS)
Andrey A. KAMASHEV (KPTI FRC KazSC RAS)
Ivan V. YATSYK (KPTI FRC KazSC RAS)
Alexei V. SHESTAKOV (KPTI FRC KazSC RAS)
Raisa R. GUSEVA (KPTI FRC KazSC RAS)
Valentina I. KHABIBULLINA (KPTI FRC KazSC RAS)
Valentina V. PUSHKOVA (KPTI FRC KazSC RAS)
Alla M. AKHMETGALIEVA (KPTI FRC KazSC RAS)
Olga O. KUPRIYANOVA (KPTI FRC KazSC RAS)
Yuriy V. OLADOSHKIN (KPTI FRC KazSC RAS)
Dilyara V. ILMATOVA (KPTI FRC KazSC RAS)
Ranis R. GARIPOV (KPTI FRC KazSC RAS)
Rodion F. LIKEROV (KPTI FRC KazSC RAS)
Daniil V. POPOV (KPTI FRC KazSC RAS)
Roman V. YUSUPOV (IP KFU)
Igor V. YANILKIN (IP KFU)
Airat G. KIIAMOV (IP KFU)
Ruslan G. BATULIN (IP KFU)
Anna S. MOROZOVA (KPTI FRC KazSC RAS)
Albina R. GAFAROVA (KPTI FRC KazSC RAS)
Amir I. GUMAROV (IP KFU)
Iskander R. VAKHITOV (IP KFU)
Almaz L. ZINNATULLIN (IP KFU)
Mikhail A. CHEROSOV (IP KFU)
Evgenii M. BEGISHEV (KPTI FRC KazSC RAS)
Alsu R. SAKHBIEVA (IP KFU)
Marina S. YATSYK (IP KFU)
German A. NOVIKOV (KPTI FRC KazSC RAS)
Tatiana N. ENDEROVA (KPTI FRC KazSC RAS)
Diana E. ZHELEZNYAKOVA (KPTI FRC KazSC RAS)

TOPICS

Plenary lectures

Section A. Spintronics and magnetic nanostructures

Section B. Spin dynamics and magnetic resonances

Section C. Low dimensional magnetism

Section D. Domain walls, vortices and skyrmions

Section E. Magnetotransport, magnetooptics and magnetophotonics

Section F. Magnetoelastic, magnetocaloric and shape memory effects

Section G. Frustrated and disordered magnetism

Section H. Magnetism of strongly correlated electron systems

Section I. Magnetism and superconductivity

Section J. Soft and hard magnetic materials

Section K. Magnetic semiconductors, multiferroics, topological insulators

Section L. Magnetic soft matter

Section M. Magnetism in biology and medicine

Section N. Instruments and techniques for studying magnetism

Section O. MAX materials

Contents

Plenary lectures 1

Pl.1
SPIN-ORBIT TRANSITION METAL COMPOUNDS
S.V. Streltsov 2

Pl.2
NEUTRON SCATTERING METHODS FOR STUDYING MAGNETISM
S.V. Grigoriev 3

Pl.3
PT-SYMMETRY AND EXCEPTIONAL POINTS IN SPINTRONICS, MAGNONICS, AND PHONONICS
S.A. Nikitov, D.V. Kalyabin, A.R. Safin, O.S. Temnaya, A.V. Dorofeenko, A.A. Zyablovsky A.V. Sadovnikov, E.A. Vilkov 4

Pl.4
SPIN CROSSOVERS IN MAGNETIC MATERIALS
V.A. Dudnikov, V.A. Gavrichkov, S.V. Nikolaev, Yu.S. Orlov, S.G. Ovchinnikov 7

Pl.5
MANIPULATION OF MAGNETISM VIA FERROELECTRIC SWITCHING
Shuai Dong 9

Pl.6
THE ELECTRIC FIELD-MODULATED SURFACE ENERGY OF MAGNETIC DOMAIN WALLS: STRIPE DOMAIN STRUCTURE "REFRACTION" AND MAGNETIC BUBBLE DOMAIN "BLOWING"
S.A. Kaminskiy, A.A. Podkletnova, A.I. Yadvichuk, D.P. Kulikova, E.P. Nikolaeva, A.P. Pyatakov 10

Pl.7
FERROMAGNET PARTICLES IN A POLYMER HARNESS. MESOSCOPIC MAGNETOMECHANICS AND MACROSCOPIC BEHAVIOR OF MAGNETOACTIVE ELASTOMERS
Yu.L. Raikher 12

Pl.8
ULTRAFAST MAGNETOPHOTONICS
V.I. Belotelov 14

Pl.9
MAGNETIC NANOPARTICLES IN MEDICINE
Y.A. Koksharov 15

Pl.10
SPIN FLUCTUATION TRANSITIONS IN THE SPIRAL MAGNET MnSi
S.V. Demishev, A.N. Samarin, M.S. Karasev, S.V. Grigoriev, A.V. Semeno 16

CONTENTS

Section A.
Spintronics and magnetic nanostructures 18

A.I1
CHIRAL HELIMAGNET AS A SPIN WIND TURBINE AND SPIN ARCHIMEDEAN SCREW
V.V. Ustinov, I.A. Yasyulevich 19

A.I2
CURRENT NOISE GEOMETRICALLY GENERATED BY A DRIVEN MAGNET
I.S. Burmistrov 21

A.I3
TUNNELING HALL EFFECT: THEORY AND EXPERIMENT
E.A. Karashtin, N.S. Gusev, I.Yu. Pashen'kin, M.V. Sapozhnikov, A.A. Fraerman . . . 22

A.I4
CONTROLLABLE THREE-STATE MAGNETIZATION SWITCHING IN EPITAXIAL $Pd_{0.92}Fe_{0.08}/Ag/Pd_{0.96}Fe_{0.04}$ HETEROSTRUCTURE
I.V. Yanilkin, A.I. Gumarov, G.F. Gizzatullina, R.V. Yusupov, L.R. Tagirov 23

A.I5
FUNCTIONAL LOW COERCIVE GMR MULTILAYERS FOR MAGNETIC SENSORS
M.A. Milyaev, L.I. Naumova, V.V. Proglyado, T.P. Krinitsina, R.S. Zavornitsyn, I.A. Naydanov, V.V. Ustinov 24

A.I6
EFFECT OF VAN HOVE SINGULARITIES ON THE EFFICIENCY OF SPIN CURRENT GENERATION BY TRAVELLING SPIN WAVES IN YIG/Pt STRUCTURES
M. Seleznev, Y. Nikulin, V. Sakharov, G. Dudko, S. Vysotskii, A. Kozhevnikov, Y. Khivintsev, Y. Filimonov 26

A.I7
INFLUENCE OF DZYALOSHINSKII-MORIYA INTERACTION ON HYSTERESIS PROCESSES IN MAGNETOELECTRIC NANOELEMENT
Z.V. Gareeva, N.V. Shulga, R.A. Doroshenko, A.K. Zvezdin 28

A.I8
MAGNONIC TRANSPORT IN 3D MULTILAYER STRUCTURES WITH BROKEN TRANSLATION SYMMETRY
A.V. Sadovnikov, E.N. Beginin, A.A. Martyshkin, S.A. Nikitov 29

A.O1
EASY-CONE STATE IN SPIN-TORQUE DIODE UNDER COMBINED ACTION OF MAGNETOSTATICS AND INTERFACIAL PERPENDICULAR MAGNETIC ANISOTROPY
A.G. Buzdakov, P.N. Skirdkov, K.A. Zvezdin 30

A.O2
FERROMAGNETIC SILICIDES AND GERMANIDES EPITAXIAL FILMS AND MULTILAYERED HYBRYD STRUCTURES: SYNTHESYS, MAGNETIC AND TRANSPORT PROPERTIES
I.A. Tarasov, I.A. Yakovlev, M.V. Rautskii, I.A. Bondarev, A.V. Lukyanenko, A.L. Sukhachev, S.N. Varnakov, S.G. Ovchinnikov, N.V. Volkov, A.S. Tarasov 31

A.O3
METASTABLE STATES IN EXCHANGE-COUPLED FERROMAGNETIC DISKS
D.A. Tatarskiy, I.Yu. Pashen'kin, E.V. Skorokhodov, S.A. Gusev 33

CONTENTS

A.O4
ULTRAFAST SIGNATURES OF MAGNETIC INHOMOGENEITY IN $Pd_{1-x}Fe_x$ ($x \leq 0.08$) EPITAXIAL THIN FILMS
R.V. Yusupov, A.V. Petrov, S.I. Nikitin, I.V. Yanilkin, A.I. Gumarov, L.R. Tagirov 36

A.O5
Co-Zn NANOFERRITES FOR HIGH FREQUENCY APPLICATIONS: CORRELATIONS BETWEEN DIELECTRIC AND MAGNETIC PROPERTIES
A. Thakur, I.S. Edelman, S.G. Ovchinnikov, A.L. Sukhachev, D.A. Petrov, P. Thakur 37

A.O6
SPACER THICKNESS AND TEMPERATURE DEPENDENCES OF THE INTERLAYER EXCHANGE COUPLING IN A Co/Pt/Co THREE-LAYER STRUCTURE
V.S. Gornakov, I.V. Shashkov, Yu.P. Kabanov 39

A.O7
SLOW DYNAMICS PHENOMENA IN MAGNETIC MULTILAYER NANOSTRUCTURES
M.M. Boldyreva, Yu.K. Evstafyeva, M.V. Mamonova, P.V. Prudnikov, V.V. Prudnikov 41

A.O8
INFLUENCE OF THE EFFECT OF LOCAL LASER HEATING ON SPIN WAVE PROPAGATION IN A BILAYER FERROMAGNETIC FILM
V.A. Gubanov, E.G. Lock, A.V. Sadovnikov, S.A. Nikitov 43

A.O9
DIFFERENT TYPES OF NANOWIRES – SYNTHESIS, STRUCTURE, PROPERTIES AND MAGNETIC PROPERTIES
D. Zagorskiy, I. Doludenko, D. Khairetdinova, R. Khaibullin, D. Cherkasov, A. Gippius, S. Zhurenko, O. Zhigalina, S. Chigarev, E. Vilkov, L. Fomin 45

A.O10
MAGNETISM AND EPR-SPECTRA OF NANOCRYSTALLINE AND AMORPHOUS TiO_2 DOPED BY Fe AND Al
L.S. Molochnikov, A.E. Yermakov, M.A. Uimin, A.S. Minin , K.I. Borodin, D.W. Boukhvalov, D.V. Starichenko, A.S. Volegov, R.M. Eremina, I.V. Yatsyk, G.S. Zakharova, M.I. Kurkin, S.F. Konev, A.M. Murzakayev, V.S. Gaviko 47

A.O11
CLASSICAL AND QUANTUM EFFECTS OF THE MAGNETIZATION DYNAMICS INDUCED BY PICOSECOND PULSE OF SPIN CURRENT
V.V. Yurlov, K.A. Zvezdin, A.K. Zvezdin 48

A.O12
THE INFLUENCE OF EXCHANGE CORRELATION FUNCTIONAL ON THE PROPERTIES OF $Mn_2V(Al,Si)$ HEUSLER ALLOYS
V.D. Buchelnikov, D.R. Baigutlin, V.V. Sokolovskiy, O.N. Miroshkina 50

A.O13
INTERFACE EFFECTS IN HETEROGENEOUS INTEGRATION OF $Bi_3Fe_5O_{12}$ FILMS
A.S. Fedorov, S.S. Safonov, A.A. Fedorova, S.A. Nikitov, A.I. Stognii, M.V. Logunov 53

A.O14
THE EFFECT OF MAGNON-MAGNON DRAG IN MAGNETIC INSULATOR LAYERS THROUGH OF NON MAGNETIC METAL LAYER
I.I. Lyapilin 55

CONTENTS

A.O15
NON-RESONANT BROADBAND SPIN-TORQUE DIODE RECTIFICATION OF MICROWAVE CURRENT IN A MTJ WITH IN-PLANE MAGNETIZATION OF THE FREE LAYER
G.A. Kichin, P.N. Skirdkov, K.A. Zvezdin 56

A.O16
SPIN VALVES FOR STUDYING HELICOIDAL STATES IN NANOLAYES OF CHIRAL Dy AND Ho HELIMAGNETS
R.S. Zavornitsyn, M.A. Milyaev, L.I. Naumova, T.P. Krinitsina, V.V. Proglyado, V.V. Ustinov 57

A.O17
MATHEMATICAL MODELLING OF THE SOT-MRAM ELEMENT BASED ON THE SPIN-HALL EFFECT
N.V. Ostrovskaya, V.A. Skidanov, Iu.A. Iusipova 59

A.O18
MAGNETIC AND MOSSBAUER STUDIES OF Fe_xCO_{1-x} NANOWIRES
I.V. Perunov, K.V. Frolov, M.A. Chuev, I.M. Doludenko, D.L. Zagorskii, N.C. Chumakov, I.S. Lyubutin 61

A.O19
MONTE CARLO SIMULATION OF MAGNETIC PROPERTIES OF SPIN-VALVE NANOSTRUCTURES
E.V. Drovorub, A.S. Egorina, N.I. Piskunova, P.V. Prudnikov, V.V. Prudnikov 62

A.O20
TUNABLE RECEIVER OF SUB-THZ SIGNALS BASED ON AN ANTIFERROMAGNET
A.R. Safin 64

A.O21
EVOLUTION OF MAGNETIC TUNNEL JUNCTION'S MODES FOR DIFFERENT DIRECTIONS OF AN EXTERNAL MAGNETIC FIELD
M.D. Shkanakina, G.A. Kichin, P.N. Skirdkov, K.A. Zvezdin 66

A.O22
FEATURES OF THE CURIE POINT BEHAVIOR IN NANOGRANULATED STRUCTURES OF THE Cd_3As_2-MnAs SYSTEM
M.H. Al-Onaizan, A.T. Morchenko 69

A.O23
SPIN REORIENTATION TRANSITION IN CoFeB/MgO/CoFeB TUNNEL JUNCTION IMPLEMENTED BY ULTRAFAST LASER-INDUCED SUPPRESSION OF PERPENDICULAR MAGNETIC ANISOTROPY
L.A. Shelukhin, R.R. Gareev, V. Zbarsky, J. Walowski, M. Münzenberg, N.A. Pertsev, A.M. Kalashnikova 71

A.O24
ELECTRONIC AND MAGNETIC PROPERTIES OF SPHERICAL CARBON SHELLS
K.B. Tsiberkin, E.I. Kovycheva 73

A.O25
SPIN TRANSPORT IN IRIDATE/MANGANITE INTERFACE
G.A. Ovsyannikov, K.Y. Constantinian, V.A. Shmakov, A.V. Shadrin, Yu.V. Kislinski, E.A. Kalachev, A.A. Klimov 75

CONTENTS

A.O26
ELECTRIC AND MAGNETIC PROPERTIES OF Co_2FeAl AND Co_2FeSi HEUSLER ALLOY FIMS GROWN ON SAPPHIRE SUBSTRATES
I.V. Malikov, V.A. Berezin, L.A. Fomin, V.V. Marchenkov 77

A.O27
MOVING SPIN-VALVE BRIDGE CONFIGURATIONS IN INHOMOGENEOUS 3D MAGNETIC FIELD
N.G. Chechenin, G.V. Babaytsev, I.O. Dzhun, I.L. Romashkina, M.G. Kozin, A.V. Makunin 80

A.O28
FEATURES OF FERROMAGNETISM IN PALLADIUM FILMS IMPLANTED WITH COBALT AND IRON IONS
R.I. Khaibullin, A.I. Gumarov, I.R. Vakhitov, N.M. Lyadov, I.I. Gumarova, I.V. Yanilkin, R.V. Yusupov, L.R. Tagirov 82

A.O29
INVESTIGATION OF THE DEPENDENCE OF THE MAGNETIC PROPERTIES OF FeNi ALLOY NANOWIRES ON THE ASPECT RATIO
I.M. Doludenko, D.L. Zagorskiy, D.R. Khairetdinova 84

A.O30
MAGNETIZATION REVERSAL MECHANISMS OF FeNi/FeMn BILAYERS DEPENDING ON GROWTH CONDITIONS
Ch. Gritsenko, V. Lepalovskij, M. Volochaev, V. Komanický, A. Gorkovenko, H. Pazniak, N. Andreev, V. Rodionova 86

A.O31
ULTRA FAST SPIN POLARIZATION SWITCHING IN A HYBRID STRUCTURE QUANTUM WELL – SPIN SPLIT BOUND STATE
V.N. Mantsevich, I.V. Rozhansky, N.S. Maslova, P.I. Arseyev, N.S. Averkiev, E. Lahderanta. 87

A.O32
THE QUANTUM MECHANICAL CALCULATION OF THE THERMAL-DRIVEN SPIN TRANSFER IN THE MTJ, BASED ON A CRYSTALLINE MgO TUNNEL SPACER
G.D. Demin, N.A. Dyuzhev 89

A.O33
HEAT-INDUCED FANO RESONANSE TUNABILITY IN MAGNONIC MICROSTRUCTURES
A.A. Grachev, E.N. Beginin, A.V. Sadovnikov. 91

A.O34
MAGNETIC ANISOTROPY AND DZYALOSHINSKII-MORIYA INTERACTION IN EPITAXIAL Pd/Co/CoO FILMS
A.G. Kozlov, G.S. Suslin, E.V. Tarasov, O.E. Ayanitov, V.S. Shatilov, A.V. Davydenko. 92

A.O35
INVESTIGATION OF MAGNETIC TUNNEL JUNCTIONS UNDER THE SIMULTANEOUS ACTION OF DIRECT AND ALTERNATING CURRENTS, BOTH IN RESONANT AND BROADBAND MODES
A.V. Duvakina, G.A. Kichin, P.N. Skirdkov, K.A. Zvezdin 94

CONTENTS

A.O36
INFLUENCE OF THE NANOCRYSTALLITE SIZE ON SPATIAL SPIN-MODULATED STRUCTURE OF $BiFeO_3$
N.E. Gervits, A.V. Tkachev, S.V. Zhurenko, A.V. Gunbin, N.A. Lomanova, D.P. Danilovich, A.V. Bogach, A.A. Gippius 96

A.P1
MAGNETIC RESONANCE PROPERTIES OF LOW-DIMENSIONAL COBALT-Al_2O_3-GERMANIUM TUNNEL CONTACT
A.V. Kobyakov, G.S. Patrin, V.I. Yushkov, Ya.G. Shiyan, R.Yu. Rudenko, N.N. Kosyrev 97

A.P2
INVESTIGATION OF CURRENT-INDUCED FIELDS IN THE YIG/COTB STRUCTURE
M.A. Bazrov, M.E. Letushev, Zh.Zh. Namsaraev, M.E. Stebliy, Wenqing He, Caihua Wan, Xiufeng Han 99

A.P3
MAGNETOPLASMONIC CRYSTAL FOR DC MAGNETIC FIELD TOPOGRAPHY
V.K. Belyaev, D.V Murzin, A.A. Grunin, A.A. Fedyanin, V.V. Rodionova 101

A.P4
MAGNETIC PROPERTIES OF COMPOSITION GRADED Co-Ni RODS
E.A. Denisova, E.A. Chekanova, S.V. Komogortsev, O.A. Li, R.S. Iskhakov, I.V. Nemtsev, S.V. Semenov 103

A.P5
FERROMAGNETIC RESONANCE INVESTIGATIONS OF EXCHANGE BIASED NiFe/IrMn/NiFe TRILAYER STRUCTURES
I.O. Dzhun, G.V. Babaytsev, I.L. Romashkina, M.G. Kozin, A.V. Makunin, N.G. Chechenin 104

A.P6
AB INITIO CALCULATIONS OF MAGNETIC PROPERTIES OF CHIRAL MONOAXIAL HELIMAGNET
D.V. Evsin, M.V. Mamonova, V.O. Borzilov, P.V. Prudnikov 106

A.P7
FEATURES OF CRYSTAL STRUCTURE AND EXCHANGE BIAS IN Cr-Mn/FeNi FILMS
A.A. Feshchenko, M.E. Moskalev, V.N. Lepalovskij, A.N. Gorkovenko, E.A. Kravtsov, V.O. Vas'kovskiy 108

A.P8
MAGNETIC AND STRUCTURAL TRANSFORMATION OF CARBON-COATED IRON OXIDE NANOCOMPOSITES
K.O. Funtov, S.S.Starchikov, I.S.Lyubutin, C.-R. Lin 110

A.P9
MAGNETIC PROPERTIES OF FeNi/V_xO_y/FeNi FILMS
G.S. Patrin, A.V. Kobyakov, V.I. Yushkov, I.O. Anisimov, S.V. Semenov, S.A. Yarikov, S.M. Zharkov 111

A.P10
MAGNETIZATION BEHAVIOR IN NICKEL NANOFILMS WITH A PERIODIC STRIPED STRUCTURE
A.V. Golov, V.S. Vlasov, L.N. Kotov, V.V. Temnov 112

CONTENTS

A.P11
THE EFFECT OF ANNEALING ON THE MICROSTRUCTURE AND MAGNETIC PROPERTIES OF FeMn/FM FILMS
A.N. Gorkovenko, V.N. Lepalovskij, N.A. Kulesh, M.E. Moskalev, V.O. Vas'kovskiy 114

A.P12
CONTROL OF SPIN-WAVE DISPERSION IN A PERMALLOY MEANDER STRUCTURE
Y.A. Gubanova, V.A. Gubanov, E.N. Beginin, N. Noginova, A.V. Sadovnikov 116

A.P13
INFLUENCE OF MAGNETIC FORCES ON THE SPATIAL DISTRIBUTION OF PARTICLES AND CELLS
A.A. Gurevich, L.V. Panina 118

A.P14
AB INITIO INVESTIGATION OF HETEROSTRUCTURES FOR SPINTRONIC APPLICATIONS
A.A. Evseev, I.I. Gumarova, O.V. Nedopekin 120

A.P15
DYNAMIC OPERATING MODES OF THE SPIN VALVE WITH IN-PLANE ANISOTROPY IN THE MAGNETIC FIELD OF THE ARBITRARY DIRECTION
Iu.A. Iusipova, N.V. Ostrovskaya, V.A. Skidanov 121

A.P16
ION-BEAM SYNTHESIS AND MAGNETIC PROPERTIES OF IRON NANOPARTICLES IN RUTILE (TiO_2)
I.R. Vakhitov, N.M. Lyadov, V.I. Vdovin, A.K. Gutakovskii, V.I. Nuzhdin, V.F. Valeev, L.R. Tagirov, R.I. Khaibullin 123

A.P17
CONTROL OF SPIN WAVE PROPAGATION MODES IN ARRAYS OF YIG STRIPES
A.B Khutieva, E.N. Beginin, A.V. Sadovnikov 125

A.P18
MAGNETIC CONDUCTIVITY OF COMPOSITE FILMS ($CoFeB+SiO_2+N_2$) IN TEMPERATURE RANGE 2–400 K
L.N. Kotov, A.A. Utkin, V.S. Vlasov, A.V. Sitnikov, Yu.E. Kalinin 127

A.P19
INVESTIGATION OF INHOMOGENEOUS CURRENT ACTION ON THE MAGNETIC STRUCTURE OF A FERRIMAGNET
M.E. Letushev, Zh.Zh. Namsaraev, M.A. Bazrov, M.E. Stebliy 129

A.P20
SIMULATION OF THE PROCESSES OF NONMONOTONIC RELAXATION OF A MULTILAYER MAGNETIC STRUCTURE
D.A. Lgotina, P.V. Prudnikov 131

A.P21
EFFECT OF SPIN CURRENT ON THE FORMATION OF BAND GAPS IN A LAYERED STRUCTURE BASED ON COUPLED MAGNONIC CRYSTALS
M.A. Morozova, O.V. Matveev, N.D. Lobanov 133

CONTENTS

A.P22
EFFECT OF SYNTHESIS CONDITIONS AND BUFFER LAYERS ON MORPHOLOGY AND PHASE FORMATION DURING THE GROWTH OF AN EPITAXIAL Mn_5Ge_3 FILM ON Si(111)
A.V. Lukyanenko, A.S. Tarasov, I.A. Yakovlev, S.N. Varnakov 135

A.P23
MAGNETIC ANISOTROPY OF FeNi THIN FILMS AND MULTILAYERED STRUCTURES PREPARED BY OBLIQUE MAGNETRON DEPOSITION
I.A. Makarochkin, V.N. Lepalovskij, A.A. Pasynkova, G.V. Kurlyandskaya, A.V. Svalov 137

A.P24
TEMPERATURE DEPENDENCE OF MAGNETIC PROPERTIES AND MAGNETIC-FIELD BEHAVIOR OF Co/Cu/Co THIN-FILM THREE-LAYER SYSTEMS
A.V. Makarov, E.E. Shalygina, A.V. Svalov 139

A.P25
SDFT INVESTIGATION OF MAGNETIC ANISOTROPY EFFECTS IN TRILAYER METAL NANOSTRUCTURES
M.V. Mamonova, M.Y. Makeev, M.M. Nurkusheva 142

A.P26
PERPENDICULAR MAGNETIC ANISOTROPY IN GRAPHENE/Fe/Ni AND GRAPHENE/Fe/h-BN
E.K. Mikhailenko, S.M. Dunaevski 145

A.P27
INFLUENCE OF COMPETITION EFFECTS FOR DIFFERENT TYPES OF ANISOTROPY ON THE BEHAVIOR OF MULTILAYER MAGNETIC STRUCTURES
A.V. Minkova, P.V. Prudnikov 148

A.P28
MAGNETIC PROPERTIES AND CURRENT-INDUCED MAGNETIZATION REVERSAL IN FERROMAGNETIC MULTILAYER STRUCTURES W/CoTb/Ru
Zh.Zh. Namsaraev, M.A. Bazrov, M.E. Letushev, M.E. Stebliy 150

A.P29
MAGNETOELASTIC FEATURES OF FLEXIBLE SPIN VALVES WITH DYSPROSIUM LAYER
L.I. Naumova, R.S. Zavornitsyn, M.A. Milyaev, N.G. Bebenin, I.K. Maksimova, A.A. Zakharov, V.V. Proglyado, A.S. Rusalina, V.V. Ustinov 152

A.P30
NONLINEAR SPIN WAVES IN MULTILAYEAR YIG WAVEGUIDE
S.A. Odintsov, E.H. Lock, E.N. Beginin, A.V. Sadovnikov 154

A.P31
PROPERTIES AND SEGREGATION TENDENCY OF Fe-Rh-Z (Z = Pt, Mn, Pd) ALLOYS
O.O. Pavlukhina, V.V. Sokolovskiy, V.D. Buchelnikov, M.A. Zagrebin 156

A.P32
MAGNETIZATION REVERSAL AND DOMAIN STRUCTURE IN THIN FILM AND ARTIFICIAL ANTIFERROMAGNET BASED ON $L1_0$-PdFe
M.V. Pasynkov, R.V. Yusupov, A.I. Gumarov, I.V. Yanilkin, L.R. Tagirov 159

CONTENTS

A.P33
FIRST PRINCIPLES INVESTIGATIONS OF HALF-METALLIC Ti-BASED HEUSLER FERROMAGNETIC ALLOYS
A.A. Raev, D.R. Baigutlin, V.V. Sokolovskiy, V.D. Buchelnikov 161

A.P34
ANOMALOUS HALL EFFECT IN AN EPITAXIAL Mn_5Ge_3 THIN FILM ON Si(111)
M.V. Rautskii, I.A. Yakovlev, S.N. Varnakov, A.S. Tarasov 163

A.P35
MAGNETIC PROPERTIES AND DOMAIN STRUCTURE OF CoFe NANOSPRINGS
K.A. Rogachev, A.Yu. Samardak, A.G. Kozlov, V.N. Kharitonov, M.E. Stebliy, M.E. Letushev, M.A. Bazrov, Y.S. Jeon, E. Jeong, A.V. Ognev, A.S. Samardak, Y.K. Kim 165

A.P36
INVESTIGATION OF MAGNETIC TRILAYER Co/Cu/Co SYSTEM IN THE FRAMEWORK OF FIRST-PRINCIPLES CALCULATIONS
R.A. Sukhachev, M.V. Mamonova 167

A.P37
MAGNETIC AND OPTICAL INVESTIGATIONS OF POTASSIUM ALUMINOBORATE GLASS WITH THE ADDITION OF IRON OXIDES SUBJECTED TO THERMORADIATION INTERACTION
E.M. Ibragimova, M.K. Salakhitdinova 169

A.P38
SPIN-WAVE COUPLER BASED ON THE YIG/FeRh STRUCTURE
E.I. Salomatova, S.A. Odintsov, S.V. Grishin, A.V. Sadovnikov 170

A.P39
MAGNETOSTATIC INTERACTIONS OF DENSELY PACKED FERROMAGNETIC SEGMENTS IN Fe/Au BARCODE NANOWIRES ARRAYS
A.Yu. Samardak, Y.S. Jeon, A.G. Kozlov, K.A. Rogachev, A.V. Ognev, E. Jeong, G.W. Kim, M.J. Ko, A.S. Samardak, Y.K. Kim 172

A.P40
MAGNETIC AND STRUCTURAL PROPERTIES OF Co-Ni-Z (Z = Al, Ga, In, Sn) HEUSLER ALLOYS
A.A. Sanosyan, V.V. Sokolovskiy, V.D. Buchelnikov 174

A.P41
INSTABILITY FIELD ANISOTROPY OF POLYCRYSTALLINE FERROMAGNETIC NANOWIRES
S.A. Satsuk, S.V. Komogortsev 176

A.P42
ELECTRICAL, MAGNETIC, AND GALVANOMAGNETIC PROPERTIES OF Mn_3X ALLOYS (X = Al, Ga, Ge, Sn)
A.A. Semiannikova, V.Yu. Irkhin, P.S. Korenistov, P.B. Terentyev, E.B. Marchenkova, V.V. Marchenkov 178

A.P43
MAGNETIC PROPERTIES OF Ni NANOWIRES SYNTHESIZED USING TEMPLATES WITH DIFFERENT PORE ORDER
M.I. Sobirov, A.Yu. Samardak, S.A. Azon, S.R. Potapova, M.B. Karibov, A.S. Samardak, A.V. Ognev 179

CONTENTS

A.P44
FERROCENE TRANSFORMATION AT HIGH PRESURE HIGH TEMPERATURE TO FORM CORE@SHELL NANOCOMPOSITES BASED ON IRON CARBIDES
S.S. Starchikov, V.A. Zayakhanov, A.L. Vasiliev, I.S. Lyubutin, K.O. Funtov, M.V. Lyubutina, N.K. Chumakov, L.F. Kulikova, V.N. Agafonov, V.A. Davydov 181

A.P45
HARD/SOFT MAGNETIC BILAYER AND TRILAYER. MONTE CARLO STUDY
T.A. Taaev, K.Sh. Khizriev, A.K. Murtazaev 182

A.P46
EXCHANGE BIAS IN Pd/Co/CoO EPITAXIAL FILM WITH PERPENDICULAR MAGNETIC ANISOTROPY
E.V. Tarasov, H.S. Suslin, A.V. Gerasimenko, I.A. Tkachenko, A.G. Kozlov 183

A.P47
STUDY OF MANETIC HETEROSTRUCTURES USING THE HARMONIC HALL VOLTAGE METHOD
A.S. Trushin, G.A. Kichin, K.A. Zvezdin 186

A.P48
SPIN-POLARIZED CURRENT IN MAGNETIC TUNNEL JUNCTION WITH NON-COPLANAR MAGNETIZED ELECTRODES
N.Kh. Useinov, L.R. Tagirov 188

A.P49
FERROMAGNETIC RESONANCE SPECTRA OF NANOCOMPOSITE METAL-DIELECTRIC FILMS
L.N. Kotov, A.A. Utkin, V.S. Vlasov, V.A. Ustyugov, M.P. Lasek, P.D. Kovalev, Yu.E. Kalinin, A.V. Sitnikov 190

A.P50
INVESTIGATION OF STRUCTURAL FEATURES OF THE SUPERCONDUCTING SPIN VALVE Fe/Nb/Fe
A.A. Validov, M.I. Nasyrova, R.R. Habibullin, I.A. Garifullin 192

A.P51
EXCHANGE BIAS AND MAGNETIC ANISOTROPY OF FILM STRUCTURES BASED ON THE ANTIFERROMAGNET FeMn
V.O. Vaskovskiy, A.A. Bykova, A.N. Gorkovenko, M.E. Moskalev 194

A.P52
ANGULAR AND TEMPERATURE DEPENDENCES OF FERROMAGNETIC RESONANCE IN EXCHANGE-COUPLED FeNi/Dy/FeNi PLANAR STRUCTURES
R.S. Iskhakov, I.G. Vazhenina, V.Y. Yakovchuk 196

A.P53
SPIN LIGHT-EMITTING DIODE WITH INTENSITY CONTROL
M.V. Ved, M.V. Dorokhin, A.V. Zdoroveyshchev, P.B. Demina, D.A. Zdoroveyshchev, Yu.A. Dudin, V.E. Kotomina 198

A.P54
INTERFACE-ENHANCED DMI INTERACTION IN Pt/Co/Ta HETEROSTRUCTURES
V.D. Bessonov, J.H. Park, T.H. Kim, G.W. Kim, A.V. Telegin, V.S. Teplov, I.G. Iliushin, A.A. Pervishko, D. Yudin, A.V. Ognev, A.S. Samardak, J.U. Cho, Y.K. Kim 200

CONTENTS

A.P55
CHIRALITY-DEPENDENT SPIN-TRANSFER TORQUE AND CURRENT-INDUCED SPIN ROTATION IN HELIMAGNETS
V.V. Ustinov, I.A. Yasyulevich 201

A.P56
FORMATION OF A DILUTED MAGNETIC SEMICONDUCTION PHASE BY THERMAL DIFFUSION IN THE METHOD OF PULSED LASER DEPOSITION
Yu.M. Kuznetsov, M.V. Dorokhin, R.N. Kryukov, A.V. Zdoroveyshchev, V.P. Lesnikov, D.A. Zdoroveyshchev 203

A.P57
HALF-METALLIC PROPERTIES OF THE Rh_2FeZ ALLOYS
D.R. Baigutlin, V.V. Sokolovskiy, V.D. Buchelnikov 205

A.P58
FIRST PRINCIPLE STUDY OF HALF-METALLIC CONNECTIONS ON THE BASIS OF HEUSLER ALLOY Fe_2RhSi
K.R. Erager, D.R. Baigutlin, V.V. Sokolovskiy, V.D. Buchelnikov 207

A.P59
CHIROMAGNETIC OXIDE COBALT NANOPARTICLES: SYNTHESIS AND MAGNITOOPTICAL PROPERTIES
A.V. Kurilova, D.I. Klimenko, E.V. Kundelev, A.L. Suhachev, K.V. Shulga, A.U. Dubavik, A.E. Sokolov 209

A.P60
PERTURBATION THEORY FOR THE SPIN-TRANSFER TORQUE TERM WITHIN THE VECTOR HAMILTONIAN FORMALISM IN THE NONLINEAR CASE
A.A. Matveev, A.R. Safin 211

A.P61
NONLINEAR LIMITATION OF RESONANCE FREQUENCY GROWTH OF SPIN WAVES IN EXCEPTIONAL POINTS
O.S. Temnaya, A.R. Safin, D.V. Kalyabin, S.A. Nikitov 214

A.P62
INVESTIGATION OF THE CONTROL OF THE MAGNETIZATION VECTOR OF A FERROMAGNETIC LAYER IN A TWO-LAYER SYSTEM FERROELECTRIC/FERROMAGNET
A.A. Kamashev, A.V. Leontyev, I.A. Garifullin, R.F. Mamin 216

A.P63
NON-RECIPROCAL PROPAGATION OF SPIN WAVES IN STRUCTURES WITH PARTIAL METALLIZATION SURFACE
A.A. Martyshkin, E.H. Lock, E.N. Beginin, A.V. Sadovnikov 218

A.P64
RESEARCHING OF PROPERTIES OF MAGNETIC THIN FILMS FOR STORAGE DEVICES
A.A. Valiullin, A.S. Kamzin, L.R. Tagirov, L.D. Zaripova 220

CONTENTS

Section B.
Spin dynamics and magnetic resonances 221

B.I1
On the theory of spin nutation
K.M. Salikhov 222

B.I2
HIGH-FIELD MAGNETIC STRUCTURE OF THE TRIANGULAR ANTIFERROMAGNET $RbFe(MoO_4)_2$ TESTED BY NMR
Yu.A. Sakhratov, L.E. Svistov, A.P. Reyes 223

B.I3
TWO TYPES OF MAGNON BOSE CONDENSATION
Yu.M. Bunkov 224

B.I4
SPIN-TORQUE DIODE EFFECT: FROM FUNDAMENTAL RESEARCH TO APPLICATIONS
P.N. Skirdkov, K.A. Zvezdin 226

B.I5
TWO-GAP SUPERCONDUCTIVITY IN $Mo_4Ga_{20}Sb$ INTERMETALLIC SUPERCONDUCTOR AS EVIDENCED BY NMR- AND NQR-SPECTROSCOPY
A.A. Gippius, A.V. Tkachev, S.V. Zhurenko, A.V. Gunbin, D.A. Iarygina, V.Yu. Verchenko, A.V. Shevelkov 228

B.I6
LOW-TEMPERATURE ROTATIONAL TUNNELING OF BH_4 GROUPS IN $Li_2(bIm)BH_4$: NUCLEAR MAGNETIC RESONANCE AND NEUTRON SPIN-ECHO STUDIES
A.V. Skripov, A.V. Soloninin, O.A. Babanova, R.V. Skoryunov, F. Morelle, Y. Filinchuk, M. Dimitrievska, A. Faraone, T.J. Udovic 230

B.O1
ELECTRONIC STRUCTURE AND HYPERFINE INTERACTIONS IN Cr_xNbSe_2 (x = 0.33, 0.5) BY DFT STUDIES
P.A. Agzamova, V.V. Ogloblichev 232

B.O2
TIME-DEPENDENT EXCHANGE CREATES THE TIME-FRUSTRATED STATE OF MATTER
V.E. Valiulin, N.M. Chtchelkatchev, A.V. Mikheenkov, V.M. Vinokour 234

B.O3
EVOLUTION OF THE MAGNETIC PROPERTIES OF $FeBO_3$ SINGLE CRYSTALS UNDER GALLIUM DOPING
N. Snegirev, I. Lyubutin, A. Bogach, M. Chuev, S. Starchikov, S. Yagupov, Yu. Mogilenec, K. Seleznyova, M. Strugatsky 237

B.O4
SPECTRUM EVOLUTION OF MAGNETOSTATIC WAVES EXITED VIA FEMTOSECOND LASER PULSES IN ANISOTROPIC FILMS
N.E. Khokhlov, Ia.A. Filatov, P.I. Gerevenkov, A.M. Kalashnikova 239

B.O5
THEORY AND EXPERIMENT OF THE FERROMAGNETIC RESONANCE IN NANOCOMPOSITE METAL-DIELECTRIC FILMS
V.S. Vlasov, L.N. Kotov, A.A. Utkin, D.A. Pleshev, F.F. Asadullin, A.V. Sitnikov 240

CONTENTS

B.O6
MAGNETIC STRUCTURE OF $FeP_{1-x}As_x$ (x = 0.33, 0.5) AS SEEN BY NMR-SPECTROSCOPY
S.V. Zhurenko, A.V. Tkachev, A.V. Gunbin, I.G. Silkin, I.V. Morozov, A.S. Moskvin, A.A. Gippius 241

B.O7
THE CONDUCTION ELECTRON SYSTEM OF A HEXABORIDE SUPERCONDUCTOR YB_6 PROBED BY ^{89}Y AND ^{11}B NMR
O.M. Vyaselev, N.E. Sluchanko, A.V. Bogach, N.Y. Shitsevalova, V.B. Filipov, A.A. Gippius 242

B.O8
SPIN WAVE SPECTRA IN PSEUDOPEROVSKITE MANGANITES WITH SUPEREXCHANGE INTERACTION COMPETITION
L.E. Gonchar 245

B.O9
VARIETY OF SPIN RESONANCE MODES IN THE MONOAXIAL CHIRAL HELIMAGNET $Cr_{0.33}NbS_2$
I.G. Bostrem, V.E. Sinitsyn, E.G. Ekomasov, A.S. Ovchinnikov 247

B.O10
MRFM STUDIES OF FERROMAGNETIC RESONANCE IN EXCHANGE-COUPLED MAGNETIC VORTICICES
D.A. Tatarskiy, V.L. Mironov, E.V. Skorokhodov 249

B.O11
THE PRECESSION OF THE EQUILIBRIUM POSITION IN THE TWO-LAYER STRUCTURE WITH THE EXCHANGE INTERLAYER INTERACTION
I.E. Abramovsky, V.S. Vlasov, L.N. Kotov, D.A. Pleshev, F.F. Asadullin 251

B.O12
SPIN-WAVE RESONANCES IN Pd-Fe ALLOY FILMS WITH CONTROLLED COMPOSITION PROFILES
I.V. Yanilkin, A.I. Gumarov, B.F. Gabbasov, A.G. Kiiamov, I.A. Golovchanskiy, R.V. Yusupov, L.R. Tagirov 252

B.O13
ANION AND CATION DYNAMICS IN NANOPOROUS SILICA SCAFFOLDS: NMR STUDIES OF $NaCB_{11}H_{12}$ IN SBA-15
O.A. Babanova, R.V. Skoryunov, A.V. Soloninin, A.V. Skripov, M.S. Andersson, V. Stavila, M. Dimitrievska, M. Karlsson, T.J. Udovic 254

B.O14
UNUSUAL DEPENDENCES OF EPR-LINE SHAPES OF Gd^{3+} CENTERS IN NARROW-BAND $Pb_{1-x}Gd_xTe$ SEMICONDUCTOR ON MICROWAVE POWER
V.A. Ulanov, I.V. Yatsyk, A.V. Shestakov 256

B.O15
DYNAMIC CHARACTERISTICS OF A NANOCOMPLEX WITH IRON IN GLASS-IONOMER CEMENT POWDER
V.V. Shapovalov, V.A. Shapovalov, Yu.A. Sluzhbin, T.V. Drokina, A.M. Vorotynov, V.G. Shavrov, V.I. Valkov 258

CONTENTS

B.O16
MAGNETIZATION DYNAMICS SIMULATION OF THE ANISOTROPIC FERROMAGNETIC FILM EXCITED BY THE NANOSECOND MAGNETIC PULSES
V.N. Shaporov, V.S. Vlasov, L.N. Kotov 261

B.O17
HIGH-FREQUENCY MAGNETIC SUSCEPTIBILITY OF THIN MAGNETIC FILMS WITH 1D AND 2D INHOMOGENEITIES
V.A. Ignatchenko, D.S. Tsikalov, D.S. Polukhin 263

B.P1
^{59}Co NMR AND ^{57}Fe MÖSSBAUER STUDIES OF CARBON ENCAPSULATED MAGNETIC NANOPARTICLES BASED ON BINARY FeCo ALLOYS
A.Yu. Germov, B.Yu. Goloborodskiy, A.S. Konev, D.A. Prokopyev, I.A. Kurmachev, E.V. Suvorkova 265

B.P2
SYNTHESIS AND CHARACTERIZATION OF EPITAXIAL Mn_5Ge_3 THIN FILMS ON A SILICON SUBSTRATE
M.V. Rautskii, I.A. Yakovlev, A.S. Tarasov, M.A. Bondarev 266

B.P3
TRANSVERSE RELAXATION IN H_2o-D_2o LIQUID ENTRAPPED IN NANOCAVITIES
G. Furman, V. Sokolovsky, D.A. Petrov 268

B.P4
SPIN POLARON MODEL OF STATIC AND DYNAMIC MAGNETIC PROPERTIES OF STROGLY CORRELATED MATERIALS
S.V. Demishev 269

B.P5
LANDAU-LIFSHITS EQATION OF MOTION MODIFIED BY QUANTUM FLUCTUATIONS AND EPR IN STRONGLY CORRELATED MATERIALS
S.V. Demishev 271

B.P6
Pd-Fe ALLOY FILM WITH HIGH GRADIENT OF IRON CONTENT: STRUCTURAL AND MAGNETIC STUDIES
G.F. Gizzatullina, I.V. Yanilkin, A.I. Gumarov, B.F. Gabbasov, A.G. Kiiamov, R.V. Yusupov, L.R. Tagirov 273

B.P7
ELECTRON SPIN RESONANCE OF ^{51}V IONS IN SCANDIUM ORTHOSILICATE MONOCRYSTAL
R.F. Likerov, I.V. Yatsyk, R.B. Zaripov, K.B. Konov, V.F. Tarasov, V.A. Shustov 274

B.P8
MAGNETIC PROPERTIES OF $Ba_xSr_{2-x}TiFeO_6$ DOUBLE PEROVSKITES AT LOW TEMPERATURES
R.M. Eremina, I.V. Yatsyk, V.A. Shustov, F.G. Vagizov, T. Maiti, D.V. Mamedov 276

B.P9
SPIN WAVES CONTROL BY SPIN-POLARIZED CURRENT IN PERIODIC HETEROSTRUCTURES
O.V. Matveev, N.D. Lobanov, M.A. Morozova 277

CONTENTS

B.P10
CRITICAL DYNAMICS OF THE QUANTUM PHASE TRANSITION IN 3D QUANTUM HEISENBERG MODEL
M.G. Vasin 278

B.P11
NMR STUDY OF Co_3C AND Fe_3C CARBIDE NANOPARTICLES
K.N. Mikhalev, A.Yu. Germov, M.A. Uimin, A.E. Yermakov, A.S. Konev, S.I. Novikov, T.V. Dyachkova, A.P. Tyutyunnik 279

B.P12
CHARACTERISTIC FEATURES OF THE DYNAMIC SUSCEPTIBILITY OF FERRITE-GARNET FILMS IN AN EXTERNAL FIELD
Yu.I. Nepochatykh, V.G. Shavrov, V.V. Koledov 280

B.P13
SPIN SWITCHING MECHANISM STIMULATED BY LINEARLY POLARIZED FEMTOSECOND OPTICAL PUMP
N.B. Orlova, P.A. Agzamova, M.I. Kurkin 282

B.P14
MAGNETIC ANISOTROPY AND "EASY AXIS-EASY PLANE" TRANSFORMATION IN $Pr_xY_{1-x}Fe_3(BO_3)_4$ SINGLE CRYSTALS STUDIED BY ANTIFERROMAGNETIC RESONANCE
A.I. Pankrats, S.M. Zharkov, G.M. Zeer, I.A. Gudim 284

B.P15
^{53}Cr NMR STUDY OF THE HALF-METALLIC FERROMAGNET CrO_2
Y.V. Piskunov, A.F. Sadykov, V.V. Ogloblichev, A.G. Smolnikov, A.P. Gerashenko, P.Z. Si 287

B.P16
THICKNESS-DEPENDENT MAGNETIC PROPERTIES IN ULTRATHIN $La_{0.7}Sr_{0.3}MnO_3$ FILMS
T.A. Shaikhulov, K.L. Stankevich, V.A. Luzanov, A.G. Temiryazev, M.P. Temiryazeva, V.E. Zhivulin, A.R. Safin, S.A. Nikitov 289

B.P17
MOBILITY OF THE PILLAR[5]ARENE COMPLEX WITH THIOCTIC ACID ACCORDING TO NMR-DATA
L.V. Sharipova, B.I. Khayrutdinov, D.N. Shurpik, I.I. Stoikov, Yu.F. Zuev 291

B.P18
NMR-SPECTROSCOPY OF CATIONIC SURFACTANT–SERUM ALBUMIN SYSTEM
L.V. Sharipova, B.I. Khayrutdinov, Yu.F. Zuev 292

B.P19
EPR STUDY OF MAGNETIC PROPERTIES OF $(Cd_{0.6}Zn_{0.36}Mn_{0.04})_3As_2$ THIN FILM
A.V. Shestakov, I.I. Fazlizhanov, I.V. Yatzyk, V.S. Zakhvalinskii, E.A. Pilyuk, R.M. Eremina 293

B.P20
FMR METHOD FOR DETERMINING THE MAGNETIZATION OF THIN COBALT FILMS
Ya.G. Shiyan, L.A. Lee 296

CONTENTS

B.P21
THE BEHAVIOR OF THE SPIN COHERENCE AFTER THE APPLICATION OF MULTI-PULSE PROTOCOLS IN SOLID-STATE ^{1}H NMR IN Cu- AND Ni-OXAMIDATO COMPLEXES
Yu. Slesareva, Yu. Kandrashkin, R. Zaripov, T. Ruffer, E. Vavilova 297

B.P22
MAGNETIC RESONANCE STUDIES OF AR-ION IMPLANTED RUTILE (TiO_2): EFFECT OF OXYGEN VACANCIES CONCENTRATION
A.A. Sukhanov, V.F. Valeev, V.I. Nuzhdin, R.I. Khaibullin 298

B.P23
THE "DARKS" STATES OF THE LEAKY MAGNON POLARONS SPECTRUM IN MAGNETIC HETEROSTRUCTURES WITH SLIDING-CONTACT INTERFACES
O.S. Sukhorukova, A.S. Tarasenko, S.V. Tarasenko, V.G. Shavrov 300

B.P24
MAGNETIC-FIELD-DRIVEN TRANSPARENCY OF MANGANITE-BASED COMPOSITES
V.A. Bessonova, V.S. Teplov, S.V. Naumov, A.V. Telegin 301

B.P25
MICROMAGNETIC SIMULATION OF MAGNETIZATION DYNAMIC IN FM FILMS
V.S. Teplov, V.D. Bessonov, A.V. Telegin 302

B.P26
SPIN DINAMICS IN $SrMnO_{3-x}$ BY ^{17}O and ^{87}Sr NMR-DATA
Z. Volkova, A. Gerashenko, K. Mikhalev, A. Trokiner 304

B.P27
FEATURES OF FMR IN THIN FILMS Fe_xNi_{100-x} AND Fe
S.A. Vysulin, N.E. Syr'iev 305

B.P28
FERRIMAGNET BASED SPIN HALL DETECTOR OF SUBTERAHERTZ FREQUENCY RANGE SIGNALS
E.E. Kozlova, A.R. Safin, S.A. Nikitov 307

B.P29
SUPERCONDUCTOR INFLUENCE ON THE FERROMAGNETIC RESONANCE PROPERTIES OF IRON-GARNET FILM NEAR THE CRITICAL TEMPERATURE
F.M. Maksimov, S.N. Polulyakh, N.G. Pugach, A.S. Pakhomov, V.N. Berzhansky, V.S. Stolyarov, V.I. Belotelov, A.I. Chernov 309

B.P30
THE DYNAMICS OF A SINGLE SPINTRONIC AFM OSCILLATOR
A.Yu. Mitrofanova, A.R. Safin, O.V. Kravchenko 311

B.P31
SPIN DYNAMICS IN FRUSTRATED QUANTUM MAGNET $BaCdVO(PO_4)_2$
T.A. Soldatov, A.I. Smirnov 314

B.P32
PARAMAGNETIC RESPONSE, AND ELECTRONIC AND MAGNETIC PROPERTIES OF OXIDIZED SPARK PLASMA SINTERED CARBON NANOTUBES
A.N. Ulyanov, E.V. Suslova, S.V. Savilov 316

CONTENTS

B.P33
MAGNETIC SENSOR BASED ON DIPOLE-EXCHANGE SPIN WAVES IN EXCHANGE-COUPLED YIG FILMS
S. Vysotskii, A. Kozhevnikov, M. Balinskiy, A. Khitun, Y. Filimonov 318

B.P34
PECULIARITIES OF THE EPR-SPECTRA OF THE PbTe CRYSTAL WITH Mn AND Cu IMPURITIES IN THE X- AND Q-BAND
I.I. Fazlizhanov, A.V. Shestakov, V.A. Ulanov 320

Section C.
Low dimensional magnetism 322

C.I1
INTERACTION OF SPINONS DETECTED BY MICROWAVE SPECTROSCOPY
A.I. Smirnov, K.Yu. Povarov, T.A. Soldatov, Ren-Bo Wang, A. Zheludev, O.A. Starykh 323

C.I2
POLARIZED NEUTRON REFLECTOMETRY IN THE STUDY OF RARE-EARTH NANOSTRUCTURES
N.O. Antropov, D.I. Devyaterikov, E.A. Kravtsov 325

C.I3
SQUARE KAGOME SYSTEMS
A.N. Vasiliev 326

C.O1
FERROMAGNETISM INDUCED BY OXYGEN VACANCIES IN MULLITE $Bi_2Fe_4O_9$
S.S. Aplesnin, L.V. Udod, M.N. Sitnikov, D.A. Velikanov, O.B. Romanova 327

C.O2
ANTIFERROMAGNETIC STATE IN $(NO)M(NO_3)_3$ (M = Co, Ni)
O.S. Volkova 329

C.O3
MAGNETOELECTRIC EFFECT IN FLEXIBLE COMPOSITE STRUCTURES CONTAINING MAGNETOACTIVE ELASTOMER
L.Y. Fetisov, G. Glavan, V.O. Belan, I.A. Belyaeva, M. Shamonin, D.V. Saveliev 330

C.O4
NEUTRON DIFFRACTION STUDIES OF HELICAL MAGNETIC ORDER IN CHIRAL $PbMnTeO_6$ WITH TRIANGULAR LATTICE
A.I. Kurbakov, A.N. Korshunov 332

C.O5
MAGNETIC PROPERTIES OF QUASI-TWO-DIMENSIONAL OXYBORATES $(Ni,Cu,Mn)_3BO_5$ WITH DIFFERENT COMPOSITION OF Cu IONS
S.N. Sofronova, E. Moshkina, E. Eremin, M. Molokeev 335

C.O6
INFLUENCE INTERFACE THICKNESS TO THE EXCHANGE INTERACTION CONSTANT BETWEEN FERRO- AND ANTIFERROMAGNET
L.L. Afremov, L.O. Brykin, I.G. Iliushin 337

CONTENTS

C.O7
STRONG AND ULTRASTRONG PHOTON-MAGNON COUPLING OF SUPERCONDUCTING PLANAR RESONATORS WITH YIG CRYSTALS
M. Maksutoğlu, A. Ghirri, C. Bonizzoni, F. Yıldız, M. Affronte, B. Rameev 339

C.O8
NEW SHORT-WAVELENGTH SPIN EXCITATIONS IN SPIN-1/2 ANTIFERROMAGNETS ON THE TRIANGULAR LATTICE
A.V. Syromyatnikov 340

C.O9
INFLUENCE OF INTERFACIAL EXCHANGE INTERACTION ON THE METASTABILITY OF MAGNETIC STATES OF CORE-SHELL NANOPARTICLES
L.L. Afremov, I.G. Iliushin, V.N. Kharitonov 342

C.O10
AGING EFFECTS IN CRITICAL BEHAVIOR OF HEISENBERG ANISOTROPIC ULTRATHIN FILMS
M.A. Shlyakhtich, P.V. Prudnikov 344

C.P1
MAGNETIC AND TEMPERATURE PROPERTIES OF LUDWIGITE $Mn_{1.17}Co_{1.83}BO_5$
D.V. Popov, T.P. Gavrilova, I.V. Yatsyk, M.A. Cherosov, E.M. Moshkina, V.A. Shustov, R.M. Eremina 346

C.P2
INVESTIGATION OF THE INFLUENCE OF COMPOSITION ON THE MAGNETIC BEHAVIOR OF Cu/Co SEGMENTED NANOWIRES FOR APPLICATION AS 3D MEMORY ELEMENTS
V.N. Kharitonov, A.Yu. Samardak, M. Yu. Pavliuk, E.V. Tepnin, D.R. Khairetdinova, I.M. Doludenko, A.S. Samardak, A.V. Ognev 348

C.P3
MONTE CARLO SIMULATION OF A PHASE TRANSITION IN A QUASI-ONE-DIMENSIONAL MULTIFERRROIC ON A SUBSTRATE
I.V. Bychkov, I.V. Maltsev 350

C.P4
FRUSTRATIONS IN THE GROUND STATE OF THE DILUTE ISING CHAIN IN A MAGNETIC FIELD
Yu.D. Panov 352

C.P5
NON-EQUILIBRIUM VORTEX COARSENING OF DISORDER IN TWO-DIMENSIONAL XY-MODEL WITH COMPLEX DILUTION MODEL
A.P. Popova, I.S. Popov, P.V. Prudnikov 353

C.P6
MAGNETIC ORDERING IN DELAFOSSITES WITH DEFECTED LATTICE
S.P. Savchenko, R.V. Skorunov, A.G. Smolnikov 355

C.P7
VIBRATIONAL PROPERTIES AND LATTICE SPECIFIC HEAT OF QUASI-1D TERNARY IRON SULFIDE $KFeSe_2$
M.D. Kuznetsov, A.G. Kiiamov, D.A. Tayurskii 356

CONTENTS

C.P8
EFFECT OF ANNEALING CONDITIONS ON MAGNETIC CHARACTERISTICS OF NANOCRYSTALLINE OXYGEN-DEFICIENT $TiO_{2-\delta}$(B)
I.A. Tkachenko, D.P. Opra, A.M. Ziatdinov, A.A. Sokolov, E.V. Tarasov 357

Section D.
Domain walls, vortices and skyrmions 360

D.I1
ZIGZAG DOMAINS IN MAGNETIC FILMS WITH ANISOTROPIC DZYALOSHINSKII-MORIYA INTERACTION
O.G. Udalov, R.V. Gorev, E.V. Skorokhodov, N.S. Gusev, A.V. Sadovnikov, M.V. Sapozhnikov 361

D.I2
INFLUENCE OF THE ROUGHNESS OF Co-LAYERS ON THE CREEP OF DOMAIN WALLS IN Pd/Co/Pd EPITAXIAL STRUCTURES
A.V. Davydenko, N.N. Chernousov, A.A. Turpak, A.G. Kozlov, A.V. Ognev, A.S. Samardak 364

D.O1
VORTEX NANOOBJECTS IN PERFORATED FERROMAGNETIC FILMS
E.B. Magadeev, R.M. Vakhitov, R.R. Kanbekov 366

D.O2
SIMULATION OF MAGNETIC SKYRMIONS ON FLAT LATTICES
A.V. Perzhu, E.V. Vasiliev, V.Yu. Kapitan 367

D.O3
THERMALLY ACTIVATED DRIFT OF MAGNETIC VORTICES IN A RANDOM FIELD OF DEFECTS
V.A. Orlov, A.A. Ivanov, I.N. Orlova, G.S. Patrin 368

D.O4
REVERSAL OF DOMAIN WALLS DRIFT DIRECTION IN HARMONIC MAGNETIC FIELD IN IRON GARNET CRYSTALS
L.A. Pamyatnykh, M.S. Lysov, S.E. Pamyatnykh, G.A. Shmatov. 370

D.O5
NONLINEAR OPTICAL STUDIES OF RESIDUAL DOMAIN STRUCTURE OF EPITAXIAL GARNET FILMS
E.A. Mamonov, D.A. Kopylov, M.P. Temiryazeva, A.G. Temiryazev, T.V. Murzina 372

D.O6
STRUCTURE AND PROPERTIES OF kπ-SKYRMIONS IN FERROMAGNETIC FILMS WITH SPATIALLY MODULATED PARAMETERS
R.M. Vakhitov, G.F. Ilyasova, R.V. Solonetsky 374

D.O7
MAGNETIC FORCE MICROSCOPY OF SKYRMION FORMATION IN THIN CoPt-FILMS
M.P. Temiryazeva, A.G. Temiryazev, M.V. Stepushkin, A.V. Zdoroveyshchev D.A. Zdoroveyshchev, A.V. Kudrin, D.A. Tatarskiy, A.V. Sadovnikov, S.A. Nikitov 376

CONTENTS

D.O8
FORMATION OF THE SKYRMIONS IN CoPt AND CoPd THIN FILMS AFTER ION IRRADIATION
I.L. Kalentyeva, O.V. Vikhrova, A.V. Zdoroveyshchev, A.V. Zdoroveyshchev, Yu.A. Dudin, Yu.A. Danilov, M.P. Temiryazeva, A.G. Temiryazev, A.V. Sadovnikov 378

D.O9
TEMPERATURE RESOLVED DEPENDENCIES OF GILBERT DAMPING IN HETEROSTRUCTURES $MnBi_2Te_4$/NiFe
P.N. Skirdkov, G.A. Kichin, F.M. Maksimov, A.I. Chernov, K.A. Zvezdin, A.S. Pakhomov 381

D.O10
MEAN-FIELD DESCRIPTION OF TOPOLOGICAL PHASES IN HEXAGONAL FRUSTRATED ANTIFERROMAGNETS
O.I. Utesov 382

D.O11
PINNING OF VORTICES DURING THE PASSAGE OF TURBULENT MAGNETIZATION REVERSAL WAVES IN ANTIDOT FILMS WITH THROUGH AND NON-THROUGH HOLES
V.V. Zverev 384

D.P1
INHOMOGENEOUS MAGNETOELECTRIC EFFECT IN (011)-ORIENTED FERRITE-GARNET FILM
R.M. Vakhitov, A.R. Yumaguzin, G.T. Akhmadeeva 386

D.P2
FLEXOMAGNETOELECTRIC EFFECT IN FERRITE-GARNET FILMS WITH (001)-ORIENTATION
R.M. Vakhitov, Z.A. Baymukhametova, R.V. Solonetsky 388

D.P3
NUMERICAL SIMULATION OF THE STRUCTURE AND DYNAMICS OF MAGNETIC VORTICES AND SOLITONS IN MULTILAYER FERROMAGNETIC NANOSTRUCTURES
K.U. Samsonov, S.V. Stepanov, G.I. Antonov, K.A. Zvezdin, E.G. Ekomasov 390

D.P4
INVESTIGATION OF THE DYNAMICS OF DOMAIN WALL MOTION IN COBALT-BASED MICROWIRES
S.A. Evstigneeva, R.I. Shamsuvaleev, N.A. Yudanov, M.G. Nematov, L.V. Panina 391

D.P5
THE STRUCTURE OF VORTEX-LIKE MAGNETIC INHOMOGENEITIES FORMED IN MODULATED FERROMAGNETIC FILMS AND THEIR BEHAVIOR IN A MAGNETIC FIELD
A.A. Akhmetova, R.M. Vakhitov, R.V. Solonetsky, M.A. Filippov 393

D.P6
INHOMOGENEOUS MAGNETOELECTRIC EFFECT IN (111)-FERRITE-GARNETS FILMS
R.M. Vakhitov, R.F. Ishmanova, A.R. Yumaguzin 395

CONTENTS

D.P7
STRIPE STRUCTURE ROTATION IN TRANSCRITICAL MAGNETIC FILMS
S.V. Komogortsev, V.A. Fel'k, A.A. Kuznetsova, A.A. Mokhov 397

D.P8
DOMAIN WALL DRIFT IN SINGLE CRYSTAL PLATES WITH COMPLEX MAGNETIC ANISOTROPY
D.S. Mekhonoshin, L.A. Pamyatnykh 399

D.P9
INFLUENCE OF THE MAGNETIC FIELD ON THE STRUCTURE AND PROPERTIES OF 0°-DWS IN UNIAXIAL FILMS WITH INHOMOGENEOUS MAGNETOELECTRIC EFFECT
R.M. Vakhitov, A.R. Nizyamova, R.V. Solonetsky 401

D.P10
FEATURES OF THE MAGNETIC STATE OF AN ORDERED ARRAY FERROMAGNETIC NANOSTRIPES
V.A. Orlov, R.Yu. Rudenko, A.V. Luk'yanenko, V.Yu. Yakovchuk, V.S. Prokopenko, I.N. Orlova 403

D.P11
PHENOMENOLOGICAL MODEL OF ACCELERATED MOTION OF A DOMAIN WALL IN FERROMAGNETIC BISTABLE AMORPHOUS MICROWIRE
V.V. Rodionova, V.V. Savin 406

D.P12
EFFECT OF INTERLAYER COUPLING ON THE DOMAIN WALL KINETICS IN ULTRATHIN Co/Pd/Co TRILAYER
I.V. Shashkov, V.S. Gornakov, Yu.P. Kabanov 408

D.P13
MAGNETIC DISSIPATION FORCE MICROSCOPY IN AMBIENT CONDITIONS
A.G. Temiryazev, M.P. Temiryazeva, Yu.V. Nikulin, N.S. Gusev, S.A. Nikitov 410

D.P14
DISORDER IN SKYRMION LATTICE INDUCED BY RANDOM MAGNETIC ANISOTROPY
V.A. Fel'k, S.V. Komogortsev, A.A. Mokhov, A.N. Pavlova 412

D.P15
STABILITY OF FLAT STRUCTURES IN FERROMAGNETIC NANOFILMS
E.B. Magadeev, R.M. Vakhitov, R.R. Kanbekov 413

CONTENTS

Section E.
Magnetotransport, magnetooptics and magnetophotonics 414

E.O1
PROXIMITY INDUCED LONG-RANGE TRANSFORMATION OF TRANSVERSE MAGNETO-OPTICAL KERR EFFECT IN BILAYERS OF MAGNETIC AND NORMAL TRANSITION METALS
V.A. Skidanov 415

E.O2
FABRICATION OF ONE-DIMENSIONAL MAGNETOPHOTONIC CRYSTALS CONTAINING METAL-ORGANIC DECOMPOSITION-PREPARED BISMUTH-SUBSTITUTED YTTRIUM IRON GARNET
S.L. Efremova, K.N. Afanasiev, A.A. Kasyanov, D.P. Kulikova, Y.M. Sgibnev, A.V. Shelaev, P.N. Tananaev, A.V. Baryshev 417

E.O3
HALL EFFECT IN HEUSLER-TYPE MAGNETIC SHAPE MEMORY ALLOYS
A.B. Granovsky, V.N. Prudnikov, M.I. Blinov, Ya.G. Rezninov, M.V. Prudnikova 420

E.O4
MAGNETO-OPTICAL SPECTROSCOPY OF $(CoFeB)_x(LiNbO_3)_{100-x}$ NANOCOMPOSITES BELOW THE PERCOLATION THRESHOLD
E.A. Ganshina, A.B. Granovsky, E.S. Kanazakova, I.M. Pripechenkov, S.N. Nikolaev, A.S. Sitnikov, V.V. Rylkov 422

E.O5
SWITCHABLE TERAHERTZ EMISSION BY MAGNETIC TUNNEL JUNCTION
A.A. Fraerman, E.A. Karashtin, F. Kholid, R.V. Mikhaylovskiy, I.Yu. Pashen'kin, Y . Saito 425

E.O6
MAGNETIC MODULATION OF HYPERBOLIC SURFACE PLASMON-POLARITONS IN UNIAXIAL METASURFACES
D.A. Kuzmin, I.V. Bychkov, V.G. Shavrov 428

E.O7
INFLUENCE OF DIMENSIONAL EFFECTS AND SIZE DISTRIBUTION OF GRANULES ON OPTICAL AND MAGNETO-OPTICAL PROPERTIES OF NANOSTRUCTURES
A.N. Yurasov, M.M. Yashin, E.A. Gan'shina, I.V. Gladyshev, M.A. Simdyanova, D.A. Saifulina, K.R. Safin 430

E.O8
MAGNETIC AND MAGNETOTRANSPORT PROPERTIES OF MnSb POLYCRYSTALS AND MnSb-BASED COMPOSITES
L.N. Oveshnikov, A.B. Granovsky, A.B. Davydov, L.A. Morgun, A.V. Bogach, A.L. Vasiliev, A.V. Ovcharov, A.M. Kharlamova, E.I. Nekhaeva, A.I. Ril', M. Jaloliddinzoda, S.F. Marenkin, B.A. Aronzon 432

E.O9
THERMAL DECOMPOSITION OF METAL OLEATES FOR FABRICATION OF Bi:YIG OPTICAL FILMS
P.N. Tananaev, A.V. Shelaev, S.L. Efremova, D.P. Kulikova, A.V. Voennov, A.V. Baryshev 434

CONTENTS

E.O10
PHOTO-INDUCED MAGNETO-OPTICAL PHENOMENA IN EPITAXIAL EuO FILMS
V.V. Pavlov, V.N. Kats, L.A. Shelukhin, P.A. Usachev, D.V. Averyanov, I.A. Karateev, O.E. Parfenov, A.N. Taldenkov, A.M. Tokmachev, V.G. Storchak 436

E.O11
EFFECT OF THE INTERPARTICLE INTERACTIONS ON SUPERPARAMAGNETIC RELAXATION
D.A. Balaev, S.V. Stolyar, A.A. Krasikov, O.A. Bayukov, R.N. Yaroslavtsev, D.A. Velikanov, R.S. Iskhakov, Yu.V. Knyazev 437

E.O12
MAGNETO-OPTICAL SPECTROSCOPY OF GaSb-MnSb COMPOSITES
E.A. Ganshina, A.B. Granovsky, E.S. Kanazakova, I.M. Pripechenkov, L.N. Oveshnikov, M. Jaloliddinzoda, A.I. Ril', B.A. Aronzon 439

E.O13
LOW TEMPERATURE OSCILATIONS OF MAGNETORESISTANCE IN ANTIMONY-DOPED SILICON
A.L Danilyuk, A.G. Trafimenko, S.L. Prischepa 441

E.O14
KINETIC AND MAGNETIC PROPERTIES OF HEUSLER ALLOYS IN THE STATES OF A HALF-METALLIC FERROMAGNET, SPIN GAPLESS SEMICONDUCTOR AND TOPOLOGICAL SEMIMETAL
V.V. Marchenkov, V.Yu. Irkhin 443

E.P1
THE THEORY OF THE PRESSURE-INDUCED INVERSION OF MAGNETORESISTANCE IN $La_{1-x}Ag_xMnO_3$
Z.Z. Alisultanov, A.G. Gamzatov, T.R. Arslanov 444

E.P2
CORRELATION BETWEEN MAGNETORESISTANCE BEHAVIOR AND MAGNETIC STATES IN LAYERED COMPOUNDS Fe_xTiS_2
N.V. Baranov, N.V. Selezneva, E.M. Sherokalova, A. Podlesnyak 445

E.P3
LOW TEMPERATURE BEHAVIOUR OF THE LATERAL PHOTOVOLTAIC EFFECT IN MULTILAYERED SILICON-BASED NANOSTRUCTURES
M.V. Rautskii, L.V. Shanidze, A.V. Lukyanenko, A.S. Tarasov, I.A. Yakovlev, I.A. Bondarev 446

E.P4
FLUCTUATION OF ELECTROMAGNETIC FIELD FROM GYROTROPIC HALF-SPACE
I.V. Bychkov, I.A. Kuznetsov, D.A. Kuzmin, V.G. Shavrov 448

E.P5
FARADAY EFFECT AND MAGNETIC CIRCULAR DICHROISM OF ULTRATHIN IRON GARNET FILMS
A.S. Fedorov, S.S. Safonov, A.A. Fedorova, V.A. Kotov, S.A. Nikitov, A.I. Stognii, M.V. Logunov 450

E.P6
VECTORIZATION OF MAGNETO-OPTICAL IMAGES OF A IN-PLANE COMPONENT OF INHOMOGENEOUS MAGNETIC FIELDS
V.E. Ivanov, A.N. Gorkovenko, V.N. Lepalovskij 451

CONTENTS

E.P7
MAGNETO-OPTICAL PROBING OF THE MAGNETIC AND PHASE STRUCTURES IN InFeAs LAYERS
E.A. Gan'shina, Z.E. Kun'kova, I.M. Pripechenkov, Yu.V. Markin 452

E.P8
LASER-PULSE-INDUCED NON-EQUILIBRIUM PHASE TRANSITIONS IN MAGNETITE Fe_3O_4
A.V. Kuzikova, L.A. Shelukhin, R.V. Pisarev, A.M. Kalashnikova 454

E.P9
PERMALLOY-BASED TWO-DIMENSIONAL MAGNETOPLASMONIC CRYSTALS FOR MAGNETIC FIELD SENSING
D.V. Murzin, V.K. Belyaev, Ch. Gritsenko, V. Komanicky, V.V. Rodionova 456

E.P10
MAGNETORESISTANCE AND ANOMALOUS HALL EFFECT IN $(CoFeB)_x(LiNbO_3)_{100-x}$ NANOCOMPOSITES GROWN ON Si SUBSTRATE
S.N. Nikolaev, A.V. Emelyanov, K.Yu. Chernoglazov, E.A. Gan'shina, A.V. Sitnikov, V.A. Demin, A.B. Granovsky, V.V. Rylkov 458

E.P11
GALVANOMAGNETIC AND OPTICAL PROPERTIES OF MOLYBDENUM AND TUNGSTEN DITELLURIDES
A.N. Perevalova, S.V. Naumov, E.I. Shreder, V.V. Chistyakov, E.B. Marchenkova, S.M. Podgornykh, J.C.A. Huang, V.V. Marchenkov 460

E.P12
ULTRAFAST LASER-INDUCED MAGNETIZATION PRECESSION IN THIN FILM AND ANTIFERROMAGNETIC BILAYER OF $L1_0$-PdFe
A.V. Petrov, M.V. Pasynkov, A.A. Busse, R.V. Yusupov, S.I. Nikitin, A.I. Gumarov, I.V. Yanilkin, A.G. Kiiamov, L.R. Tagirov 461

E.P13
MAGNETOTRANSPORT PROPERTIES OF Ni_2MnGa SINGLE CRYSTAL
I.G. Reznikov, V.N. Prudnikov, M.V. Prudnikova, A.B. Granovsky 463

E.P14
Co NANOPARTICLES LOCALIZED IN MATRICES OF VARIOUS TYPES: MAGNETOOPTICAL AND MAGNETOTRANSPORT PROPERTIES
Yu.E. Samoshkina, D.A. Petrov, M.V. Rautskii, D.S. Neznakhin, E.A. Stepanova, A.L. Stepanov 466

E.P15
ELECTRONIC STRUCTURE AND OPTICAL PROPERTIES OF Mn-BASED HEUSLER ALLOYS
E.I. Shreder, A.A. Semiannikova, E.D. Chernov, A.V. Lukoyanov, V.V. Marchenkov 468

E.P16
MAGNETIC CIRCULAR DICHROISM AND ABSORPTION OF A $HoAl_3(BO_3)_4$ CRYSTAL IN THE REGION OF $^5I_8 \longrightarrow {}^5F_3$ AND $^5F_2$ TRANSITIONS
V.V. Sokolov, A.V. Malakhovskii, A.L. Sukhachev, I.A. Gudim 470

E.P17
SPECTRALLY SELECTIVE DETECTION OF SHORT SPIN WAVES IN MAGNETOPLASMONIC NANOSTRUCTURES VIA THE FARADAY EFFECT
O.V. Borovkova, S.V. Lutsenko, D.A. Sylgacheva, A.N. Kalish, V.I. Belotelov 472

CONTENTS

E.P18
THE SECOND HARMONICS OF MAGNETIC QUANTUM OSCILLATIONS OF MAGNETIZATION AND CONDUCTIVITY IN QUASI-TWO-DIMENSIONAL METALS
T.I. Mogilyuk, P.D. Grigoriev 474

E.P19
STUDY OF HM/FM NANOSTRUCTURES WITH HIGH EFFICIENCY OF SOT
A.V. Telegin, M. Steblii, A.V. Ognev, A.S. Samardak, I.D. Lobov, S.V. Batalov, E.A. Surzhikov, V.D. Bessonov 475

E.O20
PICOSECOND MAGNETOOPTICS IN FERROMAGNETIC CHROMIUM SPINEL
A.V. Telegin, S. Changhee, H.-R. Park, S. Yu, A.V. Kimel, Yu.P. Sukhorukov. 477

E.P21
BEHAVIOR OF SURFACE PLASMON POLARITONS IN THE VANADIUM DIOXIDE-SILICON DIOXIDE-HYPERBOLIC METASURFACE STRUCTURE UNDER THE INFLUENCE OF AN EXTERNAL MAGNETIC FIELD
M.O. Usik, D.A. Kuzmin, I.V. Bychkov 478

E.P22
IRON GARNET-BASED ULTRAFAST OPTOMAGNONIC XNOR GATE
A.A. Kolosvetov, M.A. Kozhaev, V.I. Belotelov, A.I. Chernov 480

E.P23
STRUCTURE AND EFFECT OF A MAGNETIC FIELD ON THE MICROWAVE IMPEDANCE OF COMPOSITE FILMS CoFeB + SiO_2
L.N. Kotov, M.P. Lasek, A.V. Sitnikov, Yu.E. Kalinin. 482

Section F.
Magnetoelastic, magnetocaloric and shape memory effects 484

F.I1
STRUCTURE AND MAGNETIC PROPERTIES OF Fe-Ga-Al ALLOYS: AB INITIO STUDY
M.V. Matyunina, M.A. Zagrebin, V.V. Sokolovskiy, V.D. Buchelnikov. 485

F.O1
DYNAMICS OF MAGNETIZATION OSCILLATIONS AND ELASTIC DISPLACEMENT OF THE FERRITE FILM UNDER FREQUENCY-MODULATED EXCITATION
D.A. Pleshev, F.F. Asadullin, V.S. Vlasov, L.N. Kotov 487

F.O2
NEW MATERIALS FOR SOLID-STATE MAGNETIC COOLING
I.S. Tereshina, I.A. Ovchenkova, N.Yu. Pankratov 488

F.O3
INFLUENCE OF CHEMICAL IMPURUTIES ON MAGNETOTHERMAL PROPERTIES OF RARE-EARTH METALS AND PERMANENT MAGNETS
R.R. Gimaev 489

CONTENTS

F.O4
THE ISSUES OF PHASE STABILITY AND MAGNETOCRYSTALLINE ANISOTROPY IN Fe_2Ni-BASED HEUSLER ALLOYS
V.V. Sokolovskiy, O.N. Miroshkina, A.A. Sanosyan, V.D. Buchelnikov, M.E. Gruner 490

F.O5
FEATURES OF THERMAL EXPANSION IN SUBSTITUTION ALLOYS BASED ON HEAVY RARE-EARTH METALS $R^{I}_{1-x}R^{II}_{x}Fe_2$
Z.S. Umkhaeva, I.S. Tereshina, N.Y. Pankratov, I.M. Aliev 492

F.O6
NATURE OF THE FREQUENCY DEPENDENCE OF THE MAGNETOCALORIC EFFECT IN $Ni_{50}Mn_{28}Ga_{22-x}(Cu, Zn)_x$ (x = 0, 1.5) ALLOYS
A.G. Gamzatov, A.M. Aliev, Sh.K. Khizriev, A.G. Varzaneh, P. Kameli, I.A. Sarsari 494

F.O7
MAGNETIC NANORADIOSENSITIZERS IN NEUTRON THERAPY FOR ONCOLOGY
V.I. Zverev 495

F.O8
ANOMALOUS ULTRASONIC ATTENUATION NEAR THE LOW-SPIN-HIGH-SPIN CROSSOVER IN $LuCo_3$
A.A. Tereshchenko, A.S. Ovchinnikov 496

F.O9
MNAS COMPOUNDS UNDER HIGH PULSED MAGNETIC FIELDS UP TO 500 KOE
A. Kamantsev, Yu. Koshkidko, V. Koledov, V. Shavrov, A. Golovchan, A. Sivachenko, B. Todris, V. Valkov, L. Butvina 498

F.O10
ELECTRONIC STRUCTURE AND EXCHANGE INTERACTIONS IN $LaFe_{13}$-BASED ALLOYS
A.P. Kamantsev, O.E. Kovalev, A.P. Sivachenko, A.V. Golovchan 499

F.O11
WEAK FERROMAGNETISM IN SUBMICRON BARIUM TITANATE
L.N. Korotkov, N.A. Tolstykh, R.M. Eremina, N.A. Emelyanov, R.G. Batulin 501

F.O12
MAGNETOCALORIC PROPERTIES OF FeRh ALLOY UNDER MAGNETIC FIELD AND THERMAL CYCLING
A.M. Aliev, A.G. Gamzatov, G.M. Aliev, L.G. Khanov 502

F.O13
MAGNETOELASTICITY OF THE JAHN-TELLER SUB-SYSTEM IN THE CHROMIUM-DOPED II-IV CRYSTALS
M.N. Sarychev, I.V. Zhevstovskikh, Yu.V. Korostelin, V.T. Surikov, N.S. Averkiev, V.V. Gudkov 503

F.O14
MAGNETOELECTRIC EFFECT IN LAMINATED COMPOSITES $CoFe_2O_4$/PZT. DEPENDENCE ON THICKNESS OF MAGNETOSTRICTION PHASE
V.A. Astakhov, A.T. Morchenko, V.G. Kostishyn 505

CONTENTS

F.O15
MAGNETIC GLASSINESS AND CRYSTAL FIELD EFFECTS ON THERMAL AND ELECTRICAL PROPERTIES OF Er_5Pd_2-TYPE COMPOUNDS
A.A. Vaulin, E.A. Sherstobitova, D.A. Shishkin, E.M. Sherokalova, N.V. Baranov, A.F. Gubkin 506

F.O16
THE FERROMAGNETIC PHASE GROWTH MECHANISMS IN FeRh ALLOYS
A.S. Komlev, R.A. Makaryin, T.S. Ilina, D.A. Kiselev, V.I. Zverev, N.S. Perov 508

F.O17
MODELING THE DOMAIN STRUCTURE OF SQUARE FERROMAGNET MICROPARTICLES UNDER UNIAXIAL MECHANICAL STRESS
N.I. Nurgazizov, D.A. Byziaev, A.P. Chuklanov 510

F.O18
INFLUENCE OF DEFORMATION-THERMAL IMPACT ON THE STRUCTURE AND PROPERTIES OF FERROMAGNETIC ALLOYS
Yu.V. Kaletina, A.Yu. Kaletin, V.P. Pilyugin 512

F.P1
MAGNETOCALORIC EFFECT IN $LaFe_{11.1}Mn_{0.1}Co_{0.7}Si_{1.1}$ ALLOY: DIRECT AND INDIRECT MEASUREMENTS
N.Z. Abdulkadirova, A.G. Gamzatov, K.I. Kamilov, A.T. Kadirbardeev, A.M. Aliev, P. Gebara 513

F.P2
MAGNETOCALORIC EFFECT IN HEUSLER ALLOYS IN THE REGION OF MARTENSITIC TRANSITIONS UNDER CYCLIC MAGNETIC FIELDS
A.M. Aliev, A.G. Gamzatov, L.G. Khanov 516

F.P3
MAGNETIC PROPERTIES OF CRYSTALLINE POWDERS OF TERBIUM, DYSPROSIUM, HOLMIUM, ERBIUM AND YTTERBIUM TETRAFLUORIDES
G.Iu. Andreev, I.V. Romanova, S.L. Korableva, O.A. Morozov, A.S. Semakin, M.A. Cherosov, A.G. Kiiamov, M.S. Tagirov 517

F.P4
MAGNETOCALORIC EFFECT IN $Y(Co_{0.84}Fe_{0.16})_2$ AND $Lu(Co_{0.84}Fe_{0.16})_2$ COMPOUNDS
M.S. Anikin, E.N. Tarasov, N.V. Kudrevatykh, A.V. Zinin 518

F.P5
SIMULATION OF MICROWAVE SWITCHING IN THE MAGNETIC AND ELASTIC SUBSYSTEMS OF A THREE-LAYER MAGNETIC STRUCTURE
L.N. Kotov, M.Yu. Dianov, V.S. Vlasov 520

F.P6
HALL EFFECT IN Ni-Mn-Sb-BASED HEUSLER ALLOYS DOPING BY ALUMINUM
S.M. Emelyanova, V.V. Marchenkov 522

F.P7
INFLUENCE OF MAGNETIC FILM ANISOTROPY ON MAGNETOELASTIC DYNAMICS UNDER FREQUENCY-MODULATED EXCITATION
F.F. Asadullin, D.A. Pleshev, V.S. Vlasov, V.I. Shcheglov 523

CONTENTS

F.P8
CONDITIONS FOR EFFICIENT DETECTING A FREQUENCY-MODULATED ALTERNATING MAGNETIC FIELD BASED ON MAGNETOELASTIC OSCILLATIONS OF YIG FILM
M.A. Filitov, S.A. Maltseva, F.F. Asadullin, D.A. Pleshev, V.S. Vlasov, V.I. Shcheglov 524

F.P9
MAGNETOCALORIC EFFECT, HEAT CAPACITY AND EXCHANGE INTERACTIONS IN NONSTOICHIOMETRIC $Er_{0.65}Gd_{0.35}Co_2Mn_x$ COMPOUNDS
E.G. Gerasimov, A.A. Inishev, N.V. Mushnikov, P.B. Terentev, V.S. Gaviko, M.S. Anikin 525

F.P10
DEFORMATION OF A STRUCTURED MAGNETICALLY ACTIVE ELASTOMER WITH MAGNETICALLY HARD INCLUSIONS IN A 2D FORMULATION
A.A. Ignatov, O.V. Stolbov, V.V. Rodionova 526

F.P11
MAGNETOSTRICTION IN NONSTOICHIOMETRIC $TbCo_2Mn_x$ COMPOUNDS
A.A. Inishev, E.G. Gerasimov, P.B. Terentev, N.V. Mushnikov 528

F.P12
RELATIONSHIP OF THE MAGNETIC AND ELASTIC SUBSYSTEMS IN THE CASE OF THE SHEAR MODULUS IN NICKEL
E.L. Kolyvanov, I.V. Shashkov 529

F.P13
MAGNETIC PHASE TRANSITIONS AND MAGNETOCALORIC EFFECT IN COMPOUNDS BASED ON $Gd_5Si_2Ge_2$
A.A. Kurganskaya, A.V. Smirnov, I.A. Ovchenkova, A.E. Bogdanov, A.V. Morozkin, I.S. Tereshina, S.A. Nikitin 530

F.P14
INFLUENCE OF THE [011] FERRITE FILM CRYSTALLOGRAPHIC CELL ORIENTATION ON THE DETECTION OF ALTERNATING AMPLITUDE-MODULATED MAGNETIC FIELD
D.K. Lytkin, P.A. Nikiforova, D.A. Pleshev, F.F. Asadullin, V.S. Vlasov, L.N. Kotov, V.I. Shcheglov 532

F.P15
MAGNETOELASTIC EFFECTS IN THERMAL EXPANSION OF Fe_7Se_8 SINGLE CRYSTAL
S.N. Mozgovykh, V.A. Kazantsev, D.F. Akramov, E.M. Sherokalova, N.V. Selezneva 533

F.P16
MAGNETIC AND STRUCTURAL PROPERTIES OF THE $GdRu_{1-x}Cr_xSi$ COMPOUNDS
S.P. Platonov, A.G. Kuchin, V.S. Gaviko, A.S. Volegov, M.Yu. Yakovleva 534

F.P17
MODELING OF ITINERANT MAGNETOCALORIC EFFECT IN Si, Al DOPED METAMAGNETIC $LaFe_{13}$
D.I. Radzivonchik, V.I. Grebennikov 536

CONTENTS

F.P18
DEFORMATION-INDUCED INCREASE OF THE ISOTROPIC ENERGY GAP IN IRON BORATE EPITAXIAL FILM
K. Seleznyova, D. Prilepsky, Yu.A. Mogilenec, M.B. Strugatsky, S.V. Yagupov, A. Drovosekov, N. Kreines, J. Kliava 538

F.P19
EXCITATION OF MAGNETIC AND ELASTIC OSCILLATIONS IN MAGNETIC CRYSTALS WITH INVERSION AREA OF THE SIGN OF THE FIRST ANISOTROPY CONSTANT
L.N. Kotov, P.A. Severin, V.S. Vlasov 539

F.P20
MODELING THE EVOLUTION OF THE MARTENSITIC STRUCTURE OF A SHAPE MEMORY FERROALLOY IN A MAGNETIC FIELD
A.A. Rogovoy, O.S. Stolbova 541

F.P21
INVESTIGATION OF $Fe_{49}Rh_{51}$ ALLOY BY WIDE-FIELD KERR MICROSCOPY
T.A. Taaev, A.A. Amirov, A.M. Aliev, A. Chirkova, I. Soldatov, R. Schäfer 543

F.P22
THE MAGNETOSTRICTION IN GARNET FERRITE $Y_{1.8}Bi_{1.2}Fe_{3.5}Ga_{1.5}O_{12}$ SYNTHESING BY THE MODIFIED METHOD OF GEL COMBUSTION USING ETHYLENE GLYCOL
F.V. Zelenov, T.N. Tarasenko, O.E. Kovalev, Z.F. Kravchenko, V.V. Burkhovetskii, V.I. Mikhaylov, A.V. Golovchan 545

F.P23
THEORY OF COUPLED MAGNETOELASTIC WAVES IN A THIN ANTIFERROMAGNETIC FILM BASED ON SIGMA-MODEL
T.V. Bogdanova, D.V. Kalyabin, A.R. Safin, S.A. Nikitov 547

F.P24
THE MAGNETOCALORIC EFFECT IN MAGNETICALLY ORDERED COMPOUNDS $Fe_{3-x}Ni_xSe_4$
N.V. Selezneva, E.M. Sherokalova, V.A. Komarova, M.D. Klyucharev 549

F.P25
EFFECTS OF CARBON ATOMS ON MAGNETIC MOMENT IN FE-C SYSTEM: FIRST-PRINCIPLES CALCULATION
A.A. Mirzoev, Ya.M. Ridnyi 550

F.P26
VORTEX DYNAMIC MAGNETIC STRUCTURE INDUCED BY TRANSVERSE SOUND IN TRIGONAL WEAK FERROMAGNETS
M.B. Strugatsky, D.Yu. Prilepsky 551

A.P65
STRUCTURAL AND MAGNETIC PROPERTIES OF FeNi FILMS WITH OUT-OF-PLANE MAGNETIZATION COMPONENT
A.V. Svalov, A.N. Gorkovenko, A. Larrañaga, G.V. Kurlyandskaya 553

Author Index 555

Plenary

SPIN-ORBIT TRANSITION METAL COMPOUNDS

S.V. Streltsov

M.N. Mikheev Institute of Metal Physics, Ekaterinburg, Russia
E-mail: streltsov@imp.uran.ru

The spin-orbit coupling has become one of the key notions of the condensed matter physics in last decade. While most of the emphasis has been made on various topological effects, many conventional physical phenomena in transition metal compounds have been reexamined. First of all, these are "magnetic" manifestations related to pronounced anisotropy of the exchange interaction due to strong spin-orbit coupling. The most prominent examples are so-called Kitaev materials – layered systems with honeycomb lattice based on typically Ru^{5+} or Ir^{4+} ions. Second, it has been realized that there is an important class of compounds, where the metal-insulator transitions turn out to be related to the spin-orbit coupling (spin-orbit assisted Mott insulators). Third, the spin-orbit coupling can result in formation of highly non-trivial states, where not dipolar, but higher order multipoles order. Forth, even such "classical" effects as e.g. Jahn-Teller effect can be modified by the spin-orbit coupling. All these phenomena will be discussed in the present talk.

We thank Russian Science Foundation for support (№ 20-62-46047).

1. D.I. Khomskii and S.V. Streltsov, Chem. Rev. **121**, 2992 (2021).
2. S.V. Streltsov, D.I. Khomskii, Physics-Uspekhi **60**, 1121 (2017).

NEUTRON SCATTERING METHODS FOR STUDYING MAGNETISM

S.V. Grigoriev

Petersburg Nuclear Physics Institute NRC "Kurchatov institute", Gatchina, St. Petersburg, Russia
E-mail: grigoryev_sv@pnpi.nrcki.ru

Neutron scattering methods require construction and operation of large scale neutron facilities such as research nuclear reactors or spallation neutron sources. The neutron sources are surrounded by different types of neutron scattering stations based on neutron beams coming from the secondary sources – moderators providing the neutrons of a certain energy and wavelength. Neutron wave being electrically neutral but having a spin 1/2 and magnetic moment are very sensitive to and equally good scattered by both nucleus and electron magnetic moment of an atom. Tens of neutron scattering instruments are effectively operated around one neutron source. They are diffractometers for studying magnetic and crystal structure of matter, spectrometers for studying elementary magnetic and crystal excitations, small-angle neutron scattering machines for studying nanoobjects and nanostructures as well as reflectometers for studying layered structures and interfaces. We give several historically meaningful and recent examples of such studies.

Studies of the ferro-, antiferro- and ferrimagnetic structures by neutron diffraction give a direct evidence on the symmetry of the structure, nuclear and magnetic lattice parameters. As the magnetic moments are collinear and the period of magnetic structure is commensurate to the atomic structure, one may consider them as being rather simple in sense of structure determination with help of neutron diffraction. Anisotropy sometimes results in non-collinear arrangement of the magnetic moments but the magnetic structure remains commensurate. The most complicated case appears when the magnetic structure is neither collinear nor commensurate, i.e. in case of magnetic spirals, cycloids, skyrmion lattices, etc. It is the competition of strong isotropic exchange interactions along with weak that relativistic interactions that breaks spin symmetry and leads to the appearance of complex magnetic structures. Complex phenomena determined by the hierarchy of interactions include the appearance of long-period spirals of a certain chirality, the appearance of "skyrmion lattices", phase transitions with several order parameters. The fragile balance of these interactions can be easily disturbed by external forces: pressure, magnetic field, chemical substitution, which leads to quantum phase transitions in pressure, magnetic field or concentration.

As an example we present studies of non-centrosymmetric crystals, which are helicoidal cubic magnets (MnSi, $Fe_{1-x}Co_xSi$, FeGe, MnGe etc.) These compounds crystallize into a cubic non-centrosymmetric structure with space group $P2_13$. The magnetic configuration is a spin spiral with a period from 30 to 3000 Å, which is formed as a result of a balance of two interactions: a symmetric ferromagnetic exchange and an antisymmetric Dzyaloshinsky-Moriya interaction.

An ideal probe for studying such systems is the small-angle diffraction of polarized neutrons. Using this method, phase diagrams of compounds (magnetic field-temperature) were constructed and the parameters of the basic magnetic interactions were estimated. The critical phenomena during the transition from a paramagnetic state to an ordered helix were studied in fine details. The magnetic structure of a skyrmion lattice was established in tiny room of the (H-T) phase diagram. In conclusion, we generalize the experimental results within the framework of the phenomenological Back-Jensen model.

PT-SYMMETRY AND EXCEPTIONAL POINTS IN SPINTRONICS, MAGNONICS, AND PHONONICS

S.A. Nikitov[1,2,4*], D.V. Kalyabin[1,2], A.R. Safin[1,3], O.S. Temnaya[1], A.V. Dorofeenko[1,2], A.A. Zyablovsky[1,2] A.V. Sadovnikov[1,4], E.A. Vilkov[1]

[1]Kotel'nkov Institute of Radio-Engineering and Electronics of RAS, Moscow, Russia
[2]Moscow Institute of Physics and Technology, Dolgoprudny, Moscow Region, Russia
[3]Moscow Power Engineering Institute, Moscow, Russia
[4]Laboratory "Metamaterials", Saratov State University, Saratov, Russia
[*]E-mail: nikitov@cplire.ru

Recently, research in spintronics has led to discovering some new effects that have not been previously found and, therefore, have not been studied. In particular, the dynamics associated with the behavior of spins, or magnons, exhibit various phenomena inherent in other classical and quantum systems. One of them is analogous to a quantum mechanical phenomenon of parity-time symmetry (PT-symmetry [1]). It concerns quantum systems with non-Hermitian Hamiltonian, which, however, can have a real set of eigenstates with real eigenvalues. The main requirement for such a system is that its Hamiltonian has parity- and time-reversal symmetry, namely, $\hat{\mathscr{H}}(\hat{\mathbf{r}},\hat{\mathbf{p}},t) = \mathscr{H}^*(-\hat{\mathbf{r}},-\hat{\mathbf{p}},t)$, where $\hat{\mathbf{r}}$, $\hat{\mathbf{p}}$, t is momentum, radius vector, and time. PT-symmetry was discovered and studied in optics, plasmonics, and acoustics, and the first results appeared in spintronics recently [2]. In PT-symmetric systems, spontaneous violation of the symmetry of eigenstates can be observed, which occurs at exceptional points in its parameter space [3]. The exceptional points correspond to the maximum degree of non-orthogonality of eigenstates in a non-Hermitian system. In this paper, we review systems with exceptional points and implement such systems using specific examples of two magnetic waveguides. We also generalize the results to solid-state acoustic (phonon) systems.

The phase transition in PT-symmetric systems is due to the balance and controllability between intrinsic spin-wave gain and loss of propagating waves. In magnetic systems, the dynamics of spin waves, or magnons, is described by the Landau-Lifshitz equation for magnetization precession with a term in the Gilbert form, which is responsible for the intrinsic losses in the magnetic system. Several compensating for these intrinsic losses measures can have been proposed, such as parametric amplification of waves or introducing external sources (for example, spin-torque and spin-Hall moment). In recent writings concerning the manifestation of PT-symmetry in magnonic structures, attention was paid to multilayer heterostructures containing ferromagnetic layers separated, as a rule, by non-magnetic layers of heavy metals with strong spin-orbit interaction (CO, Py, and Pt). Spin torque, that occurs when direct electric current flows through the Pt layer, compensated the losses of spin waves. Thus, losses increasing during the propagation of spin waves was observed in one layer, and losses decreased in the second layer. In the next work, a similar structure was considered, in which, however, YIG ($Y_3Fe_5O_{12}$) have been chosen as a magnetic material. In both cases, the coupling between the waveguides was carried out by indirect exchange interaction (RKKY). From the point of view of implementation, such structures are complicated to fabricate; besides, the non-identity of the magnetic layers and the weak, short-range interaction between them does not make it possible to achieve PT-symmetry in the system easy.

Our work proposes at least two structures, different from those previously offered, for observing PT-symmetry and exceptional points for spin waves propagating in them. The structures consist of two identical narrow ferromagnetic waveguides (YIGs) fabricated from the same sample on a gallium gadolinium garnet substrate by laser cutting.

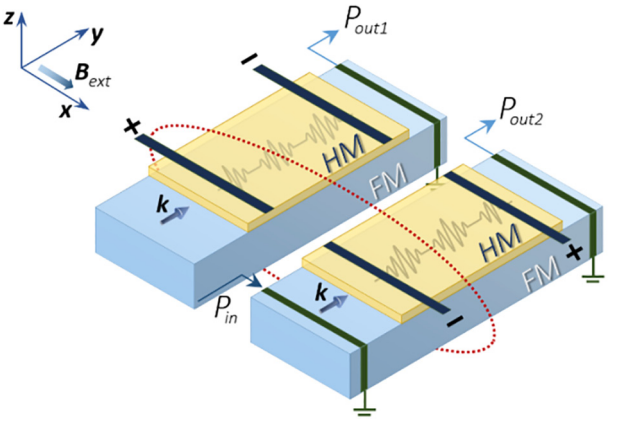

Figure 1. Coupled magnonic heterostructures “ferromagnetic-heavy metal”.

In the first case (Fig. 1), the waveguides are covered with heavy metal layers through which a current of different polarity is passed; in this case (as in the second case, Fig. 2), the coupling between the waveguides is due to the dipole-dipole interaction. Changing the current’s direction and magnitude in the heavy metal layers makes it possible to control spin-wave losses at the ferromagnet/heavy metal interface, partially compensating or amplifying it. The second structure (Fig. 2a) consists of coupled YIG waveguides coated with a semiconductor n-GaAs layer. Under normal conditions, YIG waveguides are identical; therefore, the properties of spin waves in them are also equal. When a semiconductor is irradiated with infrared light with a wavelength corresponding to the bandgap in the semiconductor, electrons will be thrown from the valence band to the conduction

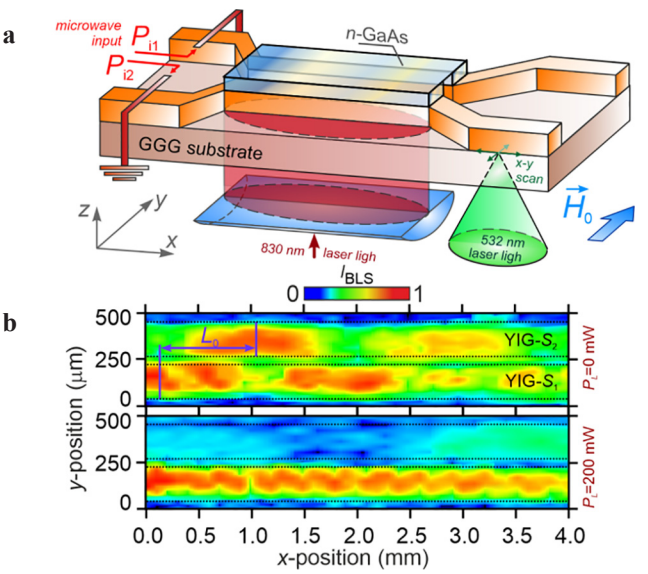

Figure 2. **a** Planar system of magnonic waveguides with a semiconductor layer; **b** spatial distribution of dynamic magnetization when changing the power of laser light focused on one of the waveguides.

band, which will lead to a change in the electrical properties of the semiconductor, namely, it will become more "metallic". This, in turn, will lead to a change in the dispersion of infrared light, so it becomes possible to control the parameters of the spin waves. By focusing light on only one of the waveguides, the parameters can be changed only in one of the waveguides without varying the properties of the second waveguide.

The results of two-dimensional maps of magnon intensities in coupled waveguides measured using the Mandelstam-Brillouin scattering of light (MBRS) on spin waves, which can be used to detect exceptional points in PT-symmetric structures, are shown in Fig. 2b. Similar calculations are also performed in this work for surface acoustic waves propagating in coupled acoustic waveguides, in which PT-symmetry can also be observed.

The work was performed in the framework of Russian Science Foundation (Grant No. 19-19-00607).

1. C.M. Bender and S. Boettcher, Phys. Rev. Lett. **80**, 5243 (1998).
2. X. Wang, Xi-guang Wang, G. Guo, and J. Berakdar, Nature Comm. **11**, 5663 (2020).
3. Miri et al., Science **362**, 42 (2019).

SPIN CROSSOVERS IN MAGNETIC MATERIALS

V.A. Dudnikov[1], *V.A. Gavrichkov*[1], *S.V. Nikolaev*[2], *Yu.S. Orlov*[1,2], *S.G. Ovchinnikov*[1,2*]

[1]Kirensky Institute of Physics, Krasnoyarsk, Russia
[2]Siberian Federal University, Krasnoyarsk, Russia
[*]E-mail: sgo@iph.krasn.ru

Experimental and theoretical results on spin crossovers in strongly correlated magnetic materials are reviewed. Due to the cooperative effect of the interatomic exchange interaction a well-known level crossing of the mulrielectron terms with different spin values transforms in the first order phase transition accompanied by a magnetization and volume drop. In transition metal oxides this phenomen is usually results from the high pressure and is studied experimentally in the diamond anvil cells, mostly at 50–100 GPa. The effect of spin crossover on the electronic structure of these Mott insulators and the Bose condensation of spin excitons near the crossover pressure are discussed. It is shown that the low energy electronic structure of strongly correlated transition metal oxides can be described within the effective Hubbard model including the electroneutral term d^n and the electron removal term d^{n-1} and the electron addition term d^{n+1} with the effective Hubbard energy $U_{\text{eff}}(n) = E_0(n + 1) + E_0(n - 1) - 2E_0(n)$, where $E_0(n)$ is the ground term of d^n configuration. Due to the competition of the Hund coupling and the crystal field a spin crossover the HS and LS terms change their order under the external pressure. Spin crossover can occur for configurations with n = 4–7, and it results in the change of the effective parameter $U_{\text{eff}}(n)$. The spin crossover effect on $U_{\text{eff}}(n)$ depends on the electron number n, for d^5 configuration the spin crossover from HS to LS results in the sharp decreasing of electron correlations, while for d^6 configuration the spin crossover from HS to LS results in the sharp decreasing of electron correlations. The most unusual effect of spin crossover on the electronic correlation strength takes place for NiO, where the electroneutral term d^8 has the stable HS term for all pressures but the virtual non-occupied term d^7 has the crossover from the HS with S = 3/2 in the LS with S = 1/2 term. This virtual spin crossover results in the kink in the $U_{\text{eff}}(P)$ dependence with a maximum at the crossover pressure 55 GPa. NiO is the last 3d-metal mono-oxcide where the insulator-metal transition under high pressure is not obtained. We predict metallization of NiO at pressures 450–600 GPa. A number of experimental studies of spin crossovers in transition metal oxides under high pressure is discussed.

A new approach to the superexchange interaction in transition metal oxides is developed that allows to calculate separate contributions from definite excited terms of magnetic ion. At low pressure the LS term is the excited one, and its contribution to the superexchange may have an opposite sign to the exchange interaction between the ground HS terms. With increasing pressure above the spin crossover the LS terms appears to be the ground one. Thus the superexchange interaction may change its value or sign due to the spin crossover. Some examples will be considered for d^5 and d^6 compounds.

In a family of the rare-earth cobaltites $RCoO_3$ the LS ground state of the Co^{+3} ion is nonmagnetic, with heating the thermal population of the HS term resulting in a set of experimentally known anomalies of magnetic, electrical, optical, thermodynamical and elastic properties with the maxima in the temperature dependences at higher temperatures for the heavier R element (the 4f-electrons compression effect). The stabilization of the HS term of the Co^{+3} ion in situations with reduced crystal field (in thin films on the stretching sublattice, at the surface of single crystal and in the intergrain borders of polycrystalline samples) results in the competition of the ferromagnetic and antiferromagnetic exchange contributions from different excited states.

Dynamical properties of spin crossover systems are discussed under sudden spin switch, at low pressure from the HS ground state to the LS initial one, and vice versa for the high pressure. The dynamics of multiplicity, magnetization and local lattice deformations is considered. At small pressure the long live periodic oscillations of magnetization is obtained.

Effect of spin crossover in the ferropericlase $Fe_xMg_{1-x}O$ with $x \sim 0.2$ that is the second abandon mineral after the $MgSiO_3$ in the Earth low mantle is considered. The experimental study of the the ferropericlase $Fe_xMg_{1-x}O$ phase diagram pressure-temperature (P, T) confirms the theoretically calculated phase diagram with spin crossover at 57 GPa at $T = 0$. Further extension of this phase diagram to high temperatures and pressures typical for the Earth low mantle results in a prediction of the insulator-metal-insulator transitions with the metallic layer at the depths 1400–1800 km. This prediction is in agreement with the temporal variations of the Earth geomagnetic field and seismic anomalies experimental data.

Support by RSF project 18-12-00022 is acknowledged.

MANIPULATION OF MAGNETISM VIA FERROELECTRIC SWITCHING

Shuai Dong

School of Physics, Southeast University, Nanjing, China
E-mail: sdong@seu.edu.cn

The converse magnetoelectric effect (CME), namely the modulation of magnetism using electric field, is very interesting science and highly promising for applications. However, because magnetism and polarity break different symmetries, it is not straightforward to obtain the CME, while delicate designs are usually required [1, 2]. In this talk, I will briefly summarize several mostly-adopted strategies in the past decades. Then I will introduce some works from our group.

First, the charge-mediated magnetoelectricity is applied to both ferrimagnetic heterostructrure [3] and bulk [4]. By tuning the charge order parameter, the net magnetic moment of ferrimagnetism can be switched for 180°. Such charge-mediated magnetoelectricity can be coined as: $(\nabla\cdot\mathbf{P})(\mathbf{M}\cdot\mathbf{L})$, where **P** denotes the polarization, **M** is the net magnetization, and **L** is the ferrimagnetic order.

Second, the dynamic magnetoelectricity is proposed for magnetic domain wall [5]. The chirality of Nèel-type domain wall is determined by the Dzyaloshinskii-Moriya interaction, which can be switched by the ferroelectric polarization. Accompanying the chirality switching, the domain wall is shifted for dozens of nanometers, rendering a dynamic CME in nanoscale.

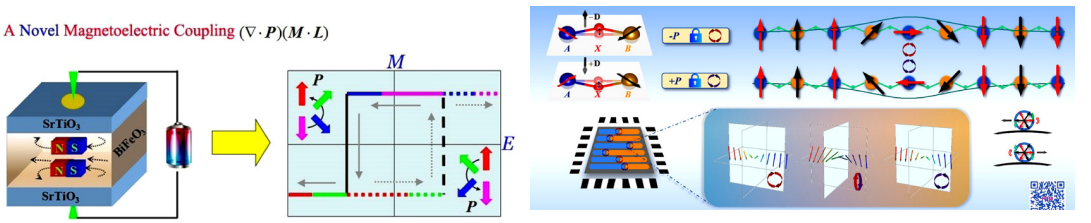

Figure 1. Schematic of converse magnetoelectric effect. Left: charge-mediated magnetoelectricity in $BiFeO_3$/$SrTiO_3$ heterostructures. The net magnetization can be reversed by electric field. Right: the chirality of magnetic domain can be reversed by the ferroelectric polarization switching, which leads the motion of domain wall.

Support by National Natural Science Foundation of China (Grant No. 11834002) is acknowledged.

1. S. Dong, J.-M. Liu, S.-W. Cheong, and Z.F. Ren, Adv. Phys. **64**, 519–626 (2015).
2. S. Dong, H.J. Xiang, and E. Dagotto, Natl. Sci. Rev. **6**, 629–641 (2019).
3. Y.K. Weng, L.F. Lin, E. Dagotto, and S. Dong, Phys. Rev. Lett. **117**, 037601 (2016).
4. L.F. Lin, Q.R. Xu, Y. Zhang, J.-J. Zhang, Y.-P. Liang, and S. Dong, Phys. Rev. Mater. **1**, 071401(R) (2017).
5. J. Chen and S. Dong, Phys. Rev. Lett. **126**, 117603 (2021).

THE ELECTRIC FIELD-MODULATED SURFACE ENERGY OF MAGNETIC DOMAIN WALLS: STRIPE DOMAIN STRUCTURE "REFRACTION" AND MAGNETIC BUBBLE DOMAIN "BLOWING"

*S.A. Kaminskiy, A.A. Podkletnova, A.I. Yadvichuk, D.P. Kulikova, E.P. Nikolaeva, A.P. Pyatakov**

Physics Department, Moscow University, Moscow, Russia
*E-mail: pyatakov@physics.msu.ru

The surface energy of magnetic domain walls and magnetostatic energy are the governing forces that give rise to a rich variety of micromagnetic structures observed in magnetic film. The magnetoelectricity of magnetic domain walls reported by several groups in last decade [1–4] provides a new playground for micromagnetism.

The surface energy of magnetic domain wall in the presence of electric field can be represented as follows [5]:

$$\sigma_{\text{eff}} = 4\sqrt{A(K + 2\pi M^2 \sin^2 \varphi(E))} - \pi\gamma E, \quad (1)$$

where A is the exchange stiffness, K is the magnetic anisotropy constant, γ is the magnetoelectric constant, E is the electric field, M is magnetization and φ is an angle that defines the structure of the domain wall (it varies from $\varphi = 0$ for the case of pure Bloch domain wall and $\varphi = \pi/2$ for Neel-type one).

Recently the refraction-like behavior of magnetic domain wall running through the topography step-like defect: in analogy to Fermat's principle the domain wall assumes the optimum path that minimizes its effective length [6]. Since the energy of the domain wall is proportional to its length, and surface energy can be modulated by the electric field, the refraction-like behavior can be expected for the domain wall running through the stripe electrode. This phenomenon is indeed observed in iron garnet films: the region near the electrode can be highlighted where the stripe domain structure changes its direction (Fig. 1a).

The analysis of domain wall "refraction" in the region of the stripe electrode for various "angle of incidence" confirms the fulfilment of Snell's law. In the case of domain wall the "refractive indexes" ratio corresponds to the ratio of surface energies of the domain wall in the vicinity of the

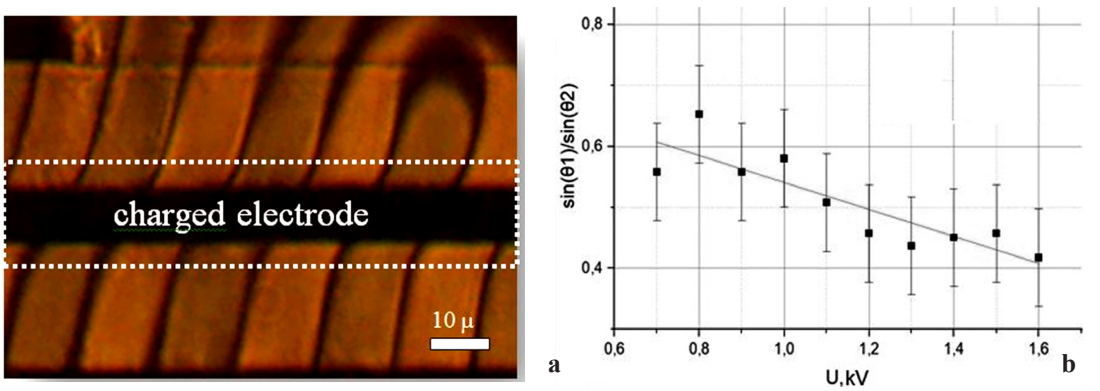

Figure 1. **a** The "refraction" of stripe domain structure in the vicinity of positively charged electrode (the region with modulated surface energy is highlighted with dotted line). **b** The dependence of the "refractive indexes" ratio on the voltage at the electrode.

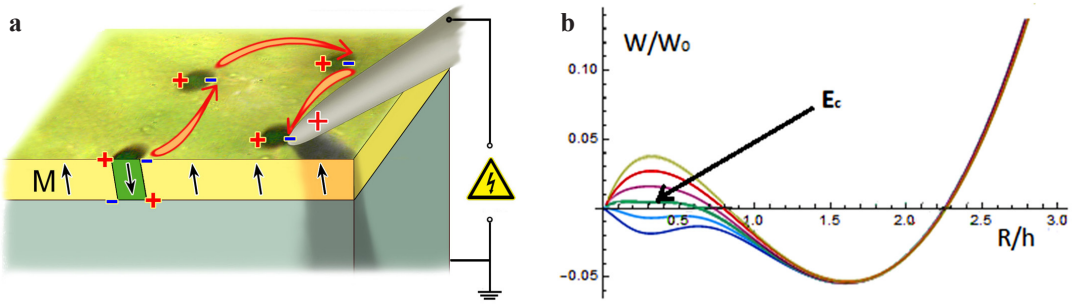

Figure 2. **a** Multiple bubble domain "blowing" with the tip electrode in iron garnet film. **b** The calculated energy dependence on the normalized radius R of the domain (h is the thickness of the film).

electrode and far from it. In accordance with (1) the surface energy and effective refraction indexes ratio should linearly decrease with electric field that agrees well with the experiment (Fig. 1b).

This dependence allows us to estimate the surface energy of magnetoelectric interaction related to the domain wall as 0.003 erg/cm^2 (the parameters of the sample: $(AK)^{1/2} \sim 0.01$ erg/cm^2, the electrode width R = 10 μm; due to the relatively low magnetization of the sample M = 5 G the magnetostatic contribution in Eq. (1) can be neglected). This value well agrees with the estimates obtained in experiments on electric field-induced magnetic domain wall dynamics [7] and statics [8, 9].

Another story related to the domain wall surface energy modulation is the nucleation of magnetic bubble domains [10–12] (Fig. 2a).

At some critical voltage (and, correspondingly, the critical electric field E_c) the energy barrier for bubble domain nucleation is suppressed (Fig. 2b). At larger electric field the local minimum appears that stabilizes the domain with the radius much smaller than the film thickness (Fig. 2b, blue curves).

A.S. Kaminskiy acknowledges the support by the Interdisciplinary Scientific and Educational School of Moscow University "Photonic and Quantum technologies. Digital medicine". D.P. Kulikova acknowledges the financial support from the Foundation for the advancement of theoretical physics and mathematics (BASIS).

1. A.S. Logginov, G.A. Meshkov, A.V. Nikolaev, and A.P. Pyatakov, JETP Lett. **86**, 115 (2007).
2. V. Koronovskyy and Y. Vakyla, Electron. Mater. Lett. **11**, 1028 (2015).
3. G.V. Arzamastseva, A.M. Balbashov, F.V Lisovskii, E.G. Mansvetova, A.G. Temiryazev, and M.P. Temiryazeva, J. Exp. Theor. Phys. **120**, 687 (2015).
4. I.S. Veshchunov, S.V. Mironov, W. Magrini, V.S. Stolyarov, N. Rossolenko, V. Skidanov, J.-B. Trebbia, A.I. Buzdin, P. Tamarat, and B. Lounis, Phys. Rev. Lett. **115**, 27601 (2015).
5. I. Dzyaloshinskii, EPL **83**, 67001 (2008).
6. N. Hedrich et al., Nat. Phys. **17**, 574 (2021).
7. A.S. Logginov, G.A. Meshkov, A.V. Nikolaev, E.P. Nikolaeva, A.P. Pyatakov, and A.K. Zvezdin, Appl. Phys. Lett. **93**, 182510 (2008).
8. A.P. Pyatakov, D.A. Sechin, A.S. Sergeev, A.V. Nikolaev, E.P. Nikolaeva, A.S. Logginov, and A.K. Zvezdin, EPL **93**, 17001 (2011).
9. A.P. Pyatakov, A.K. Zvezdin, A.M. Vlasov, A.S. Sergeev, D.A. Sechin, E.P. Nikolaeva, A.V Nikolaev, H. Chou, J. Sun, and L.E. Calvet, Ferroelectrics **438**, 79 (2012).
10. D.P. Kulikova, A.P. Pyatakov, E.P. Nikolaeva, A.S. Sergeev, T.B. Kosykh, and Z.A. Pyatakova, JETP Lett. **104**, 197 (2016).
11. M. Schott, A. Bernand-Mantel, L. Ranno, S. Pizzini, J. Vogel, H. Béa, C. Baraduc, S. Auffret, G. Gaudin, and D. Givord, Nano Lett. **17**, 3006 (2017).
12. D.P. Kulikova, T.T. Gareev, E.P. Nikolaeva, T.B. Kosykh, A.V. Nikolaev, Z.A. Pyatakova, A.K. Zvezdin, and A.P. Pyatakov, Phys. Status Solidi – Rapid Res. Lett. **12**, 1800066 (2018).

FERROMAGNET PARTICLES IN A POLYMER HARNESS. MESOSCOPIC MAGNETOMECHANICS AND MACROSCOPIC BEHAVIOR OF MAGNETOACTIVE ELASTOMERS

Yu.L. Raikher

Institute of Continuous Media Mechanics, Russian Academy of Sciences,
Ural Branch, Perm, Russia
E-mail: raikher@icmm.ru

The idea to unite strong magnetic susceptibility with high deformability but avoiding irreversible fluidity embodied itself in creation of composites now well known as magnetoactive elastomers (MAEs), one of the kinds of hybrid materials. The magnetization is ensured by employing micron-size ferromagnetic particles, the mechanical softness – by embedding these particles into weakly cross-linked polymer mesh that, however, possesses equilibrium elasticity, i.e., is capable to restore the sample shape when the magnetic and/or mechanical loads are removed. No need to mention the application potentials of such media, they are plenty [1–3].

The appetite for applications, especially hightech ones, spawned, voluntary or not, the interest on the part of practitioners to the theory of MAEs and its predictions. In other words, a task had emerged to construct fundamental material science of these composites. Certainly, the work is essentially interdisciplinary: an amalgamation of physics, chemistry, and mechanics.

If to look at this realm from the magnetic viewpoint, i.e., considering the filler particles, immediately it becomes clear that there should be a number of qualitatively different variants. Evidently, one may imagine magnetically soft (MS-MAEs), magnetically hard (MH-MAEs) and those of mixed content (MAEs-MC). Depending on that, the composites should display diverse mechanical behavior and demonstrate specific magnetomechanical effects.

All the above-mentioned species are really attainable experimentally and do exist. Moreover, a lot of experimental material has been already accumulated and available for interpretation. This makes a fertile ground for theoretical studies, a partial review of which is given in the talk. Being limited by the length of presentation we would describe just some but essential examples of the work done.

Magnetostriction effect that, although denoted by this conventional term, has very little in common with its solid-state magnetism namesake. For the MAE magnetostriction the intraparticle spin-orbit interaction is insignificant whereas the interparticle dipole-dipole one is the main source, it drives the particle rearrangement and by that entrains the matrix.

Magnetic shape memory effect, is also very different from its customary analogue. It is displayed in full by MS-MAEs and occurs in the systems where interparticle magnetostatic interaction is so intense that external magnetization leads to particle clustering.

Magnetic hysteresis in MH-MAEs, which in a way inverts the Stoner-Wohlfarth model. Here not the magnetic moment on its motion surmounts a potential barrier at rest, but the mobile potential barrier passes by the motionless magnetic moment. In this context, a problem of the strength of the particle/matrix adhesion in MAEs turns up entailing important consequences.

Formation of magnetization curves of MAEs-MC, where the interaction between MS and MH phases exists yet in the absence of any external field. Certainly, this interphase magnetic coupling affects the magnetomechanical response of a MAE-MC sample when it is subject to the action of the field and to mechanical stresses.

Contributions of numerous co-authors would be acknowledged in the course of the talk.

1. S. Samal, M. Škodová, L. Abate, and I. Blanco, Applied Sciences **10**, Art. no. 4899 (2020).
2. D. Zhalmuratova and H.-J. Chung, ACS Applied: Polymer Materials **2**, 1073–1091 (2020).
3. S. Lucarini, M. Hossain, and D. Garcia-Gonzalez, Composite Structures B, Art. no. 114800 (2022).

ULTRAFAST MAGNETOPHOTONICS

V.I. Belotelov[1,2,3]

[1]Lomonosov Moscow State University, Leninskie Gory, Moscow, Russia
[2]Vernadsky Crimean Federal University, Simferopol, Russia
[3]Russian Quantum Center, Moscow, Russia
E-mail: belotelov@physics.msu.ru

Optical control of the magnetization at ultrashort time scales attracts a significant research attention. Launching and controlling magnons with laser pulses opens up new routes for applications including optomagnetic switching and all-optical spin wave emission and enables new approaches for information processing with ultralow energy dissipation. However, subwavelength light localization within the magnetic structures leading to efficient magnon excitation that does not inherently absorb light has still been missing.

Here, we propose to marriage the laser-induced ultrafast magnetism and all-dielectric nanophotonics to efficiently excite and control spin dynamics in magnetic dielectric structures [1]. We demonstrate an all-optical excitation of spin dynamics in a specially designed nanopatterned bismuth iron-garnet film via femtosecond laser pulses. The unique feature of such a structure that was demonstrated experimentally is the possibility to excite optical modes that can increase the spin actuation efficiency and the all-optical control of the excited states. The nanopatterning of a transparent magnetic dielectric film allows localization of light in optical mode hot spots tens of nanometers in size with 25 times higher light fluence. This enables the efficient optical launching and control of exchange standing spin waves of different orders that is impossible in a smooth magnetic film. We demonstrate that the nanopatterning of the magnetic film provides advanced control over the spin wave excitations: relative amplitude of the exchange and magnetostatic spin waves can be adjusted on demand by modifying laser pulse polarization, incidence angle, or wavelength.

The nanopatterned magnetic dielectric films can serve as a unique platform for a nonthermal ultrafast excitation of spin interactions with vast opportunities for their control and manipulation that are highly demanded for novel applications including magnonic data processing, as well as quantum computation based on coherent spin oscillations.

Therefore, the magnetophotonic structures are demonstrated to be very useful for spin control and manipulation by femtosecond laser pulses [2–4].

This work was financially supported by the Russian Ministry of Education and Science, Megagrant project N 075-15-2019-1934.

1. A.I. Chernov, M.A. Kozhaev, D.O. Ignatyeva, E.N. Beginin, A.V. Sadovnikov, A.A. Voronov, D. Karki, M. Levy, V.I. Belotelov, Nano Lett. **20**(7), 5259–5266 (2020).
2. P.E. Zimnyakova, D.O. Ignatyeva, D. Karki, A.A. Voronov, A.N. Shaposhnikov, V.N. Berzhansky, M. Levy, V.I. Belotelov, Nanophotonics **11**, 119–127 (2021).
3. D.M. Krichevsky, D.O. Ignatyeva, V.A. Ozerov, V.I. Belotelov, Phys. Rev. Appl. **15**, 034085 (2021).
4. A.A. Voronov, D.O. Ignatyeva, A.K. Zvezdin, T.B. Shapaeva, V.I. Belotelov, Phys. Rev. Appl. **16**, L051001 (2021).

MAGNETIC NANOPARTICLES IN MEDICINE

Y.A. Koksharov[1,2,3]

[1]Moscow State University, Moscow, Russia
[2]Kotelnikov Institute of Radioengineering and Electronics, Russian Academy of Sciences, Moscow, Russia
[3]Faculty of Material Science, Shenzhen MSU-BIT, Shenzhen, China
E-mail: yak@physics.msu.ru

Nanomedicine has reached such a level of development that it is beginning to be considered as a separate field of life sciences. The use of magnetic nanoparticles (MNPs) and magnetic nanostructures in medicine is a complex interdisciplinary scientific and practical task that is far from being complete [1]. The goals of the search for new medicines using MNPs are diverse: improvement of the therapeutic index by increasing efficiency and/or reducing toxicity; targeted drug delivery, specific to the type of tissue or even at the cellular or sub-cellular level; improving the pharmaceutical properties of therapeutic molecules – stability, solubility, circulation time in the body, increasing the concentration of the drug in the diseased organ; the possibility of controlled release of the drug; the possibility of targeted intracellular delivery of therapeutic agents based on biological macromolecules – DNA and RNA; joint delivery of complex therapeutic agents to increase the effectiveness and overcome drug resistance; the possibility of more accurate selection of the ratio of components of a complex drug taking into account a specific patient (the so-called "personalized medicine"; the possibility of successful drug transcytosis, i.e. overcoming endothelial, for example, blood-brain and epithelial barriers; the possibility of more accurate diagnostic methods (visualization); prospects of simultaneous diagnosis and therapy, including in real time (theranostics); the possibility of using their own specific physical and chemical properties of nanocarriers for therapy. The main feature that distinguishes MNPs from other types of nanocarriers of medicines is the ability to influence them with an external physical factors, for example, electromagnetic field, and use them in various biophysical methods and approaches. For example, magnetic field can provide control over the movement of MNPs and their accumulation in the target local areas of the body and, if necessary, significant heating (in the hyperthermia method). For medical applications, MNPs based on iron oxides – magnetite and maghemite are most suitable, since nanophase iron oxides are low-toxic, widespread in living systems and can be metabolized by cells. When using MNPs in therapeutic or diagnostic methods, it is extremely important to directly control the spatial location of nanoparticles inside the patient's body. This is especially important in methods with controlled release of the drug in the target area of the body, which should be performed only after the MNPs of the target organ has been reached. A very promising experimental method that solves this problem is called MPI (magnetic particle imaging).

The disadvantages of modern medical methods using MNPs are due to their complexity, insufficient reliability and low efficiency. Only in very few cases it was possible to put into practice the methods of magnetic hyperthermia and controlled targeted drug delivery. The practical application of MNPs for diagnostic purposes is more successful, despite many problems associated with side effects. The reasons preventing the practical use of MNPs are divided into three groups: (i) scientific (fundamental or technical); (ii) clinical (medical and social); (iii) marketing. Overcoming all these challenges requires new integrated multidisciplinary approaches.

1. Y.A. Koksharov, S.P. Gubin, I.V. Taranov, G.B. Khomutov, Yu.V. Gulyaev, J. Commun. Technol. Electronics **67**, 101–116 (2022).

SPIN FLUCTUATION TRANSITIONS IN THE SPIRAL MAGNET MnSi

S.V. Demishev[1*], A.N. Samarin[1], M.S. Karasev[1], S.V. Grigoriev[2], A.V. Semeno[1]

[1]Prokhorov General Physics Institute of RAS, Moscow, Russia
[2]Petersburg Nuclear Physics Institute named by B.P. Konstantinov of NRC "Kurchatov Institute", Gatchina, Russia
[*]E-mail: sergey_demishev@mail.ru

De-facto spin fluctuation transitions in magnets were introduced about decade ago [1], however, the general character of this type of magnetic phenomena was recognised quite recently [2–3]. Typically a spin fluctuation transition (SFT) is defined as the transition at which character of spin fluctuation changes, but no long-range magnetic order (ferromagnetic, antiferromagnetic, etc.) is established. Classical example of SFT is spin nematic transition expected for systems with the hidden quadrupolar order [1]. This type of SFT is characterized by the appearance of the anisotropy of average projections of the spin fluctuation magnitude $\langle S_i^2 \rangle$ (i.e. $\langle S_x^2 \rangle \neq \langle S_y^2 \rangle$), whereas in the absence of magnetic order average spin on site remaining zero ($\langle S_x \rangle = \langle S_y \rangle = 0$). At a moment several kinds of SFTs were established experimentally and theoretically, including spin nematic transition in CeB_6, [1, 2], SFT analogous to orientation transition in magnets [2] and SFT in the Ising model on random sites [3].

The spiral magnets, MnSi and $Mn_{1-x}Fe_xSi$, are prospective objects for finding and studying SFT. This expectation is based, from one hand, on the presence of various intermediate phases of spin fluctuation nature on the magnetic phase diagrams [4–5]. Secondly, SFT at $T \sim 15$ K caused by quantum fluctuations may be expected in magnetically ordered phase of MnSi [5–7]. The latter possibility is quite unusual as long as all spin fluctuation transitions known so far occur in the phases without any long-range magnetic order.

The direct experimental method for studying SFT is electron paramagnetic resonance (EPR) as long as EPR line width provides a direct measure of the spin fluctuations magnitude [2]. In the present work a single crystal of manganese monosilicide, MnSi, was studied by high-frequency (60 GHz) EPR. In the temperature range of 2–40 K, the most detailed temperature dependences of the linewidth and g factor known to date have been obtained, which made it possible to establish several types of spin fluctuation transitions. In the magnetic field $B \sim 2$ T, the spiral magnetic order in MnSi is suppressed and the only magnetic transition is the transition at ~30 K between the paramagnetic phase (P) and spin polarized phase (SP). The latter phase is of spin polaron nature and corresponds to parallel alignment of the reduced magnetic moments of spin polarons thus demonstrating ferromagnetic type of long range magnetic order. In MnSi, spin polarons are represented by quasi-bound states of itinerant electrons and localized magnetic moments on Mn sites [7].

Two magnetic transitions corresponding to the change of spin fluctuations are revealed [8] on the temperature dependence of the EPR line width $W(T)$ (Fig. 1). The first one is the stepwise variation of W at P-SP phase boundary ($T_c \sim 29.6$ K, Fig. 1a) providing pronounced λ-anomaly of the derivative $\partial W/\partial T$ (Fig. 1b). This behavior agrees with the EPR results reported previously for magnetic transitions in a system consisting of magnetic polarons [9].

We proposed a model reasonably describing temperature dependence $W(T)$ in the range $T > T_L \sim 15$ K (line 1 in Fig. 1a). Noticeable discrepancy between theory and experiment (Fig. 1a) corresponding to the change of the slope of $\partial W/\partial T = f(T)$ curve (Fig. 1b) occurs for $T < T_L \sim 15$ K, i.e. just in the range, where SFT transition is expected. Simultaneous analysis of the temperature dependences of the EPR line width and g-factor carried out in the framework of recently developed

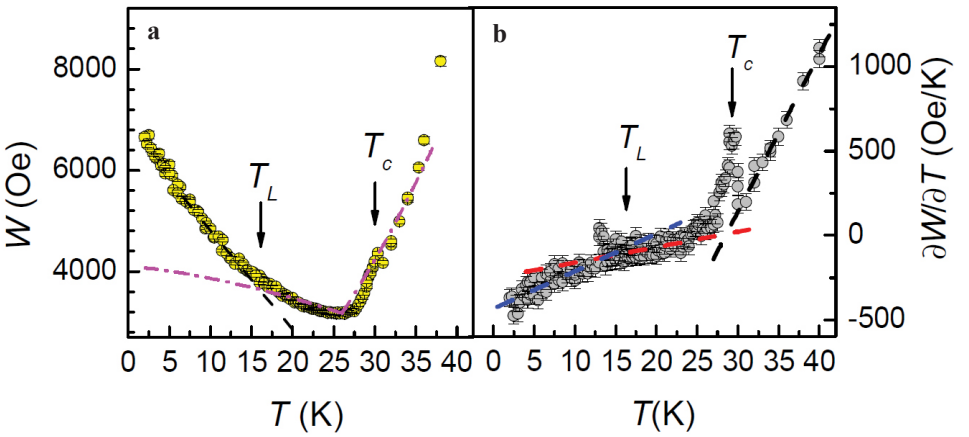

Figure 1. Temperature dependences of the EPR line width W (**a**) and the derivative $\partial W/\partial T$ (**b**). Arrows indicate characteristic temperatures T_c and T_L (see text). On panel a: points – experiment; dash-dotted line – model calculation; dashed line is the guide to the eye. On panel **b**: dots are the derivative calculated from experimental data, dashed lines are the guides to the eye.

theory [10] confirms the key role of quantum fluctuations of the magnetic moment in the genesis of this low temperature anomaly.

Thus we provide first direct experimental evidence of the new type of SFT corresponding to a change in the regime of magnetic fluctuations at a temperature $T_L \sim 15$ K much lower than the transition temperature $T_c \sim 30$ K from the paramagnetic ($T > T_c$) to the magnetically ordered phase ($T < T_c$). This result expands the range of applicability of the concept of spin-fluctuation transitions, which were previously considered only for the case of magnetic states that do not have a long-range magnetic order.

1. K. Penc, A.M. Läuchli, in C. Lacroix, P. Mendels, F. Mila (eds.), Introduction to Frustrated Magnetism, Springer-Verlag, Berlin, p. 331 (2011).
2. S.V. Demishev, Appl. Magn. Reson. **51**, 473 (2020).
3. N.A. Bogoslovskiy, P.V. Petrov, and N.S. Averkiev, Jetp Lett. **114,** 347 (2021).
4. M. Janoschek et al., Phys. Rev. B **87**, 134407 (2013).
5. S.V. Demishev et al., Pis'ma v ZhETF **98** (12), 933 (2013).
6. V.V. Glushkov et al., Phys. Rev. Lett. **115**, 256601 (2015).
7. S.V. Demishev et al., Phys. Rev. B **85**, 045131 (2012).
8. S.V. Demishev et al., Pis'ma v ZhETF **115** (11), 717 (2022).
9. A.V. Shestakov et al., IEEE Magnetics Letters **11**, 2503505 (2020).
10. S.V. Demishev, Dokl. Phys. **66**, 187 (2021).

Section A.

Spintronics and magnetic nanostructures

CHIRAL HELIMAGNET AS A SPIN WIND TURBINE AND SPIN ARCHIMEDEAN SCREW

V.V. Ustinov[*], *I.A. Yasyulevich*

Institute of Metal Physics, Ekaterinburg, Russian Federation
[*]E-mail: ustinov@imp.uran.ru

The theory of the magnetic dynamics of conductive chiral helimagnets (ChHMs) under conditions of electric and spin currents flowing through them underlies the subject of this paper. Before posing the problem of the spin transport of conduction electrons in ChHM, we would like to refresh in the reader's memory some well-known mechanical analogies of the considered magnetic phenomena related to the object of our research.

The first of those is the Archimedean screw invented by Archimedes in the 3rd century BC. It includes a simple mechanical machine for moving water using a rotating spiral screw. The rotation of the Archimedean screw causes water to move along its axis. Hence, it is quite obvious that such a screw begins rotating as water runs on it. The second analogy is a wind turbine. This is an apparatus for converting the kinetic energy of the wind flow into mechanical energy of the rotor rotation. Historically, windmills are the first implementation of the idea of converting linear air motion into rotary motion of the blades and rotor of a mill. The first written mentions of a windmill as a technical device belong to the Greek Heron of Alexandria and date back to the first century AD. The key aspect for operating both the Archimedean water screw and the Heron wind turbine is the interaction between the particle flow and a body of a special helical chiral-symmetry shape.

Let us return to the problem of the spin transport of conduction electrons in a conductive chiral helimagnet. To start with, we can draw an analogy between usual atmospheric wind that blows over the wings of a windmill and flux of spin moment of conduction electrons that transfer their rotational moment to a system of spin moments of electrons localized at the sites of the crystal lattice of a helimagnet. Bearing this analogy in mind, we will use the term "spin wind" as a poetic image of the well-known and more prosaic term "spin current" [1].

Based on the aforesaid mechanical analogies, we can expect that the spin wind "blowing" in a chiral helimagnet causes its magnetic system to rotate under certain conditions, the same as an ordinary wind turns propeller blades. This work aims to find the conditions under which the magnetic system of the conductive ChHM, termed "helicoid" hereafter for brevity, rotates as a whole when direct electric current passes through the helimagnet.

We have built a consistent theory of the Spin Transfer Torque (STT) effect in conductive chiral helical magnet (ChHM) [2]. It is shown that the STT effect induced by a spin current flowing through ChHM leads to the rotation of the ChHM magnetization spiral around its axis. The frequency of such rotation of the ChHM magnetization is found. The former is expressed in terms of the parameters of the quantum exchange Hamiltonian that specifies helical magnetic ordering in a conductive crystal. We have showcased that both the direction of rotation of the ChHM magnetization and the direction of changes in the shape of the magnetic spiral are determined by the electron flow direction and the chirality of the magnet. The theory developed accounts for the generation of an electromagnetic field when rotating the magnetic spiral in the ChHM subjected to an electric current flowing through the helimagnet.

As a result of the investigation of the spin dynamics of conductive chiral helimagnets, based on jointly solving the Bloch-Torrey equation for the magnetization of itinerant electrons, the Landau-Lifshitz-Gilbert equation for the magnetization of localized electrons, and Maxwell's equations for

an electromagnetic field, we can note the following regularities of the phenomenon of spin torque transfer from the spin system of conduction electrons to that of localized electrons:

1. A time-constant flow of electrons moving along the chiral helimagnet axis with a drift velocity *w*, due to the STT effect, induces the rotation of the magnetic spiral of the helimagnet with an angular frequency ω. The ω-frequency sign that specifies the direction of rotation of the spiral with a wave vector **q** is determined by the sign of the scalar product (**q**·**w**). The magnitude of the frequency depends on the ratio of the Gilbert damping parameter and a parameter characterizing the efficiency of the SST processes. The latter is governed by the magnitude of the constant of the exchange interaction between conduction and localized electrons. For helimagnets with extremely low Gilbert damping, the frequency ω, with an accuracy of a numerical factor of the order of unity, is equal to (**q**·**w**). All the quantities facing in the theory advanced on the pages of this paper are expressed in terms of the parameters of the quantum exchange Hamiltonian that assigns helical magnetic ordering in conductive crystals.

2. The STT effect leads to the fact that the wavelength of the helimagnet's magnetic spiral rotating under the flowing spin current, is always somewhat less than that of the stationary magnetic spiral. The spin current also gives rise to changes in conicity of the magnetic helicoid. The angle θ characterizing the conicity augments with increasing the frequency of rotation of the magnetic spiral.

3. It is found that the Poynting vector that sets the direction of propagation of the electromagnetic field energy generated by an electric current flowing in a chiral helimagnet is directed along the vector of the conduction electron flux, regardless of the helimagnet chirality. In calculating the rotation frequency of the magnetic spiral, accounting for the generation of an electromagnetic field, is reduced to an effective increase in the Gilbert damping parameter and an increase in the limiting rotation frequency of the spiral.

Figure 1 illustrates the results described above.

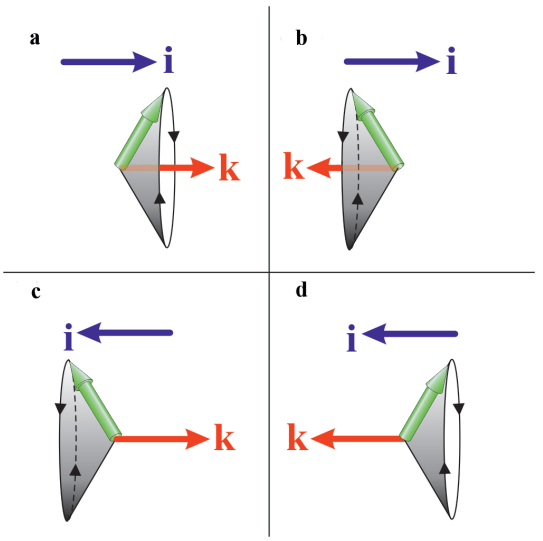

Figure 1. Schematic representation of the directions of the ChHM magnetization spiral rotation and spiral conicity depending on the directions of the chirality **k** and flow **i** vectors without an external magnetic field. **a**, **c** right-handed spiral; **b**, **d** left-handed spiral.

The authors would like to hope that the present investigation paves the way for the future of chiral conductive helimagnets to be used as a new functional component of spin devices: spin generators to convert a direct electric current into a high-frequency electromagnetic field, and spin diodes to transform a high-frequency electromagnetic field into a constant electricity.

This work has been carried out under the financial support of the Russian Science Foundation within the framework of project № 22-22-00220.

1. S. Maekawa, S.O Valenzuela, E. Saitoh, T. Kimura (ed.), Spin Current, Oxford University Press, (2017).
2. V.V. Ustinov and I. A. Yasyulevich, Chirality-dependent spin-transfer torque and current-induced spin rotation in helimagnets, (2022), to be published.

CURRENT NOISE GEOMETRICALLY GENERATED BY A DRIVEN MAGNET

I.S. Burmistrov

L.D. Landau Institute for Theoretical Physics RAS, Chernogolovka, Russia
E-mail: burmi@itp.ac.ru

We consider a nonequilibrium cross-response phenomenon, where a driven magnetization gives rise to electric shot noise (but no d.c. current). This effect is realized on a nanoscale, with a small metallic ferromagnet which is tunnel coupled to two normal metal leads. The driving gives rise to a precessing magnetization. The geometrically generated noise is related to a nonequilibrium electron distribution in the ferromagnet. Our protocol provides a channel for detecting and characterizing ferromagnetic resonance.

To describe the magnetization dynamics we use the macrospin approximation; that is, the magnetization is described by a single vector $\mathbf{M} = M(\sin\theta\cos\phi, \sin\theta\sin\phi, \cos\theta)$. We assume that the magnetization precesses in a steady state, where polar angle θ and precession frequency $\omega = d\phi/dt$ are constant. Under these assumptions, we find that the charge current vanishes on average, $I = 0$, but the current noise remains finite: $S = 4g_tT + g_t\sin2\theta[\omega\coth(\omega/2T) - 2T]$. Here g_t is the total conductance of the double tunnel junction. The results were published in [1].

1. T. Ludwig, I.S. Burmistrov, Y. Gefen, A. Shnirman, Phys. Rev. Research **2**, 023221 (2020).

A.I3

TUNNELING HALL EFFECT: THEORY AND EXPERIMENT

E.A. Karashtin[1,2], *N.S. Gusev*[1], *I.Yu. Pashen'kin*[1], *M.V. Sapozhnikov*[1,2], *A.A. Fraerman*[1*]

[1]Institute for Physics of Microstructures, Nizhny Novgorod, Russian Federation
[2]Lobachevsky State University, Nizhny Novgorod, Russian Federation
[*]E-mail: andr@ipmras.ru

Tunneling (anomalous) Hall effect consists in appearance of Hall voltage if an electric current flows through a magnetic tunnel junction (MTJ) due to the spin-orbit interaction in an insulating barrier. The mechanism of tunneling Hall effect may either be skew scattering or side jump. The former is caused by the asymmetry of the probability of tunneling of the conductance electrons through the barrier with respect to their momentum along its surface. It was theoretically considered in several papers [1–3]. The latter follows from the anomalous electron velocity that appears inside the barrier due to spin-orbit coupling (SOC). It may either be caused by SOC in a non-centrosymmetric barrier [3] or by SOC due to an electric field induced by the voltage applied to the MTJ. The Hall current inside the barrier caused by such SOC was calculated in [4]. The experiments aimed at spectroscopy were carried out [5]. We provide a consequent theory that takes into account all mechanisms of tunneling Hall effect. A simple model is used in which the barrier with Rashba spin-orbit coupling is described by the delta-function. We show that there is an additional side jump mechanism caused by the asymmetry of the electron coefficient of reflection from the barrier with respect to the electron momentum along the insulator surface. We show that the quadratic in the applied voltage V_{bias} Hall effect appears in such system. We carry out an experiment in which tunneling Hall effect is measured in an MTJ with a ferromagnet (CoFeB) and a heavy metal (Pt) layer separated by a 1.5 nm thick MgO insulator (Fig. 1a). The quadratic in V_{bias} Hall effect is observed. It is much stronger than the linear effect for a thin (1 nm) Pt (Fig. 1b). This effect becomes smaller as the platinum layer is made thicker which manifests its surface nature. It almost vanishes for a 10 nm Pt layer.

This work was supported by the Russian Science Foundation (Grant #21-12-00271).

1. S.A. Tarasenko, V.I. Perel' and I.N. Yassievich, Phys. Rev. Lett. **93**, 056601 (2004).
2. A. Matos-Abiague and J. Fabian, Phys. Rev. Lett. **115**, 056602 (2015).
3. A. Vedyayev, N. Ryzhanova, N. Strelkov and B. Dieny, Phys. Rev. Lett. 110, 247204 (2013).
4. A.V. Vedyaev, M.S. Titova, N.V. Ryzhanova et al., Appl. Phys. Lett. **103**, 032406 (2013).
5. L. Liu, C.-T. Chen and J.Z. Sun, Nature Physics **10**, 561 (2014).

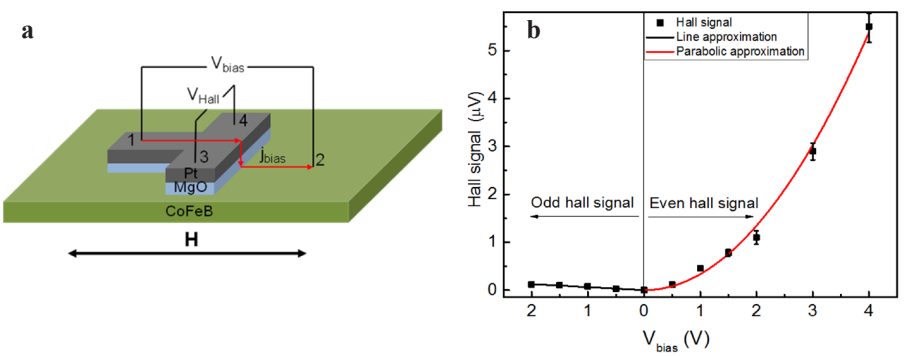

Figure 1. **a** The sample and geometry of measurement. **b** Even and odd tunneling Hall signal for Pt (1 nm).

A.I4

CONTROLLABLE THREE-STATE MAGNETIZATION SWITCHING IN EPITAXIAL $Pd_{0.92}Fe_{0.08}/Ag/Pd_{0.96}Fe_{0.04}$ HETEROSTRUCTURE

I.V. Yanilkin[1], *A.I. Gumarov*[1,2], *G.F. Gizzatullina*[1], *R.V. Yusupov*[1], *L.R. Tagirov*[2,3*]

[1]Institute of Physics, Kazan Federal University, 420008 Kazan, Russia
[2]Zavoisky Physical-Technical Institute, FRC Kazan Scientific Centre of RAS, Russia
[3]Tatarstan Academy of Sciences, Institute of Applied Research, Kazan, Russia
[*]E-mail: Ltagirov@mail.ru

Superconducting spintronics is rapidly developing branch of post-silicon electronics [1,2]. Several kinds of device physics were proposed based on Josephson junctions (JJ) [2], and recent ones deal with manipulation by spin-triplet currents (ref. [3] and references therein). We propose a magnetic actuator to switch JJ between the singlet and tripled regimes of conduction by control of magnetic configurations in the bilayer of two ferromagnetic films.

We have grown a thin-film $Pd_{0.92}Fe_{0.08}/Ag/Pd_{0.96}Fe_{0.04}$ heterostructure on the MgO(001) single-crystal substrate using ultra-high vacuum molecular beam deposition system [4]. The structural *in-situ* and *ex situ* investigations have shown that the resulting film stack is end-to-end single-crystalline and epitaxial. The low-temperature magnetotransport and magnetic properties were studied at different directions of the current and the applied magnetic field. The obtained experimental results are well described within an assumption of a single-domain magnetic state of the ferromagnetic layers. In a wide range of the applied field directions, the magnetization reversal proceeds in two steps via the intermediate easy axis. The magnetic configuration diagram has been constructed and the conditions have been determined for a controllable switching between steady parallel (P), orthogonal (OG), and antiparallel (AP) arrangements of magnetic moments of the layers (see Fig. 1, [4]).

Support by the Priority-2030 Program of KFU is acknowledged.

1. J. Linder, J.W.A. Robinson, Nat. Phys. **11**, 307–315 (2015).
2. I.I. Soloviev, N.V. Klenov, S.V. Bakurskiy, M.Yu. Kupriyanov, A.L. Gudkov, A.S. Sidorenko, Beilstein J. Nanotechnol. **8**, 2689–2710 (2017).
3. O.M. Kapran, A. Iovan, T. Golod, V.M. Krasnov, Phys. Rev. Res. **2**, 013167 (2020).
4. I.V. Yanilkin, A.I. Gumarov, G.F. Gizzatullina, R.V. Yusupov, L.R. Tagirov, Beilstein J. Nanotechnol. **13**, 334–343 (2022).

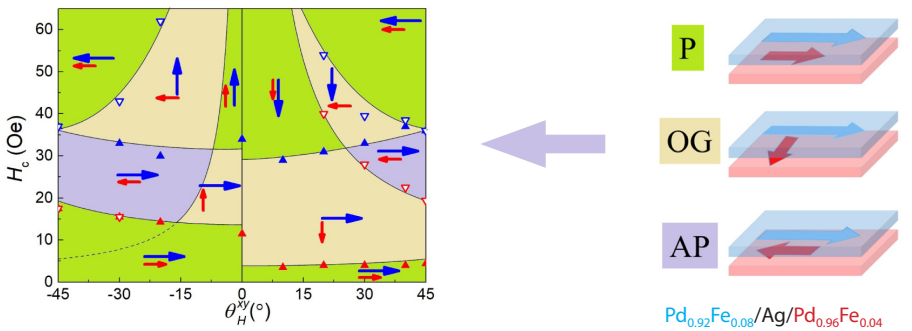

Figure 1. Phase diagram of magnetic configurations of the $Pd_{0.92}Fe_{0.08}/Ag/Pd_{0.94}Fe_{0.04}$ heterostructure on the H_c-θ plane (H_c – is a coercive field, θ is an angle between the applied magnetic field direction and the [100] crystallographic axis of the epitaxial film.)

A.I5

FUNCTIONAL LOW COERCIVE GMR MULTILAYERS FOR MAGNETIC SENSORS

*M.A. Milyaev**, *L.I. Naumova, V.V. Proglyado, T.P. Krinitsina, R.S. Zavornitsyn, I.A. Naydanov, V.V. Ustinov*

M.N. Mikheev Institute of Metal Physics, Ekaterinburg, Russian Federation
*E-mail: milyaev@imp.uran.ru

Magnetic multilayers with the effect of giant magnetoresistance (GMR) belong to modern magnetically sensitive nanomaterials and are widely used in various spintronics devices along with exchange-biased spin valves and nanostructures with tunnel magnetoresistance. The most important for practical use characteristics of these materials are: GMR ratio, saturation field, sensitivity, coercivity, and linearity of the magnetic field dependence of magnetoresistance. These characteristics can be changed considerably by variation of a multilayer composition. GMR multilayers with high magnetoresistance, low saturation field and minimal coercivity are the most expedient type of magneto-sensitive materials for development of magnetic sensors. The requirement of low coercivity is necessary to ensure an unambiguous dependence of the electrical resistance on the magnetic field.

In our studies, the main stages of improving the functional characteristics of GMR multilayers based on exchange coupled superlattices included: 1) search for a buffer layer necessary for the formation of a perfect crystal structure and ⟨111⟩ texture in a magnetic multilayer; 2) search for efficient magnetic materials based on CoFeNi ternary ferromagnetic alloys with high spin polarization of conduction electrons and low coercivity; 3) finding a special non-magnetic material based on copper, which would be used in superlattices as spacers and had a significant impact on the microstructure and size of crystallites. A decrease in the size of crystallites also leads to an additional decrease in coecivity.

In our studies, it was established that the use of the Ta/$Ni_{48}Fe_{12}Cr_{40}$ composite buffer layer makes it possible to form a perfect crystal structure of layers and interfaces in CoFe/Cu and CoFeNi/Cu superlattices. It was shown [1] that the X-ray coherent scattering length for the Ta/$Ni_{48}Fe_{12}Cr_{40}$/$[CoFe/Cu]_n$ system is comparable to the total thickness of the periodic part of the superlattice with n = 10 bilayers. In the case of n = 32, the width at half maximum of the rocking curve around the (111) Bragg peak is only FWHM = 2.5°, which indicates the presence of a sharp ⟨111⟩ texture in the

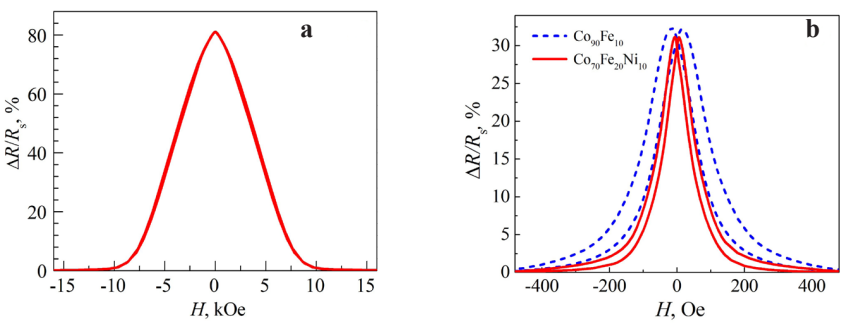

Figure 1. Magnetoresistance curves for multilayers: **a** Ta(5)/NiFeCr(5)/$[Co_{90}Fe_{10}(1.5)/Cu(0.95)]_{32}$/Ta(5), **b** glass/Ta(5)/NiFeCr(5)/[FM(1.3)/Cu(2.2)]12/Ta(5), FM = $Co_{90}Fe_{10}$, $Co_{70}Fe_{20}Ni_{10}$. Layers thickness is indicated in nm.

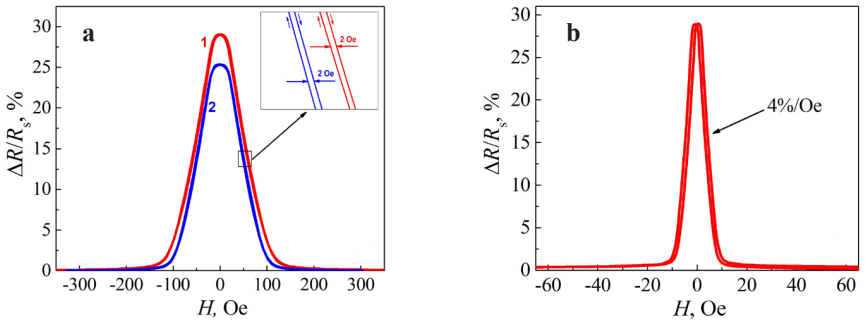

Figure 2. **a** Magnetoresistance curves for two multilayers with optimized compositions: 1 – glass/ Ta(4)/NiFeCr(3)/ $[Co_{77}Fe_{17}Ni_6(1.8)/Cu_{96.1}In_{3.9}(2)]_6/Co_{77}Fe_{17}Ni_6(1.8)/Ta(5)$; 2 – glass/Ta(4)/ NiFeCr(3)/$[Co_{70}Fe_{20}Ni_{10}(2)/Cu_{95.3}In_{4.7}(2)]_6/Co_{70}Fe_{20}Ni_{10}(2)/Ta(5)$; **b** magnetoresistance curve for the multilayer (1) measured with the using of the magnetic flux concentrator.

superlattice. In $Co_{90}Fe_{10}$/Cu superlattices with the Ta/$Ni_{48}Fe_{12}Cr_{40}$ buffer layer a record magnetoresistance of 83% at room temperature was obtained [1, 2] – Fig. 1a.

To reduce the magnetic saturation field and increase the sensitivity of the material to a magnetic field, it is necessary to use the thickness of nonmagnetic spacers corresponding to the second maximum of the interlayer exchange coupling, and also to choose an efficient ferromagnetic material with a low coercive force. When studying CoFeNi/Cu superlattices with cobalt-rich CoFeNi ternary alloys, it was found [3] that the most efficient ternary alloys are located in a narrow region of the ternary diagram near the $Co_{70}Fe_{20}Ni_{10}$ composition. Deviation of the composition of the ternary alloy from this optimal composition leads either to a decrease in the GMR ratio or to a significant increase in the coercivity. It was shown that changing the composition of the $Co_{90}Fe_{10}$ alloy to $Co_{70}Fe_{20}Ni_{10}$ leads to a decrease in the hysteresis on the magnetoresistance curve by more than 2 times while maintaining the magnetoresistance at the level of 30% – Fig. 1b.

The most difficult characteristics to optimize are the linearity of the field dependence of the magnetoresistance and hysteresis. It has been established that the linearity substantially depends on the number of bilayers (n) in a superlattice. For a large number of bilayers n = 10–20 the linearity is only 40–50%. A high linearity of 70% or more, which is one of the requirements for functional GMR materials, is observed only for superlattices with a small number of bilayers n = 3–7.

We have solved the problem of a significant decrease in hysteresis by using nonmagnetic CuIn alloys as a material of spacers. It is shown that the use of $Cu_{1-x}In_x$ alloys with an indium content of up to 5 at.% leads to a multiple decrease of crystallites size in the superlattice and a decrease in hysteresis by a factor of 5–7 compared to similar superlattices prepared with Cu spacers.

As a result of the developed approaches, GMR multilayers promising for use in magnetic sensors were synthesized with a magnetoresistance of 25–30%, saturation fields of 80–150 Oe, hysteresis of a few Oe (Fig. 2a), linearity of over 70% and sensitivity of 0.2–0.6%/Oe. When using magnetic flux concentrator, the sensitivity was increased to 4–6%/Oe – Fig. 2b.

The research was carried out within the state assignment on the theme "Spin" № 122021000036-3 and RFBR project No. 20-42-660018 p_a.

1. M.A. Milyaev, L.I. Naumova, V.V. Proglyado, T.P. Krinitsina, N.S. Bannikova, V.V. Ustinov, IEEE Trans. On Magn. **50**, 2300904 (2019).
2. V.V. Ustinov, M.A. Milyaev, and L.I. Naumova, Phys. Metals Metall. (English only) **118**, 1300 (2017).
3. M.A. Milyaev, N.S. Bannikova, L.I. Naumova, V.V. Proglyado, E.I. Patrakov, N.P. Glazunov, V.V. Ustinov, J. Alloys Comp. **854**, 157171 (2021).

EFFECT OF VAN HOVE SINGULARITIES ON THE EFFICIENCY OF SPIN CURRENT GENERATION BY TRAVELLING SPIN WAVES IN YIG/Pt STRUCTURES

*M. Seleznev, Y. Nikulin, V. Sakharov, G. Dudko, S. Vysotskii, A. Kozhevnikov, Y. Khivintsev, Y. Filimonov**

Kotel'nikov IRE RAS, Saratov Branch, Saratov, Russia
*E-mail: yuri.a.filimonov@gmail.com, yuri.a.filimonov@mail.ru

Magnon spintronics is the field of spintronics concerned with information processing devices and technologies that use spin current carried by magnons [1]. One of the most important structures for this area are yttrium iron garnet-platinum (YIG/Pt) bilayers, where moving charges are replaced by dynamic objects in the form of coherent and incoherent spin waves (SW). Due to the exchange and spin-orbit interactions, the conduction electrons in the Pt are associated with localized spins in the YIG. Such a coupling due to the spin-Hall effect (SHE) and its inverse (ISHE) [2] allows, on the one hand, to excite SW [2, 3] and control their propagation [4], and, on the other hand, to detect [2] SW as well the results of their interference [5].

The problem of efficient spin current conversion into electric current in YIG-Pt structures is important for magnon spintronics. The conversion efficiency is usually characterized by the value of the ISHE electric voltage U, generated at the edges of an electrically open Pt film upon excitation of the spin subsystem of the YIG film.

To pump spins through the YIG/Pt interface traveling SW can be used. In experiments on pumping by traveling SW, the magnon spin current density J_S through the FI film cross section S can be related to the microwave power flux P of the spin waves $J_S \sim P \approx |\vec{m}|^2 v_g S$, where $|\vec{m}|$ and v_g are, respectively, the amplitude and group velocity of the SW. The part J_S^p of the current J_S, which pumped through the interface, is determined by the processes of electron-magnon scattering at the YIG/Pt interface, the probability of which is proportional to the SW density of states in the spectrum of the magnetic film. From this point of view, frequencies f^* in the SW-spectrum that correspond to van Hove singularities in the magnon density of states and where the group velocity is low $v_g(f^*) \to 0$ [6] may be of particular interest to create an efficient spin current generation.

Note, that in the spectrum of dipole surface magnetostatic waves (MSSW) propagating in a tangentially magnetized ferromagnetic film, the frequencies f^* correspond [7] to long-wavelength ($k \to 0$) f_0 and short-wavelength ($k \to \infty$) f_s boundaries, where k is the wavenumber along the film's plane. Additional frequencies f^* of van Hove singularities in MSSW spectrum can appear at frequencies of resonance interaction with exchange modes (EM), having wavenumber along the film thickness d equal to $k_{\perp,N} = \pi N/d$, where N is the mode number [8]. In case of $k \ll k_{\perp,N}$ the spin current, carried by EM partial wave, directed almost perpendicular to the YIG/Pt interface (see color insert to Fig. 1a, which can contributes to the growth normal to the interface component $J_{S,\perp}^p$ of the spin current density J_S^p pumped by MSSW through the interface. In typical planar geometry of the ISHE measurement an increase of the $J_{S,\perp}^p$ accomplished by the growing of the in-plane electric current density $J_c^{ISHE} \sim |J_{S,\perp}^p| \cdot [\mathbf{n} \times \boldsymbol{\sigma}]$, where $\mathbf{n}$ and $\boldsymbol{\sigma}$ are, respectively, unit vectors along normal to the YIG/Pt interface and spin-current polarization. In this work we experimentally demonstrated correlation between van Hove singularities in MSSW spectrum of the YIG film and enhancement of spin current emission by the travelling MSSW in YIG/Pt structure.

We have studied ISHE in YIG/Pt structures based on YIG films with thickness from 0.9 up to 14 μm. Experimental scheme shown on Fig. 1a. On Fig. 1b typical ISHE frequency dependence

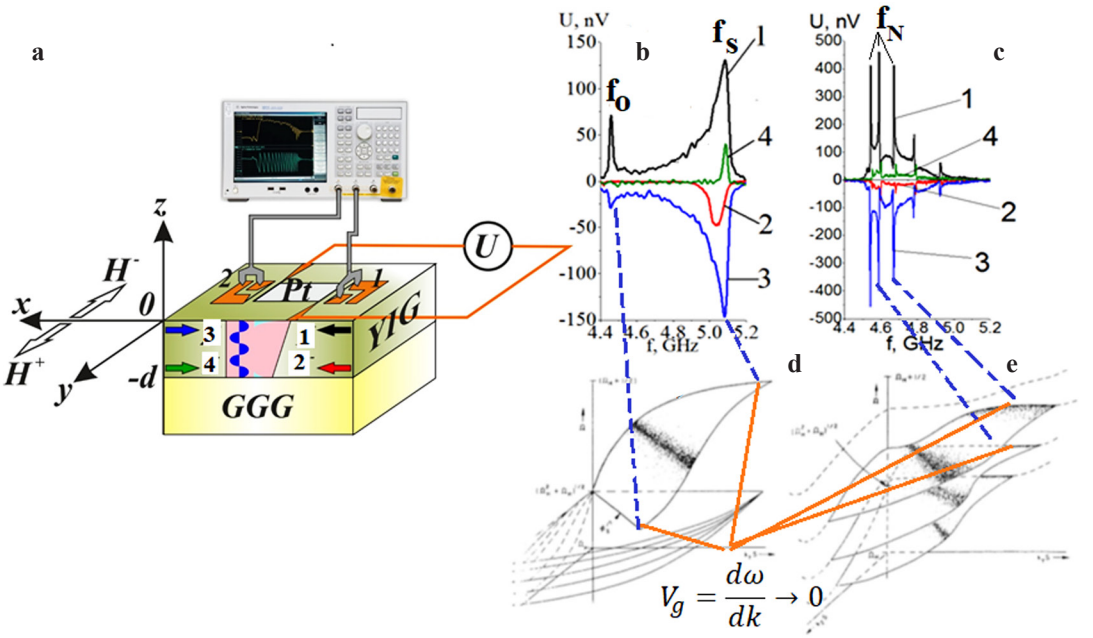

Figure 1. **a** The studied structures and the experimental scheme. Numbers 1 and 2 correspond to the input and output MSSW antennas. Position of the color arrows 1–4 near surfaces $z = 0$ and $z = -d$ correspond to position of the maximum for MSSW propagating in YIG film excited by antennas 1 or 2 for bias field H^+ directed along (1, 4) or H^- controversy (2, 3) *Oy*-axis. Color insets schematically represents thickness distributions of the partial waves, which forming dipole-exchange SW propagating in YIG film: dipole MMSW (pink), exchange volume (blue) and exchange surface (turquoise) partial waves. **b** and **c** – ISHE voltage frequency dependencies in YIG(8 μm)/Pt(8 nm) and YIG(0.9 μm)/Pt(8 nm) structures, curves 1–4 corresponds MSSW shown by arrows 1–4 on **a**, H = 943 Oe; **c** and **d** dispersion for pure dipole and dipole-exchange MSSW, red lines show position of the frequencies f^*, where $v_g(f^*) \to 0$ and van Hove singularities appear.

$U(f)$ is shown for dipole-dominated MSSW having dispersion shown on Fig. 1d. In this case two clear extremums at frequencies f_0 and f_s can be detected.

For YIG/Pt structures based on sufficiently thin YIG film the resonant enhancement takes place at frequencies correspondent to MSSW resonance interaction with EM in YIG film and reflects the growing of the normal to YIG/Pt interface spin current density component as well spin waves density of states, see Fig. 1c and d. Observed effects is promising for efficient spin-to-charge conversion in magnon spintronics devices.

Support by the Russian Science Foundation (project no. 22-19-00500) is acknowledged.

1. A. Chumak, V. Vasyuchka, A. Serga et al., Nature Phys. **11**, 453–461 (2015).
2. Y. Kajiwara, K. Harii, S. Takahashi et al., Nature **464**, 262–266 (2010).
3. M. Collet, X. de Milly, O. d'Allivy Kelly et al., Nat. Commun. **7**, 10377 (2016).
4. M. Evelt, V. E. Demidov, V. Bessonov et al., Appl. Phys. Lett. **108**, 172406 (2016).
5. M. Balinskiy, H. Chiang, D. Gutierrez, et al., Appl. Phys. Lett. 118, 242402 (2021).
6. L. van Hove, Phys. Rev. **89**, 1189 (1953).
7. R. Damon, J. Eshbach, J. Phys. Chem. Solids **19**, 308–320 (1961).
8. R.E. De Wames, T. Wolfram. J. Appl. Phys. **41**, 987 (1970).

INFLUENCE OF DZYALOSHINSKII-MORIYA INTERACTION ON HYSTERESIS PROCESSES IN MAGNETOELECTRIC NANOELEMENT

Z.V. Gareeva[1*], *N.V. Shulga*[1], *R.A. Doroshenko*[1], *A.K. Zvezdin*[2]

[1]Institute of Molecule and Crystal Physics, Subdivision of the Ufa Federal Research Centre of the Russian Academy of Sciences, Ufa, Russia
[2]Prokhorov General Physics Institute of the Russian Academy of Sciences, Moscow, Russia
[*]E-mail: zukhragzv@yandex.ru

Advances in spintronics and computer technology are forcing researchers to look for new ways to design efficient logic and memory devices [1]. In this regard, it seems promising to consider magnetoelectric materials in which the control and collective switching of magnetic states is carried out by an electric field due to the mechanisms of magnetoelectric coupling. In multicomponent structures, the magnetoelectric properties can be provided by the Dzyaloshinskii-Moriya (DMI) interaction due to interfacial effects [2].

We consider the magnetoelectric nanoelement and explore the manifestation of Dzyaloshinskii-Moriya interaction (DMI) in the reversal magnetization processes. Due to non-homogeneous magnetoelectric effect electric polarization arises in the vicinity of magnetic inhomogeneities. Simulations implemented with Object Oriented Micro Magnetic Framework (OOMMF) public code with the additional module for DMI allows us to follow polarization behavior during magnetization and remagnetization processes induced by magnetic field applied along the normal to a film (Fig. 1). The peculiar features of magnetoelectric effect including magnetoelectric coefficient and toroidal moment have been considered.

The support of from the State assignment for the implementation of scientific research by laboratories (Order MN-8/1356 of 09/20/2021), Russian Foundation for Basic Research under grant No. 19-52-80024. is kindly acknowledged.

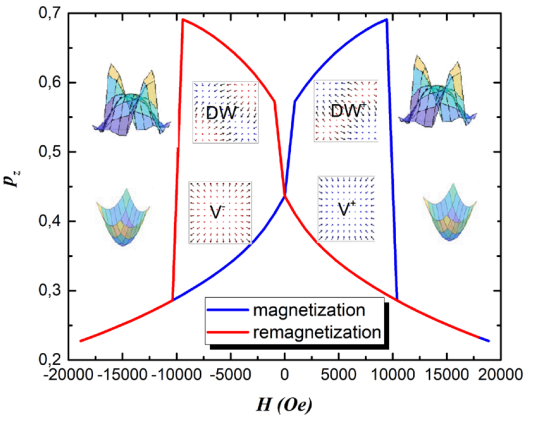

Figure 1. Electric polarization dependence on magnetic field in nanoelement 50×50×30 nm at $D = 0.6$ mJ/m^2, distributions of P_z component in the *xy*-plane and four magnetic configurations are shown.

1. S. Manipatruni et al., Nature **565**, 35–42 (2019).
2. L. Caretta et al., Nat. Commun. **11**, 1–9 (2020).

MAGNONIC TRANSPORT IN 3D MULTILAYER STRUCTURES WITH BROKEN TRANSLATION SYMMETRY

*A.V. Sadovnikov**, *E.N. Beginin, A.A. Martyshkin, S.A. Nikitov*

Laboratory "Magnetic Metamaterials", Saratov State University, Saratov, Russia
*E-mail: SadovnikovAV@gmail.com

Recently magnetic micro- and nanostructures are extensively studied due to their potentials as candidates for future magnonic devices [1, 2] and beyond-CMOS (complementary metal-oxide semiconductor) technologies, as they are free of Joule heating and, respectively, free of power loss associated with traditional electronics [3]. Magnetostatic spin waves (MSW) propagating in such structures are considered as signal carriers for information processing. In recent years much research has been directed towards the ways of the control of MSW for signal processing at microwave and subterahertz frequencies. The effect of the electric field on the magnetic configuration results from the modification of the effective internal magnetic field. The latter is changed due to inverse magnetostriction (Villary effect) as a result of the local deformation of the magnetic film.

Here we report the micromagnetic study of magnonic structures with broken translation symmetry which are shown in Fig. 1. To model the magnonic band structure of the 3D magnonic crystals the micromagnetic simulations were performed and spin-wave dispersion was then obtained by performing a 2D Fast Discrete Fourier Transform. The comparison between measured and calculated dispersion relations for the CoFeB/Ta/NiFe and CoFeB meander structures, as well as the dispersion of an equivalent planar CoFeB/Ta/NiFe magnetic bilayer was provided.

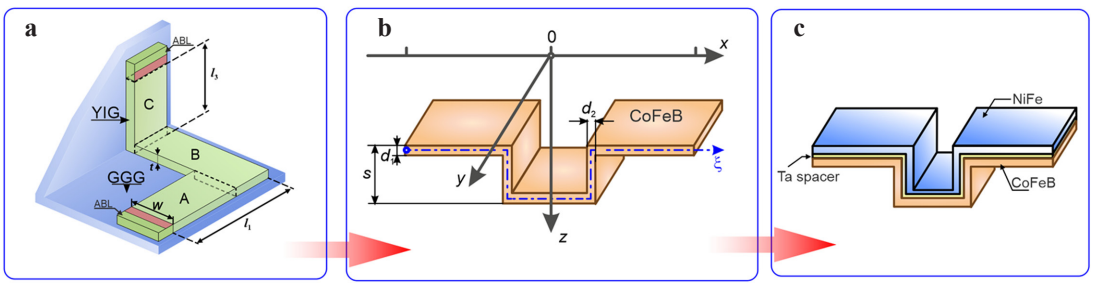

Figure 1. Magnonic structures with broken translation symmetry.

This work is supported by RSF grant (#20-79-10191).

1. A. Barman et al., J. Phys.: Condensed Matter **33**, 41, 413001 (2021).
2. S.A. Nikitov et al., Phys. Usp. **63**, 945–974 (2020).
3. G. Gubbiotti et al., Phys. Rev. Applied **15**, 014061 (2021).
4. G. Gubbiotti et al., Appl. Phys. Lett. **118**, 162405 (2021).
5. A.V. Sadovnikov et al., JMMM **544**, 168670 (2022).
6. E.N. Beginin, D.V. Kalyabin, P.A. Popov, A.V. Sadovnikov, A.Yu. Sharaevskaya, A.I. Stognij, S.A. Nikitov, 3D Magnonic Crystals in Three-Dimensional Magnonics (G. Gubbiotti, Ed.). CRC Press (Taylor&Francis), Jenny Stanford Publishing, New York.

A.O1

EASY-CONE STATE IN SPIN-TORQUE DIODE UNDER COMBINED ACTION OF MAGNETOSTATICS AND INTERFACIAL PERPENDICULAR MAGNETIC ANISOTROPY

A.G. Buzdakov[1,2], *P.N. Skirdkov*[2,3*], *K.A. Zvezdin*[2,3]

[1]Moscow Institute of Physics and Technologies, Moscow, Russia
[2]New Spintronic Technologies, Moscow, Russia
[3]Prokhorov General Physics Institute of the Russian Academy of Sciences, Moscow, Russia
[*]E-mail: petr.skirdkov@phystech.edu

Spin-torque diodes (STDs) with interfacial perpendicular magnetic anisotropy (IPMA) in the free layer (FL) demonstrate outstanding microwave signal rectification performances [1, 2]. Large sensitivity values in such systems are usually associated with an easy-cone (EC) magnetic state, when the magnetization in the FL is tilted from the normal to the plane of the film.

Firstly, we report the magnetostatically induced formation of an easy-cone magnetic state in free layers of magnetic tunneling junction (MTJ) with only first-order IPMA [3]. By means of micromagnetic modeling, we study easy-cone angle dependence on the first-order anisotropy and its impact on the microwave sensitivity of the unbiased spin-torque diode. Considered magnetization tilt can be effectively engineered by choosing the ratio of the shape and first-order surface anisotropy, defined by the free layer's thickness, in-plane MTJ shape, and interlayer magnetostatic interactions. Through micromagnetic modeling over a broad range of input powers and free-layer thicknesses, we demonstrate a significant role of nonlinearity and inhomogeneous magnetization dynamics in achieving high sensitivity levels. Our modeling for typical state-of-the-art parameters of MTJ shows a possibility to reach a record-breaking unbiased sensitivity of 1100 mV/mW and 4650 mV/mW after impedance matching, which is far beyond the parameters of commercial Schottky diodes.

Secondly, we theoretically investigate the phase diagram for the EC state in an infinite FL of the MTJ considering both IPMA (of the first and of the second order) and magnetostatic interaction [4]. We show that the increase of the magnetostatic field leads to the EC state phase expansion. Then, we consider the effect of finite sizes in the case of two different spatially oriented elliptical nanopillars of magnetic tunnel junctions (for one, the semi-major axis is directed along the x-axis, for the other, the semi-major axis is directed along the y-axis) on the obtained phase diagrams. Finally, we consider the dynamic properties and rectification of two elliptical spin-diodes under the action of a microwave current in a linear approximation [4]. To confirm the identified approach, micromagnetic modeling was carried out for two characteristic points on the phase diagrams. The obtained results of micromagnetic modeling confirmed the results obtained in the linear approximation.

Our results clarify the role of magnetostatic interaction for microwave rectification with the IPMA-based STDs and suggest approaches to the EC state effective rectification phase extension through the parameters optimization. These results will be very helpful for the development of efficient spintronic ambient energy harvesters.

Support by RSF 19-12-00432 is acknowledged.

1. B. Fang, M. Carpentieri, X. Hao, X. et al., Nature Commun. **7**, 11259 (2016).
2. L. Zhang, B. Fang, J. Cai et al., Appl. Phys. Lett. **113**, 102401 (2018).
3. A.G. Buzdakov, P.N. Skirdkov, K.A. Zvezdin, Phys. Rev. Appl. **15**, 054047 (2021).
4. A.G. Buzdakov, P.N. Skirdkov, K.A. Zvezdin, J. Phys. D: Appl. Phys. **55**, 115001 (2022).

A.O2

FERROMAGNETIC SILICIDES AND GERMANIDES EPITAXIAL FILMS AND MULTILAYERED HYBRYD STRUCTURES: SYNTHESYS, MAGNETIC AND TRANSPORT PROPERTIES

I.A. Tarasov[1], *I.A. Yakovlev*[1], *M.V. Rautskii*[1], *I.A. Bondarev*[1,2], *A.V. Lukyanenko*[1], *A.L. Sukhachev*[1], *S.N. Varnakov*[1], *S.G. Ovchinnikov*[1], *N.V. Volkov*[1], *A.S. Tarasov*[1*]

[1]Kirensky Institute of Physics, Krasnoyarsk Scientific Center, SB RAS, Krasnoyarsk, Russia
[2]Krasnoyarsk Scientific Center, SB RAS, Krasnoyarsk, Russia
[*]E-mail: taras@iph.krasn.ru

Nowadays the miniaturization of field-effect transistors (MOSFETs) is approaching its limit, and this problem has not yet been solved. The solution may lay in the creation of novel devices, which operating principle is based on the spin degrees of freedom of electrons, making it possible to reduce overall power consumption, improve the speed of RAM and expand the data processing capabilities [1–3]. The search for suitable ferromagnetic (FM) materials for these spintronic devices is a relevant and complex task. These materials must be compatible with the silicon technology that is currently dominant in the semiconductor (SC) industry, they must also have a high transition temperature to the FM state T_C, high spin polarization of electrons, and meet a number of other requirements. An example of such materials is Heusler alloys [4], such as Fe_2MnSi, Fe_3Si, Co_2FeAl, Co_2FeSi, $Co_2Fe(Al,Si)$. Based on these ferromagnets, both simple FM/SC epitaxial structures and multilayer magnetic and hybrid structures of various compositions can be grown. In particular, three-layer hybrid structures of FM/SC/FM are promising for vertical and planar devices of semiconductor spintronics [5]. We have developed approaches for the synthesis of thin $Fe_{3+x}Si_{1-x}$, epitaxial films and demonstrated the effect of spin accumulation in multiterminal devices based on $Fe_{3+x}Si_{1-x}$/Si. We also synthesized the $Fe_{3+x}Si_{1-x}$/Ge/Fe_3Si and $Fe_{3+x}Si_{1-x}$/Ge/Mn_5Ge_3 multilayer structures on the Si(111) substrate and studied their structural, magnetic and transport properties.

All samples were grown by molecular beam epitaxy at a base vacuum of $6\cdot10^{-8}$ Pa. Before the deposition, the Si(111) substrates were annealed at a temperature of 900 °C to obtain a 7×7 surface reconstruction, which was controlled using in situ RHEED. Individual materials (Fe, Si, Ge, Mn) were evaporated from separate sources at different rates to provide the required stoichiometry of binary compounds. During the growth of $Fe_{3+x}Si_{1-x}$ films, the substrate temperature was maintained at the level of 150 °C, for Ge – 300 °C, for Mn_5Ge_3 – 390 °C. The microstructure and morphology of the samples were studied using XRD, TEM and AFM. The magnetic properties were studied using VSM and FMR techniques. Electrical characteristics were measured by a Keithley 2634b SourceMeter precision multimeter over a temperature range of 4.2 to 300 K in a home-built helium flow cryostat. On the basis of some samples, multiterminal structures of special topology were prepared using standard optical lithography.

$Fe_{3+x}Si_{1-x}$ epitaxial thin films on p- and n-Si(111), substrates have been synthesized; devices for studying spin transport by the 3-T Hanle method have been fabricated on their basis [6]. The effect of spin accumulation in these structures was demonstrated [7]. A comprehensive study of the electrical properties made it possible to interpret the spin accumulation effect taking into account surface states in Fe_3Si/p-Si structures with a low-doped silicon substrate [8]. Comparing the results for n- and p-Si, as well as considering the literature data, we can conclude that the spin lifetime, as well as the magnitude of the spin signal, is more affected by the concentration of charge carriers than by their type. [9]. To study the growth features and the subsequent implementation of vertical spintronic devices, hybrid three-layer epitaxial structures $Fe_{3+x}Si_{1-x}$/Ge/Fe_3Si with different thicknesses

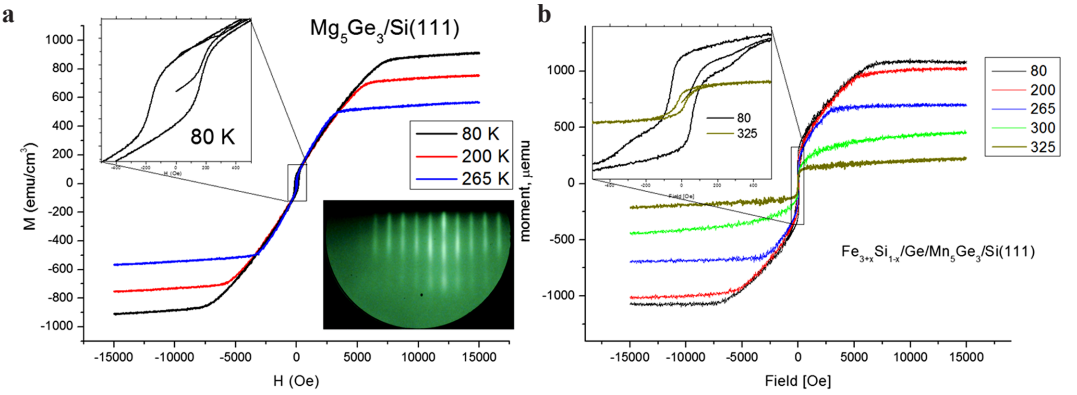

Figure 1. **a** Magnetic hysteresis loops of Mn_5Ge_3 film. Inset shows in situ RHEED pattern. **b** Magnetic hysteresis loops of $Fe_{3+x}Si_{1-x}$/Ge/Mn_5Ge_3 multilayer film.

(4 and 7 nm) of the Ge interlayer were synthesized. By comprehensive characterization it has been established that an increase in the Ge thickness causes a prolonged atomic diffusion through the interfaces, which significantly increases the lattice misfits in the Ge/$Fe_{3+x}Si_{1-x}$ heterosystem due to the incorporation of Ge atoms into the $Fe_{3+x}Si_{1-x}$ bottom layer. The resultant decrease in total free energy caused by the development of the surface roughness leads to a transition from an epitaxial to a polycrystalline growth of the upper $Fe_{3+x}Si_{1-x}$. The variation in structural order and morphology significantly changes the magnetic properties of the upper $Fe_{3+x}Si_{1-x}$ layer and causes a subtle effect on the transport properties of the Ge layer [10].

Epitaxial 180-nm-thick Mn_5Ge_3 films on Si(111) substrates were synthesized for the first time. RHEED (right inset on Fig. 1a) and XRD data are indicative of an epitaxial growth mode. An analysis of AFM images over 10×10 μm area shows that the average roughness is quite low (3.8 nm) which means that there is the coalescence of 3D-islands at the initial stages of growth. A ferromagnetic ordering temperature of the obtained films is 300 K, which is close to 296 K for bulk material, and the hysteresis loops are quite typical (Fig. 1a). Combining the growth technology of silicide-based three-layer structures and the obtained information on the nuances of Mn_5Ge_3, growth, we obtained $Fe_{3+x}Si_{1-x}$/Ge/Mn_5Ge_3/Si(111), the high quality of which is confirmed by preliminary RHEED and TEM data. Multilayer structures demonstrate more complex magnetism defined by the properties of the individual layers (Fig. 1b), which can be used in the design and construction of spintronic devices.

Support by Russian Foundation for Basic Research, the Government of the Krasnoyarsk Territory, and the Krasnoyarsk Territorial Foundation for Support of Scientific and R&D Activities, (project no. 20-42-243007) is acknowledged.

1. I. Zutic, J. Fabian, S. Das Sarma, Rev. Mod. Phys. **76**(2), 323–41 (2004).
2. R. Jansen, Nature Materials **11**, 400–408 (2012).
3. A. Hirohata, K. Yamada, Y. Nakatani, I.L. Prejbeanu, B. Diény et al., JMMM **509**, 166711 (2020).
4. L. Wollmann, A.K. Nayak, S.S. Parkin, C. Felser, Annu. Rev. Mater. Res. **47**, 247–270 (2017).
5. K. Hamaya, Y. Fujita, M. Yamada, M. Kawano et al., J. Phys. D: Appl. Phys. **51**(39), 393001 (2018).
6. A.S. Tarasov et al., Thin Solid Films **642**, 20–24 (2017).
7. A.S. Tarasov et al., J. Surf. Invest. **12**(4), 633–637 (2018).
8. A.S. Tarasov et al., Semicond. Sci. Technol. **34**, 035024 (2019).
9. A.S. Tarasov et al., Tech. Phys. Lett. **46**, 665–668 (2020).
10. A.S. Tarasov et al., Nanomaterials **12**, 131 (2022).

A.O3

METASTABLE STATES IN EXCHANGE-COUPLED FERROMAGNETIC DISKS

D.A. Tatarskiy[1,2], *I.Yu. Pashen'kin*[1], *E.V. Skorokhodov*[1], *S.A. Gusev*[1]

[1]Institute for Physics of Microstructures RAS, Department of Magnetic Nanostructures, Nizhny Novgorod, Russia
[2]Lobachevsky State University of Nizhny Novgorod, Nizhny Novgorod, Russia
*E-mail: tatarsky@ipmras.ru

Low-frequency oscillations of magnetic vortices are of interest in connection with the prospects for their use in spin-transfer vortex nanooscillators. Combining vortices into arrays will significantly increase the generated power. The generation frequency depend on the metastable configuration of magnetization in overlapping arrays of exchange-coupled disks. This paper presents the results of studies of metastable states in a system of exchange-coupled magnetic vortices by Lorentz transmission electron microscopy (LTEM) and computer simulation.

Arrays of overlapping ferromagnetic disks were fabricated by electron lithography and ion etching from a Permalloy film deposited on a 50 nm thick silicon nitride membrane by magnetron sputtering. The array consisted of double disks with a nominal diameter of 1 μm and overlaps from –10% to 80%. The LTEM measurements were carried out in a Carl Zeiss LIBRA 200MC transmission electron microscope operated at 200 kV in the low magnification mode and adapted for operation in the Fresnel mode. The geometry of the array made it possible to apply an external uniform field both along the line connecting the centers of the disks and perpendicular to it by tilting the sample in the microscope column and weak excitation of the objective lens. A part of double disks lattice with the Fresnel contrast is shown on Fig. 1a.

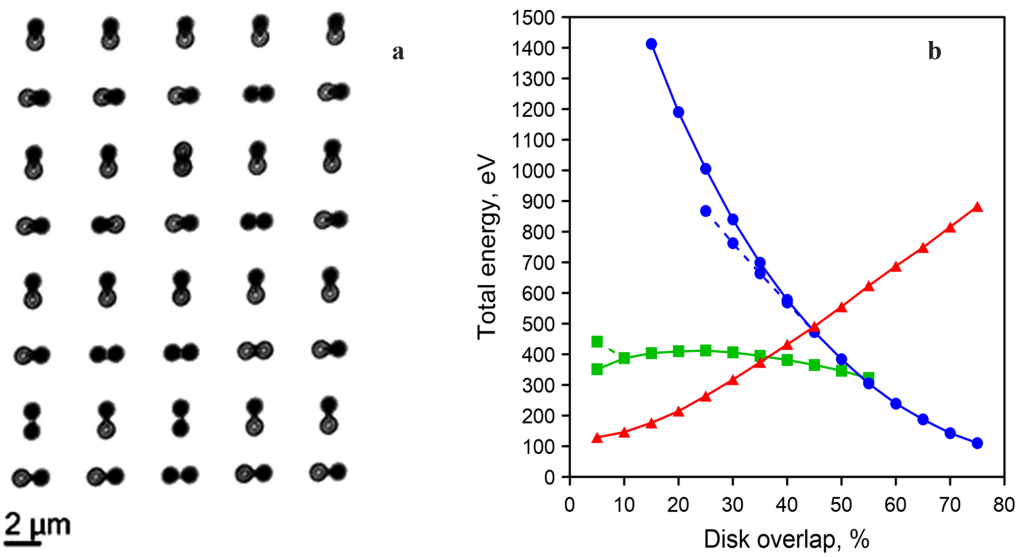

Figure 1. **a** Micrograph of Fresnel contrast in a part of the double disk lattice; **b** phase diagram of metastable states full magnetic energy in different magnetic states: red line – VV, solid green line – VAV, dashed green line – sVV, solid blue line – SV, dashed blue line – VC.

Micromagnetic modeling was performed using the MuMax3 simulator on a 512×256×1 grid with a grid step of 4.2×4.2×38 nm. In a double disk with different overlaps, different initial distributions of the magnetization were established and, after the magnetization relaxed to equilibrium, the total magnetic energy of the system was calculated. Thus, an energy diagram of metastable states was obtained (Fig. 1b).

It is known that the ground state in a mesoscopic ferromagnetic disk is a magnetic vortex. The vortex consists of a central region, where the magnetization is directed perpendicular to the disk plane (core) and an outer part, where the magnetization lies in-plane (shell). The orientation of the core determines the polarity of the vortex ($p = \pm 1$), while the clockwise/counterclockwise twist of the shell determines the vorticity ($c = \pm 1$).

Several metastable states are realized in a double overlapping disk. These states can contain both one or two magnetic vortices. There are two types of states with one vortex. In one case, the vortex core is localized at the geometric center of the overlapping disks and a supervortex (SV) is formed. Such a state is unstable for small overlaps. It passes into the second type of a single-vortex state under an infinitely small influence of an external field, when the vortex is localized in one of the disks, and the C-state is realized in the second disk (VC). There are three types of two-vortices states. First, when the shells of the vortices are curled in different directions, a state with a rhombic domain between the disks (VV) is formed. It is the ground state for small overlaps. Secondly, if the vortex shells are curled in same directions, two variants are realized. In one case, a singularity arises between the disks and an antivortex (VAV) is formed, in the other case, both vortices are displaced and the antivortex "leaves" the disks (sVV). Note that for large overlaps, VAV and sVV are unstable and go over to SV. The energy diagram of all states is shown in Fig. 1b.

Based on the Fresnel contrast in the microphotographs, we calculated the number of states in the double disks depending on both the overlap and the direction of the magnetic field application. The VV state is mainly formed up to 60% overlap during magnetization along short side. The VV

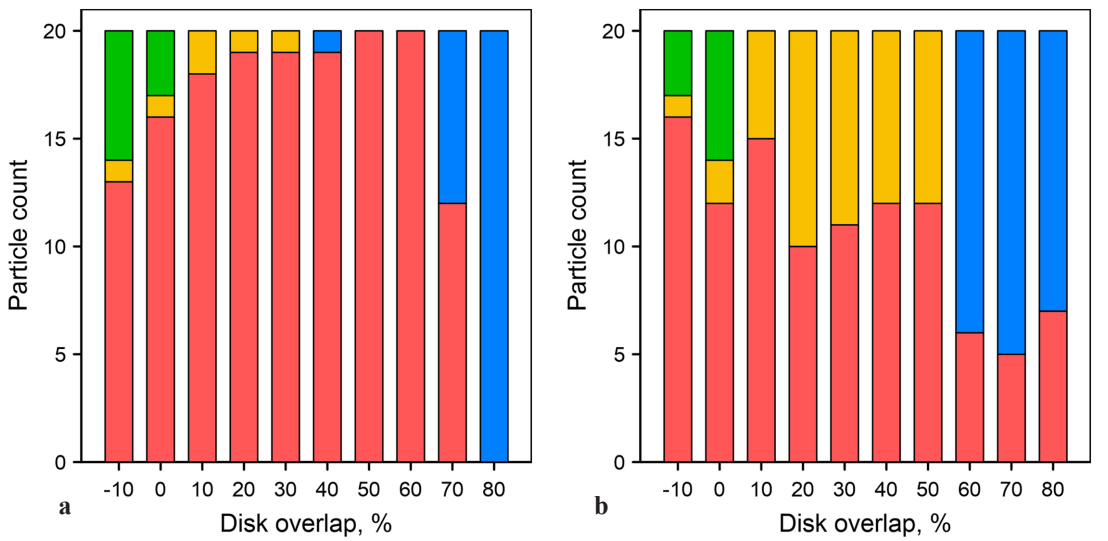

Figure 2. Statistics of metastable states versus external magnetizing field direction: **a** along short side of a double disk; **b** along long side of a double disk. Colors for states: red – VV, yellow – VAV, green – sVV, blue SV.

and VAV states are formed with equal probability up to 50% overlap when we magnetize the double disks along the long side.

Thus, we have shown that it is possible to change the state in double overlapping disks by applying an appropriate external field. The question of metastatble states and their control in double disk chains and lattices are very complicated. One should modify disks by cutting edges or alternating overlaps in chains and lattices to get an appropriate ground magnetic state with the help of shape anisotropy.

This research was performed with support from Russian Science Foundation (project No. 21–72–10176). The authors are grateful to V.L. Mironov and A.A. Fraerman for helpful discussions. The facilities of Center "Physics and technology of micro- and nanostructures" at IPM RAS were used for the fabrication and analysis of the samples.

A.O4

ULTRAFAST SIGNATURES OF MAGNETIC INHOMOGENEITY IN $Pd_{1-x}Fe_x$ ($x \leq 0.08$) EPITAXIAL THIN FILMS

R.V. Yusupov[1*], *A.V. Petrov*[1], *S.I. Nikitin*[1], I.V. *Yanilkin*[1], *A.I. Gumarov*[1], *L.R. Tagirov*[1,2]

[1]Kazan Federal University, Kazan, Russian Federation
[2]Zavoisky Physical-Technical Institute, Kazan, Russian Federation
[*]E-mail: Roman.Yusupov@kpfu.ru

Superconducting spintronics is one of the technologies promising for exaflop-scale supercomputing, big-data processing, and artificial intelligence [1–3]. The highlighting features of the superconducting spintronic systems, for example, RSFQ-logic, are the high speed and unprecedental energy efficiency [2–5]. The important components here are thin-film magnetic Josephson junctions (MJJ), which include layers of superconductors (S) and ferromagnets (F) [1–3]. The phase difference of the superconducting wave function between S-layers in the three-layer S/F/S structures is determined by the thickness and the exchange splitting of the conduction band of the F-material. Among several materials for F-layer [1–3], the palladium-rich $Pd_{1-x}Fe_x$ alloy looks attractive because of the noble-metal base robust against deterioration and the possibility to tune the magnetic properties of $Pd_{1-x}Fe_x$ alloy film by varying the iron content x and preparation conditions [6, 7]. However, the attempts to incorporate $Pd_{1-x}Fe_x$ faced the problems of small critical current and temporal instability of magnetic properties [8]. To the high extent, these problems originated from the magnetic inhomogeneity inherent to alloys. Our studies aimed at an investigation of the inhomogeneities in high-quality thin films of the palladium-rich $Pd_{1-x}Fe_x$ alloys.

A series of $Pd_{1-x}Fe_x$ alloy epitaxial films (x = 0, 0.038, 0.062, and 0.080) was prepared and studied with ultrafast optical and magnetooptical laser spectroscopies in a wide 4–300 K temperature range. It was found that the transition to the ferromagnetic state causes the qualitative modification of both the reflectivity and the magnetooptical Kerr effect transients. Nanoscale magnetic inhomogeneity of the ferromagnet/paramagnet type inherent in the palladium-rich $Pd_{1-x}Fe_x$ alloys reveals itself in an occurrence of a relatively slow, 10–25 ps, photoinduced demagnetization component following a subpicosecond one; the former vanishes at low temperatures only in the x = 0.080 sample. We argue that the 10-ps timescale demagnetization originates most probably from the d-electron diffusive transport in the conditions of the nanometer-scale magnetic inhomogeneity. The low-temperature amount of the residual paramagnetic phase can be deduced from the magnitude of the slow reflectivity relaxation component, and is estimated as ~30% for x = 0.038 and ~15% for x = 0.062 films. The minimal iron content ensuring the magnetic homogeneity of the ferromagnetic state in $Pd_{1-x}Fe_x$ alloy at low temperatures is about 7–8 at.%.

Support from the Priority-2030 program of KFU is gratefully acknowledged.

1. V.V. Ryazanov et al., Phys. Procedia **36**, 35–41 (2012).
2. S.K. Tolpygo, Low Temp. Phys. **42**, 361–379 (2016).
3. I.I. Soloviev et al., Beilstein J. Nanotechnol. **8**, 2689–2710 (2017).
4. O.A. Mukhanov, IEEE Trans. Appl. Supercond. **21**, 760–769 (2011).
5. Q.P. Herr et al., J. Appl. Phys. **109**, 103903 (2011).
6. A. Esmaeili et al., Thin Solid Films **669**, 338–344 (2019).
7. A. Esmaeili et al., Sci. China Mater. **63**, 1–10 (2021).
8. L.S. Uspenskaya, I.N. Khlyustikov, J. Exp. Theor. Phys. **125**, 875–878 (2017).

A.O5

Co-Zn NANOFERRITES FOR HIGH FREQUENCY APPLICATIONS: CORRELATIONS BETWEEN DIELECTRIC AND MAGNETIC PROPERTIES

A. Thakur[1,3*], *I.S. Edelman*[2], *S.G. Ovchinnikov*[2], *A.L. Sukhachev*[2], *D.A. Petrov*[2], *P. Thakur*[3]

[1]Centre for Nanotechnology, Amity University Haryana, India
[2]Kirensky Institute of Physics, FRC KSC SB RAS, Krasnoyarsk, Russia
[3]Department of Physics, Amity School of Applied Sciences, Amity University Haryana, India
[*]E-mail: athakur1@ggn.amity.edu

Co-Zn ferrites, especially in the form of nanoparticles, attract an increasing attention of researchers and technologists due to their intriguing physical properties and wide field of applications which are based upon their significant saturation magnetization, a high electrical resistivity, low electrical losses, and a very good chemical stability. A series of $Co_xZn_{1-x}Fe_2O_4$ nanoparticles (NPs) with x varying from 0.0 to 0.5 prepared by citrate precursor technique demonstrated a remarkable resistivity and improved dielectric properties [1]. In particular, the value of the dielectric loss tangent varied in the range 0.003-0.052 at 1 MHz for different concentration of cobalt ions; the samples were found to be good insulators with enormous resistivity values ranging from $1.4\cdot10^{10}$ Ω-cm to $1.4\cdot10^{11}$ Ω-cm. Though magnetic properties of Co-Zn ferrite NPs synthesized with other techniques were studied by several authors (e.g, [2]), there were no data on magnetic properties of this particular system. At the same time, the profound knowledge of magnetic properties and their effect in the dielectric characteristics of NPs can open new channels of their applications.

Nanoparticles were prepared by using citrate precursor technique. Stoichiometric amount of analytic grade materials, zinc nitrate hexahydrate ($Zn(NO_3)_2\cdot6H_2O$, cobalt nitrate hexahydrate ($Co(NO_3)_2\cdot6H_2O$, and iron(III) nitrate nonahydrate ($Fe(NO_3)_3\cdot9H_2O$, were dissolved in a beaker containing 125 mL distilled water. 5 g of citric acid was added into the solution of metal nitrates. The mixture was kept for stirring at 80 °C to get a homogeneous solid solution. Thereafter, the samples were pre-sintered at 700 °C for 3 h in a muffle furnace, followed by cooling to room temperature. The resultant samples were pelletized by adding 2% polyvinyl alcohol (PVA) as a binder. After that, final sintering of the pellet was done at 800 °C in a muffle furnace for another 3 h.

X-ray diffraction study confirmed the spinel phase cubic structure of the prepared ferrites with Fd3m group. The average crystallite size of the samples was found in the range 28÷36 nm. Transmission electron microscope (TEM) investigations record crystallite size in the range 30-40 nm which is in good agreement with XRD. Scanning electron microscope (SEM) imaging confirmed

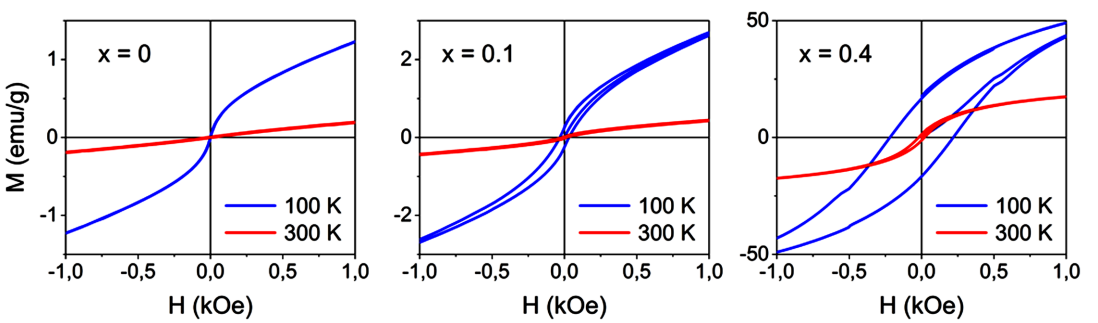

Figure 1. Magnetization dependences on magnetic field at two temperatures for samples with x = 0, 0.1, 0.4.

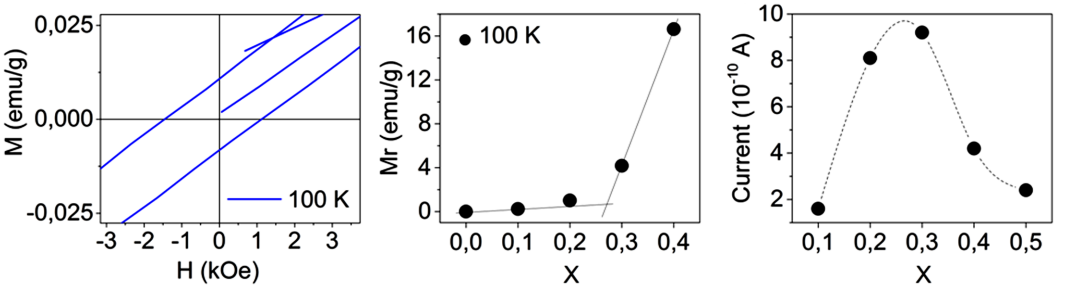

Figure 2. Low field part of hysteresis loop of the sample with x = 0 (left), remnant magnetization (central) and electric current at 3 V (right) in dependence on x.

agglomerated structure of the ferrite nanoparticles. Magnetization dependences on an external magnetic field were studied with the vibrating sample magnetometer Lake Shore 8604 in magnetic field up to 15 kOe at temperatures from 90 to 350 K. First of all note the magnetic ordering in pure Zn ferrite nanoparticles (Fig. 1, left, Fig. 2, left) revealed at lower temperatures. This phenomenon was observed previously, but not always. For example, magnetic ordering was not observed in Zn spinel nanoparticles obtained with co-precipitation method up to 50 K [2].

At low Co concentrations, formation of long-range magnetic order is impossible. Observation of hysteresis loops in this case can be associated with the inhomogeneous Co ions distribution inside NPs with formation of small areas enriched in cobalt ions. Co^{2+} and part of Fe^{3+} ions in the areas occupy the octahedral positions while other part of Fe^{3+} ions occupies the tetrahedral positions, that is, the ion distribution in these areas is close to that in the Co-ferrite. Such areas can be considered as ultrafine NPs that exhibit properties characteristic of an ensemble of superparamagnetic particles. The hysteresis which appears with decreasing temperature already for x = 0.1 indicates the formation of a certain small number of rather large particles with magnetic ordering that are blocked at 100 K. As x increases, the magnetization M and remnant magnetization M_r increase very slowly at first, and, starting from x = 0.3, very quickly. An example of such behavior is shown in Fig. 2 (center panel) for M_r. The change in the form of the dependence of the magnetic characteristics on x is probably associated with the appearance of long-range magnetic order in the NPs.

Now we can compare the magnetic characteristics dependences on the x-value with the Co concentration dependences of dielectric characteristics of the same NPs presented in [1]. No monotonic concentration dependences of the real and imaginary parts of the dielectric constant ε′ and ε″, dielectric loss tangent, ac conductivity, and the current-voltage relationship are shown in Figs. 7–11 in [1]. All these characteristics reach their maximal or minimal meanings near x = 0.3÷0.4 and then tend to return to values observed at x ~ 0.1. Figure 2 (right panel) clearly shows that the maximum in the concentration dependence of the current corresponds to a sharp change in the rate of increase in the remnant magnetization. A similar type of dependence is also observed for other characteristics. It is reasonable to assume that the appearance of a long-range magnetic order affects the dielectric properties of the material under study. The mechanisms of such influence are currently being studied.

1. D. Chahar, S. Taneja, P. Thakur, A. Thakur, J. Alloys Comp. **843**, 155681 (2020).
2. P.A. Asogekar, S.K. Gaonkar, A. Kumar, V.M.S. Verenkar, Mater. Res. Bull. **141**, 111330 (2021).

SPACER THICKNESS AND TEMPERATURE DEPENDENCES OF THE INTERLAYER EXCHANGE COUPLING IN A Co/Pt/Co THREE-LAYER STRUCTURE

*V.S. Gornakov**, *I.V. Shashkov, Yu.P. Kabanov*

Institute of Solid State Physics of RAS, Chernogolovka, Russia
*E-mail: gornakov@issp.ac.ru

Magnetic thin-film structures with perpendicular magnetic anisotropy (PMA) are promising candidates for the design of the magnetic random access memories [1] and spintronic devices [2]. The nucleation of domains with reverse magnetization and the domain walls (DWs) motion mainly determine magnetization reversal in these materials [3]. Due to interlayer exchange coupling, the process of magnetization transformation in thin heterophase films with PMA, in which two ferromagnetic (FM) layers separated by a nonmagnetic (NM) interlayer, have a significant influence on the kinetics, dynamic parameters, and relaxation of the domain structure in these films. In this FM/NM/FM multilayer, it has been found that the exchange interaction energy J demonstrates oscillatory behaviors with the gradually changing in Pt spacer thickness t. The mutual orientation of the magnetic moments in the FM layers changes alternately from parallel to antiparallel depending on the Pt thickness. However, the micromechanism of the magnetization reversal of the FM layers was not considered. Features of inhomogeneous processes of domain nucleation and domain walls motion in Co/Pt/Co films with a wedge-shaped platinum spacer were studied in [3]. In such a film, the critical thickness of the NM spacer t_{CR} was found [3]. In the heterostructure with $t > t_{CR}$, the domains nucleation in the FM layers was uncorrelated, and the DW motion in them was independent, while at $t < t_{CR}$, the domains nucleation occurred in both Co layers simultaneously and the domain walls moved together. Thus, in such three-layer structures, the magnetization reversal features can be caused both by the specifics of the magnetization reversal of single films and by interlayer exchange coupling. The magnetization reversal, kinetics and relaxation of a domain structure of such synthesized films should be depend both on the NM layer thickness and on the temperature. So far, this issue has not been studied in detail. This report presents the results of an experimental study of the domain walls motion and the exchange coupling formation between FM layers depending on the Pt thickness and temperature in ultrathin Co/Pt/Co structure.

The structure Pt(10 nm)/Co(0.6 nm)/Pt(t)/Co(0.6 nm)/Pt(3 nm) was deposited by magnetron sputtering on an oxidized silicon substrate with an area of 5×6 mm^2 at room temperature. The thickness of the platinum interlayer t changed uniformly along the side of the wedge from 6 to 5 nm (Fig. 1). The formation and evolution of domains were studied using the magneto-optical (MO) Kerr effect, which provides real-time information about the domain structure, affecting the spin distribution in the sample.

We demonstrate a measurement and analyze field-displacement responses of a single domain wall in one magnetic layer coupled to a second, saturated magnetic layer. Moving of this domain wall yields a reference a determination of the interlayer coupling. The spacer thickness dependence of the magnetization evolution in the Co/Pt/Co three-layer with perpendicular anisotropy in the magnetic field observed. Both ferromagnetic layers of the sample were previously saturated in a DC perpendicular magnetic field. The domains with opposite magnetization in the top layer were formed by a pulse magnetic field. A domain wall, which separates ferromagnetic and antiferromagnetic (AFM) areas (Fig. 1a), was formed in an AC magnetic field $H \approx H_C$, where H_C is a coercive field of the top layer. This wall is located in place, where Pt thickness $t = t_0$ and interlayer exchange coupling equals $J = J_0 = 0$ erg/cm^2.

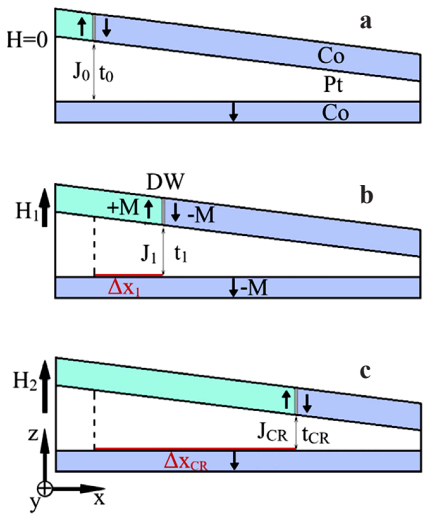

Figure 1. Schematic structure of three-layer with edge Pt spacer and domain structure in the **a** initial, **b** intermediate and **c** final states.

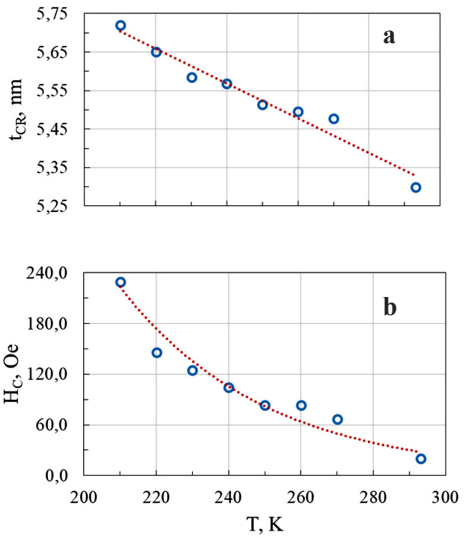

Figure 2. Temperature dependence of the **a** critical thickness of the Pt spacer t_{CR} and **b** coercive force H_C of the upper layer.

A nonlinear dependence of the displacement of domain walls Δx (Fig. 1b) on the magnitude of the external magnetic field H in this FM region of the heterostructure is found. The dependence $\Delta x(H)$ tends to saturation in the region of the heterostructure with the interlayer thickness equal to t_{CR}. After reaching the upper domain wall of the region Δx_{CR} with $t = t_{CR}$, its further independent movement with an increase in the amplitude of the magnetic field pulses stopped and remained in this position until the coordinated bound movement of a pair of domain walls began in both layers. It has been established that the equilibrium position (with Δx_{CR} at Fig. 1c) of the domain wall depends on the thickness of the nonmagnetic interlayer. This equilibrium is determined by the competition between the energy due to the displacement of this wall in an external field and the energy J of the interlayer exchange interaction in the surface of the sample ($\Delta x_{CR} \times Y$, where Y is DW-length along y) swept by the domain wall. In other words, the DW achieves equilibrium state when effective field $H - H_C - H_J = 0$, where H_J is an effective coupling field induced by the interlayer coupling J. The mechanism of stabilization of domain walls near t_{CR} in the case of independent motion of DWs in layers is considered.

The heterostructure magnetization reversal by the domain walls motion at temperature range 200–300 K was observed using MO Kerr effect. It is shown, there is a critical temperature $T_{CR} \approx 200$ K, at which $\Delta x \to 0$ and, consequently, t_{CR} cannot change. The dependence of the critical thickness t_{CR}, determined by the interlayer exchange interaction energy J_{CR}, on the temperature is obtained. It is establishes that t_{CR} is linearly decreasing with temperature increasing (Fig. 2a). This phenomena was explained by the temperature dependence of the coercive force H_C of the upper layer (Fig. 2b), which is decreasing with T decreasing as it occur in the case of $t_{CR}(T)$.

1. B. Dieny and M. Chshiev, Rev. Mod. Phys. **89**, 025008 (2017).
2. R.B. Wilson, Y. Yang, J. Gorchon, C.-H. Lambert, S. Salahuddin, and J. Bokor, Phys. Rev. B **96**, 045105 (2017).
3. R.D. Shull, Y.L. Iunin, Y.P. Kabanov, V.I. Nikitenko, O.V. Skryabina, and C.L. Chien, J. Appl. Phys. **113**, 17C101 (2013).

A.O7

SLOW DYNAMICS PHENOMENA IN MAGNETIC MULTILAYER NANOSTRUCTURES

*M.M. Boldyreva, Yu.K. Evstafyeva, M.V. Mamonova, P.V. Prudnikov, V.V. Prudnikov**

Omsk State University, Omsk, Russia
*E-mail: prudnikv@univer.omsk.su

The magnetic properties of ultrathin films and superstructures are sensitive to the effects of anisotropy generated by the crystal field of a substrate or nonmagnetic layers. The multilayer magnetic structure Co/Cu(100)/Co extensively usable in active elements of spintronic devices is characterized by anisotropy of "easy" magnetic plane type with magnetization oriented in plane of cobalt film. The structure Pt/Co/Cu/Co/Pt with cobalt films coated by ultrathin platinum films is characterized already by anisotropy of "easy" magnetic axis type with magnetization oriented perpendicularly to plane of cobalt film.

The nanoscale periodicity in magnetic multilayer structures gives rise to the mesoscopic effects of the strong spatial spin correlation with the slow relaxation dynamics of magnetization accompanying the quenching of the system in the non-equilibrium state. The experimental investigations of relaxation [1] revealed magnetic aging in a Co/Cr-based magnetic superstructure.

The nonequilibrium behavior of a system is realized via its transition at the starting instant t_0 from the initial state at temperature T_0 to the state with temperature T_s differing from T_0. The evolution of systems with slow dynamics depends on its initial state for times $t << t_{rel}(T_s)$, where $t_{rel}(T_s)$ is a relaxation time at temperature T_s. Various initial states exert noticeable inuence on time dependence of characteristic functions in systems with slow dynamics [2]. In this connection, the non-equilibrium behavior of the system depends on whether it evolves from a high-temperature $T_0 > T_s$ or a low temperature $T_0 < T_s$ initial state.

In present work, a Monte Carlo simulation of the nonequilibrium behavior of multilayer magnetic nanostructures Co/Cu(100)/Co and Pt/Co/Cu(100)/Co/Pt consisting of alternating magnetic and nonmagnetic nanolayers was carried out. We have calculated two-time dependence of the autocorrelation function for these structures with different thicknesses N of cobalt films relaxing from both high-temperature and low-temperature initial states. It were revealed aging effects characterized by a slowing down of correlation characteristics with increase of the waiting time t_w. For evolution from high-temperature initial state, the study of dependence of aging characteristics on thickness N of cobalt films reveals a weakening of the aging with increasing N at the critical temperatures $T_c(N)$ and an opposite tendency at temperatures $T < T_c(N)$ with strengthening of aging with increasing N for considered $N \leq 9$ ML. This phenomenon is connected with increasing correlation and relaxation times in nanostructures when temperature is decreased. For case of the low-temperature initial state, it is shown that correlation times are two-three orders of magnitude smaller than those in the evolution from a high-temperature initial state at the same tw values. In this case, time behavior of the autocorrelation function doesn't depend considerably on temperature for $T < T_c(N)$ and thickness N of cobalt films.

Simulation of transport properties in Co/Cu(100)/Co and Pt/Co/Cu/Co/Pt structures with current perpendicular to plane (CPP) permitted to calculate temperature dependence of their equilibrium CPP-magnetoresistance values with demonstration that magnetoresistance in Pt/Co/Cu/Co/Pt structures is higher than in Co/Cu(100)/Co structures with the same thickness N [3]. During simulation of nonequilibrium behavior of these structures with evolution from different initial states, we revealed nontrivial aging effects in the magnetoresistance $\delta(t, t_w)$ (Fig. 1) and influence of initial states on

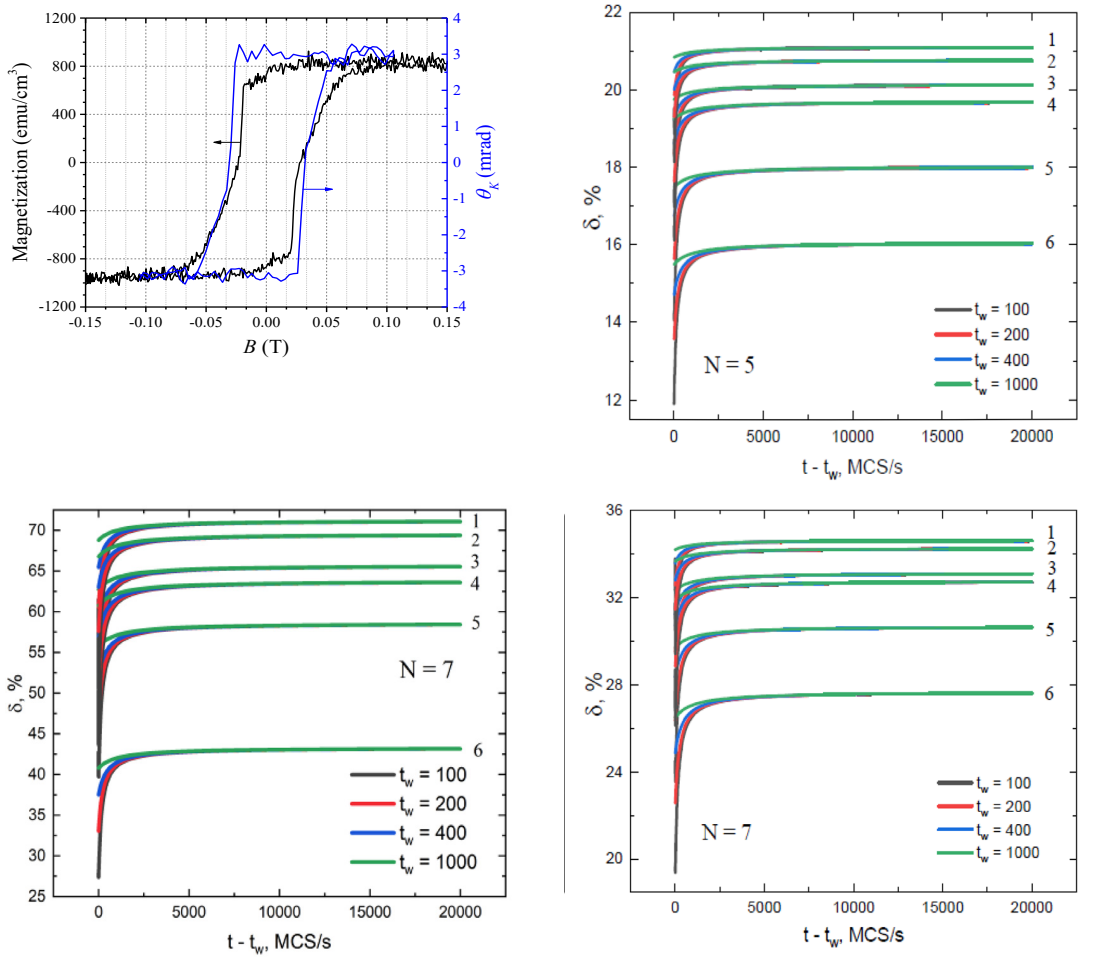

Figure 1. Time dependence of the CPP-magnetoresistance in structures Pt/Co/Cu(100)/Co/Pt (left) and Co/Cu(100)/Co (right) with the thicknesses N = 5 and 7 MLs of the cobalt films at temperatures $T_s = T_c(N)/4$ for waiting times t_w = 100, 200, 400 and 1000 MCS/s with evolution from different initial states with temperatures: 1 – $T_0 = 0$, 2 – $T_0 = T_c(N)/8$, 3 – $T_0 = 3T_c(N)/8$, 4 – $T_0 = T_c(N)/2$, 5 – $T_0 = 3T_c(N)/4$, 6 – $T_0 >> T_c(N)$.

the magnetoresistance. It has been shown that the magnetoresistance reaches plateau in asymptotic long-time regime with values $\delta^{\infty}(T_0, N, T_s)$, which depend on type of initial state, thickness of cobalt films, temperature and type of magnetic anisotropy in nanostructures.

This work was supported by RFBR according to the research project 20-32-70189, by the Ministry of Education and Science of Russian Federation in the framework of the state assignment (No 0741-2020-0002), and grant MD-2229.2020.2 of the President of the Russia.

1. T. Mukherjee, M. Pleimling and C. Binek, Phys. Rev. B **82**, 134425 (2010).
2. V.V. Prudnikov, P.V. Prudnikov and M.V. Mamonova, Phys. Usp. **60**, 762–797 (2017).
3. P.V. Prudnikov, V.V. Prudnikov, M.V. Mamonova and N.I. Piskunova, J. Magn. Magn. Mater. **482**, 201–205 (2019).

A.O8

INFLUENCE OF THE EFFECT OF LOCAL LASER HEATING ON SPIN WAVE PROPAGATION IN A BILAYER FERROMAGNETIC FILM

V.A. Gubanov[1*], *E.G. Lock*[2], *A.V. Sadovnikov*[1], *S.A. Nikitov*[2]

[1]Laboratory "Magnetic Metamaterials", Saratov State University, Saratov, Russia
[2]Institute of Radioengineering and Electronics (IRE) of Russian Academy of Sciences, Moscow, Russia
[*]E-mail: vladmeen@gmail.com

At present a large amount of research is aimed at developing an approach, which is an alternative to the well-proven method of information signal processing based on semiconductor (SC) structures. Signal generation, transmission and processing devices based on the principles of magnonics [1, 2] are of great interest due to the physical processes that take place without electron-hole transport, which allows to overcome the limitations of SC technologies associated with the ever-increasing thermal heating.

Thus, one of the signal transmission methods is based on spin wave (SW) propagation in ferromagnetic structures. At the same time, control of the SW properties is possible by varying the magnitude and direction of the magnetic field, as well as by modifying the structures: the formation of irregularities by precision laser cutting and local control by applying deformations or laser heating [3–5]. The latter method has proved to be the most promising for implementing an approach that implies performing various logical operations in magnonics networks.

In this work we consider a bilayer ferromagnetic yttrium iron garnet (YIG) film formed on a gadolinium gallium garnet (GGG) substrate. Since the film has a small width, it can be considered a magnon waveguide, shown in Fig. 1. A microstrip antenna, used in the experiment to excite spin waves, located on one edge of the film. Each of the YIG layers has a different value of saturation magnetization $M_{1,2}$. The surface of the multilayer structure is subjected to a laser beam, the power and diameter of which are varied during the study. Local laser heating changes the magnetization saturation value in each of the layers of the bilayer film, and heating that is not homogeneous in thickness of the structure is taken into account in the problem.

By scanning the film surface with a system based on the Brillouin light spectrometer, dynamic magnetization maps were plotted over the entire film surface. The creation of inhomogeneous heating in the center of the structure led both to the reflection of SW and to the localization of the SW power in the heating region. In addition, the characteristics of localization of SW in each of the layers depended on the frequency excited by the microstrip antenna signal. It is shown how the mode composition of SW in the proposed structure is transformed due to the manifestation of the anisotropy effect of the magnetic microwaveguide shape [6, 7].

Further, using the methods of micromagnetic modeling and experimental methods, the dynamics of propagating SW in a two-layer YIG film during the passage of the barrier created by laser radiation was investigated. Dispersion character-

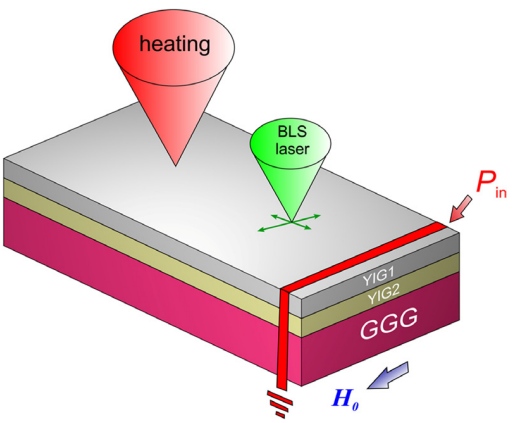

Figure 1. Sketch of bilayer YIG structure.

istics were obtained for each YIG layer and the vertical coupling of YIG layers for the transfer of SW in the region of heating by laser radiation at the expense of point change of each layer was shown. At the same time, the mechanism of short SW generation in the interface layer separating two YIG layers was found in the considered structure.

This work was supported by the Russian Science Foundation (project no. 20-79-10191).

1. A.V. Sadovnikov, A.A. Grachev, S.E. Sheshukova, S.A. Nikitov, J. Phys.: Condensed Matter **33**, 413001 (2021).
2. A.V. Sadovnikov, S.A. Nikitov, Bull. Russ. Acad. Sci. Phys. **85**, 595–598 (2021).
3. V.A. Gubanov, S.E. Sheshukova, S.A. Nikitov and A.V.Sadovnikov, J. Phys. D: Appl. Phys. **54**, 245001 (2021).
4. A.V. Sadovnikov, A.A. Grachev, A.A. Serdobintsev et al., IEEE Magnetics Lett, **10**, 1–5, (2019). Art no. 5506405.
5. M. Vogel, A.V. Chumak, E.H. Waller et al., Nature Physics **11**, 487 (2015).
6. A.V. Sadovnikov, G. Talmelli, G. Gubbiotti, E.N. Beginin, S. Sheshukova, S.A. Nikitov, C. Adelmann, F. Ciubotaru, JMMM **544**, 168670 (2022).
7. S.A. Odintsov, E.I. Salomatova, A.P. Kamantsev, A.A. Amirov, V.V. Rodionova, S.E. Sheshukova, A.V. Sadovnikov. Directional Control of Spin-Wave Transport in Tunable Spin-Photonic YIG/Fe-Rh Bilayer Structure for Signal Processing, Proceedings V. 11847. Saratov Fall Meeting 2020: Computations and Data Analysis: from Molecular Processes to Brain Functions; 118470I (2021).

DIFFERENT TYPES OF NANOWIRES – SYNTHESIS, STRUCTURE, PROPERTIES AND MAGNETIC PROPERTIES

D. Zagorskiy[1*], *I. Doludenko*[1], *D. Khairetdinova*[1,2], *R. Khaibullin*[3], *D. Cherkasov*[4], *A. Gippius*[5,6], *S. Zhurenko*[5], *O. Zhigalina*[1], *S. Chigarev*[7], *E. Vilkov*[7], *L. Fomin*[8]

[1]FSRC "Crystallography and Photonics", Russian Academy of Sciences, Moscow, Russia
[2]NUST "MISIS", Moscow, Russia
[3]Zavoisky Physical-Technical Institute, Kazan Scientific Center of RAS, Kazan, Russia
[4]Moscow Institute of Physics and Technology, Dolgoprydny, Russia
[5]Moscow State University named by M.V. Lomonosov, Moscow, Russia
[6]P.N. Lebedev Physical Institute, Russian Academy of Sciences, Moscow, Russia
[7]Fryazino branch of IRE named by V.A. Kotelnikov of RAS, Fryazino, Russia
[8]Institute of Microelectronic technology and High-purity materials of RAS, Chernogolovka, Russia
[*]E-mail: dzagorskiy@gmail.com

Nanowires (NWs) are one-dimensional threads with a diameter of several tens of nanometers and a length of several microns. Such structures are of great interest for practical applications. For example, NWs made of 3d-metals have unique magnetic characteristics. For NWs made of alloys, it is possible to change the magnetic properties over a wide range by changing the concentration of metals. For layered NWs – consisting of layers of different composition alternating along the length – properties can be varied by changing the composition and thickness of layers. These objects could be used in electronics and spintronics – for example, as sensors.

One of the promising ways to obtain arrays (ensembles) of such NWs is the method of matrix synthesis [1]. In this case, the pores of the matrix (template) are filled with the required alloy or alternating layers of different metals. The main problem here is the regulation of NWs' parameters during synthesis. Such regulation is carried out by choosing a matrix with the required pore structure, by changing the electrolyte composition and deposition conditions. At the same time, in the case of multicomponent structures, the solution of this problem can be rather complicated. It is necessary to investigate the dependence of the synthesis conditions on the structure, and the correlation of the structure with the properties.

In this work, various types of layered NWs obtained by the method of matrix synthesis based on polymer track membranes are investigated. Matrix synthesis was carried out using track membranes with pores 100 nm in diameter and the surface density of 10^9 pores per sq. cm (produced by JINR, Dubna). Electrolytes with sulfate salts of the corresponding metals and various additives were used. During deposition, both "single-bath" and "two-bath" methods were used. In the first case, the growth was carried out in a two-component electrolyte, while the alternation of layers was obtained by changing the potential. In the second case the growth electrolyte was changed in order to alternate the growth of layers with different compositions.

NWs consisting of layers of magnetic and non-magnetic metals – Co/Cu, Ni/Cu have been obtained. The geometric parameters of the layers, their composition, and the nature of the interlayer boundary were estimated by the TEM method. Methods for controlling the thickness of layers, reducing their thickness, and obtaining flat interlayer boundaries ("interfaces") are described. These include: the use of dilution of the solution, the use of special deposition modes (the method of controlling the thickness not by the duration of the pulses, but by the passed charge), the transition to the three-electrode method (with the reference electrode). The state of the interfaces between the layers was estimated. It is known that the quality of interfaces (thickness, flat shape) determines the characteristics of interlayer transitions in spintronic applications. The X-ray diffraction analysis

made it possible to determine the phase composition of the samples. In the above mentioned cases the layers in NW consist of both pure metals and solid solutions of a ferromagnetic metal with Cu.

The investigations of the direction of the easy magnetization axis in layered NWs, started in [2], are continued. The magnetic properties of layered Co/Cu NPs with different ratios of the thickness of magnetic cobalt to the thickness of the nonmagnetic copper interlayer have been studied by magnetometry. It was shown that the magnitude of the magnetic response and the magnetic anisotropy of an array of such NWs are strongly affected not only by the aspect ratio of the magnetic layer thickness to the diameter of an individual NW, but also by the magnetic dipole interaction both between the magnetic layers in the NW and between the NWs in the array. In fact, by changing the thickness of the magnetic layer of cobalt and non-magnetic copper interlayer, it is possible to change the direction of the easy magnetization axis in the NWs array.

Application of resonance methods. Previously (in [3]), Co-59 NMR was used to study layered Co/Cu NWs. A significant number of cobalt atoms with one, two or more copper atoms in the coordination of the probe nucleus was revealed. Conclusions were made about the state of the Co/Cu interfaces. In this work, we measured the NMR spectra on Fe-57 nuclei in a zero magnetic field at 4.2 K for single-component, homogeneous NWs of various diameters from 30 to 200 nm, containing only iron. The resulting spectra demonstrate a significant (up to 1 order) broadening of the line, compared with the NMR spectrum of bulk alpha iron. The possibilities of applying this approach to the analysis of iron-containing layered NWs are discussed.

Generation of electromagnetic radiation. In this work, NW arrays of another type were synthesized – consisting of alternating layers of two different magnetic metals or alloys (for example, Ni/Co or FeNi/FeCo, respectively). It was shown that in such samples, when a current is passed through them, the generation of electromagnetic radiation of the terahertz frequency is possible [4]. In this work, we compare two methods for the synthesis of such NWs and show the advantages of the “double-bath” method. It was shown that NWs with layers from alloys usually generate more intensive signal than NWs consisting of “pure-metal” layers. Various methods have been studied to “output” a signal from a sample. It is known that template matrix with NWs is usually coated on both sides with a copper film. This film absorbs the emerging radiation. In the work, a non-continuous current-carrying coating was made – contacts were deposited on the surface in the form of thin conductive strips. It is shown that the intensity of the emitted signal in this case increases many times. The angular dependence of radiation propagation has been studied. The features of the signal increase in time proved it`s “non-thermal” character. The prospects for using devices with arrays of layered NWs as generators and/or detectors of the radiation of THz frequency are discussed.

This work was supported by the Russian Science Foundation N 22-22-00983 and was done (in part) within the State Tasks of Federal Scientific Research Center (FSRC) “Cryst. and Phot.” RAS (Moscow), Zavoisky Physical-Technical Institute (Kazan), Lebedev Physical Institute (Moscow), IRE (Fryazino).

1. C.R. Martin, Science **266**(5193), 1961–1966 (1994).
2. D.A. Cherkasov, D.L. Zagorskii et al., Phys, Solid State **62**(9), 1695–1705 (2020).
3. S. Chuprakov, I. Blinov, D. Zagorskiy, D. Cherkasov, Phys. Metals Metall. **9**, 933 (2021).
4. Yu.V. Gulyaev, S.G. Chigarev et al., Techn. Phys. Lett. **45**(3), 270–272 (2019).

A.O10

MAGNETISM AND EPR-SPECTRA OF NANOCRYSTALLINE AND AMORPHOUS TiO_2 DOPED BY Fe AND Al

L.S. Molochnikov[1], A.E. Yermakov[2], M.A. Uimin[2], A.S. Minin [2], K.I. Borodin[2], D.W. Boukhvalov[3], D.V. Starichenko[2], A.S. Volegov[3], R.M. Eremina[4], I.V. Yatsyk[4], G.S. Zakharova[5], M.I. Kurkin[2], S.F. Konev[3], A.M. Murzakayev[6], V.S. Gaviko[2]*

[1]Ural State Forest Engineering University, Ekaterinburg, Russia
[2]M. N. Mikheev Institute of Metal Physics, Ural Branch of the Russian Academy of Sciences, Ekaterinburg, Russia
[3]Ural Federal University, Ekaterinburg, Russia
[4]Zavoisky Physical-Technical Institute, Federal Research Center "Kazan Scientific Center of RAS", Kazan, Russia
[5]Institute of Solid State Chemistry, Ural Branch of the Russian Academy of Sciences, Ekaterinburg, Russia
[6]Institute of Electrophysics, Ural Branch of the Russian Academy of Sciences, Ekaterinburg, Russia
[*]E-mail: yermakov.anatoly@gmail.com; yermakov@imp.uran.ru

The work is devoted to the study of the magnetic properties and electronic structure of TiO_2:Fe, Al nanopowders, which are promising for solving various applied problems. The sol-gel methods used to obtain the nanopowders in both crystalline (anatase structure with average size from 3 to 20 nm) and X-ray amorphous states. The magnetic and spectroscopic (EPR) properties of nanocrystalline TiO_2:Fe, Al samples are studied in wide temperature range.

1. The TiO_2:Fe system. The existence of an inhomogeneous magnetic state in TiO_2:Fe samples of different compositions were revealed by EPR-spectroscopy in a wide temperature range. The analysis of the EPR-spectra in the L-, X- and Q-bands allowed us to calculate the quadratic fine structure (D, E) parameters, "axial" and "rhombic" ones, respectively. The value of D turned out to be quite small, which indicates an insignificant anisotropy, which can be ignored describing the magnetic properties of TiO_2:Fe. It was shown that the temperature behavior of different separate components of the integral EPR-spectra can be qualitatively interpreted in the model of coexistence in the TiO_2:Fe system, mainly, dimers with a strong negative exchange interaction and isolated paramagnetic centers. No ferromagnetic state in TiO_2:Fe-based samples after etching of as-prepared samples were detected.

2. The TiO_2:Fe, Al system. The EPR spectra of crystalline samples TiO_2:Fe doped with aluminum exhibit resonance with a g-factor of 4.3 from Fe^{3+} ions with rhombohedral distortions. The fraction of Fe^{3+} with rhombohedral distortions increases with increasing aluminum content. For the amorphous state at Al doping, the resonance with a g-factor of 4.3 is completely dominant in the EPR-spectrum. The DFT-calculation shows that aluminum prefers to be localized near iron ions, distorting the nearest Fe^{3+} environment. The complex integral EPR-spectrum of all samples was fitted with a sufficient accuracy by three separate resonance lines with different widths and intensities. The temperature dependence of the integral intensity of above separate EPR resonance components is investigated and it was established that EPR-spectrum can be described by the coexistence of paramagnetic centers (isolated Fe^{3+} ions) and iron clusters with negative exchange interactions as well.

The support by RFBR (Grant # 20-02-00095) is acknowledged.

A.O11

CLASSICAL AND QUANTUM EFFECTS OF THE MAGNETIZATION DYNAMICS INDUCED BY PICOSECOND PULSE OF SPIN CURRENT

V.V. Yurlov[1*], *K.A. Zvezdin*[2], *A.K. Zvezdin*[2]

[1]Moscow Institute of Physics and Technology, Dolgoprudny, Russia
[2]Prokhorov General Physics Institute of the Russian Academy of Sciences, Moscow, Russia
[*]E-mail: yurlov.vv@phystech.edu

The classical dynamics of the magnetic moment in an easy-plane magnet induced by picosecond spin current pulse is considered based on earlier research [1]. Analytical expressions were obtained to describe the processes of spin reorientation for the magnetic system with weak dissipation, as well as the effective Lagrangian and thermodynamic potential of these magnetic structures. To present the magnetization switching process the magnetization switching diagrams were constructed depending on the external parameters such as the electric current density, external magnetic field, and electric current pulse duration (see Fig. 1). We can see that at a fixed electric current, both magnetization switching and its absence can be observed depending on the magnitude of the magnetic field. Note that switching is also possible at a zero magnetic field at a high electric current density (see in Fig. 1a). Figure 1b shows the switching diagram depending on pulse duration and the magnitude of the spin current. The switching pattern indicates a strong stochasticity at a small value of pulse duration. Then there is a region of complete absence of switching (yellow area in Fig. 2b). After reaching some critical current density at fixed pulse duration, magnetization switching is observed stable (blue area in Fig. 1b). The effect can be associated with the relaxation time of the system. When the pulse duration is comparable to the characteristic relaxation time, the switching process may or may not be observed depending on their ratio.

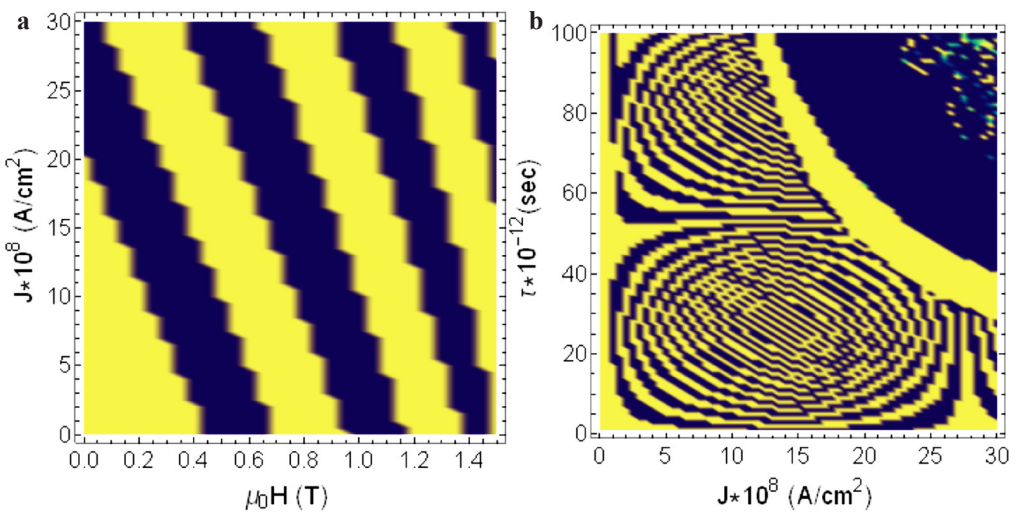

Figure 1. The switching diagrams for the classical dynamics of the magnetic moment in the coordinates electric current density – magnetic field (**a**) and electric current pulse duration – electric current density (**b**). The yellow area of the diagrams corresponds to the absence of magnetization switching and the blue area corresponds to the magnetization switching.

In the case of low temperatures and weak dissipation, quantum properties can be observed in the magnetic system [1]. The effective Lagrangian written for description of the spin dynamics makes it possible to construct a quantum bit model similar to the simplest type of charge qubit, which is considered in the framework of the Josephson junction theory [2, 3]. Quantum effects in the Josephson junction can be described by considering the charge and phase as generalized momentum and coordinate operators, respectively. In our case, these quantities are the projection of the magnetization onto the direction perpendicular to the plane of the magnetic film (or the polar angle) and the azimuthal angle, respectively.

This model makes it possible to determine the parameters of the magnetic system (dissipation time, geometrical dimensions) at which the implementation of quantum effects is possible.

The research has been supported by RSF grant No.19-12-00432.

1. A.K. Zvezdin, ZhETF **122**(4(10)), 879–885 (2002) [in Russian].
2. A. Kringhoj et al., Phys. Rev. B **97**, 060508 (2018).
3. D. Riste et al., Nat. Commun. **4**, 1913 (2013).

A.O12

THE INFLUENCE OF EXCHANGE CORRELATION FUNCTIONAL ON THE PROPERTIES OF $Mn_2V(Al,Si)$ HEUSLER ALLOYS

V.D. Buchelnikov[1*], *D.R. Baigutlin*[1], *V.V. Sokolovskiy*[2], *O.N. Miroshkina*[1,2]

[1]Chelyabinsk State University, Chelyabinsk, Russia
[2]University of Duisburg-Essen, Duisburg, Germany
[*]E-mail: buche@csu.ru

Half-metallic (HM) materials attract interest due to their potential spintronics applications involving novel thermoelectrics, spin filters, data storage, and other spin-based devices [1, 2]. The HMs exhibit metallic behavior in one spin channel and semiconducting behavior in the other spin channel around the Fermi energy. Mn_2-based Heusler alloys with HM are particularly interesting as they host Mn^{3+} ions with d^4 electronic configuration and strong ferromagnetic or antiferromagnetic correlations between the Mn atoms. These alloys have low magnetic moments and reduced stray fields, making them promising materials for spintronics applications. Mn_2VAl was the first to be proposed as a HM ferromagnet and it has been investigated both experimentally [3] and theoretically [4, 5]. One of the other potential HM ferromagnet is the Mn_2VSi alloy [6].

Recently, we reported that the implementation of electron correlation effects using the strongly constrained and appropriately normed (SCAN) meta-GGA functional yields nearly degenerate HM and metallic phases in Mn_2ScSi and Mn_2VGe [7, 8]. It has been suggested that switching between these two phases could be achieved by applying volume change within the cubic phase, by the application of an external magnetic field or doping of alloy by fourth element.

The aim of this work is to provide a theoretical description of Mn-V-Al-Si Heusler alloy, which is shown to demonstrate a switchable low (LMS) to high magnetic state (HMS) behavior. We show that such a switching mechanism can be treated via the exchange-correlation effects described within the SCAN functional. Stoichiometric Mn_2VAl and Mn_2VSi are found to display an energy difference between the LMS and HMS phases, which is too large to allow easy switching between these two phases. For this reason, we explore the effects of Si or Al doping, which drives the LMS and HMS phases into near degeneracy. It is shown that the effect of doping significantly decreases the energy between the LMS and HMS phases. These alloys are more cost effective and stable to segregation.

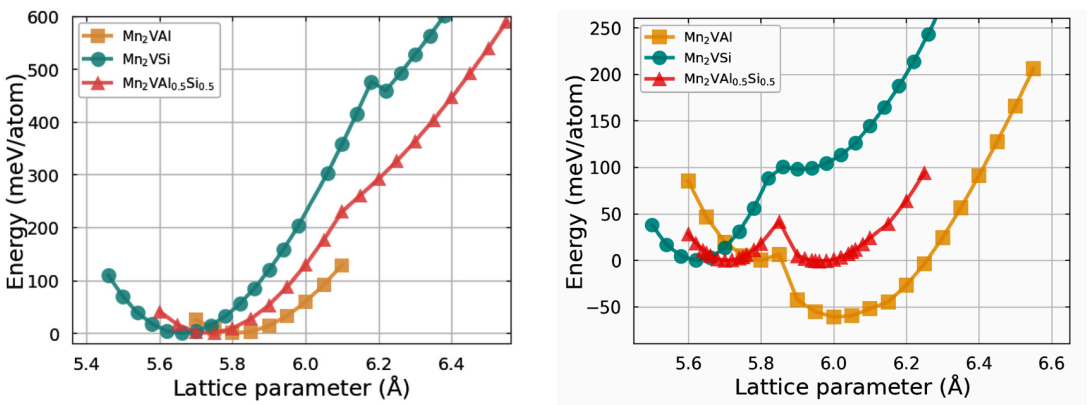

Figure 1. The dependence of energy from lattice parameter for Mn_2VAl, Mn_2VSi and $Mn_2VAl_{0.5}Si_{0.5}$ for PBE (left panel) and SCAN (right panel) functional.

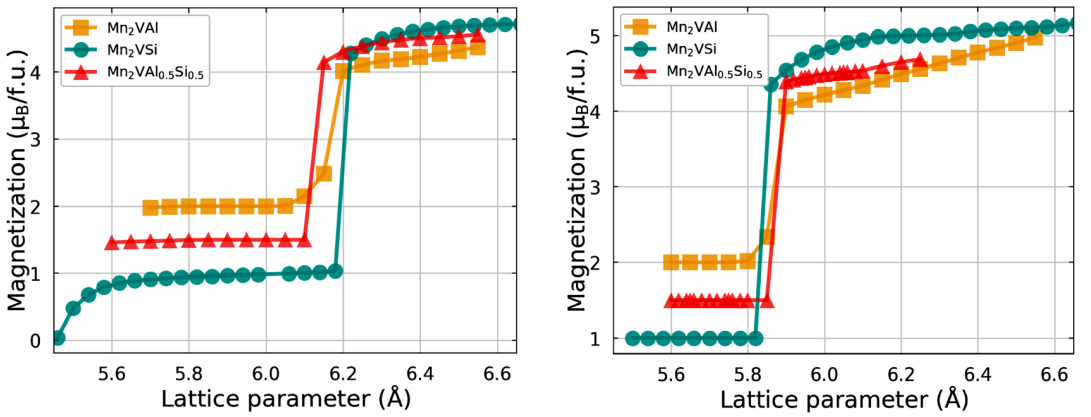

Figure 2. The dependence of magnetic moment from lattice parameter for Mn_2VAl, Mn_2VSi and $Mn_2VAl_{0.5}Si_{0.5}$ for PBE (left panel) and SCAN (right panel) functional.

Calculations were performed using the DFT scheme with the PAW method as implemented in the VASP package [9]. The PBE parametrization [10] of the GGA and the SCAN meta-GGA [11] were taken for treating exchange correlation effects. The cut-off energy of 450 eV for the plane waves was used. The Monkhorst-Pack scheme [12] was applied for generating k-points in the reciprocal space. A grid of 11×11×11 k-points was used in the relaxation procedure, while a grid of 25×25×25 k-points was used in density-of-states (DOS) and band structure computations. 16 atom cell was taken in calculations.

The results of geometry optimization for Mn_2VAl, Mn_2VSi and $Mn_2VAl_{0.5}Si_{0.5}$ are presented on the Fig. 1.

It can be seen that when using the PBE functional, the dependence of the energy on the lattice parameter has one minimum for all three alloys. In the case of the SCAN functional, this dependence has two minima, which correspond to two values of magnetic moment: LMS and HMS (Fig. 2).

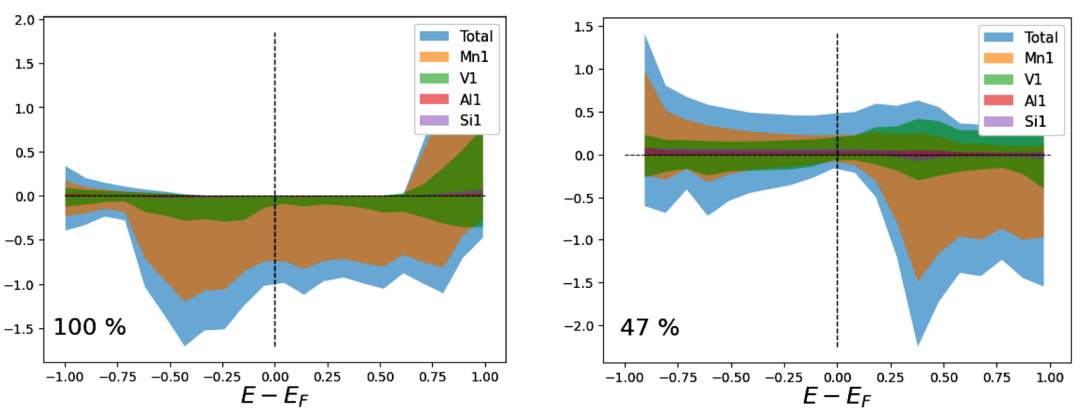

Figure 3. Total and partial DOSs of $Mn_2VAl_{0.5}Si_{0.5}$ in the LMS (left panel) and HMS (right panel) phases for SCAN functional calculated at the corresponding equilibrium volumes.

The same trend in the dependence of magnetization on the lattice parameter takes place for the PBE functional (Fig. 2, left panel). For $Mn_2VAl_{0.5}Si_{0.5}$, the energy difference between LMS and HMS is 0.65 meV. This allows the transition from LMS to HMS and vice versa. Figure 3 shows that LMS has HM behavior and HMS has metallic behavior. These properties can be used in spintronics.

Figure 3 shows that the LMS has 100% polarization at the Fermi level, which corresponds to the HM state. Polarization in HMS is about 50%, and this state is metallic. Thus, we can conclude that in $Mn_2VAl_{0.5}Si_{0.5}$ we can switch between the low magnetic HM state and the high magnetic metallic state.

Support by RSF # 22-12-20032 is acknowledged.

1. B. Dieny et al., Nat. Electron. **3**, 446 (2020).
2. J. Puebla, J. Kim, K. Kondou, Y. Otani, Commun. Mater. **1**, 1 (2020).
3. C. Jiang, M. Venkatesan, J. Coey, Solid State Commun. **118**, 513 (2001).
4. R. Weht, W.E. Pickett, Phys. Rev. B **60**, 13006 (1999).
5. R. Umetsu et al., Phys. Rev. B **99**, 134414 (2019).
6. K. Özdogan, I. Galanakis, E. ¸Sasioglu, B. Aktas, J. Condens. Matter Phys. **18**, 2905 (2006).
7. V.D. Buchelnikov et al., Phys. Rev. B **103**, 054414 (2021).
8. V.D. Buchelnikov et al., Adv. Theory and Simul. **4**, 2100311 (2021).
9. G. Kresse, J. Furthmüller, Phys. Rev. B **54**, 11169 (1996).
10. J. Perdew, K. Burke, M. Ernzerhof, Phys. Rev. Lett. **77**, 3865 (1996).
11. J. Sun, A. Ruzsinszky, J.P. Perdew, Phys. Rev. Lett. **115**, 036402 (2015).
12. H.J. Monkhorst, J.D. Pack, Phys. Rev. B **13**, 5188 (1976).

A.O13

INTERFACE EFFECTS IN HETEROGENEOUS INTEGRATION OF $Bi_3Fe_5O_{12}$ FILMS

A.S. Fedorov[1,2], *S.S. Safonov*[1], *A.A. Fedorova*[1,2], *S.A. Nikitov*[1,2], *A.I. Stognii*[3], *M.V. Logunov*[1*]

[1]Kotel'nikov Institute of Radio-Engineering and Electronics of RAS, Moscow, Russia
[2]Moscow Institute of Physics and Technology, Dolgoprudny, Moscow Region, Russia
[3]Scientific and Practical Center for Materials Science of NAS, Minsk, Belarus
[*]E-mail: logunov@cplire.ru

To use the numerous advantages of spintronics, it is necessary to integrate the corresponding materials and nanostructures with the available microelectronics technologies. The search for integration ways to expand the functional properties of promising electronic and spintronic information storage devices and artificial neural networks is actively underway [1–6]. A number of spintronics materials, including those with record values of magneto-optical effects of $Bi_3Fe_5O_{12}$, cannot be synthesized in bulk due to the absence of a stable state region in the phase diagram.

This report presents the results of the synthesis of nanoscale polycrystalline garnet films on quartz and silicon substrates by pulsed laser deposition and ion beam sputtering-deposition. To improve the quality of the $Bi_3Fe_5O_{12}$ films, sputtering of $Gd_3Ga_5O_{12}$ intermediate layer was used; to create 2D- and 3D-structures, the $Bi_3Fe_5O_{12}$ film was structured in area and thickness by ion beam sputtering with oxygen ions (Fig. 1). Since spintronics devices require nanometer thickness films, the properties of the layers on the interface are of particular importance. Figure 2 shows the temperature dependences of the magnetic circular dichroism (MCD) spectra of such an interface layer with an effective thickness of ~1 nm. The presence of a magnetic moment compensation point indicates that the intermediate $Gd_3Ga_5O_{12}$/quartz nanolayer exhibits chemical activity in the form of Gd^{3+} ions diffusion into the interface layer of the $Bi_3Fe_5O_{12}$ film, and a decrease in the Neel temperature indicates a similar process with Ga^{3+} ions. Thus, using MCD method, it is possible to obtain information about extremely thin layers of films comparable in thickness to the crystal lattice parameter.

Support by RSF (#19-19-00607) and RFBR (#18-29-27020) is acknowledged.

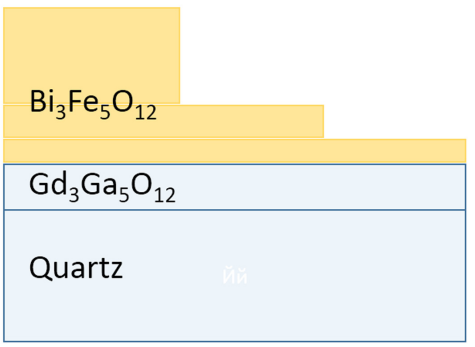

Figure 1. Garnet film on quartz substrate.

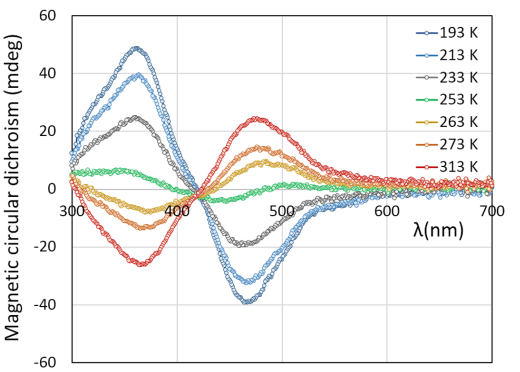

Figure 2. Temperature-dependent MCD spectra for interface layer of $Bi_3Fe_5O_{12}$ film.

1. B. Dieny, I.L. Prejbeanu, K. Garello et al., Nature Electronics **3**, 446 (2020).
2. H.S. Kum, H. Lee, S. Kim et al., Nature **578**, 75 (2020).
3. L. Caretta, S.-H. Oh, T. Fakhrul et al., Science **370**, 1438 (2020).
4. I. Razdolski, A.L. Chekhov, A.I. Stognij, A. Stupakiewicz, Phys. Rev. B **100**, 045412 (2019).
5. M.V. Logunov, S.S. Safonov, A.S. Fedorov et al., Phys. Rev. Appl. **15**, 064024 (2021).
6. Yu.B. Kudasov, M.V. Logunov, R.V. Kozabaranov et al., Appl. Phys. Lett. **120**, 122403 (2022).

THE EFFECT OF MAGNON-MAGNON DRAG IN MAGNETIC INSULATOR LAYERS THROUGH OF NON MAGNETIC METAL LAYER

I.I. Lyapilin

Institute of Metal Physics UB RAS, Ekaterinburg, Russia
E-mail: lyapilin@imp.uran.ru

As you know, the conventional Coulomb drag effect occurs in two-dimensional electron gases separated by an insulator barrier. When one of the conductive layers carries a current, the momentum transfer due to Coulomb interaction leads to a current in another conductive layer. This current drag phenomenon has been discovered in a different system with entirely different physical mechanisms [1]. In transport phenomena with spin-polarized charge carriers, subsystems of electrons with spins (up) and spins (down) have different drift velocities. In this case, the Coulomb interaction between electrons leads to the spin drag effect [2]. For two metallic layers separated by a ferromagnetic insulator (FI) layer, the drag effect can be induced by a non-equilibrium magnon current in the FI layer [3].

Here we consider the drag effect of the spin-wave (magnon) current caused by the transfer of angular momentum through the conductive layer due to the exchange interaction between localized magnetic moments and spins of conducting electrons at the interfaces of such a structure as magnetic insulator/non-magnetic metal/magnetic insulator (MI/NM/MI).

In this context, the spin transfer through the interface in the mentioned-above hybrid structures has been investigated. A distinctive feature of the considered effect is the excitation of a spin-wave current in a magnetic insulator through the interaction of magnons with an inhomogeneous electric field. Magnetic dipoles moving in an electric field acquire both the Aharonov-Casher phase and a force similar to the Lorentz force that leads to an effect analogous to the Hall effect. The non-equilibrium distribution of magnons is described by the non-equilibrium Bose-Einstein distribution [4].

The interface exchange interaction between the non-equilibrium localized moments and the spins of conducting electrons in a non-magnetic metal (NM) leads to the appearance of spin accumulation and diffusive spin current in NM [5]. The direction of the diffusive spin current can be determined by a temperature gradient applied to NM. If the latter consists of a metal with a large spin-orbit interaction, the spin current provokes a charge current in NM, the direction of which is orthogonal to the spin current. In a three-layer hybrid structure of MI/NM/MI, the spin current arising in NM gives rise to the excitation of a spin-wave current in the second layer of MI.

Thus, we have predicted a new effect: the dragging of magnons (the magnon drag) through the conductive electric layer by the exchange interaction of localized magnetic moments and spins of conducting electrons at the interfaces of the hybrid structure.

1. A.G. Rojo, J. Phys. Cond. Matter. **119**, R31–R52 (1999).
2. I. D'Amico, G. Vignale, Phys. Rev. **62**, 4854–4857 (2000).
3. S. S.-L. Zhang, S. Zhang, Phys. Rev. Lett. **109**, 096603–5 (2012).
4. F. Meier, D. Loss, Phys. Rev. Lett. **90**, 167204–4 (2003).
5. H.M. Bikkin, I.I. Lyapilin, Non-Equilibrium Thermodynamics and Physical Kinetics. Berlin: Walter de Gruyter GmbH, p. 436 (2021).

NON-RESONANT BROADBAND SPIN-TORQUE DIODE RECTIFICATION OF MICROWAVE CURRENT IN A MTJ WITH IN-PLANE MAGNETIZATION OF THE FREE LAYER

G.A. Kichin[1*], *P.N. Skirdkov*[1,2], *K.A. Zvezdin*[1,2]

[1]New spintronic technologies, Russian Quantum Center, Skolkovo Innovation Center, Moscow, Russia
[2]Prokhorov General Physics Institute of the Russian Academy of Sciences, Moscow, Russia
*E-mail: g.kichin@nst.tech

The growing interest in automatic process monitoring systems requires a large number of sensors and control devices. Special attention is paid to the size of the device and power consumption. For small sizes, ultra-low power consumption and power efficiency becomes a problem. To solve this problem, an important task is to explore new approaches that can be used to make monitoring sensors autonomous, low-power, and wirelessly powered.

A promising solution to this problem are structures based on a magnetic tunnel junction (MTJ) [1]. Devices of this type are multilayer structures of the nanometer scale in the form of nanopillars, in which the key elements are ferromagnetic layers separated by dielectric layers. MTJ proved to be promising for use as memory cells, nanooscillators, the basis for spectrum analyzers, communication devices and random bit generators, as well as nodes for neuromorphic computing systems. Recent studies have shown that these devices are also capable of converting microwave currents into DC voltage due to the spin-torque diode rectification effect [1]. In the case of low radiation power, MTJ-based devices demonstrate significantly better signal rectification characteristics than Schottky diodes [2].

Recent papers have reported that MTJ-based devices are capable of signal rectification over a wide frequency range. Theoretical [3] and experimental [4, 5] studies show that the rectification effect is usually observed in two cases. In one case, the magnetization in the sample is oriented in the plane of the layers, and an external magnetic field is additionally applied, which is directed perpendicular to the magnetization. In other case, the sample must have magnetic anisotropy and a perpendicular magnetization component must be present. Due to the high complexity, not all physical effects that are observed in MTJ-based devices have been fully studied.

In this work, we consider and analyze various mechanisms of operation of MTJ-based devices. In addition, we report a new type of broadband, nonresonant rectification mechanism with no-power threshold, where the inhomogeneity of the free layer magnetization plays an important role. We tested samples of round and elliptical shapes and investigated their rectification properties. We used the ST-FMR method to measure and analyze the rectified voltage as a function of the frequency of the input signal and the applied magnetic field. In experiments, we observed rectification in a wide frequency range, from fractions of a GHz to several GHz, which is much larger than previously reported. We also found that rectification is observed in the magnetic tunnel junction even when the free layer magnetization is orientated in the plane of the sample. The highest values of the rectification voltages are observed near the compensation point for the demagnetization and anisotropy fields and decreases with increasing external magnetic field. In addition, we present the results of micromagnetic simulations, which provide insight into the dynamics of the system's magnetization.

Support by RSF №19-12-00432 (РНФ №19-12-00432).

1. A. Tulapurkar et al., Nature **438**, 339 (2005).
2. S. Miwa et al., Nat. Mater. **13**, 50 (2014).
3. O. Prokopenko et al., J. Appl. Phys. 111, 123904 (2012).
4. B. Fang et al., Phys. Rev. Appl. **11**, 014022. (2019).
5. M. Tarequzzaman et al., Appl. Phys. Lett. **112**, 252401 (2018).

SPIN VALVES FOR STUDYING HELICOIDAL STATES IN NANOLAYES OF CHIRAL Dy AND Ho HELIMAGNETS

*R.S. Zavornitsyn**, *M.A. Milyaev, L.I. Naumova, T.P. Krinitsina, V.V. Proglyado, V.V. Ustinov*

M.N. Mikheev Institute of Metal Physics, Ekaterinburg, Russian Federation
*E-mail: zavornitsyn@imp.uran.ru

The study of nanostructures based on rare earth metals (Dy, Ho) provides information on magnetic phases in thin layers of rare earth magnets [1–5]. This information can be used in developing new nanospintronic devices.

To study the magnetic structure in ultrathin rare-earth layers, standard research methods, e.g. neutron diffraction, cannot be used because of small volume the material, therefore there is a need for new research methods. The approach we propose involves studying the magnetotransport properties of "spin valve" as well as other nanostructures containing a nanolayer of a helimagnet (HM) under study. It is important that our approach is not associated with the use of "megascience" installations, but is based on the use of conventional laboratory methods for measuring magnetoresistance.

Our spin valves consist of ferromagnetic (FM) layers of $Co_{90}Fe_{10}$, non-magnetic (NM) copper layer, HM-layer, and antiferromagnetic (AFM) $Fe_{50}Mn_{50}$. A typical spin valve is shown in Fig. 1. The FM-layer adjacent to AFM is called the "pinned" layer; we denote the magnetic moment of this layer as $\mathbf{M}_p$. Next layer is the rare earth one. The second FM-layer is called the "reference" layer, its magnetic moment is $\mathbf{M}_r$. Next comes the non-magnetic layer. The last ferromagnetic layer (with magnetic moment $\mathbf{M}_f$) is called "free" layer because it can be remagnetized in a weak field.

The change in the magnetic state of the HM-layer e.g. due to magnetic phase transition affects the magnetization reversal of a nanostructure and hence magnetoresistance.

Trilayer structures containing a rare-earth layer is also studied.

The spin valves, as well as the metal/HM/metal trilayers were fabricated by magnetron sputtering. The study of magnetic and magnetotransport properties was carried out in the temperature range of 23 to 293 K. The microstructure of the samples was investigated by X-ray diffractometry at room temperature.

It is established that the $Co_{90}Fe_{10}/Cu/Co_{90}Fe_{10}$-layers have a perfect microstructure and smooth interfaces, which is important for obtaining large values of magnetoresistance. The Dy- and Ho-nanolayers are polycrystalline with the ⟨0002⟩ axial texture, with the axis being perpendicular to the film plane. This orientation is preferable for observing changes in the magnetoresistive properties of spin valves caused by the formation of an antiferromagnetic structure in a helimagnet nanolayer.

For Dy- and Ho-nanolayers of various thicknesses, the temperature of the paramagnet-antiferromagnet transition was estimated.

The features of the formation of unidirectional anisotropy at the Dy(Ho)/$Co_{90}Fe_{10}$ interface during the paramagnet-antiferromagnet transition are studied.

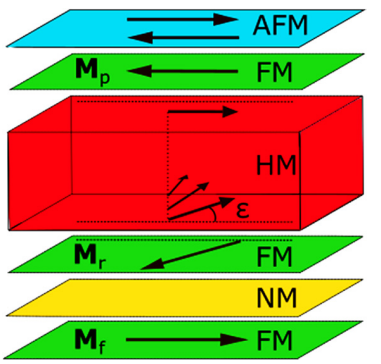

Figure 1. Schematic of a chiral spin valve. The arrows show the magnetic moments of a fragment of the helimagnet Dy(Ho)-layer, an antiferromagnetic $Fe_{50}Mn_{50}$-layer, and ferromagnetic $Co_{90}Fe_{10}$-layers: pinned $\mathbf{M}_p$, reference $\mathbf{M}_r$, and free $\mathbf{M}_f$.

An external magnetic field is found to cause the rotation of helicoid in a holmium nanolayer. The mobility of the helicoidal structure can be due to the presence of an uncompensated magnetic moment.

The magnetoresistance data obtained on the Dy-based spin valves show that the angle ε between the magnetic moments at the boundaries of the Dy-layer depends on temperature (Fig. 2). A significant change in this angle, observed in the range of existence of antiferromagnetic helicoidal ordering in Dy, reflects the change in the spatial period of the magnetic spiral with temperature.

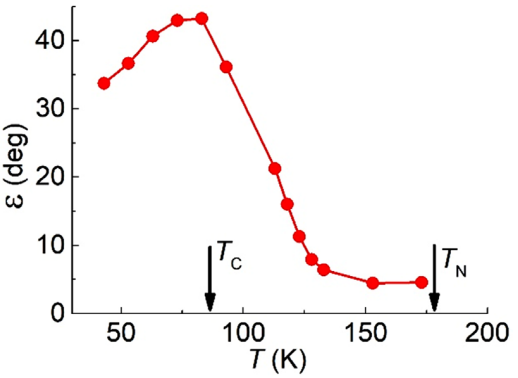

Figure 2. Temperature dependence of the angle ε between magnetic moments at the boundaries of the dysprosium layer.

The features of the deformation of an antiferromagnetic helicoid by a magnetic field in ultrathin Dy-layers are studied. In spin valves with a bottom position of the Dy-layer, the transition from low resistance to high-resistance state is observed, if temperature is decreased or magnetic field is increased. This transition is accompanied by an inversion of the field dependence of the magnetoresistance.

The fields and temperatures, at which the magnetic moments of the Dy- and $Co_{90}Fe_{10}$-layers are compensated, are estimated and it is found how these quantities depend on the Dy-nanolayer thickness.

The current research on chiral spintronics is supported by Russian Science Foundation (project No. 22-22-00220).

1. V.V. Ustinov, M.A. Milyaev, L.I. Naumova, R.S. Zavornitsyn, T.P. Krinitsina, V.V. Proglyado, J. Surf. Invest. **15**, 1278 (2021).
2. L.I. Naumova, R.S. Zavornitsyn, M.A. Milyaev, M.V. Makarova, V.V. Proglyado, V.V. Ustinov, IEEE Trans. Nanotech. **20**, 866 (2021).
3. L.I. Naumova, R.S. Zavornitsyn, M.A. Milyaev, M.V. Makarova, V.V. Proglyado, V.V. Ustinov, Phys. Metals Metall. **122**, 581 (2021).
4. R.S. Zavornitsyn, L.I. Naumova, M.A. Milyaev, M.V. Makarova, V.V.Proglyado, I.K.Maksimova, V.V. Ustinov, Current Appl. Phys. **20**, 1328 (2020).
5. R.S. Zavornitsyn, L.I. Naumova, M.A. Milyaev, M.V. Makarova, T.P. Krinitsina, V.V. Proglyado, V.V. Ustinov, Phys. Metals Metall. **121**, 624 (2020).

A.O17

MATHEMATICAL MODELLING OF THE SOT-MRAM ELEMENT BASED ON THE SPIN-HALL EFFECT

*N.V. Ostrovskaya**, *V.A. Skidanov, Iu.A. Iusipova*

Institute for Design Problems in Microelectronics RAS, Moscow
*E-mail: ost.ippm@yandex.ru

The model of the SOT-MRAM memory element was analysed using the methods of the qualitative theory of dynamical systems [1, 2]. The basis for modelling is the fundamental Landau-Lifshits equation written for the case of the uniform approximation with the dissipative term in the Gilbert form. After the normalization and algebraic transformations, this equation takes the following form resolved with respect to the temporal derivative

$$\frac{\partial \mathbf{m}}{\partial \tau} = -[\mathbf{m} \times \mathbf{f}] + \alpha \mathbf{f} - \alpha \mathbf{m}(\mathbf{m}, \mathbf{f}).$$

Here

$$\mathbf{f} = (h + km_x + bjm_z)\mathbf{e}_x - bj\mathbf{e}_y + (-bjm_x - m_z)\mathbf{e}_z$$

is the equivalent of the effective field for the rectiangle SOT-MRAM element controlled by the spin current j, $b = \theta_{SH}\eta$, θ_{SH} is the angle of the spin-Hall effect, η is the coefficient of the spin-Hall effectiveness [3]. The resulting equations for description of the magnetization dynamics in the free layer of the memory element in this case are

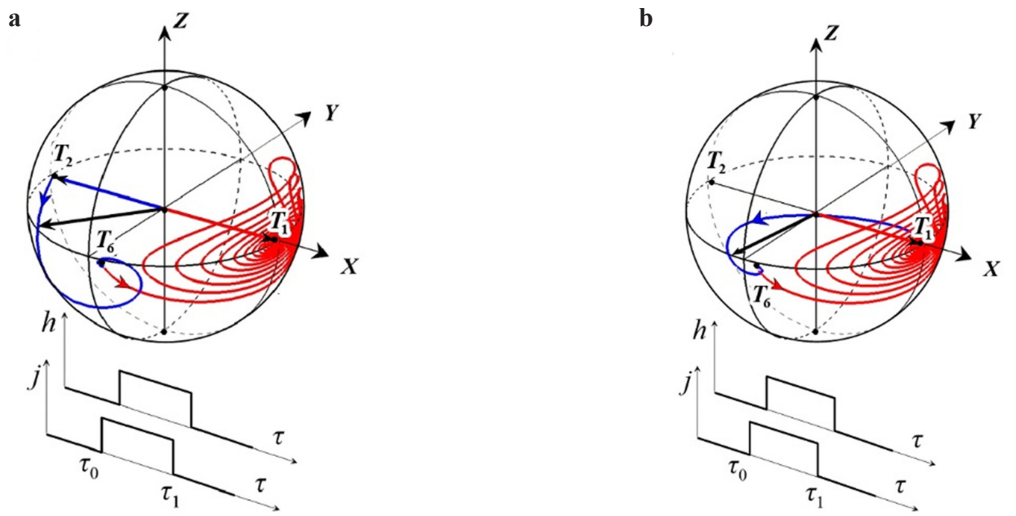

Figure 1. Switching of the SOT memory element with the positive impulses of current and field. The trajectories of the end of the magnetization vector start from the points $T_{1,2}(\pm1,0,0)$: **a** the trajectory coming from the point $T_2(-1,0,0)$ tends to the stable focus T_2 (blue line) and after the field and current were turned off, it comes to the point T_1 (red line) – switching; **b** the trajectory starting from the point T_1 tends to the stable point T_6 (blue line), and after the field and current were turned off, it returns back to the point T_1 – no switching.

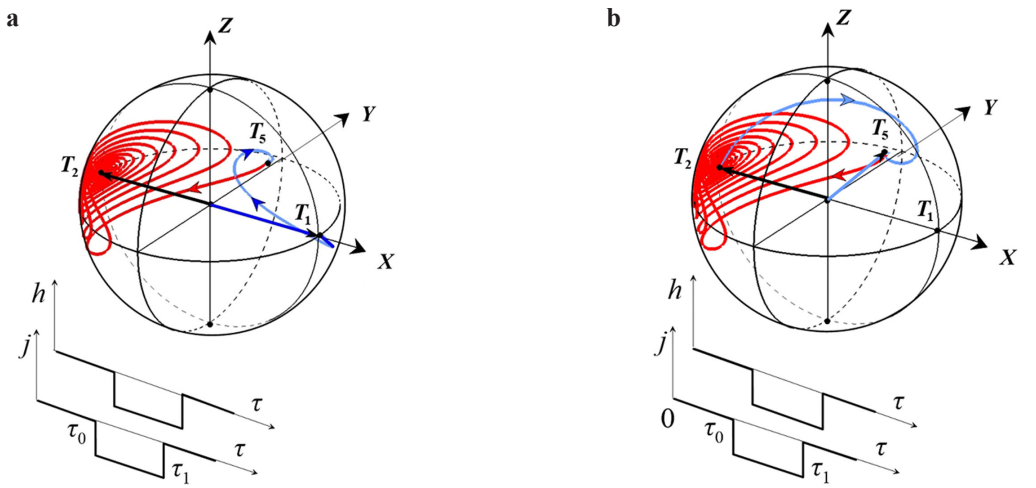

Figure 2. Switching of the SOT memory element with the negative impulses of current and field: **a** the trajectory starting from the point $T_1(+1,0,0)$ tends to the stable focus T_5 (blue line) and after the field and current were turned off, it comes to the point T_2 (red line) – switching; **b** the trajectory starting from the point T_2 tends to the stable point T_5 (blue line), and after the field and current were turned off, it returns to the point T_2 – no switching.

$$
\begin{aligned}
dm_x/d\tau &= -bjm_z + bjm_x m_y + m_y m_z + a(h + km_x + bjm_z - hm_x^2 - km_x^3 + bjm_x m_y + m_x m_z^2),\\
dm_y/d\tau &= -bjm_x^2 - m_x m_z - hm_z - km_x m_z - bjm_z^2 + a(m_y m_z^2 - hm_x m_y - km_y m_x^2 - bjm_x^2 - bjm_z^2),\\
dm_z/d\tau &= hm_y + km_x m_y + bjm_y m_z + bjm_x + a(bjm_y m_z + m_z^3 - bjm_x - m_z - hm_x m_z - km_x^2 m_z),
\end{aligned}
\tag{1}
$$

where m_x, m_y, m_z are the components of the magnetization vector in the free layer, k is the normalized anisotropy coefficient, and α is a dimensionless damping parameter. We calculated the bifurcation diagram for this system of equations and revealed the values of the control parameters h and j at which the system has two, four or six singular points. The magnetization dynamics for the parameters when there are two singular points is presented in the Figs. 1 and 2.

1. L.P. Shilnikov, A.L. Shilnikov et al., Methods of Qualitative Theory in Nonlinear Dynamics, vol. 1, 2. World Scientific (2003).
2. N.V. Ostrovskaya, Iu.A. Iusipova, Phys. Metals Metall. **120**(13), 1291–1298 (2019).
3. C. Song, R. Zhang, L. Liao et al., Prog. Mater. Sci. **118**, 100761 (2021).

A.O18

MAGNETIC AND MOSSBAUER STUDIES OF Fe_xCO_{1-x} NANOWIRES

I.V. Perunov[1*], *K.V. Frolov*[1], *M.A. Chuev*[2], *I.M. Doludenko*[1], *D.L. Zagorskii*[1], *N.C. Chumakov*[3], *I.S. Lyubutin*[1]

[1]Shubnikov Institute of Crystallography FSRC "Crystallography and Photonics" RAS, Moscow, Russia
[2]Valiev Institute of Physics and Technology RAS, Moscow, Russia
[3]National Research Centre "Kurchatov Institute", Moscow, Russia
[*]E-mail: igor_v_perunov@mail.ru

Currently, much attention is paid to the synthesis and properties of magnetic nanowires [1] due to the prospects of their applications. Such nanoobjects can be used in magnetic sensors, spintronics devices, hydrogen fuel cell electrodes and in biomedical technologies, including antitumor therapy.

Fe_xCo_{1-x} nanowires (x = 6.7; 15.7; 29.7; 38.6; 38.2; 46.5; 52.15; 54.8; 59; 64.4) were obtained by electrochemical deposition in the pores of polymer track membranes with a pore diameter of 100 nm and studied by electron microscopy, Mossbauer spectroscopy on ^{57}Fe nuclei and vibrational magnetometry. Magnetometry data and Mossbauer spectroscopic measurements show that nanowires have pronounced ferromagnetic properties, and the magnetic moments of Fe-Co nanoparticles are oriented mainly in the direction of the wire axis. Such materials can be considered as quasi-one-dimensional nanostructured ferromagnetic systems. The generalized theoretical Stoner-Wolfart model was used to describe the magnetic properties and calculate the basic physical parameters of nanowires [2, 3].

The work was supported by the Ministry of Science and Higher Education within the framework of the state tasks of the Federal Research Institute "Crystallography and Photonics" of the Russian Academy of Sciences and the K.A. Valiev Institute of Physics and Technology of the Russian Academy of Sciences. The equipment of the Center for Collective Usage of the A.V. Shubnikov Institute of Crystallography of the Federal Research Institute "Crystallography and Photonics" of the Russian Academy of Sciences and the equipment of the resource Center for Electrophysical Methods of the National Research Center "Kurchatov Institute" were used.

1. M. Vázquez (ed.), Magnetic Nano- and Microwires: Design, Synthesis, Properties and Applications. – 2nd Edn., Woodhead Publishing 997 p., 2020.
2. A.M. Afanas'ev, M.A. Chuev, J. Hesse, JETP **89**(3), 533–546 (1999).
3. M.A. Chuev, J. Hesse, J. Phys.: Condens. Matter **19**(50), 506201 (2007).

A.O19

MONTE CARLO SIMULATION OF MAGNETIC PROPERTIES OF SPIN-VALVE NANOSTRUCTURES

*E.V. Drovorub, A.S. Egorina, N.I. Piskunova, P.V. Prudnikov**, *V.V. Prudnikov*

Dostoevsky Omsk State University, Omsk, Russia
*E-mail: prudnikovpv@omsu.ru

Modern trends in studies of magnetism include a shift of fundamental interest from bulk samples to nanosized structures made of ultrathin magnetic films. Synthetic antiferromagnetic nanostructures with the GMR-effect consist of ferromagnetic layers divided by intermediate nonmagnetic metallic layers. Effective antiferromagnetic coupling between neighboring ferromagnetic layers is ensured by choosing the thickness of the intermediate layer through long-range and oscillating interlayer exchange interaction. A drawback of these structures is the high saturation field ($H_s \approx 20$ kOe) needed for the parallel orientation of magnetization in their layers and obtaining GMR.

The creation of spin-valve systems is a great improvement in structures that experience the GMR-effect. However, the direction of magnetization in one ferromagnetic layer is determined by its interaction with an additional antiferromagnetic layer. To reduce exchange coupling between magnetic layers, a nonmagnetic intermediate conductor from such noble metals as Cu, Ag, or Au is made thick enough (1.5 to 5 nm) for the orientation of magnetization in a layer not coupled with an antiferromagnetic layer to change freely under the influence of a weak external magnetic field. An advantage of the spin-valve structures are fields of saturation (H_s = 5–50 Oe) much smaller than in multilayered magnetic structures. Introduced in 1991 [1], spin-valve structures have found wide application in, e.g., read heads of HDDs with data densities of more than 100 gigabytes per square inch.

A variety of more complicated spin-valve structures have been designed [2] that contain a three-layered antiferromagnetic system Co/Ru/Co [1]. This system magnifies the effect antiferromagnetic IrMn has on a freely magnetizing ferromagnetic layer. The aim of this work was to model the magnetic properties of such spin-valve structure and identify the effect magnetic anisotropy and intra- and interlayer exchange interaction have on those of hysteresis in a spin valve upon varying the thickness of nanosized ferromagnetic films.

Exchange interaction in structures with magnetization in plane of the ferromagnetic film are characterized by the Hamiltonian of the anisotropic Heisenberg model [3]

$$\mathscr{H} = -\sum_{\langle i,j\rangle} J_{ij}\{S_i^x S_j^x + 0.8 S_i^y S_j^y + (1-\Delta_1(N)) S_i^z S_j^z\} - h\sum_i S_i^x , \quad (1)$$

and structures with magnetization normal to the plane of films are described by

$$\mathscr{H} = -\sum_{\langle i,j\rangle} J_{ij}\{(1-\Delta_2(N))(S_i^x S_j^x + S_i^y S_j^y) + S_i^z S_j^z\} - h\sum_i S_i^z . \quad (2)$$

Here, $\mathbf{S}_i = (S_i^x, S_i^y, S_i^z)$ is the classical unit vector of a spin fixed in the ith center of the FCC lattice of a ferromagnetic film (cobalt), and $\Delta_{1,2}(N)$ are parameters of anisotropy caused by the crystalline field of the substrate has on the magnetic properties of a film consisting of N monolayers, which were taken from [3]. Parameter $h = g\mu_B H$ characterizes the effect of an external magnetic field oriented in the plane of a film with weak anisotropy introduced along axis x (in Eqn. (1)) to remove degeneracy or along the easy axis (axis z) in Eqn. (2).

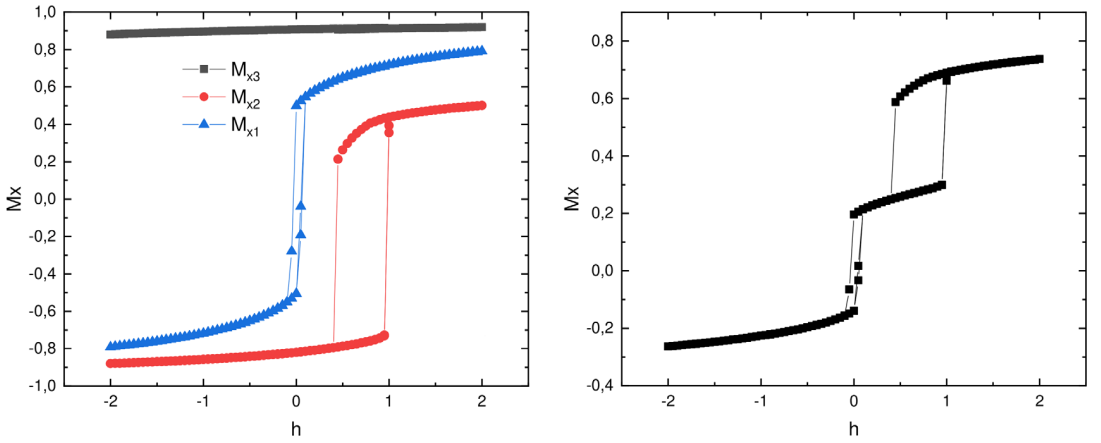

Figure 1. Hysteresis loops in a spin-valve structure with magnetization in the planes of individual films (left) with thicknesses $N_1 = N_2 = N_3 = 5$ ML and throughout a structure (right) at temperatures $T = 1.0J_1/k_B$.

To investigate hysteresis phenomena in the spin-valve structures, we modeled their magnetic properties when cycling external fields with parameter h varying from –2 to 2 and back. Temperatures slightly lower than ferromagnetic ordering point T_{c1} in the first film were chosen so that magnetization reversal in this film was achieved in weak magnetic fields with minimal hysteresis effects. Hysteresis loops obtained for structures with different type anisotropy are presented in Figs. 1 and 2.

The study was carried out with the financial support of the Ministry of Education and Science of the Russian Federation (agreement 0741-2020-0002) and grant MD-2229.2020.2 of the President of the Russian Federation. The computational research was supported in through resources provided by the Shared Services Center "Data Center of FEB RAS" (Khabarovsk).

1. B. Dieny, V.S. Speriosu, S.S.P. Parkin et al., Phys. Rev. B **43**, 1297 (1991).
2. C.H. Marrows, F.F. Stanley, B.J. Hickey, J. Appl. Phys. **87**, 5058 (2000).
3. P.V. Prudnikov, V.V. Prudnikov, M.V. Mamonova, N.I. Piskunova, JMMM **482**, 201 (2019).

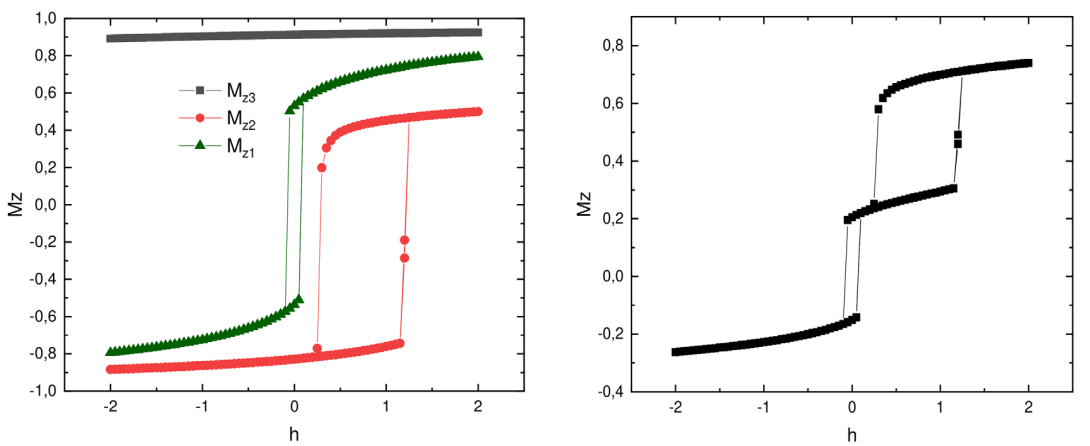

Figure 2. Hysteresis loops in structure with magnetization normal to the planes of individual films (left) with thicknesses $N_1 = N_2 = N_3 = 5$ ML and throughout a structure (right) at temperatures $T = 1.0J_1/k_B$.

TUNABLE RECEIVER OF SUB-THZ SIGNALS BASED ON AN ANTIFERROMAGNET

A.R. Safin[1,2]

[1]Kotel'nikov Institute of Radioengineering and Electronics, Russian Academy of Sciences, Moscow, Russia
[2]Moscow Power Engineering Institute, Moscow, Russia
E-mail: SafinAR@mpei.ru

Antiferromagnetic (AFM) materials have natural resonance frequencies in the sub-THz or THz frequency range. Thus, it is tempting to use antiferromagnets (AFM) as active layers in THz-frequency detectors. Recently [1], it has been shown theoretically that a dielectric AFM having bi-axial anisotropy, such as NiO, can be used for the resonance quadratic rectification of a linearly polarized AC spin current of THz frequency, and could have a sensitivity in the range of 100–1000 V/W.

Here we present both analytical and numerical data illustrating the performance of a possible electrically tunable resonance THz-frequency receiver based on an AFM crystal having the frequency of the antiferromagnetic resonance (AFMR) in the THz-frequency range [2]. The receiver is based (see Fig. 1) on a layered structure consisting of a layer of a uniaxial AFM crystal and two layers of a heavy metal (HM). The conversion of the received AC signal into an output DC signal is done using the inverse spin Hall effect in the (AFM/HM) bilayer. An additional bias DC current in the bottom HM layer can be used for the tuning of the AFMR frequency of the system, and for a partial regeneration of the system losses. The AFMR frequency can be continuously tuned in a substantial frequency interval (of about 0.5 THz) by varying the magnitude of the DC electric current. It is shown that the AC sensitivity of the proposed AFM/HM-based detector is comparable to the sensitivity of the modern sub-millimeter-wave detectors based on the Schottky and Gunn diodes, and that the received DC signals are well above the level of the thermal noise for the AC signals having power of the order of several microwatts.

By successively considering the piezoelectric effect in the piezoelectric (PE) layer, inducing elastic deformations in the layer (AFM) through deformations in the PE layer and the magnetoelastic effect (see Fig. 2a), it was found that the electric field in the PE layer can be used to induce magnetic anisotropy fields and change the frequency of the AFM resonance and change the critical current of excitation of self-oscillations. This result was demonstrated using the Pt/NiO/PZT-5H heterostructure

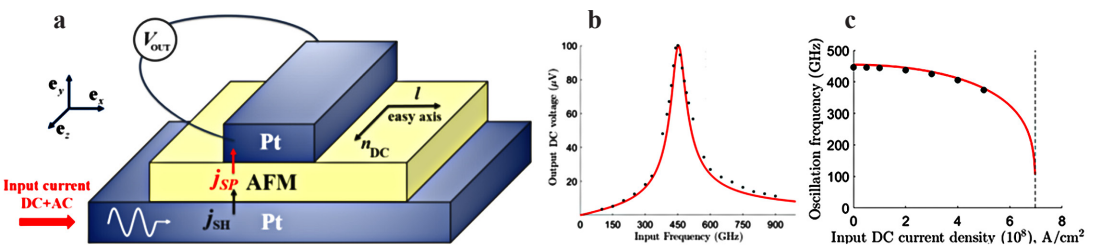

Figure 1. **a** Schematic view of the THz-frequency resonance detector based on the AFM-Pt structure, where **l** is the Néel vector oriented along the easy axis $\mathbf{n}_e = \mathbf{e}_x$ and V_{OUT} is the output DC electric voltage; **b** resonance curve of the output rectified DC voltage V_{OUT} of an AFM-based detector; **c** comparison between the results of the analytical calculations (solid line) and micromagnetic simulations (dots), showing the dependence of the AFMR oscillation frequency on the input density of the DC bias current flowing in the bottom Pt layer of the detector.

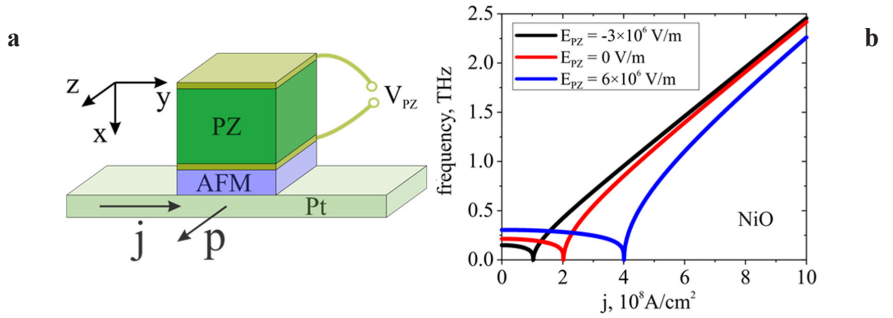

Figure 2. **a** The structure of the voltage-tunable detector of THz oscillations; **b** the dependence of the detector oscillation frequency on the magnitude of the direct current at various values of the EPZ field strength.

as an example. It was shown that the oscillation frequency of a detector built on the basis of the considered heterostructure can be tuned by an electric voltage over a wide range (Fig. 2b). The effect described in this work can find practical application in magnonic and spintronic devices based on piezoelectrics and magnetic materials or using magnetic anisotropy. Thus, it was found that the frequency of a terahertz detector can be tuned by an electric field.

Finally, we propose and theoretically study the concept of tunable microwave resonance-type quadratic detector based on the hematite (α-Fe_2O_3)/heavy metal (Pt) heterostructure (Fig. 3a) placed on the top of coplanar waveguide, which gives the linear polarization of AC magnetic field. We show that the external DC magnetic field can be used for the continuously tuning of the QFMR frequency of the AFM as shown in Fig. 3b. Finally, we calculate the dependence of the output resonance DC voltage as a function of external input power (the slope of this curve determines the sensitivity of the detector), which is shown in Fig. 3c and gives approximately 0.2 nW/mW and can be increased by changing the method of the output power collecting. We anticipate that the performance of this detector leads in the agreement with the experimental results of spin-pimping carried out in recent experiments [3, 4].

Support by RSF (Grant No. 21-79-10396) is acknowledged.

1. R. Khymyn et al., AIP Adv. **7**, 055931 (2017)
2. A. Safin et al., Appl. Phys. Lett. **117**, 222411 (2020).
3. I. Boventer et al. // Phys. Rev. Lett. **126**, 187201 (2021).
4. H. Wang H., et al., arXiv:2104.01796 (2021).

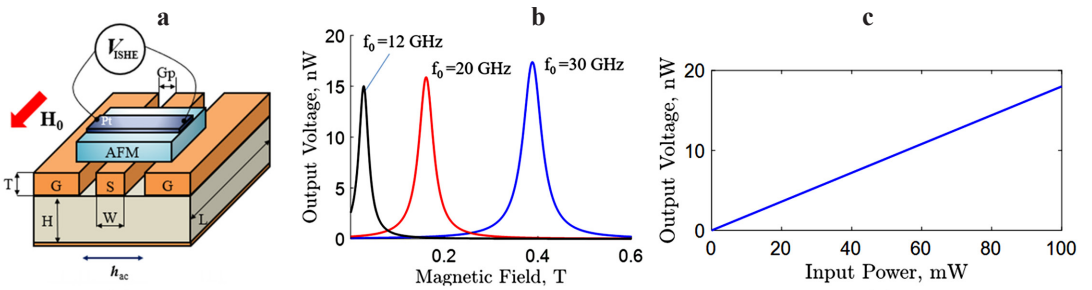

Figure 3. **a** Schematic view of the microwave detector based on the canted AFM-HM structure; **b** resonance curves of the output rectified DC voltage of an AFM-based detector for different input frequencies; **c** dependence of the output resonance DC voltage as a function of external input power.

A.O21

EVOLUTION OF MAGNETIC TUNNEL JUNCTION'S MODES FOR DIFFERENT DIRECTIONS OF AN EXTERNAL MAGNETIC FIELD

M.D. Shkanakina[1,2*], *G.A. Kichin*[2,3], *P.N. Skirdkov*[2,3,4], *K.A. Zvezdin*[2,3,4]

[1]National Research University of Electronic Technology, Zelenograd, Moscow, Russia
[2]New Spintronic Technologies, Russian Quantum Center, Skolkovo Innovation Center, Moscow Region, Russia
[3]Moscow Institute of Physics and Technology, Dolgoprudny, Moscow Region, Russia
[4]Prokhorov General Physics Institute of the Russian Academy of Sciences, Moscow, Russia
[*]E-mail: m.shkanakina@rqc.ru

Spintronics is a rapidly developing promising area of nanoelectronics. Spintronic devices [1–6] use not only the electrons' charge but also their spins for information processing and communication, which provides new functional opportunities. One of the most interesting spintronic devices is the spin-torque diode (STD) [7]. STD is based on the magnetic tunnel junction (MTJ) which consists of a free magnetic layer and a pinned magnetic layer that are separated by the MgO isolator [7]. Electrical and microwave properties of MTJ are acquired due to the magnetization dynamic processes in magnetic layers. When the frequency of the incident microwave signal on the top electrode of MTJ coincides with its ferromagnetic resonance (FMR) frequency, the dynamic excitation of the magnetization in the free layer is observed, which leads to the rectification of the input signal. The dynamics of magnetization is realized as a multimode process. The STD functioning is based on this effect, and it is studied by the ST-FMR experimental approach (spin-torque ferromagnetic resonance) [8]. In this investigation we use the ST-FMR experimental technique combined with macrospin modeling to study the free layer magnetization excitation by a microwave spin-polarized current with different directions of the external magnetic field.

Investigated MTJs are of a round shape, the free and the pinned layers of nanopillars are magnertized in-plane. Detailed information about the tunnel magnetoresistance ratio and the size of the samples, is present in the Table 1.

We present spectra of the sample S1 (Fig. 1a) at the field directions θ = 30°, 60°, 64°, 70°, 80°. We have found two V-shaped modes symmetric with respect to the external field of 140 Oe, which means that V1 and V2 modes are localized in the free layer. V1 and V2 modes exist at frequencies above 4 and 2 GHz, respectively. With increasing the angle θ of the external field, the V1 mode is transformed into a W-shaped configuration by interacting with the V2 mode, since the V1 mode is sensitive to the direction of field. The position of the FMR-peaks of V2 mode (Fig. 1b) at a fixed field value of –220 Oe shifts to higher frequencies from 5.6 to 5.88 GHz, and the V2 mode is less sensitive to the external field direction. We check the presence of insensitive mode in the samples S2–S4. Figures 1c-1e show the dependence of a rectified voltage from the frequency of incident signal at different θ. S2 has two modes V1 and V2 (Fig. 1c). With increasing θ, we observe the

Table 1. Diameter, TMR of investigated samples.

Sample	Diameter (nm)	TMR (%)
S1	100	118.5
S2	100	77.2
S3	150	93.5
S4	200	90.0

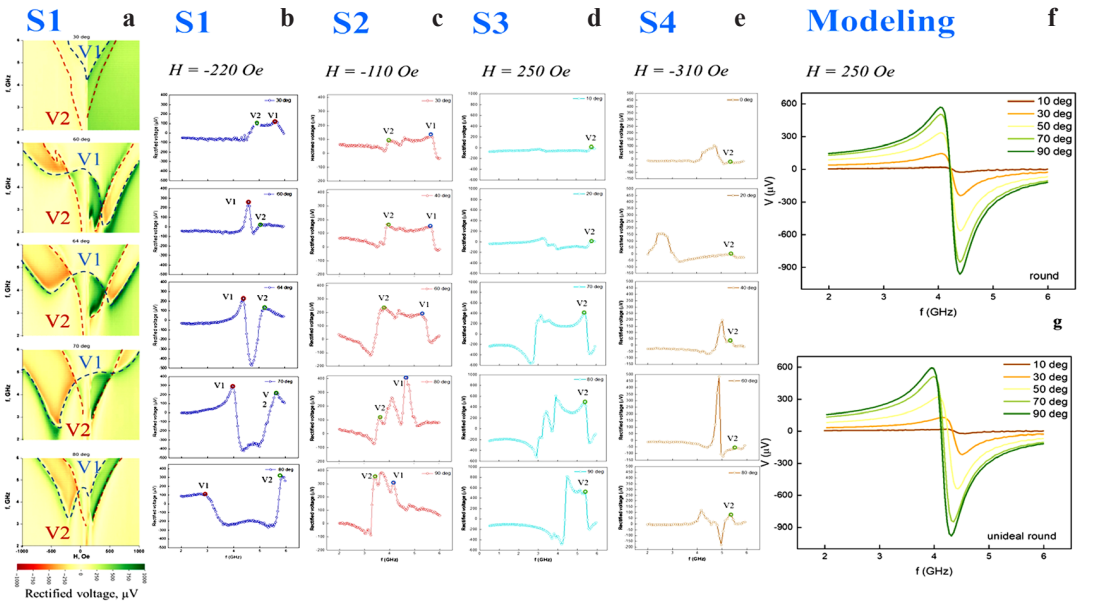

Figure 1. Spectra and slices of the ST-FMR for the different θ for samples: **a**, **b** S1: θ = 30°, 60°, 64°, 70°, 80°, contours of the spin-wave modes V1 and V2 are outlined in blue and red, respectively, fixed H = –220 Oe; **c**, S2: θ = 30°, 40°, 60°, 80°, 90°, H = –110 Oe; d, S3: θ = 10°, 20°, 70°, 80°, 90°, H = 250 Oe; e, S4: θ = 0°, 20°, 40°, 60°, 80°, H = –310 Oe. The FMR-peaks of the insensitive mode V2 are marked; **f**, **g** modeling of ideal round and unideal round samples: θ = 10°, 30°, 50°, 70°, 90°, H = 250 Oe.

displacement of the FMR peak of the V2 mode in the frequency range from 3.9 to 3.4 GHz, the FMR peak of V1 mode shifts from 5.6 to 4.1 GHz. Based on this, the V1 mode is more sensitive to the direction of the field compared to the V2 mode. With an increase in the sample size, the magnetization of the free layer becomes more inhomogeneous in low fields [10-11], since for the S3 and S4 we fix the fields 250 Oe and –310 Oe respectively (Figs. 1d, e). The FMR peak of the V2 mode for sample S3 with a change in the direction of the field θ from 0°–50° is at a frequency of 5.3 GHz and shifts to 5.5 GHz at θ = 60°, remaining in this position as θ increases to 90°. For the S4 sample, the FMR peak of the V2 mode of the sample does not change its position and is at a frequency of 5.4 GHz. Thus, we found the insensitive mode V2 to the field direction for all samples.

In order to explain the nature of the insensitive mode, we analyze the behavior of the bulk or quasi uniform mode of the free layer for different directions of the field. We use modeling of the Landau-Lifshitz-Gilbert (LLG) equation [7]. We have found that the FMR-peak of quasi uniform mode of ideal round shape sample (Fig. 1f) doesn't change its position in the frequency region with increasing θ. It means that S3 and S4 have ideal round shape. As for S1 and S2, samples have a small sizes and possibility they acquired sightly ellipticity in the manufacture. Modeling (Fig. 1g) confirmed this hypothesis. Thus, the V2 mode of S1–S4 is quasi uniform and that's insensitive to the direction of the field.

In our work we have identified the insensitive mode to direction of the field in the set of round samples. With using a macrospin modeling, we have defined that insensitive mode is a quasi uniform mode of free layer.

This work was supported by Russian Science Foundation (grant # 19-12-00432).

1. Lenz, J. Edelstein, IEEE Sens. J. **6**, 631–649 (2006).
2. S.I. Kiselev et al., Nature **425**, 380 (2003).
3. J.A. Katine et al., Phys. Rev. Lett. **84**, 3149 (2000).
4. D. Houssameddine et al., Nat. Mater. **6**, 447 (2007).
5. T. Kawahara et al., Int. Electron Devices Meet. **473**, (2006).
6. B. Fang et al., Phys. Rev. Appl. **11**, (2019).
7. P.N. Skirdkov and K.A. Zvezdin, Ann. Phys. **532**, (2020).
8. B. Fang, M. Carpentieri, S. Louis et al., Phys. Rev. Appl. **11**, (2019).
9. J.C. Sankey et al., Nat. Phys. **4**, 67 (2008).
10. Z. Zeng et al., Phys. Rev., 82 (2010).
11. A. Helmer et al., Phys. Rev. **81**, (2010).

A.O22

FEATURES OF THE CURIE POINT BEHAVIOR IN NANOGRANULATED STRUCTURES OF THE Cd_3As_2-MnAs SYSTEM

M.H. Al-Onaizan[*], *A.T. Morchenko*

Department of Electronic Materials Technology, NUST MISiS, Moscow, Russia
[*]E-mail: m1809132@edu.misis.ru, dratm@mail.ru

Hybrid nanogranular ferromagnet/semiconductor structures are promising materials for spintronics and are composites in which ferromagnet particles are dispersed in a semiconductor matrix. In such materials, the electron spins of ferromagnetic particles can be controlled by applying a magnetic field without significant energy expenditure, and the high value of the carrier path in a semiconductor (as, for example, in Cd_3As_2) makes it possible to transfer an electron from particle to particle without losing the state of spin polarization (spin current). Such composites are analogues of superlattices, surpassing them in ease of manufacture and low cost, and therefore seem to be the most promising working media for use in MRAM magnetic memory devices and the creation of microrefrigerators.

As the particle size decreases, the surface plays an increasingly important role in the formation of the resulting properties of the material [1], therefore, in the nanoscale state, surface tension forces act on the material, which leads to the approach of atoms and enhancement of exchange interactions. On the other hand, atoms located on the surface have a smaller number of bonds with neighbors (lower coordination number) and have reduced symmetry, which leads both to the decrease of exchange interactions and affects the nature of magnetic anisotropy. In addition, the effects of quantum uncertainty begin to manifest themselves in such systems, which also affects the decrease in the exchange interaction. The Curie temperature is a parameter that reflects the degree of exchange interaction and the possibility of realizing magnetic properties [2, 3].

The average distance between nanoparticles in a composite, which determines the possibility of transfer of a spin-polarized state and, accordingly, the implementation of the exchange interaction between neighboring inclusions due to conduction electrons, is determined by both the concentration of the magnetic phase and the particle size [4, 5]. In turn, the particle size can be controlled

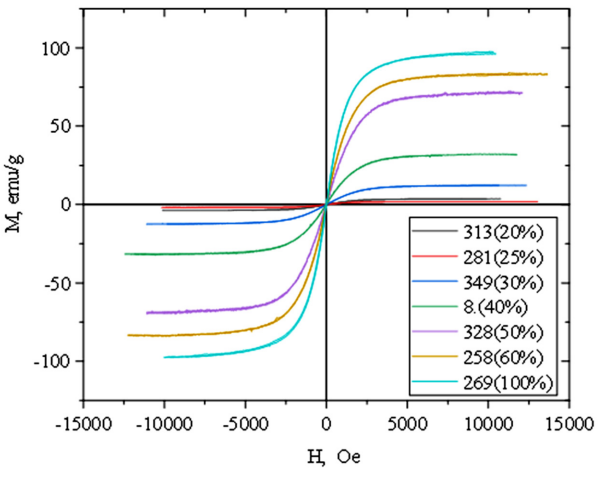

Figure 1. Hysteresis loops for samples of the Cd_3As_2-MnAs system synthesized without quenching.

Table 1. Dependence of the Curie temperature on the MnAs content in the composite.

Sample number	Concentration of MnAs, (mol. %)	Heating	Cooling
		T_c (°C)	T_c (°C)
313	20	39.5	38
281	25	38.6	38
349	30	41	38
8	40	40.6	38
328	50	43.8	38
258	60	43.5	36.5
269	100	45.5	36

by choosing the mode of nanocomposite synthesis. If during synthesis in the furnace cooling mode, the growth of particles continues even after the heating is turned off, then in the quenching mode their growth stops almost immediately.

Manganese arsenide (MnAs) is a ferromagnet at room temperature. In the range from 40 to 45 °C, a magnetic transformation was found in MnAs, which is associated with a polymorphic transformation [4]. The research included a study of the composites of the Cd_3As_2-MnAs system with composition ranging from 0 to 100 mol.% MnAs was synthesized in two ways: with quenching and without quenching. The phase composition of the samples was identified by the XRD method using a BRUKER D8 ADVANCE powder diffractometer. Recording of hysteresis loops (Fig. 1) and investigation of the temperature behavior of magnetization were carried out using a MV-07 vibration magnetometer (see Table 1).

It is determined that magnetic properties of nanogranulated composites of Cd_3As_2-MnAs system depend both on the composition of the samples and on the method of their manufacturing.

Also, the size of the crystallites of the magnetic component and their mutual arrangement, depending on the synthesis method, have a great influence on the Curie temperature, since quenching prevents the growth of crystallites. Since the resulting energy of the exchange interaction in nanogranulated structures depends on the particle size of the ferromagnetic component and on the alternating integral of exchange between individual particles through charge carriers in a semiconductor, this can lead to variations in the Curie temperature depending on the average distance between the particles of manganese arsenide.

1. L. He et al., J. Phys.: Condens. Matter **19**(3), 036216 (2007).
2. H.M. Lu et al., J. Appl. Phys. **103**(12), 123526 (2008).
3. H. Jin et al., J. Mater. Chem. C **3**(15), 3547–3551 (2015).
4. Y. Nakazawa et al., Phys. Rev. B **103**(4), 045109 (2021).
5. J. Guo et al., J. Mater. Sci. Technol. **76**, 247–253 (2021).

SPIN REORIENTATION TRANSITION IN CoFeB/MgO/CoFeB TUNNEL JUNCTION IMPLEMENTED BY ULTRAFAST LASER-INDUCED SUPPRESSION OF PERPENDICULAR MAGNETIC ANISOTROPY

L.A. Shelukhin[1*], *R.R. Gareev*[2], *V. Zbarsky*[3], *J. Walowski*[3], *M. Münzenberg*[3], *N.A. Pertsev*[1], *A.M. Kalashnikova*[1]

[1]Ioffe Institute, St. Petersburg, Russia
[2]Institute of Experimental and Applied Physics, University of Regensburg, Germany
[3]University of Greifswald, Institute of Physics, Germany
[*]E-mail: shelukhin@mail.ioffe.ru

Magnetic tunnel junctions (MTJs) are nanostructures consisting of two ferromagnetic electrodes separated by an insulating nanolayer creating a potential barrier for the charge transport [1]. MTJs with perpendicular magnetic anisotropy (PMA) are among of key elements for neuromorphic calculations [2] and high-density magnetic memory with low power consumption [3]. Therefore, magnetization control in such structures at subpicosecond timescale is crucial. For this purpose, we suggest to modulate PMA by means of femtosecond laser pulses.

In this work, we selected multilayer heterostructure with MTJ CoFeB(1.2 nm)/MgO(1.2 nm)/CoFeB(1.4 nm) grown on the thermally oxidized silicon substrate by the deposition technique described in [4]. Main feature of this structure is PMA stabilized by the interface anisotropy (IA) at the MgO/CoFeB interface which dominates over shape anisotropy (SA) if the thickness of the CoFeB layer is below 1.4 nm. Thus, both CoFeB layers are in a vicinity of the thickness-induced spin reorientation transition (SRT). The aim of our work is to induce such a SRT with femtosecond laser pulses.

Laser-induced dynamics of magnetization has been studied using the time-resolved magneto-optical Kerr effect technique. 190 fs-laser pulses with the central wavelength of 515 and 1030 nm were used as the pump and probe respectively. Laser-induced changes of magnetization were monitored by measuring the polar Kerr ellipticity of the probe pulses as a function of the pump-probe delay. The external magnetic field is applied in the sample plane.

In the experiment, the impact of femtosecond laser pulses leads to ultrafast demagnetization followed by magnetization precession in the thin CoFeB layer. Herewith, the magnetization of the thick layer with weak PMA is directed along the external magnetic field. Importantly, precession initial phase shows that change of out of plane projection of magnetization has the same sign as ultrafast demagnetization. This indicates that IA is reduced stronger than SA by ultrafast laser-induced heating of the MTJ. From the measurements of ultrafast demagnetization and precession frequency as a functions of pump fluence at fixed external field it is possible to get reliable estimate of IA parameter. Dependence of the latter on magnetization demonstrates dramatic enhancement of IA suppression by the laser-induced heating in the demagnetization range over 20%. This enables SRT at the moderate pump fluence 1.8 mJ/cm^2 when the SA exceeds the IA.

Thus, we show that femtosecond laser pulses induce SRT in CoFeB/MgO/CoFeB MTJ from perpendicular to parallel configuration already at moderate pump fluence 1.8 mJ/cm^2 due to the enhancement of IA suppression with ultrafast laser-induced heating [6].

LASh, AMK were supported by RSF (Grant No. 20-12-00309).

1. J.-G. Zhu, C. Park, Mater. Today **9**, 36–45 (2006).

2. J. Torrejon et al., Nature **547**, 428–431 (2017).
3. M. Cubukcu et al., Appl. Phys. Lett. **104**, 042406 (2014).
4. R.R. Gareev et al., Appl. Phys. Lett. **106**, 132408 (2015).
5. R.F.L. Evans, L. Rózsa, S. Jenkins, U. Atxitia, Phys. Rev. B **102**, 020412(R) (2020).
6. L.A. Shelukhin et al., Nanoscale (2022), accepted.

A.O24

ELECTRONIC AND MAGNETIC PROPERTIES OF SPHERICAL CARBON SHELLS

*K.B. Tsiberkin**, *E.I. Kovycheva*

Theoretical Physics Department, Perm State University, Perm, Russia
*E-mail: kbtsiberkin@psu.ru

We present an analysis of electron energy spectrum, evaluation of the statistical properties and approximate simulation of the magnetization dynamics for the spherical carbon shell is doped by magnetic admixture (e.g., N, F or H atoms). This composite is assumed to be perspective basement for the development of electrochemical energy storages [1, 2].

Application of the Hubbard model in continuous medium approximation permits to evaluate the energies of the electrons within carbon material for the arbitrary radius of the shell and finite number of carbon layers. Band structure matches the typical carbon bands, because the basic lattice of the wall is a hexagonal bipartite lattice (Fig. 1). The average shell radius is obtained in experiments in [2] is about 3–5 nm, and it contains up to 104 atoms. Therefore, we consider hexagonal lattice in continuous medium limits, assuming the distance between lattice nodes is much less than the shell radius and neglecting the defects. The energy levels are determined by the orbital quantum number of the electrons. All the levels have $2\times(2l + 1)$ degeneracy by magnetic quantum number and spin. Maximum possible quantum number l depends on the total amount of the lattice nodes, and, respectively, the shell radius.

There is a band gap determined by dopant concentration. If there is no admixture, the semimetal spectrum with the Dirac points exist. These results are verified by measurements of composite conductivity after functionalization. It decreases with the concentration, and the dependence matches the narrow-band semiconductor relations [3]. The optical absorption spectrum qualitatively similar

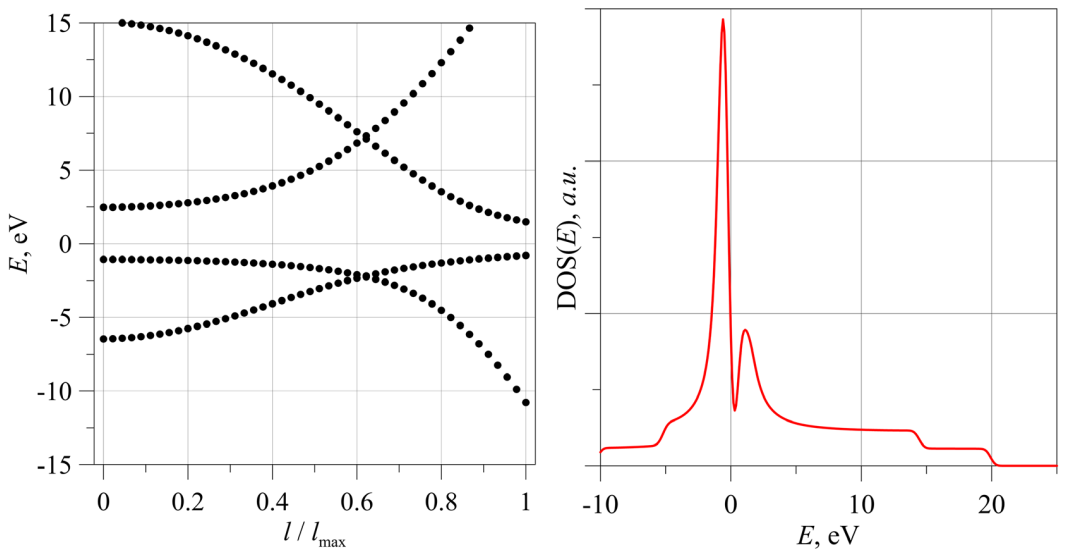

Figure 1. Energy spectrum (left) and density of states (right) of doped carbon shell evaluated from the Hubbard model with Coulomb repulsion.

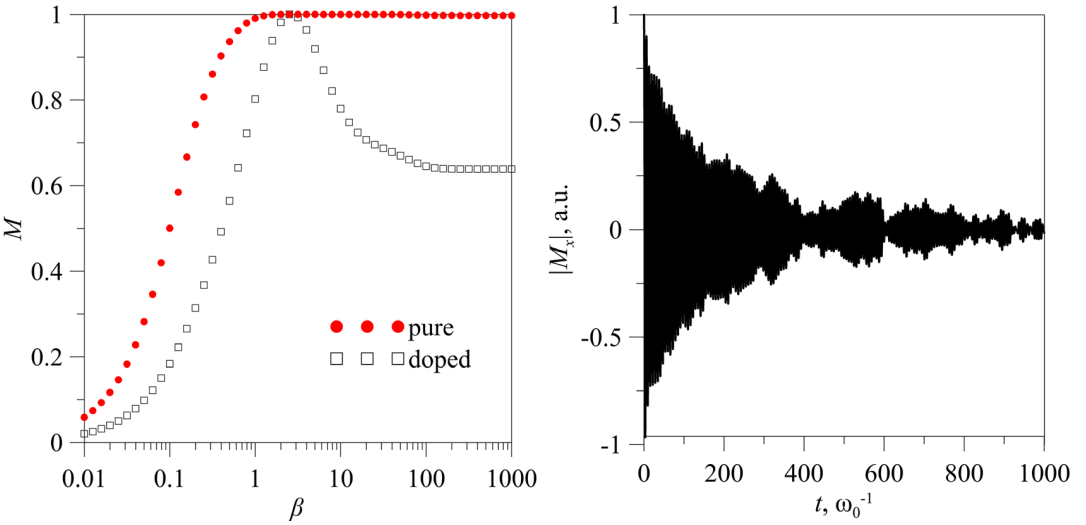

Figure 2. Thermal dependence of the static magnetization (left) and simulated free induction decay (right) of the doped spherical carbon shell.

with the established data for the fullerenes C_{60} and C_{70}. It also includes specific wide bands of the ultra-violet radiation absorption [4].

The energy dependence permits to evaluate density of states and thermodynamic properties of the array or solution of non-interacting shells. Particularly, it is the static magnetization. The pure composite shows typical paramagnetic properties. In case of the doped material, the interplay between the magnetization of the electrons localized in the carbon and admixture nodes leads to the change of maximum possible magnetization. An equilibrium state at low temperature doesn't match the full magnetic saturation (Fig. 2). We assume that it is determined by the Coulomb repulsion of the electrons at the different lattice nodes because the initial Hubbard model includes only the hopping, repulsion and Zeeman terms. There are no additional mechanisms which can change the magnetization.

In addition, we realize the quantum-based numerical simulation of the free induction decay signal from the dopant ions assuming their spins are coupled by dipole interaction. Because the simulation requires large resources, we simplify the problem considering that the spin ensemble on the spherical shell as a linear superposition of ring clusters with different orientation. The algorithm evaluates the eigenvalues and eigenvectors of the dipole Hamiltonian matrix, and built the time-dependent wave function and observable transversal magnetization from these data [5]. The FID signal decays almost exponentially (Fig. 2). The characteristic decay time is determined by dipole interaction magnitude and average radius of the ring in the whole ensemble. The additional weak exchange coupling between the spins is almost insignificant. That means that RKKY interaction of the ions deposited on the spherical carbon shell can be neglected in practice.

1. Zh. Lyu et al., Nano Research **8**, 3535–3543 (2015).
2. G.A. Rudakov, K.B. Tsiberkin, R.S. Ponomarev et al., J. Magn. Magn. Mater. **427**, 34–39 (2019).
3. A.V. Sosunov, K.B. Tsiberkin and V.K. Henner, Bull. Perm Univ. Physics **2**, 63–68 (2019) [In Russian].
4. H. Ajie, M.M. Alvarez, S.J. Anz et al., J. Phys. Chem. **94**, 8630–8633 (1990).
5. V.K. Henner, A. Klots, A.A. Nepomnyashchy et al., Appl. Magn. Reson. **52**, 859–866 (2021).

A.O25

SPIN TRANSPORT IN IRIDATE/MANGANITE INTERFACE

G.A. Ovsyannikov[1*], K.Y. Constantinian[1], V.A. Shmakov[1], A.V. Shadrin[1,2], Yu.V. Kislinski[1], E.A. Kalachev[3], A.A. Klimov[1,3]

[1]V.A. Kotelnikov Institute of Radio Engineering and Electronics, Russian Academy of Sciences, Moscow, Russia
[2]Moscow Institute of Physics and Technology (National Research University), Dolgoprudny, Russia
[3]Russian Technological University - MIREA, Moscow, Russia
[*]E-mail: gena@hitech.cplire.ru

The use of electron spins opens up new opportunities in microelectronics, especially in the field of heat dissipation from submicron-sized elements. The detection and generation of spin current requires a completely different approach to the transport problem. The spin Hall effect is used for the conversion of spin current to charge current and vice versa in paramagnetic metals [1–5]. The paper presents the results of experimental studies of the spin magnetoresistance and spin current arising in $SrIrO_3/La_{0.7}Sr_{0.3}MnO_3$ heterostructures at the presence of ferromagnetic resonance.

Thin films of strontium iridate $SrIrO_3$ (SIO_3) and manganite $La_{0.7}Sr_{0.3}MnO_3$ (LSMO) of nanometer thickness were deposited on single-crystal substrates (110)$NdGaO_3$. Epitaxial films were grown by magnetron sputtering at substrate temperatures of 770–800 °C in Ar and O_2 gas mixture at a total pressure of 0.3 mBar [4, 5].

When a ferromagnetic resonance (FMR) is excited in a ferromagnetic film, a spin current arises across the interface. The density of the spin current across a ferromagnetics/paramagnetic metal interface j_s is determined by the change of magnetization and the components proportional to the real ($\mathrm{Re}\, g^{\uparrow\downarrow}$) and imaginary ($\mathrm{Im}\, g^{\uparrow\downarrow}$) parts of spin mixing conductance of the heterostructure interface.

The FMR-spectrum was determined from the magnetic field dependence of the amplitude of the transmitted microwave radiation $S_{12}(H)$ in the frequency range F = 1–20 GHz. The shape of the $S_{12}(H)$-spectrum (inset to Fig. 1) was approximated using sum of the Lorentz line and the dispersion relation. From fitting the experimental curves with these two components it is possible to determine the resonance field H_0 and the Lorentz line width ΔH.

As can be seen from Fig. 1 for LSMO film Gilbert damping $\alpha_{LSMO} = 2.0\pm0.2\cdot10^{-4}$ as after sputtering SIO_3 increases to values $\alpha_{SIO/SMO} = 6.7\pm0.8\cdot10^{-4}$. The value of the real part of the spin conductivity is determined by the difference of these values $\mathrm{Re}\, g^{\uparrow\downarrow} = (6.0\pm0.6)\cdot10^{19}$ m^{-2}. $\mathrm{Re}\, g^{\uparrow\downarrow} = 1.3\cdot10^{18}$ m^{-2} was obtained in [6] for the SIO_3/LSMO heterostructure fabricated by laser ablation. According to [7], when the SIO_3 film thickness changes from 10 to 40 nm Re for the heterostructure changes from 1.3 до $3.6\cdot10^{19}$ m^{-2} respectively, which is close to our value.

Inverse spin Hall effect is used to detect spin current [8]. According to the effect the ratio of spin and charge currents is determined by a dimensionless parameter – the spin Hall angle θ_{SH}. Following the theory taking into account conductivity of $La_{0.7}Sr_{0.3}MnO_3$ film the expression for spin resistance (SMR) under the condition thickness SIO_3 larger then spin diffusion length [8]:

$$\frac{\Delta R}{R} = \frac{\theta_{SH}{}^2 \lambda_S g_R}{(1+\eta) t_{SIO} [1+g_R]},$$

where $g_R = h\rho_{SIO}\lambda_s \mathrm{Re}\, g^{\uparrow\downarrow}/e^2$. Using the data for the spin resistance value of the boundaries $\mathrm{Re}\, g^{\uparrow\downarrow} = 6\cdot10^{19}$ m^{-2} and λ_s = 1 nm we obtain θ_{SH} = 0.2 compare with θ_{SH} = 0.02 for Pt.

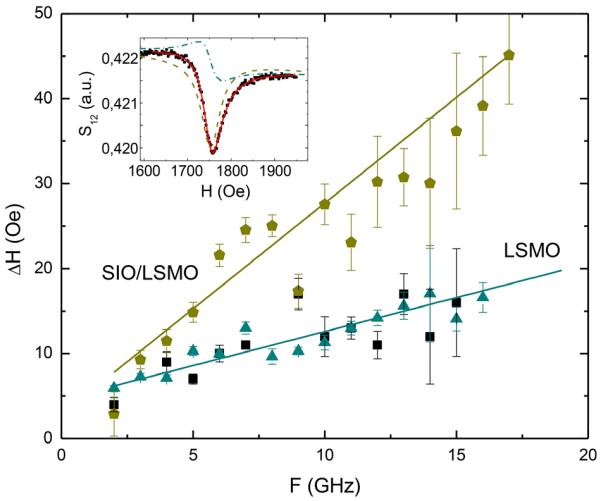

Figure 1. Frequency dependence of the FMR line-width ΔH for the LSMO film (squares and triangles) and the SIO_3/LSMO heterostructure (pentagons). The solid lines show linear approximations of the experimental data. The inset shows the spectrum of the $S_{12}(H)$ heterostructure under microwave exposure at F = 9 GHz. The solid line shows the approximation of the spectrum.

This work was carried out within the framework of the state task of the Kotel'nikov IRE RAS. The study was carried out using the Unique Science Unit "Cryointegral" (USU #352529), Project No. 075-15-2021-667.

1. Ya. Tserkovnyak, A Brataas, G.E.W. Bauer, Phys. Rev. Lett. **88**, 117601 (2002).
2. E. Saitoh, M. Ueda, H. Miyajima, and G. Tatara, Appl. Phys. Lett. **88**, 182509 (2006).
3. O. Mosendz, V. Vlaminck, J.E. Pearson, F.Y. Fradin, W.G.E. Bauer, S.D. Bader, and A.Hoffmann. Phys. Rev., B **82**, 214403 (2010).
4. T.A. Shaikhulov, G.A. Ovsyannikov, V.V. Demidov, N.V. Andreev, JETP **129**, 112 (2019).
5. G.A. Ovsyannikov, T.A. Shaikhulov; K.L. Stankevich, Yu. Khaydukov; N.V. Andreev, Phys. Rev B **102**, 144401 (2020).
6. S. Crossley, A.G. Swartz, K. Nishio, Y. Hikita, and H.Y. Hwang, Phys. Rev. B **100**, 115163 (2019).
7. X. Huang, S. Sayed, J. Mittelstaedt, S. Susarla, S. Karimeddiny, L. Caretta, H. Zhang, V. A. Stoica, T. Gosavi, F. Mahfouzi,Q. Sun, P. Ercius, N. Kioussis, S. Salahuddin, D. C. Ralph,and R. Ramesh, Adv. Mater., 20082 (2021).
8. D. Ye, T. Saburo and N. Junsaku, Phys. Rev. B **103**, 094419 (2021).

A.O26

ELECTRIC AND MAGNETIC PROPERTIES OF Co_2FeAl AND Co_2FeSi HEUSLER ALLOY FIMS GROWN ON SAPPHIRE SUBSTRATES

I.V. Malikov[1], *V.A. Berezin*[1], *L.A. Fomin*[1*], *V.V. Marchenkov*[2]

[1]Institute of Microelectronics Technology and High Purity Materials RAS, Chernogolovka, Russia
[2]M.N. Mikheev Institute of Metall Physics, Ekaterinburg, Russia
[*]E-mail: fomin@iptm.ru

Among the materials that demonstrate the property of half metallic ferromagnets (HMF), that is, one of the spin subbands, is partially occupied in equilibrium, and the other is not, the most promising are Heusler ternary alloys, which are currently being intensively studied [1].

Their use would lead to a significant increase in magnetoresistive effects in devices used in spintronics. It was predicted by means of *ab initio* calculations that Co_2FeAl and Co_2FeSi Heusler alloys possess the property of HMF and the large constants of anisotropy which more than by an order exceeds that for iron [2]. To use these alloys in spintronic devices, it is necessary to be able to grow films from them and fabricate nanostructures in such a way that the property of HMF is not lost.

In this work thin films of the ferromagnetic Co_2FeAl and Co_2FeSi Heusler alloys were grown by pulse laser deposition technique on R- and A-plane monocrystalline sapphire substrates with and without epitaxial refractory metal seed layer. The technology of their growth was similar to that used for the growth of epitaxial iron films on sapphire [3].

It was shown [4] that such a growth method preserves the target composition well, and one can expect that the properties of HMF in the film will be retained. Nonmonotonic dependences of the morphological and magnetic properties of Co_2FeAl films on their growth temperature were found (Fig. 1). The coercive fields H_c and the width of the peaks of the anisotropic magnetoresistance curves at half the maximum ΔH_c first increased sharply and then sharply decreased with increasing temperature. This indicates to the structural transformation in Heusler alloy films in different growth temperature ranges.

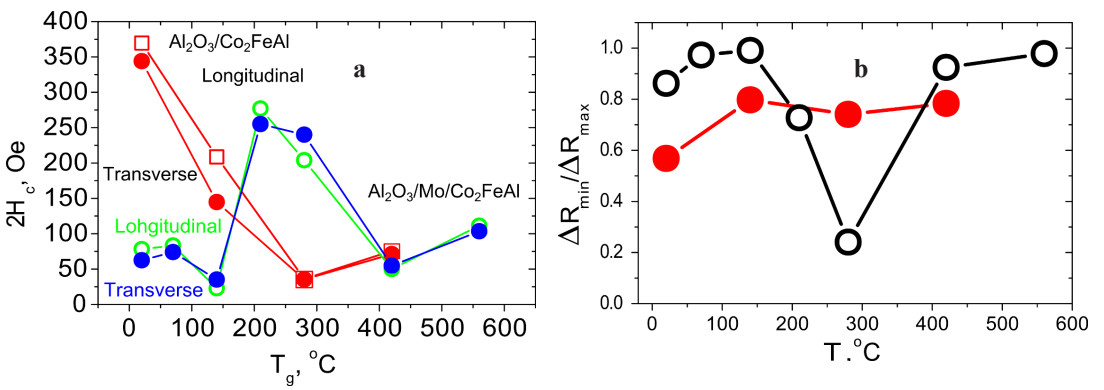

Figure 1. The dependence of the doubled value of the coercive field of films grown on the R-plane sapphire substrate in the longitudinal (open sympols) and transverse (filled symbols) magnetoresistances (**a**) and the ratio of the changes in the transverse and longitudinal magnetoresistance at the coercive field (**b**) for films with the seed layer (open symbols) and without it (filled symbols), versus the growth temperature.

Recently, a new theoretical model has been developed in which the effect of anisotropic magnetoresistance (AMR) for various ferromagnetic materials has been analyzed [5]. In this model, the s-d electron scattering that causes AMR in HMF comes mainly from the state s↑ to d↑ or from s↓ to d↓, which results in a negative sign of AMR, i.e. the electrical resistance in when the magnetization is parallel to the current is less than when it is perpendicular to the current. We have found an inverse dependence of the transverse and longitudinal magnetoresistances of the grown films, which indicates the realization of the HMF state in them. The angular dependence of the position of the extrema of the field dependence of the resistance (correlating with the magnitude of the coercive force) (Fig. 2) indicates the presence of uniaxial magnetic anisotropy.

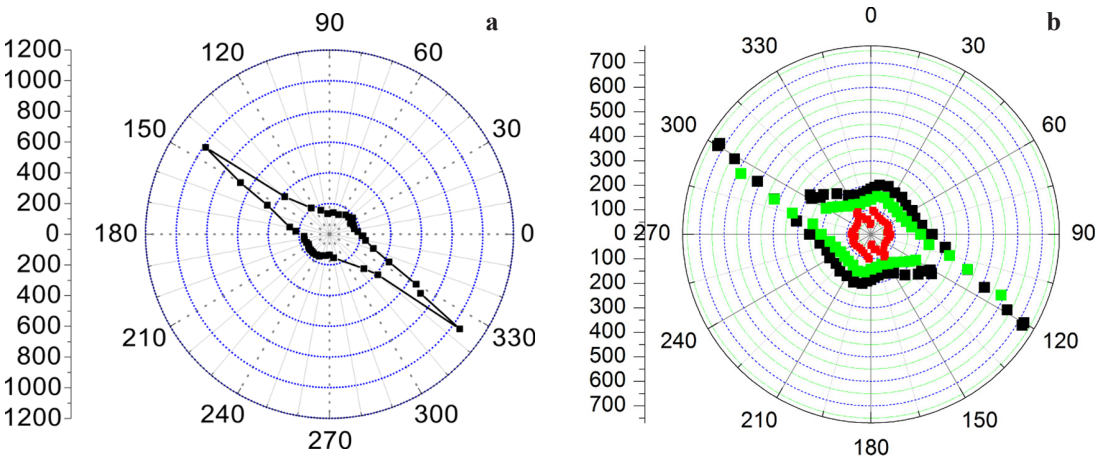

Figure 2. Polar figures of the coercive field H_c (vertical scale in Oe) against the direction of the in-plane magnetic field for films grown on A-plane of sapphire with Mo(011) seed layer: Co_2FeAl (**a**) and Co_2FeSi (**b**). Black dots are for the sample after sputtering at 280 °C, green dots after annealing at 280 °C, red dots after annealing at 400 °C.

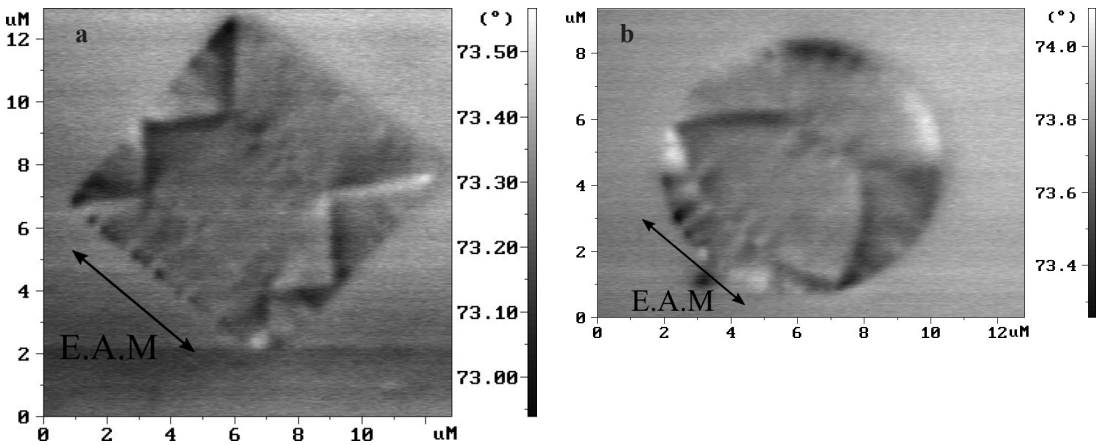

Figure 3. The magnetic force microscopy images of microstructures from Co_2FeAl films grown on the R-plane of sapphire. The arrows indicate the easy axis of magnetization.

Microstructures fabricated by subtractive technology from the Co_2FeAl films were studied by magnetic force microscopy in the presence of external magnetic field (Fig. 3). They exhibit regular magnetic domain patterns in the form of stripes, the formation of which is in agreement with the magnetic anisotropy found from magnetoresistive experiments. This could be useful for applications in magnetic storage and spin transfer torque devices.

Support by State Task № 075-00706-22-00 is acknowledged.

1. H. Schneider et al., J. Phys. D: Appl. Phys. **40**, 1548–1551 (2007).
2. Y-I. Matsushita et al., J. Phys. D: Appl. Phys. **50**, 095002 (2017).
3. G.M. Mikhailov et al., Solid State Phenom., **168-169**, 300–302 (2011).
4. I.V. Malikov, V.A. Berezin, L.A. Fomin et al., J. Phys.: Conf. Ser. **1686**, 012043 (2020).
5. S. Kokado, M. Tsunoda, J. Phys. Soc. Jpn. **88**, 034706 (2019).

A.O27

MOVING SPIN-VALVE BRIDGE CONFIGURATIONS IN INHOMOGENEOUS 3D MAGNETIC FIELD

N.G. Chechenin[1,2*], *G.V. Babaytsev*[1,2], *I.O. Dzhun*[1], *I.L. Romashkina*[1], *M.G. Kozin*[1], *A.V. Makunin*[1]

[1]Skobeltsyn Institute of Nuclear Physics, MSU, Moscow, RF
[2]Faculty of Physics, MSU, Moscow, RF
[*]E-mail: nchechenin@yandex.ru

Spin-valve (SV) sensors are one of the basic elements of modern and prospective spintronics. The sphere of applications of sensors covers almost all areas of industry and activities of daily living. Their advantages are high sensitivity, low energy consumption, low cost, small size, and high spatial and temporal resolution of the magnetic fields of the objects under study. Generally, an SV sensor is a multilayer thin-film structure consisting of two ferromagnetic (F) layers separated by a nonmagnetic layer.

The direction of the magnetization vector of one of the F-layers (pinned ferromagnetic (PF) layer) is fixed via an exchange interaction with the antiferromagnetic layer (AF). The layer with free magnetization (FF) is a sensitive element in the structure and varies the orientation of its magnetization under the action of an external magnetic field. As a result of noncollinearity of magnetic moments of PF- and FF-layers, the total resistance of the structure increases. This effect is named giant magnetoresistance (GMR). Wheatstone bridge (WB) configurations of clusters of SV sensors moving in the 3D-field of a magnetic label are considered as a sensor of the magnetic field of a label. Potentially, the WB-network is a more favorable device than a single SV-sensor, offering higher sensitivity to a weak magnetic field and to a weak space variation of the magnetic field. That is an important feature of WB-like sensors in many applications, including the localization and positioning of a moving magnetic object.

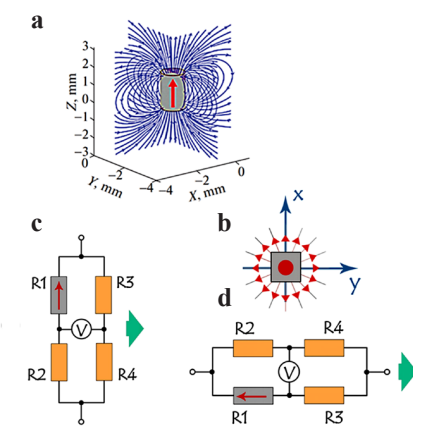

Figure 1. Schematic illustration of 3D magnetic field of the label (**a**) and 2D-projection on *XY*-plane (**b**); an example of two different WB-sensor orientations with respect to the magnetic label field. Magnetization **M** of the sensitive element R1 of the left WB-sensor **c** is perpendicular and of the bottom WB-sensor and **d** is parallel to the direction of movement along *Y*-axis, perpendicular to the orientation of the label aligned along *Z*-axis.

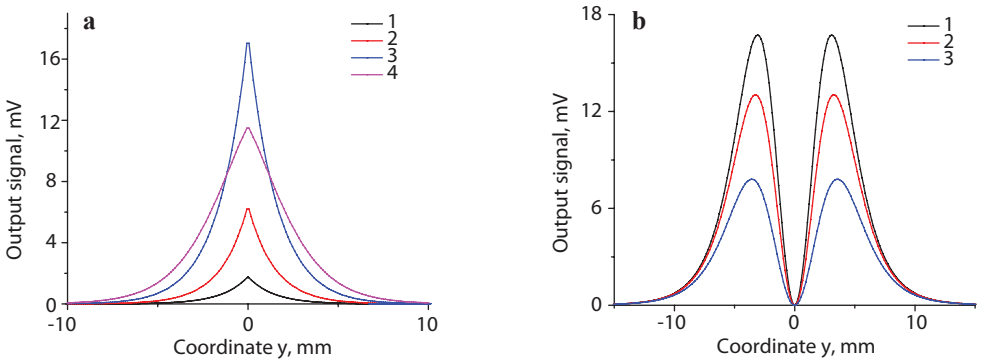

Figure 2. Position response of WB-sensors with orientations corresponding to **a** Fig. 1b and d, and **b** Fig 1b and c. Curves 1, 2, 3, 4 correspond to R1 coordinates: $\{x = x_0 = 0.5; 1; 2; 5$ mm, y = var; $z = z_0 = 6$ mm$\}$.

WB-network output signals are considered for different bridge sizes, numbers of sensitive elements, and orientations with respect to the label, see an example in Fig. 1. We demonstrate that the WB output signal, as a function of approach distance to the label, strongly depends on several factors. First is the trajectory of the sensor, i.e., the height and width of the signal strongly depend not only on the distance of the nearest approach of the sensor to the label, the so-called impact parameter, but also the position of the line of motion with respect to the geometry and orientation of the label, see examples in Fig. 2.

The design and parameters of the WB-sensor is a second factor. Here we consider WB-like sensors of rectangular design with four SV-elements, balanced in a no-field environment, with one-of-four or two-of-four sensitive SV-elements and the other SV-elements protected from the influence of a magnetic field. We show that the shape and amplitude of the output signal critically depend on the configuration of the sensitive and protected WB-arms, the size of the sensor, the number (one or two) of sensitive elements, and spacing between the sensitive arms.

A third factor is the orientation of the WB-sensor with respect to the label, compare Figs. 2a and b. In Figs. 1 and 2, we demonstrate that the response of the sensor is crucially dependent on the initial orientation of the WB basic plane and magnetic moments of the sensitive elements within the plane.

Calculations provided new information on a WB-like SV-sensor manifold response to the nonhomogeneous magnetic field of an object. This information can be used to design positioning devices for a variety of applications, including the localization and positioning of a moving magnetic object.

A.O28

FEATURES OF FERROMAGNETISM IN PALLADIUM FILMS IMPLANTED WITH COBALT AND IRON IONS

R.I. Khaibullin[1*], A.I. Gumarov[1,2], I.R. Vakhitov[2], N.M. Lyadov[1], I.I. Gumarova[2], I.V. Yanilkin[1,2], R.V. Yusupov[2], L.R. Tagirov[1,2]

[1]Zavoisky Physical-Technical Institute, FRC Kazan Scientific Center of RAS, Kazan, Russia
[2]Kazan Federal University, Kazan, Russia
[*]E-mail: rikkfti@mail.ru

Thin films of diluted $Pd_{1-x}Fex$ alloys (where $x \leq 0.1$) are of particular interest in superconducting spintronics [1]. Recently [2], we applied ion implantation technique to obtain the desired $Pd_{1-x}Fe_x$ alloys by using implantation with 40 keV Fe^+ ions into epitaxial Pd films. The ion-synthesized thin film $Pd_{1-x}Fe_x$ alloys revealed low-temperature ferromagnetism with a Curie temperature (T_C) depending on the concentration of iron implant. In the current study, we show the influence of the chemical type of the implant (Fe *vs*. Co) as well as the effect of co-implantation of both 3d-elements on the magnetic properties of epitaxial Pd films.

Samples for our research had been obtained by using implantation with 20, 40, or 80 keV Fe^+ ions and Co^+ ions into epitaxial Pd films (50–70 nm thick) to equal total dose of $1.0 \cdot 10^{16}$ ions/cm^2 for both single ion (Co or Fe) and double ion (Co with Fe) implantations. All implanted Pd films were post-annealed in UHV ($5 \cdot 10^{-9}$ mbar) at 770 K for 2 hours and then the magnetic properties were investigated by vibrating sample magnetometry (VSM). The magnetic study was supported by structure characterization of the samples by scanning electron microscopy, X-ray photoelectron spectroscopy, as well by *ab initio* calculations of impurity ferromagnetism in Pd:3d-metal system.

Figure 1 shows the influence of the chemical type of 3d-ions on the magnetic hysteresis loops $M(H)$ and thermomagnetic curves $M(T)$ of Pd films implanted with either Co^+ ions or Fe^+ ions. It can be clearly seen from the figure, at equal values of the T_C the Pd film implanted with iron exhibits a higher magnetization value and a narrow magnetic hysteresis loop with a coercive field of $H_c \cong 7$ Oe than the sample implanted with cobalt, for which the coercivity values are two orders of magnitude higher ($H_c \cong 1050$ Oe).

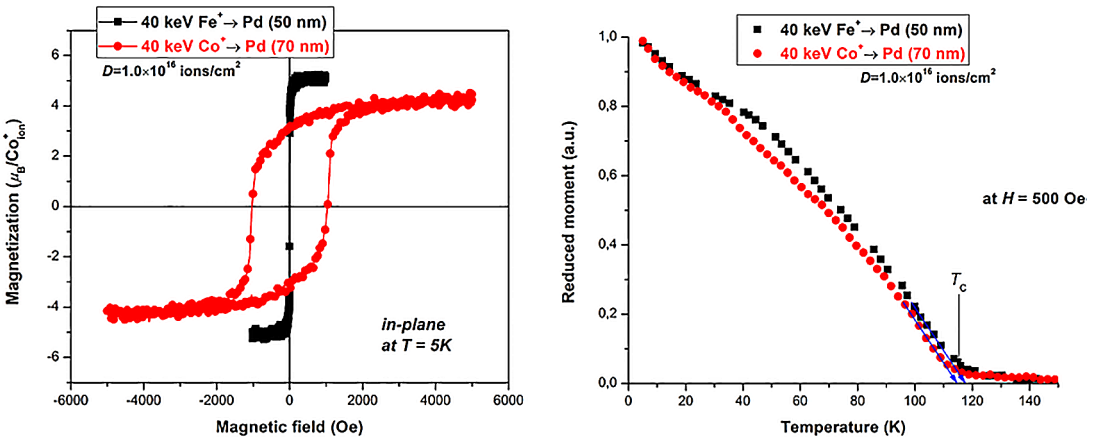

Figure 1. $M(H)$ (left) and $M(T)$ (right) curves of epitaxial 50-70 nm-thick Pd films implanted with either Fe^+ ions (squares) or Co^+ ions (circles) to a dose of $1.0 \cdot 10^{16}$ ions/cm^2.

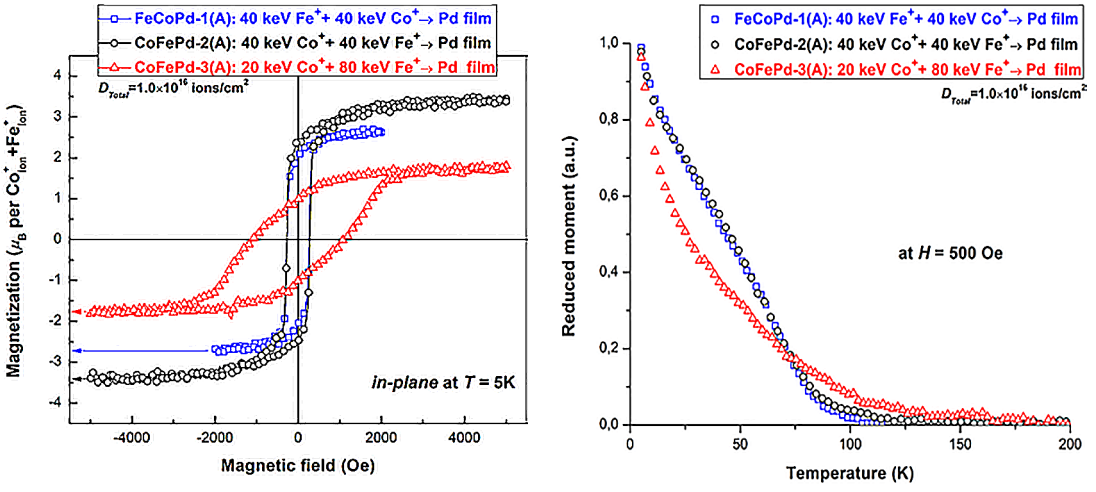

Figure 2. $M(H)$ (left) and $M(T)$ (right) curves of epitaxial 50 nm-thick Pd films co-implanted with Fe^+ and Co^+ ions at different order of ion implantation: at first 40 keV Fe^+ ions and then 40 keV Co^+ ions (squares) or vice versa (circles) as well as at first 20 keV Co^+ ions and then 80 keV Fe^{++} ions (triangles). For each type of magnetic ion, a dose of $0.5 \cdot 10^{16}$ ions/cm^2 was used.

Figure 2 shows the effect of co-implantation with Fe^+ and Co^+ ions on the magnetic properties of Pd films. In this work, three samples were studied. In the first two samples, both ions were implanted at the same energy of 40 keV (in fact, at the same depth), but with a different sequence: first iron and then cobalt in the FeCoPd-1(A) sample and *vice versa* in the CoFePd-2(A) sample. In the third sample CoFePd-3(A), iron and cobalt ions were separated in depth Pd film by using different ion energies: 20 keV for Co and 80 keV for Fe during implantation. An analysis of the results of studies of these co-implanted (composite) samples allows us to conclude that in the case of implantation of both impurities with the same energy, the iron impurity determines the value of the total magnetization (M_s) of the sample and suppresses the high coercivity from cobalt. In this case, different values of the Ms in FeCoPd-1(A) and CoFePd-2(A) samples can be associated with different coefficient of ion sputtering of Pd films during Fe or Co ion implantation. In the case of implantation of Co and Fe impurities at different ion energy (sample CoFePd-3(A)), the cobalt implant is closer to the surface of the Pd film, and ones suppresses ferromagnetic response induced by the iron impurity.

This work was supported by RFBR, grant No 20-02-00981. Authors thanks V.I. Nuzhdin and V.F. Valeev (ZPTI of FRC KSC of RAS) for technical assistance with ion implantation experiments.

1. V.V. Ryazanov, V.V. Bol'ginov, D.S. Sobanin, I.V. Vernik, S.K. Tolpygo, A.M. Kadin, O.A. Mukhanov, Phys. Procedia. **36**, 35 (2012).
2. A.I. Gumarov, I.V. Yanilkin, R.V. Yusupov, A.G. Kiiamov, L.R. Tagirov, R.I. Khaibullin, Mater. Lett. **305**, 130783 (2021).

A.O29

INVESTIGATION OF THE DEPENDENCE OF THE MAGNETIC PROPERTIES OF FeNi ALLOY NANOWIRES ON THE ASPECT RATIO

I.M. Doludenko[1*], *D.L. Zagorskiy*[1], *D.R. Khairetdinova*[1,2]

[1]FSRC "Crystallography and Photonics", Russian Academy of Sciences, Moscow, Russia
[2]NUST "MISIS", Moscow, Russia
[*]E-mail: doludenko.i@yandex.ru

Currently, nanostructures and nanoobjects are being used in an increasing number of fields of science and technology. One of the most important issues now is the correlation between the structure of the objects obtained and the methods for obtaining them. One of such methods is the matrix synthesis method. This method is based on the galvanic filling of matrix pores with certain parameters by one or another substance. The method makes it possible to widely vary the structure and, consequently, the properties of the obtained nanoobjects. In this work, a matrix based on a track membrane was filled by electrochemical deposition with FeNi metal alloys with different ratios of elements. The dependence of the structure of one-dimensional magnetic nanowires (NWs) on the production mode and the process of their growth were considered in order to create a predictable model. As part of the work, the influence of geometric parameters, namely the aspect ratio, on the magnetic properties of the resulting nanoparticles was studied.

Track membranes with the following parameters were used as a matrix: film thickness, 12 μm; pore diameter, 100 nm; pore density (set by irradiation parameters) – $1.2 \cdot 10^9$. The change in the composition of the resulting NWs was achieved by changing the composition of the electrolyte. At the first stage of the study, the deposition was carried out at a constant potential of 1.5 V using a two-electrode galvanic cell with an iron anode.

The process of filling matrices was studied in more detail on one of the compositions for obtaining NWs from $Fe_{24}Ni_{76}$, which was chosen as a model. According to the chronoampere dependences and SEM, it was found that the deposition process can be divided into 5 stages. Stage 1 – the process of the beginning of the growth of nanowires, while the current drop occurred in accordance with the Cottrell law [1]; 2nd stage – filling the matrix pores and further development of the diffusion layer; 3rd stage – partial release of the deposited metal to the surface of the matrix; 4th stage – complete filling of the matrix; 5th stage – the formation of a continuous layer of metal on the surface of the matrix. The dependences of the growth rate and current efficiency were also established for various stages of matrix filling. The resulting model made it possible to deposit NWs of a given length.

After obtaining, the structure of the samples was studied by SEM with elemental analysis. It was proved that all NWs have a similar topography determined by the geometry of the pores. The main interest in the work was the elemental analysis of the samples. For all NW from the FeNi alloy, the effect of anomalous deposition of iron is observed: the Fe content in the NW exceeded the content in the electrolyte solution. In this case, with an increase in the Fe concentration, the difference between the compositions increased from 10% to 35%.

X-ray diffraction analysis of the samples showed that, in all cases, the nanoparticles consist of solid solutions. With an increase in the iron content of more than 25%, a transition from the fcc to the bcc lattice occurs. Within the phase, with a change in concentration, a regular change in the lattice parameter occurs.

At the second stage of the work, the distribution of elements along the length of the NWs made of the $Fe_{24}Ni_{76}$ alloy was studied. At the initial deposition potential, the composition changes

along the length – the changes are about 7%: the Fe concentration increases with approaching the top of the NW. For samples of the $Fe_{24}Ni_{76}$ alloy, the dependence of the distribution of elements along the length depending on the deposition potential was studied. It was found that the uneven distribution of elements along the length of the NW strongly depends on the deposition potential. With a decrease in the potential, the difference in the concentration of iron is 16%, and under the condition of an increase in the potential, it practically reduces to zero.

It can be concluded that the diffusion rate of ions in a limited volume of matrix pores is not equal. Namely, that the rate of Ni^{+2} is less than that of Fe^{+2}. This dependence is also confirmed by the integral analysis of the elemental composition of the NWs samples obtained at different potentials.

Using the previously obtained growth model, nanowires with different lengths were grown to study their magnetic properties depending on their aspect ratio. It is shown that the coercive force decreases with decreasing aspect ratio. The coercive force can vary in this way from 100 to several hundred Oe. The nature of the dependence is not linear, which may be due to the features of the matrix. The data obtained can be used to create flexible micromagnets, sources of electromagnetic waves and nanoparticles with the effect of hyperthermia for medical applications.

This work was supported by the Russian Science Foundation N 22-22-00983 and was done (in part) within the State Task of Federal Scientific Research Center (FSRC) "Crystallography and Photonics" RAS.

1. S. Valizadeh, J.M. George, P. Leisner, L. Hultman, Electrochim. Acta. **47**, 865–874 (2001).

MAGNETIZATION REVERSAL MECHANISMS OF FeNi/FeMn BILAYERS DEPENDING ON GROWTH CONDITIONS

Ch. Gritsenko[1*], *V. Lepalovskij*[2], *M. Volochaev*[3], *V. Komanický*[4], *A. Gorkovenko*[2], *H. Pazniak*[5], *N. Andreev*[1,6], *V. Rodionova*[1]

[1]Research and Education Center "Smart Materials and Biomedical Applications", Immanuel Kant Baltic Federal University, Kaliningrad, Russia
[2]Solid State Magnetism Department, Institute of Natural Sciences and Mathematics, Ural Federal University, Ekaterinburg, Russia
[3]Kirensky Institute of Physics, Federal Research Center KSC SB RAS, Krasnoyarsk, Russia
[4]Institute of Physics, Faculty of Science, Pavol Jozef Šafárik University, Kosice, Slovakia
[5]Faculty of Physics and Center for Nanointegration Duisburg-Essen (CENIDE), University of Duisburg-Essen, Duisburg, Germany
[6]Materials Science and Metallurgy Shared Use Research and Development Center, National University of Science and Technology MISiS, Moscow, Russia
[*]E-mail: christina.byrka@gmail.com

For thin film materials with exchange-coupled ferro- and antiferromagnetic layers, below the Neel temperature and at induced uniaxial magnetic anisotropy, magnetic hysteresis loops are shifted. This phenomenon is called the exchange bias and is widely used in modern spintronics, magnetic recording, and magnetic sensorics, for example, in giant magnetoresistance (GMR)-based or giant magnetoimpedance (GMI)-based elements [1, 2]. Depending on the application, the most important property of an exchange bias system can be either the effect value [3], or layer thickness, or hysteresis loop shape [4]. This work was aimed at a better (compared to the existing) understanding of a relationship between structural and magnetic properties of NiFe/FeMn thin films with thick ferromagnetic layers up to 50 nm, which can be used in developing GMI-based elements.

We studied magnetization reversal processes in the NiFe/FeMn exchange biased structures with various antiferromagnetic layer thicknesses (0–50 nm) and glass substrate temperatures (17–600 °C) during deposition. Magnetic measurements were performed in the temperature range from 80 up to 300 K. Hysteresis loop asymmetry was found at temperatures lower than 150 K for the samples with an antiferromagnetic layer thickness of more than 10 nm. The average grain size of FeMn was found to increase with the AFM-layer increase, and to decrease with the substrate temperature increase. Hysteresis loop asymmetry was explained in terms of the exchange spring model in the antiferromagnetic layer.

The electron microscopy investigations were carried out on the equipment of Krasnoyarsk Regional Center of Research Equipment of Federal Research Center "Krasnoyarsk Science Center SB RAS".

1. R.B. Da Silva et al., Appl. Phys. Lett. **94**(4), 042501 (2009).
2. C. García et al., Appl. Phys. Lett. **96**(23), 232501 (2010).
3. G. Vinai et al., Appl. Phys. Lett. **104**(16), 162401 (2014).
4. D.N. Merenkov et al., Low Temp. Phys. **33**(11), 957–964 (2007).

A.O31

ULTRA FAST SPIN POLARIZATION SWITCHING IN A HYBRID STRUCTURE QUANTUM WELL – SPIN SPLIT BOUND STATE

V.N. Mantsevich[1*], *I.V. Rozhansky*[2,3], *N.S. Maslova*[1], *P.I. Arseyev*[4], *N.S. Averkiev*[2,3], *E. Lahderanta*[3]

[1]Lomonosov Moscow State University, Moscow, Russia
[2]Ioffe Physical Institute, Saint-Petersburg, Russia
[3]Lappeenranta Technical University, Lappeenranta, Finland
[4]P.N. Lebedev Physical Institute, Moscow, Russia
[*]E-mail: vmantsev@gmail.com

Nowadays, the research field of spintronics continues to grow covering various spin phenomena in solid-state physics [1]. The spin injection into a semiconductor remains the cornerstone of modern spintronics. The conductivity mismatch prevents an efficient spin injection from a ferromagnetic metal into a semiconductor [2]. Some ways to overcome this difficulty have been proposed based on spin-polarized transport across a heterojunction [3]. Also the widely discussed solutions of this problem include application of a dilute magnetic semiconductor as a spin injector [4] or spin injection from a ferromagnet through a tunnel barrier [5].

We considered a spin injection into a semiconductor due to spin-dependent relaxation of an initially unpolarized ensemble of charge carriers. In our model a nonequilibrium distribution of the nonpolarized carriers is assumed created instantaneously in the QW. We analyze theoretically the subsequent kinetics of the spin polarization. We have studied dynamic spin injection by the mechanism of spin-dependent relaxation in a quantum well coupled to the spin-split bound state [6]. The role of the Coulomb correlations at the bound state on the spin and sheet density kinetics in the QW were analyzed. It was revealed that the effect of the Coulomb correlations leads to an effectively larger spin splitting at the bound state and, consequently, an enhanced spin polarization of the electrons remaining in the QW. Moreover, it increases the characteristic time of the carriers relaxation in the QW since it reduces the electron tunneling into the bound state. We predicted that the interplay of these two effects would lead to the nontrivial dependence of a circular polarization degree of photoluminescence from the QW.

We propose two mechanisms for ultrafast switching of the spin polarization in the QW. One of them is based on the laser pulse frequency tuning between the bound state spin sublevels [7]. Another one is associated with remote spin-split bound states [8, 9]. A mechanism of ultrafast PL polarization switching in this case is based on tunnel barrier transparency modulation. Such modulation can be experimentally realized by applying a gate voltage to the semiconductor heterostructure. The proposed mechanism is based on the split-off state energy level position being sensitive to the transparency of the tunnel barrier. Mn-doped core/multishell nanoplatelets and hybrid bound state-semiconductor heterostructures are suggested as promising candidates to prove the predicted effect experimentally. The obtained results open the possibility to form fully polarized PL signal and is promising for applications in spintronics, in particular, for ultrafast polarization modulation in spin lasers.

The work is supported by RSF grant №18-72-10002.

1. A. Hoffmann and S.D. Bader, Phys. Rev. Appl. **4**, 047001 (2015).
2. A. Fert and H. Jaffrès, Phys. Rev. B **64**, 184420 (2001).
3. I. Žutić, J. Fabian, and S.C. Erwin, Phys. Rev. Lett. **97**, 026602 (2006).
4. T. Dietl and H. Ohno, Rev. Mod. Phys. **86**, 187 (2014).

5. E.I. Rashba, Phys. Rev. B **62**, R16267(R) (2000).
6. N.S. Maslova, I.V. Rozhansky, V.N. Mantsevich, P.I. Arseyev, N.S. Averkiev, E. Lahderanta, Phys. Rev. B **97**, 195445 (2018).
7. V.N. Mantsevich, I.V. Rozhansky, N.S. Maslova, P.I. Arseyev, N.S. Averkiev, E. Lahderanta, Phys. Rev. B **99**, 115307 (2019).
8. I.V. Rozhansky, V.N. Mantsevich, N.S. Maslova, P.I. Arseyev, N.S. Averkiev, E. Lahderanta, Phys. Rev. B **101**, 045305 (2020).
9. I.V. Rozhansky, V.N. Mantsevich, N.S. Maslova, P.I. Arseyev, N.S. Averkiev, E. Lahderanta, Physica E, **132**, 14775 (2021).

A.O32

THE QUANTUM MECHANICAL CALCULATION OF THE THERMAL-DRIVEN SPIN TRANSFER IN THE MTJ BASED ON A CRYSTALLINE MgO TUNNEL SPACER

*G.D. Demin**, *N.A. Dyuzhev*

R&D Center "MEMSEC", National Research University of Electronic Technology (MIET), Moscow, Zelenograd, Russia

*E-mail: gddemin@edu.miet.ru

The significant progress has been made since the discovery of the tunnel magneto-Seebeck effect in the MTJ in 2011 [1], which is associated with the generation of a spin-dependent thermoelectric voltage at a nonzero temperature gradient across the tunnel barrier [2]. In particular, the Seebeck coefficient in the MTJ structure increased from tens of μV/K [3] to record values close to 0.4 mV/K [4], which is several times higher than the similar parameters of modern thermoelectric materials (BiTe, Cr, NiFe), usually used in commercial prototypes of thermoelectric generators. Despite this fact, such an increase can only be achieved within a narrow temperature range (285–290 K) and strongly depends on the thickness of the antiferromagnetic layer in the MTJ, which requires further development of methods for optimizing its structure and layer composition, as well as consideration of new microscopic mechanisms for improving tunnel magneto-Seebeck effect for practical applications. According to theoretical predictions of J. Slonczewski [5], the thermal-driven spin-transfer torque (STT) that occurs during the non-uniform heating of the MTJ can be several times higher than the STT induced by the spin-polarized current, which is especially attractive for the formation of an energy-efficient concept of the STT-based magnetoresistive memory elements.

In this work, we calculated the spin-dependent Seebeck coefficient (Fig. 1) and the corresponding (field-like, damping-like) components of thermal-driven STT in the MTJ with a MgO tunnel barrier generated due to its Joule heating by a direct current.

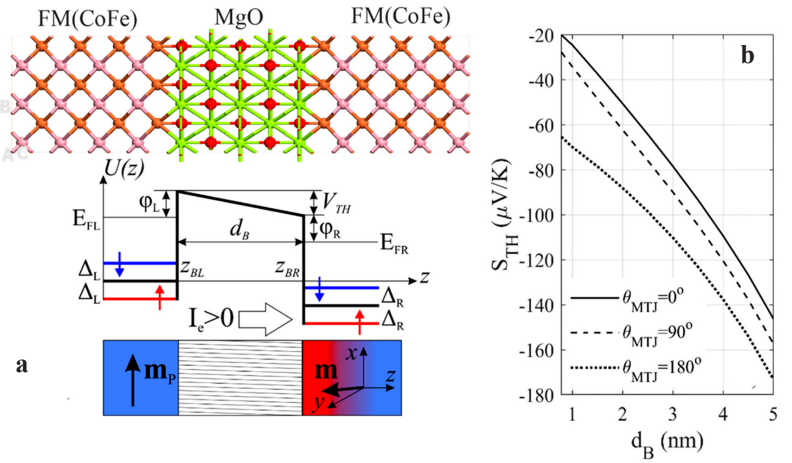

Figure 1. **a** The schematic potential profile of the MgO-based MTJ under its non-uniform heating by an external current. **b** The Seebeck coefficient as a function of the thickness of the MgO tunnel spacer in the CoFe-MgO-CoFe magnetic stack, where θ_{MTJ} is the angle between the magnetizations of the ferromagnetic (FM) layers.

The simulation was carried out both on the basis of the quantum-mechanical free-electron Sommerfeld model and first-principles model of spin transport with the non-equilibrium Green's function (NEGF) formalism to describe electron tunneling through the MgO crystalline layer. The distribution of the temperature gradient across the MTJ stack was obtained for the selected composition and thermal parameters of the MTJ layers. It was found that an increase in the Seebeck coefficient to a level above 150 μV/K is achieved by increasing the thickness of the MgO layer (up to 5 nm) and lowering the MgO barrier height (up to 1 eV and lower), which also requires high-quality technological optimization of the magnetic layer/MgO interfaces. The rise of the temperature gradient across the MgO layer is possible by including thermal barriers (CuSbSe, CuS, CuSTe, SnSe, GeSbTe) with low thermal conductivity in the region of its interfaces, which makes it possible to enhance the heating asymmetry by tens or more times and thus increase the thermal-driven STT.

The results obtained can be used in the development of new technological solutions aimed at creating highly efficient thermoelectric spintronic devices for the spin caloritronics tasks.

The work was performed based on the equipment of R&D Center "MEMSEC" (MIET) and supported by the RF Ministry of Science and Higher Education (#075-15-2021-1350).

1. M. Walter et al., Nature Mater. **10**, 742–746 (2011).
2. T. Kuschel et al., J. Phys. D: Appl. Phys. **52**, 133001 (2019).
3. T. Huebner et al., Phys. Rev. B **96**, 214435 (2017).
4. S. Tu et al., Nat. Commun. **11**, 2023 (2020).
5. J.C. Slonczewski, Phys. Rev. B **82**, 054403 (2010).

A.O33

HEAT-INDUCED FANO RESONANSE TUNABILITY IN MAGNONIC MICROSTRUCTURES

*A.A. Grachev**, *E.N. Beginin, A.V. Sadovnikov*

Laboratory "Magnetic Metamaterials", Saratov State University, Saratov, Russia
*E-mail: stig133@gmail.com

Recent advances in the creating micro- and nano-sized magnetic structures based on insulating materials open up a promising alternative to signal processing using spin waves (SW) compared to CMOS (complementary metal-oxide-semiconductor structure) technologies based on magnonic networks [1] increasing the functionality of basic units of computing systems, as well as those with low energy consumption. Micro- and nanosized magnetic structures is a promising base for the creation of magnonic integrated circuits [2], which makes it possible to overcome the limitations of CMOS electronics. In this case, the main attention is paid to the use of SWs as carriers of information signals, since in this case it is possible to implement a number of signal processing devices based on the principles of magnonics [1, 2].

Here we report about formation asymmetric Fano-type resonances in a system based on irregular magnonic microwaveguides, which consists an array of resonators. By means of Brillouin light scattering (BLS) spectroscopy and microwave spectroscopy we are measured a transmission of SW and demonstrate a formation of asymmetric resonances in transmission characteristics.

The structure (Fig. 1) is fabricated from a YIG film with a thickness of 10 μm and a saturation magnetization of $4\pi M_0$ = 1750 G. The structure consists of two identical planar microwaveguides with a width w = 200 μm. The length of the structure is 6 mm. Between the microwaveguides there is a system of resonators with a width w and length of 500 μm. The entire structure is placed in an external uniform magnetic field H_0 = 1200 Oe, directed along the y-axis, which ensures efficient excitation of surface magnetostatic waves (MSSWs).

Using a micromagnetic modeling, we developed a model that describes the formation of asymmetric Fano-type resonances. To control the transmission characteristics of spin waves in irregular microwaveguides and an array of resonators in the center of the microwaveguides, we use a laser light on resonators to change a saturation magnetization in YIG microwaveguides.

This work is supported by RSF grant (#20-79-10191).

1. A. Barman et al., J. Phys.: Condensed Matter **33**(41), 413001 (2021).
2. S.A. Nikitov et al., Phys. Usp. **63**, 945–974 (2020).

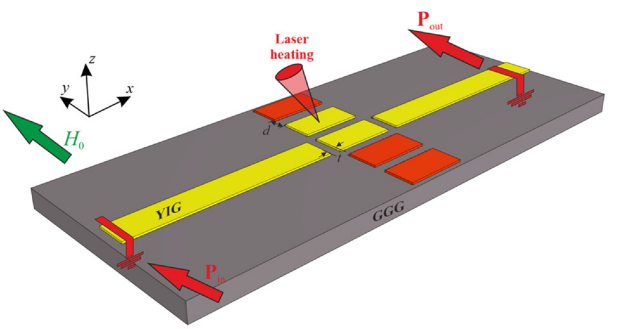

Figure. 1. Scheme of irregular microwaveguides and a system of resonators between them.

A.O34

MAGNETIC ANISOTROPY AND DZYALOSHINSKII-MORIYA INTERACTION IN EPITAXIAL Pd/Co/CoO FILMS

A.G. Kozlov[1*], *G.S. Suslin*[1], *E.V. Tarasov*[1,2], *O.E. Ayanitov*[1], *V.S. Shatilov*[1], *A.V. Davydenko*[1]

[1]Institute of High Technologies and Advanced Materials, FEFU, Vladivostok, Russia
[2]Institute of Chemistry, Far Eastern Branch of the RAS, Vladivostok
[*]E-mail: kozlov.ag@dvfu.ru

We study the dependences of magnetic parameters, such as magnetic anisotropy and the interfacial Dzyaloshinskii-Moriya interaction (DMI) on the ferromagnetic and oxide layer thicknesses in Pd(111)/Co/CoO /Pd thin epitaxial films. Epitaxial Si(111)/Cu(2 nm)/Pd(2 nm)/Co(1 nm) films were grown by molecular beam epitaxy in ultrahigh vacuum chamber. After deposition of Co layer, films were exposed via dry oxygen. Two series of samples was created: with different Co thickness and with different exposition dose (L; 1 Langmuir corresponds to a dose of 10^{-6} Torr·s). For first series we changed the Co thickness with fixed exposition dose, and in the second series we deposited Co 1 nm layer and exposed with different doses. We varied the oxide thickness and this way we changed ferromagnetic thickness. The significant mismatch of Co and Pd lattice parameters is induce a significant elastic strains on the bottom interface, which leads to strong perpendicular magnetic anisotropy [1]. Effective magnetic anisotropy reduces with Co thickness increasing up to 1,5 nm with an out-of-plane easy axis and after that increase linearly with an in-plane easy axis of magnetization. Definition of the thickness of the magnetic layers carried out by measuring the saturation magnetic moment with vibrating samples magnetometry. Oxidation of magnetic layer leads to symmetry breaking on the bottom and top magnetic interfaces in epitaxial films, which reduces compensation of interfacial DMI. To determine the interfacial DMI of the films we analyzed the velocity-curves described the asymmetrical propagation of domain walls in creep mode. Magnetic structure was investigated by a magneto-optical Kerr effect (MOKE) microscope which was equipped with a hand-made coil applying out-of-plane magnetic fields and an in-plane electromagnet. The

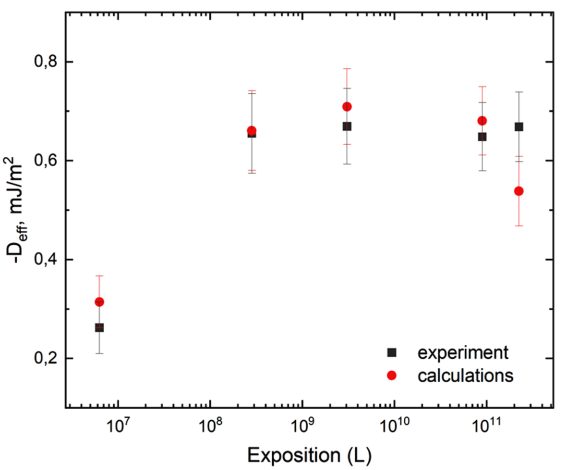

Figure 1. Interfacial DMI constant as a function of oxidation dose of Co. Experimental points ware measured by domain walls velocity-curves. Theoretical values were calculated with extended dispersive stiffness model [2].

out-of-plane coil was used in pulse mode and produced magnetic fields. Including of oxide layer is eliminate the asymmetrical contribution of chiral dumping [2]. Based of the velocity-curves, we calculated D_{eff} and compared with theoretical calculations was shown in Fig. 1.

The work was supported by the Ministry of Science and Higher Education of the Russian Federation (State Assignment No. 0657 2020 0013) and by Council for Grants of the President of the Russian Federation (project – MK-1384.2021.1.2).

1. A.V. Davydenko, A.G. Kozlov, A.V. Ognev, M.E. Stebliy, A.S. Samardak, K.S. Ermakov, A.G. Kolesnikov, L.A. Chebotkevich, Phys. Rev. B **95**, 064430 (2017).
2. A.V. Davydenko, A.G. Kozlov, M.E. Stebliy, A.G. Kolesnikov, N.I. Sarnavskiy, I.G. Iliushin, A.P. Golikov, Phys. Rev. B **103**, 094435 (2021).

A.O35

INVESTIGATION OF MAGNETIC TUNNEL JUNCTIONS UNDER THE SIMULTANEOUS ACTION OF DIRECT AND ALTERNATING CURRENTS, BOTH IN RESONANT AND BROADBAND MODES

A.V. Duvakina[1*], *G.A. Kichin*[1], *P.N. Skirdkov*[1,2], *K.A. Zvezdin*[1,2]

[1]New Spintronic Technologies, Russian Quantum Center, Skolkovo Innovation Center
[2]Prokhorov General Physics Institute of the Russian Academy of Sciences
[*]E-mail: a.duvakina@nst.tech

At present, spintronics is a promising direction in electronics due to the possibility of creating high-speed devices with low power consumption and heat release.

The magnetic tunnel junction (MTJ) is the main part of many spintronic devices. This structure consists of two thin layers of a ferromagnet, reference and free, separated by a dielectric layer. The operation of this device is based on the effects of tunneling magnetoresistance and spin transfer. A spin-polarized alternating microwave current excites magnetization precession in the free layer and can also excite ferromagnetic resonance modes, when injected into a nanoscale ferromagnetic layer. The excitation of the FMR mode in a MTJ is accompanied by a fluctuation of its resistance and leads to a rectification effect [1]. The reference layer and the state of magnetization near the edge of the sample can also be additional sources of resonant modes and affect the efficiency of microwave signal rectification. This is the description of the resonant mode of the MTJ rectification.

In addition to rectification near the FMR modes, there are large regions where microwave signal rectification is also observed. Such regions appear near magnetic transitions and have a width of several hundred Oersteds in the field. They are limited in terms of frequencies from above by the FMR mode, and from below by low frequencies with values of hundreds of megahertz. Such a broadband regime of spin diodes was theoretically predicted in 2012 [2] and presented experimentally [3].

It was demonstrated [4, 5] that the rectified voltage obtained by a MTJ increases when a DC bias current is applied. In this case the magnetization of the free layer fluctuates with a large amplitude, while in the case of only RF excitation, it exhibits only small deviations. A DC bias current increases the resulting voltage since the damping of the magnetization precession decreases.

We will consider the effect of the bias current on the spectral characteristics of a MTJ operating in both resonant and broadband modes in this report.

To study these dependencies, the following experimental measurement technique has been developed. The microwave signal and bias current were applied to the device using a signal generator and a source measure unit. The microwave signal was modulated using a modulator at a low frequency supplied from a lock-in amplifier. The rectified voltage was also measured using a lock-in amplifier.

We used a cylindrical sample with a diameter of 200 nm with a multilayer structure to study the spectral characteristics of the MTJ. Rectified voltage versus frequency curves was obtained for a range of DC bias currents from 0 to 2 mA.

It was found that for the current range from 0 to 1.3 mA, the resulting voltages increase significantly, and the spectra shift to a higher frequency. The current value of 1.4 mA corresponds to the auto-generation current (I^{th}). The maximum rectified voltage of the spectra decreases at bias currents larger than I^{th} (from 1.4 to 2 mA).

Experimental data show that broadband rectification is suppressed with increasing bias current in the region near zero fields. The broadband voltage rectification mode is most visible in the absence of a bias current.

This work was supported by Russian Science Foundation (grant № 19-12-00432).

1. A. Tulapurkar, Y. Suzuki, A. Fukushima, H. Kubota, H. Maehara, K. Tsunekawa, D. Djayaprawira, N. Watanabe, S. Yuasa, Nature **438**, 339 (2005).
2. O. Prokopenko, I. Krivorotov, E. Bankowski, T. Meitzler, S. Jaroch, V. Tiberkevich, A. Slavin, J. Appl. Phys. **111**, 123904 (2012).
3. B. Fang, M. Carpentieri, S. Louis, V. Tiberkevich, A. Slavin, I.N. Krivorotov, R. Tomasello, A. Giordano, H. Jiang, J. Cai, Y. Fan, Z. Zhang, B. Zhang, J. A. Katine, K.L. Wang, P.K. Amiri, G. Finocchio, Z. Zeng, Phys. Rev. Appl. **11**, 014022 (2019).
4. S. Miwa, S. Ishibashi, H. Tomita, T. Nozaki, E. Tamura, K. Ando, N. Mizuochi, T. Saruya, H. Kubota, K. Yakushiji, T. Taniguchi, H.Imamura, A. Fukushima, S. Yuasa, Y. Suzuki, Nat. Mater. **13**, 50 (2014).
5. B. Fang, M. Carpentieri, X. Hao, H. Jiang, J.A. Katine, I.N. Krivorotov, B. Ocker, J. Langer, K.L. Wang, B. Zhang, B. Azzerboni, P.K. Amiri, G. Finocchio, Z. Zeng, Nat. Commun. **7**, 11259 (2016).

A.O36

INFLUENCE OF THE NANOCRYSTALLITE SIZE ON SPATIAL SPIN-MODULATED STRUCTURE OF $BiFeO_3$

N.E. Gervits[1*], *A.V. Tkachev*[1], *S.V. Zhurenko*[1], *A.V. Gunbin*[1], *N.A. Lomanova*[2], *D.P. Danilovich*[3], *A.V. Bogach*[4], *A.A. Gippius*[1,5]

[1]Lebedev physical institute RAS, Moscow, Russia
[2]Ioffe Institute, St. Petersburg, Russia
[3]Saint-Petersburg State Institute of Technology, St. Petersburg, Russia
[4]Prokhorov General Physics Institute RAS, Moscow, Russia
[5]Lomonosov Moscow State University, Moscow, Russia
[*]E-mail: ngervits@gmail.com

The existence of an incommensurate cycloid type magnetic spatial spin-modulated structure (SSMS) with a period of λ = 620±20 Å [1] in bismuth orthoferrite $BiFeO_3$ (BFO) and BFO-based compounds leads to a deterioration in the magnetic properties and, accordingly, the prospects for its application as a multiferroic. Search for methods of controlled destruction, suppression, and modification of SSMS draws attention for several decades. Main ways of SSMS modification are:

- the substitution of A-site atoms in the with atoms that differ in characteristics (magnetism, ionic radius, heterovalent substitution),
- magnetic fields,
- the transition to nano-scale.

The existence of SSMS is possible only in the presence of a phase with a rhombohedral structure (R3c); however, the presence of a rhombohedral structure alone is insufficient to confirm and characterize the magnetic properties of the sample. There is contradictory information in the literature about the existence of SSMS with a decrease of nanocrystalline size, since the effect on the magnetic moment of nanoobjects can be modified not only by SSMS suppression, but also by the presence of uncompensated spins on the surface, size limitation, due to which there are uncompensated regions of the cycloid, and other reasons [2].

The samples under study were synthesized by the solution combustion method and characterized by X-ray diffraction, the sizes of nanocrystals were estimated from 170 to less than 40 nm. Previously, we developed a protocol for measuring NMR-spectra in a zero field on ^{57}Fe nuclei, which makes it possible to study SSMS even in samples with a natural ^{57}Fe isotope abundance [3].

NMR-spectroscopy revealed the presence of SSMS in all the studied samples, even in the ones with linear size less than the cycloid period. The anharmonicity parameter *m*, which characterizes the degree of harmonicity of SSMS, decreases monotonically with decreasing nanocrystallite size, and in the ~50 nm size region, the anisotropy type changes from “easy axis” to “easy plane”.

1. I. Sosnowska, T. Neumaier, E. Steichele, J. Phys. C: Solid State Physics **15**, 4835 (2000). 10.1088/0022-3719/15/23/020.
2. R. Mazumder, P. Devi, D. Bhattacharya, P. Choudhury, A. Sen, M. Raja, Appl. Phys. Lett. **91**, (2007). 10.1063/1.2768201.
3. N.E. Gervits, A.V. Tkachev, S.V. Zhurenko, A.V. Gunbin, V.S. Pokatilov, A.A. Gippius, Solid State Commun. **344**, 114682 (2022). 10.1016/j.ssc.2022.114682.

MAGNETIC RESONANCE PROPERTIES OF LOW-DIMENSIONAL COBALT-Al_2O_3-GERMANIUM TUNNEL CONTACT

A.V. Kobyakov[1,2*], *G.S. Patrin*[1,2], *V.I. Yushkov*[1,2], *Ya.G. Shiyan*[1,2], *R.Yu. Rudenko*[1], *N.N. Kosyrev*[2]

[1]Siberian Federal University, Krasnoyarsk, Russia
[2]Kirensky Institute of Physics, Krasnoyarsk Scientific Center, Siberian Branch, Russian Academy of Sciences, Krasnoyarsk, Russia
[*]E-mail: nanonauka@mail.ru

To create high-quality basic elements of spin electronics, it is necessary to solve the problems of creating spin polarization of electrons, maintaining it for a sufficiently long time, and detecting it. For example, a tunnel junction coupled to a ferromagnetic source of spin-polarized electrons is a candidate for efficient spin injection [1, 2]. The injection of spin-polarized electrons in systems of the ferromagnet/dielectric/semiconductor type has a number of features. For example, the interface should not contain the so-called "dead" – disordered layers, defects, for example, in the form of layer punctures, roughness of the previous layers [3]. Therefore, controlling the desired magnetic behavior in the synthesis of ferromagnetic complexes such as cobalt is still a big problem, and much more work is needed to expand knowledge of the structure-property relationship.

The study of magnetic properties and interfaces in the cobalt/Al_2O_3/germanium system in conjunction with the technological conditions of synthesis is of considerable interest [4]. In this work, we analyze the magnetic resonance behavior of the Al_2O_3(130 nm)/Ge(45 nm)/Al_2O_3(4.5 nm)/Co(95nm) structures, obtained by different technological methods.

The samples were obtained by ion-plasma evaporation at a base pressure of $P = 10^{-7}$ Torr in an argon atmosphere with a pressure of 3 mTorr. The substrate material was a cover glass, previously cleaned by ion-plasma etching in the working chamber, immediately before the deposition process. The deposition was carried out on a rotating substrate at its temperature $T \approx 373$ K.

Two sets of samples with different combinations of deposition rates of magnetic and non-magnetic layers were obtained. Set A is received in one cycle. Set B differs in that before the deposition of the magnetic layer, air was admitted into the system to atmospheric pressure in order to saturate the working chamber with gases (as a result of this, the roughness of the next magnetic layer increased, as can be seen from Table 1). Then pumping was carried out to the base pressure and the last Co layer was deposited.

Table 1. Sample marking, velosity, roughness.

	Cases of deposition of samples. The rate of deposition, nm/min								
	Layers:	A1	B1	A2	B2	A3	B3	A4	B4
	1 Al_2O_3	0.55				0.05			
	2 Ge	14.4				2.4			
	3 Al_2O_3	0.55				0.05			
Average roughness parameters of the cobalt surface.	4 Co	7.2		1.2		1.2		7.2	
	Rms (R_q) nm	8.3	16.5	4	12	4.4	13	5.3	14.5
	10 pt mean (R_z) nm	51.5	115	36	96	38	106	47	114

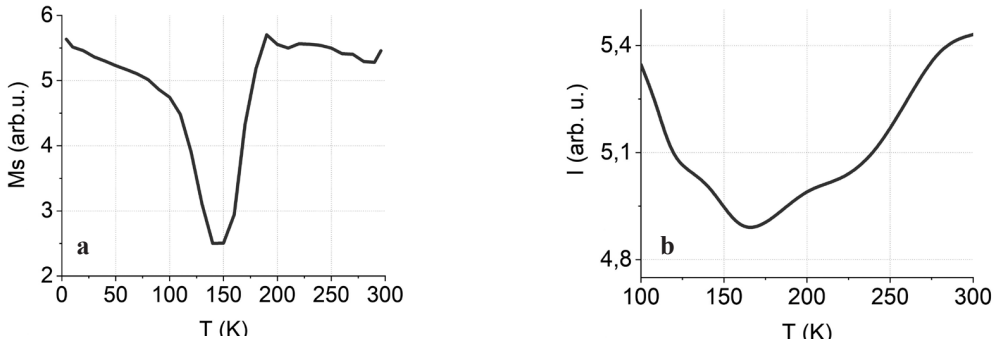

Figure 1. The temperature dependence of the saturation magnetization values (**a**) and FMR absorption line area (**b**) for samples A2 of structure $Al_2O_3/Ge/Al_2O_3/Co$.

The surface morphology of the films was studied using a VeecoMultiMode atomic force microscope (resolution 1 nm). The morphology, phase, and elemental composition of the films were studied using a JEOL JEM-2100 high-resolution transmission electron microscope equipped with an Oxford Instruments INCA x-sight (EDS) energy-dispersive spectrometer. Magnetic measurements were carried out using the method of the magneto-optical Kerr effect (NanoMOKE-2) and on a SQUID magnetometer. The magnetic field lay in the plane of the film. Before each measurement, the film was first placed in a demagnetizer and then cooled in a zero magnetic field (ZFC mode). As a result, hysteresis loops were obtained for all $Al_2O_3/Ge/Al_2O_3/Co$ samples.

Analysis of the AFM images of the cobalt surface observed in the selected region, obtained from all samples, shows that the surface contains the vast majority of cobalt grains with a diameter of 11 nm or more. The proportion consists ~90% hcp-Co to ~10% fcc-Co. There is a singularity in all temperature dependences of the saturation magnetization. At low temperatures, a minimum of the saturation magnetization value appears (see Fig. 1a for samples A2) 120 → 150 K. For case B in the area: $T = 50 \rightarrow 90$ K.

When measuring the EPR-response of cobalt for various samples, a spectrum was observed that for all samples is well approximated by a superposition of 1-2 lines of the Lorentz type (see Fig. 1b for samples A2) depending on the sample number. Since the area bounded by the resonance absorption line is proportional to the number of spins in the sample, the temperature dependences of the areas under the FMR lines were plotted. On all dependences, there is also a temperature minimum corresponding to the minimum on the temperature dependences of the saturation magnetization.

The difference in the temperatures of the magnetization minima for case A, from the side of the layers and the substrate, and for case B, shows that the growth of cobalt on the Al_2O_3 oxide layer has a direct effect on the magnetically disordered phase both at the interface and in the volume of cobalt. The effect of the Al_2O_3-layer on the temperature of the magnetization minimum can be substantiated by the following factors. First, by the diffusion of cobalt particles into the Al_2O_3-layer and the formation of a weakly magnetic interface. Secondly, the influence of the Al_2O_3-layer growth structure on the growth of the cobalt layer and, as a result, the predominance of either shape anisotropy or crystallographic magnetic anisotropy of ferromagnetic particles.

The work was carried out in the process of fulfilling the state task of the Ministry of Science and Higher Education of the Russian Federation No. FSRZ-2020-0011 "Synthesis and physical foundations of nanoscale film and granular composite materials for spintronics devices".

1. A. Fert and H. Jaffrès, Phys. Rev. B **64**, 184420 (2001).
2. A.I. Nikitchenko and N.A. Pertsev, Phys. Rev. Applied **14**, 034022 (2020).
3. N.A. Viglin, I.V. Gribov, V.M. Tsvelikhovskaya and E.I. Patrakov, Semiconductors **53**, 264 (2019).
4. A.C. Petrarca, A.M. Poma, V. Giulia, G. Bernardini, Nanotechnol. Rev. **9**(1), 1538 (2020).

A.P2

INVESTIGATION OF CURRENT-INDUCED FIELDS IN THE YIG/COTB STRUCTURE

M.A. Bazrov[1*], *M.E. Letushev*[1], *Zh.Zh. Namsaraev*[1], *M.E. Stebliy*[1], *Wenqing He*[2], *Caihua Wan*[2], *Xiufeng Han*[2]

[1]Laboratory of Spin-Orbitronics, Institute of High Technologies and Advanced Materials, Far Eastern Federal University, Vladivostok, Russia
[2]Beijing National Laboratory for Condensed Matter Physics, Institute of Physics, Chinese Academy of Sciences, Beijing, China
[*]E-mail: bazrov.ma@dvfu.ru

The development of reliable methods for local control of the magnetization orientation is a key direction in the development of spintronics. One of the promising control mechanisms is spin orbit torque (SOT) [1]. The mechanism is based on the use of a bilayer structure consisting of a metal layer, which can be a source of spin-polarized current, and a magnetically ordered layer, current injection into which leads to switching of the magnetization orientation. As a spin current source a heavy metal layer (W, Pt, Ta) is usually used whear due to spin Hall effect conduction current generat a spin current. However, there are alternative approaches when the spin current is generated as a result of the Seebeck effect [2] or the self-torque mechanism [3]. In the latter case, the spin

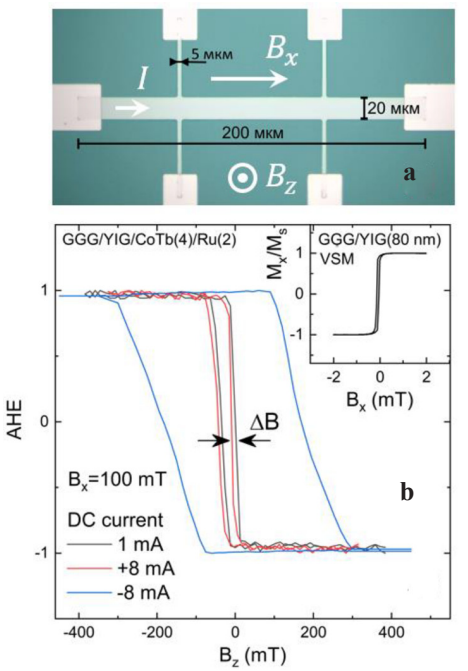

Figure 1. **a** Image of the Hall bar structure of the GGG/YIG(80)/$Co_{56}Tb_{44}$(4)/Ru(2 nm) composition with mutual orientations of the fields and current. **b** Hysteresis loops obtained by changing the perpendicular field for the different magnitude and orientations of the current propagetion through the Hall bar. In the insert VSM loop of single YIG film presented.

current is generated in the magnetically ordered layer, and then, as a result of reflection from the magnetic dielectric, it is injected back, inducing the SOT effect. To study this effect, the structure of YIG/CoTb/Ru was experimentally studied. Passing a current through the CoTb ferrimagnetic layer results in the generation of a spin current, which is reflected from the YIG dielectric ferromagnetic. The use of a ferrimagnet is due to the high efficiency of current-induced action [4].

For experimental verification of the approach, three types of structures were prepared with different percentages of Co and Tb atoms: W(4)/Co_xTb_{1-x}(4)/Ru(2), YIG(80)/Co_xTb_{1-x}(4)/Ru(2) and SiO_2/Co_xTb_{1-x}(4)/Ru(2) as a reference. The structures were deposited by magnetron sputtering. The CoTb layer was formed while sputtering mixed Co and Tb, the percentage was changed by changing the Co sputtering power. Hall bar structures were formed from the films obtained by photolithography and ion-plasma etching, Fig. 1a. The $Y_3Fe_5O_{12}$ (YIG) layer was preliminarily formed on the $Gd_3Ga_5O_{12}$ (GGG) (111) surface. The resulting layer is isotropic, the magnetization lines up along the external field at 1 mT, Fig. 1b.

To estimate the magnitude of the effective magnetic fields induced by the current, we used the method of magnetic hysteresis loops shifting [5]: the Hall bar structure was remagnetized by a perpendicular magnetic field (B_z), while a constant electric current (I) was passed through the structure in the presence of a constant field in the plane (B_x), Fig. 1a. A change in the direction of the current leads to a shift in the loops by ΔB, which is equal to the perpendicular component of the current-induced field, Fig. 1b. Effectiveness of the current-induced action estimated as the shift magnitude to current ratio. For structures based on SiO_2, there was no shift. In the structure based on the W-layer, the ratio of the magnitude of the induced field per unit current was $5\cdot10^{-13}$ T/A m^2, and for the YIG-based sample it was $0.3\cdot10^{-13}$ T/Am^2. The value obtained for YIG is relatively small respective to the W-case, such a field is insufficient for complete remagnetization of the structure. However, this confirms the assumption that the YIG-layer reflects the spin current generated in the CoTb-layer. In this work, this effect was studied depending on the composition and thickness of the CoTb-layer.

Support by the grants the Russian Science Foundation, RSF 21-42-00041.

1. I. Manchon, V. Miron, P. Gambardella, Rev. Mod. Phys. **91**, 035004 (2019).
2. A. Yagmur, S. Sumi , H. Awano, K. Tanabe, Phys. Rev. Appl. **14**, 064025 (2020).
3. N. Vlietstra, B. J. van Wees, F.K. Dejene, Phys. Rev. B **94**, 035407 (2016).
4. J. Finley, Luqiao Liu, Phys. Rev. Appl. **6**, 054001 (2016).
5. C.F. Pai, M. Mann, A.J. Tan and G.S.D. Beach, Phys. Rev. B. **93**(14), 144409 (2016).

A.P3

MAGNETOPLASMONIC CRYSTAL FOR DC MAGNETIC FIELD TOPOGRAPHY

V.K. Belyaev[1*], *D.V Murzin*[1], *A.A. Grunin*[2], *A.A. Fedyanin*[2], *V.V. Rodionova*[1]

[1]Immanuel Kant Baltic Federal University, Kaliningrad, Russia
[2]Lomonosov Moscow State University, Moscow, Russia
[*]E-mail: belyaev@lnmm.ru

Technological progress sets the direction for the development of modern fundamental and experimental approaches to the study of materials and their adaptation to various applications. One of the rapidly developing directions is the design of magnetic field sensors [1]. Nowadays tasks are aimed for balancing the sensitivity and resolution, and lowering the power consumption. It is also required to lower the price of the magnetic field sensing elements production and miniaturize their dimensions. One of the new approaches for magnetic field sensing is based on the use of magnetoplasmonic crystals (MPlCs) – plasmonic crystals made of noble and ferromagnetic materials [2, 3]. The possibility to enhance magneto-optical response by two orders of magnitude with the use of MPlCs can expand possible applications of magneto-optical effects [4].

A MPlC-based magnetic field sensor that utilize the possibility to enhance the transverse magneto-optical Kerr effect by the excitation of surface plasmon-polaritons (SPPs) can reach the sensitivity up to 10^{-7} Oe [5]. The change of an optical probe position on the MPlC's surface can be used for magnetic field topography.

Here we present the results of the magnetic field topography with the use of permalloy-based MPlCs with the diffraction scheme for SPPs excitation. The used approach is based on the dependence of the magneto-optical response on the of DC magnetic field magnitude codirected with the AC modulating magnetic field. Thus, it is possible to make magnetic field topography by moving the DC field source in the plane of MPlCs (XY) at a distance behind it (Z). As DC magnetic field sources, a wire, a flat planar induction coil with DC current and a set of permanent magnets were used.

With the use of the MPlC fabricated by the magnetron sputtering of 50 nm of Ag, 15 nm of permalloy and 20 nm of silica nitride on top of a subwavelength quasi-sinusoidal diffraction grating with the period of 320 nm and the stripe height of 20 nm, a topography of the planar coil with 10 windings and outer diameter of 15 mm was made at Z = 9, 10.5 and 12 mm. An area of

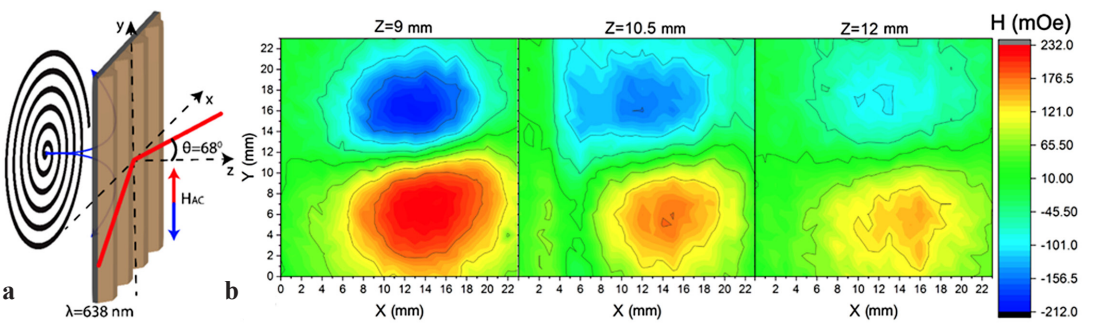

Figure 1. **a** The scheme of the experiment. **b** Measured magnetic field topographies at different distances Z between the MPlC and the planar coil.

24×24 mm was scanned with the step of 0.5 mm. During the experiment, a DC current of 400 mA was applied to the coil. The schematics of the experiment and measured topographies at different distances Z between the MPlC and the planar coil are shown in Fig. 1.

The sensitivity to the change of the DC magnetic field in the experimental configuration was 7 mOe with the incident beam focused in a round spot with the diameter of 150 um. The achieved sensitivity and resolution is enough to use the MPlC as an effective probe for magnetic flaw detection.

The work was supported by the Ministry of Science and Higher Education of the Russian Federation, grant № 13.2251.21.0143.

1. M.A. Khan, J. Sun, B. Li, A. Przybysz, J. Kosel, ERX **3**, 2 (2021).
2. G.A. Knyazev, P.O. Kapralov, N.A. Gusev, A.N. Kalish, P.M. Vetoshko, S.A. Dagesyan, V.I. Belotelov, ACS Photonics **5**(12), 4951–4959 (2018).
3. S. Chandra, J. Cozart, A. Biswas, S. Lee, D. Chanda, ACS Photonics **8**(5), 1316–1323 (2021).
4. A.A. Grunin, I.R. Mukha, A.V. Chetvertukhin, A.A. Fedyanin J. Magn. Magn. Mater. **415**, 72–76 (2016).
5. V.K. Belyaev, V.V. Rodionova, A.A. Grunin, M. Inoue, A.A. Fedyanin, Sci. Rep. **10**(1), 1–6 (2020).

MAGNETIC PROPERTIES OF COMPOSITION GRADED Co-Ni RODS

E.A. Denisova[1,2*], *E.A. Chekanova*[1], *S.V. Komogortsev*[1], *O.A. Li*[2], *R.S. Iskhakov*[2], *I.V. Nemtsev*[2,3], *S.V. Semenov*[1]

[1]Kirensky Institute of Physics, FRC KSC SB RAS, Krasnoyarsk, Russia
[2]Siberian Federal University, Krasnoyarsk, Russia
[3]Krasnoyarsk Scientific Center, FRC KSC SB RAS Krasnoyarsk, Russia
[*]E-mail: len-den@iph.krasn.ru

Our investigations concern a new class of advanced materials, known as structural and functional gradient materials, characterized by compositional or microstructural gradation over macroscopic or microscopic distances. Different types of geometrical and compositional modulations of magnetic nanowires can be used for control of the functional magnetic characteristics for the fabrication of spintronic, magnetic data storage, and sensing devices [1, 2]. In this work, we will demonstrate the possibility to control functional magnetic characteristics of rods by means of composition architecture (smooth or step-like gradient). Magnetic properties of composition modulated materials in comparison with that for homogeneous in composition samples was the subject of this report.

The multisegmented Co/Ni (MS) rods, Co-Ni alloy rods and rods with gradient Ni content along pillar axis, the rods with coaxial composition gradient (Co core-Ni shell CS) were prepared by electroless plating of ferromagnetic metals into pores of nuclear track etched polycarbonate membrane (PCTE). The PCTE membranes with diameters of pores from 0.1 up to 0.4 μm were used as the template material. The EDX analysis data confirms the composition modulation in produced samples.

The created composition gradient manifests in the features of the ferromagnetic resonance (FMR) spectra and magnetization curves. We observed a staggering difference between the FMR spectra measured on arrays of Co/Ni MS rods, Co/Ni core-shell rods and Co-Ni gradient rods as well as the difference with the homogeneous Ni rods, Ni tubes without core and Co wires without Ni shell. The FMR spectra for rods with composition gradient exhibit a clear multi-peak character, which resonance field do not match to the peaks measured independently in the homogeneous rods. According to the result of decomposition FMR spectra for Co/Ni CS and MS rods into individual resonance peaks the resonance field (H_R) value corresponding to the Ni tube increases from 1.6 kOe to 2.2 kOe, and the H_R value corresponding to the Co core decreases from 1.3 kOe to 0.9 kOe for coaxial rods. The presence of graded Co or Ni content could give rise to graded anisotropy effects (that is, local variations of the effective magnetic anisotropy along the rod axis). Such variations in magnetic anisotropy manifest in variations of resonance fields for different rod segments and increase linewidth of gradient rods. Information on local anisotropy field H_a is obtained from investigation of approach magnetization to saturation law. It turned out that the local magnetic anisotropy field in rods with a step-type gradient (~2 kOe) is significantly higher than in rods with a smooth gradient (~1 kOe). The study of the magnetization reversal processes was performed by analyzing the angular dependence of coercivity. We show that the reversal occurs by curling for both types of gradient rods (smooth or step-like).

So, the magnetic anisotropy field, the ferromagnetic resonance field, and linewidth are mainly determined by the artificially created interface boundaries for rods with composition gradient.

The research was funded by RFBR, Krasnoyarsk Territory and Krasnoyarsk Regional Fund of Science, project number 20-43-240003.

1. A. Pereira, J.L. Palma, M. Vázquez et al., Phys Chem Chem Phys., **17**, 5033–5038 (2015).
2. J. Rial, M.P. Proenca, Nanomaterials, **10**, 2403 (2020).

A.P5

FERROMAGNETIC RESONANCE INVESTIGATIONS OF EXCHANGE BIASED NiFe/IrMn/NiFe TRILAYER STRUCTURES

I.O. Dzhun[1*], *G.V. Babaytsev*[1,2], *I.L. Romashkina*[1], *M.G. Kozin*[1], *A.V. Makunin*[1], *N.G. Chechenin*[1,2]

[1]Skobeltsyn Institute of Nuclear Physics, MSU, Moscow, RF
[2]Faculty of Physics, MSU, Moscow, RF
[*]E-mail: irina.dzhun@gmail.com

Investigations of magnetization dynamics in nano scaled magnetic structures are now of great importance for several reasons. The most important one is that in low-dimensional devices, such as sensors and spin valves based on the giant magnetic resistance effect, the rate of reorientation of the magnetization of the layer is a key factor. The dynamics is determined by the damping of the precession of the magnetization towards the equilibrium state. In turn, the amount of damping depends on large number of factors, including the microstructure, presence and magnitude of exchange bias field.

Here we present our results on ferromagnetic resonance (FMR) study of NiFe/IrMn/NiFe trilayer structures with IrMn layer thickness t_{AF} varied from 2 to 50 nm. The set of experimental samples was obtained using magnetron sputtering in presence of a constant magnetic field of 420 Oe applied in substrate plain during the layer deposition. The FMR method for exchange-biased structures makes it possible to obtain a resonant field and, therefore, the value of the exchange bias. The FMR linewidth is determined by spin damping and is an important characteristic for the design of magnetic devices.

It was shown that the dependence of the exchange bias on the AF layer thickness is non-monotonic. Thus, the exchange bias that appears at t_{AF} = 4 nm increases, then, at AF thicknesses of 8–12 nm, a sharp decline is observed, after which, the exchange bias increases linearly from 22 Oe at t_{AF} = 20 nm to 48 Oe at t_{AF} = 50 nm (Fig. 1a). The angle of non-collinearity of the uniaxial and unidirectional anisotropies has a maximum value at t_{AF} = 4 nm, which corresponds to the thickness of the AF layer at which the exchange bias appears. With a further increase in the thickness of the AF layer,

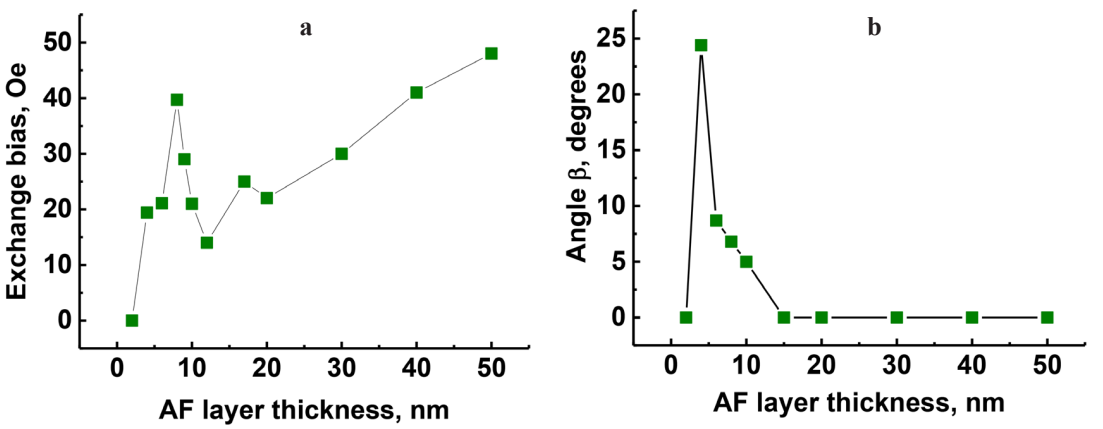

Figure 1. AF layer thickness dependence of exchange bias (**a**) and misalignment angle β (**b**) for Ni40Fe60/IrMn/Ni40Fe60 samples.

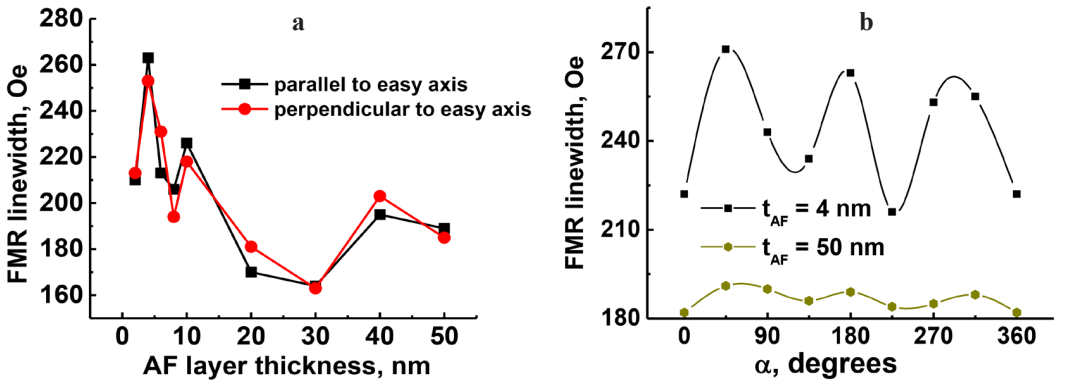

Figure 2. **a** The dependence of FMR linewidth on AF layer thickness for parallel (squares) and perpendicular (circles) sample orientations. **b** Angular dependence of FMR linewidth for the samples with 4 nm (squares) and 50 nm (circles) AF layers.

the noncollinearity angle decreases and becomes zero at t_{AF} = 15 nm (Fig. 1b). The dependence of the FMR linewidth on the thickness of the AF layer for different orientations of the sample relative to the external field of the FMR has along with small quantitative differences a single qualitative form for parallel and perpendicular orientation of the sample (Fig. 2a). It was shown that with the appearance of the exchange bias at the AF layer thickness of 4 nm, there is a sharp increase in FMR linewidth. Further, as the AF layer thickness increases, the linewidth decreases nonmonotonically and does not change significantly after the AF layer thickness of 20 nm. It is worth noting that the maximum of the FMR linewidth corresponds to small AF layer thicknesses of 4–10 nm, corresponding to the AF thicknesses at which a peak is observed depending on the exchange bias of the AF layer thickness, as well as the non-collinearity of the unidirectional and uniaxial anisotropies. This can be explained by the weak magnetic ordering of the AF layer at small thicknesses, in which defects and local structural inhomogeneities play a significant role, leading to local disorientation of the magnetic moments. The angular dependence of the FMR linewidth (Fig. 2b) for a sample with an AF layer thickness of 4 nm, corresponding to the thickness at which the exchange bias and the greatest angle of non-collinearity of the unidirectional and uniaxial anisotropies appear, is characterized by an asymmetric angular dependence of the FMR peak width and the greatest absolute change in the peak width with a change in the angle between external FMR field and easy axis of the sample. At the same time, a sample with an AF thickness of 50 nm is characterized by a small (about 10 Oe) change in the FMR linewidth when the sample orientation changes.

A.P6

AB INITIO CALCULATIONS OF MAGNETIC PROPERTIES OF CHIRAL MONOAXIAL HELIMAGNET

D.V. Evsin, M.V. Mamonova, V.O. Borzilov, P.V. Prudnikov*

Dostoevsky Omsk State University, Omsk, Russia
*E-mail: evsindv@stud.omsu.ru

Chirality is one of the basic concepts underlying the symmetry properties of nature, which manifest themselves at various scales [1]. Helimagnetic $CrNb_3S_6$ belongs to magnetic soliton crystals with layered structures that host periodic chiral helimagnetic ordering which are promising candidates for spintronic nanodevices. $CrNb_3S_6$ is unique because of it's crystallographic chirality and monoaxial Dzyaloshinskii-Moriya interaction [2]. Experimental studies showed the dependence of the period of the chiral helimagnet on the external magnetic field at a constant temperature, namely, the crossover to the state of the chiral soliton lattice in thin lamellae [3]. In this work, we calculated the magnetic properties $CrNb_3S_6$ thin film using ab initio calculations by VASP package [4].

The crystal structure of the $CrNb_3S_6$ system under study is shown in Fig. 1. In calculations of the helimagnetic film a 20-atomic supercell with a lattice constant a = 10.84892 a.u. was used [5];

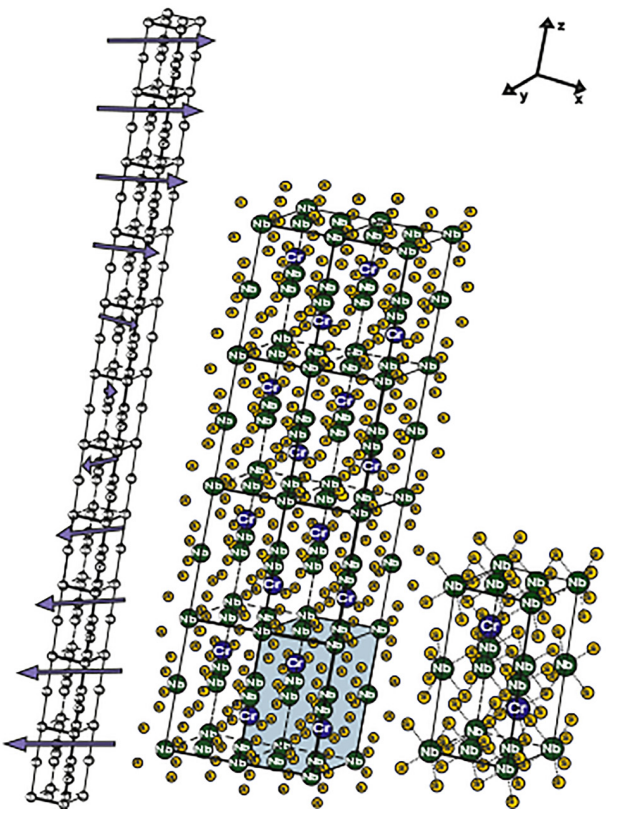

Figure 1. Crystal structure of monoaxial helimagnet $CrNb_3S_6$. The arrows indicate the direction of the magnetization of the layer.

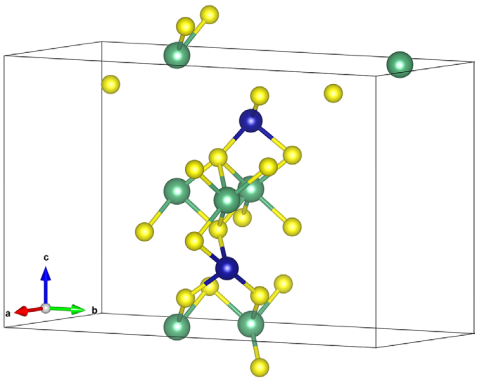

Figure 2. Crystallic structure of film of helimagnet. Blue color is for chromium atoms, green – niobium, yellow – sulfur.

the number of k-points of the Monkhorst-Pack grid was assumed to be 16; cutoff energy – 500 eV; vacuum layer – 5 Å; the helix propagation vector $q = 0.5a$ is directed along the z-axis.

During the calculations, the following values of the projections of the magnetization of the magnetic moments of two chromium atoms were obtained: $\mu_x(Cr_1) = -0.889\mu_B$, $\mu_y(Cr_1) = -1.654\mu_B$, $\mu_x(Cr_2) = 2.022\mu_B$, $\mu_y(Cr_2) = 0.109\mu_B$. The value of the total energy of the system $E_{tot} = -143.80466\mu_B$ was also obtained.

The study was carried out with the financial support of the Ministry of Education and Science of the Russian Federation (agreement 0741-2020-0002) and grant MD-2229.2020.2 of the President of the Russian Federation. The computational research was supported in through resources provided by the Shared Services Center "Data Center of FEB RAS" (Khabarovsk) [6].

1. Y. Togawa, Y. Kousaka, K. Inoue, J. Kishine, J. Phys. Soc. Jpn. **85**, 112001 (2016).
2. D. Song, L. Wang, W. Wang et al, Phys. Rev. B **102**, 64432 (2020).
3. Y. Togawa, J. Kishine, P.A. Nosov et al, Phys. Rev. L **122**, 017204 (2019).
4. G. Kresse, M. Marsman, J. Furthmuller, VASP the GUIDE, Wien: Universitat Wien, 2016.
5. N.J. Ghimire, M. Marsman, J. Furthmuller et al., Phys. Rev. B **87**, 104403 (2013).
6. A.A. Sorokin, S.V. Makogonov, S.P. Korolev, Sci. Tech. Inf. Proc. **44**, 302 (2017).

A.P7

FEATURES OF CRYSTAL STRUCTURE AND EXCHANGE BIAS IN Cr-Mn/FeNi FILMS

A.A. Feshchenko[1*], *M.E. Moskalev*[1], *V.N. Lepalovskij*[1], *A.N. Gorkovenko*[1], *E.A. Kravtsov*[1,2], *V.O. Vas'kovskiy*[1,2]

[1]Ural Federal University, Ekaterinburg, Russia
[2]Institute of Metal Physics, UB RAS, Ekaterinburg, Russia
[*]E-mail: a.a.feshchenko@urfu.ru

An important component of functional elements in modern spintronics are antiferromagnet/ferromagnet thin films due to the exchange bias effect implemented in them. It should be noted that the antiferromagnetic component determines the temperature characteristics of such films. Antiferromagnetic alloys Ir-Mn and Pt-Mn are used most often in technical devices [1], because they have high thermal stability properties and good corrosion resistance. But expensive precious metal components are not economically viable to use. At this moment a search is underway for cheaper antiferromagnetic materials that would have a high Néel temperature in the film state and that would be able to effectively interact with adjacent ferromagnetic layers. One of the candidates for this role is the Cr-Mn alloy [2]. This work is devoted to the search for conditions to obtain the antiferromagnetic state in Cr_xMn_{100-x} layers included in film structures of the glass/A/$Cr_{100-x}Mn_x$/B/Ta type.

The objects of investigation are multilayer films deposited by magnetron sputtering on Corning glass substrates. In this case, a two-component permalloy ($Fe_{20}Ni_{80}$) target and one-component Fe, Cr, Mn and Ta targets were used. The upper layer B = Fe, $Fe_{20}Ni_{80}$ served as an indicator of antiferromagnetic ordering and had a thickness of 10 nm. The thickness of each layer of buffer A = Ta, Ta/Fe, Ta/Cr was kept at 5 nm. The crystal structure of the films was studied with the help of a PANalytical Empyrean series 2 X-ray diffractometer. The magnetic properties were studied using a LakeShore vibromagnetometer, an EvicoMagnetics magneto-optical Kerr-magnetometer, and a PPMS DynaCool 9T measuring complex.

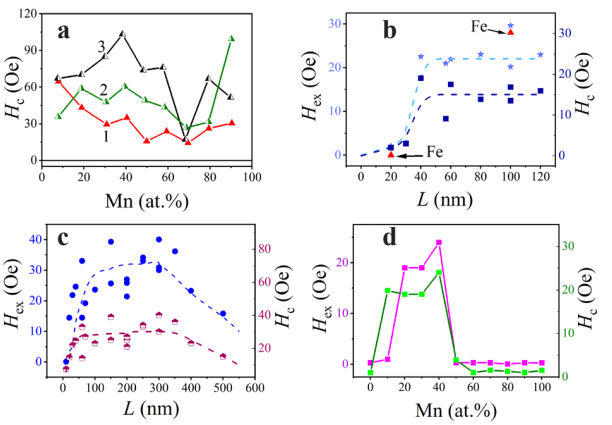

Figure 1. **a** Concentration dependences of the coercivity H_c for A/Cr_{100-x}Mn (20 nm)/Fe/Ta films (A = Ta – 1, Cr – 2, Fe – 3); thickness dependence of the exchange bias field H_{ex} and coercivity H_c for Ta/$Cr_{80}Mn_{20}$(L)/$Fe_{20}Ni_{80}$/Ta (**b**) and Ta/$Cr_{60}Mn_{40}$(L)/$Fe_{20}Ni_{80}$/Ta (**c**) films; concentration dependences of the coercivity H_c (**c**) and exchange bias field Hex (**d**) for Ta/$Cr_{100-x}Mn_x$ (50 nm)/$Fe_{20}Ni_{80}$/Ta films.

During the experiment, the composition of the $Cr_{100-x}Mn_x$ layer ($0 \leq x \leq 100$ at.%) and its thickness L = 10÷500 nm, the composition of the buffer layer (Ta, Ta/Fe, Ta/Cr), the composition of the indicator layer B = Fe, $Fe_{20}Ni_{80}$) were varied. Thus, the goal was to form such a composite-structural state of the Cr-Mn layer, in which the exchange pinning of ferromagnetic layers with different types of crystal structure is provided. It also turned out that, in contrast to other systems with antiferromagnetic ordering, the texture in the films under study is not a necessary factor for the implementation of exchange bias in the system. It has been established that the level of coercity H_c of the indicator layers, as a rule, is higher than that typical for single-layer Fe or $Fe_{20}Ni_{80}$ films (Fig. 1a and b), which can serve as an indirect sign of the antiferromagnetic ordering in the Cr-Mn layer. The presence of exchange bias, which is a direct indication of the exchange coupling present, was recorded for rather large values of $L \geq 40$ nm (Fig. 1b and c) and only in a limited range of compositions $20 \leq x \leq 40$ at.% (Fig. 1d). As can be seen, there is a significant scattering in the values of H_c and H_{ex}, the elucidation of the reasons for which requires further research.

In this work, the temperature dependences of the coercivity H_c and exchange bias field H_{ex} are determined. Possible mechanisms of the regularities established are discussed.

1. K. O'Grady et al., J. Appl. Phys. **128**, 040901 (2020).
2. W. Feng et al., J. Appl. Phys. **108**, 073915 (2010).

A.P8

MAGNETIC AND STRUCTURAL TRANSFORMATION OF CARBON-COATED IRON OXIDE NANOCOMPOSITES

K.O. Funtov[1*], S.S. Starchikov[1], I.S. Lyubutin[1], C.-R. Lin[2]

[1]Shubnikov Institute of Crystallography of FSRC"Crystallography and Photonics" RAS, Moscow, Russia
[2]Department of Applied Physics, National Pingtung University, Pingtung County, Taiwan
[*]E-mail: funtov.ko@gmail.com

Nanostructured materials are considered as promising materials for use in medicine and biotechnology. Much research interest has been focused on the core-shell iron oxide materials generally used for magnetic data storage and on the ferrofluids used as contrast agents in magnetic resonance imaging.

In the present study, carbon-coated iron oxides core@shell nanoparticles were synthesized by a one-step process of thermal pyrolysis. The influence of the synthesis temperature on the structural and magnetic properties of Fe_xO_y@carbon core-shell nanoparticles was investigated by X-ray diffraction, transmission electron microscopy (TEM), Raman and Mössbauer spectroscopy, as well as by magnetic measurements. The reaction temperature (T_R) varied from 360 to 400°C. At T_R from 360 to 385°C, spherical and nearly monodispersed nanoparticles of magnetite covered with an amorphous carbon shell were obtained. When the reaction temperature rises above 385°C, the nanoparticles of wüstite phase begin to form, and its concentration increases at the expense of the magnetite phase with further T_R increasing. In the narrow temperature range from 390 to 400°C, the wüstite concentration increases from about 10 to 40%. At that time magnetite nanoparticles become smaller in size and superparamagnetic.

The Mössbauer spectroscopy indicates, that an excess of the $[Fe^{3+}]B$ ions in octahedral B-sites of magnetite which associated with the particle surface does not participate in the electron hoping $[Fe^{3+} \leftrightarrows Fe^{2+}]B$ above the Verwey temperature. The wüstite phase appears and grows with a corresponding decrease in the fraction of $[Fe^{3+}]B$, that does not undergo the electronic exchange. This proves that the wüstite phase is generated and formed on the surface of magnetite particles under the influence of carbon. The Mössbauer data allow one to monitor the dynamics of reduction of iron oxide from Fe_3O_4 to FeO under the influence of carbon [1].

Support by the Ministry of Science and Higher Education of the Russian Federation within the State assignment FSRC "Crystallography and Photonics" RAS is acknowledged.

1. I.S. Lyubutin et al., Materials characterization **150**, 213–219 (2019).

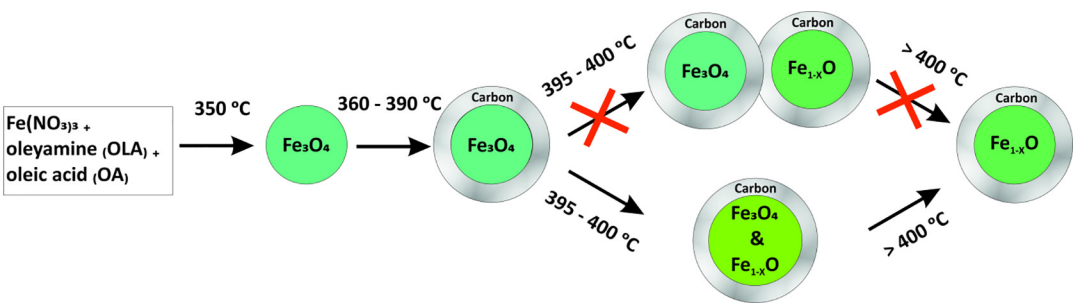

Figure 1. Schematic view of process of thermal reduction of magnetite to wustite under influence of carbon with creation of Fe_xO_y@carbon core-shell nanoparticles.

MAGNETIC PROPERTIES OF FeNi/V_xO_y/FeNi FILMS

G.S. Patrin[1,2*], *A.V. Kobyakov*[1,2], *V.I. Yushkov*[1,2], *I.O. Anisimov*[1], *S.V. Semenov*[1,2], *S.A. Yarikov*[2], *S.M. Zharkov*[1,2]

[1]Siberian Federal University, Krasnoyarsk, Russia
[2]L.V. Kirensky Institute of Physics, Federal Research Center, Siberian Branch of Russian Academy of Sciences, Krasnoyarsk, Russia
[*]E-mail: patrin@iph.krasn.ru

A wide range of properties of oxide film materials and heterostructures attracts much attention to them [1]. Such materials are promising for spintronics devices as multifunctional materials for sensor elements, magnetic memory elements, etc. [2]. The most widespread compounds have control elements based on $FeBiO_3$ and $(La,Sr)MnO_3$. Methods of properties control can be either external electric or magnetic fields, elastic stresses, light radiation, electric current, etc. At the same time, external influences can affect the volumetric properties and/or interfaces.

In this regard, structures that may include layers with a metal-dielectric transition are of a particular interest. There are some studies where the magnetic properties of films with a vanadium oxides interlayer have been studied (for example, [3]).

We have tried to study three-layer structures with an interlayer of vanadium oxide. The films were sprayed onto a glass substrate by an "Omicron" ultra-high vacuum magnetron sputtering unit (with a film thickness control system during growth) at a base pressure of 10–10 Torr. A V_2O_3 target was used to spray a layer of vanadium oxide. Electron microscopic measurements were carried out by a JEOL JEM-2100 microscope. Magnetic characteristics were studied by the MPMS-XL SQUID magnetometer in fields up to 50 kOe. A series of single-layer V_xO_y films with the thicknesses of t_{VO} = 2, 3, 4, 5, 8, 10 nm, FeNi/V_xO_y and V_xO_y/FeNi films and three-layer FeNi/V_xO_y/FeNi films with the thicknesses of t_{FeNi} = 15 nm, t_{VO} = 3–19 nm in 2 nm increments have been produced.

Electron microscopic studies of the cross-section of a three-layer FeNi/V_xO_y/FeNi film have shown that the FeNi-V_xO_y interface is blurred. This indicates the diffusion penetration of materials at the interface. The V_xO_y-FeNi interface is more pronounced. It means that the mixing of materials of different layers might not take place.

The electrical properties of films are known to depend on their thickness. The dependence of the temperature (T_C) of the metal-semiconductor transition for single-layer films on the thickness of the film has been studied. It has been found that a decrease in the film thickness results in an increase in T_C. A sharp increase starts at $t_{VO} \leq 7$ nm, and at $t_{VO} > 10$ nm its value asymptotically tends to $T_C \approx 120$ K.

The magnetic field and temperature dependences of the magnetization of three-layer films depending on the thickness of the interlayer have been studied. At temperatures $T < 40$ K, an exchange bias has been detected, its value significantly decreases at $t_{VO} > 10$ nm. Thermomagnetic effects are also observed in small fields in the ZFC mode. They appear in the form of induced negative magnetization.

This work was supported by the State order of the Ministry of Science and Higher Education of the Russian Federation (topic No. FSRZ-2020-0011).

1. Ch. Lu, W. Hu, Y. Tian, T. Wu, Appl. Phys. Rev. **2**, 021304(18) (2015).
2. H. Ben, M. Gajek, M. Bibes, A. Barthelemy, J. Phys.: Condens. Matter. **20**, 434221(11) (2008).
3. J. Lauzier, L. Sutton, J. de la Venta, J. Appl. Phys. **122**, 173902(5) (2017).

MAGNETIZATION BEHAVIOR IN NICKEL NANOFILMS WITH A PERIODIC STRIPED STRUCTURE

A.V. Golov[1*], *V.S. Vlasov*[1], *L.N. Kotov*[1], *V.V. Temnov*[2]

[1]Department of Radiophysics, Syktyvkar State University, Syktyvkar, Russia
[2]LSI, Ecole Polytechnique, CEA/DRF/IRAMIS, CNRS, Institut Polytechnique de Paris, France
[*]E-mail: antongolov@mail.ru

Today nonlinear dynamics in nanoferromagnets is of great interest in the context of practical applications and has the potential for use in non-volatile data storage and information processing. Many works now are devoted to ultrafast magnetization reversal of magnetic nanoparticles using laser and elastic pulses, with the aim of using this phenomenon for the development of new generation of ultrafast, compact and energy-efficient memory devices or in many other electronic and spintronic hardware [1]. The generation of the short acoustic pulses became possible due to the use of modern femtosecond lasers. The pulses have rather high amplitude, due to time compression of the laser energy. The strain amplitude in a pulse can be as high as several percent and is close to the plastic limit of a solid. These pulses can change significantly the magnetic properties of material by affecting the magnetic subsystem of nanostructures [1].

Experiments on generation of magnetoelastic surface waves in tangentially magnetized array of nickel nanowires using the ultrafast laser excitation were performed in [2] for the film's saturation magnetization M_s = 315 kA/m that is lower than that for bulk nickel. By tuning the magnitude of an externally applied magnetic field, optically excited surface acoustic waves can selectively excite either the upper or lower branches of a splitting in the nanowire's spin-wave spectrum [2].

In this paper we develop this work further by using micromagnetic simulations. We study the influence of the shape of nickel nanoarray to its magnetic structure and its magnetic dynamics exited by acoustic pulses. Micromagnetic simulations of the nanowire's magnetization dynamics are performed using the MUMAX3 software package [3].

The nickel nanoarrays characterized in this study have the linear dimensions of cuboid and equal to 2560×2560×40 nm. The dimensions of the film without ridges were selected as multiples of powers of two for the 5×5×5 nm mesh is used for all simulations. The notches with depth h and width a were set to create inhomogeneities in the nickel film (Fig. 1a). These notches were repeated eight times to take into account the influence of the periodicity w. The in-plane external magnetic field was applied at an angle φ align to the x-axis (Fig. 1b).

Hysteresis loops were plotted for the magnitude of the magnetization vector depending on the magnitude of the external field for various angles φ at a ratio η of the height of the ridges h to the total height of nickel film equal to 50% (Fig. 1c). It can be seen that the spatial structure has the highest coercivity when an external magnetic field is applied exactly perpendicular to the strips. The coercivity of the film decreases sharply closer to φ = 30°. Then it slowly increases as the external magnetic field rotates closer and closer to the direction parallel to the stripes. Also, hysteresis loops at different heights of the ridges for an external magnetic field directed strictly perpendicular to the strips were built (Fig. 1d). In this case, the film geometry with the notches are close to the middle of the film total height has the highest coercivity. Thus, this is the most complicated case of film magnetization reversal. The simplest case is the magnetization reversal of individual strips in the absence of any jumpers between stripes. The asymmetry in the hysteresis loops for a symmetric structure is explained by the fact that the initial magnetization of the film in the absence of an external field was directed along the y-axis.

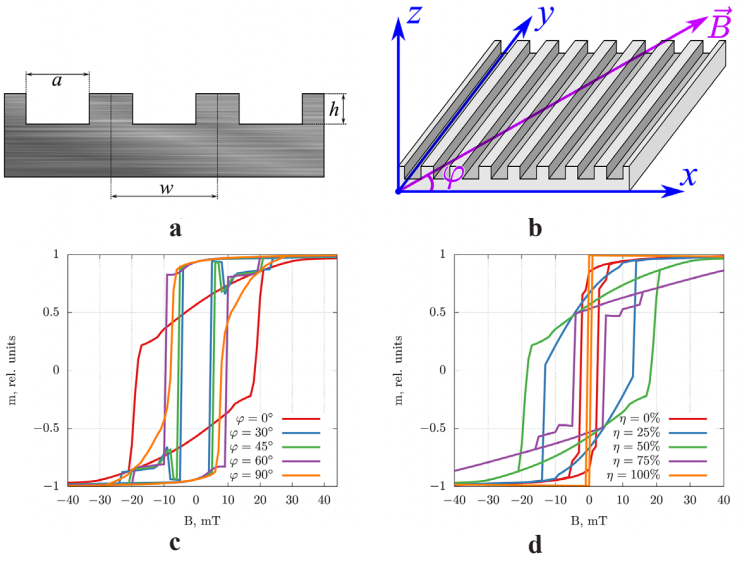

Figure 1. **a**, **b** Schematic diagram indicating the shape of nickel film, including the magnetic-field angle φ with respect to the *x*-axis. Magnetization of the nickel striped film as a function of the applied field with respect to the angle φ at η = 50% (**c**) and ratio of height of ridges to total height η at φ = 0° (**d**).

Micromagnetic simulations of the dynamic of the total magnetization of nickel striped film exited by acoustic pulses in the presence of an external magnetic field were also carried out and spin-wave spectrum of these oscillations was plotted.

This work has been supported by Russian Science Foundation (project No. 21-72-20048).

1. V.S. Vlasov, A.V. Golov, L.N. Kotov, V.I. Shcheglov, A.M. Lomonosov, V.V. Temnov, Acoust. Phys. **68**, 18–47 (2022).
2. C.L. Chang, R.R. Tamming, T.J. Broomhall, J. Janusonis, P.W. Fry, R.I. Tobey, T.J. Hayward, Phys. Rev. Applied **10**, 034068 (2018).
3. A. Vansteenkiste, J. Leliaert, M. Dvornik, M. Helsen, F. Garcia-Sanchez, B. Van Waeyenberge, AIP Advances **4**, 107133 (2014).

A.P11

THE EFFECT OF ANNEALING ON THE MICROSTRUCTURE AND MAGNETIC PROPERTIES OF FeMn/FM FILMS

A.N. Gorkovenko[1*], *V.N. Lepalovskij*[1], *N.A. Kulesh*[1], *M.E. Moskalev*[1], *V.O. Vas'kovskiy*[1,2]

[1]Ural Federal University, Ekaterinburg, Russia
[2]Institute of Metal Physics UB RAS, Ekaterinburg, Russia
[*]E-mail: A.n.gorkovenko@urfu.ru

Over the past decades, in the physics of magnetic phenomena, much attention has been paid to the study of thin-film structures that contain exchange-coupled ferromagnetic and antiferromagnetic layers and, as a result, have unidirectional anisotropy (exchange bias) [1]. Films with $Fe_{20}Ni_{80}$ as a ferromagnet and $Fe_{50}Mn_{50}$ as an antiferromagnet are a classic example of such structures [2].

The hysteresis properties of films with unidirectional anisotropy are largely determined by the features of the exchange interaction through the ferromagnet/antiferromagnet interlayer magnetic interface. In turn, the quality of this interface to some extent depends on the microstructure of the adjacent layers. Thus, the hysteresis properties of exchange-coupled films can be modified by introducing changes in their microstructure, for example, as a result of heat treatment. At the same time, the nature and quantitative side of thermally initiated changes can be influenced by the "crystalline affinity" of the layers in terms of the type and parameters of crystal lattices, as well as the presence of texture in polycrystalline conjugated layers [3]. The possibility of interdiffusion of the layers, which is activated at elevated temperatures, should also be considered. This work is devoted to revealing these bonds in films of the $Fe_{50}Mn_{50}$/FM type (where FM = Co, Fe, Ni, $Fe_{20}Ni_{80}$, $Fe_{11}Ni_{89}$, $Co_{30}Ni_{70}$). In other words, the objects under study had a common basis in terms of the antiferromagnetic (fixing) layer and a fairly wide range of ferromagnetic (fixed) layers. In other words, the objects under study had a single base in terms of the antiferromagnetic (fixing) layer and a fairly wide range of ferromagnetic (fixed) layers. This series includes the iron group metals and their alloys, which are of particular practical interest as magnetoresistive materials with low magnetic hysteresis [4].

The films studied in this work were obtained by magnetron sputtering on an Orion-8 device. Films were formed by sequential sputtering of alloy targets in the presence of a uniform magnetic field (technological field) oriented along the surface of the substrates. The main study was carried out on samples with the general structural formula glass/Ta(5)/$Fe_{20}Ni_{80}$(5)/FeMn(20)/FM(40)/Ta(5), in which the layer thicknesses in nanometers are given in brackets. Buffer layers of Ta and permalloy 5 nm thick played an auxiliary role and were responsible for the initiation of the fcc structural modification in the overlying equiatomic FeMn (γ-FeMn) layer, which is associated with the antiferromagnetic ordering of this material. In addition, the auxiliary layers contributed to texturing of the polycrystalline γ-FeMn layer according to the (111) type, which provided the necessary conditions for the formation of unidirectional anisotropy in polycrystalline ferromagnetic layers deposited on top of the antiferromagnetic layer [5]. The outer Ta layer performed a protective function. Along with this, simplified auxiliary structures of the glass/Ta(5)/FM(40)/Ta(5) and Si/FeMn(5)/FM(5) types were obtained. The former was used to test the properties of the studied ferromagnets in the film state, the latter to analyze atomic migration processes.

Thermomagnetic treatment of the samples was carried out in vacuum at a pressure of 5.10^{-7} Torr and temperatures T_a = 200 and 400 °C in the presence of a magnetic field co-directional with the axis of application of the technological field and had an accumulative character. The choice of these values of Ta is due to the intention to single out the role of relaxation processes with different

levels of activation energy. The interval up to 200 °C is primarily characterized by the removal of inhomogeneous elastic stresses, and above 300 °C – pronounced recrystallization [6].

The duration of annealing at each temperature was 1 hour. For attestation of the structural state of the films, X-ray diffractometry was used, which was carried out on a Dron-3M device modified for the study of films, in the Bragg-Brentano geometry (θ-2θ) and in Co-K_α radiation. To study interlayer diffusion, a Nanohunter X-ray fluorescence spectrometer with total external reflection was used. The investigation of magnetization reversal processes was carried out at room temperature using a high-resolution Kerr magnetometer Evico Magnetics and a VSM LakeShore. Longitudinal and transverse magneto-optical hysteresis loops were measured in a magnetic field oriented, respectively, along and perpendicular (in the plane of film samples) to the axis of application of the technological field.

In the course of the study, detailed information was obtained on the formation of the properties of films containing antiferromagnetic layers of FeMn and ferromagnetic layers of metals and alloys of the iron group in the initial state and after thermomagnetic treatment. All of the studied ferromagnets Fe, Co, Ni, $Fe_{11}Ni_{89}$, $Fe_{20}Ni_{80}$, $Co_{30}Ni_{70}$ in the composition of multilayers show the presence of an exchange coupling with the FeMn layer, which is expressed in the exchange bias effect. A larger exchange bias is observed for the Ni-containing ferromagnetic layers, and the smallest for the Fe-layer. The difference in the efficiency of interlayer exchange coupling is apparently due to the features of the crystal structures of the mating layers.

Film annealing at temperatures T_a above 200 °C initiates atomic interlayer diffusion, which leads to a redistribution of chemical elements over the thickness and a change in the magnetization and hysteresis properties of film samples. According to X-ray fluorescence analysis, the process tends to saturate at T_a above 300 °C. The migration effect is inherent in all chemical elements, but it is most pronounced in Mn. At the same time, the depth of its diffusion from the FeMn layer into neighboring ferromagnetic layers depends on the composition of these layers. It is greatest for the FeMn/Co pair, which leads to complete segregation of Mn and the disappearance of the antiferromagnetic layer, and with it the effect of the exchange bias in this sample. In the presence of other ferromagnetic layers, diffusion destruction of the antiferromagnetic layer also takes place, but occurs only partially, and to a lesser extent for the FeMn/Fe pair. As a result, the exchange bias is retained in these samples, although it decreases in magnitude.

This work was financially supported by the Russian Science Foundation in the framework of the research project No. 22-22-00814.

1. A.E. Berkowitz, K. Takano, J. Magn. Magn. Mater. **200**, 552–570 (1999).
2. Y.K. Kim, K. Ha, L.L. Rea, IEEE Trans. Magn. **31**, 3823–3825 (1995).
3. M.F. Toney, C. Tsang, K. J. Howard, J. Appl. Phys. **70**, 6227–6229 (1991).
4. F.T. Yuan, C.Y. Tsai, Jen-Hwa Hsu, K.F. Lin, J.K. Mei, Thin Solid Films **536**, 244–248 (2013).
5. F. Offi, W. Kuch, J. Kirschner, Phys. Rev. B **66**, 064419 (2002).
6. V.O. Vas'kovskiy, G.S. Kandaurova, V.N. Lepalovskij, A.N. Sorokin, E.I. Teitel, N.N. Shchegoleva, Metallofizika **13**, 107–115 (1991) [in Russian].

A.P12

CONTROL OF SPIN-WAVE DISPERSION IN A PERMALLOY MEANDER STRUCTURE

Y.A. Gubanova[1*], *V.A. Gubanov*[1], *E.N. Beginin*[1], *N. Noginova*[2], *A.V. Sadovnikov*[1]

[1]Saratov State University, Saratov, Russia
[2]Norfolk State University, Norfolk VA, USA
[*]E-mail: yulya29022095@gmail.com

Meander structures with one-dimensional modulation of the submicron period profile have been studied by the micromagnetic simulation method and the spectrum of eigenmodes has been constructed [1, 2]. Control modes of frequency ranges of Bragg bandgaps in the spectrum of spin waves depending on the parameters of the meander structure are revealed. Interest in such structures is caused by the possibility of creating functional devices of microwave electronics, as filters, noise suppressors, power limiters [3, 4].

The study of periodic structures of micron and submicron sizes based on magnetic films, in which spin waves propagate, is of great interest at the present time. A special characteristic of these structures is the presence of Bragg bandgaps in the spectrum of spin waves, which arise from the interaction of direct and counter waves.

This paper presents the results of a study of the permalloy (NiFe) meander structure. Figure 1 shows a segment of meander waveguide has the following parameters: modulation period L = 740 nm, horizontal section height n = 50 nm, vertical section thickness m = 50 nm, the height of the drop k changed from 10 to 140 nm. The external magnetic field direction was directed along the Oz axis.

The dispersion characteristics were obtained as a result of numerical simulation (Fig. 2). The frequency ranges Δf_1, Δf_2, and Δf_3 denote the Bragg gaps in which the spin waves do not propagate. For low-frequency modes the frequency range of the bandgap is the most important.

The dependences of the Bragg band gap thicknesses on the difference thickness k, which varied from 10 to 140 nm, were plotted. The maximum thickness of the sounding zone Δf_1, Δf_2 is observed at the thickness of the drop k from 75 to 90 nm. The width of the third frequency band of non-transmission Δf_3 is smallest in the region of values of the height of the difference $60 < d < 80$ nm.

Varying the modulation meander depth, it is possible to control the width of the frequency band of non-transmission in the spectrum of spin waves propagating in the meander structure, which can be used in the design and fabrication of microwave filters based on nanoscale magnon-crystalline structures fabricated in the form of meander ferromagnetic films.

Varying the modulation meander depth, it is possible to control the width of the frequency band of non-transmission in the spectrum of spin waves propagating in the meander structure, which can

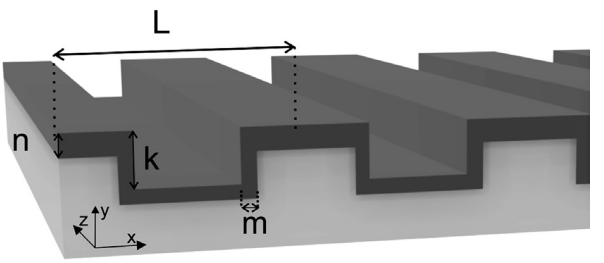

Figure 1. The segment of the periodic structure used to simulate the meander structure.

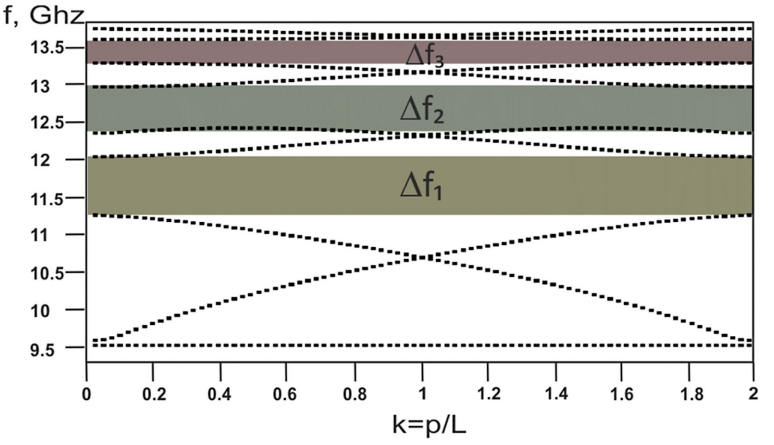

Figure 2. Dispersion characteristic of the permalloy structure.

be used in the design and fabrication of microwave filters based on nanoscale magnon-crystalline structures fabricated in the form of meander ferromagnetic films.

This work was supported by the grant from Russian Science Foundation (No 20-79-10191).

1. A.V. Sadovnikov, G. Talmelli, G. Gubbiotti, E.N. Beginin, S. Sheshukova. S.A Nikitov, C. Adelmann, F. Ciubotaru, JMMM **544**, (2022).
2. N. Noginova, V. Gubanov, M. Shahabuddin, Y. Gubanova, S. Nesbit, V.V. Demidov and A.V. Sadovnikov, Appl. Magn. Reson. **52**(7), 749–758 (2021).
3. K. Vogt, F. Y. Fradin, J. E. Pearson, T. Sebastian, S.D. Bader, B. Hillebrands, A. Hoffmann and H. Schultheiss, Nature commun. **5**(1), 1–5 (2014).
4. J. Stigloher, M. Decker, H.S. Körner, K. Tanabe, T. Moriyama, T. Taniguchi, H. Hata, M. Madami, G. Gubbiotti, K. Kobayashi, T. Ono and C.H. Back, Phys. Rev. Lett. **117**, (2016).

A.P13

INFLUENCE OF MAGNETIC FORCES ON THE SPATIAL DISTRIBUTION OF PARTICLES AND CELLS

A.A. Gurevich[1*], *L.V. Panina*[1,2]

[1]National University of Science and Technology MISiS, Moscow, Russia
[2]Immanuel Kant Baltic Federal University, Kaliningrad, Russia
[*]E-mail: gurevich-anastasia@yandex.ru

The manipulation of micro- and nano-objects such as particles or cells is being actively explored for applications in biomedical technologies. For these purposes, magnetic fields which can freely penetrate biological tissues can be used. In combination with magnetic micro- and nanoparticles they are exploited for diagnostic and therapeutic applications. Magnetic manipulation strategies are continuously developing. The main concern is related to short-range forces, since the magnetic field decreases rapidly away from the magnetic poles. Another problem is related to the same direction of particle magnetic moment and the magnetic field, which causes a paramagnetic particle to move in the direction of the highest field gradient (or the lowest for a diamagnetic particle). Therefore, magnetic systems should be specifically designed to overcome some of these problems. In this paper we analyze a number of effective field configurations with strong spatial gradients capable to impose a sufficient force on magnetic particles (paramagnetic or diamagnetic).

We consider systems of ferromagnetic microwires and microscopic washers magnetized in a certain way as sources of a magnetic field for manipulating by magnetic particles. Between two diametrically magnetized microwires, a 2D energy minimum is formed, which constitutes an effective capture of diamagnetic particles [1, 2]. When using three microwires with longitudinal magnetization located at an angle of 120 degrees, three energy maxima are formed [3]. Such a system can be used as a tweezer for capturing paramagnetic objects. A linear field gradient and a constant force can be produced with two hard-magnetic cylinders polarized oppositely. 2D-arrays of microscopic washers (shown in Fig. 1a) generate an energy landscape with arrays of potential wells for trapping diamagnetic particles. The energy profile for a unit cell, consisting of 4 washers magnetized longitudinally is shown in Fig. 1b. An energy minima are seen between the washers,

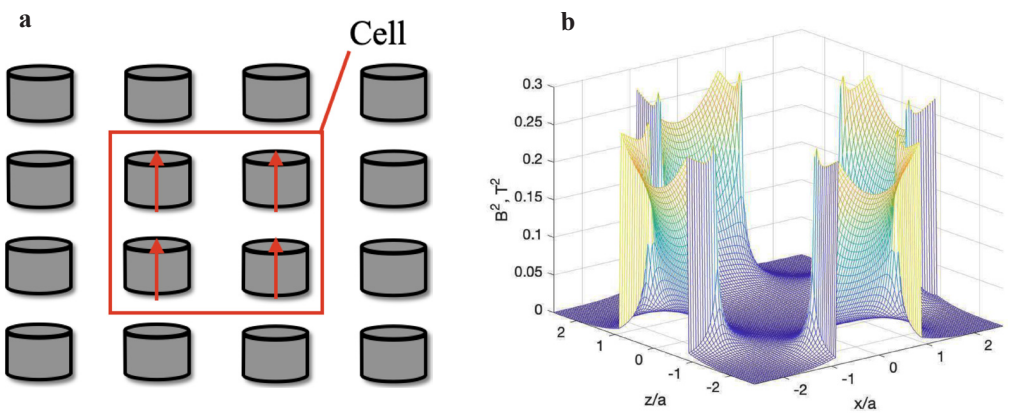

Figure 1. **a** Schematic configuration of a unit cell cylindrical micromagnet. b The distribution of the magnetic field from a system of cylindrical micromagnets in the plane (x,z), $y = 1.2a$ with magnetization $\mu_0 M = 0.6$ T, radius $a = 15$ μm, length $2L = 2a$.

where the diamagnetic particles can be trapped, while the maxima are formed on the washers, which contributes to the capture of paramagnetic particles.

1. A.V. Beklemisheva, N.A. Yudanov, A.A. Gurevich, L.V. Panina, V.A. Zablotskiy, A. Deyneka, Phys. Met. Metallogr. **120**(6), 556–562 (2019). https://doi.org/10.1134/S0031918X19060036.
2. A. Gurevich, A.V. Beklemisheva, E. Levada, V. Rodionova, L.V. Panina, IEEE Magn. Lett. **11**, 1 (2020). https://doi.org/10.1109/LMAG.2020.2974150.
3. A. Omelyanchik, A. Gurevich, S. Pshenichnikov, V. Kolesnikova, B. Smolkova, M. Uzhytchak, I. Baraban, O. Lunov, K. Levada, L. Panina, V. Rodionova, J. Magn. Magn. Mater. **512**, 166991 (2020). 0304-8853. https://doi.org/10.1016/j.jmmm.2020.166991.

AB INITIO INVESTIGATION OF HETEROSTRUCTURES FOR SPINTRONIC APPLICATIONS

A.A. Evseev[1,2], *I.I. Gumarova*[1,2*], *O.V. Nedopekin*[1]

[1]Institute of Physics, KFU, Kazan, Russia
[2]Zavoisky Physical-Technical Institute, FRC Kazan Scientific Center of RAS, Kazan, Russia
[*]E-mail: i.piyanzina@gmail.com

It is desired for materials used in spintronic devices and the detection of Majorana fermions in solids to have a large and ideal Rashba-type spin-orbit splitting. Recently, it was proposed to combine ordered surface alloying and interface engineering, that is growing alloy monolayers on an insulating polar surface [1]. The Rashba effect is reffered to as the spin-orbit splitting at surfaces/interfaces due to the broken inversion symmetry [2].

In this work, we have studied film heterostructures with different combination of components, which were expected to have spin-orbit splitting of the Rashba type [2, 3]. In these heterostructures, due to the electron density gradient at the interfaces, a current vortex arises associated with the electron spins. The structural and electronic properties of these systems were studied. An electronic calculation of DFT+U was made considering the spin-orbit coupling. All calculations were carried out using the VASP program [4] implemented into MedeA software [5].

For the CuO/Cu, Al/Si, Cu_3N/Cu, Bi/$BaTiO_3$ heterostructures, band structures were calculated considering the spin-orbit interaction, and based on this, the values of the Rashba parameter αR characterizing the values of the spin-orbit splitting [6] were extracted. An impact of interfacial contact layers, staking parameters, thickness, interface polarity and ferroelectric polarization onto the values of the Rashba parameter was investigated.

The results of this study can be used in the development of functional materials for spintronics based on the properties of these compounds.

Calculations were supported by the Kazan Federal University Strategic Academic Leadership Program (Priority-2030) within the Laboratory of Computer design of new materials and machine learning.

1. M. Chen and F. Liu, Natl. Sci. Rev. 8 (2021).
2. E.I. Rashba and V.I. Sheka, Fiz. Tverd. Tela – Collected Papers (Leningrad) **II**, 162–176 (1959) [in Russian].
3. A.D. Caviglia, M. Gabay, S. Gariglio et al., Phys. Rev. Lett. 126603 (2010).
4. G. Kresse, J. Furthmüller, Phys. Rev. B **54**, 11169–11186 (1996).
5. MedeA version 3.; MedeA is a registered trademark of Materials Design, Inc., San Diego, USA.
6. Yu.A. Bychkov, E.I. Rashba, Sov. Phys. – JETP Lett. **39**, 78–81 (1984) [in Russian].

A.P15

DYNAMIC OPERATING MODES OF THE SPIN VALVE WITH IN-PLANE ANISOTROPY IN THE MAGNETIC FIELD OF THE ARBITRARY DIRECTION

*Iu.A. Iusipova**, *N.V. Ostrovskaya, V.A. Skidanov*

Institute for Design Problems in Microelectronics RAS (IPPM RAS), Moscow, Russia
*E-mail: linda_nike@mail.ru

The large number of operating modes of spin-valve structures and compatibility with CMOS technology allows them to be used as the basic elements of a large number of microelectronic devices, such as hard magnetic disk drives (HMDD), magnetoresistive random access memory (MRAM), spin-transfer nano-oscillator (STNO), spin-valve biosensors and a p-bit stochastic neuron used to implement probabilistic spin logic (PSL) [1].

In this work, the magnetization vector **M** dynamics of the spin-valve free layer with planar anisotropy under the influence of the electric current with the density J and the magnetic field **H** of the arbitrary direction were simulated. Four hard magnetic ferromagnetic alloys ($Co_{50}Pt_{50}$, $Fe_{50}Pt_{50}$, $Fe_{50}Pd_{50}$, $Fe_{50}Ni_{50}$) and six soft magnetic materials (cobalt, iron, $Fe_{70}Co_{30}$, $Fe_{60}Co_{20}B_{20}$, $Co_{93}Gd_7$ and $Co_{80}Gd_{20}$) were considered as materials for the free and fixed layers of the valve.

As a result of the qualitative analysis of the Landau-Lifshitz-Gilbert system of equations describing the vector **M** dynamics, the equations for the coordinates of the vector **M** equilibrium points $T_{1\text{-}6}$ were obtained. Analyzing singular points types on the H-J plane, the areas with qualitatively different vector **M** dynamics were identified. Bifurcation diagrams for different values of the vector **H** guiding angles were plotted (Fig. 1).

In the paper, the vector **M** dynamic modes were classified. We identified the following types of dynamics: switching with two probable outcomes T_q and T_p ($2S_{q,p}$), switching to the single stable equilibrium positions T_q ($1S_q$), modes with stable limit cycles (LC) and modes with unstable limit cycles (ULC), dynamics of the magnetization vector with two possible outcomes — switching to the point T_q or "winding" on the limit cycle (LC + $1S_q$), where q, p are the numbers of singular points. The time dependences of the output voltage for these modes of operation.

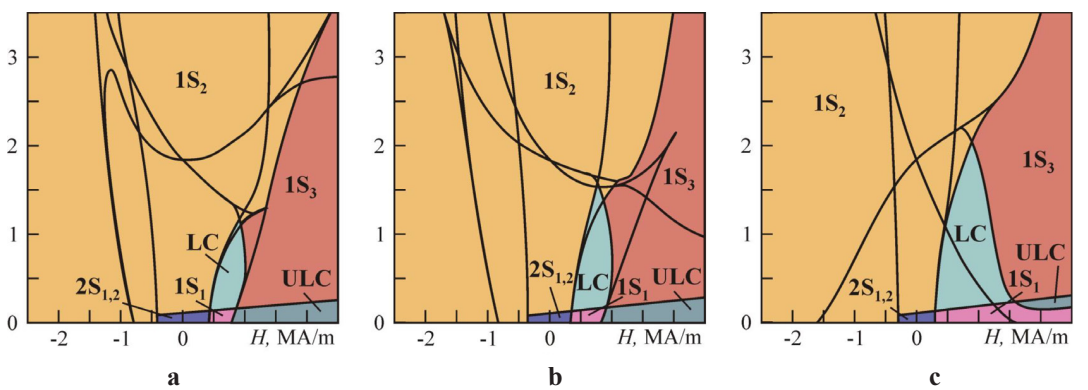

Figure 1. Bifurcation diagrams for the cobalt-based spin valve at $\varphi = \pi/4$, $\theta = \pi/4$ (**a**); $\varphi = \pi/4$, $\theta = \pi/3$ (**b**); $\varphi = \pi/4$, $\theta = \pi/2$ (**c**). The designations in the figure are listed in the text above.

The main mode of the spin-valve operation as a HMDD read head is switching from parallel to antiparallel states and *vice versa* in the applied magnetic field H. The dependence of the minimal switching field H_{min} on the guiding angles φ and θ is calculated. The orientation of the field **H** with the smallest value of H_{min} was identified for the materials listed above. In some cases, it turned out to be 1.7 times less than the anisotropy field.

The precessional mode of the vector **M** dynamics is the main operating mode of the spin valve as STNO [2]. For magnetic field with directions not perpendicular to the anisotropy axis, oscillatory modes with non-sinusoidal output signal types were found. Such modes arise due to the fact that the cyclic hodographs of the end of the magnetization vector on a spherical phase surface are asymmetrical about the axis of rotation.

The main operating mode of the spin valve as a biosensor is the vector **M** switching under the action of the magnetic-nanoparticles field acting as labels for analytes [3]. The sensitivity, nominal resistance, and reading voltage of the biosensors based on the spin valve with planar layer anisotropy for various ferromagnets were calculated. The optimal directions of the magnetic field used to orient magnetic nanoparticles, corresponding to the largest deviation of the vector **M** from the anisotropy axis, were determined.

1. Iu.A. Iusipova, A.I. Popov, Semiconductors **55**(13), 1008–1020 (2021).
2. Ch.Y. You, J. Magnetics **14**(4), 168–171 (2009).
3. E.Y. Tsymbal, I. Žutić, Handbook of Spin Transport and Magnetism. Boca Raton: CRC Press Taylor & Francis Group, 777 p. (2012).

A.P16

ION-BEAM SYNTHESIS AND MAGNETIC PROPERTIES OF IRON NANOPARTICLES IN RUTILE (TiO_2)

I.R. Vakhitov[1,2*], *N.M. Lyadov*[1], *V.I. Vdovin*[3], *A.K. Gutakovskii*[3], *V.I. Nuzhdin*[1], *V.F. Valeev*[1], *L.R. Tagirov*[1,2], *R.I. Khaibullin*[1]

[1]Zavoisky Physical-Technical Institute, FRC Kazan Scientific Center of RAS, Kazan, Russia
[2]Kazan Federal University, Kazan, Russia
[3]Rzhanov Institute of Semiconductor Physics, Novosibirsk, Russia
*E-mail: iskvakhitov@gmail.com

Magnetic nanoparticles embedded into semiconductors have current perspectives for using in semiconducting spintronics [1]. It this work we utilized the ion implantation technique in a regime of the ion-beam synthesis to form magnetic nanoparticles of iron in the semiconducting matrix of rutile ($TiO_{2)}$. Namely, 40 keV Fe^+ ions had been implanted into single-crystalline (100)- or (001)-faced rutile plates to high fluences of $(0.5\div1.5)\cdot10^{17}$ ion/cm^2 at room temperature of the irradiated substrate. Microstructure, elemental-phase composition and magnetic properties of the Fe-ion implanted samples were studied by using transmission and scanning electron microscopies (TEM and SEM), X-Ray photoelectron (XPS) and Rutherford backscattering (RBS) spectroscopies, as well as vibrating-sample magnetometry (VSM).

The high-fluence implantation with iron ions significantly changes microstructure and magnetic properties of the surface layer of rutile TiO_2. Analysis of the cross-section TEM images and electron diffraction patterns indicate clearly the formation of magnetic nanoparticles of the alpha phase of metallic iron into the irradiated layer. XPS data support that the most of implanted iron is in the metallic state and localized at the depth of ~15 nm. However, there are also extended tails in the XPS distribution profiles, up to depth of 90 nm and 120 nm for (100)- and (001)-oriented samples, respectively (Fig. 1a). This trend indicates the implant diffusion deep into the substrate during the

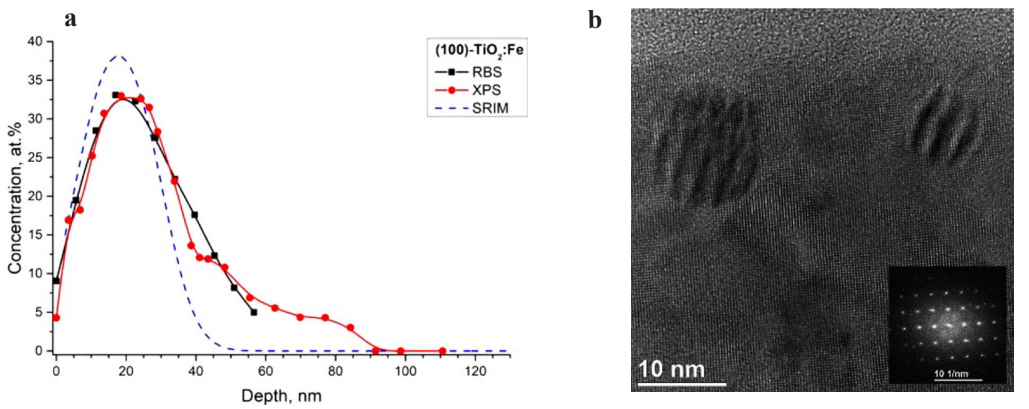

Figure 1. **a** Depth distribution profiles of iron impurity in the (100)-TiO_2 plate implanted with a dose of $1.5\cdot10^{17}$ ion/cm^2. The black squares show the profiles calculated from the RBS spectra, and the red circles show the profiles obtained from the analysis of the XPS spectra. The dash line shows the theoretical impurity distribution profile calculated using the SRIM algorithm [2], which takes into account the sputtering of the substrate during the ion irradiation. **b** High-resolution cross-section transmission electron microscopy (HRTEM) image of the surface layer of the implanted rutile TiO_2.

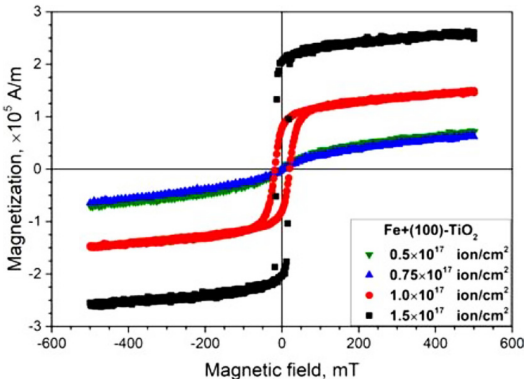

Figure 2. Evolution of the magnetic response with increasing the irradiation dose for the iron-implanted (100)-oriented rutile plates.

ion implantation. It is important to note that the ion-synthesized nanoparticles of iron have a pronounced moire' pattern on the TEM images (Fig. 1b). It indicates an endotaxial (coherent) growth of the iron nanoparticles in crystal structure of rutile

With increasing the implantation fluence, the Fe-ion implanted samples exhibit first a superparamagnetic and then a ferromagnetic response at room temperature (Fig. 2). A strong magnetic shape anisotropy have been observed at the highest implantation fluence of $1.5 \cdot 10^{17}$ ion/cm^2, which is typical for thin granular magnetic films. Furthermore, 2 or 4-fold magnetic crystallalline anisotropy is also observed in the (100)- and (001)-planes of the TiO_2 plates, respectively. The induced ferromagnetism and the observed anisotropy are associated with the coherent growth of iron nanoparticles oriented along certain crystallographic axes of the TiO_2 oxide matrix [3].

The study was supported by the Russian Science Foundation (project number 22-19-00712, https://rscf.ru/project/22-19-00712/).

1. A. Hirohata, K. Yamada, Y. Nakatani, I.-L. Prejbeanu, B. Diény, P, Pirro, B, Hillebrands, J. Magn. Magn. Mater. **509**, 166711 (2020).
2. J.F. Ziegler, J.P. Biersak, U. Littmark, The Stopping and Range of Ions in Solids, NY: Pergamon, 192 p. (1985).
3. C. Okay, I.R. Vakhitov, V.F. Valeev, R.I. Khaibullin and B. Rameev, Appl. Magn. Reson. **48**, 347–360 (2017).

A.P17

CONTROL OF SPIN WAVE PROPAGATION MODES IN ARRAYS OF YIG STRIPES

A.B Khutieva[*], *E.N. Beginin, A.V. Sadovnikov*

Laboratory of Magnetic Metamaterials, Saratov State University, Saratov, Russia
[*]E-mail: abkhutieva@gmail.com

Magnons, which are quanta of spin-wave ex-citations, can be signal carriers in the case when the mode of propagation of spin waves in ferro- or ferrimagnetic films and structures is realized. The main advantage of this approach is the range of existence of spin waves – frequencies from several GHz to hundreds of GHz [1] and wavelengths from tens of nanometers to a few millimeters. In this case, the combination of magnonic elements makes it possible to create magnon networks (MS) consisting of coupled spin-wave elements. The simplest element can be a strip of a ferromagnet limited in two directions and representing a waveguide of spin waves or, from an electrodynamic point of view, waveguides with a gyrotropic medium. In this case, the gyrotropy properties are set by the direction of the external magnetic field, along which the magnetization direction is built in the ferromagnet at sufficient magnetic field strengths to saturate. As materials for waveguides of spin waves, films of yttrium iron garnet (YIG) are currently being considered, which can be used for information processing and at the same time provide technological integration with the existing semiconductor architecture [1, 2]. It has recently been shown that a three-dimensional (3D) magnonic crystal in the shape of a meander [3, 4] can provide vertical transfer of spin waves with vertical sections of the magnonic waveguide. At the same time, it was also experimentally demonstrated that

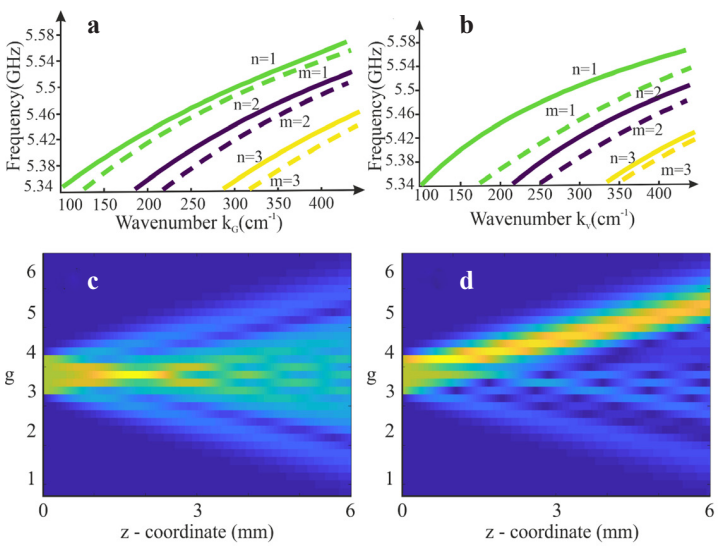

Figure. 1. Dispersion characteristics of spin waves to reveal (**a**) lateral and (**b**) vertical coupling. The dotted line shows asymmetric modes, the solid line shows symmetric modes. The order of width modes of the symmetric type is denoted by the symbol n, for the asymmetric type, by the symbol m; **c** concentration of the spinal beam in the Y-section of the structure; **d** accumulation of the spin beam concentration in the Y-section of the structure when phases appear between the source in the collimated beam mode.

the creation of multilayer topologies of three-dimensional structures with violation of translational symmetry makes it possible to consider the created elements as nodes of interconnections for vertically integrated MS topologies.

In the present work, the dipole stray fields of magnon stripes are considered for performing vertical and lateral transfer of spin waves and signal transmission between magnon strips in two mutually orthogonal directions. Each strip is made from thin YIG films. To study the dynamics of spin wave propagation in a system of coupled YIG waveguides, numerical simulation was used based on the finite element method (FEM) and micromagnetic (MM) simulation with time and frequency resolution. At the same time, a study was made of the modes of propagation of spin waves in the considered arrays of microwave guides by varying the magnetization angle.

A system of microwave guides. The scheme shows two antennas in red, which in the micromagnetic calculation corresponded to the location of the excitation region of the spin-wave signal. The magnetic field is directed along the short side of each microwaveguide.

To describe the spin transport, a system of first-order differential equations is used written in the form [4, 5]:

$$\frac{\mathrm{d}A_{ij}}{\mathrm{d}z} = \mathrm{i}\beta A_{ij} + \mathrm{i}C_{\mathrm{v}}(A_{i+1,j} + A_{i-1,j}) + iC_{\mathrm{g}}(A_{i+1,j} + A_{i-1,j}),$$

where A_{ij} is the amplitude of the n-th microwaveguide, i (laterally), j (vertically) are waveguide numbers, β is the wave number in an isolated waveguide, C_{v} is vertical, C_{g} is the lateral dipole coupling coefficients of spin waves. The numerical value of the coefficients C_{v} and C_{g} was found by the finite element method as a result of solving the system of Maxwell equations with the magnetic permeability tensor obtained from the linearization of the Landau-Lifshitz equation. At the same time, the frequency dependence of these parameters was built, as well as dependences on the orientation of the bias angle.

Next, nonlinear modes of signal propagation in an array of YIG waveguides were considered. A study was made of the features of the processes of formation of spin-wave beams in the linear and nonlinear cases for systems of systems of coupled magnetic waveguides. A study was made of the transformation of isofrequency characteristics for a system of coupled waveguides with a variation in the bias field. Features of the propagation of spin waves in a three-dimensional array of YIG films are revealed. The phenomenon of the formation of a tunable spin-wave beam in a three-dimensional magnon structure is shown, which can give a deep understanding of the physics of the lethal and vertical transfer of spin waves in an array of micro- and nanosized structures. It should be noted that the considered class of ensembles of magnonic structures can be used to expand the functionality of in-formation processing devices based on magnonic principles [5].

This work was supported by the grant from Russian Science Foundation (No. 19-29-03034)

1. A.R. Safin, S.A. Nikitov, A.I. Kruglyuk, D.V. Kalyabin, A.V. Sadovnikov, P.A. Stremoukhov, M.V. Logunov, P.A. Popov, J. Exp. Theor. Phys. **131**, 71–82 (2020).
2. S.L. Vysotskii, A.V. Sadovnikov, G.M. Dudko, A.V. Kozhevnikov, Y.V. Khivintsev V.K. Sakharov, N.N. Novitskii A.I. Stognij, Y.A. Filimonov, Appl. Phys. Lett. **117**, 102403 (2020).
3. V.K. Sakharov, E.N. Beginin, Y.V. Khivintsev, A.V. Sadovnikov, A.I. Stognij, Y.A. Filimonov, and S.A. Nikitov, Appl. Phys. Lett. **117**, 022403 (2020).
4. A.V. Sadovnikov, G. Talmelli, G. Gubbiotti, E.N. Beginin, S.E. Sheshukova, S.A. Nikitov, C. Adelmann, F. Ciubotaru J. Magn. Magn. Mat. **544** (2022).
5. A.V. Sadovnikov, S.A. Odintsov, E.N. Beginin, A.A. Grachev, V.A. Gubanov, S.E. Sheshukova, Yu.P. Sharaevsky, S.A. Nikitov, JETP Lett. **107**(1), 29–34 (2018).

A.P18

MAGNETIC CONDUCTIVITY OF COMPOSITE FILMS ($CoFeB+SiO_2+N_2$) IN TEMPERATURE RANGE 2–400 K

L.N. Kotov[1*], *A.A. Utkin*[1], *V.S. Vlasov*[1], *A.V. Sitnikov*[2], *Yu.E. Kalinin*[2]

[1]Syktyvkar State University, Syktyvkar, Russia
[2]Voronezh State Technical University, Voronezh, Russia
[*]E-mail: kotovln@mail.ru

Nanogranulated magnetic metal-dielectric composite films have both positive magnetic conductivity and negative magnetic conductivity [1, 2]. It is still not clear which mechanisms are responsible for positive and negative magnetic conductivities. This paper presents the results of studying the magnetic conductivity of composite films ($CoFeB + SiO_2 + N_2$) for different concentrations of the metal alloy. Studies of specific conductivity were carried out in a wide temperature range of 2–400 K and when the films were magnetized by a constant magnetic field $B_0 = 1$ T.

The films were deposited by ion bombardment of targets consisting of $Co_{0.44}Fe_{0.36}B_{0.2}$ metal alloys and SiO_2 dielectric onto a lavsan sheet with an area of 297×210 mm^2. The films were deposited in a nitrogen atmosphere, the targets were bombarded with nitrogen ions, which were contained in

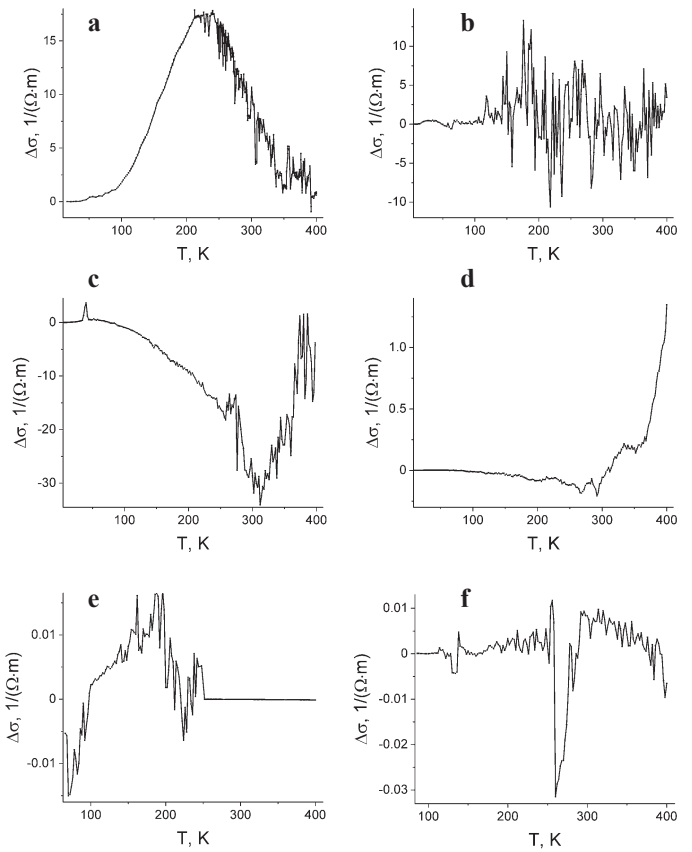

Figure 1. Temperature dependences of the magnetic conductivity of composite films ($CoFeB + SiO_2 + N_2$) at $x = 0.27$ (**a**), 0.32 (**b**), 0.37 (**c**), 0.47 (**d**), 0.62 (**e**), 0.72 (**f**).

the elemental composition of the films up to 2 at.%. The elemental composition of the films was determined using a Tescan Mira 3 scanning electron microscope.

An approximate formula for the film compositions was obtained $[(Co_{0.46}Fe_{0.4}B_{0.14})_x + (SiO_2)_y + N_{2z}]$, $0.25 < x < 0.8$, $y = (1 - x)/3$, $z = 0.01$.

The electrical resistance of the composite films was determined by the four-contact method in a wide temperature range using a PPMS-9 Quantum Design instrument in magnetic fields up to 1 T. The obtained temperature dependences of the electrical conductivity were subtracted from each other using a mathematical program. The resulting difference in specific conductivities in a magnetic field and without a field at a fixed temperature is called magnetic conductivity and is equal to $\Delta\sigma = \sigma_B - \sigma_0$. Temperature dependences of magnetic conductivity for composite films ($CoFeB + SiO_2 + N_2$) for six metal alloy concentrations x are shown in Fig. 1. As can be seen from Fig. 1, for low concentrations $x = 0.27$, positive magnetic conductivity is observed in a wide temperature range of 20–400 K. At $x = 0.32$, magnetic conductivity decreases by five times (Fig. 1b). At $x = 0.37$, negative magnetic conductivity is observed in the films in the range of 20–400 K. For films with large $x = 0.47$, positive magnetic conductivity is observed in the temperature range of 300–400 K. At $x = 0.62$, in a wide temperature range of 250–400 K, the magnetic conductivity of the films is zero. In the temperature range of 80–250 K, a maximum of positive magnetic conductivity is observed. As the temperature decreases from 80 to 50 K, the negative magnetic conductivity increases. At a very high concentration of metals $x = 0.72$ in a wide temperature range of 50–380 K, the magnetic conductivity is almost zero. In conclusion, we can say that both positive and negative magnetic conductivity is present in all films simultaneously. Their ratio strongly depends on the concentration of the metal phase and temperature, which determines the structure and, accordingly, the mechanisms of magnetic conductivity.

Scientific research were performed at the Research park of St.Petersburg State University "Center for Diagnostics of Functional Materials for Medicine, Pharmacology and Nanoelectronics". The study was supported by a grant from the Russian Science Foundation (project no. 21-72-20048).

1. O.V. Stognei, Yu.E. Kalinin, I.V. Zolotukhin et al., J. Phys.: Condens. Matter **15**, 4267–4277 (2003).
2. Yu.E. Kalinin, A.V. Sitnikov, O.V. Stognei et al., Mater. Sci. Eng. **941**, 304–306 (2001).

A.P19

INVESTIGATION OF INHOMOGENEOUS CURRENT ACTION ON THE MAGNETIC STRUCTURE OF A FERRIMAGNET

M.E. Letushev[*], *Zh.Zh. Namsaraev*[1], *M.A. Bazrov*[1], *M.E. Stebliy*[1]

Laboratory of Spin-Orbitronics, Institute of High Technologies and Advanced Materials,
Far Eastern Federal University, Vladivostok, Russia
[*]E-mail: letushev.me@dvfu.ru

Ferrimagnetic media (FIM) are a promising direction in the development of spintronics due to the possibility of being in a state of compensation of magnetic and angular momentum. The first state is characterized by stability and maximum efficiency of the spin-polarized current action [1], and the second state is characterized by the maximum speed [2]. The possibility of using a non-uniform current density to control the process of magnetization reversal under the action of a current is studied in this work: fixing the place of origin of the domain, the speed and direction of its movement.

In the simplest case, FIMs are amorphous two-component alloys (CoTb, FeGd), whose magnetic structure can be represented as two antiparallel ordered sublattices formed by atoms of two sorts. An experimental study was carried out on the example of the W(40)/Co65Tb35(40)/Ru(20) structure obtained by magnetron deposition on the Si/SiO2 surface. At room temperature, the film of the indicated composition is Tb-rich, i.e., the magnetization of the Tb sublattice is aligned along the external magnetic field. Magnetic moment compensation temperature T_M = 52°C, further heating transfers to the Co-rich state. Hall structures with a non-uniform width profile were formed by photolithography and ion-plasma etching, Fig. 1a. In such a structure, the transmission of electric current pulses leads to a number of inhomogeneities along the *x*-axis: variable current density, variable temperature, due to the Joule effect with maximum in the center and inhomogeneous magnetization since the resulting magnetic moment of the FIM depends on temperature, Fig. 1b.

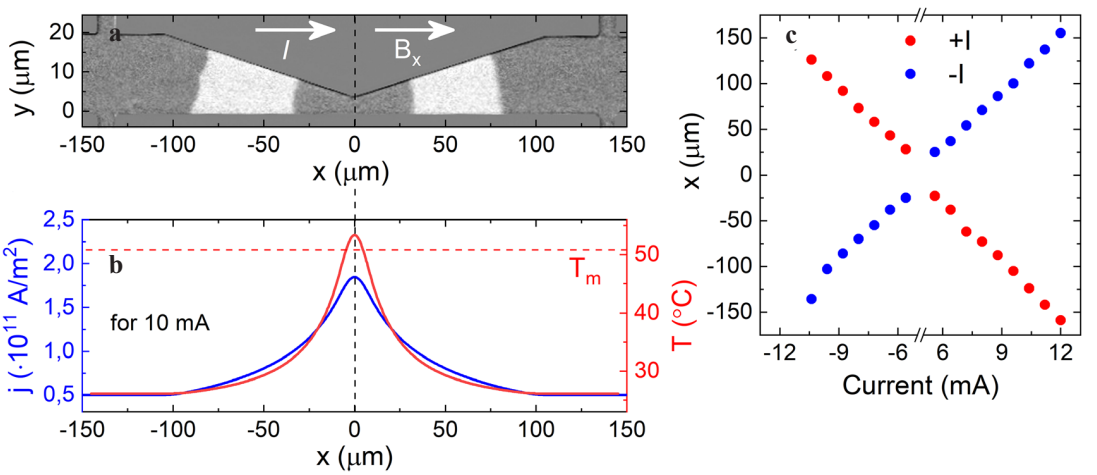

Figure 1. **a** Profile image of a Hall bar structure of an inhomogeneous profile, the magnetic structure visualized with a Kerr microscope. **b** An example of the distribution of current density and structure temperature for a 10 mA current pulse. **c** Dependence of the position of the domain wall on the current pulse amplitude for different current orientations.

To study the current-induced magnetization reversal, the standard spin-orbit torque mechanism [3] was used: current pulses of variable amplitude and direction are passed through the sample in the presence of a constant magnetic field along the x-axis B_x = 100 mT. In this case, the magnetization reversal always begins in the region with the maximum current density – in the center, and the wall moves to the periphery, Fig.1a. In this case, the position of the domain wall is uniquely determined by the amplitude of the current pulse, Fig. 1c. In addition, by adjusting the current density, it is possible to heat up the central region locally by transferring it from the Tb-rich state to the Co-rich state. Also, such a structure makes it possible to study the velocity of the domain wall under the action of a current of inhomogeneous density.

Support by the grants the Russian Science Foundation, RSF 21-72-00138.

1. J. Finley, L. Liu, Phys. Rev. Appl. **6**, 054001 (2016).
2. G. Sala, V. Krizakova, E. Grimaldi et al., Nat. Commun. **12**, 656 (2021).
3. Manchon, I.M. Miron, P. Gambardella, Rev. Mod. Phys. **91**, 035004 (2019).

A.P20

SIMULATION OF THE PROCESSES OF NONMONOTONIC RELAXATION OF A MULTILAYER MAGNETIC STRUCTURE

*D.A. Lgotina**, *P.V. Prudnikov*

Dostoevsky Omsk State University, Russia
*E-mail: lgotinada@para-lab.ru

Recently, much attention has been paid to the study of the properties of thin magnetic films of transition metals and multilayer thin-film systems obtained on their basis, which are an alternation of magnetic and non-magnetic layers. Ultrathin films of magnetic metals and alloys are constituent elements for multilayer structures, which are characterized by a wide range of applications in devices based on the giant magnetoresistance (GMR) phenomenon. At present, multilayer magnetic structures consisting of from ultrathin films are widely used: as a magnetic medium for recording and storing information in memory devices; when designing a magnetic random access memory (MRAM) to reduce the magnitude of the current density and the amount of time required to switch the magnetic state; to create sensors sensitive to the presence of ferromagnetic nanoparticles on their surface for medical applications [1].

The aim of this work is to study non-equilibrium processes of relaxation of a multilayer structure from a low-temperature initial state at different initial states – parallel and antiparallel state of the magnetization of ferromagnetic films, when changing the initial outer field h_0. The problem of numerically investigating the nonequilibrium behavior of a multilayer magnetic structure consisting of two Heisenberg ferromagnetic films with a bcc-lattice separated by a nonmagnetic metal film is considered.

The three-dimensional ferromagnetic Heisenberg model is one of the traditional statistical models used to describe phase transitions in various spin systems, including those in transition metals. From the point of view of a theoretical description, it is convenient to specify the effects of magnetic anisotropy in the form of a generalized Heisenberg model. In multilayer structures with the GMR effect, the thickness of the nonmagnetic interlayer is chosen so that the RKKY interaction between the spins of the ferromagnetic layers has an effective antiferromagnetic character. In a number of structures with a metal interlayer, where the role of the RKKY exchange interaction between ultrathin ferromagnetic layers is important, supermagnetic behavior was observed. Thus, the structure under consideration models artificially created multilayer structures characterized by the manifestation of GMR effects.

The critical temperature of the system is determined by the type of the behavior of the projection of magnetization with a change in the external magnetic field. Critical temperatures for anisotropy constant value A = 0.0, 1.0 and 2.0: T_c = 1.33, 1.63 and 1.83 respectively. With an increase in the value of the anisotropy constant, the critical temperature increases.

Four stable magnetic states are observed in hysteresis loops, which correspond to the magnetization flip of the layers in the film. Flat areas of magnetization are an important property for the creation of permanent magnets, which is associated with a change in the magnetic state of the multilayer structure, one layer in a ferromagnetic film flips over.

Various types of magnetization relaxation were obtained for an asymmetric multilayer magnetic structure and experiment [2]. Monotonic relaxation of magnetization, which goes straight from one equilibrium state to another with favorable energy. With a decrease in the value of the external magnetic field after relaxation, the behavior of the relaxation curve changes to nonmonotonic. Relaxation of the nonmonotonic magnetization is carried out from the initial magnetic state to the

equilibrium state through the third, nonequilibrium intermediate state. In addition to nonmonotonic relaxation with one extremum, there can be relaxation with two or more extrema, called oscillating. It can be concluded that the external magnetic field after relaxation affects the behavior of magnetization relaxation by changing its type of classification. The results obtained are consistent with the experimental data.

The values of the critical temperatures of magnetic ordering in ferromagnetic films of a multilayer structure were obtained by the method of the behavior of the magnetization projection with a change in the external magnetic field. With an increase in the value of the anisotropy constant, the critical temperature of magnetic ordering in ferromagnetic films of an asymmetric multilayer structure increases. The chosen method gives an approximate estimate of the values of critical temperatures. In the study of the effects of hysteresis, a strong dependence on the value of the anisotropy parameter was revealed. An increase in the value of the anisotropy constant leads to an increase in the loop width, which means that the coercive force increases, which characterizes the ability of a ferromagnet to maintain a magnetized state. The relaxation of the magnetization in multilayer magnetic structures can be of several types: monotonic, nonmonotonic, and oscillating. In the process of nonmonotonic relaxation, a two-step transition occurs from the initial magnetic state to the equilibrium state through a third, nonequilibrium intermediate state. The oscillating type of magnetization relaxation can be with two or more extremum points. The initial conditions have a significant effect on the relaxation behavior of the magnetization in a multilayer structure.

The study was carried out with the financial support of the Ministry of Education and Science of the Russian Federation (agreement 0741-2020-0002). The computational research was supported in through resources provided by the Shared Services Center "Data Center of FEB RAS" (Khabarovsk).

1. A. Ottova, V. Tvarozek et al., Membrane Science and Technology **7**, 917–961 (2003).
2. E. Shalygina, A. Kharlamova, A. Makarov, EPJ Web of Conf. **185**, 03009 (2018).
3. R.B. Morgunov, A.I. Bezverkhnii, Superlatties and Microstructures **142**, 106509 (2020).

A.P21

EFFECT OF SPIN CURRENT ON THE FORMATION OF BAND GAPS IN A LAYERED STRUCTURE BASED ON COUPLED MAGNONIC CRYSTALS

*M.A. Morozova, O.V. Matveev, N.D. Lobanov**

Institute of Physics, Saratov State University, Saratov, Russia
*E-mail: lobanov_nikita17@mail.ru

The propagation of spin waves in magnonic crystals (MC) – ferromagnetic films with periodically changing parameters, is actively studied in the problems of modern magnonics [1]. As is known, during the propagation of magnetostatic waves in a structure consisting of two coupled MCs separated by a dielectric layer, one to four band gaps are formed in the region of the first Bragg resonance. The number and characteristics of band gaps depend on the magnetic and geometric parameters of the structure [2].

On the other hand, recently spintronics (or spin-wave electronics) has been intensively developed [3]. In spintronic devices, along with the charge, the spin of particles is used, which is associated with the presence of their own mechanical moment. The spin current in a normal metal (NM), due to the transfer of spin torque at the ferromagnetic film/NM interface, can lead to an increase or weakening of magnetostatic waves in a ferromagnetic film [4, 5].

In this work, we study the effect of the spin current on the formation of band gaps during the propagation of magnetostatic waves in a layered structure consisting of two magnonic crystals separated by a layer of a normal metal (eg, platinum). The structure is placed in an external magnetic field directed tangentially to the plane of the structure, while surface magnetostatic waves propagate in the MC.

The influence of the spin current on the characteristics of the band gaps (the frequency ranges in which Im(k) increases/decreases, respectively, the regions G-1, G-4, and G-2/G-3 in Fig. 1) has been studied. In Fig. 1, the blue curves show the cases at $c = 0$, and the red curves at $c \neq 0$, where c is a parameter depending on the magnitude of the spin current in the NM. It can be seen from Fig. 1a that in the absence of a spin current, one band gap G-2/G-3 is formed, the introduction of a spin current leads to the formation of additional band gaps (G-1 and G-4). In the absence of a spin current, three band gaps (G-1, G-4 and G-2 / G-3) are formed, when the spin current is introduced, G-1 and G-4 converge, at G-2/G-3 current has no effect (Fig. 1b). The spin current of

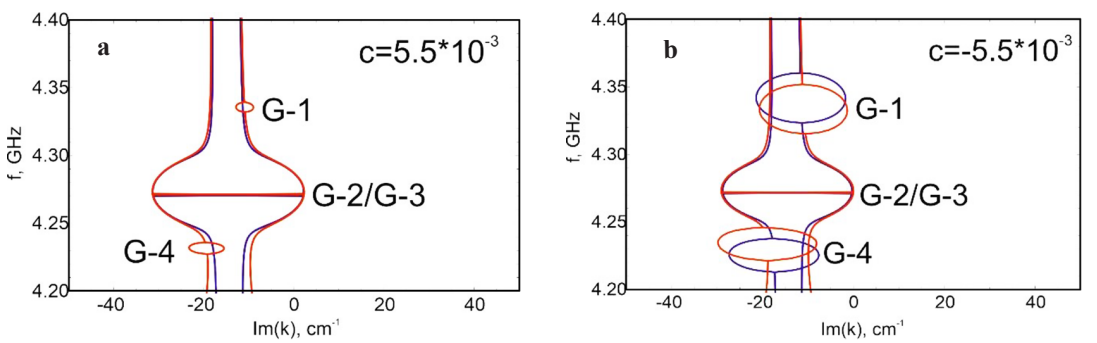

Figure 1. Dependence of frequency on Im(k) at $c = 0$ (blue curves) and $c \neq 0$ (red curves) at a shift between MCs equal to π (**a**), at a shift between MCs equal to 0.6π (**b**).

positive polarity leads to an increase in the width of the G-1 and G-4 bands, while the current of negative polarity does not affect to the width of these band gaps (Fig. 1).

These features make it possible to control the characteristics of band gaps during the propagation of magnetostatic waves in the structure under study by changing the magnitude and direction of the spin current in a normal metal. Thus, the use of an active layer in the form of a normal metal expands the functionality of devices based on magnonic crystals, which can be used in microwave electronics as tunable microwave filters, phase shifters, and delay lines.

This work was supported by the Russian Science Foundation, project № 19-79-20121.

1. M. Krawczyk, D. Grundler, J. Phys.: Condens. Matter **26**, 123202 (2014).
2. M.A. Morozova et al., J. Appl. Phys. **120**, 223901 (2016).
3. A.V. Chumak et al., Nature Physics **11**, 453 (2015).
4. J. Xiao, G.E.W. Bauer, Phys. Rep. Lett. **108**, 217204 (2012).
5. X. Wang et al., Nat. Comm. **11**, 5663 (2020).

EFFECT OF SYNTHESIS CONDITIONS AND BUFFER LAYERS ON MORPHOLOGY AND PHASE FORMATION DURING THE GROWTH OF AN EPITAXIAL Mn_5Ge_3 FILM ON Si(111)

A.V. Lukyanenko[1,2*], *A.S. Tarasov*[1,2], *I.A. Yakovlev*[1], *S.N. Varnakov*[1]

[1]Kirensky Institute of Physics, Federal Research Center KSC SB RAS, Krasnoyarsk, Russia
[2]Siberian Federal University, Krasnoyarsk, Russia
[*]E-mail: lav@iph.krasn.ru

The search for ferromagnetic (FM) materials for spintronic devices is an urgent and complex goal. These materials must be compatible with the silicon technology, which is currently dominant in the semiconductor industry, and also satisfy a number of other requirements [1]. An example of such a material is Mn_5Ge_3, which, in addition to the necessary magnetic properties, exhibits a giant magnetocaloric effect near room temperature [2] that makes it attractive both for environmentally friendly magnetic cooling and for "thinner" spin caloritronic devices [3]. The possibility of synthesizing thin Mn_5Ge_3 epitaxial films on Ge substrates [4, 5], Ge epitaxial buffer layers [6], and GaAs (111) substrates [7] has already been shown in the literature. The processes of epitaxial growth of FM Mn_5Ge_3 on Si substrates had not been studied well, but are of great interest from both fundamental and applied points of view. Growing Mn_5Ge_3 directly on Si will make it possible to study the effects of spin injection, accumulation, and detection in silicon, as was done for Ge [2]. In this work, we studied the morphological features of the formation of Mn_5Ge_3 thin films grown on Si(111) substrates.

The Mn_5Ge_3 thin films were obtained at the Angara ultra-high-vacuum molecular-beam epitaxy setup [8], during the experiment the vacuum was at least $6.5 \cdot 10^{-8}$ Pa. The synthesis was carried out on p-Si (111) (resistivity 0.02–0.04 Ohm cm), before the deposition process, the substrates were prepared in a standard way and annealed until the reconstruction of the Si surface was 7×7 [8]. In the experiment, Mn and Ge were co-deposited in given ratios from Knudsen effusion cells with boron nitride (BN) crucibles. During the synthesis, the substrate temperature was maintained constant at 390 °C. During the synthesis, the parameters of the epitaxial films were controlled *in situ* using a LEF 751M laser ellipsometer using reflection high-energy electron diffraction (RHEED). After the synthesis, the morphology of the Mn_5Ge_3 films was studied *ex situ* by atomic force microscopy (AFM) on a DPN 5000 instrument (NanoInk, U.S.) in a semi-contact scanning mode using NSG10 cantilevers (TipsNano). AFM data processing and statistical analysis of images was carried out using the free software Gwyddion (v. 2.51).

Previously, the successful synthesis of Mn_5Ge_3 films on Si substrates has not been reported, which is most likely due to a rather high lattice mismatch (8%). By decreasing the amount of manganese in the composition, one can reduce this mismatch and grow a Mn-depleted buffer layer or ultra-thin layers of silicides and germanides with the B20 structure, followed by a composition gradient and a smooth transition to a stoichiometric ratio of 5:3. Observation of changes in the RHEED intensity provides information on the growth mode and surface roughness of Mn_5Ge_3 thin films. Figure 1 shows the final RHEED (a–c) and AFM (d–f) images of Mn_5Ge_3 films deposited on a Si (111) substrate. The corresponding sample numbers are marked in the figure. It can be seen how the epitaxial growth is stabilized by adding a buffer layer and optimizing its composition. Sample №3 (thickness 56 nm) – the growth of the Mn_5Ge_3 film was carried out directly on the Si (111) substrate without using a buffer layer at the same stoichiometry of manganese and germanium. There are only reflections from a textured polycrystalline film. Sample №5 (thickness 60 nm) – the

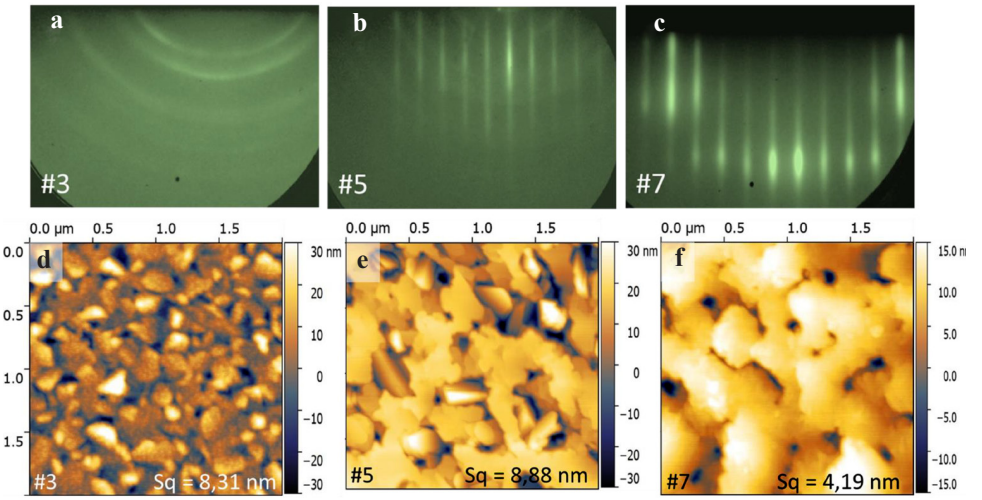

Figure 1. RHEED patterns and AFM images of the Mn_5Ge_3 thin film on Si (111). **a** Sample №3, there are only reflections from a textured polycrystalline film; **b** sample №5 shows the formation of an epitaxial film along with a polycrystalline one; **c** pattern for sample №7, formation of only an epitaxial film is observed. AFM images are shown from 2×2 μm^2 area: **d** sample №3 thickness 56 nm; **e** sample №5 thickness 60 nm; **f** sample №7 thickness 180 nm Mn_5Ge_3 film.

growth of the Mn_5Ge_3 film was carried out on a 13 nm buffer layer consisting of single-crystal germanium (5 nm) and one transition layer with a high manganese content (8 nm) deposited on Si (111). RHEED pattern for the sample №5 shows the formation of an epitaxial film along with a polycrystalline one. This can be seen in the AFM image (Fig. 1e), the fraction of the single-crystal phase is ~66% of the total area, crystallites of the side phase are visible. Sample №7 (thickness 180 nm) – the growth of the Mn_5Ge_3 film was carried out on a buffer layer (20 nm) consisting of a thin layer of germanium and several transition layers with a gradual change in the stoichiometry of manganese and germanium. RHEED pattern for the sample №7 shows the formation of only an epitaxial film. It should be noted that stable growth was observed throughout the entire synthesis. This is also confirmed by the AFM data in fig. 1f that shows the characteristic surface morphology of the Mn_5Ge_3 epitaxial film without a side phase.

Apparently, the formation of epitaxial films is achieved by the formation of buffer gradient layers, which ensure the matching of the crystal lattices of the silicon substrates and the resulting germanides. Figure 1 also shows the parameters of root-mean-square roughness (S_q) taken over the entire area of the scanning frame. It can be seen that, upon stabilization of the growth conditions for the Mn_5Ge_3 film, S_q decreases by almost a factor of two. This may also indicative of the stable growth of the Sample №7 during the entire synthesis time.

Support by Krasnoyarsk Regional Fund of Science is acknowledged.

1. I. Zutic, J. Fabian, S. Das Sarma, Rev. Mod. Phys. **76**(2), 323–41 (2004).
2. J. Tang et al., Nano Lett. **13**(9), 4036–4043 (2013).
3. S. Boona et al., Energy Environ. Sci. **7**, 885 (2014).
4. S. Olive-Mendez et al., Thin Solid Films **517**, 191 (2008).
5. M. Petit et al., Appl. Surf. Sci. **480**, 529–536 (2019).
6. S. Bechler et al., Semicond. Sci. Technol. **33**, 095008 (2018).
7. R. Cardoso de Oliveira et al., JMMM **539**, 168325 (2021).
8. I.A. Yakovlev et al., JETP Lett. **99**(9), 527–530 (2014).

A.P23

MAGNETIC ANISOTROPY OF FeNi THIN FILMS AND MULTILAYERED STRUCTURES PREPARED BY OBLIQUE MAGNETRON DEPOSITION

I.A. Makarochkin[1*], *V.N. Lepalovskij*[1], *A.A. Pasynkova*[1,2], *G.V. Kurlyandskaya*[1,3], *A.V. Svalov*[1]

[1]Institute of Natural Sciences and Mathematics, Ural Federal University, Ekaterinburg, Russia
[2]Institute of Metal Physics, Ural Branch of Russian Academy of Sciences, Ekaterinburg, Russia
[3]Depto Electricidad y Electrónica, Universidad del País Vasco UPV/EHU, Bilbao, Spain
[*]E-mail: makarochkin98@gmail.com

Oblique angle deposition is an efficient way of tailoring of magnetic anisotropy in thin films [1, 2]. The application of the oblique deposition method requires an understanding of the relationship between the thickness, structural features and the magnetic properties of these films, as well as the magnetic behaviour of exchange coupled multilayers with different orientations of the magnetic anisotropy axes in individual layers. In this work, features of magnetic anisotropy of FeNi films of different thickness and FeNi-based multilayers prepared by oblique angle magnetron deposition were studied.

FeNi films were deposited by dc magnetron sputtering onto glass substrates at room temperature using a $Fe_{20}Ni_{80}$ target. The oblique deposition angle with respect to the normal to the surface of the substrate was 35°. The thickness of the FeNi films was varying in the interval 10–500 nm. During the deposition of FeNi multilayered structures, the next layer was deposited when the substrate was rotated in the plane with respect to the previous layer in the range of angles 90–180°. Magnetic measurements were carried out by means of vibrating sample magnetometer and magneto-optical Kerr effect using the optical microscope Evico.

It was found that the angular dependencies of the coercivity and normalized remnant magnetization M_r/M_s (Fig. 1) confirmed the existence of the uniaxial magnetic anisotropy in the plane for FeNi films prepared by oblique deposition. The easy magnetization axis (EA) was perpendicular to the atomic flux direction. The bilayers obtained by rotating of the sample by 180° also had a similar

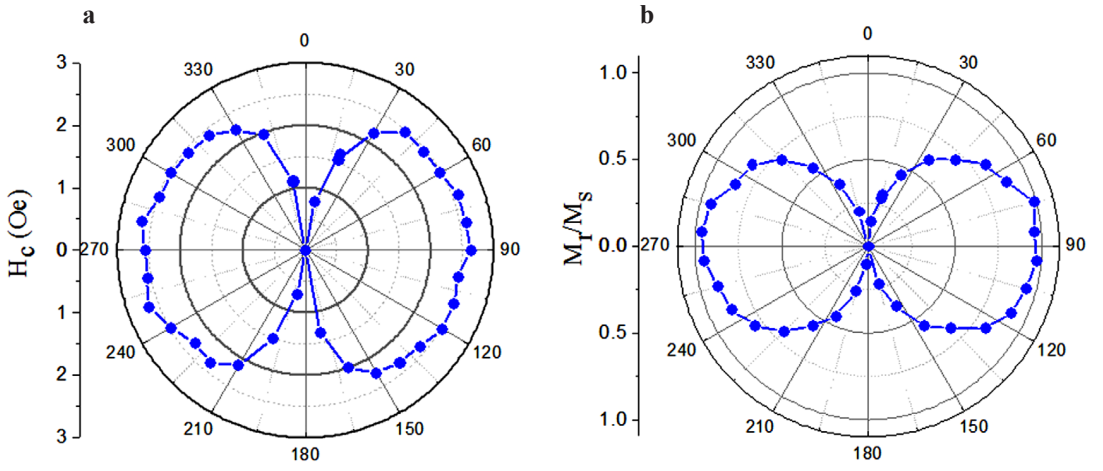

Figure 1. Coercivity (**a**) and normalized remnant magnetization (**b**) versus azimuthal angle between the applied field direction and the incident flux for 40 nm thick FeNi film.

uniaxial magnetic anisotropy. For multilayered structures obtained by rotating the sample by 90° the easy and hard magnetization directions of the effective uniaxial anisotropy were tilted by 45° and 45° from the EA of each individual layer. We discuss the relationship between the effective uniaxial anisotropy, the number and thickness of the FeNi-layers and orientation of EA in the nearest layers.

The Russian Science Foundation (RSF), project No. 22-29-00980, financially supported this work.

1. P.N. Solovev, A.V. Izotov, B.A. Belyaev, J. Magn. Magn. Mater. **429**, 45–51 (2017).
2. X. Jiang, J. Zhang, X. Song et al., J. Magn. Magn. Mater. **547**, 168946 (2022).

A.P24

TEMPERATURE DEPENDENCE OF MAGNETIC PROPERTIES AND MAGNETIC-FIELD BEHAVIOR OF Co/Cu/Co THIN-FILM THREE-LAYER SYSTEMS

A.V. Makarov[1*], *E.E. Shalygina*[1], *A.V. Svalov*[2]

[1]Moscow State University, Moscow, Russia
[2]Ural Federal University n. a. the first President of Russia B. N. Yeltsin, Ekaterinburg, Russia
[*]E-mail: andrey6257@gmail.com

In recent years, multilayer and, in particular, three-layer thin-film Co/Cu/Co systems have attracted the attention of scientists. This is due to the discovery of the exchange interaction between the layers of Co through the nonmagnetic interlayer of Cu by the polarization of conduction electrons. In the works published earlier by the authors, the magnetic properties of three-layer Co/Cu/Co samples at room temperature were studied. It was found that the saturation field of the samples oscillates in magnitude with a change in the thickness of the copper layer. The results obtained indicated the influence of the exchange interaction on the magnetic properties of the samples. For samples with copper thicknesses equal to 1.4, 2.2, and 3.2 nm, two-stage hysteresis loops were observed, the complex shape of which was explained by antiferromagnetic exchange interaction through the copper interlayer. This paper presents the results of studying the magnetic properties and magnetic field behavior of Co/Cu/Co samples at low temperatures.

The Co/Cu/Co samples under study were obtained by magnetron sputtering of Co and Cu layers on glass (Corning 2845) substrates at room temperature. The measurements were performed under the following conditions: the substrate surface roughness was about 0.5 nm, the base pressure in the vacuum chamber was $4\cdot10^{-7}$ mbar, and the argon pressure during film deposition was $3.8\cdot10^{-3}$ mbar. To create induced magnetic anisotropy, a constant magnetic field of 250 Oe was applied parallel to the plane of the substrate. Measurements at low temperatures were performed on samples with a copper layer with thicknesses of 1.4, 2.2, 3.2 and 4.0 nm, and a cobalt layer thickness of 5 nm. The length and width of the samples were 5 mm. It should be noted that three samples (t_{Cu} = 1.4 nm, 2.2 nm, and 3.2 nm) exhibited antiferromagnetic interaction at room temperature.

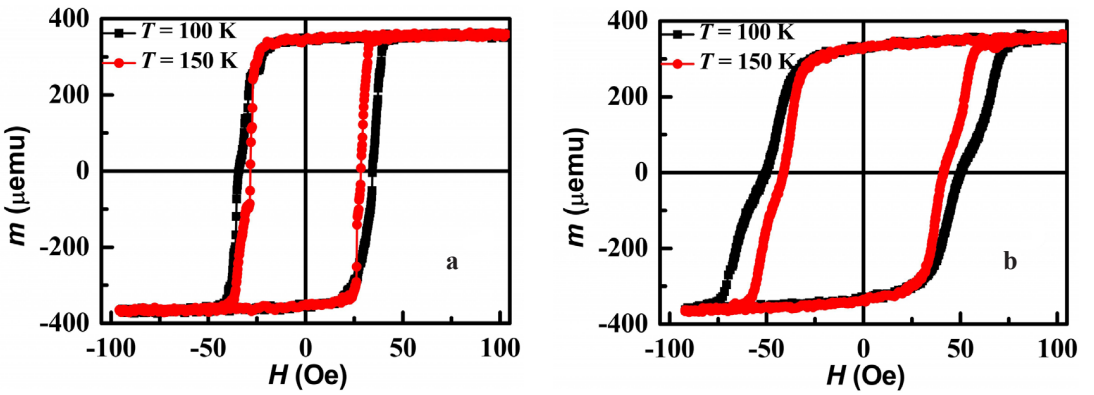

Figure 1. Hysteresis loops observed in a magnetic field parallel to the easy magnetization axis for samples with t_{Cu} = 1.4 nm (**a**) and t_{Cu} = 3.2 nm (**b**) at T = 100 and 150 K.

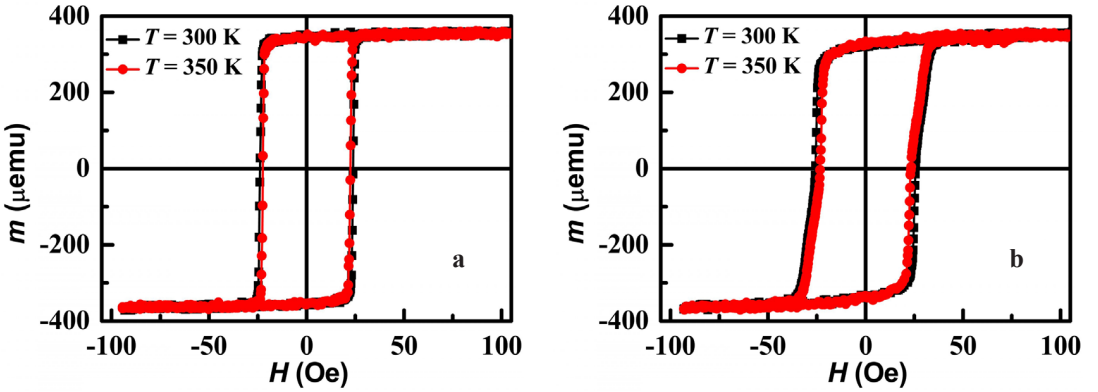

Figure 2. The hysteresis loops observed for the same samples as in Fig. 1 at room temperature (T = 300 K) and 350 K.

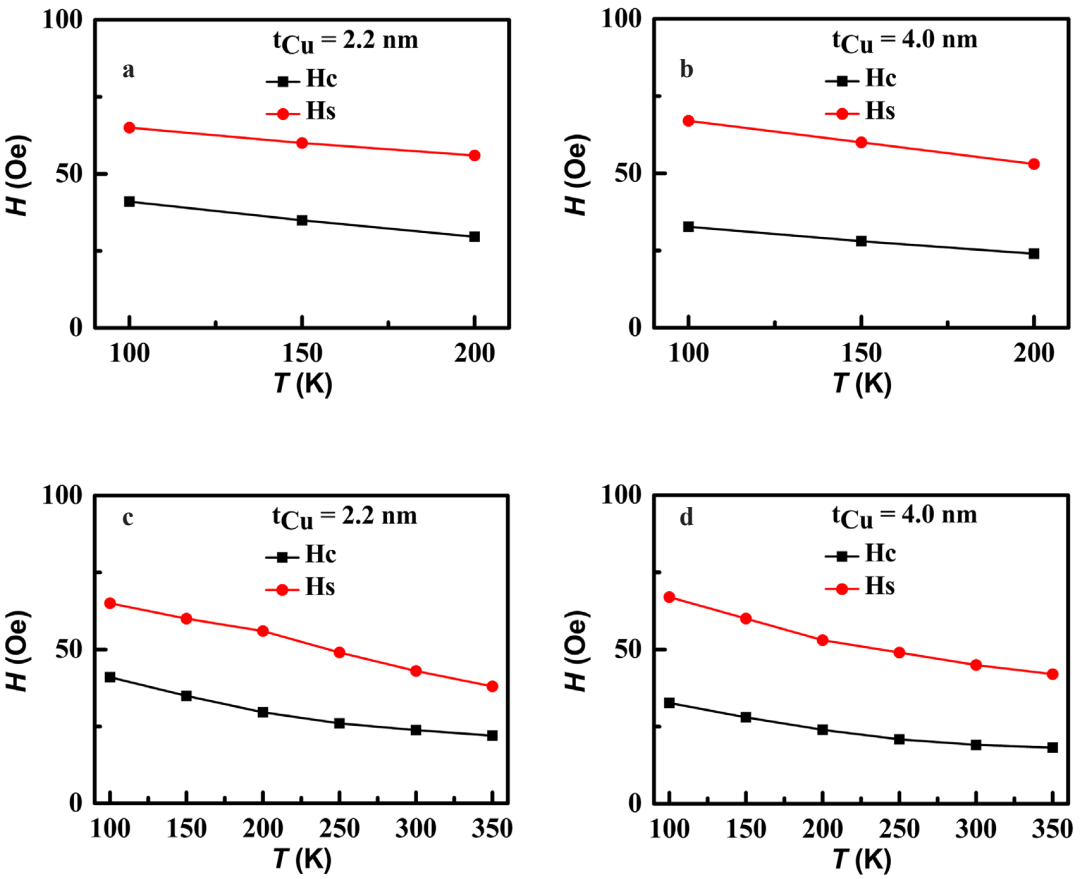

Figure 3. Temperature dependences of the coercive force H_c and saturation field H_s observed for a Co/Cu/Co sample with a Cu layer thickness of t_{Cu} = 2.2 nm (**a**, **c**) and t_{Cu} = 4.0 nm (**b**, **d**) in a magnetic field parallel to the EMA.

The hysteresis loops were measured on a vibrating magnetometer with a special low-temperature attachment. The hysteresis loops observed for the samples under study at temperatures of 100 and 150 K are shown in Figs. 1 and 2.

An analysis of the hysteresis loops observed at different temperatures T showed that a decrease in T leads to a change in the shape of the hysteresis loops. In particular, they become wider, and the saturation field and coercive force of the samples increase by about 10%. For the samples under study, the temperature dependences of the saturation field and coercive force were also determined which are shown in Fig. 3.

The following conclusions can be made as a result of this research:

1. The observed temperature dependences of the saturation field and coercive force indicate that, the values of the magnetic characteristics decrease as the temperature increases from 100 to 350 K.
2. It has been established that the saturation magnetization of the samples does not depend on temperature.
3. It has been found that with an increase in the thickness of the copper layer, the coercive force and the saturation field increase.

A.P25

SDFT INVESTIGATION OF MAGNETIC ANISOTROPY EFFECTS IN TRILAYER METAL NANOSTRUCTURES

*M.V. Mamonova**, *M.Y. Makeev, M.M. Nurkusheva*

Dostoevsky State University, Omsk, Russia
*E-mail: mamonovamv@omsu.ru

Trilayer structures with giant magnetoresistance effects consist of ferromagnetic layers separated by nonmagnetic layers and they are the key element of magnetic recording and spintronic devices [1]. In this work, in framework spin density functional theory studies of the energy and magnetic properties of the Fe/Cr/Fe, Fe/Pt/Fe, Co/Cu/Co, Co/Pt/Co systems were carried out using the software package VASP [2] and the PAW method with the (PBE) version of the generalized gradient approximation (CGA). The plane-wave basis cutoff energy was set to E_{cut} = 500 eV at a vacuum layer thickness of 5 Å and the size of the Monkhorst-Pack k-point grid of 32×32×1.

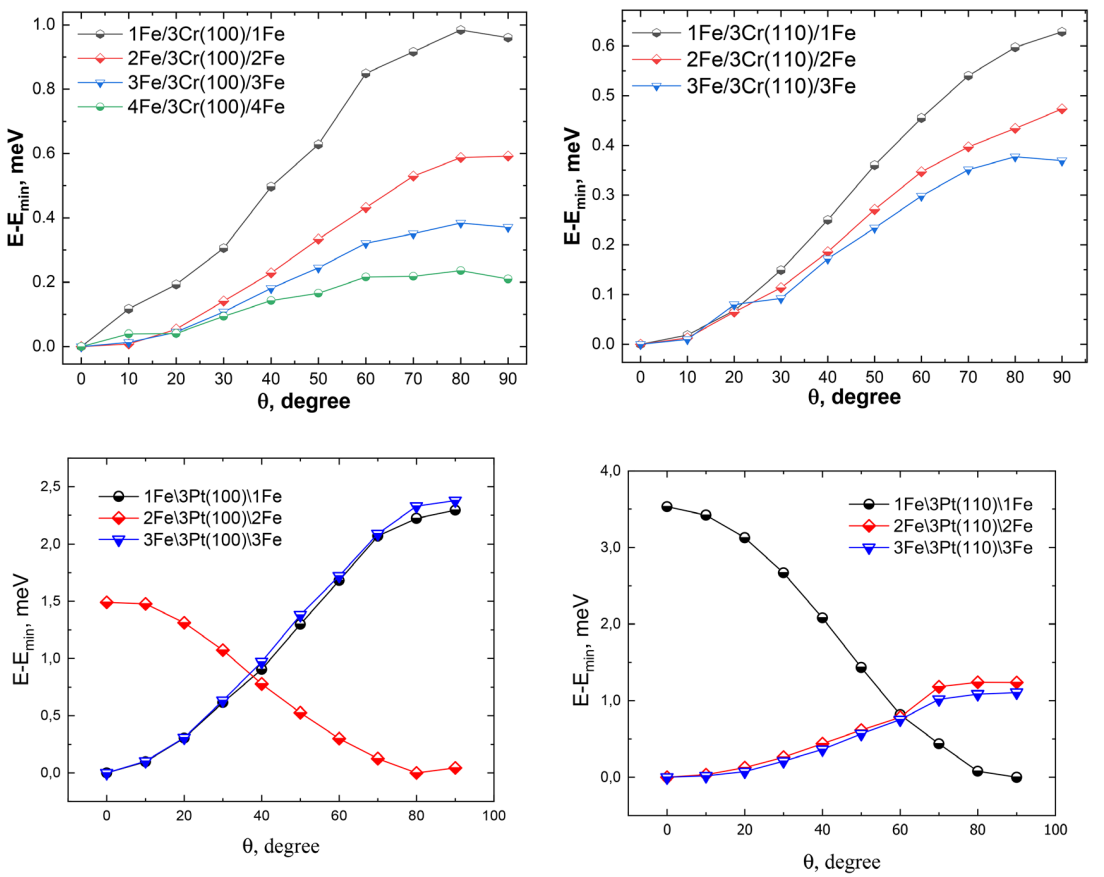

Figure 1. The dependence of the total energy difference on the azimuth angle of the magnetization direction for (100) and (110) orientations of the surface face Fe/Cr/Fe and Fe/Pt/Fe structures with Fe film thickness of 1–3 monolayers.

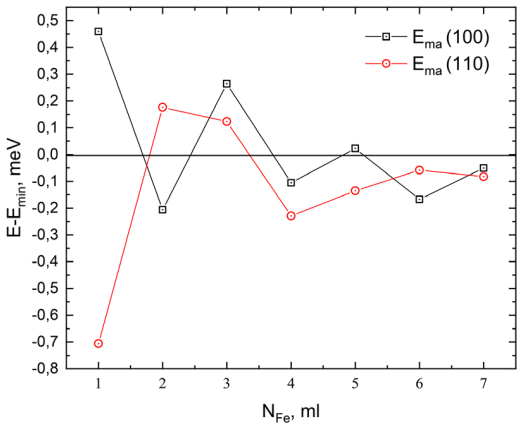

Figure 2. The dependence of the magnetic anisotropy energy on Fe film thickness for (100) and (110) orientations of the surface face Fe/Pt/Fe structure.

In order to calculate the magnetic anisotropy energy (*MAE*), we need to estimate the difference between the total energies of a magnetic material corresponding to different magnetization orientations. In this work, we present the results of calculations for structures with a non-magnetic layer thickness of 3 monolayers; the dependence of the magnetic properties of trilayer structures on the thickness of the non-magnetic layer is given in our article [3]. Calculations of the difference between the total energies depending on the azimuth angle (Fig. 1.) showed the advantage of perpendicular anisotropy ($\theta = 0$) or plane anisotropy ($\theta = 90°$) depending on the structure.

Calculations of the dependence of the total energy on the azimuth angle showed the advantage of perpendicular anisotropy for Fe/Cr/Fe for all considered thicknesses Fe films and surface orientation. For other systems, for example Fe/Pt/Fe (Fig. 2), a more complex dependence is observed.

As the ferromagnetic film thickness increases, the magnitude of the magnetic anisotropy decreases in absolute value. Therefore, we have presented in the Table 1 the values of the magnetic anisotropy energy for structures with a ferromagnetic layer thickness of 1 monolayer. At $MAE < 0$, the orientation of magnetic moments perpendicular to the surface is more energetically favorable. This corresponds to easy-axis anisotropy. At $MAE > 0$, easy-plane anisotropy is realized.

It is known from experiment [4] that the Co/Cu structure is characterized by a weak easy-plane magnetic anisotropy with magnetization oriented in the film plane, while the Fe/Cr, on the contrary, characterized by a easy-axis magnetic anisotropy. This is confirmed by our calculations. Calculations for 1Fe/3Pt/1Fe structure showed that for the (110) and (111) faces, the direction of the magnetic moments parallel to the surface plane is the most energetically favourable. For the (100) face, a perpendicular magnetic anisotropy was obtained.

Table 1. Result of calculation magnetic anisotropy energies $MAE = E_{\perp} - E_{\parallel}$, meV for different trilayer structures with 1 ml thickness of the ferromagnetic layers depend on the orientation of the surface face.

Surface	1Co/3Cu/1Co	1Co/3Pt/1Co	1Fe/3Pt/1Fe	1Fe/3Cr/1Fe
100	0.898	0.846	–2.295	–0.984
110	–0.024	5.970	3.531	–0.628
111	0.961	1.076	2.383	–0.279

Support by the Ministry of Education and Science of the Russian Federation (agreement 0741-2020-0002) is acknowledged.

1. V.V. Prudnikov, P.V. Prudnikov, M.V. Mamonova, Phys.-Usp. **60**, 8, 762 (2017).
2. P.G. Kresse, J. Furthmuller, Phys. Rev. B **54**(16), 11169 (1996).
3. M.V. Mamonova, M.Yu. Makeev, D.S. Kalinin, A.A. Zenova, Phys. Solid State, **63**(11), 67–74 (2021).
4. M.T. Johnson, P.J.H. Bloemen, F.J.A. den Broeder, J.J. de Vries, Rep. Prog. Phys. **59**, 1409 (1996).

A.P26

PERPENDICULAR MAGNETIC ANISOTROPY IN GRAPHENE/Fe/Ni AND GRAPHENE/Fe/H-BN

E.K. Mikhailenko[1,2*], *S.M. Dunaevski*[1,2]

[1]NRC "Kurchatov Institute" – PNPI, Gatchina, Russia
[2]Saint Petersburg State Electrotechnical University – LETU, Saint Petersburg, Russia
[*]E-mail: mikhailenko_ek@pnpi.nrcki.ru

Due to the unique properties of graphene and its possible usefulness in spintronic applications interface of graphene/ferromagnetic metal have attracted more attention in recent time. Experiments have shown that contact of graphene with FM metal can enlarge magnetic anisotropy of thin Co layers and stabilize perpendicular (to surface) magnetic anisotropy of thin layers of Co intercalated under graphene grown on nonmagnet Ir(111).

Another interesting system to form thin Co or Fe epitaxial layers under graphene is graphene/Ni(111). Investigations of graphene/Co/Ni and graphene/Fe/Ni have shown that thin films of Co and Fe sandwiched between graphene and Ni are pseudomorphic and reproduce fcc structure of Ni(111) substrate. It was revealed that contact of C and metal strongly modifying electronic structure of graphene. This dependence on magnetic properties still hadn't been investigated.

Because of strong magnetic interaction of Ni(111) (substrate) and thin layers of Fe, perpenducular magnetic anisotropy (PMA) is possible to relatively thin film (~ 5 ML of Fe)[1]. Thus the investigations of system graphene/Fe/h-BN (hexagonal boron nitride) become interesting because of excellent proximity of crystal structures of Fe(111) and h-BN ($a_{B\text{-}N}$ = 1.44 Å, $a_{C\text{-}C}$ = 1.42 Å) [2]. In spite of large number of experimental works of growth and investigation on monolayer and double layer of graphene on h-BN, there are only few works dedicated to intercalations on graphene/h-BN systems.

In this work we analyse magnetic properties of graphene/Fe/Ni(111) and graphene/Fe/h-BN using *ab initio* density functional theory (Quantum Espresso packet)[3].

For PMA calculations we have used general gradient approximation (GGA) in local spin density approximation for exchange-correlation potential. PBE pseudopotential was used. Energy cutoff for valence electrons had been chosen as 300 Rydberg for both – graphene/Fe/Ni and graphene/Fe/h-BN systems. Monkhorst pack mesh was set to 12×12×3.

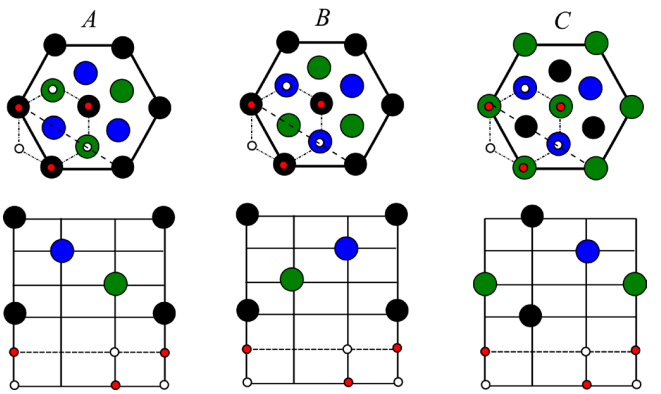

Figure 1. Possible mutual orientation of h-BN (B marked as red ball, N as white) and Fe (black ball as a closest to h-BN, green as second layer atom and blue as third layer atom).

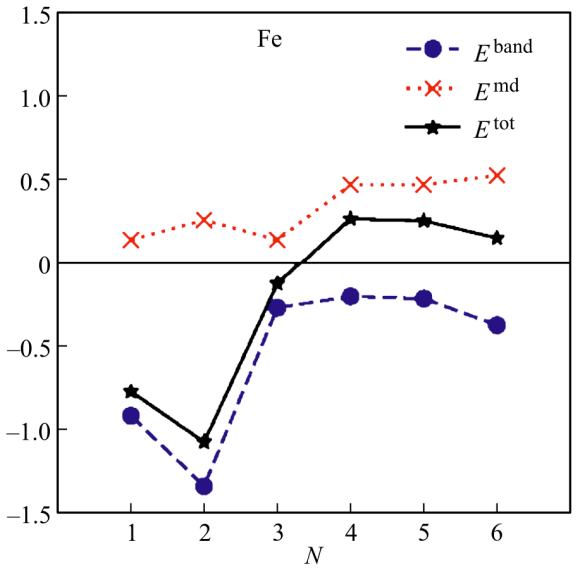

Figure 2. E_{tot}, E_{md} and E_{band} of graphene/Fe/Ni system as a function of number of Fe monolayers.

Total energy of system E_{tot} may be written as a sum of E_{band} and E_{md}, where E_{band} is band energy calculated via Kohn-Sham equations (and thus have no dependence on crystal axis directions) and E_{md} is magnetic dipolar interaction energy of all magnetic atoms in system. The sign of E_{tot} shows the possibility of PMA in considering structure.

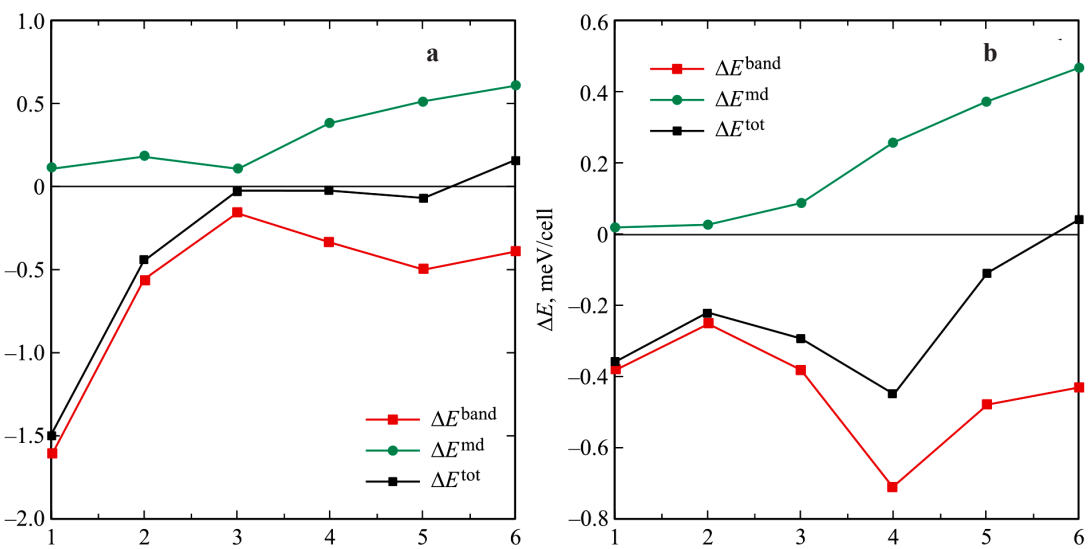

Figure 3. **a** E_{tot}, E_{md} and E_{band} of Fe/h-BN system, **b** Etot, Emd and Eband of graphene/Fe/Ni system s a function of number of Fe monolayers.

Our calculation for graphene/Fe/Ni(111) system shows the anisotropic constant $K_1^{Fe} \approx 0.92$ meV/atom (which is close to $K_1^{Fe} \approx 0.7$ meV/atom in Fe/MgO system). PMA seems possible to 5 ML of Fe, which corresponds to experimental results of Grebenyuk [4]). Calculated anisotropic constant for Fe in graphene/Fe/h-BN is $K_1^{Fe} \approx 0.72$ meV/atom, PMA is possible to 5-6 Fe ML.

Due to graphene defence properties against oxidation, this PMA structures may be useful in electronic and spintronic devices and practical applications.

1. S.M. Dunaevskii, E.Yu. Lobanova, E.K. Mikhailenko and I.I. Pronin, Surface Physics and Thin Films **61**, 1310–1315 (2019).
2. C. Oshima, A. Itoh, E. Rokuta, T. Tanaka, K. Yamashita, T. Sakurai, Solid State Commun. **116**, 37 (2000).
3. P. Giannozzi et al. J. Phys. Condens. Matter **29**, 395502 (2009).
4. G.S. Grebenyuk, S.M. Dunaevsky, E.Yu. Lobanova, D.A. Smirnov, I.I. Pronin., Appl. Surf. Sci. **470**, 840 (2019).
5. S.M. Dunaevsky and E.K. Mikhailenko, Surface Physics and Thin Films **62**, 2203–2207 (2020).

A.P27

INFLUENCE OF COMPETITION EFFECTS FOR DIFFERENT TYPES OF ANISOTROPY ON THE BEHAVIOR OF MULTILAYER MAGNETIC STRUCTURES

*A.V. Minkova**, *P.V. Prudnikov*

Department of Theoretical Physics, Dostoevsky Omsk State University, Omsk, Russia
*E-mail: minkovaav@stud.omsu.ru

The magnetic properties of ultrathin films are susceptible to the effects of magnetic anisotropy [1], which created by the crystal field of the substrate [2]. In this work, we studied the effect of two competitive types of anisotropy, single-ion and easy-plane, on the behavior of a three-layer magnetic structure Co/Cu/Co. The anisotropic Heisenberg model [3] was used for simulation by Monte Carlo methods.

The Hamiltonian of the spin system with single-ion anisotropy and easy-plane anisotropy can be introduced in the following form:

$$\mathscr{H} = -J_1 \sum_{i,j \in N_1 N_2} [\mathbf{S}_i \mathbf{S}_j - \Delta S_i^z S_j^z] - J_2 \sum_{\alpha \in N_1 \beta \in N_2} [\mathbf{S}_\alpha \mathbf{S}_\beta - \Delta S_i^z S_j^z] - A \sum_{i \in N_1 N_2} (S_i^z)^2 - \mathbf{h} \sum_{i \in N_1 N_2} \mathbf{S}_i,$$

where J_1 and J_2 is the intralayer and interlayer exchange constants, $\mathbf{S}_i$ is a three-dimensional spin in the lattice, A characterizes single-ion anisotropy in out-of-plane direction, Δ is the easy-plane anisotropy parameter depending on the film thickness N, $\mathbf{h}$ is applied magnetic field.

In this work, magnetic characteristics were calculated using different values of single-ion anisotropy parameter A = (–2.0, –1.0, 0.0, 1.0, 2.0, 3.0, 4.0)J_1 and thickness-depended easy-plane anisotropy parameter for each thin film in atomic structures of N = 3, 5, 7, 9, 11 monolayers. We measured the magnetization dependence of the applied magnetic field at different film thicknesses are shown in Fig. 1. The value of the easy-plane anisotropy parameter decreases as the film thickness N increases. One can see that, starting from N = 9, the effects of single-ion anisotropy with the value A = 2.0J_1 appear.

The behavior of the magnetization was considered as a function of the applied magnetic field with a change in the single-ion anisotropy parameter. It is found that with an increase in the value of

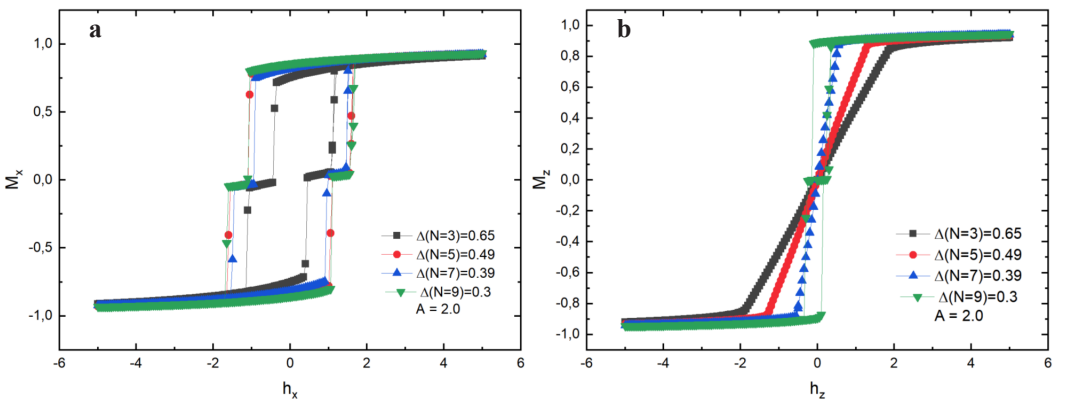

Figure 1. Dependence of the magnetization on the in-plane (**a**) and out-of-plane (**b**) applied magnetic field for different film thicknesses.

single-ion anisotropy to A = (3.0, 4.0)J_1, one can observe the appearance of a hysteresis loop when the field is directed along the Z-axis, because the effects of single-ion anisotropy become stronger than effects of the easy-plane type. Studies of effects on the influence of anisotropy contributions can be used in the design of spin-valve structures.

The study was carried out with the financial support of the Ministry of Education and Science of the Russian Federation (agreement 0741-2020-0002) and grant MD-2229.2020.2 of the President of the Russian Federation. The computational research was supported in through resources provided by the Shared Services Center "Data Center of FEB RAS" (Khabarovsk).

1. X.D. He, L.L. Zhang, G.J. Wu, J.W. Gao, P. Ran, Muhammad Sajjad, X.W. Zhou, J.W. Cao, L. Xi, YL. Zuo, Y. Ren, J. Magn. Magn. Mater. **519**, 167429 (2021).
2. C.A.F. Vaz, J.A.C. Bland, G. Lauhoff, Rep. Prog. Phys. **71**, 056501 (2008).
3. P.V. Prudnikov, V.V. Prudnikov, A.Yu. Danilova, V.O. Borzilov, G.G. Baksheev, EPJ Web Conf. **185**, 11009 (2018).

A.P28

MAGNETIC PROPERTIES AND CURRENT-INDUCED MAGNETIZATION REVERSAL IN FERROMAGNETIC MULTILAYER STRUCTURES W/CoTb/Ru

*Zh.Zh. Namsaraev**, *M.A. Bazrov, M.E. Letushev, M.E. Stebliy*

Laboratory of Spin-Orbitronics, Institute of High Technologies and Advanced Materials,
Far Eastern Federal University, Vladivostok, Russia
*E-mail: namsaraev.zhzh@dvfu.ru

Local control and detection of the magnetization orientation by the means of electric current in magnetically ordered media is an important fundamental area of research with the possibility of practical application. A promising medium for such research is ferrimagnets (FIM): multicomponent materials with antiparallel ordered magnetic sublattices formed by different atoms. Zero resulting magnetic moment – compensation point, can be obtained as a result of changing one of the three parameters, with other fixed: 1) the mutual concentration of atoms in the CoTb alloy [1]; 2) sample temperature [2]; 3) FIM layer thickness [3]. In a number of works, it is stated that in the vicinity of the compensation point, the maximum ratio of the effective magnetic field induced by the current to the conduction current density can be achieved [4]. In such works, the state of compensation is achieved by changing the composition of the alloy. In this work, the effect of current-induced magnetization reversal is considered in the case when the compensation state is achieved by changing the thickness of the FIM layer. A series of samples of the composition W(4)/$Co_{56}Tb_{44}$(x)/Ru(2 nm), x from 1.5 to 7 nm, was prepared by magnetron sputtering on Si/SiO_2 substrates, Fig. 1a. To study the magnetic transport properties the Hall bar structures were prepared by photolithography and ion-plasma etching.

A study of the magnetic properties showed that with the specified composition, the compensation state corresponds to a thickness of 4 nm, Fig. 1b. Decreasing thickness brings the sample to the Co-rich state: the magnetic moments of Co atoms are oriented along the external field, while Tb is antiparallel. An increase in thickness, on the contrary, to the Tb-rich state. The passage of current pulses through the Hall bar structure in the presence of a constant in-plane field B_x leads to a

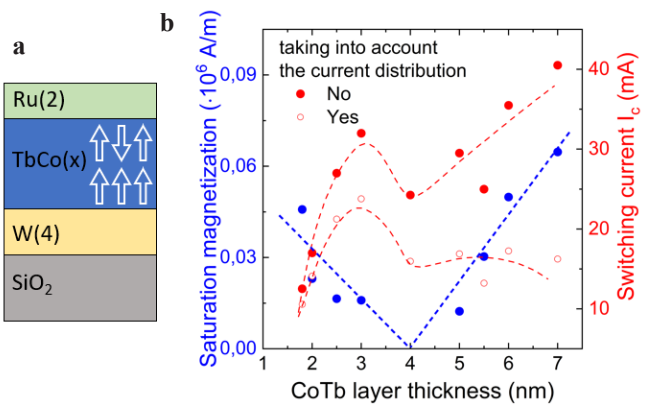

Figure 1. **a** Composition of the investigated structure, thickness in nm. **b** Saturation magnetization and switching current as a function of CoTb layer thickness.

reversible switching of the magnetization orientation in the structure from the up-state to the down, because of the spin-orbit torque effect [5]. Switching current I_c was noted as a parameter indirectly corresponding to the efficiency of current-induced magnetization reversal. In Fig.1b dependences of the magnetic moment and switching current on the FIM layer thickness are compared. The lower switching current corresponds to the minimum thickness of the FIM layer. However, there is a local minimum on the dependence, which does not coincide with the compensation point, as might be expected. The displacement can be explained by the heating of the Hall structure in the process of current. Upon heating, the magnetic moment of Tb atoms decreases, which leads to a shift in the compensation point to the region of large thicknesses. In the research, several additional studies have been carried out and the obtained results have been interpreted.

This work has been supported by the grant of the Government of the Russian Federation for state support of scientific research conducted under supervision of leading scientists in Russian institutions of higher education, scientific foundations, and state research centers of the Russian Federation (Project No. 075-15-2021-607).

1. J. Finley, L. Liu, Phys. Rev. Applied **6**, 054001 (2016).
2. Y. Hirata, T. Ono, Phys. Rev. B **97**, 220403 (2018).
3. B. Hebler, A. Hassdenteufel, M. Albrecht, Ferrimagnetic Tb–Fe alloy Thin Films: composition and Thickness Dependence of Magnetic Properties and all-Optical switching. Frontiers in Materials (2016).
4. Y. Wu, X. Zeng, J. Cao, Appl. Phys. Lett. **118**, 022401 (2021).
5. A. Manchon, I.M. Miron, P. Gambardella, Rev. Mod. Phys. **91**, 035004 (2019).

A.P29

MAGNETOELASTIC FEATURES OF FLEXIBLE SPIN VALVES WITH DYSPROSIUM LAYER

*L.I. Naumova**, *R.S. Zavornitsyn, M.A. Milyaev, N.G. Bebenin, I.K. Maksimova, A.A. Zakharov, V.V. Proglyado, A.S. Rusalina, V.V. Ustinov*

M.N. Miheev Institute of Metal Physics of the Ural Branch of the Russian Academy of Sciences, Ekaterinburg, Russian Federation
*E-mail: naumova@imp.uran.ru

Magnetosensitive materials on flexible polymer substrates are increasingly used in modern microelectronics. Devices such as flexible screens [1], electronic skin [2] and medical sensors [3] need materials that have strictly defined magnetoelastic, magnetic and transport characteristics. Functional parameters of magnetic multilayered nanostructures can be controlled by selecting the material and thickness of the layers, and changing the mutual orientation of the magnetic anisotropy axes.

Spin valve (SV) is a magnetic nanostructure that has a giant magnetoresistive effect and high magnetoresistive sensitivity in weak magnetic fields. SV includes an antiferromagnetic (AFM) layer and two ferromagnetic (FM) layers separated by a nonmagnetic one. One of the FM layers is coupled with adjacent AFM layer by exchange interaction. This FM layer is called "pinned". Another layer is called "free" (FL). FM materials are characterized by magnetostriction, so mechanical stresses and deformation can change the magnetoresistive properties of SVs. In [4, 5] based on 3d-metals SVs on polymer substrates are proposed to be used in strain and pressure sensors. One of the unique properties of rare earth (RE) 4f-metals is giant magnetostriction. Therefore, the inclusion of a RE metal layer in the SV composition can lead to a change in the magnetoelastic properties of the nanostructure. In particular, it is possible to increase the dependence of magnetoresistance on mechanical deformation.

SVs of [Ta(5 nm)/$(Ni_{80}Fe_{20})_{60}Cr_{40}$(5 nm)]$_5$/$Co_{90}Fe_{10}$(1.5 nm)/Dy($t_{Dy}$)/$Co_{90}Fe_{10}$(3 nm)/Cu(3.2 nm)/$Co_{90}Fe_{10}$(2 nm)/$Fe_{50}Mn_{50}$(12 nm)/Ta(6) composition with a layer of dysprosium in the FL were fabricated by magnetron sputtering. The nominal thickness of dysprosium layer (t_{Dy}) was varied. Polyimide (PI) film and glass were used as substrates. Micron sized stripes with the width (w) ranged

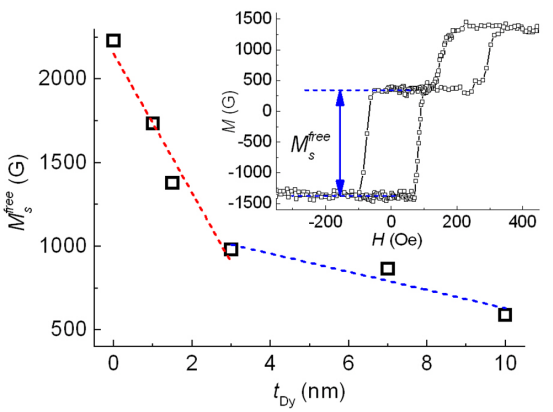

Figure 1. Dependence of the free layer saturation magnetization on nominal t_{Dy}. The inset shows field dependence of magnetization for SV with t_{Dy} = 1 nm and method of free layer saturation magnetization evaluation.

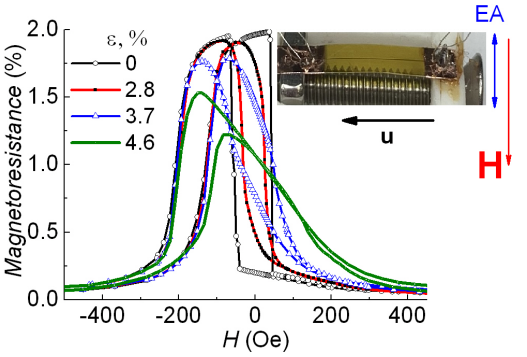

Figure 2. The magnetoresistive curves for of SV with if t_{Dy} = 3 nm stripe (w = 20 μm) in undeformed state and under the uniaxial stretching with different elongation (ε). The inset shows the SV stripe with copper contact pads on PI substrate installed in the holder.

from 20 to 100 μm were made by optical lithography. Magnetic measurements were performed by vibrating-sample magnetometer. Magnetoresistance was measured by dc four-probe method. All measurements were performed at room temperature.

Figure 1 shows the decrease of FL saturation magnetization with t_{Dy} increase. The reason of such dependence is antiferromagnetic exchange coupling between 3d- and 4f-metals in CoFe/Dy/CoFe. At $t_{Dy} \approx 3$ nm the slope of the dependence changes. We suppose that there is no pure dysprosium in CoFe/Dy(t_{Dy})/CoFe free layer if $t_{Dy} < 3$ nm. Thus, in that case the increase of t_{Dy} leads to increase of Dy-Co-Fe alloy layer in FL. This alloy is ferrimagnetic at room temperature. At $t_{Dy} > 3$ nm a pure Dy appears in FL and Dy is paramagnetic at room temperature.

Figure 2 shows the evolution of magnetoresistive curve at the uniaxial stretching of SV stripe sputtered on PI substrate. The deformation vector **u** was directed along the stripe and perpendicular to easy magnetic axis (EA) of the SV.

The strong dependence of the shape of magnetoresistive curve on the elongation was revealed. The magnetoresistance at $H \approx 0$ decreases by more than two times. The FL hysteresis loop width decreases significantly. The slope of the loop increases. Therefore, we suppose that the magnetoelastic anisotropy axis is perpendicular to EA. Magnetoelastic anisotropy constants (K_ε) for the SVs sputtered on PI substrate have been estimated using the change of the free layer coercivity at stretching. For the sample with t_{Dy} = 1 nm and w = 60 μm the value of K_ε reaches $3.6 \cdot 10^4$ at ε = 5%. After the deformation is removed, the magnetoresistive curve takes on its original shape.

Fabricated on PI substrates SVs with a layer of dysprosium in the FL are suitable sensing material for strain and stress sensors.

Support by State Assignment from the Ministry of Education and Science of Russian Federation (topic Spin, no. № 122021000036-3) and the Russian Foundation for Basic Research (project no. 20-42-660018 r_a) is acknowledged.

1. L. Zhou, A. Wang, Sheng-Chu Wu, J. Sun, S. Park, and T. Jackson, Appl. Phys. Lett. **88**, 083502 (1–3) (2006).
2. J.C. Yang, J. Mun, S.Y. Kwon, S. Park, Z. Bao, and S. Park, Adv. Mater. **31**, 1904765 (1–50) (2019).
3. S. Cardoso et al., J. Phys. D: Appl. Phys. **50**, 213001 (2017).
4. Q. Guo, X.G. Xu, Q. Zhang, Q. Liu, Y.J. Wu, Z.Q. Zhou, W.M. Zhu, Y. Wu, J. Miao, and Y. Jiang, RSC Adv. №6, 88090 (2016).
5. S. Ota, A. Ando and D. Chiba, Nature electronics **1**, 124–129 (2018).

A.P30

NONLINEAR SPIN WAVES IN MULTILAYEAR YIG WAVEGUIDE

S.A. Odintsov[1*], *E.H. Lock*[2], *E.N. Beginin*[1], *A.V. Sadovnikov*[1]

[1]Laboratory of Magnetic Metamaterials, Saratov State University, Saratov, Russia
[2]Fryazino Branch of Institute of Radioengineering and Electronics, Fryazino, Russia
[*]E-mail: odinoff@gmail.com

Multilayer films based on ferromagnetic materials that support the propagation of spin-wave signals have attracted a large number of researchers due to the constant development of both technologies for creating magnetic layers on non-magnetic substrates and the development of ideas for using magnetization waves to solve information signal processing problems [1]. Magnetic thin film structures are made in the form of single magnetic films, double magnetic films and multilayer magnetic films, with various thicknesses and arrangement of layers, among which ferromagnetic/non-magnetic multilayer structures have caused a large interest in the last decade [2]. The use of multilayer dielectric films of yttrium iron garnet (YIG) ensures the manifestation of the nonreciprocity effect and at the same time gives a greater advantage over the well-known YIG/metal layered structures due to significantly lower spin-wave losses in a two-layer YIG film consisting of layers with different values M0 of magnetization. In turn, the study of nonlinear processes in width-limited waveguide structures is an interesting task due to the use of microwaveguides as elements of interconnections in magnonic networks that perform signal processing functions based on the principles of magnon logic [3]. The consideration of nonlinear spin-wave processes in the regimes of three-magnon and four-magnon decay in YIG films made a significant contribution to the theory describing the nonlinear dynamics of dissipative systems [3].

In this work, we considered a structure consisting of a two-layer YIG microwaveguide, with different saturation magnetizations in the layers. Micromagnetic simulation of the structure under study was carried out by the finite difference method. An experimental study of the effect of nonreciprocity with a change is carried out. It is shown how the geometric parameters of waveguides affect the dynamics of spin waves in two-layer lateral structures.

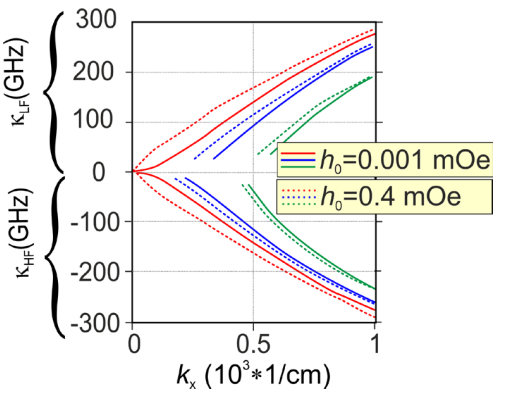

Figure 1. Nonreciprocity coefficient κ_{HF} and κ_{LF} for the HF and LF regions at different h_0.

The system under study was a ferrimagnetic two-layer ferrite YIG film. When creating a film on a GGG substrate, we first grew a pure YIG layer 7 μm thick with a saturation magnetization $4\pi M_1$ = 1738 G (YIG1), and on it a 9 μm thick YIG layer doped with gallium and lanthanum with a saturation magnetization $4\pi M_2$ = 904 G (YIG2). Next, the waveguide was placed in a uniform external magnetic field H_0 = 670 Oe, oriented along the y axis, and it was possible to change the field direction by 180 degrees. The width of the test sample was w = 200 μm. Waveguide length L = 7 mm.

We estimate the nonreciprocity phenomenon by using the nonreciprocity coefficient as $\kappa_{HF} = f_+ - f_-$, where f_+ is the frequency of SW propagation in the positive direction of the y-axis, and f_- is the frequency of SW propagation in the negative direction of the x-axis with the same wavenumber k. The coefficient of nonreciprocity for the low frequency range of the dispersion characteristic

$\kappa_{LF} = f_+ - f_-$ is also determined. Both coefficients are shown in Fig. 1 at h_0 = 0.001 mOe and h_0 = 0.4 mOe, which corresponds to the power P_{in} = –25 dBm and P_{in} = 14 dBm, respectively. Thus, with an increase in the wave number, the nonreciprocity coefficient decreases for the high frequency range and increases for the lower one, while an increase in power affects the nonreciprocity coefficient in such a way that in the LF region this leads to a decrease in κ_{LF}, and in the HF region, on the contrary, to an increase κ_{HF}.

This work was supported by the grant from Russian Science Foundation (No 20-79-10191).

1. S.A. Nikitov, A.R. Safin, D.V. Kalyabin, A.V. Sadovnikov, E.N. Beginin, M.V. Logunov, M.A. Morozova, S.A. Odintsov, S.A. Osokin, A.Yu. Sharaevskaya, Yu.P. Sharaevsky, A.I. Kirilyuk, Phys. Usp. **63**, 945–974 (2020).
2. I.V. Vetrova, M. Zelent, J. Šoltýs, V.A. Gubanov, A.V. Sadovnikov, T. Ščepka, J. Dérer, R. Stoklas, V. Cambel, and M. Mruczkiewicz, Appl. Phys. Lett. **118**, 212409 (2021).
3. D.D. Stancil. & A. Prabhakar. Spin Waves: Theory and Applications (Springer, 2009).
4. V. Sechovsky and L. Havela, in K.H.J. Buschow (ed.), Handbook of Magnetic Materials, vol. 11, Elsevier Science B.V., Amsterdam, p. 1, (1998).

A.P31

PROPERTIES AND SEGREGATION TENDENCY OF Fe-Rh-Z (Z = Pt, Mn, Pd) ALLOYS

*O.O. Pavlukhina**, *V.V. Sokolovskiy, V.D. Buchelnikov, M.A. Zagrebin*

Chelyabinsk State University, Chelyabinsk, Russia
*E-mail: pavluhinaoo@mail.ru

The Fe-Rh, Rh-Mn, Fe-Pt and Fe-Pd-based alloy have attracted a lot of attention due to the observation of shape memory effect [1], magnetocaloric effect [2] etc. Fe-Rh alloys exhibit a metamagnetic phase transition (AFM-FM) [3]. The metamagnetic phase transition in Fe-Rh succeeds also the large change in magnetization, which is responsible for a giant magnetocaloric effect upon variation of a magnetic field. The combination of Fe-Rh, Rh-Mn, Fe-Pd and Fe-Rh compounds represents a relevant study aimed to enhancement of magnetic and thermodynamic properties. For instance, the direct method investigations of magnetocaloric properties for $Fe_{49}(Rh_{1-x}Pd_x)_{51}$ (x = 0–0.09) have been performed in Ref. [4]. It has been concluded that a substitution of Pd for Rh (less than 8 at.%) realizes a wide active temperature range for the magnetocaloric effect. In this work, we present theoretical studies of the properties and phase stability of $FeRh_{1-x}Pd_x$, $FeRh_{1-x}Pt_x$ and $Fe_{1-x}RhMn_x$ ($0 \le x \le 1$) alloys using *ab initio* calculations.

In the present work we used the density functional theory as implemented in the VASP package. The generalized gradient approximation for the exchange correlation functional in the formulation of Perdew, Burke and Ernzerhof was taken into calculations. In the calculations the automatically generated uniform grid of 12×12×12 k-point as in Monkhorst-Pack grids was taken into account. The following magnetic configurations were considered: FM and three types of AFM ((I) the magnetic moment alignment in the plane alternates; (II) the magnetic moment alignment is staggered; (III) the layered magnetic moment alignment). Firstly, the ground state energy of all compounds under study was estimated. At the next stage, the stability of the alloys was assessed with respect to decomposition into individual components and with respect to decomposition into binary compounds at zero temperature.

Table 1. Total energies E, lattice constants a_0, tetragonal ratio c/a, partial magnetic moments for Fe μ_{Fe}, Rh μ_{Rh}, Pt μ_{Pt} for $FeRh_{1-x}Pt_x$ with favorable magnetic configurations.

		E (eV/cell)	a_0 (Å)	c/a	μ_{Fe} (μ_B/atom)	μ_{Rh} (μ_B/atom)	μ_{Pt} (μ_B/atom)
FeRh	AFM-II	–125.15	2.99	1.00	±3.12	0	0
$FeRh_{0.875}Pt_{0.125}$	AFM-II	–124.43	2.76	1.26	±2.91	0	0
$FeRh_{0.75}Pt_{0.25}$	AFM-II	–123.61	2.76	1.27	±2.92	0	0
$FeRh_{0.625}Pt_{0.375}$	AFM-II	–122.88	2.76	1.28	±2.94	0	0
$FeRh_{0.5}Pt_{0.5}$	AFM-II	–122.07	2.75	1.30	±2.95	0	0
$FeRh_{0.375}Pt_{0.625}$	AFM-II	–121.08	2.76	1.30	±2.97	0	0
$FeRh_{0.25}Pt_{0.75}$	AFM-III	–120.12	2.74	1.33	±2.93	0	0
$FeRh_{0.125}Pt_{0.875}$	AFM-III	–119.29	2.75	1.33	±2.96	0	0
FePt	FM	–118.46	2.73	1.38	2.94	0	0.32

In the first step, we calculated the lattice parameters, energy, partial and total magnetic moments for Fe-Rh-Z (Z = Pt, Mn, Pd) with different magnetic ordering. As can be seen from Table 1, the Pt addition in the FeRh system results in an appearance of stable tetragonal structure ordered antiferromagnetically. It is found that AFM-II order is energetically favorable for $FeRh_{1-x}Pt_x$ alloys with a Pt concentration of $0 \leq x \leq 0.625$ whereas for compounds with $x = 0.75$ and 0.875, the AFM-III order is preferable. Besides, the tetragonal ratio c/a increases with increasing Pt content. This finding also agrees with the experimental data [5]. For the FePt alloy ordered ferromagnetically with bct structure, the tetragonal ratio is found to be $c/a = 1.38$ which agrees well with the experimental ($c/a = 1.359$ [5]) and theoretical ($c/a = 1.39$ [6]) data.

The calculated optimized lattice parameters for FePd alloy ($c/a = 1.39$) is in a good agreement with experimental values ($c/a = 1.36$) [7]. For $FeRh_{1-x}Pd_x$ ($x > 0.5$) the total energies take minimum values in the ferromagnetic state that indicates on the stability of FM order. The antiferromagnetic spin configuration is energetically favorable for $FeRh_{1-x}Pd_x$ ($x \leq 0.5$) alloys. The tetragonal ratio increases with increasing palladium concentration. These results are in a consistent with experimental ones [7]. We can conclude from the obtained data that the AFM-II phase is energetically favorable for $Fe_{1-x}RhMn_x$ ($x < 1$). It was found that the FM spin configuration is energetically favorable for RhMn.

At the next stage, the possibility of the existence of the alloys described above was investigated. To determine the phase stability of Fe-Rh-Z alloys, formation energies for all the studied alloys were calculated as the difference between the total energy for each alloy and the energies of pure elements contained in the composition in proportion with their concentration. We found that the total energy for energetically favorable Fe-Rh-Z alloys is lower than the sum of the total energies of pure elements. Let's discuss further, the stability of Fe-Rh-Z alloys with respect to decomposition into two-component composites (E_{mix}). Figure 1 shows the calculated mixing energies E_{mix} as a function of the Mn concentration for $Fe_{1-x}RhMn_x$ alloys ($0 \leq x \leq 1$) with energetically favorable magnetic configurations considered. As can be seen from Fig. 1, the structure with AFM-II order is stable with respect to decomposition into two-component alloys in the concentration range of $0.25 \leq x \leq 0.625$ while other compounds show a tendency to segregate due to the positive E_{mix} energy.

This study was supported by the Ministry of Science and Higher Education of the Russian Federation within the framework of the Russian State Assignment under contract No. 075-01391-22-00.

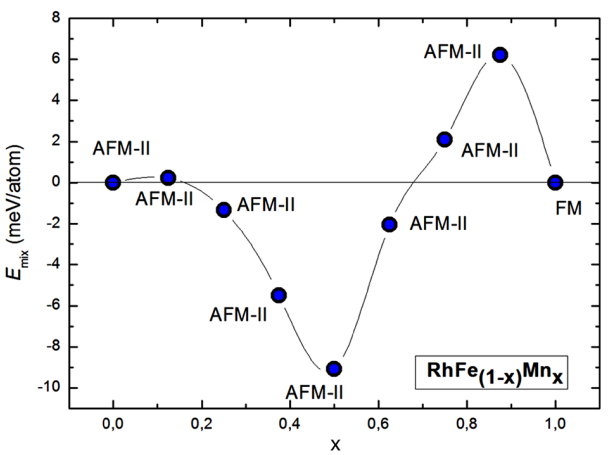

Figure 1. Mixing energy as a function of Mn content for $RhFe_{1-x}Mn_x$ alloys ($0 \leq x \leq 1$) with favorable magnetic configurations.

Dr. O.O. Pavlukhina and Dr. M.A. Zagrebin gratefully acknowledges the Advanced science research foundation of the Chelyabinsk State University.

1. J. Koeda, Y. Nakamura et al., Trans. Mater. Res. Soc. Jpn. **26**, 215–217 (2001).
2. M.P. Annaorazov, K.A. Asatryan et al., Cryog. **32**, 867–872 (1992).
3. J.S. Kouvel, C.C. Hartelius, J. Appl. Phys. **33**, 1343 (1962).
4. K. Nishimura, Y. Nakazawa, L. Li, K. Mori, Materials Transactions **49**, 1753–1756 (2008).
5. S. Yuasa, H. Miyajima, Nucl. Instrum. Methods Phys. Res. Sect. B **76**, 71–73 (1993).
6. N. Zotov, A. Ludwig, Intermetallics **16**, 113–118 (2008).
7. S. Yuasa, H. Miyajima, Y. Otani, A. Sakuma, J. Phys. Soc. Jpn. **64**, 4906–4913 (1995).

A.P32

MAGNETIZATION REVERSAL AND DOMAIN STRUCTURE IN THIN FILM AND ARTIFICIAL ANTIFERROMAGNET BASED ON $L1_0$-PdFe

M.V. Pasynkov[1*], *R.V. Yusupov*[1], *A.I. Gumarov*[1], *I.V. Yanilkin*[1], *L.R. Tagirov*[1,2]

[1]Institute of Physics, Kazan Federal University, Kazan, Russian Federation
[2]Zavoisky Physical-Technical Institute, FRC Kazan Scientific Center of RAS, Kazan, Russian Federation
[*]E-mail: mike_p95@mail.ru

Platinum and palladium based intermetallic compounds with $L1_0$-structure are ferromagnetic (FM) materials of a choice for ultrahigh density non-volatile magnetic memory. Thin-films of FePt and CoPt with high perpendicular magnetic anisotropy (PMA) are used in a new generation of hard disc drives with heat- (HAMR) and microwave-assisted magnetic recording (MAMR) technologies. Further advances in storage density and data writing and reading rates are expected from an all-optical data manipulation that has been demonstrated on the ferromagnetic GdFeCo alloys [1]. A complementary to alloy-based approach is a development of artificial ferrimagnetic structures suitable for all-optical magnetization switching. We consider here a ferrimagnetic thin-film three-layer structure with PMA, consisting of two FM layers separated by a non-magnetic layer, as a candidate for such a material, and analyze its magnetization reversal utilizing micromagnetic modelling. By adjusting the thickness of an intermediate layer in three-layer F/N/F systems (F is a ferromagnet, N is a normal metal), it is possible to obtain the structures with both the ferromagnetic and antiferromagnetic couplings. The paper presents the results of a modeling of the magnetization reversal curves and domain structures in thin films of the $L1_0$-PdFe alloy and artificial antiferromagnet based on it.

Single-layer epitaxial $L1_0$-PdFe films and trilayer PdFe/W/PdFe heterostructures with PMA have been grown by the molecular beam epitaxy in ultrahigh-vacuum setup. Quasi-static magnetization reversal curve of a single-layer film has a conventional rectangle-like shape (Fig. 1a). Magnetization curve of the artificial antiferromagnet (not shown here) differs drastically and has a butterfly-like shape. For millimeter-scale films, magnetization process and its reversal is dominated by the dynamics of magnetic domains. Therefore, the experimental data have been modelled within the micromagnetic macroscopic approach.

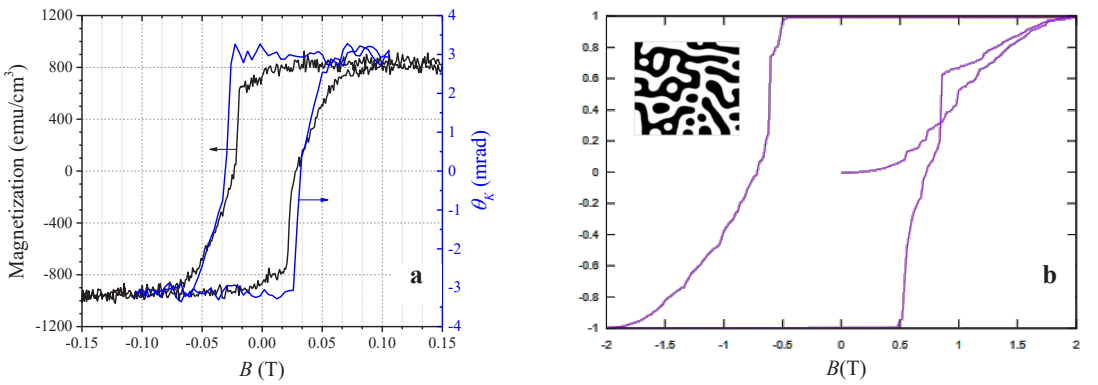

Figure 1. Magnetization curves (**a** experiment, **b** modeling) and domain structure of a thin film $L1_0$-PdFe.

The calculations were carried out using the Mumax 3 program for micromagnetic simulations [2]. For a thin film of the PdFe PMA alloy with a size of 256×256 nm^2 and a thickness of 7 nm, the following parameters were used: exchange stiffness $A = 5{\cdot}10^{-13}$ J/m, uniaxial anisotropy constant $K_u = 8{\cdot}10^5$ J/m^3, saturation magnetization $M_s = 8{\cdot}10^5$ A/m. A mesh step both in the film plain and across the thickness was 0.5 nm; larger step values bring to a different result. The magnetization curve obtained by a modeling (Fig. 1b) reproduces qualitatively the shape of the hysteresis loop at room temperature. The difference in coercivity value, in our opinion, is associated with the modeling approximation of $T = 0$ K.

In the inset to Fig. 1b, the equilibrium domain structure at zero magnetic field is shown. The dark and light regions correspond to up and down perpendicularly magnetized domains. A detailed inspection of the domain structure reveals gray-color regions at the boundaries of the domains, which are probably the visualization of the domain walls. The scale and the character of the modelled domain structure agrees nicely with the results of the magnetic force microscopy study [3] for thin films of the $L1_0$-PdFe alloy. In particular, the characteristic width of the domains is 50–70 nm.

Results of a similar modelling of the domain structure and its development in an applied perpendicular magnetic field will also be presented and analyzed.

The work was supported by Kazan Federal University within the frames of the Priority-2030 program.

1. T.A. Ostler et al. Nature Commun. **3**, 1–6 (2012).
2. A. Vansteenkiste et al., AIP Adv. **4**, 107133 (2014).
3. V. Gehanno et al. Phys. Rev. B **55**, 12552–12555 (1997).

A.P33

FIRST PRINCIPLES INVESTIGATIONS OF HALF-METALLIC Ti-BASED HEUSLER FERROMAGNETIC ALLOYS

*A.A. Raev**, *D.R. Baigutlin, V.V. Sokolovskiy, V.D. Buchelnikov*

Chelyabinsk State University, Chelyabinsk, Russia
*E-mail: landrew637@gmail.com

In recent years, half-metallic ferromagnetics have played an important role in applications in magnetoelectronics and spintronics. These materials have environmentally friendly elements, low weight, inexpensive and high power factors. There are a huge number of studies on half-metallic compounds of MNiSn and MCoSb based half-Heisler alloys, where (M = Ti, Zr, Hf) [1], which have been considered as thermoelectric materials.

In this investigation the regular, inverse, $T^{\#}$, T^{c} and T^{p} lattice of the half-metallic Heisler alloy Ti_2VZ with FM ordering have been considered. The geometric optimization of the lattice has been performed in the framework of density functional theory using the coupled plane wave approach implemented in the VASP software package [2] in the PBE functional approximation [3]. The Brillouin zone integration was performed on a k-point grid and was 7×7×7. The cut-off energy of the plane waves was 465 eV and the energy convergence parameter was 10^{-8} eV/atom.

The values of both structural and magnetic characteristics were obtained from these studies. All the alloys considered have a cubic structure, in the corresponding energy minima (Table 1).

Table 1. Equilibrium values of lattice parameters, ground state energy, magnetic moments of Ti_2VZ alloys (Z = Al, Ga, In).

№	*a* (Å)	*b* (Å)	*c* (Å)	*E* (eV/atom)	M_A (μB/f.u.)
Al	6.3274	6.3274	6.3274	–7.2470	1.1655
Ga	6.2831	6.2831	6.2831	–7.0694	1.0075
In	6.5175	6.5175	6.5175	–6.7745	1.0943

Figure 2 shows the density of states for T^{c} structure of Ti_2VGe alloy. From the data obtained it can be seen that the degree of spin polarization $P \sim 36\%$ and is quite high for the T^{c} structure in FM.

This work was supported by Russian Science Foundation Project No. 22-12-20032

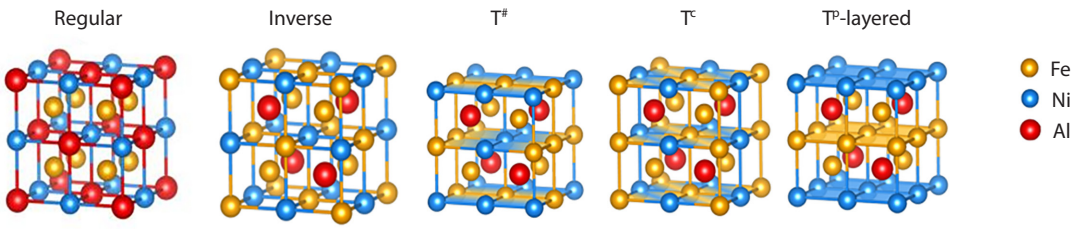

Figure 1. The five considered structures for the Fe_2NiAl Heusler alloy with cubic lattice parameters Cu_2MnAl-type Regular Heusler structure, Hg_2TiCu-type Inverse Heusler structure, $T^{\#}$, T^{c}, and T^{p} structures [4].

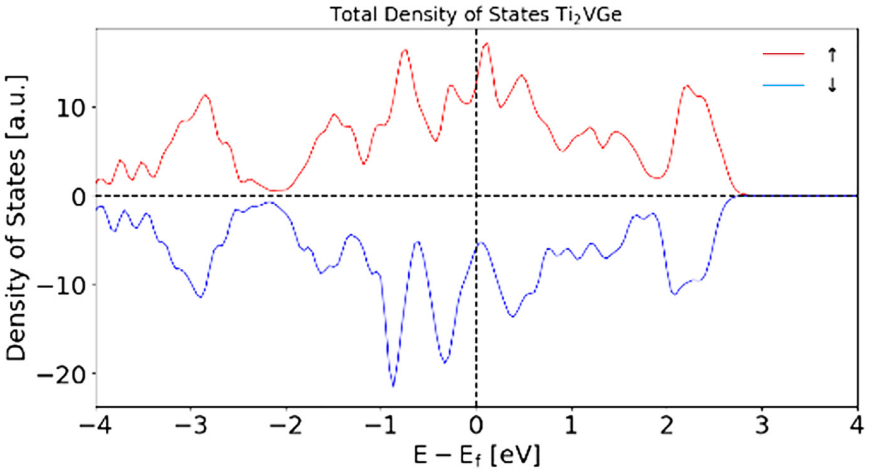

Figure 2. Electron density of Ti_2VGe states calculated with PBE functional for T^c structure.

1. C. Uher, J. Yang, S. Hu, D.T. Morelli, G.P. Meisner, Phys. Rev. B **59**, 8615 (1999).
2. G. Kresse, J. Furthmüller, Phys. Rev. B **54**, 11169 (1996).
3. J.P. Perdew, K. Burke, M. Ernzerhof, Phys. Rev. B **77**, 3865 (1996).
4. V.V. Sokolovskiy, O.N. Miroshkina, V.D. Buchelnikov, and M.E. Gruner, Phys. Rev. Mat. **6**(2), 025402 (2022).

A.P34

ANOMALOUS HALL EFFECT IN AN EPITAXIAL Mn_5Ge_3 THIN FILM ON Si(111)

*M.V. Rautskii**, *I.A. Yakovlev, S.N. Varnakov, A.S. Tarasov*

Kirensky Institute of Physics, Federal Research Center KSC SB RAS, Krasnoyarsk, Russia
*E-mail: rmv@iph.krasn.ru

The intermetallic magnetic Mn_5Ge_3 shows ferromagnetism with high Curie temperature (296 K) and spin polarization (42%). Ferromagnetic germanides are favorable due to the possible integration into semiconductor electronics and complementary metal-oxide semiconductor (CMOS) technology [1]. Mn_5Ge_3 is also an interesting material for the development of novel spintronic devices as a promising spin-injector material. Most studies about the Mn_5Ge_3 found in the literature report on the growth of it on Ge or GaAs substrates [2, 3]. However, modern semiconductor technology is based on silicon. And in our opinion, the Mn_5Ge_3/Si hybrid structures are more interesting.

In this work, was study anomalous Hall effect (AHE) of thin films Mn_5Ge_3 on Si substrate. All semples were deposited on the MBE setup "Angara" [4] by molecular beam epitaxy on a p-Si(111) substrate at a temperature T = 390 °C and a pressure of $6.5 \cdot 10^{-8}$ Pa.

Figure 1 shows Hall resistivity at 80 K. In magnetic fields close to the saturation magnetization, a hysteresis of the Hall resistance is observed. This is a well-known effect due to the fact that the oppositely magnetized domain has to reach a certain minimum dimension in order to create a stable domain configuration.

The inset in Fig. 1 shows that the Hall resistivity is nonmonotonically dependent on temperature. This is due to the fact that $\rho_H \sim \rho^2$ and $\rho(T)$ is non-monotonic. Apparently, this is due to the fact that the substrate is conductive and shunts the film. At a temperature of 3 K, when the contribution to the resistance from the substrate is minimal, the film resistance is 18 μOhm cm, which is in good agreement with the literature data [5] and indicates the high quality of the epitaxial film. In addition, an anomaly in ρ is observed near T_c which is clearly seen in the temperature dependence of dρ/dT.

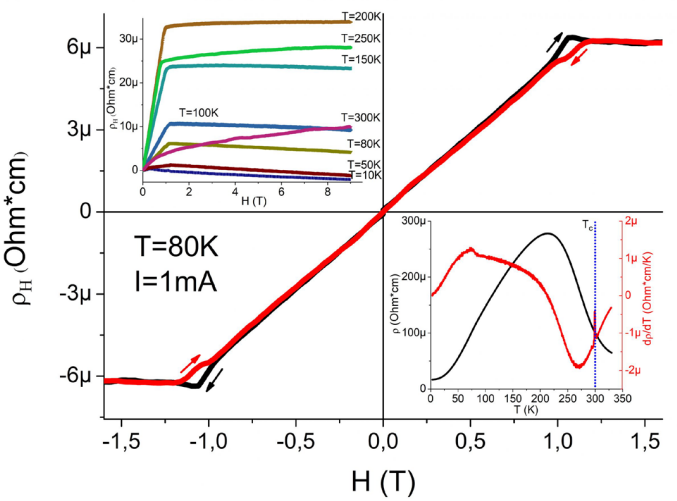

Figure 1. Anomalous Hall effect of a thin film Mn_5Ge_3 at a temperature of 80 K. The insets show Hall resistivity at other temperatures and the temperature dependences of ρ and dρ/dT.

We have investigated the Hall effect and resistivity of ferromagnetic Mn_5Ge_3 films. The anomalous Hall effect and anomaly on the temperature dependence ρ confirm the formation of a ferromagnetic layer with a Curie temperature of 300 K. The low resistivity at 3 K (18 μOhm cm) and the observed hysteresis of the Hall resistance in magnetic fields near the saturation field indicate the high quality of the Mn_5Ge_3 film. This allows us to hope for the use of this material in silicon spintronics.

Support by Russian Foundation for Basic Research, the Government of the Krasnoyarsk Territory, and the Krasnoyarsk Territorial Foundation for Support of Scientific and R&D Activities, (project no. 20-42-243007) is acknowledged.

1. Y. Zhou et al., Phys. Rev. B **84**, 125323 (2011).
2. S. Olive-Mendez et al., Thin Solid Films **517**, 191–196 (2008).
3. R. Cardoso de Oliveira et al., JMMM **539**, 168325 (2021).
4. S.N. Varnakov et al., Instrum. Exp. Tech. **47**, 839 (2004).
5. C. Surgers et al., Phys. Rev. B **90**, 104421 (2014).

MAGNETIC PROPERTIES AND DOMAIN STRUCTURE OF COFE NANOSPRINGS

K.A. Rogachev[1*], *A.Yu. Samardak*[1], *A.G. Kozlov*[1], *V.N. Kharitonov*[1], *M.E. Stebliy*[1], *M.E. Letushev*[1], *M.A. Bazrov*[1], *Y.S. Jeon*[2], *E. Jeong*[3], *A.V. Ognev*[1], *A.S. Samardak*[1], *Y.K. Kim*[3+]

[1]Institute of High Technologies and Advanced Materials, Far Eastern Federal University, Vladivostok, Russia
[2]Institute of Engineering Research, Korea University, Seoul, Republic of Korea
[3]Department of Materials Science and Engineering, Korea University, Seoul, Korea
[*]E-mail: rogachev.ka@dvfu.ru

One-dimensional ferromagnetic nanostructures are of great interest in modern material science and applications because of their unique magnetic behavior compared to bulk magnetic materials and thin magnetic films. The high aspect ratio of these nanostructures usually induced a strong uniaxial magnetic anisotropy in the direction of the long axis, with strong interactions between neighbors in the arrays [1]. Variations of such nanostructures, for example, nanotubes and nanosprings, can provide even more unusual properties, due to more complex geometry.

With the development of one-dimensional nanostructure synthesis techniques, a facile method was developed to prepare helical-shaped nanostructures [2]. Nanosprings show a completely different magnetic behavior compared to other one-dimensional nanostructures due to their complex helical shape [3]. The complex remagnetization process provides potential applications of such structures as spintronic devices or magnetic field sensor. In this study, we investigated the changes in the magnetic properties and domain structure of CoFe alloy nanosprings. An alloy of this composition was chosen because of the highest magnetic moment among 3d metals and their alloys.

Nanosprings were synthesized by electrodeposition in a commercial porous alumina template under galvanostatic conditions. The electrolyte contained cobalt sulfate ($CoSO_4 \cdot 7H_2O$), iron sulfate ($FeSO_4 \cdot 7H_2O$) and was modified with vanadium oxide sulfate ($VOSO_4 \cdot H_2O$) and ascorbic acid ($C_6H_8O_6$) to define the helical shape of the nanospring. Coil diameter was controlled by the current density of the electrodeposition.

The surface morphology was studied by scanning electron microscopy. For investigation, nanosprings were etched from AAO template using a solution of H_3PO_4 (6 wt.%) and H_2CrO4 (1.8 wt.%) solution. The element composition was studied using energy-dispersive X-ray spectroscopy.

Magnetic properties of an array of CoFe nanosprings were investigated using vibration magnetometry with recording of hysteresis loops. First-order reversal curve (FORC) diagram method was implemented to study the complex distribution of interaction and coercive fields in the nanospring array. The domain structure was investigated using magnetic force microscopy.

To investigate the magnetic configuration and define the magnetostatic interactions, the micromagnetic package MuMax3 was used. To achieve a reliable model, experimental data (hysteresis loops and MFM images) were compared with the simulation results.

The results of the surface morphology investigation are shown in Fig 1. As can be seen, the nanosprings are 210 nm in diameter and approximately 14 μm in length. The coil thickness was around 65 nm. EDX analysis showed that all samples consisted of the $Fe_{49}Co_{51}$ alloy.

Hysteresis measurements showed that the samples are isotropic. However, there are significant differences in the coercive force depending on the direction of applied magnetic field: $H_c(\perp) = 310$ Oe, $H_c(||) = 130$ Oe (($\perp$) and (||) indicate the perpendicular and longitudinal directions of the external magnetic field), which can be explained by the shape of the nanospring.

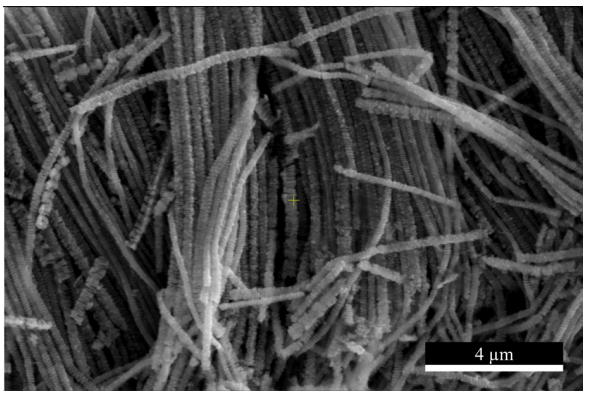

Figure 1. SEM image of nanosprings without alumina template.

The FORC diagrams showed that irreversible switching occurs mostly in the external fields, perpendicular to the main axis of the nanosprings, which is uncommon for one-dimensional nanostructures. However, the same situation was observed in the case of coercive force values obtained through FORC diagrams $H_c(\perp)^{FORC}$ = 648 Oe, $H_c(||)^{FORC}$ = 145 Oe. The interaction fields for both configurations show approximately the same values ($H_u(\perp)^{FORC}$ = 168 Oe, $H_u(||)^{FORC}$ = 190 Oe).

Micromagnetic simulation shows that the remagnetization process in the longitudinal external field configuration proceeds through coherent rotation of magnetic moments, however, in the perpendicular field, switching occurs by nucleation and annihilation of domain walls. Simulating of the residual states shows that, after magnetization in the longitudinal direction, the nanospring retains its predominant magnetization along the previously applied field, and the magnetic moments are directed along a helix. After the application of a transverse magnetic field, many domains are formed in the structure in remnant state.

Rogachev K.A. was supported by the grant of the Government of the Russian Federation for state support of scientific research conducted under the supervision of leading scientists in Russian institutions of higher education, scientific foundations, and state research centers of the Russian Federation (Project No. 075-15-2021-607).

1. L. Elbaile, R.D. Crespo, V. Vega, J.A. Garcıa, J. Nanomaterials **2012**, 198453 (2012).
2. Y.S. Jeon, B.C. Park, M.J. Ko, J.H. Moon, E. Jeong, Y.K. Kim, Nano Today **42**, 101348 (2022).
3. D.Y. Nam, A.Yu. Samardak, Y.S. Jeon, S.H. Kim, A.V. Davydenko, A.V. Ognev, A.S. Samardak, Y.K. Kim, Nanoscale **10**, 20405–20413 (2018).

A.P36

INVESTIGATION OF MAGNETIC TRILAYER Co/Cu/Co SYSTEM IN THE FRAMEWORK OF FIRST-PRINCIPLES CALCULATIONS

*R.A. Sukhachev**, *M.V. Mamonova*

Dostoevsky State University, Omsk, Russia
*E-mail: sukhachevruslan@gmail.com

In this work, numerical studies of the energy and magnetic properties of the Co/Cu/Co system were carried out using the VASP software package [1]. Calculations describing the influence of the surface facet orientation on the magnetic anisotropy energy showed that for the (100) and (111) faces, the direction of the magnetic moments parallel to the film plane is the most energetically favorable. For the (110) face, a weak perpendicular magnetoanisotropy was obtained.

Many research works on the features of ultrathin films are focused on studying the fundamental physical aspects of magnetism. However, films also have great potential for practical application of the results of scientific activity [2]. If we consider the applied value of thin magnetic films, they are widely used in microelectronics, nanoelectronics and spintronics devices. For example, they are used to store and record information in memory devices, which makes it possible to obtain high density and speed of information recording. In particular, one of the types of multilayer structures are spin valve structures. At the moment they are a popular area of study because. are part of the hard disk write heads that separate the read and write processes into an inductive write element and a magnetoresistive read sensor. The range of materials used in the spin valve is quite wide. As well as a list of other parameters that can be changed when working with it. For example, the number of layers. These reasons give rise to a whole class of giant magnetoresistance (GMR) structures that use pinned and free layers. Unsurprisingly, the hard drive industry is now rapidly moving towards the use of spin-valve structures.

Calculations of the difference between the energies of the AFM and FM configurations of Co/Cu/Co depending on the number of copper layers in 3–9 monolayers and cobalt in 1–3 monolayers showed that the ferromagnetic configuration becomes the most energetically favorable when the number of substrate layers is 9 monolayers and magnetic material in 3 monolayers.

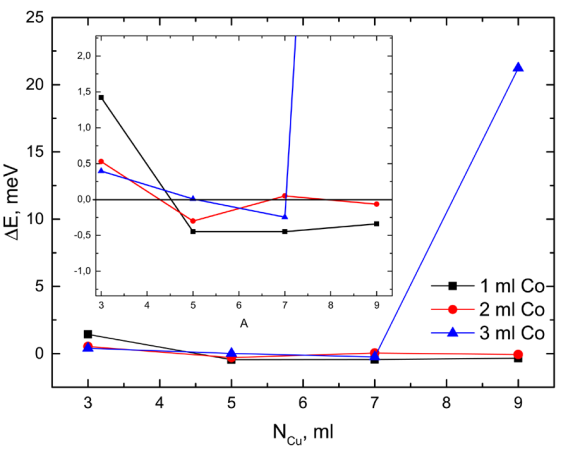

Figure 1. Dependence of the energy difference between the AFM and FM structures.

Table 1. Total energies for the Co/Cu/Co system with (100), (110), and (111) faces.

Faces	$E_{m\parallel}$ (eV)	$E_{m\perp}$ (eV)	E_{MA} (meV)
(100)	–22.717099	–22.716201	0.898
(110)	–21.663702	–1.663726	–0.024
(111)	–23.282756	–23.281794	0.961

Figure 1 shows the dependence of the energy difference between the AFM and FM structures of one supercell atom on the number of substrate layers for different numbers of magnetic material layers. The plane-wave basis cutoff energy was set to E_{cut} = 600 eV at the size of the Monkhorst-Pack k-point grid of 48×48×1.

The study of the dependence of the magnetic properties of the system on the number of Co monolayers showed that the values of the magnetic moment obtained in the course of calculations are in good agreement with the experimental data of other researchers [3].

It is known from experiment [4] that the Co/Cu structure is characterized by a weak easy plane magnetic anisotropy with magnetization oriented in the film plane. This is confirmed by our calculations. For the Co/Cu/Co structure, $E_{MA} = E_{\perp} - E_{\parallel} > 0$, which corresponds to easy plane magnetic anisotropy, except for very small values of E_{MA} = –0.02 eV for energetically unfavorable FM face configurations (110). But additional measurements [5] confirmed that the Co/Cu(111) system indeed exhibits a weak anisotropy perpendicular to the interface.

Table 1 lists the total energies for the Co/Cu/Co system with 100, 110, and 111 faces when the magnetization vectors are directed in the film plane and perpendicular to it.

The study was carried out with the financial support of the Ministry of Education and Science of the Russian Federation (agreement 0741-2020-0002)

1. P.G. Kresse, J. Furthmuller, Phys. Rev. B **54**, 16, 11169 (1996).
2. J.W. Nielsen, Annu. Rev. Mater. Sci. **9**, 87–121 (1979).
3. U.L. Pustogowa, Szunyogh, H. Ebert, P. Weinberger, Solid State Commun. **108**, 343–348 (1998).
4. M.T. Johnson, P.J.H. Bloemen, F.J.A. den Broeder and J.J. de Vries, Rep. Prog. Phys. **59**, 1409 (1998).
5. J. Kohlhepp, H.J. Elmers, S. Cordes, U. Gradmann, Phys. Rev. **45**, 12287 (1992).

MAGNETIC AND OPTICAL INVESTIGATIONS OF POTASSIUM ALUMINOBORATE GLASS WITH THE ADDITION OF IRON OXIDES SUBJECTED TO THERMORADIATION INTERACTION

E.M. Ibragimova[1], *M.K. Salakhitdinova*[2*]

[1]Institute of Nuclear Physics, Republic of Uzbekistan Academy of Sciences, Tashkent, Uzbekistan
[2]Samarkand State University, Faculty of Physics, Department of General physics, Samarkand, Uzbekistan
[*]E-mail: smaysara@yandex.ru

An important direction in the development of modern materials science is the development of materials based on multicomponent oxide glasses activated by nanoparticles of oxides of transition and rare earth metals, and approaches to their local structural modification under the action of various types of interactions. Such integrated solutions, located at the intersection of chemical technology and condensed matter physics, open the way to the creation of new materials for nanophotonics and integrated optics.

Glasses activated by metal oxide nanoparticles exhibit unique properties associated with states at the dielectric-metal interface. In such materials, the size effects of metal nanoparticles are clearly expressed, which also plays an important role in the creation of materials with desired properties [1, 2].

The aim of this work is to study of nonlinear effects observed by optical and EPR-spectroscopy in oxygen-containing glasses with additives of transition metal oxides subjected to radiation and thermoradiation treatment.

Glasses of the following composition were used as objects of study: $25[K_2O]\cdot 25[Al_2O_3]\cdot 50[B_2O_3]$ (mol. %) with additions of 1.0 and 2.0 mass.% Fe_2O_3.

The samples were in the form of polished plates with an area of 1 cm^2 and the thickness of 1×0.05 and 8×0.1 mm. Thermoradiation treatment of the samples was carried out in dry air in a uniform γ-field of ^{60}Co isotope source with dose rate of 236 R/s at temperatures of 423, 473, 523, 573 K for 2 hours.

In this case, a dose of $1.7\cdot 10^6$ R was accumulated, sufficient to achieve equilibrium between the generation and recombination of atomic displacement defects.

The interaction and simultaneous influence of thermal annealing and gamma irradiation with glass lead to nonlinear dependences of the intensity of the radiation-induced EPR-spectrum on the dose of gamma irradiation of potassium aluminoborate glass with iron oxide additives. In this case, Fe^{3+} ions serve as an EPR-probe and have paramagnetic properties at certain rather low concentrations of iron ions.

The work was supported by grants A-4-9 and OT-F2-27 of the Ministry of Higher and Secondary Specialized Education of the Republic of Uzbekistan.

1. E.M. Ibragimova, A.N. Salakhitdinov, M.K. Salakhitdinova, N.S. Saydirasulov, A.A. Yusupov, J, Magn. Magn. Mater. **459**, 12–15 (2018).
2. M.K. Salakhitdinova, A.N. Salakhitdinov, Kh.B. Mirzokulov, Bull. Russian Academy of Sciences: Physics **83**, 832–834 (2019).

A.P38

SPIN-WAVE COUPLER BASED ON THE YIG/FeRh STRUCTURE

*E.I. Salomatova**, *S.A. Odintsov, S.V. Grishin, A.V. Sadovnikov*

Saratov State University, Saratov, Russia
*E-mail: e.salomatova2016@yandex.ru

Recently, a new field spintronics – magnonics [1] – has been developing rapidly. This field is the study of spin-wave processes in irregular micron and nanoscale magnetic structures, which have advantages such as fast performance and low power consumption. Among promising structures, iron yttrium garnet (YIG) films, which exhibit record-low attenuation at ultrahigh frequencies, are being investigated. Of interest is the YIG-based microwave lateral system, which is used as an alternative approach to frequency and wave filtering methods in magnonics networks. One of the methods considered in this paper is the addition of an antiferromagnetic FeRh [2, 3] layer to the system, which has a high saturation magnetisation in the ferromagnetic phase and also has significant magnetocaloric, magnetoelectric and piezoelectric effects occurring near the type 1 metamagnetic phase transition.

In the paper a study of signal control modes in a spin-wave coupler based on two microstrips of YIG connected through the lateral side and the FeRh layer located on top is performed. Also, by changing the characteristics of the FeRh layer the mechanism of spin-wave signal switching, which is observed as a redistribution of spin waves (SW) power between lateral waveguides, is implemented in the system.

The investigated structure shown in Fig. 1 is placed in an external static magnetic field of H_0 = 1200 Oe in the direction of y-axis for effective excitation of surface magnetostatic waves (SMSW). In order to study the SMSW dynamics in such a system, micromagnetic modelling (MMM) based on numerical integration of Landau-Lifshitz-Hilbert [4, 5] equation (1) was carried out:

$$\frac{\partial \mathbf{M}}{\partial t} = -\gamma\left[\mathbf{H}_{\text{eff}} \times \mathbf{M}\right] + \frac{\alpha}{M_s}\left[\mathbf{M} \times \frac{\partial \mathbf{M}}{\partial t}\right], \quad (1)$$

where $\mathbf{M}$ is the magnetization vector, γ = 2.8 MHz/T is the gyromagnetic ratio, $\alpha = 10^{-5}$ is the damping parameter, M_s = 139 G is the saturation magnetization of the YIG, $\mathbf{H}_{\text{eff}} = -\delta\mathbf{F}/\delta M$ is the effective magnetic field. The MMM allows us to numerically solve the problem of excitation and propagation of SW in an irregular magnetic microstructure. Then, conducting one of the control methods, MMM was carried out and the obtained results were compared. When the magnetisation

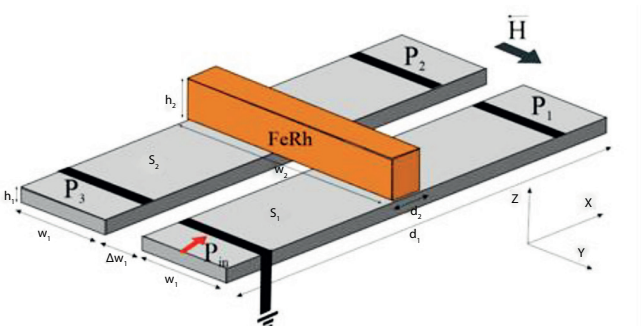

Figure 1. Schematic illustration of the structure.

of FeRh M_{fr} was changed, the amplitude-frequency response (AFR) plot showed dips and deflections on one port of P_3. When the length of FeRh layer was changed, the amplitude-frequency response also changed, namely, a drop in signal amplitude on the same port was observed. During the calculations it was found that the transmittance could be controlled by adjusting the values of the parameters to be changed.

Thus, in this paper a numerical and experimental study of a tunable spin-wave tap based on the YIG/FeRh structure has been performed. It is shown that by changing the characteristics of the FeRh antiferromagnet placed over the microwave conductors, one can modulate the microwave propagation, in particular by redirecting the spin-wave signal to one output. The special properties of the FeRh alloy allow several control paths to be used. The nonlinear switching effects in the YIG/FeRh composite system allow the design of nonlinear taps and spin-wave signal power dividers in planar magnon network topologies for selective processing of information signals.

Work supported by Russian Science Foundation 19-79-20121.

1. S.A. Nikitov, D.V. Kalyabin, I.V. Lisenkov, A.N. Slavin, Y.N. Barabanenkov, S.A. Osokin, A.V. Sadovnikov, E.N. Beginin, M.A. Morozova, Y.P. Sharaevsky, Y.A. Filimonov, Y.V. Khivintsev, S.L. Vysotsky, V.K. Sakharov, and E.S. Pavlov, Phys. Usp. **58**, 1002 (2015).
2. A.A. Amirov, V.V. Rodionov, I.A. Starkov, A.S. Starkov, A.M. Aliev, J. Magn. Magn. Mater. **470**, 77 (2019).
3. A.A. Amirov, A.S. Starkov, I.A. Starkov, A.P. Kamantsev, V.V. Rodionov, Lett. Mater. **8**(3), 353 (2018).
4. L. Landau, E. Lifshitz, Phys Z Sowj **8**, 153 (1935).
5. T.L. Gilbert and J.M. Kelly, American Institute of Electrical Engineers, 253–263 (1955).

MAGNETOSTATIC INTERACTIONS OF DENSELY PACKED FERROMAGNETIC SEGMENTS IN Fe/Au BARCODE NANOWIRES ARRAYS

A.Yu. Samardak[*1], *Y.S. Jeon*[2], *A.G. Kozlov*[1], *K.A. Rogachev*[1], *A.V. Ognev*[1], *E. Jeong*[3], *G.W. Kim*[3], *M.J. Ko*[3], *A.S. Samardak*[1], *Y.K. Kim*[2,3]

[1]Institute of High Technologies and Advanced Materials, Far Eastern Federal University, Vladivostok, Russia
[2]Institute of Engineering Research, Korea University, Seoul, Republic of Korea
[3]Department of Materials Science and Engineering, Korea University, Seoul, Republic of Korea
[*]E-mail: samardak.aiu@dvfu.ru

The latest studies in the field of nanomagnetism have led to the rebirth of magnetic memory devices. Slow, energy-consuming, and restricted by superparamagnetic limit classic magnetic memory devices, storing data in magnetic domains on thin films, are losing relevance on fast pace. To improve their properties and fix imperfections, scientists and engineers developed novel design approaches [1, 2]. Spin-Transfer Torque (STT) and Spin-Orbit Torque (SOT) magnetoresistive random-access memory (MRAM) devices are already being mass-produced, implemented, and showing good performance in specific tasks. Nevertheless, there is a possibility to improve magnetic memory even further by increasing the density of memory cells in the device, which could lead to a rapid increase of bytes located in square inch and therefore could decrease the cost of such devices significantly. To do that, a number of problems must be solved. One of these problems is due to the decrease of distance between memory cells in the device, which could result in magnetostatic interactions between them, capable of shifting desirable for data storage square hysteresis loop and changing it critical switching fields for each cell individually. To avoid such unwanted behavior in the systems of densely packed ferromagnetic elements, magnetostatic interactions, which could take complex forms due to their 3-dimensional distribution, must be studied. In this work, we present study of magnetic behavior of Fe/Au barcode nanowire arrays using variety of experimental and simulation methods with a focus on magnetostatic interactions.

Fe/Au barcode nanowires (BNWs) were synthesized using electroplating from single electrolyte method inside the porous Al_2O_3 membrane with diameters of pores 200–300 nm. To manage the segmented structure, pulses with different current densities ρ (10 and 0.01 mA cm^{-2}) were fed to the electrochemical cell. The electrolyte consisted of a mixture of deionized water and solutions of iron (II) sulfate heptahydrate ($FeSO_4 \cdot 7H_2O$) as a source of Fe-ions, and potassium dicyanoaurate ($KAu(CN)_2$) as a source of Au ions. To study the influence of segment size on magnetic properties, samples with different lengths of corresponding segments were synthesized – L_{Fe} = 100 and 200 nm, L_{Au} = 30, 50, 100 and 200 nm.

BNWs were etched from the Al_2O_3 membrane to study their geometrical parameters and elemental composition using scanning electron microscopy (SEM) ThermoScientific SCIOS2 (Fig. 1) and Energy-Dispersive X-Ray Spectroscopy (EDX) TEAM, respectively. Elemental composition analysis showed that the segments synthesized with high ρ (Fe-segments) consist of the $Fe_{90}Au_{10}$ alloy and with a low ρ – of the $Fe_{45}Au_{55}$ alloy with magnetic moments of 1000 G and 20–100 G, respectively.

Magnetic properties were measured using a LakeShore VSM 7400 vibrating sample magnetometer and showed almost isotropic behavior of Fe(100)Au(*x*) samples, and *vice versa*, strong anisotropy along the main axis of BNWs of Fe(200)Au(30) sample, which decreased with increase of L_{Au}. To study the coercive force H_c and magnetostatic fields H_u distributions, the first order reversal curve (FORC) diagram method [3] was used. As a result, a rapid increase in H_u distribution was detected

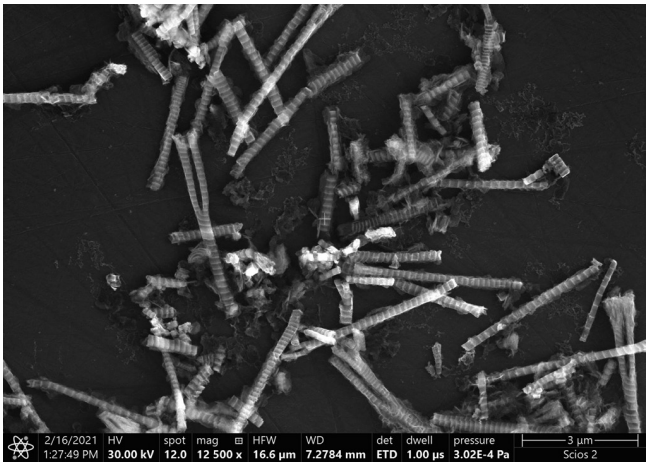

Figure 1. SEM image of segmented Fe(100)Au(30) BNWs etched from Al_2O_3 template on Si substrate.

in Fe(200)Au(x) samples, while in the Fe(100)Au(x) series H_u stayed at the same level despite the change of L_{Au}.

Magnetic force microscopy (MFM) was performed to analyze the domain structure of the samples. In the absence of an external magnetic field H, no contrast from the studied sample was detected. In the H = 800 Oe along the main axis of BNW, an alternating contrast of black and white poles on the ends of Fe segments became visible. With an appliance of perpendicular H, the poles of the stray field appeared rotated to 90° and located exclusively in the Fe segments at the edges of the nanowire.

On the basis of SEM, MFM and hysteresis results, a micromagnetic model using Mumax3 [4] was implemented. The vortex configuration of magnetic moments was confirmed in the remnant state after saturation in all samples. Analysis of distribution of magnetostatic fields revealed that dipole interactions can be divided into 3 types: interactions between opposite magnetic pole of the adjacent segment in the same nanowire (type I), opposite magnetic pole of the same segment (type II) and closest poles in the segments of the neighboring nanowires in the array (type III). Simulations of BNWs with longer L_{Au} showed that depending on L_{Fe} a different type becomes dominant – type (II) for Fe(100)Au(x) series and type (III) for Fe(200)Au(x) series.

This work was supported by the Russian Ministry of Science and Higher Education (state task No. 0657-2020-0013).

1. E Grimaldi, Nat. Nanotechnol. **15**(2), 111–117 (2020).
2. M. Baumgartner, Nat. Nanotechnol. **12**(10), 980–986 (2017).
3. I.D. Mayergoyz, J. Appl. Phys. **57**(8), 3803–3805 (1985).
4. A. Vansteenkiste, Aip Adv. **4**(10), 107133 (2014).

A.P40

MAGNETIC AND STRUCTURAL PROPERTIES OF Co-Ni-Z (Z = Al, Ga, In, Sn) HEUSLER ALLOYS

*A.A. Sanosyan**, *V.V. Sokolovskiy, V.D. Buchelnikov*

Chelyabinsk State University, Chelyabinsk, Russia
*E-mail: arthursanosyan@mail.ru

Nowadays, the Heusler alloy families have attracted a great attention from experimental and fundamental points of view due to their remarkable magnetic, mechanical, electrical and thermodynamic properties, which are reviewed in detail in [1, 2]. Most of the Heusler alloys exhibit a martensitic transformation from high-symmetry cubic austenite to lower symmetry martensite with tetragonal or orthorhombic structure. A lowering in a crystal symmetry induces a large magnetocrystalline anisotropy energy (*MAE*). As a consequence, ferromagnetic Heusler possessing a high *MAE* would be useful in the field of rare-earth free permanent-magnet technology.

The study was performed with the help of density functional theory and the projected augmented wave (PAW) method implemented in VASP [3, 4]. The exchange-correlation effects were treated in the framework of generalized gradient approximation (GGA) realized in Perdew, Burke, and Ernzerhof (PBE) functional [5].

The k-points within the Brillouin zone were generated using a uniform Monkhorst-Pack [6] mesh of 16×16×16. The cut-off energy of 450 eV for the plane waves was used. For geometry relaxations, the conjugate gradient algorithm with the energy and force convergence criteria as 10^{-6} eV and 10^{-3} eV/Å were assumed.

To describe the chemical disorder in $Co_2Ni_{1+x}Z_{1-x}$ (Z = Al, Ga, Sn, In) ($0 \le x \le 1$), the 16-atom supercell approach was treated. Crystal structure optimization was performed for five structures with cubic symmetry, which differ from each other by the atomic configurations of Co, Ni and Z, as shown in Fig. 1 together with corresponding Wyckoff positions of atoms.

To determine the *MAE*, two sets of self-consistent noncolinear magnetic calculations were performed for total energy of favorable structure, where magnetic moments oriented along [001]- and [100]-axis. The *MAE* was calculated in terms of the difference in these total energies as $MAE = E_{[100]} - E_{[001]}$, where a negative *MAE* means the preferable in-plane spin configuration, whereas a positive one indicates the out-plane direction.

To find the favorable crystal structure in both austenitic and martensitic phases of Co-Ni-Z (Z = Al, Ga, In, Sn), we calculate ground state energy E_0 and consider the influence of tetragonal distortions on regular $L2_1$, inverse, T^p, T^c, and $T^\#$ structures. $E_0(c/a)$ dependencies are depicted in Fig. 2 by an example of Co-Ni-(Al, Ga) alloys. One can see that regular $L2_1$ structure is significantly higher in energy and can not be regard as a competitor for the rest considered structures.

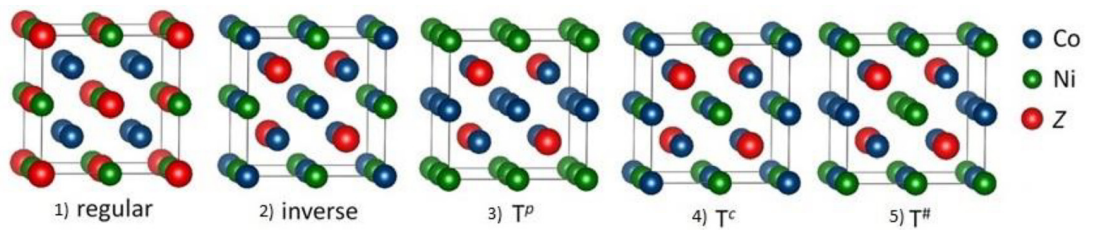

Figure 1. Structural motives considered in the study of Co-Ni-Z.

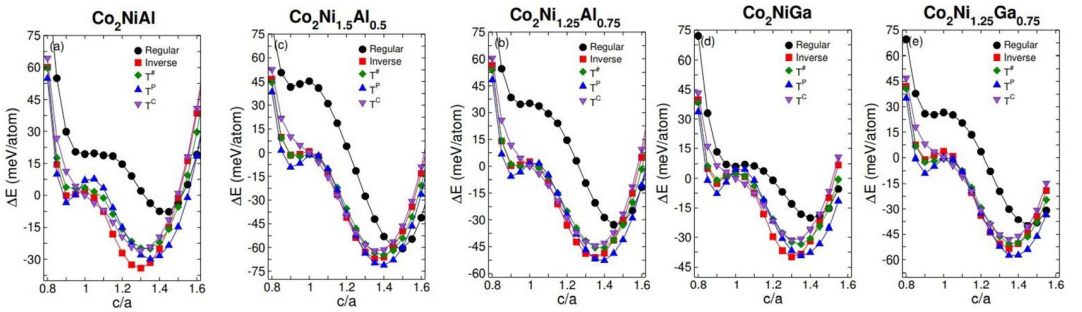

Figure 2. Ground state energy as a function of tetragonal distortions for $Co_2Ni_{1+x}(Al,Ga)_{1-x}$ alloys. The energy of T^c cubic structure is a reference one.

The absence of minima at $c/a = 1$ allows to conclude that austenitic structures of these alloys will be unstable. The martensitic phases are possible in all considered structures, which demonstrate a strong competition nearly the global $E(c/a)$ minimum. Nevertheless, the inverse structure is the most favorable for Co_2NiAl martensite with $c/a = 1.292$, while adding of Ni results in favoring of T^p structure with higher tetragonal distortions $c/a = 1.380$ for Ni excess $x = 0.25$ and 0.5.

The stable compositions can be found just in Co-Ni-Al and Co-Ni-Ga families. Moreover, the mostly stable compounds are the ternary stoichiometric $Co_2Ni(Al,Ga)$, while Ni excess x destabilizes $Co_2Ni_{1+x}(Al,Ga)_{1-x}$, and off-stoichiometric compositions become unstable at $x > 0.5$ and $x > 0.25$ in Al- and Ga-containing alloys, correspondingly.

Stoichiometric and off-stoichiometric compositions of both Co_2NiAl and Co_2NiGa families possess the *MAE* of easy plane type. *MAE* of inverse and T^p structures are equal for Co_2NiAl, while MAE^{T^p} is 7% smaller than $MAE^{inverse}$ in case of Co_2NiGa. Deviation from stoichiometry affects drastically on magnetocrystalline anisotropy and reduces *MAE* of $Co_2Ni_{1+x}(Al,Ga)_{1-x}$ by at least 1.7 times.

This work was supported by the Russian Foundation for Basic Research, № 075-01391-22-00

1. A.N. Vasil'ev, V.D. Buchel'nikov, T. Takagi, V.V. Khovailo, E.I. Estrin, Physics-Uspekhi **46**, 559–588 (2003). doi:10.1070/pu2003v046n06abeh001339.
2. V.D. Buchel'nikov, A.N. Vasiliev, V. Koledov, S. Taskaev, V.V. Khovaylo, V.G. Shavrov, Physics-Uspekhi **49**, 871 (2006). doi:10.1070/pu2006v049n08abeh006081.
3. G. Kresse, J. Furthmüller, Phys. Rev. B **54**, 11169–11186 (1996).
4. G. Kresse, D. Joubert, Phys. Rev. B **59**, 1758 (1999).
5. J. Perdew, K. Burke, M. Ernzerhof, Phys. Rev. Lett. **77**, 3865 (1996).
6. H.J. Monkhorst, J.D. Pack, Phys. Rev. B **13**, 5188–5192 (1976). doi:10.1103/PhysRevB.13.5188.

A.P41

INSTABILITY FIELD ANISOTROPY OF POLYCRYSTALLINE FERROMAGNETIC NANOWIRES

S.A. Satsuk[1*], S.V. Komogortsev[2]

[1]Federal Research Center KSC SB RAS, Krasnoyarsk, Russia
[2]Kirensky Institute of Physics, Federal Research Center KSC SB RAS, Krasnoyarsk, Russia
[*]E-mail: svetlana.satsuk@gmail.com

Ferromagnetic nanowires have been intensively studied for several decades in view of their applications as a functional element in information technology and biomedicine [1]. The transverse size of such wires varies from a few to hundreds of nanometers, while the length exceeds the transverse size by at least an order of value. In most cases, such wires are characterized by a polycrystalline structure. The applied properties of polycrystalline nanowires, such as coercive force and magnetic anisotropy, can be tuned by changing the shape, structure, and/or spatial distribution of magnetic functional units [1].

The instability field H_i, at which the magnetization patterns have an abruptly transition from one to another, depends on the magnetization reversal mechanism. The H_i exhibits a different angular dependence in nanowires with different magnetization reversal mechanisms. In some cases, the instability field is identical to the coercive field H_c. There are two analytically solved problems for the angular dependence of the instability field: the dependence with the shape of an astroid, calculated within the Stoner-Wohlfahrt model [2] of uniform magnetization rotation and the angular dependence with the shape of an ellipse by Aharoni for a curling instability [3]. The both problems do not take into account the polycrystalline structure of the wire, while it is well known that such a structural feature can significantly affect the micromagnetic states and hysteresis of the nanowires.

In this work, we performed a micromagnetic calculation in order to reveal the effect of the polycrystalline structure and the transverse size of the nanowire on the anisotropy of the instability field and the coercive field. In the micromagnetic simulation three main contributions to the magnetic energy of the wire (exchange, dipole-dipole, and crystallite anisotropy energy) were taken into account. The simulation was performed using OOMMF framework [4]. Calculation parameters were: exchange stiffness constant A = 1.106 erg/cm, cubic cell size in the finite difference method 5 nm, magnetization M_s = 1000 G. The easy axis of crystallites including form one cell (for the crystallite size of 5 nm) to the 64 cells (for the crystallite size of 20 nm) were randomly oriented. We calculated the angular dependences for the case when the local magnetic anisotropy of the crystallite is $K = 5.10^4$ erg/cm^3. We found the magnetization reversal by uniform rotation in wires of diameter less than $D = (A/M_s^2)^{1/2}$ (transverse size of 5 nm) can be well described by the Stoner-Wohlfarth like astroid, and the angular dependence of the instability field in nanowires of large diameter much more than D (transverse size of 40 nm) follows to ellipse like dependence according to the loss of stability of the magnetic state due to curling mechanism [3]. In intermediate cases, for diameters of the order of 20 nm none of two known analytical results is observed even for small values of the anisotropy constant.

We propose a universal approach to description of the behaviour of the instability field anisotropy for all diameters of nanowires, by the Lame curves (superellipse). The equation of superellipse in polar coordinates is:

$$H_i = \frac{ab}{\left((a\cos\varphi)^n + (b\sin\varphi)^n\right)^{1/n}} .$$

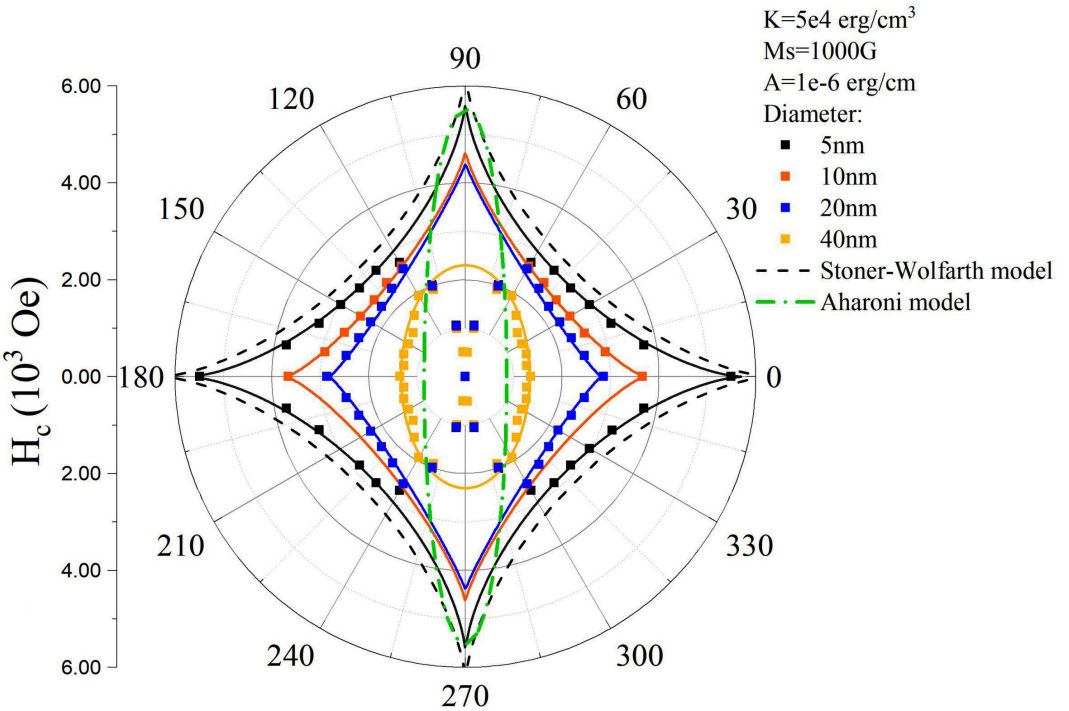

Figure 1. Model angular dependences of the coercive field for nanowires with different diameters (symbols). Corresponding Lame curves (lines of the same color) for instability field H_i. Anisotropy constant in all cases $K = 5.10^4$ erg/cm^3.

The selection of the critical index n and the coefficients a and b in the Lame equation make it possible describing the angular dependences of H_i. In the numerical experiment we have a range of angles, where instability field are equal coercive field and we can discuss both of them. As a result, we see a transition from the uniform rotation result ($n = 2/3$ and $a = b$) to the curling model result ($n = 2$ and $a \neq b$) during the changing the wire diameter and this transition can be described by the universal equation (Fig. 1). The polycrystalline structure of nanowires apparently generates a certain transition type of instability between instabilities in the curling and uniform rotation models, leading to the appearance of an angular dependence of the instability field specific for a certain set of micromagnetic constants, nanowire sizes and crystallite sizes. This means that in the future such a description of the experimental angular dependences by Lame curves can be used to judge the presence in the sample under study of a specific set of magnetic constants, nanowires sizes and crystallite sizes.

This research was funded by the RFBR, Krasnoyarsk Region and the Krasnoyarsk Regional Science Foundation (Project No. 20-42-240001).

1. L.G. Vivas, Y.P. Ivanov, D.G. Trabada, M.P. Proenca, O. Chubykalo-Fesenko, and M. Vázquez, Nanotechnology **24**, 105703 (2013).
2. E.C. Stoner and E. P. Wohlfarth, Phil.Trans. Roy. Soc. A. **240**, 559 (1948).
3. A. Aharoni, J. Appl.Phys. **82**(3), 1281–1287 (1997).
4. M. Donahue, D. Porter, Interagency Report 6376 (2006).

ELECTRICAL, MAGNETIC, AND GALVANOMAGNETIC PROPERTIES OF Mn_3X ALLOYS (X = Al, Ga, Ge, Sn)

A.A. Semiannikova[1*], *V.Yu. Irkhin*[1], *P.S. Korenistov*[1], *P.B. Terentyev*[1], *E.B. Marchenkova*[1], *V.V. Marchenkov*[1,2]

[1]M.N. Mikheev Institute of Metal Physics, UB RAS, Ekaterinburg, Russia
[2]Ural Federal University, Ekaterinburg, Russia
[*]E-mail: semiannikova@imp.uran.ru

Intermetallic compounds based on Mn_3X (X = Al, Ga, Ge, Sn) are of great interest for research, since the states of an antiferromagnet [1, 2], and a compensated ferrimagnet [3, 4], a topological semimetal, and a frustrated magnet [5] can be realized in these alloys. Such materials have unusual, very sensitive to external influences magnetic and electronic characteristics, which can be used for practical applications. With the help of magnetic and electric fields, pressure and temperature, it is possible to tune their electronic band structure and, consequently, influence their transport and magnetic properties.

It is well known that the structure of intermetallic compounds, in particular, Mn_3X, can strongly depend on the methods of preparation of alloys, which will inevitably be reflected in their electronic and magnetic state. Therefore, the study of the role of the structural state in the formation and behavior of the electronic and magnetic characteristics of intermetallic compounds based on manganese seems to be a rather important and interesting problem. Thus, the purpose of this work is to study the structure, magnetic, and electrical properties of the system of intermetallic compounds Mn_3X (X = Al, Ga, Ge, Sn), since it will make it possible to describe the evolution of the electronic structure and magnetic state of these compounds, to understand the features of the manifestation of the state of an antiferromagnet, and a compensated ferrimagnet, a topological semimetal, and a frustrated magnet, their similarity and differences.

Polycrystalline Mn_3X alloys were prepared in an induction furnace. The ingots were annealed for 72 hours at 650 °C in an argon atmosphere followed by cooling to room temperature at the rate of 100 K/h. An elemental analysis, XRD and electronic transport measurements were carried out at the Collaborative Access Center of the IMP UB RAS. Electrical resistivity was measured by the conventional four-probe method at direct current with current switching through the sample in the temperature range from 4.2 to 300 K. Field dependences of a magnetization were measured in the fields up to 50 kOe at T = 4.2 K using a Quantum Design MPMS-XL-5 SQUID-magnetometer. The galvanomagnetic properties were measured on the "Oxford Instruments" setup in magnetic fields up to 130 kOe.

As a result of studies carried out, it was found that with a variation in the X-component, the residual resistivity ρ_0, the saturation magnetization M_s, and the Hall effect change significantly. The found features of the behavior of electrical, magnetic and galvanomagnetic properties may indicate the features of the crystallographic and magnetic structure of the studied compounds, as well as the manifestation of an unusual bulk electronic topology. These results can be useful in the selection of materials for spintronic devices.

The research was supported by RSF (project No. 22-22-00935).

1. Y. Zhang et al., Phys. Rev. B **95**, 075128 (2017).
2. K. Manna et al., Nat. Rev. Mater. **3**, 244 (2018).
3. M.E. Jamer et al., Phys. Rev. Appl. **7**, 064036 (2017).
4. V.V. Marchenkov et.al., JETP **128**, 919–925 (2019).
5. H. Yang et al., New J. Phys. **19**, 015008 (2017).

A.P43

MAGNETIC PROPERTIES OF Ni NANOWIRES SYNTHESIZED USING TEMPLATES WITH DIFFERENT PORE ORDER

*M.I. Sobirov**, *A.Yu. Samardak, S.A. Azon, S.R. Potapova, M.B. Karibov, A.S. Samardak, A.V. Ognev*

Institute of High Technologies and Advanced Materials, Far Eastern Federal University, Vladivostok, Russia
*E-mail: sobirov.mi@dvfu.ru

Porous anodic aluminum oxide is a well-known nanomaterial that can be used as a template to prepare nanowires, nanocrystals, nanotubes, nanofibers, and quantum dots, in filter production, instrumentation, biomedicine, and optoelectronics [1]. By controlling the conditions of the two-step anodization method [2] one can vary the structural parameters of the porous matrix and nanostructures obtained by using them as a template. Thus, by changing the electrolyte composition, temperature, and time of first and second anodization, we can modify the geometry of the magnetic nanostructures, their spatial distribution, and order.

In this work, we investigate magnetic properties and changes in coercive forces and interaction fields of Ni nanowire arrays, synthesized using Al_2O_3 porous templates achieved with different times of first anodization, resulting in drastic changes of order of pores.

To define the effect of the first anodization time on the aluminum oxide membrane structure, porous templates were synthesized with the first anodization time of 0, 15 and 120 min using the Agilent 6030A power supply in mild potentiostatic mode at 40 V in 2–3 °C oxalic acid. After the porous Al_2O_3 membrane was achieved, Al was dissolved with 0.08M of $CuCl_2$ + 8% HCl in 20 °C at 1 h, and the barrier layer on one side of the pores was etched with 1.0 M of H_3PO_4 acid at 40–60 m. After that, a thick conducting layer of Cu was deposited on the top side of the porous membrane to avoid the formation of dendrites during the growth of the nanowires.

Templates were checked by scanning electron microscope (SEM) ThermoScientific SCIOS2. The nanowires were electrodeposited from a Watts solution containing $NiSO_4$, $NiCl_2$ and H_3BO_3 into prepared templates in potentiostatic mode at –1 V for 10 minutes using a Keithley 2460 power source. The geometrical properties and elemental composition of the synthesized nanowires were investigated and analyzed by SEM ThermoScientific SCIOS2 with EDX module. Magnetic properties were studied using a LakeShore VSM 7410 vibration magnetometer. The first order reversal curve (FORC) diagram method was used to study the distribution of coercive force and magnetostatic interactions in the arrays of Ni nanowires.

The surface of sample without the first anodization (t = 0 min) did no show any order with the average pore diameter of 30–50 nm and various interpore distances. With an increase in the time of the first anodization to t = 15 min, we observed two types of pores – with large diameters (D = 100 nm) and small diameters (D = 50–60 nm) distributed randomly. In the sample with the time of the first anodization t = 120 min, the disorder of the pore diameters vanishes with an average diameter of 70–90 nm, and the interpore distance becomes more ordered. To study the order, we used a Fourier analysis of the image of the surface of the samples after the second anodizing.

SEM images of porous Al_2O_3 templates with different time of first anodization, Fourier analysis, and FORC diagrams of massive nanowires are shown in Fig. 1.

As a result, the geometry, morphology, and magnetic properties of Ni nanowires synthesized at different time of the first anodization have been studied. In nanowires with the time of the first anodization t = 0 and 15 min, there are defects such as branching and nonuniform growth. With an increase in the time of the first anodizing, the nanowires become straighter and more ordered.

A.P43

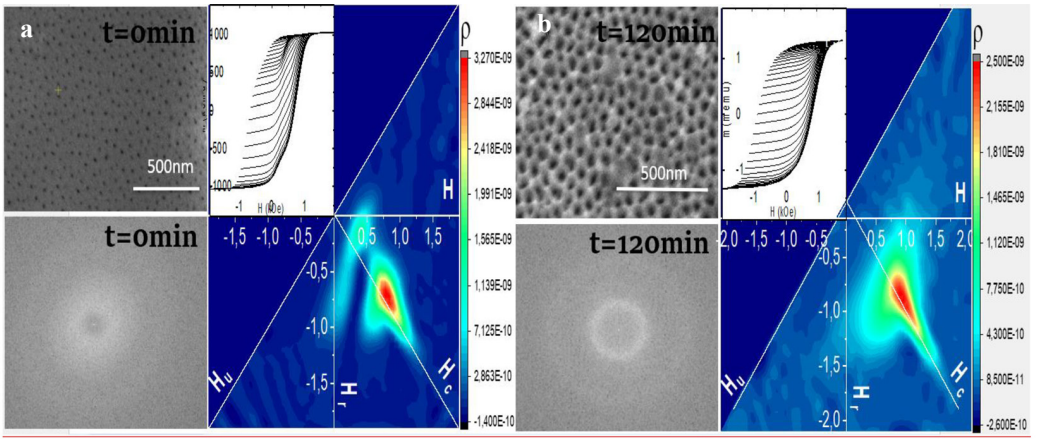

Figure 1. SEM images of porous Al_2O_3 templates with the time of the first anodization t = 0 min (**a**) and t =120 min (**b**), Fourier analysis (second row) and FORC diagrams of massive nanowires.

Hysteresis measurements showed that coercive force changes in the range of H_c = 750–950 Oe. FORC-diagram method showed changes of H_c and H_u distributions with changing the first anodization time. In Ni nanowire arrays synthesized using an Al_2O_3 template with time of first anodization t = 0 min, an additional peak appeared on FORC diagrams. With an increase in the time of the first anodizing, the coercive force increases, and the additional peak vanishes. The observed peak can be related to nanowires with smaller diameters or dendrites, formed in the beginning of electrodeposition in a disordered template.

This work was supported by the Russian Science Foundation (Project No. 19-72-20071).

1. J.M. Vargas, L.M. Socolovsky, M. Knobel, D. Zanchet, Nanotechnology **16**, 285–290 (2005).
2. H. Masuda, K. Kanezawa, K. Nishio, Chem. Lett. **31**, 6342–6346 (2002).

A.P44

FERROCENE TRANSFORMATION AT HIGH PRESURE HIGH TEMPERATURE TO FORM CORE@SHELL NANOCOMPOSITES BASED ON IRON CARBIDES

S.S. Starchikov[1*], *V.A. Zayakhanov*[1], *A.L. Vasiliev*[1], *I.S. Lyubutin*[1], *K.O. Funtov*[1], *M.V. Lyubutina*[1], *N.K. Chumakov*[2], *L.F. Kulikova*[3], *V.N. Agafonov*[4], *V.A. Davydov*[3]

[1]Shubnikov Institute of Crystallography of FSRC, "Crystallography and Photonics" RAS, Moscow, Russia
[2]National Research Center "Kurchatov Institute", Moscow, Russia
[3]L.F. Vereshchagin Institute for High Pressure Physics of RAS, Troitsk, Moscow, Russia
[4]GREMAN, UMR CNRS 7347, Francois Rabelais University, 37200, Tours, France
[*]E-mail: sergey.s.starchikov@gmail.com

Nanoparticles and nanocomposites based on iron and carbon carbides have a unique set of magnetic and chemical properties, which can be promising for application in such fields of science and technology as catalysis, Fischer-Tropsch synthesis, data storage devices, as protective coatings against corrosion, in batteries, supercapacitors, biomedical applications [1, 2]. According to some researchers [2], increased magnetization values, the absence of cytotoxicity, and the ease of chemical attachment of various functional groups to the carbon surface, provide iron carbide-based core@shell nanocomposites with a higher innovation potential compared to iron oxides.

It has recently been shown that Fe_7C_3 and Fe_3C nanoparticles encapsulated in carbon shells can be obtained during the ferrocene $Fe(C_5H_5)_2$ transformations induced by high pressure and temperature (HPHT) [3]. In this work, we discuss the mechanism of ferrocene transformation at pressure 8 GPa and high temperatures, as well as the structure and magnetic properties of the resulting $Fe_7C_3/Fe_xO_y/C$ nanocomposites. It has been shown that two main transformations were observed during the process of ferrocene HPHT treatment. These are the *in-situ* ferrocene transformation under HP-HT and the *ex-situ* transformation of obtained products after releasing the pressure and removing the samples from the high pressure cell.

Support by RSF grant 22-72-00060 is acknowledged.

1 S.S. Starchikov, V.A. Zayakhanov, A.L. Vasiliev et al., Carbon **178**, 708–717 (2021).
2. J. Yu, F. Chen, W. Gao et al., Nanoscale Horizons **2**, 81–88, (2017).
3. A.O. Baskakov, I.S. Lyubutin, S.S. Starchikov et al., Inorg. Chem. **57**, 14895–14903 (2018).

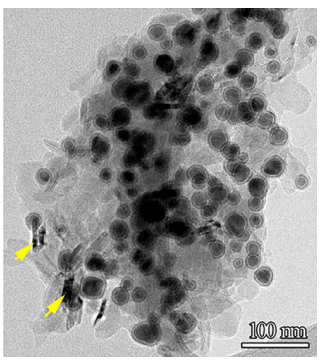

Figure 1. TEM image of Fe_7C_3@Fe_xO_y@C nanocomposites obtained during the ferrocene transformation at high pressure and temperature. Arrows show the graphitized carbon particles.

HARD/SOFT MAGNETIC BILAYER AND TRILAYER. MONTE CARLO STUDY

*T.A. Taaev**, *K.Sh. Khizriev, A.K. Murtazaev*

H. Amirkhanov Institute of Physics of the DFRC of the RAS, Makhachkala, Russia
*E-mail: taaev89@mail.ru

In 1991, it was proposed to produce permanent magnets with alternating hard and soft magnetic layers which resulted in the maximum energy product $(BH)_{max}$ [1] increase, as well as to the discovery of a very interesting phenomenon: the reversibility of the magnetization reversal curve (exchange-coupled behavior) [2]. This phenomenon is called a spin spring by analogy with the mechanical properties of solid bodies under elastic deformation. All this has led to the fact that the technological significance of these materials has acquired a new level: the production of permanent magnets with record values $(BH)_{max}$, the use as fast acting attenuators, magnetic sensors, advanced media storage with a high recording density, etc.

In the most of hard/soft magnetic heterostructures there is strong in-plane anisotropy and magnetic moments lie in plane of bilayers [2]. Therefore, field properties of magnetic hard/soft heterostructures can be estimated using a simple model integrating the standard XY-model [3–6]. The total energy of the system is represented as:

$$E = -\frac{1}{2}\sum_{i,j} J(S_i^x S_j^x + S_i^y S_j^y) - \sum_i K(S_i^x)^2 - g\mu_B\mu_0 \sum_i (H^x S_i^x + H^y S_i^y), \quad (1)$$

where the first sum takes into account the exchange interaction of each magnetic atom with its nearest neighbors inside the layers with exchanges $J = J_{hard}$ and $J = J_{soft}$ in the hard and soft magnetic layers, respectively, and the interlayer interaction with the parameter $J = J_{int}$; the second sum takes into account the contribution of anisotropy to the energy of the system, $K = K_{hard}$ and $K = K_{soft}$, respectively, the anisotropy constants of the hard and soft magnetic layers; the third sum is the contribution of the external magnetic field to the system energy, $g \approx 2$ is the Lande factor, μ_B is the Bohr magneton, μ_0 is the magnetic permeability of a substance, $H^{x,y}$ is the projections of the external magnetic field vector **H**, $S_i^{x,y}$ is the projections of the spin $\mathbf{S}_i$ localized at the node i.

The temperature dependences of magnetization M, their longitudinal and transverse components, as well as the magnetizations of each j-th magnetic monolayer M_j were investigated.

We also investigated the processes of magnetization reversal of the hard/soft bilayer and trilayers model under the action of an external magnetic field: the influence thickness of the hard magnetic layers on the magnetization reversal of the magnetic trilayers. The irreversibility field H_{irr} for both magnetic trilayers increased by 30%, and the exchange-bias field H_{ex} increased by almost 150% relative to the values for the magnetic bilayer model. Behavior of the magnetic bilayer under the external magnetic field was shown to agree with theoretical predictions well enough [7].

1. E.F. Kneller, R. Hawig, IEEE Trans. Magn. **27**, 3588 (1991).
2. E.E. Fullerton, J.S. Jiang et al., Phys. Rev. B **58**, 12193 (1998).
3. T.A. Taaev, K.Sh. Khizriev et al., JETP **129**, 277 (2019).
4. T.A. Taaev, K.Sh. Khizriev et al., J. Alloys and Comp. **785**, 1253 (2019).
5. T.A. Taaev, K.Sh. Khizriev et al., Physics of the Solid State **62**, 954 (2020).
6. T.A. Taaev, K.Sh. Khizriev et al., JMMM **524**, 167638 (2021).
7. T.A. Taaev, K.Sh. Khizriev et al., Thin Solid Films **741**, 139040 (2022).

A.P46

EXCHANGE BIAS IN Pd/Co/CoO EPITAXIAL FILM WITH PERPENDICULAR MAGNETIC ANISOTROPY

E.V. Tarasov[1,2*], *H.S. Suslin*[1], *A.V. Gerasimenko*[2], *I.A. Tkachenko*[2], *A.G. Kozlov*[1]

[1]Far Eastern Federal University, Vladivostok, Russia
[2]Institute of Chemistry, Far Eastern Branch of the RAS, Vladivostok, Russia
[*]E-mail: tarasov.ev@dvfu.ru

Exchange bias is a phenomenon that occurs at the interface when nanostructures of the FM/AFM type are cooled in the presence of a constant magnetic field to a temperature $T < T_N$, and $T_N < T_C$. This effect manifests itself, as a rule, in the displacement of the magnetic hysteresis loop in the opposite direction relative to the field applied during cooling. Due to the increased coercive force, materials with an exchange bias can be used as permanent magnets and for magnetic information storage devices with a high recording density [1, 3].

In this work, we study the exchange bias in ultrathin Pd/Co/CoO epitaxial films with different Co and $[Pd/Co/CoO]_n$ oxidation times, where n is the number of repetitions.

The magnetic properties of the samples were studied experimentally using a magnetometer based on a superconducting quantum interferometer (SQUID). Data on the structure of the samples were obtained using high-energy electron diffraction during sample deposition.

Epitaxial Pd(2 nm)/Co(1 nm) films were obtained by MBE, after that the procedure of controlled oxidation in dry oxygen was carried out. During the oxidation process, the thickness of CoO increased due to the decrease in the thickness of cobalt. As a result of the analysis of the magnetic hysteresis loops obtained at temperatures of 300, 100, (70 K for multilayer systems), 50 and 4 K, the values of the exchange bias H_{Eb} (Fig. 1a) were determined for samples with different thicknesses of cobalt oxide. It has been established that the exchange bias depends on the cobalt oxide thickness and increases with decreasing temperature. A sample with a residual cobalt oxide thickness of 0.62 nm was chosen as the base sample for obtaining a series of samples with different numbers of repetitions Pd/Co/CoO. The dependences of the magnetization on the external magnetic field, studied at different temperatures for samples with n = 1, 2, 3, made it possible to establish that a decrease in temperature leads to an increase in the exchange bias (Fig. 1b). It is known that the size factor

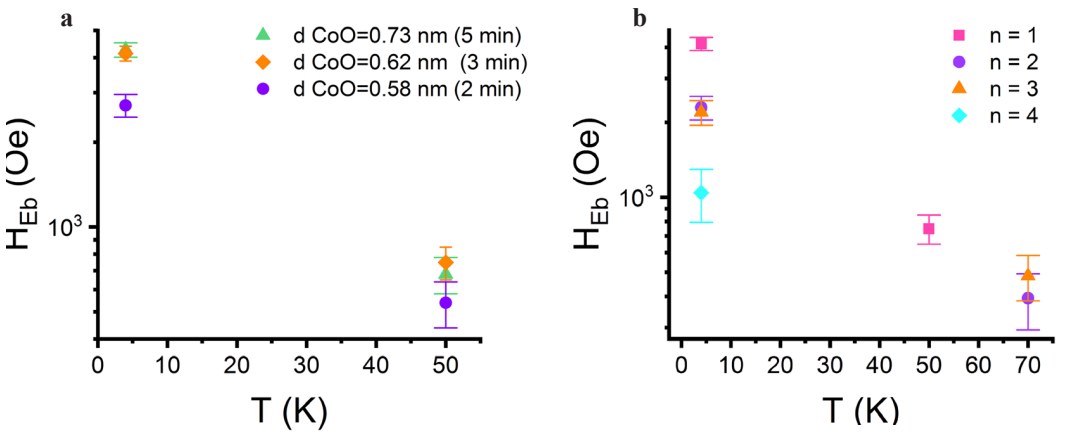

Figure 1. Temperature dependence of the exchange bias for samples with different CoO thicknesses (**a**) and with different numbers of Pd/Co/CoO repetitions (**b**). d_{CoO} = 0.62 nm.

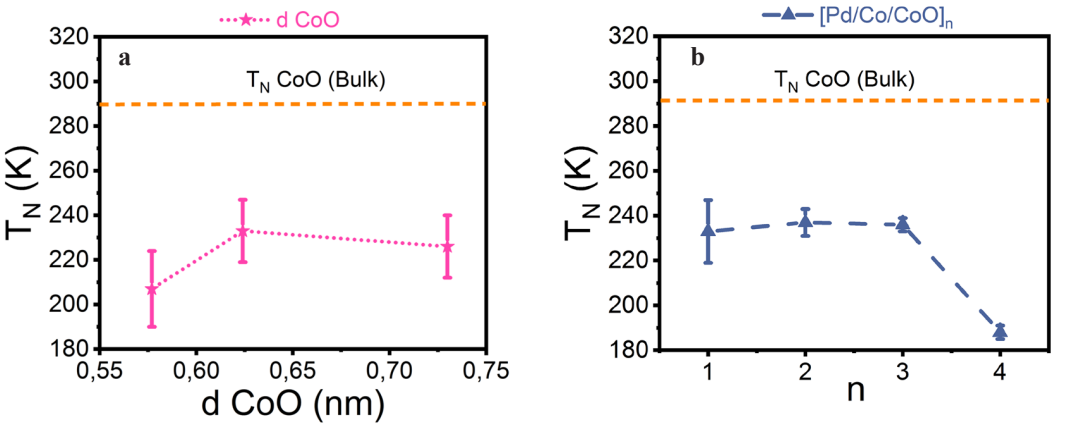

Figure 2. Dependences of the Neel temperature on the thickness *d* of CoO (**a**) and on the number of repetitions of trilayers *n* [Pd/Co/CoO] (**b**).

significantly affects the magnetic properties of a substance, for example, the transition temperature to a magnetically ordered state. In this regard, it would be reasonable to study the influence of the oxide thickness on the magnetic characteristics of these structures with temperature. The temperature dependences of the magnetization of all fabricated samples were studied. Based on the data obtained, it was found that the Neel temperature depends on the thickness of cobalt oxide and does not depend on the number of bilayers before $n = 4$ (Fig. 2). The blocking temperature was studied for two samples with different thicknesses of cobalt oxide (Fig. 3).

The possibility of the existence of an exchange bias perpendicular to the film plane in Pd/Co/CoO epitaxial structures with different CoO and [Pd/Co/CoO]n thicknesses, which are characterized by perpendicular magnetic anisotropy, is shown. The Neel temperature depends on the thickness of the Co oxide and does not depend on the number of repetitions before $n = 4$. It has been found that the blocking temperature increases significantly with increasing cobalt oxide thickness.

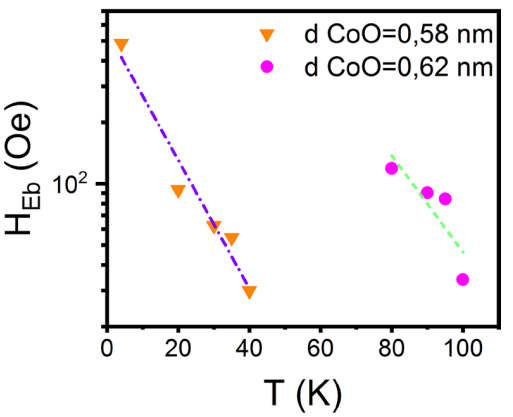

Figure 3. To search for the blocking temperature, two experiments were carried out with a small temperature step.

The work was carried out within the framework of the state assignment of the Institute of Chemistry, Far Eastern Branch of the RAS No. 0205 2021 1. This work has been supported by the grant of the Government of the Russian Federation for state support of scientific research conducted under supervision of leading scientists in Russian institutions of higher education, scientific foundations, and state research centers of the Russian Federation (Project No. 075-15-2021-607).

1. T.J. Moran, J.M. Gallego and I.K. Schuller, J. Appl. Phys. **78**(3), 1887–1891 (1995).
2. Kim, Gideok et al., Phys. Rev. Mater. **3**(8), 084420 (2019).
3. J. Nogues, I.K. Schuller, J. Magn. Magn. Mater. **192**(2), 203–232 (1999).

A.P47

STUDY OF MANETIC HETEROSTRUCTURES USING THE HARMONIC HALL VOLTAGE METHOD

A.S. Trushin[1*], *G.A. Kichin*[1], *K.A. Zvezdin*[1,2]

[1]New Spintronics Technologies, Russian Quantum Center, Skolkovo Innovation Center, Moscow, Russia
[2]Prokhorov General Physics Institute of the Russian Academy of Science, Moscow, Russia
[*]E-mail: a.trushin@nst.tech

Controlling the magnetization of nanodevices without utilizing the external magnetic fields is of great interest since this approach opens up wide opportunities for the development of new spintronic devices that can be integrated into classical electronic devices.

Magnetization can be controlled by using a spin-polarized current and/or by accumulating spin-polarized charges at the interface between a magnetic and non-magnetic material with a large spin-orbit coupling. Magnetization switching occurs either due to diffusion of the spin-polarized current or due to exchange coupling with accumulated spins.

Passing of a current through non-magnetic metal with strong spin-orbit coupling makes electrons become spin-polarized and thus causes the spin-polarized current, this effect is referred to as spin Hall effect. Alternately, the accumulation of spin-polarized electrons at the interface is caused by the Rashba-Edelstein effect.

In both cases, an effect similar to the presence of an additional "effective magnetic field" is observed, this field affects the magnetization vector of a sample. To evaluate this "effective magnetic field", the method of adiabatic (low-frequency) harmonic Hall voltage is used [1].

The magnetization dynamics is described by the Landau-Lifshitz-Gilbert equation:

$$\frac{\partial \hat{m}}{\partial t} = -\gamma \hat{m} \times \left(-\frac{\partial E}{\partial \vec{M}} + \Delta \vec{H} \right) + \alpha \hat{m} \times \frac{\partial \hat{m}}{\partial t}. \quad (1)$$

Here the effective field:

$$\Delta \vec{H} = a_J (\hat{m} \times \hat{p}) + b_J \hat{p}. \quad (2)$$

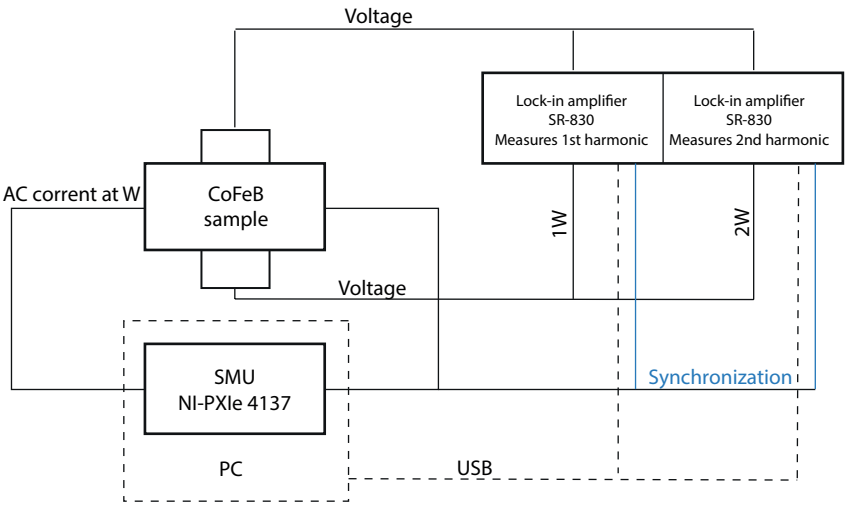

Figure 1. Scheme of the experiment.

The parameters a_J and b_J are called field-like and damping-like terms respectively, $\hat{p}$ is the direction of polarization of the upper layer of the structure. The harmonic Hall method is used for the effective measurement of these parameters.

In our work, we used this method to estimate the magnitude and direction of the effective field in magnetic heterostructures with different magnetizations. Among them, samples based on CoFeB were studied they are considered to be of significant interest due to the high spin polarization. The studied sample is a heterostructure of the following configuration: MgO(2)|CoFeB(2)|Ta(5)|Ru(5) (thickness in nm). The sample has an in-plane magnetization. We have obtained the above-mentioned parameters that match the previous studies [2, 3].

The scheme of the experiment is represented in Fig. 1.

The work was supported by the RSF No. 19-12-00432.

1. U.H. Pi et al., Appl. Phys. Lett. **97**, 162507 (2010).
2. M. Hayashi et al., Phys. Rev. B **89**, 144425 (2014).
3. H. Gamou, Y. Du, M. Kohda and J. Nitta, Phys. Rev. B **99**, 184408 (2019).

A.P48

SPIN-POLARIZED CURRENT IN MAGNETIC TUNNEL JUNCTION WITH NON-COPLANAR MAGNETIZED ELECTRODES

N.Kh. Useinov[1*], L.R. Tagirov[1,2]

[1]Department of Physics, Kazan Federal University, Kazan, Russia
[2]Zavoisky Physical-Technical Institute, FRC Kazan SC RAS, Kazan, Russia
[*]E-mail: nuseinov@mail.ru

In the past few years, when designing spintronic devices for storing and processing information, much attention has been paid to their energy efficiency. Therefore, the processes of magnetization reversal of magnetic nanostructures, in particular, magnetic tunnel junctions, which are used to implement such devices, are intensively studied [1]. Usually, it is proposed to use a heterostructure of two single-domain ferromagnetic layers separated by a dielectric nanolayer (tunnel barrier) as a magnetic tunnel junction (MTJ). In-plane rotation of magnetization of one of the ferromagnetic layers changes the resistance of such a heterostructure, and this change may be sufficient for practical use.

In this work, we study the regime of operation of the MTJ, when the magnetization of one of the ferromagnetic layers rotates on some arbitrary angle relative to the magnetization direction of the other ferromagnetic layer. To simulate the process of current flow through the MTJ, the quasiclassical theory is used in combination with a quantum-mechanical evaluation of the spin-dependent electron transmission coefficient through the potential barrier [2]. The main goal is to achieve the maximum change of the tunnel magnetresistance (TMR) upon rotation of the magnetization and under a voltage applied to the MTJ.

The quasiclassical theory of electron transport in magnetic tunnel junctions [2, 3] is generalized to calculate the dependence of the spin-polarized current I_α ($\alpha = \uparrow,\downarrow$ is the spin index) on the applied voltage to the MTJ and an arbitrary mutual orientation of magnetizations the magnetically hard FM^L and magnetically soft FM^R layers (see Fig. 1). The magnetization of the right FM^R layer can change its direction by some angle, which can be characterized by spherical angles (θ, φ). The polar angle θ is the angle between the z-axis and the direction of the magnetization vector $\mathbf{M}_R$, and the azimuthal angle φ is the one subtended with respect to the x-axis by the projection of the $\mathbf{M}_R$-vector onto the x-y plane.

Using the solutions of the Schrödinger equations for each MTJ-layer and the transfer matrix method [3], we calculate the spin-dependent transmission coefficients for conduction electrons at the non-coplanar angle between the magnetization directions. The expression for the spin-polarized current of the magnetic tunnel junction as a function of the angles θ, φ and the applied voltage V can be written as:

$$I_\alpha(V,\theta,\varphi) = \sum_{\alpha'} \frac{e^2 (k_{F,\alpha}^L)^2 A V}{4\pi^2 \hbar} \int_0^{\gamma_{cr}} \sin(\gamma_{L,\alpha})\cos(\gamma_{L,\alpha}) D_{\alpha,\alpha'}\left(V,\cos(\gamma_{L,\alpha}),\theta,\varphi\right) \mathrm{d}\gamma_{L,\alpha}\,, \quad (1)$$

where $k_{F,\alpha}^L$ is the Fermi wave vector in the FM^L-layer taking into account the spin polarization; A is the area of the contact; $\gamma_{L,\alpha} \in [0, \pi/2]$ is the polar angle determined by the electron trajectory towards the barrier in the left FM^L-electrode. The upper limit γ_{cr} is determined by the conservation law for the longitudinal components of the Fermi wave vectors at the each boundary between layers [2]. The transmission coefficient components $D_{\alpha,\alpha'}\left(V,\cos(\gamma_{L,\alpha}),\theta,\varphi\right)$ are calculated from the matrices of amplitudes of the wave functions in the three layers of MTJ: FM^L, FM^R and spacer. These matrices are coupled by linear equations. Taking into account the inclination of the quantization axis of spin-polarized conduction electrons leads to the dependence on the angles θ and φ.

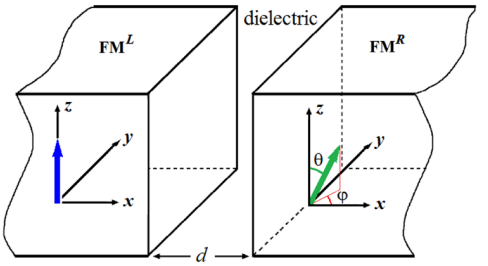

Figure 1. Schematic representation of the MTJ with a non-coplanar orientation of the magnetization of ferromagnetic FM^L- and FM^R-electrodes is shown. The direction of the magnetizations $\mathbf{M}_L$ and $\mathbf{M}_R$ are shown by bold arrows with the latter directed at a certain angle with respect to the other. The direction of $\mathbf{M}_R$ is determined by the angles θ and φ relative to the coordinate axes. Direction of the *x*-axis is perpendicular to the interfaces of the FM-electrodes. The thickness of the dielectric layer is *d*.

The spin-polarized current $I_\alpha(V,\theta,\varphi)$ for a symmetric magnetic tunnel junction was calculated at different angles θ and φ with the following parameters: the thicknesses of single-domain left FM^L and right FM^R ferromagnetic layers are arbitrary; spacer thickness, d = 2.0 nm; energy height of the barrier (spacer bandgap), U = 4.8 eV; the values of the Fermi wave vectors for the FM^L and FM^R layers were $k_{F\uparrow}$ = 1.1 Å^{-1}, $k_{F\downarrow}$ = 0.42 Å^{-1}; the effective masses of electrons of the FM layers were taken equal to the free-electron mass m_e, while the electron effective mass in the barrier, $m_{eff} = 0.4m_e$; the contact area was A = 4×4 nm^2, and the applied voltage V = 0.35 V.

Numerical calculations of the sum $I_\uparrow(V,\theta,\varphi) + I_\downarrow(V,\theta,\varphi)$ according to equation (1) show a strong dependence of the current $I(V,\theta,\varphi)$ on the applied voltage V in the range –1.0÷1.0 V and spin-dependent Fermi wave vectors $k_{F\uparrow}$, $k_{F\downarrow}$ in ferromagnetic layers. The TMR values obtained by calculating the magnetoresistance on the applied voltage and the angle between the magnetizations of the ferromagnetic layers in the MTJ are in qualitative agreement with the experimental data.

The work was supported by the Priority-2030 Program of Kazan Federal University.

1. A.A. Bukharaev, A.K. Zvezdin, A.P. Pyatakov, Yu.K. Fetisov, Phys. Usp. **61**, 1175–1212 (2018).
2. A.N. Useinov, H.-H. Lin, N.Kh. Useinov, L.R. Tagirov, JMMM **508**, 166729 (2020).
3. N.Kh. Useinov, A.P. Chuklanov, et al., Phys. of the Solid State **62**, 1706–1712 (2020).

A.P49

FERROMAGNETIC RESONANCE SPECTRA OF NANOCOMPOSITE METAL-DIELECTRIC FILMS

L.N. Kotov[1], *A.A. Utkin*[1*], *V.S. Vlasov*[1], *V.A. Ustyugov*[1], *M.P. Lasek*[1], *P.D. Kovalev*[1], *Yu.E. Kalinin*[2], *A.V. Sitnikov*[2]

[1]Syktyvkar State University, Syktyvkar, Russia
[2]Voronezh State Technical University, Voronezh, Russia
[*]E-mail: utych@yandex.ru

A great number of experimental and theoretic works today is devoted to research of magnetic characteristics of composite films and structures [1–5]. Created due to the newest nanotechnologies nanosized magnetic materials display unusual characteristics: giant magnetoresistance, intense magnetooptical response etc. [2–3]. This work is devoted to the research of ferromagnetic resonance (FMR) characteristics of the composite single layer films. The connection between the FMR and structural characteristics of the films was revealed.

The composite films were received in the argon atmosphere with pressure 0.04 Pa (A1-, B1-, B2-series), and with the addition of nitrogen with pressure 10^{-4} Pa (C1-, C2-series). The films were deposited on substrates of polyethyleneterephthalate by the ion-beam sputtering method using two targets: of ferromagnetic and dielectric. The chemical composition of the films was defined as relation of the atoms of the metal and dielectric by scanning electron microscope Tescan Mira 3. The compositions of the films were as following: $(Co)_x(SiO_2)_y$ (A1-series); $(CoFeB)_x(MgO)_y$ (B1-series); $(CoTaNb)_x(MgO)_y$ (B2-series), $(FeCoZr)_x(Zr_2O_3)_y$ (C1-series); $(FeCoZr)_x(Zr_2O)_y$ (C2-series) $0.2 < x < 0.7$.

The FMR-spectrum was obtained by an electron paramagnetic spectrometer RE-1306 on the frequency of 9.36 GHz with using a standard modulation index meter. The DC magnetic field was directed along the films plane. The alternating magnetic field was perpendicular to the DC field and also was directed along to the plane of the film.

The dependences of the FMR-field $\mu_0 H_{res}$ and width of line $\mu_0 \Delta H$ on the concentration x for 5 series of the films at temperature 300 K are shown in the Fig. 1.

For the interpretation of the experimental results the standard Kittel formula with average magnetization of the films $\langle M \rangle(x)$ for resonance field was used. The expression for ΔH taking into ac-

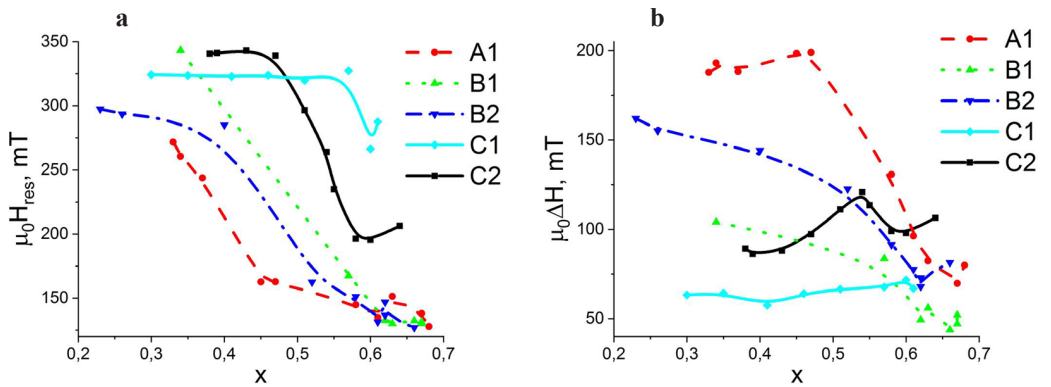

Figure 1. Dependences of the FMR field $\mu_0 H_{res}$ (**a**) and width of line $\mu_0 \Delta H$ (**b**) on the concentration x for 5 series of the films.

count the main summands caused by: ΔH_{dd} – the sum of inhomogeneity of internal magnetic fields, natural width of line ΔH_n – the magnetic losses in the granules, ΔH_a – the induced anisotropy of the film, ΔH_{SP} – spin-polarized relaxation. The contribution ΔH_{dd} by the authors of the article [6] was found with the using of the generalized Kittel's formula and performance for the metal particles as ellipsoid of rotation. Spin-polarized contribution ΔH_{SP} to width of line decreases monotonically with increasing x [7].

For composite films of series C1 we can see the weak dependence of FMR-field $\mu_0 H_{res}$ and width of line $\mu_0 \Delta H$ on the metal concentration x. Films of series C2 have the maxima on dependences $\Delta H(x)$. Maxima are well described by the equation for the $\Delta H(x)$ and caused by growth of magnetization field dispersion and line narrowing because of exchange interaction between granules. The resonance fields magnitudes for all film series (excluding series C1) decreases at increasing x (Fig. 1a) in agree with Kittel formula because $\langle M \rangle(x)$ is grown.

Research of influence of metal phase concentration x to FMR-properties of the composite films has been carried out. The data comparison of the curves of FMR-characteristics for the different series of the films was carried on. It is showed that the characteristics of FMR depend on magnetic interaction among magnetic granules in the composite layer and topology of nanogranules in composite layer. Based on the equations for the internal field and the FMR-width of line the qualitative changes in nanostructure are determined.

This work has been supported by Russian Science Foundation (project No. 21-72-20048).

1. B. Raneesh, P.M. Visakh, Metal Oxide Nanocomposites. Synthesis and Applications. Scrivener Publishing, USA, (2021).
2. A.B. Drovosekov, N.M. Kreines, A.S. Barkalova, S.N. Nikolaev, V.V. Rylkov, A.V. Sitnikov, JMMM **495**, 165875 (2020).
3. L.N. Kotov, M.P. Lasek, V.K. Turkov et al., Bull. Russ. Acad. Sci. Phys. **84**, 1065–1067 (2020).
4. S. Pokhrel, B. Waters, S. Felton et al., Phys. Rev. B **103**, 134110 (2021).
5. A. Talaat, M.V. Suraj, K. Byerly et al. J. Alloys and Comp. **870**, 159500 (2021).
6. A. Butera, J.N. Zhou, J.A. Barnard, Phys. Rev. B **60**, 12270 (1999).
7. L.V. Lutsev, Phys. Solid State **44**, 102–110 (2002).

A.P50

INVESTIGATION OF STRUCTURAL FEATURES OF THE SUPERCONDUCTING SPIN VALVE Fe/Nb/Fe

A.A. Validov, M.I. Nasyrova, R.R. Habibullin, I.A. Garifullin*

Zavoisky Physical-Technical Institute, FRC Kazan Scientific Center of RAS, Kazan, Russia
*E-mail: validov@kfti.knc.ru

In this project, new structures of superconducting spin valves are investigated, the operation of which is not based on the classical superconductor/ferromagnet proximity effect. The superconductor-ferromagnet interface is separated by an additional insulating layer. Indirect evidence of the possibility of observing the effect of a superconducting spin valve in such structures was shown in the Ref. [1].

Metallic layers were grown on the high-quality single crystalline MgO(001) substrates using classical e-gun in ultrahigh vacuum (UHV) conditions of about 10^{-9} mbar within a closed vacuum cycle. The evaporation chamber has a load-lock station, allowing us to avoid vacuum breaking before the substrate load. The thickness of the layers during the growth was controlled by a standard quartz-crystal monitor. All materials used for evaporation had a purity of better than 4N, i.e., the contamination level could be kept below 0.01 at.%. The substrates were fixed at a small rotating wheel on the sample holder. After that, the sample holder was placed inside the load-lock station. The rotating wheel system allows us to prepare a set of samples with varied thickness at the same evacuation cycle.

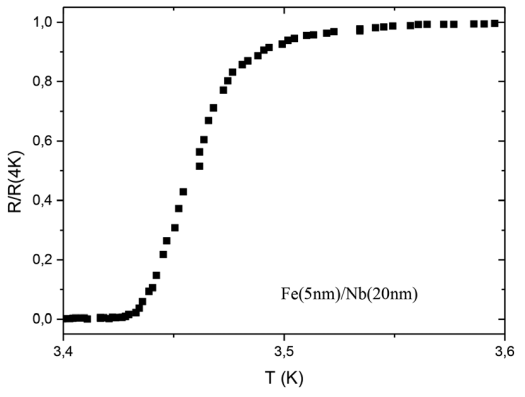

Figure 1. The transition of a superconductor from the normal to the superconducting state. The critical temperature is determined at the middle of the transition.

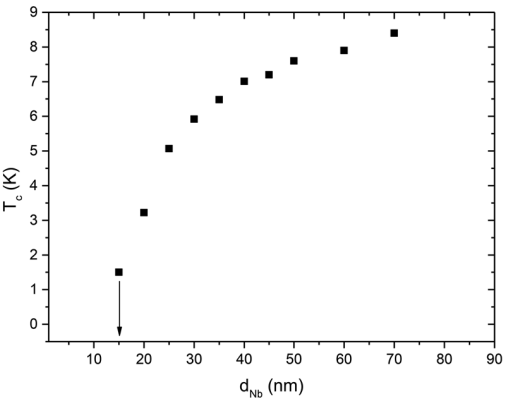

Figure 2. Temperature dependence of the transition to the superconducting state in the Fe(5 nm)/Nb system. Between the ferromagnet and the superconductor there is a non-magnetic layer 7 Å thick.

It was shown in the Ref. [2] that a so-called "dead" layer appears at the interface between iron and niobium. This is a non-magnetic region 7 Å thick. It is this property of the Fe/Nb interface that we decided to use to magnetically separate a ferromagnet and a superconductor. To initially determine the required layer thicknesses, a series of two-layer structures with a fixed iron layer thickness (5 nm) and various niobium layer thicknesses from 15 to 70 nm was fabricated. Figure 1 shows one of the normal-to-superconducting transitions measured to determine the superconducting transition temperature (T_c). Figure 2 shows the dependence of T_c on the thickness of niobium.

For us, the optimal thickness of the superconductor layer was approximately 30 nm. With such a thickness, the superconductor is already quite sensitive to the ferromagnetic layer, while T_c is still quite high, which facilitates the technical part of the research.

The next step will be the transition to the full structure of the spin valve, and further its optimization.

1. G. Deutscher and F. Meunier, Phys. Rev. Lett. **22**, 395 (1969).
2. Th. Mühge, K. Westerholt, H. Zabel, N.N. Garif'yanov, Yu.V. Goryunov, I.A. Garifullin, and G.G. Khaliullin, Phys. Rev. B **55**, 8945 (1997).

A.P51

EXCHANGE BIAS AND MAGNETIC ANISOTROPY OF FILM STRUCTURES BASED ON THE ANTIFERROMAGNET FeMn

V.O. Vaskovskiy[1,2], *A.A. Bykova*[1*], *A.N. Gorkovenko*[1], *M.E. Moskalev*[1]

[1]Ural Federal University, Ekaterinburg, Russia
[2]Institute of Metal Physics, UB RAS, Ekaterinburg, Russia
[*]E-mail: vladimir.vaskovskiy@urfu.ru

This work is devoted to the study of the temperature properties of the antiferromagnet FeMn, which provides the exchange bias effect in FeMn/$Fe_{20}Ni_{80}$ films. This phenomenon consists in the effective pinning of the magnetization of the ferromagnetic layer (in our case $Fe_{20}Ni_{80}$) on account of its exchange interaction with the antiferromagnetic layer and provokes an increased interest in connection with practical applications in the fields of magnetoelectronics and spintronics [1].

The experiment was conducted on glass/Ta(5)/$Fe_{20}Ni_{80}$(5)/FeMn(L)/$Fe_{20}Ni_{80}$(40) films deposited by magnetron sputtering. The purpose of Ta and $Fe_{20}Ni_{80}$ 5 nm thick buffer layers (thicknesses of corresponding layers are given in nm in parentheses of the structural formula) was to promote the formation of the necessary face-centered cubic crystal structure and the (111)-texture in the FeMn layer. The thickness of the antiferromagnetic layer ranged between 3÷20 nm. Measurements of magnetic properties, which consisted in determining the exchange bias field H_e of hysteresis loops of a $Fe_{20}Ni_{80}$(40) layer, were performed in accordance with the York protocol [2] with a help of a PPMS Dynacool in a temperature range T = 25÷400 °C. The dependences of $H_e(T)$ for films with different thicknesses of antiferromagnetic FeMn layers are shown in Fig. 1a. It shows that as the thickness L decreases the average blocking temperature T_b, determined as an interception of the temperature axis, decreases monotonically. This is due to a decrease in the average size of antiferromagnetic crystallites and increasing role of thermal fluctuations destabilizing the magnetic structure of the antiferromagnet.

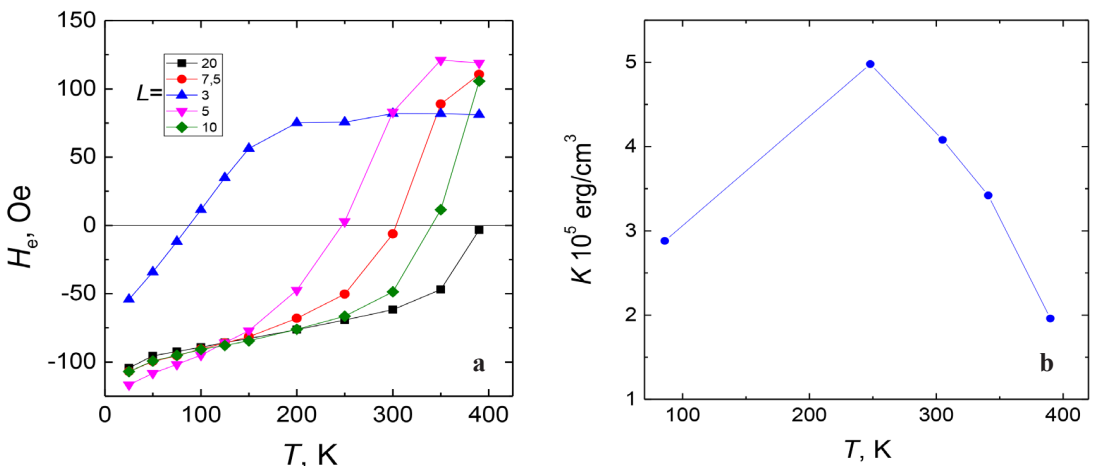

Figure 1. **a** The exchange bias field H_e as a function of temperature T for a FeMn/$Fe_{20}Ni_{80}$ film with thicknesses of FeMn ranging from 3 to 20 nm. **b** Temperature dependence of the anisotropy constant K of the antiferromagnetic FeMn layer.

Data analysis was based upon the well-known relationship between magnetic anisotropy energy and energy of thermal fluctuations $KV = CkT_b$, where K – anisotropy constant, k – Boltzmann's constant, V – grain volume, C – dimensionless constant that takes into account relaxation effects [2], the value of which in our case was 40. This equation allows to estimate the value of K for different blocking temperatures T_b and thus find its temperature dependence. Estimation results are shown in Fig. 1b. The work gives justification for the used model approximations and presents a qualitative interpretation of the temperature dependence of the magnetic anisotropy constant of the antiferromagnet FeMn.

This work was financially supported by the Ministry of Science and Higher Education of the Russian Federation, project № FEUZ-2020-0051.

1. F. Radu, H. Zabel, Magnetic Heterostructures. Springer, 97 (2008).
2. K. O'Grady, L.E. Fernandez-Outon, G. Vallejo-Fernandez, JMMM **322**, 883 (2010).

A.P52

ANGULAR AND TEMPERATURE DEPENDENCES OF FERROMAGNETIC RESONANCE IN EXCHANGE-COUPLED FeNi/Dy/FeNi PLANAR STRUCTURES

R.S. Iskhakov, I.G. Vazhenina, V.Y. Yakovchuk*

Kirensky Institute of Physics, Federal Research Center KSC SB RAS, Krasnoyarsk, Russia
*E-mail: irina-vazhenina@mail.ru

Planar three-layer structures "ferromagnetic material/interlayer/ferromagnetic material" were studied by ferromagnetic and spin-wave resonance methods in a wide temperature range. The three-layer films were obtained by the vacuum-evaporation technique (10^{-6} mm Hg). The layers $Fe_{20}Ni_{80}$ and Dy were successively sputtered on glass substrates from unrelated vapor sources with a ring-shaped cathode. The thickness of every ferromagnetic layer is about 70 nm, and the thickness of the Dy layer is about 5, 10 and 15 nm. Microwave absorption spectra were measured using the equipment of the Krasnoyarsk Regional Center of Research Equipment of the Federal Research Center "Krasnoyarsk Science Center SB RAS" (spectrometer ELEXSYS E580, Bruker, Germany). The resonator pumping frequency was $f = 9.2$ GHz. The angular dependences were measured with changing the angle between the direction of constant magnetic field and the film normal. When the temperature measurements in the range from 4 to 300 K were carried out, the constant magnetic field was applied in the plane of the film. Microwave absorption curves were divided into individual peaks using the differential Lorentz function.

The aim of our work is to study the effect of the magnetic state of the Dy-layer of the three-layer system on the parameters of the effective exchange coupling of the ferromagnetic layers.

The experimental FMR-spectra in the whole range of temperatures and angles show a complex structure and demonstrate an excitation of the exchange-coupled oscillations on the form of acoustic and optical modes (Fig. 1).

The temperature dependences of the interlayer exchange interaction constant J_{12}, the values of which were detected from experimental microwave spectra [1], have a set of the features. These are the sign change $J_{12}(-|J_{12}| \rightarrow |J_{12}|)$ and the extremum point on the curve $J_{12}(T)$. We believe that

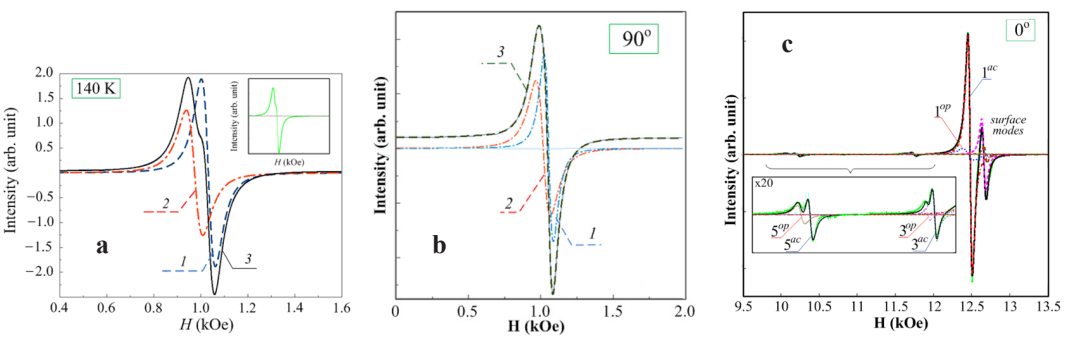

Figure 1. The experimental microwave spectra for films with the thickness of Dy equal 5 nm at 140 K (**a**), the thickness of Dy equal 10 nm at the room temperature and $\theta_H = 90°$ (**b**) and $\theta_H = 0°$ (**c**). Curves 1 and 2 are acoustic and optical modes, curve 3 is the fitting curve. The experimental curve is shown in the inset.

the behavior of the dependence $J_{12}(T)$ reflects the transformations of the magnetic structure of the Dy. The values of effective magnetization M_{eff}, exchange interaction constant A, surface anisotropy constant K_S and perpendicular anisotropy field were also defined from the angular dependences of the resonance fields.

Support by RFBR, Krasnoyarsk Territory and Krasnoyarsk Regional Fund of Science, project number 20-42-240010 is acknowledged.

1. Z. Zhang, L. Zhou, P.E. Wigen, K. Ounadjela, Phys. Rev. B **50**, 6094–6112 (1994).

A.P53

SPIN LIGHT-EMITTING DIODE WITH INTENSITY CONTROL

*M.V. Ved**, *M.V. Dorokhin, A.V. Zdoroveyshchev, P.B. Demina, D.A. Zdoroveyshchev, Yu.A. Dudin, V.E. Kotomina*

Research Institute for Physics and Technology of UNN, Nizhny Novgorod
*E-mail: mikhail28ved@gmail.com

The functional combination of the basic elements of spintronics (a magnetoresistive element and a spin light-emitting diode) is an urgent task. This will allow obtaining one of the four stable states for one cell, which will at least double the information capacity of spintronic devices. In the field of research of a combined magnetoresistive element and a light-emitting diode, several works can be mentioned. Some examples are [1, 2], in which structures that combine various elements of electronics and spintronics were studied. The structures studied in the cited papers are the schemes of a low integration level with the intensity of the optical signal be controlled by an external magnetic field. In this paper, we report on a device with an independent variation of both the emission intensity and degree of circular polarization carried out by applying external magnetic fields.

A magnetoresistive spin light-emitting diode is a combination of an emitting part based on a heterostructure with an InGaAs/GaAs quantum well (QW) with a CoPd spin injector and a spin valve consisting of Cr/Co90Fe10/Cu/Co90Fe10 layers connected in series. The semiconductor part of the studied structure was formed on the n-GaAs substrate by the MOCVD method in a hydrogen flow. The CoPd ferromagnetic injector and the magnetoresistive element were formed by electron beam evaporation in vacuum. At the final stage, using photolithography and chemical etching, contacts of a special shape were formed on the surface of the structures. The base contact to the substrate was formed by sparking of Sn foil. The device was powered in the current source mode. Figure 1 shows a scheme of a combined device. For the electrical insulation of the semiconductor structure around the mesa contacts, the parts of the structure, uncovered by the contacts, were bombarded with He^{++} ions before applying magnetoresistive layers [3].

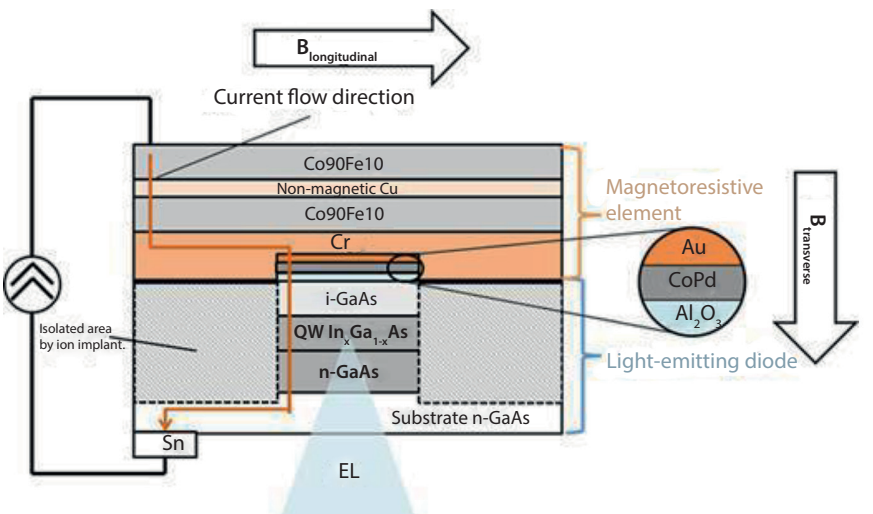

Fig. 1. Combined device scheme.

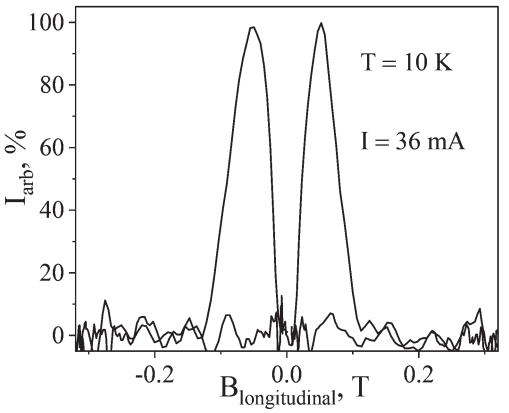

Figure 2. Magnetic field dependence of the relative emission intensity for a combined device.

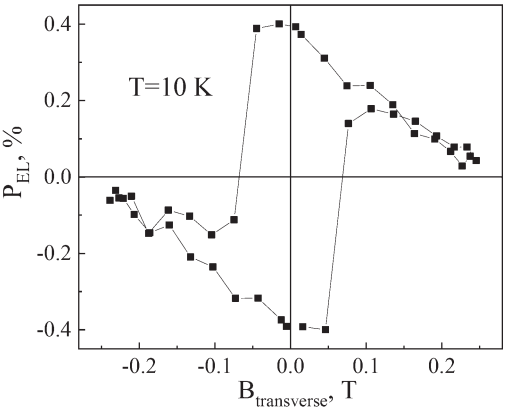

Figure 3. Magnetic field dependence of PEL for a combined device.

Figure 2 shows the magnetic field dependence of the relative electroluminescence intensity of the device. The observed EL intensity change is due to a change of the resistance for the magnetoresistive contact layer. It should be noted that at a current of 36 mA, the structure operates in the key mode: in a magnetic field of ±50 mT, the relative intensity takes on maximum values; in zero magnetic field, as well as in a field above 100 mT it is zero. The most probable mechanism for increasing the EL intensity of such a combined device in the longitudinal magnetic field is presented in [4].

When the magnetoresistive spin light-emitting diode is introduced into a transverse magnetic field, the EL becomes partially circularly polarized. The degree of circular polarization of EL is calculated by the formula:

$$P_{\mathrm{EL}} = \frac{I_1 - I_2}{I_1 + I_2} \times 100\%,$$

where I_1 and I_2 are the relative EL intensities measured for light polarized along the left and right circles respectively. Figure 3 shows the magnetic field dependence of the circular polarization degree of EL. The maximum PEL value was 0.4%. The linear slope in magnetic fields greater than 0.1 mT (in absolute value) is presumably related to the Zeeman splitting of energy levels in the QW.

As a result, we have fabricated a laboratory sample that operates not in two controlled states corresponding to a logical zero and one (high and low intensity or right- and left-circularly polarized emission), but four independently variable states (high intensity with right- and left-circularly polarized emission and low intensity with right- and left-circularly polarized emission).

The work was supported by the Ministry of Science and Higher Education of the Russian Federation (the federal academic leadership program "Priority 2030" and the basic part of the state assignment No. 0729-2020-0060).

1. I. Appelbaum, K. Russel, D. Monsma, V. Narayanamurti, C. Marcus, M. Hanson, A. Gossard, Appl. Phys. Lett. **83**, 4571 (2003).
2. D. Saha, D. Basu, P. Bhattacharya, Appl. Phys. Lett. **93**, 194104 (2008).
3. J. De Souza, I. Danilov, H. Boudinov, Appl. Phys. Lett. **68**(4), 535 (1996).
4. M. Ved, Yu. Danilov, P. Demina, M. Dorokhin, Yu. Dudin, V. Kotomina, S. Kudrin, Yu. Kuznetsov, S. Zdoroveyshchev, D. Zdoroveyshchev, Appl. Phys. Lett. **118**, 092402 (2021).

A.P54

INTERFACE-ENHANCED DMI INTERACTION IN Pt/Co/Ta HETEROSTRUCTURES

V.D. Bessonov[1*], *J.H. Park*[2,3], *T.H. Kim*[2], *G.W. Kim*[2], *A.V. Telegin*[1], *V.S. Teplov*[1], *I.G. Iliushin*[4], *A.A. Pervishko*[5], *D. Yudin*[5], *A.V. Ognev*[4], *A.S. Samardak*[4], *J.U. Cho*[6], *Y.K. Kim*[2]

[1]M. N. Miheev Institute of Metal Physics UB of RAS, Ekaterinburg, Russia
[2]Department of Materials Science and Engineering Korea University, Seoul, Korea
[3]Semiconductor R&D Center, Samsung Electronics Co. Ltd., Hwaseong, Gyeonggi-do, Korea
[4]Far Eastern Federal University, Vladivostok, Russia
[5]Skolkovo Institute of Science and Technology, Moscow, Russia
[6]Western Seoul Center, Korea Basic Science Institute, Seoul, Korea
[*]E-mail: bessonov@imp.uran.ru

Magnetic multilayers consisting of nonmagnetic normal metal/ferromagnet stacks are a host of the interfacial Dzyaloshinskii-Moriya interaction (DMI) induced because of the broken inversion symmetry and strong spin-orbit coupling of the heavy metal layer [1]. The study of the microscopic nature of DMI is subject to extensive scientific attention because this antisymmetric exchange interaction is capable of stabilizing nontrivial chiral spin textures such as skyrmions and skyrmioniums [2]. As is known, in magnetic heterostructures, bulk DMI coexists with conventional interfacial DMI contributing to the chiral magnetic behavior of the system [3].

We investigated the evolution of DMI in Pt/Co heterostructures modulated by Pt-Co alloy with various compositions, including the graded $Pt_{75}Co_{25}/Pt_{50}Co_{50}/Pt_{25}Co_{75}$ and homogeneous $Pt_{50}Co_{50}$ (in at.%) layers.

We used Brillouin light scattering spectroscopy (BLS) to estimate and separate the interfacial and bulk DMI contributions for all samples [4]. Samples with a gradual Pt-Co alloy show a higher DMI value (59.3% increase relative to a homogeneous sample without any alloy layer). From the microstructural analysis, we confirmed that the structure of face-centered cubic (111) Pt is well established and concluded that the net DMI has interfacial and compositional gradient (bulk) origins. From the first-principles *ab-initio* calculations, we also demonstrated that the DMI originates from both interlayer and intralayer interactions in the structures. While the bulk DMI strengths are nearly the same for all samples (~0.2 mJ/m^2), the sample inserted with a gradual Pt-Co alloy showed a significant enhancement (22% increase relative to homogeneous sample) in the DMI value. On the contrary, the sample with a single Pt-Co alloy had a slight decrease (8.5% drop relative to the homogeneous sample) in the DMI value. It was supposed that the $Pt/Pt_{75}Co_{25}/Pt_{50}Co_{50}/Pt_{25}Co_{75}$ structure can be considered as a system with a gradient distribution of elements, where contributions are manifested both from the interaction of atoms in one layer (bulk-DMI) and the enhanced interfacial DMI between atoms in neighboring layers. The proposed approach can be used to realize the so-called "all-interface-bulk" DMI metamaterials [5]. In such metamaterials, the controllable spatial composition will allow for manipulating the distribution of DMI vectors in three dimensions, which contributes to the design of future spin-orbitronics devices, especially skyrmion-based.

Support of the Russian Science Foundation (grant № 21-72-20160) and NRF of Korea grant funded by the MIST (2020M3F3A2A01082591) and Samsung Electronics Co. (IO201211-08104-01) is acknowledged. A.S.S. acknowledges the Russian Ministry of Science and Higher Education under the state task (Project 0657-2020-0013) and the megagrant (Project 075-15-2021-607).

1. A. Manchon et al., Solid State Physics, Academic Press (2017).
2. A. Fert et al., Nat. Rev. Mat. **2**, 17031 (2017).
3. D.H. Kim, M. Haruta, H.W. Ko et al., Nat. Mater. **18**, 685–690 (2019).
4. R.W. Damon, J.R. Eshbach, J. Phys. Chem. Solids **19**, 308-320 (1961).
5. L. Fallarino, B.J. Kirby, E.E. Fullerton, J. Phys. D: Appl. Phys. **54**, 303002 (2021).

A.P55

CHIRALITY-DEPENDENT SPIN-TRANSFER TORQUE AND CURRENT-INDUCED SPIN ROTATION IN HELIMAGNETS

*V.V. Ustinov**, *I.A. Yasyulevich*

Institute of Metal Physics, Ekaterinburg, Russian Federation
*E-mail: ustinov@imp.uran.ru

In [1], the authors of the present paper developed a theory of the electrical resistance of a helical magnet subjected to an electric current along the axis of the magnetic spiral. It was shown that, when acting on the spin of conduction electrons, an inhomogeneous exchange field induced by the magnetic moments of localized electrons that form a magnetic spiral causes an increase in the electrical resistance of the helimagnet. This result is obtained under the assumption that the electric current flowing through the helimagnet does not affect the helimagnet's magnetic system.

In [2], we constructed a theory of the Spin Transfer Torque effect (STT) in helical magnets. We demonstrated that spins of conduction electrons that create electric and spin currents along the axis of the helimagnet make its magnetic spiral rotate. To describe the magnetization dynamics of localized electrons, we used the Landau-Lifshitz-Gilbert equation. The dynamics of the magnetization of conduction electrons was expressed through the Bloch-Torrey equation. To take into account the electromagnetic field generated by the magnetization rotation, we supplemented the set of the Landau-Lifshitz-Gilbert and Bloch-Torrey equations by Maxwell's equations. It was shown that, at low currents, the rotation frequency of the helimagnet's spin spiral due to the STT effect can be defined by a simple formula:

$$\omega = \frac{\Gamma}{\alpha_{\text{eff}} + \Gamma}(\mathbf{q} \cdot \mathbf{w}). \tag{1}$$

Here $\mathbf{w}$ is a drift velocity of itinerant electrons; $\mathbf{q}$ is the wave vector of the magnetic helicoid, α_{eff} is the effective Gilbert damping parameter that takes into account the losses due to the emission of electromagnetic waves by the helimagnet. The parameter $\Gamma = \chi\Lambda\Omega_{\text{HM}}/\nu_{\text{eff}}$ is a dimensionless quantity characterizing the efficiency of the SST process in the helimagnet; χ is the Pauli susceptibility of a conduction electron gas, Λ is a dimensionless parameter characterizing the magnitude of the s-d exchange interaction, $\Omega_{\text{HM}} = \gamma\Lambda M$, γ is the gyromagnetic ratio, M is the magnitude of the magnetization of localized electrons, ν_{eff} is the effective rate of spin relaxation in a helimagnet. In helimagnets $\nu_{\text{eff}} = \nu_{\text{S}} + \nu_{\text{D}} + \nu_{\text{L}}$, where ν_{S} is the spin-lattice relaxation rate, ν_{D} is the "spin-diffusion" relaxation rate, ν_{L} is the "spin-precession" relaxation rate [1].

The present work emphasizes that the electrical resistance contribution arising from the deceleration of the electron flow by an inhomogeneous helical magnetic exchange field decreases conditional upon an electric current produces the helimagnet magnetization spiral rotation due to the STT effect. If there is no external magnetic field, the electrical resistance of a helimagnet is given by:

$$\rho = \rho_{\text{FM}} + \rho_{\text{HM}}\left(1 - \frac{\Gamma}{\alpha_{\text{eff}} + \Gamma}\right), \tag{2}$$

where ρ_{FM} is the electrical resistance of the magnet in the field of transition to the ferromagnetic state,

$$\rho_{\text{HM}} = \frac{\chi}{\nu_{\text{eff}}}\left(\frac{q\Lambda M}{eN_0}\right)^2$$

is the magnitude of the chiral magnetoresistance in the limit of small measuring currents and without spiral rotation, e is the electric charge of an electron, N_0 is the equilibrium value of the electron density.

Equation (1) implies that at the same drift velocity of electrons in helimagnets with a small Gilbert damping parameter ($\alpha_{eff} \ll \Gamma$), the rotation frequency is higher than in those with a significant value of the Gilbert damping parameter ($\alpha_{eff} \gg \Gamma$). Equation (2) shows that in the first case, the helicoid rotates without almost decelerating the electron flow in an inhomogeneous exchange field. In the second case, the helicoid rotates in such a way that the deceleration of the electron flow is close to that by an immovable helicoid. The parameter Γ of the order of 10^{-2} is typical for metallic helimagnets.

The present work also evaluates the influence of rotation of the helimagnet magnetization spiral on the Stern-Gerlach kinetic magnetoelectric effect. The kinetic magnetoelectric Stern-Gerlach effect is the effect of the emergence of non-equilibrium magnetization of conduction electrons along the spiral axis, with the magnetization being proportional to the applied current. It is shown that if an electric current flowing through a helimagnet causes the magnetization spiral to rotate, the magnitude of the non-equilibrium magnetization of conduction electrons decreases along the spiral axis. The drop in the non-equilibrium magnetization of conduction electrons along the spiral axis is similar to the above described decrease in the contribution to the resistance arising from the deceleration of the electron flow in an inhomogeneous exchange magnetic field.

This work has been carried out under the financial support of the Russian Science Foundation within the framework of project № 22-22-00220.

1. V.V. Ustinov and I.A. Yasyulevich, Phys. Rev. B **102**, 134431 (2020).
2. V.V. Ustinov and I.A. Yasyulevich, (2022), to be published.

FORMATION OF A DILUTED MAGNETIC SEMICONDUCTION PHASE BY THERMAL DIFFUSION IN THE METHOD OF PULSED LASER DEPOSITION

Yu.M. Kuznetsov[1*], *M.V Dorokhin*[2], *R.N. Kryukov*[1], *A.V. Zdoroveyshchev*[1], *V.P. Lesnikov*[1], *D.A. Zdoroveyshchev*[1,2]

[1]Scientific Research Institute of Physics and Technology of Lobachevsky State University, Russia, Nizhny Novgorod
[2]Lobachevsky State University, Russia, Nizhny Novgorod
[*]E-mail: yurakz94@list.ru

One of the main directions in the development of modern microelectronics is spintronics, which device implementation requires dilute magnetic semiconductors with both semiconductor properties and ferromagnetic ordering at room temperatures. The most promising are diluted magnetic semiconductors of the A_3B_5 group doped with atoms of transition elements. In this paper, we consider a method for obtaining the dilute magnetic semiconductor phase doped with Fe and Mn atoms.

A series of structures of various compositions was formed on a semi-insulating gallium arsenide (100) substrate by pulsed laser deposition (PLD).

The target was a 1×1 cm^2 metal plate made of Fe-Mn-C alloy. To control the ratio of the components on the target, an additional sector of high-purity manganese or iron was introduced (Table 1). Sputtering time was 30 minutes, substrate temperature was 500 °C.

Table 1. List of studied structures.

№	Target
1	Fe ~ 100% Mn ~ 0.00% C ~ 0.0%
2	Fe ~ 86.0% Mn ~ 13.0% C ~ 1.0%
3	Fe ~ 82.4% Mn ~ 16.7% C ~ 0.9%
4	Fe ~ 78.8% Mn ~ 20.3% C ~ 0.9%

The magnetic properties of the structures were studied by measuring and analyzing the magnetic field dependence of the Hall resistance, which is proportional to the perpendicular component of the thin film magnetization. Information about the chemical composition was obtained by X-ray photoelectron spectroscopy, supplemented by an ion etching technique.

Figure 1a shows the magnetic field dependences of the Hall resistance of the studied structures. The curves are marked with structure numbers (Table 1). In all of the samples a nonlinearity of the magnetic field dependence is detected, this confirms the presence of magnetic ordering in the studied films. The presence of a loop in the magnetic field dependence of the Hall resistance is obtained within structure 3 (Fig. 1a, curve 3). Figures 1b-e show the measured distribution profiles of chemical elements over depth in structures 1–4 respectively. It can be seen that the concentration profiles are “smeared”, while the presence of Fe and Mn atoms is recorded in the GaAs bulk at a relatively large distance from the boundary. The latter is associated with the diffusion of transition elements in GaAs, which obviously occurs during film formation and takes place in all structures, regardless of the target composition. Presumably, diffusion leads to the formation of $GaFe_x$ [1] and $FeAs_y$ [2], MnAs [3] phases.

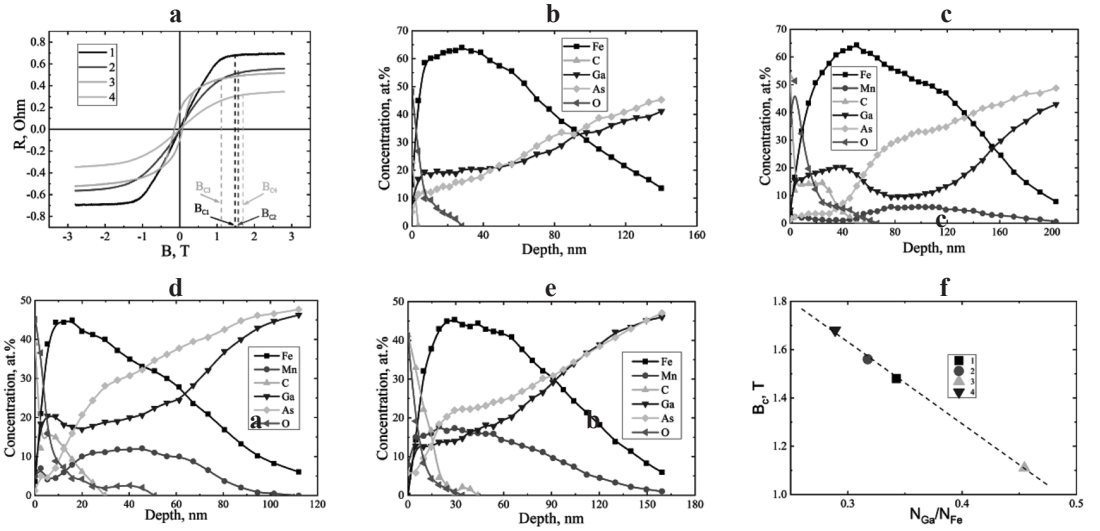

Figure 1. **a** Magnetic field dependence of the Hall resistance, **b**–**e** distribution profiles of chemical elements in structures 1–4 respectively, **f** – experimental dependence of B_c on the concentration ratio of gallium and iron atoms.

The form of the magnetic field dependence of the Hall resistance measured in the experiment is a superposition of the effects from the above phases. We also note that an increase in the Mn concentration leads to a significant change in the nature of the distribution profiles of chemical elements over the depth of the film. An increase in the manganese concentration leads to the appearance of the MnAs phase, which is accompanied with the presence of hysteresis in the magnetic field dependence of the Hall resistance (structure 3). A further increase of manganese leads to the fact that the concentration of MnAs inclusions in structure 4 is become quite high, which causes the coalescence of these inclusions (structure 4).

Figure 1f shows the calculated dependence of B_c on the ratio of the average concentration of gallium (N_{Ga}) and iron (N_{Fe}) atoms in the film. The dependence is linear, which means that the characteristics of the magnetic field dependence of the Hall resistance are determined by the Ga and Fe diffusion mixing during film deposition. Similar results were obtained in [4], where the magnetic properties of GaFe were considered.

The work demonstrates the presence of iron and manganese atoms diffusion into the GaAs substrate during the growth of the Fe-Mn-C alloy film by the PLD method. Diffusion causes mixing of film and substrate materials. It is assumed that the characteristic form of the magnetic field dependence of the Hall resistance is determined by the ratio of the concentrations of gallium and iron in the Ga_xFe_y phase. An increase in the manganese concentration and a decrease in the iron concentration in the sputtered target lead to the formation of a MnAs compound. The presence of this phase in the film leads to the appearance of a hysteresis loop in the magnetic field dependence of the Hall resistance.

The work was supported by the RFBR grant (20-32-90032).

1. B.K. Kuanr, R.E. Camley, Z. Celinski et al., J. Appl. Phys. **115**, 17C112 (2014).
2. K.A. Ziq, A.F. Salem, J. Supercond. Nov. Magn. **26**, 1185 (2013).
3. L. Daweritz, Rep. Prog. Phys. **69**, 2581 (2006).
4. V.A. Lukshina, D.A. Shishkin, A.R. Kuznetsov et al., Phys. Solid State **62**, 1746 (2020).

A.P57

HALF-METALLIC PROPERTIES OF THE Rh_2FeZ ALLOYS

*D.R. Baigutlin**, *V.V. Sokolovskiy, V.D. Buchelnikov*

Chelyabinsk State University, Chelyabinsk, Russia
*E-mail: d0nik1996@mail.ru

Half-metallic ferromagnets are a class of materials with 100% spin polarization on the Fermi level. They have attracted recently a lot of interest due to their possible applications in spintronics area [1]. Many double perovskites, $C1_b$ compounds, and Heusler compounds have half metallic behavior [2].

The first half-metallic ferromagnet among the Heysler alloys NiMnSb was predicted by de Groot et al. in 1983 [3]. The most studied half metall full Heusler alloys are based on the 3d element Mn and Co [2]. Alloys based on other 3d transition metals such as Ti, V, Cr, Fe, Ni are also quite well investigated [2]. On the contrary, there is much less information about half metals feromagnets containing 4d transition elements. Among these alloys, some Zr_2-based alloys with 3d Y elements Zr_2YZ (Y = V, Cr, Co, Ni; Z = B, Al, Ga, In, Si, Ge, Sn, Pb) are studied for $L2_1$ and X_A structure [4, 5]. In thus works have shown that X_A structure are energetically preferable for all compounds, except Zr_2VX. At the same time, the electronic structure corresponds to the half metallic state for XA structure and usual metall for $L2_1$ structures. In the work [6] yttrium-based full-Heusler alloys Y_2CrZ (Z = Al, Ga, In) was investigated using *ab-initio* methods. The authors found that the ground state for Y_2CrZ is ferromagnetic with half metallic properties. The origin of the band gap is d-d hybridization between Y and Cr atoms and the band gap is stable over a wide pressure range.

Calculations were performed using the density functional theory approach with the projector augmented-wave method as implemented in the Vienna Ab initio Simulation Package [7]. The Perdew, Burke, and Ernzerhof (PBE) parametrization [8] of the GGA and the SCAN meta-GGA [9] were used for treating exchange correlation effects. The k-points grid density of ≈5000 k-points per reciprocal lattice was considered for the calculations.

First, we consider the geometry optimization of stoichiometric Rh_2FeZ (Z = Al, Si, Ga, Ge, In, Sn) with regular and inverse Heusler structure considering ferromagnetic (FM) and two types of antiferromagnetic (AFM) orders as illustrated. Total energy as a function of the lattice constant calculated using PBE and SCAN is presented in Fig. 1, respectively. Interestingly, the FM solution is uniquely advantageous for elements of the third main group, while the FM minimum is almost

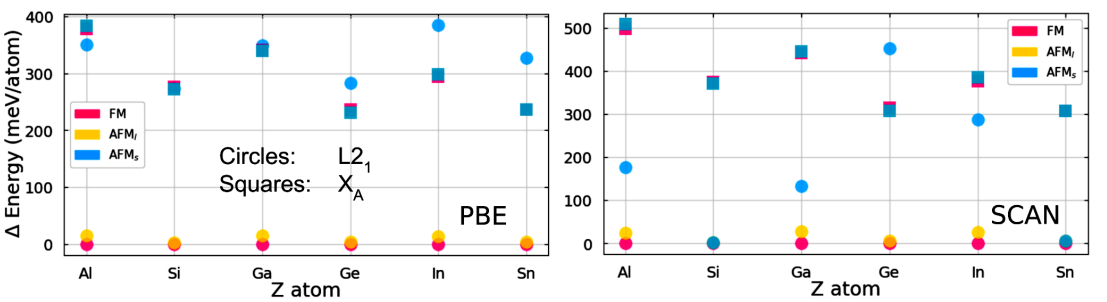

Figure 1. The total energy difference (ΔE) as a function of the lattice parameter of Rh_2FeZ (Z = Al, Si, Ga, Ge, In, Sn) for PBE and SCAN solutions. For each cases, the ΔE is plotted with respect to the $L2_1$ lattice with FM minimum.

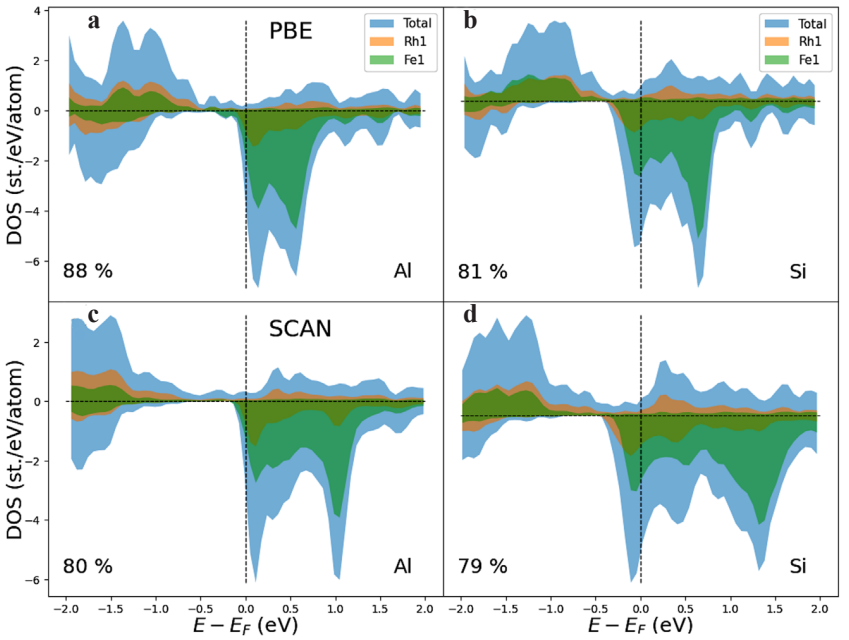

Figure 2. Total and partial DOSs for Rh_2FeAl and Rh_2FeSi calculated by PBE (**a**, **b**) and SCAN (**c**, **d**) at their equilibrium volumes.

degenerate with the AFM minimum for elements of the fourth group for both the GGA and SCAN. In addition, the possibility of martensite transition was estimated. For third group elements, only one austenitic minimum is observed. Fourth main group elements have two energy minima for both FM and AFM states.

To study the electronic properties of the alloys, we constructed full and orbital DOS and calculated the degree of polarization at the Fermi level. The Rh_2FeZ alloys for Z = Al, Ga, Ge and for Z = Si, Ge, Sn are not true half-metall, but the Fermi level for the additional elements of the third group is much closer to the pseudo-gap than for fourth main group elements. Both PBE and SCAN in this case predict similar results, except that SCAN slightly increases the pseudo band gap width. Achieving 100% spin polarization at the Fermi level is possible due to the introduction of chemical disorder, external pressure, or surface effects. In addition, the DOS shows strong hybridization between 3d Fe electrons and 4d Rh electrons, this mechanism of pseudo-gap formation differs from the 3d X_2YZ Heisler alloys, where the decisive role is played by the X-element.

The research was supported by the RSF – Russian Science Foundation project No. 22-12-20032.

1. I. Zutic, J. Fabian, and S.D. Sarma, Rev. Mod. Phys. **76**(2), 323 (2004).
2. C. Felser, G.H. Fecher, and B. Balke, Angew. Chem. Int. **46**(5), 668–699 (2007).
3. R.A. Groot, F.M. Mueller, P.G. Engen, and K.H.J. Buschow, Phys. Rev. Lett. **50**(25), 2024 (1983).
4. D. Amari, M. Mokhtari, F. Dahmane et. al., Chinese J. Phys. **60**, 450–461 (2019).
5. Z.Y. Deng and J.M. Zhang, J. Magn. Magn. Mater. **397**, 120–124 (2016).
6. X.H. Kang and J.M. Zhang, Solid State Commun. **264**, 19–25 (2017).
7. G. Kresse, D. Joubert, Phys. Rev. B **59**, 1758 (1999).
8. J. Perdew, K. Burke, M. Ernzerhof, Phys. Rev. Lett. **77**, 3865 (1996).
9. J. Sun, A. Ruzsinszky, J.P. Perdew, Phys. Rev. Lett. **115**, 036402 (2015.

A.P58

FIRST PRINCIPLE STUDY OF HALF-METALLIC CONNECTIONS ON THE BASIS OF HEUSLER ALLOY Fe_2RhSi

*K.R. Erager**, *D.R. Baigutlin, V.V. Sokolovskiy, V.D. Buchelnikov*

Chelyabinsk State University, Chelyabinsk, Russia
*E-mail: eragerk@rambler.ru

Half-metallic ferromagnetic materials are the most interesting class of materials because they exhibit an electronic structure in which one spin direction has metallic behavior and the other exhibits semiconducting behavior. A feature of this type of ferromagnetics is that electrons with one type of spin have electronic transport properties and exhibit 100% spin polarization at the Fermi level. Recently, they have attracted great interest due to their possible applications in the field of spintronics.

Ab initio calculations were performed using first-principles using from the plane-wave basis set and the projector augmented wave (PAW) method implemented in the Vienna *ab initio* simulation package (VASP) [1] in the approximations of the PBE [2] and SCAN [3] functionals. Cubic structures with regular, inverse, $T^{\#}$, T^{c} and T^{p} c.f. Fig. 1., lattices of Heusler Fe_2RhSi alloy are considered. The density of the k-grid used for geometric optimization was ~5000 points per reciprocal lattice. The plane wave cutoff energy was 470 eV, and the energy convergence parameter was 10^{-7} eV/atom. Geometric optimization of the crystal structures of the austenite and martensite phases was performed within the framework of electronic and ionic relaxation. The crystal structures of the cubic austenite were given by the 16-atomic cubic and tetragonal supercell.

We considered three structures related to the inverse Heusler type, with layer-wise and columnar ordering of Fe and Rh atoms on the 4a and 4b sites, see Fig. 1c-e, as shown by the authors of [4]. The $T^{\#}$ structure is characterized by columns of Fe and Rh atoms located at 4a and 4b sites, which change their orientation from layer to layer as shown in Fig. 1c. T^{c} consists of alternating Fe and Rh atomic columns along the [001] direction (*z*-axis) and can also be conceived as Fe and Rh layers alternating along [110], c.f. Fig. 1d. T^{p} is composed of layers of Fe and Rh atoms alternating along [001], see Fig. 1e. The latter two structures were suggested in an earlier work on quaternary stoichiometric NiCoMn(Ga,Al) alloys [5], where they proved competitive to the conventional and the inverse Heusler structure in Fig. 1a and b, in agreement with the experimental findings.

The T^{p} lattice of Fe_2RhSi alloy is energetically more favorable than other configurations, according to the data of this study. The difference of ground state energy in $c/a = 1$ between T_p and inverse lattice is ~59.3 and 47.5 meV/atom for PBE and SCAN functionals, respectively. The value of the magnetic moment takes an integer of ~5 μB/f.u. in the for SCAN approximation and ~4.8 μB/f.u. in the for PBE approximation.

From Fig. 2 it can be seen that the degree of spin polarization of Fe_2RhSi alloy is quite high, however not reaching 100%, and the energy gap does not shift relative to the Fermi energy.

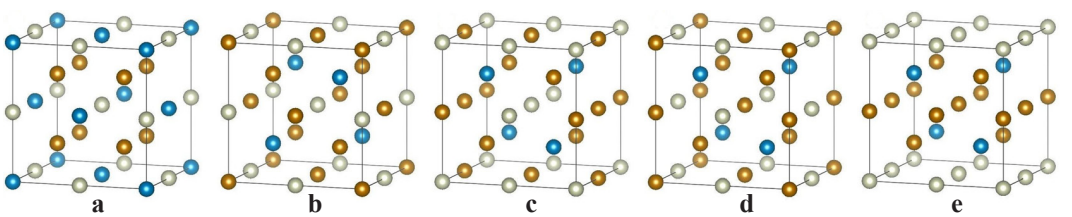

Figure 1. **a** Regular, **b** inverse, **c** $T^{\#}$, **d** T^{c} and **e** T^{p} lattices of Fe_2RhSi Heusler alloy.

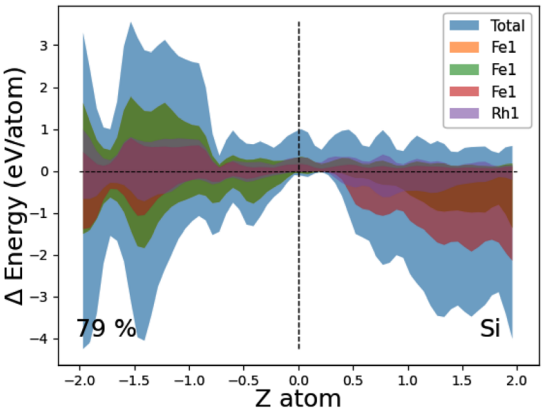

Figure 2. Density of states for configuration Fe_2RhSi at their equilibrium lattice parameter within SCAN functional for the T^p structure.

The Heusler alloy Fe_2RhSi with direct and inverse structures has been studied by the density functional theory methods. It is shown that the composition with T^p structure may be a half-metal as it possesses an integer magnetic moment, sufficiently high polarization degree and energy gap for spin-up electrons.

This work was supported by the Russian Science Foundation project No. 22-12-20032.

1. G. Kresse, J. Furthmüller, Phys. Rev. B **54**, 11169 (1996).
2. J.P. Perdew, K. Burke, M. Ernzerhof, Phys. Rev. Lett. **77**, 3865 (1996).
3. J. Sun, A. Ruzsinszky, J.P. Perdew, Phys. Rev. B **115**, 036402 (2015).
4. V.V. Sokolovskiy, O.N. Miroshkina, V.D. Buchelnikov, M.E. Gruner, Phys. Rev. Mat. B **00**, 005400 (2022).
5. P. Neibecker, M.E. Gruner, X. Xu, R. Kainuma, W. Petry, R. Pentcheva, M. Leitner, Phys. Rev. B **96,** 165131 (2017).

CHIROMAGNETIC OXIDE COBALT NANOPARTICLES: SYNTHESIS AND MAGNITOOPTICAL PROPERTIES

A.V. Kurilova[1*], *D.I. Klimenko*[1], *E.V. Kundelev*[1], *A.L. Suhachev*[2], *K.V. Shulga*[3], *A.U. Dubavik*[1], *A.E. Sokolov*[2,3]

[1]University ITMO, Sant-Peterburg, Russia
[2]Kirensky Institute of Physics, FRC KSC SB RAS, Krasnoyarsk, Russia
[3]Siberian Federal University, Krasnoyarsk, Russia
[*]E-mail: ankurilova@niuitmo.ru

The ability to identify the molecular chirality of enantiomers is important for drug development and biochemistry. It's catalysis, drug separation, biosensing, recognition, etc. The purification of racemic mixtures is based on fundamental chiral interactions that often only one enantiomer has biological activity (eutomer), the other one being not active or toxic (distomer).

Benefits of using magnetic nanoparticles for separation over more traditional methods are related to its simplicity, high activity, speed, stability, selectivity, and great cost-performance ration [1–3]. During separating enantiomers, surface-modified MNPs (usually SPION) with chiral molecules are exposed to a racemic mixture to selectively adsorb one enantiomer, which is removed by magnetic separation or deposited together with NPs, an excess of the other enantiomer leave in supernatant. Chiral ligands selected for the separation of enantiomers are subject to denaturation and renaturation under the influence of external influences, such as temperature and magnetic field, which makes them switchable and suitable for reuse [1].

NPs Co_3O_4 have spinel structure like magnetite but usually shows anti-ferromagnetic properties (p-type semiconductor). Studies of the genotoxic potential of cobalt-based materials *in vitro* have shown that cobalt nanoparticles are highly cytotoxic and genotoxic. Main, the genotoxic potential of cobalt nanoparticles is contributed primarily by its ability to generate/induce reactive oxygen species (ROS) [4]. L-cysteine-MNPs can be employed for Mannich reaction and Biginelli condensation [3] and separation enantiomers of cysteine.

Circular dichroism (CD) and magnetic circular dichroism (MCD) spectrum were measured in the range 270–800 nm using a Jasco J-1500 CD-spectrometer with a magnetic block MCD581 supplying constant magnetic field tunable from −1.5 to +1.5 T. UV−vis spectroscopy was carried out using a UV-Probe 3600 spectrophotometer (Shimadzu, Japan).

The nanoparticles were synthesized by thermal decomposition oleate cobalt in octadecene with post oxidation at 550°C. Then the hydrophobic NPs were added to a low concentrated aqueous solution L-cystine (1 mM) and vortex for the night. During annealing part of the surface group left and the vacant positions were occupied by L-cysteine molecules. The size of particles varies from 10 to 50 nm.

The absorption spectrum of our sample demonstrates some transitions as in the article [3], Fig. 1a. Optical density picks at 260, 350, 440, 560 nm belong cysteine (respectively 4.8, 3.5, 2.8, 2.2 eV). But this method is uninformative for determination of cobalt oxide transitions. The position of remaining peaks was clarified from MCD-spectrum at field 1.5 T, when saturation of magnetization is observed, Fig. 1c. There are transitions at 3.8 and 4.24 eV, which can be cases a charge transfer from ligand (oxygen anion, molecules L-cysteine) to surface NPs. Also, some bands may be attributed to d-d transitions in $Co^{3+}(O_h)$ with a contribution of ligand-to-metal charge-transfer [$p(O^{2-}) \rightarrow t_2(Co^{2+})$, $p(O^{2-}) \rightarrow e_{2g}(Co^{3+})$, $p(O^{2-}) \rightarrow t_{2g}(Co^{3+})$] such as 2.3, 2.9 and 3.21 eV [5] and metal-to-ligand charge-transfer [$t_{2g}(Co^{2+}) \rightarrow t_{2g}(Co^{3+})$] at 1.63 eV. The bands at 2.3 and 1.94 eV

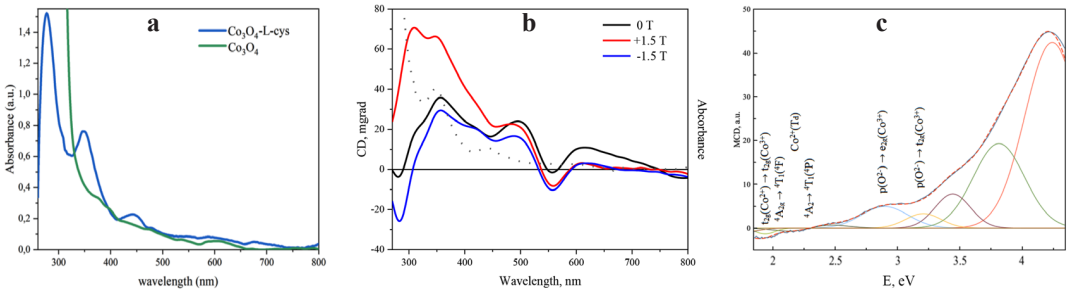

Figure 1. **a** Absorption spectrum, **b** CD-spectrum, **c** MCD-spectrum of nanosystem Co_3O_4-L-cysteine.

can be related to $^4A_2 \rightarrow {}^4T_1(^4P)$ of tetrahedral Co^{2+} [6]. The 3.44 and 1.83 eV bands correspond to transitions of octaoctahedral Co^{3+} and $^4A_{2g} \rightarrow {}^4T_1(^4F)$ of Co^{2+} respectively [7].

The circle dichroism spectrum aquas solution Co_3O_4-L-cysteine demonstrates primary absorption of right-polarized light in visible range, excluding transitions at 260, 560 nm. The chirality transfer from amino acids to the crystal lattice of the inorganic core of the NPs with crystal lattice distortions is available for the researched nanosystem Co_3O_4-L-cysteine [4].

Therefore, magnetooptical and optical properties of the composite Co_3O_4-L-cysteine prove consist of system. Significant differences from analogy sample [3] are synthesis methods, size, and changes of intensity redistribution in CD-spectrums.

Presumably, the NPs Co_3O_4 can be useful for magnetic recognition enantiomers and their separated above Neel temperature. This is due to the specific nature of the binding of molecular chains to the particle surface. Employment in vitro is questionable because mechanism of movement control has many restrictions.

The reported study was funded by RFBR, project number 20-32-90144.

1. A. Gogoi et al., Molecules **24**(6), 1007 (2019).
2. V. Angamuthu, D.F. Tai, Appl. Catalysis A: General **506**, 254–260 (2015).
3. J. Yeom et al., Science **359**(6373), 309–314 (2018).
4. V. Raman et al., Experimental and Therapeutic Medicine **11**(2), 553–560 (2016).
5. K.J. Kim, Y.R. Park, D.H. Hyun, S.H. Lee, J. Appl. Phys. **96**(4), 1975–1978 (2004).
6. Dohčević-Mitrović, D. Zorana et al., Process. Appl. Ceramics **14**(2), 102–112 (2020).
7. K. El Kabouss et al., J. Mater. Chem. **16**(25), 2453–2463 (2006).

A.P60

PERTURBATION THEORY FOR THE SPIN-TRANSFER TORQUE TERM WITHIN THE VECTOR HAMILTONIAN FORMALISM IN THE NONLINEAR CASE

A.A. Matveev[1,2*], *A.R. Safin*[1,3]

[1]Kotel'nikov Institute of Radioengineering and Electronics, Russian Academy of Sciences, Moscow, Russia
[2]Bauman Moscow State Technical University, Moscow, Russia
[3]Moscow Power Engineering Institute, Moscow, Russia
[*]E-mail: maa.box@yandex.ru

There is a necessity to study nonlinear spin-wave dynamics in micromagnetic systems with nonuniform magnetization of the ground state, such as domain walls, vortices and skyrmions [1]. Previously, such a problem was investigated using vector Hamiltonian formalism (VHF), but perturbations in the system caused by spin current were not considered [2]. In the work, VHF has been applied for the description of weakly nonlinear magnetization dynamics with spin-transfer torque (STT) excitation in the structures of current in plane (CIP) and current perpendicular to plane (CPP). So, additional term in Landau-Lifshits equation (LLE) for CIP case was considered in the form [3]

$$\mathbf{T}_{\mathrm{STT}}^{\mathrm{CIP}} = -\frac{b_j}{(1+\alpha^2)}\mathbf{m}\times[\mathbf{m}\times(\mathbf{j}\cdot\nabla)\mathbf{m}] - \frac{\xi b_j}{(1+\alpha^2)}\mathbf{m}\times(\mathbf{j}\cdot\nabla)\mathbf{m}. \tag{1}$$

where $\mathbf{m}$ is the unit magnetization vector, $\mathbf{j}$ denotes the spin current density, α is the Hilbert damping constant, ξ is the degree of nonadiabacity, $b_j = P\mu_B/(eM_s(1+\xi^2))$ is the coupling constant between the current and the magnetization, P denotes the spin polarization of the current, μ_B is the Bohr magneton, M_s denotes saturation magnetization, e is the elementary charge. In VHF spin current density vector $\mathbf{j}$ is allowed to be spatially non-uniform and also depends on time. For CPP structures Slonczewski spin transfer torque model is used. The additional term in LLE in this case has the form [4]

$$\mathbf{T}_{\mathrm{STT}}^{\mathrm{CPP}} = \beta\frac{\epsilon+\alpha\epsilon'}{1+\alpha^2}\mathbf{m}\times[\mathbf{p}\times\mathbf{m}] - \beta\frac{\epsilon'-\alpha\epsilon}{1+\alpha^2}\mathbf{m}\times\mathbf{p}. \tag{2}$$

Here $\beta = j_z\mu_B/M_s ed$, $\epsilon = P/2$, ϵ' is the Sloncewski secondary STT term parameter, $\mathbf{p}$ is the Slonczewski fixed layer polarization, d is the thickness of free layer, j_z is the z-component of vector $\mathbf{j}$. In CPP structures $\mathbf{j} = (0, 0, j_z)$ is assumed.

To simplify, the dynamics of the magnetization vector $\mathbf{m}(\mathbf{r}, t)$ was reformulated by introducing a spin excitation vector (SEV) $\mathbf{s}(\mathbf{r}, t)$. The transition from the magnetization vector $\mathbf{m}$ to the SEV was carried out using the Lambert transformation, which projects at each point the spherical space of the vector $\mathbf{m}$ into a plane perpendicular to the magnetization of the ground state $\mathbf{m}_0$. Expanding SEV in set over eigenmodes of the studied system $\mathbf{s}(\mathbf{r}, t) = \sum\mathbf{s}_\nu(\mathbf{r})c_\nu(t)$, where $c_\nu(t)$ denotes complex spin-wave amplitude while the $\mathbf{s}_\nu(\mathbf{r})$ denotes spin wave profile, allowed to obtain differential equations for dynamics of complex wave amplitudes. All spin wave profiles can be obtained from the solution of linear eigenproblem for Hamiltonian of the system $\hat{\mathscr{H}}_0$. This problem writes as

$$-i\omega_\nu\hat{\mathbf{L}}_0\mathbf{s}_\nu = \hat{\mathscr{H}}_0\mathbf{s}_\nu, \tag{3}$$

where ω_ν is eigenfrequency of mode with index ν and $\hat{\mathbf{L}}_0$ denotes the skew-symmetric operator, which is defined as $\hat{\mathbf{L}}_0\mathbf{s}_\nu = -L_s\mathbf{m}_0\times\mathbf{s}_\nu$, where $L_s = M_s/\gamma$ denotes density of spin angular momentum. The equations of motion for complex spin-wave amplitude $c_\nu(t)$ derives from the follow relation

$$\frac{\mathrm{d}c_\nu}{\mathrm{d}t} = \left(\frac{\mathrm{d}c_\nu}{\mathrm{d}t}\right)_{\mathrm{c}} + \left(\frac{\mathrm{d}c_\nu}{\mathrm{d}t}\right)_{\mathrm{nc}} + \left(\frac{\mathrm{d}c_\nu}{\mathrm{d}t}\right)_{\mathrm{STT}}. \tag{4}$$

Here $(\mathrm{d}c_\nu/\mathrm{d}t)_{\mathrm{c}}$ stands for conservative part of derivative of c_ν, which is connected with self-interactions in the system, $(\mathrm{d}c_\nu/\mathrm{d}t)_{\mathrm{nc}}$ is nonconservative correction for derivative of c_ν and it arises from presence of Hilbert damping, $(\mathrm{d}c_\nu/\mathrm{d}t)_{\mathrm{STT}}$ denotes the correction for derivative of c_ν because of STT perturbation. Conservative term $(\mathrm{d}c_\nu/\mathrm{d}t)_{\mathrm{c}}$ and linear case for damping term $(\mathrm{d}c_\nu/\mathrm{d}t)_{\mathrm{nc}}$ has been considered in [2]. It was found out that in the general case all modes are connected and for a complete description of the system it is necessary to solve a system of differential nonlinear equations of the first order. So, in case of linear damping and non-linear STT excitation equations for c_ν takes the form

$$\begin{aligned} \mathrm{i}\hbar_\nu\frac{\mathrm{d}c_\nu}{\mathrm{d}t} &= -\mathrm{i}\hbar_\nu\Gamma_\nu c_\nu + \hbar_\nu\omega_\nu c_\nu + \frac{1}{2}\sum_{\beta\gamma}V_{\nu^*\beta\gamma}c_\beta c_\gamma + \sum_{\gamma}V_{\nu^*\nu^*\gamma}c_{\nu^*}c_\gamma + \frac{1}{2}V_{\nu^*\nu^*\nu^*}c_{\nu^*}^2 \\ &+ \frac{1}{6}\sum_{\beta\gamma\delta}W_{\nu^*\beta\gamma\delta}c_\beta c_\gamma c_\delta + \frac{1}{2}\sum_{\gamma\delta}W_{\nu^*\nu^*\gamma\delta}c_{\nu^*}c_\gamma c_\delta + \frac{1}{2}\sum_{\delta}W_{\nu^*\nu^*\nu^*\delta}c_{\nu^*}^2 c_\delta + \frac{1}{6}W_{\nu^*\nu^*\nu^*\nu^*}c_{\nu^*}^3 \\ &+ \sum_{\beta}A_\beta c_\beta + \sum_{\beta\gamma}B_{\beta\gamma}c_\beta c_\gamma + \sum_{\beta\gamma\delta}D_{\beta\gamma\delta}c_\beta c_\gamma c_\delta \end{aligned}, \tag{5}$$

where Γ_ν represents damping, while the $V_{\alpha\beta\gamma}$ and $W_{\alpha\beta\gamma\delta}$ are self-interaction coefficients, A_β, $B_{\beta\gamma}$, $D_{\beta\gamma\delta}$ are STT coefficients, index ν^* is used for conjugated modes $c_{(\nu^*)} = c_\nu^*$, the norm $\hbar_\nu$ of ν mode is determined from the orthogonality condition $\int_V \mathbf{s}_\alpha\hat{\mathbf{L}}_0\mathbf{s}_\beta\mathrm{d}V = \mathrm{i}\hbar_\alpha\Delta_{\alpha\beta}$. Here $\Delta_{\alpha\beta}$ is the Kronecker delta and V denotes the volume of the studied sample. The obtained STT coefficients for ν mode in case of sufficiently small non-adiabatic component in Slonczewski spin transfer torque has the form

$$\begin{aligned} A_\beta &= a\int_V L_s(\mathbf{m}_0\cdot\mathbf{p})\mathbf{s}_\nu^*\left[\mathbf{m}_0\times\mathbf{s}_\beta\right]\mathrm{d}V, \\ B_{\beta\gamma} &= \frac{3a}{4}\int_V L_s(\mathbf{s}_\gamma\cdot\mathbf{p})\mathbf{s}_\nu^*\left[\mathbf{m}_0\times\mathbf{s}_\beta\right]\mathrm{d}V, \\ D_{\beta\gamma\delta} &= -\frac{3a}{4}\int_V L_s(\mathbf{m}_0\cdot\mathbf{p})(\mathbf{s}_\gamma\cdot\mathbf{s}_\delta)\mathbf{s}_\nu^*\left[\mathbf{m}_0\times\mathbf{s}_\beta\right]\mathrm{d}V, \end{aligned} \tag{6}$$

where $a = \beta(\epsilon + \alpha\epsilon')/(1 + \alpha^2)$. However, in many cases it is unnecessary to consider the influence of all modes. Obtained dynamical equation for complex spin wave amplitude in a single-mode approximation with linear STT excitation takes the simple form

$$\frac{\mathrm{d}c_\nu}{\mathrm{d}t} + \mathrm{i}\omega_\nu c_\nu + \Gamma_\nu c_\nu - A_\nu c_\nu = 0. \tag{7}$$

Using the vector Hamiltonian formalism, it is possible to calculate the behavior of the system with spatially nonuniform ground state under nonlinear effects, including resonance. To do this, it is necessary to find the profiles of eigenmodes by solving the eigenproblem (3), take into account

all the necessary modes in equation (5) and solve the obtained dynamics equations for complex spin wave amplitudes.

Support by RSF No. 21-79-10396 is acknowledged.

1. Q. Shao et al., IEEE Trans. Magn. **57**(7), 1–39 (2021). doi: 10.1109/TMAG.2021.3078583.
2. V. Tyberkevych, A. Slavin, P. Artemchuk, and R. Graham, Vector Hamiltonian formalism for nonlinear magnetization dynamics, arXiv:2011.13562
3. B. Krüger et al., Phys. Rev. B **75**, 054421 (2007).
4. J. Slonczewski, J. Magn. Magn. Mat. **159**, L1 (1996); *ibid* **247**, 324 (2002).

NONLINEAR LIMITATION OF RESONANCE FREQUENCY GROWTH OF SPIN WAVES IN EXCEPTIONAL POINTS

O.S. Temnaya[1*], *A.R. Safin*[1,2], *D.V. Kalyabin*[1,3], *S.A. Nikitov*[1,3]

[1]Kotel'nikov Institute of Radio-Engineering and Electronics of RAS, Moscow, Russia
[2]Moscow Power Engineering Institute, Moscow, Russia
[3]Moscow Institute of Physics and Technology, Dolgoprudny, Moscow Region, Russia
[*]E-mail: ostemnaya@gmail.com

We present a theoretical model of the PT-symmetric system of two coupled planar magnonic "ferromagnetic-normal metal" heterostructures. We explore conditions for the appearance of an exceptional point (EP). The growth of spin-wave resonance amplitudes in the EP is restricted by nonlinearity. We show a dependence of resonant amplitudes in the EP on the excitation amplitude at different values of the nonlinearity coefficient.

Micro- and nanowaveguides and heterostructures are the basic structures of magnonics. Such structures are essential for information processing problems since the frequency range of spin waves lies between units of GHz and units of THz. At the same time, standard CMOS technology is limited to a frequency range of GHz. One of the critical properties of magnonic structures is the possibility of transferring the energy of collective modes between coupled waveguides. This process can be influenced by changing the intrinsic spin-wave damping. It is shown that the magnon system can possess PT-symmetry when enhancing the spin-wave damping in one waveguide is equal to damping compensation in the other waveguide. Physical systems described by pseudo-Hermitian Hamiltonians are PT-symmetric and can have a real spectrum of eigenvalues [1]. The phase transition of the system to the broken PT-symmetry phase can occur at exceptional points (EPs), where the real eigenvalues become complex. When passing through an EP, the eigenmodes and eigenvalues of the system coalesce. Thus, PT-symmetric systems represent an exotic class of conservative systems that simultaneously have the properties of dissipative systems. In addition, the unique nature of PT-symmetric systems makes it possible to observe such unusual effects as single-mode laser generation and high magnetic permeability at EPs.

This work aims to study a PT-symmetric system of coupled magnonic waveguides with equally balanced gain and loss of spin waves. The control of the intrinsic amplification and damping of spin waves in the system is implemented using the spin Hall effect, which occurs at the ferromagnetic-normal metal interface. The attenuation varying is achieved due to the multidirectional flow of direct current through the metal [2].

Unique characteristic of PT-symmetric systems allows the creation of hypersensitive sensors because of having a strikingly narrow resonance curve in the EPs [3], as it is shown in Fig. 1a. However, nonlinear effects must play an essential role in these systems. Let us estimate the influence of these effects on the growth of the amplitude at the exceptional point. As it was mentioned before, the amplitudes of magnetic oscillations in magnonic waveguides sharply increase at the EP.

The system of equation for complex amplitudes has the following form [4]:

$$\begin{cases} \dot{c}_1 + \mathrm{i}\Omega c_1 + \Gamma_0(1+Q|c_1|^2)c_1 - \Gamma_1 c_1 = \mathrm{i}\Omega_c c_2 + \Lambda_0 \exp(-\mathrm{i}\omega t), \\ \dot{c}_2 + \mathrm{i}\Omega c_2 + \Gamma_0(1+Q|c_1|^2)c_2 + \Gamma_1 c_2 = \mathrm{i}\Omega_c c_1, \end{cases} \quad (1)$$

where Γ_0 is a linear relaxation rate of the uniform magnetization precession, Λ_0 is the amplitude of the external signal; Q is a dimensionless parameter describing nonlinear relaxation that reflects the

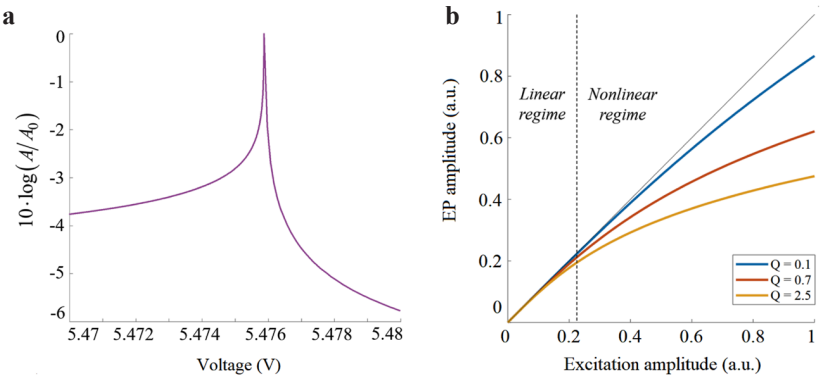

Figure 1. **a** Resonance amplitude dependence in the PT-symmetric planar magnonic system; **b** dependence of EP amplitude on excitation amplitude.

limitation of longitudinal components of magnetization vectors at sufficiently large values of the external signal's amplitudes; it is most often found phenomenologically from experimental data [4, 5].

Note that the system (1) does not include the nonlinear coefficient reflecting the ferromagnetic resonance frequency shift, which characterizes the effect of nonisochronism – the dependence of the oscillation frequency on the amplitude. It can be neglected by selecting the magnetic field magnitude and its direction.

Here we consider the influence of the introduced coefficient Q on the change in the amplitudes of the oscillations at the EP when varying this coefficient. The corresponding dependence is shown in Fig. 1b. With an increase in the amplitude of the external signal, the oscillation amplitude is limited, and it decreases with the growth of the nonlinearity parameter. Therefore, the growth of the oscillation amplitude at the EP is limited by the system's nonlinearity.

Support by RSF (Grant No. 19-19-00607) is acknowledged.

1. C.M. Bender and S. Boettcher, Phys. Rev. Lett. **80**, 5243 (1998).
2. Z. Wang, Y. Sun, M. Wu, V. Tiberkevich, and A. Slavin, Phys. Rev. Lett. **107**, 146602 (2011).
3. M.-A. Miri and A. Alù, Science **363**, 6422 (2019).
4. A. Slavin and V. Tiberkevich, IEEE Trans. Magn. **44**, 7 (2008).
5. S.R. Lake, B. Divinskiy, G. Schmidt, S.O. Demokritov, and V.E. Demidov, Phys. Rev. Appl. **17**, 034010 (2022).

A.P62

INVESTIGATION OF THE CONTROL OF THE MAGNETIZATION VECTOR OF A FERROMAGNETIC LAYER IN A TWO-LAYER SYSTEM FERROELECTRIC/FERROMAGNET

*A.A. Kamashev**, *A.V. Leontyev, I.A. Garifullin, R.F. Mamin*

Zavoisky Physical-Technical Institute, FRC Kazan Scientific Center of RAS, Kazan, Russia
*E-mail: kamandi@mail.ru

Two theoretical models of the superconducting spin valve (SSV) were proposed in the late 1990s. One of them F1/F2/S (where F1 and F2 are ferromagnetic layers, and S is a superconducting layer) was proposed by Sanjiun Oh et al. [1]. Another model F1/S/F2 was predicted by Tagirov [2]. The principle of both models is the same. It is based on the fact that the value of the exchange field from two F-layers, which acts on the Cooper pair from the S-layer, in the case of parallel (P) orientation of the magnetizations of the F-layers is bigger than in the case of antiparallel (AP) one. This difference leads to a lower value of the transition temperature in the superconducting state in the case of parallel orientation of the magnetizations of the F-layers (T_c^P) than in the antiparallel orientation (T_c^{AP}).

As our results [3, 4] and the results of other groups [5] show, the limiting values of the SSV effect have already been reached using various alloys and elemental ferromagnets in F1/F2/S structures. In this regard, it is necessary to start studying structures with non-standard approaches. One of such approaches may be the study of the structures of a SSV based on ferroelectric substrates. This should make it possible to control the superconducting current using an electric field in SSV structures.

In general, for the implementation model of SSV based on ferroelectric substrates the following task must be solved. We have to realize the mechanism of controlling direction of the magnetization of the ferromagnetic layer due to the magnetoelastic effect in a two-layer ferroelectric/ferromagnet system. The magnetoelastic effect is caused due to deformations in the ferroelectric layer caused by the reverse piezoelectric effect when an electric field is applied. Deformations in the ferroelectric layer cause stress in the ferromagnetic layer due to the ferroelectric/ferromagnet contact. This, in turn, manifests itself in the appearance of additional magnetic anisotropy.

We prepared a series of $LiNbO_3/Fe(d_{Fe})$ samples with a varying thickness of the iron layer from 5 to 10 nm on a ferroelectric lithium niobate substrate. Next, we carried out magnetic characterization of the samples using a scanning magnetopolarimetric complex based on the magneto-optical Kerr effect. We applied an electric field in the range of 10 to 50 V to the ferroelectric substrate and observed the light intensity. The most interesting result was obtained at applying electric field about 10 V for $LiNbO_3$/Fe(5 nm) sample (see Fig. 1). At point 0, there is no magnetic or electric field. At point 1, magnetic field of about 50 Oe was applied. At point 2, electric field of the order of 10 V was also applied. At point 3, electric field has been turned off. At point 4, magnetic field has been also turned off. At point 1 on Fig. 1, magnetization of the Fe layer was directed along the plane of application of the external magnetic field. In Fig. 1, this fact manifests itself in a sharp increase in light intensity. Further, at point 2 when an electric field about 10 V is applied, we observe a smooth increase in the light intensity, which may indicate a change in the direction of the magnetization vector of the Fe layer. This is also confirmed by the fact that at point 3, when the electric field is turned off, we observed a smooth decrease in the light intensity, that is, the film is magnetized again along the plane of application of the external magnetic field. At point 4, the magnetic field is turned off, and we observed a sharp decline in the intensity of light. Based on our results, we can

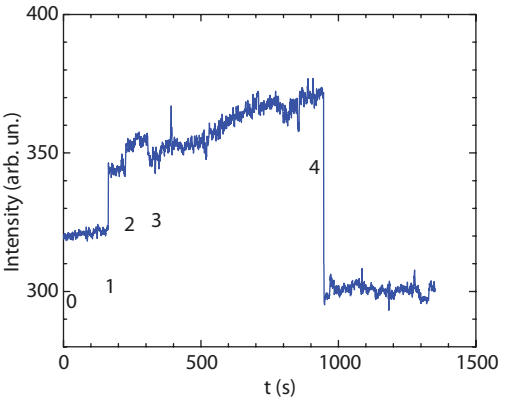

Figure 1. Time dependence of the intensity of the light passed through the polarizer for $LiNbO_3$/Fe(5nm). For a detailed description of the figure, see the text. Electric field of the order of 10 V is applied at point 2.

already say that we have managed to register a certain change in the orientation of the magnetization vector of the ferromagnetic layer. These are our first experiments in this investigation, so we could not quantitatively estimate the angle of change of the magnetization vector. Our first experiments show that an electric field of the order of 10 V is already sufficient to change the orientation of the magnetization vector of the ferromagnetic layer in a two-layer ferroelectric/ferromagnet system.

We demonstrated our first experimental results to investigate the change of the direction of magnetization of a ferromagnetic layer on a ferroelectric substrate under the action of an electric field. Our results show that electric fields of the order of 10 V are already sufficient to change the orientation of the magnetization of the ferromagnetic layer. Consequently, the model of a superconducting spin valve on a ferroelectric substrate is possible realizable.

The research was supported by the Russian Science Foundation grant No. 21-72-10178.

1. S. Oh, D. Youm, and M. R. Beasley, Appl. Phys. Lett. **71**, 2376 (1997).
2. L.R. Tagirov, Phys. Rev. Lett. **83**, 2058 (1999).
3. A.A. Kamashev et al., Beilstein J. Nanotechnol. **10**, 1458 (2019).
4. A.A. Kamashev et al., Phys. Rev. B **100**, 134511 (2019).
5. A. Singh et al., Phys. Rev. X **5**, 021019 (2015).

A.P63

NON-RECIPROCAL PROPAGATION OF SPIN WAVES IN STRUCTURES WITH PARTIAL METALLIZATION SURFACE

A.A. Martyshkin[1*], *E.H. Lock*[2], *E.N. Beginin*[1], *A.V. Sadovnikov*[1]

[1]Laboratory of Magnetic Metamaterials, Saratov State University, Saratov, Russia
[2]Fryazino Branch of Institute of Radioengineering and Electronics, Fryazino, Russia
[*]E-mail: aamartyshkin@gmail.com

In connection with the development of the technological process of manufacturing thin films of magnetic films, it is of great interest to study spin waves (SW) during their propagation in regular and irregular magnonic structures [1]. Magnonics is a scientific direction in the physics of condensed matter, which aims to study the characteristics and methods of controlling spin-wave transport in various wave-breathing systems. Currently, devices based on the principles of magnon logic demonstrating reconfigurable SW propagation in two-dimensional magnetic structures are of great interest [2]. Investigation of the control mechanisms of non-reciprocal propagation of magnetostatic spin waves in single-crystal magnetic films is an interesting area of research, since it opens up new design possibilities when creating logical reconfigurable devices [3].

The building element of reconfigurable magnon circuits can be a splitter based on the junction of a spatially limited waveguide element and an unlimited magnetic film in which directional focusing of spin waves is possible. One of the focusing requirements is the presence of anisotropy, which provides different directions of group and phase velocities [4].

In this work, caustic-like SW beams non-reciprocally propagating in a T-shaped magnetic structure with partial metallization of the surface are studied using numerical and experimental methods. Using the method of microwave Mandelstam-Brillouin spectroscopy and micromagnetic modeling, the possibility of controlling the spatial-frequency selection of SW is shown. Propagating in a T-shaped magnetic structure with partial surface metallization.

The proposed implementation of a spin-wave signal demultiplexer based on a T-shaped magnetic film of an yttrium iron garnet signal is schematically shown in Fig. 1a. For the experiment, a waveguide structure was made of yttrium iron garnet [$Y_3Fe_5O_{12}$, (111)] with a saturation magnetization of $4\pi M_s$ = 1750 G, epitaxially grown on a gallium-gadolinium garnet substrate [$Gd_3Ga_5O_{12}$, (111)]. A system of local laser ablation was used to form a T-shaped waveguide structure. A metallized layer is deposited on the surface of the waveguide in the transverse direction. Using a microstrip antenna with a width of 30 μm, located at the beginning of the waveguide structure, a spin-wave front propagating in the direction of the metallized layer was excited. Figure 1b shows the dependence of the relative output power of the signal P_n/P (n = 1,2.) at the outputs P_1 and P_2 on the frequency at on positive (+) and negative (–) direction of the uniform magnetic field H_0. With positive direction, the relative power received at the output of P_1 increases with increasing frequency, while the relative power at P_2 decreases. When changing the direction of the magnetization of the structure, one can observe a drop in power P_1/P and an increase in P_2/P with increasing frequency.

To obtain maps of the spatial distribution of dynamic magnetization by Brillouin spectroscopy, an experiment was carried out in a quasi-backscattering configuration, while the intensity of the reflected optical signal was proportional to the square of dynamic magnetization. Next, a stationary spatial distribution was obtained for various directions of the external magnetic field. Figure 1c and d show the spatial distributions of the intensity of the spin-wave signal. When the direction of the external magnetic field changes along the Oy-axis, the effect of non-reciprocal propagation of quasi-caustic beams of the spin-wave signal formed due to diffraction is observed. The presented design

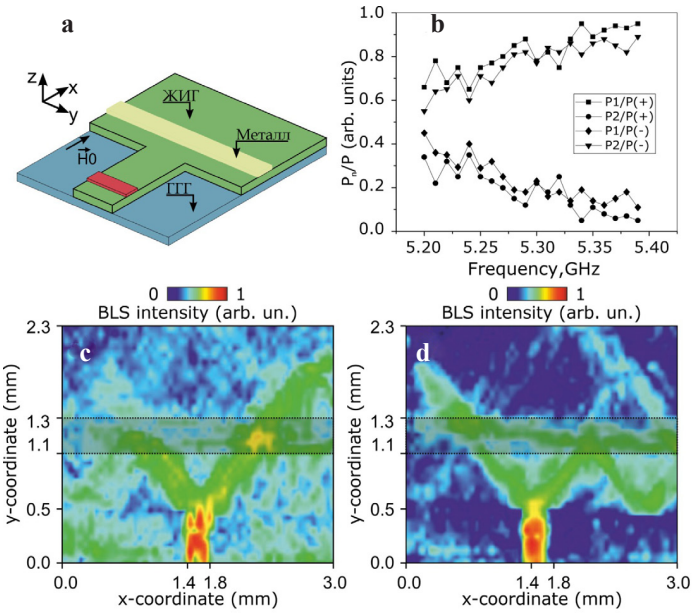

Figure 1. **a** Schematic T-shape structure with partial surface metallization. **b** Relative signal output power at outputs P_1 and P_2 on positive (+) and negative (–) direction external magnetic field. Spin waves intensity distribution maps for an external magnetic field of H_0 = 1200 G directed along the *x*-axis (**c**), against the *x*-axis (**d**).

of the device makes it possible to change the direction of propagation of the spin-wave signal due to the inhomogeneous distribution of the internal magnetic field created by the metallized layer.

This work was supported by the grant from Russian Science Foundation (No 20-79-10191)

1. F. Heussner, A. A. Serga, T. Brächer et al., Appl. Phys. Lett. **111**, 122401 (2017).
2. A. Barman A, G. Gubbiotti et al., J. Phys. Condens. Matter. **33**, 413001 (2021).
3. A.V. Sadovnikov, E.N. Beginin, S.E. Sheshukova, D.V. Romanenko, Y.P. Sharaevsky, and S.A. Nikitov, Appl. Phys. Lett. **107**, 202405 (2015).
4. A.V. Vashkovskii and E.H. Lokk, Physics-Uspekhi **47**, 601 (2004).

A.P64

RESEARCHING OF PROPERTIES OF MAGNETIC THIN FILMS FOR STORAGE DEVICES

A.A. Valiullin[1*], *A.S. Kamzin*[2], *L.R. Tagirov*[1,3], *L.D. Zaripova*[1]

[1]Kazan Federal University, Kazan, Russia
[2]Ioffe Physical–Technical Institute of RAS, St. Petersburg, Russia
[3]Zavoisky Physical-Technical Institute, FRC Kazan Scientific Center, RAS, Kazan, Russia
[*]E-mail: albert.bm@yandex.ru

A great many studies of thin film magnetic materials focus on increasing their magnetic data density. The data density is often raised by minimizing the size of grains (data storage items in a magnetic film) and by switching from longitudinal to transverse recording. However, the minimum possible size of granules is limited by the emergence of the superparamagnetic effect, which prevents the magnetic data density from increasing. The exchange interaction between granules is another limiting factor.

In this report different methods of synthesis of $L1_0$ FePt thin films are used to overcome these limitations:

1) Further study indicates that the perpendicular anisotropy in $[Fe/Pt]_n$ multilayer films has an intimate correlation with the periodicity n, and, with the increasing of periodicity n, the out-of-plane remanence ratio significantly increases and then decreases slowly. This result suggests that the enhanced perpendicular anisotropy may be caused by the interface anisotropy at the Fe/Pt interfaces in the $[Fe/Pt]_n$ multilayers.

It has been established that, in multilayer structures based on $L1_0$ FePt films obtained by RF magnetron sputtering, the evolution of texture from (111) to (001) can be effectively induced by using multilayer structure. This might be a new method to obtain perpendicular anisotropy and, at same time, to effectively reduce the exchange coupling interaction among grains in FePt films.

2) Bit-patterned media (BPM), which consist of ferromagnetic (FM) nanodots regularly arranged in a nonmagnetic matrix, are a promising candidate to replace continuous film media for ultrahigh density magnetic recording.

It is known that the magnetic properties of FePt films can be tailored by introducing additional elements into them. Adding rhodium (Rh) to the FePt alloy allows us to optimize the magnetic properties of thin films without sacrificing their magnetocrystalline anisotropy energy.

$FePt_{1-x}Rh_x$ films with different Rh concentrations ($0 \le x \le 0.4$) and a thickness of 20 nm were fabricated by magnetron sputtering. It was found that the film was paramagnetic at room temperature when $x = 0$, and the easy axis of magnetocrystalline anisotropy was perpendicular to the film surface. At rhodium concentrations of $x < 0.32$, the ferromagnetic order was preserved at room temperature in $FePt_{1-x}Rh_x$, and the high magnetocrystalline anisotropy energy that established the perpendicular magnetization orientation was retained.

3) The possibility of controlling the properties and orientation of the easy axis of magnetization of the multilayer magnetic structure by means of annealing in an external magnetic field has been investigated. The investigations have been performed on multilayer magnetic structures based on $Fe_{50}Pt_{50}$ films in the $L1_0$ phase.

Section B.

Spin dynamics and magnetic resonances

ON THE THEORY OF SPIN NUTATION

K.M. Salikhov

Zavoisky Physical-Technical Institute, FRC Kazan Scientific Center, Russian Academy of Sciences, Kazan, Russia
E-mail: kevsalikhov@mail.ru

For the simplest systems of paramagnetic particles, the response of spins to a sudden switching on of an alternating magnetic field ("nutation") is considered. A detailed analysis of the dependence of "nutation" on the excitation pattern of spins by an alternating field has been carried out. In the limiting cases of nonselective excitation of spins or frequency-selective resonance excitation of a transition between spin states, analytical solutions are obtained for the time dependence of the spin magnetization.

In the case of non-selective excitation by a strong alternating field, the motion of spins upon a sudden switching on of the field is a nutation described by Torrey. In this case, nutation in the rotating coordinate system occurs with the Rabi frequency of the alternating field, and the nutation frequency does not depend on the magnitude of the spin of paramagnetic particles.

In the case of selective excitation of a resonant transition, the end of the magnetization vector in a rotating coordinate system moves along an ellipse in a plane perpendicular to the polarization vector of the alternating field. The frequency of motion along the ellipse turns out to be greater than the Rabi frequency, for example, for particles with spin $S = 1$ it is $\sqrt{2}$ times greater. Despite the difference in the trajectory of the end of the magnetization vector in the limiting cases of non-selective excitation and selective excitation of the resonant transition, in both cases the motion of spins can be called nutation, circular and elliptical, respectively.

Under conditions when spin interactions are comparable with the energy of interaction of spins with an alternating field, the motion of the spin magnetization is not described by nutation. The movement of spins in this situation can be called "nutation" only for brevity of speech. It is shown that the motion of magnetization during "nutation" is described as the sum of contributions oscillating at different frequencies. These frequencies can be calculated numerically for any spin Hamiltonian. In this case, "nutation" is not reduced to Torrey nutation based on the Bloch equations. In this situation, the application of the Bloch equations to describe the motion of the spin magnetization vector is not justified.

Equations for the magnetization vector are proposed, which, in contrast to the Bloch equations, correctly describe the nutation of interacting spins.

On the basis of numerical calculations, a detailed analysis of nutation was carried out for two simplest systems: paramagnetic particles with spin $S = 1$ and pairs of paramagnetic particles with spins $S = 1/2$.

1. H.C. Torry, Phys. Rev. **76**, 1059 (1949).
2. A.V. Astashkin, A. Schweiger, Chem. Phys. Lett. **174**, 595–602 (1990).
3. A. Schweiger, G. Jeschke, Principle of Pulse Electron Paramagnetic Resonance, Oxford, University Press (2001).
4. S.S. Kim and S.L.Weissman, J. Magn. Reson. **24**, 167–169 (1976).
5. R. Furrer, E Fujara, C. Lange, D. Stehlik, H.M. Vieth and W. Vollmann, Chem. Phys. Lett. **75**, 332 (1980).
6. R. Hanaishi, Ya. Ohba, K. Akiyama, S. Yamauchi, M. Iwaizumi, J. Chem. Phys. **103**, 4819–4822 (1995).

HIGH-FIELD MAGNETIC STRUCTURE OF THE TRIANGULAR ANTIFERROMAGNET $RbFe(MoO_4)_2$ TESTED BY NMR

Yu.A. Sakhratov[1,2], *L.E. Svistov*[3*], *A.P. Reyes*[2]

[1]Kazan State Power Engineering University, Kazan, Russia
[2]National High Magnetic Field Laboratory, Tallahassee, USA
[3]P. Kapitza Institute for Physical Problems RAS, Moscow, Russia
[*]E-mail: svistov@kapitza.ras.ru

The magnetic H–T phase diagram of a quasi-two-dimensional antiferromagnet $RbFe(MoO_4)_2$ (S = 5/2) with an equilateral triangular lattice structure is studied with ^{87}Rb NMR. The results of neutron-diffraction experiments are described in [1]. Combination of these two experimental techniques allows to determine the ordered components of the magnetic moments on the Fe^{3+} ions within various high-field phases – the Y, UUD, V, and fan structures, stabilized in the compound by the in-plane magnetic field. It is also established that the transition from the V to the fan phase is of first order, whereas the transition from the fan phase to the polarized paramagnetic phase is continuous. Analysis of the NMR spectra shows that the high-field fan phase of $RbFe(MoO_4)_2$ can be successfully described by a periodic commensurate oscillation of the magnetic moments around the field direction in each Fe^{3+} layer combined with an incommensurate modulation of the magnetic structure perpendicular to the layers.

The second part of the report discuss the magnetic phases of $RbFe(MoO_4)_2$ for static field aligned perpendicular to triangular crystal structure ($H \| C_3$), which coincides with the hard axis of the zero field planar magnetic structure. For this field orientation umbrella like magnetic structure can be expected in the frame of the quasi-classical theory in full field range up to the transition to the polarized paramagnetic phase. However, it has recently been found that the magnetization process at this field orientation occurs within two magnet structures [2, 3]. One of them is low-field umbrella-like phase, and the second one is realized near the saturation field with an unknown structure. Our results of NMR experiments for $H \| C_3$ confirm the transition to the new high field phase and give information about the spin configuration within this phase.

The work was supported by Russian Science Foundation Grant 22-12-00259. Work at the National High Magnetic Field Laboratory is supported by the NSF Cooperative Agreement No. DMR-1157490 and the State of Florida.

1. Yu.A. Sakhratov, O. Prokhnenko, A.Ya. Shapiro, H.D. Zhou, L.E. Svistov, A.P. Reyes, and O.A. Petrenko, Phys. Rev. B **105**(1), 014431 (2022).
2. Hiroyuki Mitamura, Ryuta Watanuki, Norimichi Onozaki, Yuta Amou, Yohei Kono, Shunichiro Kittaka, Yasuyuki Shimura, Isao Yamamoto, Kazuya Suzuki, Toshiro Sakakibara, J. Magn. Magn. Mat. **400**, 70 (2016).
3. A. Zelenskiy, J.A. Quilliam, A.Ya. Shapiro, and G. Quirion, Phys. Rev. B **103**, 224422 (2021).

TWO TYPES OF MAGNON BOSE CONDENSATION

Yu.M. Bunkov

Russian Quantum Center, Moscow, Skolkovo, Russia
E-mail: Y.Bunkov@rqc.ru

Magnons are quasiparticles in magnetically ordered materials that describe elementary excitations of the ground state. They possess spin equal to 1 and accordingly obey Bose statistics. In thermal equilibrium, the density of magnons is not significant and their properties are well described in the linear approximation. However, the concentration of magnons can be enhanced up to a very high number by pumping them under magnetic resonance conditions. The first magnon Bose-condensed state was discovered in 1984 by Borovik-Romanov, Bunkov, Dmitriev and Mukharsky in antiferromagnetic superfluid 3He-B [1]. We may call this coherent magnon state the BBDM state. It is expressed in obtaining a coherent inductive signal, the duration of which can be thousands of times longer than the time of inhomogeneous relaxation. In this case, the induction signal after the excitation pulse is dephased due to the inhomogeneity of the magnetic field, and then spontaneously recovers [2]. A feature of this state is that magnons condense into a state with zero momentum, as in the case of atomic Bose condensation and in other known cases of condensation. This state exhibits all the properties of magnon superfluidity, such as the Josephson effect, the phase slippage when the critical Landau velocity is reached, Abrikosov quantum vortices, Goldstone oscillation modes (second sound), etc. [3]. The BBDM state was observed in different phase of superfluid 3He [4, 5] in antiferromagnetic crystals [6] and in Yttrium Iron Garnet (YIG) film [7].

In the YIG film, the BBDM state was observed for the case when the external magnetic film was directed perpendicular to the film surface. The minimum magnon energy in this case corresponds to stationary magnons with the wave vector $k = 0$. However, if the external magnetic field is directed along the surface, the magnon spectrum is significantly deformed. Under these conditions the magnon energy minimum corresponds to a wave vector k of about 10^5 cm^{-1} which directed along the field. In other words, magnons in this system have momentum, which fundamentally distinguishes it from classical systems with atomic BEC and magnon BBDM state. The question arose about the possibility of the formation of a magnon BEC under such conditions? Already the results of the first experiments were interpreted in favor of the formation of an exotic BEC for magnons with nonzero k [8]. The formation of an exotic magnon BEC was most obviously demonstrated in an experiment where the formation of a BEC was found some time after the parametric pump was turned off [9, 10].

Let's look at a few differences in the properties of the magnetic BEC in these configurations. In the case of the BBDM state, RF photons in the resonator excite magnons at a frequency corresponding to the energy minimum of the mBEC. A hybrid system of bound photons and magnons appears. The evaporation of magnons is compensated by the creation of new magnons by the RF field, and according to quantum mechanics, new magnons are born in the state of magnon condensate [11]. In this case, the mBEC precession phase relative to the RF field is automatically adjusted so that the number of produced magnons exactly corresponds to their relaxation. Thus, the magnon BEC exists continuously. Moreover, it propagates in a superfluid way outside the region of excitation [12].

In the case of an exotic mBEC, magnons are excited by parametric pumping at a frequency much higher than the frequency corresponding to the minimum energy. Therefore, the magnon gas is overheated during excitation and does not form a condensate. Sometime after the pumping is turned off, the magnons are thermalized and form mBECs, as was shown in [9, 10]. Another difference

of the BBDM state is that magnons with $k = 0$ are not sensitive to the boundary conditions of the sample. On the contrary, in the case of an exotic mBEC, magnons are reflected from the boundary. Therefore, the boundary conditions determine the frequencies of standing spin waves even in the case when the magnon system is overheated and, accordingly, the Bose condensate is not formed. This explains the results of observing the interference pattern of macroscopic standing spin waves under parametric pumping [13].

In conclusion, it should be noted that the magnon BEC is a quantum effect that can be used to create quantum computers capable of operating even at room temperatures. At the end of this review, the author will introduce the audience to modern approaches to solving this problem.

Support by RSF (grant № 22-12-00322) is acknowledged.

1. A.S. Borovik-Romanov, Yu.M. Bunkov, V.V. Dmitriev and Yu.M. Mukharskii, JETP Lett., **40**, 1033 (1984).
2. Yu.M. Bunkov and G.E. Volovik, J. Phys.: Condens. Matter **22**, 164210 (2010).
3. Yu. M. Bunkov and G. E. Volovik, "Spin Superfluidity and Magnon BEC" Chapter IV of the book "Novel Superfluids eds. K.H. Bennemann and J.B. Ketterson, Oxford University press (2013).
4. T. Sato, T. Kunimatsu, K. Izumina, A. Matsubara, M. Kubota, T. Mizusaki, and Yu.M. Bunkov, Phys. Rev. Lett. **101**, 055301 (2008).
5. S. Autti, V.V. Dmitriev, J.T. Makinen, T. Rysti, A.A. Soldatov, G.E. Volovik, A.N. Yudin, and V.B. Eltsov, Phys. Rev. Lett. **121**, 025303, (2018).
6. Yu.M. Bunkov, E.M. Alakshin, R.R. Gazizulin, A.V. Klochkov, V.V. Kuzmin, V.S. L'vov, and M.S. Tagirov. Phys. Rev. Lett. **108**, 177002 (2012).
7. Yu.M. Bunkov, A.N. Kuzmichev, T.R. Safin, P.M. Vetoshko, V.I. Belotelov, and M.S. Tagirov, Sci. Rep. **11**, 7673 (2021).
8. G.A. Melkov, V.L. Safonov, A.Yu Taranenko, S.V. Sholom, JMMM **132**, 180 (1994).
9. D.A. Bozhko, P. Clausen, A.V. Chumak, Yu.V. Kobljanskyj, B. Hillebrands, and A.A. Serga, Low Temperature Physics **41**, 1024 (2015).
10. D.A. Bozhko, A.J.E. Kreil, H.Yu. Musiienko-Shmarova, A.A. Serga, A. Pomyalov, V.S. L'vov & B. Hillebrands, Nature Commun. **10**, 2460 (2019).
11. R.P. Feynman, R.B. Leighton, and M. Sandsб "The Feynman Lectures on Physics" (2011).
12. P.M. Vetoshko, G.A. Knyazev A.N. Kuzmichev, A.A. Holin, V.I. Belotelov, and Yu.M. Bunkov, JETP Lett. **112**, 299 (2020).
13. P. Nowik-Boltyk, O. Dzyapko, V.E. Demidov, N.G. Berloff, & S.O. Demokritov, Sci. Rep. **2**, 1 (2012).

SPIN-TORQUE DIODE EFFECT: FROM FUNDAMENTAL RESEARCH TO APPLICATIONS

P.N. Skirdkov[1,2], *K.A. Zvezdin*[1,2]

[1]New Spintronic Technologies, Russian Quantum Center, Skolkovo Innovation Center, Moscow Region, Russia
[2]Prokhorov General Physics Institute of the Russian Academy of Sciences, Moscow, Russia
*E-mail : zvezdin.ka@phystech.edu

Interest in spintronic heterostructures based on magnetic tunnel junctions (MTJ) is primarily due to the possibility of their efficient use for information storage. However, this does not limit the range of their application. Of particular interest is the microwave dynamics of magnetization in such structures. It was shown that, using a magnetic tunnel junction, it is possible to generate an alternating (microwave) signal under the action of a direct spin-polarized current [1]. Based on this effect, there are efforts to create a new generation of alternating signal generators called spin-transfer nanooscillator (STNO) for telecommunication devices.

Of no less interest is the effect opposite to the one considered above, namely the spin-torque diode (STD) effect [2]. When an alternating spin-polarized current with a frequency close to the resonant frequency is passed through the MTJ, a direct current component is created at the output. It can obviously be used for signal detection. In the first works, the microwave sensitivity of the AC signal rectification did not exceed 1.4 mV/mW. However, already in 2014, a record microwave sensitivity of a spin-torque diode at room temperature of 12,000 mV/mW was experimentally demonstrated [3]. This sensitivity was achieved by using a DC bias current. Subsequently, the microwave sensitivity was increased up to 210,000 mV/mW [4–5] by using the bias current and

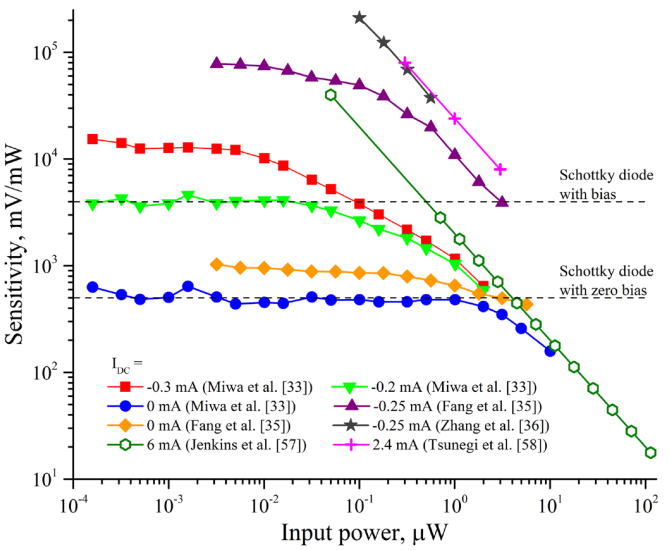

Figure 1. Summary on the dependences of the spin-torque diodes microwave sensitivity on power for different bias currents.

synchronizing the oscillations to an external signal. The summary dependences of sensitivity on power are shown in Fig. 1.

In addition to resonant spin-torque diode rectification, a broadband STD rectification mechanisms are of particular interest. This is primarily due to their potential for ambient RF energy harvesting. The broadband spin-torque rectification mode was first theoretically predicted in 2012 [6] for systems in a perpendicular magnetic field. Then it was experimentally shown that it can be realized without an external field in an MTJ with perpendicular magnetic anisotropy [7].

Another important issue in this area is the possibility of expanding the frequency range of spin-torque diodes. The expansion of the frequency range is possible in the resonant mode, due to the use of exotic micromagnetic states. For example, the vortex distribution of magnetization leads to lower frequencies [8–9], while the exchange pinning leads to higher ones [10]. In addition, unstable magnetic states (such as out-of-plane cone states) make it possible to achieve record sensitivity values, even without bias currents [11].

In this overview report, we demonstrate the development path of spin-torque diodes. Options for increasing sensitivity are be shown and the physical mechanisms behind it are explained. The possibilities of resonant frequency engineering and the transition to broadband rectification are analyzed. The influence of the magnetization distribution on the features of microwave rectification is considered. In conclusion, possible practical applications of the mentioned effects are discussed.

This work was supported by Russian Science Foundation (grant # 19-12-00432).

1. S.I. Kiselev et al., Nature **425**, 380–383 (2003).
2. A. Tulapurkar et al., Nature **438**, 339 (2005).
3. S. Miwa et al., Nat. Mater. **13**, 50 (2014).
4. B. Fang et al., Nat. Commun. **7**, 11259 (2016).
5. L. Zhang et al., Appl. Phys. Lett. **113**, 102401 (2018).
6. O. Prokopenko et al., J. Appl. Phys. **111**, 123904 (2012).
7. B. Fang et al., Phys. Rev. Appl. **11**, 014022 (2019).
8. A. Jenkins et al., Nature Nanotechnology **11**, 360–364 (2016).
9. P.N. Skirdkov et al., Appl. Phys. Lett. **113**, 242403 (2018).
10. A.A. Khudorozhkov et al., Phys. Rev. B **96**, 214410 (2017).
11. A.G. Buzdakov et al., Phys. Rev. Appl. **15**, 054047 (2021).
12. P.N. Skirdkov et al., Annalen der Physik **532**, 1900460 (2020).

TWO-GAP SUPERCONDUCTIVITY IN $Mo_4Ga_{20}Sb$ INTERMETALLIC SUPERCONDUCTOR AS EVIDENCED BY NMR- AND NQR-SPECTROSCOPY

A.A. Gippius[1*], *A.V. Tkachev*[2], *S.V. Zhurenko*[2], *A.V. Gunbin*[2], *D.A. Iarygina*[1], *V.Yu. Verchenko*[3], *A.V. Shevelkov*[3]

[1]M.V. Lomonosov Moscow State University, Faculty of Physics, Moscow, Russia
[2]P.N. Lebedev Physical Institute of the Russian Academy of Sciences, Moscow, Russia
[3]M.V. Lomonosov Moscow State University, Faculty of Chemistry, Moscow, Russia
[*]E-mail: gippius@mail.ru

Molybdenum gallide superconductor $Mo_4Ga_{20}Sb$ with T_c = 6.6 K represents a family of novel intermetallic superconductors $Mo_4Ga_{20}X$ (X = S, Se, Te and Sb) of the Mo_4Ga_{21} structure type which attracts significant scientific interest due to unusual properties of their superconducting state and enhanced electron-phonon coupling [1]. In particular, the specific heat of $Mo_4Ga_{20}Sb$ follows the BCS-derived α-model [2] with the enhanced value of $\alpha = \Delta(0)/(k_B T_c) = 1.825$ and $\Delta C_e/(\gamma_N T_c) = 1.53$ [3].

We performed an extensive study of the intermetallic superconductor $Mo_4Ga_{20}Sb$ by means of NMR and NQR spectroscopy on ^{69}Ga and ^{71}Ga nuclei to gain novel information about its normal state and superconducting properties including pairing mechanism and gap values. We succeeded to observe the complete ^{69,71}Ga NQR spectrum of $Mo_4Ga_{20}Sb$ at 4.2 K, which consists of four pairs of lines corresponding to the four nonequivalent crystallographic positions of gallium in the crystal structure. We observed an unexpected step-like increase in the ^{69}Ga1 NQR linewidth at T_c with decreasing temperature, which might indicate coexistence of several superconducting phases on a

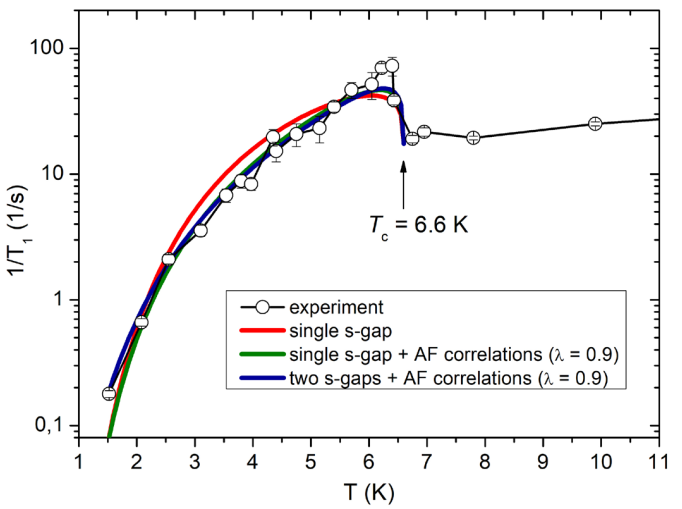

Figure 1. Temperature dependence of $1/^{69}T_1$ and simulation curves for one s-wave gap (red dotted curve), one s-wave gap with antiferromagnetic correlations (green dashed curve), and two s-wave gaps with antiferromagnetic correlations (blue solid curve).

microscopic scale with slightly different T_c values. Above 140 K, the NQR linewidth decreases rapidly with increasing temperature caused by partial averaging of the EFG spatial inhomogeneity due to oscillatory and/or rotational modes of the gallium cluster network arising at elevated temperatures.

We found that above T_c nuclear spin lattice relaxation $1/T_1$ of ^{69}Ga isotope in the Ga1 position follows the Korringa law K^2T_1T = const characteristic for the systems with good metallic conductivity. Below T_c, we observed a pronounced intensive Hebel-Slichter peak (Fig. 1) evidencing for the *s*-wave superconductivity without points or zeroing lines in the *k*-space (full gap s-wave superconductivity).

We demonstrated that the best coincidence with the experimental data is achieved assuming two s-wave superconducting gaps of 13 K and 6 K with relative weights of 0.8 and 0.2, respectively, taking into account antiferromagnetic correlations. The obtained weighted average value of 11.6 K is consistent with the literature estimate of Δ = 12.05 K [3].

Finally, by studying the ^{69}Ga nuclear spin-spin relaxation curves, we found long period oscillations of the spin echo intensity with the frequency of about 2E4 rad/s, which may correspond to internal field of ~3 gauss at all gallium sites.

This work was supported in part by the Ministry of Science and Higher Education of Russian Federation, grant No. 075-15-2021-1353.

1. V.Yu. Verchenko, A.V. Shevelkov, Dalton Trans. **50**, 5109–5114 (2021).
2. H. Padamsee, J.E. Neighbor, C.A. Shifman, J. Low Temp. Phys. **12**, (1973) 387–411.
3. V.Y. Verchenko, A.O. Zubtsovskii, D.S. Plenkin, A.V. Bogach, Z.Wei, A.A. Tsirlin, E.V. Dikarev, A.V. Shevelkov, Chemistry of Materials **32**, 6730−6735 (2020).

LOW-TEMPERATURE ROTATIONAL TUNNELING OF BH_4 GROUPS IN $Li_2(bIm)BH_4$: NUCLEAR MAGNETIC RESONANCE AND NEUTRON SPIN-ECHO STUDIES

A.V. Skripov [1*], *A.V. Soloninin*[1], *O.A. Babanova*[1], *R.V. Skoryunov*[1], *F. Morelle*[2], *Y. Filinchuk*[2], *M. Dimitrievska*[3], *A. Faraone*[3], *T.J. Udovic*[3]

[1]Institute of Metal Physics, Ural Branch of the Russian Academy of Sciences, Ekaterinburg, Russia
[2]Universite Catholique de Louvain, Louvain-la-Neuve, Belgium
[3]National Institute of Standards and Technology, Gaithersburg, MD, USA
[*]E-mail: skripov@imp.uran.ru

To investigate the dynamical properties of the novel hybrid compound, lithium benzimidazolate-borohydride $Li_2(bIm)BH_4$ (where bIm denotes a benzimidazolate anion, $C_7N_2H_5^-$), we have used a set of complementary techniques: nuclear magnetic resonance (NMR), quasielastic neutron scattering, and neutron spin echo. The unusual structural feature of $Li_2(bIm)BH_4$ is that one H atom of each tetrahedral $[BH_4]^-$ anion is anchored within a nearly square hollow formed by four coplanar Li^+ cations, while the remaining $-BH_3$ fragment extends into a relatively open space, being only loosely coordinated to other atoms (Fig. 1) [1].

For such a structure, one may expect low energy barriers for the uniaxial reorientational motion of BH_4 groups, as shown in Fig. 1. Our NMR measurements of the ^1H spin-lattice relaxation rates at different resonance frequencies have revealed the extremely fast reorientational motion at low temperatures. Interpretation of the experimental NMR results in terms of the classical thermally activated motion indicates that the H jump rate should reach 10^8 s^{-1} already at T = 28 K. However, the frequency dependence of the low-temperature spin-lattice relaxation data deviates from the predictions of the classical theory, suggesting a presence of rotational tunneling of BH_4 groups. Analysis of our low-temperature NMR results in the framework of the model [2] yields the value of 0.49 μeV for the tunnel splitting of the ground libration state. A direct evidence of the rotational tunneling could be based on observing a line splitting in low-temperature inelastic neutron scattering spectra corresponding to very high resolution in energy transfer. Our measurements performed on the backscattering neutron spectrometer HFBS at the National Institute of Standards and Technology (NIST) have appeared to be consistent with the rotational tunneling in $Li_2(bIm)BH_4$; however,

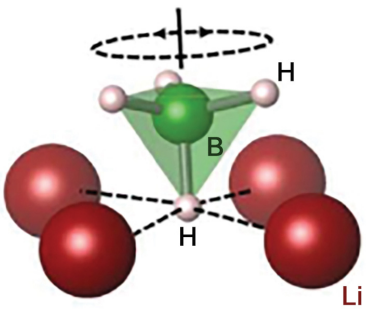

Figure 1. Schematic view of the coordination of each tetrahedral $[BH_4]^-$ anion in $Li_2(bIm)BH_4$ and the uniaxial reorientational (rotational) motion of a BH_4 group.

the observed value of the tunnel splitting is at the limit of energy resolution for this backscattering spectrometer. Therefore, we have used the neutron spin echo spectrometer NSE at NIST which is known to provide the highest available resolution in energy transfer. The NSE measurements have been performed at three temperatures (3.6 K, 20 K, and 30 K). The oscillatory form of the observed intermediate scattering function $I(Q, t)$ at 3.6 K gives the direct evidence of the rotational tunneling. The value of the tunnel splitting derived from the neutron spin-echo experiment (0.43 μeV) satisfactorily agrees with the corresponding value estimated from the NMR spin-lattice relaxation measurements. This result is the first well-documented observation of rotational tunneling of BH_4 groups in borohydrides. With increasing temperature, we have observed a gradual transition from the quantum dynamics of BH_4 groups (rotational tunneling) to the classical dynamics (thermally activated reorientational jumps). Our measurements using the time-of-flight neutron spectrometer DCS at NIST at $T = 80$ K have confirmed that the Q-dependence of the elastic incoherent structure factor corresponds to the uniaxial reorientations of BH_4 groups around its 3-fold symmetry axis, and the rate of reorientational jumps at this temperature reaches $5 \cdot 10^{11}$ s^{-1}.

1. A.V. Skripov, M. Dimitrievska, O.A. Babanova, R.V. Skoryunov, A.V. Soloninin, F. Morelle, Y. Filinchuk, A. Faraone, H. Wu, W. Zhou and T.J. Udovic, J. Phys. Chem. C **123**, 20789–20799 (2019).
2. W. Müller-Warmuth, R. Schüler, M. Prager and A. Kollmar, J. Chem. Phys. **69**, 2382–2392 (1978).

B.O1

ELECTRONIC STRUCTURE AND HYPERFINE INTERACTIONS IN Cr_xNbSe_2 (x = 0.33, 0.5) BY DFT STUDIES

P.A. Agzamova[1,2*], *V.V. Ogloblichev*[1]

[1]M.N. Mikheev Institute of Metal Physics of Ural Branch of Russian Academy of Sciences, Ekaterinburg, Russia
[2]Ural Federal University named after the first President of Russia B.N. Yeltsin, Ekaterinburg, Russia
[*]E-mail: polly@imp.uran.ru

The transition metal dichalcogenides (TMDCs) consist of hexagonal layer of metal T atoms which are sandwiched between two layers of chalcogen atoms X (S, Se, or Te). The T–X bonds in sandwiches are predominantly covalent in nature, whereas the T–X–T trilayers are connected by week van der Waals forces. The week bonding between the T–X–T sandwiches allows intercalating foreign atoms or molecules in the interlayer space and obtaining materials with new properties that differ significantly from those observed in the parent compounds. In M_xTX_2 compounds intercalated with 3d metal atoms having a magnetic moments, different magnetic states were observed depending on the concentration and type of M atoms as well as on the matrix compound TX_2.

From these points of view the intercalated compounds Cr_xNbSe_2 with Cr concentrations up to $x = 0.5$ were recently studied to reveal the effect of intercalation on the crystal structure, magnetic state, and thermal properties [1]. It was shown the presence of a magnetic moment on Nb atoms oppositely directed relative to the Cr moment. Keeping in mind that the distribution of charge and spin density is a key to understanding the mechanisms responsible for the changes in properties of compounds upon intercalation of various TMDCs. In [1] the investigations of Cr_xNbSe_2 compounds with chromium concentration $x = 0.33$ and $x = 0.5$ have been performed by means of NMR spectroscopy on ^{53}Cr and ^{93}Nb nuclei to answer the question about the effect of chromium intercalation on the distribution of spin and charge density in Cr_xNbSe_2.

The present work aims to theoretically estimate the quadrupole interactions of chromium and niobium nuclei in different environments by DFT methods and interpret the experimental NMR data.

Intercalation of the parent compound $NbSe_2$ with chromium ions leads to the formation of crystal structures with a different arrangement of chromium atoms in the lattice. So, the crystal structure of the $Cr_{0.5}NbSe_2$ compound was attributed the $P6_3/mmc$ space group, whereas in $Cr_{0.33}NbSe_2$ the coexistence of $P6_3/mmc$ and $P6_322$ space groups takes place. The parameters of quadrupole interaction of ^{53}Cr and ^{93}Nb nuclei were determined by the first-principles calculations using density functional theory (DFT) methods in the VASP program package [2] (the lattice parameters for $x = 0.33$ and $x = 0.5$ were taken from [3]). It was determined that for both structures the principal axis of the electric-field gradient V_{zz} is directed along the c axis and has the asymmetry parameter η close to zero. The values of quadrupole frequencies of chromium nuclei are determined as $\nu_Q^{calc} = 1.1$ MHz for the crystal structures with the $P6_3/mmc$ space group and $\nu_Q^{calc} = 2.85$ MHz with the $P6_322$ space group, respectively. The ^{93}Nb quadrupole frequency for the crystal structures $P6_322$ was $\nu_Q^{calc} \approx 1.2$ MHz. In the crystal structures $P6_3/mmc$, the distribution of frequencies was from 1.2 to 0.8 MHz. Such a ν_Q^{calc} distribution is associated with the existence of nonequivalent niobium positions in the structure due to the different nearest environment of chromium ions.

Thus, the *ab initio* calculations made it possible to interpret the NMR spectra on chromium. Analyzing the quadrupole parameters of the NMR spectra, it was found that two crystallographic

phases with different space groups coexist in the composition of $Cr_{0.33}NbSe_2$. At the same time, this is not observed in the composition of $Cr_{0.5}NbSe_2$.

The work was supported by RSF (project No. 22-12-00220).

1. V.V. Ogloblichev, N.V. Baranov, P.A. Agzamova et al., Phys. Rev. B **104**, 245115 (2021).
2. G. Kresse and J. Hafner. Phys. Rev. B **47**, 558 (1993).
3. N.M. Toporova, E.M. Sherokalova, N.V. Selezneva et al., J. Alloys Compd. **848**, 156534 (2020).

B.O2

TIME-DEPENDENT EXCHANGE CREATES THE TIME-FRUSTRATED STATE OF MATTER

V.E. Valiulin[1,2], *N.M. Chtchelkatchev*[1,2,3*], *A.V. Mikheenkov*[1,2], *V.M. Vinokour*[4]

[1]Vereshchagin Institute of High Pressure Physics, Troitsk, Moscow, Russia
[2]Moscow Institute of Physics and Technology, Dolgoprudny, Russia
[3]Institute of Metallurgy, Ekaterinburg, Russia
[4]Physics Department, City College of the City University of New York
[*]E-mail: chtchelkatchev@hppi.troitsk.ru

Magnetic systems governed by exchange interactions between magnetic moments harbor frustration that leads to ground state degeneracy and results in the new topological state often referred to as a frustrated state of matter (FSM). The frustration in the commonly discussed magnetic systems has a spatial origin [1, 2]. Here we demonstrate that an array of nanomagnets coupled by the real retarded exchange interactions develops a new state of matter, time frustrated matter (TFM). In a spin system with the time-dependent retarded exchange interaction, a single spin-flip influences other spins not instantly but after some delay. This implies that the sign of the exchange interaction changes, leading to either ferro- or antiferromagnetic interaction, depends on time. As a result, the system's temporal evolution is essentially non-Markovian. The emerging competition between different magnetic orders leads to a new kind of time-core frustration. To establish this paradigmatic shift, we focus on the exemplary system, a granular multiferroic, where the exchange transferring medium has a pronounced frequency dispersion and hence develops the TFM.

In granular multiferroics [3, 4] interactions occur not directly but through the mediating active dielectric or ferroelectric environment. In such materials the retardation effects are relatively large and cannot be ignored.

An elemental building block of a granular-multiferroic, two adjacent magnetic granules interacting via a ferroelectric medium as schematically shown in Fig. 1. Since the dielectric constant of a ferroelectric environment typically has significant frequency dispersion, the retardation effects are inevitable. Indeed, in a simplest approximation taking into account the dielectric screening of the Coulomb interaction, one finds, that the dielectric constant appears in the effective exchange between two magnetic moments:

$$J \sim \sum_{a,b} \int d\mathbf{r}_1 d\mathbf{r}_2 \Psi_a^*(\mathbf{r}_2)\Psi_b^*(\mathbf{r}_1)\frac{e^2}{\varepsilon\,|\mathbf{r}_1-\mathbf{r}_2|}\Psi_a(\mathbf{r}_1)\Psi_b(\mathbf{r}_2) \quad ,$$

where the sum is taken over the electron wave functions of each granule, and Ψ stand for the undisturbed electron wave functions. More precise calculation requires including the effect of the environment on the wave functions and also accounting for the spatial dispersion effects. Yet, even in this first approximation, the frequency dispersion of the exchange integral $J(\omega)$ arises due to dispersion of $\varepsilon(\omega)$ the behavior of which is straightforwardly related to the dielectric permittivity tensor of the ferroelectric environment.

Accordingly, we arrive at the model of a magnetic system with the effectively delayed exchange J. In a temporal representation, this implies the delay in the interaction of magnetic moments. In typical ferroelectrics (e.g., such as barium titanate (BTO) and lead zirconate titanate (PZT)), $\varepsilon(\omega)$ is

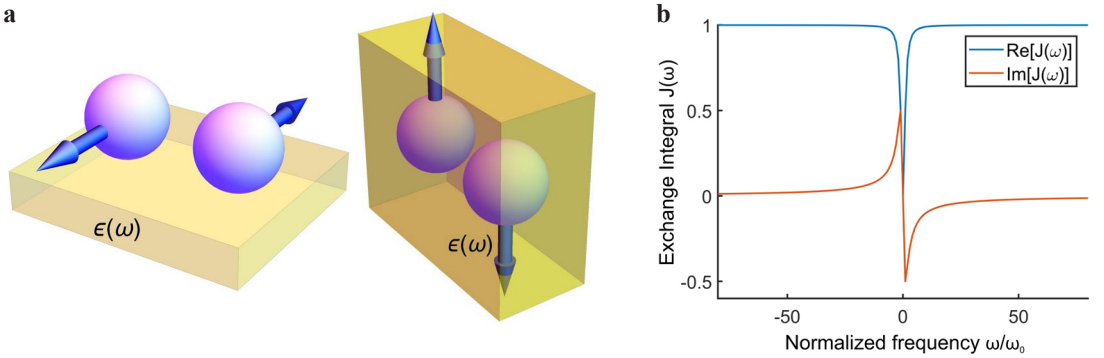

Figure 1. **a** Granular multiferroic: magnetic granules in ferroelectric medium. **b** Exchange interaction with ω-dispersion.

large (≥1000) at low frequencies, and is of the order of unity for large frequencies. The frequency threshold is set by the phonon frequency which usually does not exceed much 1 THz.

Consequently, for small frequencies, we may treat $J(\omega)$ as vanishing, while at large frequencies, $J(\omega)$ tends to finite values. Taking the simplest form of the exchange satisfying all the above-defined conditions

$$J(t) = G\left((\delta(t) - \omega_0 e^{-\omega_0|t|}\right) \ ,$$

where $\delta(t)$ is the Dirac delta function using its Fourier transform,

$$J(\omega) = G\frac{\omega}{\omega + i\omega_0} \ ,$$

which preserves the causality as the pole is in the lower half of the ω-plane, and displays a reasonable asymptotic behavior, see Fig. 1.

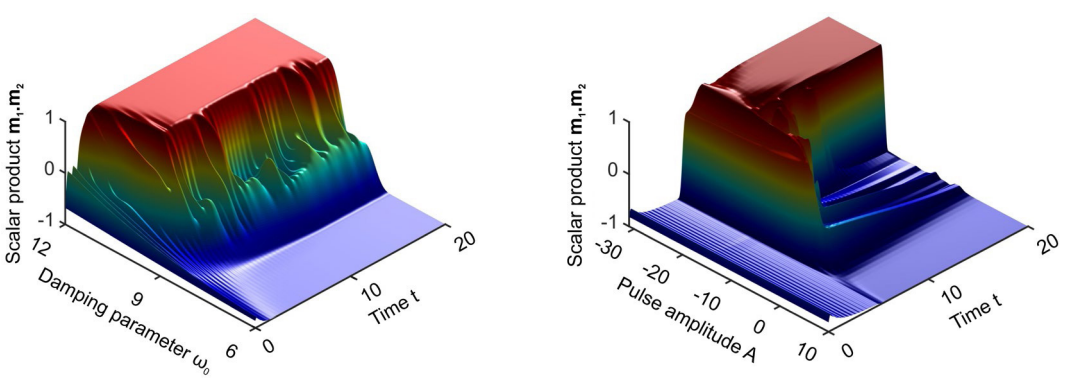

Figure 2. Control of the final stable state by the damping parameter or by the external pulse: the magnetic moments scalar product is depicted.

The magnetic granules are supposed to be semiclassical, hence granule's magnetization should obey the non-local in time Landau-Lifshitz-Hilbert (LLH) equation:

$$\dot{\mathbf{m}}_i(t) = -\gamma[\mathbf{m}_i(t)\times\mathbf{h}_i^{\mathrm{eff}}(t)] - \lambda\gamma[\mathbf{m}_i(t)\times[\mathbf{m}_i(t)\times\mathbf{h}_i^{\mathrm{eff}}(t)]] \ ,$$

$$\mathbf{h}_i^{\mathrm{eff}}(t) = \sum_j \int_{-\infty}^{t} J_{ij}(t-\tau)\mathbf{m}_j(\tau)\mathrm{d}\tau + h^{\mathrm{ext}}(t) \ .$$

While $J(\omega = 0) = 0$ (dynamical frustration) any magnetic configuration formally assumes a stationary solution of LLH. We address further the important question whether these solutions are stable with respect to small perturbations like noise or an external field, and show that only particular stationary configurations are stable. We demonstrated, see Fig. 2, that owing to the dynamic frustration, the ferromagnetic and antiferromagnetic are stable and long-living states, hence having, in fact, the same energies [5].

The work was supported by the Russian Science Foundation (grant 18-12-00438).

1. A. Kirilyuk, A.V. Kimel, and T. Rasing, Rev. Mod. Phys. **82**, 2731–2784 (2010).
2. M. Fiebig, T. Lottermoser, D. Meier, and M. Trassin, Nature Reviews Materials **1**, 16046 (2016).
3. O.G. Udalov, N.M. Chtchelkatchev, A. Glatz, and I.S. Beloborodov, Phys. Rev. B **89**, 054203 (2014).
4. O.G. Udalov, N.M. Chtchelkatchev, A. Glatz, and I.S. Beloborodov, Phys. Rev. B **90**, 054201 (2014).
5. V.E. Valiulin, N.M. Chtchelkatchev, A.V. Mikheenkov and V.M. Vinokour, Sci. Rep. 2022 (in press).

EVOLUTION OF THE MAGNETIC PROPERTIES OF $FeBO_3$ SINGLE CRYSTALS UNDER GALLIUM DOPING

N. Snegirev[1*], *I. Lyubutin*[1], *A. Bogach*[2], *M. Chuev*[3], *S. Starchikov*[1], *S. Yagupov*[4], *Yu. Mogilenec*[4], *K. Seleznyova*[4], *M. Strugatsky*[4]

[1]Shubnikov Institute of Crystallography, FSRC "Crystallography and Photonics" of RAS, Moscow, Russia
[2]Prokhorov General Physics Institute of RAS, Moscow, Russia
[3]Valiev Institute of Physics and Technology of RAS, Moscow, Russia
[4]Physics and Technology Institute, V.I. Vernadsky Crimean Federal University, Simferopol, Russia
[*]E-mail: niksnegir@yandex.ru

Iron borate $FeBO_3$ is a well-known material with interesting properties that are important for fundamental physics and materials science [1, 2]. The synthesis of $Fe_{1-x}Ga_xBO_3$ single crystals, isostructural with iron borate, determines the prospects for further practical application of such materials [2, 3]. Doping with gallium enables to synthesize crystals with desired magnetic properties, in particular, with a reduced temperature of the magnetic phase transition [3]. Thus, $Fe_{1-x}Ga_xBO_3$ crystals with a Néel point $T_N \sim 42$ °C can be used as an ultrasensitive temperature sensor in biomedicine, whereas crystals with T_N near the room temperature are important for use in nuclear resonance synchrotron experiments [4].

In this work, a series of single crystals based on iron borate was studied using SQUID magnetic measurements and Mössbauer spectroscopy. Theoretical analysis was applied for accurate processing of the magnetic properties of $Fe_{1-x}Ga_xBO_3$ single crystals.

A series of high quality $Fe_{1-x}Ga_xBO_3$ crystals was synthesized [4] by the flux-growth technique developed in references [1–3]. The exact concentration of Ga in the obtained crystals was determined using X-ray fluorescence analysis.

Figure 1 shows the magnetization curves of $Fe_{1-x}Ga_xBO_3$ single crystals with different x. The shape of the magnetization curves is well described by the conventional conception of an easy-plane antiferromagnet with weak ferromagnetism appeared due to the Dzyaloshinskii interaction. This

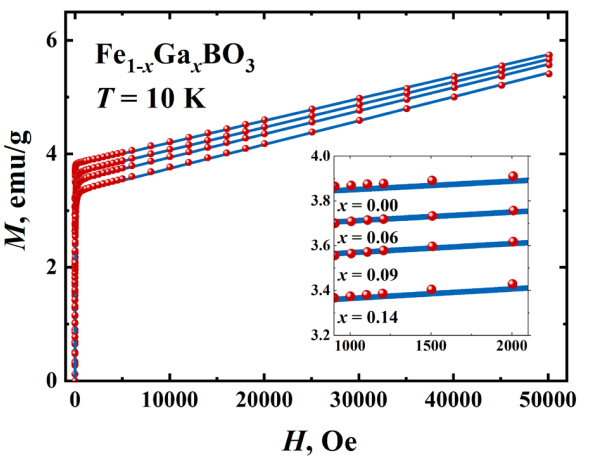

Figure 1. Magnetization curves for $Fe_{1-x}Ga_xBO_3$ single crystals with different x, obtained at 10 K ($H \parallel [001]$). The dots are experimental data and the lines are the result of theoretical modelling.

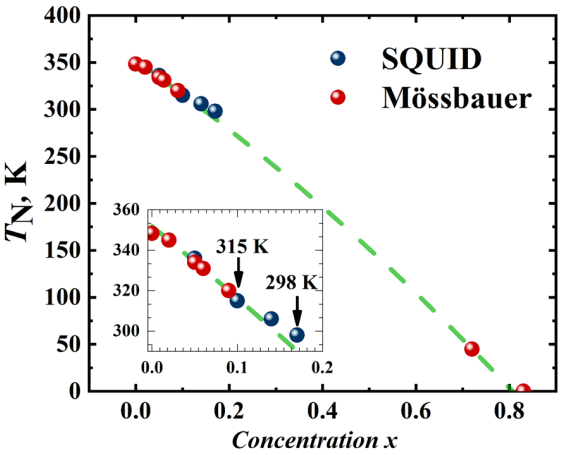

Figure 2. Magnetic phase transition temperature T_N for $Fe_{1-x}Ga_xBO_3$ single crystals with different x, obtained by SQUID measurements (blue dotes) and Mössbauer spectroscopy (red dotes). Dashed lines are guides for the eye.

results in a slight deviation of the magnetic moments of the two sublattices from the antiparallel orientation [5].

Theoretical modelling of the magnetization curves was performed in terms of uncompensated magnetic moments of two magnetic sublattices [6]. It was established that the antiferromagnetic susceptibility increases with increasing x. At 10 K it is equal to $\chi = (3.875 \pm 0.05) \cdot 10^{-5}$ g^{-1} for $FeBO_3$ and $\chi = (4.207 \pm 0.07) \cdot 10^{-5}$ g^{-1} for $Fe_{0.86}Ga_{0.14}BO_3$.

The Mössbauer spectra for $Fe_{1-x}Ga_xBO_3$ single crystals were obtained in a wide temperature range of 10–400 K. A theoretical model was developed to describe nuclear resonance transitions in iron atoms in the approximation of a combined magnetic dipole and electric quadrupole hyperfine interaction [7]. The distribution of the hyperfine magnetic field centered around the characteristic maxima of the binomial distribution was taken into account when interpreting the Mössbauer spectra for gallium-doped crystals.

The dependence of the Néel temperature of $Fe_{1-x}Ga_xBO_3$ on the gallium concentration, obtained using SQUID measurements and Mössbauer spectroscopy data, is shown in Fig. 2.

It can be concluded that the crystals with composition $Fe_{0.9}Ga_{0.1}BO_3$ and $Fe_{0.83}Ga_{0.17}BO_3$, whose Neel temperatures are about ~42 °C (315 K) and near the room temperature, respectively, can be of interest for the practical applications.

The results obtained will be important for the use of $Fe_{1-x}Ga_xBO_3$ crystals in new high-tech fields.

This work is funded by the Russian Foundation for Basic Research, project number 19-29-12016-мк.

1. S. Yagupov et al., Crystal Growth & Design **18**, 7435–7440 (2018).
2. E.S Smirnova et al., Acta Crystallographica Section B **76**, 1100–1108 (2020).
3. S. Yagupov et al., Appl. Phys. A **121**, 179–185 (2015).
4. N. Snegirev et al., Journal of Alloys and Compounds **889**, 161702 (2021).
5. S.V. Vonsovskii, Magnetism, Nauka, Moscow, (1971); Wiley, New York (1974).
6. L. Néel Comptes Rendus Hebdomadaires Des Seances De L Academie Des Sciences **252**, 4075–4080 (1961).
7. I.S. Lyubutin et al., Journal of Alloys and Compounds **906**, 164348 (2022).

SPECTRUM EVOLUTION OF MAGNETOSTATIC WAVES EXITED VIA FEMTOSECOND LASER PULSES IN ANISOTROPIC FILMS

*N.E. Khokhlov**, *Ia.A. Filatov, P.I. Gerevenkov, A.M. Kalashnikova*

Ioffe Institute, St. Petersburg, Russia
*E-mail: n.e.khokhlov@mail.ioffe.ru

In the last two decades, femtosecond laser pulses have become a powerful tool for controlling ultrafast magnetization dynamics as they have a number of significant advantages over traditional research tools [1]. The development of modern magnetism has brought femtomagnetism [1] and magnonics [2] into contact: optical excitation of spin waves (SW) has been demonstrated recently [3]. On the other hand, active optical control of SW propagation is an urgent task of magnonics [4]. But the characteristic times of such control are still far from the ultrafast regime. Thus, the use of femtosecond laser pulses in reconfigurable magnonics is a modern problem of fundamental magnetism with a potential impact on the design of data processing devices.

We present the analysis of the spectrum evolution of magnetostatic spin waves (MSWs) in uniformly magnetized film and near 180° domain wall. Firstly, we use two-color optical pump-probe technique with spatial resolution to study the influence of femtosecond laser pulses on propagation of MSWs in ferromagnetic metallic films of iron and galfenol ($Fe_{81}Ga_{19}$). The films exhibit the pronounced in-plane magnetocrystalline anisotropy. We show that the feature provides the opportunity to excite MSWs via ultrafast thermal magnetocrystalline anisotropy changes [5–7]. Moreover, we control whether the low- or high-frequency part of the spin wave spectrum is suppressed upon propagation by changing the orientation of external magnetic field with respect to the anisotropy axes. The concept of MSSW's spectrum control is extended further by analysing properties of the MSWs optically excited near a Néel domain wall in a ferromagnetic strip. Micromagnetic modelling reveals the appearance of controllable resonance peaks in the MSWs spectrum and shows that the combination of femtosecond optical excitation with magnetic nonuniformity of the film, e.g. a domain wall, serves as a tuneable source of MSWs wavepackets [8].

The presented concept of controllable modification of MSWs' spectrum will work near different types of magnetic inhomogeneities that create spatially varying stray fields and/or demagnetizing fields. Examples of such inhomogeneities are Néel or Bloch DWs, magnetic skyrmions, cylindrical magnetic domains, impurities, sample defects, etc. opening up additional possibilities for creating magnonic nanodevices.

Support by RSF (grant 22-22-00326) is acknowledged.

1. A.V. Kimel, A.M. Kalashnikova, A. Pogrebna, A.K. Zvezdin, Physics Reports **852**, 1 (2020).
2. С.А. Никитов и др., УФН **190**, 1009–1040 (2020).
3. T. Satoh et al., **6**, 662–666 (2012).
4. M. Vogel et al., Nat. Physics **11**, 487–491 (2015).
5. N.E. Khokhlov et al., Phys. Rev. Applied **12**, 044044 (2019).
6. Ia.A. Filatov et al., J. Phys. Conf. Ser. **1697**, 012193 (2020).
7. Ia.A. Filatov et al., Appl. Phys. Lett. **120**, 112404 (2022)
8. N.E. Khokhlov, A.E. Khramova, Ia.A. Filatov, P.I. Gerevenkov, B.A. Klinskaya, A.M. Kalashnikova, JMMM **534**, 168018 (2021).

THEORY AND EXPERIMENT OF THE FERROMAGNETIC RESONANCE IN NANOCOMPOSITE METAL-DIELECTRIC FILMS

V.S. Vlasov[1*], *L.N. Kotov*[1], *A.A. Utkin*[1], *D.A. Pleshev*[1,2], *F.F. Asadullin*[2], *A.V. Sitnikov*[3]

[1]Syktyvkar State University, Syktyvkar, Russia
[2]Saint-Petersburg state forest technical university named after S.M. Kirov, St. Petersburg, Russia
[3]Voronezh State Technical University, Voronezh, Russia
[*]E-mail: vlasovv78@mail.ru

Nanocomposite metal-dielectric films are promising materials for application [1]. This films have unique characteristic: giant magnetoresistance, intense magnetooptical response, high coercivity, weak noise [2]. The films can be used as medium for recording and they can be applied as magnetic sensor, for microwaves filters, read heads [1–3]. Using ferromagnetic resonance (FMR) is very useful tools to study of magnetic films. To study the spectra of uniform precession or excited modes we can get important information about the effective fields, form and distribution of the grains, the ferromagnetic exchange coupling constant, etc. [2, 3]. To solve the problem of FMR in nanocomposite films is important to choose the model for resonance films properties describe. Metal-dielectric composite films consist of many randomly oriented magnetic and dielectric particles with different size and shape. Thus, each composite film is a complex magnetic system and the FMR in such system is different from the resonance in homogeneous single-crystal films.

For description of FMR spectra of the films the averaging field method was used. We had used the mathematical model like the Netzelmann method [4]. The macroscopic demagnetization tensor of the whole film for determination of resonance fields and averaged magnetization were used. The demagnetizing factor of a single particle was also used in resonance field expression. Dubowik in the work [5] noticed that the expression of Netzelmann [4] require correction. The equations for the resonance fields from the works [4, 5] were used in present work. We develop the model for the different particle distributions cases.

We compare our model results with the experimental data of FMR in nanocomposite metal-dielectric films with same dielectric and different magnetic metal alloy. The compositions of the films were as following: $(CoFeB)_x(MgO)_y$ (B1-series); $(CoTaNb)_x(MgO)_y$ (B2-series) $0.2 < x < 0.7$. Experimental FMR data show that for these series of films, with the increase of the concentration of metal x, different percolation regimes are observed. The theoretical model developed in the work allows us to explain the differences in percolation in the films based on the different distribution of metal film granules for this films and the different topology of these granules. The behavior of the metal phase concentration dependence of the resonance field was explained particularly by the concentration dependences of the demagnetizing factors of film particles.

Thus we considered model that can be used to describe experiments on the FMR for nanocomposite metal-dielectric films. This model is suitable for thin films.

This work has been supported by Russian Science Foundation (project No. 21-72-20048).

1. B. Raneesh, P.M. Visakh, Metal Oxide Nanocomposites. Synthesis and Applications. Scrivener Publishing, USA (2021).
2. A.B. Drovosekov, N.M. Kreines, A.S. Barkalova, S.N. Nikolaev, V.V. Rylkov, A.V. Sitnikov, JMMM **495**, 165875 (2020).
3. L.N. Kotov, M.P. Lasek, V.K. Turkov et al., Bull. Russ. Acad. Sci. Phys. **84**, 1065–1067 (2020).
4. U. Netzelmann, J. Appl. Phys. **68**, 1800–1807 (1990).
5. J. Dubowik, Phys. Rev. B **54**, 1088–1091 (1996).

MAGNETIC STRUCTURE OF $FeP_{1-x}As_x$ (x = 0.33, 0.5) AS SEEN BY NMR-SPECTROSCOPY

S.V. Zhurenko[1,2*], *A.V. Tkachev*[1], *A.V. Gunbin*[1], *I.G. Silkin*[3], *I.V. Morozov*[3], *A.S. Moskvin*[4], *A.A. Gippius*[1,2]

[1]P.N. Lebedev Physics Institute, Moscow, Russia
[2]Department of Physics, Lomonosov Moscow State University, Moscow, Russia
[3]Department of Chemistry, Lomonosov Moscow State University, Moscow, Russia
[4] Ural Federal University, Ekaterinburg, Russia
[*]E-mail: Zhurenko@lebedev.ru

Scientific interest in binary pnictides of 3d-metals: FeAs, FeP, CrAs, MnP is due to the complexity of their magnetic structure in the ground state, as well as the recently discovered superconductivity in the FeAs compound at high pressures. In our recent articles, the magnetic structure of a polycrystalline and single crystal FeP was investigated in detail by means of NMR-spectroscopy [1].

The magnetic properties of poly- and single-crystal FeAs were investigated [2–4]. According to various sources, the Neel temperature is 77 K [5] or 69.6–71.5 K [3, 4, 6]. The magnetic structure of FeAs was studied earlier both by neutron diffraction [5, 6] and by Mössbauer spectroscopy [7–9]. According to these data, the magnetic structure of FeAs in the ground state is helicoidal and, in contrast to FeP, is incommensurate with the crystal lattice.

As is known, doping a compound with an ion with a different ionic radius leads to a change in the crystal lattice constant (chemical contraction). Which leads to a change in the magnetic structure. To study the effect of homovalent substitution of phosphorus on arsenic, polycrystalline samples were synthesized. To prevent the effect of sample grain rotation by high magnetic field, the samples were sealed in paraffin. We chosed the NMR-spectroscopy as the most informative local technique for the study of magnetic structures. In this paper we present the field-sweep ^{31}P NMR-spectra measurements at several fixed frequencies and zero-field NMR-spectra at 4.2 K performed on the single-phase polycrystalline sample $FeP_{1-x}As_x$ with x = 0.33 and 0.50. In contrast to Mössbauer results, we observe dramatic symmetry reduction of magnetic structure in $FeP_{1-x}As_x$ (x = 0.33, 0.50), resulting in essential narrowing ^{31}P NMR spectra. This narrowing points to phosphorous local fields decreasing compared to parent FeP.

1. A.A. Gippius et al., Phys. Rev. B **102**, 214416–214416 (2020). DOI: 10.1103/PhysRevB.102.214416.
2. K.A. Ziq, A.F. Salem, Magnetic Properties of FeAs Single Crystal. J. Supercond. Nov. Magn., **26**, 1185–1188 (2013). DOI: 10.1007/s10948-012-2013-3.
3. K. Segawa, Y. Ando, J. Phys. Soc. Japan **78** (10), 104720 (2009). DOI: 10.1143/jpsj.78.104720.
4. D. Gonzalez-Alvarez et al., FeAs: J. Chem. Thermodynamics **21** (4), 363–373 (1989). DOI:10.1016/0021-9614(89)90137-7.
5. K. Selte, A. Kjekshus, and A.F. Andresen, Acta Chem. Scand. A **26**, 3101–3113 (1972). DOI: 10.3891/acta.chem.scand.26-3101.
6. E.E. Rodriguez et al., Phys. Rev. B **83**(13) (2011). DOI:10.1103/physrevb.83.134438.
7. S.K. Kulshreshtha, P. Raj, J. Physics F: Metal Physics **9**(11), 2253–2259 (1979). DOI:10.1088/0305-4608/9/11/015.
8. M. Yuzuri, R. Tahara, Y. Nakamura, J. Phys. Soc. Japan **48**(6), 1937–1941 (1980). DOI:10.1143/jpsj.48.1937.
9. A. Błachowski, K. Ruebenbauer, J. Żukrowski, Z. Bukowski, J. Alloys and Comp. **582**, 167–176 (2014). DOI:10.1016/j.jallcom.2013.08.049.

B.O7

THE CONDUCTION ELECTRON SYSTEM OF A HEXABORIDE SUPERCONDUCTOR YB_6 PROBED BY ^{89}Y AND ^{11}B NMR

O.M. Vyaselev[1,2*], N.E. Sluchanko[3], A.V. Bogach[3], N.Y. Shitsevalova[4], V.B. Filipov[4], A.A. Gippius[5,6]

[1]Institute of Solid State Physics, Rus. Ac. Sci., Chernogolovka, Moscow region, Russia
[2]Russian Quantum Center, 100 Novaya Street, Skolkovo, Moscow Region Russia
[3]Prokhorov General Physics Institute, Rus. Ac. Sci., 38 Vavilov str., Moscow, Russia
[4]Frantsevich Institute for Problems of Materials Science, Nat. Ac. Sci. of Ukraine, Kyiv, Ukraine
[5]Faculty of Physics, M. V. Lomonosov Moscow State University, Moscow, Russia
[6]P. N. Lebedev Physical Institute, Rus. Ac. Sci., Moscow, Russia
*E-mail: vyasel@issp.ac.ru

Binary borides MeB_x are relatively simple regarding their chemical composition and crystal structure but show diverse superconducting behavior that makes them attractive model objects for studying superconducting mechanisms. Metal hexaborides MeB_6 adopt the simple CsCl-type $Pm\bar{3}m$ crystal structure. Among hexaboride superconductors only YB_6 has the transition temperature achievable by ^{4}He cryogenics. Depending on preparation conditions and methods, the reported critical temperatures of this BCS-type superconductor vary up to 8.4 K. In this report we present ^{11}B and ^{89}Y NMR study performed in 7 T field on YB_6 powder samples with T_c = 7.4 and 4.2 K prepared from single crystals grown with a slight variation of the starting charge composition. A recent study of these crystals [1] has related the change in T_c with structural peculiarities: the sample with higher T_c was reported to be slightly more disordered and less stoichiometric that the other one.

Figure 1a shows the nuclear spin-lattice relaxation (NSLR) rates of ^{89}Y, $^{89}T_1^{-1}$ for the two studied samples, plotted as a function of temperature. The relaxation shows $^{89}T_1^{-1} \propto T$ dependence indicating

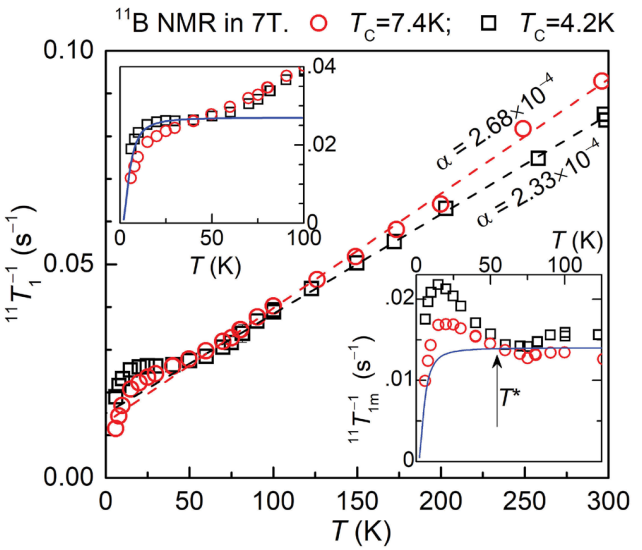

Figure 1. Temperature dependences of ^{89}Y **a** nuclear spin-lattice relaxation rate, **b** Knight shift, in two samples of YB_6, measured in the external field of 7 T.

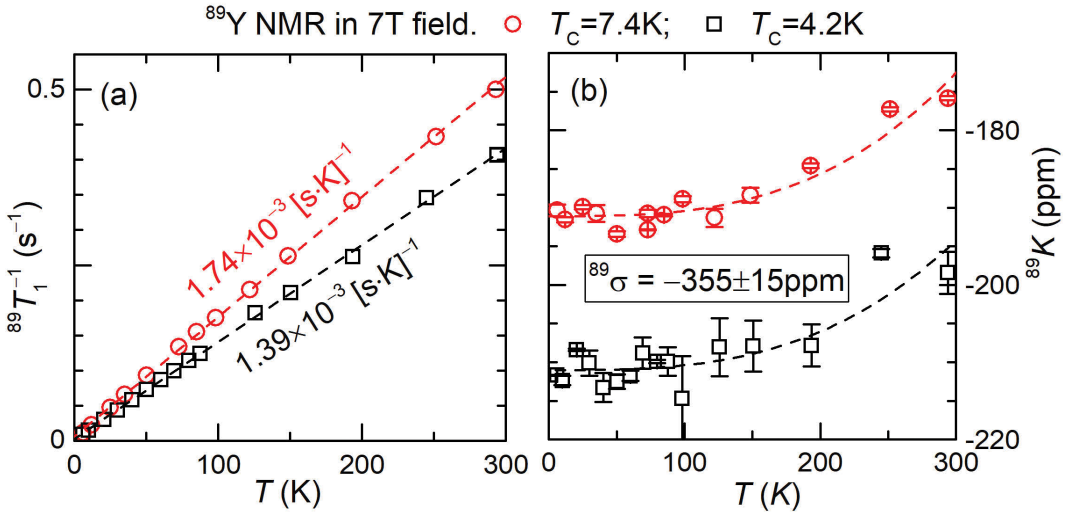

Figure 2. The temperature dependences of ^{11}B NSLR rates in the YB_6 samples. Dashed lines: linear fits for $T > 60$ K with the indicated slopes α. Top inset: zoom-in to the low-temperature part; solid line illustrates $1 - P_e^2$ (see text). Bottom inset: $^{11}T_{1m}^{-1}$ contribution, see text.

the conduction electron mediated relaxation. The NSLR of ^{89}Y in the sample with T_c = 7.4 K is 1.27 times faster than in the one with T_c = 4.2 K in the whole temperature range. For this type of the relaxation $T_1^{-1} \propto \rho_F^2$, where ρ_F is the Fermi-level density of electronic states (DOS). The change in the NSLR rate with T_c corresponds therefore to the change in ρ_F by the factor 1.13.

The temperature dependence of ^{89}Y Knight shift, ^{89}K, is presented in Fig. 1b. The diamagnetic contribution to the shift, $^{89}\sigma$, in both samples is estimated as $^{89}\sigma$ = 355 ± 15 ppm. Therefore, larger ^{89}K in the sample with higher Tc reflects the growth of the Knight shift spin part, $K_s \propto \rho_F$, hence the growth of the DOS.

The Sommerfeld coefficients obtained in the specific heat measurements of these samples [1] are γ_e = 3.8 and 2.6 mJ/(mol K) for T_c = 7.4 and 4.2 K, resp., while ρ_F is estimated [2] as ~0.7 electrons/eV. Using these numbers and the change in ρ_F found in the $^{89}T_1^{-1}$ measurements, we utilized the formula $\gamma_e = 2/3(\pi k_B)^2\rho_F(1 + \lambda)$ and determined the electron-phonon coupling constants, λ = 1.02 and 0.57, T_c = 7.4 and 4.2 K, resp. Therefore, the growth of T_c results from the growth of both ρ_F and λ. The estimates of ρ_F and λ for the two studied samples are in a good agreement with the Allen-Dynes formula [3] which relates T_c, λ and ρ_F.

^{11}B NMR is much less informative regarding the conduction electron system. This is because of the small *s* character of the wave function of the conduction electrons at the Fermi surface, which is common to conducting borides, and low p-electron DOS. This is the reason why we did not detect any difference in temperature-independent ^{11}B spectra of the two studied samples. ^{11}B NSLR however, includes a detectable contribution from the conduction electron system, as one can see in Fig. 2 as a linear component visible above 60 K. Like for ^{89}Y, the linear term in ^{11}B NSLR, $^{11}T_{1e}^{-1} = \alpha T$, is faster for the sample with higher T_c.

The non-zero intercept implies another contribution to ^{11}B relaxation, which is shown in the bottom inset in Fig. 2. In semiconducting hexaborides (e.g. SrB_6, CaB_6) ^{11}B NSLR is totally gov-

erned by magnetic centers associated with the clusters of boron vacancies, and its T-dependence is determined by the factor $(1 - P_e^2)$ with polarization $P_e = \tanh(\mu_B B_0/k_B T)$. One can see in Fig. 2 that in YB_6 ${}^{11}T_{1m}^{-1}$ below 60 K does not obey the T-dependence of $(1 - P_e^2)$ and shows a rapid increase with cooling, indicating to a build-up of yet another relaxation source. A possible explanation of this upturn in ${}^{11}T_{1m}^{-1}$ is the development of the cooperative Jahn-Teller instability of the boron B_6 clusters detected in other hexaborides [4].

This work was supported by ISSP RAS – Russian Government contracts.

1. N. Sluchanko et al., Phys. Rev. B **96**, 144501 (2017).
2. J.A. Alarco et al,. Model. Simul. Mat. Sci. Eng. **4**, 53–69 (2014).
3. P.B. Allen, R.C. Dynes, Phys. Rev. B **12**, 905–922 (1975).
4. E.S. Zhukova et al., JETP Lett. **110**, 79–84 (2019).

SPIN WAVE SPECTRA IN PSEUDOPEROVSKITE MANGANITES WITH SUPEREXCHANGE INTERACTION COMPETITION

L.E. Gonchar

Ural State University of Railway Transport, Ekaterinburg, Russia
Ural Federal University, Ekaterinburg, Russia
E-mail: l.e.gonchar@urfu.ru

The Jahn-Teller magnets with manganese sublattice are widely investigated as compounds with lattice, charge, orbital and magnetic subsystems interaction. The main application of CMR properties in these crystals awoke a vivid interest to some fundamental features including low-dimensional and frustrated magnetic structures.

The pseudoperovskite $R_{1-x}A_xMnO_3$ manganites (where R^{3+} is a rare earth ion, A^{2+} is an alkaline earth ion, and x is a doping level) are distorted to orthorhombic or nearly-orthorhombic crystal structure [1–3]. If the R^{3+} position is occupied by bismuth ions, the crystal structure distortions are mostly monoclinic without doping. The Mn^{3+} magnetic sublattice is orbitally degenerated in the non-distorted ideal crystal. The Jahn-Teller effect removes degeneration, thus the complicated superexchange interaction takes place [4]. $BiMnO_3$ has more complicated crystal structure of monoclinic symmetry, which is sharply different comparing with rare-earth undoped or doped manganites. It causes unusual orbital structure [5]. In $BiMnO_3$ compound and in doped rare-earth manganites at some doping levels, the competition of superexchange parameters is possible. This kind of magnetic non-geometric frustration leads to low-dimensional and essentially non-collinear magnetic structures [6].

The spin excitation study is the way to clarify the sign and value of superexchange parameters, because in the case of superexchange competition only resulting magnetic structure could be measured. The resulting magnetic structure could give enough information if it is essentially non-collinear, as in charge-ordered manganites [3]. In $BiMnO_3$ there is good ferromagnetic ordering, which cannot help to describe different superexchange interactions. The current study is aimed to predict spin-wave spectra within the framework of orbitally dependent magnetic interactions and supposing a regular magnetic structure.

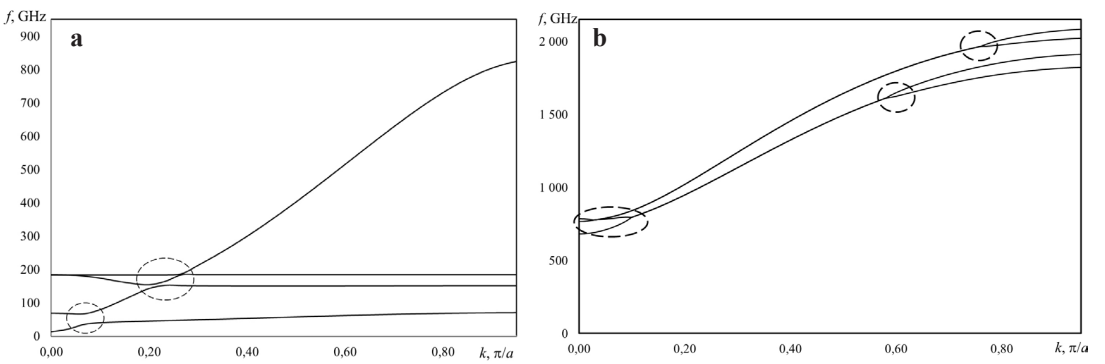

Figure 1. The low-frequency zone of spin-wave spectra dispersion dependences in $[1\ 0\ 0]_p$ direction for frustrated compounds $BiMnO_3$ (**a**), $La_{1/3}Ca_{2/3}MnO_3$ (**b**). The dashed lines show the specific features of spectra due to magnetic frustration.

The model of magnetic subsystem [6] is following:

$$\hat{\mathbf{H}}_{\text{mag}} = \sum_{i>j} J_{ij}(\Theta_i,\Theta_j)(\mathbf{S}_i \cdot \mathbf{S}_j) + \sum_{i,\alpha,\beta} D_i^{\alpha,\beta}(\Theta_i) S_i^{\alpha} S_i^{\beta}\,, \tag{1}$$

where first sum is superexchange interaction, second one is single ion anisotropy. All terms are dependent upon total manganese spins $\mathbf{S}_i$, $\mathbf{S}_j$ and orbital structure parameters Θ_i, Θ_j.

In the compounds under consideration, the role of orbital ordering in magnetic competition is crucial. It causes non-geometrical magnetic frustration with account of nearest-neighbor superexchange interaction only. In compounds $La_{1/3}Ca_{2/3}MnO_3$ and $BiMnO_3$, a calculation of spin-wave dispersion dependences along pseudoperovskite directions of inverse space is made. The peculiarities of frustrated magnetic spin-wave spectra are found. The crossing and splitting of spin-waves branches in non-symmetric points of magnetic Brillouin zone is a common feature for both frustrated manganite compounds. The spectra in $[1\ 0\ 0]_p$ pseudoperovskite direction are shown in Fig. 1. The magnetic structures with small incommensurate component are assumed to be possible. The directions without dispersion are found for $BiMnO_3$. This feature points out the quasi-low-dimensional ferromagnetism in compound. The spin-wave spectrum for $La_{1/3}Ca_{2/3}MnO_3$ with quasi-low-dimensional magnetic stripe structure differs from $La_{1/2}Ca_{1/2}MnO_3$ one [6] because of different stripes arrangements.

The spin-wave spectrum gap in Γ-point od Brillouin zone differs in different manganite crystals and does not depend upon the fact of superexchange competition.

1. J.B. Goodenough, Phys. Rev., **100**, 564–573 (1955).
2. P.G. Radaelli, D. E. Cox, M. Marezio, S.-W. Cheong, Phys. Rev. B **55**, 3015– 3023 (1997).
3. P.G. Radaelli, D.E. Cox, L. Capogna, S.-W. Cheong et al., Phys. Rev. B **59**, 14440–14450 (1999).
4. I. Bersuker, The Jahn–Teller Effect, Cambridge University Press, Cambridge (2006).
5. D.P. Kozlenko, A.A. Belik, S.E. Kichanov et al., Phys. Rev. B **82**, 014401 (2010).
6. L.E. Gonchar, J. Phys.: Conf. Ser. **1389**, 012138 (2019)

VARIETY OF SPIN RESONANCE MODES IN THE MONOAXIAL CHIRAL HELIMAGNET $Cr_{0.33}NbS_2$

I.G. Bostrem[1], *V.E. Sinitsyn*[1], *E.G. Ekomasov*[2], *A.S. Ovchinnikov*[1*]

[1]Institute of Natural Science and Mathematics, Ural Federal University, Ekaterinburg, Russia
[2]Bashkir State University, Ufa, Russia
[*]E-mail: alexander.ovchinnikov@uruf.ru

The chiral spin soliton lattice (CSL) is a highly reconfigurable and robust superstructure over a macroscopic length scale. The CSL consists of an array of chiral soliton kinks (2π magnetic kinks) periodically partitioned by ferromagnetic domains. The period of the CSL is tunable by altering the strength of an external magnetic field H. Thus, the CSL is anticipated to exhibit tunable and reconfigurable magnon dispersion, when the kinks of the CSL oscillate collectively around their equilibrium positions and produce phonon-like excitations [1]. The Brillouin zone (BZ) formed in the magnon dispersion depends on the CSL period, the dispersion branches are fold at the BZ boundaries and higher-order modes appear in a broad frequency range. Thus, the CSL phonon modes are expected to have a broad frequency range due to the CSL reconfigurability. However, although the spin dynamics of the CSL were investigated in many studies, the ponon-like excitations attributed to the CSL have not yet been experimentally observed.

In the recent study, the existence of the CSL phonon modes has been experimentally demonstrated in a bulk single crystal of the monoaxial chiral helimagnet $Cr_{0.33}NbS_2$ [2]. Three types of the resonance modes in the CSL phase are identified based on the H dependence of resonance frequency. The first noticeable feature is that multiple resonance modes were observed above 16 GHz, the resonance frequency in all the modes decreases with increasing the strength of H and converges toward the critical field H_c of the incommensurate-commensurate phase transition. The dome-shaped characteristics of the resonance frequency are similar to that derived from the analytical calculation of the CSL phonon [1]. A second type of a resonance mode, referred to as an asymmetric mode, appears between 7.8 and 11.4 GHz, and may be attributed to standing spin waves as discussed in the previous studies [3, 4] A third type of resonance modes, referred to as the Kittel-like mode, appears in the low frequency regime and shows a monotonous increase of the resonance frequency with a growth of H. This mode is naturally connected to the forced ferromagnetic phase, which is ascribed to the Kittel mode observed in conventional ferromagnetic materials.

For the forced ferromagnetic phase of the monoaxial chiral helimagnet $Cr_{0.33}NbS_2$, formed by an external magnetic field **H** directed along the chiral axis, we investigated a possibility of experimental observation of discrete breather excitations. We found that the presence of the DM interaction does not prevent their emergence but, conversely, ensures their topological protection. We demonstrate that the model Hamiltonian of the monoaxial chiral helimagnet supports several kinds of possible spatially periodic discrete breather solutions, but a specific choice depends on subtle interplay between interactions accounted for in the Hamiltonian. Using experimental data for strengths of the DM coupling and the easy-plane single-ion anisotropy in $Cr_{0.33}NbS_2$, we predict for this magnetic material the appearance of the dark breather lattice modes with frequencies lying within the linear spin-wave spectrum near to its bottom edge. Results of numerical simulations of the DB excitations on a finite-length chain are in very good agreement with the continuum approximation, which

relates the DB lattice modes and periodic solutions of the nonlinear Duffing equation. The Floquet analysis confirms the stability of the discrete breather excitations.

Support by Grant RFBR 20-02-00213 is acknowledged.

1. J. Kishine, and A. S. Ovchinnikov, Phys. Rev. B **79**, Id. 220405(R) (2009).
2. Y.Shimamoto, Y. Matsushima, T. Hasegawa, Y. Kousaka, I. Proskurin, J. Kishine, A.S. Ovchinnikov, F.J.T. Goncalves, and Y. Togawa (accepted in Physical Review Letters).
3. F.J.T. Goncalves, T. Sogo, Y. Shimamoto, Y. Kousaka, J. Akimitsu, S. Nishihara, K. Inoue, D. Yoshizawa, M. Hagiwara,M. Mito, R.L. Stamps, I.G. Bostrem, V.E. Sinitsyn, A.S. Ovchinnikov, J. Kishine, and Y. Togawa, Phys. Rev. B **95**, Id. 104415 (2017).
4. J. Kishine, Vl. E. Sinitsyn, I.G. Bostrem, I. Proskurin, F.J.T. Gonsalves, Y. Togawa, A.S. Ovchinnikov, Phys. Rev. B **100**, Id. 024411 (2019).
5. I.G. Bostrem, E.G. Ekomasov, J. Kishine, A.S. Ovchinnikov, V.E. Sinitsyn, Phys. Rev. B **104**, Id. 214420 (2021).

B.O10

MRFM STUDIES OF FERROMAGNETIC RESONANCE IN EXCHANGE-COUPLED MAGNETIC VORTICICES

D.A. Tatarskiy[1,2], *V.L. Mironov*[2], *E.V. Skorokhodov*[1*]

[1]IPM RAS, Nizhny Novgorod, Russia
[2]Lobachevsky State University of Nizhny Novgorod, Nizhny Novgorod, Russia
[*]E-mail: evgeny@ipmras.ru

The main ferromagnetic resonance in a magnetic vortex is the gyrotropic mode associated with the circular precession of the vortex core around the equilibrium position [1]. This type of magnetization oscillations is prospective in developing high-frequency vortex spin-transfer nano-oscillators [2]. The problem of individual nano-oscillator low generated power is proposed to be solved by using arrays of synchronized nanogenerators. Synchronization can be carried out due to magneto-dipole interaction, spin waves or exchange coupling which is the strongest [3]. The report presents the results of studies of metastable magnetic states and gyrotropic modes of magnetization oscillations in exchange-coupled overlapping disks by magnetic resonance force spectroscopy and Lorentz transmission electron microscopy.

An array of ferromagnetic overlapping disks with a diameter of 1 micron was fabricated by electron lithography and ion etching. Disks with an overlap of 20% of the diameter were studied. A sample was also made on a silicon nitride membrane with a thickness of 30 nm for the study of magnetic states by Lorentz transmission electron microscopy on a LIBRA 200 MC microscope (Carl Zeiss, Jena) operating at 200 kV in the Fresnel mode. The resonant properties of the disks were studied using a magnetic resonance force microscope (MRFM). Various vortex states were realized in the manufactured system: states with different vorticity of the vortex shells (states VV, Fig. 1a, c); states with the same vorticity of the vortex shells containing an anti-vortex (states VAV, Fig. 1b, d)).

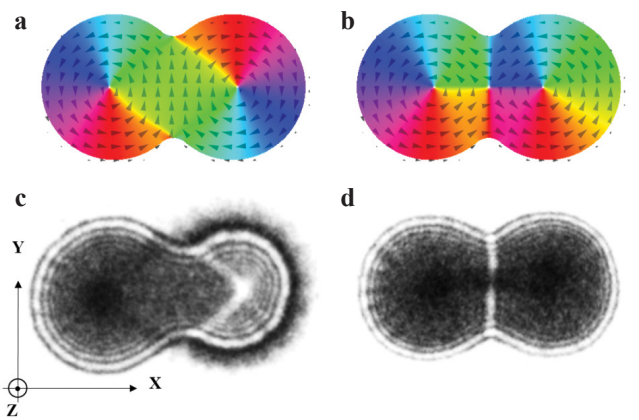

Figure 1. Model magnetization distributions in double disks and corresponding experimental images with Fresnel contrast. **a**, **c** The state VV with different vorticity of the shells; **b**, **d** the state of VAV with the same vorticity of the shells.

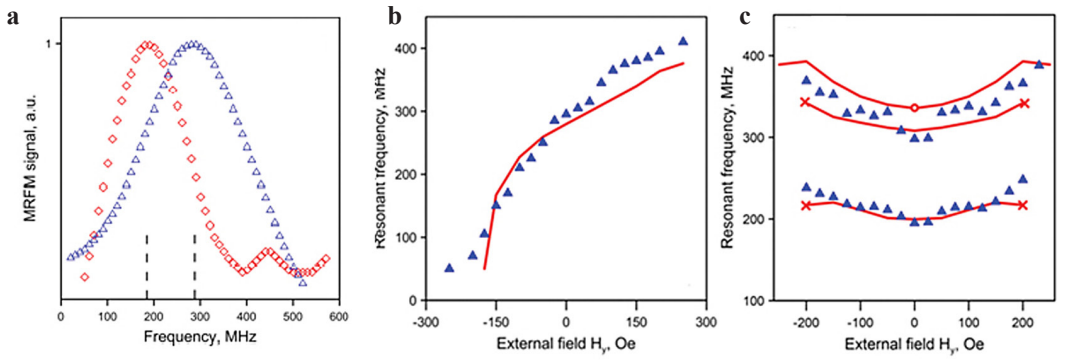

Figure 2. **a** MRFM spectra of overlapping disks in the VV (blue triangles) and VAV (red rhombuses) states. **b** Dependence of the resonant frequency of gyrotropic modes of vortices in the state of VV. The simulation results are shown by solid curves. **c** Dependence of the resonant frequency of gyrotropic modes of vortices in the VAV state. Experimental dependences are shown by triangles. The simulation results are shown by solid curves.

The MRFM spectra of VV and VAV states of exchange-coupled disks are shown in Fig. 2a. It can be seen that a change in the magnetic state leads to a shift in the resonant frequency by an amount of the order of 100 MHz.

The field dependences of the frequencies of both states were also studied. When an external permanent magnetic field is applied perpendicular to the axis connecting the disks, the frequency for the state VV will be an odd function of the external field (Fig. 2b). In the VAV state, the frequency field dependencies are much more complicated. It can be seen that the field dependence for this state is a function symmetric with respect to the direction of the field (Fig. 2c).

Thus the type of metastable state in which the double disk is located can be determined by the field dependences of the MRFM spectra.

The work is supported by the Russian Science Foundation (project No. 21-12-00271).

1. N.A. Usov, L.G. Kurkina, J. Magn. Magn. Mater. **242**, 1005 (2002).
2. V. Pribiag, I. Krivorotov, G. Fuchs, P. Braganca, O. Ozatay, J. Sankey, D. Ralph, R. Buhrman, **3**(7), 498–503 (2007).
3. A. Ruotolo, V. Cros, B. Georges, A. Dussaux, J. Grollier, C. Deranlot, R. Guillemet, K. Bouzehouane, S. Fusil, A. Fert,, Nature Nanotechnology **4**, 528–532 (2009).

THE PRECESSION OF THE EQUILIBRIUM POSITION IN THE TWO-LAYER STRUCTURE WITH THE EXCHANGE INTERLAYER INTERACTION

I.E. Abramovsky[1*], *V.S. Vlasov*[1], *L.N. Kotov*[1], *D.A. Pleshev*[1,2], *F.F. Asadullin*[2]

[1]Syktyvkar State University, Syktyvkar, Russia
[2]Saint-Petersburg state forest technical university named after S.M. Kirov, St. Petersburg, Russia
[*]E-mail: abramowsk-ivan@mail.ru

In the field of modern physics, in conditions of limited technical and laboratory equipment, the field of modeling physical processes of various levels of complexity is actively developing. One of the directions of this branch is the modeling of nonlinear magnetic effects arising in thin-film structures with various properties. The interest in this topic is explained by the fact that the physics of these structures is very specific and has unique properties that can interest various industries, and what is especially interesting is the field of computer technology. Purely electronic devices have been gradually moving into the background for a long time, giving way to new types of devices, such as magnetic-resistive memory, spin processors, spin valves, etc. [1]. The operation of these devices is based on nonlinear spin dynamics in multilayer magnetic structures. Often, the operation of such devices is also associated with spin-orientation phase transitions in planar structures [2]. Our work is devoted to the analysis of nonlinear magnetic dynamics in the two-layer structure. The analysis is carried out on the basis of numerical methods. We have modeled various modes of magnetic dynamics under the conditions of the orientation transition in the normally magnetized layered structure, which were described earlier in [3] in relation to the case of a single ferrite layer.

The calculation of the forced nonlinear precession of the magnetization vector in a normally magnetized two-layer magnetic structure having different saturation magnetization values is performed. During the calculations, the effects of small DC fields applied along the film's plane, the fields of cubic anisotropy of the orientation [011], as well as the field of interlayer interaction on the precession of the second order of the magnetization vector were considered. Surface observation suggests that with a change in the coupling constant of the layers, the oscillation frequency of the small ellipse around the large one changes in the precession portrait. This can be seen by the varying distances between the tracks of the magnetization vector, or by the position in which the magnetization vector leaves the last track during modeling. With the growth of the layer coupling constant, the small ellipse shifts along the large one in the clockwise direction (which can cause «switching» from one condensation to another). This fact may be caused by an increase in gyromagnetic forces due to the action of the interlayer exchange field. The consequence of this fact is an increase in the period of the precession in the full rotation of magnetization. In addition, we can observe that the exchange interaction field has a stabilizing effect, fixing the magnetization vector in one of the condensation caused by the cubic anisotropy field. The minimum of the potential energy becomes deeper inside the condensation caused by the cubic anisotropy field. The magnetization vector jumps from one minimum to another and this is evidenced by the vague form of condensation with fuzzy boundaries.

This work has been supported by Russian Science Foundation (project No. 21-72-20048).

1. A. Claas, Eur. Phys. J. B **92**, 120 (2019).
2. V.S. Vlasov, V.G. Shavrov, V.I. Shcheglov, J. Commun. Technol. Electron. **59**, 441–455 (2014).
3. V.S. Vlasov, M.S. Kirushev, L.N. Kotov, V.G. Shavrov, V.I. Shcheglov, J. Commun. Technol. Electron. **58**, 847–862 (2013).

B.O12

SPIN-WAVE RESONANCES IN Pd-Fe ALLOY FILMS WITH CONTROLLED COMPOSITION PROFILES

I.V. Yanilkin[1,2*], *A.I. Gumarov*[1,2], *B.F. Gabbasov*[1,2], *A.G. Kiiamov*[1], *I.A. Golovchanskiy*[3,4], *R.V. Yusupov*[1], *L.R. Tagirov*[1,2]

[1]Institute of Physics, Kazan Federal University, Kazan, Russia
[2]Zavoisky Physical-Technical Institute, FRC Kazan Scientific Center of RAS, Kazan, Russia
[3]Moscow Institute of Physics and Technology, Dolgoprudny, Russia
[4]National University of Science and Technology MISIS, Moscow, Russia
[*]E-mail: yanilkin-igor@yandex.ru

Currently, exchange spin waves (SWs) in various magnetic thin films and heterostructures are actively studied [1]. The interest to SWs is primarily due to the fact that their propagation in a magnetic material is charge-current-free. The SW wavelength is typically of the micro- and sub-micrometer scale, and the frequency range can be tuned to the sub-THz. It is known from the literature that the excitation of standing spin waves (SSWs) in thin magnetic films is mainly associated with surface anisotropy [2]. However, SSWs can also be related to the presence of magnetic inhomogeneity in the film [3]. An analysis of the literature shows that experimental studies of spin-wave resonances (SWR) in magnetically inhomogeneous materials are random and have not been carried out systematically. At the same time, this effect has been well elaborated theoretically (see, for example, V.A. Ignatchenko *et al.* [4]). In particular, it is shown that the dispersion law for spin waves depends on the character of the magnetic properties distribution in the film. Therefore, the main goal of our work was an experimental study of SWR in single-crystal films of the Pd-Fe alloy, in which the magnetic impurity is distributed non-uniformly across the thickness. Pd-Fe alloys are promising for such a study, since it is possible to fine-tune its magnetic properties, in particular,

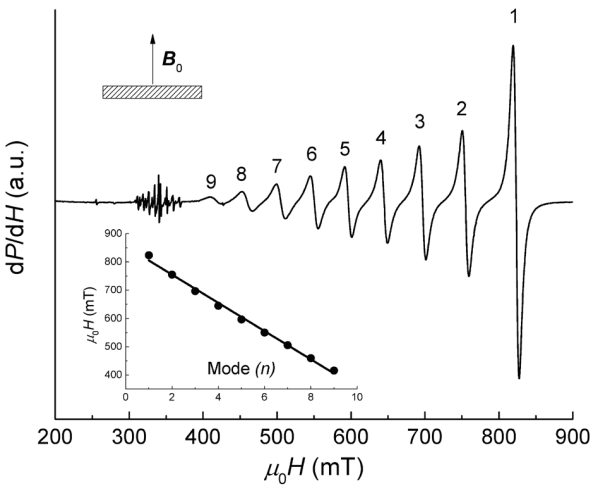

Figure 1. Spin-wave resonance spectrum obtained at T = 20 K for a 200 nm thick epitaxial Pd-Fe film with an iron-concentration across the thickness varied linearly from 2 to 10 at.%. The insets show the measurement geometry (top) and dependence of the resonant field on the mode number n (bottom).

saturation magnetization, Curie temperature, and magnetic anisotropy by varying the iron concentration in the range of 1–10 at.% [5]. In addition, epitaxial films of Pd-Fe alloys are chemically resistant and do not change structure and magnetic properties over a long period of time, which is important for practical applications. These circumstances make the Pd-Fe alloy an ideal material for elements of magnon spintronics.

In this work, we present structure and magnetic resonance studies of epitaxial films of the Pd-Fe alloy with non-uniform composition profiles across the thickness. The films were synthesized by molecular beam epitaxy by co-evaporation of the palladium and the iron from high-temperature effusion cells onto the (001)-oriented MgO substrate. The temperature of the effusion cell with palladium during the deposition stayed constant, while the temperature of the cell with Fe was varied, providing the required predetermined iron concentration profile. Using this approach, we have synthesized films with linear, sine, cosine, and other variants of iron distribution in the palladium matrix in the concentration range of 2–10 at.% and the thickness up to 200 nm.

The study of SSWs was performed using a commercial X-band Bruker ESP300 electron spin resonance spectrometer (~9.4 GHz) in different geometries and measurement temperatures (10–300 K). Figure 1 shows the SWR spectrum for a 200-nm thick Pd-Fe film with a linear distribution of the iron content. One can see from the figure that nine resonant SSW modes are excited with an essentially linear dependence of the resonant field Hres on the mode number *n*. This is a typical behavior for anomalous spin waves [6]. The obtained experimental SWR spectra were analyzed within the framework of the existing model described, for example, in [6]. Experimental results and modeling for the film with a linear distribution of the iron content are available at arxiv.org [7].

This research was supported by the Russian Science Foundation (Project № 22-22-00629, https://rscf.ru/en/project/22-22-00629/)

1. A. Barman et al., J. Phys.: Cond. Matt. **33**, 413001 (2021).
2. C. Kittel, “Introduction to Solid State Physics, 8th edition”, Wiley (2021).
3. A.M. Portis, Appl. Phys. Lett. **48**, 69 (1963).
4. V.A. Ignatchenko, D.S. Tsikalov, J. Appl. Phys. **127**, 123903 (2020).
5. A. Esmaeili et al., Sci. China Mater. **64**, 1246 (2021).
6. T.G. Rappoport et al., Phys. Rev. B **16**, 14 (2004).
7. arXiv:2203.05014 [cond-mat.mtrl-sci].

B.O13

ANION AND CATION DYNAMICS IN NANOPOROUS SILICA SCAFFOLDS: NMR STUDIES OF $NaCB_{11}H_{12}$ IN SBA-15

O.A. Babanova[1*], *R.V. Skoryunov*[1], *A.V. Soloninin*[1], *A.V. Skripov*[1], *M.S. Andersson*[2,3], *V. Stavila*[4], *M. Dimitrievska*[5], *M. Karlsson*[2], *T.J. Udovic*[5,6]

[1]M.N. Miheev Institute of Metal Physics UB RAS, Ekaterinburg, Russia
[2]Chalmers University of Technology, Göteborg, Sweden
[3]Uppsala University, Uppsala, Sweden
[4]Sandia National Laboratories, Livermore, CA, United States
[5]NIST Center for Neutron Research, Gaithersburg, MD, United States
[6]University of Maryland, College Park, MD, United States
[*]E-mail: babanova@imp.uran.ru

High-temperature disordered phases of hydroborates based on *closo*-ions $[B_{12}H_{12}]^{2-}$ and $[CB_{11}H_{12}]^{-}$ (e.g. $Na_2B_{12}H_{12}$, $Li_2B_{12}H_{12}$, and $NaCB_{11}H_{12}$) possess high superionic conductivity [1–3], therefore these systems can be applied as solid electrolytes in electrochemical batteries [4]. Nuclear magnetic resonance (NMR) studies of the dynamical properties of sodium *closo*-dodecaborate $Na_2B_{12}H_{12}$ have revealed that the phase transition from the low-temperature monoclinic to the high-temperature cubic phase is accompanied by an abrupt increase of both the reorientational motion of $[B_{12}H_{12}]^{2-}$ anions and the translational diffusion of Na^+ cations [5]. These results initiated a study of the electrical transport properties in the high-temperature phase of $Na_2B_{12}H_{12}$, which showed high values of ionic conductivity (~0.1 S/cm at 530 K) [1]. For the practical battery applications of $Na_2B_{12}H_{12}$ as a solid electrolyte, it is important to stabilize the superionic disordered phase at room temperature and below. In addition, from the fundamental point of view, it is necessary to elucidate the nature of the high ionic conductivity in the disordered phase and the relationship between the reorientational motion of anions and the translational diffusion of cations. To lower the order–disorder phase transition temperature, a combination of two strategies can be used. The first strategy is the chemical modification of the complex anion by replacing one boron atom in the divalent $[B_{12}H_{12}]^{2-}$ anion with a carbon atom to obtain the monovalent anion $[CB_{11}H_{12}]^{-}$ and, the second one is the altering the bulk properties by confinement this hydroborate within nanoporous matrices.

In the present work, we report the results of NMR studies of the reorientational motion of $[CB_{11}H_{12}]^{-}$ complex anions and the translational diffusion of Na^+ cations in sodium monocarbo-*closo*-decaborate $NaCB_{11}H_{12}$ nanodispersed within the porous high-surface-area silica matrix SBA-15. The measured temperature dependences of the proton spin-lattice relaxation rates at different resonance frequencies are consistent with thermally-activated reorientations of the $[CB_{11}H_{12}]^{-}$ anions. The corresponding activation energies derived from the experimental data are discussed in relation with the structural features of these compounds. It is found that the depositing of $Na_2B_{12}H_{12}$ into nanoporous matrix SBA-15 leads to the suppression of the order–disorder phase transition; as a result, the disordered phase with a high reorientational mobility of anions and a high diffusion mobility of Na^+ cations is retained down to low temperatures. At $T > 180$ K, the sharp ^{23}Na NMR line narrowing to the values of about 0.9 kHz is observed, which indicates the presence of translational diffusion of Na^+ cations on a frequency scale of $\sim 10^4$ s^{-1}.

The research was carried out within the state assignment of Ministry of Science and Higher Education of the Russian Federation (theme "Function" No. 122021000035-6).

1. T.J. Udovic *et al*., Chem. Comm. **50**, 3750 (2014).
2. W.S. Tang *et al*., Energy Environ. Sci. **8**, 3637 (2015).
3. W.S. Tang *et al*., Adv. Energy Mater. **6**, 1502237 (2016).
4. M. Brighi *et al*., J. Cell Reports Physical Science **1**, 100217 (2020).
5. A.V. Skripov *et al*., J. Phys. Chem. C **117**, 25961 (2013).

UNUSUAL DEPENDENCES OF EPR-LINE SHAPES OF Gd^{3+} CENTERS IN NARROW-BAND $Pb_{1-x}Gd_xTe$ SEMICONDUCTOR ON MICROWAVE POWER

V.A. Ulanov[1,2*], *I.V. Yatsyk*[1], *A.V. Shestakov*[1]

[1]Zavoisky Physical-Technical Institute, Kazan, Russian Federation
[2]Kazan State Power Engineering University, Kazan, Russian Federation
[*]E-mail: ulvlad@inbox.ru

The main component of the considered here semiconductor material that determines its physical properties is PbTe. It is a narrow direct-band semiconductor belonging to a group of lead chalcogenides ($A^{IV}B^{VI}$: PbS, PbTe, and PbSe) with the rock salt structure (NaCl) and a narrow-gap interval E_g ~ 0.23–0.42 eV [1]. The narrow direct-band gap, low effective mass and high mobility of free charge carriers, high static permittivity, and proximity of the crystal lattice to the state of thermodynamic instability [2] are characteristic of $A^{IV}B^{VI}$. These properties are responsible for initiating complex physical processes in their volumes. Doping lead chalcogenides with paramagnetic Gd^{3+} ions containing half-filled electron $4f^7$-shells produces deep states in the band gap of $A^{IV}B^{VI}$. Spin-orbit interaction of charge carriers and exchange interactions between Gd^{3+} ions and charge carriers can lead to mutual dependences between their dynamical parameters.

When using the electron paramagnetic resonance (EPR) spectroscopy to study the effect of a gadolinium doping on the defectiveness of $Pb_{1-x}Gd_xS$ crystals [3], we noticed that the shape and width of the EPR spectrum lines of cubic Gd^{3+} centers strongly depend on the microwave (MW) power in the cavity of the spectrometer. Unusual features observed were subscribed to three possibilities: (1) the notable conductivity of a given sample under study and the limited penetration of microwaves into its sample depth due to the thickness of the skin layer (the Dyson mechanism); (2) the high inhomogeneous broadening of EPR-lines; and (3) the realization of mechanisms of absorption of microwave power of a nonmagnetic nature.

The present work was devoted to EPR-study of the deep Gd^{3+} centers in $Pb_{1-x}Gd_xTe$ (x = 0.0003) crystalline sample. The dependences of EPR line shapes on MW power and temperature were the main goal of the study. X-band EPR-measurements were performed on single $Pb_{1-x}Gd_xTe$ crystals grown by vertical Bridgman method in quartz crucibles. The measurements were carried out with an EMX/plus (Bruker) spectrometer equipped with a cylindrical microwave cavity operating in the TE_{011} mode. Figure of merit of the cavity loaded with the sample under study was about 7500. Modulation of the external magnetic field ($\mathbf{B}_0$) was carried out at a frequency of 100 kHz. The magnitude of the modulating magnetic field was 1 Oe. Two types of Gd^{3+} paramagnetic centers (I and II type) with cubic symmetry were observed in a $Pb_{1-x}Gd_xTe$ crystalline sample. The centers of I type gave the spectral lines with Dysonian shapes but the centers II the lines with "inverted bell" type shapes. Positions and relative amplitudes of EPR-lines of the I and II centers were described by spin-Hamiltonian

$$H_S = \beta_e g\, S \cdot H + (b_4/60)(O_4^0 + 5O_4^4) + (b_6/1260)(O_6^0 - 21O_6^4)\,, \qquad (1)$$

where a Cartesian coordinate system with axes parallel to one of the crystallographic axes (001) was used to represent the operator (1). Despite of the I-type centers lines are much narrow, the sets of spin-Hamiltonian parameters of both the I- and II-type centers are practically equivalent at each

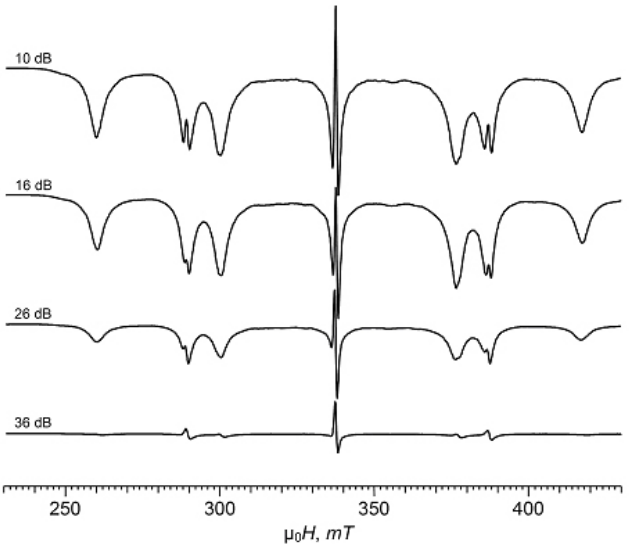

Figure 1. EPR spectra of crystalline $Pb_{1-x}Gd_xTe$ (x = 0.0003) sample ($\mathbf{B}_0$ || <001>; T = 10 K; f_{EPR} = 9.41 GHz).

temperature point in the range of 5–40 K. It was found that at temperatures higher than 40 K the EPR lines of II-type centers are unobservable.

The main result of the present study is unusual dependence of the EPR line shape parameters on temperature and MW power in the cavity with sample under investigation. Such a dependence on MW power is represented in Fig. 1 for T = 10 K. The picture presented in Fig. 1 corresponds to an $\mathbf{B}_0$ || <001> orientation of the sample under investigation in MW cavity of the spectrometer.

The temperature and power dependences of the EPR lines shapes and temperature dependences of the spin-Hamiltonian parameters were described numerically. A physical nature of the experimental facts found in the present investigation is discussed. There is considered the occurrence of spin excitation mechanisms other than magnetic dipole transitions which lead to the specific shapes of the resonance lines. Such mechanisms are realised in the cases of conducting samples where effective spin-orbit interaction of the Rashba type is realized. It is known [4] that the Rashba coupling leads to spin excitations by an MW electric current and dependence of the conductivity on spin polarization. The latest varies at the resonance and thus causes a polarization signal. In conducting samples, the spin resonance absorption due to a spin-dependent electric conductivity can exceed highly the absorption originating from magnetic dipole transitions.

1. V.I. Kaidanov and Yu.I. Ravich, Sov. Phys. Usp. [in Russian] **28**, 51–86 (1985).
2. E.S. Bozin, C.D. Malliakas, C.D., P. Souvatzis et al., Science **330**, 1660–1663 (2010).
3. V.A. Ulanov, R.R. Zainullin, T.A.N. Housheya, and I.V. Yatsyk, Bull. Russ. Acad. Sci.: Phys. **85**, 1337–1341 (2021).
4. Z. Wilamowski, W. Ungier, and W. Jantsch, Phys. Rev. B **78**, 174423 (2008).

B.O15

DYNAMIC CHARACTERISTICS OF A NANOCOMPLEX WITH IRON IN GLASS-IONOMER CEMENT POWDER

V.V. Shapovalov[1], *V.A. Shapovalov*[2*], *Yu.A. Sluzhbin*[2], *T.V. Drokina*[3], *A.M. Vorotynov*[3], *V.G. Shavrov*[4], *V.I. Valkov*[2]

[1]Organization "Math for America", New York, USA
[2]Donetsk Institute of Physics and Technology n.a. A.A. Galkin, Donetsk, DNR
[3]Institute of Physics n.a. L.V. Kirensky RAS, Krasnoyarsk, Russia
[4]Kotelnikov Institute of Radio-engineering and Electronics of RAS, Moscow, Russia
[*]E-mail: vashapovalov1@mail.ru

The study is a part of nanomedical biotechnology and is carried out by probing these systems using the Electronic Spin Resonance (ESR) method [1]. The paper investigates the glass ionomer cement powder CX-Plus Glass Ionomer Cement Triple Kit, which is widely used in dental practice. ESR radiospectroscopy is used to assess the quality of glass-ionomer cement. A new characteristic of such coordination compounds with nanocomplexes of magnetic iron ions Fe^{3+} is applied. This characteristic [2] is used in the study of powdered substances in which orientational averaging of randomly oriented nanocomplexes with magnetic ions occurs. In this case, the effect of the multiminimum potential of the crystal field is used, which manifests itself in the ESR spectra with Fe^{3+} ions [2–6]. Such a manifestation occurs when studying the temperature transformation of the ESR spectra with Fe^{3+} ions in the range from low (T = 4.2 K) to room (T = 300 K) temperatures. The research is used to assess the quality of the material. The Fe^{3+} ion is a probe and characterizes the nearest environment. The parameters of this environment change depending on the technology of applications of the material. At the same time, the properties of the material used in dental practice

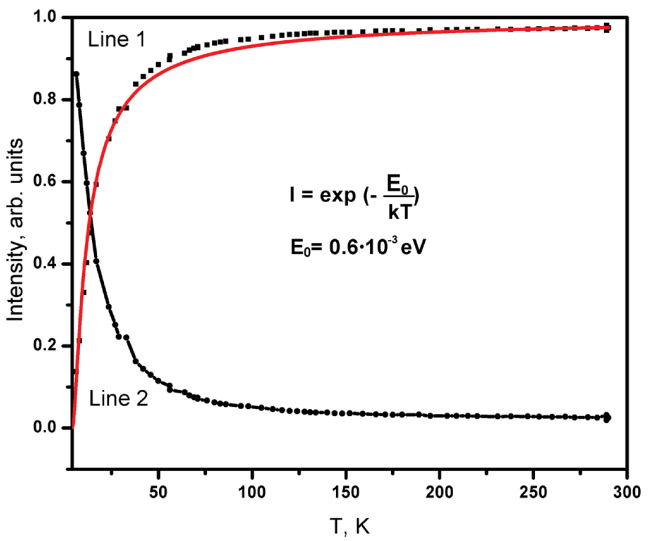

Figure 1. Temperature change in the ESR spectrum of the Fe^{3+} ion in glass-ionomer cement powder. Resonance lines 1 and 2 are shown in the order of increasing temperatures: T = 3.7; 46; 64 K.

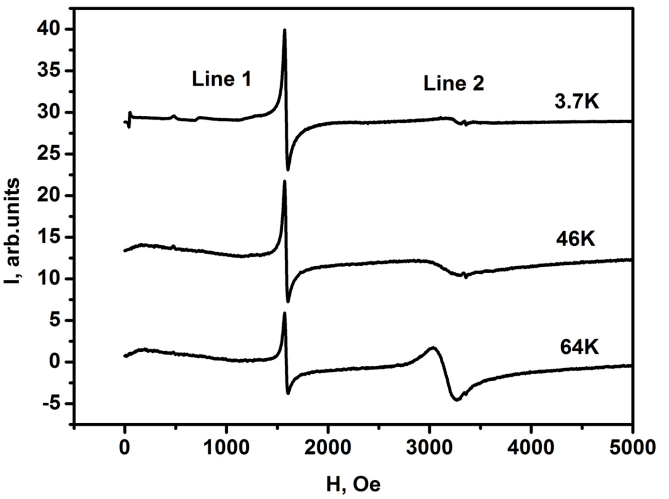

Figure 2. Temperature dependence of the reduced integral intensities of lines 1 and 2 of the ESR spectrum of Fe^{3+} ions in glass-ionomer cement powder.

and the quality of dental treatment change accordingly. The composition of CX-Plus Glass Ionomer Cement Triple Kit includes kaolinite $Al_2[Si_2O_5](OH)_4$ with an impurity iron ion Fe^{3+}, which is part of the mineral kaolinite. Impurity paramagnetic Fe^{3+} ions in kaolinite isovalently replace Al^{3+} ions. The iron content of kaolinite is typically around 0.3%. The nearest environment of the magnetic center of iron has a coordination number of 6. The investigated magnetic ion Fe^{3+} in kaolinite nanocrystals is located in an octahedron consisting of two oxygen anions O and four OH groups.

The study was carried out on a radio spectrometer with a frequency of 10 GHz in the range from low (T = 4.2 K) to room (T = 300 K) temperatures. The spectrum consists of two lines belonging to the Fe^{3+} iron ion. The effect of the multi-minimum potential of the crystal field manifests itself in the temperature dependence of the EPR spectrum of the Fe^{3+} ion as a result of orientational averaging from the ±5/2 – ±3/2 and ±3/2 – ±1/2 transitions. The spectrum does not depend on the orientation of the external field. The value of the g-factor of line 1 at the temperature T = 4.2 K is g_1 = 4.13±0.16. The value of the g-factor of line 2 at the temperature T = 4.2 K is equal to g_2 = 2.15 ± 0.1. As the temperature changes, a change in the shape of the ESR spectrum is observed. The temperature dependence of the intensities of lines 1 and 2 is shown in Fig. 1. The redistribution of the intensities of line 1 with $g \cong 4$ and line 2 with $g \cong 2$ of the EPR spectrum of Fe^{3+} ions is observed in the range from low (T = 4.2 K) to room (T = 300 K) temperatures (Fig. 1). According to Fig. 1, as the temperature increases, the intensity of resonance line 1 decreases, while the intensity of line 2 increases. The nature of this redistribution of intensities is determined by the barrier height of the crystal field potential $E_0 \cong kT$ (Fig. 2). The barrier height E_0 of the crystal field potential is determined from experimental studies of the temperature dependences of the ESR spectra. For each temperature, the sum of the reduced intensities of lines 1 and 2 is a constant and equal to 1.

The barrier height E_0 depends on the symmetry of the nearest environment of the Fe^{3+} ions. The Fe^{3+} ion is located in an octahedron consisting of two oxygen anions O and four OH groups. The parameters of the nearest environment depend on the production technology and can be set by the barrier height of the crystal field potential $E_0 \cong kT$ (Fig. 2).

1. R.G. Saifutdinov, Electron Paramagnetic Resonance in Biochemistry and Medicine. New York, pp. 276, (2019).
2. V.A. Shapovalov, V.V. Shapovalov, M. Rafailovich, S. Piechota, A. Dmitruk, E. Aksimentyeva, A. Mazur, The Journal Physical Chemistry C **117**, 7830−7834, (2013).
3. V.V. Shapovalov, S.A. Schwarz, V.A. Shapovalov, Mol. Cryst. Liq. Cryst. **468**, 245–256 (2007).
4. V.N. Vasyukov, V.V. Shapovalov, V.A. Shapovalov, J. Magn. Reson. **154**, 15–21 (2002).
5. V.N. Vasyukov, V.P. Dyakonov, V.A. Shapovalov, Low Temp. Phys. **26**, 265–269 (2000).
6. V.N. Vasyukov, V.A. Shapovalov, V.P. Dyakonov, Int. J. Quantum Chem. **88**, 425–529 (2002).

MAGNETIZATION DYNAMICS SIMULATION OF THE ANISOTROPIC FERROMAGNETIC FILM EXCITED BY THE NANOSECOND MAGNETIC PULSES

V.N. Shaporov, V.S. Vlasov, L.N. Kotov*

Syktyvkar State University, Syktyvkar, Russia
*E-mail: shaporov@mail.ru

The development of spintronics and research in the ultrafast magnetoacoustics causes interest in the study of the magnetic dynamics of ferromagnetic films. One of the tasks of these areas is to search the ultrafast magnetization reversal conditions in ferromagnetic films to create devices based on the transfer or reversal of their working elements magnetizations as an individual magnetic bits at the nanoscale [1–3].

In this paper, the simulation of the magnetization dynamics of the ferromagnetic film excited by magnetic pulses with a duration of up to one nanosecond is performed and the conditions where the magnetization reversal occurs are found. For calculations, a sample of yttrium-iron garnet (YIG) $Y_3Fe_{4.97}Co_{0.03}O_{12}$ was taken as the thin ferromagnetic plate with a cubic lattice that one of the easy magnetization axes is perpendicular to the film plane, and the external magnetizing and exciting fields are in the film plane as shown in Fig. 1a.

The total magnetic energy U of the ferromagnetic film was taken as the sum of energies: the energy of the external field U_Z, the energy of the demagnetizing field of the film U_d and the energy of the magnetic anisotropy U_a: $U = U_Z + U_d + U_a$ [2]. Magnetic anisotropy creates the energy

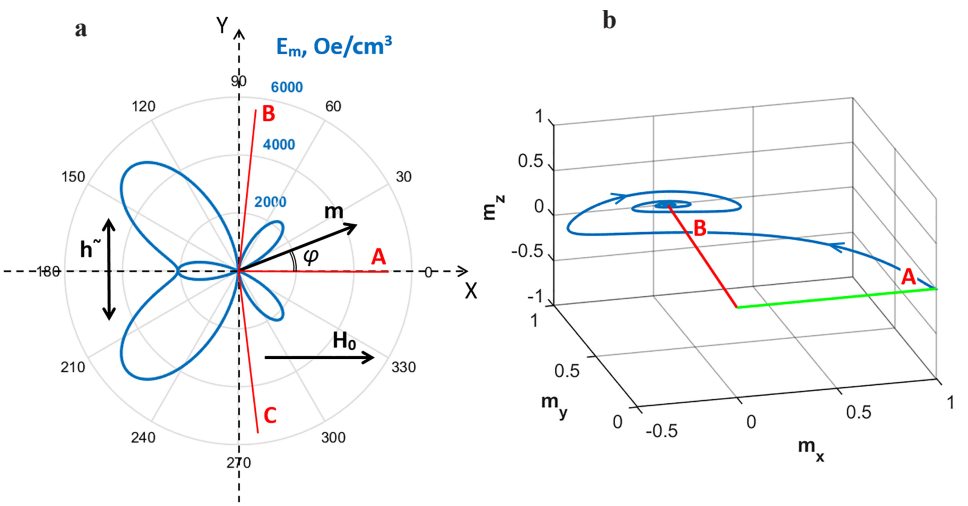

Figure 1. **a** Orientations of external magnetic fields and distribution of magnetic energy density in the film plane with the applied magnetizing field H = 15 Oe in the plane of the YIG film $Y_3Fe_{4.97}Co_{0.03}O_{12}$. The red lines show the directions of the minimum magnetic energy density E which the magnetization can be reoriented after the end of the action of the pulse field and the relaxation process. **b** The trajectory of the magnetization transition obtained within 6 ns from position A to position B at the magnetizing field H = 15 Oe, pulse amplitude h =200 Oe, pulse duration τ = 0.8 ns.

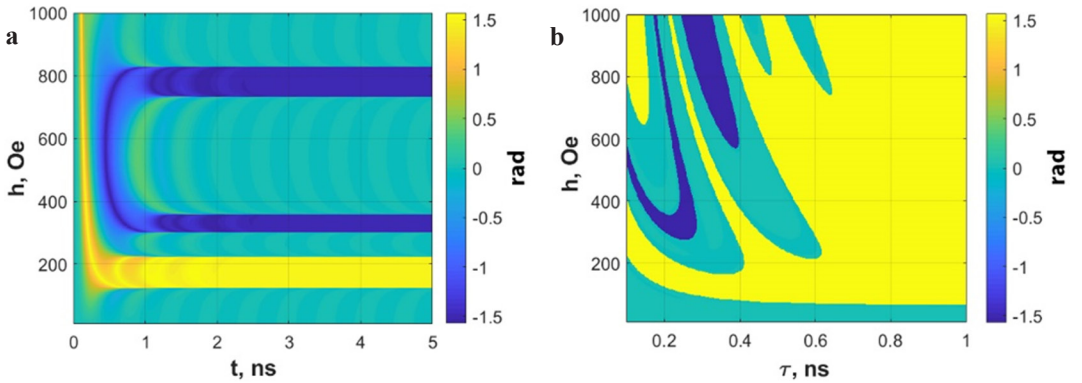

Figure 2. Position of the angle φ between of axes X (along [100]) and unit magnetization vector **m** in the film plane depending on: **a** time t and pulse magnitude h when pulse duration is $\tau = 0.2$ ns; **b** pulse duration τ and pulse magnitude h at the end of process when time moment is $t = 6$ ns. Magnitude of the magnetizing field is $H = 15$ Oe.

spatial minima in the film plane along the easy magnetization axes. When the magnetizing field is smaller than the magnetic anisotropy field, energy minima are formed in the crystal lattice space and magnetization are oriented in their direction (Fig. 1).

The magnetization dynamics is calculated using the Landau-Lifshitz equation with the relaxation term in the Gilbert form [3, 4]. The solution of this equation for the components $\mathbf{m}_{x,y,z}$ of the unit magnetization vector was carried out by the numerical Dorman-Prince method of the 8th order. This equation used the expression for the magnetic energy of a crystal with cubic anisotropy. Calculations of the magnetization position excited by short magnetic pulses which have a different durations and amplitudes in the magnetizing field applied along the magnetic easy direction are made (Fig. 2).

Calculations of the magnetization m position after relaxation passes into one of the three energy minima A, B, C, passing either through one barrier to the neighboring minimum or passing through several potential barriers are showed. There are relatively large continuous areas of variants combinations of pulse magnitude h and pulse duration τ when it stops at the same energy minimum. The boundaries of these regions correspond to the orientation transitions [5] as well as complex precession modes which were observed in [6] are shown in the switching diagram in the Fig. 2b. The dynamics of the magnetization orientation during 6 ns is shown in the Fig. 2a when the pulse duration is $\tau = 0.2$ ns.

This work has been supported by Russian Science Foundation (project No. 21-72-20048).

1. O. Kovalenko, T. Pezeril, V. Temnov, Phys. Rev. **110**, 266602 (2013).
2. V.S. Vlasov, A.V. Golov, L.N. Kotov, V.I. Shcheglov, A.M. Lomonosov, and V.V. Temnov, Acoust. Phys. **68**, 18–47 (2022).
3. V.S. Vlasov, A.M. Lomonosov, A.V. Golov, L.N. Kotov, V. Besse, A. Alekhin, D.A. Kuzmin, I.V. Bychkov, V.V. Temnov, Phys. Rev. B **101**, 024425 (2020).
4. A.G. Gurevich, Magnitnyi rezonans v ferritakh i antiferromagnetikakh (Magnetic Resonance in Ferrites and Antiferromagnets), Moscow: Nauka, 1973. [In Russian]
5. V.G. Shavrov, V.I. Shcheglov, Ferromagnitnyi rezonans v usloviyakh orientatsionnogo perekhoda (Ferromagnetic Resonance under Conditions of Orientational Transition), Moscow: Fizmatlit, 2018. [In Russian]
6. A.M. Ferona, R.E. Camley, Phys. Rev. B **95**, 104421 (2017).

B.O17

HIGH-FREQUENCY MAGNETIC SUSCEPTIBILITY OF THIN MAGNETIC FILMS WITH 1D AND 2D INHOMOGENEITIES

V.A. Ignatchenko, D.S. Tsikalov, D.S. Polukhin*

Kirensky Institute of Physics, Federal Research Center KSC SB RAS, Krasnoyarsk, Russia
*E-mail: d_tsikalov@iph.krasn.ru

It was shown in [1, 2] that 2D phase inhomogeneities in a magnetic superlattice in the plane *xy* at wave propagation along the axis *z* lead to an asymmetric broadening of the resonance peak of the Green's function. These results were obtained in the approximation of single scattering of waves by inhomogeneities (the Bourret approximation [3]). The aim of this work is to investigate effects of amplitude 1D and 2D inhomogeneities in a magnetic film in a plane *xy* at wave propagation along the *z* axis on the high-frequency magnetic susceptibility of the film and, in particular, to check whether the effect of the asymmetry of the Green's function peaks found for a superlattice manifests itself in the spin-wave resonance in a thin film. In contrast to works [1, 2], the study is carried out taking into account the processes of multiple scattering of waves by inhomogeneities. To take into account the processes of multiple wave scattering, the method of self-consistent approximation (SCA) is used both in the standard form and in the form of a higher level in relation to the standard SCA, taking into account both the first and second terms of the series for the vertex function, derived and studied in the works [4, 5]. The equation for spin waves in a ferromagnetic medium with a nonuniform uniaxial magnetic anisotropy parameter β can be represented as

$$\nabla^2 m + \left[\nu + \gamma\rho(\mathbf{x})\right] m = 0\,, \tag{1}$$

where $m = M_x + iM_y$, $\nu = (\omega - \omega_0)/g\alpha M_0$, $\gamma = \Delta\beta/\alpha$, $\Delta\beta$ are standard deviations, ω is the frequency, $\omega_0 = g[H + (\beta - 4\pi)M_0]$ is the frequency of homogeneous ferromagnetic resonance, *g* is the gyromagnetic ratio, α is the exchange constant, and $\rho(\mathbf{x})$ is a centered ($\langle\rho(\mathbf{x})\rangle$, 0) and normalized ($\langle\rho^2(\mathbf{x})\rangle$, 1) random function. The directions of the external magnetic field **H**, the constant component $\mathbf{M}_0$ of

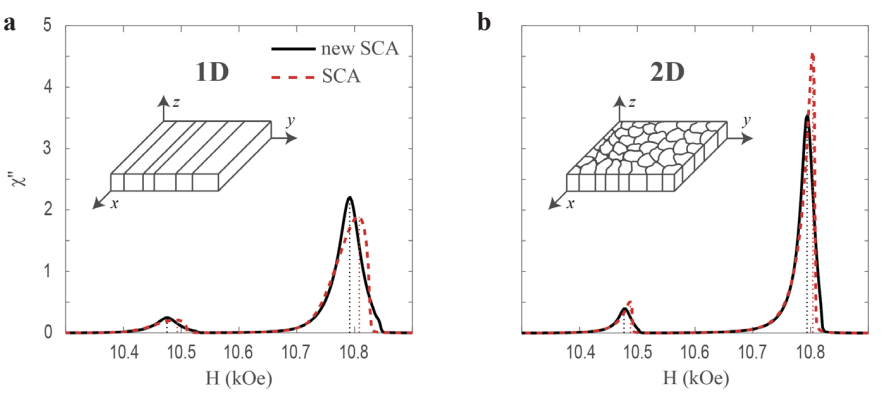

Figure 1. High-frequency magnetic susceptibility of spin-wave resonances χ″ as a function of the external magnetic field *H* for the cases of 1D (**a**) and 2D (**b**) inhomogeneities. $\Delta\beta M_0$ = 40 Oe, k_c/k_r = 1.5, $k_r = \pi/d$, ω/γ = 3283 Oe, βM_0 = 800 Oe, M_0 = 800 Gs, *d* = 200 nm, $\alpha = 2\cdot10^{-12}$ cm^2.

the magnetization **M**, and the magnetic anisotropy axis **l** coincide with the direction of the z axis. We consider a film that is unbounded in the (x, y) plane, the boundary conditions for pinning the magnetization at the edges of the film along the z axis $m(-d/2) = m(d/2) = 0$ and we believe that the random function $\rho(\mathbf{x})$ depends only on the coordinates (x, y) in the film plane. Further development of the SCA method was carried out and it was shown that for the situation under consideration, the averaged Green's function is represented in the form

$$G(z,z_0,\mathbf{k}_\perp) = \frac{2}{d}\sum_n \cos\left(\frac{n\pi}{d}z\right)\cos\left(\frac{n\pi}{d}z_0\right)G_n(\mathbf{k}_\perp) \ , \tag{2}$$

where each coefficient of the series is a 2D Green's function $G_n(\mathbf{k}_\perp)$ and must be found by the standard or new SCA method. Unlike the standard one, the new SCA is described by a coupled system of two nonlinear integral equations for the Green's function $G_n(\mathbf{k}_\perp)$ and the vertex function $\Gamma_n(\mathbf{k}_\perp)$ [4]:

$$G_n(\mathbf{k}_\perp) = \frac{1}{g_n^{-1}(\mathbf{k}_\perp) - \gamma^2(2\pi)^{-2}\int S(\mathbf{k}_\perp - \mathbf{k}_{\perp 1})G_n(\mathbf{k}_{\perp 1})\Gamma_n(\mathbf{k}_{\perp 1},\mathbf{k}_\perp - \mathbf{k}_{\perp 1})\mathrm{d}\mathbf{k}_{\perp 1}} \ , \tag{3}$$

$$\Gamma_n(\mathbf{k}_{\perp 1},\mathbf{k}_\perp - \mathbf{k}_{\perp 1}) \approx$$

$$\approx \frac{1}{1 - \gamma^2(2\pi)^{-2}\int S(\mathbf{k}_{\perp 1} - \mathbf{k}_{\perp 2})G_n(\mathbf{k}_{\perp 2})G_n(\mathbf{k}_\perp - \mathbf{k}_{\perp 1} + \mathbf{k}_{\perp 2})\Gamma_n(\mathbf{k}_{\perp 2},\mathbf{k}_{\perp 1} - \mathbf{k}_{\perp 2})\mathrm{d}\mathbf{k}_{\perp 2}} \ , \tag{4}$$

where $g_n(\mathbf{k}_\perp) = [\nu - (n\pi/d)^2 - k_\perp^2]^{-1}$ is the original Green's function of each n-th harmonic of the Fourier series, $S(\mathbf{k}_\perp)$ is the spectral density of inhomogeneities, and $k_\perp = \sqrt{k_x^2 + k_y^2}$. Neglecting in the denominator of Eq. (4) a term of the order γ^2 we would get $\mathbf{\Gamma}_n(\mathbf{k}_{\perp 1}, \mathbf{k}_\perp - \mathbf{k}_{\perp 1}) = 1$. Substituting this value in Eq. (3) turns it into the equation of the standard SCA. If in equation (3) we set $G_n(\mathbf{k}_{\perp 1})$ equal to $g_n(\mathbf{k}_{\perp 1})$, along with $\mathbf{\Gamma}_n(\mathbf{k}_{\perp 1}, \mathbf{k}_\perp - \mathbf{k}_{\perp 1}) = 1$, we obtain the equation (not selfconsistent) of the Bourret approximation [3].

The magnetic susceptibility is proportional to the integral of the Green's function $\chi'' \propto \iint G''(z,z_0,\mathbf{k}_\perp = 0)\mathrm{d}z\,\mathrm{d}z_0$ over the film thickness. Figure 1 shows the high-frequency susceptibility χ'' for 1D (Fig. 1a) and 2D (Fig. 1b) inhomogeneities. The difference between the results obtained in the standard (red dashed curves) and the new SCA (black solid curves) is clearly seen.

Main results. Effects of 1D and 2D inhomogeneities in a magnetic film in the xy plane on the high-frequency magnetic susceptibility χ'' is studied by both the standard and the new self-consistent approximation (SCA) methods. The development of the SCA method for the case of a film with boundary conditions for pinning oscillations on the film surfaces has been carried out. It is shown that the width of the χ'' peaks in the case of 2D inhomogeneities is smaller than for 1D inhomogeneities. The asymmetry of the first peak for 2D inhomogeneities in the new SCA has been obtained. The asymmetry of peaks for 1D inhomogeneities obtained in the standard SCA is a consequence of the imperfection of the method.

The reported study was funded by Russian Foundation for Basic Research, Government of Krasnoyarsk Territory, Krasnoyarsk Regional Fund of Science to the research project № 20-42-240010.

1. V.A. Ignatchenko, Yu.I. Mankov, D.S. Tsikalov, Zh. Eksp. Teor. Fiz. **134**, 706–715 (2008).
2. Yu.I. Mankov, D.S. Tsikalov, Fiz. Tverd. Tela **52**, 505–513 (2010).
3. R.C. Bourret, Nuovo Cimento **26**, 1 (1962); Can. J. Phys., **40**, 782 (1962).
4. V.A. Ignatchenko, D.S. Polukhin, J. Physics A: Mathem. and Theor. **49**, 095004 (2016).
5. V.A. Ignatchenko, D.S. Polukhin, D.S. Tsikalov, J. Magn. Magn. Mat. **440**, 83–86 (2017).

^{59}Co NMR AND ^{57}Fe MÖSSBAUER STUDIES OF CARBON ENCAPSULATED MAGNETIC NANOPARTICLES BASED ON BINARY FeCo ALLOYS

A.Yu. Germov[1*], *B.Yu. Goloborodskiy*[1], *A.S. Konev*[1], *D.A. Prokopyev*[1], *I.A. Kurmachev*[1], *E.V. Suvorkova*[2]

[1]M.N. Mikheev Institute of Metal Physics of Ural Branch of Russian Academy of Sciences, Ekaterinburg, Russian Federation
[2]Ural Federal University, Ekaterinburg, Russian Federation
[*]E-mail: germov@imp.uran.ru

Magnetic nanoparticles are now widely used [1] due to exotic properties and processability. Iron oxide-based magnetic particles are mainly used in biology and medicine, since their safety has been proven. The magnetic characteristics of such particles are low. Therefore, of particular interest are particles of the core-shell type, which contain a metal or an alloy [2]. The carbon coating of metal nanoparticles reliably protects the particles from oxidation, but leads to a decrease in the magnetic properties due to the penetration of carbon atoms into the particles, forming metal-carbon solid solutions [3]. In this study we improved magnetic properties of the carbon encapsulated nanoparticles.

The main methods for investigating nanoparticles are magnetization measurements and electron microscopy. Other conventional methods are found to be inefficient or expensive due to very small particle sizes. Local nuclear resonance methods allow us to solve several problems including phase analysis [4], analysis of the atomic environment, observation of ordered structures, tracking transitions to a single-domain or superparamagnetic state [5].

Magnetic Fe_xCo_{1-x}@C (x = 0.4–0.8) nanoparticles were prepared by gas-phase synthesis [2, 3]. Parent materials were obtained by sintering Fe and Co powders at 1050 °C in vacuum ($P = 10^{-4}$ Torr). This material was put into the induction levitation melting chamber, forming a molten droplet which was in a gas mixture (P = 150 Torr) of argon and isobutane. For the part of the samples, homogenizing annealing (540 °C) was carried out in a vacuum chamber for 4 hours.

In this work, nanoparticles based on Fe_xCo_{1-x}@C (x = 0.4–0.8) were studied using ^{59}Co NMR (powder sample in ampule) and ^{57}Fe Mössbauer spectroscopy (sample in polystyrol). The samples were powders with an average particle size of 6 nm before and 10 nm after annealing. A complex analysis of the induced hyperfine fields has shown that the ordered phase of the binary alloy is absent after synthesis according to ^{59}Co NMR data and ^{57}Fe Mössbauer spectroscopy.

Small part (5%) of iron atoms is oxidized and composition $Fe_{0.6}Co_{0.4}$@C become close to equiatomic. Nanoparticles without heat treatment also contain γ-iron and solid solutions FeC_x and $Fe_{1-y}Co_yC_x$ according to Mössbauer spectroscopy data. Annealing has removed most part (at least 90%) of these configurations. After the homogenizing annealing of $Fe_{0.6}Co_{0.4}$@C, an ordered alloy (probably $Fe_{0.5}Co_{0.5}$) without dissolved carbon inside has been obtained according to the ^{59}Co NMR data. Small part of $Fe_{1-y}Co_yC_x$ is preserved after heat treatment. These results are also confirmed by the very high magnetization (M = 192 emu/g) of $Fe_{0.6}Co_{0.4}$@C nanoparticles which contain 17 wt.% of carbon.

This study was supported by the Russian Science Foundation, project No. 21-72-00007.

1. D.L. Huber, Small **1**, 482–501 (2005).
2. M.A. Uimin et al., Phys. Met. Metallogr. **120**, 228–232 (2019).
3. A.Y. Yermakov et al., Materials Letters **254**, 202—205 (2019).
4. K.N. Mikhalev et al., Mater. Res. Express **5**, 055033 (2018).
5. A.Yu. Germov et al., Materials Today Communications **27**, 102382 (2021).

B.P2

SYNTHESIS AND CHARACTERIZATION OF EPITAXIAL Mn_5Ge_3 THIN FILMS ON A SILICON SUBSTRATE

M.V. Rautskii[1], *I.A. Yakovlev*[1], *A.S. Tarasov*[1], *M.A. Bondarev*[1,2*]

[1]Kirensky Institute of Physics, Federal Research Center KSC SB RAS, Krasnoyarsk, Russia
[2]Institute of Engineering Physics and Radio Electronics, Siberian Federal University, Krasnoyarsk, Russia
[*]E-mail: bondarevmisha99@gmail.com

Ferromagnetic Mn_5Ge_3 thin films are the promising materials for spintronics applications due to the high spin polarization and Curie temperature T_C = 296 K. At present, there are a number of works on the deposition of Mn_5Ge_3 thin films on semiconductor substates, such as Ge [1], GaAs (111), and on Ge epitaxial buffer layers [2].

The films under study were synthesized by molecular beam epitaxy on a Si(111) substrate at a temperature T = 390 °C and a pressure of $6.5 \cdot 10^{-8}$ Pa using different buffer layers. Ferromagnetic resonance (FMR) spectra were measured on a Bruker Elexsys E580 spectrometer in the temperature range from 110 K to 330 K. For all samples, an easy-plane magnetic anisotropy was observed, which is typical for thin films. The FMR spectra are shown in Fig. 1.

An analysis of the angular and temperature dependences of the parameters of the FMR lines allowed determining the optimal composition of the buffer layer. Based on the obtained experimental data one can conclude that the crystalline axis c in the Mn_5Ge_3 films is strongly ordered perpendicular to the substrate plane.

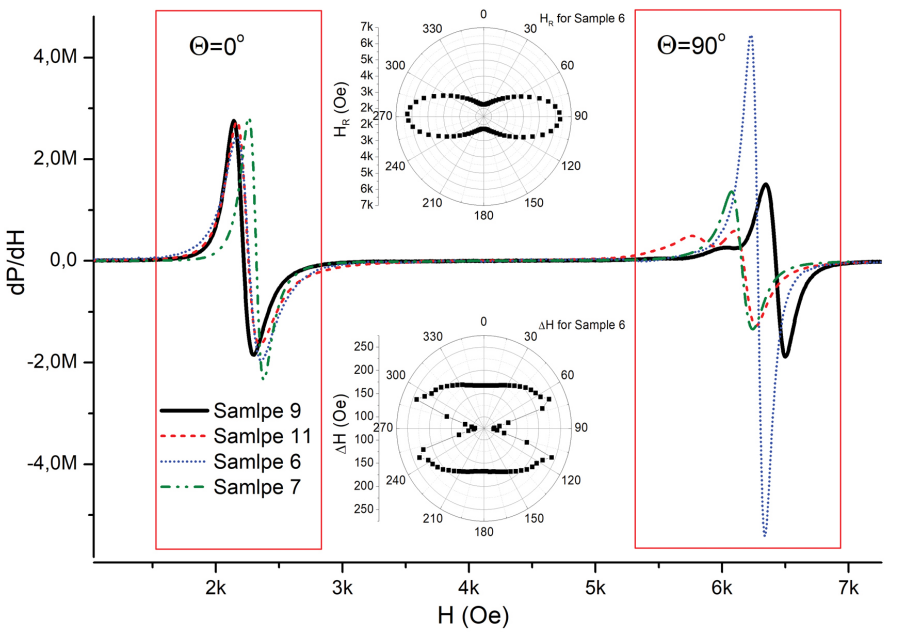

Figure 1. FMR spectra of the Mn_5Ge_3 films at T = 290 K in two orientations (the inset shows the polar angular dependences of the resonance field and FMR linewidth for one of the samples).

Support by Russian Foundation for Basic Research, the Government of the Krasnoyarsk Territory, and the Krasnoyarsk Territorial Foundation for Support of Scientific and R&D Activities, (project no. 20-42-243007) and support by Krasnoyarsk Regional Fund of Science is acknowledged.

1. A. Spiesser et al., Phys. Rev. B **84**, 165203 (2011).
2. S. Bechler et al., Semicond. Sci. Technol. **33**, 095008 (2018).

TRANSVERSE RELAXATION IN H_2O-D_2O LIQUID ENTRAPPED IN NANOCAVITIES

G. Furman[1], *V. Sokolovsky*[1], *D.A. Petrov*[2*]

[1]Physics Department, Ben Gurion University of the Negev, Beer Sheva, Israel
[2]Physics of Phase Transitions Department, Perm State University, Perm, Russia
[*]E-mail: petrovda@bk.ru

One approach to investigate the contributions of dipolar interactions to the transverse spin relaxation and its orientational dependence in NMR experiments is to replace some of the water with deuterium oxide, thereby creating an equilibrium mixture of H_2O, D_2O, and HDO.

We have proposed a model that allows us to simulate the spin-spin relaxation in a connective tissue which forms ordered hierarchical structures [1]. In the frame of this model a tissue is represented as a set of nanocavities containing H_2O-D_2O liquid. Taking into account the restricted Brownian motion of water and deuterium molecules in nanocavities the analytical expression for the rate of transverse relaxation as a function of the molar fraction of deuterium has been obtained.

The results obtained make it possible to explain the available experimental data [2], where the anisotropy of transverse relaxation was observed regardless of the degree of deuteration of an articular cartilage. Collagen fibrils in the connective tissue form ordered hierarchical long structures of hydrated nano-cavities with characteristic diameter from 1 nm to several tens of nanometers and length of about 100 nm. A well agreement between the experimental data and theoretical results was obtained due to averaged orientation of the main axes of the nanocavities about some “preferred direction”.

Our approach can be used to characterize a fine fibrillar structure of biological samples using the results of NMR/MRI experiments. Since during degradation the water concentration in a tissue can vary, the present theoretical study could benefit in future development of experimental protocols in clinical MRI.

This research was supported by the Israel Binational Science Foundation (BSF No. 2019033).

1. G. Furman, V. Meerovich, D. Petrov, V. Sokolovsky, Y. Xia, Hyperfine Interactions **242**, 19 (2021).
2. S. Tadimalla, K.I. Momot, PLoS One **9**, e115288 (2014).

SPIN POLARON MODEL OF STATIC AND DYNAMIC MAGNETIC PROPERTIES OF STROGLY CORRELATED MATERIALS

S.V. Demishev

Prokhorov General Physics Institute of RAS, Moscow, Russia
E-mail: sergey_demishev@mail.ru

In various strongly correlated materials, an effective magnetic moment μ^* describing field dependence of magnetization $M(B, T) = M_0\varphi(\mu^* B/k_B T)$ acquires anomalously high value (here B denotes magnetic field and function $\varphi(x)$ satisfies conditions $\varphi(x \to 0) \sim x$ and $\varphi(x \to \infty) \to 1$). For example in the spiral magnet MnSi, μ^* lies within (5–12)μ_B depending on the $\varphi(x)$ form used for data analysis [1, 2]. The magnetic response of the surface of topological Kondo insulator SmB_6 includes paramagnetic contribution described $\mu^* \sim 14\mu_B$ ($J = 5/2$), $\mu^* \sim 12\mu_B$ ($J = 3/2$), $\mu^* \sim 7\mu_B$ ($J = 1/2$) under assumption that $\varphi(x)$ is given by Brillouin function [3]. In both cases, the values of μ^* noticeably exceed those expected for an isolated magnetic ion [1–3].

We suggest the model explaining this anomalous behavior by formation of the many-body spin polaron state driven by antiferromagnetic (AFM) interaction [2, 4]. According to [2] this spin polaron may be treated as a ferrimagnetic cluster containing n_1 electrons with the magnetic moments μ_1 and n_2 localized magnetic moments (LMM) with the magnetic moments μ_2 (it assumes that $\mu_1^1 \neq \mu_2$). The "sublattices" in this ferrimnagnet M_1 and M_2 are formed by electrons and LMM respectively. Magnetic interactions in cluster result in parallel alignment on the sublattice magnetization and local magnetic field vectors for any external magnetic field [2]. This leads to a canted configuration of the sublattices magnetization, and it is supposed that the sum of the sublattices magnetization always has non zero projection on the direction of the magnetic field only [2]. The number of LMM and electrons in the cluster is controlled by thermodynamic stability condition, which reduces to $\mu_1^2 n_1 = \mu_2^2 n_2$. Calculation shows that such spin cluster behaves as a paramagnetic center with enhanced (with respect to elementary magnetic moments in each sublattice) the effective magnetic moment μ^* in the field dependence of magnetization.

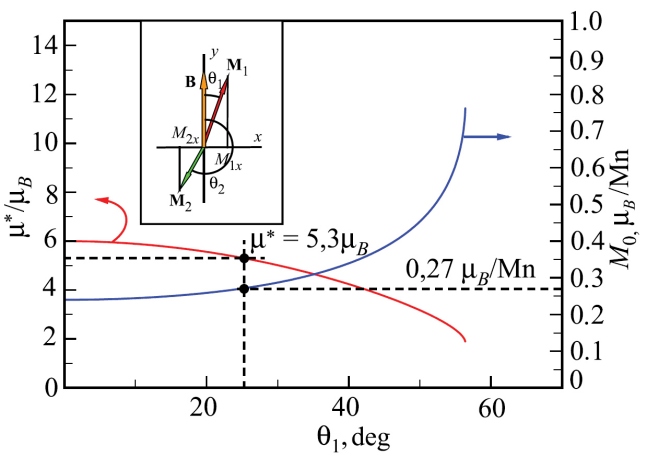

Figure 1. Spin configuration (inset) and the calculated values of the effective magnetic moment and saturation magnetization in the spin-polaron model for MnSi.

In the considered model the value of μ^* is given by [2, 4]

$$\mu^* = \frac{\mu_+}{\cos\theta_1 - \sqrt{(\mu_+/\mu_-)^2 - \sin^2\theta_1}} = \frac{\mu_+}{\cos\theta_1 - \sqrt{(n_-/n_+)^2 - \sin^2\theta_1}} \quad , \tag{1}$$

where indexes + and – denote two sublattices, which have positive and negative projection of magnetization on external magnetic field direction respectively. The angle θ_1 in Eq. (1) is the angle between the external magnetic field and magnetization of the sublattice with positive projection (inset in Fig. 1). It is visible that if $\mu_- = \mu_+ + \Delta\mu$ and $\Delta\mu < \mu_+, \mu_-$ the Eq. (1) reduces to $\mu^* \approx \mu_+^2\cos\theta/\Delta\mu$ and paramagnetic response of spin cluster ($\mu^* > 0$) is possible when $\Delta\mu > 0$ and hence sublattice with the biggest magnetic moments is aligned antiparallel to the external field and contains fewer members due to aforementioned stability condition. For strong enhancement of μ^* it is necessary to have small $\Delta\mu$ or, equivalently, $n_+ \approx n_-$ ($n_+ < n_-$).

The considered model was successfully applied for quantitative accounting of the enhancement of μ^* accompanied by a simultaneous reduction of saturating magnetization M_0 in MnSi [2] (Fig. 1). In SmB_6, the use of the model allowed finding parameters of the spin polaron states at the topological surface, formed by several Kondo singlets which are binding one excessive electron [4]. Following the classical model of a ferrimagnet [5] it is possible to estimate g-factor from the g-factors of electrons g_1 and LMM g_2 describing dynamic magnetic properties of spin polaron

$$g_{SP} = \frac{g_1\mu_1 n_1 - g_2\mu_2 n_2}{\mu_1 n_1 - \mu_2 n_2} = g_2\frac{g_1\mu_2/g_2\mu_1 - 1}{\mu_2/\mu_1 - 1} \quad . \tag{2}$$

Our recent experiments on electron paramagnetic resonance in MnSi support the validity of the Eq. (2).

We believe that applicability of the spin polaron model [2, 4] is not limited to the cases considered above and may be applicable for an explanation of static and dynamic magnetic properties of strongly correlated electron systems of different nature.

1. S.V. Demishev, V.V. Glushkov, I.I. Lobanova, M.A. Anisimov, V.Yu. Ivanov, T.V. Ishchenko, M.S. Karasev, N.A. Samarin, N.E. Sluchanko, V.M. Zimin, and A.V. Semeno, Phys. Rev. B **85**, 045131 (2012).
2. S.V. Demishev, T.V. Ishchenko, A.N. Samarin, Low Temp. Phys. **41**, 971 (2015).
3. S.V. Demishev, A.N. Azarevich, A.V. Bogach, M.I. Gilmanov, V.B. Filipov, N.Yu. Shitsevalova, V.V. Glushkov, JETP Lett. **109**, 150 (2019).
4. S.V. Demishev, Appl. Magn. Reson. **51**, 473 (2020).
5. R.K. Wangsness, Phys. Rev. **91**, 1085 (1953).

LANDAU-LIFSHITS EQATION OF MOTION MODIFIED BY QUANTUM FLUCTUATIONS AND EPR IN STRONGLY CORRELATED MATERIALS

S.V. Demishev

Prokhorov General Physics Institute of RAS, Moscow, Russia
E-mail: sergey_demishev@mail.ru

In the present work we consider a system, which spin dynamics may be described by semi-classical Landau-Lifshits (LL) equation of motion. We argue that accounting of the quantum fluctuations of magnetic moment changes significantly dynamical response of a strongly correlated materials and gives rise to new regulations linking parameters of electron paramagnetic resonance (EPR).

It is possible to show that in semi-classical approximation Heisenberg uncertainty principle leads to the link between fluctuation $\Delta\omega$ of the rotation frequency of magnetization around external magnetic field H and fluctuation of the magnetization M_z along field direction are related

$$\frac{\Delta\omega}{\omega} = \frac{2\Delta M_z}{\mu_B} \quad . \tag{1}$$

In the LL equation,

$$\frac{d\mathbf{M}}{dt} = \gamma[\mathbf{M},\mathbf{H}] - \frac{\alpha\gamma}{M_0}[\mathbf{M},[\mathbf{M},\mathbf{H}]] \ , \tag{2}$$

the frequency fluctuations may be taken into account by replacing $\gamma \to \gamma + \Delta\gamma$, where $\Delta\gamma$ corresponds to fluctuations of the gyromagnetic ratio, which are of a quantum nature. The Eq. (1) suggests that the correlator $t <\Delta\gamma\Delta\mathbf{M}> = <\Delta\gamma\Delta M_z>\mathbf{k}$ is non-zero (hereafter we assume experimental geometry shown in Fig. 1). Averaging of LL Eq. (2) leads to the following expressions for oscillating magnetization $\mathbf{m}$ [1]

$$\frac{dm_x}{dt} = \gamma H_0 m_y - \gamma M_0(1+a)h_y - \nu \cdot m_x(1+a)\,,$$
$$\frac{dm_y}{dt} = -\gamma H_0 m_x + \gamma M_0(1+a)h_x - \nu \cdot m_y(1+a)\,,$$

where H_0 and M_0 stands for external field magnitude and magnetization respectively, h_x and h_y are components of the oscillating magnetic field $\mathbf{h}$. Here a is the parameter describing effect of quantum fluctuations $a = <\Delta\gamma\Delta M_z>/\gamma M_0 \sim 2\Delta M_x{}^2/\mu_B M_0$. From Eq. (3) it is possible to find power adsorbed in the EPR

$$P \sim \mathrm{Im}\{\mathbf{m}\cdot\mathbf{h}^*\} = \chi(1+a)h_0{}^2 \frac{2\omega_H\omega\nu(1+a)}{[\omega_H^2 - \omega^2 + \nu^2(1+a)^2]^2 + 4\omega^2\nu^2(1+a)^2} \tag{4}$$

Here $\chi = H_0/M_0$, $h_0^2 = h_x^2 + h_y^2$ and ω are the square of the amplitude of the alternating magnetic field and its frequency, respectively. We also use notations $\omega_H = \gamma H_0$ for reduced magnetic field and $\nu \approx \alpha\gamma H_{res}$ for the relaxation frequency at the resonant field H_{res}.

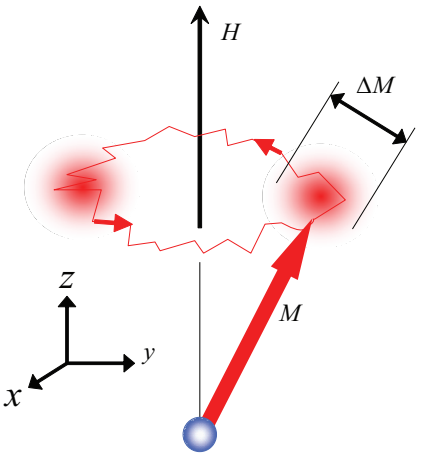

Figure 1. The movement of the magnetic moment (M) in an external magnetic field (H) in the presence of spin fluctuations. The end of vector trajectory M has a random character and is located in the spatial region corresponding to the uncertainty ΔM.

This result leads to enhancement of the integrated intensity I by the factor ~$(1 + a)$, appearance of the g-factor shift together with the additional contribution to the EPR line width ΔH. Interesting that these parameters are linked by the universal relation [1]

$$\frac{(\Delta H_{\mathrm{QF}}/H_{\mathrm{res}})^2}{-\Delta g_{\mathrm{QF}}/g} \approx \frac{\Delta I_{\mathrm{QF}}}{I} \approx a\,,$$

where ΔH_{QF}, Δg_{QF} and ΔI_{QF} stand for variation of the EPR line width, g-factor and integrated intensity caused by quantum fluctuations. Analysis shows that the relation (5) may be applicable for accounting of the experimental data on EPR in such strongly correlated systems like MnSi and CeB_6.

1. S.V. Demishev, Dokl. Phys. **66**, 187 (2021).

Pd-Fe ALLOY FILM WITH HIGH GRADIENT OF IRON CONTENT: STRUCTURAL AND MAGNETIC STUDIES

G.F. Gizzatullina[1], *I.V. Yanilkin*[1,2*], *A.I. Gumarov*[1,2], *B.F. Gabbasov*[1,2], *A.G. Kiiamov*[1], *R.V. Yusupov*[1], *L.R. Tagirov*[1,2]

[1]Institute of Physics, Kazan Federal University, Kazan, Russia
[2]Zavoisky Physical-Technical Institute, FRC Kazan Scientific Center, Russian Academy of Sciences, Kazan, Russia
[*]E-mail: yanilkin-igor@yandex.ru

Creation and studies of ferromagnetic materials with controlled inhomogeneities, e.g., smoothly varying value of a certain magnetic parameter, attract an increasing attention of the researchers involved in the field of magnetic phenomena investigations. The aim of this work was to study the structural and magnetic properties of an artificially created film with a high fixed gradient of iron concentration across the thickness.

The synthesis of an inhomogeneous single-crystal film of the Pd-Fe alloy with a thickness of 116 nm was carried out with an ultrahigh-vacuum setup by the molecular beam epitaxy method. A single crystal MgO (100) was used as a substrate. To obtain a sample with the required distribution of the iron content across the thickness (from 2% to 50%), the temperature of the effusion cell with Pd was kept constant, while that of the Fe was varied with time. The magnetic properties of the sample were studied with the vibrational magnetometry and ferromagnetic resonance spectroscopy. According to the data obtained by X-ray diffraction, the $L1_0$ phase, which is characterized by a large perpendicular uniaxial magnetic anisotropy, is present. Additionally, the change in film properties after several etching steps was studied.

This research was supported by the Russian Science Foundation (Project № 22-22-00629, https://rscf.ru/en/project/22-22-00629/).

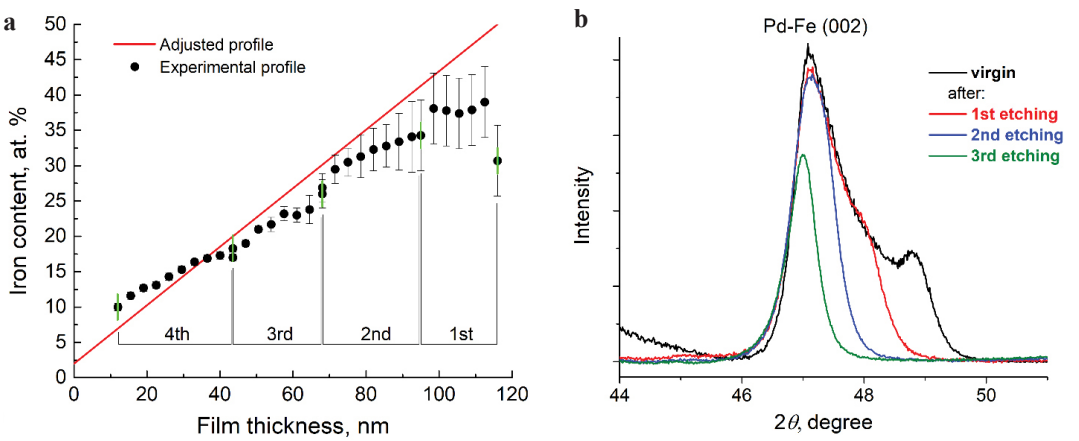

Figure 1. Adjusted by deposition process (line) and measured by XPS (symbols) iron concentration profile. Etching stages are marked by 4 segments (**a**); XRD (002)-maximum from the as prepared Pd-Fe film as well as after argon ion etchings (**b**).

B.P7

ELECTRON SPIN RESONANCE OF ^{51}V IONS IN SCANDIUM ORTHOSILICATE MONOCRYSTAL

R.F. Likerov, I.V. Yatsyk, R.B. Zaripov, K.B. Konov, V.F. Tarasov, V.A. Shustov*

Zavoisky Physical-Technical Institute, FRC Kazan Scientific Center, Russian Academy of Sciences, Kazan, Russia
*E-mail: rodionlikerov@gmail.com

Active search for suitable materials has a significant role in the quantum communications development. Such materials will be used as a medium for quantum memory devices. Key requirements for these devices are long phase memory time enough to complete manipulations with the quantum information and simplified method of interaction with the quantum memory through various protocols.

For example, scandium and yttrium orthosilicate (YSO, SSO) monocrystals doped with monoisotopic rare-earth ions such as ^{143}Nd, ^{145}Nd, ^{171}Yb were studied for quantum memory applications [1, 2]. Alternatively, similar studies were carried out for monoisotopic ^{53}Cr doped YSO and SSO monocrystals [3, 4].

In this work we study scandium orthosilicate monocrystal with monoisotopic Si ($Sc_2{}^{28}SiO_5$) and doped with monoisotopic ^{51}V ions (0.001 at.%). This crystal was not studied before in the literature and the closest to our work was done for vanadium doped forsterite (Mg_2SiO_4) by authors in [5].

We measured CW ESR spectra and orientational dependencies of the ESR transitions from the rotation angle in the external magnetic field in X-band at the temperature T = 10 K (Fig. 1) and in Q-band at the temperatures T = 20 K and T = 30 K. On spectra from both bands, we observed the group of lines from paramagnetic centers of vanadium ions V^{4+} ($3d^1$). Since there is only 1 electron on the d-shell responsible for one ESR transition and the nuclear magnetic moment of ^{51}V

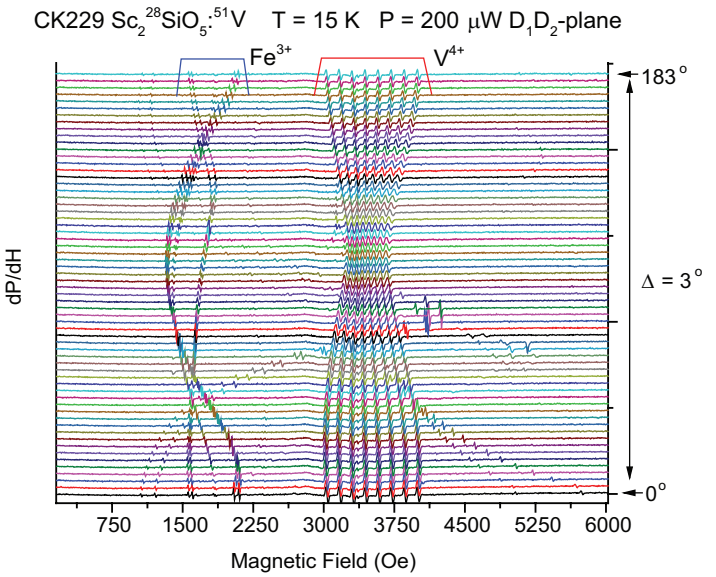

Figure 1. Orientational dependence of ESR spectra for ^{51}V: $Sc^{228}SiO_5$ (0.005 at.%) measured at T = 15 K with $\mathbf{B}_0 || D_1D_2$.

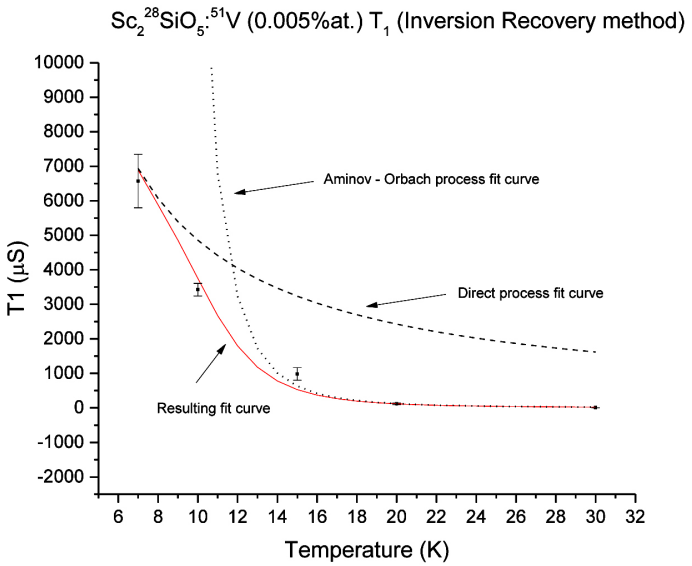

Figure 2. Temperature dependence of the spin-lattice relaxation time for $^{51}V:Sc_2{}^{28}SiO_5$ (0.005 at.%) measure with inversion recovery method.

isotope is $I = 7/2$ resulting in $2I + 1 = 8$ lines of hyperfine structure. The group of lines in the 1000–2250 Oe magnetic field range belongs, presumably to Fe^{3+} ions, which are presented in the crystal as unwanted impurity.

We also measured spin dynamics by pulsed ESR methods, such as spin-lattice and phase coherence times and their temperature dependencies. The temperature dependence for spin-lattice relaxation time of V^{4+} centers is shown at Fig. 2. The experimental points were approximated by the sum of direct phonon relaxation process and Aminov-Orbach process. The spin-lattice relaxation time $T_1 \approx 6.5$ ms.

Authors acknowledge the financial support from the government assignment for FRC Kazan Scientific Center of RAS.

1. A.A. Sukhanov et al., Journal of Magnetic Resonance **295**, 12–16 (2018)
2. R.F. Likerov et al., Magn. Reson. Solids **22**, 20201 (2020)
3. A.A. Sukhanov et al., Appl. Magn. Reson. **52**, 1175–1185 (2021)
4. V.F. Tarasov et al., Appl. Magn. Reson. **52**, 5–14 (2021)
5. I.N. Gracheva et al., Appl. Magn. Reson. **44**, 561–570 (2013)

MAGNETIC PROPERTIES OF $Ba_xSr_{2-x}TiFeO_6$ DOUBLE PEROVSKITES AT LOW TEMPERATURES

R.M. Eremina[1], *I.V. Yatsyk*[1], *V.A. Shustov*[1], *F.G. Vagizov*[2], *T. Maiti*[3], *D.V. Mamedov*[1*]

[1]Zavoisky Physical-Technical Institute, FRC Kazan Scientific Center, Russian Academy of Sciences, Kazan, Russia
[2]Institute of Physics, Kazan Federal University, Kazan, Russia
[3]Department of Materials Science and Engineering Indian Institute of Technology Kanpur, Kanpur, India
[*]E-mail: javi-m@yandex.ru

Currently, thermoelectric materials such as chalcogenides (Bi_2Te_3, Sb_2Te_3, Zn_4Sb_3, Bi_2Se_3, SnTe and others) and intermetallics are mainly used to convert heat into electricity [1]. They have significant disadvantages, such as toxicity, decomposition, at high temperatures ($T > 600$ K), evaporation, melting and oxidation. As a result, the efficiency of converting heat to electricity at high temperatures is low. However, most of the heat is generated by various sources at temperatures above 900 K. For these temperatures, oxides are a more suitable alternative because of their greater stability at high temperatures, lower cost, and higher oxidation resistance. Among oxide materials, good thermoelectric properties are shown, for example, by Na_xCoO_2, $Ca_3Co_4O_9$ and others [2]. Several oxides of double perovskites have shown promising high temperature thermoelectric properties.

Double perovskite oxides have the formula $A_2B'B''O_6$, where A is alkaline earth metals, lanthanides; B′, B″ are transition metals.

In this work, we investigate the magnetic properties of double perovskite oxides $Ba_xSr_{2-x}TiFeO_6$ (x = 0, 0.1, 0.15, 0.25). This substance has a cubic structure $Pm\bar{3}m$ with parameters a = 3.8986 Å; 3.8986 Å; 3.8982 Å; 3.9000 Å for x = 0; 0.1; 0.15; 0.25 respectively.

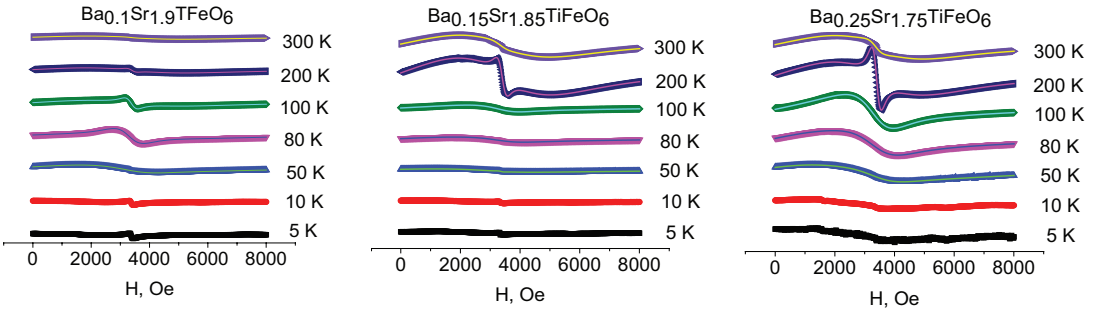

Figure 1. EPR temperature dependence of $Ba_xSr_{2-x}TiFeO_6$ double perovskites.

Electron paramagnetic resonance (EPR) (Fig. 1) and Mössbauer studies of the samples were carried out. From the EPR and Mössbauer spectroscopy data, we have shown the presence of two magnetic centers of iron (Fe^{3+}, Fe^{4+}) in this substances. The temperature dependences of the magnetization were obtained. It can be seen from the dependence that the phase transition to antiferromagnetic or ferrimagnetic ordering occurs at temperatures of about ~ 17.5 K, 14.5 K, 13.5 K, and 13.0 K for x = 0, 0.1, 0.15, 0.25, respectively.

This work is supported by RSF-22-42-02014.

1. T. Maiti, M. Saxena, and P. Roy, J. Mater. Res. **34**, 107 (2019).
2. P. Roy, V. Waghmare, and T. Maiti, RSC Adv. **6**, 54636 (2016).

B.P9

SPIN WAVES CONTROL BY SPIN-POLARIZED CURRENT IN PERIODIC HETEROSTRUCTURES

O.V. Matveev[1*], *N.D. Lobanov*[1], *M.A. Morozova*[1,2]

[1]Saratov State University, Saratov, Russia
[2]Moscow Institute of Physics and Technology, Dolgoprudny, Moscow Region, Russia
[*]E-mail: olvmatveev@gmail.com

Recently magnon spintronics, a new branch in spin-wave electronics, attracts the attention of researchers. The basis of magnon spintronics is the interaction of magnons (spin waves) with a spin-polarized current [1, 2]. This interaction is most effective in layered ultrathin structures based on the ferromagnetic materials and normal metals. Spin-polarized current is the flow of angular momentum that can be mediated by electrons. Spin current, due to the transfer of the angular momentum from the electrons spin to the ferromagnetic magnetization at the ferromagnetic/normal metal interface, allows to control gain and attenuation of spin waves [3].

In this work, we study the opportunities of using the spin-polarized current to control the characteristics of the Bragg band gaps in two types of periodic structures: a magnonic crystal with grooves (Fig. 1a) and a ferromagnetic film with metal stripes (Fig. 1b).

We show that in the first type of structures (a magnonic crystal with grooves), the formation of a band gap is possible. Depending on the direction of the spin current, a gain or attenuation of MSSW is possible, in the frequency range both outside and inside the band gap. When using the second type of structures (ferromagnetic film with metal stripes), it is possible to create a so-called dynamic magnonic crystal, which can turn its periodic waveguide properties on and off, in this case, depending on the presence and magnitude of the spin-polarized current in the metal strips.

Thus, we have shown that in periodic composite structures based on ferromagnetic materials and normal metals, it is possible to control the gain/attenuation of spin waves in ferromagnetic films due to the interaction with a spin-polarized current, as well as the formation and parameters of the Bragg band gaps for spin waves.

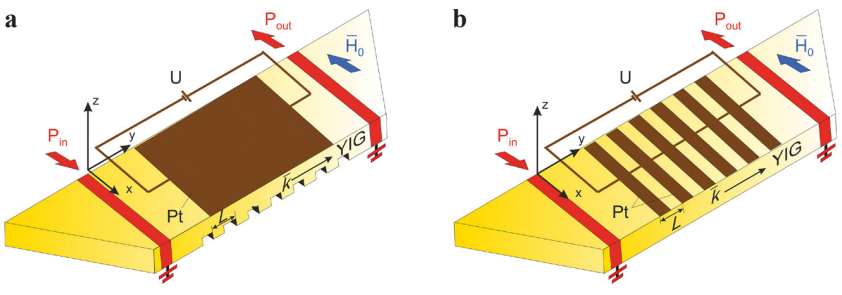

Figure 1. Two types of periodic structures: a magnonic crystal with grooves (**a**) and a ferromagnetic film with metal stripes (**b**).

The work was supported by Russian Foundation for Basic Research (\textnumero 19-29-03049-mk).

1. A.V. Chumak et al., Nature Physics **11**, 453 (2015).
2. A. Hoffmann, S.D. Bader, Phys. Rev. Applied **4**, 047001 (2015).
3. P. Pirro et al., Appl. Phys. Lett. **104**, 012402 (2014).

CRITICAL DYNAMICS OF THE QUANTUM PHASE TRANSITION IN 3D QUANTUM HEISENBERG MODEL

M.G. Vasin

Vereshchagin Institute of High Pressure Physics, Russian Academy of Sciences, Moscow, Russia
E-mail: dr_vasin@mail.ru

It is known that quantum phase transitions are dynamic in nature [1]. However, at present only non-dissipative quantum dynamics is described in detail, the application of which in the case of a complex multi-particle system is limited by the coherence time of this system. At the same time, the question remains how dissipation affects the critical behavior near the quantum critical point. And such an influence exists, which, for example, is indicated by a continuous change in the critical indices of quantum systems undergoing a phase transition when approaching $T = 0$ [2–5].

In this paper, we consider a new theoretical approach [6, 7] that allows us to consider both adiabatic and dissipative processes in various magnetic systems through a unified theory based on the Keldysh-Schwinger technique. In particular, the critical dynamics of the 3D quantum Heisenberg model near the quantum critical point is considered.

For this, using the Majorana fermions formalism the quantum Heisenberg model is reduced to the standard Ginsburg-Landau second order phase transition model. Then it is shown that in the system during the transition from the high-temperature regime, in which thermal fluctuations prevail, to the quantum regime, in which only quantum fluctuations remain, the system acquires an effective dimension $d + z\Lambda(T)$, where z is the dynamic index, and $\Lambda(T)$ increases from 0 to 1 when the temperature approaches to zero. It is shown that during the transition from the high-temperature regime, in which thermal fluctuations prevail, to the quantum regime, in which only quantum fluctuations remain, the system acquires an effective dimension $d + z\Lambda(T)$, where z is the dynamic index, and $\Lambda(T)$ increases from 0 to 1 when the temperature approaches to zero (Fig. 1).

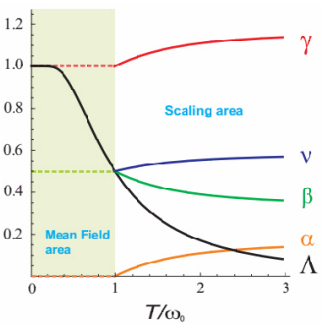

Figure 1. Critical exponents crossover close to $T = 0$ (T/ω_0 is the thermal fluctuation energy to the quantum zero-point fluctuation energy ratio).

1. S.M. Stishov, Physics-Uspekhi **47**(8), 789 (2004).
2. W.A. Erkelens et al., Europhys. Lett. **1**, 37–44 (1986).
3. J.J.M. Steijger et al., J. Magn. and Magn. Mat. 3**1–34**, 1091–1092 (1983).
4. S.M. Stishov et al., Phys. Rev. B **91**, 144416 (2015).
5. F.B. Carneiro et al., Phys. Rev. B **101**, 195135 (2020).
6. M.G. Vasin, V.N. Ryzhov, V.M. Vinokur, Sci. Rep. **5**, 18600 (2015).
7. M.G. Vasin, V.M. Vinokur, Physica A **575**, 126035 (2021).

NMR STUDY OF Co_3C AND Fe_3C CARBIDE NANOPARTICLES

K.N. Mikhalev[1*], *A.Yu. Germov*[1], *M.A. Uimin*[1,2], *A.E. Yermakov*[1,2], *A.S. Konev*[1], *S.I. Novikov*[1], *T.V. Dyachkova*[3], *A.P. Tyutyunnik*[3]

[1]M.N. Mikheev Institute of Metal Physics, Ural Branch, Russian Academy of Sciences, Ekaterinburg, Russia
[2]Ural Federal University, Ekaterinburg, Russia
[3]Institute of Solid State Chemistry, Ekaterinburg, Russia
E-mail: mikhalev@imp.uran.ru

Magnetic nanoparticles are of considerable interest both from the fundamental point of view, and in connection with the possibility of their practical application in medicine, spintronics, sensor devices, supercapacitors, etc. [1].

Transition metal carbides themselves are no less interesting [2, 3]. Their study is complicated by a complex synthesis procedure, as a result of which heterophase systems in the form of nanocrystals are most often obtained [2]. The absence of single-phase samples leads to significant contradictions in the published data. For example, the magnitudes of magnetic moments on cobalt ions in Co_3C given in [2] and [4] differ by more than 1.5 times! The ^{59}Co, ^{57}Fe NMR data in Co_3C and Fe_3C, respectively, are practically absent in literature.

Carbides Co_3C and Fe_3C are ferromagnetic intermetallic compounds [2, 3] with orthorhombic structure (*Pnma*) and metallic conductivity. Their Curie temperatures are also very close ($T_C \sim 500$ K).

We have obtained and analyzed the ^{59}Co NMR spectra of Co_3C nanoparticles with an average size about 40 nm in a local field in the temperature range 77–300 K and the ^{57}Fe NMR spectra of Fe_3C nanoparticles (average size about 50 nm) in the temperature range 4.2–300 K.

The ^{59}Co NMR spectra of Co_3C nanoparticles recorded in a zero external magnetic field consist of several inhomogeneously broadened lines. The complex analysis of the ^{59}Co NMR spectra and magnetic measurement data shows that Co_3C is the ferromagnet with a Curie temperature $T_C = 498$ (10) K. This result confirms the previous data obtained for heterophase Co_xC samples [2].

A comprehensive analysis of the ^{59}Co NMR spectra allowed us to determine the hyperfine magnetic fields for two non-equivalent positions of cobalt in this carbide: 203 kOe for Co_1 and 187 kOe for Co_2 (at room temperature). These hyperfine fields correspond to the spin state of cobalt ions $S = 1$. The components of the electric field gradient tensor (EFG) for two non-equivalent positions of cobalt are also obtained.

An analysis of the ^{59}Fe NMR spectra in Fe_3C also allowed us to obtain the hyperfine fields for two nonequivalent positions of iron atoms, which correspond to spin state $S = 1$.

The study was performed within the state assignments of the Mikheev Institute of Metal Physics of the Ural Branch of the Russian Academy of Sciences: state program "Function" No 122021000035-6 and state program "Magnit" No 122021000034-9.

1. E.G. Sharoyan, A.A. Mirrahkanyan, H.T. Gyulasaryan, A.N. Kocheryan, A.S. Makuryan, J. of Contemporary Phys. **52**, 147 (2017).
2. Y. Zhang, G.S. Chaubey, C. Rong, Y. Ding, N. Poudyal, P. Tsai, Q. Zhang, J.P. Liu, J. of Magnetism and Magnetic Mat. **323**, 1495 (2011).
3. Xing-Wu Liu, Shu Zhao, Yu Meng, Qing Peng, Albert K. Dearden, Chun-Fang Huo, Yong Yang, Yong-Wang Li, Xiao-Dong Wen. Scientific Rep. **6**, 26184 (2016).
4. K.J. Carroll, Z.J. Huba, S.R. Spurgeon, M. Qian, S.N. Khanna, D.M. Hudgins, M.L. Taheri, E.E. Carpenter, Appl. Phys. Lett. **101**, 012409 (2012).

B.P12

CHARACTERISTIC FEATURES OF THE DYNAMIC SUSCEPTIBILITY OF FERRITE-GARNET FILMS IN AN EXTERNAL FIELD

Yu.I. Nepochatykh[1*], *V.G. Shavrov*[2], *V.V. Koledov*[2]

[1]Donetsk Institute for Physics and Engineering named after A.A. Galkin, Donetsk, DPR
[2]Kotelnikov IRE RAS, Moscow, Russia
[*]E-mail: nepo@bk.ru

Obtaining a large change in the characteristics of an object and a high signal response to a small impact is possible when the control signal acts as a trigger for unblocking the flow of external energy through this object or releasing the energy stored in its system. The second is typical of magnetic materials with an abrupt change in properties during their magnetization reversal. Such effects are in demand and are already widely used. The influence of a high-frequency (HF) field on an object during its magnetization reversal and, especially, in the range of values of an external field causing a magnetization jump, when the HF field can significantly influence its course, excite an additional jump, and at the same time also reproduce the process of jumps by its measurable change, is investigated.

Figure 1 shows the dependences on the field of the controlled parameters of an autodyne [1] with a film of yttrium iron garnet (YIG) in a measuring cell when magnetized by a field perpendicular to its plane. A characteristic form of their modification for field orientation more precisely than 0.1 degree to the normal to the film plane is given. The shape of the experimental curves changes rapidly as the field is disoriented. The shape of the experimental curves rapidly changes as the field is disoriented. The effect of deviations in the orientation of the [111] axis and growth uniaxial anisotropy from the normal to the plane for different samples is also very large. However, obtaining similar curve shapes is reproducible for samples of the same composition and was carried out in our experiments by additional field orientation. The behavior of the curves with high sensitivity reflects the change in the magnetic structure when the sample is magnetized. Irregular

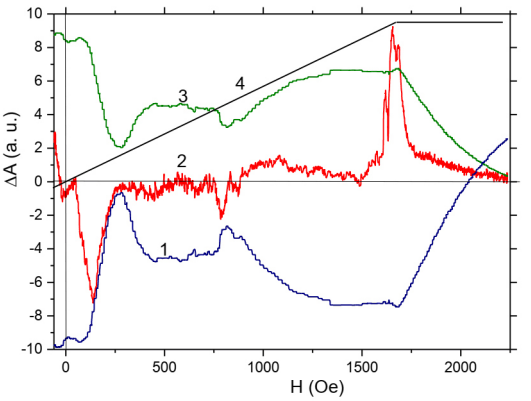

Figure 1. Dependences of autodyne parameters on the field perpendicular to the plane of the YIG film: 1 – frequencies in the range 6.0÷6.124 MHz, 2 – derivative of the change in the amplitude of HF oscillations, 3 – susceptibility (calculated from frequency data), 4 – calculated [2] magnetization.

jumps in the autodyne amplitude are observed in the range of the fields of extremes of curve 2 and the corresponding susceptibility maxims on curve 3. They reflect stepwise changes in the magnetic structure upon rearrangement of domain structure and upon saturation of the magnetization.

Near the value of the saturation field of the film magnetization and the corresponding maxima on curves 2, 3, even a regular change in the autodyne amplitude can be installed, that is, its self-modulation with a frequency of 1–10 kHz. This self-modulation is interconnected with the resonant low-frequency vibration of the magnetization. It is induced by the HF field, since it shows a strong dependence on the parameters of the HF field. The resonance also demonstrates the achievement of conditions for the appearance of a magnetization jump and the possibility of stabilizing the conditions for the generation of self-oscillations.

The work is supported by Russian Science Foundation Grant No 20-19-00745.

1. N.I. Mezin, Yu.I. Nepochatykh, N.Yu. Starostyuk, S.V. Yampolskii, JMMM **476**, 447–452 (2019).
2. V.G. Shavrov, V.I. Shcheglov, Ferromagnetic resonance under conditions of orientation transition, Fizmatlit, Moscow (2018) [in Russian].

SPIN SWITCHING MECHANISM STIMULATED BY LINEARLY POLARIZED FEMTOSECOND OPTICAL PUMP

N.B. Orlova[1*], *P.A. Agzamova*[2], *M.I. Kurkin*[2]

[1]Novosibirsk State Technical University, Novosibirsk, Russia
[2]Institute of Metal Physics, Ural Branch of Russian Academy of Sciences, Ekaterinburg, Russia
[*]E-mail: n.b.orlova@corp.nstu.ru

The spin reversal after the femtosecond linearly polarized pumping in the absence of an external magnetic field was experimentally observed by the authors of [1]. Since under these conditions both opposite directions for magnetization are equivalent, the magnetization reversal discovered by the authors of [1] is possible only with spontaneous symmetry breaking. This violation is not the only feature of the effect under discussion. Another feature is its occurrence near the magnetic compensation temperature of the sublattices of f and d electrons in the considered Gd–Fe–Co film. Besides that, the authors of [2] encountered that the discussed magnetization reversal is accompanied by the destruction of the sublattices after optical exposure followed by restoration in the reoriented direction in the relaxation process. Moreover, the uncompensated spin in the intermediate state is uniformly distributed between the sublattices. As a result, their magnetic moments become parallel like if their exchange interaction turned from antiferromagnetic to ferromagnetic.

This report is about the new mechanism for the optical magnetization reversal of the spin sublattices with all the listed anomalous properties The mechanism is based on the spin sublattice model proposed by M. I. Kurkin and N. B. Orlova in 2019 [3]. This model assumes the formation of spin sublattices with the obligatory participation of magnetic anisotropy eliminating degeneracy in the spectrum of the exchange interaction operator. In a two-sublattice antiferromagnet near the temperature magnetic compensation is the S_1 and S_2 sublattices:

$$S_1 + S_2 \ll S_1 .$$

According to our model the spin switching is stimulated by the femtosecond linearly polarized optical pumping and consists of three stages. The first stage is the formation of a transient state in the process of relaxation of electrons excited by optical pumping with a duration τ_p. During the relaxation the electrons stay in excited states with an excitation energy ΔE determined by the Heisenberg uncertainty relation:

$$\Delta E \approx \hbar/\tau_p .$$

Spin switching is provided by the electrons with energies ε above the Fermi energy E_F in the interval:

$$E_F < E < E_F + \Delta E ,$$

and the holes with energies E below E_F in the interval $E_F - \Delta E < E < E_F$. The recombination of the electrons with the holes decreases their kinetic energy $\Delta E_{kin} < 0$. This decrease can compensate the increase in the magnetic anisotropy energy $\Delta E_{an} < 0$ upon spin switching:

$$\Delta E_{kin} + \Delta E_{an} = 0 .$$

As a result, the degeneracy in the spectrum of the operator $V_{kin} + V_{an}$, which was violated by V_{an} before optical pumping is now restored. Here V_{ex} is the exchange interaction operator, V_{an} is the energy operator of magnetic anisotropy. The spin sublattice model proposed by M. Kurkin and N. Orlova [3] predicts the destruction of the sublattices after such restoration of degeneracy. Destruction of sublattices in the transient state after femtosecond optical pumping is the second stage of the optical spin switching process. The article discusses the conditions that ensure a uniform distribution of the excess spin S between both sublattices with their incomplete magnetic compensation ($S \neq 0$). Uniform distribution means that the spins of both sublattices S_1 and S_2 satisfy the condition:

$$S_1 = S_2 = S/2 \ .$$

This equality corresponds not only to the destruction of the sublattices, but also to the partial restoration of the shorter sublattice S_2 in the direction of the initial spin S and a spin with a longer sublattice S_1. The state corresponding to the condition $S_1 = S_2 = S/2$ is the initial condition for the third stage of spin switching. This stage is associated with the relaxation of the transient state, which is accompanied by the restoration of the sublattices. If the shorter S_2 sublattice is restored faster with a longer S_1, then the restored ferrite structure turns out to be switched with respect to the original structure before pumping.

1. T.A. Ostler et al., Nature Commun. **3**, 666 (2012).
2. I. Radu et al., Nature **472**, 205 (2011).
3. D.C. Mattis, The Theory of Magnetism (Made Simple. Word Scientific Publishing Co. Singapore, 2006).
4. M.I. Kurkin, N.B. Orlova, JMMM **474**, 287 (2019).

B.P14

MAGNETIC ANISOTROPY AND "EASY AXIS-EASY PLANE" TRANSFORMATION IN $Pr_xY_{1-x}Fe_3(BO_3)_4$ SINGLE CRYSTALS STUDIED BY ANTIFERROMAGNETIC RESONANCE

A.I. Pankrats[1,2,*], *S.M. Zharkov*[1,2], *G.M. Zeer*[2], *I.A. Gudim*[1]

[1]Kirensky Institute of Physics, Federal Research Center KSC SB RAS, Krasnoyarsk, Russia
[2]Siberian Federal University, Krasnoyarsk, Russia
[*]E-mail: pank@iph.krasn.ru

In the pure $PrFe_3(BO_3)_4$ the easy-axis (EA) contribution of the Pr^{3+} ion subsystem to the total magnetic anisotropy dominates over the easy-plane (EA) contribution of the Fe^{3+}+ ion subsystem, determining the EA antiferromagnetic structure of the crystal below the Néel temperature T_N = 32 K [1]. The diamagnetic dilution of the Pr subsystems changes the ratio of the contributions to the total magnetic anisotropy. The high resolution neutron powder diffraction [2] show that the transition from the EA antiferromagnetic structure to the EP one occurs in these crystals through the forma-tion of inclined magnetic structures in the region of the Pr concentration x = 0.45 ÷ 0.67. The present study is devoted to the investigation of spin dynamics, magnetic structures and magnetic anisotropy of the $Pr_xY_{1-x}Fe_3(BO_3)_4$ single crystals using antiferromagnetic resonance (AFMR).

In the $Pr_xY_{1-x}Fe_3(BO_3)_4$ crystals with x = 0.25 and 0.45, the AFMR study for both **H**||c and **H**⊥c orientations shows frequency-field dependences (FFD) which are characteristic for EP antiferromagnets and qualitatively close to the FFD of pure $YFe_3(BO_3)_4$.

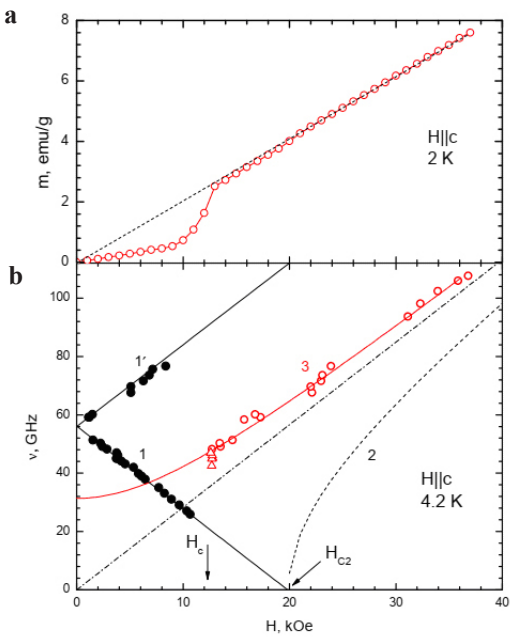

Figure 1. **a** FFD in $Pr_{0.67}Y_{0.33}Fe_3(BO_3)_4$ measured at T = 4.2 K, **H** || c; **b** – magnetization as a function of the magnetic field **H**||c at T = 2 K.

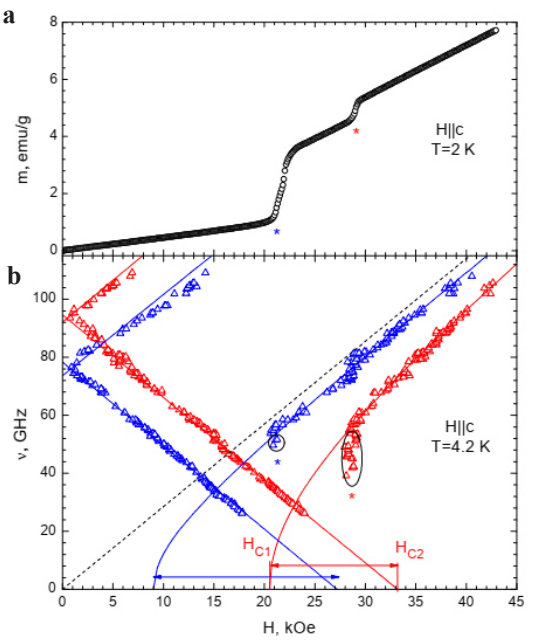

Figure 2. **a** FFD in $Pr_{0.75}Y_{0.25}Fe_3(BO_3)_4$ measured at T = 4.2 K, **H** || c; **b** magnetization as a function of the magnetic field **H** || c at T = 2 K.

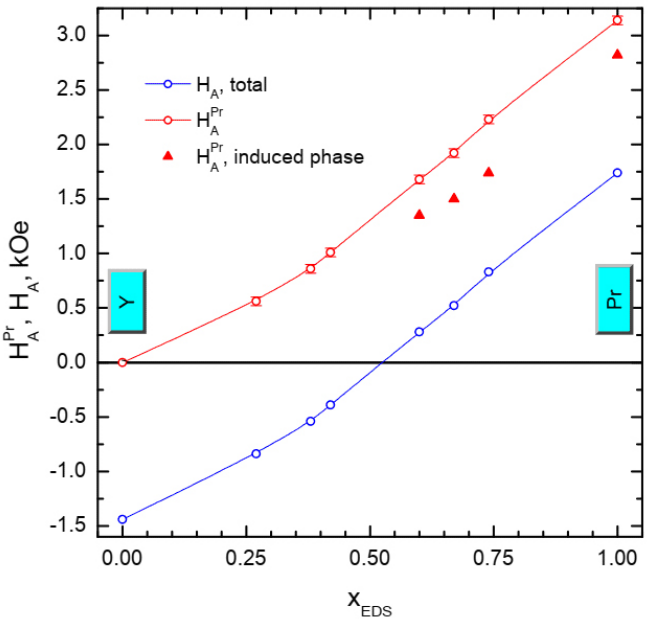

Figure 3. Concentration dependences of the total anisotropy fields (blue circles), anisotropy fields of Pr in the low-field (red circles) and field-induced (red triangles) states.

The $Pr_{0.67}Y_{0.33}Fe_3(BO_3)_4$ crystal belongs to the most interesting range of Pr concentrations, in which the competing contributions to the total magnetic anisotropy from Pr and Fe subsystems are close in absolute value and almost compensate each other. In the low magnetic fields applied at T = 4.2 K along the trigonal axis of the crystal, one can observe the FFD 1 and 1′ (see Fig. 1a) which are characteristic for the EA antiferromagnet. These dependences are observed only up to some critical field $H_c \approx 12$ kOe. Above this field, there appears branch 3 (red circles in Fig. 1a) with the FFD which is typical for the EP antiferromagnet magnetized along the trigonal axis. Thus, the reso-nance data indicate that in the $Pr_{0.67}Y_{0.33}Fe_3(BO_3)_4$ crystal, upon reaching the critical field Hc, the effective field of the total magnetic anisotropy changes its sign, which results in the spin reorienta-tion transition from the EA to the EP state and in the jump of magnetization in Fig. 1b. The reason for the transition is assumed to be the field dependence of the Pr contribution to the total anisotropy field of the crystal.

The magnetization data [3] show that, in terms of magnetic properties, the crystal with x = 0.75 is the closest to pure $PrFe_3(BO_3)_4$. The AFMR study was carried out on a sample on which an unusual two-step spin-flop transition were found in a magnetic field applied along the trigonal axis (see Fig. 2b). The AFMR study shows two groups of FFD (Fig. 2a) with different energy gaps: ~75 GHz (blue dots) and ~94 GHz (red dots); each of these groups has a shape characteristic of the EA antiferromagnet. The existence of two groups of FFD with different gaps suggests that the studied single crystal consists of at least two macroscopic areas with different content of Pr. The electron microscopy studies of the $Pr_{0.75}Y_{0.25}Fe_3(BO_3)_4$ crystal surface were carried out, and the EDS analysis evidences that two areas can actually be distinguished in the sample with the real content of Pr amounts to x = 0.67 and x = 0.74. Consequently, the jumps found in the field dependence of

the magnetization of this crystal are due to the spin-flop transitions sequentially occurring in the areas of the crystal with different Pr content.

In the crystals with $x = 0.75$ and $x = 1$, large lability intervals were found with the coexistence of the collinear and spin-flop states. In the Fig. 2a, these intervals are marked with red and blue arrows. The analysis [4] shows, that the existence of such an interval can be ac-counted for by the joint action of the second anisotropy constant of the Fe subsystem and by the dif-ference in the effective anisotropy fields of Pr in the collinear and spin-flop states, with the latter contribution being dominant.

From AFMR data, the total effective anisotropy fields of the crystals and the Pr contributions to the total anisotropy are calculated for the entire $Pr_xY_{1-x}Fe_3(BO_3)_4$ family. Figure 3 shows that both the effective total anisotropy fields and the praseodymium contribution depend almost linearly on the Pr concentration x. In the crystals with $x = 0.67 \div 1.0$, a significant (up to 20%) decrease in the effective anisotropy fields of the Pr subsystem in the field-induced both EP and spin-flop states was found as compared to the collinear EA state.

1. C. Ritter, A. Vorotynov, A. Pankrats et al., J. Phys.: Condens. Matter **22**, 206002 (2010).
2. C. Ritter, A.I. Pankrats, A.A. Demidov et al., Phys. Rev. B **91**, 134416 (2015).
3. A.I. Pankrats, A.A. Demidov, C. Ritter et al., J. Phys.: Condens. Matter **28**, 396001 (2016).
4. A.I. Pankrats, S.M. Zharkov, G.M. Zeer, I.A. Gudim, J. Alloys Compd. **909**, 164821 (2022).

B.P15

^{53}Cr NMR STUDY OF THE HALF-METALLIC FERROMAGNET CrO_2

Y.V. Piskunov[1], *A.F. Sadykov*[1*], *V.V. Ogloblichev*[1], *A.G. Smolnikov*[1], *A.P. Gerashenko*[1], *P.Z. Si*[2]

[1]M.N. Mikheev Institute of Metal Physics of Ural Branch of Russian Academy of Sciences, Ekaterinburg, Russia
[2]Zhejiang Key Lab of Magnetic Materials, China Jiliang University, Hangzhou, PR China
[*]E-mail: Sadykov@imp.uran.ru

We investigated the static and dynamic properties of Cr ions in the CrO_2 ultra-high purity polycrystalline sample using ^{53}Cr nuclear magnetic resonance (NMR). Two ^{53}Cr NMR lines, corresponding to magnetically non-equivalent Cr nuclei, were observed in the ferromagnetic phase of CrO_2 in spite of all Cr ions are situated on the crystallographic equivalent sites, as in earlier works [1, 2]. The authors [1] assumed the presence of two positions of Cr with different spontaneous magnetic moments, and the authors [2] believed that two Cr sites do not have different valence states, but the occupation numbers of the 3d orbit differ from each other.

We have measured for the first time the temperature dependences of the ^{53}Cr spin-lattice relaxation rate $(T_1)^{-1}$ in the ferromagnetic phase for the temperature range T = 4.2–360 K. It was found that at low temperatures (T > 60 K) the relaxation of nuclear magnetic moments is determined mainly by the temperature-proportional orbital contribution due to the fluctuation of the orbital currents of d-band electrons. It is shown that at temperatures T > 60 K, the main mechanism leading to nuclear spin-lattice relaxation is the process of three-magnon scattering, in which nuclear spin relaxation is accompanied by magnon absorption and the production of two magnons. The analysis of the temperature dependences $(T_1)^{-1}$ for two non-equivalent Cr ions made it possible to establish that their

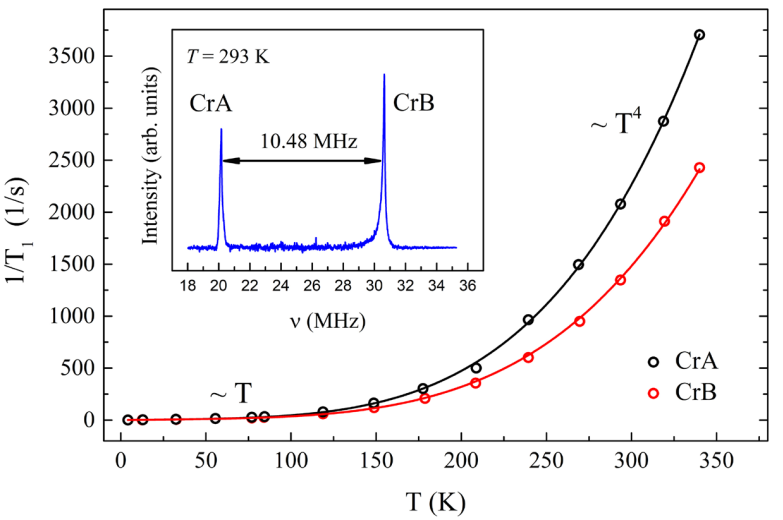

Figure 1. Temperature dependences of the nuclear spin-lattice relaxation rates of chromium nuclei in the CrA and CrB positions (see inset). The data are approximated by the function $1/T_1 = AT + BT^n$. Inset: ^{53}Cr NMR spectra at temperature T = 293 K.

valence state is the same and corresponds to Cr^{4+}, and the difference in the resonant frequencies of the nuclei of these ions is associated with different local magnetic fields at their location.

The research was carried out within the state assignment of Ministry of Science and Higher Education of the Russian Federation (theme "Funktsiya" No. 122021000035-6).

1. J.H. Shim, S. Lee, J. Dho, D-H. Kim Phys. Rev. Lett. **99**, 057209 (2007).
2. H. Takeda, Y. Shimizu, Y. Kobayashi, M. Itoh, T. Jin-no, M. Isobe, Y. Ueda, S. Yoshida, Y. Muraoka, T. Yokoya, Phys. Rev. B **93**, 235129 (2016).

B.P16

THICKNESS-DEPENDENT MAGNETIC PROPERTIES IN ULTRATHIN $La_{0.7}Sr_{0.3}MnO_3$ FILMS

T.A. Shaikhulov[1*], *K.L. Stankevich*[1,2], *V.A. Luzanov*[1], *A.G. Temiryazev*[1], *M.P. Temiryazeva*[1], *V.E. Zhivulin*[3], *A.R. Safin*[1], *S.A. Nikitov*[1]

[1]Kotel'nikov Institute of Radio Engineering and Electronics of Russian Academy of Sciences, Moscow, Russia
[2]Moscow State University, Moscow, Russia
[3]South Ural State University, Chelyabinsk, Russia
[*]E-mail: shcaihulov@hitech.cplire.ru

The manganite with the optimized stoichiometry $La_{0.7}Sr_{0.3}MnO_3$ (LSMO) is one of the most promising material among the $La_{1-x}Sr_xMnO_3$ manganites due to its unique magnetic and magneto-transport properties. LSMO is a conducting ferromagnet with a strong spin-orbit interaction that makes it a promising material for a use as a spintronics element. In the process of a film growth, the mismatch between the lattices of the film and the substrate leads to a stress in the LSMO layer that influences on its magnetic and magnetotransport properties. In this research, we study the thickness dependence of the LSMO out-of-plane lattice constant and the corresponding magnetic properties, namely magnetization, cubic and uniaxial magnetic anisotropy. For this purpose we have grown thin-film epitaxial heterostructures $La_{0.7}Sr_{0.3}MnO_3$ by a magnetron sputtering on singlecrystal (110) neodymium galate substrates ($NdGaO_3$).

Figure 1 shows the results of X-ray diffraction measurements on lattice parameters of the LSMO films. Thickness of the sample is shown on the *X*-axis, the value of the mismatch between the lattices of the LSMO and the substrate in the perpendicular direction $\varepsilon = (a_{LSMO} - a_{NGO})/a_{NGO}$ is shown on

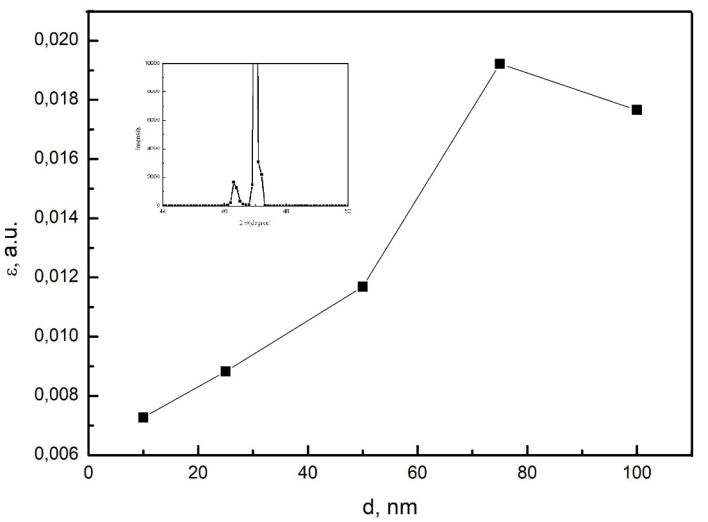

Figure 1. Thickness dependence of the mismatch between the lattices of the $La_{0.7}Sr_{0.3}MnO_3$ and the substrate in the perpendicular direction. The inset shows X-ray 2θ-ω scans for LSMO film with thickness 100 nm.

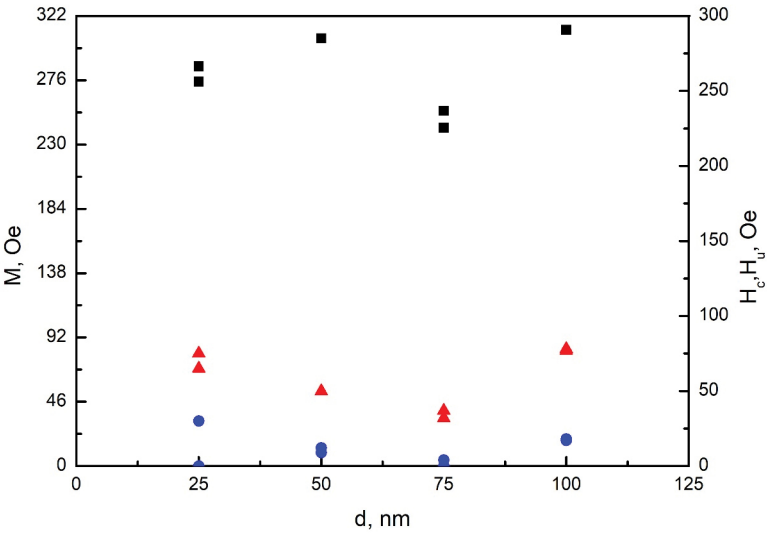

Figure 2. Thickness dependence of magnetization(black squares), uniaxial anisotropy H_u (red triangles) and cubic anisotropy H_c (blue circles).

the *Y*-axis (where *a* is a out-of-plane lattice constant). The structure and the lattice parameters were determined from the peak positions. The resulting thickness dependence qualitatively repeats the results of [1] at small thicknesses. However, at the film thickness 75 nm we observed the maximum value of the out-of-plane lattice constant of the LSMO layer.

Figure 2 shows the thickness dependences of the LSMO magnetic parameters, namely magnetization (left axis), cubic and uniaxial magnetic anisotropy (right axis). Peaks are clearly visible in all dependences for the film with a thickness of 75 nm. It can be assumed that the reason of the observed peaks is the strain caused both by the substrate itself and by the film thickness (see [1, 2]).

On the basis of the results obtained, it can be assumed that the thickness of the transition layer in LSMO films exceeds 100 nm. Also within our research we will discuss the obtained dependence of the LSMO magnetic properties upon an out-of-plane lattice constant and corresponding stress in the LSMO layer.

This work was supported by the Russian Science Foundation No. 21-79-10396, The study was carried out using the Unique Science Unit "Cryointegral" (USU #352529), which was supported by the Ministry of Science and Higher Education of Russia (Project No. 075-15-2021-667).

1. S.J. Sun, D.W. Abraham, R.A. Rao, C.B. Eom, Applied Physics Letters **74**, 3017–3019 (1999).
2. J. Dho, N.H. Hur, I.S. Kim, Y.K. Park, Journal of Applied Physics **94**, 7670–7674 (2003).

B.P17

MOBILITY OF THE PILLAR[5]ARENE COMPLEX WITH THIOCTIC ACID ACCORDING TO NMR-DATA

L.V. Sharipova[1,2*], *B.I. Khayrutdinov*[1,2], *D.N. Shurpik*[3], *I.I. Stoikov*[3], *Yu.F. Zuev*[1]

[1]Kazan Institute of Biochemistry and Biophysics, FRC Kazan Scientific Center of RAS, Kazan, Russian Federation
[2]Institute of Physics, Kazan Federal University, Kazan, Russian Federation
[3]Institute of Chemistry, Kazan Federal University, Kazan, Russian Federation
[*]E-mail: lv.sharipova@yandex.ru

The development of modern supramolecular chemistry has led to the creation of new macrocyclic compounds – pillar[n]arenes capable of forming "guest-host" complexes. Pillar[n]arenes show good biocompatibility and lack of cytotoxicity. They are promising as transport systems, using a hydrophobic macrocyclic cavity to encapsulate small molecules into it. These properties of supramolecular chemistry in biomedicine make it possible to increase bioavailability, prolong the action of the drug, prevent its premature degradation, which reduces the number of side effects and increases the therapeutic efficacy of the drug.

The object of study was the compound of decaammonium salt 4,8,14,18,23,26,28,31,32,35-deca(carboxymethoxy)-pillar[5]arene with encapsulated biologically active substance thioctic acid. Thioctic acid is a coenzyme that regulates aerobic processes of energy production in the cell.

In this work, high-resolution nuclear magnetic resonance was used to study the intermolecular complex of pillar[5]arene with thioctic acid encapsulated in a macrocyclic cavity. Two-dimensional NOESY spectroscopy confirmed the formation of the pillar[5]arene-thioctic acid complex. Based on the analysis of the NMR spectra, a three-dimensional model of the complex was obtained. The thermodynamic parameters of the proton mobility of the hydroquinone fragment of pillar[5]arene are found from the temperature dependence of the chemical exchange rate constant determined from the dispersion dependence of the relaxation rate R_2 measured using a Carr-Purcell-Meiboom-Gill pulse sequence.

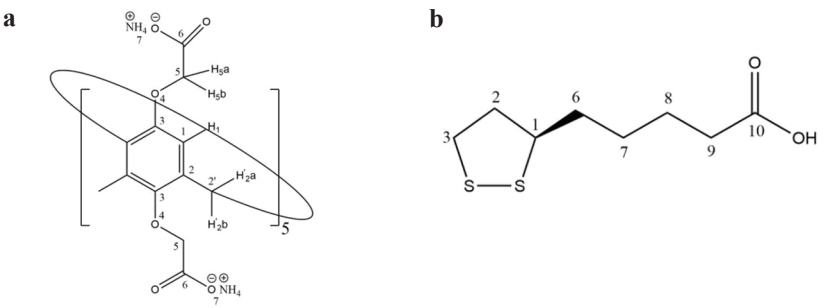

Figure 1. Chemical structural formulas of pillar[5]arene (**a**) and thioctic acid (**b**).

The authors gratefully acknowledge the Assigned Spectral-Analytical Center of FRC Kazan Scientific Center of RAS for possibility to fulfill the NMR experiments.

B.P18

NMR-SPECTROSCOPY OF CATIONIC SURFACTANT–SERUM ALBUMIN SYSTEM

L.V. Sharipova[1,2*], *B.I. Khayrutdinov*[1,2], *Yu.F. Zuev*[1]

[1]Kazan Institute of Biochemistry and Biophysics, FRC Kazan Scientific Center of RAS, Kazan, Russian Federation
[2]Institute of Physics, Kazan Federal University, Kazan, Russian Federation
[*]E-mail: lv.sharipova@yandex.ru

The study of interaction between low-weight amphiphilic compounds and macromolecules is of great fundamental and applied importance. One of the impaortant characteristics of surfactants in terms of their potential as drug and gene carriers is their ability of complexation with respect to biological systems. Bovine serum albumin, which has a unique ability of selective binding of hydrophobic substances, is often used as a model system.

In this work, a system based on a cationic surfactant (tetradecylmethylmorpholinium bromide) and bovine serum albumin (BSA) was studied using nuclear magnetic resonance methodology by varying the surfactant concentration under a fixed protein concentration. Translational diffusion was determined using the NMR method with a pulsed magnetic field gradient. From the analysis of high-resolution ^{1}H NMR spectra, changes in the chemical shifts and spectral linewidths of surfactant protons in the presence and absence of BSA were obtained. The displacement of surfactant chemical shifts of protons to the region of weak fields under an increase in surfactant concentration and the narrowing of their spectral lines proves the interaction of amphiphilic compound with protein. The obtained NMR data was used to speculate about structural details of surfactant-protein complexation.

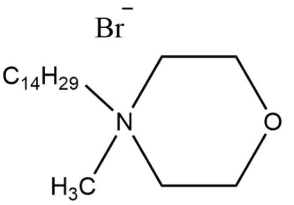

Figure 1. Chemical structure of the surfactant tetradecylmethylmorpholinium bromide.

This work was partly supported by the government assignment for Federal Research Center Kazan Scientific Center of Russian Academy of Sciences and Russian Foundation for Basic Research [Grant N 20-04-00157]. Authors gratefully acknowledge the Assigned Spectral-Analytical Center of FRC Kazan Scientific Center of RAS for possibility to fulfill the NMR experiments.

B.P19

EPR STUDY OF MAGNETIC PROPERTIES OF $(Cd_{0.6}Zn_{0.36}Mn_{0.04})_3As_2$ THIN FILM

A.V. Shestakov[1*], *I.I. Fazlizhanov*[1], *I.V. Yatzyk*[1], *V.S. Zakhvalinskii*[2], *E.A. Pilyuk*[2], *R.M. Eremina*[1]

[1]Zavoisky Physical-Technical Institute, FRC Kazan Scientific Center, Russian Academy of Sciences, Kazan, Russia
[2]Belgorod National Research University, Belgorod, Russia
[*]E-mail: Aleksey665@gmail.com

The main field of application of magnetic semiconductors is spintronics, where employ the spin degree of freedom of electrons in addition to their charge. The use of materials with a high temperature Curie T_C expands the capabilities of modern microelectronics and gives impetus to the development of spintronics. The magnetic properties of the $ZnMn_2As_2$ semiconductor connected with the presence of magnetic Mn ions in its crystal lattice. The $ZnMn_2As_2$ compound exhibits the so-called spin-glass-like and ferromagnetic properties and, at the same time, has a disordered layered structure at temperatures below 32 K [1]. The deluted magnetic semiconductor group based on the 3D Dirac semimetal Cd_3As_2 is of particular interest. The study of solid solutions based on Cd_3As_2 will allow us to trace the evolution of topological properties and create the prerequisites for the practical application of this unique material [2]. Existence of a linear in magnetic field contribution into the magnetoresistance in $(Cd_{1-x}Zn_x)_3As_2$ solid solutions was associated with the manifestation of the properties of the Weyl semimetal [3]. In the range of helium temperatures, hopping conductivity with a variable long hopping according to Shklovsky-Efros is manifested, and the radius of localization of charge carriers for these samples is calculated [4]. The Dingle temperature in the CZMA

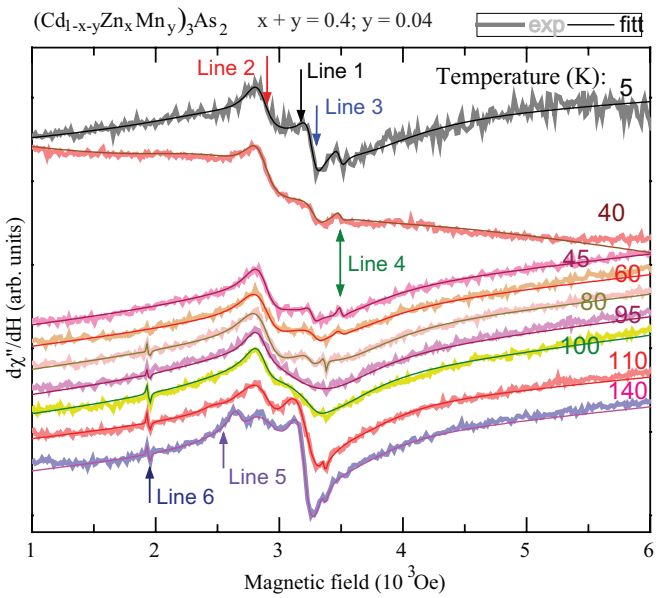

Figure 1. Temperature dependencies of ESR spectra of the thin film $(Cd_{0.6}Zn_{0.36}Mn_{0.04})_3As_2$.

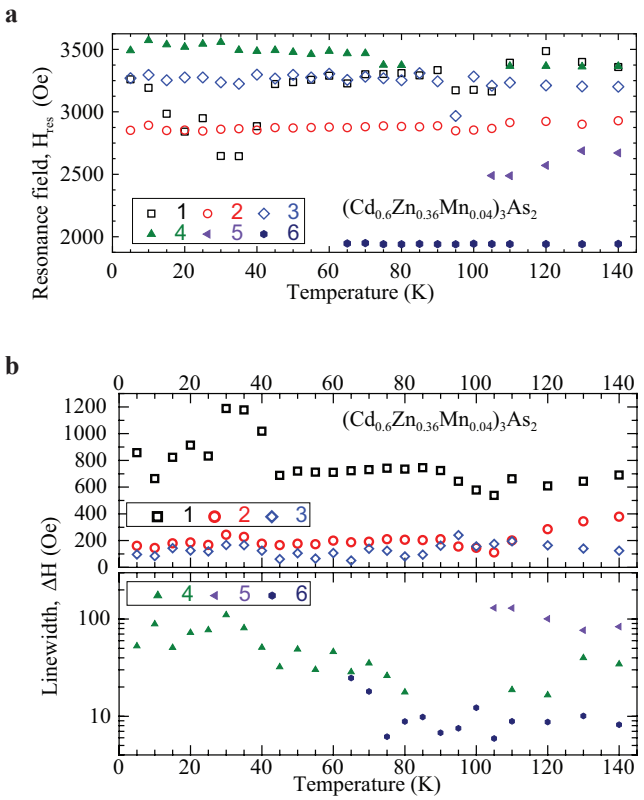

Figure 2. Temperature dependence of the resonance field (**a**) and linewidth (**b**) the thin film CZMA.

compound ($x + y = 0.3$; $0 \le y \le 0.08$) was determined from an analysis of the Shubnikov-de Haas oscillations and its values are in the range from 32 to 44 K [5]. Further research is focused on the study of the high quality thin film of $(Cd_{1-x-y}Zn_xMn_y)_3As_2$ ($x + y = 0.4$; $y = 0.04$) (CZMA).

In this work, we investigate the thin film of $(Cd_{1-x-y}Zn_xMn_y)_3As_2$ ($x + y = 0.4$; $y = 0.04$) by the ESR method. The thin film was obtained by sputtering on an unheated silicon substrate and was annealed in Ar vapor at a temperature of 300 °C. The EPR measurements were carried out with an EMX/plus (Bruker) spectrometer in the temperature range from 5 to 140 Kelvin and at a MW frequency ~9.34 GHz. The EPR spectra are shown in Fig. 1. Six lines are observed. The EPR lines were fitted with broad asymmetric Dysonian spectra (Eq. 5 of Joshi's article [6]). The first is a wide line, with a g-factor that depends on temperature. And there are two narrow lines with $g_2 = 2.3 \pm 0.03$ ($H_{res2} = 2898$ Oe) и $g_3 = 2.06 \pm 0.03$ ($H_{res3} = 3236$ Oe). In addition to the described lines, three more lines are observed at some temperatures $g_4 \approx 1.88$ ($H_{res4} = 3546$ Oe), $g_5 \approx 2.6$ ($H_{res5} = 2564$ Oe), $g_6 \approx 3.43$ ($H_{res6} = 1943$ Oe).

The temperature dependencies of resonant fields and linewidths of EPR-lines are presented in Fig. 2a and b, respectively. Three temperature regions can be distinguished: below 40 K, from 40 to 100 K, and above 100 K for first EPR-line. In the region of 40–100 K, the resonant fields and linewidths do not change comparatively.

Below 40 K, the g-factor of the broad line was increased from g_1 = 2.04 (H_{res1} = 3260 Oe) to g_1 = 2.52 (H_{res1} = 2644 Oe). Maximum of g-factor was reached at 30–35 K. We believe that the first exchange narrowed line is observed from the system of spins of manganese ions and charge carriers.

At temperatures above 100 K, the g-factor of the broad line was decreased. A minimum ($g_1 \approx 1.91$) was reached at 120 K. The broadening of the first line with temperatures above 100 K occurs according to the linear Korringa law [7].

It is assumed that EPR lines with number 2–6 was caused by the fine structure of manganese ions Mn^{2+} with S = 5/2. The symmetrical angular dependence of a group of lines was also found.

1. O. Ivanov et al., Mater. Res. Express **6**, 105908 (2019).
2. V.S. Zakhvalinskii et al., Proc. of the Southwest State Uni. Series: Engineering and Technologies **9** (4), 131–141 (2019).
3. O. Ivanov et al., Phys. Status Solidi (RRL) **12**(12), 1800386 (2018).
4. V.S. Zakhvalinskii et al., App. Mathematics & Physics **52**(3), 224–233 (2020) [in Russian].
5. R. Laiho et al., J. Phys. Chem. Solids **57**(1), l–5 (1996).
6. J.P. Joshi, and S.V. Bhat, J. of Magn. Res. **168**(2), 284–287 (2004).
7. S.E. Barnes, Adv. Phys. **30**(6), 801–938 (1981).

FMR METHOD FOR DETERMINING THE MAGNETIZATION OF THIN COBALT FILMS

Ya.G. Shiyan[1,2*], *L.A. Lee*[2]

[1]Siberian Federal University, Krasnoyarsk, Russia
[2]L.V. Kirensky Institute of Physics, FRC KSC, Siberian Division, Russian Academy of Science, Krasnoyarsk, Russia
[*]E-mail: ysh@iph.krasn.ru

A growing level of research and development is focused on cobalt thin film structures, which find many new applications in various industries [1] and this interest based on its attractive electrical, physical and mechanical properties [2]. To study their magnetic properties, among other things, researchers try to analyze the magnetization behavior of films in the required temperature range. However, sometimes the magnetometer is not available for whatever reasons: the unit is being repaired or under long-term maintenance, or there is a long queue to this unit. In such cases, one can make a qualitative analysis of the magnetization behavior using the method of electron magnetic resonance. It is known [3–5] that the intensity of the magnetic resonance signal is proportional to the magnetization of the film. In this case, if the magnetization (e.g. mesured at a temperature of 300 K) of one of the films of the series is known in absolute units, then the magnetic resonance method will also allow to carry out a quantitative analysis of the temperature behavior of the magnetization of the series of films. The work is devoted to the experimental verification of this statement and the further use of the results to describe the films produced.

A series of cobalt films of various thicknesses from 5 to 20 nm with a step of 2.5 nm was obtained by ion-plasma sputtering at a base pressure of $P = 10^{-6}$ Torr in an argon atmosphere. Glass was used as the substrate material, and the substrate temperature during deposition was 373 K. Then, the magnetic resonance properties of the films were studied on a Bruker EleXsys E 500 CW EPR spectrometer operating at frequency 9.4 GHz, in the temperature range from 120 K to 300 K, the magnetic field was parallel to the film plane.

The magnetic resonance spectra were processed by fitting the experimental integral absorption curve to the Lorentzian line to extract data on the resonant field, linewidth, and its integral intensity. As a result, the dependences of the integral intensities of cobalt films on temperature were obtained. The magnetization values measured on a vibrating magnetometer at a temperature of 300 K were taken as reference points to plot the temperature dependences of the magnetization in absolute units.

This work was supported by the State order of the Ministry of Science and Higher Education of the Russian Federation (topic No. FSRZ-2020-0011).

1. A.E. Kaloyeros et al., ECS J. Solid State Sci. Technol. **8**, P119 (2019).
2. A.R. Ivanova et al., J. Electrochem. Soc. **146**, 2139 (1999).
3. C.P. Slichter, Principles of Magnetic Resonance / Ed. Springer-Verlag R58 (1980).
4. X.Y. Yue et al., Phys. Rev. B **97**, 054417 (2018).
5. A.K. Shukla (ed.) EMR/ESR/EPR Spectroscopy for Characterization of Nanomaterials, Springer, India, p. 159 (2017).

B.P21

THE BEHAVIOR OF THE SPIN COHERENCE AFTER THE APPLICATION OF MULTI-PULSE PROTOCOLS IN SOLID-STATE ^{1}H NMR IN Cu- AND Ni-OXAMIDATO COMPLEXES

Yu. Slesareva[1*], *Yu. Kandrashkin*[1], *R. Zaripov*[1], *T. Ruffer*[2], *E. Vavilova*[1]

[1]Zavoisky Physical-Technical Institute, FRC Kazan Scientific Center, Russian Academy of Sciences, Kazan, Russia
[2]Technische Universität Chemnitz, Chemnitz, Germany
[*]E-mail: julia18.slesarev@gmail.com

The probable future scope of application of the metal−(bis)oxamidato complexes, as precursor materials for the synthesis of the corresponding polynuclear complexes, pertains to spintronics and quantum computing. Carr-Purcell pulse protocol usually serves to increase the coherence time in presence of the spectral diffusion [1]. Here we present the results of ^{1}H NMR study of Cu(II)-oxamidato complex compared to its diamagnetic Ni-containing counterpart. The experiments have shown the influence of the inhomogeneous broadening on the process of suppression of the nuclear spin decoherence and registration of parasitic echo components. An improved Carr-Purcell pulse protocol suggested in [2] was applied for elimination of unwanted echoes.

1. R. Zaripov et al., Phys. Rev. B **88**, 094418 (2013).
2. R. Zaripov et al., Beilstein J. Nanotechnol. **8**, 943–955 (2017).

MAGNETIC RESONANCE STUDIES OF AR-ION IMPLANTED RUTILE (TIO_2): EFFECT OF OXYGEN VACANCIES CONCENTRATION

*A.A. Sukhanov**, *V.F. Valeev, V.I. Nuzhdin, R.I. Khaibullin*

Zavoisky Physical-Technical Institute, FRC Kazan Scientific Center, Russian Academy of Sciences, Kazan, Russia
*E-mail: ansukhanov@mail.ru

Titanium dioxide (TiO_2) in both rutile and anatase crystal structures is a wide-band-gap semiconductor of n-type with many applications ranging from solar energy conversion, power electronic and spintronics to nonvolatile memristor memory. Although TiO_2 has been extensively studied, a detailed understanding of the role of point defects in controlling its optical, magnetic and electrical properties still none exists [1, 2].

The long-time purpose of our work is a modification of electron band structure, magnetic and electrical properties of TiO_2 by using ion implantation with various chemical type of ions accelerated to the energy up to 100 keV. The ion implantation with various chemical implants into TiO_2 results in both ions doping of TiO_2 with donor or acceptor impurity and the formation of different type of point defects in its structure. In the given work we implanted ions of inert gas (argon) into single crystalline plates of rutile (TiO_2) to exclude ion doping process during implantation and in details to study the process of point defect formation in Ar-ion implanted TiO_2. We have used the electron paramagnetic resonance (EPR) method that is well suited for studying point defects in different crystals [3, 4], including TiO_2 [5, 6].

The implantation with 40 keV Ar^+ ions into (001)- and (100)-face oriented plates of rutile (TiO_2) was carried out on an ILU-3 ion-beam accelerator at an ion current density $j \cong 8$ μA/cm^2 to the dose of $1.5 \cdot 10^{17}$ ion/cm^2 at an elevated substrate temperature (900 K) during ion irradiation. EPR spectra of samples under study were recorded in X-band (9.8 GHz) at different orientation of the applied magnetic field with respect to crystallographic axes of TiO_2 plate in the wide temperature range of 5–300 K.

It was established that initially colorless plates TiO_2 are coloring in sky-blue tone due to the formation of oxygen vacancies in Ar-ion implanted TiO_2 rutile (Fig. 1). Moreover, we developed original methods of oxygen vacancies migration under an applied DC electric field with the aim of changing the concentration of these point defects in the sample. In fact, after this electromigration procedure, the initial sky-blue color of the samples changed into the dark blue-grey around the negative electrode, while the region around the positive electrode lost the coloration due to decreasing the content of oxygen vacancies in this part of sample. Then all samples under study were divided in two parts with dark blue and a light blue color, respectively, for subsequent EPR studies.

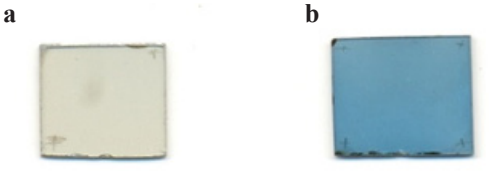

Figure 1. Photographs of virgin colorless TiO_2 plate (left) and the similar TiO_2 plate after ion implanted with 40 keV Ar^+ ions to a dose of $1.5 \cdot 10^{17}$ ion/cm^2.

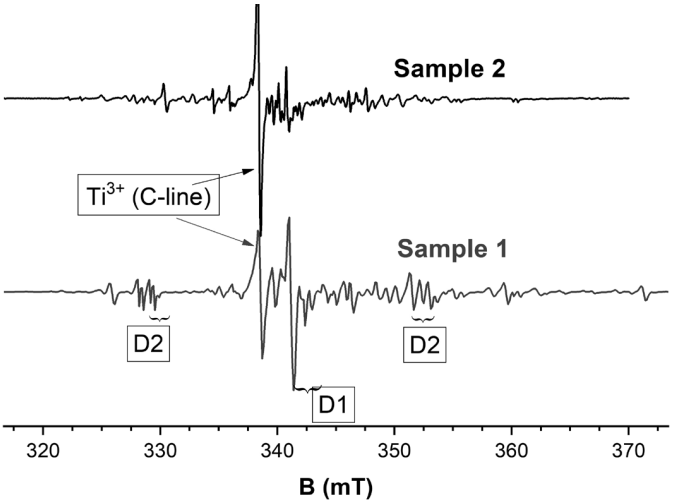

Figure 2. EPR spectra of (001)-TiO_2 plate implanted with Ar^+ ions to the dose of $1.5 \cdot 10^{17}$ with high (Sample 1) and low (Sample 2) content of oxygen vacancies. Spectra are taken at temperature of 11 K for magnetic field directed along the crystallographic axis of [001].

EPR spectra of two parts for Ar-implanted (001)-TiO_2 plate with both increased (sample 1) and reduced (sample 2) content of oxygen vacancies are shown in Fig. 2. A preliminary analysis of the presented spectra shows that the observed signals can be attributed to paramagnetic Ti^{3+} ions (electron spin S = 1/2 and magnetic nucleus titanium with natural abundance) and oxygen vacancies with one (V_O^+, center D1, S = 1/2) or two captured electrons (V_O^0, center D2, S = 1). Note that EPR lines related to oxygen vacancies vanish when the sample temperature rises above 30 K. We concluded that the EPR lines disappearance is a result of the oxygen vacancy recharging at $T > 30$ K due to the transition of an electron trapped by the vacancy to the conduction band of rutile. Moreover, in sample 1 with a high content of vacancies, we observed signals previously not described in the literature, which are absent in sample 2 with a low content of vacancies. A more detailed interpretation of the observed signals is the subject of our subsequent research.

The study was supported by the Russian Science Foundation (project number 22-19-00712, https://rscf.ru/project/22-19-00712/).

1. M.K. Nowotny, L.R. Sheppard, T. Bak, and J. Nowotny, J. Phys. Chem. C **112**, 5275 (2008).
2. V.N. Kuznetsov and N. Serpone, J. Phys. Chem. B **110**, 25203 (2006).
3. S.A. Altshuler and B.M. Kozyrev, Electron Paramagnetic Resonance in Compounds of Transition Elements (Nauka, Moscow, 1972) [in Russian].
4. J.-M. Spaeth, J.R. Niklas, and R.H. Bartram, Structural Analysis of Point Defects in Solids: An Introduction to Multiple Magnetic Resonance Spectroscopy (Springer Berlin Heidelberg) (1992).
5. L.N. Shen, O.W. Johnson, W.D. Ohlsen, and J.W. DeFord, Phys. Rev B **10**, 1823 (1974).
6. J.M. Cho, J.M. Seo, J.-K. Lee, H. Zhang, R. Lam, Physica B **404**, 127 (2009).

B.P23

THE "DARKS" STATES OF THE LEAKY MAGNON POLARONS SPECTRUM IN MAGNETIC HETEROSTRUCTURES WITH SLIDING-CONTACT INTERFACES

O.S. Sukhorukova[1], *A.S. Tarasenko*[1], *S.V. Tarasenko*[1*], *V.G. Shavrov*[2]

[1]Donetsk Institute for Physics and Engineering named after Galkin, Donetsk, Ukraine
[2]Institute of Radio Engineering and Electronics named after Kotelnikov, Russian Academy of Sciences, Moscow, Russia
[*]E-mail: s.v.tarasenko@mail.ru

Active research interest in the magnetoacoustics of hybrid magnetic structures has been refreshed in recent years in view of problems of production of new classes of controlled acoustic metamaterials and the fast development of magnon spintronics [1, 2], implying the replacement of charge currents by spin currents that can f low without transfer of mass and electric charge. It is expected that this will allow fabricating more compact and higher speed information storage and processing devices. Spin currents can be due not only to conduction electrons but also magnons, which are quasiparticles of the spectrum of spin waves, and the class of accompanying dynamic effects, which are not only of purely academic but also of applied interest, is continuously expanding. However, although various aspects of the interaction between spin currents and the lattice in multilayer and multicomponent magnetic materials are studied in numerous works, the majority of these works are in fact focused on various aspects of the interaction of magnons with the field of emitting phonons in layered magnetic heterostructures and the possibility of using the corresponding effects in practice. Meanwhile, unlike optics and acoustics of composite conducting and dielectric nonmagnetic materials, the conditions of formation of "dark" magnon modes in the spectrum of the phonon radiation field of a multilayer magnetic structure, as well as accompanying dynamic anomalies, are still unclear.

In this context, the aim of this work is to determine in the dissipationless limit necessary conditions under which the indirect spin-spin interaction through the field of virtual phonons polarized in the plane of incidence (Lamb phonons) even in an acoustically subwavelength-thick AFM layer in the elastically isotropic nonmagnetic environment can even in the nonexchange approximation lead simultaneously to the collapse of the acoustic Fano resonance and to the formation of "dark" states in the phonon radiation spectrum of the leaky bulk magnon polarons.

In particular it is shown that the linewidth associated with the radiative damping of the corresponding leaky wave near points of the "dark" state existence can be arbitrarily small within the considered dissipationless model. In the case of bounded low-temperature antiferromagnets, the hybridization of the phonon and inhomogeneous exchange mechanisms of the spin– spin interaction can result in the formation of additional magnon polaron bound states in the continuum of radiative phonon modes. The conditions have been determined under which the spectrum of radiative magnon polarons in the finite acoustically coupled system of identical magnetic layers with the slip boundaries can additionally exhibit the formation of not only a series of "dark" states of nonexchange Lamb magnon polarons, but also the acoustic superradiance of the longitudinal bulk elastic wave by a light Lamb magnon polaron. It has been shown that the angular Shoch effect for the longitudinal or transverse vertically polarized elastic wave reflected from the magnetic layer and transmitted through it can increase sharply when the quasiplane bulk elastic P- or SV-wave is incident from outside on the magnetic layer

1. K. Yu, N.X. Fang, G. Huang, and Q. Wang, Adv. Mater. **30**, 1706348 (2018).
2. P. Liu, X. Chen, W. Xu, and Y. Pei, J. Appl. Phys. **127**, 18510, 4 (2020).

MAGNETIC-FIELD-DRIVEN TRANSPARENCY OF MANGANITE-BASED COMPOSITES

V.A. Bessonova, V.S. Teplov, S.V. Naumov, A.V. Telegin*

M.N. Mikheev Institute of Metal Physics of Ural Branch of Russian Academy of Sciences, Ekaterinburg, Russia
*E-mail: vbessonova@imp.uran.ru

Single crystals and thin films of doped lanthanum manganites with the effect of colossal magnetoresistance (CMR) have been considered as promising functional optical materials in connection with the observed giant effect of magnetotransmission (MT) of unpolarized light in the infrared (IR) region [1, 2]. The applied application of the MT effect in manganites is limited by a number of factors: the need for thermal stabilization near the Curie temperature (T_C), the increase of optical efficiency, the simplification of a mass-production technology etc. Doped manganites have high light absorption in the infrared region due to the free charge carriers contributions below T_C. In this view composite materials are one of the possible solutions [3]. This paper presents the results of studying of the MT of light in composites made of a mixture of manganite with an organics matrix.

The initial polycrystals of manganites $La_{1-x}A_xMnO_3$ (A – Ba, Ca) were grown by solid-phase synthesis. The microsize powders of manganites were obtained by grinding in a ball mill. Polymer composites were prepared by fixing the powder of manganite on a transparent adhesive tape.

First of all, the noticeable change of transparency of polymer composites under an external magnetic field applied MT effect has been detected for the first time. The MT effect reaches 10% for $La_{0.7}Ca_{0.3}MnO_3$ composition and 2% for $La_{0.7}Ba_{0.3}MnO_3$ in the magnetic field H = 8 kOe at temperatures close to T_C of manganites. The spectral dependences of optical absorption and MT in such composites are similar to that for the films and pressed composites of similar composition. It is worth to notice the transparency of the obtained polymer composites is close to one for pressed composites and lower than for thin films, which is primarily due to the dominate contribution of light scattering processes and higher optical density. Within the experimental errors any variations of the orientation of both magnetic field and polarization of light do not affect the behavior of MT in the polymer composites. It is also interesting that the low thermal conductivity of the used polymer leads to the self-thermally stabilized MT effect in composites independently on external conditions in our experimental setup.

Finally, accounting for specific mechanical and thermal properties of polymer composites and high value of magnetotransmission one can recommend them as new IR magneto-optical materials.

The research was carried out within the state assignment of Ministry of Science and Higher Education of the Russian Federation (theme "Spin" No. 122021000036-3).

1. N.G. Bebenin, N.N. Loshkareva, A.A. Makhnev, E.V. Mostovshchikova, L.V. Nomerovannaya, E.A. Gan'shina, A.N. Vinogradov, Ya.M. Mukovskii, J. of Phys.: Cond. Matt. **22**, 096003 (2010).
2. A.V. Telegin, V.A. Bessonova, Yu.P. Sukhorukov, A.P. Nosov, E.A. Gan'shina, Optics and Spectroscopy **128**, 42–48 (2020).
3. E.V. Mostovshchikova, N.N. Loshkareva, A.V. Telegin, S.V. Naumov, B.A. Gizhevskii, L.I. Naumova, J. of Appl. Phys. **113**, 043503 (2013).

B.P25

MICROMAGNETIC SIMULATION OF MAGNETIZATION DYNAMIC IN FM FILMS

*V.S. Teplov**, *V.D. Bessonov, A.V. Telegin*

M.N. Mikheev Institute of Metal Physics of Ural Branch of Russian Academy of Sciences, Ekaterinburg, Russia

*E-mail: teplov@imp.uran.ru

Nonlinear effects of magnetization dynamics are promising area of physics of high-frequency and non-linear resonance phenomena. To excite large amplitudes of the magnetization deviation in a ferromagnet, either large values of the pumping magnetic field or high spin current densities are used, both methods are energy unprofitable. Another method of magnetization excitation is based on nonlinear excitation of magnetic subsystem by the rapidly changing of the frequency of low-amplitude exciting field. This phenomenon called as an autoresonance was theoretically predicted almost ten years ago [1, 2]. It seems to be interesting to determine the necessary parameters for the experimental observation of this effect by using the methods of micromagnetic modeling in the MUMAX[3] software.

In this work, numerical simulation of autoresonance excitation of magnetization in a thin FM layer with perpendicular magnetic anisotropy was carried out. The contribution of demagnetizing fields, uniaxial and cubic magnetic anisotropy, and complex damping in magnetization dynamic was evaluated.

It was shown for yttrium iron garnet film that the autoresonance can be achieved at GHz frequency range by applying a sweeping external magnetic field 0.1 mT perpendicular to permanent saturating field 0.2 T [3]. The phase locking between weak pumping magnetic field and eigen magnetization oscillations in the film was shown to be of high importance for observing the threshold behavior of magnetization oscillations. Numerical simulations were in good agreement with analytical predic-

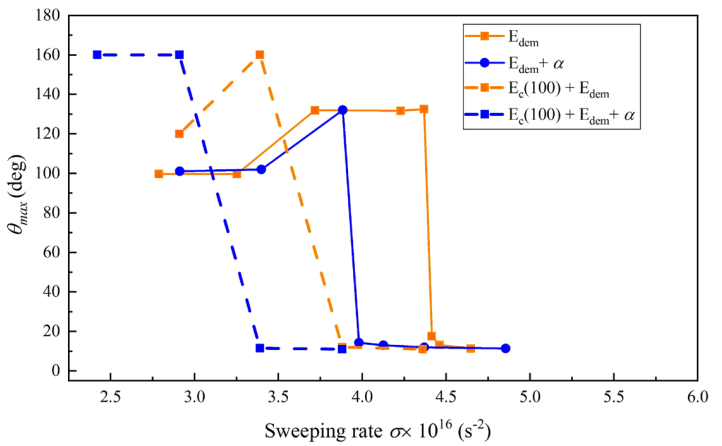

Figure 1. Threshold dependence maximum the magnetization deflection angle θ_{max} on sweeping rate of the exciting magnetic field in a case demagnetizing fields (E_{dem}), gilbert damping α and cubic anisotropy ($E_c(100)$).

tions [1, 2]. The one of the promising results was a high angular deflection of magnetization (up to 160°) achieved in the volume of normally magnetized YIG film at the sweep rate of excitation field $\sigma_{th} = 3.5 \cdot 10^{16}$ s^{-2} (Fig. 1).

The introduction of surface anisotropy made it possible to correctly consider spin pinning and obtained a discrete spectrum of resonance oscillations. Accounting for the dipole-dipole interaction and damping had little effect on the static magnetization behavior, but led to a both noticeable low-frequency shift in the spectrum of dynamic magnetization oscillations and decreasing of the sweep rate of excitation field in the FM film. The results are promising for observing the autoresonance phenomena in FM in experiments.

Support by RSF № 21-72-20160 is acknowledged.

1. S.V. Batalov, A.G. Shagalov, The Physics of Metals and Metallography **109**, no. 1, 1–6 (2010).
2. S.V. Batalov, A.G. Shagalov, The Physics of Metals and Metallography **114**, no. 1, 115–119 (2013).
3. S.V. Teplov et al., accepted for publication in JSNM (2022).

B.P26

SPIN DINAMICS IN $SrMnO_{3-x}$ BY ^{17}O AND ^{87}Sr NMR-DATA

Z. Volkova[1*], A. Gerashenko[1], K. Mikhalev[1], A. Trokiner[2]

[1]M.N. Mikheev Institute of Metal Physics, UB RAS, Ekaterinburg, Russia
[2]ESPCI Paris, PSL Research University, Paris, France
[*]E-mail: volkovazn@imp.uran.ru

In the paramagnetic phase of cubic antiferromagnet $SrMnO_{3-x}$ ($x < 0.01$, $T_N = 236$ K) the spin susceptibility of the localized Mn(t_{2g}) electrons exhibits a gapped behavior with $d\chi_s(T) \geq 0$, suggesting the existence of a low-dimensional short-range magnetic order above T_N [1]. In this work we study the time-dependent part of the hyperfine fields $^{17}\mathbf{h}_{hf}$, $^{87}\mathbf{h}_{hf}$ of ^{17}O and ^{87}Sr nuclei at low frequencies by measuring the spin-lattice relaxation rate T_1^{-1} and the spin-spin relaxation rate T_2^{-1}. The results enable to shed light on the slow-fluctuating short-range correlations between the localized Mn spins, $S(t_{2g})$, in the PM phase of a lightly electron doped cubic $SrMnO_{3-x}$.

^{17}O being involved in a Mn–O–Mn bond, the echo decay rate $^{17}T_2^{-1}$ probes the fluctuations of the two neighboring $S(t_{2g})$ spins at low frequency, $\omega \leq 10^3$ s^{-1}. In the temperature range $T < 350$ K an anomaly in the ^{17}O spin-spin relaxation rate (Fig. 1) shows that there exist local changes of the double-exchange interaction, which favor FM correlated pairs of neighboring $S(t_{2g})$ spins in the Mn–^{17}O–Mn bond. The unusual thermal behavior of $^{17}T_2^{-1}(T)$ indicates low-frequency fluctuations of the short-range magnetic order which may include the change of AF ↔ FM spin alignment of neighboring magnetic ions.

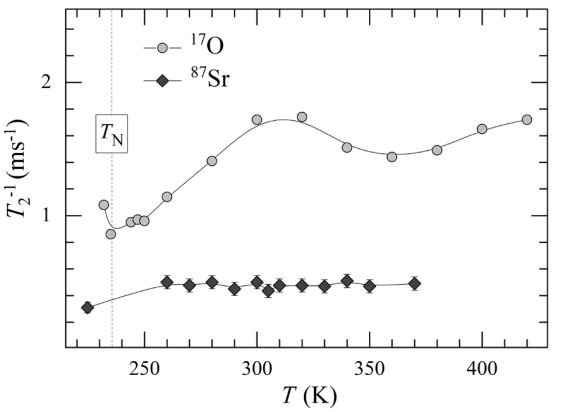

Figure 1. Thermal behavior of ^{17}O and ^{87}Sr spin-spin relaxation rates in $SrMnO_{3-x}$ ($x < 0.01$).

In contrast to ^{17}O, for ^{87}Sr nuclei, which probe the spin configuration of eight neighboring Mn in the cubic unit cell, $^{87}T_2^{-1}$ has no such anomaly (Fig. 1), implying that FM order should be excluded within the cubic unit cell. With both NMR probes, it is deduced that the only magnetic orders which may exist in the cubic unit cells are the following: AF – G [$\mathbf{q} = \pi/a$ (1, 1, 1)], AF – C [$\mathbf{q} = \pi/a$ (1, 1, 0)] and AF – A [$\mathbf{q} = \pi/a$ (0, 0, 1)] so that the slow fluctuating short-range magnetic order is built from these three AF ordered unit cells.

1. A. Trokiner et al., Phys. Rev. B **93**, 174413 (2016).

B.P27

FEATURES OF FMR IN THIN FILMS Fe_xNi_{100-x} AND Fe

S.A. Vysulin[1*], *N.E. Syr'iev*[2]

[1]Higher Military School named after General of the Army S.M Shtemenko, Krasnodar, Russia
[2]Faculty of Physics, Lomonosov Moscow State University, Moscow, Russia
[*]E-mail: vyzulin@mail.ru

The ferromagnetic resonance (FMR) method is one of the most effective ways to study the magnetic properties of material samples, including nanometer-thick films. It allows, without special sample preparation, to establish the relationship between the observation data of ferromagnetic resonance and microscopic material parameters of nanofilm systems.

The theory of homogeneous FMR developed by Kittel [1] is known for massive ellipsoidal ferromagnetic bodies magnetized to saturation. Within the framework of Kittel's theory, the dependence of the resonant field on the orientation of the magnetization field with respect to the film plane is continuous. Traditionally, it is considered that Kittell's FMR theory is also applicable to thin films, including nano-thick films.

The aim of the work is to study the features of the FMR phenomenon in permalloy nanofill films depending on the orientation of the magnetization field relative to the surface of the sample under study.

Single-layer film structures from Fe_xNi_{100-x} and Fe are investigated. Synthesis methods: 1) magnetron sputtering at direct current; 2) thermal evaporation. The thickness of the magnetic layers in the Fe_xNi_{100-x} film samples ranges from 25 to 150 nm. The structures were synthesized at the L.V. Kirensky Institute of Physics SB RAS [2]. The thickness of the magnetic layer in Fe films was 270 nm. The samples were synthesized by the Institute for Theoretical and Applied Electromagnetics RAS [3]. Samples of 3×3 mm^2 in size were made from the synthesized structures.

A technique for observing the FMR phenomenon was used, based on recording the derivative of the absorption signal when scanning the spectrum along the magnetization field. The measurements were carried out by a resonator method at a frequency of 9.14 GHz at room temperature.

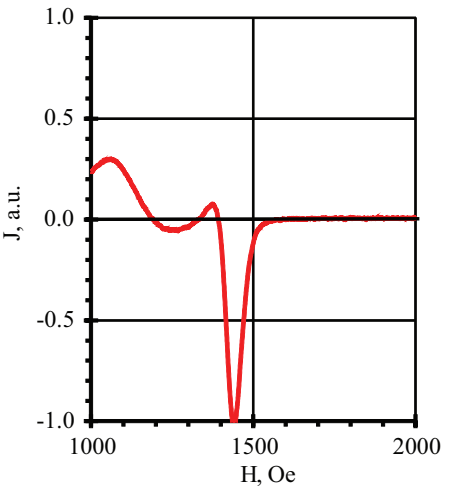

Figure 1. View of the FMR spectrum.

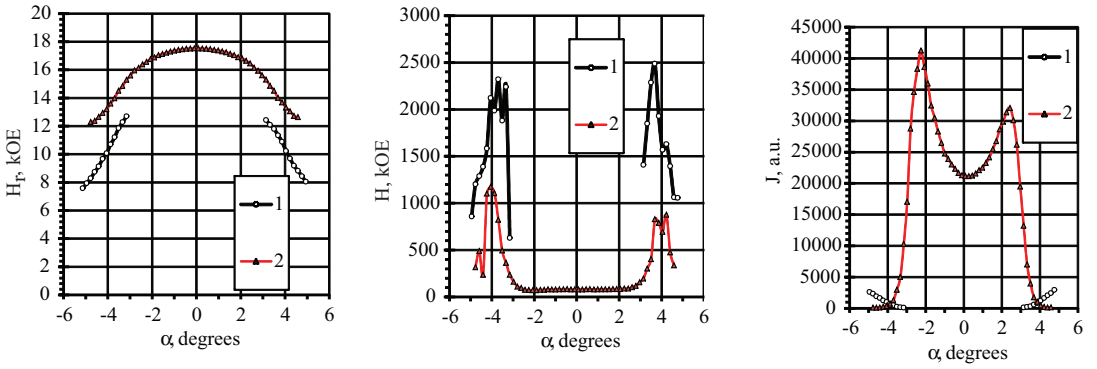

Figure 2. Angular dependences of $H_r(\alpha)$, $\Delta H(\alpha)$ and $J(\alpha)$ near normal magnetization.

FMR spectra have been studied for various values of the angle α between the external magnetic field H and the normal to the sample surface n. The angle α could be changed from 0 to 360°. The resonant field H_r, the width of the absorption line ΔH and the intensity of the first derivative of the absorption signal J were determined from the spectra.

The following is characteristic of all the samples studied.

Only one absorption line is observed in the spectrum at tangential (α = 90°) and normal (α = 0) magnetization of films. The dependencies $H_r(\alpha)$, $\Delta H(\alpha)$ and $J(\alpha)$ are symmetric with respect to the axis α = 0. The resonant field at α = 90° is minimal, and at α = 0 it is maximal. When changing α from 0 to 90°, the H_r value monotonically decreases.

There are such α_i at which the absorption lines are more than 10 times wider than at tangential magnetization (α = 90°). The intensity of the first derivative of the absorption signal J differs at α_i and α = 90° by almost two orders of magnitude. For the Fe_xNi_{100-x} sample synthesized by magnetron sputtering with x = 80 and a magnetic layer thickness of about 25 nm (sample 1), the values are $\alpha_i \approx$ 8, 172, 188 and 352°. A similar pattern of changes in $\Delta H(\alpha)$ and $J(\alpha)$ was observed earlier [1] for massive samples. However, the dynamic range of changes in ΔH and J from α for the studied Fe_xNi_{100-x} and Fe thin films is significantly (not less than an order of magnitude) larger. This circumstance was the reason for a more thorough study of the spectra of Fe_xNi_{100-x} and Fe thin films in the vicinity of α_i. A more thorough study is understood as recording spectra in smaller increments. The used measuring complex "JEOL JES FA-300" had an automatically tunable goniometer. The minimum angle change step α in our complex was 0.18°.

For some of the studied samples, both Fe_xNi_{100-x} and Fe in the vicinity of α_i, two resonances were observed simultaneously (Fig. 1). One of the resonances has a continuation in the region close to normal magnetization (marked in Fig. 1 with the digit 2), and the other in the region close to tangential magnetization (marked with the digit 1).

Splitting of the FMR spectrum in the vicinity of α_i could not be observed for all the samples studied. For a number of studied samples, there is simply a broadening of the FMR line with inhomogeneities that cannot be interpreted as resonances.

Figure 2 shows the dependencies $H_r(\alpha)$, $\Delta H(\alpha)$ and $J(\alpha)$ for sample 1, observed at $|\alpha| < 6°$. It can be seen that when the magnetization field approaches the normal (relative to the film plane) orientation in the spectrum, mode 2 appears together with mode 1. The intensity of the first derivative of the absorption signal J decreases with a decrease in the value of $|\alpha|$ for mode 1 decreases (becomes less than the level of recorded interference), and for mode 2 increases (it becomes comparable in magnitude to the signal for mode 1 observed during tangential magnetization).

FERRIMAGNET BASED SPIN HALL DETECTOR OF SUBTERAHERTZ FREQUENCY RANGE SIGNALS

E.E. Kozlova[1,2*], *A.R. Safin*[1,2], *S.A. Nikitov*[1,3]

[1]Kotel'nikov Institute of Radioengineering and Electronics, Russian Academy of Sciences, Moscow, Russia
[2]Moscow Power Engineering Institute, Moscow, Russia
[3]Moscow Institute of Physics and Technology, Dolgoprudny, Moscow Region, Russia
[*]E-mail: KozlovaYY@mpei.ru

A model of a detector of subterahertz oscillations based on a ferrimagnet/heavy metal (FiM/HM) heterostructure has been studied. In the work, 2 types of magnetic anisotropies of a FiM were considered: "easy axis" and "easy plane". A mathematical model was considered that describes the dynamics of the Neel vector magnetization in a FiM [1]:

$$\mathbf{l}\times\left[\frac{d^2\mathbf{l}}{dt^2}+\gamma_{eff}\frac{d\mathbf{l}}{dt}+\frac{\partial W_{AFM}}{\partial \mathbf{l}}\right]=\left[\mathbf{l}\times\frac{d\mathbf{h}_{AC}}{dt}\right]\times\mathbf{l}-\bar{\nu}\frac{d\mathbf{l}}{dt}\ , \tag{1}$$

where $\gamma_{eff} = \alpha_{eff}\omega_{ex}$ is the spectral linewidth of the ferrimagnetic resonance, α_{eff} is the effective damping, including the contributions from the Hilbert damping and spin pumping, $\gamma = 2\pi\cdot 28$ GHz/T is the gyromagnetic ratio, $\mathbf{h}_{AC} = h_{AC}\mathbf{e}_{AC}e^{i\omega t}$ is the magnetic component of the variable linearly polarized electromagnetic (EM) wave incident on the structure, $\mathbf{e}_{AC}$ is the unit vector characterizing the polarization of the field of the external EM waves $\mathbf{h}_{AC}$, h_{AC} and ω are the amplitude and frequency of the alternating magnetic field, respectively. The decompensation term includes $\bar{\nu} = \nu\omega_{ex}$, where ν is the uncompensation parameter of the magnetic moments of the FiM sublattices, which changes the dynamic properties of magnetic nanoparticles during antiferromagnetic interaction. The magnetic energy density $W_{AFM}(\mathbf{l})$ present in Eq. (1) is expressed as:

$$W_{AFM} = \pm\frac{\omega_{ex}\omega_A}{2}(\mathbf{l}\cdot\mathbf{e}_A)^2\ , \tag{2}$$

where $\omega_{ex} = \gamma H_{ex}$ and $\omega_A = \gamma H_A$ are the characteristic frequencies, H_{ex} is the internal exchange field of the FiM, H_A is the anisotropy field of the FiM. In Eq. (2), the sign "+" corresponds to the case of magnetic anisotropy "easy plane", and the sign "–" to the case "easy axis".

An equation was obtained that describes the dynamics of small amplitudes:

$$\frac{d^2\mathbf{s}}{dt^2}+\gamma_{eff}\frac{d\mathbf{s}}{dt}+\left[\hat{\Omega}-(\mathbf{l}_0\cdot\hat{\Omega}\mathbf{l}_0)\hat{I}\right]\mathbf{s}=-\hat{\theta}\cdot\gamma\frac{d\mathbf{h}_{AC}}{dt}+\bar{\nu}\cdot\left(\hat{\theta}\cdot\frac{d\mathbf{s}}{dt}\right)\ , \tag{3}$$

here $\hat{\Omega}=\omega_{ex}\omega_A e_A\otimes e_A$, $\hat{I}=\mathrm{diag}(1,1,1)$. The matrix $\hat{\theta}$ can be written as:

$$\hat{\theta}_1=\begin{pmatrix}0&0&0\\0&0&-1\\0&1&0\end{pmatrix},\hat{\theta}_2=\begin{pmatrix}0&-1&0\\1&0&0\\0&0&0\end{pmatrix}\ , \tag{4}$$

where index "1" corresponds to the "easy plane" case, and index "2" to the "easy axis".

The eigenfrequencies of the ferrimagnet for the "easy axis" and "easy plane" cases, respectively, were determined from the low damping condition, i.e. $\gamma_{eff} = 0$:

$$\omega_\pm^2=\omega_0^2+\frac{\bar{\nu}^2}{2}\pm\frac{\bar{\nu}}{2}\sqrt{4\omega_0^2+\bar{\nu}^2}\ ,\ \omega_\pm^2=\left[\begin{matrix}\omega_0^2+\bar{\nu}^2\\0\end{matrix}\right.\ , \tag{5}$$

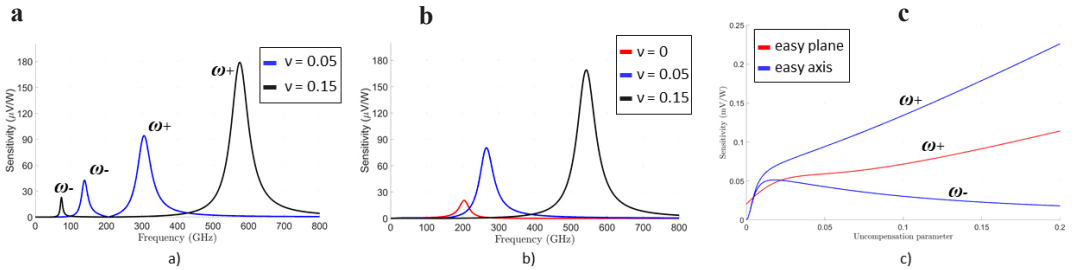

Figure 1. Sensitivity as a function of frequency with different uncompensation parameter for the "easy axis" anisotropy (**a**) and "easy plane" anisotropy (**b**), dependence of the detector sensitivity on the uncompensation parameter at resonant frequencies for "easy axis" and "easy plane" anisotropy (**c**).

where $\omega_0 = \sqrt{\omega_{ex}\omega_A}$.

The sensitivity of the detector to the frequency of the external EM wave was found as follows:

$$R(\omega) = \frac{|V_{out}(\omega)|}{P_{AC}} \tag{6}$$

where $V_{out1,2} = 2i\omega\kappa[s^*_{1,2}s_{2,3} - s^*_{2,3}s_{1,2}]$ is the output rectified voltage [2], $\kappa = Lg_r\theta_{SH}e\lambda_{Pt}\rho/2\pi d_{Pt}\tanh(d_{Pt}/2\lambda_{Pt})$ is the coefficient of proportionality, L is the distance between the output contacts, g_r is the real part of the conductivity at the boundary of the FiM/HM layer, θ_{SH} is the Hall spin angle in the heavy metal, e is the electron charge, λ_{Pt} is the spin diffusion length in the heavy metal, ρ is the electrical resistance of the heavy metal, d_{Pt} is the thickness of the heavy metal layer, $P_{AC} = cSh^2_{AC}/2\propto_0$ is the input power of the variable EM wave, where c is the speed of light, μ_0 is the magnetic permeability, S is the area of the ferrimagnet layer.

On Fig. 1a, b shows the dependence of the detector sensitivity on the frequency of the external EM wave. In the case of an "easy axis" we see two resonant peaks, and the value of the resonant peak corresponding to the frequency ω_+ is greater than the value of the resonant peak corresponding to the frequency ω_-. In addition, an increase in the value of the uncompensation parameter leads to an increase in the distance between the resonant peaks. In the case of an "easy plane" we have one resonant peak, the value of which increases with the growth of the uncompensation parameter. In contrast to the "easy axis" case, in the "easy plane" case, we have a non-zero sensitivity value with a zero uncompensation parameter. On Fig. 1c shows the dependence of the detector sensitivity on the uncompensation parameter. It is obtained by substituting Eq. (5) into Eq. (6). In the case of an "easy plane", the detector sensitivity has a non-zero value equal to 0.02 mV/W, with a zero uncompensation parameter due to attenuation. However, the lower the attenuation, the narrower the spectral linewidth and, accordingly, the lower the sensitivity. It can be seen that at small values of the uncompensation parameter, the sensitivity increases non-linearly, and at a value greater than 0.07, the dependence becomes linear. In the case of "easy axis" magnetic anisotropy, we have two curves corresponding to the frequencies ω_+ and ω_-. At small values of the uncompensation parameter, the dependence is non-linear, however, at a value of the uncompensation parameter greater than 0.02, we have a linear character.

Support by RSF (Grant No. 21-79-10396) is acknowledged.

1. B.A. Ivanov, Low Temp. Phys. **45**, 935–963 (2019).
2. A. Safin, S. Nikitov, A. Kirilyuk et al., Magnetochemistry **8**, no. 26 (2022).

B.P29

SUPERCONDUCTOR INFLUENCE ON THE FERROMAGNETIC RESONANCE PROPERTIES OF IRON-GARNET FILM NEAR THE CRITICAL TEMPERATURE

F.M. Maksimov[1,2*], *S.N. Polulyakh*[3], *N.G. Pugach*[4], *A.S. Pakhomov*[1,2], *V.N. Berzhansky*[3], *V.S. Stolyarov*[5], *V.I. Belotelov*[1,6], *A.I. Chernov*[1,2]

[1]Russian Quantum Center, Skolkovo, Moscow, Russia
[2]Center for Photonics and 2D Materials, Moscow Institute of Physics and Technology, Dolgoprudny, Russia
[3]Vernadsky Crimean Federal University, Simferopol, Russia
[4]National Research University Higher School of Economics, Moscow, Russia
[5]Center for Advanced Mesoscience and Nanotechnology, Moscow Institute of Physics and Technology, Dolgoprudny, Moscow, Russia
[6]Faculty of Physics, Lomonosov Moscow State University, Moscow, Russia
[*]E-mail: maksimov.fm@phystech.edu

In general, experiments in the field of magnonics are performed at room temperature, however, during the last several years the new subdiscipline, that deals with magnetization dynamics at cryogenic temperatures, is rapidly developing. One of the aims is to obtain further advances in applications based on hybrid magnetic-superconducting systems. In the recent works on the ferromagnet/superconductor systems [1–3], the peculiar properties due to the hybridization have been revealed.

In this work, we study in detail the effects that originate due to the interaction between thin magnetic dielectric films with niobium layer on top in the broad temperature range.

We investigate the changes in the magnetic properties of Bi-Gd-Sc iron garnet films of 250 nm thickness with a sputtered niobium superconductor layer of 20 nm and 160 nm. The critical

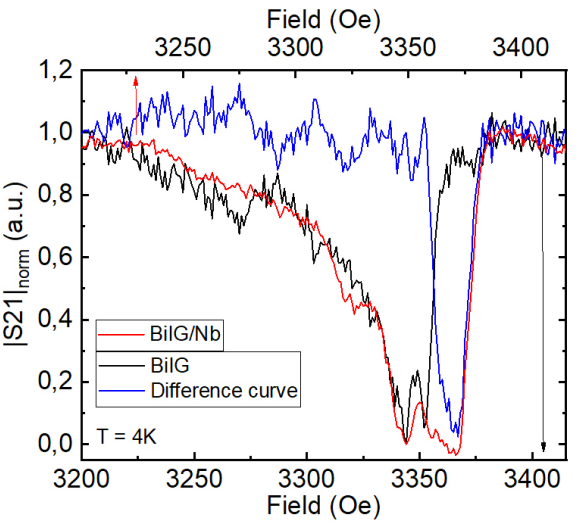

Figure 1. Transmission spectra obtained at 4 K for the Bi-substituted iron garnet with a 250 nm thickness (black) and BiIG(250 nm)/Nb(160 nm) – red color, and their difference (blue color), specifically demonstrating the appeared new component.

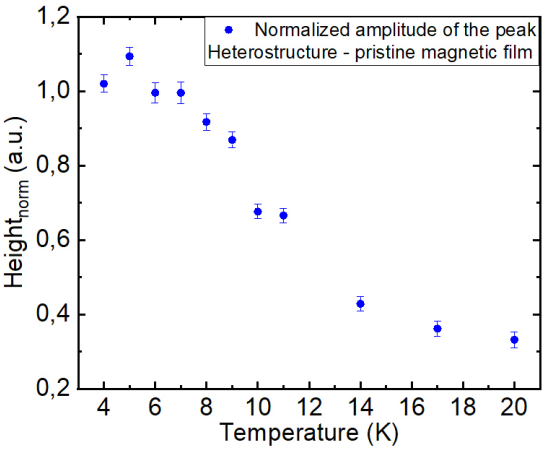

Figure 2. Temperature dependence of the normalized height of the right (difference) peak that is attributed to the influence of the niobium layer. The T_c for the niobium layer in the sample is 9 K.

temperature for the niobium layer is 9 K. The measurements were performed using the vector network analyzer (VNA) – ferromagnetic resonance (FMR) technique in the flip chip geometry. The samples were studied in the temperature range of 4–300 K.

Figure 1 demonstrates the obtained FMR spectra measured at 4 GHz for the pristine dielectric magnetic film (black) and heterostructure of the very same film and 160 nm niobium layer (red), measured at 4 K (below the transition). The spectrum of the hybrid structure is characterized by the appearance of the new spectral component located at larger field (blue color curve). The appearance of the new component depends on temperature (Fig. 2) and the behavior coincides with the transition of the niobium layer to the superconducting state. We attribute the experimental findings to the inverse proximity effect [4], that stems at the boundary between the ferromagnet and the niobium layer.

The new finding proves the possibility to manipulate the magnetic properties in the hybrid structures at low temperatures. It can be further developed for the controlled manipulation of the magnetic state in thin layered structures.

1. I.A. Golovchanskiy et al., Adv. Funct. Mater. **28**, 1802375 (2018).
2. O.V. Dobrovolskiy et al., Nat. Phys. **15**, 477–482 (2019).
3. I.A. Golovchanskiy et al., Phys. Rev. Applied **11**, 044076 (2019).
4. V.O. Yagovtsev, N.A. Gusev, N.G. Pugach, M. Eschrig, Supercond. Sci. Technol. **34**, 025003 (2021).

B.P30

THE DYNAMICS OF A SINGLE SPINTRONIC AFM OSCILLATOR

A.Yu. Mitrofanova[1*], *A.R. Safin*[1,2], *O.V. Kravchenko*[3]

[1]Kotel'nikov Institute of Radioengineering and Electronics, RAS, Moscow, Russia
[2]Moscow Power Engineering Institute, Moscow, Russia
[3]Federal Research Center "Computer Science and Control" of RAS, Moscow, Russia
[*]E-mail: nastya_mitrofanova_2000@mail.ru

The purpose of this work was to determine a locking band of a single antiferromagnetic (AFM) spin-Hall oscillator, using analytical approximations and numerical modeling. Such an oscillator is described by the following differential equation

$$\frac{1}{\omega_{ex}}\ddot{\varphi}+\alpha\dot{\varphi}+\frac{\omega_e}{2}\sin 2\varphi=\sigma j \quad . \tag{1}$$

Here $\omega_{ex} = \gamma H_{ex}$, $\omega_e = \gamma H_e$ are the exhange and easy anisotropy fields and γ is a gyromagnetic ratio, α is a damping constant, σj is a spin torque, where $\sigma = (2\pi)4.32$ Hz$\cdot$cm^2/A is a spin-torque efficiency and j is an electric current density. Analytical approximations were applied to the dimensionless equation

$$\frac{d^2\Phi}{d^2\tau}+\delta\frac{d\Phi}{d\tau}+\sin\Phi=\gamma \quad , \tag{2}$$

where $\omega_0=\sqrt{\omega_{ex}\omega_e}$, $\tau = \omega t$, $\sigma = \alpha\omega_e/\omega_0$, $\gamma = 2\sigma j/\omega_e$, $\Phi = 2\varphi$. Defining $y = d\Phi/d\tau$, $x = \Phi - \Phi_0^s$, and Φ_0^s as a saddle point, one can rewrite equation (2) in the form

$$y\frac{dy}{dx}+\delta y+\sin(x+\Phi_0^s)=\gamma \quad .$$

The applied approximation method [1] consists in the assumption that

$$y(x)=\sum_{n=1}^{N}b_n\sin\left(\frac{nx}{2}\right) \quad .$$

By the approximation method one can obtain

$$j_2^{(th)}\approx 0.631\frac{\alpha\omega_0}{\sigma}=1.1215(10^8)\ \mathrm{A/cm^2} \quad . \tag{3}$$

On the other hand, the harmonic balance method suggests looking for a solution of equation (2) in the following form

$$\Phi = \Omega\tau + \Phi_0(\tau) + A(\tau)\sin(\Omega\tau + \Psi(\tau)) \ .$$

where Φ_0 is the initial phase difference of the reference and adjustable oscillators, A is the amplitude of the phase difference deviation, Ψ is the initial phase and Ω is the beat frequency. For more details see [2]. For stationary mode when $A_0 = 1$ one can obtain

$$j_2^{(th)}\approx 0.605\frac{\alpha\omega_0}{\sigma}=1.0753(10^8)\ \mathrm{A/cm^2} \quad ,$$

that is close to (3). Expressions (3) and (4) are also close to that in [3].

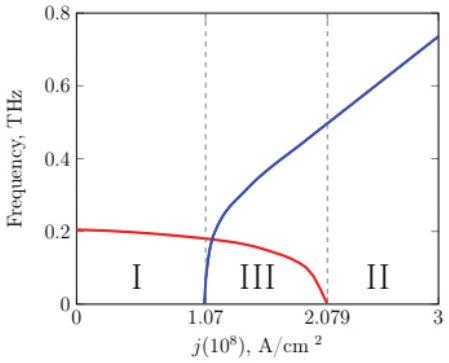

Figure 1. The results of modeling equation (1), that are subcritical stable damping mode in region I, postcritical self-oscillating mode in region II and transitional mode depending on initial conditions in region III. Critical currents are $j_2^{(th)} = 1.07$ and $j_1^{(th)} = 2.079$.

We have studied the model of a single AFM oscillator using numerical methods with $\omega_{ex} = (2\pi)27.5$ THz, $\omega_e = (2\pi)1.75$ GHz, $\alpha = 3.5 \cdot 10^{-3}$ and found out that the behavior of its frequency depends on the initial conditions. On the interval $j \in (0, 1.07)$, corresponding to region I in Fig. 1, as the current increases, the frequency decreases. For $j \in (2.079, 3)$, which corresponds to region II in Fig. 1, the frequency of the AFM oscillator increases with increasing DC current. For region III in Fig. 1, where $j \in (1.07, 2.079)$, the behavior of the frequency depends on the initial conditions. The found regions correspond to three modes of AFM oscillations, which are represented by phase portraits in Fig. 2. In region I, the AFM oscillator is in a subcritical stable damping mode, in Fig. 2 this region corresponds to a spiral source and a saddle. Region II corresponds to the postcritical regime, which is characterized by self-oscillating rotational motion in the easy plane, Fig. 2 demonstrates a limit cycle for this region. Region III is the so-called hysteresis. The oscillator regime in this region is transitional, and its stability depends on the initial conditions, which is confirmed by Fig. 2, where the separatrices of the saddle form a loop, in the domain of which we fall into a spiral source and obtain a damping regime. Outside the domain of the loop, the mode of the AFM oscillator will be self-oscillating.

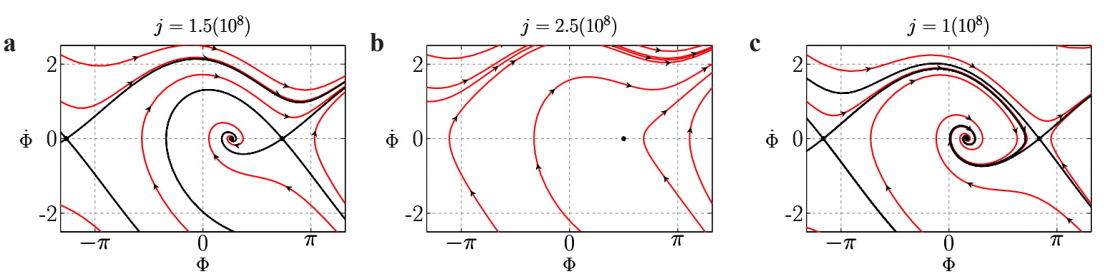

Figure 2. Phase portraits of Eq. (2): **a** spiral source corresponding to region I; **b** limit cycle corresponding to region II; **c** a loop formed with saddle separatrices and a spiral source.

It should be noted that the critical currents obtained by numerical methods, namely by modeling equation (1) with different initial conditions and creating a phase portrait of equation (2), $j_2^{(th)} = 1.07$ and $j_2^{(th)} = 1.0775$ are close to expressions (3) and (4) and $j_1^{(th)} = 2.079$ is close to the one in [3]. The fact that in order to get a representation of the dynamics of a single oscillator, we only needed to calculate the locking band and perform some numerical calculations is also worthy of mention.

Support by RSF No. 21-79-10396 is acknowledged.

1. V.V. Shachgild'an and A.A.Lyachovkin, Ripol Classic (1972) [in Russian].
2. M.V. Kapranov, MPEI Publ. (2006) [In Russian].
3. R. Khymyn et al., Sci. Rep. **7**, 1–10 (2017).

SPIN DYNAMICS IN FRUSTRATED QUANTUM MAGNET $BaCDVO(PO_4)_2$

T.A. Soldatov, A.I. Smirnov*

P.L. Kapitza Institute for Physical Problems RAS, Moscow, Russia
E-mail: tim-sold@yandex.ru

Frustrated spin systems have attracted great interest as their low-temperature properties are governed by strong quantum fluctuations. The special type of frustration provided by competing ferro- and antiferromagnetic interactions may lead to the formation of the novel nematic spin ordering near the saturation field, as it was shown by numerical and analytical calculations [1–3]. This magnetic order spontaneously breaks spin-rotational symmetry but conserves time-reversal symmetry [4]. Nematic state has no long range ordering and demonstrates anisotropic spin-spin correlations.

In recent papers [5–8] a novel presaturation quantum phase presumed to be a quantum spin nematic state was observed in quasi-2D $BaCdVO(PO_4)_2$ crystal. This material has layered magnetic structure with arrangement of magnetic ions V^{4+} carrying spin $S = 1/2$ on a distorted square lattice. At room temperature $BaCdVO(PO_4)_2$ belongs to orthorhombic P_{bca} space group with V^{4+} layers parallel to (a,b)-planes.

Below Neel temperature $T_N = 1.05$ K spins order collinearly along a-axis forming so-called "up-up-down-down" antiferromagnetic state. Neutron scattering experiments as well as magnetisation, specific heat and magnetocaloric effect measurements show that antiferromagnetic ordering disappears at field $H_{c1} = 4$ T whereas at higher fields additional phase transitions are found at $H^* = 5.5$ T and $H_{c2} = H_{sat} = 6.5$ T. In field H_{c1} the magnet is saturated by 98%.

In our work we performed electron spin resonance investigation of $BaCdVO(PO_4)_2$ in both ordered and high-field phases including field region between H_{c1} and H_{sat} tracing changes in excitation spectra. Frequency-field diagrams measured at 0.5 K for $\mathbf{H} \parallel a, b, c$ are shown in Figs. 1, 2. Two modes of resonance absorption with zero-field gaps $\Delta_1 = 12.8$ GHz and $\Delta_2 = 17.3$ GHz are observed. Measured

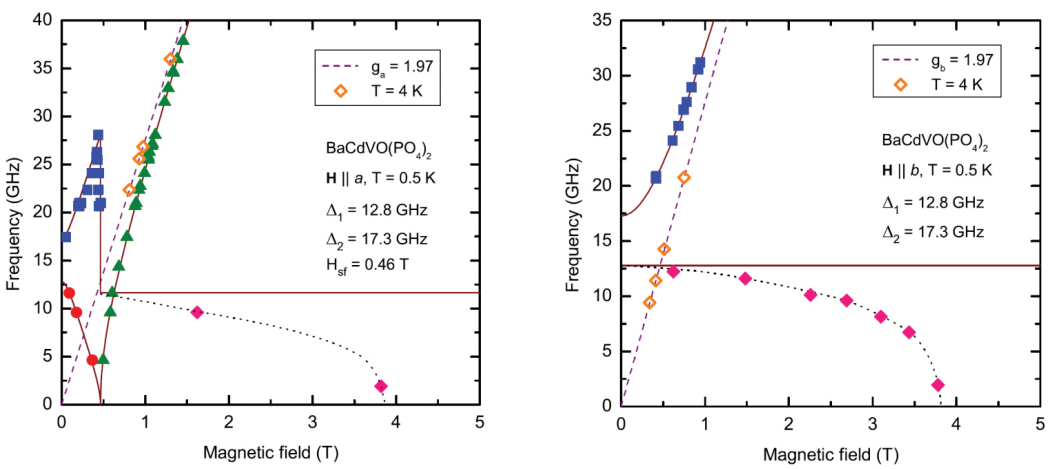

Figure 1. Frequency-field diagrams for $\mathbf{H} \parallel a, b$.

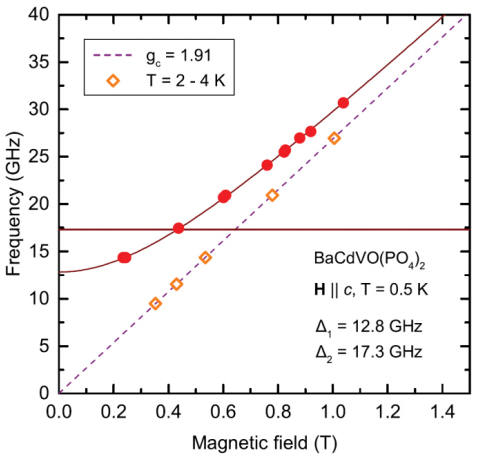

Figure 2. Frequency-field diagram for **H** || *c*.

spectrum is fully consistent with that expected for collinear antiferromagnet with biaxial anisotropy. Its behavior allows to identify *a*-axis as an easy axis and the *b*-axis as a hard axis of the spin ordering [9].

The remarkable feature of our work is observation of spin-flip mode softening at H_{c1} rather than at H_{sat}. The theory of spin excitations in a quantum spin-nematic state developed in ref. [4] shows that the macroscopic magnetic properties of spin nematics are the same as those of conventional antiferromagnets including all the phenomena typical to antiferromagnets. As the result, the magnetic resonance spectra of spin nematics should be similar to that of antiferromagnets. Thus at crossing phase transition from the ordered to spin nematic phase at H_{c1} in $BaCdVO(PO_4)_2$ we expect insignificant reconstruction of ESR spectra accompanied by the kinks or steps in frequency-field dependencies with the softening of spin-flip mode exactly at saturation field. We suppose that the transition at field H_{c1} is accompanied by a strong reduction of nematic order parameter comparing to the antiferromagnetic one resulting in an abrupt decrease of the resonance frequency for spin-flip mode.

An alternative explanation of premature softening of the spin-flip mode is that the magnetic evolution of $BaCdVO(PO_4)_2$ within the field range between H_{c1} and H_{c2} is not related to the formation of a spin nematic state but is associated with a small number of defects such as spin vacancies which contribute to the magnetization in strong fields and lead to peculiarities observed in specific heat and magnetocaloric effect measurements. Thus the true saturation field should be H_{c1} at which softening of spin-flip mode is expected. This hypothesis is also consistent with our results. The same problem was previously highlighted in ref. [10].

This work is supported by RSCF Grants № 17-12-01505 and № 22-02-00259.

1. A.V. Chubukov, Phys. Rev. B **44**, 4693 (1991).
2. N. Shannon, T. Momoi, P. Sindzingre, Phys. Rev. Lett. **96**, 027213 (2006).
3. M.E. Zhitomirsky, H. Tsunetsugu, Europhys. Lett. **92**, 37001 (2010).
4. A.F. Andreev, I. A. Grishchuk, Sov. Phys. JETP **60**, 267 (1984).
5. K.Yu. Povarov et al, Phys. Rev. B **99**, 024413 (2019).
6. M. Skoulatos et al, Phys. Rev. B **100**, 014405 (2019).
7. V.K. Bhartiya el al, Phys. Rev. Research **1**, 033078 (2019).
8. V.K. Bhartiya el al, Phys. Rev. B **103**, 144402 (2021).
9. T. Nagamiya, K. Yosida, R. Kubo, Advances in Physics **13**, 1 (1955).
10. N. Büttgen et al, Phys. Rev. B **90**, 134401 (2014).

PARAMAGNETIC RESPONSE, AND ELECTRONIC AND MAGNETIC PROPERTIES OF OXIDIZED SPARK PLASMA SINTERED CARBON NANOTUBES

*A.N. Ulyanov**, *E.V. Suslova, S.V. Savilov*

Chemistry Department, Lomonosov Moscow State University, Moscow, Russia
*E-mail: a-ulyanov52@yandex.ru

Carbon nanotubes (CNTs) attract high attention because of their interesting fundamental properties and potential application. The properties of CNTs depend on their synthesis procedure. The oxygen content and, consequently, oxidation state of carbon atoms plays an important role for the CNTs properties. Consolidation of CNTs by spark plasma sintering (SPS) increases conductivity [1] and improves mechanical properties [1, 2] of the materials that are important in electrode and constructive materials and application in fuel cells, electromagnetic shielding and magnetic separation [3].

The electron paramagnetic resonance (EPR) is widely used method to study the electronic and magnetic properties of carbon fibers, graphene oxides and nanoflakes. At the same time, this method was rarely applied for the studying the CNTs, and the various assignments of the absorption EPR lines to delocalized and localized electrons were noted. Here we report the EPR study of electronic local structure of oxidized CNTs, synthesized by pyrolytic decomposition of hexane and consolidated with SPS, to shed light on their properties. EPR measurements were carried out at a frequency of 9.8–9.9 GHz using a BRUKER EMX 6/1 spectrometer. The number of spins (N_i) in the sample (i) was deduced using the double integrated intensities of the resonance line of the studied and standard samples, respectively. TEMPO (2,2,6,6-tetramethyl-1-piperidinyloxyl) in toluene solution with $N_{st} = 2.0792 \cdot 10^{16}$ spins was used as a standard sample.

The EPR-measurements showed that the line intensity, g-factor and linewidth changes with temperature and depend on the oxidation states of CNTs. Figure 1 shows the absorption EPR spectrum measured at 150 K for the consolidated CNT oxidized at 3 h. The absorption spectra lines are split into narrow and broad components. The different g-factors of the lines indicate the different surrounding of paramagnetic centers attributed to them.

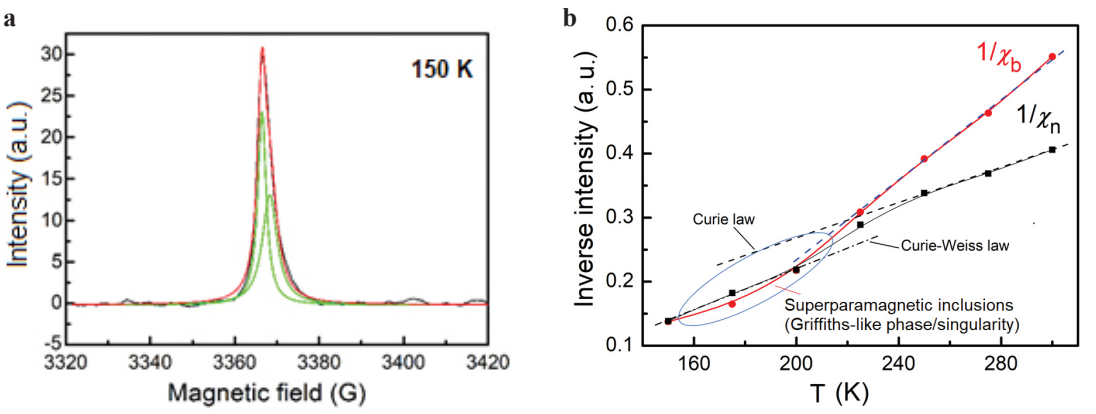

Figure 1. **a** Absorption EPR spectra of consolidated CNT oxidized 3 h. **b** Temperature dependence of inverse intensites of narrow and broad EPR adsorption lines.

The inverse intensity of narrow component ($1/\chi_n(T)$) can be well fitted by two lines and attributed to Curie law at high temperature and to Curie-Weiss law at low temperature with Curie temperature (T_c) equaled to ≈40.0 K (Fig. 1). The transfer of inverse intensity from Curie law to Curie-Weiss law was also observed in partially reduced graphene oxide [4].

The temperature dependence of inverse intensity for the broad line ($1/\chi_b(T)$) deviates from the Curie-Weiss law. It can be associated with a paramagnetic matrix with superparamagnetic conducting inclusions. The conclusion corresponds to the results for the oxidized graphene nanoflakes [5]. The similar $1/\chi(T)$ dependence was also observed in perovskite-like manganites and called a Griffiths-like singularity [6–7].

The EPR-measurements were performed for the consolidated CNTs oxidized at different time and the results will be carefully discussed.

The work was supported by the Russian Science Foundation (project No 21-43-00023).

1. C. Laurent, G. Chevallier, A. Weibel, A. Peigney, C. Estournès, Carbon **46**, 1812–1816 (2008).
2. G. Yamamoto, Y. Sato, T. Takahashi, M. Omori, T. Hashida, A. Okubo, K. Tohji, J. Mater. Res. **21**, 1537–1542 (2006).
3. S.V. Savilov, S.A. Chernyak, M.S. Paslova, A.S. Ivanov, T.B. Egorova, K.I. Maslakov, P.A. Chernavskii, Li Lu, and V.V. Lunin, ACS Appl. Mater. Interfaces **10**, 20983 (2018).
4. M.A. Augustyniak-Jabłokow, R. Strzelczyk, R. Fedaruk, Carbon **168**, 665–672 (2020).
5. P. Tong, B. Kim, D. Kwon, T. Qian, S.I. Lee, S.W. Cheong, B.G. Kim. Phys. Rev. B **77**, 184432 **(**2008).
6. A.N. Ulyanov, S.V. Savilov, A.V. Sidorov, A.V. Vasiliev, N.E. Pismenova, E.A. Goodilin, J. Alloys Compd. **722**, 77–82 (2017).

MAGNETIC SENSOR BASED ON DIPOLE-EXCHANGE SPIN WAVES IN EXCHANGE-COUPLED YIG FILMS

S. Vysotskii[1*], A. Kozhevnikov[1], M. Balinskiy[2], A. Khitun[2], Y. Filimonov[1]

[1]Kotelnikov Institute of Radioengineering and Electronics RAS, Saratov Branch, Saratov, Russia
[2]University of California-Riverside, Riverside, USA
[*]E-mail: vysotsl @gmail.com, vysotsl@yandex.ru

Interest in research and development of spin-wave (SW) interferometers is associated with the prospects for their wide application in devices for information processing, energy-efficient memory and logic devices [1], magnonic holographic memory [2] and special task processors [3]. Also, a magnetic field sensor based on a spin wave interferometer using spin wave interference in a cross junction was reported [4, 5]. A possibility of increasing of spin-wave magnetometer's sensitivity was shown in [6] where two interfered SW counter-propagate in magnetic film and the operating frequency was chosen near one of the frequencies of the resonant interaction of SW with elastic waves where SW's transmission characteristic $S(f)$ demonstrates narrow frequency regions of increasing of propagation losses. The similar features can be found in $S(f)$ dependencies of dipole-exchange SW near spin-wave resonance (SWR) frequencies [7]:

$$f_N = \sqrt{(f_H + f_{\text{ex}})(f_H + f_{\text{m}} + f_{\text{ex}})}\,, \tag{1}$$

where $f(H) = \gamma H$, $f_{\text{ex}} = 2\gamma A q_N^2/\text{M}$, $q_N = \pi N/d$, $N = 1, 2, .., f_m = \gamma 4\pi M$, H is bias magnetic field, A is the exchange stiffness, q is SW wavenumber, M and d – saturation magnetization and thickness of the film, respectively, $\gamma = 2.8$ MHz/Oe. SWR can be observed in the cases of forward volume (FVMSW) and surface (MSSW) magnetostatic waves. However, their use of and for interferometry meet some problems: FVMSW required high bias magnetic field and dipole-exchange MSSW is characterized by non-reciprocity [7], which requires to align the amplitudes of counter-propagating MSSW. Backward volume MSW (BVMSW) are free from mentioned problems but they cannot interact with exchange modes because their frequency band $[f_H, f_0 = \sqrt{f_H(f_H + f_{\text{m}})}]$ is lower than SWR frequencies (1). However, BVMSW can interact with exchange SW in the structure consisting of two exchange-coupled YIG films with different saturation magnetizations ($4\pi\text{M}_1 > 4\pi\text{M}_2$) because spectra of dipole BVMSW in a layer with a magnetization of $4\pi\text{M}_1$ and frequency band of exchange modes of a layer with a magnetization of $4\pi\text{M}_2$ are overlapped in the frequency region $[f_{01}, f_{02}]$ [8]. In this work, we study the interference of BVMSW's counter-propagating in a structure with two exchange-coupled YIG films from the point of view for potential application in magnetic field sensors.

We used a two-layer yttrium-iron garnet (YIG) film epitaxially grown by liquid phase epitaxy on a gadolinium gallium garnet (GGG) substrate with crystallographic orientation (111). First layer of composition $Y_3Fe_5O_{12}$ (YIG1) was grown on the substrate, and then a layer doped with gallium and scandium of composition $Y_3Fe_4Ga_{0.8}Sc_{0.2}O_{12}$ (YIG2) was grown. Parameters of the layers were as follows: thicknesses $d_1 = 8$ μm and $d_2 = 6$ μm, saturation magnetizations $4\pi M_1 = 1750$ G and $4\pi M_2 = 640$ G, exchange stiffnesses $A_1 = 3.85 \cdot 10^7$ erg/cm $A_2 = 2 \cdot 10^7$ erg/cm for YIG1 and YIG2, respectively. The interlayer exchange parameter $A_{12} \approx 0.03$ erg/cm^2 was found using numerical modeling of BVMSW propagation in the studied structure as a fitting parameter providing a similarity of experimental data and results of calculation [8].

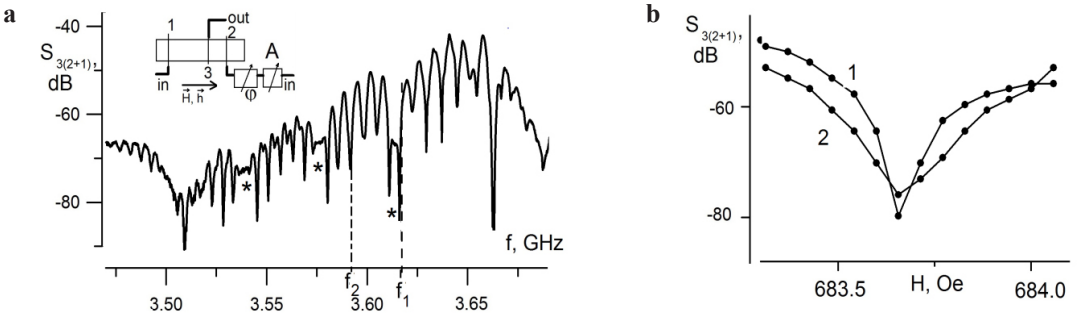

Figure 1. **a** S3(1+2)(f) characteristic correspondent to phase difference $\Delta\phi_{12}$ providing destructive interference of BVMSW at frequency $f^* = 3616$ MHz; **b** $S_{3(1+2)}(H)$ dependence for frequency f^*.

The measurements of transmission characteristics $S(f)$ were carried out in the delay line at the BVMSW configuration (see inset in Fig. 1a) with the sample of the lateral dimensions approximately 6 mm × 10 mm. Two antennas 1 and 2 were used for excitation of the BVMSW and antenna 3 was used as an output one. A width and a length of the antennas were ≈50 μm and 4 mm, respectively. The microwave signal from the vector network analyzer was fed to the power divider and then to the input antennas, while the phase shifter and attenuator were switched on between the divider and antenna 2.

Fig. 1a shows $S_{3(1+2)}(f)$ characteristic correspondent to tuning of phase difference $\Delta\phi_{12}$ between BVMSW excited antennas 1 and 2 providing destructive interference of BVMSW at frequency $f_1 = 3616$ MHz at $H \approx 683.7$ Oe. The frequency f_1 is chosen close to one of SWR frequency (1) marked in the Fig. 1a by asterisks. The curve 1 in the Fig 1b shows the dependence of level of $S_{3(1+2)}$ while tiny variation of H. One can see that the sensitivity $S_{3(1+2)}(H)$ exceeds 250 dB/Oe in the vicinity of the resonance $H \approx 683.7 \pm 0.1$ Oe that can be useful for sensors design. Note that at frequencies out of SWR regions (see for example f_2 in the Fig. 1a) the sensitivity does not exceed 60 dB/Oe (see curve 2 in the Fig. 1b).

We also study the sensitivity of the sensor to alternating magnetic field. To carry out these measurements, an alternating magnetic field h with a frequency of $\tilde{f} = 10$ kHz created by a single-turn coil was applied to the delay line model in addition to the bias magnetic field H. The coil was preliminarily calibrated in a constant magnetic field. The output signal from antenna 3 was amplified and detected and measured using nanovoltmeter synchronized by frequency $\tilde{f}$. The measurement results showed the possibility of measuring the h value down to $3 \cdot 10^{-2}$ Oe, which was limited by the noise of the used equipment.

Support by the Russian Foundation for Basic Research (project no. 20-07-00973) is acknowledged.

1. A. Khitun, M. Bao, K. L. Wang K.L., J. Phys. D: Appl. Phys. **43**, 264005 (2010).
2. F. Gertz, A. Kozhevnikov, Y. Filimonov, A. Khitun, IEEE Trans. Magn. **51**, 1–19 (2014).
3. G. Csaba, A. Papp, W Porod, Journ. of Appl. Phys. **115**, 17C741 (2014).
4. M. Balynsky, D. Gutierrez, H. Chiang et al., Sci Rep. **7**, 11539 (2017).
5. M. Balinskiy, H. Chiang, A. Kozhevnikov, J. Magn. Magn. Mater. **514**, 167046 (2020).
6. S.L. Vysotskii., A.V. Kozhevnikov and Y.A. Filimonov, Phys. Solid State **63**, 1579-1583 (2021).
7. A.G. Gurevich, G.A. Melkov, Magnetization Oscillations and Waves, N.Y.: CRC Press, 1996.
8. S.L. Vysotskii, G.T. Kazakov, Yu.A. Filimonov, Technical Physics **43**, 834–845 (1998).

B.P34

PECULIARITIES OF THE EPR-SPECTRA OF THE PbTe CRYSTAL WITH Mn AND Cu IMPURITIES IN THE X- AND Q-BAND

I.I. Fazlizhanov[1], *A.V. Shestakov*[1*], *V.A. Ulanov*[1,2]

[1]Zavoisky Physical-Technical Institute, FRC Kazan Scientific Center, Russian Academy of Sciences, Kazan, Russia
[2]Kazan State Power Engineering University, Kazan Russia
[*]E-mail: Aleksey665@gmail.com

The PbTe direct narrow band semiconductor belongs to the group of lead chalcogenides PbS, PbSe and PbTe with the cubic rock salt structure. It was the subject of a vast amount of theoretical and experimental work. These works were motivated not only by its technological applications, but also by their unusual physical properties. PbTe is a narrow gap semiconductor with strong ionic character. It has a positive temperature coefficient of the gap width ($dE/dT > 0$), the high static dielectric constant, and the large carrier mobility. These properties make it unique among polar compounds and make it important applications in many fields, such as infrared detectors, light-emitting devices, infrared lasers, thermoelectric materials and solar energy panels. Studies of quantum wires, dots, and wells in the bodies of PbTe semiconductors and possibilities of its applications have caused much attention in the past decades. But, a little of these studies were performed by EPR method. The reason of the latest fact is that most of the paramagnetic impurity centers form resonant levels in the conduction or valence band in the lead chalcogenides and all such centers are not observable by EPR method.

But it was found [1, 2] that the Mn^{2+} ions embedded in PbTe are well localized at the Pb sites and form local magnetic moments. Owing to the direct exchange interaction between the d-electrons and Bloch electrons of the valence and conducting bands, the latter are magnetically polarized. Through

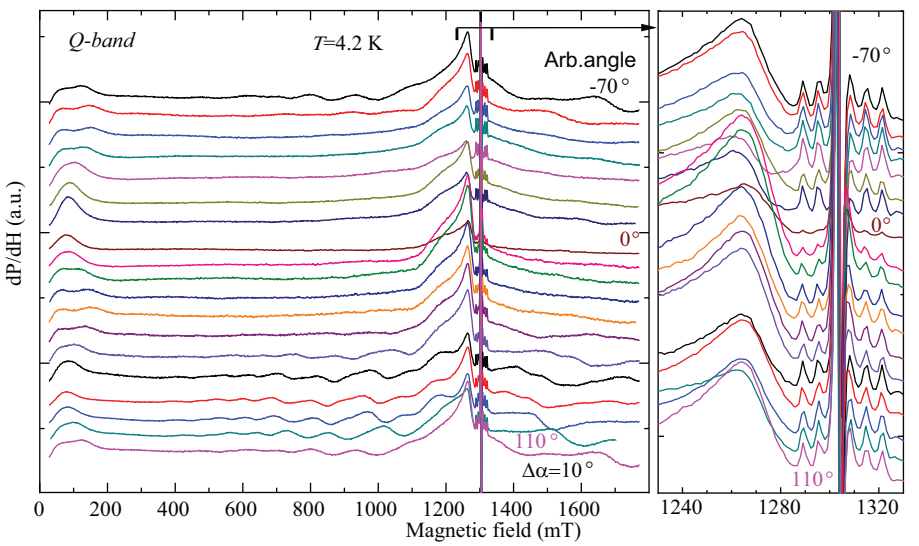

Figure 1. A series of EPR-spectra of a sample in (001) plane at various angles in the Q-band.

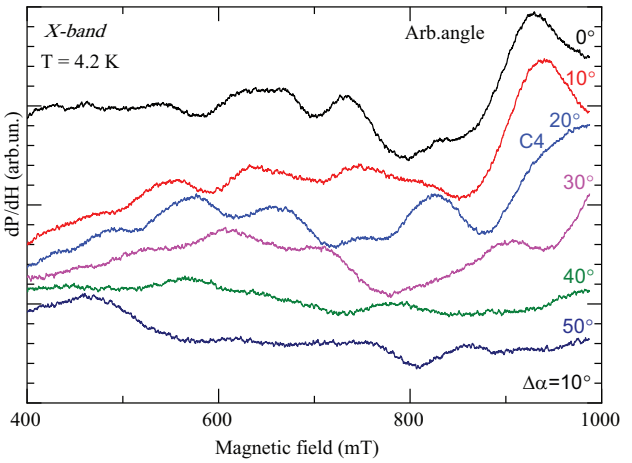

Figure 2. A series of EPR-spectra of a sample in (111) plane at various angles in the X-band (**B**⊥(100) plane if angle = 20°).

these polarized electrons, the local spins of Mn^{2+} ions interact with each other. Consequently, the manganese impurity centers can be used as paramagnetic probes to study some physical properties of PbTe semiconductors.

We report here the X-band (9.36 GHz) and Q-band (36.5 GHz) EPR data on deep Mn^{2+} centers in PbTe (Mn, Cu) crystalline sample ($x_{Mn} \approx 0.0005 \div 0.001$) grown by vertical Bridgman method in quartz crucibles. This low concentration of Mn ions was chosen with the aim that the impurity ions work as a probe.

In the X-band EPR-experiment, the sample rotated in the (111) plane. If the angle is 20 degrees, then the direction of the magnetic field coincides with the direction of the (001) axis. In the Q-band EPR experiment the sample was mounted in center of bottom of a cylindrical cavity resonator (with TE_{012} mode) and rotated in the (100) crystallographic plane. All measurements were carried out at liquid helium temperature (4.2 K).

The Q-band EPR-spectrum of this sample is very rich (see Fig. 1). We immediately note that the line at 1303 mT due to coal that was added as a reference point. Six principal Mn^{2+} hyperfine lines were observed in the EPR-spectra. The field intervals between the lines were found to be isotropic under rotation in the (100) plane within the experimental error of about 0.1 mT, where $A = 165 \div 202$ MHz. The EPR broad line with $B_{res} \sim 1275$ mT was observed presumably from Cu ions. The nature of signal in the region 0–200 mT is discussed. Quantum oscillations are also observed in the X-band (Fig. 2) and Q-band (Fig. 1) ERP-spectra, the period of which increases with increasing magnetic field. It is assumed that these oscillations are due to the de Haas-van Alphen effect.

All experimental facts observed in this study are discussed.

The financial support was provided by the FRC Kazan Scientific Center of RAS.

1. Ven-Chung Lee, Phys. Rev. B **34**, 5430 (1986).
2. J.H. Pifer, Phys. Rev. **157**, 272 (1967).

Section C.

Low dimensional magnetism

INTERACTION OF SPINONS DETECTED BY MICROWAVE SPECTROSCOPY

A.I. Smirnov[1*], K.Yu. Povarov[2], T.A. Soldatov[1], Ren-Bo Wang[3], A. Zheludev[2], O.A. Starykh[3]

[1]P. L. Kapitza Institute for Physical Problems RAS, Moscow, Russia
[2]Laboratory for Solid State Physics, ETH Zürich, Zürich, Switzerland
[3]Department of Physics and Astronomy, University of Utah, Utah, USA
[*]E-mail: smirnov@kapitza.ras.ru

The $S = 1/2$ Heisenberg antiferromagnetic spin chain has quantum critical ground state with absence of the ordered spin components and power law decay of the correlation function. This ground state and it's excitations are often described in terms of quantized fractionalized dynamic spin structures referred to as spinons, see, e.g. [1–3]. The theory of free fermions in spin $S = 1/2$ antiferromagnetic chains is supported by numerous experiments, e.g., by observation of the continuum of $S = 1$ excitations (so called two-spinon continuum) in neutron scattering experiments [4] or by finding the field-dependent soft modes appearing within the continuum of longitudinal fluctuations in a magnetic field [3].

A specific fine structure of the two-spinon continuum was predicted for a spin $S = 1/2$ chain with a uniform Dzyaloshinsky-Moriya (DM) interaction. This interaction causes a shift of the continuum in q-space by a characteristic wavevector $q_{DM} = D/(Ja)$. Here D is the Dzyaloshinsky-Moriya parameter and a – interspin distance. The shift results in an energy gap $\Delta = \pi D/2$ and a doublet of electron spin resonance (ESR) frequencies

$$\nu_{\pm} = (g\mu_B H \pm \Delta)/2\pi\hbar \ . \tag{1}$$

The frequencies $\nu_{\pm}$ correspond to lower and upper boundaries of the continuum of a purely Heisenberg (i.e. $D = 0$) chain at the wavevector q_{DM}. The ESR doublet $\nu_{\pm}$ was indeed experimentally observed in, e.g., [5], confirming the fermion nature of the ground state and its excitations.

Now we report the measurements of ESR spinon doublet for an almost ideal 1D $S = 1/2$ Heisenberg antiferromagnet $K_2CuSO_4Br_2$ in a strong magnetic field, where we observe a significant deviation of ESR modes $\nu_{\pm}$ from the simple relation (1).

According to a recent theoretical study [6], the continuum boundaries should be shifted from the positions corresponding to noninteracting spinons due to the interaction of the backscattering type. The parameter of this interaction u is defined by a Hamiltonian term

$$\begin{aligned} V = &-\frac{u}{2}\int dx\left(\psi^{\dagger}_{R\uparrow}\psi_{R\downarrow}\psi^{\dagger}_{L\downarrow}\psi_{L\uparrow} + \psi^{\dagger}_{R\downarrow}\psi_{R\uparrow}\psi^{\dagger}_{L\uparrow}\psi_{L\downarrow}\right) \\ &-\frac{u}{4}\int dx\left(\psi^{\dagger}_{R\uparrow}\psi_{R\uparrow} - \psi^{\dagger}_{R\downarrow}\psi_{R\downarrow}\right)\left(\psi^{\dagger}_{L\uparrow}\psi_{L\uparrow} - \psi^{\dagger}_{L\downarrow}\psi_{L\downarrow}\right), \end{aligned} \tag{2}$$

which describes backscattering interaction between right/left moving spinons $\psi_{R/Ls}$ (here s is the spin index ↑,↓), living near the right/left Fermi points of the one-dimensional Fermi surface, correspondingly [6, 7]. The additional interaction-induced gap between the lower and upper boundaries of the continuum is represented by $\Delta_{int} = uM/\mu_B$, where M is the magnetic moment per unit length. Using these relations we can explain [7] the deviation of the experimentally observed frequencies of the spinon doublet from the above interaction-neglecting relation (1). Figure 1 demonstrates the difference between the observed ESR frequencies and Larmor frequency $\nu_{Lar} = g\mu_B H/2\hbar$ measured

in different magnetic fields. This difference should be constant when the interaction between spinons is neglected (this behavior is illustrated by horizontal dashed lines at ±8.7 GHz). The fit according to the predictions of [6] with the parameter $u = 3.5 \cdot 10^5$ cm/s demonstrates a good quantitative correspondence of the experimental doublet frequencies to the theory with a reasonable value of the parameter u which is about 50% larger than spinon velocity. The fit is presented by solid lines. Figure 2 shows the frequency dependence of the intensity ratio of the components of the ESR doublet along with the theoretical prediction [7] for this ratio. At $u = 0$, i.e. without spinon interaction, this ratio should be equal to one in this frequency range. A good correspondence of the data and theory on this graph explains the dramatic vanishing of the upper component of the doublet, which was a puzzling result of the experiment [5].

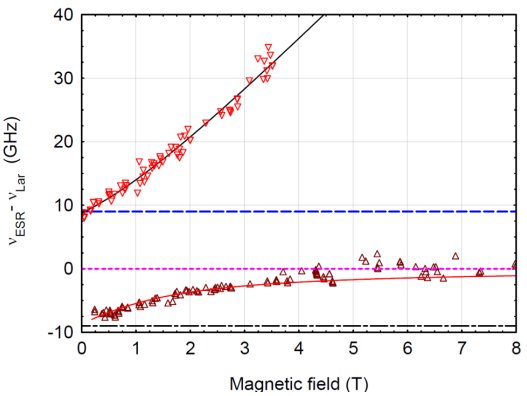

Figure 1. $\nu_{ESR} - \nu_{Lar}$ *vs* magnetic field at $T = 0.5$ K. Solid lines – theory, dashed – see text.

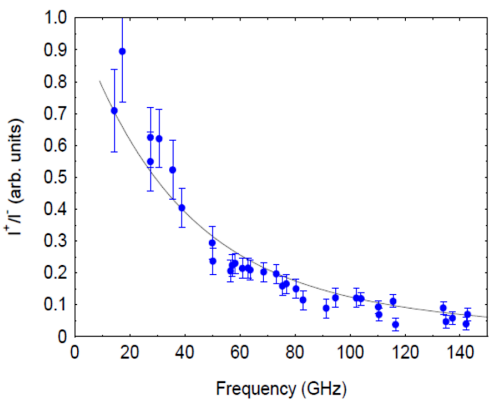

Figure 2. Ratio of intensities within spinon doublet *vs* frequency. $T = 0.5$ K.

These observations confirm the fundamental concept of interacting fractionalized fermions-spinons as a basic feature of the ground state of $S = 1/2$ Heisenberg antiferromagnetic chains in a dielectric crystal. The value of the spinon backscattering parameter is found experimentally. These experimental consequences of the spinon-spinon interaction reveal a Fermi-liquid (not a Fermi-gas) behavior of quasi-particles in a 1D antiferromagnet. Thus the collective excitations of 1D Heisenberg $S = 1/2$ antiferromagnetic chain demonstrate amazing analogy with the ensemble of electrons in a normal metal and specific Silin spin waves [8] in a normal metal.

Support of RSCF Grant 22-02-00259 is acknowledged.

1. L. Faddeev and L. Takhtajan, Phys. Lett. A **85**, 375 (1981).
2. G. Müller et. al., Phys. Rev. B **24**, 1429 (1981).
3. D. Dender et. al., Phys. Rev. Lett. **79**, 1750 (1997).
4. D. Tennant et. al., Phys. Rev. B **52**, 13368 (1995).
5. A. Smirnov et. al., Phys. Rev. B **92**, 134417 (2015).
6. A. Keselman et. al., Phys. Rev. Lett. 125 (2020).
7. K. Povarov et. al., Phys. Rev. Lett 2022. accepted March 2022.
8. V. Silin, Sov. Phys. JETP **6**, 945 (1958); V. Silin, Sov. Phys. JETP **8**, 870 (1959).

POLARIZED NEUTRON REFLECTOMETRY IN THE STUDY OF RARE-EARTH NANOSTRUCTURES

N.O. Antropov[1], *D.I. Devyaterikov*[1], *E.A. Kravtsov*[1,2*]

[1]M.N. Mikheev Institute of Metal Physics, Ural Branch of RAS, Ekaterinburg, Russia
[2]Ural Federal University, Ekaterinburg, Russia
[*]E-mail: kravtsov@imp.uran.ru

Heavy rare-earth metals (from Gd to Tm) are known to display rich magnetic phase diagrams depending on temperature and magnetic field. These include temperature-dependent magnetic anisotropy in Gd, long-range helicoidal magnetic ordering in Dy and Ho, etc. When heavy rare-earth metals are used as constituents of planar multilayered nanostructures, complex magnetic structures never observed in bulk systems may appear due to dimensional effects, proximity effects from neighboring layers, interfacial effects, epitaxial strains, long range exchange coupling, and others.

Since conventional techniques to probe magnetic ordering in rare-earth nanostructures like neutron diffraction are difficult to apply due to insufficient amount of scattering material, we discuss application of polarized neutron reflectometry (PNR) to study magnetic rare-earth multilayers. We give a short review of PNR technique as applied to determine long-range magnetic ordering in multilayers and report on our recent results on magnetic multilayers composed of 4f, 3d, and 5d metals received by complementary application of polarized neutron reflectometry and x-ray scattering.

In particular, we consider antiferromagnetic exchange ordering in Fe/Gd superlattices and its modification with introducing paramagnetic (Pd) spacers between Fe and Gd. By combined application of PNR and SQUID-magnetometry we have systematically investigated magnetic configurations in Fe/Pd/Gd multilayers with Pd spacer thickness in the range 8–28 Å. It was shown that by introducing Pd spacer of 10–14 Å in thickness it is possible to decrease the spin-flop transition field up to 2 orders of magnitude upon keeping antiferromagnetic Fe-Gd ordering in small magnetic field below 500 Oe at $T = 50$ K.

We show that in magnetic multilayers composed of alternating heavy rare-earth metals Dy/Gd and Dy/Ho there appears coherent magnetic structure propagating throughout the entire multilayer. In Dy/Gd superlattices, magnetic moments in ferromagnetically ordered Gd-layers are oriented out-of-plane, while Dy magnetic moments form a fun structure propagating coherently throughout all the Dy-layers. This complex interlayer and intralayer magnetic ordering causes to additional Bragg peak detected with polarized neutron reflectometry in limited temperature region.

In Dy/Ho superlattices, we observed two different magnetic helicoidal structures in Dy- and Ho-layers alternating coherently in all the structure. The magnetic helix periods are different in Dy and Ho, the magnetic phase transition observed in bilk Dy and Ho at low temperatures does not occur in Dy/Ho-multilayers, so the helicoidal ordering exists down to very low temperatures.

The work was supported by The Ministry of Science and Higher Education of Russian Federation (Project No. 075-10-2021-115) and RFBR (project No. 20-42-660024).

SQUARE KAGOME SYSTEMS

A.N. Vasiliev[1,2]

[1]Low Temperature Physics and Superconductivity Department, Moscow State University, Moscow, Russia
[2]Functional Quantum Materials Laboratory, National University of Science and Technology "MISiS", Moscow, Russia
E-mail: vasil@lt.phys.msu.ru

A quantum antiferromagnet with a square kagomé lattice (SKL) represents the rare case when it is possible to establish precisely the origin of a new physical concept. In 2001, Siddharthan and Georges introduced a two-dimensional network of corner-sharing triangles with square lattice symmetry [1]. In variance with kagomé lattice, which is a two-dimensional network of corner-sharing triangles with hexagonal voids, SKL is a two-dimensional network of corner-sharing triangles with alternative square and octagonal voids. There are two non-equivalent positions for the magnetic ions, α and β, being in ratio one to two. The shape of the unit cell resembles shuriken, a Ninja concealed weapon of ancient time. It has been shown numerically that the properties of a square kagomé antiferromagnet should be similar to those on a kagomé lattice. For the spin-1/2 Heisenberg quantum antiferromagnet, a resonating valence bond ground state has been predicted with a triplet gap filled by a continuum of low-lying singlet states.

In the large-N limit, N being the number of lattice sites, a finite temperature phase transition into a phase with ordered resonance loops and broken translational symmetry has been predicted. This exotic transition is not forbidden by the Mermin-Wagner theorem since it stems from the breaking of a translational symmetry. Recently, it has been shown that the model of geometrically frustrated SKL possesses just single thermodynamically stable solution for arbitrary values of model parameters. The very existence of this unique solution means that the model cannot exhibit either first order or second order phase transitions, at least, at non-zero temperatures [2]. The temperature dependence of the specific heat of spin-1/2 Heisenberg SKL antiferromagnet has been analyzed by Tomczak and Richter who predicted the broad peak located at $T \sim 0.85J$ which is a correlation one typical for any low-dimensional magnetic systems, and the second one, at $T \sim 0.10J$, which indicates an additional energy scale relevant to SKL being ascribed to the energy of the lowest spin triplet excitation [3].

For a long time, the studies of the thermodynamic properties of compounds with SKL or its derivatives were carried out exclusively by theoretical methods, albeit the nature provided such patterns in some rare minerals. Among these minerals are nabokoite $KCu_7(SO_4)_5(TeO_3)OCl$, atlasovite $KCu_6FeBiO_4(SO_4)_5Cl$, elasmochloite $Na_3Cu_6BiO_4(SO_4)_5$ and favreauite $PbCu_6BiO_4(SeO_3)_4(OH)H_2O$. The intrinsic properties of SKL in nabokoite and atlasovite are masked by the presence of magnetic ions extraneous to this network. Recently, the iron-free sibling of atlasovite, $KCu_6AlBiO_4(SO_4)_5Cl$, has been synthesized and thoroughly investigated in measurements of thermodynamics, muon spin relaxation and neutron scattering. It has been established that down to 58 mK this compound persists in a gapless quantum spin liquid state. Additionally, a novel sodium bismuth oxo-cuprate phosphate chloride, $Na_6Cu_7BiO_4(PO_4)_4Cl_3$, containing both square kagomé layers and interlayer Cu^{2+} ions has been synthesized by hydrothermal technique. This material shows no magnetic ordering down to 50 mK forming quantum spin liquid state similar to $KCu_6AlBiO_4(SO_4)_5Cl$. Here, we present the results of various measurements on synthetic $KCu_6AlBiO_4(SO_4)_5Cl$, $Na_6Cu_7BiO_4(PO_4)_4Cl_3$ and $KCu_7(SO_4)_5(TeO_3)OCl$.

1. R. Siddharthan and A. Georges, Phys. Rev. B **65**, 014417 (2001).
2. E. Jurčišinová and M. Jurčišin, Physica A **492**, 1798 (2018).
3. P. Tomczak and J. Richter, J. Phys. A: Math. Gen. **36**, 5399 (2003).

C.O1

FERROMAGNETISM INDUCED BY OXYGEN VACANCIES IN MULLITE $Bi_2Fe_4O_9$

S.S. Aplesnin[1,2*], *L.V. Udod*[1,2], *M.N. Sitnikov*[2], *D.A. Velikanov*[1], *O.B. Romanova*[1]

[1]Kirensky Institute of Physics, Federal Research Center KSC SB RAS, Krasnoyarsk, Russia
[2]Reshetnev Siberian State University of Science and Technology, Krasnoyarsk, Russia
[*]E-mail: apl@iph.krasn.ru

Mullite $Bi_2Fe_4O_9$ is a multifunctional material, which is used in chemical industry and promising for microelectronics. The magnetic properties of polycrystalline bismuth ferrite $Bi_2Fe_4O_9$ depend on a synthesis method used and a crystallite size. At room temperature, the sample with a grain size of 200–450 nm synthesized using ethylene diamine tetra acetic acid behaves like a weak ferromagnet [1]. The $Bi_2Fe_4O_9$ sample with micron grains obtained by melting exhibits the magnetization hysteresis and undergoes a magnetic phase transition at 250 K [2]. Despite the great amount of the available data on the magnetic properties of the $Bi_2Fe_4O_9$ compound, the temperature dependence of the $M(H)$ hysteresis for this composite remains unexplored. The hysteresis exists above the Néel temperature in the polycrystals with a subcritical grain size and is explained by the uncompensated sublattices magnetic moments. In the paramagnetic state, only a short-range order exists, which cannot cause the hysteresis and residual magnetic moment.

We suppose that, at room temperature, the oxygen defects cause the formation of a divalent state of iron ions. Via creating oxygen vacancies artificially, one can improve the ferromagnetic and ferroelectric characteristics. To do that, the $Bi_2(Sn_{0.7}Fe_{0.3})_2O_{7-x}/Bi_2Fe_4O_9$ (BSFO/BFO) composite was synthesized, in which bismuth pyrostannate contains ~4% of oxygen vacancies.

The temperature dependence of the magnetic susceptibility of the BSFO/BFO composite measured in the ZFC mode and in a magnetic field of H = 600 Oe have anomalies in the temperature ranges of 30–40 K and 225–235 K (Fig. 1). The temperature dependence of the inverse magnetic susceptibility is nonlinear and does not obey the Curie-Weiss law over the entire temperature range. In the ZFC curve, the $1/\chi$ nonlinearity weakens. At a temperature of 5 K, the polycrystalline $Bi_2Fe_4O_9$

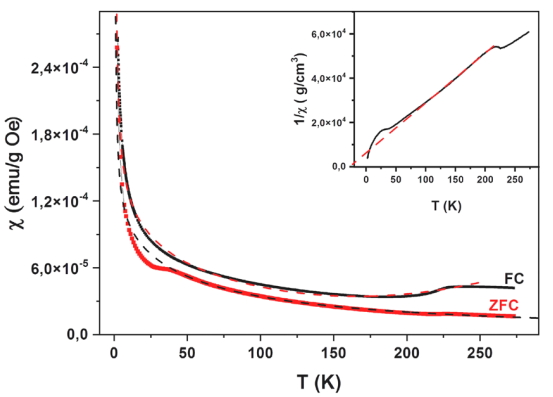

Figure 1. The temperature dependence of magnetic susceptibility of BSFO/BFO. Dashed lines corresponds to theoretical calculations of expressions

$$\chi = (1-x)\chi_2 + \chi_2 + \frac{xM_r}{H} = \frac{(1-x)C_2}{T-\theta} + \frac{C_1}{T} + \frac{xM_r}{H} \quad \text{and} \quad \chi = (1-x)\chi_2 + \chi_1 = \frac{(1-x)C_2}{T-\theta} + \frac{C_1}{T}.$$

Inset corresponds to the temperature dependence of the inverse susceptibility of BSFO/BFO.

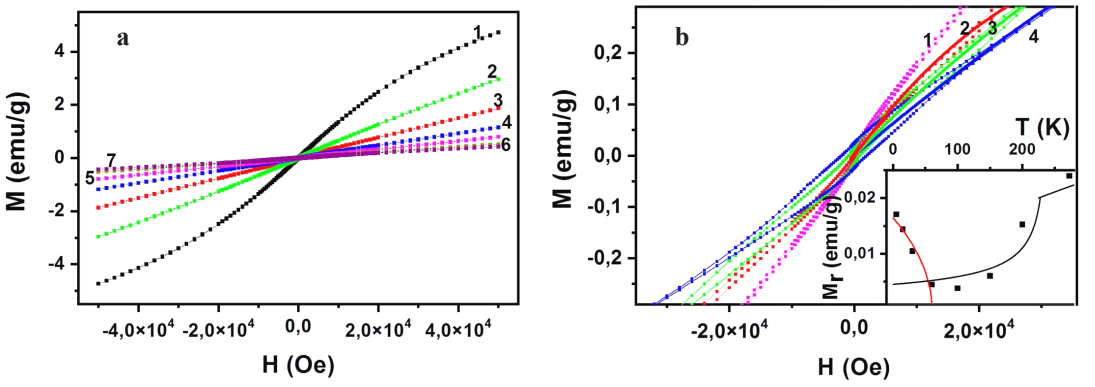

Figure 2. The field dependence of magnetization of BSFO/BFO at different temperature: **a** curve 1 corresponds to 5 K, 2 – 15 K, 3 – 30 K, 4 – 60 K, 5 – 100 K, 6 – 200 K, 7 – 273 K. **b** The field dependence of hysteresis magnetization. Curve 1 corresponds to 100 K, 2 – 150 K, 3 – 200 K, 4 – 273 K. Solid lines 2, 3, 4 show the theoretical calculations at temperatures 150, 200, 273 K. Inset **b**: the temperature dependence of remanence of magnetization

compound is a weak ferromagnet with canting of the magnetic moments of iron ions in the antiferromagnetic lattice [2]. The $\chi(T)$ anomaly at 225–235 K is caused by the magnetic phase transition of the $Bi_2Fe_4O_9$ compound from the antiferromagnetic to paramagnetic state.

Upon cooling in a strong magnetic field (H = 50 kOe), the weak ferromagnetic moments M_r of crystallites orient along the field. The paramagnetic contribution to the susceptibility is made by structural defects ($\chi_1 = C_1/T$) and bismuth stannate ($\chi_2 = C_2/(T - \theta)$). The resulting susceptibility of the BSFO/BFO composite is described by a fitting function with three parameters: the Curie temperature θ and the Curie-Weiss constants C_1 and C_2.

The ZFC magnetic susceptibility of the sample is lower by ~40% due to the absence of remanent magnetization. Figure 2 shows the field dependence of the magnetization, which is hysteretic at all temperatures. The hysteresis is symmetric about axes. The $M(H)$ dependence for the BSFO/BFO composite is convex and qualitatively differs from the field dependence of the magnetization of an antiferromagnet. Upon heating to T = 100 K, the remanent magnetization decreases by a factor of 4 and then increases by a factor of 6. At a temperature of T = 5 K, the remanent magnetization is M_r = 0.017 emu/g; at T = 273 K, M_r = 0.024 emu/g; and its minimum value is M_r = 0.0038 emu/g [3]. Upon heating, the coercivity increases from 200 Oe at T = 100 K to 2000 Oe at T = 273 K.

The above facts can be explained in the model of magnetic polarons in an antiferromagnetic matrix. The ferromagnetic microregion (the ferron radius) is determined by the competition between the kinetic energy of charge carriers and the exchange energy of localized spins. Below T_c = 60 K, a noncollinear arrangement of the sublattices with a weak ferromagnetic moment of M_{r0} = 0.018 emu/g is formed in mullite. In the molecular field approximation, the magnetization is described by the power function $M_r = M_{r0}(1 - T/T_c)^{0.5}$. This model satisfactorily describes the experimental data.

So the previously unknown temperature dependences of the magnetic hysteresis and remanent magnetization and the absence of magnetization saturation in mullite were determined. The impedance jump at the Néel temperature in mullite caused by the spin polaron-type conductivity was discovered. The remanent magnetization of mullite in the oxygen-deficient matrix is higher than the magnetization of polycrystalline $Bi_2Fe_4O_9$ by an order of magnitude.

1. J. Zhao, T. Liu, Y. Xu, Y. He, W. Chen, Mater. Chem. Phys. **128**, 388–391 (2011).
2. G. Alvarez, J. Contreras, A. Conde-Gallardo, H. Montiel, R. Zamorano, JMMM **348**, 17–21 (2013).
3. M. Pooladi, I. Sharifi, M. Behzadipour, Ceram. Int. **46**, 18453 (2020).

C.O2

ANTIFERROMAGNETIC STATE IN $(NO)M(NO_3)_3$ (M = Co, Ni)

O.S. Volkova[1,2]

[1]Lomonosov Moscow State University
[2]National University of Science and Technology MISiS
E-mail: CorrespondingAuthor@email

Two novel complex transition metal nitrates $(NO)M(NO_3)_3$ (M = Co, Ni) have been characterized in thermodynamic measurements. The structure of these compounds provides a unique opportunity for accommodation of Jahn-Teller cations with even number of electrons Co^{2+} ($3d^7$), and non-Jahn-Teller ones with odd number of electrons Ni^{2+} ($3d^8$), in similar crystallographic position. Transition metals may occupy two different crystallographic positions. The distances between transition metals within *ac*-plane are equal to 5.21/5.66 Å for nickel and 5.19/5.64 Å for cobalt compounds. While along *b*-axis transition metals are separated by 6.06 and 6.24 Å for nickel and cobalt, correspondingly. The Ni^{2+} ion with $S = 1$ may demonstrate both Ising- and Heisenberg-like behavior in various compounds [1]. The Co^{2+} ($S = 3/2$, $L = 1$) may act as highly anisotropic pseudo spin-1/2 cation and nowadays it is considered as promising candidate for low dimensional magnetism [2].

Both compounds order antiferromagnetically at $T_N^{Co} = 12.8$ K and $T_N^{Ni} = 23.8$ K. The single ion anisotropy of Co^{2+} and Ni^{2+} provides qualitatively different behavior under external magnetic field. The magnetization of cobalt nitrate demonstrates sharp metamagnetic transition at $B_M = 2.2$ T while the magnetization of nickel nitrate evidences smooth deflection at spin-flop transition BSF ~6 T. To gain microscopic understanding of the magnetic properties of $(NO)M(NO_3)_3$ the first principles density functional theory calculations have been performed providing values of the main exchange interaction parameters and single-ion anisotropy.

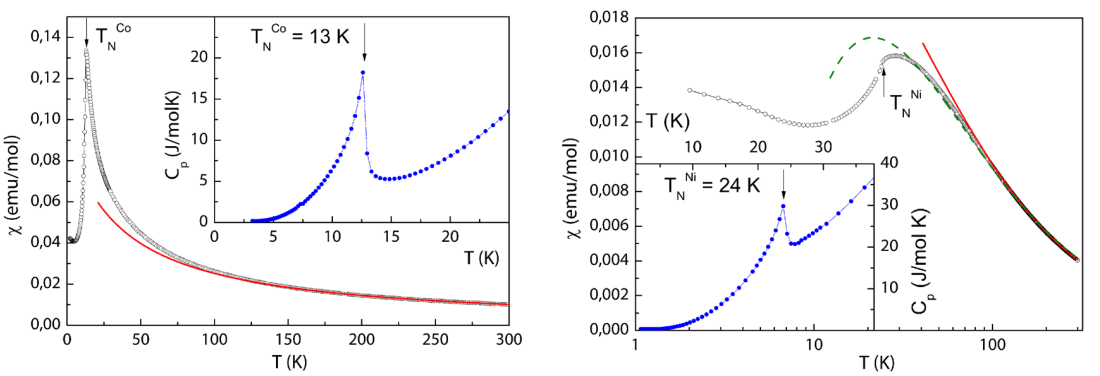

Figure. 1. The temperature dependences of magnetic susceptibility of $(NO)Co(NO_3)_3$(left panel) and $(NO)Ni(NO_3)_3$ (right panel). Solid lines are the Curie-Weiss fit. Dotted line is a fit with antiferromagnetic square lattice model. The insets represent temperature dependences of specific heat of same compounds. Arrows highlight the temperatures of antiferromagnetic ordering.

This work is supported by RSF grant No. 22-42-08002.

1. L.J. De Jongh, A.R. Miedema, Adv. Phys. **50**(8), 947–1170 (2001).
2. H. Liu, G. Khaliullin, Phys. Rev. B **97**, 014407 (2018).

C.O3

MAGNETOELECTRIC EFFECT IN FLEXIBLE COMPOSITE STRUCTURES CONTAINING MAGNETOACTIVE ELASTOMER

L.Y. Fetisov[1], *G. Glavan*[2], *V.O. Belan*[1], *I.A. Belyaeva*[2], *M. Shamonin*[2], *D.V. Saveliev*[1*]

[1]Scientific and Educational Center "Magnetoelectric materials and devices",
MIREA – Russian Technological University, Moscow, Russia
[2]East Bavarian Centre for Intelligent Materials (EBACIM), Ostbayerische Technische Hochschule (OTH) Regensburg, Regensburg, Germany
[*]E-mail: dimsav94@gmail.com

Magnetoelectric (ME) effect manifests itself as a change of polarization in external magnetic field. The effect in composite structures consisting of mechanically bonded piezoelectric (PE) and ferromagnetic (FM) layers arises due to combination of magnetostriction of FM layer and piezoelectricity in PE layer. The highest ME coefficients were obtained in structures with a highly magnetostrictive FM layer [1]. In this work, it is proposed to use magnetoactive elastomers (MAE) as an FM layer, which have high values of magnetodeformations, reaching tens of percent [2]. In the first works, in which MAEs were used as the FM layer, ME effects were observed in pulsed magnetic fields [3, 4]. In this work, the resonant ME effect is investigated. The influence of the MAE layer thickness on the resonance parameters and the magnitude of the ME voltage is shown.

Schematic view of the investigated ME composite structure is shown in Fig. 1. A composite structure based on piezopolymer PVDF (LDT0-028K, Measurement Specialties) was used as a PE layer. For better adhesion between PE and MAE layers a silicone-based adhesive was used. Then, MAE layers with dimensions 16.2×14.2 mm and different thicknesses changing from 0.85 to 4 mm were deposited on the PE surface. The manufacturing technology is described in [4, 5]. The structures were rigidly fixed inside the excitation coil, which created alternating magnetic field $h\cos(2\pi ft)$ with an amplitude h = 2.8 Oe. Bias magnetic field H up to 3 kOe was generated by an electromagnet. The frequency dependencies of ME voltages were measured. On this basis, ME voltage, resonant frequency and quality factor dependencies on magnetic field were obtained.

Figure 2 shows ME voltage dependence on frequency for sample with MAE thickness t = 0.85 mm, measured at H = 0.7 kOe. Two resonance peaks at frequencies $f_1 \approx 58$ Hz and $f_2 \approx 328$ Hz correspond to the lowest bending modes along structure's length and width, correspondingly. The value of ME

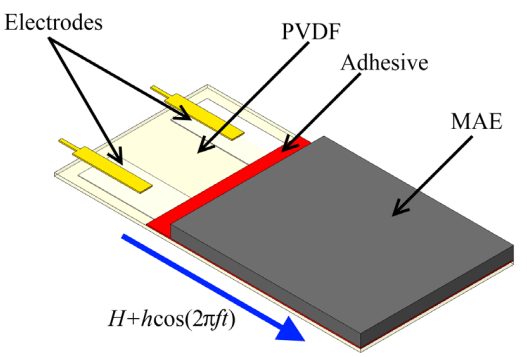

Figure 1. Schematic view of the ME composite structure.

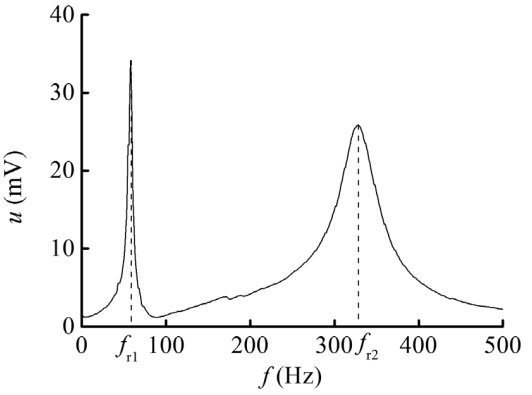

Figure 2. ME voltage dependence of a composite structure.

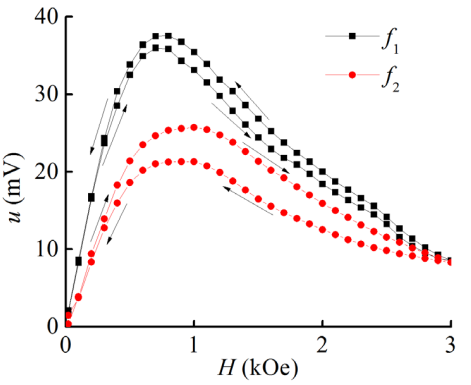

Figure 3. ME voltage dependencies on bias magnetic field at f_1 and f_2.

coefficients reached $\alpha_1 \approx 4.9$ V/(Oe·cm) and $\alpha_2 \approx 3.3$ V/(Oe·cm), correspondingly. An increase in the constant magnetic field led to a nonlinear increase in the resonance frequency of the structure as a result of the magnetorheological effect.

Figure 3 shows ME voltage at resonance frequency dependencies on bias magnetic field for the frequencies f_1 and f_2. The dependencies have a classical view [1]. It should be noted a hysteresis in the dependence of the ME voltage on the magnetic field. The hysteresis behavior in a magnetic field is characteristic of MAE and is caused by the influence of the prehistory of the sample on the distribution of magnetic particles in it [2].

Similar results were obtained for other composite structures. A decrease of the resonant frequencies f_1 and f_2 as well as the magnitude of the ME coefficients at frequency f_2 decreased with an increase of the MAE layer thickness were observed. At the same time, at frequency f_1 the highest value of ME coefficient was obtained for a sample with a MAE thickness of 1.93 mm and reached $\alpha \approx 6.2$ V/(Oe·cm).

Thus, the resonant ME effect in composite structures based on PVDF and a magnetoactive elastomer was investigated. The effect of the MAE layer thickness on the parameters of the ME effect is found. The highest ME coefficient was $\alpha \approx 6.2$ V/(Oe·cm).

This work was supported by the Russian Foundation of Basic Research, grant number 20-32-90-190 and the Deutsche Forschungsgemeinschaft (DFG, German Research Foundation), project number 466920132, The State Conference of Women and Equality Officers at Bavarian Universities (LaKoF Bayern).

1. C.W. Nan, M.I. Bichurin, S. Dong, D. Viehland, G. Srinivasan, J. Appl. Phys. **103**, 031101 (2011).
2. D.V. Saveliev, I.A. Belyaeva, D.V. Chashin, L.Y. Fetisov., D. Romeis., W. Kettl, E.Yu. Kramarenko, M. Saphiannikova., G.V. Stepanov, and M. Shamonin, Materials **13**(15), 3297 (2020).
3. L.A. Makarova, Yu.A. Alekhina, D.A. Isaev, M.F. Khairullin, N.S. Perov, J. Phys. D **54**, 015003 (2020).
4. G. Glavan, I.A. Belyaeva, K. Ruwisch, J. Wollschlager, and M. Shamonin, Sensors **21**(19), 6390 (2021).
5. I.A. Belyaeva, E.Y. Kramarenko, M. Shamonin, Polymer **127**, 119–128 (2017).

NEUTRON DIFFRACTION STUDIES OF HELICAL MAGNETIC ORDER IN CHIRAL $PbMnTeO_6$ WITH TRIANGULAR LATTICE

*A.I. Kurbakov**, *A.N. Korshunov*

NRC "Kurchatov Institute" – PNPI, Gatchina, Russia
*E-mail: kurbakov_ai@pnpi.nrcki.ru

Careful analysis of neutron diffraction data of the $PbMnTeO_6$ powder collected on a high-resolution diffractometer HRPT (PSI, Switzerland) unambiguously determined octahedral (trigonal antiprismatic) coordination for all cations within chiral space group P312 [1] in contrast to previously announced space group P-62m with trigonal prismatic coordination for all three atom species [2]. This result (Fig. 1) was obtained through the use of neutron diffraction, since both structural models have identical arrangement of cations and only differ in positions of oxygen, which was difficult to see by X-ray diffraction. The combination of a quasi-two-dimensional layered structure and triangular arrangement of Mn^{4+} magnetic ions leads to a complex magnetic system with a significant role of short-range correlations far above $T_N \sim 20$ K. All of the above makes $PbMnTeO_6$ a promising material with possible unique multiferroic properties. We traced the occurrence of long-range magnetic ordering in $PbMnTeO_6$ using a low-temperature neutron powder diffraction experiment on DMC diffractometer (PSI, Switzerland), which has a high angular resolution at low scattering angles, where magnetic scattering is mainly concentrated. Neutron diffraction data demonstrate an absence of any structural phase transition in $PbMnTeO_6$ between RT and 1.6 K and the appearance of additional reflections related to an antiferromagnetic long-range ordering below T_N. The presence of residual diffuse neutron scattering in the first magnetic peaks region is clearly visible above 15 K. Similar behavior is usually observed for low-dimensional systems where short-range spin correlations increase with transition temperature approaching. Processing of low-temperature neutron diffraction data shows that to describe a rather complex spin ordering in $PbMnTeO_6$, it is necessary to use two incommensurate modulations with respect to the triangular crystal system of magnetic ions Mn^{4+}, which are determined by the propagation vectors $\mathbf{k}_1$ and $\mathbf{k}_2$ (Fig. 2). The ob-

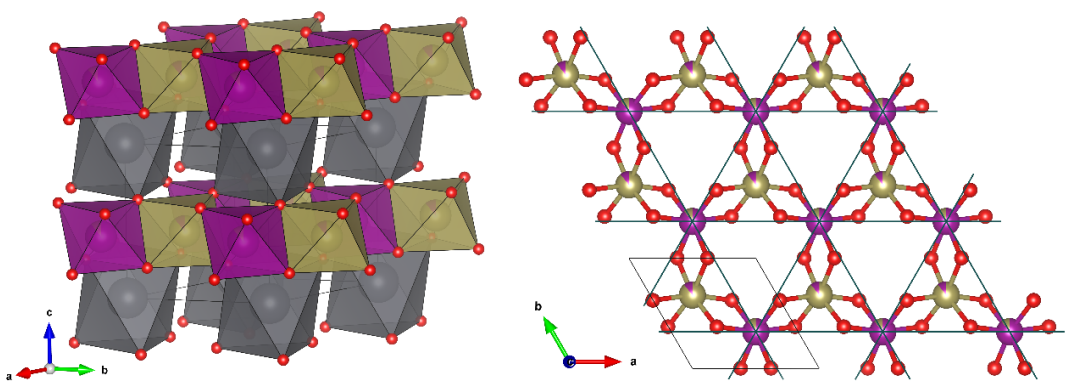

Figure 1. Refined crystal structure of $PbMnTeO_6$ at $T = 1.6$ K with the octahedral environment of oxygens (red balls). Purple, brown, and grey balls show the Mn, Te, and Pb sites respectively. The Mn^{4+} magnetic ions are forming triangular lattice in *ab*-layers. Mn/Te mixing at ~10% level is indicated as partial color filling of corresponding balls.

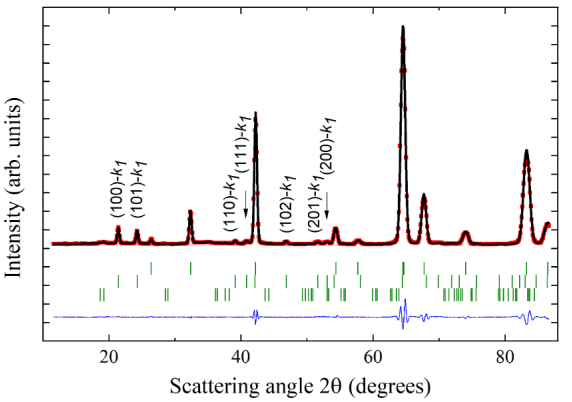

Figure 2. The refinement of the magnetic structure with propagation vector $\mathbf{k}_1$ = (1/3 1/3 0.4077) and irreducible representation Γ^2 (middle sequence of green ticks) and additional phase with propagation vector $\mathbf{k}_2$ = (1/3±δ_1 1/3±δ_1 0.15375±δ_2) (bottom sequence of green ticks). Indexation of the strongest magnetic Bragg peaks of the main magnetic phase is written.

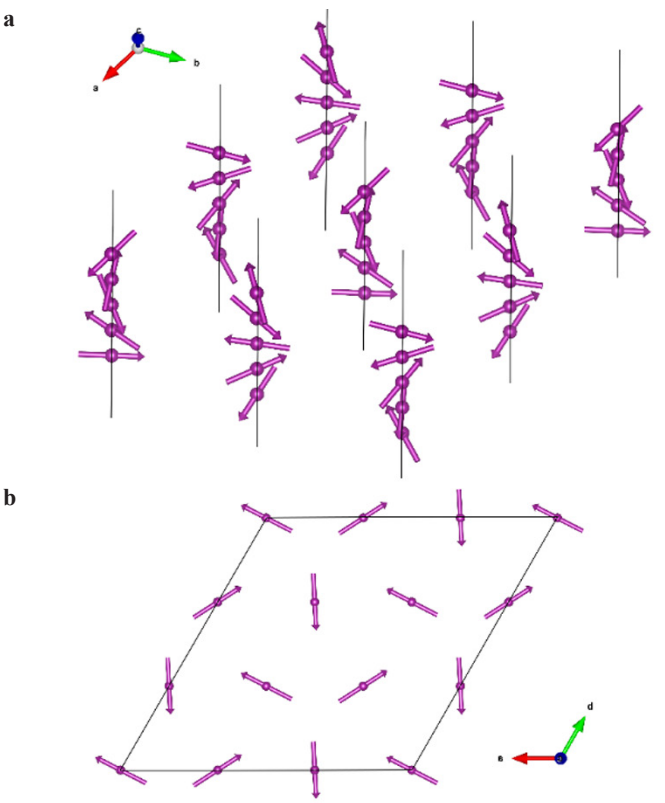

Figure 3. **a** General view of the spiral magnetic structure with propagation vector $\mathbf{k}_1$ = (1/3 1/3 0.4077) and irreducible representation Γ^2; **b** a separate *ab*-layer, forming a 120-degree spin ordering.

served result strongly indicates the complicated frustrated origin of spin ordering in $PbMnTeO_6$. The observed ground state presents a non-collinear 120-degree spin structure, that is helically modulated along the *c*-direction. The best agreement to the experimental data was obtained for the propagation vector $\mathbf{k}_1$ = (1/3 1/3 0.4077(2)), which corresponds to the commensurate magnetic unit cell in the *ab*-plane and a spiral ordering along the layers stacking direction with a characteristic period of spiral equal to ~13.2 Å (Fig. 3). Besides, we also observed the second incommensurate modulation for magnetic structure with the propagation vector $\mathbf{k}_2$ = ($1/3\pm\delta_1$ $1/3\pm\delta_1$ $0.15375\pm\delta_2$). An additional nontrivial magnetic contribution to the magnetic neutron scattering reflects the complex nature of the noncentrosymmetric chiral crystal structure.

Support by Russian Science Foundation according to the research projects № 18-12-00375 is acknowledged.

1. M.D. Kuchugura, A.I. Kurbakov, E.A. Zvereva et al., Dalton Trans. **48**, 17070–17077 (2019).
2. S.W. Kim, Zh. Deng, M.-R. Li, et al., Inorg. Chem. **55**, 1333−1338 (2016).

C.O5

MAGNETIC PROPERTIES OF QUASI-TWO-DIMENSIONAL OXYBORATES $(Ni,Cu,Mn)_3BO_5$ WITH DIFFERENT COMPOSITION OF Cu IONS

*S.N. Sofronova**, *E. Moshkina, E. Eremin, M. Molokeev*

L.V. Kirensky Institute of Physics FIC KSC SB RAS, Krasnoyarsk, Russian Federation
*E-mail: ssn@iph.krasn.ru

At present, the study of physical properties of magnetic quasi-low-dimensional compounds intensively developed. Oxyborates with ludwigites structure are the members of such type of compounds due to the presence of quasi-two-dimensional elements in their structure. The unit cell of ludwigites includes 4 non-equivalent positions which can be occupied by magnetic cations. The interesting effect such as the magnetization reversal is occur in $(Ni,Mn)_3BO_5$ [1].

In this work, single crystals of $(Ni,Cu,Mn)_3BO_5$ with different composition were synthesized by flux method, using the fluxes based on bismuth trimolybdat. Structural characterization of all samples was carried out using the X-ray diffraction method. The composition was refined by the EXAFS method. The results of refinement are presented in Table 1.

Table 1. Composition of different samples $(Ni,Cu,Mn)_3BO_5$.

Ion	Sample 1	Sample 2	Sample 3
Mn	1.04	1.06	1.22
Ni	1.85	1.73	1.57
Cu	0.11	0.21	0.21

The magnetic characterization of all samples was carried out. Magnetic transition in all samples occurs at the temperature below 75 K (Fig. 1a). *M-H* curves measured at 10 K are presented on Fig. 1b. Indirect exchange interactions calculation was held for the all compound $(Ni,Cu,Mn)_3BO_5$

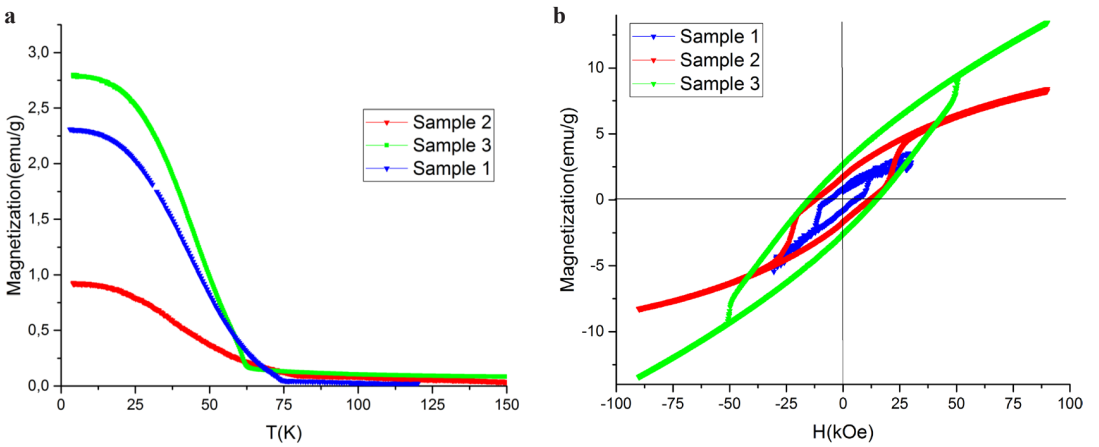

Figure 1. The temperature (**a**) and field (**b**) dependencies of magnetization of $(Ni,Cu,Mn)_3BO_5$.

in frameworks of the Anderson-Zavadskiy indirect exchange interactions model. Calculation results showed that ferromagnetic and antiferromagnetic interaction competition presents between ions in plane and ions connected planes.

The research was funded by RFBR, Krasnoyarsk Territory Krasnoyarsk Regional Fund of Science, project number 20-42-240011.

1. L.N. Bezmaternykh, E.M. Kolesnikova, E.V. Eremin et al., J. Magn. Magn. Mater. **364**, 55 (2014).

C.06

INFLUENCE INTERFACE THICKNESS TO THE EXCHANGE INTERACTION CONSTANT BETWEEN FERRO- AND ANTIFERROMAGNET

L.L. Afremov[1,2], *L.O. Brykin*[2*], *I.G. Iliushin*[1,2]

[1]Laboratory of Spin-Orbitronics, Institute of High Technologies and Advanced Materials, Far Eastern Federal University, Vladivostok, Russia
[2]Far Eastern Federal University, Vladivostok, Russia
[*]E-mail: afremov.ll@dvfu.ru

Abstract. In the "average spin" approximation, a system for determining the average magnetic moments of atoms in an extended interphase boundary between a ferromagnet and an antiferromagnet is constructed. The solution of the system of equations presented makes it possible to simulate the dependence of the interfacial exchange interaction constant on the temperature and thickness of the interface.

We generalize the model presented in [1, 2] To calculate the dependence of the interfacial exchange interaction energy on the width of the interface between a ferro- and antiferromagnetic. The following model was considered.

We use the interface of area s between a ferro- and an antiferromagnetic consisting of N_F ferromagnetic layers and N_{AF} layers of the antiferromagnetic with average values of the magnetic moments of atoms in the layers $\mu_{N_F} m_{N_F}(T)$, …, $\mu_1^F m_1^F(T)$, $\mu_1^{AF} m_1^{AF}(T)$, …, …, $\mu_{N_{AF}} m_{N_{AF}}(T)$. The magnetic moments $\mu_1^F m_1^F(T)$ и $\mu_1^{AF} m_1^{AF}(T)$ are located at the boundary between a ferromagnet and an antiferromagnet. For simplicity, we assume that the concentration of magnetic atoms n in the antiferromagnetic layer is given and there are z neighbors of the ferromagnet per such atom.

The energy of interfacial exchange interaction can be estimated as follows:

$$E_{ex} = -\alpha\mu_1^{(F)}\mu_1^{(AF)} znsd\left(m_1^{(F)}(T), m_1^{(AF)}(T)\right) = -\alpha\mu_1^{(F)}\mu_1^{(AF)} zndm_1^{(F)}(T)m_1^{(AF)}(T)\cos(\vartheta^{(F)} - \vartheta^{(AF)})s. \quad (1)$$

Here α – temperature-independent constant with the dimension of reciprocal volume, and d – distance between boundary ferromagnetic and antiferromagnetic layers, ϑ^F and ϑ^{AF} – angles defining the orientation of the average magnetic moments $\mu_1^F m_1^F$ and $\mu_1^{AF} m_1^{AF}$.

Let us compare (1) with the general expression for the exchange energy $E_{ex} = -2A_{in}\cos(\vartheta^{(1)} - \vartheta^{(2)})s/a_0$ [3]. We obtain the expression for the constant of interfacial exchange interaction:

$$A_{in}(T) = \frac{\alpha\mu_1\mu_2 znd^2}{2} m_1^{(F)}(T)m_1^{(AF)}(T) = Am_1^{(F)}(T)m_1^{(AF)}(T). \quad (2)$$

Here $A = \alpha\mu_1\mu_2 znd^2/2$. We use the equations obtained by the method of random interaction fields to estimate $m_1^F(T)$ and $m_1^{AF}(T)$, as well as in articles [1, 2]:

$$m_{N_F} = \sum_{k_1=0}^{z_{N_F,N_F}} \sum_{k_2=0}^{z_{N_F,N_F-1}} C_{z_{N_F,N_F}}^{k_1} C_{z_{N_F,N_F-1}}^{k_2} (1+m_{N_F})^{k_1} (1-m_{N_F})^{z_{N_F,N_F}-k_1} (1+m_{N_F-1})^{k_2} \frac{(1-m_{N_F-1})^{z_{z_{N_F,N_F-1}}-k_2}}{2^{z_{N_F,N_F}+z_{N_F,N_F-1}}}$$
$$\times \mathrm{th}\left(\frac{(2k_1 - z_{N_F,N_F}) + (2k_2 - z_{N_F,N_F-1})i_{N_F,N_F-1}}{t}\right), \quad (3)$$

$$m_n = \sum_{k_1=0}^{z_{n-1,n}} \sum_{k_2=0}^{z_{n,n}} \sum_{k_3=0}^{z_{n,n+1}} C_{z_{n,n-1}}^{k_1} C_{z_{n,n}}^{k_2} C_{z_{n,n+1}}^{k_3} (1+m_{n-1})^{k_1} (1-m_{n-1})^{z_{n-1,n}-k_1} (1+m_n)^{k_2} \times \frac{(1-m_n)^{z_{n,n}-k_2} (1+m_{n+1})^{k_3} (1-m_{n+1})^{z_{n,n+1}-k_3}}{2^{z_{n-1,n}+z_{n,n}+z_{n,n+1}}} \times \mathrm{th}\left(\frac{(2l_1-k_1)i_{n-1,n}+(2l_2-k_2)i_{n,n}+(2l_3-k_3)i_{n,n+1}}{t}\right), \quad (4)$$

$$m_{N_{\mathrm{AF}}} = \sum_{k_1=0}^{z_{N_{\mathrm{AF}}N_{\mathrm{AF}}}} \sum_{k_2=0}^{z_{N_{\mathrm{AF}}N_{\mathrm{AF}}-1}} C_{z_{N_{\mathrm{AF}}N_{\mathrm{AF}}}}^{k_1} C_{z_{N_{\mathrm{AF}}N_{\mathrm{AF}}-1}}^{k_2} \frac{(1+m_{N_{\mathrm{AF}}})^{k_1} (1-m_{N_{\mathrm{AF}}})^{z_{N_{\mathrm{AF}}N_{\mathrm{AF}}}-k_1}}{2^{z_{N_{\mathrm{AF}},N_{\mathrm{AF}}}+z_{N_{\mathrm{AF}},N_{\mathrm{AF}}-1}}} (1+m_{N_{\mathrm{AF}}-1})^{k_2} (1-m_{N_{\mathrm{AF}}-1})^{z_{N_{\mathrm{AF}},N_{\mathrm{AF}}-1}-k_2} \times \mathrm{th}\left(\frac{(2k_1-z_{N_{\mathrm{AF}},N_{\mathrm{AF}}})i_{N_{\mathrm{AF}},N_{\mathrm{AF}}}+(2k_2-z_{N_{\mathrm{AF}},N_{\mathrm{AF}}-1})i_{N_{\mathrm{AF}},N_{\mathrm{AF}}-1}}{t}\right). \quad (5)$$

Here in equations (3)–(5) $i_{n,n} = J_{n,n}m_{0n}/J_{N_F}m_{0N_F}$, $i_{n-1,n} = J_{n-1,n}m_{0n-1}/J_{N_F}m_{0NF}$, $i_{n,n+1} = J_{n,n+1}m_{0n+1}/J_{N_F}m_{0NF}$, $t = kT/J_{N_F}m_{0N_F}$, $z_{n,n}$, $J_{n,n}$ – the number of nearest neighbors and exchange interaction constants between atoms in the layer with number n, $z_{n\pm1,n}$ – the number of neighbors nearest to the k-th atom, located in the $(n \pm 1)$-layer, $J_{n\pm1,n}$ exchange interaction constant between atoms in neighboring monolayers, m_{0n} – the magnetic moment n-th atom.

The equations (3)–(5) make it possible to calculate the dependence of the interfacial exchange interaction constant on temperature and interface thickness.

This study was supported by the grant of the Russian Science Foundation project № 22-22-00492.

1. S. Anisimov, L. Afremov, A. Petrov, J. Magn. Magn. Mater. **500**, 166366 (2020).
2. S.V. Anisimov, L.L. Afremov and A.A. Petrov, J. Phys.: Conf. Series **138**, 012027 (2019).
3. J.-S. Yang, C.-R. Chang, J. Appl. Phys. **69**(11), 7756 (1991).

STRONG AND ULTRASTRONG PHOTON-MAGNON COUPLING OF SUPERCONDUCTING PLANAR RESONATORS WITH YIG CRYSTALS

M. Maksutoğlu[1], A. Ghirri[2], C. Bonizzoni[3], F. Yıldız[1], M. Affronte[2,3], B. Rameev[1,4,5]*

[1]Physics Department, Gebze Technical University, Gebze, Kocaeli, Turkey
[2]Istituto Nanoscienze-CNR, Modena, Italy
[3]Dipartimento FIM, Università di Modena e Reggio Emilia, Modena, Italy
[4]Zavoisky Physical-Technical Institute, FRC Kazan Scientific Center of RAS, Kazan, Russia
[5]Kazan State Power Engineering University, Kazan, Russian Federation
E-mail: mmaksutoglu@gtu.edu.tr

We present the results of photon-magnon coupling studies of Yttrium Iron Garnet (YIG) crystals with various planar superconducting (SC) resonators. Coupling strengths reaching the ultrastrong coupling regime have been obtained in the studies of various hybrid systems consisting of an MW resonator and YIG material in the form of thin film or bulk crystal. Two different resonator structures have been used, namely CoPlanar Waveguide (CPW) resonator and Inverse Anapole Resonator (IAR). Two versions of the CPW resonator have been used: a linear one and a meander-shaped CPW. The fundamental harmonic frequency for the linear resonator is around 9.4 GHz, while it is in the range of 0.9-2.4 GHz for the relatively longer meander resonators. The photon-magnon coupling between 5 microns thick YIG thin films grown on Gadolinium Gallium Garnet (GGG) substrate and the high order harmonics of the CPW resonators (up to 15 GHz) was analyzed by fitting the 2D transmission maps (S21 parameter as a function of frequency and magnetic field) with a theoretical model based on an input/output formalism. For these hybrid structures, photon-magnon coupling strengths reaching 2 GHz have been obtained, and this value is larger than 0.1 of the resonance frequency for many harmonics of CPW resonators. This means that the ultrastrong coupling regime has been achieved. We also studied the multi-mode strong and ultrastrong photon-magnon couplings of SC IARs with various shaped YIG bulk crystals. We have also obtained multi-mode strong photon-magnon couplings of magnetostatic modes of YIG microspheres with the IAR resonators at all resonance frequencies up to 15 GHz. In addition, ultrastrong coupling regimes have been achieved in the hybrid structures in the case of the IARs coupled to sub-mm-sized YIG prisms.

The results obtained for both hybrid structures have higher coupling strengths than YIG crystals of similar sizes in the literature. It has been shown that these structures have high prospects for many applications, including the detection of dark matter particles (axions) and quantum information/communication.

The work has been supported by the H2020-FETOPEN "Supergalax" project (grant agreement n. 863313) and by the SPS project No. G5859. M.M. also acknowledges the TUBITAK BIDEB for the support under 2219 Scholarship Program.

NEW SHORT-WAVELENGTH SPIN EXCITATIONS IN SPIN-1/2 ANTIFERROMAGNETS ON THE TRIANGULAR LATTICE

A.V. Syromyatnikov

National Research Center "Kurchatov Institute" B.P. Konstantinov Petersburg Nuclear Physics Institute, Gatchina, Russia
E-mail: asyromyatnikov@yandex.ru

In the modern theory of strongly correlated systems, many collective phenomena are described in terms of elementary excitations (quasi-particles). Therefore, the search for and characterization of elementary excitations is of fundamental importance. The interpretation of numerical and experimental data is largely based on the conclusions of existing analytical approaches that operate with suitable quasi-particles.

It can be said that today the properties of long-wavelength elementary excitations (magnons) in the ordered phases of quantum spin systems are well understood. However, more and more experimental and numerical evidence appear that in (quasi-)two-dimensional collinear and non-collinear quantum systems, standard analytical methods do not even qualitatively describe short-wavelength spin excitations. For example, in a series of recent experiments on inelastic neutron scattering carried out by three groups in $Ba_3CoSb_2O_9$, the complete inability was demonstrated of the standard theoretical approaches to the description of short-wavelength spin excitations in a Heisenberg antiferromagnet (HAF) with spin 1/2 on the triangular lattice [1–3]. In particular, at least four peaks can be distinguished in the scattering cross section at the boundary of the Brillouin zone, while, for example, the spin-wave theory predicts only two magnon peaks and a high-energy excitation continuum.

To eliminate this and a number of other gaps in the theory, we have recently proposed and tested on a number of systems a new method based on the cluster representation of spin operators 1/2 in terms of Bose operators [4–7]. This approach is very close in spirit to the standard spin-wave theory, but it more accurately takes into account short-range spin correlations and makes it possible, along with magnons, to quite easily study high-energy excitations that arise in the standard spin-wave theory as bound states of several magnons.

The method is based on the idea of expanding the unit cell in order to take into account all the spin degrees of freedom in it. The proposed cluster spin representation contains not one Bose operator, as the well-known Holstein-Primakoff representation for one spin, but several Bose operators, each of which creates or annihilates one of the quantum states of the entire unit cell. We emphasize that such a representation reproduces the commutation algebra of all spin operators in the unit cell. [4] In addition, it contains a formal parameter n, the maximum number of bosons that can occupy a unit cell. This parameter plays the same role in the cluster representation as the value of the spin S in the Holstein-Primakoff representation: all observable quantities can be represented as series in $1/n$, which are found using the standard diagram technique. Of course, the value of such an approach may seem doubtful, since the physical results correspond to the case of $n = 1$ (however, the value of the spin-wave theory, which operates with $1/S$ series at $S \sim 1$, should also seem low from the same considerations). However, a comparison of the results obtained by our method with numerous results of numerical calculations performed earlier in simple models showed that the series for the observables in $1/n$ converge surprisingly quickly: often, the first terms of the series in $1/n$ are enough to obtain quantitative agreement with the numerical results.

We present the results of [7], in which we used a three-spin version of the cluster spin representation proposed in [4] (for three spins in the magnetic unit cell) to study HAF on the triangular

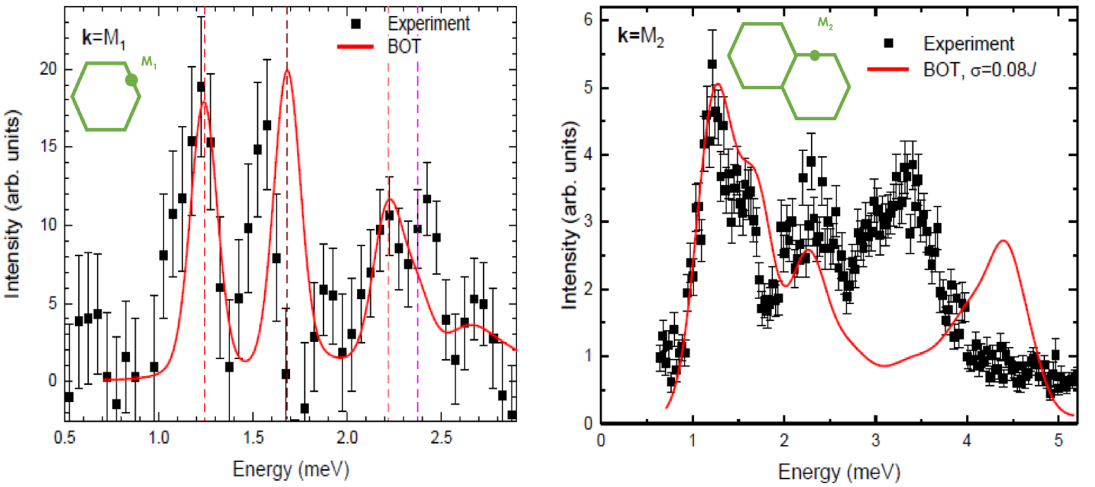

Figure 1. Neutron data obtained in $Ba_3CoSb_2O_9$ at points M on the boundary of the Brillouin zone in [1] (left) and, with a lower resolution, but in a larger energy range, [2] (right). This compound is well described by the model of spin-1/2 HAF on the triangular lattice. Spin-wave theory cannot explain these experimental results even qualitatively. On the contrary, our approach describes these experiments well (red line on the graphs): it can be said that the agreement is quantitative at $\omega < 2.4$ meV and qualitative at large ω.

lattice. This gives rise to seven Bose operators, three of which correspond to ordinary magnons. Our calculations have successfully reproduced the 120-degree structure of the magnetic moments in the ground state, and the magnetization of the three magnetic sublattices, found in the first order in $1/n$, is in excellent agreement with previous numerical results. Our calculations of dynamical spin correlators have shown that quantum fluctuations remove the degeneracy of the magnon spectrum along certain directions in the Brillouin zone and lead to the appearance of a new quasi-particle. We have also demonstrated the appearance of new high-energy well-defined quasi-particles built on the excited states of the magnetic unit cell, which give a distinct anomaly at high energies in the neutron spectra. These conclusions are in good agreement with the results of recent neutron studies (see Fig. 1).

Support by RSF grant № 22-22-00028 is acknowledged.

1. J. Ma et al., Phys. Rev. Lett. **116**, 087201 (2016).
2. S. Ito, N. Kurita, H. Tanaka et al., Nature Commun. **8**, 235 (2017).
3. D. Macdougal, S. Williams, D. Prabhakaran et al., Phys. Rev. B **102**, 064421 (2020).
4. A.V. Syromyatnikov, Phys. Rev. B **98**, 184421 (2018).
5. A.V. Syromyatnikov and A.Yu. Aktersky, Phys. Rev. B **99**, 224402 (2019).
6. A.V. Syromyatnikov, Phys. Rev. B **102**, 014409 (2020).
7. A.V. Syromyatnikov, arXiv:2107.00256, to appear in Phys. Rev. B.

INFLUENCE OF INTERFACIAL EXCHANGE INTERACTION ON THE METASTABILITY OF MAGNETIC STATES OF CORE-SHELL NANOPARTICLES

L.L. Afremov[1,2], *I.G. Iliushin*[*1,2], *V.N. Kharitonov*[1,2]

[1]Laboratory of Spin-Orbitronics, Institute of High Technologies and Advanced Materials, Far Eastern Federal University, Vladivostok, Russia
[2]Institute of High Technologies and Advanced Materials, Far Eastern Federal University.
[*]E-mail: iliushin.ig@dvfu.ru

In this article, we present the model of core/shell nanoparticle with random orientation of the axes of magnetic anisotropy of magnetic phases. The resulting expression for the total energy makes it possible to study the effect of geometric parameters (phase size, its elongation, and orientation long axes) and interfacial exchange interaction on the metastability of magnetic states core/shell nanoparticles.

Model of core/shell nanoparticle. We will use the model described in detail in [1]. The main features of this model are as follows:

- We consider a uniformly magnetised ellipsoidal nanoparticle (phase (1)) of volume V with an elongation Q and minor semiaxis B containing a uniformly magnetised ellipsoidal core (phase (2)) of volume $v = \varepsilon V$ and elongation q and minor semiaxis b. The long axes of both phases are oriented along the axis Oz (see Fig. 1).
- We assume the crystallographic anisotropy axes to be parallel to the long axes of the ferromagnetic nanoparticle and the core.
- The spontaneous magnetisation vectors of both phases $\mathbf{M}_s^{(1)}$ and $\mathbf{M}_s^{(2)}$ are located in the plane xOz containing the long axes of the magnetic phases and make the angles $\vartheta^{(1)}$ and $\vartheta^{(2)}$ with the axis Oz, respectively.
- An external magnetic field $\mathbf{H}$ is applied along the axis Oz.

The assumption that the distribution of the magnetic moment is uniform in the shell leads to a limitation of its thickness. The shell thickness cannot be greater than the width of the domain wall.

Results and discussions. The energy of a nanoparticle E located in an external field H can be represented as the sums of the energy crystallographic anisotropy E_A, the energy of the demag-

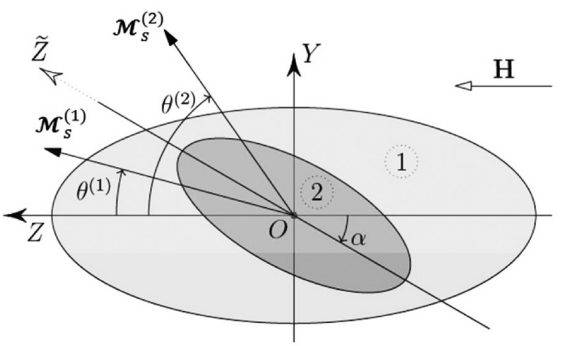

Figure 1. Model of core/shell nanoparticle.

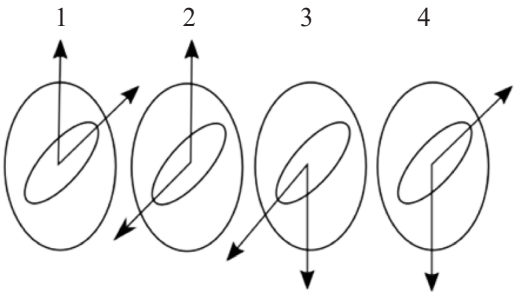

Figure 2. Illustration of equilibrium states of core/shell nanoparticles.

netizing field E_m, the energy of interfacial exchange interaction E_{ex}, and the Zeeman energy E_H: $E = E_A + E_m + E_{ex} + E_H$ [2].

Energy minimization E with respect to $\vartheta^{(1)}$ and $\vartheta^{(2)}$ together with the minimum conditions leads to a system of equations that allows one to determine the ground and metastable states of the magnetic moments of the nanoparticle phases.

The core/shell equilibrium states of nanoparticles have been : in the first "(↖↗)-state", the magnetic moments of both phases form sharp ($-\pi/2 < \vartheta^{(1)} < \pi/2$, $-\pi/2 < \vartheta^{(2)} < \pi/2$) with the O$z$-axis; in the second "(↗↘)-state", the magnetic moments of the core and the shell form the angles ($-\pi/2 < \vartheta(1) < \pi/2$, $-3\pi/2 < \vartheta(2) < \pi/2$) ; the third "(↙↘)-" and the fourth "(↙↖)-" states are the inverse of the first and second, respectively (see Fig. 2).

We used the diagram $\{b, q\}$, each point of which is associated with a nanoparticle (with given values B and Q) containing a core with semi-minor axis b and elongation q (see Fig. 3). The dot nanoparticles are fell into the dark region can be in one of the four basic or metastable states listed above. The light area corresponds to nanoparticles in basic equilibrium states.

This study was supported by the grant of the Russian Science Foundation project № 22-22-00492.

1. G.C. Lavorato, E. Lima Jr, D. Tobia, D. Fiorani, H.E. Troiani, R.D. Zysler, E.L. Winkler, Nanotechnology **25**, 355704 (2014).
2. L. Afremov, S. Anisimov, I. Iliushin. J. Magn. Magn. Mater. **447**, 88–95 (2018).

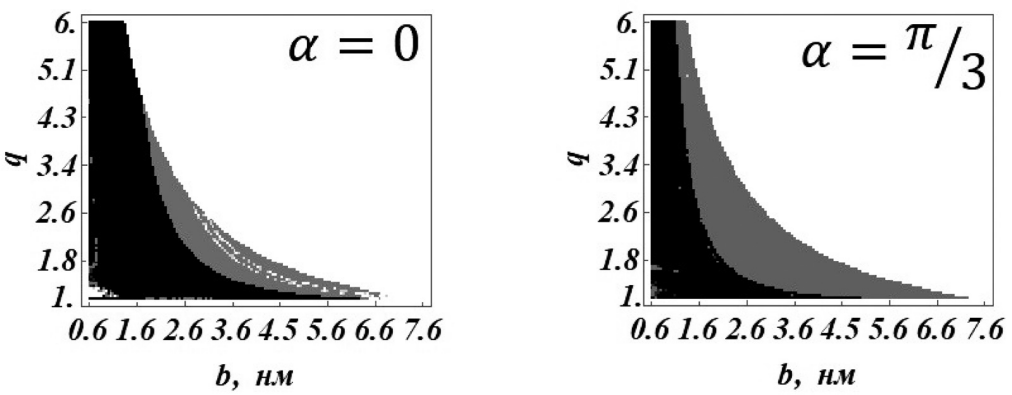

Figure 3. Diagrams $\{b, q\}$ of magnetic states of nanoparticles Fe_3O_4-$Fe_{2.44}Ti_{0.56}O_4$ for different angles α between the long axes of the cores and nanoparticle.

AGING EFFECTS IN CRITICAL BEHAVIOR OF HEISENBERG ANISOTROPIC ULTRATHIN FILMS

M.A. Shlyakhtich[1,2*], *P.V. Prudnikov*[2]

[1]Department of Theoretical Physics and Wave Phenomena, Siberian Federal University, Krasnoyarsk, Russia
[2]Department of Theoretical Physics, Dostoevsky Omsk State University, Omsk, Russia
[*]E-mail: mshlyakhtich@sfu-kras.ru

Statistical systems with slow dynamics have recently attracted considerable theoretical and experimental interest, in view of the rich scenario of phenomena they display: dramatic slowing down of relaxation processes, memory effects, etc. After a perturbation a system with slow dynamics does not generically achieve equilibrium even after long times and its dynamics is not invariant either under time translations or under time reversal, as it should be in thermal equilibrium. During this never-ending relaxation ageing occurs: two-time quantities such as response and correlation functions depend on the two times t_w and $t > t_w$ not via $t \to t_w$ only and their decays as functions of t are slower for larger t_w. At variance with one-time quantities (e.g. the order parameter) – converging to asymptotic values in the long-time limit – two-time quantities clearly bear the signature of ageing.

In the spin system the critical slowing down, i.e. an increase of the autocorrelation time τ_{cor} as the critical point T_c is approached, is governed by the universal dynamical critical exponent z: $\tau \sim |T - T_c|^{-\nu z}$, with the correlation length critical exponent ν.

Autocorrelation function clear demonstrates the presence of the three characteristics regimes: quasi-equilibrium regime at times $(t - t_w) << t_w$ and non-equilibrium regime at times $(t - t_w) >> t_w$. At times $(t - t_w) \sim t_w$ there is a crossover regime with the dependence of correlation characteristics of the waiting time.

In this work we study the ferromagnetic thin film with Heisenberg hamiltonian

$$\mathscr{H} = -J\sum_{ij} [(1 - \Delta)(S_i^x S_j^x + S_i^y S_j^y) + S_i^z S_j^z],$$

where (S_i^x, S_i^y, S_i^z) is a unit vector in the direction of the classical magnetic moment at lattice site i; $J > 0$ – ferromagnetic exchange constant; Δ characterizes the amount of anisotropy; $\Delta = 0$ corresponds to the isotropic Heisenberg case; $\Delta = 1$ – the Ising case. Periodic and free boundary conditions are used for the in-plane and out-plane directions, respectively.

The effective anisotropy constant Δ [1, 2] as a function of film thickness N was chosen from experimental studies of the Curie temperature T_c for thin films of Ni(111)/W(110) [3] with different thicknesses of Ni film.

The simulations were carried out for systems of size $N_s = L \times L \times N$, where N is number of layers and L is linear size of layer. We used the Metropolis algorithm for updating spin configurations. Simulation was carry out at critical temperature $T_c = 1.15$ K for $N = 3$, $T_c = 1.31$ K for $N = 5$, $T_c = 1.39$ K for $N = 7$ [1, 2, 4] and different initial state $m_0 = 1$, $m_0 = 0.0001$. Data for autocorrelation function $C(t, t_w)$ are presented in Fig. 1a. This data are plotted over against the time difference $t - t_w$ are displayed for the Heisenberg thin film with $N = 3$ for different values of the waiting time $t_w = 200, 100, 70, 50, 20, 0$.

In order to estimate correlation time of our systems we calculate dimensionless dynamic correlation function $R(t, t_w)$ [5] for different film thickness $N = 3, 5, 7$ and for different waiting time $t_w = 20, 50, 70, 100, 200$. Time dependencies of dimensionless dynamic correlation function $R(t, t_w)$ are presented in Fig. 1b. At times large enough $R(t, t_w)$ decays exponentially: $R(t, t_w) \sim \exp(-t/\tau_{cor})$.

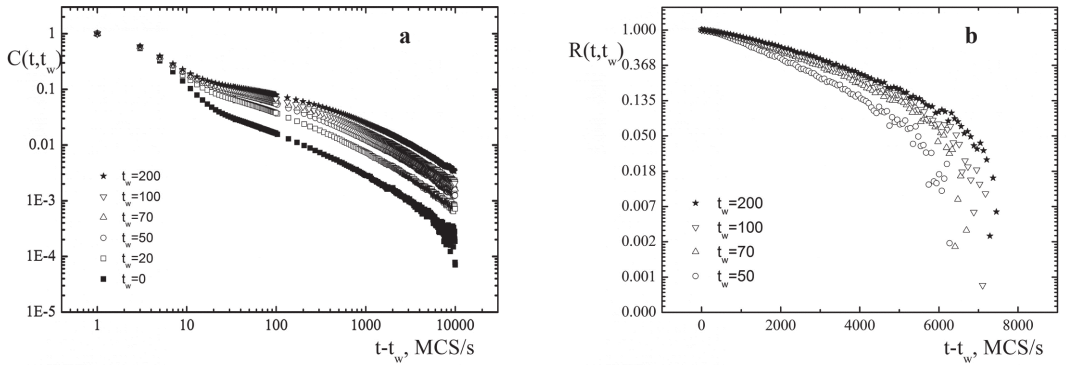

Figure 1. Time dependencies of autocorrelation function $C(t, t_w)$ (**a**) and dimensionless dynamic correlation function $R(t, t_w)$ (**b**) for film with thickness $N = 3$ for different values of the waiting time $t_w = 200$, 100, 70, 50, 20, 0.

Value of autocorrelation time demonstrate existence of aging effect in our system. The increasing of system age t_w lead to increasing of value τ_{cor}. Values of autocorrelation time presented in the Table 1 for different thickness and waiting time.

Table 1. Values of autocorrelation time.

N	$t_w = 50$	$t_w = 70$	$t_w = 100$	$t_w = 200$
3	2255(47)	2704(5)	2835(6)	3039(8)
5	1858(3)	2326(3)	2398(4)	2626(4)
7	1498(2)	1987(3)	2074(3)	2237(4)

The study was carried out with the financial support of the Ministry of Education and Science of the Russian Federation (agreement 0741-2020-0002) and grant MD-2229.2020.2 of the President of the Russian Federation. The computational research was supported in through resources provided by the Shared Services Center "Data Center of FEB RAS" (Khabarovsk) [6].

1. P.V. Prudnikov, V.V. Prundikov, M.A. Medvedeva, JETP Lett. **100**, 501 (2014).
2. P.V. Prudnikov, M.A. Menshikova et al., J. Magn. Magn. Mater. **387**, 77 (2015).
3. Y. Li, K. Baberschke, Phys. Rev. Lett. **68**, 1208 (1992).
4. M.A. Medvedeva, P.V. Prudnikov, J. Phys.: Conf. Ser. **510**, 012024 (2014).
5. R.N. Bhatt, A.P. Young, EPL **20**, 59 (1992).
6. A.A. Sorokin, S.V. Makogonov, S.P. Korolev, Sci. Tech. Inform. Process. **44**, 302 (2017).

MAGNETIC AND TEMPERATURE PROPERTIES OF LUDWIGITE $Mn_{1.17}CO_{1.83}BO_5$

D.V. Popov[1*], *T.P. Gavrilova*[1], *I.V. Yatsyk*[1], *M.A. Cherosov*[3], *E.M. Moshkina*[2], *V.A. Shustov*[1], *R.M. Eremina*[1]

[1]Zavoisky Physical-Technical Institute, FRC Kazan Scientific Center of RAS, Kazan, Russia
[2]Kirensky Institute of Physics, Federal Research Center KSC SB RAS, Krasnoyarsk, Russia
[3]Institute of Physics, Kazan Federal University, Kazan, Russia
[*]E-mail: kazan-city.dvpopoff@yandex.ru

Ludwigites are oxyborates with structural formula $(M^{2+})_2(M^{3+})BO_5$, with (M^{2+}) and (M^{3+}) being metallic ions of corresponding valence. These metallic ions create zigzag walls in crystal structure with four non-equivalent positions for them, therefore producing unusual magnetic properties, such as random magnetic ions distribution, mixed valence, strong electronic correlations, uncommon charge ordering, etc. Bimagnetic ludwigites are of particular interest, since one can easily observe evolution of said properties in dependence of relative concentrations of magnetic ions [1–3].

The aim of this work is investigation of magnetic properties of $Mn_{1.17}Co_{1.83}BO_5$ ludwigite. X-ray diffraction analyses were performed using DRON-7 diffractometer. Crystallographic unit parameters were obtained. Crystal has Pbam space group with a = 9.2039(9) Å, b = 12.4944(9) Å, and c = 3.0732(2) Å. Diffractograms were fitted using Rietveld method.

Magnetization dependences from temperature and external magnetic field were measured using PPMS-9 device in Kazan Federal University. Temperature dependences of magnetization were measured in zero-field cooling (ZFC) and field cooling (FC) modes at range 2–300 K. A magnetic transition was obtained at T = 43.9 K in this compound. Most likely this is ferrimagnetic transition. Magnetization dependences from external magnetic field were measured in fields up to 9 T. Hysteresis loops were obtained at temperatures below 50 K in this ludwigite along a- and b-axis. In addition, specific heat measurements were made, using the same device. One Debye and three Einstein terms were obtained via approximation with temperatures: θ_D = 165 K, θ_{E1} = 270 K, θ_{E2} = 620 K, θ_{E3} = 1650 K and α ratio being $\alpha_D:\alpha_{E1}:\alpha_{E2}:\alpha_{E3}$ = 0.92:2.04:3.02:3.02. Figure 1 shows measured and approximated lines for specific heat temperature dependences. The magnetic contri-

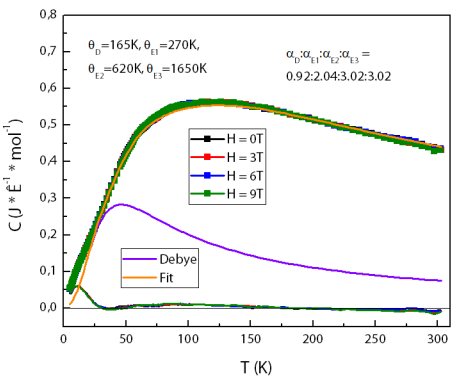

Figure 1. Specific heat temperature dependences for $Mn_{1.17}Co_{1.83}BO_5$. Lines show difference between experiment and fit data.

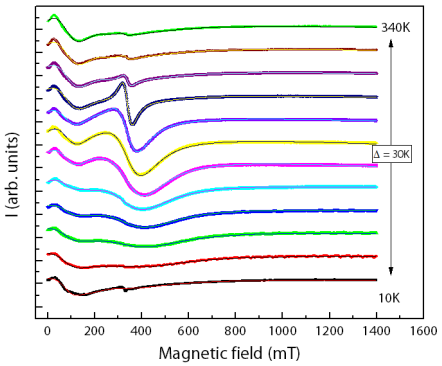

Figure 2. ESR spectra for $Mn_{1.17}Co_{1.83}BO_5$.

bution to the specific heat was obtained after subtracting the lattice contribution. The maximum magnetic contribution is observed at 12 K.

EPR-spectra were also measured using a Bruker spectrometer. Figure 2 shows obtained ESR-spectra in $Mn_{1.17}Co_{1.83}BO_5$ ludwigite. The measurements were performed at temperature range from 5 to 340 K. Spectra were approximated using three Lorentz lines. With these measurements several points of interest were obtained at temperatures 50, 100 and 250 K. It is possible, that these points mark different phase and structural transitions.

Electron spin resonance measurements were performed with the financial support from the government assignment for FRC Kazan Scientific Center of RAS.

1. D.V. Popov et al., J. Phys. Chem. Solids **148**, 109695 (2021).
2. D.C. Freitas et al., Phys. Rev. B **94**, 174409 (2016).
3. M.A.V. Heringer et al., Phys. Rev. Mat. **4**, 064412 (2020).

INVESTIGATION OF THE INFLUENCE OF COMPOSITION ON THE MAGNETIC BEHAVIOR OF Cu/Co SEGMENTED NANOWIRES FOR APPLICATION AS 3D MEMORY ELEMENTS

V.N. Kharitonov[1], *A.Yu. Samardak*[1], *M. Yu. Pavliuk*[1], *E.V. Tepnin*[1], *D.R. Khairetdinova*[2,3], *I.M. Doludenko*[2], *A.S. Samardak*[1], *A.V. Ognev*[1]

[1]Far Eastern Federal University, FEFU
[2]Federal State Institution "Federal Research Center "Crystallography and Photonics" of the Russian Academy of Sciences
[3]Moscow Steel and Alloys Institute
*E-mail: kharitonov.vn@dvfu.ru

One-dimensional metallic nanowires (NWs) have drawn scientific attention due to a broad spectrum of their possible applications in biomedicine, energy storage, optoelectronics, and nanomagnetism [1]. Multisegmented NWs possess even more exotic behavior due to the alternation along the length of parts from different elements and the possibility of combining effects from the each elements or due their interactions. Ferromagnetic segmented NWs has the unique magnetic properties [2] and can be used as high-density 3D magnetic memory devices [3], as agents for cancer therapies [4] and for various biomedical applications [5].

In this work, we present study of magnetic properties of segmented Cu/Co NWs electrodeposited in porous track membranes, with different lengths of nonmagnetic Cu spacer between ferromagnetic Co segments.

Porous membranes used as templates for the growth of segmented nanowires. The templates within cylindrical channels were made by bombarding the surface of the polymer film by high-energy krypton ions, which penetrate the polymer membrane through. Diameter of pores can be controlled by dissolution of the polymer film in the range of 5–1000 nm. After covering one side of the template with conducting layer, electrodeposition method can be implemented to grow nanostructures with geometries defined by the porous template. The image of a porous template for electrodeposition of nanowires is shown in Figure 1.

Segmented (or layered) one-dimensional nanostructures can be obtained using the single-bath electrodeposition method. In this method the elemental composition of corresponding segments can be regulated by the current density in electrochemical cell: the ferromagnetic segments synthesized

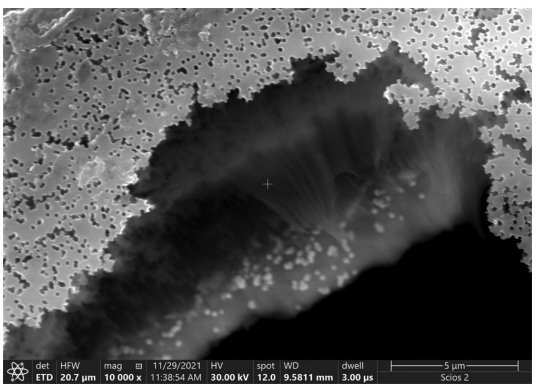

Figure 1. The image of a porous template.

by high current densities and nonmagnetic – by low current densities. The electrolyte with Co and Cu ions was used in this work. The length of the segments was controlled by the time of impulses with corresponding current density. The size of the ferromagnetic part of the wires was 200 nm while the size of the non-magnetic parts were 20, 50 or 200 nm. Scanning electron microscopy study showed that porous matrix does not have a long-range order, and the distance between the pores varies from 50 to 500 nm, with median diameter D = 100 nm. Random distribution of pores formed agglomerates which can be filled with ferromagnetic material and influence the magnetic behavior of whole array.

The magnetic properties of all samples were studied using LakeShore VSM 7410 vibrating magnetometer in the range of external magnetic fields from –7 to 7 kOe. Integral hysteresis loops for sample with 50 nm Cu segment length showed the coercive force in both directions of the field H_c = 200 Oe, and the ratio of remnant magnetization to saturation magnetization m_r/m_s = 0.12 and 0.04 for the longitudinal and transverse directions of the field, respectively. With an increase in the length of the Cu segment to 200 nm, the coercive force of the sample sharply increases in the longitudinal direction of the field up to H_c = 350 Oe, together with the value of m_r/m_s increasing to 0.24 and remains unchanged in the transverse direction. This effect can be associated with the weakening of dipole interaction between segments in one wire, which leads to an increase in the energy of the external field required to switch individual nanowires in the array. For analysis of coercive forces and interaction fields distributions in samples First Order Reversal Curves (FORC) measurements were implemented.

To analyze the possible micromagnetic configurations in NWs the simulations in MuMAX3 package were implemented. The magnetic parameters were set as for bulk Co with a 10% correction for the polycrystalline structure and the possible presence of impurities in the composition of the nanowires. To obtain a reliable model, the simulation results were compared with experimental data. The magnetic hysteresis loops obtained by micromagnetic modeling were compared with experimental data and showed good agreement between the developed model and the samples under study. Simulation in remanent state revealed vortex configuration of micromagnetic structure, deformed by influence of magnetocrystalline anisotropy and magnetostatic interactions between the segments and NWs in the array.

We acknowledge the Russian Ministry of Science and Higher Education for state support of scientific research conducted under the supervision of leading scientists in the Russian Institution of Higher Education, scientific foundation, and state research centers (Project No. 075-15-2021-607) and the state task (Project No. 0657-2020-0013). The sample growth was supported by State Task of FRSC "Crystallography and photonics" of RAS.

1. Y.J. Xia, K. Sun and J.Y. Ouyang, Adv Mater. **24**(18), 2436–2440 (2012).
2. S. Moraes, D. Navas, F. Beron, M.P. Proenca, K.R. Pirota, C.T. Sousa and J.P. Araujo, Nanomaterials-Basel **8**(7) (2018).
3. S. Bochmann, A. Fernandez-Pacheco, M. Mackovic, A. Neff, K.R. Siefermann, E. Spiecker, R.P. Cowburn, and J. Bachmann, Rsc Adv. **7**(60), 37627 (2017).
4. Z. Nemati, J. Urn, M.R.Z. Kouhpanji, F. Zhou, T. Gage, D. Shore, K. Makielski, A. Donnelly and J. Alonso, Acs Appl. Nano. Mater. **3**(2), 2058–2069 (2020).
5. H.J. Jung, Y. Kim, H. Hong, J. Shin, M.J. Ko, H.S. Ko, T. Kim, J.H. Moon, J.J. Song, V.P. Dravid, Y.K. Kim and H. Kang, Nano. Lett. **20**(10), 7272–7280 (2020).

MONTE CARLO SIMULATION OF A PHASE TRANSITION IN A QUASI-ONE-DIMENSIONAL MULTIFERRROIC ON A SUBSTRATE

*I.V. Bychkov, I.V. Maltsev**

Chelyabinsk State University, Chelyabinsk, Russia
*E-mail: malts_iv@mail.ru

We present a theoretical study of the substrate influence on the critical behavior of a one-dimensional multiferroic. We used Ca_3CoMnO_6 as a model multiferroic. The one-dimensional Ising model with axial next-nearest neighbor interactions (ANNNI model) was used in the simulation. The study was performed using Monte Carlo simulation with the standard Metropolis algorithm. The periodic Frenkel-Kontorova potential modeling the effect of the substrate.

Ca_3CoMnO_6 consists of $CoMnO_6$ parallel chains separated by Ca^{2+} ions. Interactions within $CoMnO_6$ chains are much stronger than interactions between chains, so the Ca_3CoMnO_6 composite can be described by the one-dimensional ANNNI model with competing ferromagnetic and antiferromagnetic interactions. Competitive interaction parameter $|J_{AF}/J_{FM}| > 1/2$ for this substance, so the ground state of the magnetic lattice is up-up-down-down [1]. The magnetoelectric interaction leads to a reduction in the distance between parallel spins and an increase in the distance between antiparallel ones. As a result, an electrical polarization occurs along the $CoMnO_6$ chain. The appearance of ferroelectricity because of changing Co-Mn distances and up-up-down-down magnetic ordering was confirmed using the density functional theory and first-principles *ab initio* calculation of the electronic structure [2, 3]. Choi and colleagues [4] experimentally found the appearance of ferroelectricity in the $Ca_3Co_{2-x}MnO_6$ crystal ($x = 0.96$).

The Hamiltonian of the system under study is as follows:

$$\mathscr{H} = -\sum_{i,j} J_{FM}(r_{ij}) S_i S_j - \sum_{[i,k]}^{Mn} J_{AF_{Mn}} S_i S_j - \sum_{[i,k]}^{Co} J_{AF_{Co}}(r_{ij}) S_i S_j - hg\mu_B \sum_i S_i$$
$$-E\sum_i q d_i + \frac{1}{2} k \sum_i d_i^2 - a_{FK} \sum_i \cos\left(\frac{2\pi(i+d_i)}{b_{FK}}\right),$$

where the first three terms describe the competing ferromagnetic and antiferromagnetic interactions, the fourth and fifth terms are the energies of the magnetic and electric fields, respectively, the sixth term is the elastic energy, and the last term describes the periodic potential of the substrate.

The simulation results for the system without taking into account the substrate influence are shown in Fig. 1. It shows the obtained temperature dependences of the electric polarization P, magnetic susceptibility χ, permittivity ε and the corresponding experimental curves from [4]. Comparison of simulation results with experimental data indicates their qualitative agreement.

In this work, we studied the effect of the periodic substrate potential on the thermodynamic parameters with a small deviation of the period of the substrate potential from the interatomic distance in the $CoMnO_6$ chain. The discrepancy between the substrate period and the interatomic distance leads to the spins chain deformation, i.e. changing the distance between atoms in the $CoMnO_6$ chain. This leads to a change in the exchange integrals of the spins interaction J_{AF} and J_{FM}.

The substrate potential shifts the magnetic phase transition temperature and affects the appearance of electric polarization along the chain.

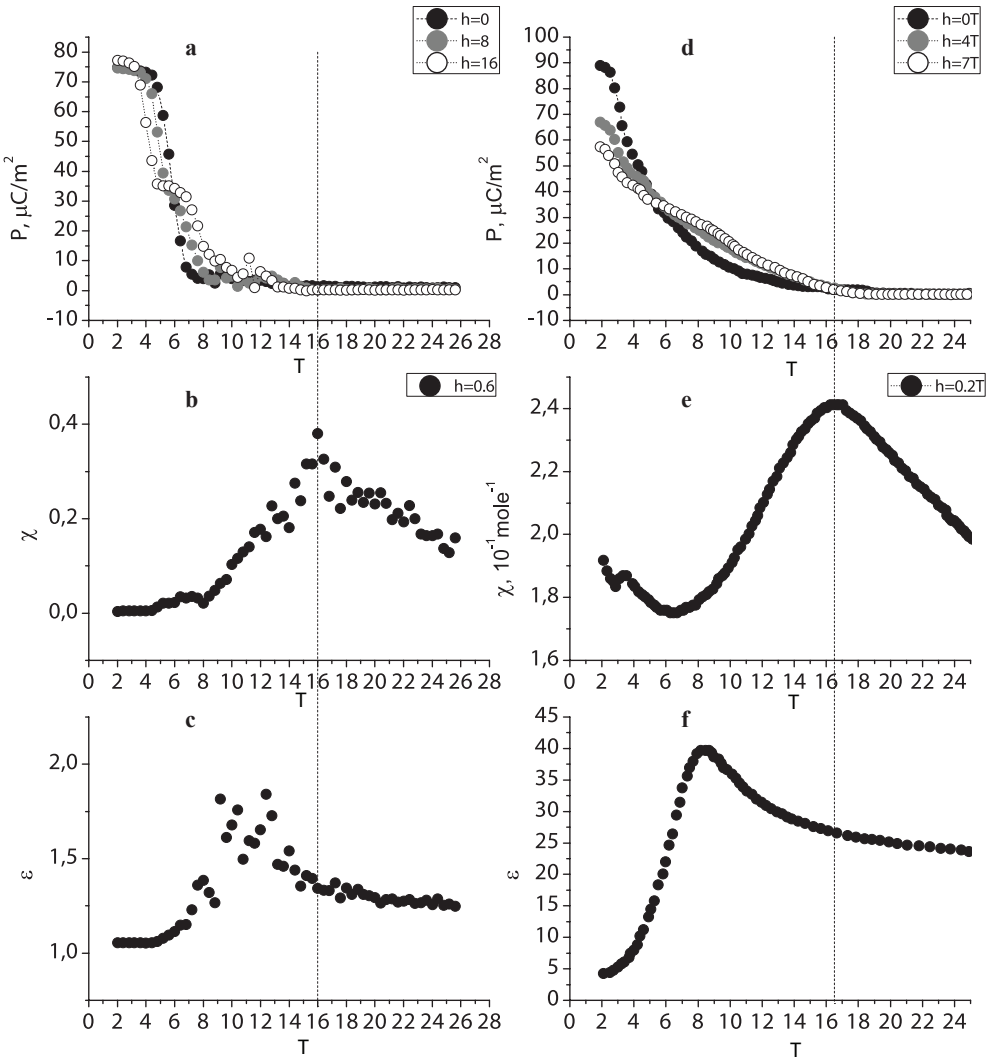

Figure 1. Temperature dependences of the polarization, magnetic susceptibility and permittivity without the periodic substrate potential obtained by simulation (**a-c**) and from experiment [4] (**d-f**).

This study was funded by the Russian Science Foundation, project number 22-19-00355.

1. M.E. Fisher, W. Selke, Phys. Rev. Lett. **44**, 1502–1505 (1980).
2. H. Wu, T. Burnus, Z. Hu, C. Martin, A. Maignan, J.C. Cezar, A. Tanaka, N.B. Brookes, D.I. Khomskii, and L.H. Tjeng, Phys. Rev. Lett. **102**, 026404 (2009).
3. Y. Zhang, H.J. Xiang, and M.-H. Whangbo, Phys. Rev. B **79**, 054432(2009).
4. Y.J. Choi, H.T. Yi, S. Lee, Q. Huang, V. Kiryukhin, and S.-W. Cheong, Phys. Rev. Lett. **100**, 047601 (2008).

FRUSTRATIONS IN THE GROUND STATE OF THE DILUTE ISING CHAIN IN A MAGNETIC FIELD

Yu.D. Panov

Institute of Natural Sciences and Mathematics, Ural Federal University, Ekaterinburg, Russia
E-mail: yuri.panov@urfu.ru

Frustrated magnetic systems have recently attracted an attention of researchers due to the enhanced magnetocaloric effect [1]. Besides to geometric factors, the impurities are also the reason for the existence of frustrations in the magnetic system. Impurities can be one of the sources of frustration in the magnets. The simplest model of this type of system is an Ising chain diluted with non-magnetic charged impurities:

$$\mathcal{H} = -J\sum_j \sigma_j\sigma_{j+1} + V\sum_j P_{0,j}P_{0,j+1} - h\sum_j \sigma_j - \mu\sum_j P_{0,j}. \quad (1)$$

Here the pseudospin operator is used, where the states of conventional spin doublet and non-magnetic impurity correspond to the $\sigma = 1$ pseudospin z-projections $\sigma = \pm 1$ and $\sigma = 0$, respectively, J is the exchange constant, V is the inter-site interaction for impurities, $P_0 = 1 - \sigma^2$ is the projection operator onto the $\sigma = 0$ state, h is the external magnetic field and μ is the chemical potential.

The ground state phase diagram shows in Fig.1a the frustrated antiferromagnetic (FR-AFM) and frustrated ferromagnetic (FR-FM) phases in a weakly diluted case, and in Fig.1b the frustrated

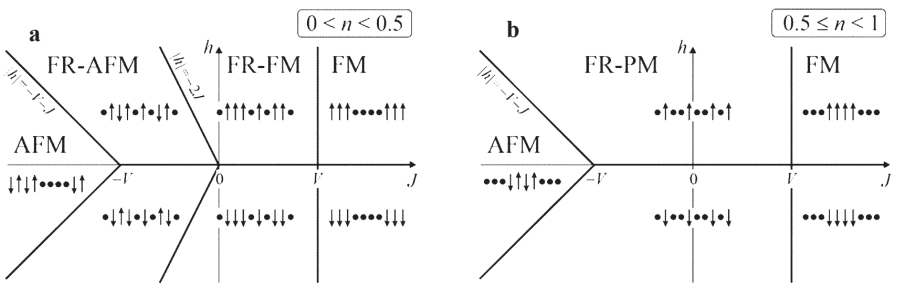

Figure 1. The ground state phase diagrams of the dilute Ising chain in a longitudinal magnetic field for a) weak dilution, b) strong dilution. Here n is the concentration of non-magnetic impurities.

paramagnetic (FR-PM) phase in a strongly diluted case. The magnetocaloric effect and the influence of impurities on the magnetic Gruneisen parameter for this system were considered in [2]. In the present work, the dependence of the residual entropy S_0 of the model (1) on the concentration of impurities is investigated. An analytical method for calculating S_0 based on the isomorphism of the model (1) to the Markov chain [3] is presented, and exact expressions of S_0 are obtained for all phases of the ground state and at the boundaries between phases.

This work was supported by the Ministry of Education and Science of the Russian Federation, project FEUZ-2020-0054.

1. M.E. Zhitomirsky, A. Honecker, J. Stat. Mech.: Theory and Experiment **2004** (07) P07012 (2004).
2. A.V. Shadrin, Y.D. Panov, JMMM **546**, 168804 (2022).
3. Y.D. Panov, JMMM **514**, 167224 (2020).

NON-EQUILIBRIUM VORTEX COARSENING OF DISORDER IN TWO-DIMENSIONAL XY-MODEL WITH COMPLEX DILUTION MODEL

*A.P. Popova**, *I.S. Popov, P.V. Prudnikov*

Department of Theoretical Physics, Dostoevsky Omsk State University, Omsk, Russia
*E-mail: anka_omsk@mail.ru

Non-equilibrium relaxation processes in complex systems of statistical mechanics are often accompanied by non-equilibrium direct and indirect interaction of internal degrees of freedoms, that leads to formation of non-equilibrium coherent structures and pattern formation and dynamics [1–3].

A two-dimensional XY-model is a classical spin model of statistical mechanics. This model is known to undergo the Berezinskii-Kosterlitz-Thouless (BKT) topological phase transition, related to dissociation of vortex pairs at the transition point at temperature $T = T_{BKT}$, and there exists a low-temperature Berezinskii phase at $T < T_{BKT}$. The model is used to describe some properties of a wide range of planar magnets and ultrathin magnetic films [4, 5]. Inclusion of structural disorder into the model results in pinning of the vortices on defects, that changes significantly low-temperature equilibrium and non-equilibrium relaxation properties of the system [4, 5]. In work [6] a formation of coherent structures such as stripes and clumps has been revealed in the two-dimensional XY-model, resulted from composition of inter-vortex interaction potential and effective potential of pinning of vortices on structural defects. In [7, 8] the effect was achieved by introducing of additional potentials in the Hamiltonian. It has been shown [6], that there is non-equilibrium vortex annealing of structural disorder in the system, accompanied by growth of defect clusters in cores of non-equilibrium vortices, and this process has nature of non-equilibrium critical coarsening.

This work is devoted to investigation of influence of dilution on non-equilibrium critical properties and on formation of non-equilibrium coherent structures in the two-dimensional XY-model with a complex dilution model, with subsystems of mobile and fixed defects with concentrations c_a and c_q respectively. Monte-Carlo simulations were performed as in [4–6]. To investigate non-equilibrium critical coarsening in detail, distributions of clusters of defects have been calculated. Dependencies of relative amount of clusters of mobile defects $N_M(n, t)$ and full clusters (of mobile and fixed defects) $N_F(n, t)$ on time t, for temperatures $T \leq T_{BKT}(p)$, for a wide range of spin concentrations $p = 1 - c_a - c_q$ have been obtained. Snapshots of configurations of defects in non-equilibrium critical relaxation of the system in Fig. 1 demonstrate clearly formation and growth of stripes of defects and of clumps of defects.

Dynamic dependencies $N_M(n, t)$ and $N_F(n, t)$, shown in Fig. 2, allow clearly distinguish the process of non-equilibrium critical coarsening of mobile defects in non-equilibrium relaxation of the

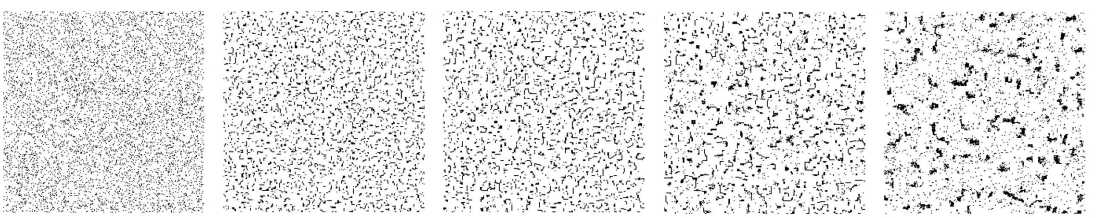

Figure 1. Snapshots configuration of defects in non-equilibrium critical relaxation of the system at observation times $t = 0$ (initial state), 100, 1000, 5000 and 20000 MCS/s. Formation and growth of stripes of defects are observed, following by formation and enlargement of clumps of defects.

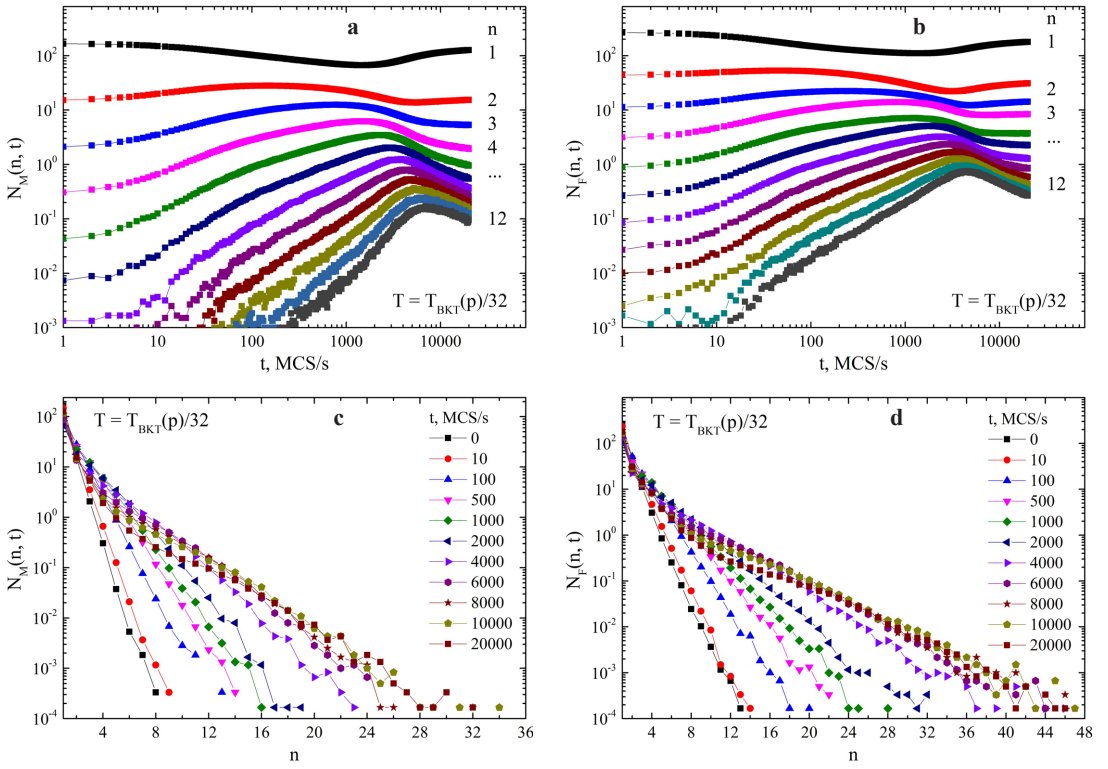

Figure 2. Dependencies of relative amount of clusters of mobile defects $N_M(n, t)$ and full clusters (of mobile and fixed defects) $N_F(n, t)$ on time t for different sizes of clusters n (top) and on size of clusters n for different moments of time t (bottom).

system – clusters of larger sizes appear as a result of merging and absorbing of smaller clusters, and a time scale of the maximum amount of clusters shifts to a region of larger times with increase of cluster size. Dependencies $N_M(n, t)$ and $N_F(n, t)$ on cluster size n, at small times demonstrate exponential distribution function, with effective scale increasing with t. This allows to conclude that coarsening of clusters of defects has "inertial" character. Quantitative relations and dependencies, characterizing spatial and dynamical scales of cluster growth with respect to time, temperature and spin concentration p have been obtained.

Support by the Russian Foundation for Basic Research (project No. 20-32-90207) is acknowledged. The simulations were supported in through computational resources provided by the Laboratory of Applied Theoretical Physics and Parallel Computation of Dostoevsky Omsk State University.

1. U.C. Tauber, Critical Dynamics: A Field Theory Approach to Equilibrium and Non-Equilibrium Scaling Behavior. Cambridge University Press, Cambridge, (2014).
2. S.N. Patitsas, Phys. Rev. E **100**, 022116 (2019).
3. J. Yan, H. Touchette and G.M. Rotskoff, Phys. Rev. E **105**, 024115 (2022).
4. V.V. Prudnikov, P.V. Prudnikov and I.S. Popov, JETP **131**, 768 (2020).
5. V.V. Prudnikov, P.V. Prudnikov and I.S. Popov, JETP **126**, 369 (2018).
6. I.S. Popov, A.P. Popova and P.V. Prudnikov, EPL **128**, 26002 (2020).
7. A.W. Sandvik, S. Daul, R.R.P. Singh and D.J. Scalapino, Phys. Rev. Lett. **89**, 247201 (2002).
8. D. Valdez-Balderas and D. Stroud, Phys. Rev. B **72**, 214501 (2005).

MAGNETIC ORDERING IN DELAFOSSITES WITH DEFECTED LATTICE

*S.P. Savchenko**, *R.V. Skorunov, A.G. Smolnikov*

IMP UB RAS, Yekaterinburg, Russia

*E-mail: sergeysavch@imp.uran.ru

The report is devoted to the study of frustrated magnetic systems. In such magnetic materials, the competition of exchange interactions leads to the degeneration of the ground state and the appearance of additional orientational degrees of freedom of the interacting spins. These materials have complicated phase diagrams with unusual examples of long-range and short-range magnetic order, making them good experimental objects for the solution of fundamental problems in the physics of phase transitions and magnetic phenomena.

A well known example of frustrated magnetic systems are materials with triangular antiferromagnetic ordering. They include compounds with ABO_2 delafossite structure, where the layers of monovalent metal A are separated by correlated BO_2 layers. Moreover, these compounds attract additional interest, because some of them are multiferroics of the same structure where the magnetic ordering and the magnitude of observed effects are significantly different [1, 2].

In some delafossites, unusually elongated incommensurate spin spirals are observed. They exist in different crystallographic directions below the Neel point. Herewith, the authors of a number of experimental works come to the conclusion that neighboring triangular lattices have a collinear ordering [3, 4]. Thus, the question of coexistence of two oppositely directed spin helicoids in one triangular lattice remains to be clariffed. It is also difficult to predict the inuence of defects on the emerging long-range magnetic order in such complex magnetic systems.

Based on a simple cellular-automata model [5] and energy minimization algorithm for a triangular lattice of quasi-classical spins, we investigated the magnetic ordering in delafossites and it's dependence on the concentration of non-magnetic impurity and on the external magnetic field. It was found that initial ordered helicoidal state progressively collapses with increase in non-magnetic impurity concentration from 0 up to 30%. Higher concentration of impurity reaches a threshold, destructs the exchange inuence to magnetic order and triggers the increasing role of anisotropy and external magnetic field. The variation of external field showed that spiral angles and spiral directions can be varied by field's direction and it's absolute value. E.g. if the field is directed along [100] direction, the 120° spiral directions tend to [010]. Introduction of both external field and non-magnetic impurity allows to observe rather more complex behaviour of magnetic order, namely small clusters of magnetic ions feel the field stronger than entirely filled magnetic lattice.

The research was carried out within the President's of Russia grant No.MK-6094.2021.1.2.

1. K. Kimura et al., Phys. Rev. B **78**, 140401 (2008).
2. E. Mun et al., Phys. Rev. B **89**, 054411 (2014).
3. V.V. Ogloblichev et al., JMMM **504**, 166668 (2020).
4. A.G. Smol'nikov et al., PMM **118**, 134 (2017).
5. S.V. Krivovichev, Acta Crystallogr. A **60**, 257 (2004).

VIBRATIONAL PROPERTIES AND LATTICE SPECIFIC HEAT OF QUASI-1D TERNARY IRON SULFIDE $KFeSe_2$

*M.D. Kuznetsov**, *A.G. Kiiamov, D.A. Tayurskii*

Insitute of Physics, Kazan Federal University, Kazan, Russia
*E-mail: steam.kuznetsov@yandex.ru

The $AFeX_2$ compounds crystallize into monoclinic structure with C2/c space group [1]. The main motif of the crystal structure is a chain of $[FeX_4]$ tetrahedra sharing a common edge and aligned along the crystallographic axis *c* [1]. These chains are cross-linked by alkali atoms to form a three-dimensional structure. The chains are characterized by the short Fe-Fe distance (2.815 Å) [1]) not much exceeding the Fe-Fe iron distance of metallic iron (2.48 Å). Previous neutron diffraction experiments on powdered samples [1] have shown that $KFeSe_2$ is a three-dimensional antiferromagnet with T_N = 310 K.

We have performed *ab initio* calculations of vibrational properties of $KFeS_2$ compound utilizing density functional theory. Total and element specific phonon densities of states (PDOS) were calculated within a direct approach of harmonic approximation. We used phonon density of states to calculate lattice contribution to the specific heat. The calculated phonon density of states shows a large number of high-frequency vibrational modes of Fe and Se atoms, which strongly restricts application of the Debye model for analysis of thermodynamical properties of $KFeSe_2$.

Inset on Fig. 1 represents calculated total phonon DOS. The calculated lattice contribution to the specific heat is presented in Fig. 1. The lattice heat capacity reaches a value of 95 $JK^{-1}mol^{-1}$ at a temperature of 300 K and does not exceed Dulong-Petit law's limit (about 99 $JK^{-1}mol^{-1}$). At low temperatures lattice specific heat demonstrates cubic dependence on temperature.

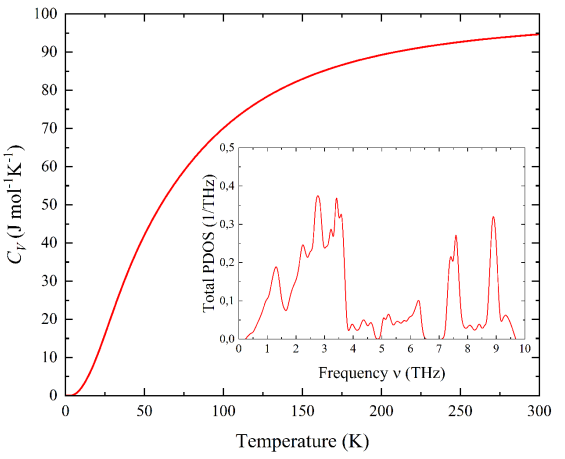

Figure 1. Temperature dependence of the calculated lattice specific heat. Inset represents calculated total PDOS.

The reported study was funded by Priority-2030 Program.

1. W. Bronger et al., J. Solid State Chem. **70**, 2 (1987).

EFFECT OF ANNEALING CONDITIONS ON MAGNETIC CHARACTERISTICS OF NANOCRYSTALLINE OXYGEN-DEFICIENT $TiO_{2-\delta}$(B)

*I.A. Tkachenko**, *D.P. Opra, A.M. Ziatdinov, A.A. Sokolov, E.V. Tarasov*

Institute of Chemistry FEB RAS, Vladivostok, Russia
*E-mail: tkachenko@ich.dvo.ru

Recently, a huge number of works have been devoted to nanoscale titanium oxides. In 2014, Chemical Reviews published 21 reviews on the preparation, properties and application of nanoscale titanium oxides [1].

The study of magnetic properties began intensively after the possibility of obtaining a magnetic semiconductor with room ferromagnetism based on TiO_2 was shown in [2].

In this paper, we investigated the effect of annealing conditions on the magnetic properties of nanocrystalline oxygen-deficient titanium dioxide in bronze modification, obtained by combining the method of hydrothermal synthesis and ion exchange, with final annealing in air, sample W-TiO_2(B), or in vacuum, sample G-TiO_2(B).

The diffraction patterns of the W-TiO_2(B) and G-TiO_2(B) samples are close, and indicate that the bronze phase of titanium dioxide (JCPDS 74-1940) of monoclinic syngony (C2m) with unit cell parameters a = 12.208 Å, b = 3.749 Å, c = 6.535 Å and β = 107.36° dominates in the samples. Based on this, we can say that the phase composition of the studied samples is determined by the conditions of hydrothermal synthesis and does not depend on the type of medium in which the final heat treatment is carried out.

The obtained EPR-spectra contain an intense narrow symmetric component with a value of g = 2.0037(1), a low-intensity asymmetric component with a value of g ~ 4.32, and a group of three nearby low-intensity resonances “a”, “b” and “c” with g-factor values of 2.063, 2.056 and 2.044, respectively. The value of the g-factor of the main component of the EPR spectra is close to the value of the g-factor of electrons localized in oxygen vacancies of titanium dioxide (so-called F-centers) [3, 4]. The values of the g-factors of the resonances “a”, “b” and “c” are close to the values of the g-factors of the radicals O– and OH– in titanium dioxide [3].

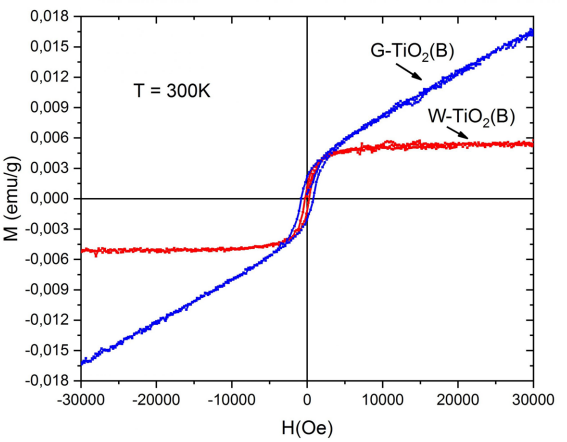

Figure 1. Curves $M(H)$ at T = 300 K.

According to the data obtained by spectroscopy in the ultraviolet and visible regions (UV View), a change in the band gap is observed in the studied samples, with a change in annealing conditions, so for G-TiO_2(B) it is 3.04 eV, and for the sample W-TiO_2(B) – 3.23 eV.

The results of the study of the field dependences of the magnetization of samples with different annealing methods at room temperature are shown in Fig. 1. According to the data presented, the studied samples have a magnetic ordering at room temperature. It should be noted that the change in the conditions of the final annealing leads to the fact that the hysteresis loop of the sample G-TiO_2(B) ceases to reach saturation, and the value of the coercive force increases from 270 to 800 Oe. Now, there are several views on the causes of ferromagnetic ordering in such materials. Most of the developed theories associate ferromagnetism with magnetic moments localized on impurity atoms, which are ordered by indirect exchange interactions [5–7]. However, ferromagnetism is associated with the spin polarization of electrons localized in a narrow defect zone of a semiconductor [8–10] in another point of view. In our case, both of these options are implemented simultaneously, since the presence of electrons localized in oxygen vacancies of titanium dioxide is confirmed by EPR data, and the presence of impurity atoms in the samples is due to the purity of commercial titanium dioxide (Alfa Aesar) at 99.7%. The fact of an increase in the values of magnetization can be explained within the framework of the model proposed by the authors of the work [11]. Within the framework of this model, ferromagnetism is spatially inhomogeneous in the sample and can exist only in the region of percolation of defects. Consequently, an increase in the total number of defects, as a special case of oxygen vacancies, will lead to an increase in the spatial regions of the material included in the ferromagnetic ordering, and in general to an increase in the total magnetic moment of the substance.

Lowering the temperature to 4 K leads to the fact that the field dependences of the samples W-TiO_2(B) and G-TiO_2(B) become similar and differ little from each other (Fig. 2). This behavior of hysteresis loops is explained by the fact that with a decrease in temperature, the electron population of the vacancy zone located near the bottom of the conduction band, and, consequently, the contribution from the exchange interaction between these electrons to the magnetic characteristics of the material decreases. The contribution from impurity ions becomes predominant, and since the amount of impurity in both samples is the same, the magnetic properties of the studied samples, in the low temperature region, become similar.

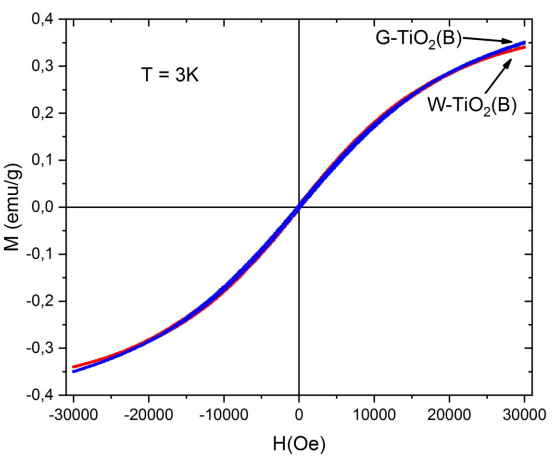

Figure 2. Curves $M(H)$ at T = 3 K.

In conclusion, we can say that the magnetic properties of titanium dioxide in the bronze phase, at room temperature, depend on the nature of the final annealing, or, in other words, on the number of oxygen vacancies. In the low temperature region, the magnetic properties of the studied samples begin to determine the impurity atoms.

The work was carried out within the framework of the state assignment of the Institute of Chemistry, Far Eastern Branch of the RAS No 0205 2021 0001, the synthesis of samples was carried out with the support of the RSF (grant No. 19-73-10017).

1. M. Dahl, Y. Liu, and Y. Yin, Chem. Rev. **114**(19), 9853–9889 (2014).
2. Y. Matsumoto, M. Murakami, T. Shono, et al., Science **291**(5505), 854–856 (2001).
3. G. Yang, Z. Jiang, H. Shi, T. Xiao, Z. Yan, J. Mat. Chem. **20**(25), 5301–5309 (2010).
4. E. Serwicka, R.N. Schindler, Z. Naturforsch. A **36**(9), 992–995 (1981).
5. P. Ding, F. Liu, C. Zhou et al., Chinese Physics B **19**(11), 118102 (2010).
6. S. Sharma, S. Chaudhary, S.C. Kashyap, S.K. Sharma, J. Appl. Phys. **109**(8), 083905 (2011).
7. P. Ding, F. M. Liu, C. C. Zhou, et al., Chinese Physics B **19**(11), 11811025 (2010).
8. A.E. Ermakov, M.A. Uimin, A.V. Korolev et al., Phys. Solid State **59**(3), 469–482 (2017).
9. J.M.D. Coey, P. Stamenov, R.D. Gunning, M. Venkatesan, K. Paul, New J. Phys. **12**, 11–14 (2010).
10. J.M.D. Coey, M. Venkatesan, C.B. Fitzgerald, Nature Materials **4**, 173–179 (2005).
11. A.A. Achkeev, I.R. Vakhitov, R.I. Khaibullin, Uchenye Zapiski Kazanskogo Universiteta. Seriya Fiziko-Matematicheskie Nauki **154**(3), 11–25 (2012) (in Russian).

Section D.

Domain walls, vortices and skyrmions

ZIGZAG DOMAINS IN MAGNETIC FILMS WITH ANISOTROPIC DZYALOSHINSKII-MORIYA INTERACTION

O.G. Udalov[1,2], *R.V. Gorev*[1], *E.V. Skorokhodov*[1], *N.S. Gusev*[1], *A.V. Sadovnikov*[3], *M.V. Sapozhnikov*[1,2*]

[1]Institute for Physics of Microstructures RAS, Nizhny Novgorod, Russia
[2]Department of Physics and Astronomy, California State University Northridge, USA
[3]Saratov State University, Saratov, Russia
[*]E-mail: msap@ipmras.ru

A new type of domain walls and domain structures in thin magnetic films with perpendicular anisotropy are theoretically predicted and experimentally discovered. The observed oriented stripe domains and zigzag-shaped domains are a consequence of the anisotropy of the interfacial Dzyaloshinskii-Moriya interaction (iDMI). The possibility to change a domain structure in Co/Pt films by manipulating the iDMI under the application of uniaxial mechanical deformations is demonstrated.

Previously it was shown that labyrinthine domain structures with an arbitrary orientation of domain walls are realized in demagnetized films with perpendicular magnetic anisotropy and with iDMI. Depending on the value of iDMI, the domain wall itself can have a Bloch, Neel, or intermediate inclined structure.

In this work, the problem of a domain wall in a ferromagnetic film with an anisotropic iDMI is analytically solved. It is shown that the orientation of the magnetization ϕ in the domain wall is determined by a simple expression $\cos(\phi) = (D_x + D_y)/\alpha$, where $D_{x,y}$ are iDMI coeficients, and α is a certain parameter characterizing the magnetostatic energy of the system. In this case, the domain wall itself has a minimum of energy at a certain orientation (which is characterized by the angle β)

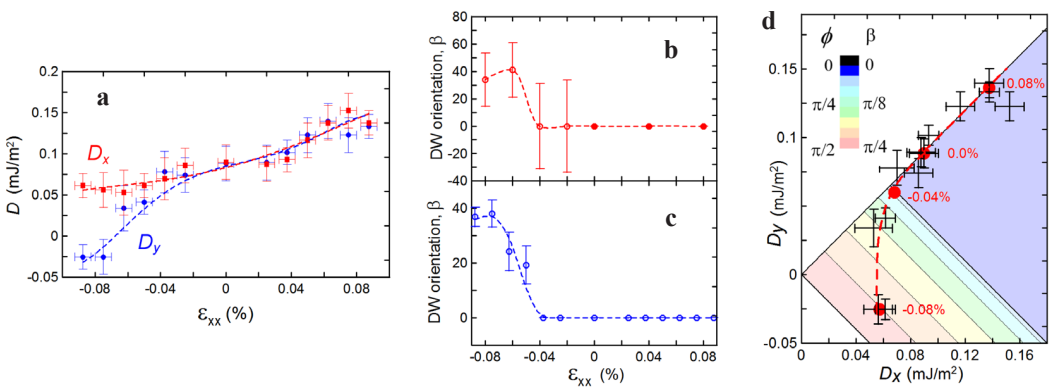

Figure 1. **a** iDMI constants ($D_{x,y}$) measured along the x and y directions as a function of the applied strain. **b** Mean wall orientation angle β and its variance as a function of strain obtained from MFM measurements. Solid red circles denote labyrinthine domain structures with no preferred orientation. The vertical segments show the variance of β. **c** Values of β calculated from the BLS data. **d** Diagram of equilibrium orientation of domain walls as a function of $D_{x,y}$ (quadrant $|D_y| < D_x$ shown). The colors show the theoretically calculated dependence for β and ϕ. The line $D_y = D_x$ corresponds to an isotropic labyrinth domain structure. The red circles correspond to the MFM images shown in Fig. 2. The black crosshairs correspond to the values of the iDMI constants given in **a**.

relative to the principal axes of the iDMI tensor. At that ϕ and β are related by a simple relation $\beta = \phi/2$, the diagram of equilibrium orientations is shown in Fig. 1d. Due to the degeneracy of the energy of the domain wall with respect to $\pm\beta$, the resulting domain structure should be zigzag, which is confirmed by the methods of micromagnetic simulations (Fig. 2).

To experimentally verify the obtained theoretical predictions samples of multilayer magnetic films (Co 0.7 nm/Pt 1 nm)$_4$ with easy anisotropy axis are fabricated and investigated. The iDMI anisotropy is induced by uniaxial tension and compression of the samples, which is achieved by bending the substrate, on which a multilayer magnetic film is deposited (Fig. 2). Indeed, direct measurements of the iDMI constants performed by the Mandelstam-Brillouin scattering method (BLS) confirms that the compression of the sample leads to anisotropy of the iDMI (Fig. 1a). The observed changes in the iDMI constants are large (~100%), and the D_y value even changes its sign. When stretched, the iDMI changes in magnitude, but remains isotropic.

The resulting domain structures at different strains are studied by magnetic force microscopy (MFM) with subsequent Fourier analysis of the obtained images (Fig. 2). In the undeformed sample a labyrinth isotropic domain structure with a period of 200 nm is observed, which corresponds to the ring symmetry of the spatial Fourier spectrum. When the film is compressed, the form of the

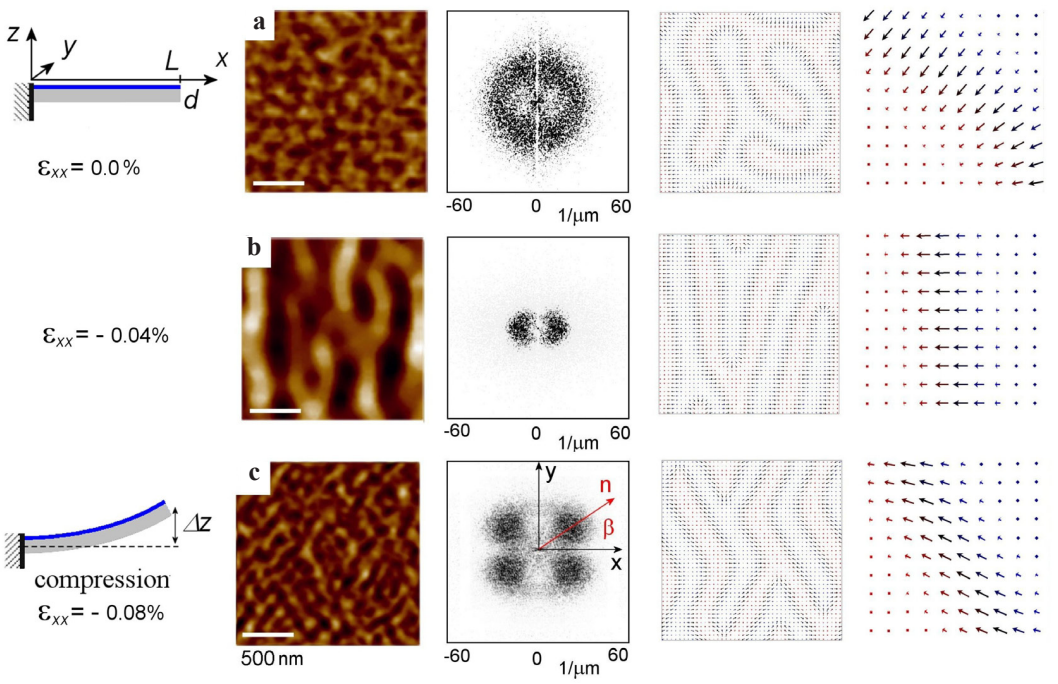

Figure 2. First column: measurement geometry. The gray part of the sample is the substrate and the blue part is the multilayer magnetic film. One end of the sample is fixed, while the other can be bent, causing mechanical deformation of the magnetic film. The displacement Δz determines the amount of deformation. The corresponding strains ε_{xx} are indicated. The images in each row are given for the strain values indicated in the first column. Second column: MFM-images of domain structures obtained under the corresponding deformations. Third column: corresponding spatial Fourier spectra of domain structures. The deformation is applied along the x axis. Fourth column: domain structures obtained by micromagnetic modeling methods. Fifth column: enlarged image of domain walls.

domains changes. First, it becomes a stripe, with 2 maxima appearing in the Fourier image. Further compression leads to the formation of a zigzag domain structure. This manifests in the spatial Fourier spectrum as the formation of four maxima. An analysis of the Fourier spectra makes it possible to extract the average value of the angle β, which characterizes the orientation of the domain walls with respect to the principal axes of the iDMI tensor and its dispersion.

The obtained BLS data for the constants of the iDMI make it possible to calculate the values of β for various strains using the analytically obtained expression for the equilibrium β. The calculated β are in good agreement with the values obtained from the analysis of the Fourier spectra of MFM-images of domain structures. (Fig. 1b, c). In addition, the experimentally obtained data for β are jointly presented in the theoretically calculated diagram of the dependence of β on D_x, D_y (Fig. 2d). The estimations made in our work and the given symmetry considerations demonstrate that the observed rearrangement of the domain structure cannot be due to a possible change in the magnetic anisotropy of the system.

Support by RSF (#21-12-00271) is acknowledged.

INFLUENCE OF THE ROUGHNESS OF Co-LAYERS ON THE CREEP OF DOMAIN WALLS IN Pd/Co/Pd EPITAXIAL STRUCTURES

*A.V. Davydenko**, *N.N. Chernousov, A.A. Turpak, A.G. Kozlov, A.V. Ognev, A.S. Samardak*

Laboratory of Spin-Orbitronics, Far Eastern Federal University, Vladivostok, Russia
*E-mail: davydenko.av@dvfu.ru

Investigation of the dynamics of domain walls (DWs) in the creep regime is widely used for characterization of the Dzyaloshinskii-Moriya interaction (DMI). The velocities of DWs in the creep regime are generally less than 0.1 m/s, therefore, measurements may be conducted quite easily. In the creep regime, the velocity of the DWs depends exponentially on the driving magnetic field and temperature. Propagation of DWs is determined by a pinning of DWs on different types of defects. Thermal fluctuations with constantly applied driving magnetic field provide enough energy for a local propagation of segments of the DWs between potential barriers in the pinning disorder landscape.

Despite the relatively simple experimental characterization of the creep of DWs, accurate analytical description of the measurements is still a difficult problem. Several analytical models exist in literature [1, 2] which describe some particular cases but they are not universal. In this work, we modify the pinning disorder landscape in the Pd/Co/Pd(111) epitaxial system by changing the interface roughness of Co-layers and apply the latest analytical model for an analysis of the obtained results.

Pd(3–10 nm)/Co(0.7 nm)/Pd(3 nm) structures were epitaxially grown on a Si(111) substrate with a Cu(2 nm) buffer layer. The root-mean-square (RMS) roughness of the bottom Pd/Co and top Co/Pd interfaces increased from 0.25 to 0.8 nm with increasing of the bottom Pd-layer thickness (Fig. 1a). The values of RMS roughness of the bottom and top interfaces are nearly the same in the sample with the fixed bottom Pd-layer thickness. However, an average diameter of Co-islands grown on the top of the Si(111)/Cu/Pd surface is larger than the diameter of bottom Pd-islands. This fact may be explained by nonuniform distribution of Co and planarization of the surface of underlying Pd-islands.

All investigated samples reveal a perpendicular magnetic anisotropy. The perpendicular magnetic anisotropy field increases from 1.25 to 1.35 T with an increase in the bottom Pd-layer thickness, while a saturation magnetization slightly decreases. A decrease in the saturation magnetization with increasing in the RMS roughness is a common fact observed in different systems [3]. Coercive force increases with increasing RMS roughness from 11 to 19 mT nearly twice. This fact corroborates a large contribution of the roughness to the coercive force and hence to the pinning of the DWs.

The velocity of DWs was measured by means of a Kerr microscope. Before measurements, an artificial nucleation center was created by a focused ion beam etching system in the center of each sample. DWs were propagated under the influence of pulses of constant driving out-of-plane magnetic field with simultaneously applied variable in-plane magnetic field. Time-length of a single pulse was taken as 2 ms. The in-plane magnetic field was varied from –0.25 to 0.25 T. The scheme for the measurement of the DW velocity was as follows. A circular domain was nucleated around the artificial center. A constant in-plane magnetic field was switched on. The pulse of the out-of-plane magnetic field was applied. The distance at which the DW propagated was measured from a snapshot of differential magnetic contrast made by the Kerr microscope.

The velocity curves $v(H_x)$ were measured for the series of samples. They were averaged for the left and right DWs and fitted by the extended dispersive stiffness model [4]. The velocity curves

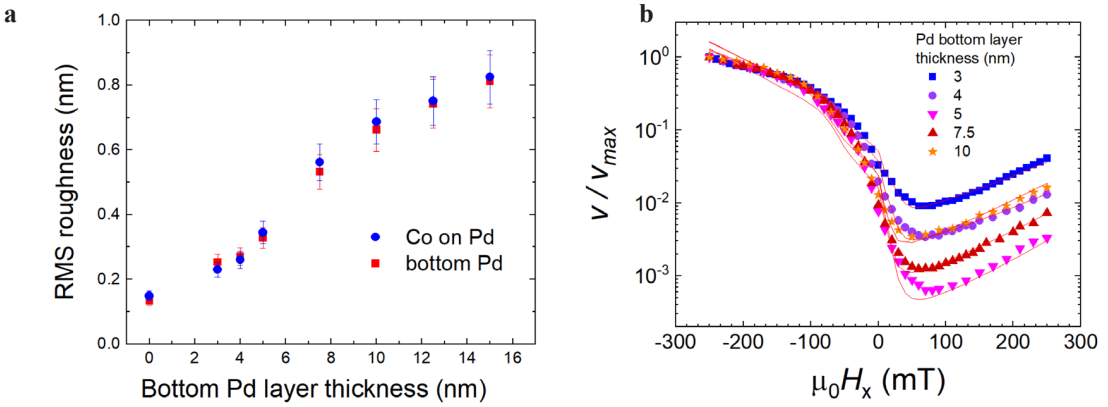

Figure 1. **a** Pd bottom layer thickness dependencies of RMS roughness of the Pd-layers deposited on Si(111)/Cu(2 nm) surface and Co-layers, deposited on the top of Pd-layers. **b** Averaged for the left and right DWs velocity curves normalized to their maximal values as a functions of the in-plane magnetic fields. Solid lines denote calculations by the analytical model.

normalized to the maximal value are shown in Fig. 1b. Calculated curves well fit experimental results. The central result of this work is that the largest asymmetry A (the largest relation of $v(-H_x)/v(H_x)$ from a single $v(H_x)$ curve) increases 13.5 times with an increase in the thickness of Pd bottom layer from 3 to 5 nm. The largest asymmetry in the velocities of the left and right domain walls in the Pd(5 nm)/Co(0.7 nm)/Pd(3 nm) sample reaches 540 in the in-plane magnetic field of 130 mT, that means that the propagation of the domain wall in the direction opposite to the in-plane magnetic field under the influence of positive out-of-plane magnetic field is almost blocked. However, a further increase in the Pd bottom layer thickness greater than 5 nm does not lead to larger asymmetries.

The result of application of the extended dispersive stiffness model are values of DMI fields, HDMI, and chiral damping parameter, χ^*, that is responsible for the asymmetry in the velocity curves. The DMI field increases with an increase in the RMS roughness from 16 to 30 mT. Similar qualitative behavior was observed in the polycrystalline systems deposited on the same Si(111)/Cu/Pd surface with different RMS roughness [5]. The chiral damping parameter expectedly reaches maximal value at the Pd bottom layer thickness of 5 nm. Thus, the roughness of the interfaces strongly influences on the DMI field and the asymmetry of the DWs propagation.

We acknowledge the support of the Russian Science Foundation (Project No. 21-42-00041).

1. D. Lau, J.P. Pellegren, H.T. Nembach, J.M. Shaw, and V. Sokalski, Phys. Rev. B **98**, 184410 (2018).
2. D.M.F. Hartmann, R.A. Duine, M.J. Meijer, H.J.M. Swagten, and R. Lavrijsen, Phys. Rev. B **100**, 094417 (2019).
3. J.-H. Kim, S.-C. Shin, J. Appl. Phys. **80**, 3121 (1996).
4. A.V. Davydenko, A.G. Kozlov, M.E. Stebliy, A.G. Kolesnikov, N.I. Sarnavskiy, I.G. Iliushin, and A.P. Golikov, Phys. Rev. B **103**, 094435 (2021).
5. A.S. Samardak, A.V. Davydenko, A.G. Kolesnikov, A. Yu. Samardak, A.G. Kozlov, Bappaditya Pal, A.V. Ognev, A.V. Sadovnikov, S.A. Nikitov, A.V. Gerasimenko, I.H. Cha, Y.G. Kim, G.W. Kim, O.A. Tretiakov, and Y.K. Kim, NPG Asia Materials **12**, 51 (2020).

D.O1

VORTEX NANOOBJECTS IN PERFORATED FERROMAGNETIC FILMS

*E.B. Magadeev**, *R.M. Vakhitov, R.R. Kanbekov*

Bashkir State University, Ufa, Russia
*E-mail: magadeeveb@gmail.com

In this paper we consider a new type of vortex-like inhomogeneities (VLI) that arise in thin ferromagnetic films with artificially created holes (antidotes [1]) and strong uniaxial easy-plane anisotropy [2]. In this case, the inhomogeneities that form in the vicinity of two antidotes (Fig. 1) are (like skyrmions [1]) topologically protected structures and have sufficient spatial localization, as well as stability with respect to external disturbances, which indicates the possibility of their use for recording and storing data. Since the structures under consideration can be in one of three non-equivalent states (one homogeneous and two symmetrical inhomogeneous), one pair of holes in the magnetic film makes it possible to encode not a bit, but a trit (trinary digit) of information, which opens up opportunities for a significant increase in the density of information recording on media through the use of ternary representation of numbers.

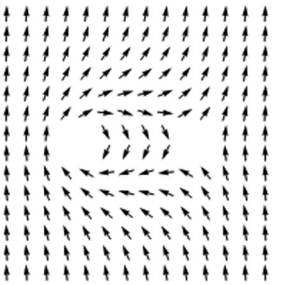

Figure 1. Solitary inhomogeneity localized at two holes.

The structure of the inhomogeneities under consideration was studied within the framework of both continuum and discrete models. The stability of VLI is studied by numerical simulation and it is shown that the work required to destroy an inhomogeneous state is comparable to the energy of the state itself. Similar studies were also carried out with respect to inhomogeneities localized on four holes. They have additional binding energy and demonstrate greater stability with respect to external influences.

An important feature of the studied VLIs is the ability to control their state using currents. In particular, it is shown that when a current of a certain value is passed through one of the holes, the change in the magnetic structure in the vicinity of the second hole can occur spontaneously due to their exchange coupling. The resulting inhomogeneity is stable and retains its topology after the current is turned off.

It was also shown that the influence of demagnetizing fields contributes to the localization of the studied inhomogeneities, the corresponding corrections to the energy and structure of inhomogeneities were obtained, and conditions were derived under which the influence of demagnetizing fields can be neglected.

1. J. Muller, A. Rosch, Phys. Rev. B **91**, 054410 (2015).
2. E.B. Magadeev, R.M. Vakhitov, JETP Lett. **115**, 114 (2022).

SIMULATION OF MAGNETIC SKYRMIONS ON FLAT LATTICES

A.V. Perzhu[1], *E.V. Vasiliev*[1,2], *V.Yu. Kapitan*[1,2*]

[1]Far Eastern Federal University, Vladivostok, Russian Federation
[2]Institute of Applied Mathematics, Far Eastern Branch, Russian Academy of Science, Vladivostok, Russian Federation
*E-mail: kapitan.vyu@dvfu.ru

Crystals with a certain symmetry and magnetic films are of particular interest from the practical point of view due to the formation in these systems of stable spiral formations – magnetic skyrmions. Individual skyrmions can be stabilized using the Dzyaloshinskii-Moriya (DM) interaction. Recent demonstrations of control of individual nanoscale skyrmions – including their creation, detection, manipulation, and annihilation – have raised expectations for their use in future spintronic devices.

In the simulation of spin systems, the Metropolis algorithm, one of the numerical Monte Carlo methods, has proven itself well. It allows to successfully study the critical properties of systems with complex Hamiltonians in a wide range of temperatures and other external parameters.

The relevance of studying of spin systems with DM interaction using computer simulation lies in the possibility of studying phase transitions, critical phenomena, and thermodynamic and magnetic properties of such systems. Understanding these properties is important because of the development of data storage devices that use magnetic spin systems to store information.

In this work, we developed a model and software on C++ and Rust programming languages for independent simulation of magnetic skyrmions considering the DM interaction on different flat lattices. We used the next Hamiltonian in our research:

$$\mathscr{H} = \mathscr{H}_J + \mathscr{H}_{\mathrm{DMI}} + B + A.$$

$$\mathscr{H}_J = -J\sum_r S_r \cdot (S_{r+\hat{x}} + S_{r+\hat{y}} + S_{r+\hat{z}}),$$

$$\mathscr{H}_{\mathrm{DMI}} = -D\sum_r S_r \times S_{r+\hat{x}} \cdot \hat{x} + S_r \times S_{r+\hat{y}} \cdot \hat{y} + S_r \times S_{r+\hat{z}} \cdot \hat{z},$$

$$B = -B_z \sum_r S_r,$$

$$A = A_z \sum_r S_r^2.$$

The ferromagnetic-exchange interaction (the first term), the Dzyaloshinskii-Moriya interaction (the second term), the Zeeman coupling (the third term) and magnetic anisotropy (the fourth term) were used [1].

We studied skyrmions of various types, determined the values of the external and internal simulation parameters, which are necessary for the creation and stabilization of skyrmions in magnetic two-dimensional ferromagnetic films. We have demonstrated switching between different stable skyrmionics states depends on various external and internal parameters, e.g. a value of DMI or external magnetic field. Also, we applied a convolutional neural network for recognition of different phases which depended on simulation parameters and plotted phase diagrams. We have proposed a method for creating and controlling the motion of magnetic skyrmions in 2D-films.

This work has been supported by the grant of the Russian Science Foundation # 21-72-00058 "High-performance intelligent approaches to the study of complex magnetic systems".

1. V. Kapitan et al., AIP Advances **11**(1), 015041 (2021).

D.O3

THERMALLY ACTIVATED DRIFT OF MAGNETIC VORTICES IN A RANDOM FIELD OF DEFECTS

V.A. Orlov[1,2*], A.A. Ivanov[1], I.N. Orlova[3], G.S. Patrin[1,2]

[1]Siberian Federal University, Krasnoyarsk, Russia
[2]Kirensky Institute of Physics, Federal Research Center KSC SB RAS, Krasnoyarsk, Russia
[3]Krasnoyarsk State Pedagogical University after V.P. Astafev, Krasnoyarsk, Russia
[*]E-mail: vaorlov@sfu-kras.ru

In thin low-dimensional magnets (nanowires, nanostripes), as a rule, there are defects that create a random or modulated force field, where the vortex moves as a particle. Here, we present a statistical description of the time evolution of a conglomerate of magnetic vortices/skyrmions as a gas of non-interacting quasiparticles involved in one-dimensional motion in the field of magnetic structure defects under the influence of a constant external force.

To describe the nature of the vortices displacement under the influence of a driving force in a random field of defects, we calculate the average number of trajectories of the $\rho(x,t)$ cores, resulting in a favorable outcome, i.e., the core is in the x coordinate at the t time. The elementary event: the core is in the x coordinate at the t time. The probability of such an elementary event can be written as:

$$\mathrm{d}\rho_n^{(\mathrm{el})}(x,t) = \prod_{k=1}^{n} \rho(\Delta x_k)\rho(\Delta t_k)\rho(W_k)\,\mathrm{d}x_k\,\mathrm{d}t_k\,\mathrm{d}W_k\,\delta\left(x - \sum_{k=1}^{b}\Delta x_k\right)\delta\left(t - \sum_{k=1}^{n}\Delta t_k\right). \quad (1)$$

$\rho(W_k)$ is the density of the distribution of the barriers heights; $\rho(\Delta x_k) = \mu\exp(-\mu\Delta x_k)$, $\rho(\Delta t_k) = \nu_k\exp(-\nu_k\Delta t_k)$ are the distribution densities of the jump lengths and their durations, respectively (Poisson's law); μ is the linear coordinate density of the distribution of the anchoring centers; ν_k is the frequency of attempts of the core disruption from the defect, which is determined by the Arrhenius law.

Based on calculations (1), analytical expressions were obtained for the average drift velocity, diffusion coefficients depending on temperature, and the degree of chaos in barrier heights. Calcula-

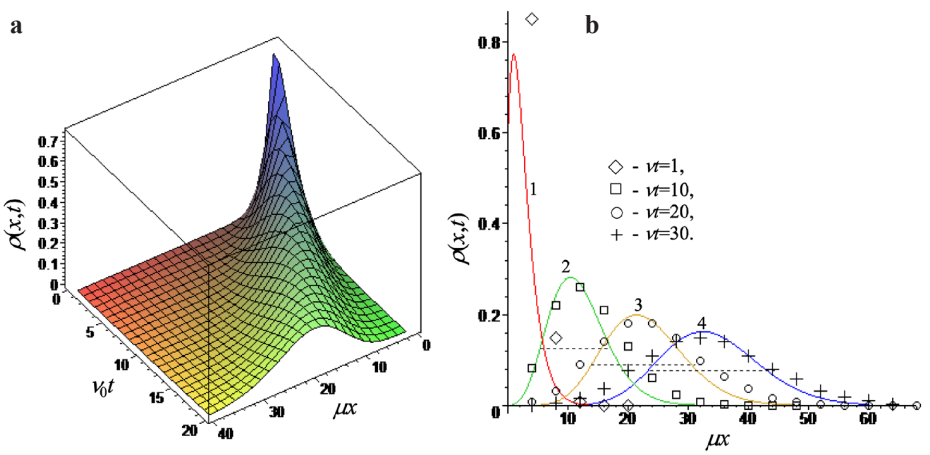

Figure 1. **a** The distribution of the vortex gas depending on the coordinate and time; **b** shows sections of the $\rho(x,t)$ surface at some moments of time. Points – simulation result.

tions were carried out for three models: 1) Identical defects (model 1), 2) Smooth distribution of activation energy (model 2), 3) Normal activation energy distribution (model 3). After integration equation (1) expression for models, it is obtained. Characteristic surface ρ(*x*,*t*) is shown in Fig. 1.

The Fig. 2 shows the main results of the comparative blooms of the three models. In the low temperature range, when the energy of thermal motion is much less than the average value of the energy barriers height, the features of the dependence of the diffusion coefficient on the dispersion of the activation energy of the anchoring centers have been found, i.e., nonmonotonicity associated with the determining role of the magnet defects with the maximum value of the barrier height.

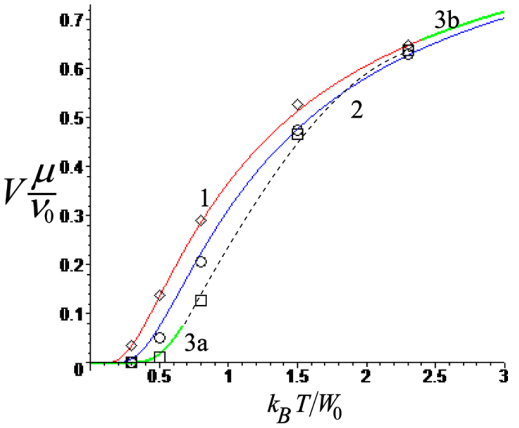

Figure 2. Temperature dependences of the velocity displacement of the maximum coordinate of the ρ(*x*,*t*) function for the models under study.

An interesting fact is that the graphs in Fig. 3 are nonmonotonic. With a small value of the ($\zeta \ll \beta_{mid}$ or $\sigma W \ll W_0$) activation energy spread, when almost all defects are the same in their effect on vortices, a slight increase in accompanied by a natural increase in σ^2, as a response of the system to a more chaotic "input signal". But with the growth of chaos in the barriers heights of the anchoring centers at low temperatures, a significant role is played by rare but more rigid defects, where the quasiparticles gas can fix itself and slows down the expansion of its localization area. It results in the diffusion coefficients decrease. The motion of the vortices gas in this case looks as if most of the quasiparticles are delayed at one (several) high barrier with the growth of ζ (or σ), that limits the spread of coordinates and the drift velocity.

The study has been carried out within the framework of the state task of the Ministry of Science and Higher Education of the Russian Federation (topic No.FSRZ-2020-0011).

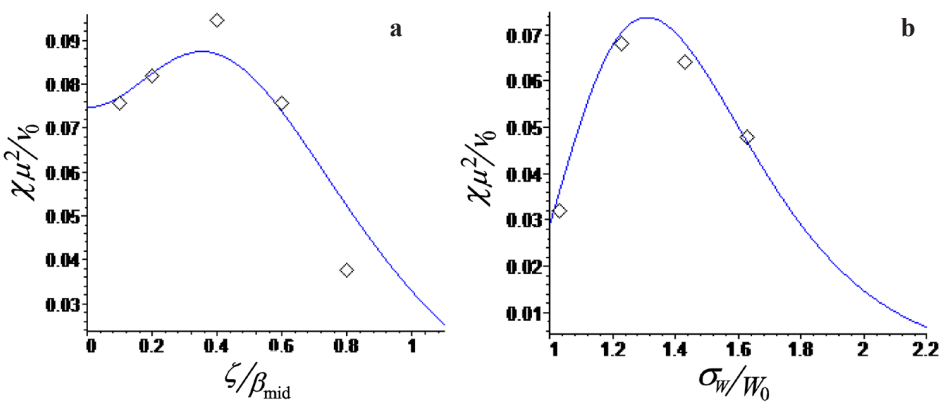

Figure 3. The dependence of the dimensionless diffusion coefficients of the vortex gas on the value of the activation energy spread for the model of smooth distribution of barrier heights (**a**) and for the normal distribution (**b**).

REVERSAL OF DOMAIN WALLS DRIFT DIRECTION IN HARMONIC MAGNETIC FIELD IN IRON GARNET CRYSTALS

*L.A. Pamyatnykh**, *M.S. Lysov, S.E. Pamyatnykh, G.A. Shmatov*

Institute of Natural Sciences and Mathematics, Ural Federal University, Ekaterinburg, Russia
*E-mail: Lidia.Pamyatnykh@urfu.ru

Domain wall (DW) control (control of the parameters and position of the DW) is a topical problem both from the point of view of fundamental science and possible technical applications [1].

The task of controlling the directed motion of domains and DWs includes the search for conditions under which the direction of motion of the DWs can be changed and the required level of speed of the translational motion of the DWs can be obtained. This work develops a possible approach to solving this control problem.

One of the factors determining the form of domain structure and its behavior in magnetic fields is the shape of the sample. In this work, a sample with obvious shape anisotropy was selected for the study. Two regions are distinguished: a wedge-shaped region (CDE) and a rectangular-shaped region (ABCE) (Fig. 1). DW drift [2] is observed in the sample in a harmonic field applied perpendicular to the plane of the sample.

The results for iron garnet $(TbErGd)_3(FeAl)_5O_{12}$ single crystal (110) plate with thickness $L = 70$ µm, saturation magnetization $M_s = 3.9\cdot10^4$ A/m, cubic anisotropy constant $K_1 = -3.0\cdot10^2$ J/m^3, uniaxial anisotropy constant $K_u = 2.0\cdot10^2$ J/m^3, and orthorhombic anisotropy constant $K_p = 7.5\cdot10^2$ J/m^3 are presented.

Domain structures were revealed using the magneto-optical Faraday effect. DW drift speed measurements were performed using an optical microscope with diode CW-laser and specifically designed stroboscopic setup based on a pulsed solid-state Nd:YAG-laser with a wavelength $\lambda = 532$ nm and a pulse duration $\tau = 10$ ns. Images of dynamic domain structure were captured with a high-speed camera with a recording rate up to 2000 fps. External harmonic magnetic field had frequencies $f = 3$–1000 Hz and amplitudes up to $H_0 = 2.2\cdot10^4$ A/m. During the measurements the sample temperature was kept constant at 295 K using LINKAM thermo-cryostat.

The DW drift velocities V_{dr} and intensities I_{MD} of nucleation centers A, E, D (Fig. 1) of magnetic dislocations (MDs) were measured. Intensity of a nucleation center IMD is a number of MDs nucleated in a certain nucleation center during one second.

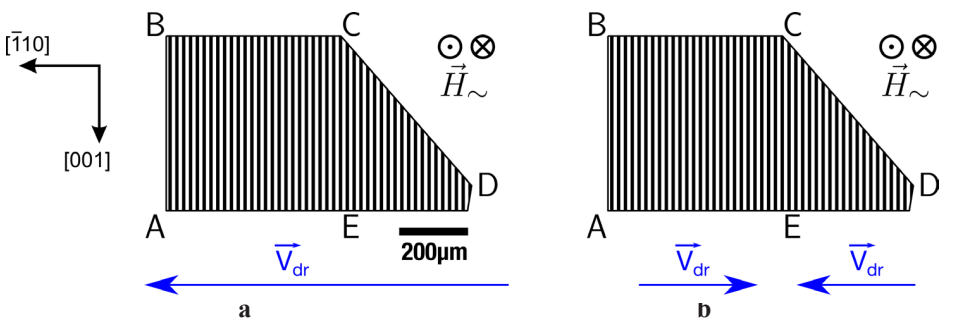

Figure 1. Approximate shape of the sample plate. **a** Drift in the whole sample in one direction. **b** The direction of the drift changes in ABCE region to the opposite.

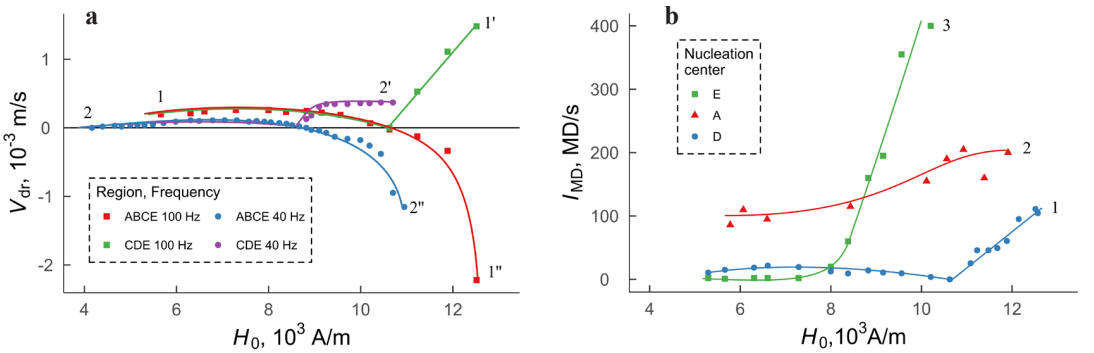

Figure 2. **a** Dependences of DW drift velocity V_{dr} on harmonic magnetic field amplitude. Curves 1 and 2 are DW drift velocities in the entire sample before the drift stops at $f = 100$ and 40 Hz, respectively. After the stop of the drift: V_{dr} in the CDE region at $f = 100$ Hz (curve 1′), at $f = 40$ Hz (curve 2′); V_{dr} in the ABCE region at $f = 100$ Hz (curve 1″), at $f = 40$ Hz (curve 2″). **b** Dependences of intensity of MD nucleation centers E, A, D on harmonic magnetic field amplitude at frequency $f = 100$ Hz.

It is established experimentally that the drift of DWs in the CDE and ABCE regions is not the same. In the frequency range 3–1000 Hz with an increase of the field amplitude from the field of the beginning of the drift H_{dr} in the ABCE region the direction of the drift changes to the opposite, while in the CDE region the direction of the DW drift remains unchanged [3].

Figure 2a shows the dependences of the DW drift velocity on the field amplitude for frequencies $f = 100$ and 40 Hz for the entire sample (curves 1 and 2, respectively). The dependence of the drift velocity on the field amplitude correlates with the results of measurements of the intensity of the MD nucleation centers. Figure 2b shows the amplitude dependences of the intensity of the MD nucleation centers for the frequency $f = 100$ Hz.

It can be assumed that the direction of the DW drift observed at low field amplitudes in the entire sample is determined by the gradient of demagnetizing fields that appears due to the anisotropy of the sample shape.

With an increase of the field amplitude, a change in the activity of the MD nucleation centers is observed (at $f = 100$ Hz in a field $H_0 = 10.4 \cdot 10^3$ A/m about 400 MDs per second nucleate in one center), which may indicate a change in the configuration of the internal field in the rectangular part of the sample and lead to a change of direction of the field gradient.

Using numerical simulations it was established that the direction of the DW drift can be determined by the direction of the magnetic field gradient in the sample. According to the model, the drift is caused by the presence of a magnetic field gradient in the sample, and the reversal of the direction of the drift is caused by a change of the field gradient direction to the opposite.

This work was performed within the framework of the state assignment of the Ministry of Science and Higher Education of the Russian Federation (Project FEUZ-2020-0051).

1. K.W. Moon, D.H. Kim, S.C. Yoo, S.G. Je, B.S. Chun, W. Kim, B.C. Min, C. Hwang and S. B. Choe, Sci. Rep. **5**(1), 1–5 (2015).
2. L.A. Pamyatnykh, B.N. Filippov, L.Y. Agafonov and M.S. Lysov, Sci. Rep. **7**, 18084 (2017).
3. L. Pamyatnykh, M. Lysov, S. Pamyatnykh and G. Shmatov, JMMM **542**, 168561 (2022).

NONLINEAR OPTICAL STUDIES OF RESIDUAL DOMAIN STRUCTURE OF EPITAXIAL GARNET FILMS

E.A. Mamonov[1], *D.A. Kopylov*[1], *M.P. Temiryazeva*[2], *A.G. Temiryazev*[2], *T.V. Murzina*[1*]

[1]Lomonosov Moscow State University, Department of Physics, Moscow, Russia
[2]Kotel'nikov Institute Radioengineering and Electronics of RAS, Fryazino Branch, Russia
[*]E-mail: murzina@mail.ru

Dielectric magnetic films and crystals, and especially their domain structure are a subject of intense studies already for quite a time [1]. It is well known that even in the case of epitaxial films their domain structure being quite complicated governs the main magnetic and magnetooptical effects, which is important for applications. Common experimental techniques such as polarization microscopy and magnetooptical (Faraday and Kerr) effect studies provide the averaged over the films' thickness information on the magnetic structure of the transparent dielectric magnetic films such as iron-garnets, while the composition of the magnetization close to the surfaces or interfaces remains less studied. Quite interesting information here was obtained when using the magnetic force microscopy (MFM) technique; as an example we can mention a paper by F. Lisovsky and co-workers [2], where a complicated surface magnetic structure of garnet films was reported. On the other hand, high surface and interface sensitivity is an attribute of the nonlinear optical method of optical second harmonic generation (SHG) [3], which is symmetry forbidden in the bulk of centrosymmetric media in the electric dipole approximation [4]. As garnet crystal is a m3m symmetric crystal, SHG-probe can be applied for the investigation of its structure and surface magnetic properties.

Here we study the magnetic properties of the subsurface layer of epitaxial $(LuBi)_3Fe_5O_{12}$ film, (111) facet, by two surface-sensitive techniques: second harmonic generation and MFM. Atomic force and magnetic force microscopy were performed using SmartSPM (AIST-NT). SHG-microscopy studies were carried out when using the setup based on a femtosecond OPO (pulse duration 150 fs, repetition rate 70 MHz, mean power 50 mW) at 850 nm wavelength, equipped with focusing and collecting objectives Mitutoyo M Plan Apo 100$^{\times}$ with NA = 0.7 that operated in transmission geometry at normal incidence, the resolution being about 500 nm. The SHG radiation transmitted through the films was spectrally selected by appropriate set of filters, passed through the Glan analyzer and detected by a photomultiplier. It is worth noting that the pump wavelength of 850 nm corresponds to the transparency band of the garnet film, while the SHG at 425 nm is far in the absorption range, thus the SHG signal could appear from a subsurface garnet layer of the thickness of several hundreds of nanometers.

The SHG anisotropy studied performed in transmission and at normal incidence demonstrate that the crystallographic garnet structure corresponds to the (111) surface symmetry. Strong SHG intensity is caused by partial breaking down the inversion symmetry of garnet layer due to the presence of Lu and Bi ions, which is known for this type of material [5]. Figure 1 shows the intensity maps of the transmitted SHG intensity polarized parallel (panel a) and perpendicular to the polarization plane of the pump radiation. One can see that in the first case the SHG map reveals a set of parallel dark and bright stripes of approximately 2.5 μm in width, which correspond to magnetic domains magnetized in the opposite directions. In addition, a periodic modulation of the SHG intensity is the direction parallel to the domains is seen, similarly to the results of the MFM studies. This periodicity is even more evident in the case of perpendicular combination of pump and SHG polarizations (Fig. 1b). Importantly, that a rather complicated magnetic structure is observed at the boundaries of the domains. This correlates again with the MFM images, where fine distribution of magnetization is attained closer to the boundaries of the magnetic domains in zero external magnetic field.

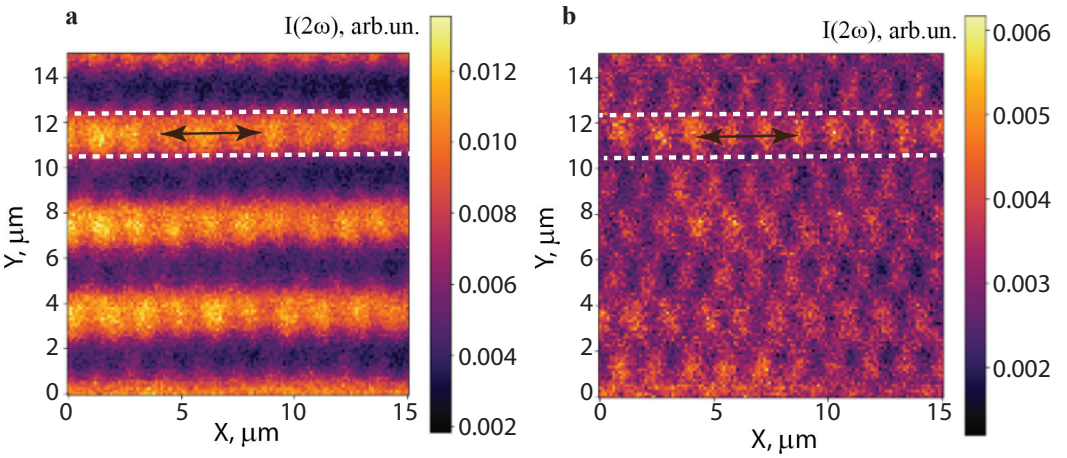

Figure 1. SHG microscopy images of the $(BiLu)_3Fe_5O_{12}$ film measured for the pump polarization parallel to the domains (shown by arrow), as the polarization of the SHG wave is (**a**) parallel or (**b**) perpendicular to that of the pump; dashed lines indicate the approximate boundaries of magnetic domains.

When discussing the obtained results, we should underline that the MFM method is sensitive to the component of magnetization normal to the film surface, whereas nonlinear SHG microscopy method is induced predominantly by the in-plane component of magnetization. Simultaneous use of these techniques allows restoration of complex picture of film surface magnetization. Namely, we suppose that the subsurface magnetic structure contains both in-plane and out-of plane magnetized substructures, especially closer to the domains' boundaries. This may be due to a zigzag like domain structure with closing domains, as well due to inclined orientation of magnetization within the domains. Further studies on the polarization plane rotation of the SHG wave can provide more details to this picture.

Support by RSF, grant No 19-72-20103 is greatly acknowledged.

1. A. Hubert, and R. Schäfer. Magnetic domains: the analysis of magnetic microstructures. Springer Science & Business Media, 2008.
2. F.V. Lisovskii, E.G. Mansvetova, M.P. Temiryazeva et al., JETP Lett. **96**, 596–600 (2013).
3. I.A. Kolmychek, V.L. Krutyanskiy, T.V. Murzina, M.V. Sapozhnikov, E.A. Karashtin, V.V. Rogov, and A.A. Fraerman, J. Opt. Soc. Am. B **32**, 331–338 (2015).
4. Y.R. Shen, The Principles of Nonlinear Optics. Wiley, Hoboken, NJ (1984).
5. A.K. Zvezdin and V.A. Kotov, Modern Magnetooptics and Magnetooptical Materials. Inst. of Phys. Publ. Bristol and Philadelphia (1997).

STRUCTURE AND PROPERTIES OF kπ-SKYRMIONS IN FERROMAGNETIC FILMS WITH SPATIALLY MODULATED PARAMETERS

R.M. Vakhitov, G.F. Ilyasova, R.V. Solonetsky*

Bashkir State University, Ufa, Russia
*E-mail: galiya.siraeva2014@yandex.ru

At present, the scale of research on magnetic skyrmions has increased significantly: their possible types, properties, magnetic materials in which they are stabilized, etc. Such interest in them is explained not only by the prospects for their application in spintronic devices, but also by their unusual properties, which are demonstrated in various works [1]. For the first time, magnetic skyrmions were discovered in chiral magnets, in which, due to the presence of the Dzyaloshinskii-Moriya interaction, they form stable states [2]. In most subsequent studies, magnetic skyrmions were understood as vortex-like inhomogeneities in which the unit magnetization vector **m** rotates by 180° as the radial variable r increases from 0 to ∞ (π-skyrmions). At the same time, studies appeared in which the possibility of the existence of $k\pi$-skyrmions ($k \in 1, 2, 3...$) was predicted [3].

Due to the fact that in chiral magnets [4] certain difficulties arose (for various reasons) with the stability of magnetic skyrmions, a demand arose for alternative methods of their stabilization in other materials, i.e. in non-chiral magnets. One of the possible ways to implement this approach was proposed in [4, 5], where it was shown that such materials can be ferromagnetic films with spatially modulated uniaxial anisotropy. Later it was established (both experimentally [4] and theoretically [5]) that magnetic skyrmions can exist in such materials in a wide range of temperature and magnetic fields.

In this paper, we study the stable states of magnetic $k\pi$-skyrmions formed on columnar defects of the "potential well" type in uniaxial ferromagnetic films [5]. Such studies in non-chiral magnets have not yet been practically carried out, with the exception of [6], in which the influence of a magnetic field on $k\pi$-skyrmions ($k \in 2, 3, 4$) that appear in Fe_3Sn_2 magnetic nanodisks was studied. As a defect model, we consider the structural inhomogeneity of a magnet, in which the material parameters $P = \{A, K_u, M_s\}$, change abruptly in the region of the defect:

$$P = \begin{cases} P_1, r < R_0 \\ P_2, r < R_0 \end{cases}, \tag{1}$$

where $P_i = \{A_i, K_{ui}, M_{si}\}$ are the material parameters outside the columnar defect ($i = 1$) and in the region of the defect ($i = 2$). Here A is the exchange parameter, K_u is the uniaxial anisotropy constant, and M_s is the saturation magnetization.

Numerical analysis of the Euler-Lagrange integro-differential equation, which describes the distribution of magnetization in the region of a defect, taking into account the energy of magnetic inhomogeneities [5], makes it possible to find the distribution of the magnetization **m** of $k\pi$-skyrmions (Fig. 1) in the region of a columnar defect and its characteristics: the characteristic dimensions of the magnetic inhomogeneity and her energy. It follows from the above calculations of the structure and stability of $k\pi$-skyrmions that they can exist as stable formations in magnetically uniaxial films on columnar defects of the potential well type. The topology and dimensions of these inhomogeneities essentially depend on the characteristics of the defect (A_2, K_{u2}, M_{s2}, R_0) and, above all, on its radius R_0 and the depth of the potential well K_{u2}. It can be noted that the initial profiles of the

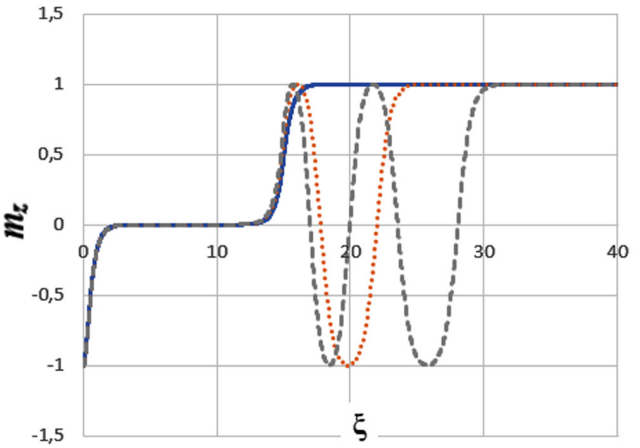

Figure 1. Distribution of the magnetization of $k\pi$-skyrmions, depending on the reduced coordinate $\xi = r/\Delta_0$, $(\Delta_0 = (A_1/K_{u1})^{1/2}$ for the following values of material parameters, $K_{u2} = -4K_{u1}$, $L = 15$, $Q = 100$, $A_2 = A_1$, $M_{s2} = M_{s1}$. Here the solid line (blue line) corresponds to the π-skyrmion, the dotted line (red line) to the 3π-skyrmion, and the dashed line (gray line) to the 5π-skyrmion.

magnetization distribution for all three types of $k\pi$-skyrmions ($k \in 1, 3, 5$) coincide with each other regardless of R_0. Studies show that the π-skyrmion is more energetically favorable, and 3π, 5π-skyrmions exist as metastable states. In this case, the lower stability threshold of π-skyrmions with respect to defect sizes starts from small R_0 ($R_0 \geq 1$), 3π-skyrmions from large R_0 ($R_0 \geq 14$), and 5π-skyrmions from even larger R_0 ($R_0 \geq 25$).

According to calculations, the stability region is practically independent of the saturation magnetization value in the M_{s2} defect region. At the same time, studies show that the exchange parameter in the defect region A_2 has a greater effect on the boundary of the stability region: as it decreases (compared to A_1), the curve $Q = Q_1(R_0)$, which characterizes the lower boundary of the region in Q, shifts downward. This behavior of the curve as a function of A_2 is explained by the fact that a decrease in the influence of the exchange interaction leads to an increase in the contribution of magnetostatic fields to the total energy of the magnet, which affects the stability region of skyrmions.

1. K. Everschor-Sitte, J. Masell, R.M. Reeve et al., J. Appl. Phys. **124**, 240901 (2018).
2. S. Muhlbauer, B. Binz, F. Jonetz, A. Neubauer, R. Georgii, P. Böni, Science **323**, 915 (2009).
3. J. Hagemeister, A. Siemens, L. Rózsa, E.Y. Vedmedenko, and R. Wiesendanger, Phys. Rev. B **97**, 174436 (2018).
4. M.V. Sapozhnikov, S.N. Vdovichev, O.L. Ermolaeva, N.S. Gusev, A.A. Fraerman, S.A. Gusev, Y.V. Petrov, Appl. Phys. Lett. **109**, 042406 606 (2016).
5. R.M. Vakhitov, R.V. Solonetsky, A.A. Akhmetova, J. Appl. Phys. **128**, 229901 (2020).
6. J. Jiang, Y. Wu, L. Kong, Y. Wang, J. Li ,Y. Xiong, J. Tang, Acta Materialia **215**, 117084 (2021).

MAGNETIC FORCE MICROSCOPY OF SKYRMION FORMATION IN THIN CoPt-FILMS

M.P. Temiryazeva[1*], *A.G. Temiryazev*[1], *M.V. Stepushkin*[1], *A.V. Zdoroveyshchev*[2]
D.A. Zdoroveyshchev[2], *A.V. Kudrin*[2], *D.A. Tatarskiy*[3,4],
A.V. Sadovnikov[5], *S.A. Nikitov*[6]

[1]Fryazino Branch of the Kotelnikov Institute of Radio Engineering and Electronics RAS, Fryazino, Russia
[2]Physico-Technical Research Institute of Lobachevsky State University of Nizhny Novgorod, Nizhny Novgorod, Russia
[3]Institute for Physics of Microstructures RAS, Nizhny Novgorod, Russia
[4]Physical faculty, Lobachevsky State University, Nizhny Novgorod, Russia
[5]Laboratory of Magnetic Metamaterials, Saratov State University, Saratov, Russia
[6]Kotelnikov Institute of Radio Engineering and Electronics RAS, Moscow, Russia
[*]E-mail: mtemiryazeva@gmail.com

Film structures prepared in high vacuum by the method of electron-beam evaporation with alternate deposition of Co (3 or 2 Å) and Pt (5 Å) layers were studied. The number of bilayers was 10, and the total films thickness was 7 or 8 nm. The resulting structures are multilayered films with blurred (diffuse) layer boundaries. They have magnetic anisotropy perpendicular to the film surface and a coercivity field of several hundred oersteds. According to measurements of the Mandelstam-Brillouin scattering, the films show the presence of the Dzyaloshinskii-Moriya interaction. All these properties determine the possibility of the existence of skyrmions. Studies using Lorentz microscopy demonstrate a special black-white dipolar contrast in the Fresnel mode. It can be interpreted as homochiral Néel-type textures: skyrmions and 360-degree domain walls – 1D skyrmions. In the demagnetized state, the films have a labyrinthine domain structure.

To study of magnetization reversal special methods of magnetic force microscopy (MFM) have been developed, which make it possible to obtain series (several hundred) of MFM images under external influence. Such series were used to create films visualizing magnetization reversal under the influence of an external magnetic field (both normal and tangential). In the absence of an external field, this technique made it possible to analyze the change of the domain structure under the action of a spatially localized field of the magnetic probe of an atomic force microscope.

The results of measurements showed that both free-standing skyrmions (Fig. 1) and 360-degree domain walls – 1D skyrmions, can be formed under the action of the magnetic field of the probe in films with different Co content. The mechanism of their formation is related to the interaction of the domain walls. The movement of the probe along the surface leads to displacement of the domain wall; when two walls approach each

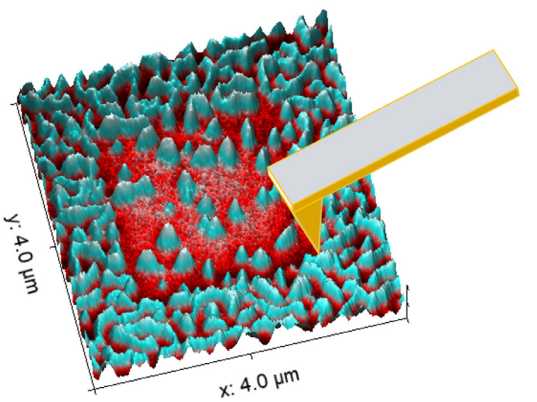

Figure 1. The skyrmions formed from a labyrinthine domain structure by the local magnetic field of an atomic force microscope probe

other, skyrmions can be formed. In an external magnetic field directed along the normal to the film surface, skyrmions are formed at fields close to saturation. When a tangential field is applied to a pre-saturated film, individual skyrmions first appear, and as the field increases, individual skyrmions merge, forming a labyrinth structure.

We have carried out experiments to measure the Hall effect with the simultaneous MFM registration of the domain structure. It is shown that the creation or destruction of one skyrmion corresponds to a change in the Hall resistance by approximately 0.6-1 mΩ.

Support by RSF (project No. 21-79-20186) is acknowledged.

FORMATION OF THE SKYRMIONS IN CoPt AND CoPd THIN FILMS AFTER ION IRRADIATION

I.L. Kalentyeva[1*], *O.V. Vikhrova*[1], *A.V. Zdoroveyshchev*[1], *A.V. Zdoroveyshchev*[1], *Yu.A. Dudin*[1], *Yu.A. Danilov*[1], *M.P. Temiryazeva*[2], *A.G. Temiryazev*[2], *A.V. Sadovnikov*[3]

[1]Lobachevsky State University of Nizhny Novgorod, Nizhny Novgorod, Russia
[2]Kotel'nikov Institute of Radioengineering and Electronics of RAS, Fryazino Branch, Fryazino, Russia
[3]Kotel'nikov Institute of Radioengineering and Electronics of RAS, Moscow, Russia
[*]E-mail: istery@rambler.ru

As is known, ion irradiation of CoPt thin films leads to asymmetric mixing of Co and Pt atoms, which causes a decrease in the perpendicular anisotropy of magnetization in the structures, leads to an increase in the Dzyaloshinskii-Moriya interaction, and promotes the activation of the formation of skyrmions [1]. This work is devoted to the study of the effect of ion irradiation on the domain structure of ferromagnetic CoPt(Pd) thin films and on the appearance of skyrmion states in such structures.

The studied samples were $Co_{0.35}Pt_{0.65}$ and $Co_{0.35}Pd_{0.65}$ films which were obtained by electron-beam evaporation at 200 °C on i-GaAs substrates: layers of Pt(Pd) (0.5 nm) and Co (0.2 nm) were deposited in turn with a tenfold repetition. The total thickness of the CoPt(2/5) and CoPd(2/5) metal films in this case was ~7 nm. The structures were then irradiated at ILU-3 accelerator with He^+ ions at an energy of 20 keV, the fluence (F) was varied from $1\cdot10^{14}$ to $3\cdot10^{15}$ cm^{-2}. The magnetic field dependences of the Faraday angle ($Q_F(H)$) (at wavelengths of 980 nm) and the Hall effect (ordinary and planar) were studied at room temperature in the range of magnetic fields (±2.5 T). The study of changes in the domain structure, leading to the formation of skyrmions, was carried out during MFM scanning with a probe with a high magnetic moment according to the method described in [2]. The paper also presents an estimate of the Dzyaloshinskii-Moriya interaction energy (EDM), obtained as a result of studying the samples by the Mandel'shtam-Brillouin spectroscopy method.

For the original CoPt(2/5) film, the MFM image (Fig. 1a) shows 1D skyrmions (360-degree domain walls ~100 nm wide). After the films are irradiated, there is a transition to round skyrmions (at $F = 3\cdot10^{14}$ cm^{-2}) and an increase in their number with increasing F (Fig. 1b). For a sample with a fluence of $7\cdot10^{14}$ cm^{-2}, a very dense lattice of individual round skyrmions is observed (Fig. 1c). At $F \geq 1\cdot10^{15}$ cm^{-2}, the lateral component of the magnetization vector begins to dominate (Fig. 1d).

This fact is confirmed by measurements of the Hall and Faraday effects: the resulting dependences $Q_F(H)$ and $R_H(H)$ contain a hysteresis loop with a coercive field H_C ~ 700 Oe, in this case, the Q_F in the zero field coincides with the value in the saturation field up to a fluence $5\cdot10^{14}$ cm^{-2} (Fig. 2). At higher values of F, a narrowing of the hysteresis loop and a decrease in the value of Q_F in zero magnetic field are observed, while at the maximum F the $Q_F(H)$ dependence becomes linear. At the same time, according to measurements of the planar Hall effect, a monotonous decrease in the saturation field is observed from 8000 Oe for the initial sample to 1500 Oe for the structure after irradiation with $F = 3\cdot10^{15}$ cm^{-2}.

CoPd(2/5) demonstrates a similar trend: one-dimensional skyrmions observed in the original sample become shorter with increasing fluence, and at $F = 1\cdot10^{15}$ cm^{-2} turn into "chains of round skyrmions" (Fig. 1e–g). Apparently, ion irradiation changes the structure of domain walls. The initial CoPd film has a larger labyrinthine domain structure and, unlike CoPt, the state when the magnetization vector lies in a plane is not achieved for CoPd in the fluence range under consideration,

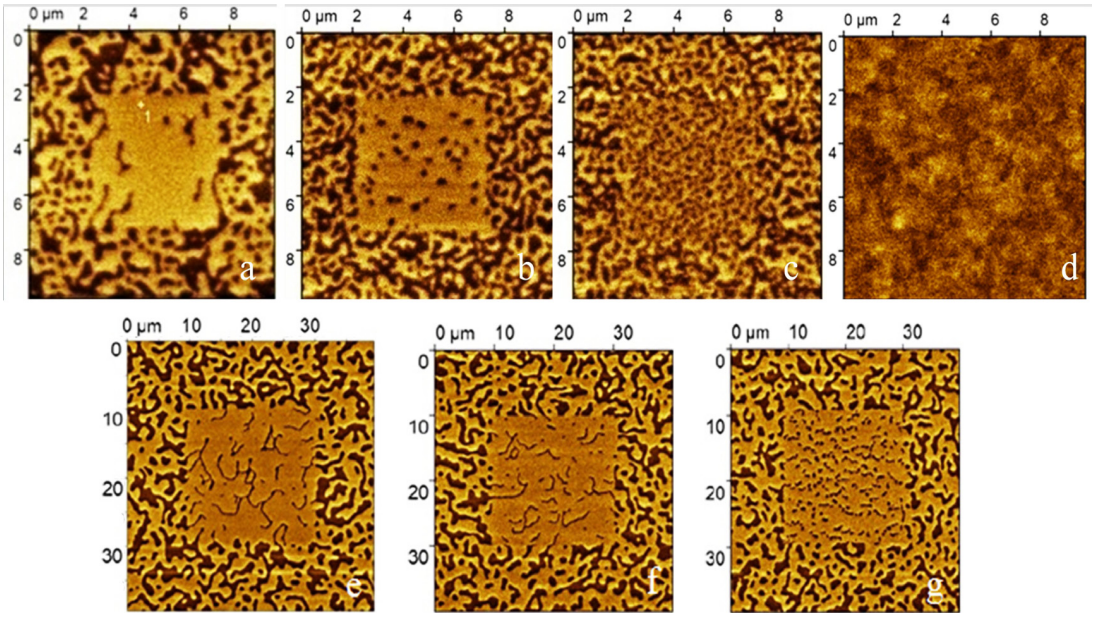

Figure 1. MFM images for irradiated CoPt films with different ion fluences F, cm^{-2}: a) 0, b) $5{\cdot}10^{14}$, c) $7{\cdot}10^{14}$, d) $1{\cdot}10^{15}$ and CoPd: e) 0, f) $5{\cdot}10^{14}$, g) $1{\cdot}10^{15}$.

however, there is a gradual increase in the lateral component of the easy magnetization axis with increasing F, as indicated by measurements of the Hall effect.

For irradiated CoPt(2/5) layers, the EDM constant (D) increases for the range of He^+ fluence from 0 to (5-7)$\cdot10^{14}$ cm^{-2} and reaches a maximum value of 0.685 mJ/m^2. At a higher fluence, the value of D sharply decreases, which corresponds to the disappearance of the perpendicular anisotropy of the magnetization of the CoPt film and the pinning of its vector in the plane. The highest values D = 0.639 mJ/m^2 are recorded for the CoPd(2/5) film irradiated with a fluence $1{\cdot}10^{15}$ cm^{-2} (at this F a transition to round skyrmions was observed on MFM images). This effect can be associated with

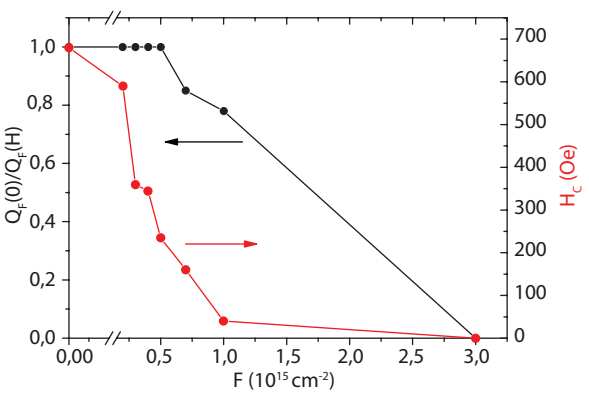

Figure 2. Dependences of the coercive field H_C and the relative values of the Faraday angle $Q_F(0)/Q_F(H)$ on the H^+ fluence for the CoPt(2/5) structure.

a decrease in the energy of the domain wall, which leads to an increase in the EDM constant and the appearance of optimal conditions for the formation of skyrmion-type domain structures under the influence of the local field of a magnetic probe. The obtained results can be used to create information storage and processing devices.

This work was supported by Russian Science Foundation (Project No. 21-79-20186) and the federal academic leadership program "Priority 2030" of the Ministry of Science and Higher Education of the Russian Federation.

1. I.L. Kalentyeva, O.V. Vikhrova, Yu.A. Danilov et al., Phys. Solid State **62**, 386–394 (2021).
2. A.G. Temiryazev, M.P. Temiryazeva, A.V. Zdoroveyshchev et al., Phys. Solid State **60**, 2200–2208 (2018).

TEMPERATURE RESOLVED DEPENDENCIES OF GILBERT DAMPING IN HETEROSTRUCTURES $MnBi_2Te_4$/NiFe

P.N. Skirdkov[1,2], *G.A. Kichin*[1], *F.M. Maksimov*[3], *A.I. Chernov*[3], *K.A. Zvezdin*[1,2], *A.S. Pakhomov*[1,3*]

[1]"New Spintronic Technologies" LLC, Skolkovo Innovation Center, Moscow, Russia
[2]Prokhorov General Physics Institute of the Russian Academy of Sciences, Moscow, Russia
[3]Moscow Institute of Physics and Technology, Dolgoprudny, Russia
[*]E-mail: a.pakhomov@nst.tech

Huge value of the spin-orbit coupling makes topological insulators (TIs) a very attractive and promising material for use in future spintronic devices. One of such materials is the recently discovered topological insulator $MnBi_2Te_4$, which has antiferromagnetic properties at low temperatures. In this work, we studied samples of heterostructures topological insulator/ferromagnet, where $MnBi_2Te_4$ was taken as a topological insulator and a widespread iron-nickel alloy, permalloy, was used as a ferromagnet. The permalloy thickness was varied from 20 to 4 nm, the TI thickness is 10 nm, which corresponds to 7 SL (septuple layer).

In this work, the parameter S21 was measured as a function of the external magnetic field at different ferromagnetic resonance frequencies in the temperature range from 5 to 295 K. The Hilbert damping parameter of the heterostructure was studied at different temperatures. In addition, the voltage of the inverse spin Hall effect was measured for the same sample at the same temperatures, but at a frequency of 4 GHz.

Anomalous behavior has been detected. The Hilbert damping parameter exhibits extremes around 80 and 150 K. Similar behavior is also observed for the inverse spin Hall effect voltage. A similar behavior of the Gilbert damping parameter was observed earlier in the work [1].

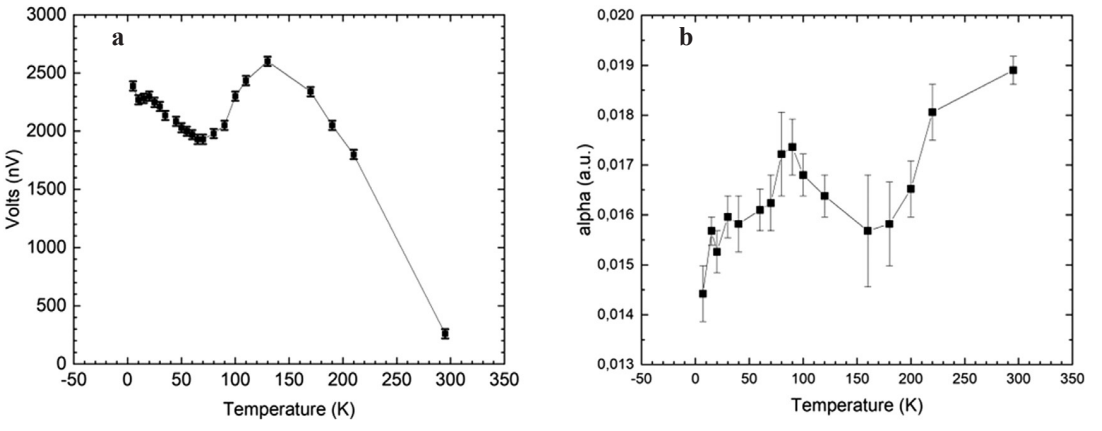

Figure 1. Temperature dependence of $MnBi_2Te_4$ (10 nm)/NiFe(20 nm): **a** ISHE voltage, **b** Gilbert-damping parameter.

Support by RSF №19-12-00432 is acknowledged.

1. Y. Zhao, Q. Song, S.H. Yang et al., Sci. Rep. **6**, 22890 (2016).

MEAN-FIELD DESCRIPTION OF TOPOLOGICAL PHASES IN HEXAGONAL FRUSTRATED ANTIFERROMAGNETS

O.I. Utesov[1-3]

[1]Department of Physics, Saint Petersburg State University, St. Petersburg, Russia
[2]National Research Center "Kurchatov Institute", B.P. Konstantinov Petersburg Nuclear Physics Institute, Gatchina, Russia
[3]St. Petersburg School of Physics, Mathematics, and Computer Science, HSE University, St. Petersburg, Russia
*E-mail: utiosov@gmail.com

Magnetic skyrmions and their ordered arrays, skyrmion lattices (SkL), are extensively studied in the present time. It is well-known that such topological structures can be stabilized in noncentrosymmetric helimagnets with Dzyaloshinskii-Moriya interaction [1] and in centrosymmetric ones due to exchange interaction frustration [2]. In the former case, skyrmion size and SkL parameter are usually large, whereas in the latter case one can expect nanometer-sized spin structures. Importantly, skyrmions of small size have an advantage from the practical point of view, e.g., in possible usage as information carriers [3].

Skyrmion lattice phase properties (including the phase diagram domain, where it is stable) are usually described numerically within the models including various anisotropic interactions and/or thermodynamic fluctuations [1, 4]. However, in the high-temperature part of the phase diagram, a simple mean-field description is possible due to a small average value of the ordered magnetic moment, which was shown in Ref. [5] for tetragonal frustrated helimagnets.

In the present study, we adapt the mean-field approach from Ref. [5] to the case of hexagonal systems. We assume that the exchange interaction Fourier-transform has three equivalent minima, which is relevant to experimental observation in Gd_2PdSi_3 [6]. Moreover, exchange coupling provides

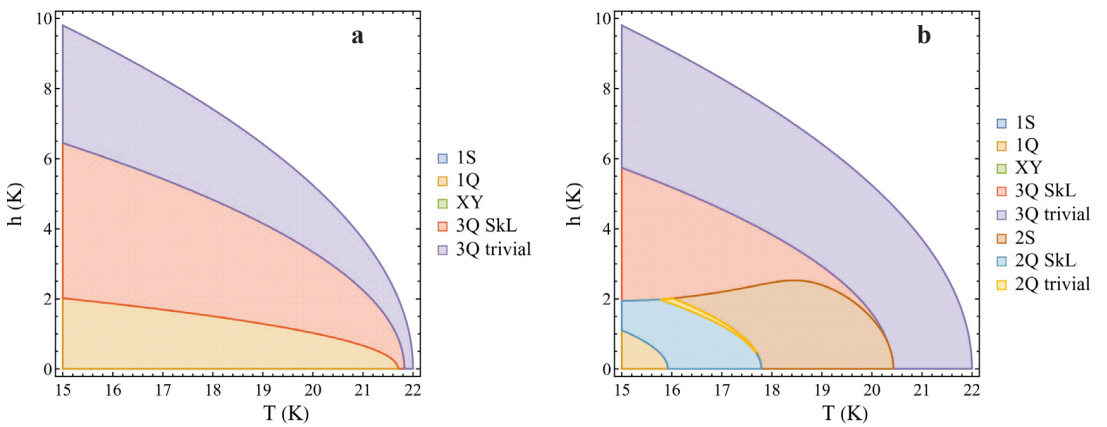

Figure 1. Several types of phase diagrams can be observed in the proposed model. The external magnetic field is along the *c*-axis. **a** Only magnetodipolar interaction-induced anisotropy is taken into account. When magnetic field grows up screw helicoid phase is substituted by the hexagonal lattice of Bloch-type skyrmions, which become topologically trivial at larger fields. **b** In the presence of additional anisotropic exchange, double-Q phases can be stable in the low-field part of the phase diagram at high temperatures.

a large energy scale, in comparison with small anisotropic interactions. The latter can be presented by magnetodipolar interaction (which is usually important for magnetic ions with $L = 0$) or anisotropic exchange. Importantly, dipolar forces provide biaxial momentum-dependent anisotropy for spiral magnetic structures, which in general favors screw helicoids [7]. Moreover, this axes hierarchy is crucial for SkL stabilization in the external magnetic field along the *c*-axis of the system.

In our mean-field calculations we compare free energies of various modulated spin structures, including single modulated spin density wave (1S), screw helicoid (1Q), conical helicoid (XY), double modulated vortical phase (2S), and the superposition of two screw helicoids (topologically non-trivial 2Q SkL and 2Q trivial structure), and finally triple-modulated structures (topologically non-trivial 3Q SkL and 3Q trivial structure). As a result, when only magnetodipolar interaction was taken into account we observe the phase diagram shown in Fig. 1a using parameters estimated for Gd_2PdSi_3. One can see that only three phases are present in this figure: screw helicoid and 3Q phase in its topologically trivial and non-trivial forms. Importantly, 3Q SkL (hexagonal Bloch-type skyrmions lattice) is stable in the large region of the phase diagram at moderate external fields. If the additional anisotropic exchange terms are included in the model, one can observe the phase diagram shown in Fig. 1b, where additional double-modulated phases emerge in the low-fields region. We argue that this type of phase diagram can be relevant to the Gd_2PdSi_3 compound [6].

To conclude, a simple mean-field description of topologically non-trivial phases in frustrated hexagonal antiferromagnets is proposed [7]. Importantly, the majority of the results are presented in the analytical form, which allows their further use in experimental data interpretation.

We are grateful to V.A. Ukleev for valuable discussions. This work is supported by the Russian Science Foundation (Grant No. 22-22-00028).

1. S. Mühlbauer, B. Binz, F. Jonietz, C. Pfleiderer, A. Rosch, A. Neubauer, R. Georgii and P. Böni, Science **323**, 915 (2009).
2. T. Okubo, S. Chung and H. Kawamura, Phys. Rev. Lett. **108**, 017206 (2012).
3. A. Fert, V. Cros and J. Sampaio, Nat. Nanotechnol. **8**, 152–156 (2013).
4. A. Leonov and M. Mostovoy, Nat. Commun. **6**, 8275 (2015).
5. O.I. Utesov, Phys. Rev. B **103**, 064414 (2021).
6. T. Kurumaji, T. Nakajima, M. Hirschberger, A. Kikkawa, Y. Yamasaki, H. Sagayama, H. Nakao, Y. Taguchi, T.-h. Arima and Y. Tokura, Science **365**, 914 (2019).
7. O.I. Utesov, Phys. Rev. B **105**, 054435 (2022).

D.O11

PINNING OF VORTICES DURING THE PASSAGE OF TURBULENT MAGNETIZATION REVERSAL WAVES IN ANTIDOT FILMS WITH THROUGH AND NON-THROUGH HOLES

V.V. Zverev[1,2]

[1]Ural Federal University n.a. the first President of Russia B.N. Yeltsin, Ekaterinburg, Russia
[2]M.N. Miheev Institute of Metal Physics of Ural Branch of Russian Academy of Sciences, Ekaterinburg, Russia
E-mail: vvzverev49@gmail.com

After more than two decades of study, magnetic films with arrays of holes (antidot arrays) continue to be interesting for research [1]. Holes act as pinning centers that prevent the motion of domain walls (DWs). Therefore, the geometric arrangement of holes strongly affects the coercive field of the film and predetermines the features of magnetic switching and hysteresis behavior [2]. Domain-walls pinning on holes leads to the appearance of complex domain structures and to various scenarios of transformations of the film magnetization. Many papers emphasize that controlled switching between magnetic configurations could be used for data storage. The need to increase the switching speed requires the study of dynamic processes, including the region of unstable dynamics and turbulence.

In the majority of works on antidot arrays, magnetic films are thin (10–40 nm) and the magnetization distribution is actually two-dimensional (2D). However, despite the general trend to focus on low-dimensional systems, three-dimensional (3D) nanomagnetism remains an intriguing and promising area of research. Bloch lines and Bloch points [3], vortex structures with tube-like cores

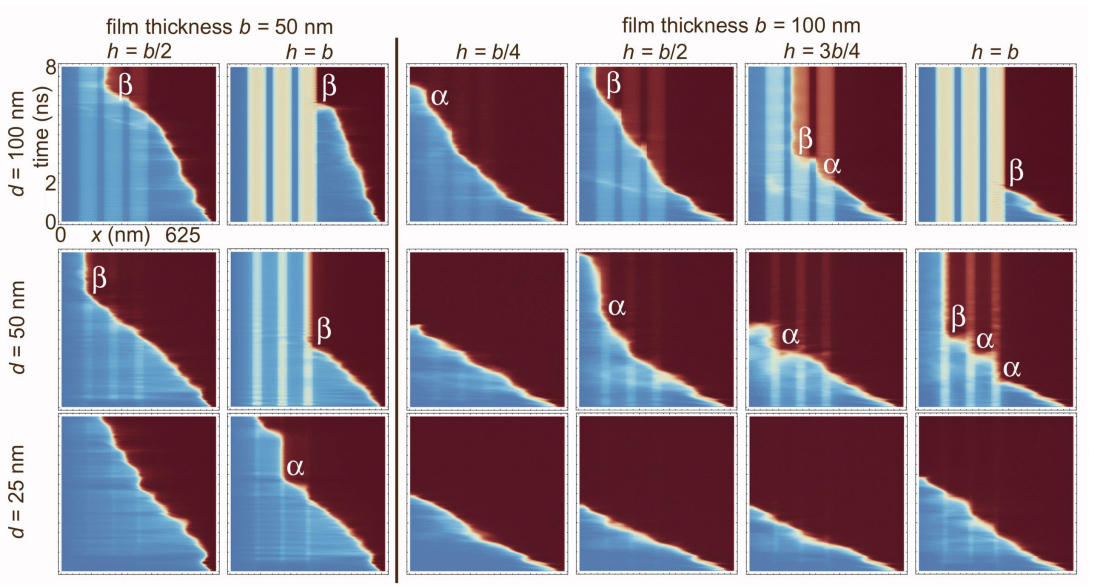

Figure 1. Time and x-coordinate dependence of the z-component of the magnetization vector averaged over the yz cross section of the sample. The images correspond to different film thicknesses b, hole sizes d and hole depths h. The transition from a blue (light) to red (dark) tone corresponds to the rotation of the average magnetization from the direction opposite to the magnetic field to the direction along the field.

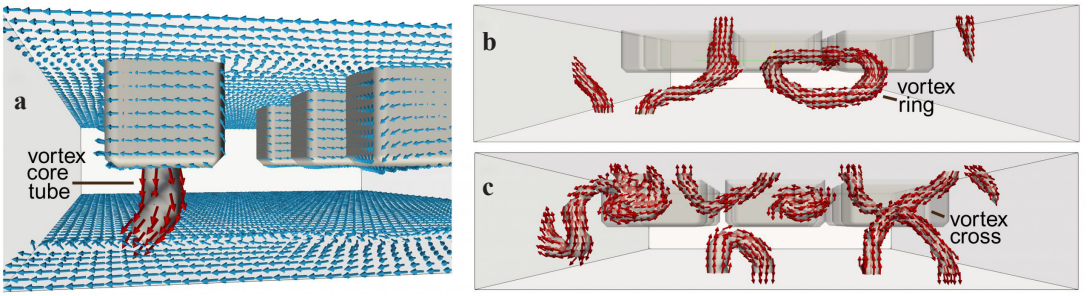

Figure 2. Snapshots of vortex structures in the antidot film. The pinning of a vortex on a non-through hole (**a**), which is the cause of slowing down and stopping the movement of the remagnetization wave. Spatio-temporal transformations of vortex configurations lead to the appearance of unstable transitional ring (**b**) and cruciform (**c**) vortex structures. The magnetization field is shown by blue (light) arrows, and the gyrovector (vorticity) field is shown by red (dark) arrows.

[4] and vortex loops [5, 6] belong to 3D topological objects; they are excluded from consideration in 2D models. An important achievement stimulating the development of 3D nanomagnetism is the improvement of electron and X-ray nanotomography methods [6, 7].

In Ref. 8 it was shown that the DW dynamics in a permalloy ($Ni_{80}Fe_{20}$) film can be unstable and irregular, accompanied by the generation of vortex structures. This paper presents the results of computer simulation of the motion of turbulent magnetization reversal waves in permalloy cuboids with dimensions L_x = 800 nm, L_y = b = 50 and 100 nm (film thickness) and L_z = 400 nm. The samples contain antidote arrays consisting of nine rectangular holes with depths $h = b/4$, $b/2$, $3b/4$, b and side lengths d = 25, 50, and 100 nm. Micromagnetic simulations were performed by solving the Landau-Lifshitz-Gilbert equation using the mumax3 solver [9]. The initial magnetization distribution includes a C-shaped (Labonte) DW lying along the anisotropy axis z. The magnetization reversal wave moves along the x-axis under the action of a DC magnetic field H = 200 Oe directed along the z-axis.

The movement of the remagnetization wave can be slowed down (Fig. 1, α) or completely stopped (Fig. 1, β) due to the transfer of the magnetization structure of the vortex (antivortex) to the hole (the case of through holes [4]). If the holes are not through, a similar effect arises due to the fixation of vortices (antivortices) at the ends of the holes (vortex pinning, Fig. 2a).

It was found that in a thicker film (b = 100 nm) the vortex cores are more often parallel to the film boundaries, so that the vortices look like segments of a C-shaped DW. In a thinner film (b = 50 nm), the lines of vortex cores usually have ends lying on opposite film boundaries. As a rule, vortices of the latter type can be fixed on holes, which slows down and stops the remagnetization process.

1. N. Tahir, M. Zelent, R. Gieniusz et al., J. Phys. D: Appl. Phys. **50**, 025004 (2017).
2. B. Van de Wiele, A. Manzin, A. Vansteenkiste et al., J. Appl. Phys. **111**, 053915 (2012).
3. A.P. Malozemoff, J.C. Slonczewski, Magnetic Domain Walls in Bubble Materials. Academic Press, New York, 1979.
4. V.V. Zverev, I.M. Izmozherov, IEEE Trans. Magn. **58**, 4300805 (2022).
5. P. Sutcliffe, Phys. Rev. B **76**, 184439 (2007).
6. C. Donnelly, K.L. Metlov, V. Scagnoli et al., Nat. Phys. **17**, 316–321 (2021).
7. C. Donnelly, V. Scagnoli, J. Phys.: Condens. Matter 32, 213001, (2020).
8. V.V. Zverev, E.Z. Baikenov, I.M. Izmozherov, Phys. Solid State **61**, 2041–2054 (2019).
9. A. Vansteenkiste, J. Leliaert, M. Dvornik et al., AIP Advances **4**, 107133–1-22 (2014).

D.P1

INHOMOGENEOUS MAGNETOELECTRIC EFFECT IN (011)-ORIENTED FERRITE-GARNET FILM

R.M. Vakhitov, A.R. Yumaguzin, G.T. Akhmadeeva*

Department of Physics, Bashkir State University, Ufa Russia
*E-mail: vakhitovrm@yahoo.com

It is known that garnet-ferrite films have a number of unique magnetic properties, which are becoming in demand or are already finding practical application in micro- and nanoelectronic devices [1–4]. One such property that confirms their status as promising materials is their magnetoelectric properties exhibited at room temperature [5]. Another effect of the same nature, referred to in the literature as flexomagnetoelectric [2], was revealed in [6], where the phenomenon of domain wall displacement (DW) in ferrite garnet films under the action of a significantly inhomogeneous electric field was found. Unusual in this experiment was the dependence of degree of manifestation of this effect on film orientation: if in (210)-oriented film a strong attraction (or repulsion) of DW to the field source was observed, then in (011)-film – weaker, and in (111)-film no effect was observed. It has been suggested [2] that the results obtained can be explained by the presence in (210)- and (011)-films of a rhombic component of induced uniaxial anisotropy, which may lead to magnetization escape from the DW plane, whereas in (111)-film there is no such component. To explain this dependence, it is necessary to investigate the possible types of micromagnetic structures present in each of the films under consideration and to reveal their topological features. Thus, the analysis of the domain structure possible in a plate of the (210) type showed [5] that, regardless of the values of the magnetic anisotropy constants and other material parameters of the sample, the DWs with the noncircular trajectory of the magnetization vector **M** are always realized in it, which creates conditions for manifesting the flexomagnetoelectric effect [1]. However, such a detailed representation

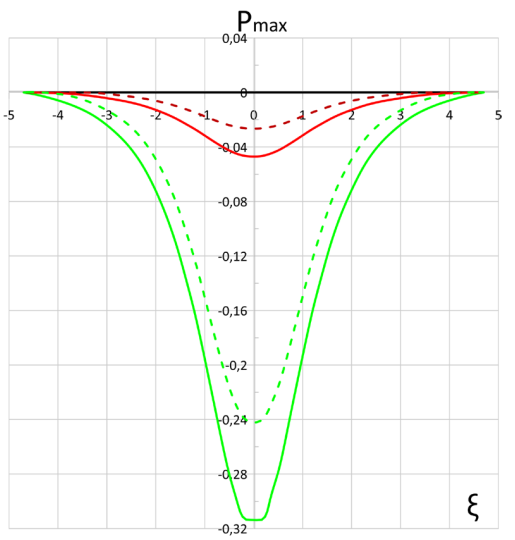

Figure 1. Dependence of the maximum polarization value on the reduced coordinate ξ. Here, the red line corresponds to the electric field $\lambda = 0.1$, the green line to – $\lambda = 0.3$, with the dotted line corresponding to $æ_p = æ_1 = 0.3$, the solid line to – $æ_p = æ_1 = 0$.

of the domain structure possible in the (011)-film is absent in the literature. For this purpose, the structure and properties of 180°-DW in the region of material parameters (011)-film in which the magnetic phase with M||[011] is stable were studied in this work. It was found that in this region ($-2 < æ_1 < 1 + æ_p$; $-1 < æ_1 < 3$; $-2 < æ_1 < 4$; $æ_p > 3$; $æ_1 = K_1/K_u$; $æ_p = K_p/K_u$; K_u, K_p, K_1 – are the constants of perpendicular, rhombic and cubic anisotropy, respectively) 180°-DW has two orientations: $\psi = 0$ and $\psi = \pi/2$ (ψ – is the angle between the DW plane and $(01\bar{1})$), which are realized in two different regions that do not intersect each other. The analysis of the Euler-Lagrange equations corresponding to the magnetic inhomogeneity energy of the film (011) shows that in this intermediate section the 180°-DW reorientation from one direction ($\psi = 0$) to another ($\psi = \pi/2$), takes place, with the transformation of its structure accompanied by the departure of the magnetization vector **M** from the DW plane. According to calculations, the maximum value of the angle of exit from the DW plane $\varphi_m < 10°$. Accordingly, in the presence of inhomogeneous magnetoelectric interaction in the vicinity of the DG, bound charges are induced. In this case, the polarization distribution $P = P(y)$ is an even function with the maximum value of P_{max}, reached in the center of the wall (Fig. 1). However, the P_{max} values decrease as $|æ_1|$ и $|æ_p|$ increase. This means that the presence of cubic anisotropy in a given problem geometry (for a given symmetry of the magnetic system) weakens the manifestation of the flexomagnetoelectric effect in (011)-oriented films.

1. V.V. Randoshkin, A.Ya. Chervonenkis, Applied Magneto-Optics. Moscow: Energoatomizdat (1990), 320pp.
2. A.P. Pyatakov, A.S. Sergeev, E.P. Nikolaeva, A.V. Nikolaev, T.B. Kosykh, K.A. Zvezdin, UFN **185**, 1077 (2015).
3. S. Tkachuk, D. Bowen, I. Nistor, C. Krafft, I. Mayergoyz, J. Appl. Phys. **103**, 07E503 (2008).
4. P. Vetoshko, V. Skidanov, A. Stempkovskiy, Sensor Letters **11**, 59 (2013).
5. B.B. Krichevtsov, V.V. Pavlov, R.V. Pisarev, JETF Lett. **49**, 466 (1989).
6. A.S. Logginov, G.A. Meshkov, A.V. Nikolaeva, E.P. Nikolaeva, A.P. Pyatakov, A.K. Zvezdin, Appl. Phys. Lett. **93**, 182510 (2008).

FLEXOMAGNETOELECTRIC EFFECT IN FERRITE-GARNET FILMS WITH (001)-ORIENTATION

R.M. Vakhitov, Z.A. Baymukhametova, R.V. Solonetsky

Bashkir State University, Ufa, Russia
E-mail: CorrespondingAuthor@mail.ru

The article considers the peculiarities of the flexomagnetoelectric effect (FE) manifesting in a (001)-oriented ferrite-garnet film under exposed to an inhomogeneous electric field. Previously, it was experimentally found that the FE in these materials significantly depends on the orientation of the developed surface of the film relative to the crystallographic axes [1]. While a displacement (to one degree or another) of domain walls (DW) under the action of the electric field $\mathcal{E}$ was observed in (210)- and (011)-oriented ferrite-garnet films, this effect was not there in (111)-oriented films. At the same time, in [2], using a method based on fluorescence spectroscopy of single molecules, local electric fields generated by the domain wall were investigated and, based on the analysis of the results thus obtained, the flexomagnetoelectric nature of the observed effect was confirmed. At the same time, it should be noted that the experiments were carried out in a (001)-oriented ferrite-garnet film (i.e., there is a FE in the films of this orientation). However, due to the specifics of these studies, there is practically no data on the structure of the DW and its possible transformation under the action of an electric field on it. Due to lack of such information, it became necessary to theoretically investigate the behavior of magnetic inhomogeneities which can occur in a film of the (001) type in an inhomogeneous electric field.

An analysis of the Euler-Lagrange equations [3] describing the structure of inhomogeneities for the magnet under consideration (i.e., taking into account the presence of cubic anisotropy in [3]) shows that if the inhomogeneous magnetoelectric interaction is neglected, the solutions corresponding to the 180-degree DWs (180°-DWs) with a non-Bloch structure will be absent, unlike those the same films with the (210), (011) and (111) orientations, in which there is an exit of the magnetization **M** from the wall plane [4]. In this case, there are only such solutions that correspond to the 180°-DW of Bloch or Neel types with **M**||[001] in the domains and with the orientation of the DW-plane characterized by the angle ψ: $\psi = \pi n/2$, $n \in Z$, if $æ > 0$ and $\psi = \pi/4 + \pi n/2$, if $-1 < æ < 0$. Here, $æ = K_1/K_u$, where K_u, K_1, respectively, are the constants of the induced uniaxial and cubic anisotropies. In the presence of an inhomogeneous magnetoelectric interaction ($\mathcal{E} \neq 0$, $\mathcal{E}$||Oz), the magnetization distribution of **M** in the 180°-DW is transformed and the latter turns into an 180°-DW with a quasi-Bloch structure [3]. Accordingly, due to the flexomagnetoelectric mechanism, polarization is induced in the vicinity of the DW, the value of which is an even function of the y-coordinate, reaching its maximum p_m in the center of the wall ($y = 0$). As the magnitude of the electric field $\mathcal{E}$ increases, the maximum angle of exit of the magnetization from the wall plane φ_m increases. Accordingly, the value of p_m also increases, which in turn leads to an increase in the integral value of polarization P (the total value of DW-polarization). Calculations show that all the FE regularities found in [3] for a magnetically uniaxial film (the dependences $\varphi = \varphi(y)$, $p = p(y)$, as well as φ_m, p_m and P on the $\mathcal{E}$-field) are exactly the same in this case. At the same time, an analysis of the influence of the value of the cubic anisotropy on the above-mentioned parameters of the FE shows that with increasing æ the value of the integral polarization increases, but to only a small extent (by about 1-2%). It can also be noted that with negative values of æ ($-1 < æ < 0$) with an increase in its absolute value, the value of the integral polarization also increases and also slightly. Such a manifestation of FE in a (001)-oriented film can be explained by the symmetry of

its magnetic system: at æ > 0, the easy axes of cubic anisotropy are the ⟨100⟩-axes, which make approximately the same contribution to both the uniaxial and the easy-plane anisotropy. A similar situation occurs in the case of æ < 0.

1. A.S. Logginov, G.A. Meshkov, A.V. Nikolaev, E.P. Nikolaeva, A.P. Pyatakov, A.K. Zvezdin, Appl. Phys. Lett. **93**, 182510 (2008).
2. I.S. Veshchunov, S.V. Mironov, W. Magrini, V.S. Stolyarov, A.N. Rossolenko, V.A. Skidanov, J.-B. Trebbia, A.I. Buzdin, Ph. Tamarat, B. Lounis, Phys. Rev. **115**, 027601 (2015).
3. R.M. Vakhitov, Z.V. Gareeva, R.V. Solonetsky, F.A. Mazhitova, Phys. Sol. St. **61**, 1043–1051 (2019).
4. R.M. Vakhitov, R.R. Iskhakova, A.R. Yumaguzin, Phys. Sol. St. **60**, 925–935 (2018).

NUMERICAL SIMULATION OF THE STRUCTURE AND DYNAMICS OF MAGNETIC VORTICES AND SOLITONS IN MULTILAYER FERROMAGNETIC NANOSTRUCTURES

K.U. Samsonov[1], *S.V. Stepanov*[2], *G.I. Antonov*[2], *K.A. Zvezdin*[3], *E.G. Ekomasov*[1,2*]

[1]Tyumen State University, Tyumen, Russia,
[2]Bashkir State University, Ufa, Russia
[3]General Physics Institute A.M. Prokhorov RAS, Moscow, Russia
[*]E-mail: EkomasovEG@gmail.com

The structure and dynamics of magnetization in a vortex spin-transfer nanooscillator, which is a three-layer spin-valve magnetic nanopillar with a small diameter, is studied during the passage of a spin-polarized current and the presence of an external magnetic field. Using micromagnetic simulation [1], we studied the dynamic change in the vortices structure, the formation of the C-structure vortex state and edge vortices, the trajectory of movement and the time it takes to reach different dynamic modes. The time needed for the vortices to reach different dynamic modes was found. The possibility of the dynamic generation of radial edge vortices without the presence of a Dzyaloshinsky field or an external inhomogeneous magnetic field is shown. We demonstrate that a vortex in a thick magnetic layer can be a generator of spin waves in a thin magnetic layer with an adjustable oscillation frequency. We consider also multilayer magnetic structures, which are periodically alternating layers of two materials with different physical properties. In such systems it is possible to generate localized magnetization waves (LMW) of the magnetic solitons and breathers type [2]. Special interest in magnetic solitons and breathers is currently associated with the appearance of new experimental techniques that allow to study formation and propagation of localized magnetization waves of nanometer dimensions and their interaction with domain walls (DW). The possibility of controlling the structure and dynamic parameters of magnetic solitons and breathers using an external magnetic field is shown [3]. Dependences of the center of the DW and amplitudes of the LMW on time are constructed and analyzed in the presence of three, five and seven layers. It is shown that LMW oscillations for the case of five layers can be described by a model with two harmonic oscillators, and for the case of seven layers – with three harmonic oscillators. The possibility of controlling the dynamic parameters of coupled magnetic solitons and breathers by an external magnetic field in an autoresonant mode is investigated.

Support by Grant RFBR 20-31-90048 is acknowledged.

1. A.E. Ekomasov et al., J. Magn. Magn. Mat. **471**, 513–520 (2019).
2. E.G. Ekomasov et al., Lett. Mat. **10**(2), 141–146 (2020).
3. E.G. Ekomasov et al., Tech. Phys. Lett. **47**, 491–494 (2021).

D.P4

INVESTIGATION OF THE DYNAMICS OF DOMAIN WALL MOTION IN COBALT-BASED MICROWIRES

S.A. Evstigneeva[1*], *R.I. Shamsuvaleev*[1], *N.A. Yudanov*[1], *M.G. Nematov*[1], *L.V.Panina*[1,2]

[1]National University of Science and Technology, MISiS, Moscow, Russia
[2]Immanuel Kant Baltic Federal University, IKBFU, Kaliningrad, Russia
[*]E-mail: s.evstigneeva@rqc.ru

Recently, much attention has been drawn to the creation of miniature magnetic materials for use as labels, temperature and mechanical stress sensors with remote interrogation. The development of sensing elements based on a non-linear magnetic dynamics is especially perspective. Cobalt-based ferromagnetic microwires, which have a high sensitivity of magnetic structure to external magnetic and mechanical stimuli, demonstrate such dynamic effects as magnetic bistability, fast domain wall propagation [1] and magnetoimpedance. In this work, we studied the effect of mechanical stress on the behavior of the harmonic spectrum of a signal occurring due to propagation of a single domain wall (DW) in a glass coated $Co_{71}Fe_5B_{11}Si_{10}Cr_3$ microwire (magnetic core diameter was 25 μm, glass coating thickness was 1.5 μm). This microwire had a unique combination of predominant axial anisotropy with negative magnetostriction.

Domain wall propagation was studied by the Sixtus-Tonks method. The decomposition of the signal in the detection coil due to passing DW into a harmonic spectrum was carried out using a lock-in amplifier SR830.

The magnetostriction of these wires sensitively depends on the external stress and becomes more negative with increasing stress, which leads to a sharp change in the type of the magnetic anisotropy. As a result, the shape of magnetic hysteresis loops sharply changes from rectangular to inclined [2]. This effect leads to a strong dependence on applied stress of the spectral characteristics of the induced voltage signal when the wire is remagnetized via DW-propagation.

In the presence of a tensile stress, the surface energy of the DW and the spin relaxation decrease due to a decrease in the total anisotropy. Then, the DW-mobility increases, as shown in Fig. 1a.

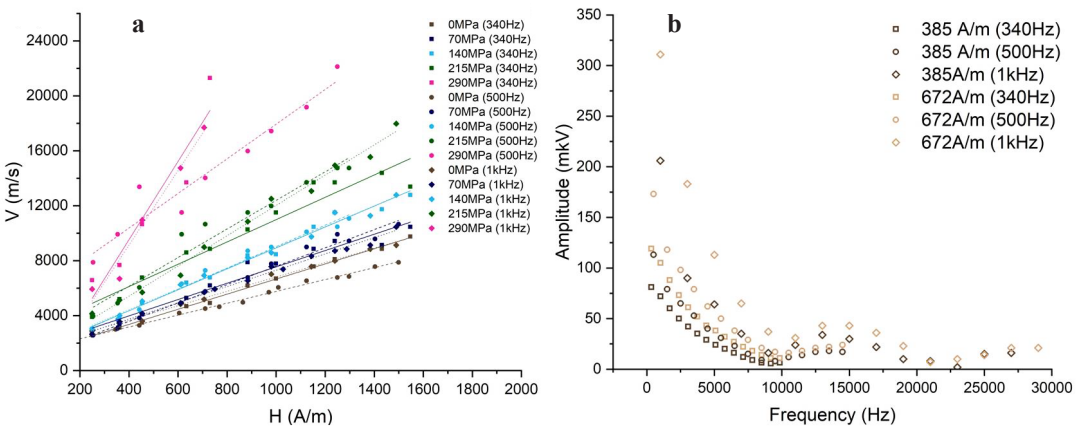

Figure 1. **a** Dependence of the DW velocity in the microwire $Co_{71}Fe_5B_{11}Si_{10}Cr_3$ under the application of different tensile stresses; **b** dependence of the odd harmonics amplitudes on the frequency and magnitude of the applied field (without applying stress).

The data obtained were approximated linearly from the assumption that the DW propagates at a constant speed ($V = S(H - H_0)$, where V is the DW-velocity, S is the DW-mobility, H_0 is the critical propagation field).

The amplitudes of odd harmonics were well recorded and the values were in the range from 4 to 300 μV. The signal increased with increasing frequency and amplitude of the driving magnetic field (Fig. 1b) while the peaks of the original signal decrease in amplitude and expand. The analysis of the obtained data revealed a non-monotonic behavior with respect to harmonic number.

The sensitivity of higher odd harmonics is of interest for use in sensor systems, since they will not contain information about instrumental noise. In the harmonic spectrum of the microwire $Co_{71}Fe_5B_{11}Si_{10}Cr_3$, the amplitude of harmonic No. 23 decreases by twice with increasing stress to 360 MPa, which can be seen on Fig. 2.

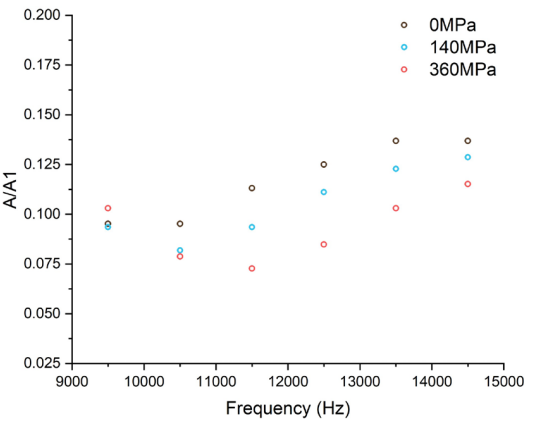

Figure 2. Influence of tensile stress on the behavior of the reduced amplitudes of higher harmonics (normalized to the amplitude of the fundamental mode), external magnetic field: 672 A/m, f = 500 Hz.

The discovered effects may be promising for the development of miniature embedded sensors of mechanical stresses.

The reported study was funded by RFBR according to the research project № 20-32-90145.

1. P. Klein et al., J. Alloys and Comp. **550**, 31–34 (2013).
2. M.G. Nematov et al., Phys. Solid State **60**, 328–333 (2018).

THE STRUCTURE OF VORTEX-LIKE MAGNETIC INHOMOGENEITIES FORMED IN MODULATED FERROMAGNETIC FILMS AND THEIR BEHAVIOR IN A MAGNETIC FIELD

*A.A. Akhmetova, R.M. Vakhitov, R.V. Solonetsky, M.A. Filippov**

Bashkir State University, Ufa, Russia
*E-mail: mikhail.filippov.99@mail.ru

Magnetic skyrmions are topologically protected vortex-like magnetic inhomogeneities that have a number of unique properties: nanoscale dimensions, ease of manipulation with a low-density electric current, and other unique spin-electronic properties [1]. Due to this, skyrmions are very promising for use in new generation memory devices and neuromorphic computing systems. First discovered in chiral magnets [1], they are stabilized in them due to the interaction of Dzyaloshinskii-Moriya (DMI). However, there are methods for stabilizing magnetic skyrmions in magnets and in the absence of DMI in them. In this paper, one of such methods is considered – the nucleation of a stable skyrmion on a columnar defect of the "potential well" type in a uniaxial ferromagnetic film [2]. A similar idea was implemented in the work [3]. It experimentally obtained a multilayer Co/Pt film with locally altered regions in which the perpendicular anisotropy constant had a reduced value.

In [2], a theoretical analysis of micromagnetic structures arising in the considered magnetic films in the region of columnar defects was carried out. According to calculations, there are four types of magnetic structures, two of which are non-topological solitons, and the other two are magnetic skyrmions. They have a Bloch magnetization distribution and differ in core polarity and configuration. Magnetic skyrmions have a topological charge $q = 1$, and there are three inflection points in the magnetization distribution profile, while non-topological solitons have $q = 0$, and the profile contains only two inflection points. At the same time, they also have common topological peculiarities. In their structure, three sections of rotation of magnetic moments can be conditionally distinguished: core (central region), intermediate and boundary sections.

Studies show that the skyrmion states are energetically more advantageous than the states corresponding to a non-topological soliton, i.e. the latter are metastable micromagnetic structures. Therefore, it is much more difficult to implement them experimentally or using numerical methods than skyrmions. However, non-topological solitons can exist as stable states (Fig. 1) when the skyrmion is magnetized in a perpendicular field [4]. In particular, when a magnetic field **H** is applied, directed normally to the plane of the film and opposite to the orientation of the core, the transformation of the structure of the skyrmion occurs. It is remagnetized in three stages: first, the size of the core decreases, then, at a certain field, the orientation of the core switches, and the skyrmion turns into a non-topological soliton. The latter decreases in size with increasing **H**, and eventually, as it were, "evaporates" and disappears. The non-topological soliton has a slightly different remagnetization scenario. As **H** increases, the size of the core increases, and the size of the intermediate section decreases. As a result, it also "evaporates", decreasing in size. In a planar field, the remagnetization scenario for both types of solitons is approximately the same. Under the action of the field, the core shifts to the edge of the defect and flies out of it, and the defect area becomes magnetized along the field [2].

The stable states of skyrmions localized on a columnar defect of a disk-shaped film were studied using the OOMMF [5] open access software package. They are completely consistent with the above-described scenarios of magnetization reversal in planar and perpendicular fields [4]. In addition, we

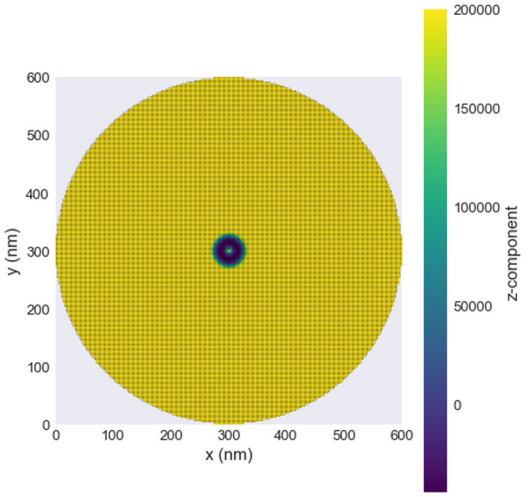

Figure 1. Non-topological soliton formed during skyrmion remagnetization [4].

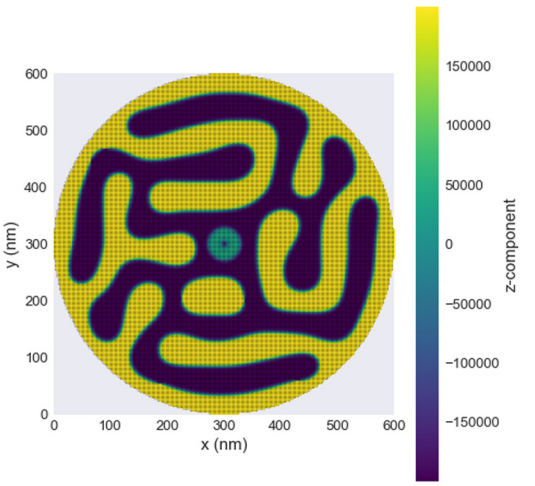

Figure 2. Stabilization of a non-topological soliton in the absence of a magnetic field.

obtained a metastable state of a non-topological soliton, which was formed on a defect in the absence of a magnetic field, and investigated its transformation under the action of a planar field. For micromagnetic modeling, the following material parameters and sample sizes were set: $K_{u1} = 3{\cdot}10^4$ J/m^3 (outside the defect), $K_{u2} = -0.5{\cdot}10^4$ J/m^3 (on the defect), $M_s = 6.6{\cdot}10^5$ A/m, $A = 2.5{\cdot}10^{-13}$ J/m [3], disc diameter 600 nm, defect diameter 60 nm, disc thickness 12.5 nm. The resulting image of a non-topological soliton and the resulting labyrinth domain structure is shown in Fig. 2.

Support by State Assignment for the performance of scientific research by laboratories (Order MN-8/1356 of 09/20/2021).

1. K. Everschor-Sitte, J. Masell, R.M. Reeve, M. Kläui, J. Appl. Phys. **124**, 240901 (2018).
2. R.M. Vakhitov, R.V. Solonetsky, A.A. Akhmetova, J. Appl. Phys. **128**, 153904 (2020).
3. M.V. Sapozhnikov, S.N. Vdovichev, O.L. Ermolaeva, N.S. Gusev, A.A. Fraerman, S.A. Gusev, Yu.V. Petrov, J. Appl. Phys. **109**, 042406 (2016).
4. R.M. Vakhitov, R.V. Solonetsky, A.A. Akhmetova, M.A. Filippov, Symmetry **14**, 612 (2022).
5. M.J. Donahue, D.G. Porter, OOMMF User's Guide, Version 2.0a3, NIST, Gaithersburg, (2021).

D.P6

INHOMOGENEOUS MAGNETOELECTRIC EFFECT IN (111)-FERRITE-GARNETS FILMS

*R.M. Vakhitov, R.F. Ishmanova, A.R. Yumaguzin**

Department of Physics, Bashkir State University, Ufa Russia
*E-mail: azyum@rambler.ru

Ferrite-garnets films have the widest prospects for application in spintronics and nanoelectronics. In addition, ferrite-garnet films are the most convenient object for studying micromagnetic structures by magnetooptical methods, which is important in studying the flexomagnetoelectric effect in magnets [1].

It was found that one of the features of the observed effect is the dependence of the degree of its manifestation on the orientation of the developed surface of the film: in the (210)-oriented film, the effect manifests itself most strongly, in the (011)-film more weakly, and in the (111)-film, it does not appear at all observed. An analysis of the domain structure possible in a plate of the (210) type showed [2] that 180°-domain walls (DWs) are always realized in it with a non-circular trajectory of the magnetization vector **M**, which creates conditions for the manifestation of the flexomanetoelectric effect [3].

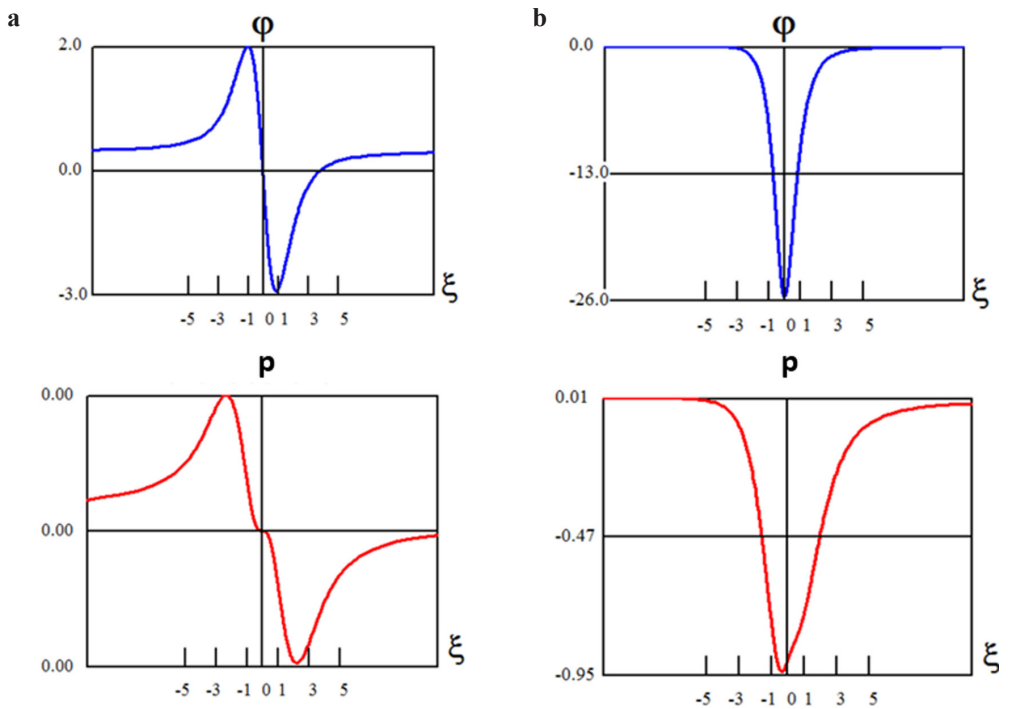

Figure 1. Dependence of the angle φ and polarization p on the coordinate ξ for two field values: **a** $\lambda = 0.3$; **b** $\lambda = 1.0$. $æ_1 = 1.0$, $Q = 0.2$. Here $\lambda = \varepsilon/\varepsilon_0$, $æ_1 = K_1/K_u$, where ε, ε_0 – are the applied and characteristic electric fields, respectively, K_u, K_1 – are the constants of perpendicular and cubic anisotropy, respectively, Q – the quality factor of magnetics.

Therefore, a theoretical study of magnetic structures in a (111)-ferrite-garnet plate is of scientific interest. To this end, in this work, we studied the structure and properties of 180°-DW in the range of material parameters of the (111)-film, in which the magnetic phase with **M**||[111] is stable. It is shown that for certain material parameters of the (111)-plate and values of the external electric field, nonuniform electric polarization occurs.

The distribution of magnetization depending on the electric field was obtained, from which it follows that the structure of the domain wall is quasi-Bloch with the dependence $\varphi = \varphi(y)$, which is an odd function in low electric fields. In large fields, it transforms and becomes even.

The polarization distribution as a function of y in low fields is also an odd function. This means that in low fields a double electric layer is formed, which, due to the screening of electric fields, leads to the absence of integral polarization. In high fields, the dependence of the differential polarization on y becomes an even function. In this case, the integral polarization is nonzero. Thus, the flexomagnetoelectric effect arises in the (111)-film, but in low fields, due to the mutual screening of electric fields, it is absent and becomes significant in high fields.

1. Y. Kajiwara et al., Nature **464**(7286), 262–6 (2010).
2. A.K. Zvezdin, A.P. Pyatakov, Phys. Usp. **52**, 845–851 (2009).
3. R.M. Vakhitov, R.R. Iskhakova, A.R. Yumaguzin, Phys.of the Sol. State **60**, 925–935 (2018).
4. V.V. Randoshkin et al., Sov. Tech. Phys. Lett. **15**, 553 (1989).

STRIPE STRUCTURE ROTATION IN TRANSCRITICAL MAGNETIC FILMS

S.V. Komogortsev[1-3*], *V.A. Fel'k*[2], *A.A. Kuznetsova*[3], *A.A. Mokhov*[1]

[1]Kirensky Institute of Physics, Federal Research Center KSC SB RAS, Krasnoyarsk, Russia
[2]Reshetnev Siberian State University of Science and Technology, Krasnoyarsk, Russia
[3]Siberian Federal University, Krasnoyarsk, Russia
[*]E-mail: komogor@iph.krasn.ru

Magnetic microstructure in a magnetic film with perpendicular magnetic anisotropy shows a transition to the so-called transcritical mode if the film thickness is greater than $L_{cr} = 2\pi(A/K_{op})^{1/2}$, where A is the exchange stiffness and K_{op} is the out of plane magnetic anisotropy constant. The transition to the transcritical state is accompanied by the appearance of stripe domains running parallel to the field previously applied to the film. The magnetic hysteresis of the transcritical film increases sharply in comparison with the hysteresis of a thin subcritical film, and the magnetic anisotropy in the film plane becomes extremely weakly pronounced, which is due to the appearance of the so-called rotatable magnetic anisotropy [1, 2]. The idea of rotatable magnetic anisotropy in this case helps to explain observable axis along the stripes and the fact that the stripe domains can be aligned with an external field in any direction in the film plane [3]. The similar idea is used to explain the independence of the mechanical torque from the angle of the external field in some films [4]. The concept of rotational magnetic anisotropy helps to explain these facts, but does this mean that such anisotropy actually exists? The phenomenon of magnetic anisotropy is primarily understood as the dependence of the magnetic properties of a ferromagnet on the direction of applied field with respect to certain axes of the object under study. The questions arise in this regard: is an arbitrarily small field capable of turning the axis of the stripe structure, and how does the anisotropy of the stripe structure manifest itself in the magnetic response of the film? This report is an attempt to answer these questions using micromagnetic modeling of a film in a transcritical state.

The calculations were performed in the OOMMF environment for a disc-shaped film element. The plane element with 700 nm diameter and 70 nm thickness was divided into 10 nm cubic cells. The easy axis of magnetic anisotropy was oriented trasnverse to the disk plane. The field was applied a in the plane of the disk. The special set of magnetic constants ($A = 5\cdot10^{-12}$ J/m, $K_{op} = 5\cdot10^{4}$ J/m^3, $M_s = 5\cdot10^{5}$ A/m) provides the film in transcritical state with stripe magnetic microstructure. The starting axis of stripe structure was set by decreasing field from saturation to the zero value and then the set of loops with diferent field magnitude was calculated.

As a result of numerical studies, we found that, first, to rotate the axis of the stripe structure with external field in the film plane, the threshold field, which is several times lower than the field of perpendicular magnetic anisotropy is necessary. Second, the change in the orientation of the stripe structure in a field above the threshold value occurs through the appearance of a dislocation dipole in the stripe pattern. Thirdly, when the field is rotated, the average orientation of the stripe structure axis may somewhat lag behind the direction of the external field, which exceeds the threshold field. This provides some clarification of the nature of the threshold field, as the field necessary for the nucleation of an edge dislocation in a system of stripe domains. Some features of the magnetic response in fields below the threshold are also discussed.

This research was funded by the RFBR, Krasnoyarsk Region and the Krasnoyarsk Regional Science Foundation (Project No. 20-42-240001).

1. N. Saito, H. Fujiwara, Y. Sugita, J. Phys. Soc. Jpn. **19**, 1116–1125 (1964).
2. A.V. Svalov, G.V. Kurlyandskaya, H. Hammer, P.A. Savin, O.I. Tutynina, Tech. Phys. **49**, 868–871 (2004).
3. G.V. Kurlyandskaya, L. Elbaile, F. Alves, B. Ahamada, R. Barrué, A.V. Svalov, V.O. Vas'kovskiy, J. Phys. Condens. Matter **16**, 6561–6568 (2004).
4. V.G. Myagkov, V.S. Zhigalov, L.E. Bykova et al., JETP Lett. **102**, 355–360 (2015).

DOMAIN WALL DRIFT IN SINGLE CRYSTAL PLATES WITH COMPLEX MAGNETIC ANISOTROPY

*D.S. Mekhonoshin, L.A. Pamyatnykh**

Institute of Natural Sciences and Mathematics, UrFU, Ekaterinburg, Russian Federation
*E-mail: Lidia.Pamyatnykh@urfu.ru

The key phenomenon required to develop new types of memory devices based on a movement of magnetic domain walls (DWs) is a unidirectional motion of the array of DWs as a whole as a result of a certain impact: an electric currant [1], a magnetic [2] or electric field [3]. A unidirectional motion of a system of stripe magnetic domains under the action of an alternating magnetic field is well known in iron garnet single crystals as an drift of DWs [4]. Revealing of the mechanisms of DWs drift in iron garnets is important to development of new principles of controlled DWs displacement in real magnetic memory devices. This work is devoted to the study of DWs drift in single-crystal plates of iron garnets with a complex magnetic anisotropy, combining four-axis magnetocrystal cubic anisotropy and induced uniaxial anisotropy, by method of micromagnetic simulation.

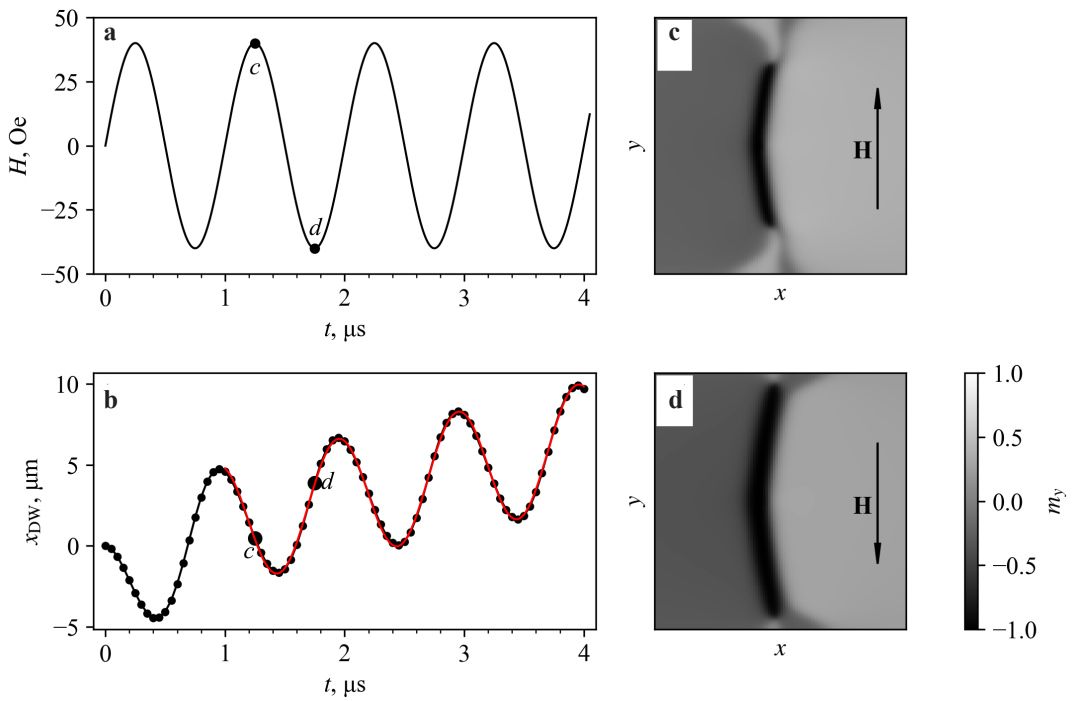

Figure 1. The dependencies of the applied magnetic field H with frequency $f = 10^6$ Hz and amplitude $H_0 = 40$ Oe (**a**) and domain boundary coordinate x_{DW} (**b**) on time. The states corresponding to **c** and **d** are highlighted by dots. The solid red line is the approximation of the dependence of the DW coordinate by the sum of the sinusoidal and linear functions. The distributions of the vertical component m_y of the normalized magnetization near the DW at the instantaneous value of the magnetic field $H(t) = 40$ Oe (**c**) and $H(t) = -40$ Oe (**d**). Horizontal area size $l_x = 5$ μm, vertical area size $l_y = 10$ μm. The arrows show the directions of the magnetic field.

The results of 2D micromagnetic simulation of a domain structure of a thick (111)-plate (L_y = 10 μm) are presented. The plate had cubic anisotropy with constant $K_1 = -6\cdot10^{-3}$ erg/cm^3 and uniaxial induced anisotropy with constant $K_u = 0.9\cdot10^{-3}$ erg/cm^3, the easy axis of which was directed along $[1\bar{1}1]$. Domain walls in the plate were directed along $[2\bar{1}1]$ axis. The parameters of the model corresponded to the parameters of real iron garnet plates with DWs drift. The section of the plate with $(2\bar{1}1)$ plane was considered, the x-axis of the model was along $[0\bar{1}1]$, the y-axis was along the plate normal [111], periodic boundary conditions were set to the x-axis. The Landau-Lifshitz-Hilbert equation was solved numerically, the simulation was performed using the Mumax3 package [5].

The initial state contained two DWs. Asymmetric Bloch DWs have minimal free energy in this case, the magnetization in the center of the DW can be directed either along the y-axis or opposite, which corresponds to the opposite directions of magnetization reversal in the wall. The DW contains regions of magnetic flux closure near the surface of the sample (Fig. 1c and d). We specified a structure with opposite directions of magnetization in the domain wall. The plate was subjected to a harmonic magnetic field of frequency $f = 10^6$ Hz and amplitude H_0 in the range 0–50 Oe, directed along the y-axis (Fig. 1a).

The results of the micromagnetic simulation are presented on Fig. 1. The dependence of DWs coordinate x_{DW} on time is shown on Fig. 1b. The DW oscillates with the field frequency and simultaneously shift along the x-axis, i.e. the drift of DW occurs. The results of the approximation of $x_{DW}(t)$ with the sum of the sinusoidal and linear functions is shown on Fig. 2b with solid red line to emphasize the onward motion of DW. The snapshots of DW structure at the instantaneous value of the magnetic field $H(t)$ = +40 Oe (Fig. 1c) и $H(t)$ = –40 Oe (Fig. 1d) are shown on Fig. 1c and d. When the magnetic field direction and direction of magnetization in DW center do not coincide (Fig. 1c), the size of the DW along the y-axis decreases by an expansion of the magnetic closure region, and the size of the DW along the y-axis increases in opposite case (Fig. 1d). Thus, the shape of the DW changes during its oscillations, which leads to asymmetry in the movement of the DW with the direction of the magnetic field, which leads to the drift motion of the DWs. The paper compares the results obtained by micromagnetic simulation with the experimentally established patterns of DW drift in iron garnet single crystals.

This work was performed within the framework of the state assignment of the Ministry of Science and Higher Education of the Russian Federation (Project FEUZ-2020-0051).

1. S.S.P. Parkin, M. Hayashi and L. Thomas, Science **320**, 190 (2008).
2. K.W. Moon et al., Sci. Rep. **5**, 9166 (2015).
3. M. Chuang et al., Nano Lett. **19**, 353–361 (2018).
4. L.A. Pamyatnykh et al., Phys. Solid State **61**, 350–360 (2019).
5. A. Vansteenkiste et al., AIP Advance **4**, 107133 (2014).

D.P9

INFLUENCE OF THE MAGNETIC FIELD ON THE STRUCTURE AND PROPERTIES OF 0°-DWS IN UNIAXIAL FILMS WITH INHOMOGENEOUS MAGNETOELECTRIC EFFECT

R.M. Vakhitov, A.R. Nizyamova, R.V. Solonetsky*

Bashkir State University, Ufa, Russia
*E-mail: alya.nizyamova.96@mail.ru

Studies of magnetoelectric phenomena in magnetic materials, as a rule, arouse increased interest, which is associated with the possibility of their application when developing various spintronics devices with low energy consumption [1]. One of these effects, which attracted the attention of many researchers, is the phenomenon of displacement of domain walls (DWs) in ferrite-garnet films under the action of an inhomogeneous electric field [2] (flexomagnetoelectric effect (FE) [1]). Subsequent studies of this effect revealed new aspects of its manifestation and, in particular, it was found the FE is significantly influenced by the magnetic field which under certain conditions can lead to its strengthening [3,4]. This paper, theoretically studies the influence of a magnetic field on micromagnetic structures of the 0-degree DW type in uniaxial films with inhomogeneous magnetoelectric interaction (IMEI), the energy density ε of which is taken as [3]

$$\varepsilon = M_s^2\mathcal{E}(b_1\mathbf{m}\,\mathrm{div}\mathbf{m} + b_2(\mathbf{m}\times\mathrm{rot}\,\mathbf{m})),$$

where b_1, b_2 are magnetoelectric constants, M_s is the saturation magnetization, **m** is the unit magnetization vector, $\mathcal{E}$ is the electric field ($\mathcal{E}\,||Oz$). In addition, the energy of the magnet under study E takes into account the exchange interaction (characterized by the exchange parameter A), uniaxial anisotropy (K_u), the Zeeman interaction ($\varepsilon_H = -M_s\mathbf{mH}$, **H** is the external magnetic field) and demagnetizing fields in the Winter approximation [3].

An analysis of the Euler-Lagrange equations which correspond to the energy E shows that their solutions in the absence of a magnetic field are not only 180°-DWs, but also 0°-DWs with a quasi-Bloch structure and 0°-DWs of the Neel type [3]. It should be stated here that the possibility of the existence of 0°-DW of the first type is of a threshold nature, because it occurs when the value of the electric field exceeds a certain critical value: $\mathcal{E} > \mathcal{E}_n$. At the same time, the second type 0°-DW can only originate in an inhomogeneous electric field. According to the calculations, in both cases bound charges (polarization) are induced in the vicinity of the DW. In the first case, however, their integral value N (the total charge of the wall) is different from zero, whereas in the second case it is zero ($N = 0$), because mutual shielding of charges takes place. The presence of a magnetic field leads to the fact that for each type of micromagnetic structures there is always such a direction of the field **H**, at which the integral value of the polarization of the wall increases. The latter means an increase in the manifestation of the flexomagnetoelectric effect in the magnet under study.

The most significant (multiple) amplification of the effect will take place when electric and magnetic fields act on 180°-DWs in the following geometry: $\mathcal{E}\,||Oz$, $\mathbf{H}\,||Oy$, and the greatest amplification effect can be achieved even in small fields. This is consistent with the experimental data [3, 4], from which it follows that the greatest displacement of the DW in an inhomogeneous electric field occurs under the action of a magnetic field perpendicular to the wall plane. In the case of a quasi-Bloch type 0°-DW, such an effect can be achieved in weak magnetic fields directed along Oz. However, the value of the electric field should not be small: $\lambda > 1.5$, where $\lambda = \mathcal{E}/\mathcal{E}_0$, $\mathcal{E}_0 = 2(AK_u)^{1/2}/M_s^2b$ is the characteristic value of the electric field. In both cases, the effect of increasing the value of the

integral polarization N is achieved by increasing the magnitude of the angle at which the magnetization vector exits from the DW plane.

If an external magnetic field with $\mathbf{H}||Ox$ acts on 0°-DW of the Neel type, then a flexomagnetoelectric effect ($N \neq 0$) also occurs sufficient for it to be observed under experimental conditions. However, this can be achieved only in strong electric ($\lambda \sim 1.5$–2) and magnetic ($h \sim 1$–1.5) fields. Here, $h = H/H_u$, $H_u = 2K_u/M_s$ is the uniaxial anisotropy field. The mechanism of the occurrence of integral polarization in this case is more complex, since contributing to it are the partial portions of the IMEI containing both div**m** and rot**m**. Obviously, the first part of the IMEI is affected by transformations in the structure of the Neel 0°-DW caused by the action of a planar magnetic field (more precisely, changes in the dependence $\varphi = \varphi(\xi)$), and the second part is affected by deviations of magnetic moments from the plane yOz under the action of the applied field, which causes the appearance of the dependence $\theta = \varphi(\xi)$ (in the absence of a field $\theta = 0$). It should be noted that the action of a magnetic field on the 0°-DW of the quasi-Bloch type can change the critical field of nucleation $\mathcal{E}_n$, in one direction or another. Moreover, by switching the orientation of the magnetic field to the opposite, it is possible to achieve that there is no threshold of nucleation of this type of the 0°-DW, i.e. $\mathcal{E}_n = 0$. These and other results obtained allow us to assert that an external magnetic field can effectively regulate the processes of nucleation and transformation of micromagnetic structures in magnetically uniaxial films in an inhomogeneous electric field, as well as influence the nature of the flexomagnetoelectric effect manifestation in them.

The work was carried out with the financial support of the State Task for the performance of scientific research by laboratories (Order MN-8/1356 of 09/20/2021).

1. A.P. Pyatakov, A.K. Zvezdin, Phys.-Usp. **55**, 557 (2012).
2. A.S. Logginov, G.A. Meshkov, A.V. Nikolaev, E.P. Nikolaeva, A.P. Pyatakov, A.K. Zvezdin, Appl. Phys. Lett. **93**, 182510 (2008).
3. A.P. Pyatakov, A.S. Sergeev, E.P. Nikolaeva, T.B. Kosykh, A.V. Nikolaev, K.A. Zvezdin, and A.K. Zvezdin, Phys.-Usp. **58**, 981 (2015).
4. F.A. Maksutova, R.V. Solonetsky, R.M. Vakhitov, A.P. Pyatakov, EPL **129**, 27004 (2020).
5. R.M. Vakhitov, R.V. Solonetsky, V.R. Gurjanova, A.R. Nizyamova, D.A. Sechin, T.T. Gareev, A.P. Pyatakov, Phys. Rev. B **104**, 144407 (2021).

D.P10

FEATURES OF THE MAGNETIC STATE OF AN ORDERED ARRAY FERROMAGNETIC NANOSTRIPES

V.A. Orlov[1,2,*], *R.Yu. Rudenko*[1], *A.V. Luk'yanenko*[2], *V.Yu. Yakovchuk*[2], *V.S. Prokopenko*[3], *I.N. Orlova*[3]

[1]Siberian Federal University, Krasnoyarsk, Russia
[2]Kirensky Institute of Physics, Federal Research Center KSC SB RAS,, Krasnoyarsk, Russia
[3]Krasnoyarsk State Pedagogical University after V.P. Astaf'ev, Krasnoyarsk, Russia
[*]E-mail: vaorlov@sfu-kras.ru

Low-dimensional objects like ferromagnetic nanostripes are considered promising objects for use in information storage devices and other new generation spintronic devices. In storage devices a new generation of bit carriers are topological inhomogeneities magnetization in magnetic tapes/wires: magnetic vortices/skyrmions, domain walls of different types. On the static magnetic state and processes magnetization reversal is significantly affected by inhomogeneities of stray fields, for the existence of which surface defects (roughness) are responsible nanowires/nanostripes.

For our study, arrays of parallel oriented tapes were formed by explosive lithography. The film was deposited thermal method from alloy 80HXC on a silicon substrate coated photoresist. Arrays of tapes of size (4×4 mm^2) were obtained. Thickness stripe b = 180 nm. The distance between the tapes in different arrays varied from 4 to 0.3 μm.

It was found that the state of the tapes is practically single-domain with the flow closure at ends of the tapes by means of combined domain walls, including magnetic vortices (see Fig. 1). We assume that when the field is turned on, the vortex objects formed at the ends stripe and separating domains, come into motion, moving along the long axis tapes. In this case, the vortex walls move in a random potential of stray fields, created by surface irregularities.

Far from the ends, a magnetization ripple is observed, which practically repeats roughness of the side surfaces of the tapes (see Fig. 2). This is valid for samples a and b, where the distance between the ribbons is relatively large and the role of the interaction of magnetic subsystems of different ribbons is small.

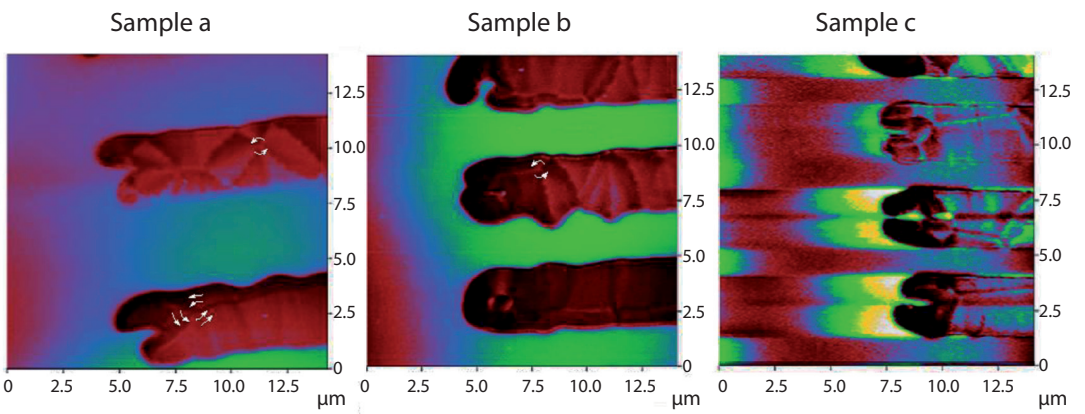

Figure 1. Magnetic force contrast near the ends of nanoribbons in arrays a, b, c. The light arrows show the approximate orientation. magnetization near vortex formations.

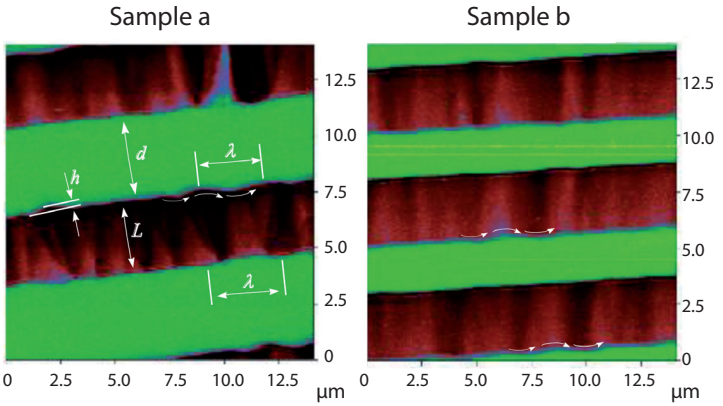

Figure 2. Magnetic force contrast far from the ends of nanostripes for arrays a, b. Light arrows near the side surfaces show the approximate orientation magnetization.

An important circumstance is the fact that in an array with closely spaced stripes (samples c and d, see Fig. 3 of ripple distribution magnetization in different stripes significantly correlates, which allows us to conclude on a significant magnetostatic mechanism of interaction of magnetic subsystems. This allows us to estimate the average constant of the effective random anisotropy, acting as a fixing factor:

$$K_{\text{eff}} = H_{\text{M}} M_{\text{S}} \approx 2M_{\text{S}}^2 \frac{\pi^2 h^2}{\sqrt{2}\lambda L} \sum_{n=1}^{\infty} \exp\left(-\frac{2\pi\sqrt{2}dn}{\lambda}\right) = M_{\text{S}}^2 \sqrt{2}\, \frac{\pi^2 h^2}{\lambda L} \left[\exp\left(-\frac{2\pi\sqrt{2}dn}{\lambda}\right) - 1\right]^{-1}.$$

Here M_{S} is the saturation magnetization, h and λ are the average depth irregularities and their average period, respectively, L – width magnetic (width of tapes), d – width of non-magnetic gap (distance between stripes), H_{M} is the stray field created by all array elements due to long-range nature of the magnetostatic interaction.

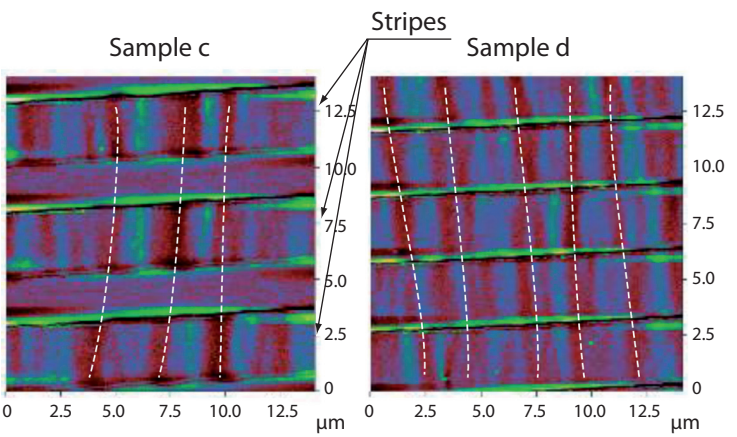

Figure 3. Magnetic force contrast far from the ends of the nanostripes for arrays c, d. The light dash-dotted lines show the synchronized parts of the ripple magnetizations belonging to different stripes.

Thus, the effects associated with the interaction between array elements, significantly affect the magnetic states. These effects should be taken into account when designing storage devices especially based on dense arrays packed items.

The study was carried out with the financial support of the Russian Foundation for Basic Research within the framework of scientific project No. 20-02-00696.

PHENOMENOLOGICAL MODEL OF ACCELERATED MOTION OF A DOMAIN WALL IN FERROMAGNETIC BISTABLE AMORPHOUS MICROWIRE

*V.V. Rodionova, V.V. Savin**

Immanuel Kant Baltic Federal University, Kaliningrad, Russia
*E-mail: savin_vv@bk.ru

Magneto-bistable amorphous microwires in a glass shell, due to their size and magnetic softness, are a promising material for the creation and development of sensor devices and magnetic memory [1]. The purpose of this work is to search for the causes that affect the dynamics of the domain wall motion during the process of magnetization reversal of the microwire and cause accelerated motion of the domain wall.

The geometric sizes and amorphous state of the microwire do not allow a detailed study of the process of its magnetization reversal: the features of the micromagnetic structure and its change in an external magnetic field. Therefore, most modern research in this direction is focused on studying the dynamics of the motion of domain walls in the process of its motion, as well as indirect estimates of this motion (the energy balance equation, the area and shape of the induced EMF peaks during the remagnetization of a microwire, the shape of hysteresis loops, the distribution of local nucleation and etc. [2–4]).

The Sixtus-Tonks method is a classical method for measuring the velocity of a domain wall in a microwire [5]. This method is based on successive detection of the EMF signal induced in two receiving coils during the remagnetization of the microwire.

In the process of investigation by this method, three types of motion were detected: accelerated uniform and decelerated of the domain wall in microwires with a metal core composition $Fe_{77.5}Si_{7.5}B_{15}$, $Fe_{77}Si_{10}B_{10}C_3$, $Fe_{47.42}Ni_{26.6}B_{12.99}Si_{11}C_{1.99}$ with different transverse dimensions.

A phenomenological model is proposed to explain the positive and negative accelerations of the domain wall during the remagnetization of a microwire.

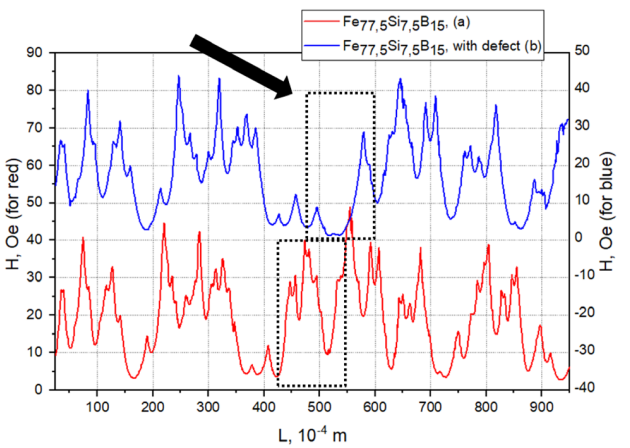

Figure 1. Distribution of local fields of nucleation of the $Fe_{77.5}Si_{7.5}B_{15}$ sample, d/D = 13/26: **a** before the infliction of the defect, **b** after the infliction of the defect.

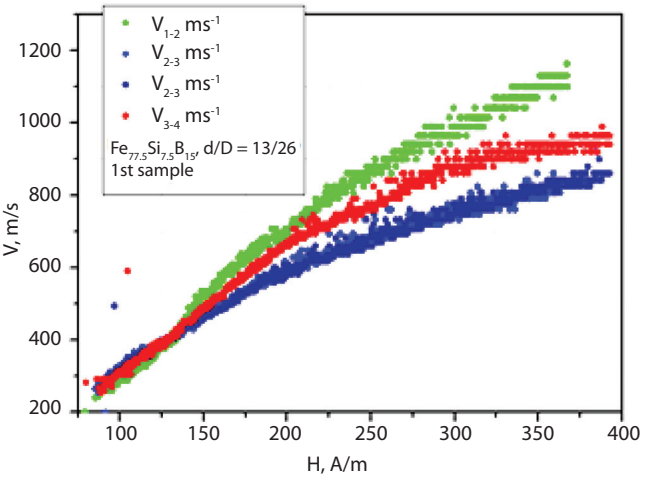

Figure 2. Deformation of an elastic matrix by hard magnetic particles in an external magnetic field.

1. M. Ipatov, Studies of Magnetic Properties of Amorphous Microwires with High Technological Interest. Dissertation. San Sebastián, (2008).
2. Zhukov et al., J. Appl. Phys. **115**, 17A305 (2014).
3. P. Corte-Leon, V. Zhukova et al., Appl. Mat. Today 101263 (2021).
4. S. Chikazumi. Physics of Ferromagnetism. Oxford University Press (1997).
5. K.J. Sixtus, L. Tonks, Phys. Rev. 42 (1932).

EFFECT OF INTERLAYER COUPLING ON THE DOMAIN WALL KINETICS IN ULTRATHIN Co/Pd/Co TRILAYER

*I.V. Shashkov**, *V.S. Gornakov, Yu.P. Kabanov*

Institute of Solid State Physics RAS, Chernogolovka, Russia
*E-mail: shav@issp.ac.ru

Magnetic multilayer thin films with perpendicular magnetic anisotropy are intensively studied in last decades due to their relevance in fundamental science and their potential use in high-density data recording applications [1]. The processes of magnetization reversal in ferromagnetic layers are determined not only by the magnetic properties of an individual ferromagnetic layer, but also by the interaction between layers. The resulting interaction is governed by several mechanisms: direct exchange via pin-hole coupling; magnetostatic (orange peel) coupling that decays exponentially with increasing Pd-spacer thickness t; coupling via conduction electron that oscillates and decreases as $1/t^2$ [2].

We studied the magnetization reversal of an ultrathin Co/Pd/Co structure, with Co-layers of equal thickness (0.4 nm) and a wedge-shaped Pd-spacer (0–10 nm), in a perpendicular magnetic field using polar magneto-optical Kerr microscopy. The sample was cut along the wedge into ten pieces. The nonmonotonic dependence of the domain nucleation field in the perpendicular field on the spacer thickness has been revealed in the thickness range 1.2–10 nm, where the perpendicular magnetization anisotropy is observed. Along with quantitative variation of coercivity, a qualitative change in the reversal mode is revealed. Structures with the spacer thickness in the range 1.2–4.5 nm show nucleation at the same field and bound motion of domain walls in both Co-layers, which may attribute to the ferromagnetic (attractive) interlayer coupling [3]. An abrupt transition to the layer-by-layer reversal with independent domain wall motion in the layers is observed at thicknesses of about 4.5 nm. In the Pd-spacer thickness range $t > 4.5$ nm nucleation and spreading fields for each layer become different. The layer with small (high) domain nucleation field we will call the "soft" ("hard") layer respectively.

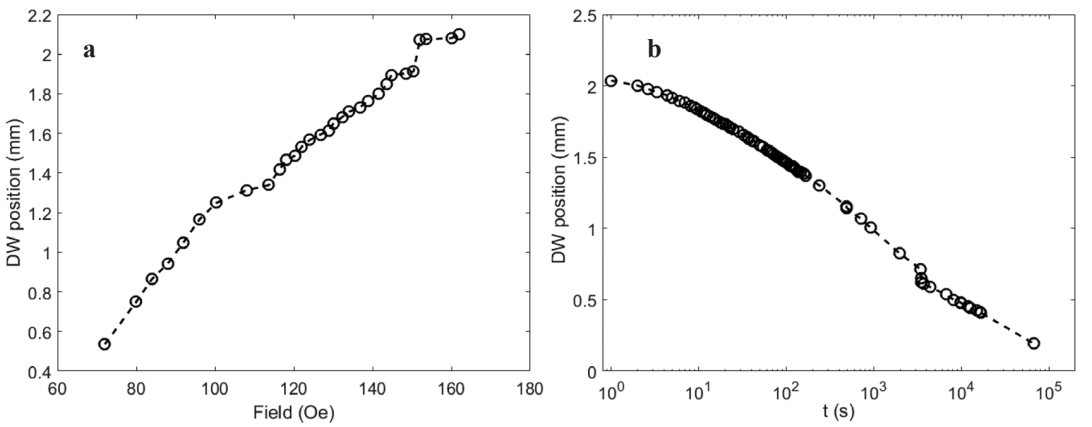

Figure 1. **a** Dependence of domain wall position in "soft" layer on the amplitude of applied magnetic field. **b** Dependence of domain wall position in "soft" layer on time without magnetic field. Zero DW position corresponds to Pd-spacer thickness t = 5 nm.

The transition region from coupled to uncoupled nucleation and spreading of domains in different layers at a Pd thickness of t = 4.5 nm was also studied. In this region the magnetization reversal of the "soft" layer leads to formation of metastable state with antiparallel magnetization of the layers. The domain of new phase in "soft" layer nucleate near edge of the film with thick Pd-spacer and spread toward edge with thin Pd-spacer. The domain wall (DW) spreading slows down and stops near the film center that corresponds to the spacer thickness t = 4.5 nm. The stop coordinate of DW depends on external field as shown on Fig. 1a. The spreading will continue after magnetization reversal of hard layer. The transition behavior from uncoupled magnetization reversal of the layers to correlated indicates increasing of ferromagnetic coupling between the layers. Moreover, our experiment shows coupling interaction almost linearly increases with spacer thinning. Figure 1b shows the DW position in "soft layer at zero magnetic field. The dependency also testifies ferromagnetic coupling between layers that decreases with growth of spacer thickness. The nature of observed effects is discussed.

The study was carried out as a part of state assignment at Institute of Solid State Physics, Russian Academy of Sciences

1. B. Lu, T. Klemmer, K. Wierman, G.P. Ju, D. Weller, A.G. Roy, D.E. Laughlin, C.H. Chang and R. Ranjan, J. Appl. Phys. **91**, 8025 (2002).
2. R.D. Shull, Y.L. Iunin, Y.P. Kabanov, V.I. Nikitenko, O.V. Skryabina and C.L. Chien, J. Appl. Phys. **113**, C101 (2013).
3. P.J. Metaxas et al., Phys. Rev. Lett. **104**, 237206 (2010).

MAGNETIC DISSIPATION FORCE MICROSCOPY IN AMBIENT CONDITIONS

A.G. Temiryazev[1*], *M.P. Temiryazeva*[1], *Yu.V. Nikulin*[2], *N.S. Gusev*[3], *S.A. Nikitov*[4]

[1]Fryazino Branch of the Kotelnikov Institute of Radioengineering and Electronics RAS, Fryazino, Russia
[2]Saratov Branch of the Kotelnikov Institute of Radioengineering and Electronics RAS, Saratov, Russia
[3]Institute for Physics of Microstructures RAS, Nizhny Novgorod, Russia
[4]Kotelnikov Institute of Radio Engineering and Electronics RAS, Moscow, Russia
[*]E-mail: temiryazev@gmail.com

Magnetic films can have a great variety of possible topologically stable magnetic structures: vortices, skyrmions, bimerons, as well as configurations localized inside the domain wall: Bloch lines, Bloch points, and even bimerons, as shown in a recent paper [1]. The combination of topological protection and the extremely small volume occupied by such structures may be of interest for the development of a new class of information storage devices and spintronics. At the same time, modern research methods cannot always reliably detect the presence of small magnetic features. We believe that indirect confirmation of their existence can be obtained on the basis of dissipative atomic force microscopy. A similar technique was previously used only for measurements in vacuum and made it possible to record the transition of a single electron to a quantum well at cryogenic temperatures [2], as well as the generation of a Josephson vortex at the superconductor-normal metal-superconductor contact [3]. Such a high sensitivity of the method is explained by the fact that the processes occurring in rhythm with the oscillations of the AFM probe are recorded, that is, in the case of the Josephson junction, a vortex is born and destroyed at each oscillation period. A characteristic feature of these measurements is the appearance of ellipses in the AFM images of the resonant frequency and amplitude. They correspond to the positions of the probe at which such a connection of the probe oscillations with the measured object occurs. Similar features were also found when measuring permalloy discs using magnetic force microscopy (MFM) in vacuum [4], where they were explained by the magnetization switching occurring at the apex of the MFM tip itself due to the strong stray field of the magnetic disc.

We performed MFM measurements in air at room temperature. Films of various compositions (Co, CoCr, Py), both patterned and unstructured, were studied. Despite the fact that the Q-factor of the probe is significantly lower in air compared to measurements in vacuum, characteristic features in the form of ellipses were found in the MFM images (Fig. 1). Their appearance is not related to the switching of the probe magnetization, since in some cases the stray fields were extremely small. On some samples, as for example in the case shown in Fig. 1, the presence of such features is strongly pronounced. In most cases, however, the effect is rather weak and can be observed in a narrow range of external magnetic fields. To reveal it and visually demonstrate it, we made a series of MFM images with a small step change in the external magnetic field. Further, a film was made from this series, which in dynamics allows you to see the smallest details of the change in neighboring images. An analysis of the data obtained (dependence upon the amplitude of the probe oscillations and the its height above the surface) allows us to assume that in certain places of the samples, at certain values of external fields, conditions arise that, in a small volume of the sample, the direction of magnetization is switched in time with the mechanical oscillations of the probe. Moreover, these are precisely switchings, and not linear oscillations of the magnetization. The observed ellipses show the position of such places with respect to domain walls, sample edges, etc. Probably, a more accurate description of such phenomena can be obtained using micromagnetic calculations.

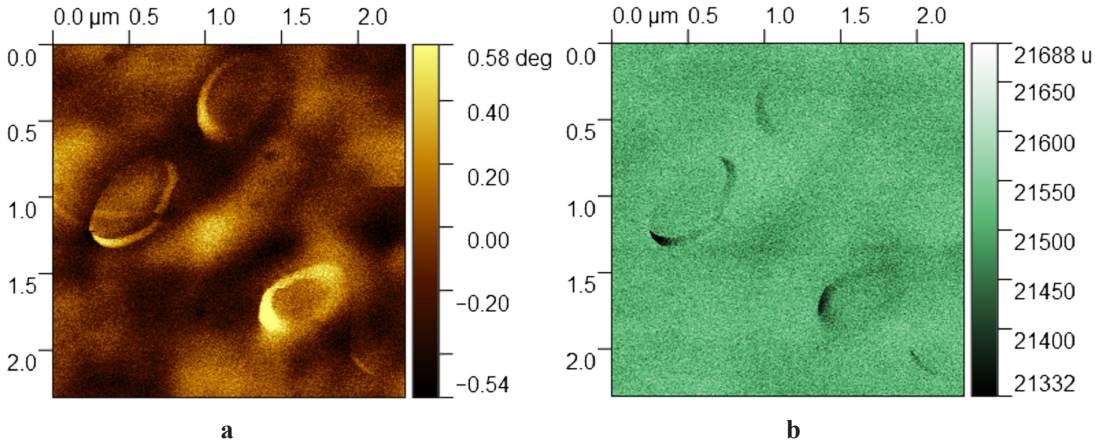

a **b**

Figure 1. **a** Phase image reflecting the resonant frequency shift; **b** amplitude image.

Support by RSF (project No. 19-19-00607) is acknowledged.

1. T. Nagase et al., Nat. Commun. **12**, 3490 (2021).
2. M.T. Woodside, P.L. McEuen, Science **296**, 1098 (2002).
3. V.V. Dremov et al., Nat. Commun. **10**, 4009 (2019).
4. O. Iglesias-Freire et al., Appl. Phys. Lett. **102**, 022417 (2013).

DISORDER IN SKYRMION LATTICE INDUCED BY RANDOM MAGNETIC ANISOTROPY

V.A. Fel'k[1*], *S.V. Komogortsev*[1,2], *A.A. Mokhov*[2], *A.N. Pavlova*[1]

[1]Reshetnev Siberian State University of Science and Technology, Krasnoyarsk, Russia
[2]Kirensky Institute of Physics, Federal Research Center Krasnoyarsk Science Center, Siberian Branch, Russian Academy of Sciences, Krasnoyarsk, Russia
[*]E-mail: vlaf80@mail.ru

In recent years, skyrmions have been actively studied since their peculiar dynamics in external fields is promising for applications in spintronics. Skyrmions are topological magnetization defects or topological solitons with a topological charge equal to unity and appear in magnetic structures without an inversion center (chiral ferromagnets) [1, 2]. In thin magnetic films with positive exchange interaction and the Dzyaloshinskii-Moriya interaction, in addition to noncollinear or noncoplanar spin structures such as magnetic vortices, domain walls, and spirals, an ordered skyrmion lattice can be formed. The region on the phase diagram external field – film thickness, in which an ordered skyrmion lattice is realized, is specified by a certain set of magnetic constants of the film. In films with a polycrystalline structure, the magnetic properties and magnetic microstructure can undergo cardinal changes in comparison with homogeneous films. In theory, the effect of a polycrystalline structure in ferromagnets is described by a random magnetic anisotropy model.

In this work, we investigated the effect of random distribution of the easy magnetization axes of crystallites on disordering in the skyrmion lattice formed in a film with positive exchange interaction and Dzyaloshinskii-Moriya interaction using micromagnetic simulation.

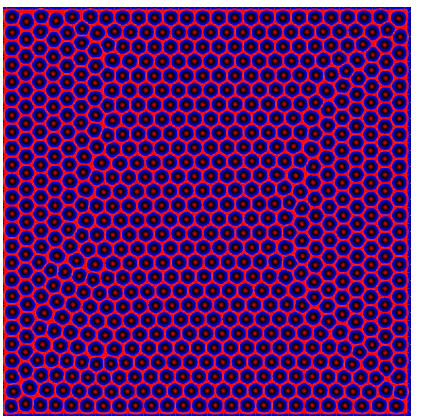

Fig. 1. Skyrmion lattice with dislocations.

It has been found that skyrmion lattices contain structural defects of the dislocation type even at a small crystallite magnetic anisotropy constant K (Fig. 1). The latter plays the role of a static stochastic parameter. Quantitatively, the order in the lattice was estimated using the correlation function and the two-dimensional Fourier transform. We observe how the order in the skyrmion lattice is destroyed as K increases. The observed behavior of the order parameter on K differs significantly from the behavior associated with approaching the melting point of the two-dimensional lattice.

This research was funded by the RFBR, Krasnoyarsk Region and the Krasnoyarsk Regional Science Foundation (Project No. 20-42-240001).

1. A.B. Borisov, A.R. Safin, D.V. Kalyabin et al., Phys. Usp. **63**, 269–288 (2020).
2. A.A. Belavin, A.M. Polyakov, Pis'ma Zh. Eksp. Teor. Fiz. **22**, 503–506 (1975).

STABILITY OF FLAT STRUCTURES IN FERROMAGNETIC NANOFILMS

E.B. Magadeev, R.M. Vakhitov, R.R. Kanbekov*

Bashkir State University, Ufa, Russia
*E-mail: magadeeveb@gmail.com

It was shown in [1] that in thin ferromagnetic films with artificially created holes (antidotes [2]) vortex-like inhomogeneities (VLI) of a new type can appear, which are of great practical interest. The condition for the occurrence of such VLIs is the presence of a strong uniaxial anisotropy of the "easy plane" type, due to which the magnetic structures under consideration are characterized by the absence of a magnetization vector leaving the film plane. This paper is devoted to determining the specific values of the anisotropy constant, at which the stability of flat structures is ensured, and also considers possible scenarios for the loss of stability. In order to carry out such an analysis, three approaches have been developed: analytical, numerical, and also empirical.

The analytical approach to the study of the stability of flat structures turns out to be effective in a number of the simplest situations and allows, firstly, to obtain universal rough estimates of the minimum allowable value of the anisotropy constant, and secondly, to calculate correction factors for this value, for example, for the case of a single antidote. With a more complex sample geometry, however, the application of the analytical approach becomes difficult, which requires the involvement of numerical and empirical approaches. The first of them is based on calculations related to the use of a lattice model of a magnet, and the second one is based on a series of numerical experiments in which the dependence of the energy of the system under study on time is studied. The combination of these approaches makes it possible to obtain estimates of the minimum allowable value of the anisotropy constant for the case of an inhomogeneous structure localized in the vicinity of two antidotes, depending on the distance between them (Fig. 1).

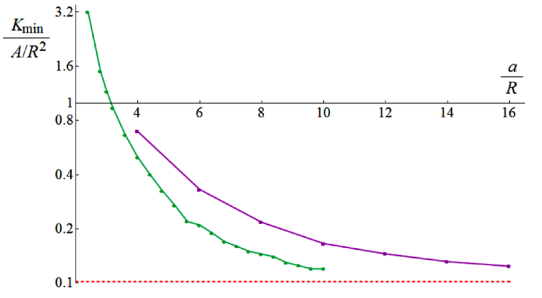

Figure 1. Dependence of the minimum allowable value of the anisotropy constant on the distance between the antidotes. The green line is obtained using the empirical approach, the purple line is obtained using the numerical approach, and the red dashed line shows the lower estimate obtained analytically.

It should be noted that, from a mathematical point of view, the calculations associated with the use of analytical and numerical approaches represent the solution of problems for the eigenvalues of a linear differential operator and a symmetric matrix, respectively.

1. E.B. Magadeev, R.M. Vakhitov, JETP Lett. **115**, 114 (2022).
2. J. Muller, A. Rosch, Phys. Rev. B **91**, 054410 (2015).

Section E.
Magnetotransport, magnetooptics and magnetophotonics

PROXIMITY INDUCED LONG-RANGE TRANSFORMATION OF TRANSVERSE MAGNETO-OPTICAL KERR EFFECT IN BILAYERS OF MAGNETIC AND NORMAL TRANSITION METALS

V.A. Skidanov

Institute for Design Problems in Microelectronics RAS, Moscow, Russia
E-mail: skidanov@ippm.ru

Phenomena at the interface between magnetic and nonmagnetic media attract growing attention during last two decades [1]. The possibility of spin ordering transfer from ferromagnetic metal F to normal metal N is of particular interest in view of important applications.

Spin diffusion from iron into tin 6 nm thick layer was observed experimentally in Fe/Sn/Fe film structure by Mössbauer effect observation in Sn^{119} [2]. The author of Electron Spin Resonance (ESR) discovery E. K. Zavoisky predicted then that long-range diffusion of polarized electrons from ferromagnetic metal can provide possibility to observe ESR signal even from diamagnetic metals [3]. In present report optical transverse Kerr effect is used to investigate polarized electrons diffusion through interface in N/F bilayer of transition normal N and ferromagnetic F metals.

Objects for investigation were fabricated by magnetron sputtering of metallic targets. Parallel strips of ferromagnetic metals (permalloy Ni80-Fe20 or pure Fe) with various thicknesses t in the range 5–40 nm were evaporated on glass substrates with use of masking coatings. Evaporation of ferromagnetic layers was made in external magnetic field to create anisotropy with easy axis in plane of the layer. Then perpendicular strips of non-magnetic transition metal with various thicknesses h in the range 5–150 nm were evaporated to form regular matrix of bi-layered rectangles (5×5 mm) with a set of thickness values pairs (t, h). Kerr effect measurements were implemented at the same intensity level of reflected white light which was strictly maintained by lamp current to avoid uncertainty caused by difference in objects thickness and transparency values. Since reflection factor increases with metal film thickness the intensity of incident light was accordingly reduced for thicker structures. All of measured magnetooptical signals are normalized by the value of the signal from the thick opaque single Py film ($t \geq 40$ nm).

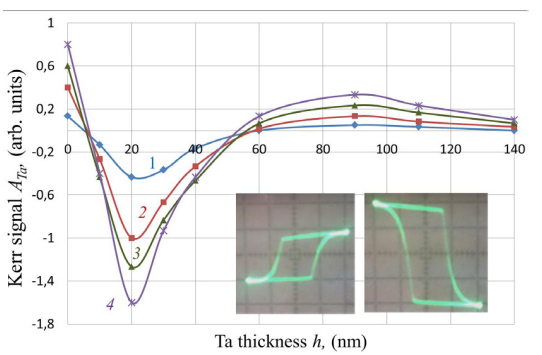

Figure 1. Dependences of normalized Kerr signals $A_{Ta}(h,t)$ from the side of Ta film on Ta thickness h for the set of Py thickness values t: 1 – t = 5 nm, 2 – t = 10 nm, 3 – t = 20 nm, 4 – t = 30 nm. Insert: left photo – Kerr signal from single Py layer, t = 20 nm; right photo – Kerr signal from Ta/Py bilayer, h = t = 20 nm.

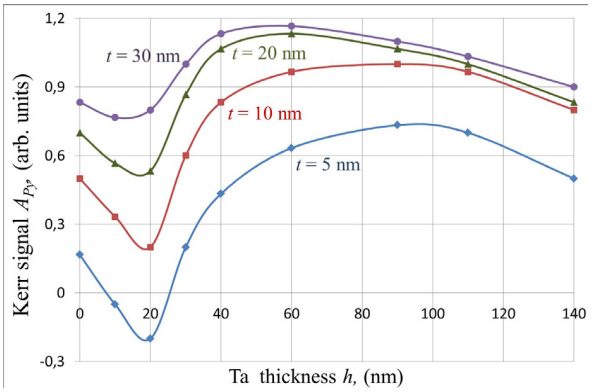

Figure 2. Normalized Kerr signals from Py layer side dependences $A_{Py}(h,t)$ for Py/Ta structure on Ta layer thickness h for the set of Py thickness values t.

Experimental investigation of transverse Kerr effect in two-layered Ta/Py structures reveals non-monotonic dependence of magnetooptical signal on nanoscale thickness (up to 150 nm) instead of exponential reduction expected due to light absorption in nonmagnetic transition metal layer. These striking dependences for a set of Py thickness values t are shown in Fig. 1. Rapid decrease and inversion of Kerr signal is seen when Ta thickness h reaches the range 7–10 nm and then inversed signal attains its maximal amplitude at $h \sim 20$ nm. The further increase of Ta layer thickness is accompanied by reduction of inverted signal amplitude to zero at h in the range 50–60 nm where signal surprisingly changes its sign once again. Then signal rises with h up to $h \sim 90$ nm although Ta film is entirely opaque if $h \geq 40$ nm and light doesn't reach Py layer.

The influence of inverted signal from Py/Ta bilayer was observed in configuration when light falls on the Py layer with Ta layer underneath and is shown in Fig. 2. Kerr signal decreases for all Py thickness values in the range $t \leq 30$ nm where permalloy layer is partially transparent. The signals reach minimum at $h \sim 20$ nm in consistency with inverted signal minimum values in Fig. 1.

The total signal from Py/Ta bilayer even changes sign for well transparent Py at which inverted signal from Ta layer exceeds signal from Py film (t = 5 nm). The increase of Ta thickness in the range $h \geq 20$ nm causes enhancement of the magnetooptical signals which exceed initial signals from single Py film (h = 0). Signal magnitudes increase even at $h \geq 40$ nm and $(t + h) \geq 70$ nm where intensity of light is negligible. The highest 5-fold enhancement of the signal is achieved for thinnest Py film. So Ta layer produces its own Kerr signal tied with magnetization in Py layer.

The probable mechanism of Kerr effect transformation is long-range diffusion of unexcited polarized minority and majority electrons through bilayer interface from ferromagnetic metal. Theoretical considerations of diffusive relaxation in transition metals [5] concern optically excited electrons and hint that spin diffusion length goes to infinity if energy of excitation approaches zero.

Results of investigation can be used in designing and analysis of multilayered spin structures and application in magnetooptical and magnetoplasmonic sensors.

1. F. Hellman et al., Rev. Mod. Phys. **89** (2), (2017).
2. V.Ya. Gamlitskii et al., JETP **40**(2), 374 (1975).
3. E.K. Zavoiskii, JETP Lett. **21**(7), 191 (1975).
4. V.P. Zhukov and E.V. Chulkov, Physics – Uspekhi **52**(2), 105 (2009).

FABRICATION OF ONE-DIMENSIONAL MAGNETOPHOTONIC CRYSTALS CONTAINING METAL-ORGANIC DECOMPOSITION-PREPARED BISMUTH-SUBSTITUTED YTTRIUM IRON GARNET

S.L. Efremova[1,2*], *K.N. Afanasiev*[1,3], *A.A. Kasyanov*[1], *D.P. Kulikova*[1,2], *Y.M. Sgibnev*[1], *A.V. Shelaev*[1], *P.N. Tananaev*[1], *A.V. Baryshev*[1]

[1]Dukhov Automatics Research Institute (VNIIA), Moscow, Russia
[2]Lomonosov Moscow State University, Moscow, Russia
[3]Institute for Theoretical and Applied Electromagnetics of RAS, Moscow, Russia
[*]E-mail: svetlana.efr96@gmail.com

Magnetophotonic crystals (MPCs) are periodic dielectric structures that are widely used to enhance magneto-optical response of media [1]. The key aspect underlying the enhancement of magneto-optical effects lies in the localization of light in a periodic structure. MPCs commonly contain layers of bismuth-substituted yttrium iron garnet (Bi:YIG), since it is a transparent material with large values of Faraday rotation and magneto-optical figure of merit. Deposition of garnets can pose a difficulty in fabrication of MPCs or other photonic structures. Most garnet fabrication techniques include thermal annealing needed for crystallization which can lead to deterioration of photonic devices' structure and degradation of their optical properties. In this regard, it appears important to study the thermal stability of Bragg mirrors (one-dimensional photonic crystals) composing MPCs, as well as to improve the Bi:YIG manufacturing technology.

In the present work we investigate thermal stability of Bragg mirrors composed of different pairs of oxides in order to determine the optimal composition for one-dimensional MPC fabrication. Also, an approach for garnet crystallization by using laser annealing is demonstrated, which can help one to avoid the undesirable effects caused by the thermal annealing. The Bragg mirrors under study were made of alternating layers of ZrO_2/SiO_2, HfO_2/SiO_2 and Ta_2O_5/SiO_2 pairs prepared by means of electron beam evaporation (EBE) on quartz substrates. These samples were subjected to thermal annealing at the temperatures ranging from 300 to 750 °C. Transmittance spectra and surface optical images were obtained for the as-deposited and annealed Bragg mirrors. The transmittance spectra revealed that the annealing of the EBE-prepared Bragg mirrors led to a spectral shift of their photonic bandgap into the shorter wavelength range. The $(ZrO_2/SiO_2)^7$ structure turned out to be the most stable one, therefore, it was chosen for MPC manufacturing. The fabricated MPC had the structure $(ZrO_2/SiO_2)^7$/Bi:YIG/$(SiO_2/ZrO_2)^7$ with a Bi:YIG layer prepared using metal-organic decomposition (MOD) method including thermal annealing at 750 °C for 45 minutes. The layer thicknesses of the MPC were chosen in such a way that the increase in Faraday rotation was observed at the wavelength of about 610 nm. The second Bragg mirror (denoted as BM2) was fabricated to have the same optical properties as the first Bragg mirror after the annealing (BM1).

Figure 1 shows the transmission and Faraday rotation spectra obtained for the resulting MPC. As one can see from plot Fig. 1b, a resonant increase in Faraday rotation was observed for the MPC as compared with the single garnet film. Nevertheless, the obtained peak value was significantly smaller than the calculated one. The thermal annealing led to a mismatch in optical properties of the Bragg mirrors composing the MPC, which led to the difference between the experimental and calculated spectra. Plot Fig. 1a reveals that the thermal annealing of BM1 resulted in a decrease in the interference fringes intensity in the short-wavelength range. To prevent degradation of photonic crystals' optical properties caused by thermal annealing, a different method of garnet crystallization is preferred.

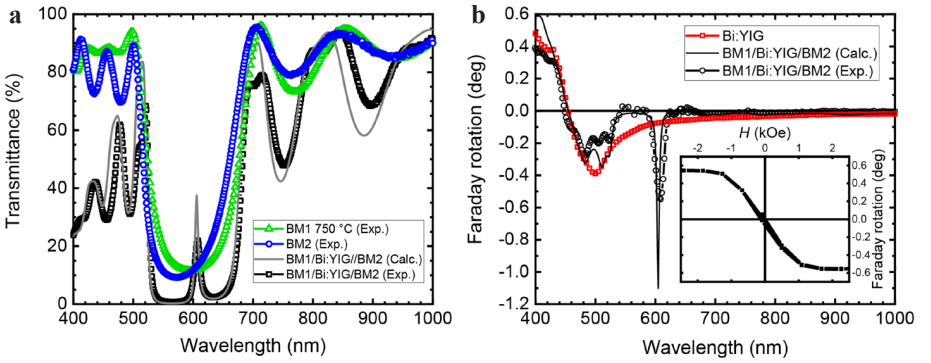

Figure 1. **a** Transmittance spectra of annealed BM1, as-deposited BM2 and the MPC (calculated and experimental). **b** The Faraday rotation angle of the single Bi:YIG film and MPC (calculated and experimental). The inset illustrates a hysteresis loop of Faraday rotation for the MPC at 610 nm [2].

We demonstrate the local crystallization of MOD-prepared oxide films performed on a micron scale by using a focused laser beam. The crystallization was carried out using femtosecond laser pulses [3], as well as a continuous-wave (CW) laser. In the first case a film of composition $Bi_{1.5}Y_{1.5}Fe_5O_{12}$ was transformed into seven 2×2 mm^2 structures consisting of 16 stripes by using the laser with a pulse energy in the range 9–24 nJ. Irradiation wavelength, pulse duration, and repetition rate were 525 nm, 200 fs, and 80 MHz, respectively. The laser beam diameter on the sample surface was 150 µm. A CW-laser emitting at a wavelength of 405 nm was used in order to crystallize a MOD-prepared $Bi_{0.5}Y_{2.5}Fe_5O_{12}$ film. The laser beam was focused into a spot with a diameter of about 1 µm. A set of strips with a length of 20 µm was obtained by using the laser power varying from 6.4 to 24.6 mW. Also, we examined the effect of different gases' presence on the crystallization process. The annealing procedure was carried out in a gas cell at a constant gas flow of O_2, N_2, Ar, or dry synthetic air.

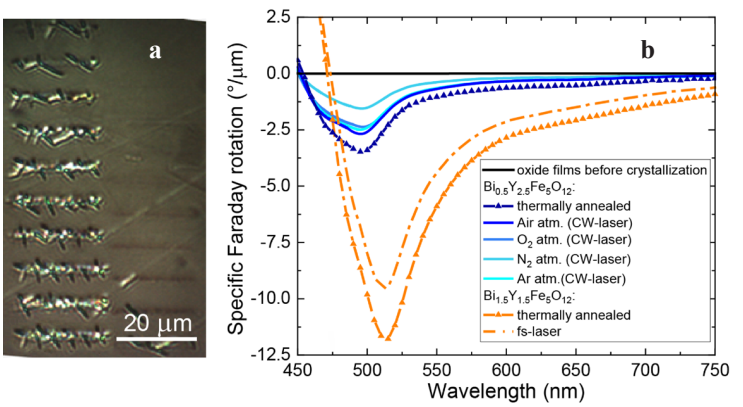

Figure 2. **a** Cross-polarized optical microscope images of the strips produced by using a CW-laser in air. The right column corresponds to the power range from 6.4 mW (the upper strip) to 15 mW (the lower one). The left column corresponds to the power range 16–24.6 mW. **b** Faraday rotation spectra measured for the garnet samples crystallized employing fs laser pulses, CW-laser and thermal annealing in air.

Figure 2a shows the cross-polarized optical microscope images of the strips produced by using a CW-laser with various powers in the air atmosphere with no magnetic field applied. One can see that the annealing led to formation of a domain structure. Figure 2b demonstrates the Faraday rotation spectra obtained for the garnet samples crystallized with a femtosecond laser, a continuous wave laser and thermal annealing of the oxide films. It can be seen that the locally crystallized garnet samples and thermally annealed ones had comparable Faraday rotation values. The Raman spectra measured for the crystallized structures confirmed the presence of the Bi:YIG phase. The presented technology can be employed to integrate garnets to non-garnet substrates, including semiconductors and photonic crystals. Thus, the processes accompanying photonic crystals' thermal treatment have been studied. A garnet crystallization method has been proposed which makes it possible to avoid the difficulties arising during thermal annealing.

1. M. Inoue, M. Levy and A.V. Baryshev, Magnetophotonics: From Theory to Applications, Springer (2013).
2. S.L. Efremova et al., J. Phys. D: Appl. Phys. **54**, 505305 (2021).
3. Y. Sgibnev et al., Crystal Growth & Design **22**, 1196–1201 (2022).

HALL EFFECT IN HEUSLER-TYPE MAGNETIC SHAPE MEMORY ALLOYS

*A.B. Granovsky**, *V.N. Prudnikov, M.I. Blinov, Ya.G. Rezninov, M.V. Prudnikova*

Faculty of Physics, Lomonosov Moscow State University, Moscow, Russia
*E-mail: granov@magn.ru

Heusler alloys have multifunctional properties that are important for a variety of practical applications. It determines the continuously growing interest in these systems. Ternary alloys of the Ni-Mn-X family, where X = Ga, In, Sb, and also quaternary alloys Ni-Mn-X-Z, of a certain concentration composition, experience a martensitic transition (MT) from a high-temperature cubic phase (austenite) into a low-temperature phase with tetragonal distortions (martensite). This transition can be magnetically induced, accompanied or not accompanied by a change in the magnetic order, and it is responsible for many properties, in particular, giant deformations, giant magnetocaloric effect, giant anomalous Hall effect (AHE), magnetic shape memory effect, etc. Recently, skyrmions and the corresponding topological Hall effect were found. in Ni-Mn-Ga and Ni-Mn-In alloys [1, 2].

It is generally accepted that MT is associated with the collective Jahn-Teller effect, in which the gain in energy due to a decrease in the symmetry of the lattice is compensated by the loss in energy of the electronic subsystem. Although a number of experimental facts and theoretical calculations confirm this concept, there are data that contradict it. Thus, the electronic contribution to the heat capacity proportional to the density of states at the Fermi level in Ni-Mn-In alloys changes insignificantly during MT, the changes in the magneto-optical Kerr effect are also small, and the electronic contribution to the magnetocaloric effect was not found. This points to a rather complex, and not fully understood, nature of the rearrangement of the electronic structure during MT. Magnetotransport effects, such as magnetoresistance, the normal Hall effect (NHE) and the anomalous Hall effect (AHE), are among of the most effective probes-indicators of phase transitions and changes in the electronic and magnetic structure. The study of the AHE, which is central to the group of spontaneous galvanomagnetic phenomena and a prominent representative of spin-dependent transport phenomena, is also of independent importance, since discussions about the role of various mechanisms in formation of this effect, especially in Heusler alloys ([3-6] and references therein).

The report analyzes experimental data on structural, magnetic and magnetotransport properties for several Heusler magnetic shape memory alloys with focus on behavior of NHE and AHE in a wide temperature range including MT. We studied $Ni_{48}Co_2Mn_{35}In_{15}$, $Ni_{50}Mn_{34.8}In_{15.2}$, $Ni_{50}Mn_{35}In_{15-x}Si_x$ (x = 1.0, 3.0, 4.0), $Ni_{50}Mn_{35}In_{15-x}B_x$ (x = 0, 0.5, 0.75), $Ni_{45}Cr_5Mn_{37}In_{13}$, $Ni_{49}BiMn_{35}In1_5$ bulk samples, fabricated by arc-melting, $Ni_{47.3}Mn_{0.6}Ga_{22.1}$ and $Ni_{49.7}Fe_{17.4}Co_{4.2}Ga_{28.7}$ thin films, obtained by magnetron scattering. Normal and anomalous Hall effect coefficients were determined by fitting the field dependencies of the Hall resistivity using magnetization data.

Magnetoresistance for all samples is negative, exhibit negative peaks near phase transitions and is more sensitive to changes in magnetic structure than resistivity. In the austenite phase, the temperature dependence of the AHE coefficient is satisfactorily described by the developed AHE theory, and there is a correlation between the temperature dependences of the AHE coefficient R_s and resistivity ρ in the form $R_s = a\rho + b\rho^2$. As a rule, the NHE coefficient R_0 in studied samples with magnetostructural MT is negative in martensitic phase, depends on temperature and changes its sign during MT [3–6], that is evidence of the change in the type of current carriers during MT.

The behavior of the AHE coefficient in the martensitic phase and during MT is not universal and strongly depends on the composition and microstructure of the alloys. The general correlation

between R_s and ρ considered as applicable for all crystalline and amorphous ferromagnetic alloys breaks down in martensitic phase and during MT. For example, in $Ni_{45}Cr_5Mn_{37}In_{13}$ the anomalous Hall coefficient R_s was found to increase with temperature in martensite while the resistivity ρ decreases. We supposed that this behavior is connected with different types of current carries responsible for resistivity and AHE, the redistribution of spin-up and spin-down d-states even at small changes in total density of states at the Fermi level and antiferromagnetic correlations.

Both coefficients R_0 and R_s in $Ni_{47.3}Mn_{0.6}Ga_{22.1}$ strongly depend on the magnetic field. To determine these coefficients we fit the total Hall resistivity curves $\rho_H = R_0B_z + 4\pi R_sM_z$ in several magnetic field ranges (100–1000 Oe, 0–5 kOe, 8–16 kOe, 0–16 kOe) using magnetization data while considering R_0 and R_s as the fitting parameters. We also fit the Hall effect resistivity with the expression $\rho_H = R_0B_z + 4\pi R_sM_z + \Delta\rho_H$ with the coefficients R_0 and R_s obtained from high field interval (8–16 kOe), where the last term $\Delta\rho_H$ was considered to correspond either to the topological Hall effect or to the antiferromagnetic Hall effect. The obtained temperature dependence and magnitude of $\Delta\rho_H$ discard the presence of the skyrmions or antiskyrmions. We conclude that unconventional field dependences of both NHE and AHE are due to both the antiferromagnetic correlations and to the influence of the magnetic field on the electronic structure.

MT in $Ni_{49.7}Fe_{17.4}Co_{4.2}Ga_{28.7}$ films is latent, since it occurs in a wide temperature range, is not accompanied by a magnetic phase transition, and the magnetizations of the martensitic and austenitic phases differ insignificantly. In this case the AHE coefficient is well described by the relation $R_s = a\rho + b\rho^2$ with the second term much smaller than the first one. This indicates the dominant role of asymmetric scattering and interference impurity-phonon scattering for the considered low-resistance composition.

Magnetic and magnetotransport properties of Heusler alloys drastically depend on even 0.5–1.0% of forth element Z, especially for Z = B, Cr, Bi. In the case of Z = Bi we observed non-monotonic temperature dependence of AHE at $T < 100$ K that might be due to metastable state.

Our experimental data can be considered as an evidence of electronic structure transformation during MT with redistribution between spin-up and spin-down d-states and insignificant change of total density of states at the Fermi level.

A.G. acknowledges support from the Russian Ministry of Science and Education grant No. 075-15-2021-1353 and the Academy of Finland (grant No.333805).

1. C. Phatak, O. Heinonen, M. De Graef, A. Petford-Long, Nano Lett. **16**, 4141 (2016).
2. W. Zhang, B. Balasubramanian, A. Ullah et al., Appl. Phys. Lett. **115**, 172404 (2019).
3. M. Blinov, A. Aryal, S. Pandey et al., Phys. Rev. B **101**, 094423 (2020).
4. S. Pandey, M.l Blinov, A. Aryal et al., J. Magn. Magn. Mater. **481**, 25 (2019).
5. M.I. Blinov, V. Chernenko, V.N. Prudnikov et al., Phys. Rev. B **102**, 064413 (2020).
6. M.I. Blinov, V. A. Chernenko, V.N. Prudnikov et al., JETP **159**, 546 (2021).

MAGNETO-OPTICAL SPECTROSCOPY OF $(CoFeB)_x(LiNbO_3)_{100-x}$ NANOCOMPOSITES BELOW THE PERCOLATION THRESHOLD

E.A. Ganshina[1*], *A.B. Granovsky*[1], *E.S. Kanazakova*[1], *I.M. Pripechenkov*[1], *S.N. Nikolaev*[2], *A.S. Sitnikov*[3], *V.V. Rylkov*[2]

[1]Faculty of Physics, Lomonosov Moscow State University, Moscow, Russia
[2]National Research Centre "Kurchatov Institute", Moscow, Russia
[3]Voronezh State Technical University, Voronezh, Russia
[*]E-mail: eagan@mail.ru

We present results of magneto-optical (MO) investigations of $(CoFeB)_x(LiNbO_3)_{100-x}$ thin film nanocomposites with metal volume fraction x = 17–48 at.% below the percolation threshold x_{per} focusing on magnetic structure gradual change from non-interacting superparamagnetic nanoparticles to superferromagnetic state and long-range ferromagnetic order.

Magnetic nanocomposites, or nanogranular magnetic films "ferromagnetic metal-insulator", in which ultrafine single-domain ferromagnetic particles are embedded in oxide matrix, exhibit numerous magnetic, transport, optical, MO and high-frequency properties that are promising for application in information storage technology, magnetic sensors, high-frequency shielding, etc. [1]. Recently, it has been shown that $(CoFeB)_x(LiNbO_3)_{100-x}$ nanocomposites below the percolation threshold show also the effects of reversible resistive switching that is very promising for creation of memristor arrays to emulate synapses in neuromorphic systems [2].

At a very low volume fraction of ultrafine ferromagnetic particles they do not interact via exchange and dipole-dipole interaction and therefore they form an ensemble of superspins at $T < T_b$ and an ensemble of superpamagnetic particles at $T_C > T > T_b$, where T_b is the blocking temperature and T_C is the Curie temperature of the single particle. With increasing x the interaction between particles at $T < T_S$ leads to superferromagnetic state, that in ideal case is an ensemble of ferromagnetically aligned nanoparticles, and to superparamagnetic state at $T_C > T > T_S$. In non-ideal case the system will consist of both ferromagnetically aligned volumes and superparamagnetic particles. With further increase of metal volume fraction up to x_{ferro} long-range ferromagnetism will arise across the whole system. There are three critical concentration $x_{ferro} < x_{MI} < x_{per}$, where x_{MI} corresponds to the metal-insulator transition, The presence of magnetic ions between granules makes possible various scenarios. Superferromagnetic state can be dentified by magnetic measurements, Mossbauer studies and MO spectroscopy [3].

$(CoFeB)_x(LiNbO_3)_{100-x}$ films with x = 17–48 at.% were produced by the ion-beam sputtering technique onto Si substrates. The compositions of the targets were $Co_{40}Fe_{40}B_{20}$ and $LiNbO_3$. Details of sample fabrication and structural characterization are similar to those given in [2]. Transport measurements showed that x_{MI} is about 48 at.%. MO investigations were carried out in transverse Kerr effect (TKE) geometry at T = 20–300 K in the spectral range 0.5–4.0 eV and magnetic field up to 2.5 kOe. We used p-polarized light, the incident angle being 69.5°. Two types of measurements were performed for each concentration: field dependences of TKE signal at selected wavelengths and spectral dependences in fixed magnetic field. We used the dynamic MO method in which the TKE parameter δ is the relative change of intensity of reflected light under magnetization in an applied alternating magnetic field with 40 Hz frequency. Some results are shown in Fig. 1.

The TKE field dependence for sample with x = 17 at.% tends to saturate at low temperatures but is strictly linear at room temperature (Fig. 1b). The temperature dependence follows $1/T$ law above 40 K (Fig. 1c) that means that this sample is superparamagnetic at least above T_b ~ 30–40 K.

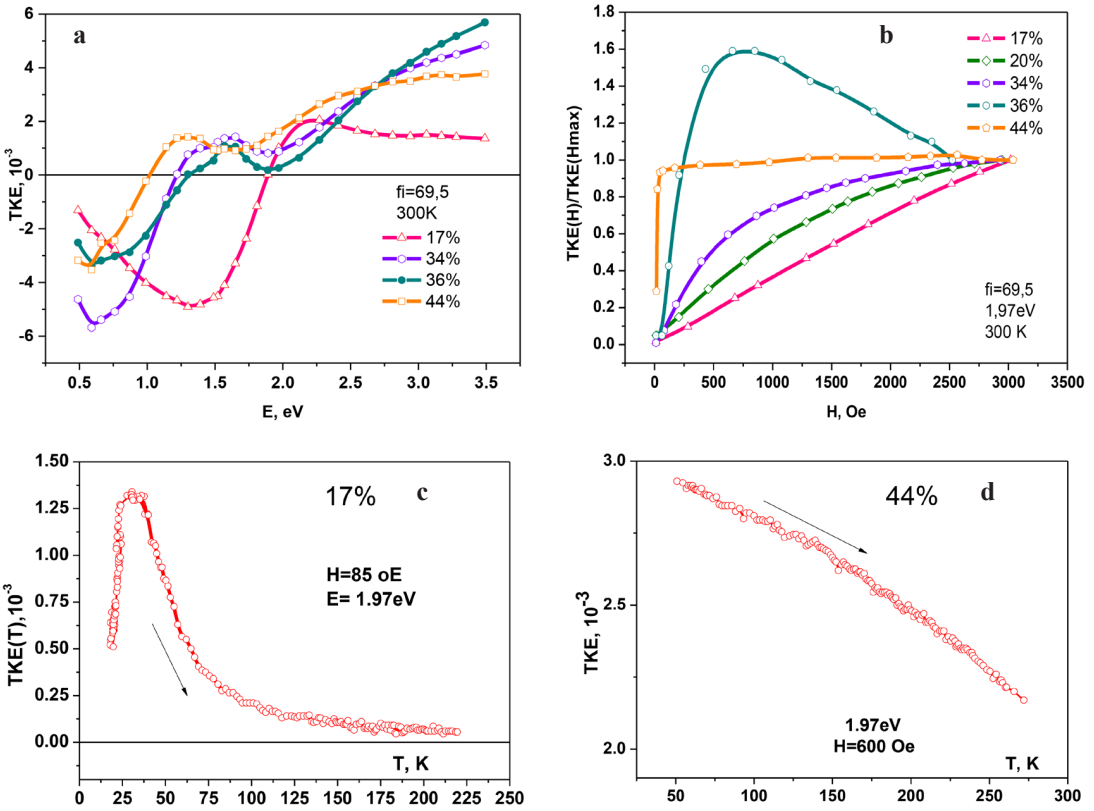

Figure 1. The spectral (**a**), field (**b**) and temperature (**c**, **d**) dependences of TKE $(CoFeB)_x(LiNbO_3)_{100-x}$ films with x = 17–44 at.%.

This value is in a good agreement with magnetic measurements. It means that samples are homogeneous across their thickness since TKE signal is due to the surface layers. Surprisingly, already at x = 20 at.% the TKE signal becomes slightly nonlinear at room temperature (Fig. 1b). It indicates on appearance of interaction between nanograins. This tendency increases with x and the field dependence of TKE signal becomes more and more similar to ferromagnetic response instead of $1/T$ law (Fig. 1b).

Quite strong decrease of the TKE signal with increase of temperature (Fig. 1d) shows that the Curie temperature of nanoparticles differs significantly from that for amorphous or crystalline $Co_{40}Fe_{40}B_{20}$. This is probably related to composition in nanoparticles different from the target composition.

MO spectra for $(CoFeB)_x(LiNbO_3)_{100-x}$ nanocomposites with $17 \le x \le 44$ at.% are shown in Fig. 1a. Their profile differs from those for $(CoFeB)_x(Al_2O_3)_{100-x}$ [3]. In spite MO spectra depend on type of matrix, substrate, granular size, granular size distribution and so on, the main features are determined by magnetic entity. The obtained difference in MO spectra clearly indicates on strong influence of technological parameters on electronic structure of magnetic nanoparticles.

An anomalous field dependence of the TKE was found for a sample with x = 36 at.% (Fig. 1b). This is a clear evidence of superferromagnetic state when the sample consists of both large soft ferromagnetic regions and superparamagnetic particles.

Support by RSF (grant № 22-29-00392) is acknowledged.

1. V.V. Ryl'kov, A.V. Emel'yanov, S.N. Nikolaev et al., JETP **131**, 161 (2020).
2. M.N. Martyshov, A.V. Emelyanov, V.A. Demin et al., Phys. Rev. Appl. **14**, 034016 (2020).
3. E. Ganshina, A. Granovsky, D. Shevyakov et al., IEEE Magnetics Lett. **11**, 2500504 (2020).

SWITCHABLE TERAHERTZ EMISSION BY MAGNETIC TUNNEL JUNCTION

A.A. Fraerman[1], *E.A. Karashtin*[1,2*], *F. Kholid*[3], *R.V. Mikhaylovskiy*[3], *I.Yu. Pashen'kin*[1], *Y. Saito*[3]

[1]Institute for Physics of Microstructures RAS, Nizhny Novgorod, Russia
[2]University of Nizhny Novgorod, Nizhny Novgorod, Russia
[3]Department of Physics, Lancaster University, Bailrigg, Lancaster, UK
[*]E-mail: eugenk@ipmras.ru

In 2016, it was first demonstrated that a multilayer magnetic nanostructure consisting of a magnetic layer (FM) which is adjacent to a non-magnetic (preferrably, heavy metal, HM) layer may act as an efficient broadband THz emitter [1]. Irradiation of such system by a femtosecond optical pulse of high intensity leads to the flow of a short spin current pulse from FM to HM, mainly due to local heating of the sample. This, in turn, causes the electric current due to the inverse spin Hall effect in HM, which emits a short and broadband electromagnetic wave pulse.

Magnetic tunnel junctions (MTJ) are used as effecient spintronic devices to control the electric current flow by applying a small magnetic field (tens of Oe) [2]. This is governed by the fact that the electric current that flows from one ferromagnet to another under an applied voltage is spin-polarized. The spin polarization depends on the magnetic state of one FM layer, while the electron transition probability depends on the magnetic state of the other FM. Thus, the resistance of the structure depends on relative magnetic state of the FM layers. Based on this property, such devices are used to create the magnetic memory (MRAM). Usually, these are plane-layered nanostructures that consist of two ferromagnetic layers (typically CoFeB) split by a thin insulator (MgO). Magnetization of one of the FM layers (fixed layer) is pinned at the antiferromagnet (IrMn), while the other FM layer is referred to as a free layer. This allows to easily control relative magnetizations of the FM layers by applying a small magnetic field which is enough to magnetize the free layer, but too small to act on the fixed layer.

In our work, we study the THz emission from MTJ structures IrMn(10)/CoFeB(4)/MgO(1.5)/CoFeB(4)/Ta(3)/Pt(10), where layer thicknesses are in nm. A sample with only one (fixed) layer is also investigated as a reference. Similar structure with two Fe layers separated by a 4-nm-thick Pt (HM) layer were studied recently [3]. In [3], the FM layers do not interact, but inject spin current into Pt. The electric current produced by it either (almost) cancels for a ferromagnetic state or adds up for an antiferromagnetic one which allows to control the THz signal emission by an external magnetic field. We further show that an MTJ structure demonstrates similar effect, but the emission is effective in a ferromagnetic state rather than an antiferromagnetic one. Besides, we show that the pump pulse of high fluence applied together with a magnetic field may control the direction of the pinning axis of the fixed layer, thus providing a possibility to locally modify the MTJ structure properties.

The samples are fabricated by magnetron sputtering. They are irradiated by optical pump pulses (wavelength 800 nm, duration 50 fs, pulse repetition rate 500 Hz, fluence 0.6–2.7 mJ/cm^2, focused into a ~3-mm region). First, we study the IrMn(10)/CoFeB(4)/Ta(3)/Pt(10) structure. The hysteresis loop of this structure measured via the magnetooptical Kerr effect (MOKE) is shown in Fig. 1a. It is exchange shifted from zero field due to pinning by an antiferromagnet. The same loop is obtained via the THz signal measurement at small pump fluence (0.6 mJ/cm^2, Fig. 1b). However at higher fluence (2.7 mJ/cm^2) the loop shift vanishes and the coercive field becomes smaller. This

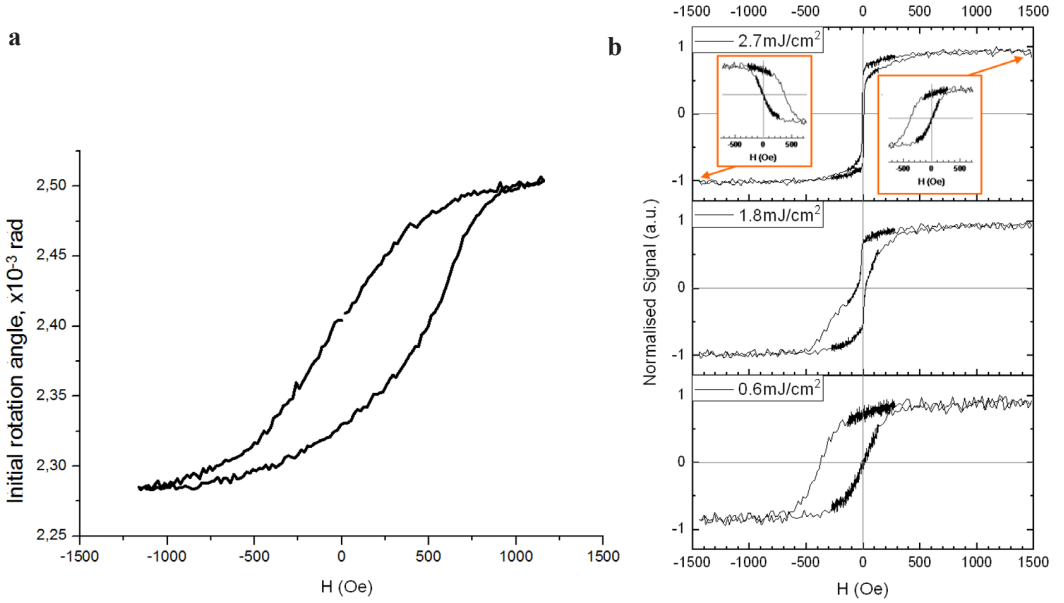

Figure 1. MOKE hysteresis loop (**a**) and THz signal measurement at different pump fluence (**b**) for IrMn(10)/CoFeB(4)/Ta(3)/Pt(10).

is attributed to local sample heating above the blocking temperature of IrMn. If the sample is rotated at an arbitrary angle (in its plane), an external field (1.5 kOe) is applied and then the sample is irradiated by pump pulses (for 10 s) the pinning is induced along the direction of the applied magnetic field (inset in Fig. 1b).

The IrMn(10)/CoFeB(4)/MgO(1.5)/CoFeB(4)/Ta(3)/Pt(10) MTJ structure demonstrates similar properties for high fluence which indicates that the MTJ may be locally annealed by pump. Besides, we see with small pump fluence that the measured signal (amplitude of electric field generated in the

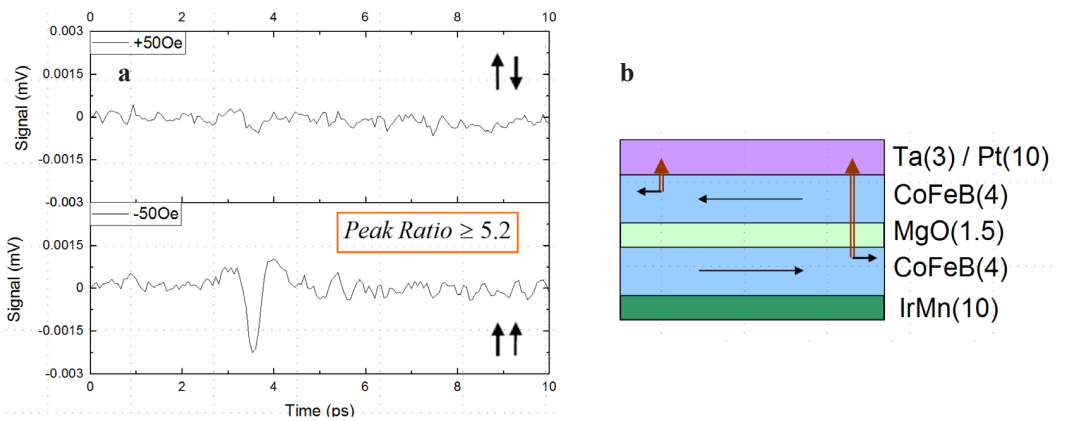

Figure 2. Signal versus time for MTJ in antiferromagnetic and ferromagnetic state (**a**) and schematic of possible explanation of the observed cancellation of signal in antiferromagnetic state (**b**).

system) contains almost no peak for the antiferromagnetic state of MTJ, while there is a pronounced peak in the ferromagnetic state (Fig. 2a). Possible explanation is that the spin current is converted to the electric current in the capping Ta layer. The top CoFeB layer is quite thin (4 nm) so the spin current from the bottom CoFeB layer reaches the Ta cap as well as the spin current from the top CoFeB layer (see e.g. [4] where spin current flows through a several nanometers thick IrMn layer). Therefore in antiferromagnetic state the currents almost compensate each other (Fig. 2b), while in ferromagnetic state the currents add up and give the observed peak. Thus the MTJ may be used as a broadband THz source with controllable properties.

This work was supported by Center of Excellence "Center of Photonics" funded by The Ministry of Science and Higher Education of the Russian Federation , contract #075-15-2020-906.

1. T. Seifert et al., Nat. Photonics **10**, 483 (2016).
2. I.Yu. Pashen'kin et al., Technical Physics **64,** 11, 1642–1645 (2019).
3. M. Fix et al., Appl. Phys. Lett. **117**, 132407 (2020).
4. O. Gueckstork et al., Appl. Phys. Lett. **120**, 062408 (2022).

MAGNETIC MODULATION OF HYPERBOLIC SURFACE PLASMON-POLARITONS IN UNIAXIAL METASURFACES

D.A. Kuzmin[1*], *I.V. Bychkov*[1], *V.G. Shavrov*[2]

[1]Chelyabinsk State University, Chelyabinsk, Russia
[2]Kotel'nikov institute of radio engineering and electronics of RAS, Moscow, Russia
[*]E-mail: kuzminda@csu.ru

Nowadays, hyperbolic plasmonics attracts researchers' attention by its exciting optical properties [1–6]. Hyperbolic metasurfaces (HMSs) support highly localized low-loss surface plasmon-polaritons (SPPs), providing drastic increase of the light-matter interactions near the surface. Moreover, HMSs allow the very effective manipulation by SPPs varying from routing them towards specific directions within the sheet, dispersion-free propagation (canalization), and to the negative refraction.

The usual realization of HMSs is constructing the surface which behaves as a dielectric (has a capacitive impedance) in one direction and as a metal (has an inductive impedance) in the orthogonal one. In the hyperbolic regime plasmons propagate as a very narrow beam along the specific direction and electromagnetic energy became localized near metasurface even stronger than for "usual" elliptic SPPs.

The general trend of increasing light-matter interactions near the surface in hyperbolic regime allows us to suppose that magneto-plasmonic effects in magneto-plasmonic HMSs should have some non-trivial features as well. Here we propose and investigate plasmonic properties of HMS on the magnetic dielectric substrate.

Let us consider HMS consisting of gold strips with the width W separated each other by gaps with the width G (see left panel on Fig. 1). Such a metasurface may be described by 2D conductivity tensor $\hat{\sigma}$ [1–6]:

$$\hat{\sigma} = \begin{pmatrix} \sigma_{xx} & 0 \\ 0 & \sigma_{yy} \end{pmatrix},$$

$$\sigma_{xx} = \sigma_{\text{gap}}\sigma_{\text{gold}} L / W\sigma_{\text{gap}} + G\sigma_{\text{gold}}, \qquad \sigma_{yy} = \sigma_{\text{gold}} W / L,$$

$$\sigma_{\text{gap}} = -\mathrm{i}\omega\varepsilon_0\varepsilon_{\text{gap}}d_{\text{eff}}, \qquad d_{\text{eff}} = -(L / \pi)\ln[\sin(\pi G / 2L)].$$

In the equations above, $\sigma_{\text{gold}} = -\mathrm{i}\omega\varepsilon_0\varepsilon_{\text{gold}}d$ is 2D complex conductivity of gold layer with thickness d, σ_{gap} is effective conductivity of gap caused by near-field coupling between neighboring strips. The metasurface is placed over magnetic substrate (YIG, for example) which electromagnetic response may be described by antisymmetric dielectric permittivity tensor $\hat{\varepsilon}$:

$$\hat{\varepsilon} = \varepsilon_0 \begin{pmatrix} \varepsilon_\perp & 0 & -\mathrm{i}\varepsilon_a \\ 0 & \varepsilon_{||} & 0 \\ \mathrm{i}\varepsilon_a & 0 & \varepsilon_\perp \end{pmatrix}.$$

Solving Maxwell's equations in each medium and considering the metasurface as a boundary condition

$$(\mathbf{E}_2 - \mathbf{E}_1)\times\mathbf{n}_{12} = 0, \qquad (\mathbf{H}_2 - \mathbf{H}_1)\times\mathbf{n}_{12} = \hat{\sigma}\mathbf{E}_1,$$

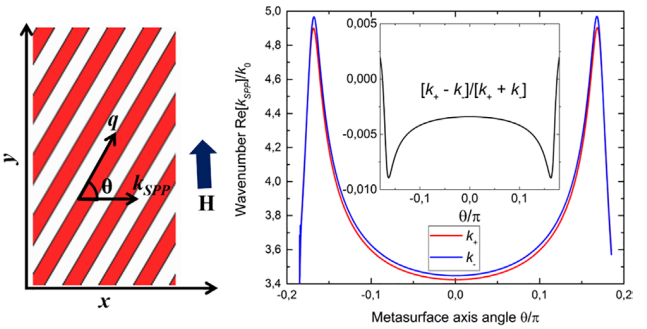

Figure 1. Scheme of the gold-based uniaxial metasurface (left) consist of gold stripes (red) with the gaps (white) in between. Dependence of the SPPs wavenumber on the metasurface axis angle for two opposite external magnetic field orientations (right). On the inset a magnetic SPPs modulation is shown.

where, indexes "1" and "2" correspond to the top medium and substrate, consequently, one may obtain a dispersion relation for surface plasmon polaritons, propagating along such a metasurface. This dispertion relation is quite cumbersome, so we will restrict ourselves just by numerical calculations. Let us consider a telecom frequency of propagating SPPs corresponding to the wavelength 1560 nm. Geometrical parameters of the metasurface will be chosen as follows W = 45 nm, L = 50 nm, d = 10 nm. For magnetic substrate we will use the parameters corresponding to YIG $\varepsilon_\perp \approx \varepsilon_\parallel = 3$, $\varepsilon_a = \pm 0.01$. Sign of ε_a depends on the direction of external magnetic field. We will consider SPPs propagating along x-axis with the magnetic field collinear to y-axis. Let us analyze how plasmonic properties of such a structure depends on HMS orientation and magnetic field direction. Results of calculations are shown on Fig. 1 (right).

One can see, that for some angles of metasurface orientation there are peaks of SPPs wavenumber. This means that a metasurface work in hyperbolic regime [1–6]. Switching the magnetic field direction led to slightly shift of the wavenumber curve. We should note that bulk electromagnetic wave is unsensitive to magnetic field direction in such geometry (Voight geometry). The change in SPPs wavenumber by switching the magnetic field direction leads to the possibility of SPPs modulation by external magnetic field. For analyze this effect we have plotted the magnetic modulation factor $[k_+ - k_-] / [k_+ + k_-]$ (see inset on Fig. 1 right panel). One can see, that maximal values correspond to the metasurface orientation when SPPs are propagating along hyperbolae asymptotes.

In conclusion, we have demonstrated the possibility of magnetic modulation in the HMS on magnetic dielectric substrate. For practical implementation of this effect, it is necessary to increase the magnetic modulation factor. So, the further investigation of magneto-plasmonic hyperbolic metasurface with more complex geometry should be provided.

Support by RFBR (grant # 20-07-00466) is acknowledged. Numerical calculations were performed with support by RSF (grant # 22-19-00355).

1. J.S. Gomez-Diaz, M. Tymchenko, A. Alù, Phys. Rev. Lett. **114**, 233901 (2015).
2. J.S. Gomez-Diaz, M. Tymchenko, A. Alù, Optical Materials Express **5**, 2313–2329 (2015).
3. J.S. Gomez-Diaz, A. Alù, ACS Photonics **3**, 2211–2224 (2016).
4. A. Nemilentsau, T. Low, G. Hanson, Phys. Rev. Lett. **116**, 066804 (2016).
5. A.V. Kildishev, A. Boltasseva, V. M. Shalaev, Science **339**, 1232009 (2013).
6. A.A. High, R.C. Devlin, A. Dibos et al., Nature **522**, 192 (2015).

INFLUENCE OF DIMENSIONAL EFFECTS AND SIZE DISTRIBUTION OF GRANULES ON OPTICAL AND MAGNETO-OPTICAL PROPERTIES OF NANOSTRUCTURES

A.N. Yurasov[1*], *M.M. Yashin*[1], *E.A. Gan'shina*[2], *I.V. Gladyshev*[1], *M.A. Simdyanova*[1], *D.A. Saifulina*[1], *K.R. Safin*[1]

[1]RTU MIREA, Institute of Advanced Technologies and Industrial Programming, Department of Nanoelectronics
[2]Faculty of Physics, Lomonosov Moscow State University
[*]E-mail: Alexey_yurasov@mail.ru

Annotation. Dimensional effects are clearly manifested in nanostructures and have a significant impact on their optical and magneto-optical properties, especially in the IR region of the spectrum, which is associated with intraband transitions. Taking into account the dimensional effects and particle size distribution allows us to improve the description of promising nanostructures. The solved problem is very important and relevant, both from the fundamental point of view – the study of magneto-optical, optical and transport phenomena in nanostructures, and from the point of view of applied applications in modern electronics and nanoelectronics.

In recent years, nanostructures have aroused great fundamental and practical interest, as they allow for changes. geometric structure and topology to obtain the required properties of materials taking into account the amplification of optical and magnetic effects [1]. One of the tools that allows us to study nanocomposites is the transverse Kerr effect. It consists in the fact that when linearly polarized radiation falls on a magnetized sample (and the magnetization vector is perpendicular to the plane of incidence of radiation), the intensity and phase of this radiation change. The effect in this case is remarkable in that it allows us to obtain information about the components of the dielectric constant tensor. The approximation of the effective medium is often used for the theoretical description of nanocomposites [1].

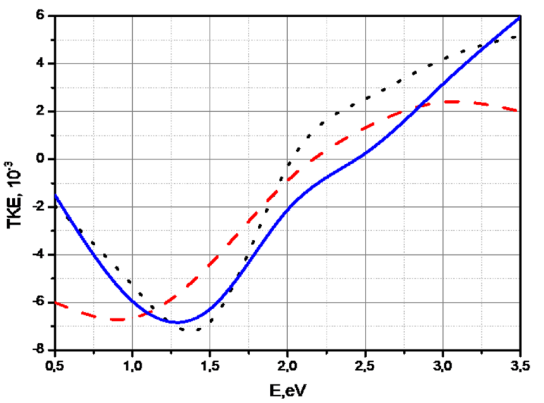

Figure 1. Experimental (dots) and calculated spectra of the transverse Kerr effect of the sample (x = 0.62) of the nanocomposite $(Co_{45}Fe_{45}Zr_{10})_x(Al_2O_3)_{1-x}$ Bruggeman (dotted line) and the symmetrized Maxwell-Garnett approximation (solid line) (the parameter of the anomalous Hall effect is 1.5, the form-factors of the particles of the medium L_B = 0.2; L_A = 0.57).

The results are presented on the example of nanocomposites $(CoFeZr)_x(Al_2O_3)_{1-x}$ (Fig.1). The main result can be considered to take into account the size distribution of granules within the lognormal distribution, both in optical and magneto-optical spectra of nanostructures, which made it possible to improve the description of experimental spectra.

Within the framework of the theory of an effective medium, taking into account the size distribution of granules, optimal parameters such as the size of granules and the parameter of the extraordinary Hall effect are selected, which makes it possible to describe experimental spectra well.

It is important to note that the approach used can be applied to any nanostructures.

During the simulation, when describing the TKE-spectra, we took into account the averaging of the TDP-components of the metal component with the distribution function, which allowed us to describe the experimental data quite well. The solved problem is very important and relevant, both from the fundamental point of view – the study of magneto-optical, optical and transport phenomena in nanocomposites, and from the point of view of possible applications in modern electronics and nanoelectronics. Taking into account dimensional effects and particle size dispersion makes it possible to find new promising functional materials, control their properties in a wide spectral range, and use them in various spheres of human activity [2–4].

1. A. Yurasov, E. Gan'shina, A. Sokolov, N. Granovsky, D. Zazymkina, EPJ Web of Conferences 185, 02009 (2018).
2. E. Lima, T. Tanaka, I. Toyoda, Progress In Electromagnetics Research M **75**, 141–148 (2018).
3. V.R. Tkacheva, Technic, Technologies. Engineering No.1, 37–40 (2016).
4. N.V. Medvedeva, O.M. Ipatova, Yu.D. Ivanov, A.I. Drozhzhin, A.I. Archakov, Nanobiotechnology and nanomedicine **52**(6) 529–546 (2006).

MAGNETIC AND MAGNETOTRANSPORT PROPERTIES OF MnSb POLYCRYSTALS AND MnSb-BASED COMPOSITES

L.N. Oveshnikov[1*], *A.B. Granovsky*[2], *A.B. Davydov*[1], *L.A. Morgun*[1], *A.V. Bogach*[3], *A.L. Vasiliev*[4], *A.V. Ovcharov*[4], *A.M. Kharlamova*[2], *E.I. Nekhaeva*[1], *A.I. Ril'*[5], *M. Jaloliddinzoda*[5], *S.F. Marenkin*[5], *B.A. Aronzon*[1]

[1]P.N. Lebedev Physical Institute RAS, Moscow, Russia
[2]Faculty of Physics, Lomonosov Moscow State University, Moscow, Russia
[3]Prokhorov General Physics Institute RAS, Moscow, Russia
[4]National Research Centre "Kurchatov Institute", Moscow, Russia
[5]Kurnakov Institute of General and Inorganic Chemistry RAS, Moscow, Russia
[*]E-mail: oveshln@gmail.com

Implementation of effective ways to control the properties of a system with spin polarized current have been the goal of numerous studies over the last three decades. The basic approach was to realize a spin-polarized current in a semiconducting system that can be controlled by external stimuli. Intensive studies of diluted magnetic semiconductors revealed that such systems are not suitable for actual applications, as the concentration of magnetic atoms in this case is very limited and correlated magnetic state can be realized only at low temperatures. An alternative approach consisted of incorporating ferromagnetic (FM) inclusions of the second phase in the semiconductor matrix. In this case, FM state may occur at substantially higher temperatures. In particular, pronounced FM response was observed in various MnSb based composites above room temperature [1, 2]. However, such studies often consider systems with relatively low volume fraction of MnSb, while at higher MnSb content the effect of FM inclusions on charge carriers in semiconducting matrix should be more pronounced. In the limiting case, MnSb inclusions separated by the thin semiconductor interlayer can be considered as a spin valve device, which should result in a substantial electrical response of such material to the external magnetic field.

In this work we studied magnetic and magnetotransport properties of GaSb-MnSb and InSb-MnSb composites with hypereutectic composition (relative to MnSb content). We also studied properties of the reference MnSb polycrystals. It should be noted that, prior to our study, magnetotransport properties of the MnSb compound had not been characterized properly. Studied composite samples were obtained via melt-quenching of polycrystalline precursors. Preliminary structural studies suggest that the semiconducting components retain lattice parameters of pristine materials, which is associated with low solubility limits of Mn in respective compounds. The MnSb phase retain hexagonal symmetry, while estimated lattice parameters suggest small deviation from equatomic composition towards the excess of Mn. Microstructural studies suggests that composite systems contain large MnSb inclusions, which, apparently, do not form a percolation cluster (inclusions are separated by the interlayers of matrix material), despite high MnSb content. All

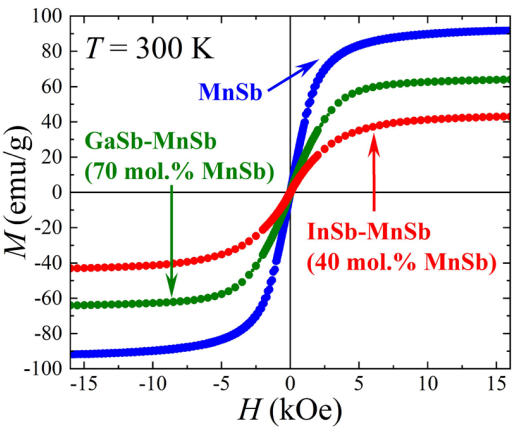

Figure 1. Room temperature magnetization curves for studied samples.

studied samples are FM at room temperature (Fig. 1), and estimated T_C values are above 500 K. The latter implies that the excess of Mn in the MnSb phase in studied composites is rather small. Observed magnetization values (see Fig. 1) correspond to the MnSb content in studied samples, suggesting the absence of secondary magnetic phases.

Studied composite samples demonstrate a metallic character of the temperature dependence of resistivity, similar to the MnSb reference. As it can be seen from the Fig. 2, the resistivity of the GaSb-MnSb sample is higher than that of the InSb-MnSb samples, despite lower content of the metallic MnSb phase in the latter. This implies that the conductivity of composite samples contains substantial contribution related to the semiconductor matrix, which agrees with the results of microstructural studies, as the formation of continuous MnSb cluster should result in the inverse conductivity ratio. The low temperature magnetoresistance (MR) of studied composites is negative, which contrasts with the positive MR observed for the MnSb polycrystal. The latter also implies a considerable role of matrix component, in which negative MR may occur due to spin-dependent scattering on the magnetic moments of diluted Mn atoms.

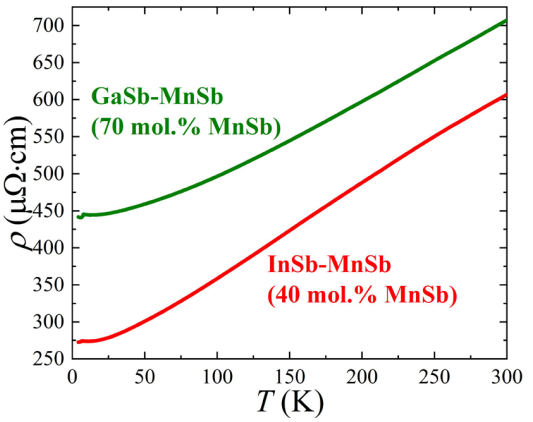

Figure 2. Temperature dependence of resistivity for studied MnSb-based composite systems.

All studied samples demonstrate pronounced anomalous Hall effect (AHE) at room temperature. The amplitude of AHE decreases with temperature, which can be related to the corresponding decrease in resistivity of the system. However, our results suggest that at low temperatures the AHE amplitude in composite samples may become vanishingly small or even negative, in contrast to the finite positive amplitude of AHE observed for the MnSb sample. Thus, our results suggest that both components in studied composites provide considerable contributions to the overall magnetotransport properties.

Support by RSF (grant № 21-73-20220) is acknowledged.

1. E.I. Yakovleva, L.N. Oveshnikov et al., JETP Lett. **101**(2), 130–135 (2015).
2. L.N. Oveshnikov, E.I. Nekhaeva et al., Beilstein J. Nanotechnology **9**, 2457–2465 (2018).

THERMAL DECOMPOSITION OF METAL OLEATES FOR FABRICATION OF Bi:YIG OPTICAL FILMS

P.N. Tananaev[1*], *A.V. Shelaev*[1], *S.L. Efremova*[1,2], *D.P. Kulikova*[1,2], *A.V. Voennov*[1], *A.V. Baryshev*[1]

[1]FSUE VNIIA, Moscow, Russia
[2]Lomonosov Moscow State University, Moscow, Russia
[*]E-mail: peternt@gmail.com

Bismuth-substituted yttrium iron garnet (Bi:YIG) is a well-known magneto-optical material characterized by large magnitudes the Faraday rotation. We present a wet chemical route to fabricating of polycrystalline Bi-substituted yttrium iron garnet films of optical quality via thermal decomposition of metal organic salts and subsequent crystallization of oxide layers at rapid thermal annealing. To fabricate initial oxide films with stoichiometry of Bi:YIG, the metal organic decomposition (MOD) method was used [1].

Our variation of the MOD method was as follows. Iron and bismuth oleates and yttrium 2-ethylhexanoate were dissolved in n-alkanes and spin-coated on quartz substrates. Metal-organic layers were then oxidated at 400 °C in air to obtain porous metal oxide films. Some instability of Bi-oleate and formation of excess oleic acid was mitigated by PMMA sublayers. Thickness was controlled in a range of 5–50 nm per each single spin-coating step. Crystallization at 650–760 °C during 30–45 min resulted in formation of clean $Bi_xY_{3-x}Fe_5O_{12}$ films characterized by the specific Faraday rotation of –4°/µm@510 nm (x = 0.5) and –12.5°/µm@510 nm (x = 1.5), which exceeded recently reported data [2].

Polycrystalline nature of thin films was confirmed by XRD, showing sporadic presence of oxide impurities in some areas of crystallized films. They were most probably due to errors in stoichiometry at the spin-coating stages. However, prolonged crystallization or overheating of all garnet films above 770 °C caused formation of metal oxides or ferrites, as seen by Raman spectroscopy, and disappearance of garnet phase. Composition range of $x > 1.5$ allows to obtain even higher rotation, however Bi:YIG formation may be accompanied by by-products crystallization. After crystalliza-

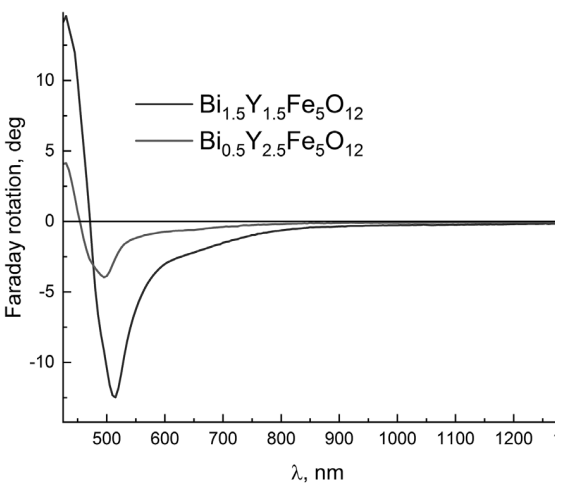

Figure 1. Specific Faraday rotation spectra of thin Bi:YIG films.

tion, thinning of the initial oxide films up to 30% was observed. For fabricated Bi:YIG films, their roughness was of 1–2 nm for $x = 0.5$ and became larger for $x = 1.5$.

Oxide Bi:YIG films were porous and were easily etched in HNO_3 and HCl acids. When Bi:YIG was crystallized, it cannot be dissolved by the acids. Thus, laser crystallization [3] and lithography can be used to create magneto-optical waveguides and other magnetophotonic micro- and nanostructures.

1. T. Ishibashi, A. Mizusawa, M. Nagai, S. Shimizu, K. Sato, N. Togashi, T. Mogi, M. Houchido, H. Sano, K. Kuriyama. J. Appl. Phys. **97**(1), 013516 (2005).
2. I. Nadinov, O. Kovalenko, J.L. Rehspringer, M. Vomir, and L. Mager, Ceramics International **45**(17), 21409–21412 (2019)
3. Y. Sgibnev, A. Shelaev, D. Kulikova, A. Salatov, P. Tananaev, G. Yankovskii, A. Baryshev, Cryst. Growth Des. **22**(2), 1196–1201 (2022).

PHOTO-INDUCED MAGNETO-OPTICAL PHENOMENA IN EPITAXIAL EuO FILMS

V.V. Pavlov[1*], *V.N. Kats*[1], *L.A. Shelukhin*[1], *P.A. Usachev*[1], *D.V. Averyanov*[2], *I.A. Karateev*[2], *O.E. Parfenov*[2], *A.N. Taldenkov*[2], *A.M. Tokmachev*[2], *V.G. Storchak*[2]

[1]Ioffe Institute, St. Petersburg, Russia
[2]National Research Center "Kurchatov Institute", Moscow, Russia
[*]E-mail: pavlov@mail.ioffe.ru

The ferromagnet EuO has the highest Curie temperature T_C = 69 K among the magnetic semiconductors EuX (X = O, S, Se, Te). Furthermore, T_C can be increased by proximity to a ferromagnetic metal [1] or doping with Gd [2], tailoring its magnetic, electric and optical properties [3]. The physical properties of EuO are determined by the electronic structure of Eu^{2+} ions having strongly localized $4f^7$ electrons with the spin S = 7/2. Here, we report photo-induced magneto-optical effects measured by a two-color pump-probe technique with and without a time resolution.

Magnetic field and temperature dependences of the photo-induced magneto-optical Kerr and Faraday effects were studied in epitaxial EuO films on YSZ substrates using a two-color pump-probe technique. A femtosecond laser with a photon energy of 1.19 eV generated pulses with a duration of 190 fs and repetition rates 72 MHz or 5 kHz. The laser beam was split into pump and probe beams. The photon energy of the pump beam was doubled (to 2.38 eV) by a BBO crystal; it was then mechanically modulated. The photo-induced magneto-optical effects were measured using a differential photodetector for the probe beam (1.19 eV).

The photo-induced Faraday rotation was studied as a function of light intensity, magnetic field and temperature. We have established that a resonance excitation of the optical electric-dipole transition $4f^75d^0 \rightarrow 4f^65d^1$ in EuO gives rise to formation of magnetic fluctuons with a high magnetic moment exceeding 100000 μ_B at a temperature of 69 K. A magnetic fluctuon is a composite quasi-particle formed in the medium by an electron localized in a potential well resulting from some fluctuation of the magnetic order parameter – magnetization [4].

Based on the photo-induced Kerr effect, magnetization precession has been observed for circularly polarized light excitation. The experiments reveal a laser-induced coherent ferromagnetic response in external magnetic field. The phase of the magnetization precession in the EuO-based films depends on the helicity of the pump beam. We set the experimental data against two potential mechanisms, the inverse Faraday effect and the optical orientation effect. Numerical estimates and comparison between EuO and Eu(Gd)O both point at the optical orientation effect, orienting spins via the $4f^75d^0 \rightarrow 4f^65d^1$ transition, as the mechanism triggering the magnetization precession. Thus, a new approach to the optical control of magnetic states in EuO has been demonstrated.

V.V.P., V.N.K., L.A.S, P.A.U. acknowledge support from RFBR – DFG (19-52-12063/ TRR160-C8), D.V.A., I.A.K., O.E.P., A.N.T., A.M.T., V.G.S. acknowledge support from NRC "Kurchatov Institute" (2753) and the Russian Science Foundation (20-79-10028; 19 19-00009).

1. D.V. Averyanov, A.M. Tokmachev, O.E. Parfenov, et al., Appl. Surf. Sci. **488**, 107–114 (2019).
2. D.V. Averyanov, O.E. Parfenov, A.M. Tokmachev, et al., Nanotechnology **29**, 195706 (2018).
3. V.N. Kats, S.G. Nefedov, L.A. Shelukhin, et al., Appl. Mater. Today **19**, 100640 (2020).
4. M.A. Krivoglaz, Sov. Phys. Usp. **16**, 856-877 (1974).

EFFECT OF THE INTERPARTICLE INTERACTIONS ON SUPERPARAMAGNETIC RELAXATION

D.A. Balaev[2], *S.V. Stolyar*[1,2], *A.A. Krasikov*[1], *O.A. Bayukov*[1], *R.N. Yaroslavtsev*[1,2], *D.A. Velikanov*[1], *R.S. Iskhakov*[1], *Yu.V. Knyazev*[1*]

[1]Kirensky Institute of Physics, Federal Research Center KSC SB RAS, Krasnoyarsk, Russia
[2]Krasnoyarsk Scientific Center, Federal Research Center KSC SB RAS, Krasnoyarsk, Russia
[*]E-mail: yuk@iph.krasn.ru

It is essential that the direction of the resulting magnetic moment of magnetic nanoparticles may rotate. Despite the magnetic ordering inside the particle, the anisotropy (magnetic) energy maybe not be enough to stabilize the magnetic moment. The frequency of this rotation completely depends on the external conditions. Dominantly, the thermal energy forces this rotation. In this way, two regimes are possible. The temperature that divides both regimes is called blocking temperature (T_B) when the magnetic energy is comparable with the thermal energy [1]. Relaxation time is associated with the energy barrier. This parameter depends on the characteristic measuring time of a certain experimental technique. Nevertheless, the blocking process seems to be abrupt, it is useful to study the relaxation dynamics of a system of nanoparticles at different temperatures.

In this study, we used ferrihydrite ultra-fine particles with narrow size distribution as a probe to investigate the effect of the interparticle interactions on superparamagnetic relaxation time by magnetization and Mössbauer methods. To modify interparticle interactions, we synthesized magnetic particles with different thicknesses of polysaccharide coating. Firstly, a "biogenic" sample was obtained from *Klebsiella oxytoca* strain [2]. "Annealed" sample was produced after calcination at 150 °C of the latter. "Uncoated" sample was synthesized by chemical process [3]. And the "coated" sample was obtained after coating of the mentioned chemical sample. The coating process was controlled by XPS.

According to our TEM data, the average particle size is slightly varying from 2.3 nm (for biogenic sample) to 3.0 nm (for coated and annealed samples). Therefore, we suppose a negligible influence of the size on the magnetization behavior. The relaxation time dependence is shown in Fig. 1.

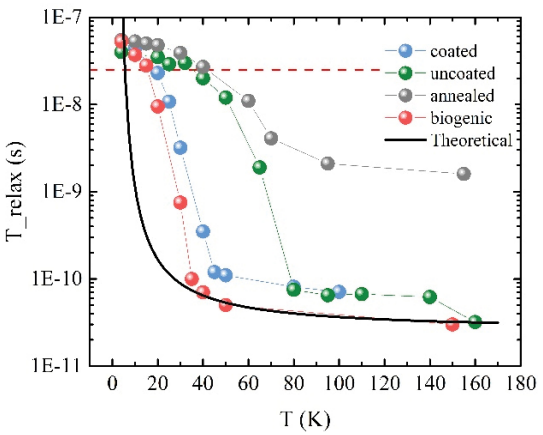

Figure 1. Relaxation time dependence for different ferrihydrite samples. Solid line depicts the theoretical curve according Néel-Brown equation. Dashed line shows Mössbauer technique characteristic time.

This study was supported by the Russian Science Foundation, Project No. 21-72-00025 (https://rscf.ru/project/21-72-00025/).

1. S. Mørup et al., J. Phys.: Condens. Matter., **19**, 213202 (2007).
2. Y.V. Knyazev et al., J. Alloys Compd., **851**, 156753 (2021).
3. Y.V. Knyazev et al., J. Alloys Compd., **889**, 161623 (2021).

MAGNETO-OPTICAL SPECTROSCOPY OF GaSb-MnSb COMPOSITES

E.A. Ganshina[1*], A.B. Granovsky[1], E.S. Kanazakova[1], I.M. Pripechenkov[1], L.N. Oveshnikov[2], M. Jaloliddinzoda[3], A.I. Ril'[3], B.A. Aronzon[2]

[1]Faculty of Physics, Lomonosov Moscow State University, Moscow, Russia
[2]P.N. Lebedev Physical Institute RAS, Moscow, Russia
[3]Kurnakov Institute of General and Inorganic Chemistry RAS, Moscow, Russia
[*]E-mail: eagan@mail.ru

We present the results of magneto-optical (MO) investigations of GaSb-MnSb composites, as well as of MnSb and Mn_2Sb compounds for comparison.

Because of a very low solubility of Mn in GaSb it was not possible to obtain dilute magnetic semiconductor GaMnSb with high Curie temperature. This problem can be overcome in composites GaSb-MnSb because MnSb has high Curie temperature ($T_c \approx 585$ K), high degree of spin polarization and large magnetization (up to 105–110 emu/g). Recently, GaSb-MnSb thin films composites have been fabricated with Curie temperature above 300 K [1]. There is a hope that charge carriers in GaSb matrix will be spin-polarized by Mn or MnSb entities and as a result a promising material for spintronics will be created.

The GaSb-MnSb samples were synthesized in two stages: obtaining a polycrystalline precursor by the vacuum-ampoule method from high-purity components and obtaining a melt-quenched polycrystalline samples. In this work we studied $(GaSb)_{100-x}(MnSb)_x$ polycrystals with x = 70, 50 and 30 mol.%. In the last two cases samples were doped with a small amount of Zn. As a reference we also studied properties of MnSb and Mn_2Sb polycrystals, obtained by direct fusion of elemental precursors.

MO investigations were carried out in transverse Kerr effect (TKE) geometry at T = 20–300 K in the spectral range 0.5–4.0 eV and magnetic field up to 2.5 kOe. We used p-polarized light, the incident angle being 66°. Two types of measurements were performed for each compound: field dependences of TKE signal at selected wavelengths and spectral dependences in fixed magnetic field.

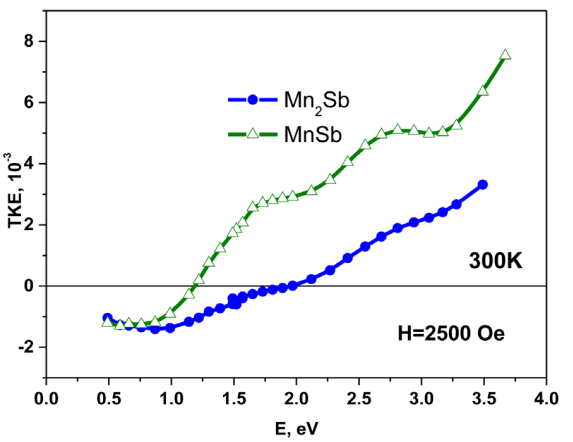

Figure 1. TKE spectra for MnSb and Mn_2Sb samples at room temperature.

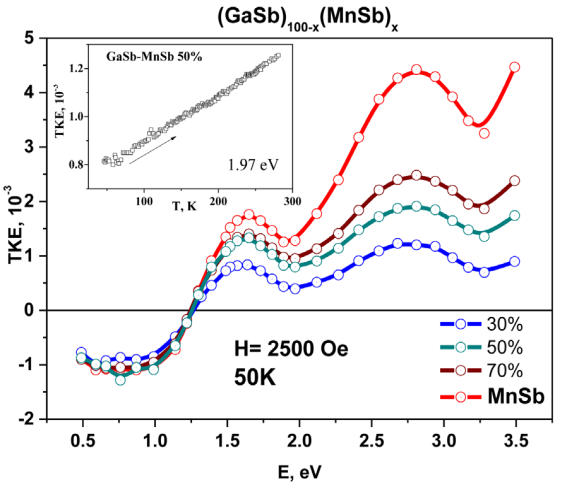

Figure 2. TKE spectra for the $(GaSb)_{100-x}(MnSb)_x$ composites at low temperature. The inset shows the temperature dependence of TKE intensity at 1.97 eV for the sample with x = 50 mol.%.

We used the dynamic MO method, in which the TKE parameter is the relative change of intensity of reflected light under magnetization in an applied alternating magnetic field with 40 Hz frequency.

Figure 1 shows MO spectra obtained for MnSb and Mn_2Sb alloys. These spectra are quite different. There are characteristic features for the MnSb sample in the vicinity of 2.0 and 3.0 eV, which are well pronounced at low temperatures and can be observed at 300 K, but these features are absent for the Mn_2Sb sample. Therefore, MO spectroscopy can be used for MnSb and Mn_2Sb phase identification in MnSb-based materials. We observed anomalous temperature dependence of MO spectra for the MnSb sample, namely, instead of decrease with increasing temperature (following the variation of magnetization), the intensity of TKE signal increases at specific wavelengths.

Figure 2 shows MO spectra for studied $(GaSb)_{100-x}(MnSb)_x$ composites. It is clearly seen that they exhibit all features characteristic for the MnSb compound and no new MO transitions can be observed. It means that the high-T_c ferromagnetism in these composites is associated with large in size entities of MnSb. Effects associated with the GaSb/MnSb interfaces or spin-polarized matrix were not detected.

Support by RSF (grant № 21-73-20220) is acknowledged.

1. L.N. Oveshnikov, E.I. Nekhaeva, A.V. Kochura et al., Beilstein J. Nanotechnology **9**, 2457 (2018).

E.O13

LOW TEMPERATURE OSCILATIONS OF MAGNETORESISTANCE IN ANTIMONY-DOPED SILICON

A.L Danilyuk[1], *A.G. Trafimenko*[1], *S.L. Prischepa*[1,2*]

[1]Belarussian State University of Informatics and Radioelectronics, Minsk, Belarus
[2]National Research Nuclear University MEPhI, Moscow, Russia
[*]E-mail: prischepa@bsuir.by

The relevance of studies of magnetotransport processes in silicon and silicon-based nanostructures is still very attractive. This is due to the development of silicon spintronic information processing devices using nonlinear and quantum effects. In this work, the processes of magnetotransport in silicon doped with antimony with a concentration of 10^{18} cm^{-3} and in the temperature range of 2.0–3.5 K are considered. The magnetic field is applied perpendicular to the direction of current flow. In this temperature range, as our previous studies have shown, the Si:Sb system exhibits nontrivial electron properties [1, 2], which are determined by neutral and negatively charged impurity atoms, i.e. the states in the lower and upper Hubbard bands. Nonlinear current-voltage characteristics (CVC), instability of the electron system, negative differential resistance (NDS) were observed [1]. Thus, Si:Sb has the characteristics of an electron correlated system [2].

The magnitude of the magnetoresistance, MR = $[R(H) - R(0)]/R(0)$, was determined from the CVC depending on the current density j in a magnetic field strength H up to 80 kOe. Here $R(H)$, $R(0)$ are the specific differential resistances of Si:Sb in the presence and absence of an external magnetic field, respectively. The performed elaboration of the CVC showed that the MR is characterized by oscillations, the amplitude of which increases with an increase in j and H, as well as with a decrease in temperature. The oscillations also have no periodicity but are random in nature.

Figure 1a shows the dependences of MR on the current density in the range of H = 60–80 kOe at T = 2 K. At a current density of up to 0.007 A/cm^2, MR fluctuations occur in the region of MR > 0, and with an increase in j, at j > 0.007 A/cm^2, fluctuations between positive and negative MR are observed. The amplitude of MR oscillations increases with increasing current density, its maximum spread is from –12 to +8.

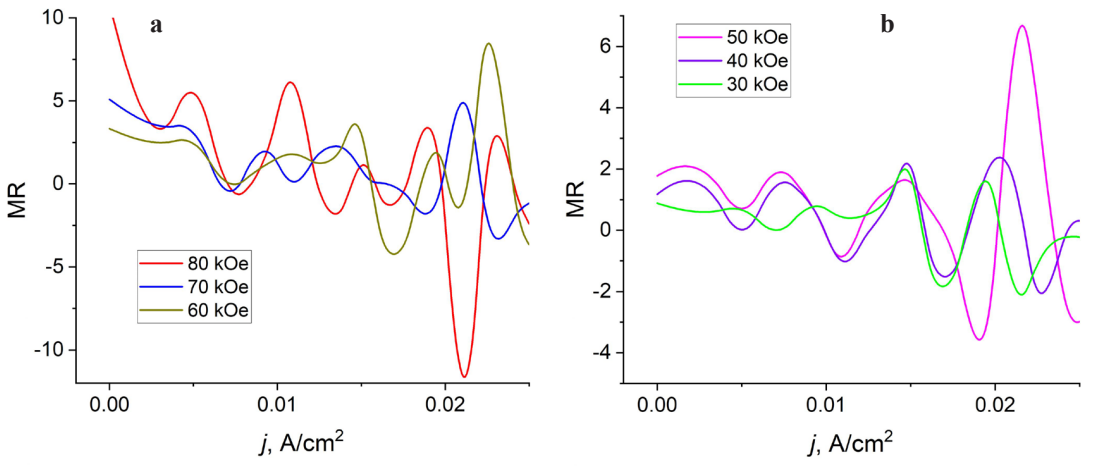

Figure 1. MR of Si:Sb as a function of j at T = 2 K: **a** H = 60–80 kOe, **b** H = 30–50 kOe.

The oscillations at different values of H are not synchronized in amplitude. With a decrease in the magnetic field strength, Fig.1b, the amplitude of the oscillations decreases slightly at $j < 0.015$ A/cm^2, but then increases and in the region of 0.02 A/cm^2, the maximum spread is from –4 to +7. With temperature increase up to 3.5 K, the amplitude of MR oscillations decreases on average. The maximum in the region of negative MR does not exceed 2, and in the region of positive MR it is no more than +8, Fig. 2.

We associate the obtained results mainly with the presence of instability of the electron system in Si:Sb at a given impurity concentration. At $T = 2$ K, the value of $R(0)$ also oscillates with an increase in j, remaining a positive value. However, the application of a magnetic field leads to the appearance of oscillations of $R(H)$ such that even at a current density of 0.007 A/cm^2, the amplitude of the MR oscillations becomes negative. This region of currents is not the region of NDR, but only adjacent to it. At $T = 3.5$ K, the picture does not change qualitatively. However, similar MR oscillations in this case are caused by smaller values of $R(H)$ and $R(0)$, and the amplitude of resistivity oscillations in a magnetic field becomes negative at a slightly higher current density (0.012 A/cm^2), which is also not yet the region of the NDR, but is adjacent to it.

Thus, we associate MR oscillations and the appearance of negative values of MR with the instability of the electron system, which is determined by the interaction of electrons localized on neutral Sb atoms (D^--states of the upper Hubbard band) with conduction electrons. The absence of any periodicity in the obtained dependences suggests that, with a change in j the concentrations of both conduction electrons and D^0- and D^--states of the Hubbard bands change. This leads to a change in the electron exchange rates between the conduction band and the Hubbard bands. At the same time, the filling of the Landau quantization levels also changes. Possible mechanisms may be associated with the transformation of one-dimensional Landau bands into sets of quasi two-dimensional layers due to the formation of charge density waves or a Wigner crystal. These mechanisms are only hypotheses and require further research.

1. A.L. Danilyuk, A.G. Trafimenko, A.K. Fedotov, I.A. Svito and S.L. Prischepa, Appl. Phys. Lett. **109**, 222104 (2016).
2. A.L. Danilyuk, S.L. Prischepa, A.G. Trafimenko, A.K. Fedotov, I.A. Svito and N.I. Kargin, J. Phys.: Condens. Matter **32**, 225702 (2020).

KINETIC AND MAGNETIC PROPERTIES OF HEUSLER ALLOYS IN THE STATES OF A HALF-METALLIC FERROMAGNET, SPIN GAPLESS SEMICONDUCTOR AND TOPOLOGICAL SEMIMETAL

V.V. Marchenkov[1,2*], *V.Yu. Irkhin*[1]

[1]M.N. Mikheev Institute of Metal Physics, UB RAS, Ekaterinburg, Russia
[2]Ural Federal University, Ekaterinburg, Russia
[*]E-mail: march@imp.uran.ru

A study of the electronic structure, kinetic and magnetic properties of various systems of Heusler alloys, which are in the states of a half-metallic ferromagnet, spin gapless semiconductor or topological semimetal, is presented [1–5]. These materials have unusual magnetic and electronic characteristics that are very sensitive to external influences, which is associated with the presence of energy gaps and exotic excitations in them. The features of the behavior and evolution of the electronic structure and properties in each of these states, as well as under transition between them, are considered. The ability to control purposefully the properties of such materials opens up prospects for their applications.

1. T. Graf et al., Prog. Solid State Chem. **39**, 1 (2011).
2. M.I. Katsnelson et al., Rev. Mod. Phys. **80**, 315 (2008).
3. X.L. Wang, Phys. Rev. Lett. **100**, 156404 (2008).
4. K. Manna et al., Nat. Rev. Mater. **3**(8), 244 (2018).
5. V.V. Marchenkov, V.Yu. Irkhin, Phys. Metal. Metallogr. **122**, 1133 (2021).

THE THEORY OF THE PRESSURE-INDUCED INVERSION OF MAGNETORESISTANCE IN $La_{1-x}Ag_xMnO_3$

Z.Z. Alisultanov[*], *A.G. Gamzatov, T.R. Arslanov*

Dagestan Federal Research Center of RAS, Institute of Physics, Makhachkala, Russia
[*]E-mail: zaur0102@gmail.com

In this paper, we present a theory of compression-induced sign reversal of the magnetoresistance of $La_{1-x}Ag_xMnO_3$ alloys.

It is known that the metallic spinless resistance caused by scattering by non-magnetic impurities increases when a magnetic field is applied. Those the magnetoresistive effect (MR) is positive in non-magnetic metals. Such magnetoresistance arises due to the action of the Lorentz force on the trajectory of electrons. On the other hand, the resistance caused by the spin-dependent scattering of carriers in a magnetic material is reduced by spin ordering. In this case, MR is negative.

Our measurements show that under comprehensive compression of $La_{1-x}Ag_xMnO_3$, the negative MR first increases, and then the growth of the negative MR changes to a decrease in this value, and at a certain pressure value, the sign of the MRE changes from negative to positive. We assumed that as the pressure increases, the Lorentz MR prevails over the spin one. On the other hand, an increase in the field at a given pressure leads to an increase in the spin part of the MR.

This result is qualitatively explained by the kinetic theory in the framework of the Born approximation and the theory of spin-dependent electron scattering.

Briefly, we offer the following qualitative explanation. As the pressure increases, the crystal lattice constant decreases, which leads to an increase in the hopping integral between atoms. This, in turn, leads to metallization due to the greater overlap of atomic orbitals. On the other hand, a decrease in the interatomic distance leads to an increase in the Fermi momentum, due to which the conductivity increases, since the Fermi speed increases. In addition, a decrease in the interatomic distance leads to a decrease in the density of states, which leads to an increase in the scattering time ($\tau \sim \rho^{-1}$), and, consequently, to an increase in the Lorentz MR. It should be noted that pressure can lead to an increase in the exchange integral and thereby change the spin MR.

In this report, we will present a detailed theory of this effect.

CORRELATION BETWEEN MAGNETORESISTANCE BEHAVIOR AND MAGNETIC STATES IN LAYERED COMPOUNDS Fe_xTiS_2

N.V. Baranov[1,2*], *N.V. Selezneva*[2], *E.M. Sherokalova*[2], *A. Podlesnyak*[3]

[1]M.N. Miheev Institute of Metal Physics, UB of RAS, Ekaterinburg, Russia
[2]Institute of Natural Sciences and Mathematics, Ural Federal University, Ekaterinburg, Russia
[3]Neutron Scattering Division, Oak Ridge National Laboratory, Oak Ridge, USA
[*]E-mail: baranov@imp.uran.ru

Transition metal (T) dichalcogenides TX_2 (X = chalcogen) with a layered crystal structure of the NiAs-type are known as starting compounds for a large family of objects with new interesting properties and potential for various applications. The intercalation of TX_2 with 3d transition metal atoms (M) having non-fully filled 3d electronic shells makes it possible to obtain structures with alternating layers of magnetic and nonmagnetic atoms [1, 2]. The magnetic properties of these intercalated compounds are controlled by combination of reduced dimensionality, ordering effects, magnetocrystalline anisotropy, and exchange interactions of different types. The M_xTX_2 compounds demonstrate a rich variety of magnetic states depending on the type and concentration of M atoms as well as on the type of a parent compound TX_2. Thus, spin-cluster glass state, antiferromagnetic (AFM) and ferrimagnetic FIM) orderings are suggested to exist in the Fe_xTiS_2 system at various Fe concentrations [3].

The present work aims to study how the change in the magnetic state of Fe_xTiS_2 with increasing Fe content affects the magnetoresistance behavior. Polycrystalline Fe_xTiS_2 samples (x = 0–0.75) were synthesized by the two-stage solid-phase reaction method. Structural characterization of the obtained samples was done using a Bruker D8 Advance x-ray diffractometer. Neutron powder diffraction (NPD) measurements were performed in magnetic fields up to 5 T by using WAND diffractometer installed at the High Flux Isotope Reactor at Oak Ridge National Laboratory (ORNL). The transversal magnetoresistance was measured by a four-contact ac method in magnetic fields up to 10 T.

It has been found that changes in the magnetic state of Fe_xTiS_2 with Fe concentration are accompanied by nonmonotonic dependencies of the magnetoresistance and coercivity with maximal absolute values in compounds with $x \sim 0.25$ and $x \sim 0.5$. The behavior of the magnetoresistance in compounds with a low Fe content ($x \leq 0.25$) is observed to be characteristic of magnetically inhomogeneous cluster glass or granular systems. The ordering of Fe atoms and formation of superstructure at $x = 0.25$ and $x = 0.5$ results in the appearance of an AFM order, as evidenced by NPD measurements. In these compounds, the field-induced phase transition from AFM to the metastable ferromagnetic (FM) state is accompanied by a sharp decrease in the electrical resistivity ($\Delta\rho/\rho \sim -35\%$). The irreversibility of the AFM to FM transition is associated with the contribution of magnetoelastic interactions [4]. The $Fe_{0.33}TiS_2$ compound exhibits the magnetization and magnetoresistance behaviors typical of cluster glass due to the formation of a triangular network of Fe atoms located between S-Ti-S tri-layers and frustrations of exchange interactions of different signs. Absence of a long-range magnetic order in $Fe_{0.33}TiS_2$ is confirmed by NPD measurements. The ferrimagnetic order in compounds with $x > 0.5$ is attributed Fe-Ti mixing in cationic layers. The enhanced coercivity observed in compounds with the AFM virgin state is ascribed to the intrinsic exchange bias together with the Ising-type spin state of Fe ions.

The present work was supported by the Russian Science Foundation (Grant No 22-13-00158).

1. A.B. Kaul, J. Mater. Res. **29**, 348 (2014).
2. N.V. Baranov, E.G. Gerasimov, N.V. Mushnikov, Phys. Metals. Metallogr. **112**, 711 (2011).
3. N.V. Selezneva, N.V. Baranov, N.V. Sherokalova et al., Phys. Rev. B **104**, 064411 (2021).
4. N.V. Baranov, N.V. Selezneva, E.M. Sherokalova et al., Phys. Rev. B **100**, 024430 (2019).

LOW TEMPERATURE BEHAVIOUR OF THE LATERAL PHOTOVOLTAIC EFFECT IN MULTILAYERED SILICON-BASED NANOSTRUCTURES

M.V. Rautskii[1], *L.V. Shanidze*[1], *A.V. Lukyanenko*[1], *A.S. Tarasov*[1], *I.A. Yakovlev*[1], *I.A. Bondarev*[1,2*]

[1]Kirensky Institute of Physics, Federal Research Center KSC SB RAS, Krasnoyarsk, Russia
[2]Krasnoyarsk Scientific Center, Federal Research Center KSC SB RAS, Krasnoyarsk, Russia
*E-mail: bia@iph.krasn.ru

Multilayered hybrid nanostructures which consist of different metallic, semiconducting and insulating layers had attracted considerable scientific attention due to their unique combination of electronic and magnetic properties. Various effects, such as giant magnetoresistance, spin injection and spin accumulation were discovered in hybrid structures [1, 2], and since then these materials had been applied in the creation of magnetic sensors and magnetoresistive random-access memory elements. The use of the silicon substrates as semiconducting layers allows easily integrating hybrid structures into the modern electronics which is already silicon-based.

Lateral photovoltaic effect (LPE) was firstly discovered by Schottky [3] and expanded upon by Wallmark in floating Ge p-n junctions [4]. It is widely applied in position sensitive detectors and solar batteries. Study of the LPE in multilayered hybrid nanostructures opens up an opportunity to expand the potential of the latter, giving the possibility to control magnetic and electronic transport inside the system via the optical irradiation.

Several hybrid structures were prepared for the present study. Silicon substrates were used as a basis for the samples. There were two types of substrates, p-Si and n-Si which were doped with boron and phosphorus respectively. On the top of some of the substrates, the 1.5-nm-thick SiO_2 layers were formed by exposing in aqueous solution of H_2O_2 and NH_4OH. Then the 10-nm-thick Fe film and the 15-nm-thick Mn film were deposited on the substrates with SiO_2 layers. Also, the 21-nm-thick Fe_3Si film was grown epitaxially on the substrate without oxide layer. As a result, Mn/SiO_2/n-Si, Fe/SiO_2/p-Si and Fe_3Si/p-Si structures were obtained. All films were deposited on the MBE setup "Angara" [5] via the method of thermal evaporation in ultrahigh vacuum. Further details on sample fabrication can be found in [6, 7].

Temperature dependences of the lateral photovoltage (LPV) under the irradiation wavelength of λ = 668 nm for all the samples are presented on Fig. 1, where signal was measured from the substrate backsides. The effect of magnetic field on the LPV is observed mostly below 30 K. The LPV(T) curve for Fe_3Si/p-Si (red one) have a single maximum which shifts slightly in a magnetic field. More peculiar dependences, however, appear for the Fe/SiO_2/p-Si and Mn/SiO_2/n-Si samples. For Mn/SiO_2/n-Si (black curve) there is a low-temperature peak, which is almost suppressed by a magnetic field of 800 mT. We already addressed this issue in [8], where we suggested that this peak occurs due to the surface states localized at the semiconductor/insulator interface. Large LPV at low T occurs when the Fermi level in n-Si start crossing the interface states, so the "hot" electrons are transferred from these states into the silicon conduction band. These electrons have a high drift velocity, so that they quickly leave the space charge region, which means that the probability of their recombination is lower than that of the regular electrons. As a result, the most part of the hot electrons reach the illuminated contact, and the LPV-value increases. Magnetic field effect on LPV in low temperature region is most likely due to the Lorentz force, which bends the trajectories of the hot electrons, decreasing the photovoltage. This interpretation also explains why such effect occurs only in the structure with the n-type substrate.

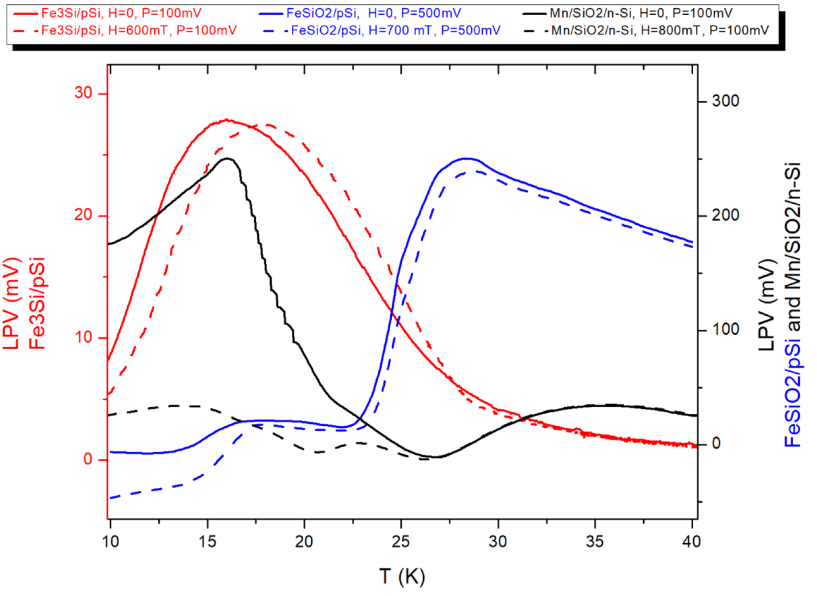

Figure 1. Temperature dependences of the LPV for three samples: $Fe_3Si/p/Si$ (red); $Fe/SiO_2/p$-Si (blue) and $Mn/SiO_2/n$-Si (black). The solid lines are the dependences in zero magnetic fields while the dashed lines are the dependences in external magnetic fields. Irradiation wavelength is λ = 668 nm. LPV was measured from the substrate backsides.

One more interesting feature is observed for the $Fe/SiO_2/p$-Si (blue curve). Above 20 K, the LPV(T)-behavior seems to be similar to that of $Mn/SiO_2/n$-Si. However, at $T > 20$ K the magnetic field causes the change of sign of the LPV, which is not observed in any other samples. The nature of this phenomenon remains unclear and requires further investigations.

Support by Krasnoyarsk Regional Fund of Science is acknowledged.

1. S.S.P. Parkin, Annu. Rev. Mater. Sci. **25.1** 357–388 (1995).
2. V.F. Motsnyi, J. De Boeck, J. Das, W. Van Roy, G. Borghs, E. Goovaerts and V.I. Safarov, Appl. Phys. Lett. **81.2** 265–267(2002).
3. W. Schottky, Phys. Z. **31**, 913–925 (1930).
4. J.T. Wallmark, Proc. IRE **45**, 474 (1957).
5. S.N. Varnakov, A.A. Lepeshev, S.G. Ovchinnikov, A.S. Parshin, M.M. Korshunov, P. Nevoral, Instrum. Exp. Tech. **47**, 839 (2004).
6. N.V. Volkov, A.S. Tarasov, M.V. Rautskii, A.V. Lukyanenko, I.A. Bondarev, S.N. Varnakov and S.G. Ovchinnikov, J. Magnet. Magnetic Mater. **451**, 143 (2018).
7. A.S. Tarasov, I.A. Bondarev, M.V. Rautskii, A.V. Lukyanenko, I.A. Tarasov, S.N. Varnakov and N.V. Volkov, J. Surf. Investigat. X-ray Synchr. Neutron Techniq. **12**(4) 633 (2018).
8. I.A. Bondarev, M.V. Rautskii, I.A. Yakovlev, M.N. Volochaev, A.V. Lukyanenko, A.S. Tarasov, and N.V. Volkov, Semiconductors. **53**(14), 1954–1958 (2019).

FLUCTUATION OF ELECTROMAGNETIC FIELD FROM GYROTROPIC HALF-SPACE

I.V. Bychkov[1*], *I.A. Kuznetsov*[1], *D.A. Kuzmin*[1], *V.G. Shavrov*[2]

[1]Chelyabinsk State University, Chelyabinsk, Russia
[2]Kotel'nikov institute of radio engineering and electronics of RAS, Moscow, Russia
[*]E-mail: bychkov@csu.ru

Electromagnetic fluctuations are an important research topic for both fundamental and applied physics. Electromagnetic fluctuations are responsible for such phenomena as van der Waals friction, the Casimir effect, vacuum heat exchange between bodies and other phenomena that occur near the surface of condensed media [1, 2].

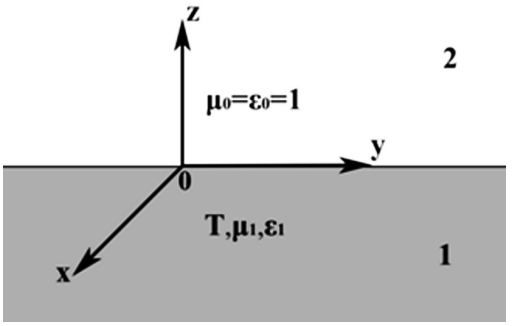

Figure 1. Geometry of the problem. 1 – half-space filled with gyrotropic medium, 2 – half-space filled with vacuum.

Dedkov and Kyasov in their work [3] obtained an expression for the spectral energy density of the fluctuation field emitted by an isotropic half-space into vacuum, which is the sum of the equilibrium radiation density constant throughout the vacuum half-space and the radiation density exponentially dependent on the distance from the emitting body. In this work, the problem of determining the spectral density of fluctuation radiation of a gyrotropic medium into a vacuum in the half-space-half-space geometry (Fig. 1) is considered. The interest of considering a gyrotropic medium is associated with the presence of a birefringence effect in such a medium, which affects the fluctuation field of this medium.

The gyrotropic medium is described by the following parameters: T is the temperature of the medium, μ_1 is the magnetic permeability,

$$\hat{\varepsilon}_1 = \begin{pmatrix} \varepsilon_1 & -ig_1 & 0 \\ ig_1 & \varepsilon_1 & 0 \\ 0 & 0 & \eta_1 \end{pmatrix}$$

is the permittivity tensor characterizing the gyrotropy of the medium.

For determine the spectral energy density of the fluctuation field, we used the fluctuation-dissipation theorem (FDT) as applied to the electromagnetic field. This method was described in detail in the work of Landau and Lifshitz [4].

We have obtained the following expression for the spectral energy density of the fluctuation electromagnetic field of the selected gyrotropic medium per unit volume of the vacuum space for ω > 0:

$$U(z,\omega)=\frac{1}{16\pi^3}\int_0^\infty\left[(E^2)_{\omega k}+(B^2)_{\omega k}\right]k\mathrm{d}k,$$

$$(E^2)_{\omega k}=-8\pi\hbar\,\mathrm{Coth}\left(\frac{\hbar\omega}{2k_\mathrm{B}T}\right)\mathrm{Im}\left(\frac{\mathrm{e}^{-2q_0z}(F_1k^4k_0{}^2\eta_1-F_2\chi)}{F_5q_0}\right)$$
$$-8\pi\hbar\,\mathrm{Coth}\left(\frac{\hbar\omega}{2k_\mathrm{B}T}\right)\mathrm{Im}\left(\frac{(q_0-k_0{}^2)(k^2k_0{}^2\eta_1(-F_3+(q_{1e}-q_{1o})\epsilon_1\mu_1(\eta_1\mu_1-1))+F_4\chi)}{F_5q_0}\right),$$

$$(B^2)_{\omega k}=-8\pi\hbar\,\mathrm{Coth}\left(\frac{\hbar\omega}{2k_\mathrm{B}T}\right)\mathrm{Im}\left(\frac{\mathrm{e}^{-2q_0z}(F_1k^4k_0{}^2\eta_1+F_2\chi)}{F_5q_0}\right)$$
$$-8\pi\hbar\,\mathrm{Coth}\left(\frac{\hbar\omega}{2k_\mathrm{B}T}\right)\mathrm{Im}\left(\frac{k_0{}^2(k^2k_0{}^2\eta_1(F_3+(q_{1e}-q_{1o})\epsilon_1\mu_1(1-\eta_1\mu_1))-F_4\chi)}{F_5q_0}\right),$$

$$F_1=n_e{}^2(-q_{1o}+q_{1e}\eta_1\mu_1)+n_o{}^2(q_{1e}-q_{1o}\eta_1\mu_1)-\big((q_{1e}-q_{1o})\eta_1\mu_1(1+\epsilon_1\mu_1)\big),$$
$$F_2=q_0{}^3(q_{1e}q_{1o}\eta_1-Q_1^2\mu_1),$$
$$F_3=n_e{}^2(q_{1o}+q_{1e}\eta_1\mu_1)-n_o{}^2(q_{1e}+q_{1o}\eta_1\mu_1),$$
$$F_4=q_0(q_{1e}q_{1o}\eta_1+Q_1^2\mu_1)-k_0{}^2(q_{1e}+q_{1o})\eta_1\mu_1,$$
$$F_5=k^4(q_{1e}-q_{1o})(\epsilon_1-\eta_1)(\eta_1\mu_1-1)+2q_0\chi(q_{1e}q_{1o}\eta_1\chi+Q_1^2\mu_1)$$
$$+(q_{1e}+q_{1o})(Q_1^2+q_0{}^2\eta_1\mu_1)\chi,$$

$$k=\sqrt{k_x^2+k_y^2},q_0=\sqrt{k^2-k_0{}^2},Q_1=\sqrt{k^2-k_0{}^2\eta_1\mu_1},q_{1e}=\sqrt{k^2-k_0{}^2n_e^2},q_{1o}=\sqrt{k^2-k_0{}^2n_o^2},$$

$$n_o{}^2=\frac{k^2(\eta_1-\epsilon_1)+2k_0{}^2\epsilon_1\eta_1\mu_1+\chi}{2k_0{}^2\eta_1},n_e{}^2=\frac{k^2(\eta_1-\epsilon_1)+2k_0{}^2\epsilon_1\eta_1\mu_1-\chi}{2k_0{}^2\eta_1},$$

$$\chi=\sqrt{k^4(\eta_1-\epsilon_1)^2-4g_1{}^2k^2k_0{}^2\eta_1\mu_1+4g_1{}^2k_0{}^4\eta_1{}^2\mu_1{}^2}.$$

It can be seen that resulting expression contains an exponential dependence on z, as well as combinations of the refractive indices of the ordinary and extraordinary waves. The result obtained can be used to determine the density of thermal radiation near a gyrotropic material.

Study were performed with support by RSCF, grant №20-19-00745.

1. G.V. Dedkov and A.A. Kyasov. Phys. Solid State **52**(2), 409, (2010).
2. E.A. Vinogradov and I.A. Dorofeyev. Physics-Uspekhi **52**(5), 425, (2009).
3. G.V. Dedkov, A.A. Kyasov. Pis'ma JTF **32**(5), (2006).
4. L.D. Landau and E. M. Lifshitz, Course of Theoretical Physics, Vol. 9: Statistical Physics (Fizmatlit, Moscow, 2002; Butterworth–Heinemann, Oxford, 2002), Part 2.

E.P5

FARADAY EFFECT AND MAGNETIC CIRCULAR DICHROISM OF ULTRATHIN IRON GARNET FILMS

A.S. Fedorov[1,2*], *S.S. Safonov*[1], *A.A. Fedorova*[1,2], *V.A. Kotov*[1], *S.A. Nikitov*[1,2], *A.I. Stognii*[3], *M.V. Logunov*[1]

[1]Kotel'nikov Institute of Radio-Engineering and Electronics of RAS, Moscow, Russia
[2]Moscow Institute of Physics and Technology, Dolgoprudny, Moscow Region, Russi
[3]Scientific and Practical Center for Materials Science of NAS, Minsk, Belarus
[*]E-mail: fedorov.andrei@phystech.edu

Magneto-optical effects are used in numerous application devices. Iron garnet films with the addition of bismuth have record values of the Faraday effect, which allows them to be used as one of the main materials for applied devices and used as a model medium for the study of ultrafast processes [1–4].

This report presents the results of studies of polycrystalline bismuth-containing iron garnet films of various thicknesses. The films were obtained by ion-beam sputtering on garnet and quartz substrates. This method, in contrast to the method of pulsed laser deposition, allows to obtain films of a large area – up to 100 cm^2. The spectral dependences of the Faraday effect and magnetic circular dichroism have been studied in a wide temperature range. It is shown that the film's parameters have a high repeatability of magneto-optical properties when the thickness of the films *h* varies from a few to hundreds of nanometers (Fig. 1 and 2). This report also presents the results of the implementation of film post-processing for the formation of magneto-optical mesostructures.

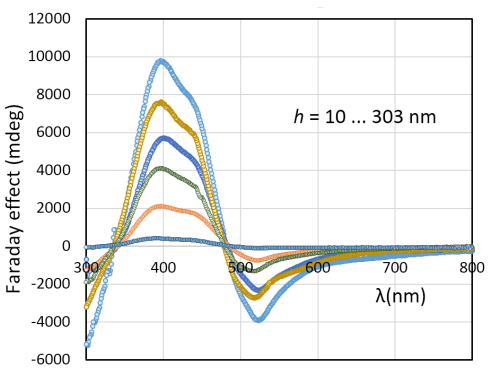

Figure 1. Faraday effect spectra for bismuth-containing iron garnet films.

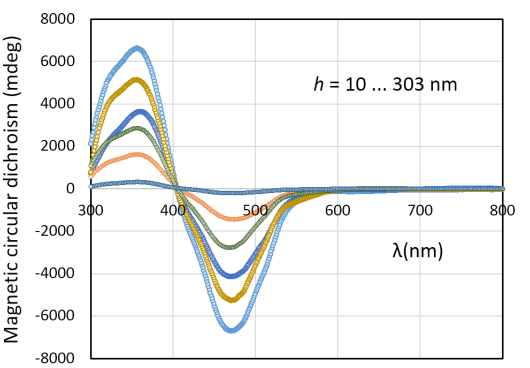

Figure 2. Magnetic circular dichroism spectra for bismuth-containing iron garnet films.

Support by RSF (#19-19-00607) and RFBR (#18-29-27020) is acknowledged.

1. A.K. Zvezdin and V.A. Kotov. Modern Magnetooptics and Magnetooptical Materials. IOP Publishing, Bristol, Philadelphia, (1997).
2. P. Němec, M. Fiebig, T. Kampfrath et al., Nature Physics **14**, 229–241 (2018).
3. R. Vidyasagar, O. Alves Santos, J. Holanda, et al., Appl. Phys. Lett. **109**, 122402 (2016).
4. M.V. Logunov, S.S. Safonov, A.S. Fedorov et al., Phys. Rev. Appl. **15**, 064024 (2021).

VECTORIZATION OF MAGNETO-OPTICAL IMAGES OF A IN-PLANE COMPONENT OF INHOMOGENEOUS MAGNETIC FIELDS

*V.E. Ivanov**, *A.N. Gorkovenko, V.N. Lepalovskij*

Ural Federal University, Ekaterinburg, Russia
*E-mail: vladimir.ivanov@urfu.ru

The paper [1] shows the possibility of topography of the in-plane component of the inhomogeneous field by fixing the coordinates of singular points of the inhomogeneous field of the magnet. In this paper, we present the results of transforming experimental magneto-optical images of an inhomogeneous magnet field into directional vector fields.

A rectangular NdFeB magnet with dimensions of 1×2×1 mm was chosen as the field source. Visualization of magneto-optical images was carried out using a Finmet-type indicator film with in-plane anisotropy. Magneto-optical images of the inhomogeneous field were obtained using the Evico Magnetics Kerr-magnetometer in overview mode. Vectorization of magneto-optical images was carried out according to the technique developed in [2] to determine the directions of magnetization in the domains of Fe films.

To execute the algorithm, it is necessary to obtain 2 magneto-optical images. One of them should reflect the intensity distribution corresponding to the coordinate dependence of the projection of the magnetization onto the light incidence plane in the longitudinal sensitivity (Fig. 1a), the other, in the transverse one (Fig. 1b). Both images should include areas reflecting the directions of magnetization parallel and perpendicular to the direction of magneto-optical sensitivity. The value of these intensities is used to calibrate the magnetization components of unit magnetization directions. In ideal magnetically soft films, the magnetization coincides in direction with the inhomogeneous field. If this assumption is correct, then one can obtain a picture of the distribution of the directions of the inhomogeneous field (Fig. 1c, d). The field direction maps obtained in this way agree with model calculations for our magnet.

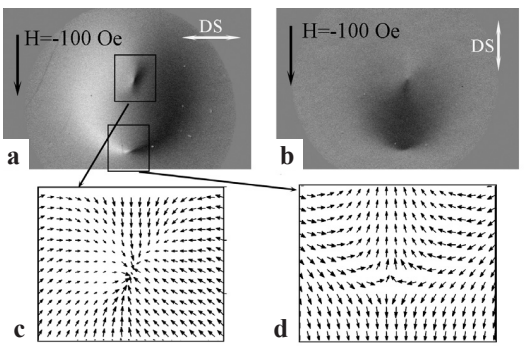

Figure 1. Magneto-optical images of the magnetic field of the magnet in the presence of a uniform constant magnetic field H = 100 Oe (**a**) in the longitudinal sensitivity, **b** in the transverse sensitivity and the corresponding vector plots of directions near the features of the magneto-optical images (**c**, **d**). DS – direction of magneto-optical sensitivity.

1. V.E. Ivanov, N.A. Kulesh, J. Magn. Magn. Mater. **513**, 167067, (2020).
2. T. von Hofe, N.O. Urs, B. Mozooni, T. Jansen, C. Kirchhof, D.E. Bürgler, E. Quandt, J. McCord, Appl. Phys. Lett. **103**, 142410 (2013).

MAGNETO-OPTICAL PROBING OF THE MAGNETIC AND PHASE STRUCTURES IN InFeAs LAYERS

E.A. Gan'shina[1], *Z.E. Kun'kova*[2*], *I.M. Pripechenkov*[1], *Yu.V. Markin*[2]

[1]Lomonosov Moscow State University, Moscow, Russia
[2]Kotel'nikov Institute of Radioengineering and Electronics, Fryazino Branch, Fryazino, Russia
[*]E-mail: z.kunkova@gmail.com

Recently, significant progress has been made in preparing diluted ferromagnetic semiconductors, DFS, (III,Fe)V (III = Ga, In; V = Sb, As). (III,Fe)V layers with the Fe content up to 35%, whose the Curie temperature (T_C) exceeds room one (T_{room}), have been obtained using low-temperature molecular beam epitaxy [1]. (In,Fe)As is unique in the (III,Fe)V family since both p- and n-type of conductivity have been realized in it. However in (In,Fe)As when doping is close to homogeneous, it is not possible to obtain $T_C > 70$ K. The method of ion implantation followed by pulsed laser melting (II+PLM) has been also used to fabricate (In,Fe)As layers. In the obtained II+PLM (In,Fe)As layers, an anisotropic Fe distribution in the semiconductor matrix and nonzero magnetization at T_{room} were detected [2]. It is known that in DFS, inclusions of secondary magnetic phases can appear during nonequilibrium growth conditions [3]. Highly sensitive SQUID-magnetometers are usually used when studying the DFS thin films, and the presence of the smallest amount of undesirable magnetic phases (iron, for example) can make a significant contribution to the magnetic signal leading to wrong conclusions. For this reason, control of the phase composition of such samples is critically important. We used magneto-optical spectroscopy to ascertain the phase composition and magnetic structure of II+PLM (In,Fe)As layers.

The samples under study were prepared by implantation of Fe ions (with the energy of 100 keV and fluence of $1\cdot10^{16}$ cm^{-2}) into InAs(001) wafers and followed laser melting at the different laser pulse energies, $W = 0.1$–0.4 J/cm^2 (the rise step $\Delta W = 0.05$ J/cm^2). The formed layers thickness is ≈90 nm. Information on the fabrication details and results of the previous studying of such samples is contained in [2]. The transversal Kerr effect (TKE) value $\delta = [I(H) - I(-H)]/2I(0)$, where $I(H)$ and $I(0)$ are the intensities of reflected light in the presence and absence of a magnetic field, respectively, was measured in the energy range of $E = 1.5$–3.5 eV at the applied magnetic fields up to 3500 Oe and temperatures of 20–300 K. TKE dependences on temperature, $\delta(T)$, and magnetic field, $\delta(H)$, were measured at several fixed energies. The measurements were carried out for two orientations of the magnetic field relatively the InAs crystallographic axes: $\mathbf{H}||[110]$ and $\mathbf{H}||[1\bar{1}0]$. To control the optical properties of the layers the spectra of the ellipsometry parameters, $\Psi(E)$ and $\Delta(E)$, were recorded in the range of $E = 1.24$–4.5 eV at T_{room}.

According to the ellipsometry data, the crystal structure of the parent InAs semiconductor is conserved in the samples under study. We have found that the laser pulse energy strongly influences the TKE spectrum shape, signal magnitude and TKE dependences on the temperature and magnetic field. The TKE spectra display the presence of an insignificant amount of Fe-rich inclusions in all samples, the TKE signal from these inclusions being negligible only for a sample prepared at the minimum pulse energy, $W = 0.1$ J/cm^2 (sample s0.1).

Figure 1a shows the TKE spectra of sample s0.1 at $T = 20$ K for two orientations of the magnetic field: 1 – $\mathbf{H}||[110]$, 2 – $\mathbf{H}||[1\bar{1}0]$. The energies of the E_1 and $E_1 + \Delta_1$ transitions near the L-critical point of InAs are denoted by dashed lines. The $\delta(T)$ and $\delta(H)/\delta_{max}$ dependences of sample s0.1 are displayed in insets (b) and (c), respectively. In the TKE spectra of sample s0.1, characteristic features in the region of the E_1 and $E_1 + \Delta_1$ transitions as well as the band in the intermediate range

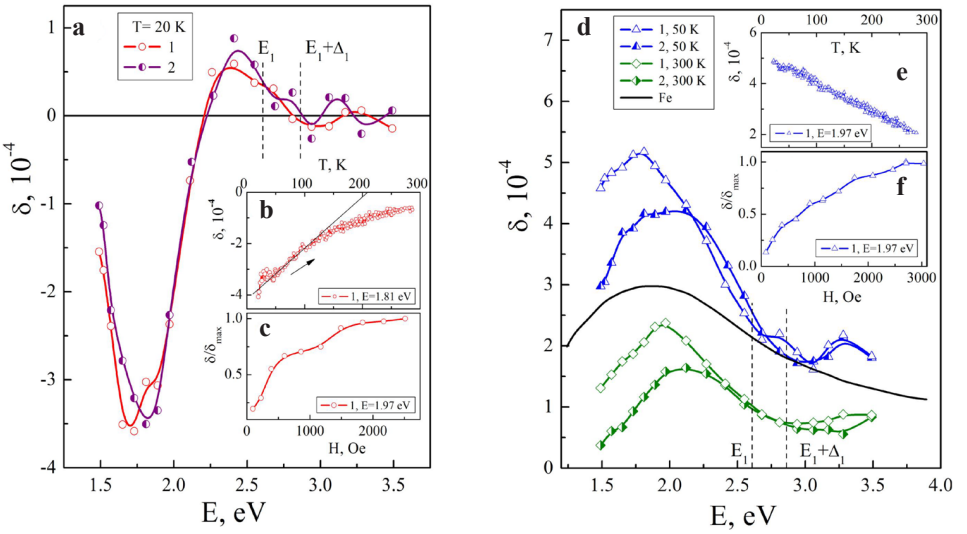

Figure 1. **a** The TKE spectra of sample s0.1 at T = 20 K for the orientations of the magnetic field 1 – **H**||[110] and 2 – **H**||[1$\bar{1}$0]. The dashed lines mark the energies of the E_1 and $E_1 + \Delta_1$ transitions in InAs. Insets: **b** $\delta(T)$ dependence of sample s0.1, H = 2500 Oe; **c** $\delta(H)/\delta_{max}$ dependence for sample s0.1 at T = 20 K. **d** The TKE spectra of sample s0.2 for the **H** orientations 1 and 2 at T = 50 and 300 K. The TKE spectrum of the reference Fe film (δ_{Fe}/30) is also shown, d_{Fe} = 100 nm. Insets: **e** $\delta(T)$ dependence of sample s0.2, H = 2500 Oe; **f** $\delta(H)/\delta_{max}$ dependence for sample s0.2 at T = 20 K.

($E \approx$ 1.5 – 2.2 eV) previously observed in the TKE spectra of DFS (In,Mn)As are present. The character of the TKE spectra as well as the TKE dependences on magnetic field and temperature show that sample s0.1 is magnetically inhomogeneous: there are local ferromagnetic (In,Fe)As regions ($T_C \approx$ 200 K) in the weakly doped paramagnetic host. Small values of the TKE signal indicate an insignificant amount of the FM (In,Fe)As phase. The magnetic field orientation weakly influences the signal values and TKE spectrum shape. At the same time a step in the $\delta(H)/\delta_{max}$ curve may be resulted of the shape anisotropy and/or orientation anisotropy of the FM (In,Fe)As inclusions.

The TKE spectra of sample s0.2 for two **H** orientations at T = 50 and 300 K together with the spectrum of the reference Fe film (δ_{Fe}/30) are shown in Fig. 1d. Insets (e) and (f) display the $\delta(T)$ and $\delta(H)/\delta_{max}$ dependences for sample s0.2, respectively. As seen from Fig. 1d, at low temperature there are also features in the region of the E_1 and $E_1 + \Delta_1$ transitions, but at the lower energies, the spectra of sample s0.2 are similar to the Fe film spectrum. At the same time, the $\delta(T)$ and $\delta(H)/\delta_{max}$ curves differ noticeably from the curves for bulk Fe. The $\delta(E)$, $\delta(T)$ and $\delta(H)/\delta_{max}$ dependences for samples prepared at W = 0.15 and 0.25–0.4 J/cm^2 are similar to those of sample s0.2. From the data analysis we can conclude that the TKE spectra of samples s0.15–s0.4 are the superposition of contributions from the (In,Fe)As and near surface Fe-rich nanoregions. The predominance of the Fe-like contribution in the spectra of samples s0.15–s0.4 indicates an enhancement of the Fe diffusion to the layer surface with increase in the pulse energy. The TKE anisotropy is apparently caused by the anisotropic spinodal decomposition earlier found in similar II+PLM (In,Fe)As samples.

The authors are grateful to Dr. S. Zhou and Dr. Ye Yuan for the DFS samples provided.

1. N.T. Tu, P.N. Hai, L.D. Anh et al., Appl. Phys. Express **12**, 103004-1–103004-5 (2019).
2. Ye Yuan, R. Hübner, M. Birowska et al., Phys. Rev. Materials **2**, 114601-1–114601-14 (2018).
3. L.M.C. Pereira, J. Phys. D: Appl. Phys. **50**, 393002 (2017).

LASER-PULSE-INDUCED NON-EQUILIBRIUM PHASE TRANSITIONS IN MAGNETITE Fe_3O_4

*A.V. Kuzikova**, *L.A. Shelukhin, R.V. Pisarev, A.M. Kalashnikova*

Ioffe Institute, St. Petersburg, Russia
*E-mail: anna.kuzikova@mail.ioffe.ru

Phase transitions in solids can be employed for realization of strong changes of electric, optical, magnetic, and other properties by using moderate external impact. With the development of femtosecond-pulse lasers, it was demonstrated that a medium can be switched from one phase state to another at picosecond timescales, and these observations naturally raised a question about mechanisms of ultrafast photo-induced transitions (PIPT) and their link to equilibrium ones [1]. The path by which the medium follows during PIPT is especially intriguing in materials, where several transitions can occur simultaneously. Examples of such transitions are those in FeRh and VO_2. Up to now, scientists have been actively arguing about the "chicken-or-egg" causality dilemma in FeRh whether structural transition causes a magnetic one, or vice versa [2, 3]. In VO_2, it is not yet completely clear whether the insulator-to-metal transition entails a change in the crystallographic structure or vice versa [4].

In this work we aim at studying ultrafast PIPT in a model ferrimagnet Fe_3O_4 in which the magnetic phase transition may have a coupling to electronic and structural ones. It is well-established that the magnetite possesses a first-order Verwey transition from a monoclinic insulating to a cubic metallic phase at a temperature of 123 K. Dynamics and mechanism of the laser-driven Verwey transition in Fe_3O_4 is the subject of many works [5, 6]. At temperature of 130 K, Fe_3O_3 possesses a spin-reorientation transition (SRT) when the sign of the magnetic cubic anisotropy parameter changes. The relationship between the Verwey transition and the SRT still remains open [5]. Our goal was to study how SRT is connected to the Verwey transition during ultrafast laser excitation.

To study PIPT, a sample prepared from a bulk single crystal of magnetite with the [110] orientation was chosen. The measurements were performed in the temperature range of 80–140 K and in an external magnetic field of 0.25 T applied along the easy magnetization axis of the sample in the low-temperature phase. This geometry is optimal for observing laser-induced spin-reorientation transitions. The magneto-optical femtosecond pump-probe setup was used. Laser pulses with a central wavelength of 1030 nm and a duration of 170 fs excite the material, and its transient optical and 515 nm probe laser pulses detect magneto-optical response. This approach enables revealing of both the SRT and Verwey transitions. As a result, the laser-induced magnetization precession and reflectivity changes were registered at different initial sample temperatures at a fixed pump fluence. Additionally, experiments were performed different pump fluences at a fixed initial temperature.

Based on the characteristic thresholds of the reflectivity change as a function of the pump fluence, it could be reliably concluded that a laser pulse induces the ultrafast Verwey transition only when its fluence exceeds certain threshold. At the same time, observation of laser-induced magnetization precession yielded counterintuitive result, showing that SRT is induced at fluences well below the threshold for a Verwey transition. However, by carefully examining evolution of the precision parameters with temperature and pump fluence, as well as of equilibrium magnetic hysteresis loops, we unambiguously show that this result does not indicate that the SRT and Verwey transitions are independent when induced by the laser pulses.

We further demonstrate that ultrafast spin-reorientation and Verwey transitions are clearly coupled. The magnetization precession at a low pump fluence is associated with the presence of domains of cubic metallic phase in the monoclinic insulating material, whose presence is elusive in the reflectivity measurements. However, above the threshold both the laser-induced reflectivity and magnetization precession follow the same trends with temperature and pump fluence.

The magnetite sample used in our study was prepared from a magnetite single crystal grown by A. M. Balbashov. Support of the Russian Foundation for Basic Research (grant No. 20-02-00938) is acknowledged.

1. S. Koshihara, et al., Physics Reports **942**, 1–61 (2022).
2. G. Ju, et al., Phys. Rev. Lett. **93**, 197403 (2004).
3. G. Li, et al., arXiv:2001.06799.
4. D. Wegkamp and J. Stähler, Prog. Surf. Sci. **90**, 464 (2015).
5. S. de Jong, et al., Nature Materials **12**, 882 (2013).
6. J.E. Lorenzo, et al., Phys. Rev. Lett. **101**, 226401 (2008).

E.P9

PERMALLOY-BASED TWO-DIMENSIONAL MAGNETOPLASMONIC CRYSTALS FOR MAGNETIC FIELD SENSING

D.V. Murzin[1*], *V.K. Belyaev*[1], *Ch. Gritsenko*[1], *V. Komanicky*[2], *V.V. Rodionova*[1]

[1]Immanuel Kant Baltic Federal University, Kaliningrad, Russia
[2]Pavol Jozef Šafárik University, Slovakia
[*]E-mail: dvmurzin@yandex.ru

One of the emerging topics in active plasmonics is the combination of plasmonic and ferromagnetic materials for excitation of magneto-optical surface plasmonic resonances [1]. Such resonances are the combination of surface plasmon polaritons and magneto-optical effects simultaneously exited on the metal/dielectric interface. Their excitation appears as a Fano-shaped resonant feature in the spectra of the magneto-optical response, depending on metal/dielectric structure's permittivity, permeability and polarizability. This feature is proposed to be used for localized and effective magnetic field [2, 3] or biomedical [4, 5] sensing with the use of structures, exhibiting magneto-optical surface plasmonic resonances. One of the ways to excite and control magneto-optical surface plasmonic resonances is the use of magnetoplasmonic crystals – photonic crystals made of noble and ferromagnetic materials. Demonstrated configurations of magnetoplasmonic crystals for magnetic field sensing, based on one-dimensional plasmonic structures, have sensitivity of about several nT [2, 3] and are sensitive to a single magnetic field direction, defined by the magnetoplasmonic crystal periodicity. Because of this drawback, the use of magnetoplasmonic crystal-based sensors for biomagnetic sensing or magnetic flux leakage detection is limited to a list of specified tasks. To overcome it, two-dimensional magnetoplasmonic crystals can be used for simultaneous excitation of magneto-optical surface plasmonic resonances in two orthogonal directions. Thus, this configuration opens a way to detect orthogonal components of the magnetic field.

Substrates for the fabrication of two-dimensional magnetoplasmonic crystals used in this work were made by the electron beam lithography to create two-dimensional diffraction gratings with the period d = 610±20 nm and height h = 80–90 nm. Atomic force microscopy image of a fabricated

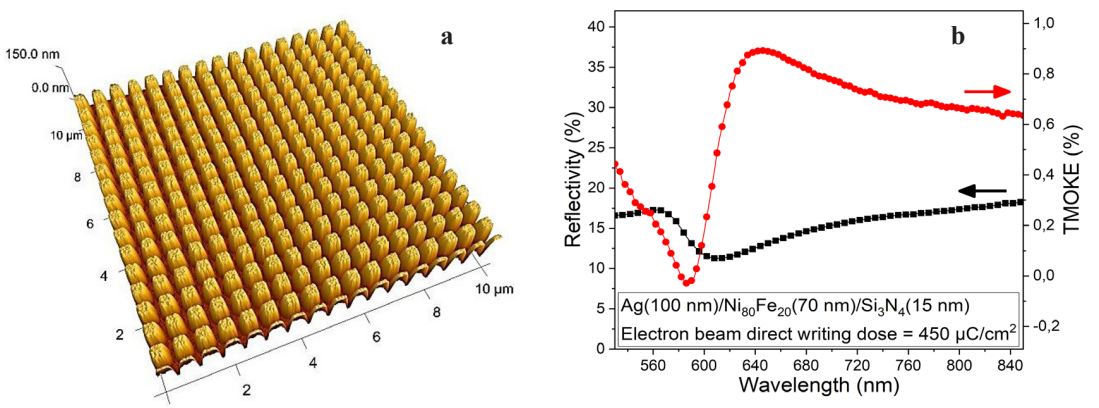

Figure 1. **a** Atomic force microscopy image of a fabricated diffraction grating. **b** Reflectivity (black) and transversal magneto-optical Kerr effect (red) spectra for the two-dimensional magnetoplasmonic crystal based on the substrate made with the electron beam direct writing dose of 450 µC/cm^2.

structure is shown in Fig. 1a. The electron beam direct writing was performed with the doses of 200, 250, 300, 350, 400, 450, 500, 550 and 600 μC/cm^2. Magnetoplasmonic crystals were made by the magnetron sputtering forming the Ag(100 nm)/$Ni_{80}Fe_{20}$(70 nm)/Si_3N_4(15 nm) multilayered structure on the top of fabricated substrates. Optical properties and magneto-optical response for fabricated permalloy-based magnetoplasmonic crystals were studied with the use of a lock-in detection method in the visible and near-infrared spectral regions. Figure 1b demonstrates spectral dependences of reflectivity and transversal magneto-optical Kerr effect for a sample with electron beam direct writing dose of 450 μC/cm^2.

In conclusion, this report demonstrates optical and magneto-optical properties' dependance of permalloy-based two-dimensional magnetoplasmonic crystals on the electron beam direct writing dose. The optimal dose for the studied set of magnetoplasmonic crystals was found to be 450 μC/cm^2. Possibility to detect enhanced magneto-optical Kerr effects in two orthogonal directions of light incidence opens a way to develop a magnetoplasmonic crystal-based magnetic field sensor sensitive simultaneously to several directions of a magnetic field.

The work was supported by the Russian Science Foundation, grant № 22-22-00997 and the Slovak Research and Development Agency under the contract No APVV-20-0324.

1. C. Rizal, IEEE Transactions on Magnetics **57**(2), 1–5 (2020).
2. V.K. Belyaev, V.V. Rodionova, A.A. Grunin, M. Inoue, A.A. Fedyanin, Scientific Reports **10**(1), 1–6 (2020).
3. G.A. Knyazev, P.O. Kapralov, N.A. Gusev, A.N. Kalish, P.M. Vetoshko, S.A. Dagesyan, V.I. Belotelov, ACS Photonics **5**(12), 4951–4959 (2018).
4. S. Chandra, J. Cozart, A. Biswas, S. Lee, D. Chanda, ACS Photonics **8**(5), 1316–1323 (2021).
5. A.A. Grunin, I.R. Mukha, A.V. Chetvertukhin, A.A. Fedyanin, J. Magn. Magn. Mat. **415**, 72–76 (2016).

E.P10

MAGNETORESISTANCE AND ANOMALOUS HALL EFFECT IN $(CoFeB)_x(LiNbO_3)_{100-x}$ NANOCOMPOSITES GROWN ON Si SUBSTRATE

S.N. Nikolaev[1*], *A.V. Emelyanov*[1], *K.Yu. Chernoglazov*[1], *E.A. Gan'shina*[2], *A.V. Sitnikov*[1,3], *V.A. Demin*[1], *A.B. Granovsky*[2], *V.V. Rylkov*[1,4]

[1]National Research Center "Kurchatov Institute", Moscow, Russia
[2]Lomonosov Moscow State University, Moscow, Russia
[3]Voronezh State Technical University, Voronezh, Russia
[4]Kotel'nikov Institute of Radio Engineering and Electronics RAS, Fryazino, Russia
[*]E-mail: niklser@list.ru

This paper presents the results of the magnetotransport properties study of $(CoFeB)_x(LiNbO_3)_{100-x}$ film nanocomposites (NCs) with x = 20–50 at.% fabricated by ion beam sputtering of composite targets on silicon substrate. Previously, we investigated similar NCs grown onto glass-ceramic substrates and observed the superferromagnetic ordering effects, presumably associated with the presence of dispersed magnetic ions (Fe^{2+}, Co^{2+}) [1]. In the case of more technologically advanced Si substrates, additional amplification of these effects can be expected, for example, due to a lower film growth temperature caused by the high thermal conductivity of Si. In addition, Si substrates are crystalline in contrast to amorphous glass-ceramic, which may lead to a different NC structure.

The transport and magnetic properties were studied using a magnetic system PPMS Dynacool-14 in the temperature range T = 4.2–200 K at magnetic field up to 14 T. For the NCs with a metal content of $x \approx$ 44–48 at.% the conductivity in a wide temperature range is described by the $\sigma \propto \ln T$ law, characteristic for a strong tunneling coupling between granules, probably, due to the presence of metal ions in the intergranular gaps [2]. For samples with x < 44%, the temperature dependence of σ obeys the 1/2 law, $\ln\sigma \propto -(T_0/T)^{1/2}$, which describes the hopping conductivity below the metal-insulator transition.

Negative magnetoresistance (NMR) is observed in the studied samples (Fig. 1). The value of NMR increases with a decrease of the metal content and reaches ~5%, at $x \approx$ 40 at.%. The observed

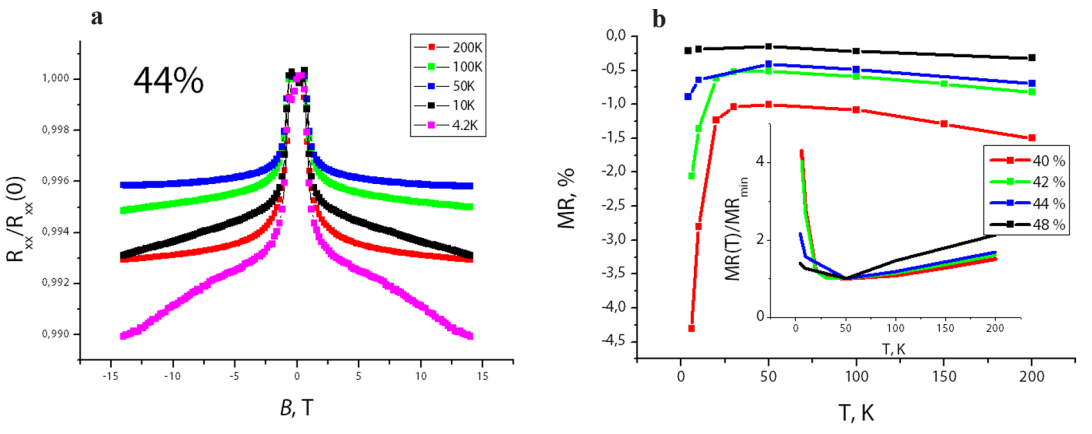

Figure 1. **a** Magnetoresistance of $(CoFeB)_x(LiNbO_3)_{100-x}$ structures with x = 44 at.% in the temperature range T = 4.2–200 K, and **b** temperature dependences of MR value for NCs with different metal content. The insert shows normalized temperature dependences of MR, i.e. $MR(T)/MR_{min}$.

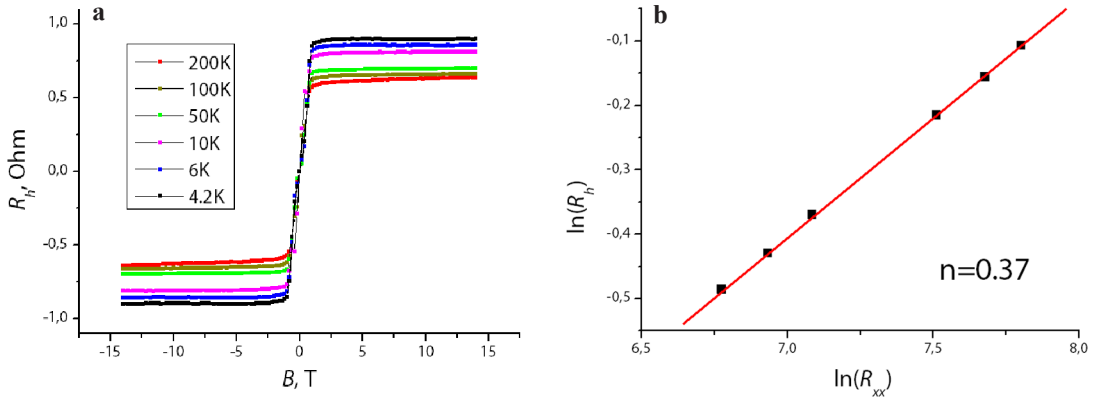

Figure 2. **a** Anomalous Hall effect resistance vs magnetic field in the temperature range T = 4.2–200 K. **b** Dependence of ln(R_h) on ln(R_{xx}) of the $(CoFeB)_x(LiNbO_3)_{100-x}$ structure with x = 48%.

NMR in granular films is usually explained by spin-dependent scattering and spin-dependent tunneling [3], which is stronger the lower the temperature. In our case, however, the NMR value does not change monotonically with temperature and has a minimum at 50 K (Fig. 1b).

Surprisingly, at $T > 50$ K, the NMR value increases. We believe that dipole-dipole interactions and exchange interactions between superparamagnetic particles gradually decrease as the temperature rises that makes the magnetic system more disordered with enhanced NMR.

In the range of compositions x = 40–48 at.%, positive magnetoresistance is also observed in relatively small fields. The observed two peaks in the field dependence of resistance at low temperatures (Fig. 1a) combine into one at temperatures above 100 K. In [3], such a behavior of the positive magnetoresistance was explained by the formation of a superferromagnetic regions with the ordering of the magnetic moments of the granules by exchange interaction. Thus, the movement of the domain walls under the influence of a magnetic field can lead to the occurrence of hysteresis in MR, which disappears during the transition of the system from a superferromagnetic state to a superparamagnetic one.

The studied samples demonstrate the anomalous Hall effect (AHE) whose magnitude increases with decreasing temperature (Fig. 2). One of the most interesting lines in the AHE research in magnetic systems is the study of a relation between the anomalous component of the Hall resistivity $\rho_{AHE} = 4\pi R_s M$ and longitudinal resistivity $\rho_{xx} = \rho$, i.e., the so-called scaling behavior $\rho_{AHE} \propto \rho^n$, where n is the power-law index determined by the definite mechanism of the AHE [4].

For all the studied structures, the law of $\rho_{AHE} \propto \rho^n$ is observed, with values of n from 0.37 to 0.45. These values are close to $n \approx 0.4$, typical for high-resistive (so called "dirty") magnetic metallic materials [4]. A similar dependence was observed by us earlier in nanogranular CoFeB-Al-O films [5].

This work was financially supported by Russian Science Foundation, grant No. 22-19-00171. Measurements were carried out on the equipment of the Resource centers under support of the NRC "Kurchatov Institute".

1. V.V. Rylkov, A.V. Sitnikov, S.N. Nikolaev et al., J. Magn. Magn. Mater. **459**, 197 (2018).
2. V.V. Rylkov, A.V. Emelyanov, S.N. Nikolaev et al., JETP **131**, 160 (2020).
3. A. Glatz, I.S. Beloborodov and V.M. Vinokur, EPL **82**, 47002 (2008).
4. N. Nagaosa, J. Sinova, S. Onoda, A.H. MacDonald, and N.P. Ong, Rev. Mod. Phys. **82**, 1539 (2010).
5. V.V. Rylkov, S.N. Nikolaev, K.Yu. Chernoglazov et al., Phys. Rev. B **95**, 144202 (2017).

GALVANOMAGNETIC AND OPTICAL PROPERTIES OF MOLYBDENUM AND TUNGSTEN DITELLURIDES

A.N. Perevalova[1*], *S.V. Naumov*[1], *E.I. Shreder*[1], *V.V. Chistyakov*[1], *E.B. Marchenkova*[1], *S.M. Podgornykh*[1], *J.C.A. Huang*[2], *V.V. Marchenkov*[1,3]

[1]M.N. Mikheev Institute of Metal Physics, UB RAS, Ekaterinburg, Russia
[2]National Cheng Kung University, Tainan, Taiwan
[3]Ural Federal University, Ekaterinburg, Russia
[*]E-mail: domozhirova@imp.uran.ru

In recent years, the search and study of topological materials have become an important area of condensed matter physics and materials science. In addition, topological semimetals, including Weyl semimetals, attract special attention of researchers. In Weyl semimetals, the valence and conduction bands cross each other at discrete points near E_F, i.e., Weyl nodes, and disperse linearly in all three momentum space directions. The corresponding low-energy excitations are condensed-matter analogues of Weyl fermions in relativistic high-energy physics. The nontrivial topology of the band structure of such materials leads to unusual transport and optical responses, which are currently being intensively studied. This work presents the results of studying the features of the galvanomagnetic and optical properties of Weyl semimetal $MoTe_2$ and WTe_2 single crystals.

$MoTe_2$ and WTe_2 single crystals were grown by the chemical vapor transport technique using bromine as a transport agent according technique described in [1]. Since the $MoTe_2$ single crystal can crystallize in three different structures [2], to obtain the semimetallic phase, the single crystal was quenched from 910 °C. The chemical composition and surface microstructure were investigated using a FEI Quanta 200 scanning electron microscope equipped with an EDAX attachment. Electronic transport properties were measured by the four-contact technique in the temperature range from 2 to 300 K in magnetic fields of up to 9 T using a PPMS-9 system (Quantum Design). The measurements were carried out when an electric current flowed in the (00*l*) plane of the sample, and a magnetic field was directed perpendicular to it. The optical properties were measured by the polarimetric Beattie method with a reflection from the (00*l*) plane of the samples in the spectral range of 0.2–5.0 eV at room temperature in air.

The behavior of the resistivity in a magnetic field and the Hall resistivity of $MoTe_2$ and WTe_2 was analyzed using a two-band model. This made it possible to estimate the densities of electrons n_e and holes n_h and their mobility. The transition from high effective magnetic fields to weak ones, which is observed in compensated conductors with a closed Fermi surface, was proposed as a possible explanation for the minimum on the temperature dependence of resistivity of WTe_2 in magnetic field. The mean free path l of current carriers was estimated based on data on electronic transport. Optical studies, the dispersions of the optical conductivity, reflectivity, real and imaginary parts of the complex permittivity, did not reveal features characteristic of metals.

The research was carried out within the state assignment of Ministry of Science and Higher Education of the Russian Federation (themes "Spin", No. 122021000036-3 and "Electron", No. 122021000039-4), supported in part by RFBR (Project No. 20-32-90069) and Scholarship of the President of the Russian Federation for young scientists and graduate students (SP-2705.2022.1).

1. A.N. Domozhirova, S.V. Naumov, S.M. Podgornykh, E.B. Marchenkova, V.V. Chistyakov, A.A. Semiannikova, J.C.A. Huang, and V.V. Marchenkov, J. Phys.: Conf. Ser. **1851**, 012023 (2021).
2. Y.Y. Lv et al., Sci. Rep. **7**, 44587 (2017).

E.P12

ULTRAFAST LASER-INDUCED MAGNETIZATION PRECESSION IN THIN FILM AND ANTIFERROMAGNETIC BILAYER OF $L1_0$-PdFe

A.V. Petrov[1*], *M.V. Pasynkov*[1], *A.A. Busse*[1], *R.V. Yusupov*[1], *S.I. Nikitin*[1], *A.I. Gumarov*[1], *I.V. Yanilkin*[1], *A.G. Kiiamov*[1], *L.R. Tagirov*[1,2]

[1]Kazan Federal University, Kazan, Russian Federation
[2]Zavoisky Physical-Technical Institute, Kazan, Russian Federation
[*]E-mail: flypetrov@yandex.ru

Magnetic materials based on thin-film structures with perpendicular magnetic anisotropy (PMA) are promising for high-capacity non-volatile magnetic memory. In trilayer F/N/F systems (F – ferromagnet, N – normal metal), by varying the thickness of the intermediate N-layer one can obtain structures with both ferromagnetic and antiferromagnetic couplings between the F-layers. Here, we report on a synthesis, static and dynamic magnetic properties of the F/N/F-type structure with antiferromagnetic coupling and high PMA, which can be used in data storage media with the information recorded by ultrafast laser pulses [1].

A trilayer structure of $L1_0$-PdFe/W/PdFe with layer thicknesses of 12/0.7/12 nm, respectively, was synthesized on a single crystal MgO (001) substrate. Thin continuous layers of the ordered $L1_0$-phase of PdFe compound were deposited by co-evaporation of Fe and Pd from high-temperature effusion cells in ultrahigh vacuum setup. For the tungsten layer deposition, the electron beam evaporation process was used. Each PdFe layer was deposited with the substrate temperature of 150 °C and annealed after deposition at 650 °C for 1 hour. The tungsten interlayer was grown with a substrate temperature of 300 °C. Epitaxial growth of the PdFe layers on both the chromium underlayer and tungsten interlayer with the tetragonal *c*-axis perpendicular to the film plane was verified by X-ray diffractometry.

Magnetization reversal curves (hysteresis loops) were measured at room temperature with a vibrating sample magnetometry (with the magnetic field applied both out-of-plane and in the plane of the structure) and with the magneto-optical Kerr effect (MOKE) setup in polar geometry (Fig. 1). A butterfly-like shape of the hysteresis loop in the out-of-plane geometry clearly indicates the PMA

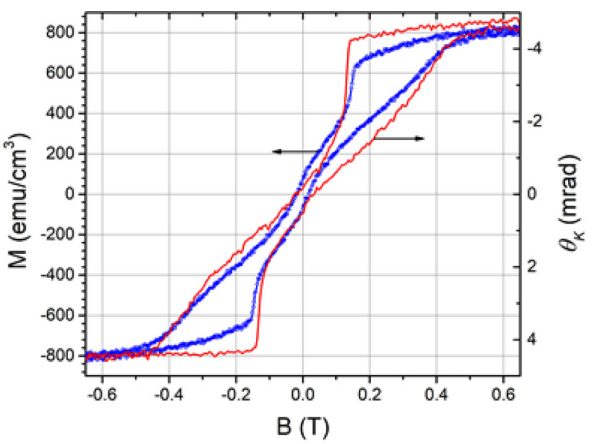

Figure 1. Magnetization hysteresis loop of the $L1_0$-structure-based PdFe/W/PdFe heteroepitaxial trilyer structure.

of the film and the AFM coupling between the PdFe layers that can be overcome by the applied magnetic field. Comparison of the $M(H)$ loops for a single-layer $L1_0$-PdFe and trilayer FePd/W/FePd structure measured with the field lying in the sample plane allowed to estimate the principal magnetic parameters of the sample: magnetocrystalline anisotropy constants K_{u1}, K_{u2}, saturation magnetization M_s and the interlayer exchange interaction integral J.

Further, magnetization precession in the $L1_0$-PdFe film and PdFe/W/PdFe artificial antiferromagnet induced by the femtosecond laser pulses was studied with time-resolved MOKE spectroscopy. It was found that the precession frequency is different for the $L1_0$-PdFe film and studied F/N/F structure. The dependence of the frequency on the applied magnetic field for both samples was studied.

Mathematical modeling of the magnetization precession within the Landau-Lifshitz-Gilbert approach was performed. As it was expected for a system of coupled FM-layers, two precessional modes coexist in the investigated three-layer structure, the oscillations of the magnetization of the FM-layers occurring either in-phase or out-of-phase. The experimental dependence of the precession frequency on the magnitude of the applied magnetic field has been successfully described. The results show that the experimentally observed Kerr angle oscillations correspond to the antiphase low-frequency mode.

The possibility of creating an artificial ferrimagnet with PMA based on L10-FePd, a prototype medium for an optically driven magnetic storage of ultrahigh density and speed, has been demonstrated.

Support by the Priority-2030 program via Kazan Federal University is acknowledged.

1. A.V. Petrov et al., Magn. Reson. Solids **21**, 19503 (2019).

MAGNETOTRANSPORT PROPERTIES OF Ni_2MnGa SINGLE CRYSTAL

*I.G. Reznikov**, *V.N. Prudnikov, M.V. Prudnikova, A.B. Granovsky*

Faculty of Physics, Lomonosov Moscow State University, Moscow, Russia
*E-mail: reznikov.jg15@physics.msu.ru

We present results of magnetic properties, resistivity, magnetoresistance and Hall effect of $Ni_{50.4}Mn_{25.9}Ga_{23.7}$ [001] single crystal.

The samples were grown in Lappeenranta University of Technology by a directional solidification using [001] oriented seed crystal. To make the ingot chemically homogenous, a heat treatment at 1300 K during four days was used. Slow cooling of the ingots from 1300 K to ambient temperature with the rate of 50 K/h was applied to guarantee complete atomic ordering of the Heusler type structure and to avoid appearance of cracks. The sample's composition was determined with 0.15 at.% precision using an X-ray fluorescence technique. The crystal structure is cubic with Heusler ordering down to 258 K. The lattice parameter decreases with decreasing temperature and matches well literature data, a = 0.583 nm, measured at room temperature. At temperatures below 253 K, the [400] peak for cubic structure is spited on four peaks, indicating structure phase transformation. Two new peaks correspond to lattice parameters for 10M martensite with shot c-axis, and $a = b > c$. Two more peaks, with corresponding lattice parameters that differ slightly from the cubic lattice parameter, are likely high intensity satellite peaks or adaptive unknown phases that exist only near phase transition, because they disappear with decreasing temperature. Magnetic measurements were carried out using Lake Shore VSM. Magnetotrasport measurments were performed by the four-probe method in magnetic field up to 20 kOe.

Figure 1 shows the temperature dependence of magnetization measured at zero-field cooling (ZFC), field-cooling (FC) and field-warming (FW) regimes. One can see that the Curie temperature T_C is about ≈380 K and martensitic transition (MT) starts at about T_M ≈ 260 K that is in a good agreement with literature [1] and structural data. Figure 2 shows the temperature dependence of

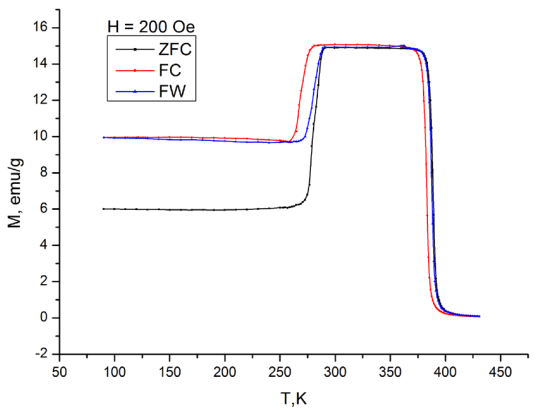

Figure 1. Temperature dependence of magnetization: zero-field cooled (black), field warmed (blue), field cooled (red) on the 200 Oe.

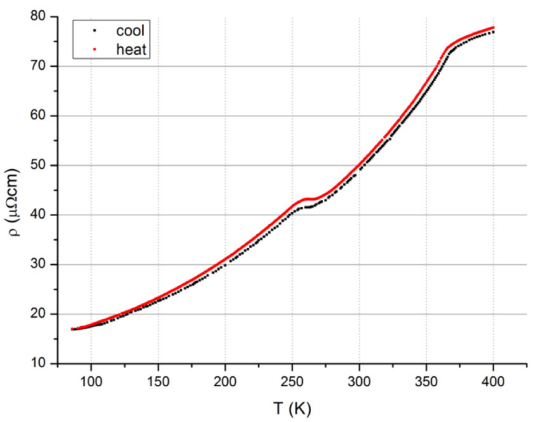

Figure 2. Temperature dependence of resistivity.

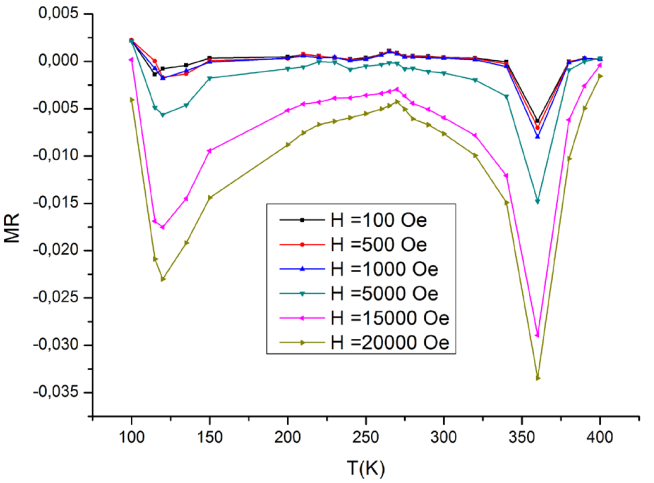

Figure 3. Temperature dependence of magnetoresistance at different fields.

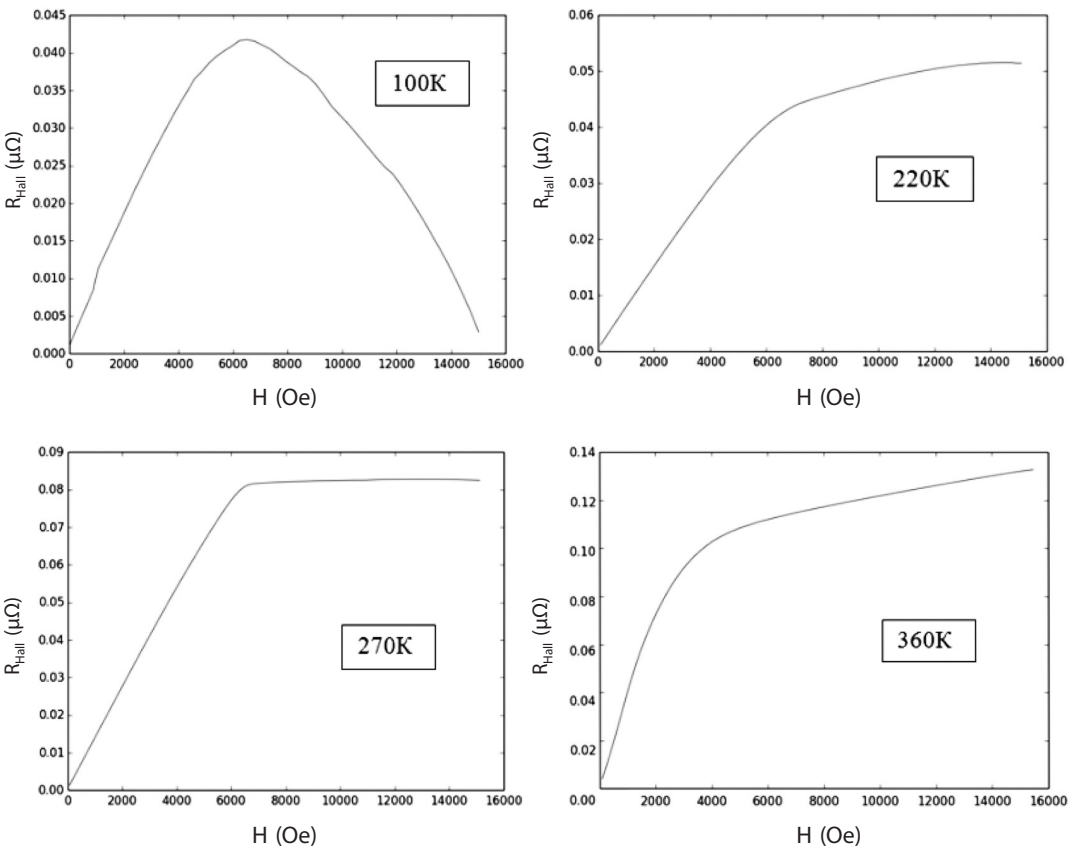

Figure 4. Field dependence of Hall resistivity at different temperatures.

resistivity that also confirms the obtained values by change of slopes at T_C and hysteresis during MT. It is worth mentioning that resistivity decreases at MT and is rather small by contrast to resistivity behavior of Ni-Mn-In Heusler alloys [2].

Figure 3 shows magnetoresistance measured at different fields. The negative peak around 260 K corresponds to second order phase transition, namely it is due to suppression of spin-disorder around T_C by strong magnetic field. Magnetoresistance around MT is also negative, at least about 500 Oe, that is typical for Heusler alloys, but by contrast to NiMnIn alloys is very small and exists in a large temperature range. Probably, it is a consequence of several phases around MT and small difference of resistivity in martensitic and austenitic states (Fig. 2). Surprisingly, there is a large negative peak of MR around 125 K in spite of there is no any noticeable changes in magnetization or in resistivity at this temperature. We think that this feature is due to intermartensitic transition.

Figure 4 shows the typical field dependences of Hall resistivity. Hall effect was measured for samples with magnetic field oriented perpendicular to [100] direction. There is clear evidence of ordinary Hall effect and anomalous Hall effect for all temperatures. In austenite above MT the slope of Hall resistivity curves in high field is positive that means that the ordinary Hall effect coefficient is negative while below MT the slope is negative that indicates on change of type of main current carriers. It is typical for all Heusler-type shape memory alloys [3–5] around MT and confirms that MT is accompanied with electronic structure transformation. Anomalous Hall effect coefficient does not change its sign at MT. It means that ordinary Hall effect and anomalous Hall effect are due to different groups of current carriers.

The authors are grateful to O. Sozinov and M. Vinogradova (Lappeenranta University of Technology, Finland) for sample fabrication and structural investigations. A.G. acknowledges support from the Russian Ministry of Science and Education grant No. 075-15-2021-1353 and the Academy of Finland (grant No.333805). The work was supported in part by M.V. Lomonosov Moscow State University Program of Development.

1. A.N. Vasiliev, V.D. Buchel'nikov, T. Takagi, et al., UFN **173**, 577 (2003).
2. I. Dubenko. N. Ali, S. Stadler, et al., in Novel Functional Magnetic Materials, Springer Series in Materials Science, Ed. A. Zhukov, 2016, pp. 41–82.
3. M. Blinov, A. Aryal, S. Pandey et al., Phys. Rev. B **101**, 094423 (2020).
4. S. Pandey, M. Blinov, A. Aryal et al., J. Magn. Magn. Mater. **481**, 25 (2019).
5. M.I. Blinov, V. Chernenko, V.N. Prudnikov et al., Phys. Rev. B **102**, 064413 (2020).

Co NANOPARTICLES LOCALIZED IN MATRICES OF VARIOUS TYPES: MAGNETOOPTICAL AND MAGNETOTRANSPORT PROPERTIES

Yu.E. Samoshkina[1*], *D.A. Petrov*[1], *M.V. Rautskii*[1], *D.S. Neznakhin*[2], *E.A. Stepanova*[2], *A.L. Stepanov*[3]

[1]Kirensky Institute of Physics, Federal Research Center KSC SB RAS, Krasnoyarsk, Russia
[2]Institute of Natural Sciences and Mathematics, Ural Federal University, Ekaterinburg, Russia
[3]Department of Nanooptics and Nanoplasmonics, FRC Kazan Scientific Center, Zavoisky Physical-Technical Institute, Russian Academy of Sciences, Kazan, Russia
[*]E-mail: uliag@iph.krasn.ru

The study of ensembles of transition metal nanoparticles in dielectric or semiconductor matrices is a promising task for the development of high-speed optical and magnetic recording devices [1–3]. Magneto-optical (MO) properties of such materials are of particular interest in this direction [4]. The MO effects such as Kerr and Faraday rotation for Co-NPs in different dielectric matrices have been investigated previously [5–7]. A significant difference in the spectral dependences of these effects compared with a solid Co film was founded. In addition, the MO spectra depended on the size and concentration of Co-NPs. This behavior was associated with conduction electrons inside particles and was explained by size effects.

The present work is devoted to the study of Co-NPs using magnetic circular dichroism (MCD) spectroscopy in the visible and near-infrared range of light. This MO effect is more informative, since it is observed directly at the electron transition frequency and allows you to exclude the contribution from the non-magnetic substrate. Two types of matrices are considered for Co-NPs, namely dielectric SiO_2 and semiconductor ZnO. The study of hydrogenated (20–50% H_2) Co-doped ZnO films [8] showed that due to the chemical reaction of H_2 with ZnO, metallic cobalt is formed in the samples as a secondary phase. It should be noted that at the highest hydrogen concentrations (40–50% H_2), the internal magnetism in the films increased and overlapped the contribution of the secondary phase. Thus, in this work we consider the Co-doped ZnO films with a lower hydrogen concentration (20–30% H_2).

Co^+ ions have been implanted in SiO_2 plates with an energy of 40 keV and dose (D) in the range of $(0.5–1.25)\cdot10^{17}$ ions/cm^2. Co-doped ZnO films have been synthesized by the radio frequency magnetron sputtering in a mixed atmosphere of Ar + 20–30% H_2. Field and temperature dependences of the samples magnetization indicate the typical behavior of an ensemble of superparamagnetic particles with a blocking temperature near and below room temperature. A significant difference in the shape of the magnetic circular dichroism (MCD) spectrum for Co-NPs compared to solid Co film and Co^{2+} ions in the ZnO lattice has been revealed. The MCD spectrum shape for Co-NPs does not depend on the matrix type

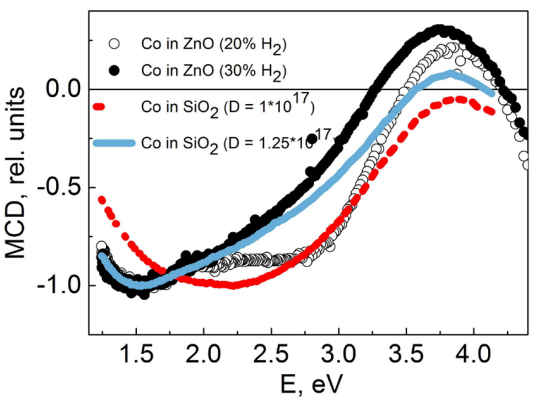

Figure 1. MCD spectra at room temperature and H = 12 kOe for the Co-doped ZnO films and Co-NPs in SiO_2.

in which they are dispersed (Fig. 1). Magneto-optical activity of Co-NPs in different matrices has been estimated at room temperature in the visible and near-infrared range of light as an indicator for practical applications. The presence of a MCD maximum near 3.8 eV indicates an improvement in the magnetotransport properties of these materials. This assumption has been tested.

This research was funded by the Russian Science Foundation grant No. 21-72-00061.

1. A. Tamion, C. Raufast, M. Hillenkamp, et al., Phys. Rev. B **81**, 144403 (2010).
2. J. Leveneur, J. Kennedy, G.V.M. Williams, et al., Appl. Phys. Lett. **98**, 053111 (2011).
3. M. Anand, J. Carrey, V. Banerjee, J. Mag. Mag. Mater. **454**, 23 (2018).
4. A.K. Zvezdin and V.A. Kotov, Modern Magneto-Optics and Magneto-Optical Materials, 1st edn. Taylor & Francis Group, New York, pp. 1–109, (1997).
5. C. Clavero, B. Sepúlveda, G. Armelles, et al., J. Appl. Phys. **100**, 074320 (2006).
6. I.S. Edelman, O.V. Vorotynova, V.A. Seredkin, et al., Phys. Solid State **50**, 2088 (2008).
7. Sh. Ozaki, H. Kura, H. Maki, et al., J. Appl. Phys. **105**, 113913 (2009).
8. I.S. Edelman, H. Chou, Yu.E. Samoshkina, et al., J. Mag. Mag. Mater. **489**, 165461 (2019).

ELECTRONIC STRUCTURE AND OPTICAL PROPERTIES OF Mn-BASED HEUSLER ALLOYS

E.I. Shreder[1*], *A.A. Semiannikova*[1], *E.D. Chernov*[1,2], *A.V. Lukoyanov*[1,2], *V.V. Marchenkov*[1,2]

[1]Institute of Metal Physics, Ural Division RAS, Ekaterinburg, Russia
[2]Ural Federal University, Ekaterinburg, Russia
[*]E-mail: shreder@imp.uran.ru

The Heusler alloys Mn_2MeAl (Me – transition metals) are intermetallic compounds with a structure of the $L2_1$, XA or β-Mn type. They initially attracted attention as ferromagnetic alloys, consisting of non-magnetic elements, having high Curie temperatures. Important a feature of this system of alloys is that their electronic structure can be easily changed using various elemental substitutions. This allows you to customize the functional properties of alloys for a wide range applications. The band structure calculations indicate that some of these alloys are half-metallic ferromagnets (HMF) and appear to be promising for spintronic devices. Previously, the electrical, magnetic, and galvanomagnetic properties of Heusler alloys Mn_2MeAl (Me = Ti, V, Cr, Mn, Fe, Co, and Ni) were investigated [1]. It was shown that the alloys under consideration demonstrate strong ferromagnetism or compensated ferrimagnetism, and phase transitions with a change in the magnetic structure are possible. Some alloys exhibit the electrical resistivity behavior abnormal for metals; in particular, there are regions with positive, negative, or zero temperature coefficient in different temperature ranges. The presence of a negative temperature coefficient may indicate proximity to the state of a spin gapless semiconductor (SGS) with a vanishingly small energy gap.

Currently, an urgent problem is the search for materials that are effective for use in solid-state devices for generating electricity, for waste heat recovery systems. Recent theoretical studies reveal the potential of some Heusler alloys as new thermoelectric materials [2]. Finding and obtaining ideal materials with high thermoelectric figure of merit remains a serious problem. Experimental studies of the thermoelectric properties of Heusler alloys have not yet led to the discovery material with high thermoelectric figure of merit. In this paper, we conduct a study to obtain information about the electronic structure of Mn-based Heusler alloys from theoretical calculations and experimental studies of optical properties.

We studied the optical properties of Mn_2MeAl (Me = Ti, V, Cr, Co, and Ni) Heusler alloys. The main focus of our attention is on the study of spectral dependence of the real (ε_1) and imaginary (ε_2) parts of the dielectric constant and optical conductivity (σ) in a range of wavelengths $\lambda = 0.3–13$ μm using the ellipsometric Beattie technique. Substitution of an atom Me in the 3d metal series is accompanied by a significant change in the optical conductivity spectrum (Fig. 1). We see on the optical conductivity curve an intense absorption band in the energy range (0.3–4) eV for alloys with Me = Ti, V, Cr. Alloys with Co, Ni have an almost structureless spectrum in the entire studied area. The main feature of the optical absorption spectrum of alloys is the absence of Drude's rise in the σ(ω) curve up to the boundary of the investigated range. This kind of behavior is abnormal for metallic systems. Only Mn_2TiAl has Drude-like growth at energies $E < 0.2$ eV (Fig. 1).

This anomalous behavior of σ(ω) indicates a weakening of the metallic properties of alloys compared to good metals. Optical conductivity dispersion σ(ω) is determined by the structure of the electronic band spectrum of the substance; therefore, we analyze it on the basis of the results of calculating the band spectrum and the $N(E)$ density of states.

The electronic structure and magnetic properties of the alloys were calculated with Quantum ESPRESSO (QE) package [3] using generalized gradient approximation (GGA) in the Perdew-Burke-Ernzerhof (PBE) form. Wave functions were expanded in plane waves. For all elements, we

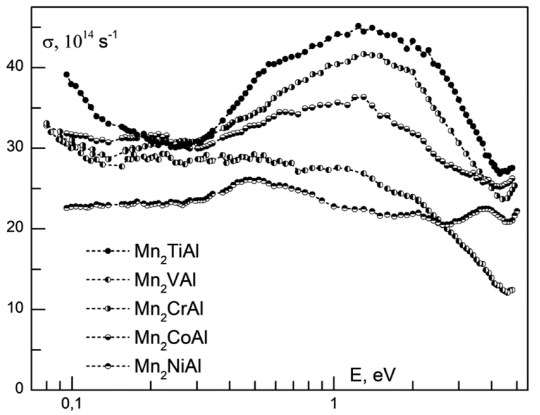

Figure 1. Dispersion of optical conductivity of alloys.

took standard ultrasoft pseudopotentials from the QE library. The kinetic energy cutoff of 60 Ry for plane waves was used. The integration was performed over an 8×8×8 k-point grid. As an example, we present here the curves of the density of states for alloys (Fig. 2). It should be noted, the occupations of the subbands with spins oriented along the magnetization direction (↑) and against it (↓) differ strongly, which can be clearly seen from the $N(E)$ curves. The cases where the states with spins up and down differ sharply is of interest for the general theory of the magnetism of itinerant electrons [4].

We see significant changes in the band-energy spectrum and density of states $N(E)$ – the principal difference is the position of the Fermi level. For Mn_2TiAl and Mn_2VAl our calculations yield HMF, for Mn_2CoAl – nearly SGS states. For Mn_2CrAl we have ferrimagnetic state (close to half-metallic) with appreciable magnetic moments. For Mn_2NiAl Fermi level lies on the peak $N(E)$ for spin down (↓) band and on the slope of the peak $N(E)$ for spin up (↑) band, thus usual FM. These changes are accompanied by considerable variations in the optical characteristics of alloys.

The research was supported by RSF (project No. 22-22-20109).

1. V.V. Marchenkov et al., JETP **128**, 919–925 (2019).
2. S.A. Sofi, D.C. Gupta, Physica B: Cond. Mat. **577**, 411792 (2020).
3. P. Giannozzi et al., J. Phys.: Condens. Matter. **29**, 465901 (2017).
4. V. Yu. Irkhin and M. I. Katsnelson, Phys. Usp. **37**, 659–676 (1994).

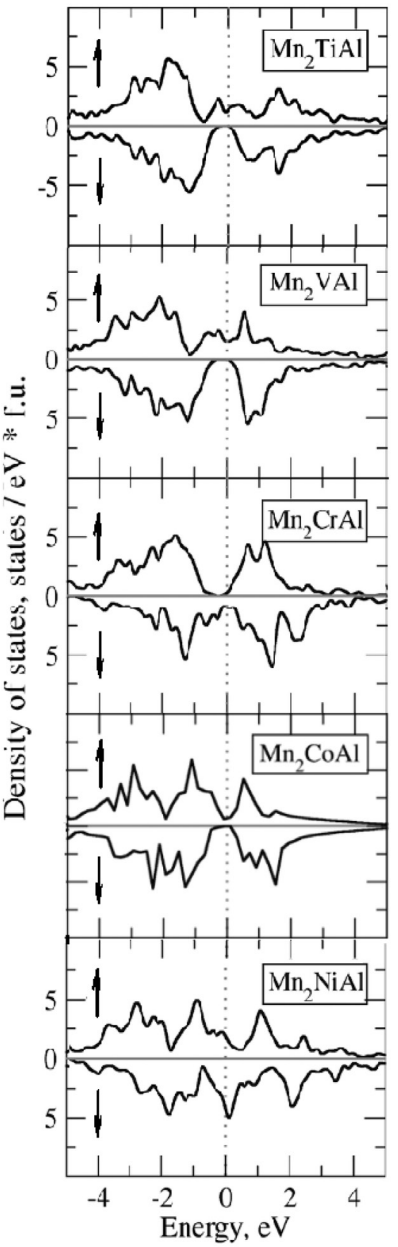

Figure 2. Density of states of alloys for spin up (↑) and spin down (↓) bands.

MAGNETIC CIRCULAR DICHROISM AND ABSORPTION OF A $HoAl_3(BO_3)_4$ CRYSTAL IN THE REGION OF $^5I_8 \rightarrow {}^5F_3$ AND $^5F_2$ TRANSITIONS

*V.V. Sokolov**, *A.V. Malakhovskii, A.L. Sukhachev, I.A. Gudim*

Kirensky Institute of Physics, Federal Research Center KSC SB RAS, Krasnoyarsk, Russian Federation
*E-mail: valer963@iph.krasn.ru

Magnetic circular dichroism (MCD) spectra and polarized absorption spectra of $HoAl_3(BO_3)_4$ crystal were measured in the region of f-f transitions $^5I_8 \rightarrow {}^5F_3$ and $^5F_2$ at a temperature of 5 K. Figure 1 shows the spectra of the $^5I_8 \rightarrow {}^5F_3$ transition (F-band). The excited $^5F_3$ state splits in the cubic and trigonal fields as follows:

$$J = 3 \rightarrow A_2 + T_1 + T_2 \rightarrow A_2 + (A_2 + E) + (A_1 + E) \ . \qquad (1)$$

The holmium ion in the $HoAl_3(BO_3)_4$ crystal is located in the position with local D_3 symmetry down to 5 K [1]. In work [2] from magnetic measurements and crystal field calculation, and in work [3] from the EPR-spectrum, it was shown that the ground state of holmium in $HoAl_3(BO_3)_4$ is doublet E. Based on these data, transitions from the ground state are identified based on the polarization of transitions, using selection rules in symmetry D_3 (Table 1) and equality (1). The uppercase letters in Fig. 1 designate transitions from the ground state, and lowercase letters indicate transitions from the upper sublevels of the ground multiplet.

During the identification, features not previously observed in [3] were found in a number of bands. Transitions F3, F5 of type E → A are not split, but transition F1 of the same type is split (Fig. 1). Consequently, the observed splitting of the f-f absorption line is not a consequence of the static distortion of the crystal in the ground state, but is caused by the distortion that occurs in the process of light absorption. The same is evidenced by the fact that the splittings are different for different transitions and vary from 2 to 7 cm^{-1}. This means, that the splitting of the ground state

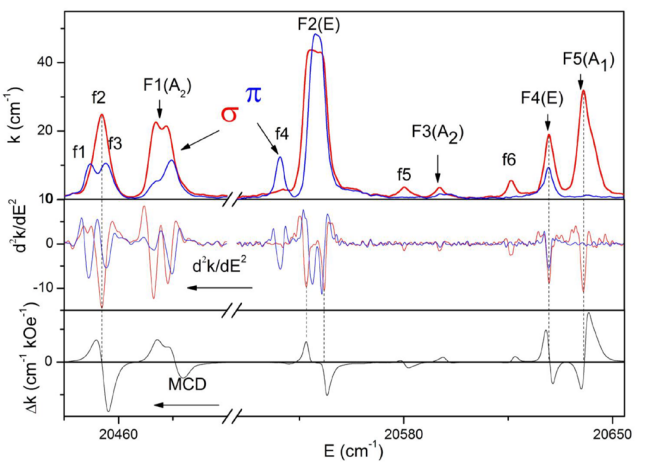

Figure 1. Polarized absorption spectra (k), second absorption derivative (d^2k/dE^2) and magnetic circular dichroism (Δk) spectra of the $^5I_8 \rightarrow {}^5F_3$ transition in $HoAl_3(BO_3)_4$ at a temperature of 5 K.

Table 1. D_3 symmetry selection rules for electric dipole transitions.

	A_1	A_2	E
A_1	—	π	σ(α)
A_2	π	—	σ(α)
E	σ(α)	σ(α)	π, σ(α)

depends on the electron transition. Indeed, the electron transition occurs due to the mixing of the initial and final states by the electromagnetic excitation of light. As a result the initial state and its interaction with the environment are changed.

The polarizations of the splitting components of the F1 transition do not correspond to the selection rules in the D_3 symmetry (Table 1), which can be explained by the lowering of the symmetry to C_2. Then the state transformation takes place:

$$E = A_1 + A_2,\ A_1 = A_1,\ A_2 = A_2\ . \quad (2)$$

The selection rules for C_2 symmetry are shown in Table 2.

Table 2. C_2 symmetry selection rules for electric dipole transitions.

	A_1	A_2
A_1	*a*	*b*,*c*
A_2	*b*,*c*	*a*

It follows from Table 2 that the transitions $A_1 \rightarrow A_1$ and $A_2 \rightarrow A_2$ correspond to σ lines. Transitions from a split doublet ($A_1 + A_2$) to singlet states (A_1 or A_2) will correspond to σ + πσ polarized lines. The F1 transition splits into πσ + σ + π lines. This means that thew symmetry drops below C_2.

The F4 transition (Fig. 1) of the E → E type does not split, while the F2 transition of the same type splits into σ + π + π + σ lines (0, 2, 5, 6 cm^{-1}). The purely π-polarized absorption lines observed in this and in the previous case can only be explained by the fact that the splitting depends on the polarization of the light as well.

In transitions where no splitting by the crystal field is observed, the Zeeman splitting is clearly seen in the MCD spectra. In particular, using the MCD and absorption spectra, we find the Zeeman splittings of the transitions. Using the Zeeman splitting of transitions in a magnetic field, experimental changes in the Lande factor Δg_C during transitions were found. For line F5 (A1) $\Delta g_C = +4$, at the theoretical value $\Delta g_{CM} = +2.5$, and for line F4 (E1) $\Delta g_C = -6.5$ at $\Delta g_{CM} = -5$. At the same time, there is no Zeeman splitting of lines in the F2 transition (Fig. 1), since both the initial and final states are split to singlets. The observed MCD in this transition is a paramagnetic mixing effect (B-term) due to the mixing of the splitting components in the crystal field by the magnetic field.

1. H. Zhang, et al. J. Phys.: Condens. Matter **31**(50), 505704 (2019).
2. A.I. Begunov, A.A. Demidov, I.A. Gudim, and E.V. Eremin, JETP Lett. **97**, 528–534 (2013).
3. A.V. Malakhovskii, V.V. Sokolov, et al., Phys. Lett. A **383**(16), 1960–1966 (2019).
4. A. Baraldi, et al., Phys. Rev. B **76**(16), 165130 (2007).

SPECTRALLY SELECTIVE DETECTION OF SHORT SPIN WAVES IN MAGNETOPLASMONIC NANOSTRUCTURES VIA THE FARADAY EFFECT

O.V. Borovkova[1,2], *S.V. Lutsenko*[1,2], *D.A. Sylgacheva*[1,2,3*], *A.N. Kalish*[1,2,4], *V.I. Belotelov*[1,2,3]

[1]Faculty of Physics, M.V. Lomonosov Moscow State University, Moscow, Russia
[2]Russian Quantum Center, Skolkovo IC, Moscow, Russia
[3]Research Center for Functional Materials and Nanotechnologies, V.I. Vernadsky Crimean Federal University, Simferopol, Russia
[4]NTI Center for Quantum Communications, National University of Science and Technology MISiS, Moscow, Russia
[*]E-mail: sylgacheva.darjja@physics.msu.ru

Optical characteristics of functional magnetic structures can be managed by the nanostructuring [1] or by controlling of the dielectric properties via illumination by powerful optical beam, short optical pulses, heating, application of the external magnetic field, etc. The latter case is relevant when a nanostructure contains magnetic components [2], and is the most interesting in context of this work.

Until now the magneto-optical effect in polar configuration of the magnetic field has been addressed for uniformly magnetized samples. The magnetization was supposed to be constant in the plane of the sample. However, the spatial modulation of the magnetization opens up new opportunities for the control of magneto-optical effects. It can be created in by different ways and by spin waves (waves of magnetization in a continuous magnetic medium) too [3]. They have a rather wide range of wavelengths, which is not always good. In this work we are interested in the properties of the magneto-optical Faraday effect in the magnetoplasmonic nanostructure with periodic spatial modulation of the magnetization in the ferrimagnetic layer. Such a study can solve the problem of searching for short spin waves with a wavelength of less than 1 μm, which is of particular interest for modern quantum and magnon technologies.

The addressed magnetoplasmonic nanostructure is given in Fig. 1. The ferrimagnetic layer of bismuth-substituted yttrium iron garnet (BIG) (its magnetic properties can be found, e.g., in [4]) of thickness h_{BIG} = 100 nm is on top of the nonmagnetic substrate of gadolinium gallium garnet (GGG). The ferrimagnetic layer is covered by the subwavelength gold grating of thickness h_{Au} = 80 nm. The period is varied to explore the magneto-optical properties. The air gap between the gold stripes is varied. To address the Faraday effect the magnetoplasmonic nanostructure is illuminated from top by linearly TE- or TM-polarized light with the wavevector normal to the surface of the sample. We are interested in how the variation of the magnetization modulation period influences the resulting Faraday effect.

Electromagnetic simulations of the optical properties of the structure was carried out by the method of rigorous coupled-wave analysis (RCWA), adapted for the case when the gyration vector proportional to the magnetization vector and specifying the off-diagonal components of the permittivity tensor changes laterally in space according to a harmonic law. In this case, the period of the structure is a multiple of the period of gyration variation in space and the corresponding directions of the periodicity coincide. The direction of the gyration vector can be arbitrary, which makes it possible to calculate the magneto-optical effects in any configuration.

Due to the plasmonic grating, waveguide modes and surface plasmon polaritons are excited in the structure under consideration, which leads to resonances in the transmission spectra, the Faraday angle. Resonances in these spectra are optimized by selecting the parameters of the grating: the height, the width of the air gap and the period. The dependencies of the angle Faraday at a

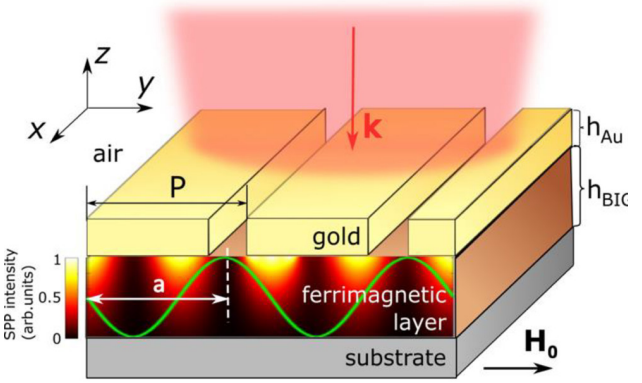

Figure 1. The scheme of the analyzed magnetoplasmonic nanostructure with spatial modulation of the magnetization in the ferrimagnetic layer. To address the Faraday effect the structure is illuminated by linearly TE- or TM-polarized light with the wavevector normal to the surface of the sample. An example of the spatial distribution of the electromagnetic field in ferrimagnetic layer is shown by yellow-red-black colormap. It corresponds to the excitation of the SPP optical modes at the [metal]/[ferrimagnetic layer] interface.

fixed resonance wavelength on the relative position of the slit and the maximum of the gyration demonstrate a harmonic appearance analogous to the dependence of the gyration in the film on the coordinate. Moreover, the extrema of these dependences of the Faraday angle arise when the extremum of the gyration coincides with the center of the gap.

Thus it was discovered that the nonuniform distribution of the gyration in the ferrimagnetic material combined with the excitation of the plasmonic and waveguide optical modes provide the significant resonant enhancement of the Faraday rotation when the effective wavelength of the optical mode coincides with the period of the magnetization modulation. The effect was shown for both TM- and TE-polarized input light. This will provide information about the amplitude, wavelength, and frequency of the spin wave propagating in the material much more effectively.

The work was supported by Russian Science Foundation (project no. 20-72-10159).

1. S. Maier, Plasmonics: Fundamentals and Applications, Springer, New York, (2007).
2. J. Park, M. Inoue, J. Cho, K. Nishimura, and H. Uchida, J. Magn. **8**, 50 (2003).
3. O. Borovkova, S. Lutsenko, M. Kozhaev, A. Kalish, and V. Belotelov, Nanomaterials **12**, 405 (2022).
4. E. Popova, L. Magdenko, H. Niedoba, M. Deb, B. Dagens, B. Berini, M. Vanwolleghem, C. Vilar, F. Gendron, A. Fouchet, J. Scola, Y. Dumont, M. Guyot, and N. Keller, J. Appl. Phys. **112**, 093910 (2012).

THE SECOND HARMONICS OF MAGNETIC QUANTUM OSCILLATIONS OF MAGNETIZATION AND CONDUCTIVITY IN QUASI-TWO-DIMENSIONAL METALS

T.I. Mogilyuk[1*], *P.D. Grigoriev*[2,3]

[1]NRC Kurchatov Institute, Russia, 123098, Moscow
[2]Landau Institute for Theoretical Physics, Russia, Moscow Region, Chernogolovka
[3]National University of Science and Technology MISiS, Moscow, Russia
[*]E-mail: 5taras@mail.ru

We find expressions for the second harmonics of magnetic quantum oscillations of interlayer magnetoconductivity and of magnetization in quasi-two-dimensional metals. The expressions obtained are useful, since in some experiments with quasi-two-dimensional metals, the second harmonic of magnetic quantum oscillations is also observed. We analyze the effect of magnetic oscillations of the real part of electron self-energy part ReΣ on the shape of the quantum magnetization oscillations and on the magnetoresistance of quasi-two-dimensional conductors. In the limit of strong quantum oscillations, which is possible only in two-dimensional or quasi-two-dimensional metals, the real part of electron self-energy function ReΣ also oscillates strongly. Usually it is neglected, taking into account only its imaginary part ImΣ, since it is assumed that ReΣ only shifts the chemical potential and does not affect the observed properties. However, ReΣ cannot be neglected if it also oscillates. As our calculations show, ReΣ oscillations affect the observed properties, since they shift the chemical potential toward the nearest Landau level even on average over the period of quantum oscillations.

Oscillations of ReΣ affect the shape of the quantum magnetization oscillations [1, 2], which is used to experimentally determine the regime of quantum oscillations: constant chemical potential or a constant electron density [3, 4]. Also, these oscillations change the monotonic part in a strong field by a coefficient of the order of 2 [5, 6], the angular dependence and the shape of the quantum oscillations of the magnetoresistance [7, 8]. Therefore, despite attempts in organic metals to achieve a constant electron density regime, the shape of the magnetization oscillations remained consistent with the constant chemical potential [3, 4]. This question is not only of great practical importance for the analysis of numerous experiments, but also of substantial interest for the development of the theory of magnetic quantum oscillations.

T. I. M. acknowledges the RFBR grant 21-52-12027.

1. P.D. Grigoriev, JETP **92**, 1090 (2001).
2. T. Champel and V. P. Mineev, Phys. Rev. B **66**, 195111 (2002).
3. J. Wosnitza, Fermi Surfaces of Low-Dimensional Organic Metals and Superconductors, Springer-Verlag, Berlin, 1996.
4. S.A.J. Wiegers, M. Specht, L.P. Lévy, M.Y. Simmons, D.A. Ritchie, A. Cavanna, B. Etienne, G. Martinez, and P. Wyder, Phys. Rev. Lett. **79**, 3238 (1997).
5. A.D. Grigoriev, P.D. Grigoriev, Low Temp. Phys. **40**, 367 (2014).
6. P.D. Grigoriev, T.I. Mogilyuk, Phys. Rev. B **90**, 115138 (2014).
7. P.D. Grigoriev, T.I. Mogilyuk, Phys. Rev. B **95**, 195130 (2017).
8. P.D. Grigoriev, T.I. Mogilyuk, J. Phys.: Conf. Ser. **1038**, 012123 (2018).

STUDY OF HM/FM NANOSTRUCTURES WITH HIGH EFFICIENCY OF SOT

A.V. Telegin[1*], *M. Steblii*[2], *A.V. Ognev*[2], *A.S. Samardak*[2], *I.D. Lobov*[1], *S.V. Batalov*[1], *E.A. Surzhikov*[1], *V.D. Bessonov*[1]

[1]M.N. Miheev Institute of Metal Physics UB of RAS, Ekaterinburg, Russia
[2]Far Eastern Federal University, Vladivostok, Russia
[*]E-mail: telegin@imp.uran.ru

HM/FM multilayered nanostructures show promise for enhancing the current-spin converting efficiency in SOT-based devices. It is reasonable to assume that the Dzyaloshinskii–Moriya interaction (DMI) can be controlled in these structures by using DC current. To study the spin momentum transfer processes in nanostructures on the value of interlayer exchange interaction a set of HM/FM samples with Hall bridges was fabricated. The samples (e.g. Ru(10)/Co(0.8)/Ru(2)/W(4), W(4)/[Tb(0.6)/Co(1.4)]$_3$/Ru(2), Pt(5)/Co(0.8)/MgO(2)/Pt(2)) were grown by magnetron sputtering, electron beam, photolithography and ion-plasma etching. The magnetic properties were studied using the vibrating magnetometer.

According to the magnetometric data, all the obtained samples have a perpendicular magnetic anisotropy and demonstrate a response to the transmission of a direct current due to a spin-polarized current (SOT) induced in the structures [1]. The processes of magnetization reversal of nanostructures under the action of DC current were confirmed using Kerr microscopy. As a result of research and numerical calculations, the following parameters were determined: resistivity, the proportion of current flowing through the layer responsible for the generation of spin current, saturation magnetization, energy of perpendicular magnetic anisotropy, coercive force, current density required for magnetization reversal. It is important, all samples demonstrate a linear dependence of the specific current-induced field and the efficiency of current-induced switching ξ [1] is about 40% (see, for example, Table 1 and Fig. 1).

The results of the research of current-controlled DMI in the obtained nanostructures by the methods of Mandelstam-Brillouin light scattering will be presented in the report.

Table 1. Experimental results for Pt(15)/Co(0.8)/MgO(2)/Pt(2).

Parameter	Value
Saturation magnetization, M_s	0.87e6
Anisotropy field, B_a	590
Energy of magnetic anisotropy, K_u	1.77e5
Coercive force, B_c	75
Threshold current, I_c	38
Density of current, j_c	1e11
Share of current through HM, p	79
Specific current-induced field, β	0.16
Efficiency of current-induced magnetization reversal, ξ	0.4

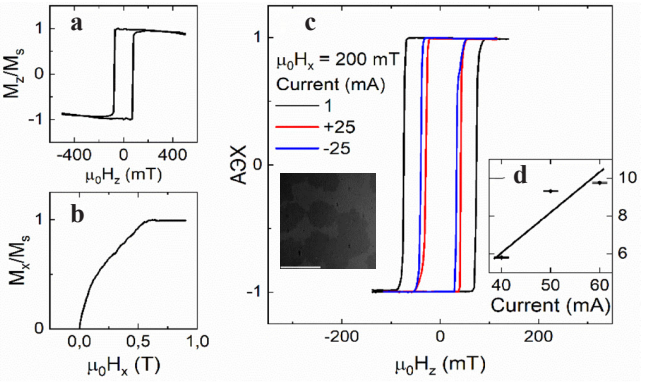

Figure 1. Curves of magnetization in the field: **a** perpendicular and **b** parallel to the film, **c** hysteresis loops of the Hall effect as a function of current, **d** dependence of the current-induced field in the Hall structure. On the left – domain structure of the sample.

Support of the Russian Science Foundation (№ 21-72-20160) and the Russian Ministry of Science (№ 0657-2020-0013) and Megagrant (№ 075-15-2021-607) is acknowledged.

1. A. Manchon, J. Železný, I.M. Miron et al., Rev. Mod. Phys. **91**, 035004 (2019).

PICOSECOND MAGNETOOPTICS IN FERROMAGNETIC CHROMIUM SPINEL

A.V. Telegin[1,2*], S. Changhee[1], H.-R. Park[1], S. Yu[1], A.V. Kimel[2], Yu.P. Sukhorukov[3]

[1]UNIST, Ulsan, S. Korea
[2]IMM Radboud University, Nijmegen, the Netherlands
[3]IMP UB of RAS, Ekaterinburg, Russia
[*]E-mail: andrei@unist.ac.kr

The development of spintronics requires new materials with ultrafast magnetooptical (MO) phenomena and spin transport at terahertz (THz) frequencies. Yet being underestimated magnetic semiconductors can be one of the promising materials. For example, chromium spinels have high charge carrier mobility, giant infrared MO effects, high spin polarization level and numerous applied applications [1]. We present the data on the absorption and high-frequency transport of carriers for single crystals of $Hg_{1-x}Cd_xCr_2Se_4$ ($0 \le x \le 1$).

The pronounced IR response to an external magnetic field in the form of the magnetoabsorption effect was demonstrated in spinel [1, 2]. The sign and magnitude of the effect are defined by the peculiarities of electronic structure of spinel and depend on the type of conductivity, level of substitution etc. [3]. A fine structure of the peak of absorption (quartet) was detected at low temperatures in the region of intracenter transitions within V_{Se^+}–Cr^+ complexes (E = 0.2–0.3 eV). Strong dependence of the peak structure from both the magnetic field and temperature confirms that 3dCr ions play a decisive role in transitions and leads to a distinct anomaly in the magnetoabsorption in spinel [4]. The dynamic of these electronic intracenter transitions was studied by an optical pump-probe method. The estimated signal risen front was about 1 ps and the decay time – about 3-6 ps depending on the temperature (Fig. 1).

The effects of magnetic linear birefringence and dichroism were observed in spinel crystals in the frequency range 0.5–2.5 THz at temperatures below the magnetic ordering by an THz pump-probe method. The maximal rotation of the light polarization plane induced by 1 kOe magnetic field reaches about 4.3 rad/cm and is associated with a high-frequency response to the DC anisotropic magnetoresistance in spinel [5]. Therefore, chromium spinels can be applied for studying various ultrafast IR and THz phenomena.

Support by the program "Spin" No. AAAA-A18-118020290104-2 and BP Program through the NRF funded by the MSIT No. 2021H1D3A2A01096552 is acknowledged.

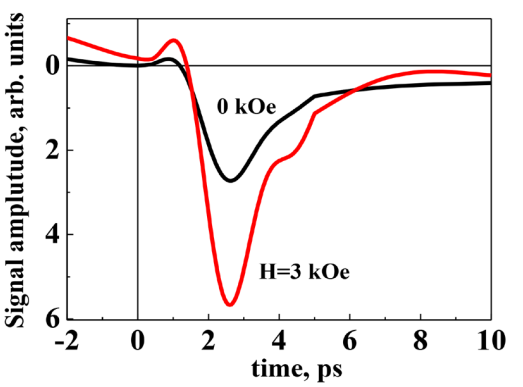

Figure 1. The temporal profile of the absorption of light in spinel single crystal at energy 0.23 eV and T = 6 K with and without an external magnetic field.

1. Yu.P. Sukhorukov et al., JETP Lett. **98**, 313–316 (2013).
2. Yu.P. Sukhorukov et al., JETP **121**, 437–445 (2015).
3. M.I. Auslender and N.G. Bebenin, Sol. State Comm. **69**, 761 (1989).
4. S. Barsaume et al., J. of Phys. Cond. Matt. **29**, 325502 (2017).
5. T.J. Huisman et al., Appl. Phys. Lett. **106**, 132411 (2015).

BEHAVIOR OF SURFACE PLASMON POLARITONS IN THE VANADIUM DIOXIDE-SILICON DIOXIDE-HYPERBOLIC METASURFACE STRUCTURE UNDER THE INFLUENCE OF AN EXTERNAL MAGNETIC FIELD

M.O. Usik, D.A. Kuzmin, I.V. Bychkov*

Chelyabinsk State University, Chelyabinsk, Russia
*E-mail: usikmo95@gmail.com

In this paper, we studied the behavior of surface plasmon polaritons (SPPs) in the vanadium dioxide-silicon dioxide-hyperbolic metasurface structure under the influence of an external magnetic field (Fig. 1). Since the influence of phase transitions on the excitation pattern of surface plasmons is of particular interest, vanadium dioxide was taken as one of the layers, since its phase transition from the dielectric state to the metallic state occurs at temperatures close to room [1].

A lattice of graphene strips was taken as a hyperbolic metasurface [2]. Such a surface is capable of supporting the propagation of both TM- and TE-polarized plasmons.

When taking into account the phase transition of vanadium dioxide, we took the already known data on the behavior of vanadium dioxide and performed a linear approximation, using the Drude theory [3], which allowed us to obtain a model that is quite simple to describe.

In order to investigate the behavior of surface plasmons, one should solve Maxwell's equations with the corresponding boundary conditions at each interface. For monochromatic wave $\mathbf{E}_{\alpha+},\mathbf{H}_{\alpha+} \sim \exp[-i\omega t + i\mathbf{k}_\alpha x \pm \gamma_a]$ [4], where ω is an angular frequency, $\mathbf{k}_\alpha$ is a propagation constant, and $\pm\gamma_a$ is a localization constant ($\alpha = VO_2, SiO_2, a$ denotes "vanadium dioxide", "silicon dioxide" and "air", consequently). With these notations, Maxwell's equation for the waves in each medium is read:

$$[\mathbf{k}_{\alpha+},\mathbf{E}_{\alpha+}] = i\omega\mathbf{B}_{\alpha+}, \quad [\mathbf{k}_{\alpha+},\mathbf{H}_{\alpha+}] = -i\omega\mathbf{D}_{\alpha+},$$

$$\mathbf{B}_{\alpha+} = \mu_0\mathbf{H}_{\alpha+}, \quad \mathbf{D}_{\alpha+} = \varepsilon_0\hat{\varepsilon}_{\alpha+}\mathbf{E}_{\alpha+}, \quad \alpha = VO_2, SiO_2, a.$$

Boundary conditions should be satisfied for total fields $(\mathbf{E}_\alpha,\mathbf{H}_\alpha) = (\mathbf{E}_{\alpha-},\mathbf{H}_{\alpha-}) + (\mathbf{E}_{\alpha+},\mathbf{H}_{\alpha+})$:

$$\mathbf{H}_{VO_2,\tau}|_{z=-t_1} = \mathbf{H}_{SiO_2,\tau}|_{z=-t_1}, \quad \mathbf{E}_{VO_2,\tau}|_{z=-t_1} = \mathbf{E}_{SiO_2,\tau}|_{z=-t_1},$$

$$[\mathbf{n},\mathbf{H}_{SiO_2,\tau}|_{z=0} - \mathbf{H}_{a,\tau}|_{z=0}] = \hat{\sigma}\mathbf{E}_{a,\tau}|_{z=0}, \quad \mathbf{E}_{SiO_2,\tau}|_{z=0} = \mathbf{E}_{a,\tau}|_{z=0},$$

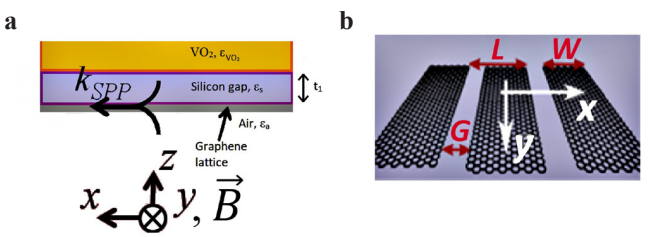

Figure 1. Schematic model of vanadium dioxide-silicon dioxide-hyperbolic metasurface structure under the influence of a magnetic field directed along the *y*-axis (**a**) and graphene-based hyperbolic metasurface (**b**).

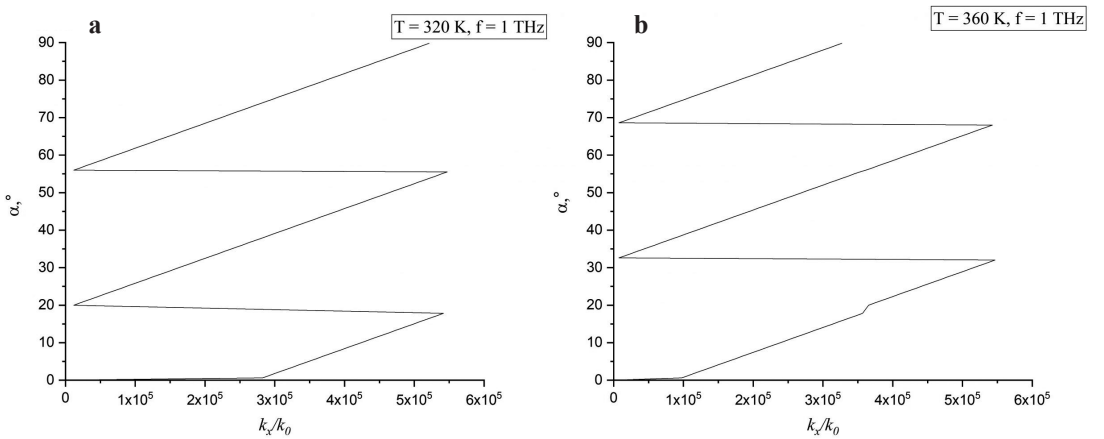

Figure 2. Propagation constant depending on the rotation angle of the hyperbolic metasurface for vanadium dioxide before the state transition (**a**) and after the phase transition (**b**).

where **n** is the unitary vector perpendicular to the interface, $\hat{\sigma}$ is tensor of graphene conductivity, $\hat{\varepsilon}_\alpha$ is a tensor of permittivity under the influence of an external magnetic field.

Solving this system of equations, we found the propagation constant depending on the rotation angle of the hyperbolic metasurface for various phase states of vanadium dioxide in an external magnetic field.

We believe that our research can help to study the behavior of surface plasmons in systems with external magnetic field, and also opens up new possibilities for controlling electromagnetic radiation at the nanoscale.

Support by RSF (22-19-00355) is acknowledged.

1. Tobias Peterseim, Martin Dressel, Marc Dietrich and Angelika Polity, J. Appl. Phys. **120**, 075102 (2016).
2. J. Sebastian Gomez-Diaz, Mykhailo Tymchenko, and Andrea Alù, Phys. Rev. Lett. **114**, (2015).
3. M. Tazawa, P. Jin and S. Tanemura, Appl. Optics **37**(10), (1998).
4. I.V. Bychkov, D.A. Kuzmin, V.A. Tolkachev, P.S. Plaksin, V.G. Shavrov, Optics Lett. **3**(1), (2018).

IRON GARNET-BASED ULTRAFAST OPTOMAGNONIC XNOR GATE

A.A. Kolosvetov[1,2*], M.A. Kozhaev[2], V.I. Belotelov[2,3], A.I. Chernov[1,2]

[1]Center of Photonics and 2D Materials, Moscow Institute of Physics and Technology, Dolgoprudny, Russia
[2]Russian Quantum Center, Moscow, Russia
[3]Faculty of Physics, Lomonosov Moscow State University, Moscow, Russia
*E-mail: kolosvetov.aa@phystech.edu

Studies of recent decades showed that ultrafast non-thermal control of the magnetization dynamics demonstrates the new prospects for Ohmic heating-free applications operating at (sub)picosecond timescales [1]. First predicted almost a century ago by Bloch, spin waves (SW) are now considered as promising information carriers, due to the absence of Ohmic heating, various nonlinear phenomena, and large propagation distances in specific materials [2]. All these advantages make SWs a prospective platform for spin wave-based computing [3]. Optomagnetism paves the way for further progress in spin wave excitation. The technique of ultrafast coherent control with circularly polarized femtosecond laser pulses provides an efficient, fast and flexible way to excite spin waves in terms of spatial location of a spin wave source, types of spin waves, directional emission pattern, phase, and wavelength [4]. The new approach may provide the solution to overcome the principal challenge of applied magnonics: manipulation of sub-100 nm wavelength spin waves at nanoscale. In this work we demonstrate the concept of the XNOR logic circuit built on the basis of ultrafast optical excitation technique.

We built XNOR gate on the base of the in-plane magnetized 46 μm-thick bismuth-substituted iron garnet (BIG) film and optical pump-probe scheme. Femtosecond laser pulses launch spin waves from several spots via Inverse Faraday Effect, while arrangement of the laser beams (Fig. 1a) is controlled by a spatial light modulator (SLM). Single linearly polarized laser beam probes the out-of-plane component of magnetization via Faraday effect. The XNOR gate can be effectively represented as a circuit with two pumping beams. When both pump spots are located at the same distance equal to an integer number of half-waves from the probing zone, the spin waves launched from two sources will come to the probing zone in phase. Moreover, one can add a phase difference of π by switching the helicity of one of the beams to the opposite, which will lead to the switching from the constructive interference to destructive one or vice versa. Logical circuit, designed in this way, will take the beam helicities as a logical input, while the logical output will be determined by constructive and destructive spin-wave interference.

In our experiment we observed the excitation and, subsequently, robust interference of backward volume magnetostatic spin waves (BVMSWs). For further confirmation we built a numerical model of our system in Mumax3 framework [5], which provided an excellent agreement with the experimental data. On the basis of the same model, we simulated the possible implementation of the logic gates – a functional XNOR logic circuit based on a thinner 1 μm film. Studying (σ+; σ−) and (σ+; σ−) pump beam configurations we revealed the opposite interference patterns with high interferential contrast, meaning that we can effectively control the "sign" of the spin-wave interference and recreate the XNOR gate truth table.

In conclusion, we present the concept of scalable, ultrafast Boolean logic made possible by the recent progress in data processing with spin waves and the advances in ultrafast coherent control of the magnetic order. We gradually proved the presented concept, first by confirming the constructive interference of BVMSWs, when the spacing between local sources was equal to an integer number of wavelengths, and further by constructing a numeric model and observing the constructive interference of BVMSWs in simulation. The numeric model was later used to build an ultrafast magnon logical

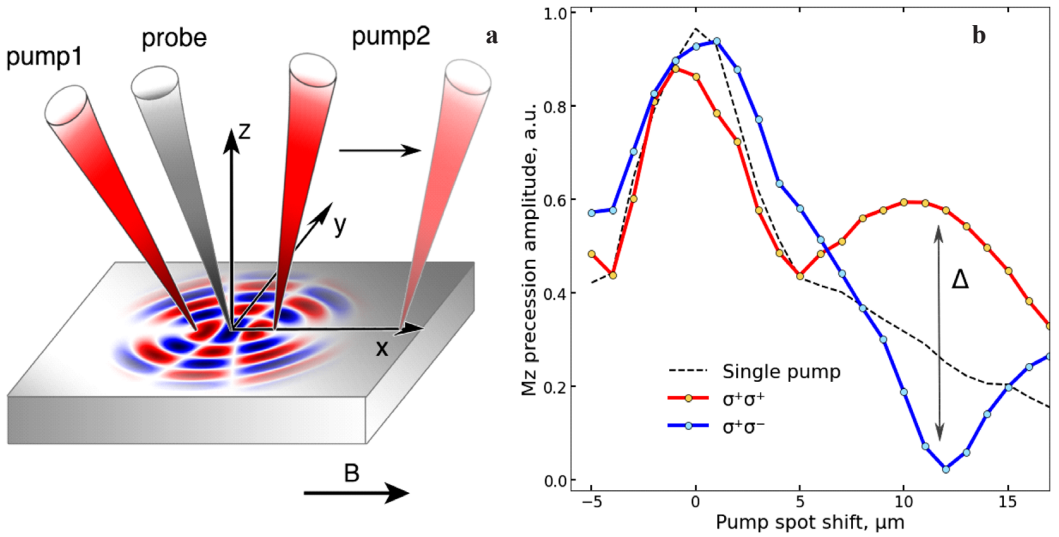

Figure 1. **a** The pump and probe beams were focused at the sample surface with a micro-objective lens in 6-μm and 4-μm spots, respectively. The center of the probing spot was at zero; the center of the first pumping spot was shifted along the *x*-axis by 12 μm in the negative direction. During the experiment, the first pump beam and the probing beam were fixed in place, while the second pump beam was shifted along the *x*-axis. **b** 0-order BVMSW amplitude at zero in a 1.1-μm BIG film as a function of the second pump position shift. The first pump was constantly located at –12 μm. The result for the two σ+ polarized pump beams (red color line), two pump beams of the opposite polarization (blue color line) and for one σ+ polarized pump beam (gray dotted line).

gate XNOR, based on the spin-wave interference. The designed XNOR serves as a building block for further implementations of optomagnonics logic. It demonstrates the advantages of optomagnonic devices in general: ultrafast operation, absence of Ohmic losses and potential for scalability.

Support by RSF project № 21-12-00316 is acknowledged.

1. A.V. Kimel et al., Nature **435**, 655–657 (2005).
2. V. Cherepanov, I. Kolokolov, and V. L'vov, Phys. Rep. **229**, 81 (1993).
3. G. Csaba, Papp, and W. Porod, Physics Letters A **381**, 1471–1476 (2017).
4. T. Satoh, Y. Terui, R. Moriya et al., Nature Photon **6**, 662–666 (2012).
5. A. Vansteenkiste et al., AIP Adv. **4**, 107133 (2014).

STRUCTURE AND EFFECT OF A MAGNETIC FIELD ON THE MICROWAVE IMPEDANCE OF COMPOSITE FILMS CoFeB + SiO_2

L.N. Kotov[1*], *M.P. Lasek*[1], *A.V. Sitnikov*[2], *Yu.E. Kalinin*[2]

[1]Syktyvkar State University, Syktyvkar, Russia
[2]Voronezh State Technical University, Voronezh, Russia
[*]E-mail: kotovln@mail.ru

Wide electrical resistance variations and a high ability to absorb UHF radiation favor application of composite films in UHF electronics devices [1, 2]. It is necessary to study influence of static magnetic fields on UHF resistivity of thin composite films to explain mechanisms of electrical transfer, absorption of electromagnetic waves, and to understand contribution of nano- and microstructure of composite films to these properties. The work is devoted to the study of the effect of a magnetic field on the impedance of composite films with the following compositions $[(Co_{0.46}Fe_{0.4}B_{0.14})_x + (SiO_2)_y]$, $0.46 < x < 0.86$, $y = (1 - x)/3$. The relationship between the magnetic structure of composite films and the behavior of the impedance as a function of the constant magnetic field and the frequency of the alternating field in the range 0.2–3 GHz is also investigated.

The composite films were fabricated in vacuum by bombarding CoFeB alloy targets and SiO_2 dielectric plates with argon ions. Nano- and microparticles of targets at a pressure of 10^{-4} Torr [4] were deposited on a lavsan sheet. The elemental compositions of the films were determined using a Tescan Mira 3 scanning electron microscope. The concentration of the metal phase x from 0.48 to 0.88 in the films varied. Images of the magnetic phase contrast and surface relief of the samples were obtained using an Integra Prima atomic force microscope (NT-MDT, Russia) before and after the films were magnetized in a constant magnetic field. A silicon probe coated with CoCr magnetic alloy, 40 nm thick, was used in a microscope. The probe tip radius was 20 nm. The oscillation frequency of the external force acting on the cantilever with the probe was selected in the frequency range of 47–90 kHz. The phase difference $\Delta\varphi$, which varied depending on the strength of the magnetic interaction of the probe with the surface of the films, was recorded by the microscope apparatus.

Change in the modulus of microwave impedance of composite films depending on the frequency of the current and the magnetic field applied to the films at different concentrations of the metal

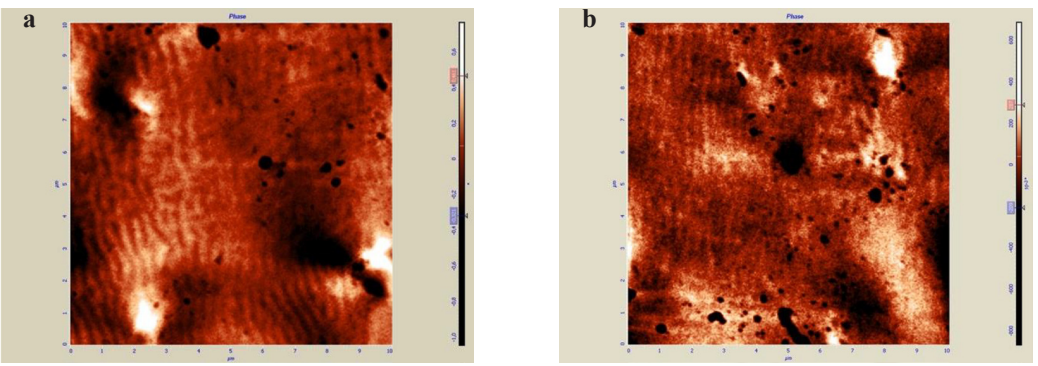

Figure 1. The magnetic structure of composite films at $x = 0.67$: before magnetization of the film (**a**), after magnetization of the film in a field of 0.2 T (**b**).

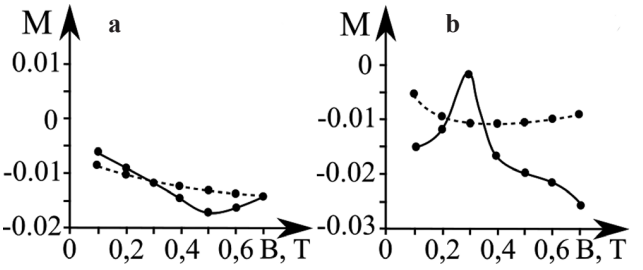

Figure 2. Dependences of the magnetic resistance on the field: before the film magnetization at x = 0.67 (**a**), after the film magnetization at x = 0.84 (**b**). Solid curve – initial orientation of the film in the field, f = 1.0 ГГц; dotted curve – after turning the film by 90 degrees, f = 2.2 ГГц.

alloy was determined experimentally. The magnetic field varied from 0.005 to 0.7 T. Magnetic field in the plane of the film parallel to the microwave current was applied. A coplanar transmission line with films to a GSP-7830 spectrum analyzer with a built-in sweeper was connected. The current frequency varied in the frequency range from 0.2 to 3.0 GHz. The power transfer coefficient spectrum was recorded by a spectrum analyzer. Then the spectrum of the film impedance modulus at different values of magnetic field induction was calculated. All measurements were carried out at room temperature. changes in the microwave module of the magnetic impedance $M(f)$ (hereinafter referred to as the microwave magnetoresistance) of the films at a frequency f was calculated using the formula $M(f) = (|Z(f)|_B - |Z(f)|)/|Z(f)|$, where $|Z(f)|_B$ and $|Z(f)|$ are the film impedance moduli in the magnetic field B and in the absence of the field, respectively.

Images of the magnetic phase contrast of composite films of the compositions $\{(Co_{0.42}Fe_{0.38}B_{0.2})_x + (SiO_2)_{(1-x)/3}\}$, where x = 0.54, are shown in Fig. 1. The stripe magnetic structure with the opposite direction of the magnetization vector of adjacent stripes is visible in the images. Films after magnetization are characterized by an indistinct image of magnetic stripes, which corresponds to the initial stage of formation of the magnetic structure. For films with $0.55 < x < 0.8$, the length of the magnetic stripes can reach more than 3 μm with an average width of about 0.13 μm.

Microwave resistance spectra for films with different metal alloy concentrations were obtained in different constant magnetic fields. After recording the resistance spectra, the films were rotated by 90 degrees with respect to a constant magnetic field. From the obtained spectra of the microwave magnetoresistance, it was determined that in the frequency range from 0.3 to 3.0 GHz, a decrease in the impedance modulus is observed with an increase in the constant magnetic field (Fig. 2a). The presence of a section of impedance decrease from the magnetic field corresponds to a negative microwave magnetoresistance. At a higher concentration x = 0.84 at low frequencies, a maximum is observed in the dependence of the film impedance on the field (Fig. 2b). This maximum is explained by the presence of positive and negative magnetoresistances in the film of the same order. A change in the concentration of the metal alloy x leads to a change in the maximum of the negative microwave magnetoresistance.

The study was supported by a grant from the Russian Science Foundation (project no. 21-72-20048).

1. L.N. Kotov, V.S. Vlasov, V.K. Turkov et al., J. Nanoscience and Nanotechnology **12**, 1696–1699 (2012).
2. L.N. Kotov, M.P. Lasek, V.S. Vlasov et al., Bulletin of the RAS: Physics **86**, 588–591 (2022).

Section F.

Magnetoelastic, magnetocaloric and shape memory effects

STRUCTURE AND MAGNETIC PROPERTIES OF Fe-Ga-Al ALLOYS: AB INITIO STUDY

*M.V. Matyunina**, *M.A. Zagrebin, V.V. Sokolovskiy, V.D. Buchelnikov*

Chelyabinsk State University, Chelyabinsk, Russia
*E-mail: matunins.fam@mail.ru

Iron-based functional alloys are of interest to the scientific community because of their unusual mechanical, magnetic, and electrical properties. The small addition of nonmagnetic atoms, such as Ga and Al, leads to a significant increase in the magnetostriction value as compared to pure iron [1]. The Fe-Ga alloys have the highest tetragonal magnetostriction values λ_{001}. The unusual two-peak dependence of the magnetostriction on the Ga concentration is interpreted on the basis of a rapid increase in the magnetoelastic energy $-B_1$ for low concentrations up to 19 at.% and a significant softening of the elastic shear constant C' to at least 27 at.% [2]. The Fe-Al alloys have a similar trend in the magnetostriction behavior in the concentration range up to 25 at.% Al with a lower magnitude, and they do not exhibit the second peak [1, 3]. The shear modulus of Fe-Al alloys decreases not so intensively as in Fe-Ga alloys when a non-magnetic element is added, and it is higher by a factor of two in the composition around 25 at.%. Evaluation of the effect of substitution of Ga atoms by Al atoms in the Fe-Ga binary alloys up to 23 at.% Ga content [1] showed that the tetragonal magnetostriction of the Fe-Ga-Al ternary alloys decreases insignificantly. This can be explained by a simultaneous increase in both the magnetoelastic constant and the tetragonal modulus of elasticity. In spite of the existing studies in this field, there is no unequivocal interpretation of the mechanisms of the influence of alloying with a third element, for example Al, on the magnetic properties and Curie temperatures in Fe-Ga alloys with high Ga concentration. In this paper, we study the effect of Al addition on the elastic, magnetic, and magnetoelastic properties in Fe-Ga alloys using first-principles calculations.

The *ab initio* electronic structure calculations and structural relaxations were performed with the Vienna ab initio simulation package VASP [4, 5]. The spin-polarized generalized gradient ap-

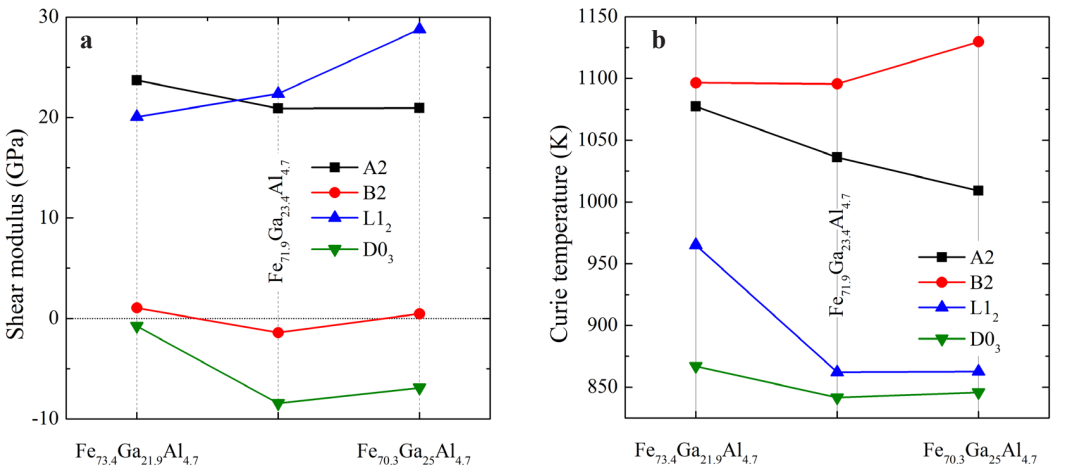

Figure 1. **a** The calculated shear modulus and **b** Curie temperature for A2, B2, $D0_3$ and $L1_2$ structures of $Fe_{73.4}Ga_{21.9}Al_{4.7}$, $Fe_{71.9}Ga_{23.4}Al_{4.7}$, and $Fe_{70.3}Ga_{25}Al_{4.7}$ alloys.

proximation was employed to describe the exchange and correlation interactions among electrons. $Fe_{73.4}Ga_{21.9}Al_{4.7}$, $Fe_{71.9}Ga_{23.4}Al_{4.7}$, and $Fe_{70.3}Ga_{25}Al_{4.7}$ compositions were considered in the present study with A2 (Im-3m, #229), B2 (Pm-3m, #221), $D0_3$ (Fm-3m, #225) and the $L1_2$ (Pm-3m, #221) structures. Non-stoichiometric compositions and structural disorders were created with special quasi-random structures by the ATAT (Alloy Theoretic Automated Toolkit) package [6]. For the 64-atom unit cells, an 8×8×8 Monkhorst-Pack k-point mesh in the Brillouin zone was used to evaluate integrals in the reciprocal space. Curie temperature was estimated from the *ab initio* calculations of magnetic exchange interactions obtained using the SPR-KKR software package (A spin-polarized relativistic Korringa-Kohn-Rostoker code) [7] and Monte Carlo simulation of three-dimensional Heisenberg model [8].

As a result, the addition of Al reduces the equilibrium lattice constants of the B2, $D0_3$, and $L1_2$ structures. The $L1_2$ phase is the most energetically preferable for the considered compositions. The addition of Al increases the total magnetic moment in the B2 and $D0_3$ structures and has no significant effect on the $L1_2$ system. As shown in Fig. 1a, the shear modulus increases slightly in the ternary composition with Ga content over 23 at.%. The Curie temperature is a decreasing function of the non-magnetic atoms for the B2, $D0_3$, and $L1_2$ phases (see Fig. 1b).

Support by the Ministry of Science and Higher Education of the Russian Federation within the framework of the Russian State Assignment under contract No. 075-01391-22-00 is acknowledged.

1. J.B. Restorff, M. Wun-Fogle, K.B. Hathaway et al., J. Appl. Phys. **111**(2), 023905 (2012).
2. A.E. Clark, K.B. Hathaway, M. Wun-Fogle et al., J. Appl. Phys. **93**(10), 8621-8623 (2003).
3. A.E. Clark, J.B. Restorff, M. Wun-Fogle et al., J. Appl. Phys. **103**(7), 07B310 (2008).
4. G. Kresse, J. Furthmüller, Phys. Rev. B **54**(16), 11169 (1996).
5. G. Kresse, D. Joubert, Phys. Rev. B **59**, 1758 (1999).
6. A. Van De Walle, M. Asta, G. Ceder, Calphad. **26**(4), 539–553 (2002).
7. H. Ebert, D. Koedderitzsch, J. Minar. Rep. Prog. Phys. **74**(9), 096501 (2011).
8. D.P. Landau, K. Binder, A Guide to Monte Carlo Simulations in Statistical Physics, Cambridge, (2014).

F.O1

DYNAMICS OF MAGNETIZATION OSCILLATIONS AND ELASTIC DISPLACEMENT OF THE FERRITE FILM UNDER FREQUENCY-MODULATED EXCITATION

D.A. Pleshev[1,2*], *F.F. Asadullin*[2], *V.S. Vlasov*[1], *L.N. Kotov*[1]

[1]Syktyvkar State University, Syktyvkar, Russia
[2]Saint-Petersburg state forest technical university named after S.M. Kirov, St-Petersburg, Russia
[*]E-mail: dpleshev@gmail.com

The application of thin magnetic periodic structures, composite and single-component films with minimal weight and size parameters are used in a wide range of radio engineering devices [1]. The method of detection on a nonlinear element is used to receive and register ultrahigh-frequency signals in traditional radio engineering. But, their use has low efficiency in the microwave range, as their interelectrode capacitance is high. The use of magnetoelastic signal detectors makes it possible to circumvent this limitation, and the application of the normally magnetized thin film geometry makes it possible to avoid the influence of exchange spin waves during their parametric excitation [2].

We show the possibility of separating the transmitted message materials from the microwave signal in a magnetostrictive transducer in linear and nonlinear modes in our work.

The general approach to the detection of magnetic fields generally and amplitude-modulated magnetic fields specifically is presented in a series of works [3, 4]. The scheme of a frequency-modulated magnetic field detecting based on a thin-film ferrite magnetoacoustic transducer is described in detail in [5]. However, the dependence of the magnetic and elastic subsystems dynamics on the type of polarization and the amplitude of the alternating magnetic field, as well as the amplitude-frequency characteristics of the magnetization vector and elastic displacement oscillations, are incompletely described.

This work is deal with the consideration of the magnetization and elastic displacement components oscillations excitation, as well as the structure of their parametric portraits in various excitation modes by a frequency-modulated alternating magnetic field. The detection of a frequency-modulated signal based on the magnetic films resonant magnetoacoustic properties, which consists in the excitation of elastic oscillations at the modulation frequency, is considered. The dependence of the parametric portraits structure of the magnetization vector and elastic displacement oscillations on the amplitude-frequency characteristics of an alternating magnetic field is determined. The features of the magnetoelastic oscillations dynamics depending on the ratio of the ferromagnetic and acoustic resonances frequencies, the frequency of modulation and frequency deviation are revealed.

Support by Russian Science Foundation (project no. 21-72-20048) is acknowledged.

1. W.-G. Yang and H. Schmidt, App. Phys. Rev. **8**, 021304 (2021).
2. R.L. Comstock and R.C. LeCraw, J. Appl. Phys. **34**(10), 3022–3027 (1963).
3. I.A. Chuprov, F.F. Asadullin, D.A. Pleshev, V.S. Vlasov, L.N. Kotov, V.I. Shcheglov, Chelyab. Phys. and Math. J. **6**(2), 237–245 (2020) [in Russian].
4. D.A. Pleshev, V.S. Vlasov, F.F. Asadullin, L.N. Kotov, I.A. Chuprov and V.I. Shcheglov, Phys. Metals Metallogr. **123**(3), 299–304 (2022).
5. V.S. Vlasov, D.A. Pleshev, V.G. Shavrov, V.I. Shcheglov, Journal of Radio Electronics 7 (2020) [in Russian].

F.O2

NEW MATERIALS FOR SOLID-STATE MAGNETIC COOLING

*I.S. Tereshina**, *I.A. Ovchenkova, N.Yu. Pankratov*

Faculty of Physics, M.V. Lomonosov Moscow State University, Moscow, Russia
*E-mail: irina_tereshina@mail.ru

Solid-state magnetic refrigeration can help reduce the world's energy consumption and avoid the use of environmentally harmful refrigerants like freon [1, 2]. Thanks to the significant efforts made by scientists from different countries, the prerequisites for a qualitative breakthrough in the development of this technology have been created [3].

While most prototype refrigeration equipment operating at room temperature uses the rare earth metal gadolinium, materials like it for use at other vital temperatures (e.g., storage temperatures for biomaterials, vaccines, drugs, etc.) have so far time is not clearly identified. Such materials are very promising as working fluids of refrigeration plants, for example, for the economical long-term storage and transportation of biomedical preparations, as well as for the creation of compact, silent and efficient refrigerators with the possibility of their use in medicine and biology, as well as in other areas (for example, in military or space development) [4].

In this work, we set a goal to develop highly efficient materials for solid-state magnetic cooling at temperatures below room temperature, namely 180–280 K. To do this, we synthesized new compositions of the $R(Co,T)_2$-, R(Mn,T)Si-, $(RT)_5(Ge,Si)_4$-type with a high magnetocaloric effect (MCE). We also synthesized new compositions of the $R_2(Fe,T)_{17}$-type with alternating MCE. It should be noted that *T* are weakly magnetic substitutional atoms, such as Al or Ti and highly magnetic atoms such as Fe or Co. $R_2(Fe,T)_{17}$ compounds can be useful for devices that stabilize the temperature when it deviates from the specified values.

All obtained samples were certified by X-ray diffraction phase analysis and optical metallography. Experimental data on the features of the field and temperature dependences of the magnetocaloric effect have been obtained and analyzed. MCE-measurements were performed using special equipment (automated complex for studying the magnetic properties of materials "MagEq AMS" manufactured by OOO "PMTC"). The results obtained in this work for new compositions form the basis for modeling cooling processes in prototypes of refrigeration equipment, for creating devices for storing and transporting various objects of animate and inanimate nature, as well as for making the transition to high-tech healthcare using cooling systems and developing a strategy for finding materials with improved magnetocaloric characteristics for a wider range of applications.

The study was supported by the Russian Science Foundation grant No. 22-29-00773, https://rscf.ru/project/22-29-00773/.

1. A.M. Tishin and Y.I. Spichckin, The Magnetocaloric Effect and Its Applications. Institute of Physics Publishing, Bristol and Philadelphia (2003).
2. V. Franco et al., Prog. Mater. Sci. **93**, 112–232 (2018).
3. A. Kitanovski et al., Magnetocaloric Energy Conversion from Theory to Applications. Springer International Publishing, Switzerland, Cham, (2015).
4. V.B. Chzhan et al., Acta Materialia **154**, 303–310 (2018).

F.O3

INFLUENCE OF CHEMICAL IMPURUTIES ON MAGNETOTHERMAL PROPERTIES OF RARE-EARTH METALS AND PERMANENT MAGNETS

R.R. Gimaev

Dukhov Research Institute of Automatics (VNIIA), Moscow, Russia
E-mail: vizverev@vniia.ru

Since the 1990s VNIIA has been developing and manufacturing a new class of electrophysical and nuclear-physical devices – portable neutron generators and equipment based on them. Modern portable neutron generators are based on the use of nuclear fusion of hydrogen isotopes: deuterium-tritium or deuterium-deuterium. These nuclear reactions are realized in a miniature linear accelerator of deuterium and tritium ions, and the generation of these ions is done in a Penning ion source.

The Penning source uses a magnetic system based on rare-earth permanent magnets. This paper presents the results of chemical impurities effect on the magnetic and magnetothermal properties of rare-earth metals (REMs).

Here we show the presence of a phase transition shift to lower temperatures for samples with higher impurity content (in the case of the predominance of magnetic impurities), which facilitates the formation of magnetic ordering with a large value of moment (for example, ferromagnetic ordering) in low fields' region. The influence of impurities explains the presence of local spin defects (spin slip type structures).

The studies have shown that the existence of allotropic modifications of REM is explained by the presence of chemical impurities. In addition, the influence of impurities on the formation of new REM phases as a result of the response to the external magnetic field of the impurity atom (rather than the REM atom) was shown.

The paper also analyzes the wide set of experimental data on single-crystalline samples of terbium, dysprosium, and holmium to prove the revealed mechanisms of the impurities' influence on magnetothermal properties of REM.

THE ISSUES OF PHASE STABILITY AND MAGNETOCRYSTALLINE ANISOTROPY IN Fe_2Ni-BASED HEUSLER ALLOYS

V.V. Sokolovskiy[1*], *O.N. Miroshkina*[2], *A.A. Sanosyan*[1], *V.D. Buchelnikov*[1], *M.E. Gruner*[2]

[1]Faculty of Physics, Chelyabinsk State University, Chelyabinsk, Russia
[2]Faculty of Physics, University of Duisburg-Essen, Duisburg, Germany
[*]E-mail: vsokolovsky84@mail.ru

The demand for permanent magnets for modern application technology is very high. Permanent magnets are used in the automating and robotics industry, and they constitute parts of electric vehicles, wind turbines, drives, and storage and magnetic cooling devices [1–3]. Nowadays, the most powerful commercial permanent magnets, such as $(Nd,Pr)_2Fe_{14}B$ and $Sm_2(Co,Cu,Fe,Zr)_{17}$, are based on rare-earth elements, which are comparatively scarce and expensive. Therefore the search for inexpensive rare-earth free permanent magnets consisting of abundant elements with similar performance is a central topic for modern materials science [1–3]. One of the most intensely discussed candidates is equiatomic FeNi [4] in the tetragonally ordered $L1_0$ structure (tetratenite). It is characterized by a large magnetocrystalline anisotropy energy (MAE) of ≈0.32–1.3 MJ/m^3 [4]. However, the pure $L1_0$-FeNi is found only in meteorites, and its synthesis under laboratory conditions would take geological order time. On the other side, FeNi compound is final point of Ni-excess Fe_2Ni-based Heusler alloys in accordance with a phase diagram. Therefore it is of interest to consider the parent compounds.

In the present work we focus on the stoichiometric and off-stoichiometric compositions $Fe_2Ni_{1+x}Z_{1-x}$ (Z = Al, Ga, In, Sn) with the framework of *ab initio* calculations. Ground state properties are calculated in the framework of density functional theory using the plane-wave basis set and the projector augmented wave (PAW) method as implemented in VASP [5]. The generalized gradient approximation (GGA) in the formulation of Perdew, Burke, and Ernzerhof (PBE) [6] is applied as exchange-correlation functional together with corresponding PAW potentials. The energy cut-off for the plane wave basis set were set to 750 eV. The Brillouin zone integration was performed with the 1st order Methfessel-Paxton method using uniform Monkhorst-Pack 15×15×15 k-point grid. We considered regular ($L2_1$) and inverse (XA) Heusler structures together with three types of layered atomic ordering, which are depicted in Fig. 1. Three new types of atomic ordering based on the inverse structure – tetragonal symmetry structures T^p, T^c, $T^\#$ – obtained by rearrangement of atom pairs according to the type of antisite defect. All these structures were modeled using the 16-atom supercells.

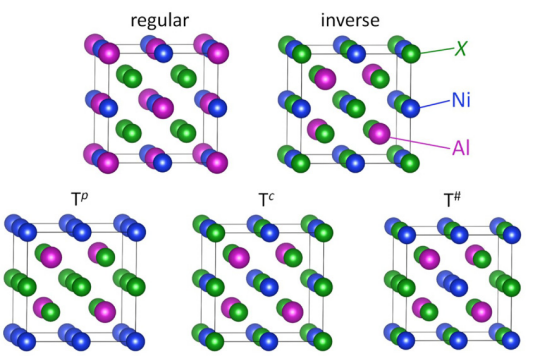

Figure 1. Types of crystal ordering considered for Fe_2NiZ (Z = Al, Ga, In, Sn). The full description of each structure can be found in [7].

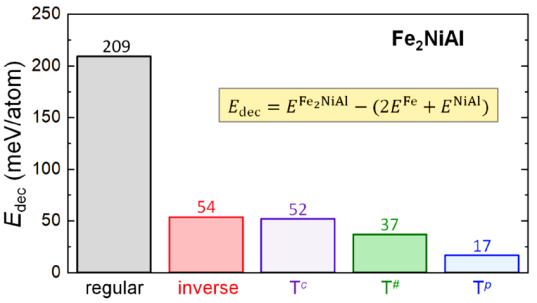

Figure 2. Decomposition energy E_{dec} for the stoichiometric Fe_2NiAl compound with different crystalline structures against the segregation into a dual phase mixture of Fe and NiAl.

For all these structures the dependences of the total energy and magnetic moments on the lattice parameter and the degree of tetragonal distortion are calculated. The possibility of martensitic transition in these alloys is determined. Equilibrium parameters are calculated for cubic and tetragonal lattices. For the favorable crystalline structures the MAE as a difference in the energies between the two directions of the spin magnetic moments is also calculated: $MAE = E_{tot}[100] - E_{tot}[001]$, where $E_{tot}[100]$ and $E_{tot}[001]$ are the total energies of the structure for the cases of orientation of magnetic moments [100] and [001]. Positive *MAE*-values indicate that anisotropy of the "easy axis" type is preferable (out-of-plane), while negative values indicate a preference for in-plane direction ("easy plane").

Stability of the considered alloys in relation to the decomposition into their constituent elements and stable binary and ternary compounds is evaluated by calculating the decomposition energy as the energy difference of the considered system and the corresponding stable compounds: $E_{dec} = E_{tot} - \Sigma E_i$, where i is the possible single-component, binary and ternary compounds. Negative values of E_{dec} indicate the stability of the compound, while positive values indicate that the system is disintegrating into the corresponding stable components.

Figure 2 illustrates the calculated E_{dec} for all considered structures of Fe_2NiAl. According to the phase stability estimation, the T^p structure reveals the most likely stability with respect to decomposition into a mixture of stable phases. As one can see from Fig. 2, this energy difference is about ten times smaller than for the regular Heusler structure and two times smaller than for the inverse Heusler structure, respectively, meaning that the layered T^p structure is significantly less prone to a decomposition into pure Fe and binary NiAl systems as compared to the other structures. Regarding the other compositions Fe_2NiZ (Z = Al, Ga, In, Sn), we received the similar tendency.

In general, we consider the fundamental understanding of the role of atomic arrangement in a crystalline structure in Heusler alloys and believe that the T^p structure in Fe_2NiZ could be interesting and promising candidates for systems exhibiting a large *MAE*, saturation magnetization, and high Curie temperature, suitable for a potential application in low-cost hard magnets.

Support by the Ministry of Science and Higher Education of the Russian Federation within the framework of the Russian State Assignment under Contract No. 075-01391-22-00 is acknowledged.

1. R. Skomski and J. Coey, Scr. Mater. **112**, 3–8 (2016).
2. K. Skokov and O. Gutfleisch, Scr. Mater. **154**, 289–294 (2018).
3. J. Coey, Engineering **6**, 119–131 (2020).
4. E. Poirier et al., J. Appl. Phys. **117**, 17E318 (2015).
5. G. Kresse and J. Furthmuller, Phys. Rev. B **54**, 11169 (1996).
6. J. Perdew, K. Burke, and M. Ernzerhof, Phys. Rev. Lett. **77**, 3865 (1996).
7. V.V. Sokolovskiy et al., Phys. Rev. Mater. **6**, 025402 (2022).

F.O5

FEATURES OF THERMAL EXPANSION IN SUBSTITUTION ALLOYS BASED ON HEAVY RARE-EARTH METALS $R^{I}_{1-x}R^{II}_{x}Fe_2$

Z.S. Umkhaeva[1,2*], *I.S. Tereshina*[3], *N.Y. Pankratov*[3], *I.M. Aliev*[1,2]

[1]Department of Material Science, CI RAS, Grozny, Russia
[2]Institute of Mathematics, Physics and Computer Science, the A.A. Kadyrov Chechen State University, Grozny, Russia
[3]Faculty of Physics, Lomonosov Moscow State University, Moscow, Russia
[*]E-mail: zargan.umhaeva@yandex.ru

Intermetallic compounds of rare-earth metals with RFe_2 stoichiometry are known to be in magnetically ordered state in a certain temperature range. These are the so-called Laves phases, which in compounds with light rare-earth elements (REE) are characterized by ferromagnetic ordering of spin magnetic moments, and in compounds with heavy rare-earth elements – ferrimagnetic ordering. The transition of intermetallic compounds to a magnetically ordered state is often accompanied by distortion-type structural phase transitions, which lead to change of certain features in the magnetic properties of alloys with the change in the temperature and anomalies in thermal expansion.

This paper presents the results of a study of thermal expansion and magnetostriction in substitutional alloys based on the known $TbFe_2$ compound: the $TbFe_2$ compound itself, the substitutional alloy $Tb_{0.8}Zr_{0.2}Fe_2$, in which 20% of the magnetically active atoms of the heavy rare earth element terbium are replaced by nonmagnetic zirconium atoms; $Tb_{0.8}Sm_{0.2}Fe_2$, in which a similar substitution of Tb atoms by weakly magnetic samarium Sm atoms was carried out. An alloy based on the heavy rare earth element gadolinium $Gd_{0.8}Sm_{0.2}Fe_2$ was also studied.

The choice of alloys was made considering the fact that the $TbFe_2$ compound is a ferrimagnet with a Curie temperature T_c = 711 K, while $ZrFe_2$ is a ferromagnet with T_c = 630 K. The spontaneous magnetic moment vectors in both compounds are oriented along the crystallographic direction [111]. Due to the "enormous" magnetostriction inherent in terbium atoms, the atomic crystal lattice of $TbFe_2$ has rhombohedral distortions up to room temperature. It was of interest to study the effect of the substitution of terbium atoms by nonmagnetic zirconium atoms in the $Tb_{0.8}Zr_{0.2}Fe_2$ alloy on the structural and magnetostrictive properties of $TbFe_2$, as well as on thermal expansion.

On the other hand, the $Tb_{0.8}Sm_{0.2}Fe_2$ alloy is interesting due to the fact that it contains two types of intersublattice exchange interactions Tb-Fe and Sm-Fe. The interactions are in the opposite directions. Therefore, the entire range of magnetic properties of the given alloy, including magnetostrictive properties, will be determined by the sign and magnitude of the dominant R-Fe interaction in a given temperature range.

The Gd element is the only one of the heavy rare earth elements that is in the S state and the effect of the crystal field on the element is negligible. Therefore, it is interesting to find out what is the cause of the significant magnetostrictive deformations in its alloys, in particular, in $Gd_{0.8}Sm_{0.2}Fe_2$. Accordingly, it is important to elucidate the effect of these deformations on the coefficient of thermal expansion of the alloy.

Phase analysis performed on DRON-3 ($TbFe_2$ и $Tb_{0.8}Zr_{0.2}Fe_2$) and Empyrean Panalytical ($Tb_{0.8}Sm_{0.2}Fe_2$ и $Gd_{0.8}Sm_{0.2}Fe_2$) X-ray diffractometers showed that the above compounds are single-phase. All compounds have a cubic Laves C15 phase structure. Measurements of the thermal expansion coefficient and magnetostriction were carried out by the tensometric method in the temperature range from 85 to 400 K.

In this range, anomalies of thermal expansion of the $TbFe_2$ and $Tb_{0.8}Zr_{0.2}Fe_2$ alloys are observed. The thermal expansion coefficient calculated from the experimental curves $\Delta l/l(T)$ turned out to be

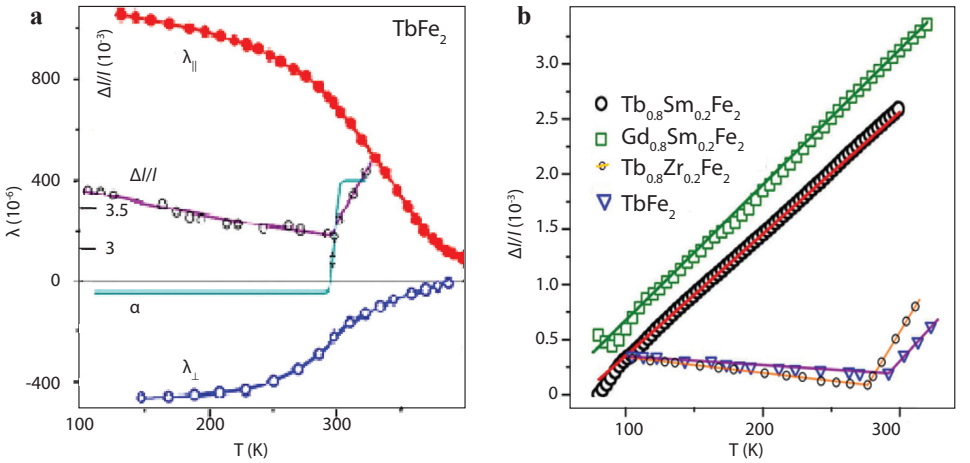

Figure 1. **a** Temperature dependence of longitudinal and transverse magnetostriction, thermal expansion and coefficient of thermal expansion of the compound $TbFe_2$. **b** Temperature dependence of thermal expansion of compounds $Sm_{0.2}Gd_{0.8}Fe_2$, $Sm_{0.2}Tb_{0.8}Fe_2$, $Tb_{0.8}Zr_{0.2}Fe_2$ и $TbFe_2$.

negative at temperatures below 293.4 and 262.8 K for $TbFe_2$ and $Tb_{0.8}Zr_{0.2}Fe_2$, respectively. To determine the nature of these anomalies, we measured the longitudinal and transverse magnetostriction. Magnetostriction, which reaches high values at low temperatures ($\approx 10^{-3}$), sharply decreases upon heating in the temperature range: from 280 to 330 K in $TbFe_2$, from 260 to 300 K in $Tb_{0.8}Zr_{0.2}FFe_2$ (Fig. 1a).

According to our data, the introduction of zirconium atoms into the rare-earth sublattice of $Tb_{0.8}Zr_{0.2}Fe_2$ is accompanied, on the one hand, by a decrease in rhombohedral distortions. On the other hand, as the temperature rises from nitrogen to room temperature, the spontaneous magnetostriction inherent in terbium atoms decreases, and the distortions of the crystal lattice caused by it decrease as well. At a temperature for which the coefficient of thermal expansion $\alpha = 0$, distortions are completely removed. Consequently, thermal expansion anomalies in these alloys are associated with the existence of a contribution to thermal expansion from spontaneous magnetostriction, which, superimposed on the phonon part of thermal expansion, overlaps the thermal expansion effect.

Figure 1b shows the thermal expansion of the $Tb_{0.8}Sm_{0.2}Fe_2$ sample (black dots). It can be seen that at low temperatures (at $T \approx 100$ K), an anomaly is observed in the $\Delta l/l(T)$ curves. As our studies show, this anomaly is associated with different temperature behavior of the magnetization of individual sublattices of the alloy (Fe, Tb, and Sm).

On the same figure the thermal expansion curve for the $Gd_{0.8}Sm_{0.2}Fe_2$ composition is shown (green curve). It shows two anomalies: in the region of 90 K the anomaly is clearly visible and a slightly noticeable anomaly at 180 K. According to the results obtained by us in the course of a comprehensive study of the magnetic and magnetostrictive properties of this alloy, the anomaly of the $\Delta l/l$ curve at high temperatures is most likely a spin-reorientation transition from the state [111] to the state [110], and the second anomaly in the low-temperature region is the rotation of the magnetic moment vector during the magnetization process near the transition boundary during spin reorientation.

This work was supported by a grant from Russian Science Foundation № 22-22-00313, https://rscf.ru/project/22-22-00313/.

NATURE OF THE FREQUENCY DEPENDENCE OF THE MAGNETOCALORIC EFFECT IN $Ni_{50}Mn_{28}Ga_{22-x}(Cu, Zn)_x$ (x = 0, 1.5) ALLOYS

A.G. Gamzatov[1*], *A.M. Aliev*[1], *Sh.K. Khizriev*[1], *A.G. Varzaneh*[2], *P. Kameli*[2], *I.A. Sarsari*[2]

[1]Amirkhanov Institute of Physics of DFRC of RAS, Makhachkala, Russia
[2]Department of Physics, Isfahan University of Technology, Isfahan, Iran
[*]E-mail: gamzatov_adler@mail.ru

Magnetic cooling based on the magnetocaloric effect (MCE) represents a promising energy-efficient and environmentally friendly alternative to traditional cooling. Recent studies show that the traditional requirements for magnetocaloric materials (large MCE values, convenient operating temperatures, and high cooling capacities) are insufficient conditions for identifying suitable materials for magnetic cooling technology. To them should be added such properties as the independence of the above parameters from the frequency of changes in the magnetic field, as well as temporary and mechanical stability under long-term cyclic exposure to a magnetic field. The prototypes of magnetic refrigerating machines created to date operate at relatively low frequencies (4–10 Hz), therefore, it is important to study the MCE depending on the frequency of the cyclic magnetic field. Until now, studies of the magnetocaloric properties of materials have been carried out at quasi-stationary fields, or at one-time cycles of changes in the magnetic field, or even estimated by indirect methods.

One of the brightest representatives of magnetocaloric materials is Heusler alloys, in which magnetic and magnetostructural phase transitions are observed. The paper presents the results of direct measurement MCE of the $Ni_{50}Mn_{28}Ga_{22-x}(Cu, Zn)_x$ (x = 0, 1.5) in cyclic magnetic fields 0.62 and 1.2 T with frequences up to 30 Hz. It is shown that the partial replacement of Ga atoms by Zn or Cu atoms leads to a convergence of magnetic and martensitic phase transition temperatures. Such convergence of the temperature of the martensite-austenite phase transition and the ferromagnetic transition leads to the coexistence of the AFM-FM phases.

Figure 1 shows the temperature dependences of the MCE in a cyclic magnetic field of 1.2 T at frequencies up to 20 Hz. As we can see, the partial replacement of gallium atoms by Cu and Zn atoms leads to a decrease in the effect. Also, such a substitution leads to a stronger frequency dependence of the MCE value. This is rather due to the fact that phase boundaries play an important role in dynamic processes. The substitution leads to an increase in the volume fraction of coexisting phases, and thus to an increase in the volume fraction of phase boundaries, which act as an additional channel of thermal relaxation.

The study was supported by the Russian Science Foundation grant No. 22-19-00610.

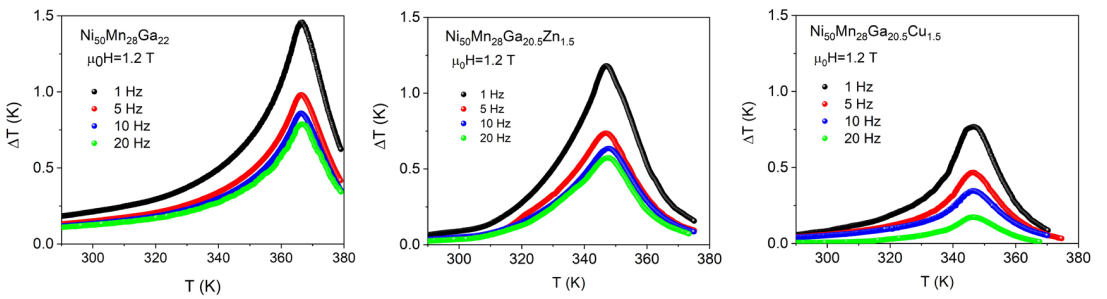

Figure 1. MCE in a cyclic magnetic field of 1.2 T for $Ni_{50}Mn_{28}Ga_{22-x}(Cu, Zn)_x$ (x = 0; 1.5).

MAGNETIC NANORADIOSENSITIZERS IN NEUTRON THERAPY FOR ONCOLOGY

V.I. Zverev

Dukhov Research Institute of Automatics (VNIIA), Moscow, Russia
E-mail: vizverev@vniia.ru

Magnetic hyperthermia using nanoparticles (MNP) is a clinically proven method of cancer treatment. MNPs could also be a promising target for combining hyperthermia with radiosensitization of the tumor. However, such applications of MNPs are poorly understood, and it is unclear what particle compositions can be relied upon. Therefore, the present work focuses on the search for materials that combine alternating magnetic field induced heating and the ability to increase the radiation dose associated with high atomic number. A theoretical evaluation of 24 promising compositions was carried out: values of the dose enhancement factor (DEF) for kilovoltage X-ray spectra were determined, and values of the specific absorption rate (SAR) were calculated for various combinations of elemental composition and particle size distribution. For alternating magnetic fields with an amplitude of 75–200 Oe and a frequency of 100 kHz, the maximum SAR values obtained ranged from 0.35 to 6000 W/g, and the DEF values for the studied compounds ranged from 1.07 to 1.59. Increasing the monodispersity of the MNPs led to an increase in SAR, which confirms the known experimental data. Four types of SAR dependences on the external magnetic field amplitude and the anisotropy constant were found for particles of different sizes. The most predictable SAR behavior corresponds to larger MNPs (~70-100 nm). Thus, based on these calculations, the following compositions $La_{0.75}Sr_{0.25}MnO_3$, Gd_5Si_4, $SmCo_5$, and $Fe_{50}Rh_{50}$ are the most promising for combining magnetic hyperthermia with radiation therapy. The greatest increase in dose is expected for surface radiotherapy.

The results of the work are important for the successful introduction of new equipment for combined radiation therapy into clinical practice. For this type of therapy with the use of heavy particles (in particular, neutrons), as well as to replace currently used nuclear reactors, cyclotrons *etc*. a compact, portable and powerful neutron generator NG-24 (weight 140 kg, dimensions 42×110 cm, nuetron flux 10^{11} n/s) has been manufactured in VNIIA.

ANOMALOUS ULTRASONIC ATTENUATION NEAR THE LOW-SPIN-HIGH-SPIN CROSSOVER IN $LuCO_3$

A.A. Tereshchenko[1*], *A.S. Ovchinnikov*[1,2]

[1]Institute of Natural Science and Mathematics, Ural Federal University, Ekaterinburg, Russia
[2]Institute of Metal Physics, Ural Division, Russian Academy of Sciences, Ekaterinburg, Russia
[*]E-mail: alexey.tereshchenko@urfu.ru

Recent studies of the binary intermetallic compound $LuCo_3$ in superstrong magnetic fields (up to 60 T) have revealed a sharp jump in the field dependence of the magnetization in the region of ~50 T, which is associated with a change in the state of cobalt from a low-spin state to a high-spin state [1]. It is widely known that magnetic phase transitions are easily detected by ultrasonic methods for studying magnetic materials, based on measurements of the velocity and attenuation coefficient of ultrasound [2]. Traditionally, sound waves are used either for temperature magnetic phase transitions, for example, near the Curie or Neel temperature, or for spin-reorientation phase transitions that occur under the influence of an external magnetic field (usually less than 1 T in magnitude). To our best knowledge, the situation of the low-spin-high-spin crossover found in $LuCo_3$ has not yet been discussed.

The Ising ferromagnet $LuCo_3$ contains 9 formula units in each elementary cell. To model elastic and magnetic subsystems, one may consider a model lattice formed by $LuCo_3$ translation vectors, and assign values of the mass and the magnetic moment of the whole elementary cell to each of the nodes. To describe interaction of the sound waves with magnetic ions the Waller mechanism is used [3], when the sound wave modulates a distance between two magnetic ions. The propagation of ultrasound in a specimen is described with aid of the linear response theory [4] and the Green's functions formalism [5].

This approach makes it possible to obtain an equation for the ultrasound wave vector **k** and an expression for calculating the ultrasound attenuation coefficient α

$$\omega_e^2 \approx \omega_s^2(k) + 2\omega_s(k)\Pi'_{ret}(k_s,\omega_e) \ ,$$

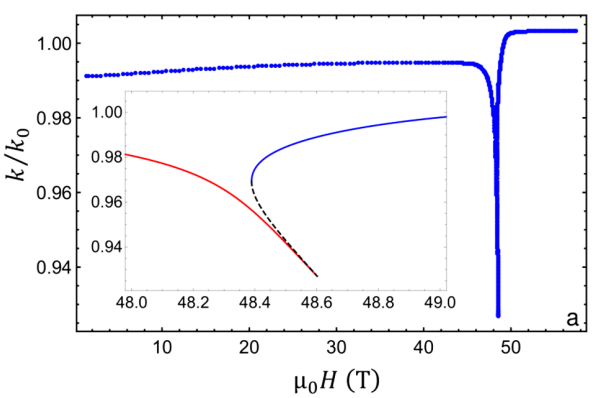

Figure 1. Wave vector of the propagating ultrasound mode measured in k_0 units as a function of the magnetic field directed along the [100]-axis of $LuCO_3$. The $k(H)$ behavior near the low-spin-high-spin crossover are zoomed in insets. The wave vector $k_0 = 42.059 \cdot 10^3$ m^{-1}.

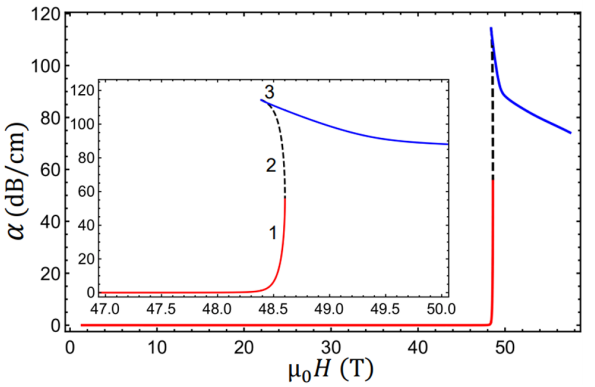

Figure 2. Attenuation coefficient α with respect to the magnetic field for the ultrasonic wave propagating along the [100]-axis. Inset: attenuation becomes multivalued near the the low-spin-high spin crossover with three branches: 1 (red solid), 2 (black dashed) and 3 (blue solid).

$$\alpha(k_s,\omega_e) \approx -\Pi''_{ret}(k_s,\omega_e)/v_s\ ,$$

where ω_e – experiment frequency, $\omega_s(k)$ – spectrum of noninteracting phonons, v_s – speed of sound corresponding to mode s, Π'_{ret} and Π''_{ret} – real and imaginary parts of the polarization operator due to the interaction between phonons and magnons. Numerical analysis of these equations enables to obtain dependences of the ultrasound wave vector (Fig. 1) and the ultrasound attenuation coefficient (Fig. 2) on the applied magnetic field. There are two regimes of ultrasound propagation: off-resonant and resonant ones. The first regime is realized in small magnetic fields and exhibits almost no ultrasound attenuation due to lack of direct magnon-phonon collisions. The second one corresponds to high fields and characterized by appreciable increase of ultrasound attenuation due to magnon-phonon scattering processes with a loss of phonon energy. In vicinity of the low-spin-high-spin crossover, there is a change of these two regimes with an intermediate region, where multi-channel ultrasound propagation occurs. In the magnetic transition region, the wave vector exhibits a sharp dip with a simultaneous increase of the attenuation coefficient.

The work was supported by the Foundation for the Advancement of Theoretical Physics and Mathematics "BASIS".

1. D.S. Neznakhin, D.I. Radzivonchik, D.I. Gorbunov, A.V. Andreev, J. Sebek, A.V. Lukoyanov, and M.I. Bartashevich, Phys. Rev. B **101**, 224432 (2020).
2. A.E. Petrova and S.M. Stishov, Phys. Rev. B **91**, 214402 (2015).
3. B. Luthi, Physical Acoustics in the Solid States. Springer-Berlin (2007).
4. P.C. Kwok, Green's Function Method in Lattice Dynamics, in Solid State Physics, vol. 20, edited by F. Seitz and D. Turnbull. Academic Press, New York (1968).
5. G. Mahan, Many-Particle Physics. Plenum, New York (1990).

MNAS COMPOUNDS UNDER HIGH PULSED MAGNETIC FIELDS UP TO 500 KOE

A. Kamantsev[1*], *Yu. Koshkidko*[1,2], *V. Koledov*[1], *V. Shavrov*[1], *A. Golovchan*[3], *A. Sivachenko*[3], *B. Todris*[3], *V. Valkov*[3], *L. Butvina*[4]

[1]Kotelnikov Institute of Radioengineering and Electronics RAS, Moscow, Russia
[2]Institute of Low Temperature and Structure Research of PAS, Wrocław, Poland
[3]Donetsk Institute for Physics and Engineering named after A.A. Galkin, Donetsk, DPR
[4]Prokhorov General Physics Institute of RAS, Dianov Fiber Optics Research Center, Moscow, Russia
[*]E-mail: kama@cplire.ru

We present the results of a systematic study of a series of MnAs samples under high pulsed magnetic fields up to 500 kOe. MnAs as a compound has attracted the interest of researchers over the years. It is relatively inexpensive and offers high magnitude of magnetocaloric effect (MCE). It is recognized as a promising candidate for the working body of the magnetic refrigerator [1].

The MCE ΔT-effect in the MnAs-based composite sample was measured using a microthermocouple in a pulsed magnetic field of 40 kOe with successive heating of the sample to 311.5–329.5 K and successive cooling of 328.2–306 K. The maximum values of the ΔT-effect were: ΔT = 6.2 K at T_0 = 318.4 K during heating, and ΔT = 9.2 K at T_0 = 314 K during cooling. In higher pulsed magnetic fields, the experiments were carried out with thermal cycling – preliminary heating of the sample to 350 K and cooling to the desired initial temperature. With this measurement protocol, the maximum values of the ΔT-effect were:
ΔT = 12.5 K at T_0 = 311.9 K in the field H = 100 kOe;
ΔT = 16.4 K at T_0 = 312.9 K in the field H = 200 kOe;
ΔT = 17.6 K at T_0 = 313.6 K in the field H = 300 kOe.

The MCE values obtained for MnAs-based composite in pulsed fields of 100–300 kOe are comparable with the results obtained in single-crystal MnAs in a steady magnetic field H = 100 kOe [1]: ΔT = 15 K at T_0 = 311 K.

We show that whole magnetoinduced magnetostructural phase transition can be finished under 100 kOe magnetic field. The kinetics of phase transition and the value of magnetocaloric effect strongly depend on the composition of the sample. The use of the optical research methods gives more reliable results than the contact methods of temperature measurement [2].

Support by RSF is acknowledged by project № 22-29-01201.

1. Yu.S. Koshkid'ko et al., J. Alloy Compd. **798**, 810 (2019).
2. A.P. Kamantsev et al., Chelyabinsk Physical and Mathematical Journal **5**(4) 537 (2020).

ELECTRONIC STRUCTURE AND EXCHANGE INTERACTIONS IN $LaFe_{13}$-BASED ALLOYS

A.P. Kamantsev[1], *O.E. Kovalev*[1,2], *A.P. Sivachenko*[1,2], *A.V. Golovchan*[1,2*]

[1]Kotelnikov Institute of Radioengineering and Electronics of RAS, Moscow, Russia
[2]Donetsk Institute for Physics and Technology named after A.A. Galkin, Donetsk, DPR
[*]E-mail: golovchan1@yandex.ru

Recently, the magnetic refrigeration technology which is based on the magnetocaloric effect of the magnetic solids has been considered as one of the most promising alternative methods to our present well used gas compression/expansion technology due to its high efficiency [1, 2]. The $LaFe_{13-x}Si_x$ system has been widely investigated in recent years because of the giant magnetocaloric effect that was observed for compositions $1.0 \leq x \leq 1.8$ [1, 2]. A potential application of materials exhibiting a gigantic magnetocaloric effect is magnetic refrigeration – a technology that has the prospect of replacing conventional gas compressor refrigerators due to higher efficiency and environmental sustainability [3].

In the presented work, an *ab initio* calculation of the electronic structure and an estimation of the parameters of interatomic exchange interactions were performed using the fully-relativistic SPR-KKR package v.8.6 [4, 5] for selected $LaFe_{13-x}Si_x$ alloys (Table 1). The VWN exchange-correlation energy density functional was used [6]. For the crystal potential, the atomic sphere approximation was used. The $LaFe_{13-x}Si_x$ alloys have the $NaZn_{13}$-type cubic crystal structure (space group $Fm\bar{3}c$) [7], Fe atoms occupy two nonequivalent sites, that is, $8b(Fe_I)$ and $96i(Fe_{II})$, respectively. The Fe_I atom is surrounded by an icosahedron with 12 Fe_{II} atoms, and the Fe_{II} atom has one Fe_I atom and nine Fe_{II} atoms as the nearest neighbors. According to thermodynamic theory, the Si atoms tend to occupy the Fe_{II} sites to stabilize the crystal structure [7]. The lanthanum atoms occupy $8a$ positions. The crystal lattice parameters are taken from [7] (a = 11.461 Å, y = 0.179, z = 0.1168). The interatomic exchange integrals were calculated by the method [8], based on the calculation of the second derivative of the total energy functional from the deviations of the selected pair of spins from equilibrium.

The typical dependence of the basic exchange integrals on the interatomic distance for $LaFe_{11.5}Si_{1.5}$ are shown on left side of Fig. 1. As can be seen from the figure, the exchange integrals decrease quite rapidly with increasing interatomic distance and do not exceed 1 meV already at a distance of $0.5a$. The most significant is the exchange interactions between Fe_{II} atoms, which form a regular icosahedron around Fe_I (~18 meV). The Fe_{II}-Fe_I interaction (between the shell of the icosahedron

Table 1. Dependence of the main exchange integrals on the Si-content (J_{ij} in meV).

Exchange type	Fe_{II}-Fe_{II}	Fe_I-Fe_{II}	Fe_{II}-Fe_{II}	Fe_{II}-Fe_{II}	Fe_{II}-Fe_{II}	La-Fe_{II}	Fe_{II}-Fe_{II}	Fe_I-Fe_{II}
R_{ij}/a	0.213	0.214	0.218	0.223	0.234	0.292	0.302	0.342
$LaFe_{13}$	20.3	6.5	22.9	20.2	7	1.8	–1.6	4
$LaFe_{12}Si$	16.8	5.6	19.1	15	4.5	0.5	0.5	3.2
$LaFe_{11.8}Si_{1.2}$	17.0	5.8	18.5	14.8	4.1	0.5	0.9	3.1
$LaFe_{11.5}Si_{1.5}$	17.1	6	18	14.4	3.9	0.5	1.3	3
$LaFe_{11}Si_2$	17.9	6.1	16.9	13.6	3.5	0.5	2	2.5
$LaFe_{10}Si_3$	18.6	6.5	15.6	12.5	2.6	0.4	2.5	1.6

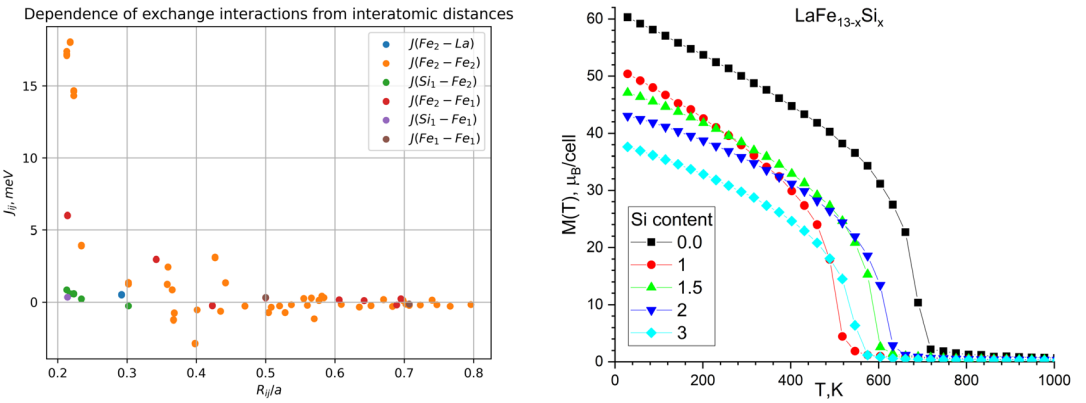

Figure 1. Isotropic exchange interactions for $LaFe_{11.5}Si_{1.5}$ (left) and obtained from Monte-Carlo simulation temperature dependence of magnetization for selected $LaFe_{13-x}Si_x$ alloys (right).

and its center) is approximately three times less (~6 meV). Increasing the silicon concentration in the range x = 0–3 leads to a decrease in J_{ij} (Table 1).

Based on the calculated exchange integrals in the framework of the classical Heisenberg model, the Monte Carlo method was used to calculate the temperature dependences of the magnetization and evaluate the effect of silicon on the Curie temperature of the alloys under study (Fig. 1, right). The obtained results are in qualitative agreement with the experimental data. According to the analysis carried out according to the Bertaut method [9], the ground magnetic state in all alloys is ferromagnetic (Fig. 2).

Support by RSF (grant № 22-29-01201) is acknowledged.

1. A.M. Tishin, Handb. Magn. Mater. **12**, 395–524 (1999).
2. L. Li, M. Yan, J. Alloys and Comp. **823**, 153810 (2020).
3. S. Fujieda, A. Fujita, K. Fukamichi, Appl. Phys. Lett. **81**, 1276–1278 (2002).
4. The Munich SPR-KKR package, version 8.6, H. Ebert et al, https://www.ebert.cup.uni-muenchen.de/sprkkr.
5. H. Ebert, D. Kodderitzsch, J. Minar, Rep. Prog. Phys. **74**, 096501 (2011).
6. S.H. Vosko, L. Wilk, Phys. Rev. B **22**, 3812 (1980).
7. X.B. Liu, Z. Altounian, D.H. Ryan, J. Phys. Cond. Matt. **15**, 7385–7394 (2003).
8. A.I. Liechtenstein, M.I. Katsnelson et.al, JMMM **67**, 65 (1987).
9. E.F. Bertaut, C.R. Acad. Sc. Paris, B **277**, 583 (1999).

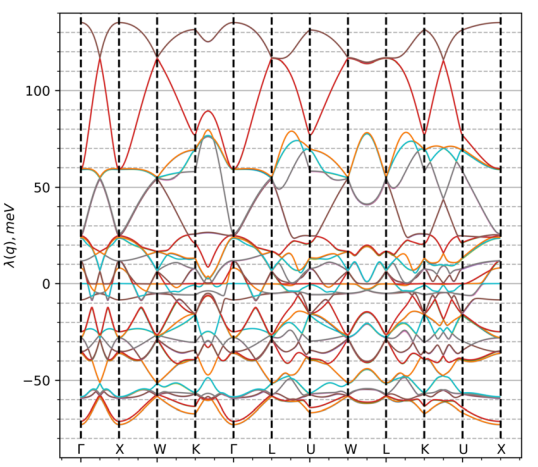

Figure 2. Dispersion of Bertaut exchange matrix eigenvalues for $LaFe_{11.5}Si_{1.5}$.

WEAK FERROMAGNETISM IN SUBMICRON BARIUM TITANATE

L.N. Korotkov[1*], *N.A. Tolstykh*[1], *R.M. Eremina*[2], *N.A. Emelyanov*[3], *R.G. Batulin*[4]

[1]Voronezh State Technical University, Voronezh, Russia
[2]Zavoisky Physical-Technical Institute, FRC Kazan Scientific Center of RAS, Kazan, Russia
[3]Institute for Problems of Chemical Physics, Russian Academy of Sciences, Chernogolovka, Russia
[4]Institute of Physics, Kazan Federal University, Kazan, Russia.
[*]E-mail: l_korotkov@mail.ru

Barium titanate ($BaTiO_3$) is a well-known ferroelectric of the perovskite family. The electronic structure of barium titanate [$Ba^{2+}(6s^0)$, $Ti^{4+}(3d^0)$, $O^{2-}(2s^22p^6)$] is characterized by zero magnetic moment. At the same time, weak ferromagnetism is observed in submicron $BaTiO_3$ particles. It is believed that a high concentration of oxygen atoms vacancies, localized on the surface of particles, leads to the appearance of magnetic ordering, owing to of decrease of titanium cations oxidation from Ti^{4+} to Ti^{3+}. The Ti^{3+} ions have uncompensated spins that interact with each other at a sufficiently high concentration, which can eventually lead to their ferromagnetic ordering.

The purpose of this work is to discuss the experimental data obtained in the course of studying the magnetic properties of nanostructured $BaTiO_3$ subjected to heat treatment under various conditions.

For the experiments, we used ultrafine commercial barium titanate powders and powders obtained by grinding of preliminarily synthesized materials in a planetary mill. The particle sizes varied within d = 50–400 nm. The pressed samples were subjected to thermal annealing at various temperatures in oxidizing, reducing, and inert atmospheres. Typical magnetic hysteresis loops $M(H)$ obtained during the experiment are shown in the Fig. 1.

Analysis of experimental data, in particular, showed:

(1). The saturation magnetization of nanocrystalline $BaTiO_3$ depends on its thermal prehistory. Thermal annealing at temperatures below 700 °C in an atmosphere of H_2 or Ar leads to a noticeable increase in the saturation magnetization M_s.

(2). The saturation magnetization of the material is approximately ~1/d, where d is the average crystallite diameter. This shows that the magnetization M_s is proportional to the total surface area of the grains in the sample.

(3). An increase in the concentration of oxygen vacancies during prolonged annealing in hydrogen leads to a noticeable increase in the diamagnetic response and a decrease in the magnetization M_s.

(4). An increase in the sintering temperature of $BaTiO_3$ nanocrystalline samples in an oxidizing atmosphere causes a decrease in both ferromagnetic and diamagnetic responses due to an increase in the crystallite size and a decrease in the concentration of lattice defects.

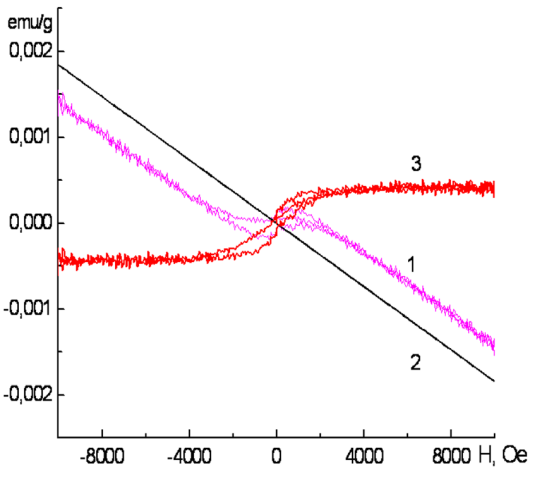

Figure 1. Dependences of $M(H)$ for nanocrystalline $BaTiO_3$ ($d \approx 120$ nm): 1 – initial curve, 2 – diamagnetic response, 3 – ferromagnetic component of magnetization.

MAGNETOCALORIC PROPERTIES OF FeRh ALLOY UNDER MAGNETIC FIELD AND THERMAL CYCLING

*A.M. Aliev**, *A.G. Gamzatov, G.M. Aliev, L.G. Khanov*

Amirkhanov Institute of Physics of Dagestan Federal Research Center RAS, Makhachkala, Russia
*E-mail: lowtemp@mail.ru

Refrigerating machines are devices with periodic sweeps of cycles, so there is a substantial need to study the magnetocaloric properties of materials under repeated cyclic exposures to magnetic fields. Magnetocaloric properties of the materials under single and repeated application of the cyclic magnetic fields can exhibit significantly different behavior for a variety of reasons. Furthermore, the magnetocaloric properties of materials with a magnetostructural phase transition in cyclic fields can degrade over time. Obviously, practical applications require materials with time-stable magnetocaloric properties.

In this work, we present results of studying the magnetocaloric properties in FeRh alloy under magnetic field and temperature cycling. We have previously established that cycling in magnetic fields can lead to the degradation of the magnetocaloric properties of some magnetic materials [1, 2]. In this work, we present the results of the influence on the magnetocaloric properties not only of a cyclic magnetic field but also of thermal cycling. During thermal cycling, the samples were rapidly heated and cooled in the region of magnetostructural phase transitions. It has been found that thermal cycling in the FeRh alloy results in a significant decrease in the MCE, as well as a shift in the temperature of the magnetostructural phase transition.

It is shown that both in the case of thermal and magnetic cycling, the initial properties of the material can be restored after the material is overheated above the Curie temperature. This indicates the same degradation mechanism in both cases. Various possible mechanisms of degradation of the magnetocaloric properties of materials are presented.

The reported study was funded by RFBR and NSFC, project number 21-58-53046.

1. A.M. Aliev, A.B. Batdalov, L.N. Khanov et al., Appl. Phys. Lett. **109**, 202407 (2016).
2. A.M. Aliev, A.B. Batdalov, L.N. Khanov et al., Phys. Solid State **62**, 837–840 (2020).

MAGNETOELASTICITY OF THE JAHN-TELLER SUB-SYSTEM IN THE CHROMIUM-DOPED II-IV CRYSTALS

M.N. Sarychev[1], *I.V. Zhevstovskikh*[1,2], *Yu.V. Korostelin*[3], *V.T. Surikov*[4], *N.S. Averkiev*[5], *V.V. Gudkov*[1*]

[1]Institute of Physics and Technology, Ural Federal University, Ekaterinburg, Russia
[2]M.N. Miheev Institute of Metal Physics, Ural Branch, RAS, Ekaterinburg, Russia
[3]P.N. Lebedev Physical Institute, RAS, Moscow, Russia
[4]Institute of Solid State Chemistry, Ural Branch, RAS, Ekaterinburg, Russia
[5]Ioffe Institute, RAS, St. Petersburg, Russia
[*]E-mail: v.v.gudkov@urfu.ru

Ultrasonic experiments proved to be a very informative tool for investigating the properties of the Jahn-Teller (JT) complexes in doped crystals. They make it possible to determine the symmetry properties of the global minima and saddle points (the energy barriers) of adiabatic potential energy surface (APES) and to study the dynamic properties of the JT sub-system (i.e., relaxation time and the mechanisms which define its temperature dependence) (see, e.g., [1] and references therein). Much less papers were devoted to influence of magnetic field on the manifestation of the JT effect (JTE) in an ultrasonic experiment or, in other words, to magneto-elasticity of the JT-sub-system [2]. Among II-IV doped crystals, to our best knowledge, a detailed study in this field has been done only on ZnSe:Cr^{2+} [3] with magnetic induction vector and wave vector parallel to the binary crystallographic axis: **k**||**B**||[110]. ZnSe is sphalerite-type crystal and the Cr^{2+} ion substitutes Zn^{2+} in tetrahedral coordination. It has $^2T_5(e^2t^2)$ high-spin ground state and subject to the $T \otimes (e + t_2)$ JTE problem [4] revealing tetragonal deformation of the cube in which the tetrahedral JT-complex is inserted. In [5], it was shown that magnetic field effects on the elastic modulus: it transforms isothermal modulus to the modulus defined at constant temperature T and constant magnetic induction B (i.e., $c_{ij}^{B,T}$), whereas the relaxation time also becomes a magnetic-field-dependent one. Here we present the results of magnetoacoustic investigation (i) of ZnSe:Cr^{2+} single crystals with another magnetic field direction **B**||[001] and the same $(c_{11} - c_{12})/2$ normal mode and (ii) of one more crystal, namely CdSe:Cr^{2+}, in which we found influence of magnetic field on c_{55} mode when **B**||[10$\bar{1}$0] and on c_{66} mode when **B**||[1000]. CdSe is a wurtzite-type crystal and Cr^{2+} ion has the same ground state and coordination as in ZnSe:Cr^{2+}, moreover, the JTE problem and the symmetry properties of the global minima and saddle points are also similar [5].

The studied crystals were grown in P.N. Lebedev Physical Institute RAS and had concentrations of the dopand $n = 3.8 \cdot 10^{18}$ cm^{-1} (in ZnSe) and $n = 1.4 \cdot 10^{18}$ cm^{-1} (in CdSe). Ultrasonic experiments were done at the Dresden High Magnetic Field Laboratory (HLD-EMFL), Helmholtz-Centrum Dresden-Rossendorf with the use of a phase-sensitive detection technique at low temperature (1.4 K). The measured variation of attenuation $\Delta\alpha(B)$ and phase velocity $\Delta v(B)/v_0$ represent the magnetic field dependences of the imaginary and real parts of dynamic (frequency dependent) elastic modulus: $\Delta\alpha(B)/k_0 = (1/2)\mathrm{Im}(\Delta c(B)/c_0)$ and $\Delta v(B)/v_0 = (1/2)\mathrm{Re}(\Delta c(B)/c_0)$, the wave number being defined as $k = \omega/v - i\alpha$, ω is the circular frequency of the wave. The variables with the subscript 0 are the reference values defined at $B = 0$. Figure 1 shows the examples of the experimental curves obtained on CdSe:Cr^{2+} crystal for the c_{66} normal mode (**k**||**B**||[10$\bar{1}$0], wave polarization along [$\bar{1}$2$\bar{1}$0]) at $\omega/2\pi = 31.5$ MHz and $T = 1.5$ K. The curves given in Fig. 1 have some common features with obtained earlier on ZnSe:Cr for the $(c_{11} - c_{12})/2$ mode, **k**||**B**||[110] [3]: they have attenuation peak in lower fields and increase in higher the magnetic fields. Both attenuation and velocity do not exhibit saturation in high fields. On the contrary, the dependences obtained for the $(c_{11} - c_{12})/2$ mode at

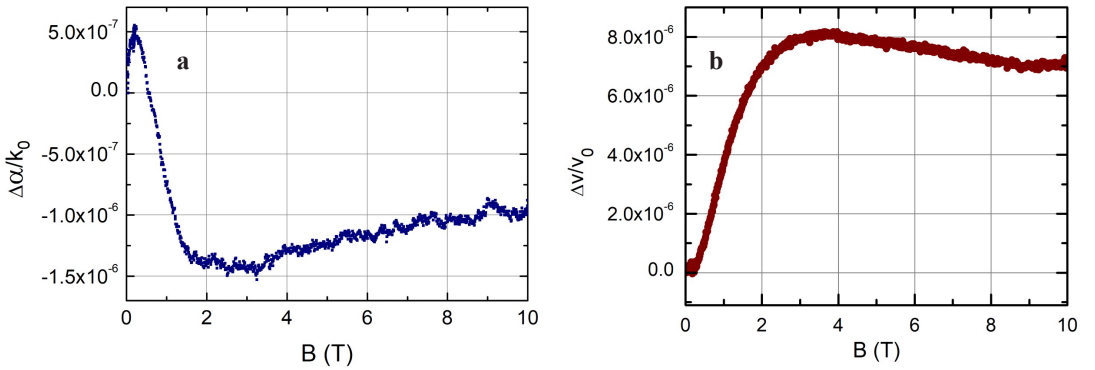

Figure 1. Magnetic field dependences of attenuation (**a**) and phase velocity (**b**) of the c_{66} ultrasonic normal mode in CdSe:Cr crystal. **B**||**k**||[10$\bar{1}$0], frequency 31.5 MHz, T = 1.5 K.

k||110], **B**||[001] in ZnSe:Cr and for c_{66} mode at **B**||[1000] revealed asymptotic behavior and tended to constant values in high magnetic fields.

This result was unexpected since the JT-complexes in both the crystals are tetrahedral ones and both have tetragonal JT-deformation, however, their position with respect to crystallographic axes are very different. All the edges of the cube associated with the JT-complex in ZnSe crystal are parallel to the cubic crystalline axes while in CdSe no one edge of the cube associated with the JT-complex is parallel to any crystalline axis of high symmetry. The second principal question that should be answered is: why in the II-IV crystals doped with Cr^{2+} ions we do observe magneto-elasticity, whereas in the fluorite-type crystals (SrF_2, CaF_2) even with higher concentration of Cr^{2+} ions we do not observe it, in spite of many common features such as orbital ground state and cubic coordination of the JT ion which is described like tetrahedral one.

Support by RSF (project № 22-22-00735) is acknowledged.

1. M.N. Sarychev et al., J. Phys.: Condens. Matter **34**, 225401 (2022).
2. K. Lasmann and Hp. Schad, Sol. State Commun **18**, 449–452 (1976).
3. N.S. Averkiev et al., Phys. Rev. B **96**, 094431 (2017).
4. V.V. Gudkov et al., J. Phys.: Condens. Matter **23**, 115401 (2011).
5. V.V. Gudkov et al., Phys. Stat. Sol. A 1800589, (2018).
6. N.S. Averkiev et al., J. Exp. Theor. Phys. **129**, 87–97 (2019).

MAGNETOELECTRIC EFFECT IN LAMINATED COMPOSITES $CoFe_2O_4$/PZT. DEPENDENCE ON THICKNESS OF MAGNETOSTRICTION PHASE

*V.A. Astakhov**, *A.T. Morchenko, V.G. Kostishyn*

NUST MISIS, Moscow, Russian Federation
*E-mail: astakhov-of@mail.ru, dratm@mail.ru

The magnetoelectric effect (MEE) has been actively attracting the close attention of scientists over the past 30 years [1]. The field of application of such materials, both single-phase and composite, with a pronounced MEE extends from classical magnetic field sensors with impressive sensitivity indicators to biomedical fields [2–6].

The investigated magnetoelectric materials are mainly represented by class 2-2 structures (layered structures) due to the greater effect magnitude than composites of 0-3 class (particles in a matrix) and greater ease of fabrication than composites of 1-3 class (rods in a matrix). Glues are usually used to join the magneto- and electroactive phases of samples with layer thicknesses of 50 μm or more, although hot pressing can be used in the case of usage organic piezoelectrics. The use of soldering in production of layered composites for joining ceramics looks more promising due to the electrical conductivity and in an order of magnitude higher elastic modulus of solders, in contrast to glues, which theoretically makes it possible to reduce losses due to the transfer of mechanical deformations between active phases.

Measurements of the magnetoelectric effect were carried out at the installation consisting of an electromagnet FL-1 with a power supply, a measuring cell, a lock-in voltmeter with generator Stanford Research Systems SR830, an low-frequency amplifier, and an AKIP-2403 AC voltmeter. The magnetostriction of cobalt ferrite was measured using BF-350AA strain gauges on a setup consisting of the same electromagnet FL-1 with a power supply, a G3-111 LF Generator, and an Unipan 237 selective nanovoltmeter. The magnetostriction measurements were calibrated using the nickel reference.

The samples were represent by soldered ceramic disks with 9.2 mm diameter and different thickness. The piezoelectric phase is represented by disks of lead zirconate-titanate of PZT-42 mark (JSC Research Institute "Elpa", Zelenograd) 0.39 mm thick with deposited copper electrodes with 8 mm in diameter on two surfaces. Polarization of the piezoceramics was carried out after the soldering process. M613CA polycrystalline ferrites (Kuznetsk factory of devices and ferrites, Kuznetsk) were grinding and polished up to 12 surface cleanliness grade, then copper (with chromium underlayer) covered by vacuum-thermal method. The thickness of the ferrite disks amounted 0.2; 0.3; 0.4; 0.5; 0.7; 1 mm. Soldering process was carried out in an oven at a temperature about 200 °C, the thickness of the solder layer was 0.025-0.04 mm.

The features of the influence of the soldering process on the magnetoelectric coefficient of composites are studied. It has been demonstrated that the magnetoelectric coefficient of 3-layer composites is significantly higher than that of 2-layer ones.

1. X. Liang et al., IEEE Trans. Magn. **57**(8), 1–57 (2021), doi: 10.1109/TMAG.2021.3086635.
2. J.F. Scott, J. Mater. Chem. **22**. 4567–4574 (2012).
3. A.P. Pyatakov, A.K. Zvezdin, Physics-Uspekhi **55**(6), 557–581 (2012) doi: 10.3367/UFNr.0182.201206b.0593.
4. M. Fiebig, J. Phys. D: Appl. Phys. **38**, 123–152 (2005).
5. J. Gao et al., "Review of Magnetoelectric" Sensors. Actuators **10**(6), 109. (2021) https://doi.org/10.3390/act10060109.
6. N.A.Spaldin et al., Nature Mater. **18**, 203–212 (2019). https://doi.org/10.1038/s41563-018-0275-2.

MAGNETIC GLASSINESS AND CRYSTAL FIELD EFFECTS ON THERMAL AND ELECTRICAL PROPERTIES OF Er_5Pd_2-TYPE COMPOUNDS

A.A. Vaulin[1], *E.A. Sherstobitova*[1], *D.A. Shishkin*[1,2], *E.M. Sherokalova*[2], *N.V. Baranov*[1,2], *A.F. Gubkin*[1,2*]

[1]M.N. Mikheev Institute of Metal Physics, UB RAS, Ekaterinburg, Russia
[2]Institute of Natural Sciences and Mathematics, Ural Federal University, Ekaterinburg, Russia
[*]E-mail: agubkin@imp.uran.ru

Binary R_5Pd_2 (R = Tb, Dy, Ho, Er) compounds are known to exhibit absence of the long-range magnetic order while the short-range antiferromagnetic correlations gradually enhance on cooling until a cluster-glass magnetic state emerges at low temperatures [1, 2]. Some of the members of R_5Pd_2 family (R = Ho, Er) meet the criteria for large magnetic heat capacity at the low temperature range formulated by K.A. Gschneidner et al. [3]. However, there is no detailed study of the heat capacity of Er_5Pd_2 in the literature. In this work, we present a detailed study of the thermal expansion, heat capacity and electrical resistivity of the $Er_{4.8}Pd_2$ cluster-glass compound in external magnetic fields up to 140 kOe.

The thermal expansion rate $\Delta l/l_0$ and the coefficients of linear thermal expansion (CTE) α plotted as a functions of temperature are shown in Fig. 1a for both $Er_{4.8}Pd_2$ and $Lu_{4.8}Pd_2$. An excess contribution to the volumetric CTE $\Delta\beta(T)$ of $Er_{4.8}Pd_2$ has been obtained by subtraction of the $\beta(T)$ curves obtained for the cluster-glass $Er_{4.8}Pd_2$ and paramagnetic isostructural compound $Lu_{4.8}Pd_2$ (see Fig. 1b). This contribution arises when the magnetic order associated with exchange interactions affects the lattice below the temperature of a magnetic phase transition and when the crystal electric field (CEF) lifts the degeneracy of the multiplet of Er^{3+} ion (Shottky effect). Approximating of the $\Delta\beta(T)$ curve in the high temperature range above 25 K with equation for Shottky effect [4], we obtained good description of the experimental data for the following CEF scheme: $\delta_1(\Gamma_6) = 0$, $\delta_2(\Gamma_8^1) = 42$ K, $\delta_3(\Gamma_7) = 94$ K, $\delta_4(\Gamma_8^2) = 163$ K and $\delta_5(\Gamma_8^3) = 281$ K, where Γ_6 and Γ_7 are doublets and Γ_8^1, Γ_8^2, Γ_8^3 are quartets (see the insert in Fig. 1b).

The temperature dependence of the heat capacity $C_p(T)$ measured for $Er_{4.8}Pd_2$ and paramagnetic isostructural compound $Lu_{4.8}Pd_2$ in a wide temperature range 1.8–200 K are shown in Fig. 1c. The excess contribution ΔC_p to the total heat capacity of magnetic compound $Er_{4.8}Pd_2$ has been obtained using a simple subtraction of $C_p(T)$-curves for cluster-glass $Er_{4.8}Pd_2$ and paramagnetic isostructural $Lu_{4.8}Pd_2$ compounds. Again, the excess contribution ΔC_p consists of Shottky-type component and a broad anomaly associated with cluster-glass magnetic state in $Er_{4.8}Pd_2$. Approximating of the $\Delta\beta(T)$ curve in the high temperature range above 25 K with equation for Shottky effect [5] almost the same CEF scheme has been obtained: $\delta_1(\Gamma_6) = 0$, $\delta_2(\Gamma_8^1) = 51$ K, $\delta_3(\Gamma_7) = 112$ K, $\delta_4(\Gamma_8^2) = 160$ K and $\delta_5(\Gamma_8^3) = 249$ K (see Fig. 1d). Subtracting Shottky component from the excess contribution $\Delta C_p/T$, we were able to extract pure magnetic contribution to the total heat capacity of $Er_{4.8}Pd_2$ and integrate it in order to estimate magnetic entropy associated with the cluster-glass magnetic state. It can be seen from Fig. 1e that the magnetic part of the entropy reaches the saturation value $\Delta S_{mag}(T) = 4.8R\ln 2 = 27.7$ J mol^{-1}K^{-1} above $T = 23$ K. This value corresponds to a doublet ground state of the $^4I_{15/2}$ multiplet of Er^{3+} ion, which is involved in the formation of the short-range magnetic order in $Er_{4.8}Pd_2$. Estimation of the theoretical magnetic entropy of $Er_{4.8}Pd_2$ associated with the thermal population of the ground doublet state and the first excited quartet state in the low temperature range below 50 K gives $S_M = 4.8R\ln 6$. Additionally, the short range antiferromagnetic

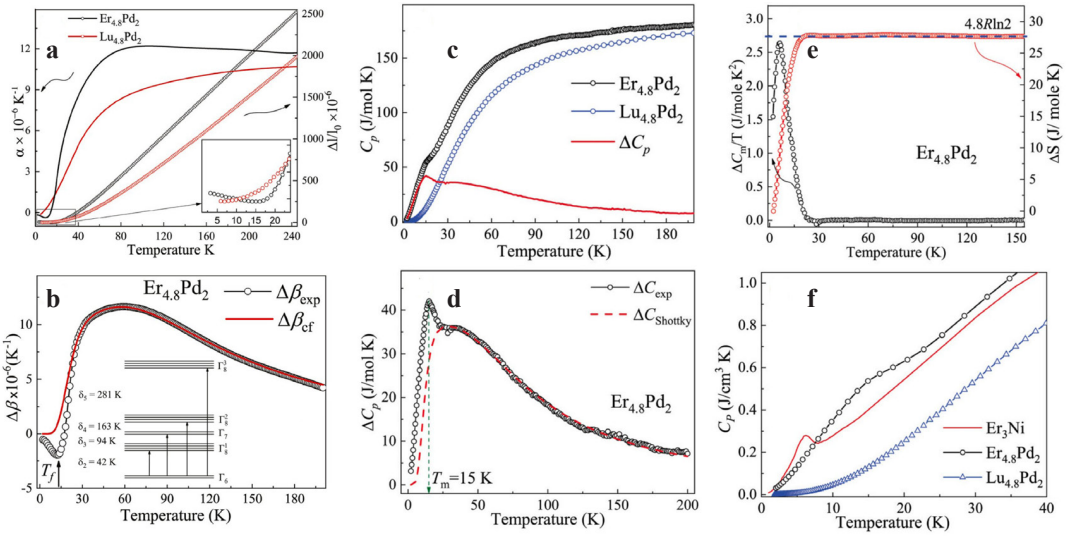

Figure 1. **a** The temperature dependence of the thermal expansion rate $\Delta l/l_0$ of $Er_{4.8}Pd_2$ and $Lu_{4.8}Pd_2$ (open circles) and calculated linear CTE α (solid line). **b** Excess CTE Δβ obtained for $Er_{4.8}Pd_2$ and the result of its approximation. Splitting scheme of Er^{3+} ion $^4I_{15/2}$ multiplet by a cubic crystal electric field in $Er_{4.8}Pd_2$ is shown in the inset. **c** Heat capacity curves $C_p(T)$ of the $Er_{4.8}Pd_2$ and $Lu_{4.8}Pd_2$ compounds as well as their difference curve $\Delta C_p(T)$, **d** difference curve $\Delta C_p(T)$ and its approximation by a Shottky-type contribution, **e** $\Delta C_M/T$ and ΔS_M curves as a function of temperature for $Er_{4.8}Pd_2$, **f** heat capacity curves for $Er_{4.8}Pd_2$, $Lu_{4.8}Pd_2$ and one of the best low temperature regenerator material Er_3Ni [6].

order developing on cooling in $Er_{4.8}Pd_2$ gives rise to a broad anomaly on the heat capacity data at T_m = 15 K. Estimation of the magnetic entropy associated with the short-range magnetic order provides $S_M = 4.8R\ln 2$. Both of these contributions result in a very high volumetric heat capacity in the low temperature range below 50 K. A comparison of the volumetric heat capacity of $Er_{4.8}Pd_2$ and well known regenerator material Er_3Ni revealing high theoretical magnetic entropy $S_M = 3R\ln 16$ is shown in Fig. 1f.

The electrical resistivity of $Er_{4.8}Pd_2$ exhibits a metallic behaviour at high temperatures and an upturn of the $\rho(T)$ curve on cooling below T^* = 40 K. This non-metallic behaviour was ascribed to an inhomogeneous electronic state due to the formation of clusters with the AFM short-range correlations.

This work was partly supported by RFBR № 20-32-90047 and by the state assignment of the Ministry of Science and Higher Education (theme "Flux" No. AAAA-A18-118020190112-8).

1. A.F. Gubkin, E.A. Sherstobitova, P.B. Terentyev, A. Hoser, N.V. Baranov, J. Phys. Condens. Matter **25**, 236003 (2013).
2. M.K. Sharma, K. Yadav, K. Mukherjee, J. Phys. Condens. Matter **30**, 215803 (2018).
3. K.A. Gschneidner, A.O. Pecharsky, V.K. Pecharsky, Low Temperature Cryocooler Regenerator Materials, Springer US, Boston, MA, pp. 457–465, (2003).
4. T. Barron, J. Collins, G. White, Adv. Phys. **29**, 609–730 (1980).
5. A. Tari, The Specific Heat of Matter at Low Temperatures. Imperial college press, London (2003).
6. A. Takahashi, Y. Tokai, M. Sahashi, T. Hashimoto, Jpn. J. Appl. Phys. **33**, 1023–1026 (1994).

THE FERROMAGNETIC PHASE GROWTH MECHANISMS IN FeRh ALLOYS

A.S. Komlev*[1], R.A. Makaryin[1], T.S. Ilina[2], D.A. Kiselev[2], V.I. Zverev[1], N.S. Perov[1]

[1]Department of Magnetism, Lomonosov Moscow State University, Moscow, Russia
[2]National University of Science and Technology "MISiS", Moscow, Russia
*E-mail: komlev.as16@physics.msu.ru

Materials which exhibit first-order magnetic phase transitions are interesting objects for research from a practical point of view. The structural, caloric, and magnetic properties of these compounds significantly change near the phase transition temperature. Such alloys can be used as an elements in magnetocaloric cooling devices [1], thermomagnetic generators [2], various types of sensors and actuators [3]. However, the time behavior of nucleation and growth of the ferromagnetic phase are still not clearly understood. Therefore, the study of the nucleation, growth, and merging of ferromagnetic clusters processes in magnetocaloric materials is a key task for constructing the theory of first-order phase transitions [4]. Previously, general approaches to the study of magnetization relaxation processes in thin films were proposed. Investigations of bulk alloys are analyzed in this work.

A first-order phase transition from the antiferromagnetic to the ferromagnetic state is observed in iron-rhodium based compounds with near equiatomic elemental composition. Additionally, the alloys crystal lattice increases in volume approximately about 1% during the phase transition. The emerged local stresses affect to the phase formation temperature [5]. Therefore, it is difficult to separate the mechanisms of nucleation and phase growth from each other in static measurements. The authors carried out temperature studies of magnetization using MFM (Fig. 1) and VSM. The combined analysis allows us to identify temperature ranges where various mechanisms of the ferromagnetic phase formation dominated.

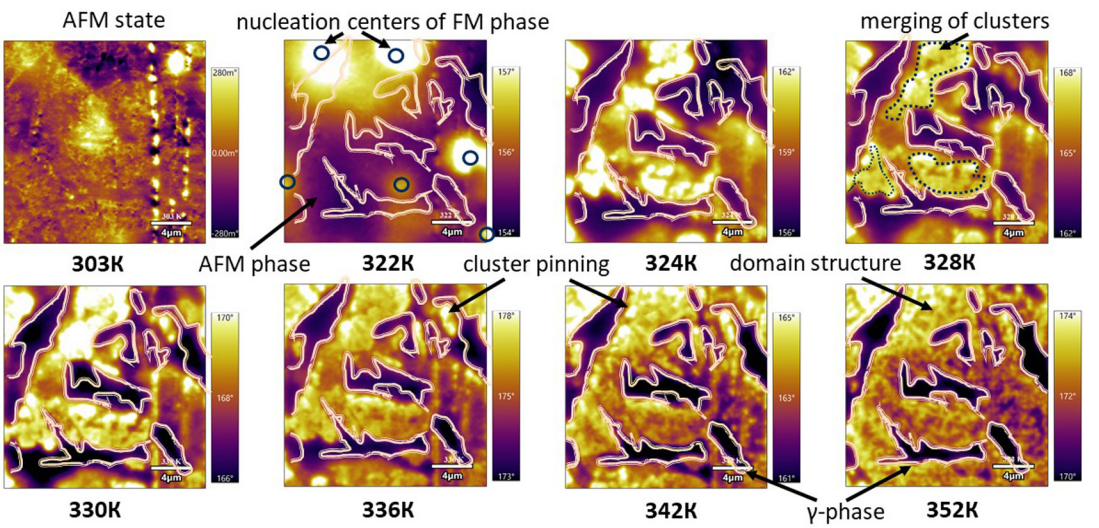

Figure 1. MFM images of the $Fe_{49}Rh_{51}$ (35%) sample surface taken at different temperatures (during heating). The pictures were taken from the same area. Light lines mark the paramagnetic gamma-phase localization sites.

Magnetizing processes have also been studied. The anomalously long-term magnetization relaxations for FeRh alloy are experimentally measured in order to separate the mechanisms of the ferromagnetic phase nucleation from its growth. A model was proposed according to which the magnetic transition process from one state to another is inextricably coupled with the crystal lattice constant. Comprehensive analysis of phase transition temporal behavior allows us investigate this processes in detail. Numerical simulation demonstrates a high degree of agreement between experimental and theoretical results. A detailed study of the ferromagnetic phase formation, based on the simulation results, allowed to determine the conditions under which various mechanisms of phase evolution dominate. The correlation between the model and experimental results makes it possible to verify the hypnoses about phase transition driving forces.

The authors hope that detailed studies of the ferromagnetic phase dynamic behavior will make it possible to improve the theory of first-order phase transitions.

The research was carried out with the financial support of the Russian Science Foundation within the framework of project 22-22-00291. Komlev A.S. thanks the BASIS Foundation for scholarship support. Perov N.S. acknowledges support from Russian Ministry of Science and Education grant No. 075-15-2021-1353.

1. A.M. Tishin, Y.I. Spichkin, V.I. Zverev, P.W. Egolf, Int. J. Refrigeration **68**, 177–186 (2016). https://doi.org/10.1016/j.ijrefrig.2016.04.020.
2. A. Waske, D. Dzekan, K. Sellschopp, D. Berger, A. Stork, K. Nielsch, S. Fähler, Nat. Energy **4**, 68–74 (2019). https://doi.org/10.1038/s41560-018-0306-x.
3. R. Modak, M. Murata, D. Hou, A. Miura, R. Iguchi, B. Xu, R. Guo, J. Shiomi, Y. Sakuraba, K. Uchida, Appl. Phys. Rev. **9**, 011414 (2022). https://doi.org/10.1063/5.0077497.
4. A.S. Komlev, D.Y. Karpenkov, D.A. Kiselev, T.S. Ilina, A. Chirkova, R.R. Gimaev, T. Usami, T. Taniyama, V.I. Zverev, N.S. Perov, J. Alloys and Comp. **874**, 159924 (2021). https://doi.org/10.1016/j.jallcom.2021.159924.
5. L.I. Vinokurova, V.G. Veselago, The Magnetic and Electron Structures of Transition Metals and Alloys **3**, 45 (1986).

MODELING THE DOMAIN STRUCTURE OF SQUARE FERROMAGNET MICROPARTICLES UNDER UNIAXIAL MECHANICAL STRESS

N.I. Nurgazizov[*], *D.A. Byziaev, A.P. Chuklanov*

Zavoisky Physical-Technical Institute, FRC Kazan Scientific Center of RAS, Kazan, Russia
[*]E-mail: niazn@mail.ru

Recently, the possibility to control the magnetization direction of single-domain or uniformly magnetized micro- and nanoparticles have been attracted the attention of scientists. If the control of magnetization carried out by magnetoelastic effect, the new class of devices for storing and processing information with ultra-low power consumption can be designed [1]. Searching for materials whose magnetic properties strongly depends on applied mechanical stress is one of the tasks of such the studies. In this work, the modifications in the domain structure of planar microparticles under the applied uniaxial mechanical stresses were studied.

Such the microparticles can be a good test structures for studying the common patterns of the stresses effects on a magnetic structure. It was shown in previous works [2] that domain structure of planar square-shaped microparticles are modified under mechanical stresses and the magnitude of the mechanical stress can be found by analyzing this modification. In this work, the effect of saturation magnetostriction of various materials on domain structure modifications under mechanical stresses was studied. For this, the changes of the domain structure of microparticles made from various materials was simulated: Py (Fe18%, Ni82%), CoNi (Co18%, Ni82%), Ni, CoFe (Co50%, Fe50%). According to data [3], the saturation magnetostriction for the materials used is: Py $-3\cdot10^{-6}$, CoNi $-25\cdot10^{-6}$, Ni $-35\cdot10^{-6}$, CoFe $60\cdot10^{-6}$.

The OOMMF [4] was used to simulate the magnetization distribution in microparticles. For simulation purposes the microparticle size was assumed to be $7.5\times7.5\times0.04$ μ^3, it was split into cells with size $10\times10\times40$ nm^3. The uniaxial mechanical stress was directed along one of the microparticle sides and was modeled by introducing the uniaxial anisotropy constant into the simulation (K_{eff}).

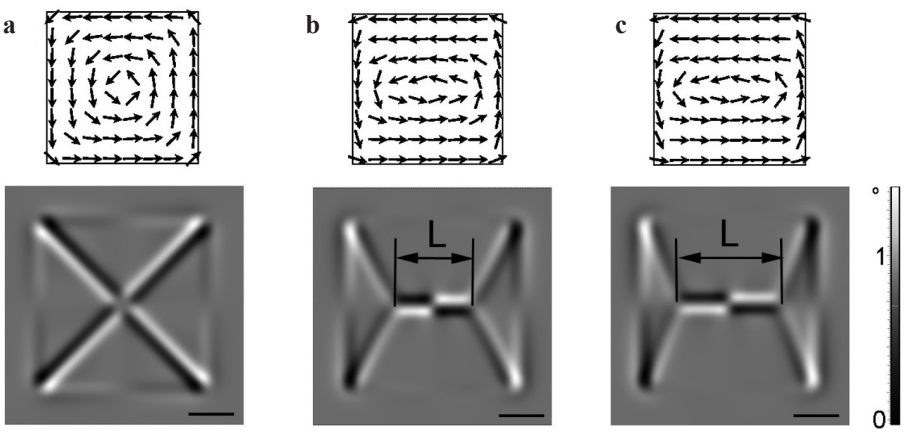

Figure 1. Scheme of magnetization distribution in CoNi microparticle modelling by OOMMF (top) and its virtual MFM image (bottom) in case: without mechanical stress (**a**), at stress 35 MPa (**b**), at stress 70 MPa (**c**). Bar on MFM images – 2 μm. *L* – length of domain wall.

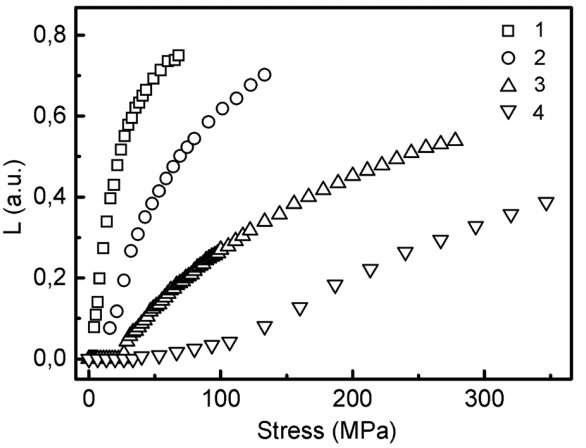

Figure 2. Dependence of domain wall length (L) on the applied stress for Ni (1), CoNi (2), CoFe (3), Py (4).

The value increased from 0 to 5000 J/m^3 with a step of 200 J/m^3. The mechanical stress (σ) applied to the particle was calculated from K_{eff} on the base of formula $\sigma = 2/3 \cdot K_{eff}/\lambda_s$, where λ_s is the saturation magnetostriction constant. In the absence of mechanical stress, the domain structure of the particles has 4 identical triangle-shaped domains, the direction of magnetization in each domain was parallel to the side at which it located (Fig. 1a). When mechanical stress, the size of two opposite domains increases and a characteristic domain wall formed between them, the length of this wall proportional to the stress applied (Fig. 1b and c). Since the domain structure of microparticles can be visualized by magnetic force microscopy (MFM), the length of this wall can be determined from MFM (Fig. 1). The dependence of domain wall length (L) on the applied stress for set of materials from which microparticle made are in Fig. 2. The length of the domain wall was normalized to the length of the microparticle side. One can note that as the saturation magnetostriction increases, the sensitivity of the magnetic structure to the applied stress also increases. For Py, the stress range required to increase L from 0.1 to 0.3 is 150–280 MPa, and for Ni is 5–13 MPa. CoFe alloy is an exception. It has the highest magnetostriction among the materials under study but at the same time reacts very weakly to mechanical stress. The stress range required to change L from 0.1 to 0.3 is 40–120 MPa. This is due to the CoFe alloy has the highest saturation magnetization 1950 kA/m, while for Ni it is 490 kA/m.

The results obtained shows, when a searching for material to design straintron devices, the most optimal material may be one that will have high saturation magnetostriction and low saturation magnetization at the same time.

The work was supported by RSF (grant №22-29-00352).

1. A.A. Bukharaev, A.K. Zvezdin, A.P. Pyatakov, Y.K. Fetisov, Physics – Uspekhi **61**, 1175–1212 (2018).
2. N.I. Nurgazizov, D.A. Bizyaev, A.A. Bukharaev et al., Tech. Phys. **64**, 1573–1578 (2019).
3. A.P. Babichev et al., Physical values: Handbook. Energoatomizdat. Moscow, (1991) [in Russian].
4. M. Donahue, D. Porter: OOMMF User's Guide, Ver. 1.0. National Institute of Standards and Technology, Gaithersburg, MD, USA (1999). 83 p. http://math.nist.gov/oommf.

INFLUENCE OF DEFORMATION-THERMAL IMPACT ON THE STRUCTURE AND PROPERTIES OF FERROMAGNETIC ALLOYS

*Yu.V. Kaletina**, *A.Yu. Kaletin, V.P. Pilyugin*

Institute of Metal Physics named after M.N. Mikheev of the Ural Branch of the Russian Academy of Sciences, Ekaterinburg, Russian Federation
*E-mail: kaletina@imp.uran.ru

The structure, functional and physical and mechanical properties of ferromagnetic alloys depend on the technology of their production and processing [1–3]. One of the effective methods of changing the structure of materials is the deformation by torsion under pressure.

In this work the influence of plastic deformation by high-pressure torsion at room and cryogenic temperatures on the structure, fracture pattern, microhardness, and magnetic properties of the Heusler ferromagnetic alloy has been researched. In the studied $Ni_{47}Mn_{42}In_{11}$ alloy of nonstoichiometric composition, shape memory effects controlled by a magnetic field and a magnetocaloric effect are realized, which is associated with structural phase transformations and their special sequence [1–3].

The $Ni_{47}Mn_{42}In_{11}$ alloy was smelted by electric arc melting in an argon atmosphere. Aftersmelting, it was subjected to homogenizing annealing in vacuum at a temperature of 1123 K for 24 h, followed by furnace cooling. Then plastic deformation was carried out in Bridgman anvils at a pressure of 8 GPa at room and cryogenic temperatures (77 K). The angle of rotation of the anvil was varied from 0 to 5 revolutions. Using the methods of optical metallography, scanning and transmission electron microscopy, the structure of the alloy after deformation was studied, the microhardness was measured, and magnetic measurements were performed.

It was shown that after deformation by torsion under high pressure, the crystal structure is refined to a submicro- and nanocrystalline state with the size of individual crystallites from 10 to 50 nm. Structure refinement leads to an increase in microhardness and a change in the nature of fractures in deformed specimens.

Differences in microhardness after deformation at room and cryogenic temperatures were found for the number of revolutions of the anvil from 2.5 to 5. The microhardness at room temperature is 1000 MPa higher than at T = 77 K. A decrease in the deformation temperature slows down thermally activated processes, leads to a change in deformation mechanisms, deformation stacking faults appear, localized deformation bands are formed, the process of fragmentation to submicro- and nanocrystalline structures is significantly slowed down, having high rates of self- and heterodiffusion.

It has been experimentally established that after plastic deformation by torsion under pressure, the magnetic susceptibility becomes small in magnitude, and no anomalies are observed in the range of critical temperatures of the structural and magnetic phase transitions. Reversible magnetically controlled shape memory effects disappear due to atomic disorder and a significant reduction in grain size and nanostructuring in deformed samples.

The work was carried out within the framework of the state task on the topics "Structure", No. 122021000033-2 and "Pressure" No. 122021000032-5 with partial support from the Russian Foundation for Basic Research (project No. 20-03-00056).

1. V.D. Buchelnikov and V.V. Sokolovskiy, Phys. Metals Metallogr. **112**, 633 (2011).
2. Yu.V. Kaletina and E.G. Gerasimov, Phys. Solid State **56**, 1634 (2014).
3. V.M. Schastlivtsev, Yu.V. Kaletina, E.A. Fokina, Martensitic Transformation in a Magnetic Field, Ural'skoe otdelenie Rossiiskoi akademii nauk, Ekaterinburg (2007) [in Russian].

MAGNETOCALORIC EFFECT IN $LaFe_{11.1}Mn_{0.1}Co_{0.7}Si_{1.1}$ ALLOY: DIRECT AND INDIRECT MEASUREMENTS

N.Z. Abdulkadirova[1*], *A.G. Gamzatov*[1], *K.I. Kamilov*[1,2], *A.T. Kadirbardeev*[1], *A.M. Aliev*[1], *P. Gebara*[3]

[1]Amirkhanov Institute of Physics of DFRC of RAS, Makhachkala, Russia
[2]Faculty of Physics, M.V. Lomonosov Moscow State University, Moscow, Russia
[3]Institute of Physics, Częstochowa University of Technology, Częstochowa, Poland
[*]E-mail: nnurizhat@mail.ru

In recent years, several new types of magnetocaloric materials with giant MCE values have been obtained, which greatly contributed to the development of magnetic cooling technology at room temperature (these are compounds Fe-Rh [1], Gd-Si-Ge [2], Ni-Mn-Ga [3], La(Fe,Si) [4], (Mn,Fe)-(As,P) [5]). In most of these materials, giant values of the MCE are observed due to magneto-structural phase transitions, where the overall effect includes the effect of the magnetic and lattice subsystems. It should be noted that in materials in which first-order phase transitions take place, temperature and magnetic hysteresis are inevitably observed. This leads to the irreversible release of latent heat of transition, which reduces the efficiency of the magnetic cooling cycle.

From the point of view of the use of materials in magnetic cooling technology, materials with second-order phase transitions are of greater interest, due to the absence of strong lattice changes and hysteresis phenomena in the region of phase transitions. An excellent example of such materials is pure Gd, which shows a maximum entropy change of ΔS = 9.7 J/kgK in a magnetic field of 50 kOe at T_C = 294 K. However, the high cost of Gd limits its widespread use, with a number of compounds represented by La-Fe-Co-Si with a phase transition of the second kind show high values of magnetocaloric characteristics, which are not inferior to Gd and its alloys [6].

This paper presents the results of studying the specific heat, magnetization, and magnetocaloric effect (direct and indirect estimates) of the $LaFe_{11.1}Mn_{0.1}Co_{0.7}Si_{1.1}$ alloy in the temperature range of 80–300 K and in magnetic fields up to 175 kOe (see Fig. 1a and b). The effect of the frequency of a cyclic magnetic field of 1.2 T on the value of the MCE was also studied. The magnetization was measured in the temperature range 80–275 K with a step of 5 K in pulsed fields up to 175 kOe. Further, using the Maxwell relation

$$\Delta S_M(T,\Delta H) = \mu_0 \int_{H_1}^{H_2} \left(\frac{\partial M}{\partial T}\right)_{P,H} dH,$$

the change in magnetic entropy was estimated, which are shown in Fig. 1c. The maximum value of ΔS_M for the $LaFe_{11.1}Mn_{0.1}Co_{0.7}Si_{1.1}$ alloy in a field of 175 kOe is 38 J/kg K. In addition to the main maximum, the dependences $\Delta S_M(T)$ at different fields exhibit small anomalies that are characteristic of the La-Fe-Si and indicate magnetic inhomogeneity or the presence of second phases [7]. The temperature dependence $\Delta S_M(T)$ for $LaFe_{11.1}Mn_{0.1}Co_{0.7}Si_{1.1}$ is symmetrical, which corresponds to a second-order phase transition. The second-order phase transition in this sample is the result of a weakening of the metamagnetic transition of itinerant electrons, and a similar effect was observed in [8, 9]. The insert in Fig. 1c shows $\Delta S_{max}(H)$ at T = 252.5 K. As was shown in [10], the field dependence of the MCE near T_C in materials with second-order phase transitions has a power dependence: $\Delta S \sim H^n$, where n = 1 at $T << T_C$, n = 2 at $T >> T_C$ and n = 0.75 near T_C. The dependence $\Delta S_{max}(H)$ for $LaFe_{11.1}Mn_{0.1}Co_{0.7}Si_{1.1}$ also follow well the regularities $\Delta S_{max}(H) \sim H^n$, where n = 2/3

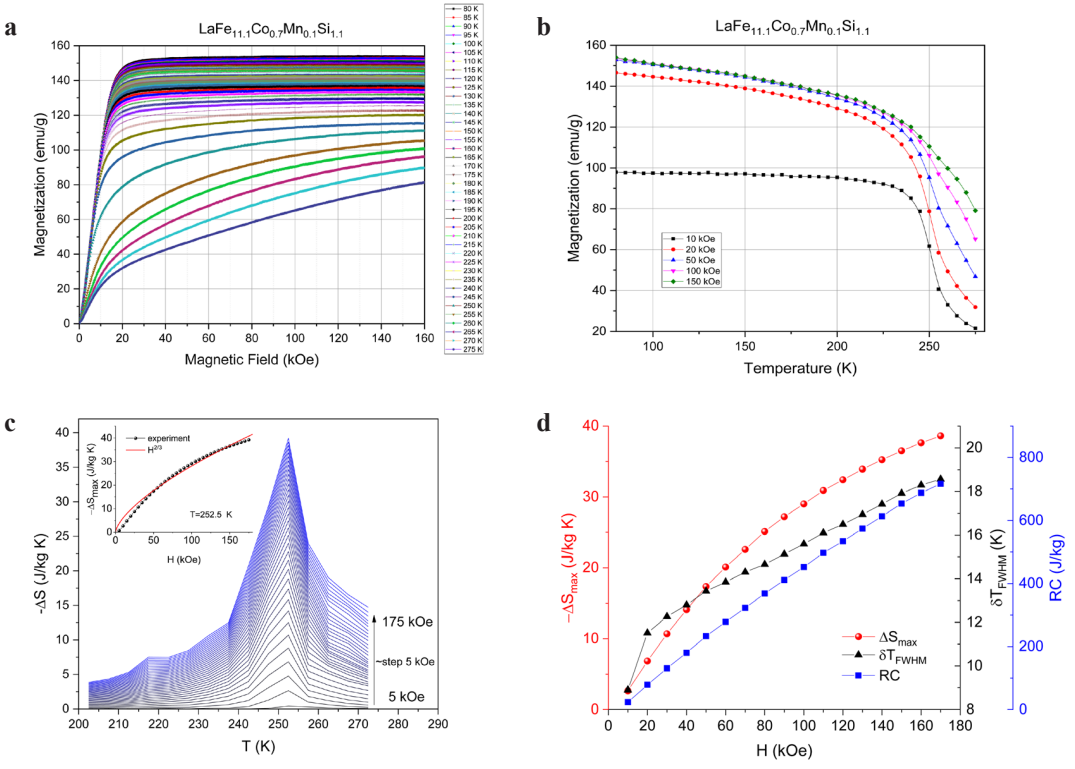

Figure 1. **a** *M-H* curves for the $LaFe_{11.1}Mn_{0.1}Co_{0.7}Si_{1.1}$ sample in the temperature range 80–275 K with a step of 5 K in pulsed fields up to 175 kOe. **b** *M*(*T*) dependences in fields 10, 20, 50, 100 and 150 kOe. **c** Temperature dependence of ΔS in fields up to 175 kOe. **d** Field dependences of parameters ΔS_{max}, δT_{FWHM} and *RC* at $T = 252$ K.

(see the line in the inset of Fig. 1c). This behavior is in good agreement with the predictions of the mean field theory, which gives the dependence $\Delta S \sim H^{2/3}$ [11].

The *RC* is an important parameter to evaluate the magnetocaloric materials which is determined by the value of ΔS_M and its full width at half maximum ($\delta T_{FWHM} = T_2 - T_1$). It is given by the expression

$$RC = \int_{T_1}^{T_2} \Delta S_M(T, \Delta H)\mathrm{d}T.$$

Figure 1d shows the field dependences of the parameters ΔS_{max}, δT_{FWHM} and *RC* near the maximum of the effect at $T = 252$ K. The dependence *RC*(*H*) increases monotonically with increasing magnetic field without signs of saturation. In a magnetic field of 175 kOe, the *RC*-value for the $LaFe_{11.1}Mn_{0.1}Co_{0.7}Si_{1.1}$ alloy reaches its maximum value and is equal to ~732 J/kg.

The reported study was funded by RFBR and NSFC, project number 21-58-53046.

1. S.A. Nikitin, G. Myalikgulyev, A.M. Tishin et al., Phys. Lett. A **148**, 363 (1990).
2. V.K. Pecharsky and K.A. Jr. Gschneidner, Phys. Rev. Lett. **78**, 4494 (1997).
3. V.D. Buchelnikov, V.V. Sokolovskiy, et al., Phys. Rev. B **81**, 094411 (2010).

4. F.X. Hu, B.G. Shen, J.R. Sun, et al., Appl. Phys. Lett. **78**, 3675 (2001).
5. H. Wada and Y. Tanabe, Appl. Phys. Lett. **79**, 3302 (2001).
6. P. Gębara, P. Pawlik, J. Magn. Magn. Mat. **442**, 145–151 (2017).
7. P. Gębara, M. Cesnek, J. Bednarcik, Current Applied Physics **19**(2), 188–192 (2019).
8. M. Balli, D. Fruchart et al., J. Magn. Magn. Mat. **313**, 43–46 (2007).
9. P. Gębara, J. Kovac, Materials & Design **129**, 111–115 (2017).
10. V. Franco, J.S. Blázquez, and A. Conde, Appl. Phys. Lett. **89**, 222512 (2006).
11. H. Oesterreicher, F.T. Parker, J. Appl. Phys. **55**, 4334–4338 (1984).

MAGNETOCALORIC EFFECT IN HEUSLER ALLOYS IN THE REGION OF MARTENSITIC TRANSITIONS UNDER CYCLIC MAGNETIC FIELDS

*A.M. Aliev**, *A.G. Gamzatov, L.G. Khanov*

Amirkhanov Institute of Physics of Dagestan Federal Research Center RAS, Makhachkala, Russia
*E-mail: lowtemp@mail.ru

Recently, there has been a great interest in the search and study of magnetocaloric materials for magnetic cooling technology. Until now, almost all studies of the magnetocaloric properties of materials have been carried out either in quasi-stationary fields or under single cycle of the magnetic field change. The magnetocaloric properties of materials under single application of the magnetic field and under continuously applied alternating fields can differ significantly for several reasons, which include relaxation phenomena during magnetization processes, the irreversibility of magnetostructural transitions induced by a magnetic field, the value of heat exchange, etc.

Despite active research into the magnetocaloric properties of various Heusler alloys over the past 20 years, there are still many unresolved issues in this area. In particular, there is no generally accepted explanation for the difference in the magnetocaloric effect values in the region of martensitic phase transitions in the heating and cooling runs. The problem of estimating the contributions of the structural and lattice subsystems to the total magnetocaloric effect (MCE) in these materials remains unsolved. In many Heusler alloys, there is a strong dependence of the MCE on the frequency of changes in the magnetic field, which also does not find a reasonable explanation at the moment. In addition, the effect of long-term exposure to a cyclic magnetic field on the stability of the magnetocaloric properties of Heusler alloys has not yet been studied, and this is a very important task from a practical point of view.

This report presents the results of a study of the magnetocaloric properties of Ni-Mn-X (X = In, Sn) Heusler alloys in the region of magnetostructural (martensitic) phase transitions in cyclic (alternating) magnetic fields. To better understand the effects occurring in Heusler alloys, the thermal expansion of these materials in constant magnetic fields, as well as magnetostriction in cyclic magnetic fields, were also studied. Based on the results obtained, explanations are given for the difference in the magnitude of the MCE in the heating and cooling regimes, and estimates for the contributions of the structural and magnetic subsystems to the overall MCE are given. Possible mechanisms of a decrease in the MCE with an increase in the frequency of field changes are discussed. Some experimental results are presented that testify to long-term relaxation phenomena and the degrading effect of long-term exposure to an alternating magnetic field on the properties of the materials under study.

The study was supported by the Russian Science Foundation grant no. 22-19-00610.

MAGNETIC PROPERTIES OF CRYSTALLINE POWDERS OF TERBIUM, DYSPROSIUM, HOLMIUM, ERBIUM AND YTTERBIUM TETRAFLUORIDES

G.Iu. Andreev[1*], *I.V. Romanova*[1], *S.L. Korableva*[1], *O.A. Morozov*[1,2], *A.S. Semakin*[1], *M.A. Cherosov*[1], *A.G. Kiiamov*[1], *M.S. Tagirov*[1,3]

[1]Institute of Physics, Kazan Federal University, Kazan, Tatarstan, Russia
[2]Zavoisky Physical-Technical Institute, FRC Kazan Scientific Center of RAS, Kazan, Tatarstan, Russia
[3]Institute of Applied Research, Tatarstan Academy of Science, Kazan, Tatarstan, Russia
[*]E-mail: ujif28@mail.ru

Lithium-rare-earth double fluorides attract interest as model objects in physics of dipolar magnetism. These fluorides share scheelite type, I41/*a* crystal symmetry, unit cell contains two magnetically equivalent rare-earth Re^{3+} ions at sites with the S_4 point symmetry that compose two sublattices. $LiTbF_4$ and $LiHoF_4$ are Ising ferromagnets, magnetic moments order in along [001]-axis, Curie temperature is 2.89 and 1.53 K, respectively. $LiDyF_4$, $LiErF_4$ and $LiYbF_4$ are XY-antiferromagnets, magnetic moments order in (001) plane, Neel temperature is 0.62, 0.37 and 0.13 K, respectively [1–5].

Microsized powders of double fluorides are synthesized by sintering powders of fluorides taken in proportions according to the phase diagrams [5–7]. Nanosized powder of $LiTbF_4$ is synthesized using hydrothermal method [8]. Magnetization of the samples is measured by vibration sample magnetometer VSM at PPMS system at the temperature range 2–300 K and applied magnetic field range 0–9 T. Theoretical analysis is performed within exchange charge model, using Hamiltonian of rare earth ion, diagonalized in the full space of the free ion energy states [3].

Qualitative agreement of calculations and experimntal data is achieved for all samples of all compounds. Magnetization measurements at B = 10 mT show transition of $LiTbF_4$ samples in ferromagnetic state; Curie temperature of nanosized powder decreases in comparison with single crystal and microsized powder.

$LiDyF_4$ microsized powder sample reveals anomalous magnetic properties: magnetic hysteresis in paramagnetic state (butterfly hysteresis) and slow magnetic relaxation, at $T < 7$ K. $LiDyF_4$ single crystal magnetisation measurements prove existence of these phenomena, while diluted single crystal $LiYF_4$:Dy 1% experiments do not display any magnetic hysteresis and slow magnetic relaxation at 2–10 K. Presumably, observed anomalies are connected with the giant magnetostriction of the $LiDyF_4$ crystal, observed at T = 4.2 K [3].

Support by Russian Science Foundation (project №22-22-00257) is acknowledged. The authors are grateful to Prof. B.Z. Malkin for helpful discussions and to Prof. R.V. Yusupov for kind permission to use laboratory computer for calculations.

1. L.K. Aminov et al., in K.A. Gshneider, Jr. and L.R. Eyring (ed.), Handbook on the Physics and Chemistry of Rare Earths, vol. 22, Elsevier Science B.V., p. 295, (1996).
2. P. Babkevich et al., Phys. Rev B **92**, 144422 (2015).
3. I.V. Romanova and M.S. Tagirov, Magn. Res. Solids **21**, 19412 (2019).
4. C. Keller and H. Schmutz, J. Inorg. Nucl. Chem. **27**, 900–901 (1965).
5. R.E. Thoma et al., Inorg. Chem. **9**, 1096–1101 (1970).
6. P.P. Fedorov, Russian J. Inorg. Chem. **44**, 1703–1727 (1999).
7. P.P. Fedorov et al., in E.I. Givargizov and A.M. Mel'nikova (ed.), Growth of Crystals, vol. 21, Springer Science+Business Media, New York, p. 141, (2001).
8. Q. Zhang, B. Yan, Inorg. Chem. **49**, 6834–6839 (2010).

MAGNETOCALORIC EFFECT IN $Y(Co_{0.84}Fe_{0.16})_2$ AND $Lu(Co_{0.84}Fe_{0.16})_2$ COMPOUNDS

*M.S. Anikin**, *E.N. Tarasov, N.V. Kudrevatykh, A.V. Zinin*

Ural Federal University, Ekaterinburg, Russia
*E-mail: maksim.anikin@urfu.ru

Previously, when studying the $(Er_{1-x}Y_x)(Co_{0.84}Fe_{0.16})_2$ compounds (x = 0–1), plateau-like temperature dependences of the magnetic entropy change (ΔS_m) for all samples were found [1]. Such dependences of the magnetocaloric effect (MCE) were explained by the Er magnetic moments ordering in the Er sublattice under the action of an external magnetic field. This sublattice is partially disordered even in the temperature range lower its Cuire temperature (T_C) due to the weak Er-3d intersublattice exchange interaction. It was found, that besides of the MCE maximum directly in the T_C region, a "low-temperature" maximum on the $\Delta S_m(T)$ dependence are observed. In the $Y(Co_{0.84}Fe_{0.16})_2$ compound with a "non-magnetic" yttrium ion, the appearance of a "low-temperature" maximum was rather unexpected. The observed broadening of the $\Delta S_m(T)$ peak at temperatures below T_C was attributed due to the partial paramagnetism in the cobalt atoms subsystem [1]. In this work, in order to clarify the reasons for the MCE occurrence at low temperatures in Laves phases with "non-magnetic" R-ions and 3d-metals, the $Y(Co_{0.84}Fe_{0.16})_2$ and $Lu(Co_{0.84}Fe_{0.16})_2$ compounds were synthesized and their magnetic and magnetocaloric properties were studied.

The alloys were synthesized in an arc furnace followed by homogenizing annealing. Using X-ray diffraction analysis of the synthesized samples, it was established that the samples belong to the face-centered cubic Fd-3m space group. The refined values of the crystal lattice parameter a were 7.2522(4) Å and 7.1405(2) Å for $Y(Co_{0.84}Fe_{0.16})_2$ and $Lu(Co_{0.84}Fe_{0.16})_2$, respectively. The magnetic properties of the samples were determined using a PPMS DynaCool (Quantum Design) instrument. The single-phase state of the investigated samples was established from the analysis of the spesific magnetization (σ) temperature dependences. The determined T_C values were 200 and 264 K for compounds with Y and Lu, respectively. Evidently that the higher T_C in the compound with lute-

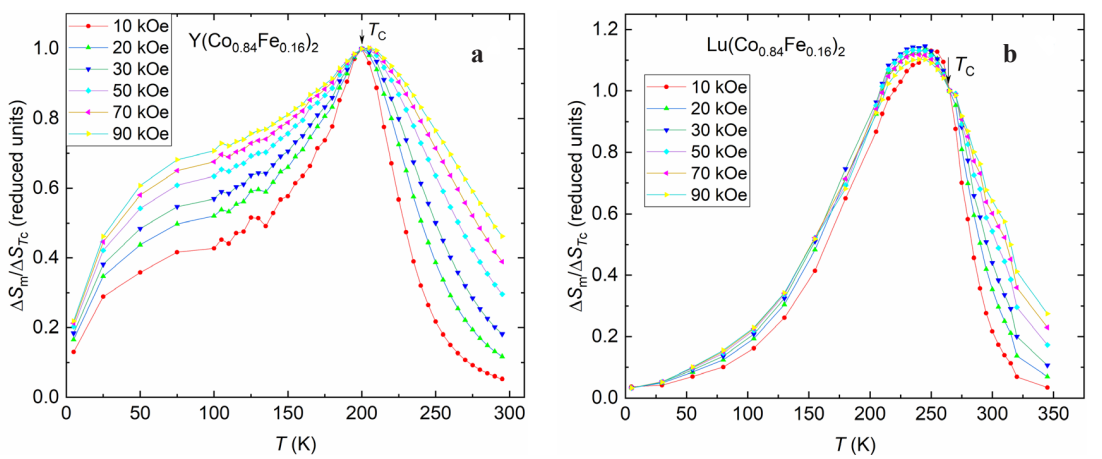

Figure 1. Temperature dependences of ΔS_m reduced to ΔS_{T_C} values at T_C for compounds: **a** $Y(Co_{0.84}Fe_{0.16})_2$ and **b** $Lu(Co_{0.84}Fe_{0.16})_2$ at different values of ΔH.

tium is due to the higher its exchange interaction energy caursed by the smaller lattice parameter. A similar enhancement of the d-d exchange interaction upon replacing Y by Lu was observed earlier in the $R(Co\text{-}Al)_2$ system, where R = Y, Lu [2]. Thus, we have two compounds with different values of d-d exchange interaction energy.

It is known that in the mictomagnetic $Y(Co_{0.97}Fe_{0.03})_2$ compound there are clusters of Fe-atoms that polarize the Co-atoms [3]. With an increase in the iron content above ≈14%, the percolation limit is reached and the $Y(Co\text{-}Fe)_2$ compound passes from the short-range magnetic order state to the long-range one and becomes a ferromagnet [4]. It can be assumed that the $Y(Co_{0.84}Fe_{0.16})_2$ compound is close to the percolation limit, and the energy of the d-d exchange interaction may not be sufficient to maintain the magnetic order of all cobalt atoms subsystem, especially at intermediate temperatures below T_C due to the strong influence of a thermal fluctuations. As a result, a situation of partial disordering of cobalt atoms magnetic moments or a transition of some of them to a paramagnetic state is possible. The application of a magnetic field leads to the ordering of them. As the d-d exchange interaction increases, the "low-temperature" maximum should be suppressed and/or its temperature apperance should shifts to the higher temperatures values. This conclusion is visually confirmed by comparing the $\Delta S_m(T)$ dependences of the $Y(Co_{0.84}Fe_{0.16})_2$ and $Lu(Co_{0.84}Fe_{0.16})_2$, compounds, shown in Fig. 1.

The $\Delta S_m/\Delta S_{Tc}(T)$ dependence of the $Y(Co_{0.84}Fe_{0.16})_2$ compound exhibits a plateau in the vicinity of 100 K, which corresponds to the "low-temperature" maximum. With an increase in magnetic field change (ΔH) up to 90 kOe, the level of the plateau rises.

The $\Delta S_m/\Delta S_{Tc}(T)$ dependence of the $Lu(Co_{0.84}Fe_{0.16})_2$ compound near 240 K exhibits a "low-temperature" broadened maximum. With an increase in the magnetic field, the value of the ΔS_m "low-temperature" maximum increases with a field increase only up to 30 kOe, which may indicate a complete ordering of the cobalt magnetic moments in this temperature range.

The values exchange energy in the studied compounds can be indirectly judged looking on the $\sigma(H)$ curves measured at 5 K. A strong paraprocess is observed for $Y(Co_{0.84}Fe_{0.16})_2$. In particular, as H increases from 10 to 90 kOe, the magnetic moment increases linearly from 1.76 to 1.92μ_B, while a very moderate paraprocess is observed in the compound with lutetium, where the magnetic moment increases from 2.24 to 2.26μ_B in the same magnetic fields range. A similar weak increase in the magnetic moment is also observed in the $Y(Co_{0.50}Fe_{0.50})_2$ compound [3], where the exchange energy is much higher due to a larger amount of iron.

According to the results of magnetic and magnetocaloric properties study of the $Y(Co_{0.84}Fe_{0.16})_2$ and $Lu(Co_{0.84}Fe_{0.16})_2$ compounds, it was shown that the transition from compound with Y to one with Lu at the same Fe-Co content ($Co_{0.84}Fe_{0.16}$) leads to an increase in the exchange interaction energy in Co-Fe atomic system accompanied by an increase in T_C. This leads to the suppression of the "low-temperature" anomaly in the $\Delta S_m(T)$ dependence. This phenomenon is similar to that observed in ferrimagnets $R(Co_{0.88}Fe_{0.12})_2$ compounds with magneto-active rare-earth elements (R) [5]. Here an increase in the energy of the exchange R-3d interaction leads to $\Delta S_m(T)$ dependence transformation and a such R magnetic sublattice was called a "weak" sublattice. By analogy with this, in the studied compounds, the role of the "weak" sublattice is played by the cobalt atoms subsystem.

The work was supported by the State Contract FEUZ-2020-0051 between Ural Federal University and the Ministry of Science and Higher Education of the Russian Federation.

1. M.S. Anikin, E.N. Tarasov, N.V. Kudrevatykh, D.S. Neznakhin, M.A. Semkin, N.V. Selezneva, S.V. Andreev and A.V. Zinin, J. Phys.: Condens. Matter **33**, 275801 (2021).
2. I.S. Dubenko, R.Z. Levitin and A.S. Markosyan, J. Magn. Magn. Mater. **111**, 146–148 (1992).
3. Z. Sniadecki, M. Kopcewicz, N. Pierunek and B. Idzikowsk, Appl. Phys. A **118**, 1273–1277 (2015).
4. S.H. Kilcoyne, Physica B **276-278**, 660–661 (2000).
5. M.S. Anikin, E.N. Tarasov, N.V. Kudrevatykh, A.A. Inishev and A.V. Zinin, Met. Sci. Heat Treat. **60**, 522–527 (2018).

SIMULATION OF MICROWAVE SWITCHING IN THE MAGNETIC AND ELASTIC SUBSYSTEMS OF A THREE-LAYER MAGNETIC STRUCTURE

L.N. Kotov, M.Yu. Dianov, V.S. Vlasov*

Syktyvkar State University, Syktyvkar, Russia
*E-mail: dianovmy@yandex.ru

Recently, the field of straintronics has been rapidly developing, in which the possibility of creating information recording/reading devices based on electro- and magnetoacoustic effects in multilayer structures is being considered [1, 2]. For the first time, the principle of high-frequency recording and reading of information based on a magnetoacoustic echo in an ensemble of magnetic particles was proposed in an invention in 1987 [1], the claims of which were described in detail in the monograph [2]. In order to improve the efficiency of control and increase the speed, this principle of recording and reading information can be implemented in multilayer magnetic structures, but also using microwave fields.

In the work, calculations of the time dependences of magnetic and elastic components for three magnetic layers of a planar structure were carried out. For the components of the magnetization vector and the equation for elastic displacements of the layers of the structure, a system of Landau-Lifshitz-Gilbert differential equations was compiled. Boundary conditions for all components between layers and at the interface with air were used [3, 4]. The constant magnetic field was directed perpendicular to the outer plane of the layers (z-axis), while the alternating field lay in the xy-plane and had circular polarization. A system of 37 first-order differential equations has been obtained. The system of equations was solved by the Runge-Kutta-Felberg method of 4-5 orders. In calculations, the constant magnetic field varied from 200 to 500 Oe, the amplitude of the alternating field varied from 0.1 to 100 Oe, and the frequency of the alternating field was chosen to be 0.8 or 2.8 GHz. At a frequency of 2.8 GHz, the conditions of ferromagnetic resonance (FMR) and acoustic resonance were satisfied for a three-layer structure. The thicknesses of the first and second layers were the same and equal to 0.1 μm, and the thickness of the third layer was 0.48 μm. The fulfillment of the conditions of magnetic and acoustic resonances ensures the maximum transfer of energy from the magnetic subsystem to the elastic subsystem. The remaining parameters of the layers were as follows: density $\rho = 5.17$ g cm^{-3}; layer elasticity constants $C_{44} = 7.64 \cdot 10^{11}$ erg cm^{-3}; the saturation magnetization of all three layers was chosen to be the same and equal to $4\pi M_0 = 280$ G; magnetic dissipation parameter $\alpha = 0.3$, elastic loss constant $\beta = 10^9$ s^{-1}. The magnetoelastic coupling constants of the first two layers p and d were taken equal and equal to $B_{p2} = B_{d2} = 6.96 \cdot 10^6$ erg cm^{-3}, and for the third r layer the magnetoelastic coupling constant varied from 0 to $1.2B_{p2}$.

As a result of the numerical solution of the system of Landau-Lifshitz-Gilbert equations and equations for elastic displacements of layers [3, 4], graphs of the time dependences of the components of the unit vector of magnetization and elastic displacements r of a layer of a three-layer structure were obtained, as well as their precessional portraits (Fig. 1). At zero magnetoelastic coupling constant of the r layer, slowly damped magnetic oscillations are observed at an ac magnetic field frequency of 0.8 GHz (Fig. 1a and c). At the magnetoelastic constant $B_{r2} = 1.2B_{p2} = 8.35 \cdot 10^6$ erg cm^{-3}, the magnetization vector rapidly switches from one magnetic position ($m_{rx} = 0$) to another position ($m_{rx} = 0.45$) (Fig. 1b and d). A change in the magnetic and elastic subsystems of a three-layer structure that occurs under the action of an alternating magnetic field can be called an act of microwave recording. At a low amplitude of the alternating magnetic field ($h < 0.1$ Oe), no recording occurs,

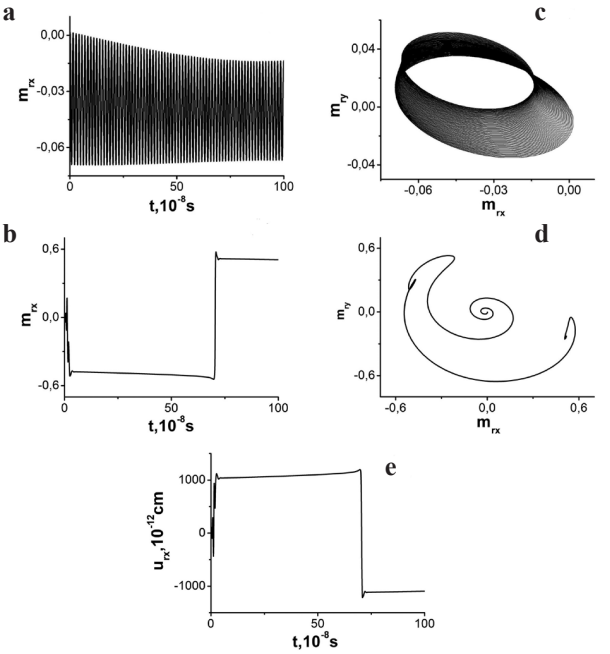

Figure 1. Time dependences of the amplitudes of the magnetic component of the r layer (**a**, **b**), elastic displacement components (**e**), and precessional portraits of magnetic oscillations (**c**, **d**). B_{r2} = 0 erg cm^{-3} (**c**, **d**). B_{r2} = 8.35·10^6 erg cm^{-3} (**b-e**). h_0 = 1 Oe. H_0 = 250 Oe.

so information can be read from the three-layer structure. At a large amplitude of the alternating magnetic field (h > 1 Oe, at B_{r2} = 8.35·10^6 erg cm^{-3}), it is possible to record information by changing the magnetic and elastic states of the layers in a three-layer structure.

This work was supported by the Russian Science Foundation, project no. 21-72-20048.

1. V.A. Shutilov, L.N. Kotov, V.L. Andzhikovich, V.L. Komashnya, Memory Element, AS USSR, No. 1332379, Class G11C11/16, BI No. 31, (1987).
2. B.A. Goldin, L.N. Kotov, L.K. Zarembo, S.N. Karpachov, Spin-Phonon Interactions in Crystals. Leningrad, Nauka (1991) [in Russian].
3. M.Yu. Dianov, L.N. Kotov, V.S. Vlasov et al., Bulletin of the RAS: Physics **83**, 1707–17011 (2019).
4. V.S. Vlasov, M.S. Kirushev, L.N. Kotov et al., J. Com. Techn. Electron. **58**, 847 (2013).

HALL EFFECT IN Ni-Mn-Sb-BASED HEUSLER ALLOYS DOPING BY ALUMINUM

S.M. Emelyanova[1*], *V.V. Marchenkov*[1,2]

[1]Institute of Metal Physics of the Ural Branch of the Russian Academy of Sciences, Ekaterinburg, Russia
[2]Ural Federal University, Ekaterinburg, Russia
[*]E-mail: emelyanova@imp.uran.ru

The magnetic properties of Heusler alloys based on Ni-Mn-Z (Z = Ga, In, Sb, Sn) are closely related to the structural state of the alloy, which, in turn, is closely related to the martensitic transition temperatures (MTT). There is a relationship between MTT and the number of valence electrons per atom e/a, but it is not always observed [1, 2], especially in complex four-component alloy systems [3]. Thereby, the search of the universal parameter, which could unambiguously predict the behavior of the MTT, is a very urgent task. For example, it is proposed to describe the behavior of the MTT using the valence electron density [4]. The authors of this work proposed to consider electronic characteristics: the coefficients of the normal R_0 (NHE) and anomalous R_S (AHE) Hall effect, concentration of charge carriers n as such possible parameter.

The $Ni_{50}Mn_{35}Sb_{15-x}Al_x$ (x = 0, 1, 2) ingots were prepared by arc melting in an inert atmosphere. The elemental analysis was performed using an Inspect F scanning electron microscope (FEI Company, USA). The structural analysis was performed at the Collaborative Access Center "Testing Center of Nano-technology and Advanced Materials" of the Institute of Metal Physics, UB RAS. The magnetic and galvanomagnetic properties were measured at MPMS-XL-5 SQUID magnetometer and PPMS-9 setup (Quantum Design). The magnetic properties were measured in magnetic fields of up to 50 kOe in the temperatures range from 4.2 to 350 K. The Hall effect was measured by the standard dc four-probe method at temperature 4.2 K and in magnetic fields of up to 50 kOe.

The MTT and the value of the temperature hysteresis were determined using the temperature dependences of the electrical resistivity $\rho(T)$ and magnetization $M(T)$, for all investigated aluminum doping alloys the MTT is increase as the aluminum content in the alloy increases. It was shown that with decreasing parameter e/a the MTT increases, although between them there should be a direct relationship. It was found that the NHE coefficient is negative, i.e., the main type of charge carriers are electrons, and the AHE is positive.

This work was partly supported by the state assignment of Ministry of High Education and Science of Russia (theme "Spin" No. AAAA-A18-118020290104-2) and by the Government of the Russian Federation (decision No. 211, contract No. 02.A03.21.0006).

1. T. Kanomata, T. Nozawa, D. Kikuchi et al., Int. J. Appl. Electromagn. Mech. **21**, 151–157 (2005).
2. Z.H. Liu, M. Zhang, W.Q. Wang et al., Appl. Phys. Lett. **92**, 5006–5010 (2002).
3. Comtesse, M.E. Gruner, V.V. Sokolovsky et al., Phys. Rev. B **89**, 184403(1–6) (2014).
4. X.Q. Chen, F.J. Yang, X. Lu et al., Phys. Stat. Sol. (b) **3**, 1047–1053 (2007).

INFLUENCE OF MAGNETIC FILM ANISOTROPY ON MAGNETOELASTIC DYNAMICS UNDER FREQUENCY-MODULATED EXCITATION

F.F. Asadullin[1*], *D.A. Pleshev*[1,2], *V.S. Vlasov*[2], *V.I. Shcheglov*[3]

[1]Saint-Petersburg State Forest Technical University named after S.M. Kirov, St-Petersburg, Russia
[2]Syktyvkar State University, Syktyvkar, Russia
[3]Institute of Radioengineering and Electronics of the RAS, Moscow, Russia
[*]E-mail: asadullin.fanur@yandex.ru

Magnetostrictive transducers based on thin films are used in hydroacoustics, flaw detection, ultrasonic technology, and information processing in the microwave range [1–3]. The excitation of magnetoelastic oscillations in a magnetostrictive transducer makes it possible to use them for recording the transmitted signal. The work [4] shows the possibility of using a converter for detecting a microwave signal with frequency modulation. It describes the main characteristics of the detection process, but the dependencies on the material parameters of the films have not been sufficiently studied.

The paper considers the magnetization vector and elastic displacement oscillations in a normally magnetized ferrite film with crystallographic anisotropy. The resonance magneto-acoustic properties of this film make it possible to detect frequency-modulated alternating magnetic fields. The paper analyzes the effect of crystallographic cell orientation on the nature of the dynamics of magnetization and elastic displacement oscillations, the establishment of various oscillation modes, and the detection process.

The time evolution of magnetization vector oscillations and elastic displacement oscillations caused by a frequency-modulated alternating magnetic field is analyzed in the case of [001] and [111] crystallographic cell orientations. The amplitude-frequency characteristics of these oscillations are determined in various modes, caused by the characteristics of the excitation field and the material parameters of the film.

Support by RFBR and Komi Republic (project No. 20-42-110004) is acknowledged.

1. R.L. Comstock and R.C. LeCraw, J. Appl. Phys. **34**(10), 3022 (1963).
2. E. Kikuchi, Ultrasonic Transducers. Mir, Moscow, p. 424 (1972) [in Russian].
3. F.F. Asadullin, S.M. Poleshchikov, D.A. Pleshev, L.N. Kotov, V.S. Vlasov, V.G. Shavrov, V.I. Shcheglov, Journal of Siberian Federal Universit. Mathematics and Physics **10**(1), 36–39 (2017).
4. W.-G. Yang and H. Schmidt, App. Phys. Rev. **8**, 021304 (2021).
5. V.S. Vlasov, D.A. Pleshev, V.G. Shavrov, V.I. Shcheglov, Journal of Radio Electronics **7** (2020).

CONDITIONS FOR EFFICIENT DETECTING A FREQUENCY-MODULATED ALTERNATING MAGNETIC FIELD BASED ON MAGNETOELASTIC OSCILLATIONS OF YIG FILM

M.A. Filitov[1*], *S.A. Maltseva*[1], *F.F. Asadullin*[1], *D.A. Pleshev*[1,2], *V.S. Vlasov*[2], *V.I. Shcheglov*[3]

[1]Saint-Petersburg State Forest Technical University named after S.M. Kirov, St-Petersburg, Russia
[2]Syktyvkar State University, Syktyvkar, Russia
[3]Institute of Radioengineering and Electronics of the RAS, Moscow, Russia
[*]E-mail: filitovm@bk.ru

Magnetostrictive transducers based on single-crystal and composite thin-film ferrite structures are widely used. In this regard, special attention has been given to materials based on yttrium iron garnet (YIG), which have a high quality factor [1]. The use of the geometry of a normally magnetized thin plate makes it possible to avoid parametric excitation of exchange waves and increase the power of excited hypersonic oscillations by more than two orders of magnitude [2, 3].

The work [2] shows the possibility of implementing the detection of a frequency-modulated alternating magnetic field based on resonance magnetoacoustic properties of thin film. However, despite the deep study of the topic, a number of issues were not considered. The paper investigates a model based on a system of ordinary differential equations similar to that presented in work [4]. This system was solved numerically by the Runge-Kutta method of 7-8 orders with integration control at each step.

The relationships between the dynamics of the magnetic and elastic subsystems of magnetic films and their material characteristics when exited by constant and frequency-modulated alternating magnetic fields are found.

The paper considers the dependencies of ferromagnetic film magnetization oscillations and elastic displacements on the frequency modulation index and the amplitude of a perturbing external frequency-modulated magnetic field. The material parameters of the film and the excitation characteristics necessary for efficient detection of a frequency-modulated alternating field are determined.

Support by RFBR and Komi Republic (project No. 20-42-110004) is acknowledged.

1. R.L. Comstock and R.C. LeCraw, J. Appl. Phys. **34**, 3022 (1963).
2. V.S. Vlasov, D.A. Pleshev, V.G. Shavrov, V.I. Shcheglov, Journal of Radio Electronics **7** (2020).
3. V.S. Vlasov, L.N. Kotov, V.G. Shavrov, V.I. Shcheglov, J. Commun. Technol. Electron. **54**, 821–832 (2009).
4. M.S. Kirushev, V.S. Vlasov, D.A. Pleshev, F.F. Asadullin, L.N. Kotov, V.G. Shavrov, V.I. Shcheglov, Solid State Phenom. **233-234**, 73–78 (2015).

F.P9

MAGNETOCALORIC EFFECT, HEAT CAPACITY AND EXCHANGE INTERACTIONS IN NONSTOICHIOMETRIC $Er_{0.65}Gd_{0.35}Co_2Mn_x$ COMPOUNDS

E.G. Gerasimov[1,2*], *A.A. Inishev*[1,2], *N.V. Mushnikov*[1,2], *P.B. Terentev*[1,2], *V.S. Gaviko*[1,2], *M.S. Anikin*[2]

[1]Mikheev Institute of Metal Physics of Ural Branch of Russian Academy of Sciences, Ekaterinburg, Russia
*2*Institute of Natural Sciences and Mathematical, Ural Federal University, Ekaterinburg, Russia
[*]E-mail: gerasimov@imp.uran.ru

In nonstoichiometric compounds, new possibilities open up for influencing the magnetic properties that were previously unavailable in conventional substitutional solid solutions. In this work we determined the exchange interactions in nonstoichiometric compounds of the RCo_2Mn_x-type (R is Er, $Er_{0.35}Gd_{0.65}$ and Tb) within a two-sublattice mean field model. We extended plateau-like temperature dependence of the field induced magnetic entropy change ΔS_m, which was observed earlier for nonstoichiometric $ErCo_2Mn_x$ alloys [1], to temperatures above room temperature. To do it we partially substitute Gd for Er for the $Er_{0.65}Gd_{0.35}Co_2Mn_x$ compounds. This substitution results in increasing of the Curie temperature from 170 K up to 324 K with preservation of plateau-like shape of $\Delta S_m(T)$ and high value of Relative Cooling Power up to 235 J/kg, the full width at half maximum of ΔS_m (ΔT_{FWHM}) up to 310 K and refrigerant capacity (R_C) up to 196 J/kg. In theory, this allows to use these compounds for magnetic cooling starting from room temperature up to 50 K since they keep unchanged their ΔS_m and ΔT in this temperature range. However, the maximal values of ΔS_m (~0.8 J/kgK) and ΔT (~0.6 K) with magnetic field change 0–20 kOe are quite small. The origin of plateau-like shape of $\Delta S_m(T)$ in the compounds is linear temperature dependence of the magnetization $M(T)$ over a wide temperature range [2].

The research was carried out within the state assignment of Ministry of Science and Higher Education of the Russian Federation (themes "Magnet" and "Alloys") and supported in part by RFBR (project No. 20-42-660008) and government of Sverdlovsk region.

1. E.G. Gerasimov, N.V. Mushnikov, A.A. Inishev, P.B. Terentev, V.S. Gaviko. J. Alloys and Compounds **680**, 359–365 (2016).
2. E.G. Gerasimov, A.A. Inishev, N.V. Mushnikov, P.B. Terentev, V.S. Gaviko, M.S. Anikin. Intermetallics **140**, 107386 (2022).

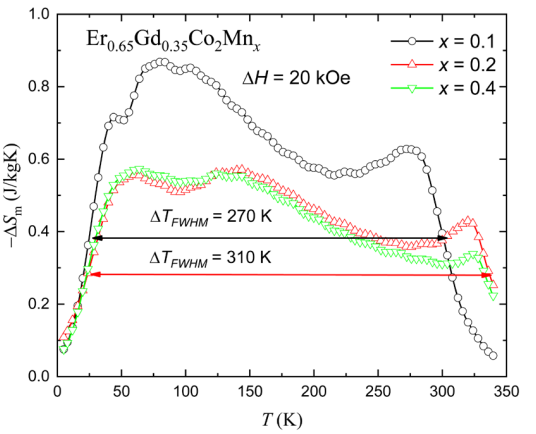

Figure 1. Temperature dependences of magnetic entropy change ΔS_m for magnetic field change $\Delta H = 20$ kOe in $Er_{0.35}Gd_{0.65}Co_2Mn_x$ ($x = 0.1$, 0.2, 0.4). The arrows show the full width ΔT_{FWHM} at half maximum of ΔS_m.

DEFORMATION OF A STRUCTURED MAGNETICALLY ACTIVE ELASTOMER WITH MAGNETICALLY HARD INCLUSIONS IN A 2D FORMULATION

A.A. Ignatov[1*], *O.V. Stolbov*[2], *V.V. Rodionova*[1]

[1]Immanuel Kant Baltic Federal University, Kaliningrad, Russia
[2]Institute of Continuum Mechanics, Ural Branch of the Russian Academy of Sciences, Perm, Russia
[*]E-mail: artem.ignatov98@gmail.com

In the last few years, there has been an increased interest in "smart" materials based on a polymer with magnetic inclusions [1, 2]. Numerical methods are used to study the quantitative properties of such materials [3]. This work is devoted to the calculation of deformations in an external field of a structured magnetically active elastomer with magnetically hard inclusions in a 2D formulation by the finite element method using the FEniCS package.

In the initial state, the particles (Fig. 1) were located at the nodes of a 4×4 rectangular grid with square cells and had a "checkerboard" orientation of magnetic moments – any neighboring particles in a vertical column or horizontal row have an antiparallel orientation of magnetic moments.

Another simulated series of configurations (Fig. 2) was a rectangular parallelogram with an aspect ratio of varying from 6 to 12. The particles were located at the nodes of a 2×12 rectangular grid. 12 particles were located along the long side. The distance between particles located along the short side (r_x) did not change. Only the distance between the particles located along the long side (r_y) changed from $r_x = r_y$ to $r_x = 2r_y$. In the initial state, the magnetic moments of all particles were codirectional and oriented along the long side. In the course of the experiment, the dependences of the relative strain on the applied field were obtained for configurations with different r_y.

The Neo-Hooke potential [4] was used to describe the hyperelastic matrix material. In modeling, the shape of the particles was assumed to be an ideal circle, and the particles themselves were considered to be single-domain. Also, during the simulation, the possibility of destruction of the matrix-particle boundary was excluded, i.e. full adhesion of particles and matrix was assumed.

As a result, the deformations of the material were calculated depending on the initial orientation of the magnetization of the particles and the magnitude of their magnetic moments.

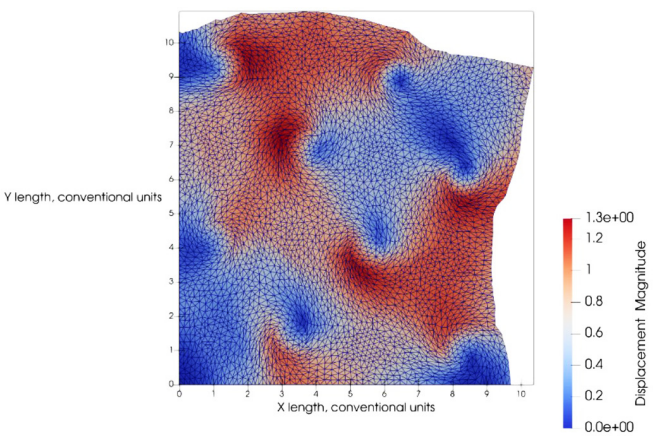

Figure 1. Deformation of an elastic matrix with hard magnetic particles.

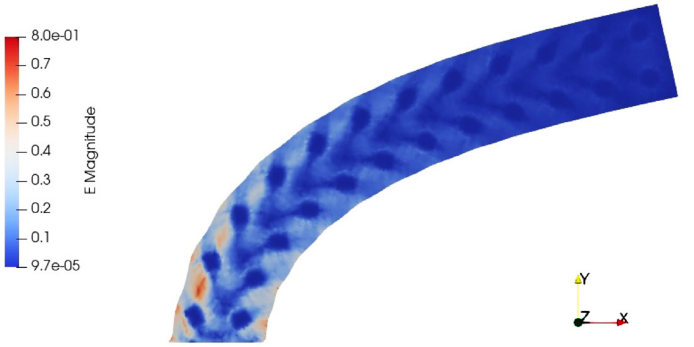

Figure 2. Deformation of an elastic matrix by hard magnetic particles in an external magnetic field.

The reported study was funded by Russian Science Foundation, project number 21-72-30032.

1. A. Allue, P. Corte-León, K. Gondra, V. Zhukova, M. Ipatov, J. Maria Blanco, A. Zhukov, Composites Part A: Applied Science and Manufacturing (2019).
2. Z. Varga, G. Filipcsei, M. Zrínyi, Polymer **46**(18), 7779–7787 (2005).
3. G. Sossou, F. Demoly, H. Belkebir, H.J. Qi, S. Gomes, G. Montavon, Materials and Design **181**, 108074 (2019).
4. A.I. Lurie, Theory of Elasticity. Nauka, 1970, published in Russian.

MAGNETOSTRICTION IN NONSTOICHIOMETRIC $TbCo_2Mn_x$ COMPOUNDS

A.A. Inishev[1,2*], *E.G. Gerasimov*[1,2], *P.B. Terentev*[1,2], *N.V. Mushnikov*[1,2]

[1]Institute of Metal Physics UB RAS, Ekaterinburg, Russia
[2]Institute of Natural Sciences and Mathematical, Ural Federal University, Ekaterinburg, Russia
[*]E-mail: inishev@imp.uran.ru

The cubic Laves phases RCo_2 (R – is a rare earth metal) compounds possess gigantic magnetostriction values and are promising materials for various magnetostriction applications [1]. In these compounds, band magnetism of 3d cobalt sublattice provides large volume magnetostriction whereas localized magnetism of 4f rare-earth sublattice leads to existence of giant single-ion anisotropic magnetostriction at low temperatures [2].

Recently, the existence of new nonstoichiometric compounds RCo_2Mn_x with a structure of the $MgCu_2$-type was discovered [3]. In contrast to traditional substitutional $RCo_{2-x}M_x$ solid solutions, in which atoms of 3d transition metals occupy only positions (16*d*), in nonstoichiometric RCo_2M_x compounds atoms also partially occupy positions of a rare-earth metal (8*a*). In particular, it was shown that, in the concentration range $x < 0.4$, there exist single-phase $TbCo_2M_x$ compounds with $MgCu_2$ type structure. Manganese atoms in these compounds occupy up to 9% of the rare earth positions of Tb (8*a*). With an increase in the concentration of manganese, the Curie temperature rises from 235 K for $TbCo_2$ to 350 K for $TbCo_2Mn_{0.4}$. The synthesis of nonstoichiometric compounds makes it possible to simultaneously change both the magnetism of the 3d sublattice of cobalt and the magnetic anisotropy of the 4f sublattice of the rare earth metal. Magnetostriction in such nonstoichiometric compounds has not yet been investigated. The purpose of this work was to study magnetostriction in nonstoichiometric $TbCo_2M_x$ ($0 \le x \le 0.6$) compounds.

According to X-ray diffraction analysis data, $TbCo_2M_x$ compounds with $x < 0.4$ are single-phase and crystallize in a $MgCu_2$ type crystal structure. When the temperature drops below the Curie temperature, magnetic ordering occurs, which leads to rhombohedral distortions of the cubical crystal lattice (Fd-3m space group), and the formation of a rhombohedral structure (R-3m space group). In the alloy with $x = 0.4$, along with the phase with the $MgCu_2$ structure, there is a small amount of the phase with the $PuNi_3$ type structure. The alloy with $x = 0.6$ is already significantly non-single-phase and, in addition to the phase with the $MgCu_2$ structure, it contains phases with structures of the $PuNi_3$ (R-3m space group) and Th_6Mn_{23} (Fm-3m space group) [3, 4].

In our work [5], it is shown that with an increase in the manganese concentration, the volume contribution to the magnetostriction of compounds decreases, which is due to an increase in the localization of the magnetic moment of the 3d sublattice. An increase in the concentration of manganese in nonstoichiometric compounds leads to a significant increase in linear magnetostriction at room temperature, which makes it possible to consider nonstoichiometric $TbCo_2M_x$ compounds as potential promising materials for various magnetostrictive applications.

The research was carried out within the state assignment of Ministry of Science and Higher Education of the Russian Federation (theme ("Magnet" 122021000034-9), supported in part by RFBR (project No. 20-42-660008).

1. N.H. Duc, Anh D.T. Kim, and P.E. Brommer, Phys. B **319**, 1–8 (2002).
2. E. Gratz and A.S. Markosyan, J. Phys.: Condens. Matter **13**, 385–413 (2001).
3. C. Fang et al., Phys. Rev. B **96**, 064425 (2017).
4. A.A. Inishev et al., Phys. Metals and Metall. **118**(11), 1036–1042 (2018).
5. E.G. Gerasimov et al., JMMM **523**, 167628 (2021).

F.P12

RELATIONSHIP OF THE MAGNETIC AND ELASTIC SUBSYSTEMS IN THE CASE OF THE SHEAR MODULUS IN NICKEL

*E.L. Kolyvanov**, *I.V. Shashkov*

Institute of Solid State Physics RAS, Chernogolovka, Russia
*E-mail: kolyvan@issp.ac.ru

In polycrystalline nickel, the temperature dependences of the shear modulus and damping and the effect of a magnetic field with an amplitude of up to 150 Oe were determined by the method of an inverse torsion pendulum at frequencies of about 40 Hz.

In the temperature range from approximately 200 to 400 K, a decrease in the shear modulus was found, accompanied by a broad peak of internal friction, which is characteristic of the relaxation process, Fig. 1. In this case, the shear modulus defect is about 2.5%. The maximum peak of internal

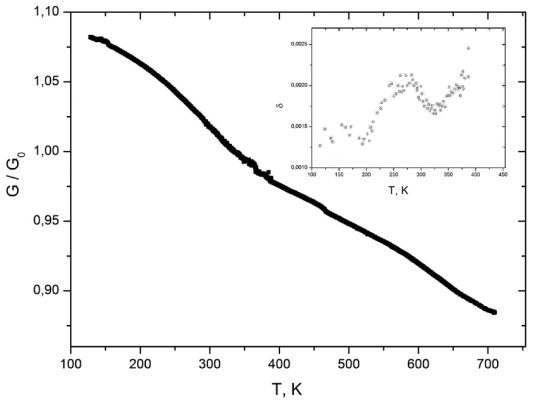

Figure 1. Temperature dependences of internal friction δ (on insert) and the shear modulus *G* normalized with its value at room temperature

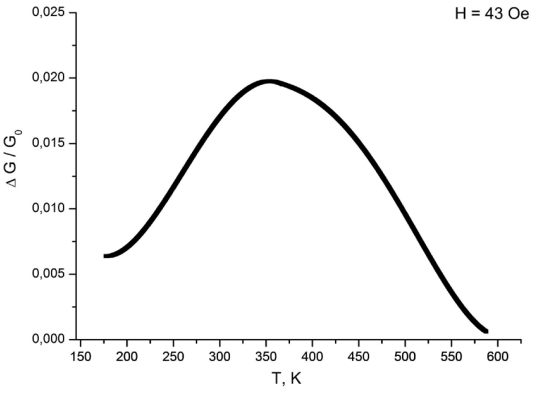

Figure 2. Temperature dependence of magnetic field contribution to the shear modulus, i.e. the difference between dependence without a magnetic field and with a field of 43 Oe.

friction lies near 270 K. From the resonance condition $\omega\tau = 1$ at this temperature, the Gibbs activation energy is estimated to be $G = 0.6$ eV. The study of the influence of a constant magnetic field at different temperatures, Fig. 2, showed that, starting from temperatures from about 250-270 K, the contribution of the magnetic field to the shear modulus (magnetoelastic effect) begins to increase rapidly. That is, in principle, the observed relaxation process can be associated with the thermally activated mobility of the boundaries of magnetic domains. On the other hand, the same activation energies are characteristic of the interaction of dislocations with point defects (Hasiguti peaks). In order to determine which mechanism is predominant (the Hasiguti process or the magnetoelastic effect), it is necessary to made comparative studies for samples with different degrees of deformation.

MAGNETIC PHASE TRANSITIONS AND MAGNETOCALORIC EFFECT IN COMPOUNDS BASED ON $Gd_5Si_2Ge_2$

A.A. Kurganskaya[1*], *A.V. Smirnov*[1], *I.A. Ovchenkova*[1], *A.E. Bogdanov*[1], *A.V. Morozkin*[2], *I.S. Tereshina*[1], *S.A. Nikitin*[1]

[1]Department of Physics, Lomonosov Moscow State University, Moscow, Russia
[2]Department of Chemistry, Lomonosov Moscow State University, Moscow, Russia
[*]E-mail: kurganskaia.aa17@physics.msu.ru

$Gd_5(Si_{1-x}Ge_x)_4$ compounds are of great interest, due to the giant magnetocaloric effect, colossal magnetostriction, and giant magnetoresistance, which are caused by the magnetostructural phase transitions detected in these compounds [1–3]. However, despite the observed record MCE values, compounds based on $Gd_5Si_2Ge_2$ have a number of significant limitations. A large temperature hysteresis, the presence of high values of the MCE only when the sample is cooled, and the absence of repeatability of the effect during thermal cycling significantly limit the possibilities of practical application of these materials. In addition, high values of the MCE obtained from measurements of magnetization and heat capacity using the Maxwell relations do not always agree with direct measurements of the MCE (perhaps due to the non-reproducibility of the results with hysteresis). In our previous works we observed that some compounds based on $Gd_5(Si_{1-x}Ge_x)_4$ with a second-order phase transition can demonstrate magnetothermal properties better than the compounds with the first order phase transition [4]. Usually, this effect can be achieved with very small substitutions in the parent compounds with a first-order phase transition. In this work, we carried out a number of substitutions in both the rare-earth and the p-sublattices in order to change the order of the phase transition and study the effect of the transition order on the MCE.

$Gd_{5-x-y}Tb_xTi_ySi_2Ge_2$ (x = 0, 0.5, 1, y = 0, 0.1), and $Gd_5(SiGe)_{2-x}Sn_x$ (x = 0, 0.05, 0.1) samples were prepared by electric arc melting in a laboratory electric arc furnace. The samples were annealed in a quartz ampoule in an argon atmosphere at a temperature of 800 °C for a week, followed by quenching in ice water. Local X-ray spectral analysis of the samples was carried out using a scanning electron microscope. According to the data of X-ray diffraction analysis for all compounds, the main phase is the monoclinic phase $Gd_5Si_2Ge_2$. The content of the main phase exceeds 90 wt.% for $Gd_{5-x-y}Tb_xTi_ySi_2Ge_2$ and 80 wt.% for $Gd_5(SiGe)_{2-x}Sn_x$ series. The insertion of Tb and Ti monotonically decreases the lattice parameters, while Sn expands the crystal lattice.

The magnetization measurements detected a typical ferromagnetic behavior for all the studied compounds. $Gd_5Si_2Ge_2$ compound shows large magnetization values at temperatures below 260 K, while above 260 K magnetization decreases rather quickly with increasing temperature. In this case, in the region of the magnetization decrease, the curves taken during heating and cooling of the sample do not coincide, indicating a significant temperature hysteresis. The temperature hysteresis was also obtained on the temperature dependences of the MCE of $Gd_5Si_{1.95}Ge_{1.95}Sn_{0.1}$ and $Gd_5Si_{1.975}Ge_{1.975}Sn_{0.05}$. The magnitude of the MCE of the samples while cooling is much greater than that while heating, and the temperature at which the maximum MCE was observed is slightly lower in the former case. Moreover, it has been found that when the samples are cooled, the magnitude of the MCE decreases, if successive measurements are made at the same temperature. When measuring the hysteresis loops in the region of the phase transition, it was also found that when the magnetic field is removed, there is no spontaneous magnetization of the sample, i.e., the decrease in the MCE during cyclic measurements cannot be attributed to the residual magnetization. The observed effect can be explained by the presence of an irreversible structural phase transition that occurs in

a magnetic field when it is first turned on. The maximal value of MCE for $Gd_5Si_{1.95}Ge_{1.95}Sn_{0.1}$ is close to the value obtained for $Gd_5Si_2Ge_2$.

We have found previously [4] that a small introduction of Ti into $Gd_5Si_2Ge_2$ increases the magnetic ordering temperature and changes the order of the phase transition while maintaining the values of the high magnetocaloric effect. At the same time, the large temperature and field hysteresis observed for the ΔT_{ad} effect in $Gd_5Si_2Ge_2$ significantly decreases with the addition of Ti. In this work, we attempted to change the type of phase transition by introducing Tb and Ti into the rare earth sublattice. When Gd is replaced by Tb, the transition temperature decreases monotonically with increasing terbium concentration. With an increase in the concentration of terbium in the rare earth sublattice up to 20%, the temperature hysteresis disappears and the type of transition changes. At the same time, a sharp reversible change in the magnetic moment remains in the region of the Curie temperature. The insertion of Ti into the $Gd_{5-x}Tb_xSi_2Ge_2$ compounds allows one to raise the transition temperature to values similar to those of the initial $Gd_5Si_2Ge_2$ composition, and in this case, there is no temperature hysteresis and the sharp reversible change in the magnetic moment is preserved.

According to X-ray diffraction data, the $Gd_5Si_2Ge_2$ compound crystallizes into a monoclinic structure of the $Gd_5Si_2Ge_2$-type at room temperature. Upon cooling, this compound undergoes a structural phase transition from a monoclinic to an orthorhombic structure. The structural transition leads to a first-order magnetic phase transition at the same temperature. With the introduction of a small amount of Ti the unit cell volume decreases. The magnetic ordering temperature increases with decreasing unit cell volume. The change in the Curie temperature with the addition of Ti or Tb leads to the fact that, in contrast to the parent compound, the magnetic and structural phase transitions are not coupled. Therefore, in doped compounds upon cooling first a magnetic phase transition takes place, and then a structural transformation from the monoclinic to the orthorhombic phase occurs. A similar separation of the magnetic and structural phase transitions was observed for the $Gd_5Si_{2-x}Ge_{2-x}In_{2x}$ [5] $Gd_{5-x}Ti_ySi_2Ge_2$ [4]. The presence of both structural and magnetic transitions retains high values of the MCE, while a separation of these transitions in temperature makes these transitions reversible.

This work was supported by a grant from the Russian Science Foundation № 22-29-00773, https://rscf.ru/project/22-29-00773/.

1. V.K. Pecharsky and K.A. Gschneidner, Jr., Phys. Rev. Lett. **78**, 4494 (1997).
2. L. Morellon, P.A. Algarabel, M.R. Ibarra, J. Blasco, B. Garcıa-Landa, Z. Arnold, and F. Albertini, Phys. Rev. B **58**, R14721 (1998).
3. W. Choe, V.K. Pecharsky, A.O. Pecharsky, K.A. Gschneidner, Jr., V.G. Young, Jr., and G.J. Miller, Phys. Rev. Lett. **84**, 4617 (2000).
4. S.A. Nikitin, A.V. Smirnov, I.A. Ovchenkova, et al., J. Appl. Phys. **124**, 083902 (2018).
5. S.A. Nikitin et al., Solid State Phenomena, vol. 233–234, Trans Tech Publications, Ltd., July 2015, pp. 208–211. Crossref, doi:10.4028/www.scientific.net/ssp.233-234.208.

INFLUENCE OF THE [011] FERRITE FILM CRYSTALLOGRAPHIC CELL ORIENTATION ON THE DETECTION OF ALTERNATING AMPLITUDE-MODULATED MAGNETIC FIELD

D.K. Lytkin[1*], *P.A. Nikiforova*[1], *D.A. Pleshev*[1,2], *F.F. Asadullin*[1], *V.S. Vlasov*[2], *L.N. Kotov*[2], *V.I. Shcheglov*[3]

[1]Saint-Petersburg State Forest Technical University named after S.M. Kirov, St-Petersburg, Russia
[2]Syktyvkar State University, Syktyvkar, Russia
[3]Institute of Radioengineering and Electronics of the RAS, Moscow, Russia
[*]E-mail: daniil352002@gmail.com

Magnetoacoustic converters operating in the microwave range find applications in many fields of science and technology [1]. The normally magnetized monocrystalline and composite thin-film ferrite structures are used as converters. This makes it possible to increase the power of excited hypersonic oscillations [2, 3].

Magnetoelastic oscillations of a ferrite film with crystallographic anisotropy excited by an amplitude-modulated alternating magnetic field are considered. The conditions for the oscillations detection at the modulation frequency due to the magnetostrictive properties of the magnetic film are determined. The dependencies of the excitation of magnetic and elastic dynamics on the material parameters and excitation parameters are shown.

The general scheme of the detection is described in detail in work [4]. The influence of the orientation of the crystallographic cell [001] and [111] on the magnetoelastic dynamics is considered in work [5]. However, the dependence of the magnetic and elastic subsystem dynamics on the orientation of the crystallographic cell [011] under applied an amplitude-modulated alternating magnetic field, as well as the nature of parametric portraits of magnetization and elastic displacement are not described.

This work is deal with the research of the detection possibility of an amplitude-modulated alternating magnetic field and the study of the excitation mode of magnetization components and the elastic displacement oscillations of a ferrite film with the [011] crystallographic cell orientation, as well as the parametric portraits of their oscillations in various excitation modes.

Support by Russian Science Foundation (project no. 21-72-20048) is acknowledged.

1. W.-G. Yang and H. Schmidt, App. Phys. Rev. **8**, 021304 (2021).
2. D.I. Sementsov, A.M. Shuty, Physics Uspekhi **50**(8), 793 (2007).
3. V.S. Vlasov, L.N. Kotov, D.A. Pleshev, F.F. Asadullin, S.M. Poleshikov, V.G. Shavrov, V.I. Shcheglov, Solid State Phenomena **233-234**, 480–484 (2015).
4. V.S. Vlasov, D.A. Pleshev, V.G. Shavrov and V.I. Shcheglov, Journal of Radio Electronics **3** (2019) [in Russian].
5. D.A. Pleshev, F.F. Asadullin, V.S. Vlasov, L.N. Kotov and V.I. Shcheglov, Phys. of Metals and Metall. **123**(3), 297–302 (2022).

MAGNETOELASTIC EFFECTS IN THERMAL EXPANSION OF Fe_7Se_8 SINGLE CRYSTAL

S.N. Mozgovykh[1*], *V.A. Kazantsev*[2], *D.F. Akramov*[1], *E.M. Sherokalova*[1], *N.V. Selezneva*[1]

[1]Institute of Natural Sciences and Mathematics, Ural Federal University, Ekaterinburg, Russia
[2]M.N. Miheev Institute of Metal Physics, UB of RAS, Ekaterinburg, Russia
[*]E-mail: Stepan.Mozgovykh@urfu.ru

The pyrrhotite-type compound Fe_7Se_8 has a layered superstructure of the NiAs type with alternating layers of iron and selenium. The magnetic moments of iron atoms in Fe_7Se_8 are arranged ferromagnetically inside each layer, but coupled antiferromagnetically between successive layers, the presence of vacancies results in incomplete compensation of magnetic moments and leads to ferrimagnetism. Two magnetic transitions were found in the Fe_7Se_8 compound with a change in temperature. The high-temperature transition from paramagnetic to the ferrimagnetically ordered phase occurs at $T_N \sim 450$ K regardless of the nature of the ordering of vacancies. At a temperature $T_{SO} \sim 120$ K, another magnetic transition is observed associated with spin reorientation from the easy *c*-plane toward the *c*-axis upon cooling. The temperature and character of the spin-reorientation transition depend both on the content and ordering of vacancies [1, 2], pressure [3] and microstresses [4]. In the temperature range from 630 to 670 K, a number of order-order and order-disorder structural phase transitions were observed as well [1, 2]. The magnetocaloric effect is observed in Fe_7Se_8 not only in the vicinity of the magnetic ordering temperature, but also around the spin-reorientation transition [4, 5].

The aim of this work is to study the thermal properties of Fe_7Se_8 single crystals. The single crystalline samples of $Fe_{7-\delta}Se_8$ were prepared from high purity selenium (99.999) and iron (99.98) in a vertical gradient furnace using a modified Bridgman method. The control of the orientation of single crystals was carried out by the Laue method. Thermal expansion measurements were performed by means of a DL-1500 RHP dilatometer (ULVAC-SINKU RIKO, Japan) in the temperature range from 80 to 700 K. The temperature and field dependences of the magnetization were measured in the temperature range 2–380 K using a MPMS SQUID-magnetometer (Quantum Design) in magnetic fields up to 70 kOe.

For the first time, thermal expansion was studied by the dilatometry method on a single crystalline sample. The anisotropic nature of the deformations of the crystal lattice upon cooling below magnetic ordering temperature was revealed; in contrast to the contraction of the lattice in the basal plane, a significant expansion along the *c*-axis was observed with decreasing temperature. It has been found that spin-reorientation transition is accompanied by a sharp change in the linear thermal expansion coefficients. Based on the low-temperature heat capacity data for the paramagnetic compound Co_7Se_8, the Debye temperature is determined as $\Theta_D = 300$ K; and this Θ_D value is used to determine the magnetic contributions to thermal expansion. It is found that the value of spontaneous magnetostriction in Fe_7Se_8 is about $\omega_s = -5.1 \cdot 10^{-3}$. An anomalous change in ω_s is also observed during the spin-reorientation transition, which implies a possible change in the value of the magnetic moment of Fe. The results obtained in the present work indicate a strong interplay between lattice deformations and changes in the magnetization in Fe_7Se_8. An increase in the concentration of vacancies has a significant effect on the low-temperature magnetic phase transition.

The present work was supported by the Russian Science Foundation (Grant No 22-13-00158).

1. T. Kamimura, J. Phys. Soc. Japan **43**, 1594 (1977).
2. K. Hirakawa, J. Phys. Soc. Japan **12**, 929 (1957).
3. Y. Konopelnyk et al., JMMM **543**, 168626 (2022).
4. Д.Ф. Акрамов и др., ФММ **123**, 305 (2022).
5. I. Radelytskyi et al., J. Appl. Phys. **124**, 143902 (2018).

MAGNETIC AND STRUCTURAL PROPERTIES OF THE $GdRu_{1-x}Cr_xSi$ COMPOUNDS

S.P. Platonov[1*], A.G. Kuchin[1], V.S. Gaviko[1,2], A.S. Volegov[1,2], M.Yu. Yakovleva[1]

[1]Institute of Metal Physics UB RAS, Ekaterinburg, Russia
[2]Ural Federal University, Ekaterinburg, Russia
[*]E-mail: platonov@imp.uran.ru

The RTX family of materials, where R is a rare earth metal, T is a transitional metal and X is a p-block element, consists of many compounds with interesting fundamental properties and application potential [1]. Relevant is the search for new magnetocaloric materials in magnetic refrigerates due to high efficiency, reliability, and environmental safety. For instance, the GdFeSi compound exhibits rather a large value of the magnetocaloric effect MCE of 6 J/kgK in a field changing to 20 kOe at Curie temperature T_C = 130 K [1]. Partial substitution of Cr for Fe made it possible to raise T_C to 250 K in $GdFe_{0.6}Cr_{0.4}Si$, but the MCE decreases to 2.4 J/kgK due to the inhomogeneity of the substitutional alloy [2].

It is of interest to study the magnetic and magnetothermal properties of the $GdRu_{1-x}Cr_xSi$ substitutional alloys with different atomic radii of Ru 4d and Cr 3d components. The $GdRu_{1-x}Cr_xSi$, x = 0–0.3 intermetallic compounds with a tetragonal structure of the CeFeSi (P4/nmm) type have been synthesized for the first time. The lattice parameters a and c slightly decreases and increases, respectively, as is seen in Fig. 1. This means that Cr is presented in the $GdRu_{1-x}Cr_xSi$ compounds. The magnetization curves $M(H)$ at 4 K for the $GdRu_{1-x}Cr_xSi$ compounds can be interpreted considering a collinear ferromagnetic structure.

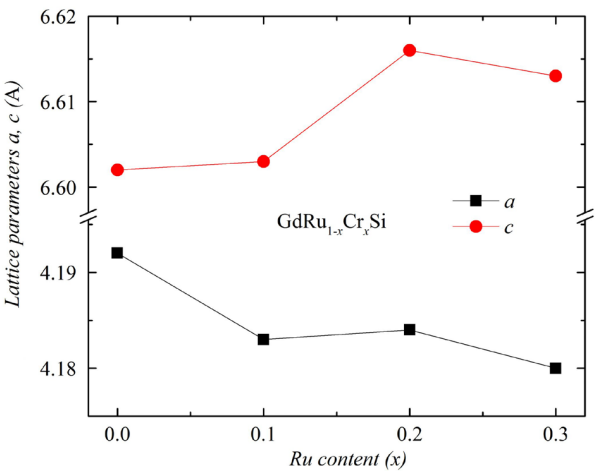

Figure 1. Concentration dependences of the lattice parameters a and c of the $GdRu_{1-x}Cr_xSi$ compounds.

The isothermal magnetic entropy change $-\Delta S_M$ (i.e. the magnetocaloric effect MCE) for the $GdRu_{1-x}Cr_xSi$, x = 0, 0.2 compounds was calculated for the first time from the magnetization isotherms M(H) using the well-known Maxwell relation. Figure 2 illustrates the isothermal magnetic

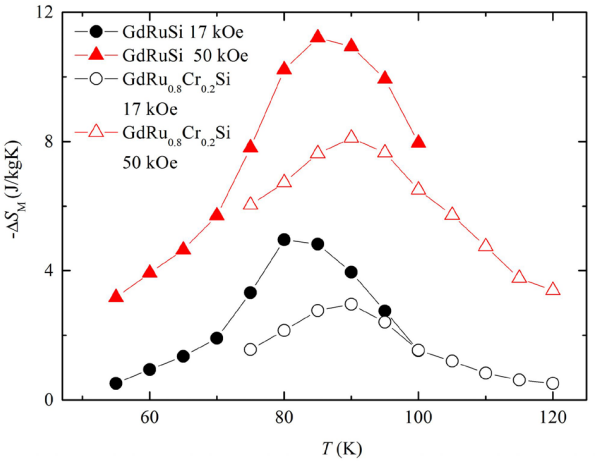

Figure 2. Temperature dependences of the change in magnetic entropy $-\Delta S_M(T)$ in a field changing to 17 kOe or 50 kOe for the compounds $GdRu_{1-x}Cr_xSi$ x = 0, 0.2.

entropy changes $-\Delta S_M$ for $GdRu_{1-x}Cr_xSi$, x = 0, 0.2 as a function of temperature in a field changing to 17 or 50 kOe. They are typical of the second-order magnetic phase transitions.

The value of MCE is rather large for both compounds. Also the Curie temperature (the position of the peak of $-\Delta S_M(T)$) somewhat increases from 85 to 90 K in the substitutional compound.

Support by RSF 18-72-10098, https://rscf.ru/en/project/18-72-10098/ is acknowledged.

1. S. Gupta and K. Suresh, J. Alloys Compd. **618**, 562–606 (2015).
2. A.G. Kuchin, S.P. Platonov, A.V. Lukoyanov, A.S. Volegov, V.S. Gaviko, R.D. Mukhachev and M.Yu. Yakovleva, Intermetallics **133**(6), 107183 (2021).

MODELING OF ITINERANT MAGNETOCALORIC EFFECT IN Si, Al DOPED METAMAGNETIC $LaFe_{13}$

D.I. Radzivonchik[1*], *V.I. Grebennikov*[1,2]

[1]IMP UB RAS, Ekaterinburg, Russia
[2]Ural State University of Railway Transport, Ekaterinburg, Russia
[*]E-mail: radzivonchik@mail.ru

The itinerant electron metamagnetic $LaFe_{13}$ compound with Si, Al-doping have revealed wide diversities of remarkable properties such as giant magnetocaloric effect (MCE). With increasing temperature, the compounds having ferromagnetic (FM) ground state undergo a first order transition to antiferromagnetic (AFM) state followed by a second order AFM to paramagnetic (PM) transition or only a first order FM-PM transition depending on the doping concentration.

At present, there is no modeling of the itinerant MCE based on the electronic structure of the real materials. In this work, we demonstrate a temperature modeling of the magnetization and MCE by means of the dynamic spin fluctuation theory [1], using the density of electronic states (DOS) of the doped $LaFe_{13}$ obtained from density functional theory calculations. Theory considers a system of itinerant 3d electrons with a strong intra-atomic interaction – $\sum_j u_j s_j^2$ (s_j is the electron spin operator of subsystem j-type; intra-atomic interaction parameter of electrons u_j takes two values $\{u_1, u_2\}$ with probabilities $c_j = \{c_1, c_2\}$ by which the effect of a diverse atomic environment is simulated). Reducing the many-body problem to a one-particle problem via the introduction of Hubbard-Stratonovich fields allows us to get the computable system of equations for local characteristics. Thus one can calculate the magnetic moment (m_j), susceptibility, entropy for each j-subsystem at an arbitrary temperature and also describe the magnetic states (ferromagnetic or ferrimagnetic) of the system and transitions between them. The temperature DOS from the theory obtained can be compared with the corresponding spectra of X-ray photoelectron spectroscopy. The dynamic spin fluctuations provide the main thermal mechanism of the magnetic moments disordering with increasing temperature, which leads to significant decrease of Curie temperature compared to the typical results (over 4000 K) of the mean field theory.

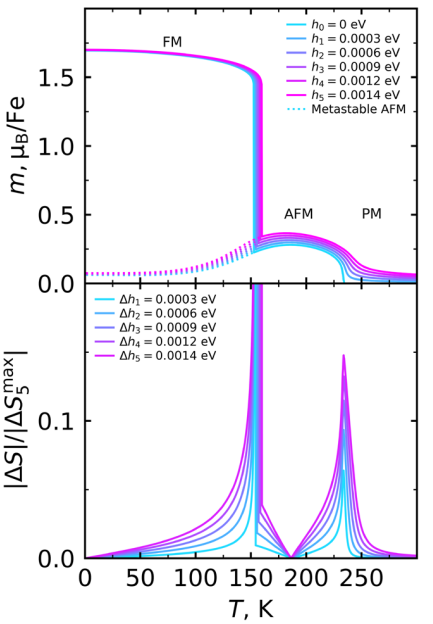

Figure 1. The calculated magnetization m and $|\Delta S|$ *vs* temperature in magnetic field h for $u_{1,2} = \{0.84, 0.76\}$ eV and $c_{1,2} = \{0.4, 0.6\}$.

Figure 1 shows an example of calculated magnetization and absolute isothermal entropy change $|\Delta S|$ within MCE as a function of temperature for $La(Fe_{0.89}Al_{0.11})_{13}$ in the finite magnetic field h. The full entropy (sum of electronic and magnetic contributions) was calculated by mean of an analytical formula derived from the theory. The results exhibit two successive magnetic transitions: FM-AFM and AFM-PM at T = 150 and 230 K,

respectively. The magnetization increase of AFM phase is due to a stronger thermal disordering of the magnetic moment in the second subsystem. The results generally reproduce the experimental behavior of the magnetization m ($m = c_1m_1 + c_2m_2$). However, for a more reasonable results, it is necessary to take into account phase separation. The report will present the calculations taking into account phase separation for various doped $LaFe_{13}$, including systems in which the first order FM-PM phase transition is revealed.

The research was carried out within theme "Quantum" No. AAAA-A18-118020190095-4, supported in part by RFBR (project No. 20-02-00541).

1. V.I. Grebennikov, Phys. Solid State **40**, 79–86 (1998).

DEFORMATION-INDUCED INCREASE OF THE ISOTROPIC ENERGY GAP IN IRON BORATE EPITAXIAL FILM

K. Seleznyova[*1], *D. Prilepsky*[1], *Yu.A. Mogilenec*[1], *M.B. Strugatsky*[1], *S.V. Yagupov*[1], *A. Drovosekov*[2], *N. Kreines*[2], *J. Kliava*[3]

[1]Physics and Technology Institute, Crimean Federal University, Simferopol
[2]P.L. Kapitza Institute for Physical Problems RAS, Moscow, Russia
[3]LOMA UMR 5798 CNRS-Université de Bordeaux, Talence, France
[*]E-mail: kira_seleznyova@mail.ru

Iron borate, $FeBO_3$ films epitaxially deposited on isostructural diamagnetic $GaBO_3$ substrate form unique transparent functional materials [1]. Moreover, from the standpoint of fundamental science, these films allow detailed studies of surface magnetism, previously observed in bulk single crystals of $FeBO_3$ [1]. The existence of the surface magnetism allows to consider these materials as active elements of magnetic memory [1]. Recently, the liquid phase epitaxy technique for synthesizing such thin magnetic films has been developed and the films have been synthesized for the first time by some of the present authors [1]. Our XRD-measurements of these films have shown that both the film and the substrate possess D^6_{3d} space group, and the mismatch between the crystal lattice parameters is *ca*. 2%. Antiferromagnetic resonance (AFMR) studies of these materials have shown that their Néel temperature is close to that previously determined for $FeBO_3$ single crystal. The AFMR spectra at room temperature measured in the microwave frequency ν range from 15.0 to 35.7 GHz are described by the low-frequency AFMR mode [1]: $\nu = \gamma[H(H + H_D) + H_\Delta^2]^{1/2}$, γ, H, H_D and H_Δ^2 being the gyromagnetic ratio, applied magnetic field, the Dzyaloshinskii-Moriya field and the isotropic energy gap, respectively. For $FeBO_3$ film, H_D is in good accordance with that for iron borate single crystal; on the other hand, H_Δ^2 in the film is several times larger than in the single crystal [1].

The aim of the present work is to provide an explanation of this unusual behaviour of H_Δ^2. This quantity is determined by the ratio of the elastic, μ_i and magnetoelastic, λ_i constants [2]:

$$H_\Delta^2 \propto \frac{4\lambda_3^2\mu_5 + \lambda_4^2\mu_3 - 4\lambda_3\lambda_4\mu_0}{4(\mu_3\mu_5 - \mu_6^2)}. \quad (1)$$

One can reasonably assume that the behaviour of H_Δ^2 is caused by mechanical deformations induced by the mismatch between the lattice parameters of the film and the substrate. However, as one can see from equation (1), H_Δ^2 does not *explicitly* depend on deformations; therefore the latter should be present in equation (1) in an *implicit* way. One can assume μ_i to be independent on deformation, see e.g. [3]; therefore, the deformation should significantly affect λ_i. The microscopic origin of λ_i is acomplicated interplay of dipole-dipole, exchange and spin-orbit couplings [4]. As all these interactions significantly decrease with increasing interatomic distances, in linear approximation one gets: $\lambda_i = \lambda_i^0 + \lambda_i^1 U$, where U is the deformation, and λ_i^0 and λ_i^1 are expansion coefficients. The latter equation allows explaining the discrepancy between H_Δ^2 for $FeBO_3$ single crystal and film: indeed, U occurs only in the latter case.

A support by the RSCF and the Ministry of Education, Science and Youth of the Republic of Crimea, in the framework of scientific project Grant no. 22-22-20112 is acknowledged.

1. S. Yagupov, M. Strugatsky et al., J. Magn. Magn. Mater. **417**, 338 (2016).
2. A.S. Borovik-Romanov and E.G. Rudashevskii, Soviet Physics JETP **20**, 1407 (1965). 3. D.P. Dandekar, Phys. Rev. **172**, 873 (1968).
4. R. Diehl, W. Jantz, B.I. Nolang et al., in Current Topics in Materials Science, E. Kaldis (ed.), vol. 11. Elsevier, New-York, pp. 241–387, (1984).

EXCITATION OF MAGNETIC AND ELASTIC OSCILLATIONS IN MAGNETIC CRYSTALS WITH INVERSION AREA OF THE SIGN OF THE FIRST ANISOTROPY CONSTANT

*L.N. Kotov**, *P.A. Severin*, *V.S. Vlasov*

Syktyvkar State University, Syktyvkar, Russia
*E-mail: kotovln@mail.ru

This work is devoted to the study of the magnetoelastic dynamics of manganese-zinc spinel (MZS) crystals in the region of a spin-reorientation phase transition. The system of ordinary differential equations describing magnetic and elastic oscillations was taken from the work [1]. The magnetic anisotropy constants and other material parameters as the functions of temperature was taken from the work [2]. MZS crystal with composition $Mn_{0.61}Zn_{0.35}Fe_{2.04}O_4$ is characterized by the presence of an inversion point of the sign of the first anisotropy constant K_1 [3, 4]. In the absence of DC magnetic field, the reorientation of the magnetization vector from the [100] easy magnetization axis to the [111]-axis is observed with decreasing temperature at $K_1 < -K_2/9$, where K_2 is the second magnetic anisotropy constant.

The magnetic vibrations were excited by the alternating magnetic field on frequency about tens of MHz with an amplitude of 0.1 Oe and a pulse duration in order of $3\cdot10^{-6}$ s. In calculations, the damping constant of elastic vibrations was assumed to be $\beta = 1.5\cdot10^{6}$ s^{-1}, and the damping parameter of magnetic vibrations was slightly exceeded the similar one for a real crystal. DC magnetic field no exceeded the maximum demagnetization field. Thus, the observed resonances are mainly due to the magnetic anisotropy fields. The calculations were made away from acoustic resonance, that is, when the elastic wave length is much smaller than the plate thickness. The dependences of the component of the unit magnetization vector m_x and elastic displacements u_x depending on the ratio of the magnetic anisotropy constants K_1/K_2 for this case were obtained (Fig. 1). The investigated range of values of the ratio of the magnetic anisotropy constants K_1/K_2 corresponds to their change in a real crystal in the temperature range from 100 to 350 K. The transition of the first anisotropy

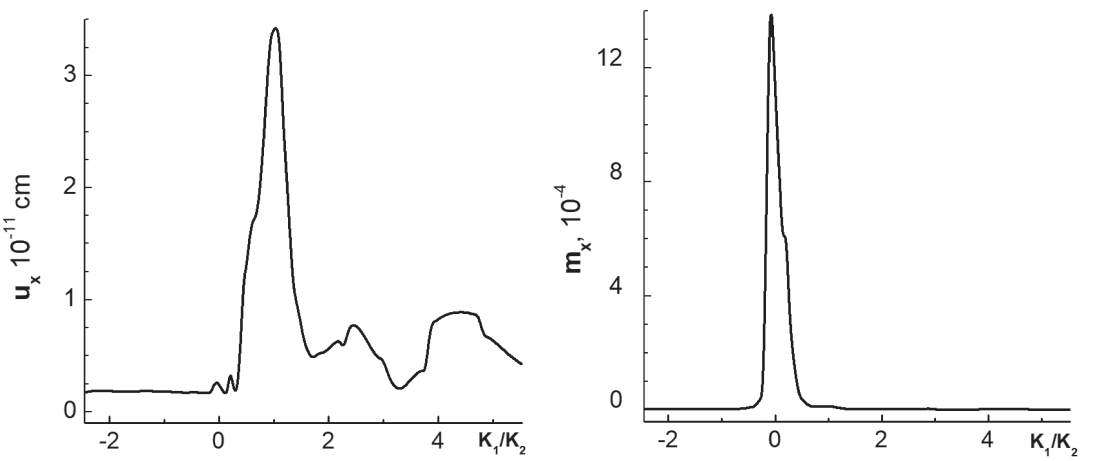

Figure 1. Dependences of amplitudes of elastic displacement u_x and magnetic component m_x versus K_1/K_2 ratio for normally magnetized plates.

constant through zero ($K_1 = 0$) occurs at $T \approx 263$ K. The obtained experimental and theoretical temperature dependences of the damping constant of acoustic waves in the MZS crystal have a good correlation.

This work was supported by the Russian Science Foundation, project no. 21-72-20048.

1. V.S. Vlasov, L.N. Kotov, V.G. Shavrov, V.I. Scheglov, J. Comm. Tech. El. **54**(7), 821–832 (2009).
2. L.N. Kotov, P.A. Severin, V.S. Vlasov, D.S. Beznosikov, E.L. Kotova, V.G. Shavrov, Phys. Solid State **60**(6), 1153–1157 (2018).
3. B.A. Goldin, L.N. Kotov, L.K. Zarembo, S.N. Karpachov, Spin-Phonon Interactions in Crystals. Leningrad, Nauka (1991) [in Russian].
4. V.A. Shutilov, L.N. Kotov, X. Mirzoahmetov, V.M. Sarnatsky, Phys. Solid State (6), 1783–1787 (1986).

MODELING THE EVOLUTION OF THE MARTENSITIC STRUCTURE OF A SHAPE MEMORY FERROALLOY IN A MAGNETIC FIELD

*A.A. Rogovoy, O.S. Stolbova**

Institute of Continuous Media Mechanics, Perm, Russia
*E-mail: sos@icmm.ru

Ferromagnetic alloys with shape memory effect (Heusler alloys) refer to the class of functional (smart) materials. They are able to change shape and size, due to the fact that large strains (up to 10%) occur in them under the action of external forces and magnetic fields [1]. In the absence of the applied mechanical load the austenite-to-martensite forward (direct) phase transformation from a cubic high-temperature phase (austenite) to a tetragonal low-temperature phase (martensite) leads to the formation of several twin-related "self-accommodated" variants of martensitic state. In these martensitic variants, magnetic domains arise, in which the magnetization vectors are directed along or against the easy magnetization axis of this domain. These domains are organized in such a way that they minimize the magnetostatic energy of the martensitic variants. The application of an external magnetic field to ferromagnetic alloys causes the motion of magnetic domain walls, the rotation of the magnetization vector and the reorientation (detwinning) of martensite variants (the last process is inherent only in the shape memory alloys). The process of detwinning is accompanied by a significant deformation 6-10 times higher than elastic.

Since the processes of detwinning, movement of the magnetic domains walls and rotation of the magnetic vector moment in each mesoelement representing a grain of material occur at the level of the structure of the material, it is necessary to build micromechanical models [2, 3]. We construct a microstructural model of ferromagnetic shape memory alloys within the framework of the theory of micromagnetism [4], in which one of the structural elements is a domain wall of a certain thickness. The dynamics of the magnetic process is described by the Landau-Lifshitz-Gilbert equation. Using the Galerkin procedure, variational equations (weak problem statement) corresponding to the differential relations of the problem are constructed [5].

The structure of the "herringbone"-type is considered, when the axes of easy magnetization in the magnetic domains belonging to two variants of martensitic plates forming the twin, are located relative to the plane separating the martensitic variants (the plane of habitus) at an angle of 90-degrees to each other, while inside each martensitic variant these axes in the magnetic domains are located at an angle of 180-degrees. The boundaries of the twins act as 90-degree magnetic domain walls. The finite element method is used to simulate the formation of these walls and the distribution of the magnetization vector in them. The evolution of this magnetic structure is investigated, namely the movement and interaction of 180-degree magnetic domain walls when an external magnetic field is applied in various directions. First, in the absence of an external magnetic field, 90- and 180-degree magnetic domain walls are constructed numerically by the finite element method within the framework of the theory of micromagnetism and the distribution of the magnetization vector in them is found. Then, taking the obtained magnetic structure as the initial one, the evolution of this magnetic structure is investigated, namely the movement and interaction of 180-degree magnetic domain walls when an external magnetic field is applied in various directions.

After that, the problems of the formation of twins from the martensite variants (the twinning problem) and their disappearance (the detwinning problem) in an external magnetic field are considered. On the plane separating the two variants of martensite, the Hadamard compatibility condition

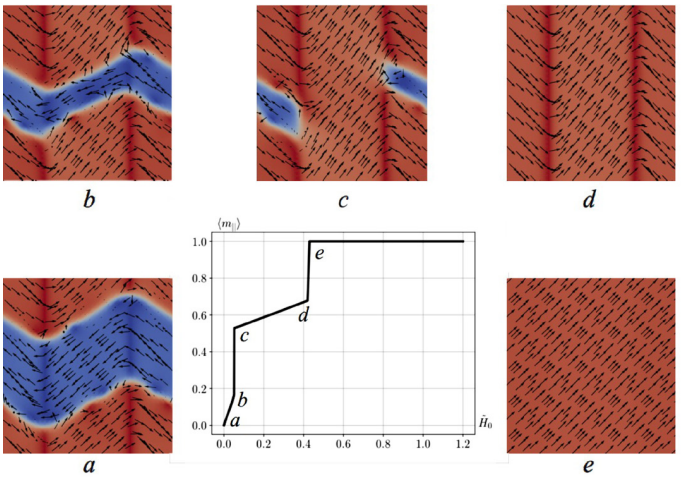

Figure 1. The magnetization curve for the magnetic field applied along one of the anisotropy axis and the evolution of the magnetization vector distribution in the magnetic field.

(or twinning equation) is written out. The kinematics of the twinning process, which reduces to a simple shift, is considered. The solution of the twinning (compatibility) equation is given and concretized for the Heusler alloy Ni_2MnGa. The processes, that this equation describes, are considered in detail. The detwinning condition for a ferroalloy with the shape memory in a magnetic field is proposed and the processes related to the reorientation (detwinning) of the martensitic variants forming a twin are discussed. The problems considered without taking into account the detwinning process are supplemented by this process. Given the process of reorientation of the martensitic variants forming a twin, the magnetization curves are constructed and the components of the strain tensor are determined. The results obtained showed good agreement with known experiments.

Figure 1 shows the dependences of $\langle m_{\|} \rangle$ (the average value of the magnetization projection on the axis, along which the external magnetic field is directed) on the modulus of the applied magnetic field $\tilde{H}_0$ in the case when the external field is directed along the anisotropy axis of the middle part of the cell. The magnetization vector distributions are presented for various values of the applied magnetic field (a – $\tilde{H}_0 = 0$, b – $\tilde{H}_0 = 0.12$, c – $\tilde{H}_0 = 0.13$, d – $\tilde{H}_0 = 0.4$, e – $\tilde{H}_0 = 0.43$). Blue and red regions are separated by 180-degree walls of magnetic domains. In the absence of an external magnetic field the average value of the magnetization is zero (Fig.1, a). When a magnetic field is applied, the average value of the magnetization increases due to movement of the walls of the magnetic domains (Fig. 1, b and c), the rotation of the magnetization vectors (Fig. 1, d) and the reorientation (detwinning) of martensite variants (Fig. 1, e). The points on the magnetization curve a, b, etc. correspond to figures a, b, etc. (Fig. 1).

This work was fulfilled under financial support of the Russian Foundation for Basic Research through Grant 20-01-00031.

1. V.D. Buchel'nikov et al., Physics-Uspekhi Adv. Phys. Sci. **49**, 871–877 (2006).
2. Y.M. Jin, Acta Mater. **57**, 2488–2495 (2009).
3. C. Mennerich, F. Wendler, M. Jainta and B. Nestler, Arch. Mech. **63**, 549–571 (2011).
4. W.F. Brown, Micromagnetics. Interscience Publisher (1963).
5. A.A. Rogovoy, O.S. Stolbova and O.V. Stolbov, J. Appl. Mech. Tech. Phys. **62**, 870–881 (2021).

INVESTIGATION OF $Fe_{49}Rh_{51}$ ALLOY BY WIDE-FIELD KERR MICROSCOPY

T.A. Taaev[1*], *A.A. Amirov*[2], *A.M. Aliev*[1], *A. Chirkova*[3], *I. Soldatov*[4], *R. Schäfer*[4,5]

[1]H. Amirkhanov Institute of Physics of the DFRC of the RAS, Makhachkala, Russia
[2]Immanuel Kant Baltic Federal University, Kaliningrad, Russia
[3]Materials Science, TU Darmstadt, Darmstadt, Germany
[4]Leibniz Institute for Solid State and Materials Research (IFW) Dresden, Institute for Metallic Materials, Dresden, Germany
[5]Institute for Materials Science, TU Dresden, Dresden, Germany
[*]E-mail: taaev89@mail.ru

The wide-field Kerr microscopy has emerged to become a well-established, most versatile and flexible laboratory technique for the investigation of magnetic domains. The method is based on the magneto-optical Kerr effect [1] i.e., small alterations of the polarization plane of linearly polarized light upon reflection from a non-transparent magnetic specimen, which are then detected and used for magnetic domain image formation. A typical wide-field Kerr microscope is based on an optical polarization reflection microscope that applies the Köhler illumination technique for homogeneously illuminated samples [2].

FeRh alloys (with the Rh content from 47 to 53%) serve as the most convenient model objects for studying the nature of magnetic phase transitions (PT) in materials showing giant magnetocaloric effect (MCE) [3–5]. Metamagnetic (PT) from the antiferromagnetic (AFM) to the ferromagnetic (FM) state is observed in FeRh alloys. This discovery led to the suggestion of using FeRh as a magnetic refrigerant.

The microstructure of FeRh alloys is consisted of α′(B2)- and γ(A1)-phases (paramagnetic, fcc, γ-phase was redistributed in the magnetic, bcc, α′-phase by diffusion) [3]. Images of the magnetic domain structure were obtained by using a Kerr microscope. The paramagnetic γ-phase surrounded by cylindrical magnetic domains of α′-phase is clearly showed in the images (Fig. 1) [6].

Analysis of the obtained intensity of magnetic contrast as a function of the temperature was allowed to see the phase transition from the FM to the AFM state $T_1 \approx 323.5$ K and of the inverse AFM–FM transformation $T_2 \approx 317$ K in zero magnetic field. The width of the temperature hysteresis was $\Delta T = 6.5$ K. And in an applied magnetic field of 0.5 T, the temperature hysteresis shifts to lower temperatures by 4 K (Fig. 2) [6].

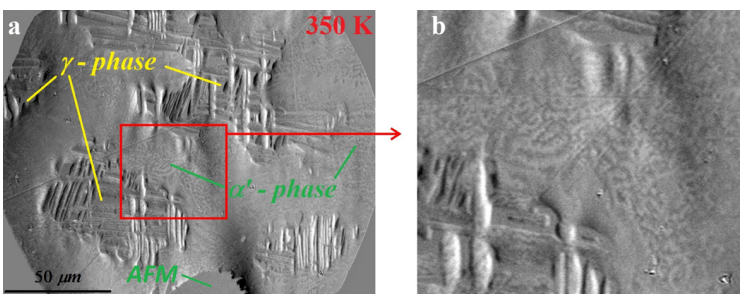

Figure 1. Polar magnetic domains of the $Fe_{49}Rh_{51}$ alloy in ferromagnetic state at 350 K in zero magnetic field (**a**); magnified image of the region with polar domains (**b**). α′-phase is a magnetic phase, γ-phase is a paramagnetic phase. AFM is a residual region of the antiferromagnetic phase.

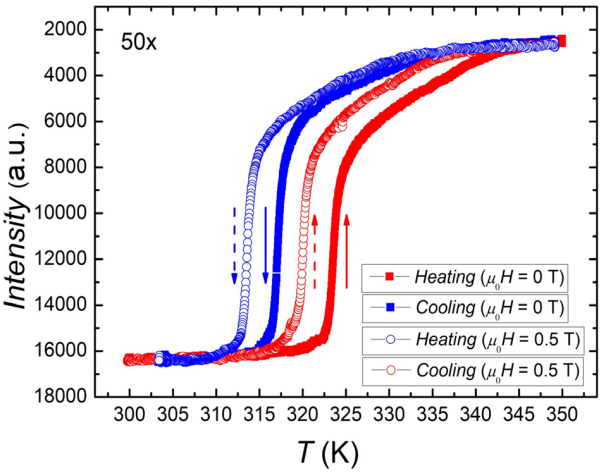

Figure 2. Magnetic contrast intensity on the $Fe_{49}Rh_{51}$ surface in zero (solid squares) and 0.5 T (open cicles) magnetic field. Magnification is 50×.

This work was supported by funding under the joint program of the Ministry of Science and Higher Education of the Russian Federation and the German Academic Exchange Service DAAD "Mikhail Lomonosov/Immanuel Kant" (project passport № 2295-21)

1. A. Hubert, R. Schäfer, Magnetic Domains: The Analysis of Magnetic Microstructures (Springer, New York, 1998) p. 696.
2. I.V. Soldatov, R. Schäfer, Rev. Sci. Instrum. **88**, 073701 (2017).
3. A. Chirkova, K.P. Skokov et al., Acta Mater. **106**, 15 (2016).
4. A. Chirkova, F. Bittner et al., Acta Mater. **131**, 31 (2017).
5. A.P. Kamantsev, A.A. Amirov et al., Phys. Solid State **62**, 160 (2020).
6. T.A. Taaev, A.A. Amirov et al., Physics of Metals and Metallography **123**, 402 (2022).

F.P22

THE MAGNETOSTRICTION IN GARNET FERRITE $Y_{1.8}Bi_{1.2}Fe_{3.5}Ga_{1.5}O_{12}$ SYNTHESING BY THE MODIFIED METHOD OF GEL COMBUSTION USING ETHYLENE GLYCOL

F.V. Zelenov[1*], *T.N. Tarasenko*[2], *O.E. Kovalev*[2], *Z.F. Kravchenko*[2], *V.V. Burkhovetskii*[2], *V.I. Mikhaylov*[2], *A.V. Golovchan*[2]

[1]Reshetnev Siberian State University of Science and Technology, Russia
[2]Public Institution "Donetsk Institute for Physics and Engineering named after A.A. Galkin", Donetsk, DPR
[*]E-mail: Fyodor.Zelenov@yandex.ru

Bismuth-substituted iron yttrium garnet films are used in creating magneto-optical memory devices based on Faraday and Kerr effects [1] and exhibit magnetoelectric effect and multiferroic properties [2]. In the region of room temperature in bismuth garnet ferrite films the magnetostriction constant changes sign. The sign change is related to the magnetic anisotropy field change. According to first-principle calculations, part of electron density (δ) from Bi^{3+} ions is transferred to $Fe^{3\pm\delta}$ ions, which leads to degenerate states of iron ions. This degeneracy can be removed by the Jahn-Teller channel for iron ions in tetrahedral positions or due to spin-orbit interaction for Fe-ions in octahedrons. The Curie temperature, magnetic anisotropy, and magnetostriction can be varied by replacing iron ions with nonmagnetic ions with different ionic radii.

The aim of the research: to increase the magnetostriction constant of bismuth garnet ferrite without using rare-earth elements, to determine the temperature of spin-orientation transition. The solution of this problem was achieved by replacing the iron ions in the tetrahedral positions with gallium ions, because the ionic radius of Ga^{3+} is smaller than that of Fe^{3+}.

The synthesis of samples based on iron-yttrium garnet ferrites by solid-phase reaction is ineffective because of its high power consumption; moreover, the synthesis process is often accompanied by the formation of a side phase with the perovskite structure of $YFeO_3$ [3]. In order to eliminate this drawback and to reduce the synthesis temperature, the gel combustion method using polyvinyl alcohol was applied to obtain bismuth-containing ferrogarnate $(Bi\text{-}Y)_3(Fe\text{-}Ga)_5O_{12}$ in [3].

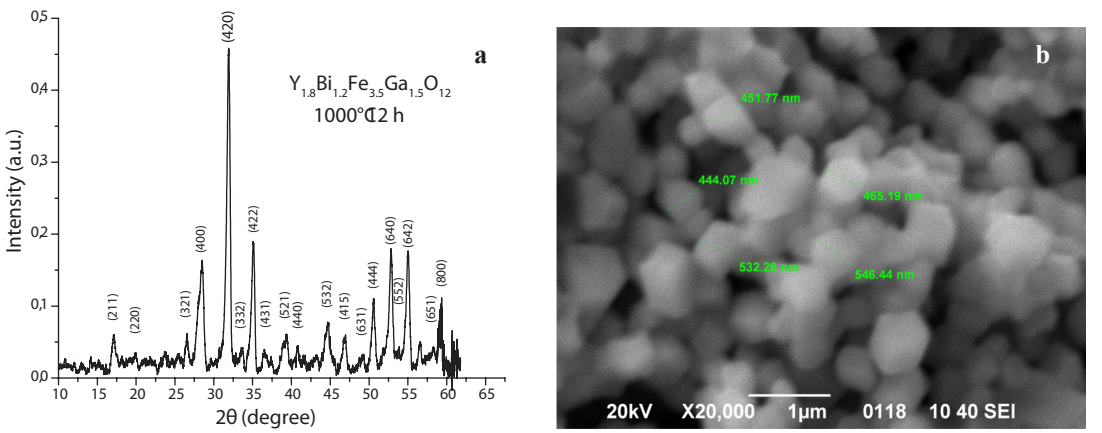

Figure 1. Structural studies of polycrystalline $Y_{1.8}Bi_{1.2}Fe_{3.5}Ga_{1.5}O_{12}$ synthesized by gel combustion using ethylene glycol: **a** X-ray diffractogram obtained at T_{room}; **b** results of the study of the morphology of the sample break surface.

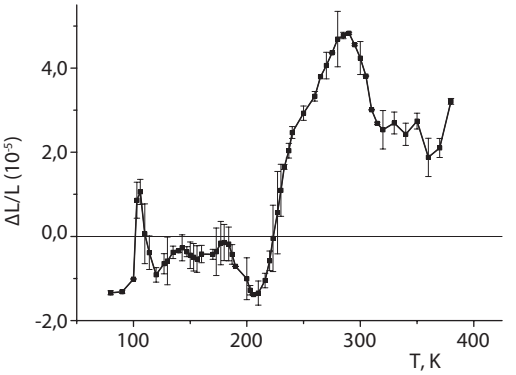

Figure 2. Relative change of linear dimensions of the sample $Y_{1.8}Bi_{1.2}Fe_{3.5}Ga_{1.5}O_{12}$ in the magnetic field of 12.6 kOe from temperature.

To obtain single-phase garne$Y_{1.8}Bi_{1.2}Fe_{3.5}Ga_{1.5}O_{12}$ the gel combustion method was modified. The starting substances were yttrium and bismuth oxides, metallic gallium, and carbonyl iron (all of high purity), stoichiometric amounts of which were dissolved in dilute nitric acid. After dissolution, excess nitric acid was evaporated and citric acid was added to the nitrate solution as a complexing agent and ethylene glycol as a gelling component. The reaction mixture was evaporated (~100ºC) with continuous stirring to a gel state in which the primary components were homogenized at the molecular level.

As the temperature increased, there was slow combustion of the gel to form a homogeneous mixture of chemically active oxides in the form of a finely dispersed powder. After cooling the powders were grinded, pressed into tablets and annealed at temperatures of 780 and 1000 °C with different holding times. In this manner were obtained three samples of composition $Y_{1.8}Bi_{1.2}Fe_{3.5}Ga_{1.5}O_{12}$ at the regimes: I – 780 °C (5 h), II – 780 °C (12 h) and III – 1000 °C (12 h).

Single-phase samples were obtained, the position of the diffraction reflexes of which correspond to the cubic structure of garnet. No extraneous phases were detected. The best mode was mode No. III: there are sharp diffraction peaks on the X-ray image, indicating good crystallization (Fig. 1a). Microstructure studies revealed the dependence of the average grain size d_{av} on temperature and annealing time: (I) ≈170 nm, (II) ≈230 nm, and (III) ≈500 nm. The results of the study of the fracture surface morphology of the sample $Y_{1.8}Bi_{1.2}Fe_{3.5}Ga_{1.5}O_{12}$ in mode III are shown in Fig. 1,b.

The magnetostriction constant was determined by the change in resistance of the ZFLA-3-11 strain gauge in the magnetic field $\lambda = (R(H) - R(0))/R(0) = (L(H) - L(0))/L(0)$. Resistance measurements were performed at a fixed temperature for 120 s without a field and in a magnetic field H = 12.6 kOe. Average values of resistance changes are shown in Fig. 2. The magnetostriction constant changes sign at 220 K. The magnetostriction constants are the product of magnetoelastic constants and spin-correlation functions, which determine the temperature and field dependence of magnetostriction [4]. A change in the sign of the magnetostriction constant is caused by a change in the sign of the magnetoelastic constants, which will lead to a change in the sign of the anisotropy constant. It is possible that a spin-orientation transition occurs at this temperature.

1. K.H. Chung et al., J. Appl. Phys. **107**, 09A930 (2010).
2. A.S. Logginov et al., JETP Lett. **86**, 115–118 (2007).
3. M.N. Smirnova et al., Ceramics International **45**, 4509–4512 (2019).
4. K.P. Belov et al., Physics-Uspekhi **140**, 271–313 (1983).

THEORY OF COUPLED MAGNETOELASTIC WAVES IN A THIN ANTIFERROMAGNETIC FILM BASED ON SIGMA-MODEL

T.V. Bogdanova[1,2*], *D.V. Kalyabin*[1,2], *A.R. Safin*[1,4], *S.A. Nikitov*[1–3]

[1]Kotel'nikov Institute of Radioengineering and Electronincs, Russian Academy of Sciences, Moscow, Russia
[2]Moscow Institute of Physics and Technology, Moscow, Russia
[3]Saratov Chernyshevsky State University, Saratov, Russia
[4]Moscow Power Engineering Institute, Moscow, Russia
[*]E-mail: bogdanova.tv@phystech.edu

Magnetoelastic (ME) Love wave propagation in a heterostructure containing antiferromagnetic film (NiO) on a piezoelectric substrate (LiNbO3) is investigated within sigma model [1]. We consider antiferromagnet with easy-plane-type anisotropy and weak ferromagnetism in an external magnetic field parallel to the film surface. The easy-plane is perpendicular to the crystal axis, which is directed along the z-axis. In the first approximation, it is possible to reduce the system of Landau-Lifshitz magnetization equations to the Neel vector equation , which is derived from the Lagrangian of the total energy of antiferromagnet [2]:

$$\left(\frac{\partial^2}{\partial t^2} - V_m^2\nabla^2\right)\bar{l}\times\bar{l} = 2g\left(\bar{l}\cdot\bar{H}\right)\frac{\partial\bar{l}}{\partial t} + g^2\left\{\left(\bar{l}\cdot\bar{H}\right)\left(\bar{l}\times\bar{H}\right) - H_D l^2\left(\bar{l}\cdot\bar{H}\right)\overline{e_z} - l_z\bar{H}\right\}$$
$$-g^2\left\{l_z\left(l_y\overline{e_x} - l_x\overline{e_y}\right)H_{\mathrm{D}} + 2bl_z\left(\bar{l}\times\overline{e_z}\right)M_0H_{\mathrm{E}} + \left(\bar{l}\times\frac{\partial F_{me}}{\partial\bar{L}}\right)H_{\mathrm{E}}\right\},$$

where $\bar{L} = \bar{M}_1 - \bar{M}_2 = 2\bar{l}M_0$ is the antiferromagnetic vector with $|\bar{M}_1| = |\bar{M}_2| = M_0$, $V_{\mathrm{m}} = (\alpha g M_0 H_{\mathrm{E}})^{1/2}$ is the characteristic velocity of spin wave, g is the gyromagnetic ratio, α, b are the nonuniform exchange constans. For simplicity the antiferromagnet is assumed to be magnetoelastically and elastically isotropic.

The thickness of the ferromagnetic layer is equal to d, while the thickness of the substrate is much larger.

The total energy of an antiferromagnet consists of magnetic, elastic, magnetoelastic, and Zeeman energies. The total energy is minimized for the ground state and this direction corresponds to the direction of the easy axis (y-axis). The Neel vector will be directed along this axis. We will consider in such an approximation.

We assume that lithium niobate is considered as a substrate. This is done to match the elastic parameters of the materials and provide waveguiding properties for propagating Love waves. This condition for the velocity of transverse bulk waves in the layer (1) and the substrate (2) is expressed in the form [3]: $\upsilon_1 < \upsilon_2$. In such a case, surface Love waves can be localized in the NiO layer.

The acoustic wave dynamics is described as follows:

$$\rho\frac{\partial^2 u_i}{\partial t^2} = \frac{\partial\sigma_{ik}}{\partial x_k},$$

where σ_{ik} is the tensor of the mechanical stresses and defined in terms of the total energy of the aniferromagnet (elastic energy based on the symmetry).

Love wave is a shear surface acoustic wave. To connect the longitudinal and transverse wave numbers, we substitute the test functions for $l_x = \exp[\mathrm{i}(ky - \omega t) + qz]$ and for $u_x = \exp[\mathrm{i}(ky - \omega t) + \kappa z]$ into the equations of motion and obtain the conditions:

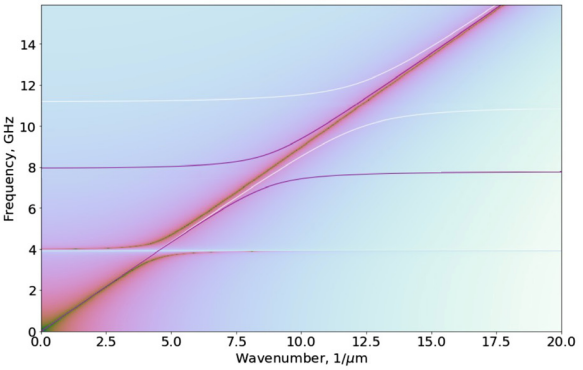

Figure 1. Dependence of the spectrum on the external applied field (green – 200 Oe, purple – 700 Oe, white – 1300 Oe).

$$\kappa_1 = \left[\frac{\omega^2}{St_1^2} - k^2\right]^{-\frac{1}{2}}, \quad \kappa_2 = \left[-\frac{\omega^2}{St_2^2} + k^2\right]^{-\frac{1}{2}}.$$

$$q = \frac{\left[\omega^4 + \left(k^2+\kappa^2\right)\left(\omega^2 St^2 + V_m^2 St^2 - V_m^2 k^2 St^2 - \omega_{sk} St^2\right) - V_m^2 k^2 - \omega_{me}\omega_e\omega_{tk}^2\right]}{V_m^2\omega^2\left[1 + \frac{St^2}{\omega^2}\left(k^2+\kappa^2\right)\right]},$$

where $S_t = (C_{44}/\rho)^{1/2}$ is velocity of the transverse sound, and ω_{me}, ω_e ($\omega_{sk} = V_m^2k^2 + \omega_H(\omega_H - \omega_D) + \omega_e\omega_{me})^{-1/2}$), $\omega_{tk} = S_t k$, are ME, elastic frequencies, respectively.

To find the dispersion, we will use the harmonic form of the function $l_x = [A\sin(qz) + B\cos(qz)]\exp[i(ky - \omega t)]$, $u_{1x} = [C\sin(\kappa_1 z + D\cos(\kappa_1 z)]\exp[i(ky - \omega t)]$ and for substrate the hyperbolic form $u_{2x} = [E\exp(\kappa_2 z)]\exp[i(ky - \omega t)]$ for the decay of elastic waves in the substrate.

The obtained forms of functions are substituted into the boundary conditions on l (the spin pinning on parameter in the formalism of the Neel vector), on σ for the antiferromagnetic layer on the substrate:

$$\sigma_1 + 4bM_0^2 l_x = 0, \quad z = d;$$
$$\sigma_1 + 4bM_0^2 l_x = \sigma_2, \quad z = 0;$$
$$u_{z1} = u_{z2}, \quad z = 0;$$
$$l_y \frac{\partial l_x}{\partial z} - l_x \frac{\partial l_y}{\partial z} = 0, \quad z = d;$$
$$l_y \frac{\partial l_x}{\partial z} - l_x \frac{\partial l_y}{\partial z} = 0, \quad z = 0.$$

Solving the matrix 5×5 , we obtain the dispersion characteristic by numerically calculation.

The effect of a change an external field on the dispersion relation (Fig. 1) has also been studied.

This work was financially supported by the RSF project No. 19-19-00607.

1. I.E. Dikshtein, S-H.S. Salk, Nonlinear Self-Localized Magnetoelastic Surface Waves in Antiferromagnetic Media, Departament of Physics, 1996.
2. V.I. Ozhogin, Preobrazhenskii, Sov. Phys., J. Magn. Magn. Mater, 1991.
3. T. Dai, D.V. Kalyabin, S.A. Nikitov, Hypersonic Magnetoelastic Waves in Inhomogeneous Structures, Ultrasonics, 2022.

THE MAGNETOCALORIC EFFECT IN MAGNETICALLY ORDERED COMPOUNDS $Fe_{3-x}Ni_xSe_4$

N.V. Selezneva, E.M. Sherokalova, V.A. Komarova, M.D. Klyucharev[*]

Institute of Natural Sciences and Mathematics, Ural Federal University, Ekaterinburg, Russia
[*]E-mail: maksim.klucharev@urfu.ru

The study of the magnetocaloric effect (MCE) is of fundamental interest both from the point of view of physics of materials and from the point of view of engineering. In addition to the most commonly used materials that have a large MCE and contain noble or rare earth elements, materials without these elements are of interest due to their availability. Fe_3Se_4 alloy is one of such materials. The Fe_3Se_4 compound has a layered monoclinic structure (space group I12/m1), selenium and iron ions occupy alternating layers along the *c*-axis, and vacancies appear in the unit cell in every second Fe-layer. This feature of the crystal structure leads to the fact that the magnetic moments on the iron atoms, which are oriented ferromagnetically in the layer and antiferromagnetically in neighboring layers, are not compensated. Below the critical temperature T_c ~ 320 K, a long-range ferrimagnetic order is formed in the Fe_3Se_4 compound. It is also known that the substitution of iron by other 3d-elements (M) makes it possible to significantly influence the magnetic characteristics of compounds of the form $Fe_{3-x}M_xSe_4$ [1].

This paper presents the results of a study of the crystal structure and physical properties of $Fe_{3-x}M_xSe_4$ compounds. Based on the magnetic properties of the initial Fe_3Se_4 composition [2], the compounds of this system can be considered as promising magnetocaloric materials, since they have a convenient operating temperature near room temperature, are easily synthesized, are chemically stable, and do not contain rare and expensive elements.

Samples of $Fe_{3-x}M_xSe_4$ (x = 0, 0.03, 0.5, 1) were obtained by the method of solid-phase reactions in evacuated quartz ampoules. The crystal structure was certified on a Bruker D8 Advance diffractometer using the X-ray powder diffraction. The magnetic properties were studied by measuring the field and temperature dependences of the magnetization in the range of 2–370 K on an MPMS SQUID magnetometer and in the range of 300–1000 K using a Lake Shore VSM 7407 vibrating sample magnetometer. The temperature dependences of the electrical resistance were measured by the 4-contact method using an autonomous closed-loop cryostat CryoFree 204.

The obtained samples are isostructural to the initial Fe_3Se_4 composition. When iron is replaced by nickel up to x = 1, an anisotropic change in the crystal lattice parameters is observed. The temperature dependences of the electrical resistance $\rho(T)$ for the synthesized compounds above the magnetic ordering temperature have the form characteristic of the metallic type of conductivity, and the value of ρ at room temperature decreases by two orders of magnitude compared to the value for Fe_3Se_4. An analysis of the temperature and field dependences of the magnetization showed that all the obtained compounds, like Fe_3Se_4, are ferrimagnets. However, the temperature of magnetic ordering when iron is replaced by nickel decreases significantly and amounts to T_c ~ 290 K for the composition x = 0.03 and T_c ~ 104 K for x = 1. For the compound $Fe_{2.97}Ni_{0.03}Se_4$, with T_c ~ 290 K, a set of $M(T)$ dependences was obtained at various values of the magnetic field in the range from 500 Oe to 15 kOe, which were subsequently used to calculate the change in magnetic entropy ΔS_M. The small substitution in the cationic sublattice led to an increase in the absolute value of the isothermal change in the magnetic entropy. At ΔH = 15 kOe for the composition x = 0 it equals ΔS_M = 0.20 J kg^{-1}K^{-1}, for x = 0.03 it equals ΔS_M = 0.22 J kg^{-1}K^{-1}.

The present work was supported by the Russian Science Foundation (Grant No 22-13-00158).

1. J.R. Regnard and J. Chappert, J. Phys. **34**(8–9), 721–731 (1973).
2. M.S. Bishwas and P. Poddar, J. Phys. D: Appl. Phys. **49**(19), 195003 (2016).

F.P25

EFFECTS OF CARBON ATOMS ON MAGNETIC MOMENT IN Fe-C SYSTEM: FIRST-PRINCIPLES CALCULATION

*A.A. Mirzoev**, *Ya.M. Ridnyi*

South Ural State University, Chelyaminsk, Russia
*E-mail: mirzoevaa@susu.ru

Tetragonality has a remarkable influence on the strength and mechanical properties of steels. Since the determination of the magnetic characteristics of a material is routine, it is of interest to study the relationship between the magnetic properties and the tetragonality of bcc Fe-C alloys. It is well known [1] that the addition of carbon increases the magnetic moment of Fe, but the mechanism of the magnetic moment increase is not well understood at present. In the work [2] an attempt was made to study this problem by methods of first-principles computer simulation. However, supercells containing one and two carbon impurities were considered, in addition the DFT calculations were used by the plane-wave base and pseudo-potential VASP package. In the present work, we performed a more detailed analysis of the problem by increasing the number of carbon atoms in a supercell to three and using a more accurate full potential package WIEN-2k. It was shown that the tetragonality and magnetic moments of the Fe-atoms depends on the configuration of the carbon atoms. The average magnetic moment on iron atoms depends linearly on the carbon concentration (Fig. 1). The change in the magnetic moment can be caused by two reasons – the magneto-volume effect, as well as the presence of a tetragonal lattice distortion. We studied in detail the effect of both factors. but is not clearly dependent on the tetragonality.

As follows from Fig. 2, the most significant factor is the magneto-volume effect, while the effect of tetragonality is not so important. The obtained conclusion differs significantly from the result presented in work [2].

1. K. Mitsuoka, H. Miyajima, H. Ino and S. Chikazumi, J. Phys. Soc. Jpn. **53**, 2381–2390 (1984).
2. H. Ohtsuka et al., ISIJ International. **55**, 2483–2491 (2015).

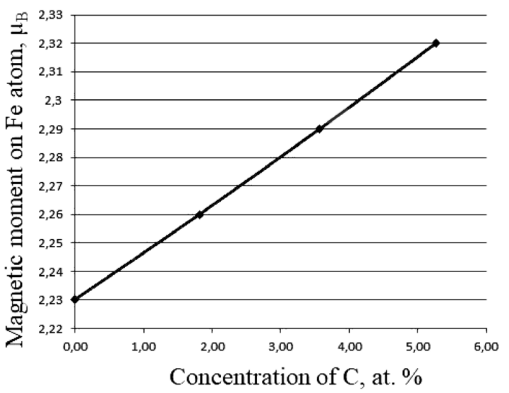

Figure 1. Dependence of the average magnetic moment on Fe-atoms on the carbon concentration

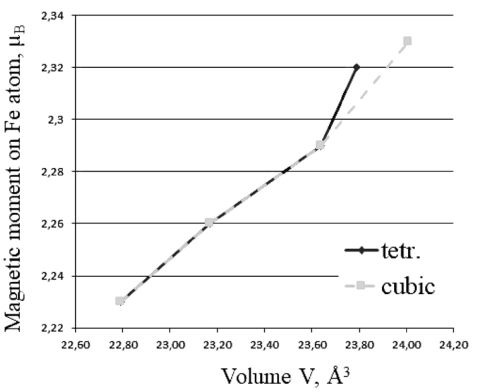

Figure 2. Dependence of the average magnetic moment on iron atoms on equilibrium cell volume at different C-contents for the cubic and tetragonal lattices.

VORTEX DYNAMIC MAGNETIC STRUCTURE INDUCED BY TRANSVERSE SOUND IN TRIGONAL WEAK FERROMAGNETS

M.B. Strugatsky[*], *D.Yu. Prilepsky*

Physics and Technology Institute, V.I. Vernadsky Crimean Federal University, Simferopol, Russia
[*]E-mail: rockaroller@mail.ru

In papers [1–4], the influence of the magnetic subsystem on the propagation of a plane transverse acoustic wave in easy-plane weakly ferromagnetic trigonal crystals, such as iron borate, hematite, was studied. When sound propagates along a threefold axis, this effect consists in the occurrence of magnetic linear birefringence of transverse sound, which is an acoustic analog of the magneto-optical Cotton-Mouton effect. The effect is explained by the magnetoelastic coupling [5], which is anomalously strong in easy-plane weak ferromagnets.

It is important to note that there is also an opposite effect: an acoustic wave propagating in a crystal generates magnetization oscillations. In this case, magnetic oscillations quasi-statically follow acoustic oscillations, the frequency of which is much lower than the AFMR frequency. Magnetic oscillations were explicitly observed during the propagation of a longitudinal plane acoustic wave in iron borate induced by femtosecond laser pulses [6].

In the works mentioned above, plane acoustic waves with transverse or longitudinal polarization were propagated. Therefore, the oscillations of the magnetic vector also represented a wave with a flat front. In this paper, we theoretically study the quasi-static magnetic dynamics in a trigonal weak ferromagnet induced by a transversely polarized acoustic wave in the form of a vortex. We have obtained the following expression for the dynamic angle representing the deviation of the magnetization vector from the equilibrium position (Fig. 1):

$$\varphi = \frac{A_r k_r \Delta C}{2B_{14}} \cdot e_r \quad . \tag{1}$$

The angle φ is determined from the quasi-static condition: $\partial F/\partial\varphi = 0$. Here F is the thermodynamic potential of the crystal, including the magnetic, elastic, and magnetoelastic contributions; B_{14} is the magnetoelastic constant; ΔC is the magnetoelastic addition to the elastic modulus; e_r is the magnetic mode of the acoustic wave; k_r is the wave vector of the magnetic mode. The modes of an acoustic wave generating magnetic oscillations in a crystal are determined by the wave equations:

$$\rho\ddot{e}_i = \frac{\partial^2 F}{\partial(\partial e_i / \partial x_j)\partial x_j} \quad . \tag{2}$$

For a vortex transverse acoustic wave propagating along the threefold axis of a trigonal crystal, the solution of Eq. (2) is reduced to two modes, magnetic (extraordinary) e_r and nonmagnetic (ordinary) e_q:

$$e_r = A_r r e^{-\alpha r^2} e^{\mathrm{i}m\psi} e^{\mathrm{i}(\omega t - k_r z)} \quad , \tag{3}$$

$$e_q = A_q r e^{-\alpha r^2} e^{\mathrm{i}m\psi} e^{\mathrm{i}(\omega t - k_q z)} \quad . \tag{4}$$

Here, the mode wave vectors are defined as follows:

$$k_r = \sqrt{\frac{\rho\omega^2}{C_{44} - \Delta C}}, \quad k_q = \sqrt{\frac{\rho\omega^2}{C_{44}}}.$$

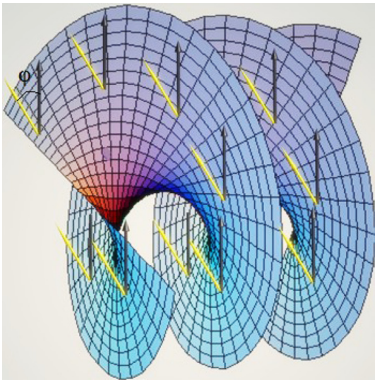

Figure 1. Schematically, vortex structure of induced magnetic oscillations (yellow lines – equilibrium position of the magnetization vector)

As can be seen from Eq. (1), magnetic oscillations are induced namely by the magnetic mode of an acoustic wave and inherit its vortex structure.

The results of this work will be important for further fundamental research and high-tech applications.

The study was supported by the Russian Science Foundation, Grant No. 22-22-20112, https://rscf.ru/project/22-22-20112/, and Ministry of Education, Science and Youth of the Republic of Crimea.

1. Yu.N. Mitsay, K.M. Skibinsky, M.B. Strugatsky, A.P. Korolyuk, V.V. Tarakanov, and V.I. Khizhnyi, JMMM, **219**, 340–348 (2000).
2. I.Sh. Akhmadullin, S.A. Migachev, M.F. Sadykov, M.M. Shakirzyanov, PSS **46**, 305 (2004).
3. I.Sh. Akhmadullin, S.A. Migachev, M.F. Sadykov, M.M. Shakirzyanov, PSS **47**, 506 (2005).
4. M. Strugatsky, K. Skibinsky, PSS **52**, 1331 (2010).
5. E.A. Turov, A.V. Kolchanov, V.V. Men'shenin, I.F. Mirsaev and V.V. Nikolaev, Symmetry and the Physical Properties of Antiferromagnets. Fizmatlit, Moscow (2001).
6. D. Afanasiev, I. Razdolski, K.M. Skibinsky, D. Bolotin, S.V. Yagupov, M.B. Strugatsky, A. Kirilyuk, Th. Rasing, and A.V. Kimel, Phys. Rev. Lett. **112**, 147403 (2014).

STRUCTURAL AND MAGNETIC PROPERTIES OF FeNi FILMS WITH OUT-OF-PLANE MAGNETIZATION COMPONENT

A.V. Svalov[1*], *A.N. Gorkovenko*[1], *A. Larrañaga*[2], *G.V. Kurlyandskaya*[1,3]

[1]Institute of Natural Sciences and Mathematics, Ural Federal University, Ekaterinburg, Russia
[2]SGIKER, Basque Country University UPV/EHU, Leioa, Spain
[3]Depto Electricidad y Electrónica, Universidad del País Vasco UPV/EHU, Bilbao, Spain
[*]E-mail: andrey.svalov@urfu.ru

Soft ferromagnetic films are used in various types of magnetoelectronic devices. One of the ways to increase the magnetic softness of thin films is to create the layers with helical magnetic anisotropy [1]. The helical variation of the orientation of the easy magnetization axis can be obtained by the deposition of the films in the rotating magnetic field in the plane of the substrate [1, 2]. Stable helical profile may occur for film thickness greater than the critical value defined as $2\pi(AK)^{1/2}$, where K is the anisotropy constant and A is the exchange constant. For FeNi films, a critical thickness depends on the deposition conditions but it is approximately equal to 1 μm [2]. However, at a thickness of several hundreds of nanometres, FeNi films can demonstrate the transition into the so-called "transcritical" state, which is accompanied by an increase in the coercive force H_c [3, 4]. The perpendicular anisotropy responsible for the formation of the "transcritical" state in FeNi films prepared by sputtering might be a strain-caused consequence of magnetostriction and magnetoelastic contribution and/or the columnar structure of the films [3]. Laminating of the thick FeNi film with various non-magnetic and weakly magnetic spacers allows to avoid the transition into the "transcritical" state [3, 5]. The use of interlayers of magnetically strong materials with a crystal structure different from that one of the permalloy is much less studied. In addition, the question about the change in the value of the perpendicular magnetic anisotropy constant K_p with a change of the thickness of the FeNi films still remains open. In this work, structural and magnetic properties of FeNi films of different thickness and FeNi/(Fe, Co)/FeNi trilayers were studied with the focus on the out-of-plane magnetic anisotropy formation.

The samples were deposited by dc magnetron sputtering onto Corning glass substrates at room temperature using the $Fe_{20}Ni_{80}$, Fe and Co targets. A constant magnetic field of 250 Oe was applied parallel to the film plane during deposition in order to induce a uniaxial magnetic anisotropy. The thickness of the FeNi films L was varying from 50 to 1000 nm and the thickness of Fe and Co spacers was a subject of variation in the interval from 5 to 20 nm. The phase analysis and average grain size was defined by X-ray diffraction technique using a PHILIPS X'PERT PRO automatic diffractometer operating with Cu radiation. Magnetic measurements were carried out by means of vibrating sample magnetometer and magneto-optical Kerr effect (MOKE) using the optical microscope Evico.

It was found that the grain size of the FeNi films was slightly increased with the increase of the thickness being of order of 10–15 nm in all cases. For Fe and Co spacers the average grain size was approximately equal to the thickness value but it did not exceed 15 nm. In the Co spacers, cubic and hexagonal phases were observed, the relative amount of the hexagonal phase increased with the increase of the Co spacer thickness. The high degree of texture observed for all samples did not allows us to unambiguously determine the lattice type (fcc or bcc) for the Fe spacers.

The critical thickness for FeNi films Lcr was about 200 nm. Thicker films had a specific shape of the hysteresis loop, the stripe domain structure (Fig. 1a), and a rotatable magnetic anisotropy in the sample plane. The thickness dependence of the saturation field H_s is well described by Murayama's model [6, 7] taking K_p value to be as high as $5{\cdot}10^4$ erg/cm^3 (Fig. 1b). Separation of "transcritical"

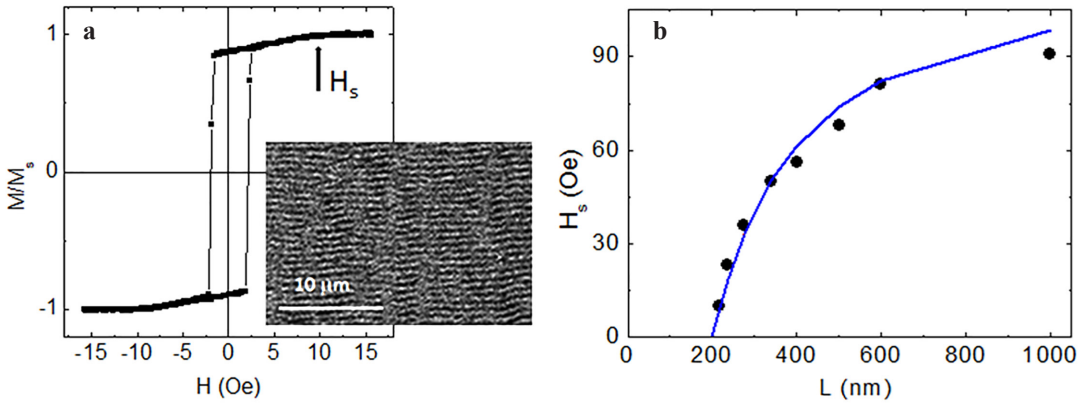

Figure 1. MOKE hysteresis loops for FeNi(220 nm) film (**a**); experimental (dots) and calculated on the basis of Murayama's model [6] (line) thickness dependence of the saturation field H_s for FeNi films (**b**); the inset – MOKE-image of the stripe magnetic domain structure for FeNi(220 nm) film.

films from the substrate does not change either the shape of the hysteresis loop or the value of H_s. In addition, the annealing of the separated film at 300 °C during one hour did not change the magnetic properties of the sample either. All these facts can serve for indirect evidence that the main source of perpendicular magnetic anisotropy in these films is the columnar microstructure [3, 4] rather than the magnetostriction effect [8].

The nanostructuring of thick FeNi films into multilayered structures having magnetic layers with $L < L_{cr}$ by Fe and Co interlayers does not prevent the occurrence of the "transcritical" state. An increase in the interlayer thickness leads to an increase in H_s and H_c for FeNi/(Fe, Co)/FeNi trilayers, especially in the case of Co spacers.

The Russian Science Foundation (RSF), project No. 22-29-00980, financially supported this work.

1. M. Gloanec, S. Dubourg, O. Acher, F. Duverger, D. Plessis, and A. Bonneau-Brault, Phys. Rev. B **85**, 094433-8 (2012).
2. D.A. Thompson, L.A. Finzi, H. Chang and P. Albert, J. Appl. Phys. **37**, 1274–1276 (1966).
3. N. Amos, R. Fernández, R. Ikkawi, B. Lee, A. Lavrenov, A. Krichevsky, D. Litvinov, and S. Khizroev, J. Appl. Phys. **103**, 07E732-3 (2008).
4. A.V. Svalov, E. Fernandez, A. Garcia-Arribas, J. Alonso, M.L. Fdez-Gubieda, and G.V. Kurlyandskaya, Appl. Phys. Lett. **100**, 162410-4 (2012).
5. S.F. Cheng, P. Lubitz, Y. Zheng, A.S. Edelstein, J. Magn. Magn. Mater. **282**, 109–114 (2004).
6. Y. Murayama, J. Phys. Soc. Japan **21**, 2253–2266 (1966).
7. P.N. Solovev, A.V. Izotov, B.A. Belyaev, N.M. Boev, Physica B **604**, 412699 (2021).
8. Y. Sugita, H. Fujiwara, T. Sato, Appl. Phys. Lett. **10**, 229–231 (1967).

Author Index

Abdulkadirova, N.Z. 513
Abramovsky, I.E. 251
Afanasiev, K.N. 417
Afremov, L.L. 337, 342
Agafonov, V.N. 181
Agzamova, P.A. 232, 282
Akhmadeeva, G.T. 386
Akhmetova, A.A. 393
Akramov, D.F. 533
Aliev, A.M. 494, 502, 513, 516, 543
Aliev, G.M. 502
Aliev, I.M. 492
Alisultanov, Z.Z. 444
Al-Onaizan, M.H. 69
Amirov, A.A. 543
Andersson, M.S. 254
Andreev, G.Iu. 517
Andreev, N. 86
Anikin, M.S. 518, 525
Anisimov, I.O. 111
Antonov, G.I. 390
Antropov, N.O. 325
Aplesnin, S.S. 327
Aronzon, B.A. 432, 439
Arseyev, P.I. 87
Arslanov, T.R. 444
Asadullin, F.F. 240, 251, 487, 523, 524, 532
Astakhov, V.A. 505
Averkiev, N.S. 87, 503
Averyanov, D.V. 436
Ayanitov, O.E. 92
Azon, S.A. 179

Babanova, O.A. 230, 254
Babaytsev, G.V. 80, 104
Baigutlin, D.R. 50, 161, 205, 207
Balaev, D.A. 437
Balinskiy, M. 318
Baranov, N.V. 445, 506
Baryshev, A.V. 417, 434
Batalov, S.V. 475
Batulin, R.G. 501
Baymukhametova, Z.A. 388
Bayukov, O.A. 437
Bazrov, M.A. 99, 129, 150, 152, 165
Bebenin, N.G. 152
Beginin, E.N. 29, 91, 116, 125, 154, 218
Belan, V.O. 330
Belotelov, V.I. 309, 480
Belyaev, V.K. 101, 456
Belyaeva, I.A. 330
Berzhansky, V.N. 309
Bessonov, V.D. 200, 302, 475
Bessonova, V.A. 301
Blinov, M.I. 420
Bogach, A.V. 96, 237, 242, 432
Bogdanov, A.E. 530
Bogdanova, T.V. 547
Boldyreva, M.M. 41
Bondarev, I.A. 31, 446
Bondarev, M.A. 266
Borodin, K.I. 47
Borzilov, V.O. 106
Bostrem, I.G. 247
Boukhvalov, D.W. 47
Brykin, L.O. 337
Buchelnikov, V.D. 50, 156, 161, 174, 205, 207, 485, 490
Bunkov, Yu.M. 224
Burkhovetskii, V.V. 545
Burmistrov, I.S. 21
Busse, A.A. 461
Butvina, L. 498
Buzdakov, A.G. 30
Bychkov, I.V. 350, 428, 448, 478
Bykova, A.A. 194
Byziaev, D.A. 510

AUTHOR INDEX

Changhee, S. 477
Chechenin, N.G. 80, 104
Chekanova, E.A. 103
Cherkasov, D. 45
Chernoglazov, K.Yu. 458
Chernousov, N.N. 364
Chernov, E.D. 468
Chernov, A.I. 309, 381, 480
Cherosov, M.A. 346, 517
Chigarev, S. 45
Chirkova, A. 543
Chistyakov, V.V. 460
Cho, J.U. 200
Chtchelkatchev, N.M. 234
Chuev, M.A. 61, 237
Chuklanov, A.P. 510
Chumakov, N.K. 181
Chumakov, N.C. 61
Constantinian, K.Y. 75

Danilov, Yu.A. 378
Danilovich, D.P. 96
Danilyuk, A.L 441
Davydenko, A.V. 92, 364
Davydov, A.B. 432
Davydov, V.A. 181
Demin, V.A. 458
Demina, P.B. 198
Demin, G.D. 89
Demishev, S.V. 16, 269, 271
Denisova, E.A. 103
Devyaterikov, D.I. 325
Dianov, M.Yu. 520
Dimitrievska, M. 230, 254
Doludenko, I.M. 45, 61, 84, 348
Dong, Shuai 9
Dorofeenko, A.V. 4
Dorokhin, M.V. 198, 203
Doroshenko, R.A. 28
Drokina, T.V. 258
Drovorub, E.V. 62
Drovosekov, A. 538
Dubavik, A.U. 209
Dudin, Yu.A. 198, 378
Dudko, G. 26
Dudnikov, V.A. 7
Dunaevski, S.M. 145
Duvakina, A.V. 94
Dyachkova, T.V. 279
Dyuzhev, N.A. 89
Dzhun, I.O. 80, 104

Edelman, I.S. 37
Efremova, S.L. 417, 434
Egorina, A.S. 62
Ekomasov, E.G. 247, 390
Emelyanov, A.V. 458
Emelyanov, N.A. 501
Emelyanova, S.M. 522
Erager, K.R. 207
Eremina, R.M. 47, 276, 293, 346, 501
Eremin, E. 335
Evseev, A.A. 120
Evsin, D.V. 106
Evstafyeva, Yu.K. 41
Evstigneeva, S.A. 391

Faraone, A. 230
Fazlizhanov, I.I. 293, 320
Fedorov, A.S. 450, 53
Fedorova, A.A. 450, 53
Fedyanin, A.A. 101
Fel'k, V.A. 397, 412
Feshchenko, A.A. 108
Fetisov, L.Y. 330
Filatov, Ia.A. 239
Filimonov, Y. 26, 318
Filinchuk, Y. 230
Filipov, V.B. 242
Filippov, M.A. 393
Filitov, M.A. 524
Fomin, L. 45
Fraerman, A.A. 22, 425
Frolov, K.V. 61
Funtov, K.O. 110, 181
Furman, G. 268

Gabbasov, B.F. 252, 273
Gamzatov, A.G. 444, 494, 502, 513, 516
Gan'shina, E.A. 422, 430, 439, 452, 458
Gareev, R.R. 71
Gareeva, Z.V. 28
Garifullin, I.A. 192, 216
Gaviko, V.S. 47, 525, 534
Gavrichkov, V.A. 7
Gavrilova, T.P. 346

AUTHOR INDEX

Gebara, P. 513
Gerashenko, A.P. 287, 304
Gerasimenko, A.V. 183
Gerasimov, E.G. 525, 528
Gerevenkov, P.I. 239
Germov, A.Yu. 265, 279
Gervits, N.E. 96
Gimaev, R.R. 489
Gippius, A.A. 45, 228, 242, 241, 96
Gizzatullina, G.F. 273, 23
Gladyshev, I.V. 430
Glavan, G. 330
Goloborodskiy, B.Yu. 265
Golov, A.V. 112
Golovchan, A.V. 498, 499, 545
Golovchanskiy, I.A. 252
Gonchar, L.E. 245
Gorev, R.V. 361
Gorkovenko, A.N. 108, 114, 194, 451, 553
Gorkovenko, A. 86
Gornakov, V.S. 39, 408
Grachev, A.A. 91
Granovsky, A.B. 420, 422, 432, 439, 458, 463
Grebennikov, V.I. 536
Grigoriev, S.V. 3, 16
Grigoriev, P.D. 474
Grishin, S.V. 170
Gritsenko, Ch. 86, 456
Gruner, M.E. 490
Grunin, A.A. 101
Gubanov, V.A. 43, 116
Gubanova, Y.A. 116
Gubkin, A.F. 506
Gudim, I.A. 284, 470
Gudkov, V.V. 503
Gumarov, A.I. 23, 252, 461, 273, 36, 159, 82
Gumarova, I.I. 82, 120
Gunbin, A.V. 96, 228, 241
Gurevich, A.A. 118
Gusev, N.S. 22, 361, 410
Gusev, S.A. 33
Gutakovskii, A.K. 123

Habibullin, R.R. 192
Han, Xiufeng 99
He, Wenqing 99
Huang, J.C.A. 460

Iarygina, D.A. 228
Ibragimova, E.M. 169
Ignatchenko, V.A. 263
Ignatov, A.A. 526
Ilina, T.S. 508
Iliushin, I.G. 200, 337, 342
Ilyasova, G.F. 374
Inishev, A.A. 525, 528
Irkhin, V.Yu. 178, 443
Ishmanova, R.F. 395
Iskhakov, R.S. 103, 196, 437
Iusipova, Iu.A. 59, 121
Ivanov, A.A. 368
Ivanov, V.E. 451

Jaloliddinzoda, M. 432, 439
Jeon, Y. S. 165, 172
Jeong, E. 165, 172

Kabanov, Yu.P. 408, 39
Kadirbardeev, A.T. 513
Kalachev, E.A. 75
Kalashnikova, A.M. 239, 454, 71
Kalentyeva, I.L. 378
Kaletin, A.Yu. 512
Kaletina, Yu.V. 512
Kalinin, Yu.E. 127, 190, 482
Kalyabin, D.V. 547, 4, 214
Kamantsev, A.P. 498, 499
Kamashev, A.A. 216
Kameli, P. 494
Kamilov, K.I. 513
Kaminskiy, S.A. 10
Kamzin, A.S. 220
Kanazakova, E.S. 422, 439
Kanbekov, R.R. 366, 413
Kandrashkin, Yu. 297
Kapitan, V.Yu. 367
Karasev, M.S. 16
Karashtin, E.A. 425, 22
Karateev, I.A. 436
Karibov, M.B. 179
Karlsson, M. 254
Kasyanov, A.A. 417
Kats, V.N. 436
Kazantsev, V.A. 533
Khaibullin, R.I. 45, 82, 123, 298

AUTHOR INDEX

Khairetdinova, D.R. 45, 84, 348
Khanov, L.G. 502, 516
Kharitonov, V.N. 165, 342, 348
Kharlamova, A.M. 432
Khayrutdinov, B.I. 291, 292
Khitun, A. 318
Khivintsev, Y. 26
Khizriev, Sh.K. 494
Khizriev, K.Sh. 182
Khokhlov, N.E. 239
Kholid, F. 425
Khutieva, A.B 125
Kichin, G.A. 56, 66, 94, 186, 381
Kiiamov, A.G. 252, 273, 356, 461, 517
Kim, G.W. 172, 200
Kim, T.H. 200
Kim, Y.K. 165, 172, 200
Kimel, A.V. 477
Kiselev, D.A. 508
Kislinski, Yu.V. 75
Kliava, J. 538
Klimenko, D.I. 209
Klimov, A.A. 75
Klyucharev, M.D. 549
Knyazev, Yu.V. 437
Ko, M.J. 172
Kobyakov, A.V. 97, 111
Koksharov, .A. 15
Koledov, V.V. 280, 498
Kolosvetov, A.A. 480
Kolyvanov, E.L. 529
Komanický, V. 86, 456
Komarova, V.A. 549
Komlev, A.S. 508
Komogortsev, S.V. 103, 176, 397, 412
Konev, A.S. 265, 279
Konev, S.F. 47
Konov, K.B. 274
Kopylov, D.A. 372
Korableva, S.L. 517
Korenistov, P.S. 178
Korostelin, Yu.V. 503
Korotkov, L.N. 501
Korshunov, A.N. 332
Koshkidko, Yu. 498
Kostishyn, V.G. 505
Kosyrev, N.N. 97
Kotomina, V.E. 198
Kotov, L.N. 112, 127, 190, 240, 251, 482, 487, 520, 532, 539, 261
Kotov, V.A. 450
Kovalev, O.E. 499, 545
Kovalev, P.D. 190
Kovycheva, E.I. 73
Kozhaev, M.A. 480
Kozhevnikov, A. 26, 318
Kozin, M.G. 80, 104
Kozlov, A.G. 92, 165, 172, 183, 364
Kozlova, E.E. 307
Krasikov, A.A. 437
Kravchenko, Z.F. 545
Kravchenko, O.V. 311
Kravtsov, E.A. 108, 325
Kreines, N. 538
Krinitsina, T.P. 24
Kryukov, R.N. 203
Kuchin, A.G. 534
Kudrevatykh, N.V. 518
Kudrin, A.V. 376
Kulesh, N.A. 114
Kulikova, D.P. 10, 417, 434
Kulikova, L.F. 181
Kundelev, E.V. 209
Kun'kova, Z.E. 452
Kurbakov, A.I. 332
Kurganskaya, A.A. 530
Kurilova, A.V. 209
Kurkin, M.I. 47, 282
Kurlyandskaya, G.V. 137, 553
Kurmachev, I.A. 265
Kuzikova, A.V. 454
Kuzmin, D.A. 428, 448, 478
Kuznetsov, I.A. 448
Kuznetsov, Yu.M. 203
Kuznetsov, M.D. 356
Kuznetsova, A.A. 397
Lahderanta, E. 87
Lasek, M.P. 482, 190
Lee, L.A. 296
Leontyev, A.V. 216
Lepalovskij, V.N. 86, 108, 114, 137, 451
Lesnikov, V.P. 203
Letushev, M.E. 99, 129, 150, 165

AUTHOR INDEX

Lgotina, D.A. 131
Li, O.A. 103
Likerov, R.F. 274
Lin, C.-R. 110
Lobanov, N.D. 133, 277
Lobov, I.D. 475
Lock, E.G. 43
Lock, E.H. 154, 218
Logunov, M.V. 450, 53
Lomanova, N.A. 96
Lukoyanov, A.V. 468
Lukyanenko, A.V. 31, 135, 446
Luk'yanenko, A.V. 403
Luzanov, V.A. 289
Lyadov, N.M. 82, 123
Lyapilin, I.I. 55
Lysov, M.S. 370
Lytkin, D.K. 532
Lyubutin, I.S. 61, 110, 181, 237
Lyubutina, M.V. 181

Magadeev, E.B. 366, 413
Maiti, T. 276
Makarochkin, I.A. 137
Makarov, A.V. 139
Makaryin, R.A. 508
Makeev, M.Y. 142
Maksimov, F.M. 309, 381
Maksimova, I.K. 152
Makunin, A.V. 80, 104
Malakhovskii, A.V. 470
Maltseva, S.A. 524
Maltsev, I.V. 350
Mamedov, D.V. 276
Mamin, R.F. 216
Mamonov, E.A. 372
Mamonova, M.V. 41, 106, 142, 167
Mantsevich, V.N. 87
Marchenkov, V.V. 178, 443, 460, 468, 522
Marchenkova, E.B. 460, 178
Marenkin, S.F. 432
Markin, Yu.V. 452
Martyshkin, A.A. 29, 218
Maslova, N.S. 87
Matveev, A.A. 211
Matveev, O.V. 133, 277
Matyunina, M.V. 485
Mekhonoshin, D.S. 399
Mikhailenko, E.K. 145
Mikhalev, K.N. 279, 304
Mikhaylov, V.I. 545
Mikhaylovskiy, R.V. 425
Mikheenkov, A.V. 234
Milyaev, M.A. 24, 152
Minkova, A.V. 148
Mironov, V.L. 249
Miroshkina, O.N. 50, 490
Mirzoev, A.A. 550
Mitrofanova, A.Yu. 311
Mogilenec, Yu.A. 237, 538
Mogilyuk, T.I. 474
Mokhov, A.A. 397, 412
Molochnikov, L.S. 47
Molokeev, M. 335
Morchenko, A.T. 505, 69
Morelle, F. 230
Morgun, L.A. 432
Morozkin, A.V. 530
Morozov, O.A. 517
Morozov, I.V. 241
Morozova, M.A. 277, 133
Moshkina, E. 335, 346
Moskalev, M.E. 108, 114, 194
Moskvin, A.S. 241
Mozgovykh, S.N. 533
Münzenberg, M. 71
Murtazaev, A.K. 182
Murzakayev, A.M. 47
Murzin, D.V 101, 456
Murzina, T.V. 372
Mushnikov, N.V. 525, 528

Namsaraev, Zh.Zh. 99, 129, 150
Nasyrova, M.I. 192
Naumov, S.V. 301, 460
Naumova, L.I. 24, 152
Naydanov, I.A. 24
Nedopekin, O.V. 120
Nekhaeva, E.I. 432
Nematov, M.G. 391
Nemtsev, I.V. 103
Nepochatykh, Yu.I. 280
Nikiforova, P.A. 532
Nikitin, S.I. 461, 36

AUTHOR INDEX

Nikitin, S.A. 530
Nikitov, S.A. 4, 29, 43, 53, 214, 376, 289, 307, 410, 450, 547
Nikolaev, S.N. 422, 458
Nikolaev, S.V. 7
Nikolaeva, E.P. 10
Nikulin, Yu.V. 410
Nikulin, Y. 26
Nizyamova, A.R. 401
Noginova, N. 116
Novikov, S.I. 279
Nurgazizov, N.I. 510
Nurkusheva, M.M. 142
Nuzhdin, V.I. 123, 298

Odintsov, S.A. 154, 170
Ogloblichev, V.V. 232, 287
Ognev, A.V. 165, 172, 179, 200, 348, 364, 475
Opra, D.P. 357
Orlov, V.A. 368, 403
Orlov, Yu.S. 7
Orlova, N.B. 282
Orlova, I.N. 368, 403
Ostrovskaya, N.V. 59, 121
Ovcharov, A.V. 432
Ovchenkova, I.A. 488, 530
Ovchinnikov, S.G. 7, 31, 37
Ovchinnikov, A.S. 247, 496
Oveshnikov, L.N. 432, 439
Ovsyannikov, G.A. 75

Pakhomov, A.S. 309, 381
Pamyatnykh, L.A. 370, 399
Pamyatnykh, S.E. 370
Panina, L.V. 118, 391
Pankratov, N.Yu. 488, 492
Pankrats, A.I. 284
Panov, Yu.D. 352
Parfenov, O.E. 436
Park, H.-R. 477
Park, J.H. 200
Pashen'kin, I.Yu. 425, 33, 22
Pasynkov, M.V. 159, 461
Pasynkova, A.A. 137
Patrin, G.S. 97, 111, 368
Pavliuk, M.Yu. 348
Pavlov, V.V. 436
Pavlova, A.N. 412
Pavlukhina, O.O. 156
Pazniak, H. 86
Perevalova, A.N. 460
Perov, N.S. 508
Pertsev, N.A. 71
Perunov, I.V. 61
Pervishko, A.A. 200
Perzhu, A.V. 367
Petrov, A.V. 36, 461
Petrov, D.A. 37, 268
Pilyugin, V.P. 512
Pilyuk, E.A. 293
Pisarev, R.V. 454
Piskunov, Y.V. 287
Piskunova, N.I. 62
Platonov, S.P. 534
Pleshev, D.A. 240, 251, 487, 523, 524, 532
Podgornykh, S.M. 460
Podkletnova, A.A. 10
Podlesnyak, A. 445
Polukhin, D.S. 263
Polulyakh, S.N. 309
Popov, D.V. 346
Popov, I.S. 353
Popova, A.P. 353
Potapova, S.R. 179
Povarov, K.Yu. 323
Prilepsky, D.Yu. 538, 551
Pripechenkov, I.M. 422, 439, 452
Prischepa, S.L. 441
Proglyado, V.V. 24, 152
Prokopenko, V.S. 403
Prokopyev, D.A. 265
Prudnikov, P.V. 41, 62, 106, 131, 148, 344, 353
Prudnikov, V.N. 420, 463
Prudnikov, V.V. 41, 62
Prudnikova, M.V. 420, 463
Pugach, N.G. 309
Pyatakov, A.P. 10

Radzivonchik, D.I. 536
Raev, A.A. 161
Raikher, Yu.L. 12
Rautskii, M.V. 31, 163, 266, 446
Reyes, A.P. 223
Reznikov, I.G. 463
Rezninov, Ya.G. 420
Ridnyi, Ya.M. 550

AUTHOR INDEX

Ril', A.I. 432, 439
Rodionova, V.V. 86, 101, 406, 456, 526
Rogachev, K.A. 165, 172
Rogovoy, A.A. 541
Romanova, I.V. 517
Romanova, O.B. 327
Romashkina, I.L. 80, 104
Rozhansky, I.V. 87
Rudenko, R.Yu. 403, 97
Ruffer, T. 297
Rusalina, A.S. 152
Rylkov, V.V. 422, 458

Sadovnikov, A.V. 29, 43, 91, 116, 125, 154, 170, 218, 361, 376, 378
Sadykov, A.F. 287
Safin, A.R. 4, 64, 211, 214, 289, 307, 311, 547
Safin, K.R. 430
Safonov, S.S. 450, 53
Saifulina, D.A. 430
Saito, Y. 425
Sakharov, V. 26
Sakhratov, Yu.A. 223
Salakhitdinova, M.K. 169
Salikhov, K.M. 222
Salomatova, E.I. 170
Samardak, A.S. 165, 172, 179, 200, 348, 364, 475
Samardak, A.Yu. 165, 172, 179, 348
Samarin, A.N. 16
Samsonov, K.U. 390
Sanosyan, A.A. 174, 490
Sapozhnikov, M.V. 22
Sapozhnikov, M.V. 361
Sarsari, I.A. 494
Sarychev, M.N. 503
Satsuk, F.A. 176
Savchenko, S.P. 355
Saveliev, D.V. 330
Savilov, S.V. 316
Savin, V.V. 406
Schäfer, R. 543
Seleznev, M. 26
Seleznyova, K. 237, 538
Selezneva, N.V. 445, 533, 549
Semakin, A.S. 517
Semeno, A.V. 16
Semenov, S.V. 103, 111
Semiannikova, A.A. 178, 468
Severin, P.A. 539
Sgibnev, Y.M. 417
Shadrin, A.V. 75
Shaikhulov, T.A. 289
Shalygina, E.E. 139
Shamonin, M. 330
Shamsuvaleev, R.I. 391
Shanidze, L.V. 446
Shapovalov, V.V. 258
Shapovalov, V.A. 258
Shaporov, V.N. 261
Sharipova, L.V. 291, 292
Shashkov, I.V. 39, 408, 529
Shatilov, V.S. 92
Shavrov, V.G. 258, 280, 300, 428, 448, 498
Shcheglov, V.I. 523, 524, 532
Shelaev, A.V. 417, 434
Shelukhin, L.A. 71, 436, 454
Sherokalova, E.M. 445, 506, 533, 549
Sherstobitova, E.A. 506
Shestakov, A.V. 228, 256, 293, 320
Shishkin, D.A. 506
Shitsevalova, N.Y. 242
Shiyan, Ya.G. 296, 97
Shkanakina, M.D. 66
Shlyakhtich, M.A. 344
Shmakov, V.A. 75
Shmatov, G.A. 370
Shreder, E.I. 460, 468
Shulga, N.V. 28
Shulga, K.V. 209
Shurpik, D.N. 291
Shustov, V.A. 274, 276, 346
Silkin, I.G. 241
Simdyanova, M.A. 430
Sinitsyn, V.E. 247
Si, P.Z. 287
Sitnikov, A.S. 422
Sitnikov, A.V. 127, 190, 240, 458, 482
Sitnikov, M.N. 327
Sivachenko, A.P. 498, 499
Skidanov, V.A. 415, 121, 59
Skirdkov, P.N. 30, 56, 66, 94, 226, 381
Skorokhodov, E.V. 33, 249, 361
Skorunov, R.V. 355
Skoryunov, R.V. 230, 254
Skripov, A.V. 254
Slesareva, Yu. 297

AUTHOR INDEX

Sluchanko, N.E. 242
Sluzhbin, Yu.A. 258
Smirnov, A.I. 314, 323
Smirnov, A.V. 530
Smolnikov, A.G. 287, 355
Snegirev, N. 237
Sobirov, M.I. 179
Sofronova, S.N. 335
Sokolov, A.A. 357
Sokolov, A.E. 209
Sokolov, V.V. 470
Sokolovskiy, V.V. 50, 156, 161, 174, 205, 207, 485, 490
Sokolovsky, V. 268
Soldatov, T.A. 314, 323
Soldatov, I. 543
Solonetsky, R.V. 374, 388, 393, 401
Soloninin, A.V. 230, 254
Stankevich, K.L. 289
Starchikov, S.S. 110, 181, 237
Starichenko, D.V. 47
Starykh, O.A. 323
Stavila, V. 254
Steblii, M. 475
Stebliy, M.E. 99, 129, 150, 165
Stepanov, S.V. 390
Stepushkin, M.V. 376
Stognii, A.I. 450, 53
Stoikov, I.I. 291
Stolbov, O.V. 526
Stolbova, O.S. 541
Stolyar, S.V. 437
Stolyarov, V.S. 309
Storchak, V.G. 436
Strugatsky, M.B. 237, 538, 551
Suhachev, A.L. 209
Sukhachev, A.L. 31, 37, 470
Sukhachev, R.A. 167
Sukhanov, A.A. 298
Sukhorukova, O.S. 300
Sukhorukov, Yu.P. 477
Surikov, V.T. 503
Surzhikov, E.A. 475
Suslin, G.S. 92
Suslin, H.S. 183
Suslova, E.V. 316
Suvorkova, E.V. 265
Svalov, A.V. 137, 139, 553
Svistov, L.E. 223
Syr'iev, N.E. 305
Syromyatnikov, A.V. 340

Taaev, T.A. 182, 543
Tagirov, L.R. 23, 36, 82, 123, 159, 188, 220, 252, 273, 461
Tagirov, M.S. 517
Taldenkov, A.N. 436
Tananaev, P.N. 417, 434
Tarasenko, A.S. 300
Tarasenko, S.V. 300
Tarasenko, T.N. 545
Tarasov, A.S. 31, 135, 163 266, 446
Tarasov, E.V. 92, 183, 357
Tarasov, I.A. 31
Tarasov, E.N. 518
Tarasov, V.F. 274
Tatarskiy, D.A. 33, 249, 376
Tayurskii, D.A. 356
Telegin, A.V. 301, 302, 200, 475, 477
Temiryazev, A.G. 289, 376, 372, 378, 410
Temiryazeva, M.P. 289, 372, 376, 378, 410
Temnaya, O.S. 4, 214
Temnov, V.V. 112
Teplov, V.S. 200, 301, 302
Tepnin, E.V. 348
Terentev, P.B. 525, 528
Terentyev, P.B. 178
Tereshchenko, A.A. 496
Tereshina, I.S. 488, 492, 530
Thaku, P. 37
Thakur, A. 37
Tkachenko, I.A. 183, 357
Tkachev, A.V. 228, 241, 96
Todris, B. 498
Tokmachev, A.M. 436
Tolstykh, N.A. 501
Trafimenko, A.G. 441
Trokiner, A. 304
Trushin, A.S. 186
Tsiberkin, K.B. 73
Tsikalov, D.S. 263
Turpak, A.A. 364
Tyutyunnik, A.P. 279

Udalov, O.G. 361
Udod, L.V. 327
Udovic, T.J. 230, 254

AUTHOR INDEX

Uimin, M.A. 47, 279
Ulanov, V.A. 256, 320
Ulyanov, A.N. 316
Umkhaeva, Z.S. 492
Usachev, P.A. 436
Useinov, N.Kh. 188
Usik, M.O. 478
Ustinov, V.V. 19, 24, 152, 201
Ustyugov, V.A. 190
Utesov, O.I. 382
Utkin, A.A. 127, 190, 240

Vagizov, F.G. 276
Vakhitov, I.R. 82, 123
Vakhitov, R.M. 366, 374, 386, 388, 393, 395, 401, 413
Valeev, V.F. 123, 298
Validov, A.A. 192
Valiulin, V.E. 234
Valiullin, A.A. 220
Valkov, V.I. 258, 498
Varnakov, S.N. 31, 135, 163
Varzaneh, A.G. 494
Vasiliev, A.L. 181, 432
Vasiliev, A.N. 326
Vasiliev, E.V. 367
Vasin, M.G. 278
Vas'kovskiy, V.O. 108, 114, 194
Vaulin, A.A. 506
Vavilova, E. 297
Vazhenina, I.G. 196
Vdovin, V.I. 123
Ved, M.V. 198
Velikanov, D.A. 327, 437
Verchenko, V.Yu. 228
Vikhrova, O.V. 378
Vilkov, E.A. 4, 45
Vinokour, V.M. 234
Vlasov, V.S. 112, 127, 190, 251, 240, 487, 523, 524, 520, 532, 539, 261
Voennov, A.V. 434
Volegov, A.S. 47, 534
Volkov, N.V. 31
Volkova, O.S. 329
Volkova, Z. 304
Volochaev, M. 86
Vorotynov, A.M. 258
Vyaselev, O.M. 242
Vysotskii, S. 26, 318
Vysulin, S.A. 305
Walowski, J. 71
Wan, Caihua 99
Wang, Ren-Bo 323

Yadvichuk, A.I. 10
Yagupov, S.V. 237, 538
Yakovchuk, V.Yu. 196, 403
Yakovlev, I.A. 31, 135, 163, 266, 446
Yakovleva, M.Yu. 534
Yanilkin, I.V. 23, 252, 461, 273, 36, 159, 82
Yarikov, S.A. 111
Yaroslavtsev, R.N. 437
Yashin, M.M. 430
Yasyulevich, I.A. 19, 201
Yatsyk, I.V. 47, 256, 274, 276, 293, 346
Yermakov, A.E. 47, 279
Yu, S. 477
Yudanov, N.A. 391
Yudin, D. 200
Yumaguzin, A.R. 386, 388
Yurasov, A.N. 430
Yurlov, V.V. 48
Yushkov, V.I. 97, 111
Yusupov, R.V. 23, 36, 82, 159, 252, 273, 461

Zagorskii, D.L. 45, 61, 84
Zagrebin, M.A. 485, 156
Zakharova, G.S. 47
Zakharov, A.A. 152
Zakhvalinskii, V.S. 293
Zaripov, R. 297
Zaripova, L.D. 220
Zaripov, R.B. 274
Zavornitsyn, R.S. 24, 152
Zayakhanov, V.A. 181
Zbarsky, V. 71
Zdoroveyshchev, A.V. 198, 203, 376, 378
Zdoroveyshchev, D.A. 198, 203, 376
Zeer, G.M. 284
Zelenov, .V. 545
Zharkov, S.M. 111, 284
Zheludev, A. 323
Zhevstovskikh, I.V. 503
Zhigalina, O. 45
Zhivulin, V.E. 289
Zhurenko, S.V. 45, 96, 228, 241

AUTHOR INDEX

Ziatdinov, A.M. 357
Zinin, A.V. 518
Zuev, Yu.F. 291, 292
Zverev, V.I. 495, 508
Zverev, V.V. 384
Zvezdin, A.K. 28, 48
Zvezdin, K.A. 30, 48 56, 66, 94, 186, 226, 381, 390
Zyablovsky, A.A. 4

VIII Euro-Asian Symposium «Trends in MAGnetism»
EASTMAG–2022
August 22–26, 2022, Kazan, Russia

BOOK OF ABSTRACTS. VOLUME I

Titles and abstracts are given in the author's edition

The layout and design of EASTMAG-2022 Book of Abstracts – Polina A. Agzamova
The editing of EASTMAG-2022 Book of Absracts – Sergey G. L'VOV, Olga B. YANDUGANOVA

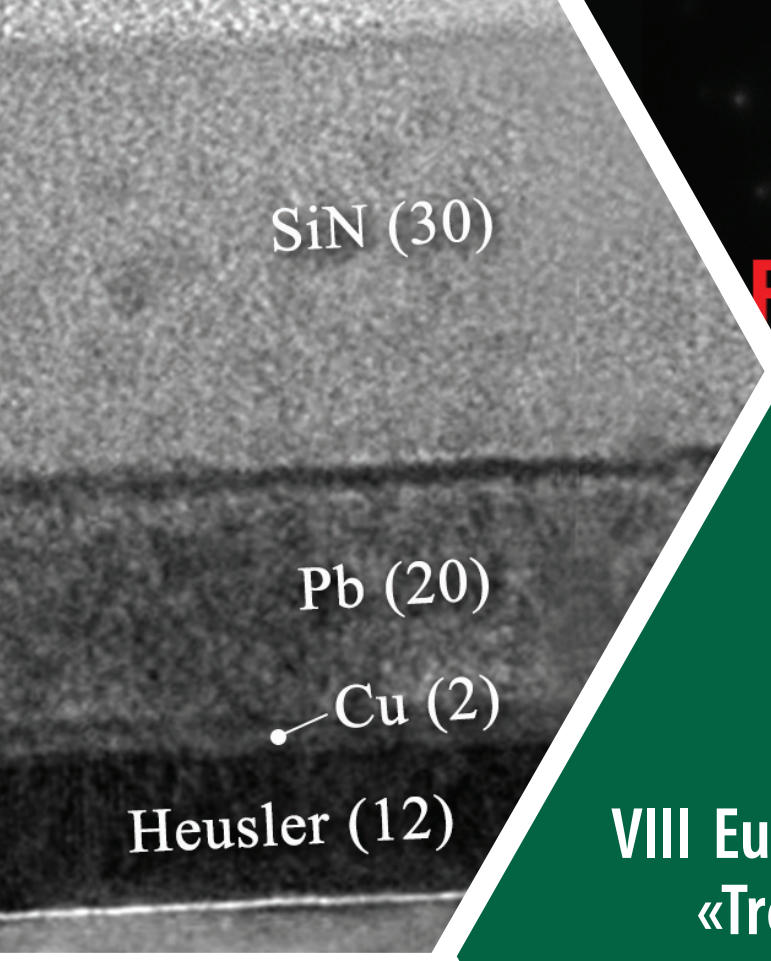

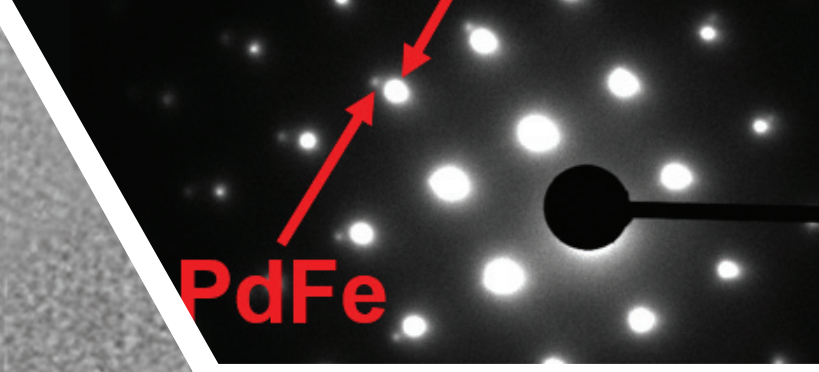

VIII Euro-Asian Symposium «Trends in MAGnetism»
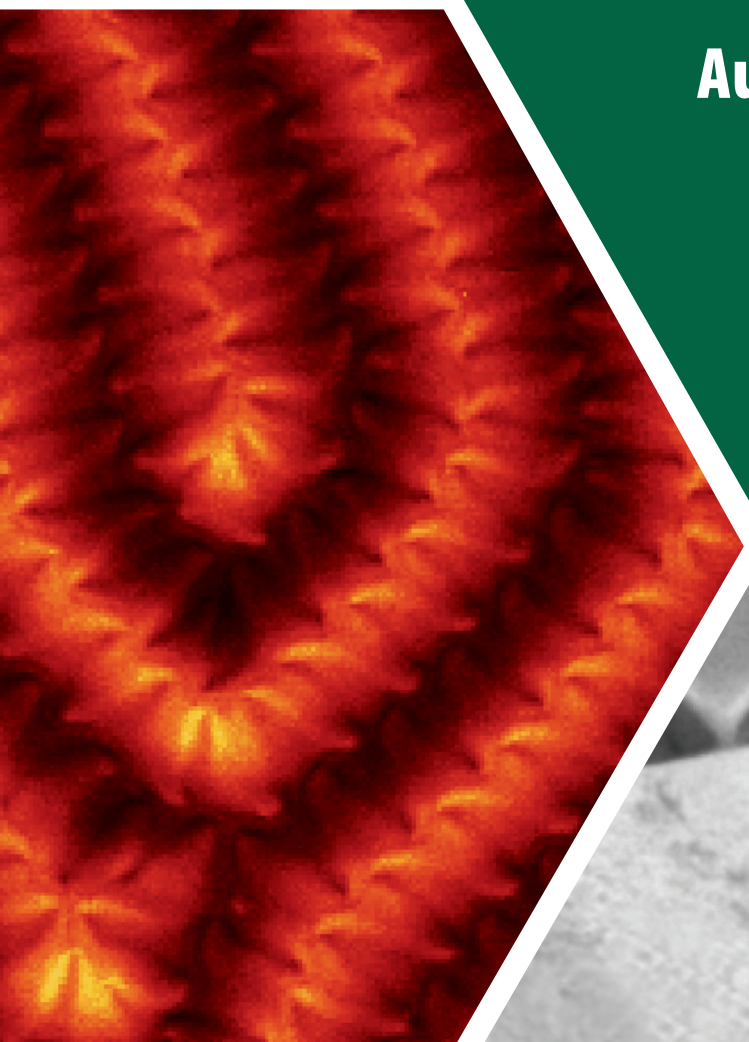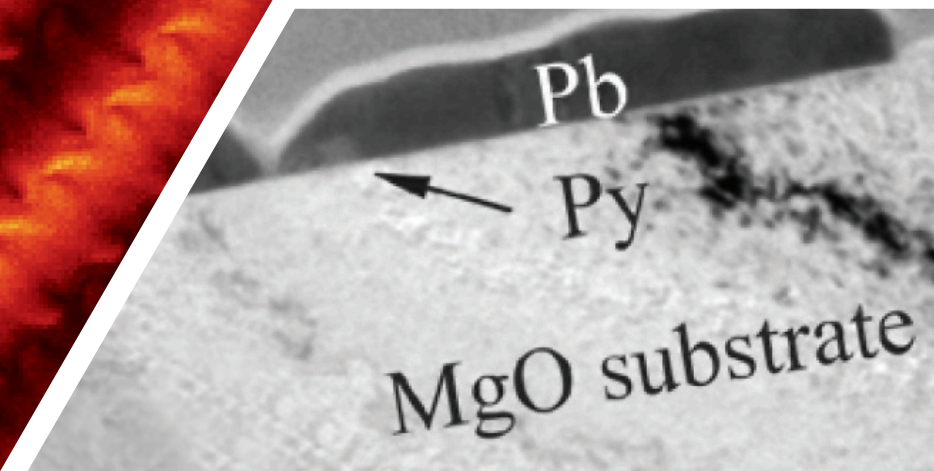
August 22–26, 2022, Kazan, Russia